Geosynthetics '97
Conference Proceedings

Volume 1
High-Strength Reinforcement
Marine
Geosynthetics Durability
Student Session
Remediation and Containment
Erosion Control

GEOSYNTHETICS
9 7
CONFERENCE
Long Beach, California USA

SOLMAX

Geosynthetics '97

Conference Proceedings

Volume 1

High-Strength Reinforcement
Marine
Geosynthetics Durability
Student Session
Remediation and Containment
Erosion Control

GEOSYNTHETICS '97 CONFERENCE
Long Beach, California USA

Geosynthetics '97 *Conference Proceedings*

Conference Organizers

The Industrial Fabrics Association International (IFAI) is extensively involved in the
geosynthetics industry, and serves its membership by facilitating the worldwide
development, application and proper utilization of products manufactured by the
geosynthetics industry.

The North American Geosynthetics Society (NAGS) is a professional society dedicated to
advancing the use of geosynthetics as engineering materials, and providing forums to
facilitate communication among geosynthetics-related interests.

The International Geosynthetics Society (IGS) is the international professional society that
brings together individuals and organizations involved with geosynthetics. The IGS has
members in 58 countries.

GEOSYNTHETICS '97 CONFERENCE
Long Beach, California USA

Foreword

The contributions and success of the previous geosynthetics conferences presented the Geosynthetics '97 Organizing Committee with outstanding precedents to meet. The technical papers published in past proceedings from the geosynthetics conference series have proven to be valuable reference documents for the industry. The 76 papers published in these proceedings provide up-to-date contributions to that heritage. The papers that were accepted to this conference were eligible for the Awards of Excellence sponsored by NAGS and industry partners. This program was initiated to recognize excellence in the state-of-the-art and state-of the-practice of geosynthetics in North America.

The papers in these proceedings were selected from 167 abstracts received by the Organizing Committee in response to an international call for papers in 1995. The Technical Review Committee that reviewed the abstracts was composed of prominent members of the geosynthetics community representing academia, manufacturers, design and construction consultants, government, and a testing laboratory. Ten topic leaders in the Technical Review Committee were engaged to run eleven topics, which were presented in 17 sessions at the conference. The selected papers were reviewed by a minimum of two qualified individuals under the direction of the technical session leaders.

The Geosynthetics '97 challenge was to continue the tradition of disseminating the most current state of knowledge and practice in the geosynthetics industry, in the form of focused topics. Topics such as durability, filtration, interface friction, soil reinforcement and pavement systems continue to be of great value as advances are made in design approaches, laboratory studies, and documented case histories. Specialty topics on economics, marine, mining, and seismic design are fresh to the geosynthetics conference series, and were included to provide new focus areas for this venue.

We are pleased to continue the Student Paper Competition that was started at Geosynthetics '95. Under the leadership of Dr. Andre Rollin, a panel of industry, academic and government professionals selected five student papers which were presented at the conference and are published in these proceedings. IFAI and NAGS provided expense-paid trips to the students to participate in the conference as part of their efforts to support the future of our industry.

We must recognize the individuals comprising the Technical Review Committee, session leaders, paper reviewers, and advisors who donated their time to maintain the high standard of technical contribution provided in geosynthetics conference series. The dedication, cooperation, and quality efforts from these individuals is not only invaluable to the benefit of these proceedings, but is symptomatic of the actual and potential value and importance that geosynthetics play in the basic infrastructure of our society.

Larry Well
Co-Chairman, Technical Committee
Geosynthetics '97

Richard Thiel
Co-Chairman, Technical Committee
Geosynthetics '97

Geosynthetics '97
Organizing Committee

Organizing Committee Chairman
John N. Paulson
Strata Systems Inc.
Cumming, Georgia USA

Technical Committee Co-chairman
Larry W. Well
CH2M Hill
Portland, Oregon USA

Technical Committee Co-chairman
Richard S. Thiel
Thiel Engineering
Oregon House, California USA

Advisor
Richard J. Bathurst
Royal Military College Of Canada
Kingston, Ontario Canada

Advisor
Y. Grace Hsuan
Geosynthetic Research Institute
Drexel University
Philadelphia, Pennsylvania USA

Panel Session Chairman
Rick Thomas
TRI/Environmental Inc.
Austin, Texas USA

Secretary General
Danette R. Fettig
Industrial Fabrics Association International
St. Paul, Minnesota USA

Geosynthetics '97
Technical Review Committee

Technical Committee Chairman
Larry W. Well
CH2M Hill
Portland, Oregon USA

Technical Committee Chairman
Richard Thiel
Thiel Engineering
Oregon House, California USA

High-Strength Reinforcement
Barry Christopher
Roswell, Georgia USA

Mining
Brian Simpson
Golder Associates
Lakewood, Colorado USA

Remediation & Containment
Gregory Richardson
G.N. Richardson & Associates
Raleigh, North Carolina USA

Seismic Design and Construction
Edward Kavazanjian, Jr.
GeoSyntec Consultants
Huntington Beach, California USA

Interface Friction Testing
Allen Marr
GeoTesting Express
Acton, Massachusetts USA

Pavement Systems
Mark Marienfeld
Amoco Fabrics & Fibers Co.
Atlanta, Georgia USA

Economics
Alice Comer
Bureau of Reclamation
Materials Engineering
& Research Lab
Denver, Colorado USA

Erosion Control & Marine
Marc Theisen
Synthetic Industries Inc.
Chatanooga, Tennessee USA

Durability
Donald Bright
The Tensar Corp.
Morrow, Georgia USA

Filtration
Shobha K. Bhatia
Syracuse University
Syracuse, New York USA

Table of Contents: Volume 1

HIGH-STRENGTH REINFORCEMENT

MARINE

Table of Contents: Volume 1

GEOSYNTHETICS DURABILITY

STUDENT SESSION

Table of Contents: Volume 1

REMEDIATION AND CONTAINMENT

Table of Contents: Volume 1

EROSION CONTROL

Table of Contents: Volume 2

PAVEMENT SYSTEMS

ECONOMICS

Table of Contents: Volume 2

Table of Contents: Volume 2

MINING

FILTRATION

High Strength Reinforcement

GEOSYNTHETICS 97

CONFERENCE

Long Beach, California USA

PRESTRESSED GEOSYNTHETIC REINFORCEMENTS FOR SOIL-BEARING SYSTEMS

R. FLOSS
TECHNICAL UNIVERSITY, MUNICH, GERMANY
G. GOLD
CRYSTAL GEOTECHNIK, UTTING, GERMANY

ABSTRACT

For the foundation of sports fields on very compressible and inhomogeneous subsoils a concept was developed and realized, which included prestressed geosynthetics to reduce differential settlements and to increase bearing capacity of insitu soil.

For analyzing the effectiveness and performance of the prestressing, calculations based on the Finite Element Method have been carried out. Different systems were examined by variation of the properties for the subgrade, thickness of the granular layer, stiffness of the geosynthetic and the degree of prestressing.

INTRODUCTION

The load and deformation behavior of earth constructions can be strongly improved by using geosynthetic reinforcements of high tensile strength. The fundamentals of this infacing mechanics and the principles of stability and deformation analyses are given (Floss, 1987).

The efficiency of the reinforcement is due to the anisotropic characteristics of the soil system. The performance increase is achieved by the introduction of stresses to the geosynthetic. To invoke these stresses, considerable system deformations are required. These deformations often can not be accepted because of the limited allowable deformations of soils (shear failure) as well as because of the usability of the system. Therefore the performance of the reinforcement with low system deformations is often on low level. Because of this and having a load input into the geosynthetic without system deformations the idea was developed, to prestress the reinforcement on a defined level until the system is loaded

At the institute of foundation engineering, soil and rock mechanics of the Technical University Munich the load and deformation behavior of the reinforced two-layer system is a theme of extensive investigations. Based on these research results (Bauer, 1989; Gold, 1993) the influence of different degrees of prestressing of the reinforcement were analyzed using the Finite Element Method (FEM). For idealizing the prestressing and analyzing the effect of prestressing a solution was found which is in good accordance to the procedure during construction. First of all a technology for prestressing the geosynthetics was developed and large scale was performed for the first time in the construction of sports grounds on very soft subgrade in Prien/Chiemsee (in the south of Germany).

FOUNDATION WITH PRESTRESSED GEOGRIDS FOR SPORTS GROUNDS

On an area of about 70 000 m² the municipality Prien/Chiemsee dedicated their new leisure and sport facility in1994. The territory is situated in the terrain of the Chiemsee glacier. The sedimentations of the glacier were eroded and replaced by river gravel and geologically very young flood sedimentations. Therefore the subsoil was very soft and inhomogeneous and had a low ultimate bearing capacity.

Soil and groundwater protection was required so that the institute of foundation engineering, soil and rock mechanics of the Technical University Munich suggested to avoid injuries of the the outcropped soils and disturbances of the ground-water level but to build up a load spreading foundation layer, reinforced with geogrids of high tensile strength and joint stiffness. This solution was planned and realised after soil investigations and large scale in-situ tests were carried out (Figure 1).
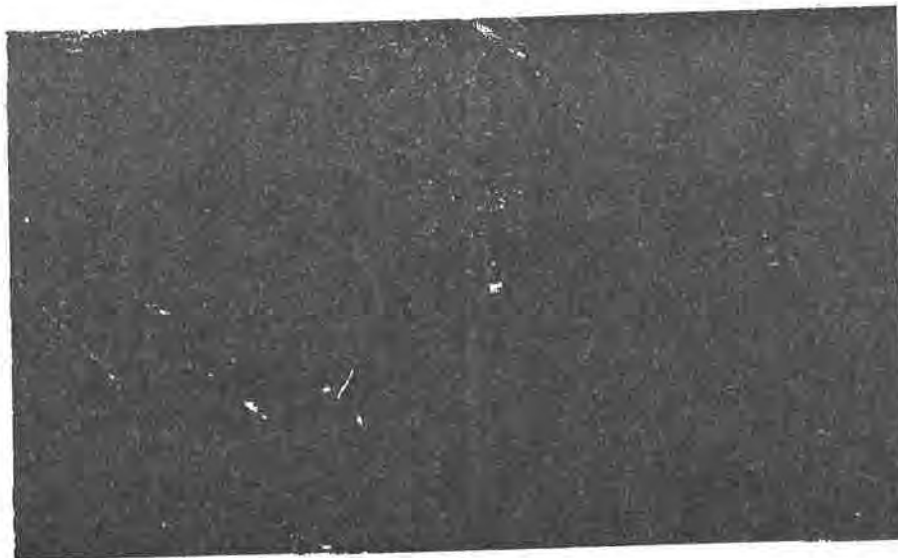
Figure (1): Arial view during prestressing of the lower layer of the reinforcement with the help of two plants over the whole width of the field

The main fields of the sports ground received a foundation as described below:

- The surface soil, which has a better shear strength because of roots of plants, was not removed, but after grass mowing directly used as substructure. Interventions in subsoil and ground water system could be avoided and cost saving were achieved.
- Spreading of a nonwoven geotextile to separate the granular layer from subgrade soil. This is important with increasing rotting of the grassland.
- Sand-gravel mixture with about 20 % clay and silt as barrier layer to the subgrade with very low permeability ($k \approx 10^{-8}$ m/s) in a thickness of about 10 - 15 cm. Furthermore this layer was the base for the reinforced gravel layer.
- Spreading the lower layer of geogrids and mechanical prestressing. On this prestressed geosynthetic a granular layer (gravel) in a thickness of 50 cm was constructed and compressed (Figure 2).

Figure (2): Unit with arrangement for prestressing of the reinforcement and subsequently covering with gravel

- Spreading of the upper layer of geogrids as second bed of reinforcement and prestressing. This reinforcement layer is to connect mechanically with the lateral pulled up lower reinforcement layer.
- Covering with gravel with a height of 25 cm as upper frost protection and bedding layer for the surface of the sport grounds.
- For adsorbing and draining off rain and surface water in the upper gravel layer trenches were included.

Prestressing and connecting of the both reinforcement layers resulted in a very stiff carrying pad. The prestressing level was chosen between 1 and 5 % in dependence on air temperature and according to first trials. A measurement program was carried out to document the behavior of the foundation. The vertical settlements were controlled with gauges. Under the sport grounds horizontal measuring tubes were installed. After termination of the construction work in 1994 and two years of utilisation the novel type of construction seems to be very successful.

ANALYTICAL EXAMINATIONS OF PRESTRESSED SYSTEMS

Modeling of the System and Prestressing. Leaning upon the construction work in Prien, the calculations were carried out using the reinforced two-layer system. Because of the symmetry only one half of the system had to be modeled (see Figure 3).
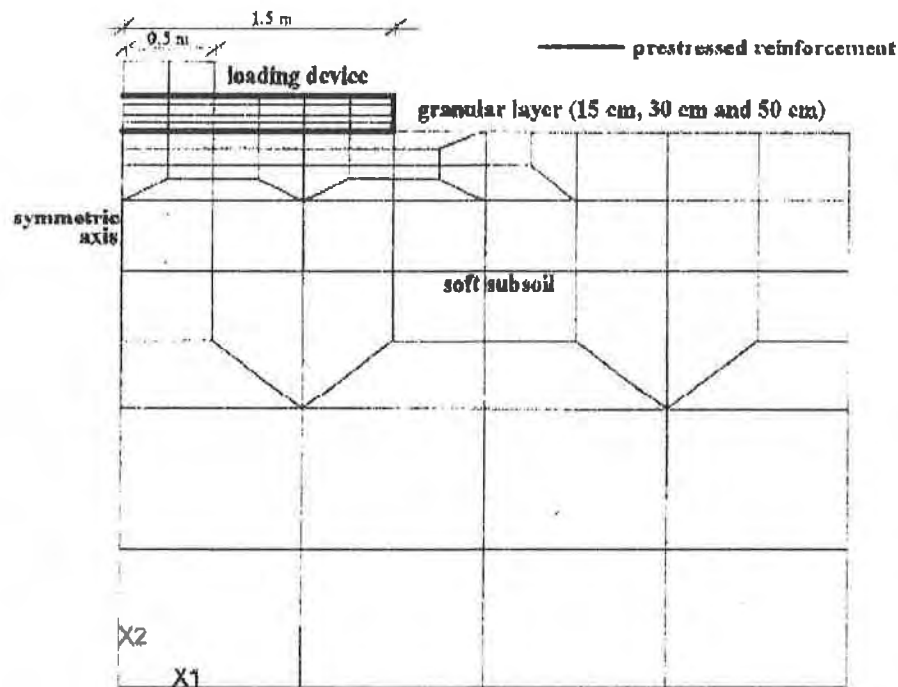
Figure 3: Prestressed Finite Element Model

The width of the loading device was 50 cm; the width of the granular layer was 1.5 m. The soil continuum is modeled by eight node isoparametric elements with quadratic shape functions. For the geosynthetics three node isoparametric bare elements were used. Calculations without bare elements were carried out for analyzing unreinforced systems (for reference).

The prestressing of the reinforcement was modeled numerically by the load-case "temperature drop constant over the sectional area". By choosing the coefficient of expansion for temperature α_t and the difference in temperature δ, well nearly any prestressing may be simulated. For

systems which are statically determinate the prestressing of the reinforcement $\varepsilon_{reinforcement}$ can be calculated by

$$\varepsilon_{reinforcement} = \alpha_t \cdot \delta t . \tag{1}$$

Because the systems are statically indeterminate, the temperature gradient of the reinforcement can't be computed using equation (1). In different areas of the reinforcement the temperature gradients must be slightly varied to reach the same prestressing of the geosynthetic, depending on the system geometry, the parameters for the idealized soils and geosynthetics, etc.. Furthermore the calculations are to carry out non linear. The used numerical iteration algorithms of the FEM-calculation are given (Gold, 1993). Usually the estimated extensions are smaller compared to equation (1). Carrying out the first calculations a multiplier of 1,2 for the temperature gradient was found to accelerate the computations. For reaching equal prestressings everywhere in the reinforcement an iterative procedure, as described below, is necessary for each system:

1. Non-linear calculation for load-case 1 (consolidation considering the own weight of the system)
2. Load-case 2: determination of a constant temperature drop δ_t for the proposed prestressing $\varepsilon_{reinforcement}$ using the equation

$$\delta_t = \left(\frac{\varepsilon_{reinforcement}}{\alpha_t} \right) \cdot 1,2 \tag{2}$$

3. Non-linear calculation for load-case 2 (−prestressing)
4. Control, if

$$\varepsilon_{reinforcement, calculation} \approx \varepsilon_{reinforcement} \tag{3}$$

for each element of the reinforcement. In the case, that

$$\left| \frac{\varepsilon_{reinforcement, calculation}}{\varepsilon_{reinforcement}} \right| > Tol , \tag{4}$$

$\delta_{t,new}$ is set to

$$\delta_{t,new} = \delta_t \cdot \frac{\varepsilon_{reinforcement, calculation}}{\varepsilon_{reinforcement}} . \tag{5}$$

Tol is estimated from the ratio of the calculated and the proposed prestressing of the reinforcement. For the practical work, values between 5 and 10 % for Tol are approved.
5. If equation (4) is true for one or more elements of the reinforcement, continue at point 4. Otherwise the process for simulating the prestressing is completed and the load-cases 1 and 2 are primary load-cases.

<u>Material Properties and Calculations.</u> Five basic systems were examined, as presented in Table 1:

- Granular layer 15 cm; very soft sub soil
- Granular layer 15 cm; soft sub soil
- Granular layer 30 cm; very soft sub soil
- Granular layer 30 cm; soft sub soil
- Granular layer 50 cm; very soft sub soil

The essential material properties are given in Table 1.

Table 1: Material Properties

		Deformation modulus E [kPa resp. KPa·m]	Friction angle ϕ' [°]	Cohesion c' [kPa]
Subsoil	very soft	750	0,0	10
	soft	2000	20	5
Granular layer	not varied	80000	37.5	0
Reinforcement	mean tensile strength	200	-	-
	high tensile strength	1000	-	-

For analyzing the degree of prestressing, two different levels of prestressing (3 % and 6%) were idealized for each basic system. Furthermore two reinforcements with different stiffnesses (200 kN/m and 1000 kN/m) were examined. Including the unreinforced and the reinforced, but not prestressed system, seven variants for each basic system had to be computed:

- unreinforced
- reinforcement stiffness: 200 kN/m; not prestressed
- reinforcement stiffness: 200 kN/m; prestressing: 3 %
- reinforcement stiffness: 200 kN/m; prestressing: 6 %
- reinforcement stiffness: 1000 kN/m; not prestressed
- reinforcement stiffness: 1000 kN/m; prestressing: 3 %
- reinforcement stiffness: 1000 kN/m; prestressing: 6 %

Altogether 35 systems were calculated.

The loading of the system was done incrementally. For each new load-case 20 kPa on the loading device was defined and the last load-case was considered as primary load-case (always including the own weight and prestressing). Altogether 10 load-cases per system were required, to reach 160 kPa. Until 2000 iterations were to carry out for single load-cases.

Results of Analysis. Figures 4 and 5 present the load-deformation data for the system with 0.5 m granular layer, a cohesion for the subsoil of 10 kPa and a friction angle of 0° and for reinforcement moduli of 200 kN/m respectively 1000 kN/m.
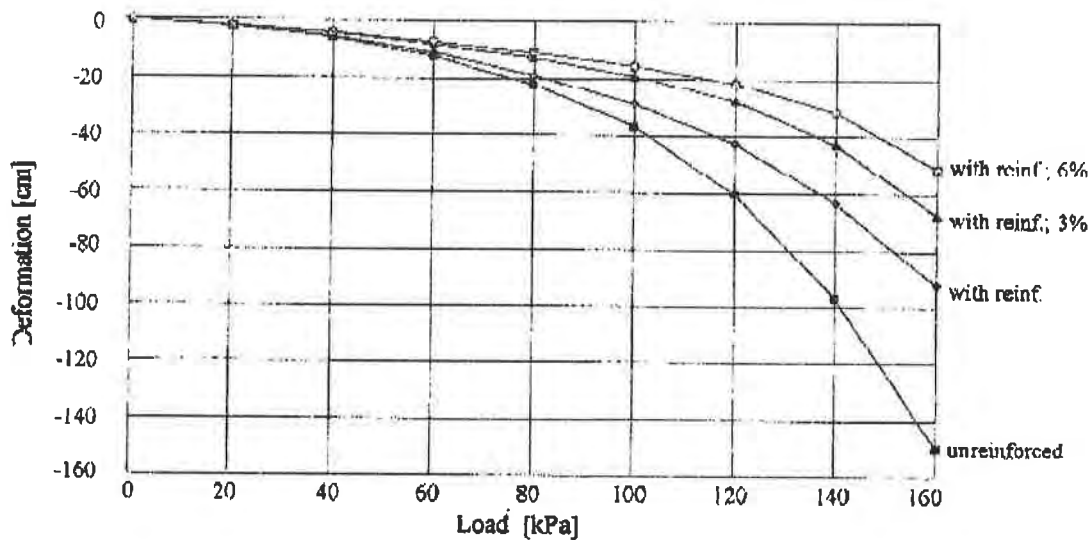
Figure 4: Load-deformation data for systems with 0.5 m granular layer, very soft subsoil ($c' = 10$ kPa, $\phi = 0°$) and a stiffness of the reinforcement of 200 kN/m
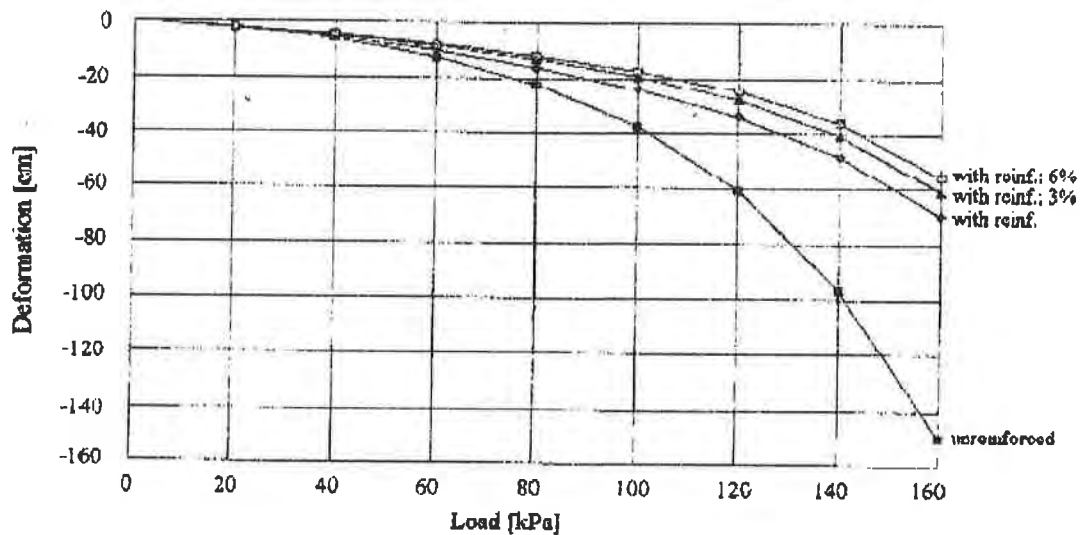
Figure 5: Load-deformation data for systems with 0.5 m granular layer, very soft subsoil ($c' = 10$ kPa, $\phi = 0°$) and a stiffness of the reinforcement of 1000 kN/m

The influence of the reinforcement is significant for both systems. In addition to lower stiffness of the reinforcement there is to remark a strong influence of the prestressing of the reinforcement (Figure 4). With increasing stiffness of the reinforcement their prestressing is of secondary importance. The deformations of the reinforced, not prestressed system amount to 62 % of the deformations of the unreinforced system (=100 %) at lower stiffness of the reinforcement At a prestressing of 3 % about 45 %, at a prestressing of 6 % approximate 38 % of the deformations of the unreinforced system were calculated.

Figures 6 and 7 present the calculated load-deformation data for 0.15 m and 0.3 m granular layers, at a stiffness of the reinforcement of 200 kN/m and very soft subsoil conditions ($c' = 10$ kPa, $\phi = 0°$).

Basically at the lower thickness of the granular layers the load-deformation data presents a similar characteristic compared to the 0.5 m granular layer system. At higher stiffness of the reinforcement there was also for lower thickness of the granular layer a smaller influence of the prestressing.

Lower absolute values for the deformations were estimated for better subsoil conditions (see Table 1). But the influence of the reinforcement and of their prestressing showed a comparable relation as given above. Therefore the load-deformation graphics are not explicitly documented in this paper, but the main results are shown in Table 2 and Figure 8.
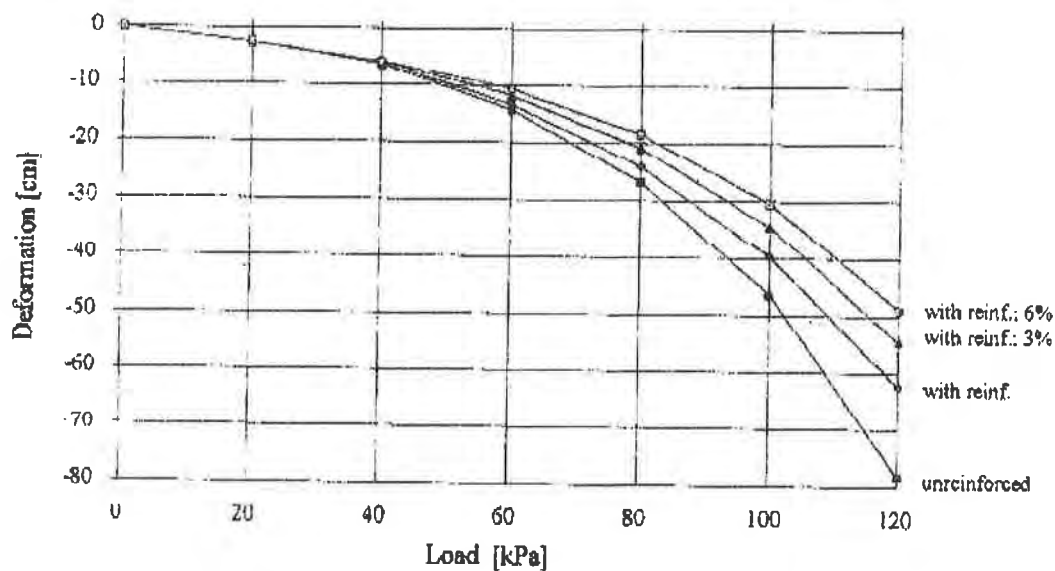
Figure 6: Load-deformation data for systems with 0.15 m granular layer, very soft subsoil ($c' = 10$ kPa, $\phi = 0°$) and a stiffness of the reinforcement of 200 kN/m
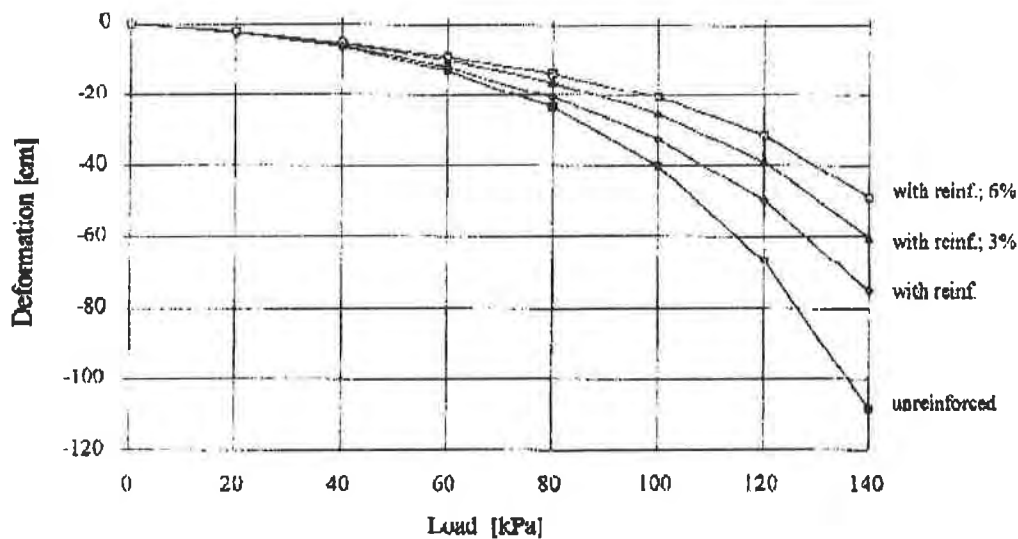
Figure 7: Load-deformation data for systems with 0.3 m granular layer, very soft subsoil
($c' = 10$ kPa, $\phi = 0°$) and a stiffness of the reinforcement of 200 kN/m

In Table 2 and Figure 8 the calculated deformations of all analyzed systems are compared, always referred to the accompanying unreinforced basic system and for the highest load-case.

Table 2: Deformations (in per cent), always referred to the accompanying unreinforced system

Kind of reinforcement/	Subsoil: $\varphi' = 0°$; $c' = 10$ kPa			Sub.: $\varphi' = 20°$ $c' = 5$ kPa	
Level of prestressing	Lay.: 15 cm	Lay.: 30 cm	Lay.: 50 cm	Lay.:15 cm	Lay.: 30 cm
unreinforced	100,00	100,00	100,00	100,00	100,00
reinforced 200 kN/m	74,59	66,39	61,53	84,57	81,90
reinforced 200 kN/m; 3 %	67,96	55,12	44,96	70,39	60,34
reinforced 200 kN/m; 6 %	62,77	46,27	38,17	62,22	51,77
reinforced 1000 kN/m	65,00	52,73	46,73	78,32	74,87
reinforced 1000 kN/m; 3 %	65,44	47,89	40,74	71,77	64,73
reinforced 1000 kN/m; 6 %	57,72	45,90	37,10	67,77	58,21

The most significant reduction of the vertical deformation by using a reinforcement was calculated by the systems with the thickest granular layer (= 0.5 m). The prestressing of the reinforcement generally shows better effects with decreasing stiffness of the reinforcement. The reason for this is, that reinforced systems with a high stiffness of the reinforcement shows a good performance even without prestressing. The effect of the prestressing is less dominant compared with systems with a lower stiffness of the reinforcement.
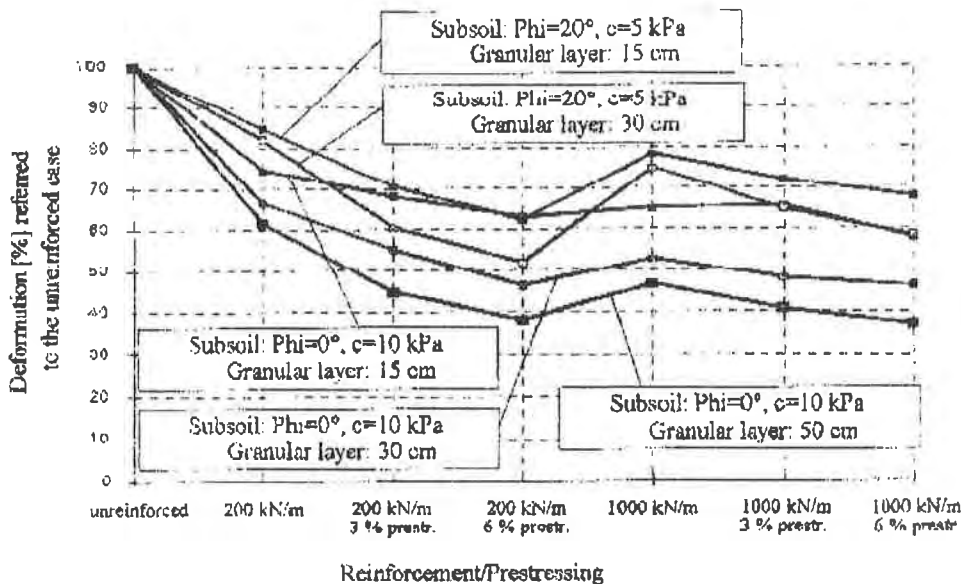
Figure 8: Calculated deformations in per cent, referred to the unreinforced system

Conclusions and valuation.

The discovered kind of simulating the prestressing of the reinforcement by using the load case „temperature reduction" is well suited to calculate the stress and deformation behavior of prestressed systems. For the practical design, it seems to be necessary, to develop a software extension to simplify the described iteration process.

For practical applications the decrease in bearing behavior can be estimated. Calculated reductions in deformation up to 50 %, referred to the unreinforced system and up to 38 % (6 % prestressed system, 0.5 m granular layer and a stiffness for the reinforcement of 200 kN/m), referred to the reinforced, not prestressed system show, that there are considerable load carrying reserves for earth systems, strengthened with prestressed geosynthetics.

The relevant reasons for the improvement of the bearing and deformation characteristics by prestressing the reinforcement can be summarized as follows:

- By prestressing the reinforcement, the stress situation of the granular layer is modified. The prestressing operates mainly in horizontal direction. Therefore the horizontal stresses are increased by prestressing the reinforcement. When the loading (in vertical direction) is brought on the system, there is an increase in vertical stresses. Several load steps can be brought up, until a stress situation, comparable to the hydrostatic stress situation; is achieved again. The increase of the second invariant of the stress deviator, which is important for the yielding of the system, happens on higher load level. The results are:

- The deformations of the granular layer itself are reduced, because plastic deformations are only reached on a higher load level.
- Because of the higher load level in the granular layer, there is given a better load spreading in this layer and it has a character comparable to a beam. Therefore bigger areas of the subsoil are claimed and smaller deformations result for the whole system. This is the essential effect for the reduction of the system deformations, because the main parts of the deformations result from the soft subsoil.

- Because of the system deformation, the geosynthetic layer is able to overtake a part of the vertical loading, depending on the stiffness of the reinforcement and the geometrical figure of the deformed system. The model for this load carrying behavior is well-known in the geosynthetic literature and called the membrane effect. The membrane effect is favored by prestressing the reinforcement. Furthermore the prestressed systems have two layers of reinforcement to overtake vertical stresses. Therefore the height of the membrane effect is to take into consideration surely more than once but less than twice.

ACKNOWLEDGEMENTS

REFERENCES

Floss, R., (1987) "Soil systems with geotextile reinforcements - State of the art on stability analyses", The Post Vienna Conference on Geotextiles, pp. 202-212

Bauer, A., (1989) "Beitrag zur Analyse des Tragverhaltens von einfach bewehrten Zweischichtensystemen", Schriftenreihe des Lehrstuhls und Prüfamtes für Grundbau, Bodenmechanik und Felsmechanik der Technischen Universität München, Vol. 15

Gold, G., (1993) "Untersuchungen zur Wirksamkeit einer Bewehrung im Zweischichtensystem", Schriftenreihe des Lehrstuhls und Prüfamtes für Grundbau, Bodenmechanik und Felsmechanik der Technischen Universität München, Vol. 19

BRIDGING A SINK-HOLE BY HIGH-STRENGTH HIGH-MODULUS GEOGRIDS

Dimiter A. Alexiew, Dr.-Ing.
HUESKER Synthetic GmbH & Co.
Gescher, GERMANY

ABSTRACT

A section of 'Federal Roadway B 180' at Neckendorf near Eisleben, Germany, is once again in service after being blocked for years. The roadway was destroyed across its entire width in 1987 by a sink-hole. The sink-hole, located along the centerline of the roadway, is 30 meters deep and 8 meters in diameter. Although the hole has been re-filled, the danger of a new subsidence due to deep underground caverns still exists. In order to put the road into operation again, the sink-hole had to be bridged to ensure acceptably low deflection values of the roadbase even under heavy truck loads.

Due to lower costs and 'ductile' deformation behavior, a geogrid-reinforced gravel cushion was preferred to a concrete bridging plate. A geogrid with very high strength (UTS = 1200 kN/m) and high modulus (40 000 kN/m at 3% elongation) was chosen. The project is the first of its kind using high-modulus geogrids in Germany for road construction. The road has been in use since October 1993 without any further deformations.

This paper describes the reinforcement concept, design philosophy, dimensioning, materials used and safety measures (control system) installed, and provides details and photographs of the reconstructed roadway.

INTRODUCTION

Problem description. In the region of Eisleben, Germany, stable soil layers of 20 m up to 40 m thick often overlie water-soluble soils. Due to ground-water flow in these soils natural caverns up to ten meters wide can develop. This well known phenomena may result in the creation of nearly vertical cylindrical "chimneys" in the soil mass above the cavern. The soils above can collapse into the cavern with a resulting sink-hole at the surface.

The collapsed soil material leaves an irregular shaped crater at the ground surface with dimensions of up to 20 m wide and 10 m deep. The subsidence occurs over relatively short periods of time while additional settlements may continue due to the loose nature of the collapsed soils within the "chimney".

A large sink-hole which developed due to this phenomena distroyed the 'Federal Roadway 180' at Neckendorf near Eisleben in 1987. The roadway collapsed across is entire width with the loss of soils initially in the lower portion of zone 1 and later settlement occurring in zone 2 as seen in Figure 1. A temporary bypass for the heavily traveled Roadway B 180 was built in 1987 – 1988, however, the bypass caused serious difficulties for the existing levels of traffic. A more permanent solution had to be developed which provided a smooth flow of traffic along the original roadway alignment in addition to creating a non-hazardous roadway for the commuters.

Zone 1 = lower subsidence probability
Zone 2 = higher subsidence probability
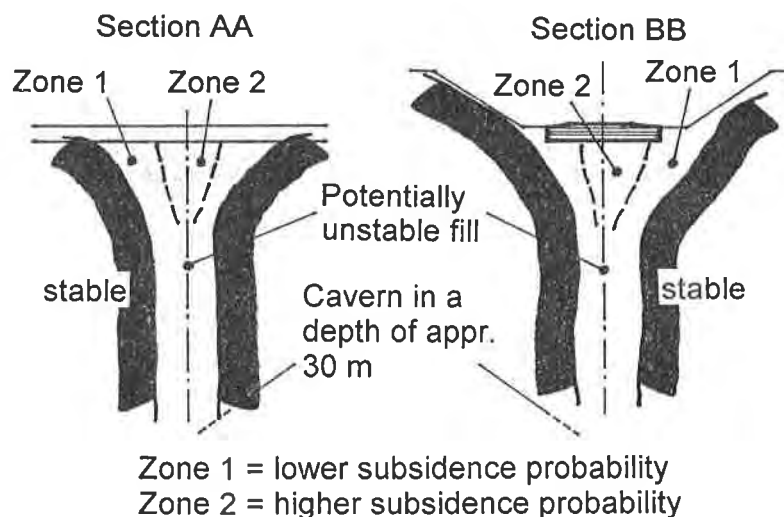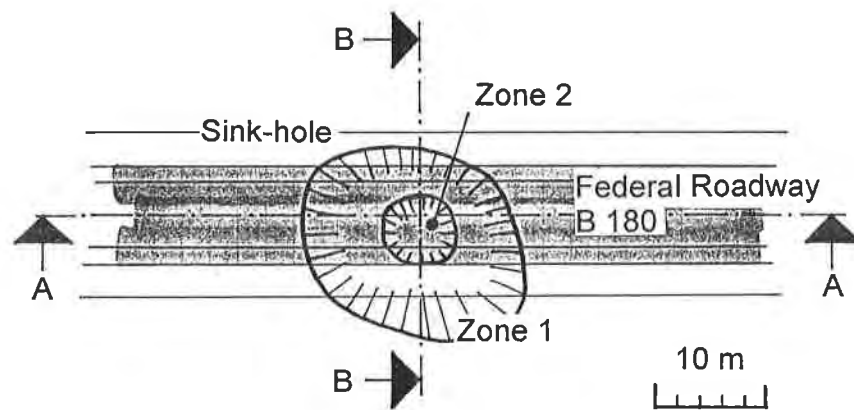
Figure 1: Geometry and zones of the sink-hole

In order to stabilize the upper part of the "chimney" the crater was completely filled by loosely placed imported stone/sand materials. After about two years it was determined by geodetical measurement that no further settlements occurred on the surface of the fill. However, information was not available regarding the density and stability of the collapsed soil and the new fill in the sink-hole, nor about the ongoing processes in the deep cavern due to ground-water flow. Therefore, for reasons of safety, the roadway remained blocked until 1993.

RECONSTRUCTION

Concept and design philosophy. In 1992,'Straßenbauamt', the administration responsible for Roadway B 180, decided to put Roadway B 180 into adequate operation again because the provisory bypass was not considered to be acceptable any longer due to increasingly intensive traffic.

The present understanding regarding the global mechanical behavior of the filled sink-hole over time was not sufficient. A reliable long-term prognosis was not possible. However, based on the history of the sink-hole and measurements after filling it seemed to be plausible to predict a higher probability for a new collapse in zone 2 and a lower subsidence probability in zone 1. The worst case scenario would be for a catastrophic failure of the complete "chimney" consisting of zones 1 and 2 (See Figure 1).

Generally two possible technical solutions were in discussion: a steel-reinforced concrete bridging plate and a geosynthetic-reinforced gravel cushion. The concrete plate was not considered an acceptable solution for two reasons: the extremely high costs for materials and construction and the possibility of a "brittle" rupture behavior in the event of exceeding the bearing capacity. It was determined that the advantage of small deformations in a pre-rupture stage did not compensate for the disadvantages described above. Consequently, the consultant 'KUHN-Engineering GmbH, Leipzig', preferred the solution with a strongly geosynthetic-reinforced gravel cushion. The preliminary design calculation resulted in the requirement of a very high tensile strength, tensile stiffness and low creep of the reinforcement.

Dimensioning, design and materials. The final dimensioning and design by the engineering consultant took place in early 1993 in collaboration with the engineers at HUESKER Synthetic GmbH & Co. Generally three possible dimensioning procedures were analysed: Giroud (1982), Giroud et al. (1990) and British Standard 8006 (1995), all based on the well established "membrane theory" for the reinforcement layer. BS 8006 was at this time still a draft.

The method in accordance with Giroud (1982) seemed to be very conservative. Further it has the disadvantage, that no prognosis for the deflection of the road surface can be made.

The method in accordance with Giroud (1990) is less conservative, because soil arching has been assumed. Unfortunately there is again no possibility to predict or to take into account the deflection of the road surface according to this method. In addition, it seems very risky to assume a stable soil arching under the dynamic influence of traffic.

The method in accordance with BS 8006 (1995) – res. the draft in 1993 – is based on the experience in Great Britain in mining and similar areas prone to subsidence. First, no arching and, second, another failure mechanism are assumed in the ultimate limit state (See Figure 2 according to Figure 73 and 74 in BS 8006 (1995)).
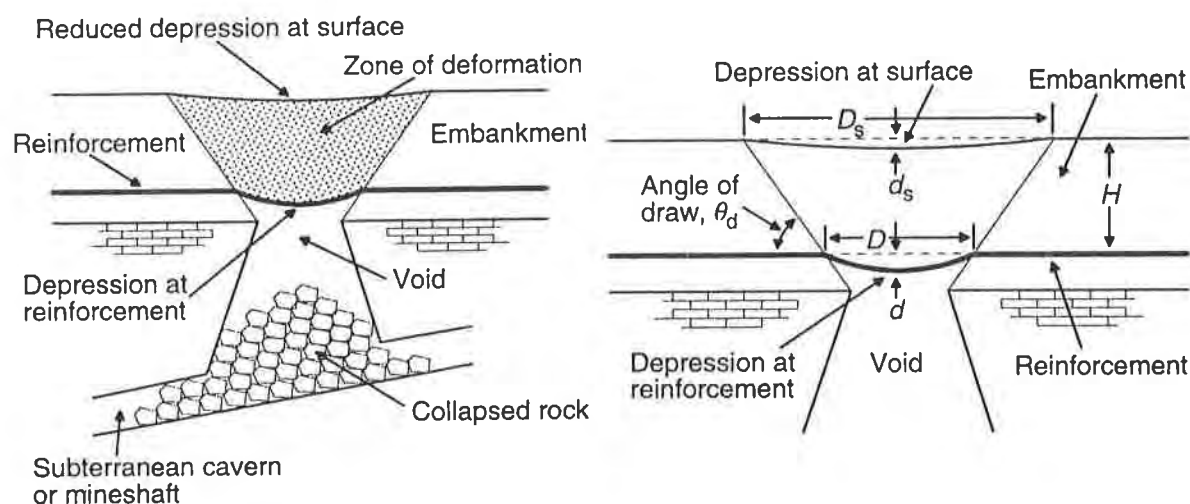
Figure 2: Dimensioning concept in accordance with BS 8006 (1995)

Further details about dimensioning equations etc. can be seen in BS 8006 (1995).

Notice, that only the method in accordance with BS 8006 (1995) allows for a prediction of the surface deflection (depression), connecting failure mode, reinforcement extension and surface depression.

Summarizing the typical assumptions, results and background experience of the methods mentioned above, logically the method in accordance with BS 8006 was found to be the most suitable for the final dimensioning of the system.

It was decided that a geogrid was preferred as the geosynthetic reinforcement as opposed to a geotextile due to the generally higher bond coefficients (anchorage capacity) achieved with geogrids over geotextiles. Notice, that in all dimensioning procedures mentioned above, formally the bond coefficient is not taken into account. Nevertheless, from the engineering point of view a better system behavior

has to be expected due to the immediate mobilizing of the tensile forces in a reinforcement with a high bond coefficient. Additionally, in the case described herewith, the good interaction is of greater importance than usually due to the limited "anchorage" lengths. The partial factors of safety for the reinforcement were adopted here from FGSV (1994), which was a draft in 1993. FGSV (1994) does not include dimensioning procedures for overspanning voids.

The logic of dimensioning and design can be shortly described as follows: The geogrid-reinforced cushion had to bridge over the more probable potential failure-zone 2 in cross and longitudinal directions (See Fig. 1) with a maximum relative deflection of (d_S/D_S, See Fig. 2) 0.015 perpendicular and/or parallel to the road axis. In this case a two-way spanning was required with sufficient anchorage length in both directions. The geogrid reinforced gravel cushion was supported in both directions along the edges of zone 2.

In the worst case where total failure of zone 1 would occur the geogrid-reinforced cushion had to bridge only the longitudinal direction (parallel to the road axis). This case was required to span the sink-hole only one-way, because the "edges" of zone 1 are too far away from the cushion to maintain a relative deflection of less than 0.015. In this worst case a relative deflection of 0.07 parallel to the road axis can be accepted only temporarily. At the first indications of the sink-hole the traffic would be stopped immediately. The deflection (bending) in cross direction was not a concern due to the linear alignment of the roadway at the area of reconstruction.

As shown in Figure 1, the axis of the road is positioned excentrically to the zone 2. It could lead to negative bending moments (tension of the upper side of the reinforced cushion in cross direction) and/or to local torsional deformations. Also, a torsion could take place under asymmetric traffic load in the worst case of collapse of the complete zone 1.

An exact dimensioning of the reinforced cushion for these cases is not possible. So it was decided to lengthen the "wrapped-back" ends of the second reinforcement layer (machine-direction = cross to the road axis) more than the required "usual" anchorage length (See Figure 4) to achieve a reinforcement for tension on the cushions upper side and a closed cross-reinforcement "ring" against torsion.

The analysis and dimensioning for both cases resulted in the need for an uniaxial geogrid with a tensile strength in machine direction of approximately 1180 kN/m tension force at 3.0 % strain (case: failure zone 1) and at least 470 kN/m at 1.8 % strain (case: failure zone 2). A five meter wide uniaxial geogrid was developed and produced in accordance to these specifications. The load-strain curve for this product in the machine direction is shown on Figure 3.
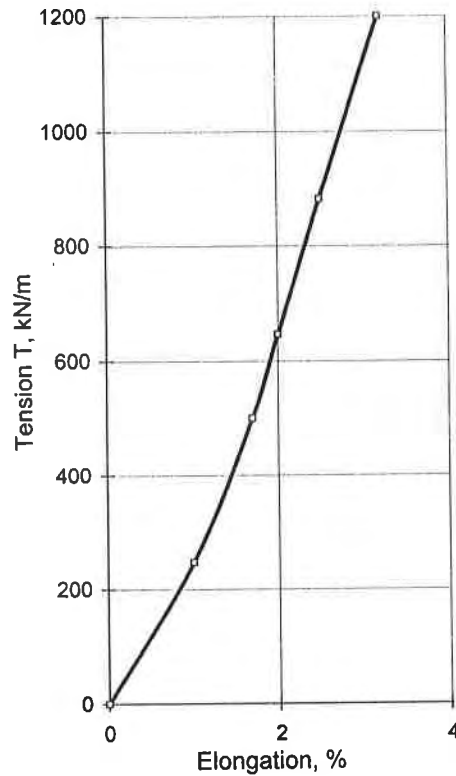
Figure 3: Load-strain curve of geogrid-reinforcement (MD)

The cross-section of the roadway and reinforced cushion is shown on Figure 4, while plan views of the geogrid reinforcement and control wires are shown on Figure 5. The lowest layer of geogrid reinforcement (longitudinal) was designed primarily for the one-way spanning reinforcement required in the " zone 1 failure case" and secondarily as half of the two-way spanning reinforcement required for the "zone 2 failure case". The second layer of geogrid was designed to provide the second half of the two-way spanning reinforcement required for the "zone 2 failure case". The upper layers are the wrapped back ends of geogrid from the second layer which ensure adequate anchoring and creation of a closed reinforcement ring for resistance against torsion.

For the cushion soil a well graded pure gravely sand (GW) according to German standard DIN 18196 with minimum grain size 0.1 mm and maximum grain size 56 mm was prescribed. It had to be compacted to a relative proctor density of $D_{pr} \geq 103$ %, ensuring good mechanical properties and compound behavior of the gravel-geogrid system.
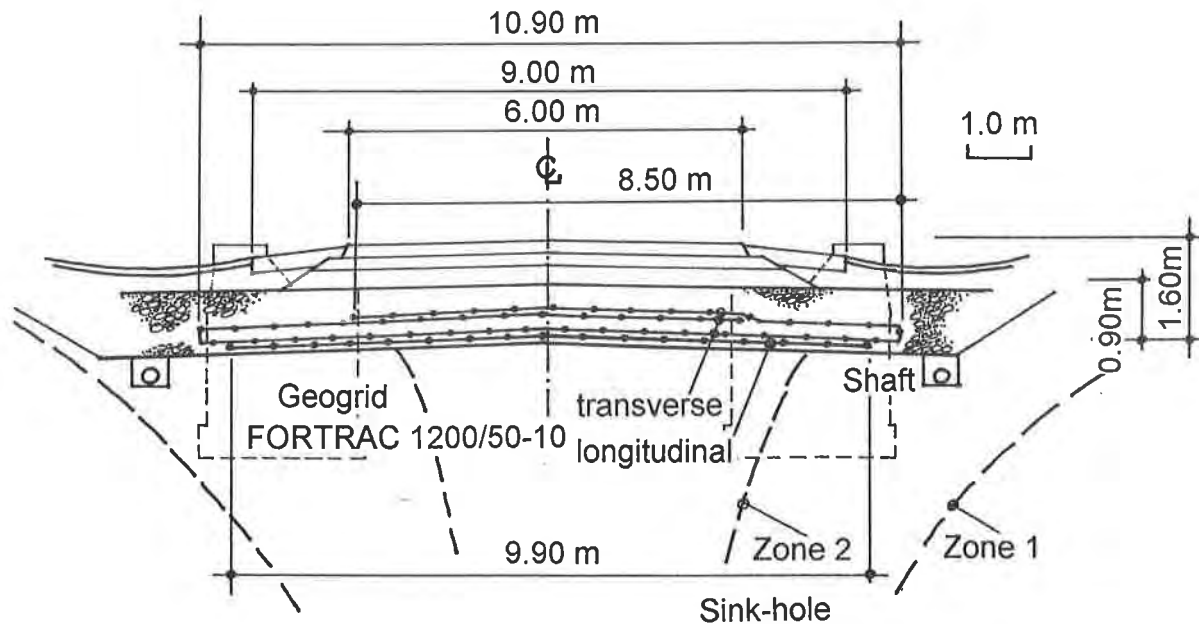
Figure 4: Cross section of reinforced gravel cushion

CONTROL SYSTEM

Due to the importance and the heavy levels of traffic on the Federal Roadway B 180, the complexity of the problem and the impossibility to analyse exactly all theoretical possible situations (the modes "failure zones 1/2" are more or less predictions of probabilistic type) the road administration and the consultant decided to install a control and warning system, consisting of steel wires and control shafts as shown on Figure 4 + 5. The nearly inextensible wires are connected to electrical gauges in the shaft. The wires (before pulling tight) can be seen on Figure 8. If the elongation /displacement of any of the four wires indicates a deflection and/or bending of the reinforced structure corresponding to an elongation of 3 %, a warning system will be activated and the traffic will be stopped in both directions at a safe distance on both sides of the critical area. The critical 3 % was selected in accordance with the dimensioning predictions and the stress-strain curve of the geogrid reinforcement.

EXPERIENCE IN THE STAGE OF CONSTRUCTION.

The geogrids were delivered with the project installation lengths pre-fabricated. The geogrids flexibility and relatively low mass per unit area (high specific strength) resulted in an easy handling and installation on site (See Fig. 6, 7, 8 + 9) by a four man construction crew. The grid's flexibility made it possible to fabricate the measurement/control shafts (See Fig. 9). Additional partial layers of grid cut to smaller widths were installed in both directions around the shafts to compensate the cut-offs in these zones.

Left diagram labels:
- Roadway
- Overlapp. 0.10 m
- 5.0 m
- Control wires on sec. geogr. layer
- Second (upper) geogrid layer; MD = transv. road dir.
- 58.8 m
- Shaft
- Road axis
- 10 m
- 5.45 m | 5.45 m
- 10.9 m

Right diagram labels:
- Roadway
- Shaft
- 12.0 m
- First geogrid layer; MD = road-axis direction
- 5.0 m
- Sink-hole
- 5.0 m
- 0.10 m overlapp.
- 50.0 m
- 31.0 m
- Road axis
- 7.0 m
- 4.95 m | 4.95 m
- 9.90 m
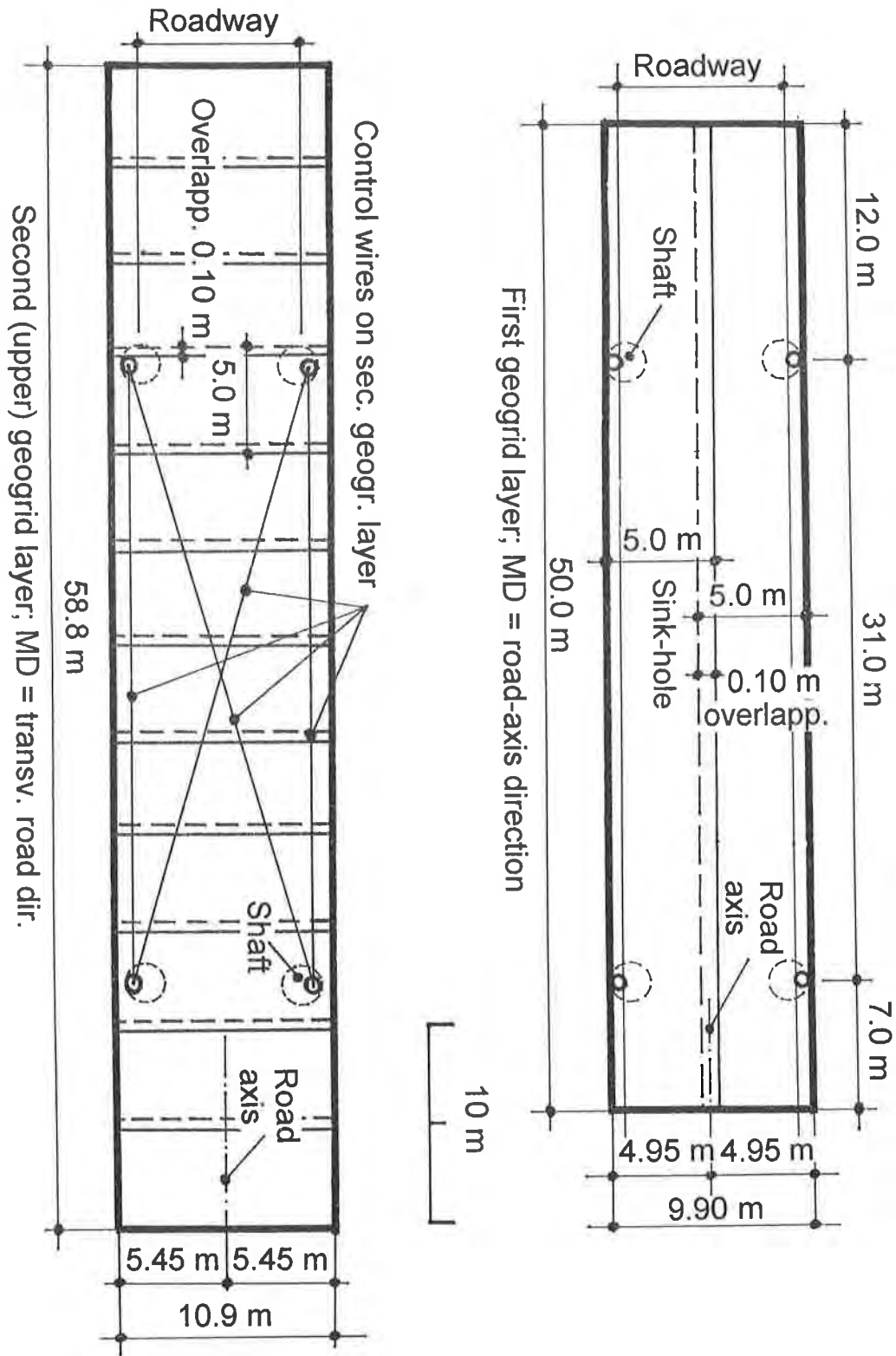
Figure 5: Plan view of reinforced gravel cushion and control system
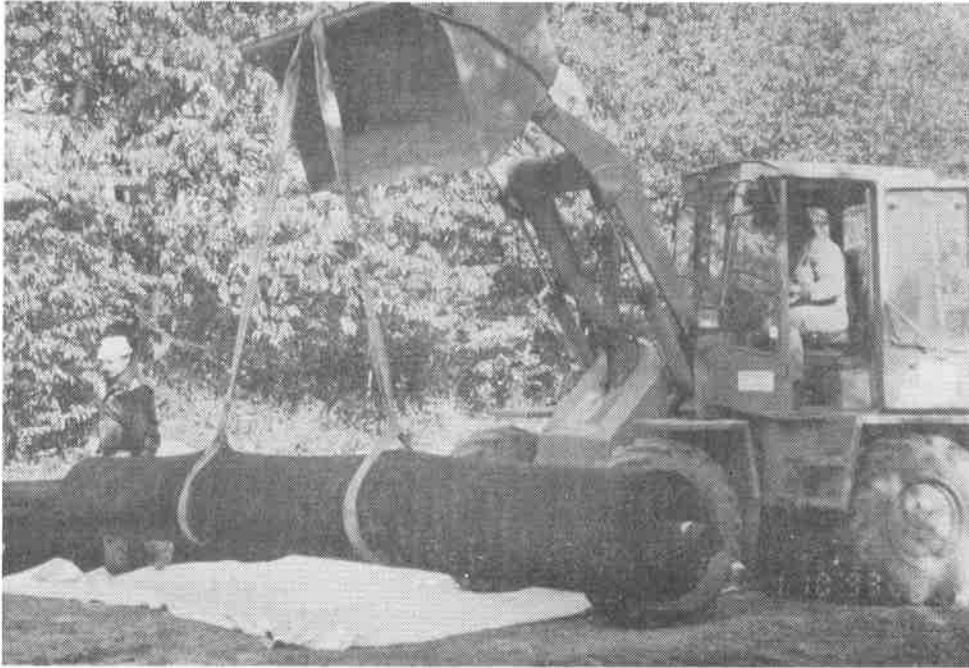
Figure 6: Handling of the 5 m wide geogrid rolls on site

Figure 7: Installation of the first geogrid layer

The 0.30 m thick fill layer (See Fig. 4) was placed on the second geogrid layer over the entire reinforced area without driving directly on the grids (See Fig. 10) and then compacted by a vibrating roller. A relative Proctor density of $D_{pr} > 103$ % was achieved, corresponding to a plate load modulus of $E_{v2} > 120$ MN/m² after re-loading according to German standard DIN 18134. These high compaction and strength values were easy and rapidly to achieve due to the effective support by the high-modulus grids. Then the free lengths of the second geogrid layer (See Fig. 8) were wrapped back, tensioned and temporarily fixed by steel pins, generating the third reinforcement layer. The same procedure for placement and compaction of the fill was executed in 2 x 0.30 m lifts up to the full height of 0.90 m of the cushion (See Fig. 4). The cushion was overlaid by a standard road structure for German Class II-roadways, including gravel and asphalt layers. The asphalt overlay was reinforced by a biaxial polyester grid to prevent cracks due to small deformations of the structure. The reinforced cushion was completed in less than a week by the German contractor TEERBAU GmbH in October 1993.
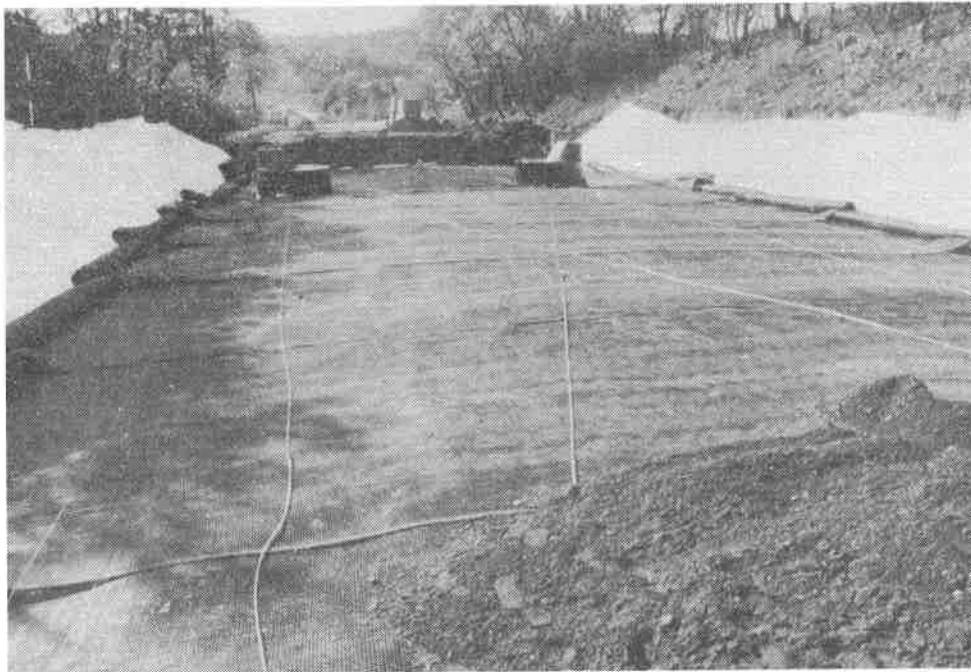
Figure 8: Second geogrid layer and measurement wires
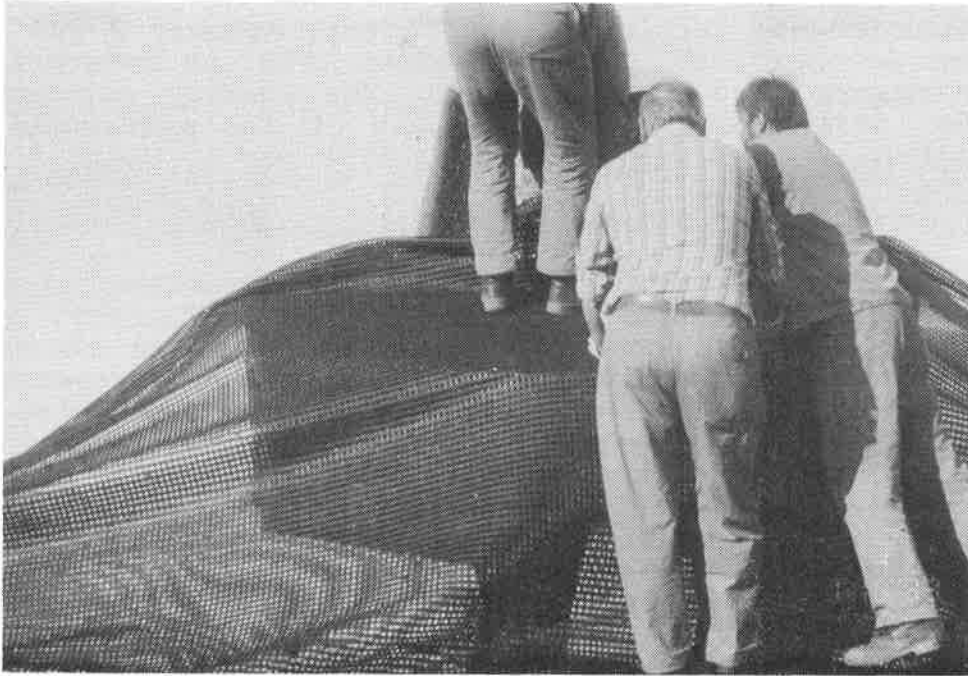
Figure 9: Field fabrication of geogrids around the measurement/control shafts
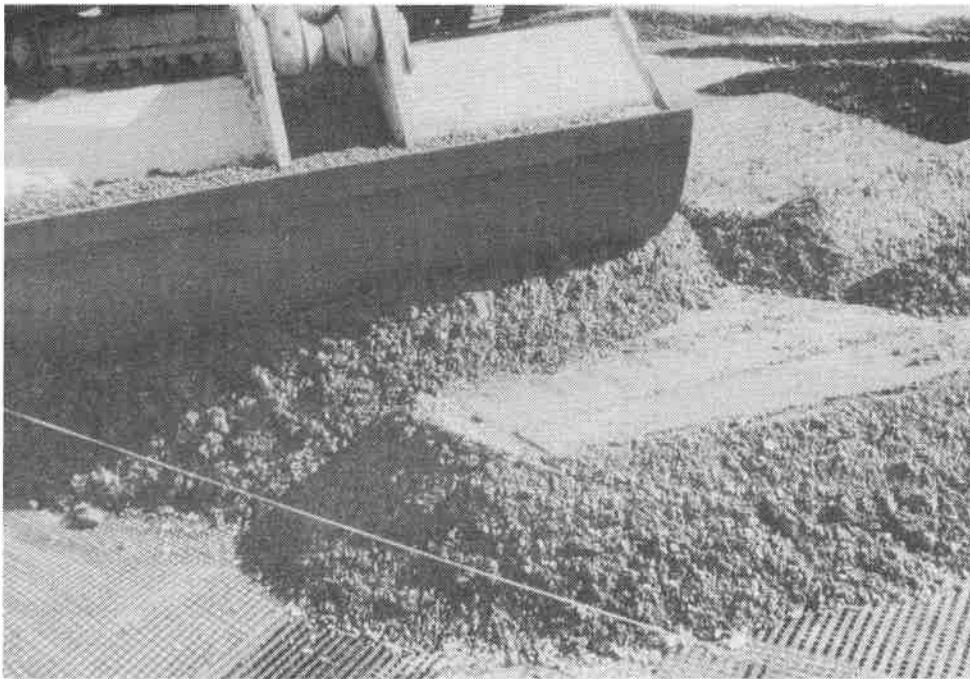
Figure 10: Placing the fill layer on the second geogrid layer

EXPERIENCE UNDER TRAFFIC

The reconstructed section of the Federal Roadway B 180 is in operation since October 1993. As of December 1996, no deformation, settlement, or cracks have been observed. The roadway continues to be monitored for deflection through the use of the measurement/control shafts.

CONCLUSION

A deep sink-hole was refilled and bridged by a geogrid-reinforced soil cushion. Briefly described are the design philosophy, soil reinforcement materials, and construction technique used to repair the collapsed roadway. The geogrid design methodology, according to English and German guidelines and standards resulted in the need for an extremely high-modulus high-strength uniaxial geogrid having a machine direction UTS of 1200 kN/m and elongation at break of 3 %, A measurement/control system was installed to monitor potential future deflection due to the safety requirements for the Federal Roadway B 180. The geogrid reinforced gravel cushion which was constructed without difficulty was the first structure of its kind in Germany.

ACKNOWLEDGMENTS

REFERENCES

British Standard BS 8006 (1995) "Code of practice for strengthened/ reinforced soils and other fills", British Standard Institution, London Great Britain.

FGSV (1994) "Merkblatt für die Anwendung von Geotextilien und Geogittern im Erdbau des Straßenbaus" (Guidelines for the use of geotextiles and geogrids for (the) application in road construction), Köln, Germany.

HUESKER Synthetic GmbH & Co. (1993) "Data sheet and specification for geogrid Fortrac®—1200/50-10", Gescher, Germany.

Giroud, J.P., (1982) "Designing of geotextiles associated with geomembranes". Proceedings of the Second International Conference on Geotextiles, Vol. 1, Las Vegas, P. 37-42.

Giroud, J.P., Bonaparte,R., Beech, J.F., Gross, B.A., (1990) "Design of soil layer-geosynthetic system overlaying voids". Geotextiles and Geomembranes 9, P. 11-50.

THE USE OF GEOTEXTILES FOR ROADWAY EMBANKMENTS OVER SOFT SOILS

SCOTT SHIMEL
SHANNON AND WILSON, INC., SEATTLE, WA, USA
HENRY GERTJE
WASHINGTON STATE DEPARTMENT OF TRANSPORTATION, USA

ABSTRACT

The State Route (SR) 509 East-West Corridor Project in Tacoma, Washington, was conceptually designed as a 2.4-km (1.5-mi)-long elevated structure spanning a waterway, a railroad yard, a wastewater treatment plant, and a river. Costly deep foundations were initially chosen because thick deposits of very soft soils were present. Project costs were reduced by selecting an alternate design in which a portion of roadway was supported by two embankments up to 12 m (40 ft) high. However, maintaining embankment stability and a reasonable construction schedule became a primary concern. An innovative embankment design that incorporated high-strength geotextiles in conjunction with staged construction was developed.

To evaluate stability, settlement, lateral movement, and rates of consolidation, a 4.3-m (14-ft)-high, fully instrumented test embankment was constructed in January 1992 and was subsequently monitored for approximately two years. This test embankment was one of the first of its kind in Washington State to use inexpensive and unobtrusive instrumentation such as horizontal profilers and pneumatic piezometers. The data was used to verify the design parameters, confirm the constructability, and better predict the behavior of the roadway embankments.

Construction of the SR-509 roadway embankments began in May 1994. Instrumentation was installed and monitored during the construction of the two embankments to aid in determining safe stage heights and appropriate delay periods. Temporary geotextile walls were constructed at the bridge abutments to facilitate surcharge placement. To date, settlements of up to 1.7 m (5.7 ft) have been observed during the successful construction of the two embankments. An overview of the geotextiles used and the performance of one of the two embankments are discussed.

BACKGROUND

The Washington State Department of Transportation (WSDOT) constructed a new east-west SR-509 corridor from I-705 to Marine View Drive in Tacoma, Washington, as shown in Figure 1. The realignment was necessary because the previous SR-509 four-lane arterial crossed several waterways with bridges, which affected Port of Tacoma ship traffic. The new SR-509 alignment shifted vehicle traffic south, so that bridges that restrict modern container ship traffic can be removed and other port facilities expanded.

The new alignment was conceptually designed as a 2.4-km (1.5-mi)-long elevated structure spanning the Thea Foss Waterway, the Burlington Northern Railroad Yard, the Tacoma Wastewater Treatment Plant, and the Puyallup River. Deep foundations were initially chosen to support the elevated structure because very soft soils up to 15 m (50 ft) thick were present. During the design phase, studies indicated that an alternate design in which approximately 1,000 m (3,200 ft) of the roadway would be supported by two embankments up to 12 m (40 ft) high was feasible. It is estimated that project costs were reduced approximately $9 million by selecting this alternate design.

The final design included two bridges and two embankments. One bridge crosses the Thea Foss Waterway, and the other crosses part of the Burlington Northern Railroad Yard, the Tacoma Wastewater Treatment Plant, and the Puyallup River. One embankment connects the two bridges, while the other embankment is located east of the Puyallup River. The latter embankment was the first to be built and its construction is the main focus of this paper. The plan and profile of this embankment are shown on Figure 2.
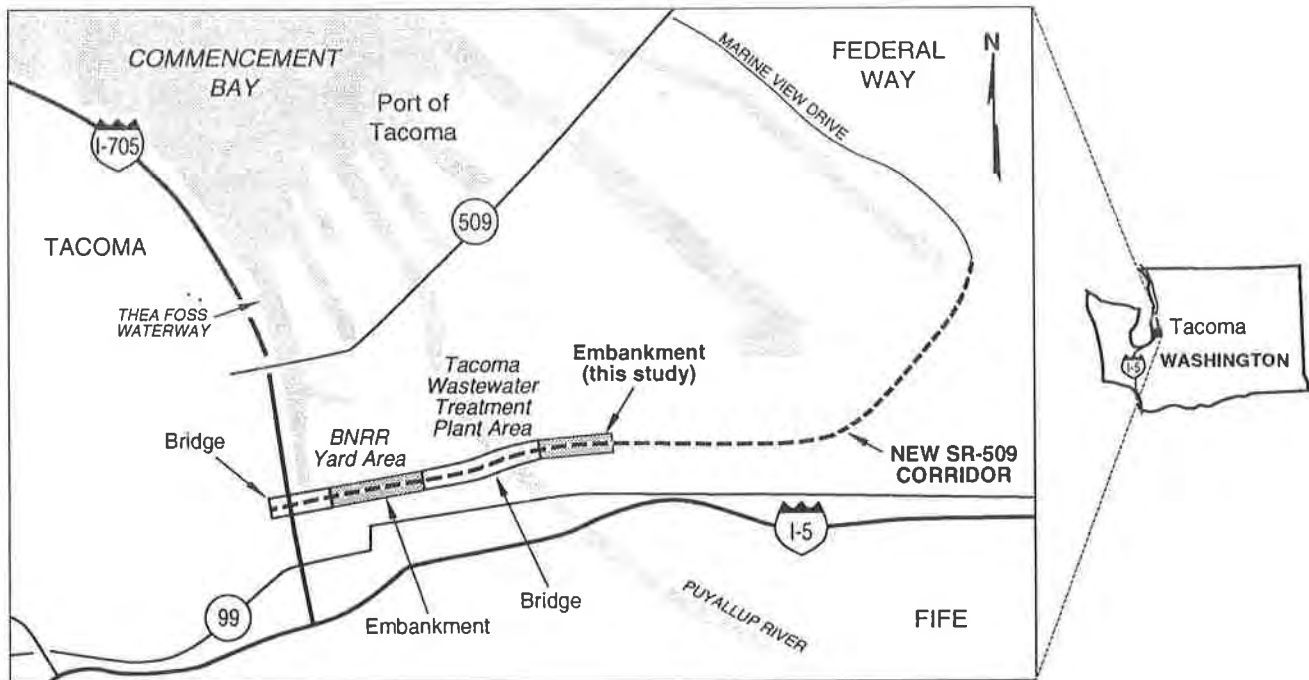
Figure 1. Vicinity Map
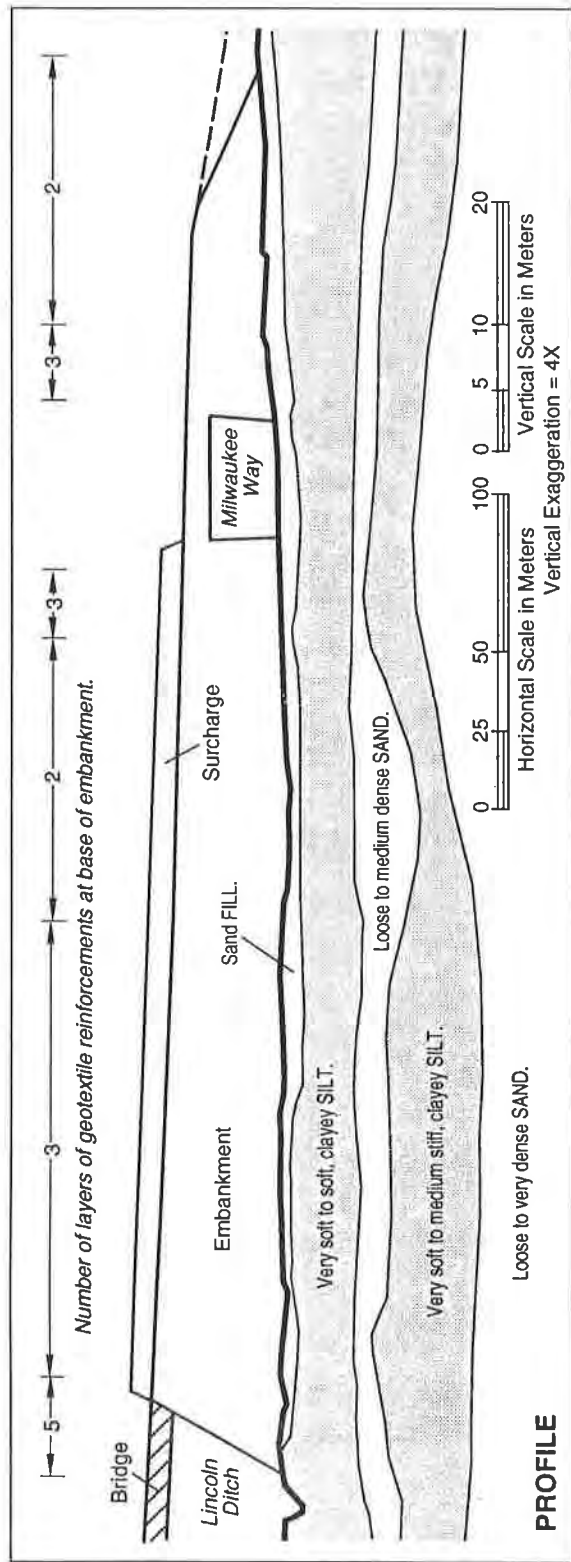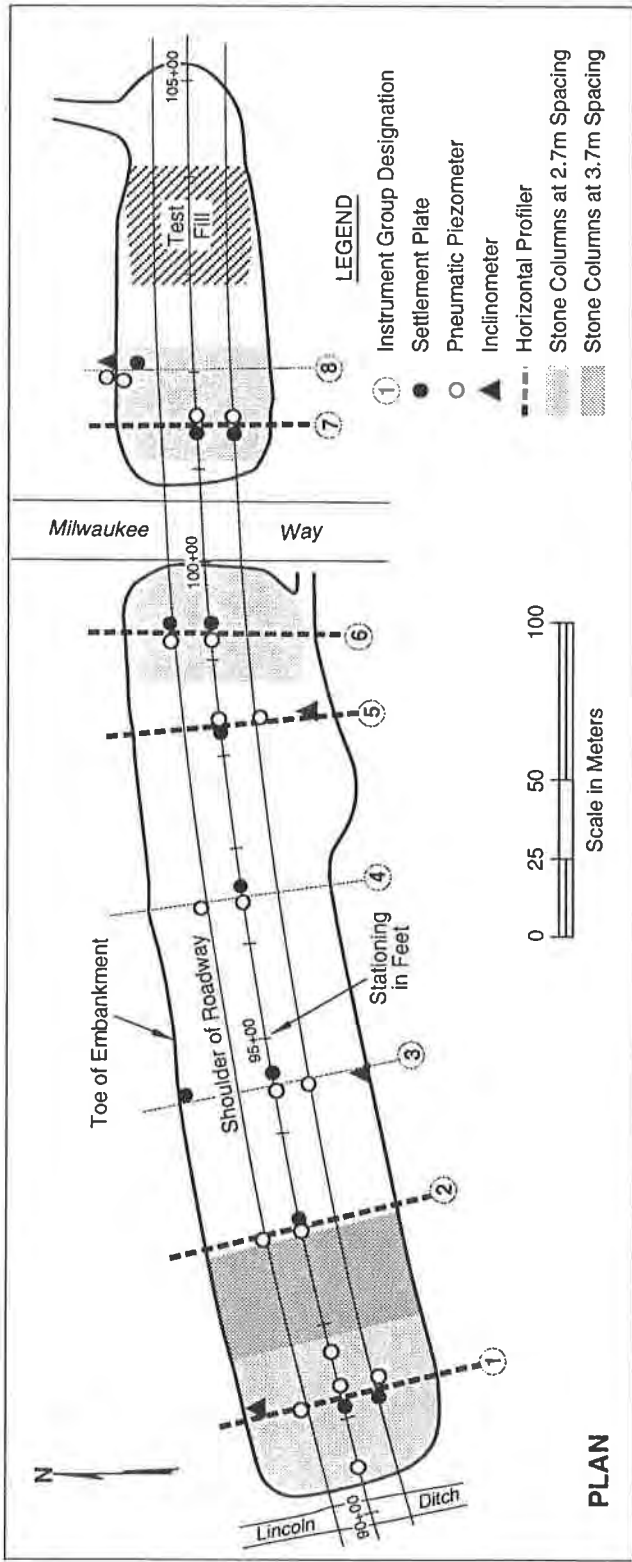
Figure 2. Lincoln Ditch to Milwaukee Way Embankment, Plan and Profile

GEOLOGY AND SUBSURFACE CONDITIONS

The project site is located on the tide flats and floodplain of the Puyallup River, approximately 3.2 km (2 mi) inland of its confluence with Puget Sound at Commencement Bay. This area is in the southeastern portion of the Puget Sound Lowland, an elongated structural and topographic depression bounded by the Cascade Mountains to the east and the Olympic Mountains to the west. Overlying the bedrock of the Puget Sound Lowland are glacial and non-glacial sediments of the Pleistocene Epoch. The last glacier retreated from the Tacoma area about 14,000 years ago, uncovering the Puyallup trough, which is the topographic low presently occupied by the Puyallup River.

The geology of the Puyallup trough is not well defined because of the limited number of deep borings as well as the variability of river discharge and relative sea level. However, in general, the Puyallup River Valley is filled with as much as 150 m (500 ft) of normally consolidated Holocene marine and alluvial sediments overlying glacially consolidated Pleistocene sediments. The alluvial and shallow marine deposits consist of interbedded clay, silt, sand, and organic layers. Because of the shifting of the Puyallup River channel and the complexities of floodplain deposition, individual strata are commonly discontinuous and interfingered with adjacent deposits.

As shown on Figure 2, the subsurface conditions beneath the Lincoln Ditch to Milwaukee Way embankment generally consist of a relatively thin layer of sandy fill material underlain by 9 to 15 m (30 to 50 ft) of very soft to soft, lacustrine, clayey silt. This clayey silt unit contains sandy silt interbeds and a 1- to 5-m (3- to 17-ft)-thick layer of loose to medium dense, silty, fine sand in the middle of the unit. The soft lacustrine deposits are underlain by loose to very dense, clean to silty, fine to medium sand. Glacial deposits were assumed to underlie the sand; however, they were not encountered in the borings (some up to 75 m [250 ft] deep) in this area.

ENGINEERING PROPERTIES OF SOFT, CLAYEY SILT

The engineering properties of the soft, clayey silt were estimated from the results of field explorations, laboratory testing, and a previous embankment study. In the vicinity of the Lincoln Ditch to Milwaukee Way embankment, five mud rotary borings with Standard Penetration Testing and thirteen electric piezocone probes were completed.

Laboratory testing was conducted on relatively undisturbed, thin-walled (Shelby) tube samples of the soft, clayey silt obtained from the borings to estimate index and strength properties, and deformation characteristics. Consolidated, undrained, triaxial compression tests and one-dimensional consolidation tests were performed. The results of the laboratory testing on the soft, clayey silt are shown in Table 1.

Table 1. Summary of Properties of Soft, Clayey Silt

Property	Laboratory Test Results
Moist Unit Weight	15-16 kN/m^3 (96-103 pcf)
Liquid Limit	32-74
Plasticity Index	3-36
Undrained Shear Strength	10-19 kPa (200-400 psf)
Total Stress Friction Angle	13-16°
Compression Index	0.56
Recompression Index	0.06
Coefficient of Consolidation	4 x 10^{-7} m^2/s (50 in^2/day)

The strength and deformation characteristics of the soft, clayey silt were also back-calculated from the results of the River Street Viaduct Project completed in 1973 (Mikkelsen and Bestwick, 1976). Estimates were obtained by reviewing construction records and instrumentation data for the fill placement just west of the Tacoma Wastewater Treatment Plant.

EMBANKMENT DESIGN

Staged Construction. Because of the thick deposits of soft soils, stable embankments could not be built to the required heights in one stage. Staged construction, therefore, had to be used. During staged construction, the embankment is built to the maximum possible stable height, the construction is temporarily stopped, and the soft cohesive soils are allowed to consolidate and increase in strength over time. After a sufficient amount of time has elapsed (the length of which is determined by the results of the field instrument measurements), the construction is continued and the embankment is built to the next maximum stable height. The sequence of filling and waiting is continued until the required height of the embankment is achieved.

Stability analyses were conducted to determine the stable heights to which the embankment could be built during successive stages. To maintain a stable embankment over the existing soft soil conditions, it was determined that approximately 3.4 m (11 ft) of fill could be placed during the first stage of construction. A delay of approximately three months would then be required to allow 60 percent consolidation of the soft, cohesive soils. The analyses indicated that after 60 percent consolidation, the strength of the soft, cohesive soils directly underneath the embankment would increase from 14 kPa (300 psf) to approximately 29 kPa (600 psf). Soil strengths outside the stress influence of the embankment were assumed to remain unchanged. With improved soil conditions, it was determined that approximately 1 m (3 ft) of additional fill could be placed in the second stage. A delay of approximately one to two months would be required to allow consolidation to take place.

At this rate, the embankments would take at least one to two years to construct. Since the project called for a six- to nine-month embankment construction time, this standard method of staged construction was not feasible. Therefore, staged construction in combination with high-strength geotextile reinforcements was proposed to allow for a shorter construction period.

High Strength Soil Reinforcement. Reinforcing the base of the proposed embankment with several layers of high-strength geotextile soil reinforcement allowed greater embankment heights to be constructed during each stage. Stability analyses were conducted to determine the most cost-effective combination of geotextile reinforcement and staged construction. The embankment was designed so that the geotextile reinforcements would only be temporarily relied upon to improve stability until the strength of the soft soils had increased enough through consolidation to support the embankment. The analyses followed the general procedures recommended in the Geotextile Design and Construction Guidelines Manual (Christopher and Holtz, 1988) for the design of reinforced embankments on soft foundations.

Three modes of failure were considered: internal stability, overall bearing capacity, and sliding. Internal stability, failure through the embankment, was evaluated at the end of each stage of construction and controlled the design of most embankment sections. Conventional slope stability analyses were used to analyze this failure mode; however, the additional resisting moment provided by the geotextile reinforcements was considered. Several construction sequences were analyzed by varying properties and number of layers of reinforcements and the delay times required for consolidation of the soft soils. A minimum factor-of-safety of 1.2 was chosen for the end of each stage of construction. Overall bearing capacity was evaluated according to a method developed by Rowe and Soderman (Rowe and Soderman, 1987), which accounts for the presence of a stronger layer at a finite depth. The factor-of-safety for the highest embankment at the most critical stage, end of construction, was calculated to be greater than 1.5. Sliding was also evaluated at the end of construction for two conditions: (1) failure between the geotextile reinforcement and the embankment soils, and (2) failure below the geotextile reinforcement through the soft foundation soil. All factors-of-safety against sliding were greater than 1.5 under static loading conditions. Seismic stability was also satisfied for all three modes of failure.

The results of the design for the number of layers of geotextiles installed at the base of the embankment from Lincoln Ditch to Milwaukee Way are shown on Figure 2. In general, the design called for successive geotextile reinforcement layers to be placed approximately 0.3 m (1 ft) apart, with their strongest direction (machine direction) perpendicular to the roadway alignment. However, near the abutments, additional layers were included parallel to the alignment to increase the stability at the ends of the embankment. No seams were allowed perpendicular to the machine direction. The final analyses indicated that the embankment, reinforced as shown, could be built in four stages in approximately five to six months.

<u>Stone Columns.</u> Stone columns were used to mitigate the potential for liquefaction of the loose, granular soil layers beneath the fill embankment within 30 to 60 m (100 to 200 ft) of the bridge abutments, as shown on Figure 2. The free-draining granular soil of the stone columns aids in minimizing the generation of excess porewater pressures in the surrounding loose soils during a seismic event, decreasing the potential for liquefaction. In general, stone columns also increase the effective modulus of loose or soft compressible layers and improve overall soil strength characteristics.

GEOTEXTILE REINFORCEMENT

The soil reinforcement chosen and specified for the construction of the embankments consisted of a high-strength, woven polyester geotextile with a minimum wide-width tensile strength of 180 kN/m (1,000 lb/in). Specifications for furnishing and placing the reinforcements followed the WSDOT standard for High Strength Geotextile for Soil Stabilization. The property requirements for the high-strength geotextiles are shown in Table 2.

Table 2. Summary of Specified Geotextile Properties

Property	WSDOT Test Method	ASTM Equivalent	Requirement
Apparent Opening Size, max.	922	D 4751	0.6 mm
Water Permeability, min.	924	D 4491	0.005 cm/s
Tensile Strength, min.	917	D 4595	
machine direction			180 kN/m
cross direction			90 kN/m
Secant Modulus at 10% strain, min.			70,000 kPa
Seam Breaking Strength, min.	917 and 918	D 4595 and D 4632	35 kN/m
Puncture Resistance, min.	921	D 4833	0.5 kN
Trapezoidal Tear Strength, min.	919	D 4533	0.3 kN

The manufacturer's advertised wide-width tensile strength of the geotextile actually used for the production embankments was 201 kN/m (1,150 lb/in) in the machine direction and 123 kN/m (700 lb/in) in the cross direction. The geotextile reinforcements were delivered to the site in 4.6-m (15 ft)-wide rolls, and butterfly type seams were field-sewn using hand-held sewing machines. Samples were taken randomly at the job site to confirm that the geotextile met the property values specified. Approval was based on testing samples from each lot. Seams sewn with the same equipment and procedures as used to sew the production seams were also obtained and tested.

INSTRUMENTATION

Instrumentation was installed to monitor pore water pressures and vertical and lateral movements in the soft soils beneath the test fill and the production embankments. The following paragraphs give a brief description of these instruments.

Pneumatic piezometers were installed within the soft, clayey silt unit to measure the buildup of porewater pressure during fill placement and the dissipation thereafter. This type of piezometer was chosen because the installations do not interfere with embankment construction, and readings can be taken without interrupting construction activities.

Settlement plates were installed at the base of the embankments to measure the settlement of the original ground surface during and after fill placement. As the embankments were constructed, the steel extension pipes were extended such that the top of the pipe would be accessible above the elevation of the fill.

Inclinometers were installed near the crest or at the toe of the embankment sideslopes to measure the lateral movement in the soft, clayey silt unit during and after fill placement. As the embankments were constructed, the inclinometer casing was extended such that the top of the casing would be accessible above the elevation of the fill. Fully extended telescoping couplings were used to connect casing sections through the soft, clayey silt unit to allow the casing to compress with the surrounding settling soils.

Horizontal profilers were installed beneath the embankments to measure the settlement of the original ground on a continuous profile at selected locations across the embankment during and after fill placement. The profilers were also chosen because of their unobtrusive nature. Fully compressed telescoping couplings were used to connect casing sections to allow the casing to elongate during settlement. Each end of each profiler was fixed into a concrete vault, and a nylon string, which extended through the casing from vault to vault, was used to pull the probe through the casing prior to data reading.

TEST FILL

To confirm the feasibility of the embankment design, a 4.3-m (14 ft)-high, fully instrumented test fill was constructed on the proposed alignment just east of Milwaukee Way in January 1992, as shown in Figure 2. The footprint of the test fill was approximately 37 m (120 ft) square and the sideslopes were 2 Horizontal to 1 Vertical (2H:1V). Two layers of high-strength geotextile reinforcement (with properties similar to those specified for the production embankments, as listed in Table 2) were placed at the base of the test fill with their machine directions perpendicular to each other. The geotextile reinforcements were factory-sewn into two, 37-m (120-ft)-square panels, and then accordion-folded, rolled into cylinders, and delivered to the site.

Settlement plates, horizontal profilers, inclinometers, and pneumatic piezometers were used to observe the performance of the test fill. Probe extensometers were also installed for the test fill; however, they were not used during production embankment construction. The test fill was monitored from January 1992 through December 1993. The layout of the test fill and the instruments is shown in Figure 3 along with selected horizontal profiler and inclinometer results. The data from horizontal profiler H-2 helped to confirm the estimated shape and magnitude of deformations across the embankment, and data from inclinometer IX-2 clearly shows lateral deformation of the two distinct layers of soft, clayey silt. The plot in Figure 4 shows the response of the porewater pressure and the resulting settlement from the placement of fill over time.

During the initial stages of the test fill study, a computer model was developed to predict settlement and lateral movement using a proprietary, finite-difference computer program. Soil parameters for the model were estimated primarily from piezocone penetration tests and laboratory data. These parameters and conventional settlement calculation theories were used to make predictions for primary, secondary, and total settlements so that appropriate surcharge heights could be determined. Data obtained from the test fill was used to calibrate the computer model so that better predictions could be made for the production embankments.

CONSTRUCTION

Embankment construction on the Lincoln Ditch to Milwaukee Way contract began in May 1994, following completion of stone column installation near the bridge abutments, and the final surcharge elevation was achieved in October 1994. The fill consisted of gravel borrow underlain by a clean sand drainage blanket. All fill areas greater than 3.7 m (12 ft) high were reinforced using high-strength geotextiles. Temporary geotextile walls were constructed at the abutments to facilitate surcharge placement.

Of the two embankments constructed for the project, the Lincoln Ditch to Milwaukee Way contract involved construction to the greatest fill heights over the softest ground conditions and had the largest associated subsurface deformation. Staged construction was coordinated by frequent communication between the contractor, the WSDOT Construction Project Office, and the WSDOT Geotechnical Branch staff. WSDOT personnel could not direct where and when fill could be placed; however, they had the authority to stop filling at any time without notice, based on instrumentation data.

Construction of the fill did not usually occur at a uniform and predictable rate across the embankments. The contractor mobilized from 8 to 20 trucks with tandem trailers, at times running two 8-hour shifts continuously. Early on, fill placement was concentrated in a short segment east of Milwaukee Way while stone column work was being completed west of Milwaukee Way. This resulted in an unanticipated increase in fill height from 2.4 m (8 ft) to over 6.1 m (20 ft) within four days. A rapid increase in pore pressures and a distinct

INSTRUMENTATION LAYOUT

HORIZONTAL PROFILER H-2

INCLINOMETER IX-2
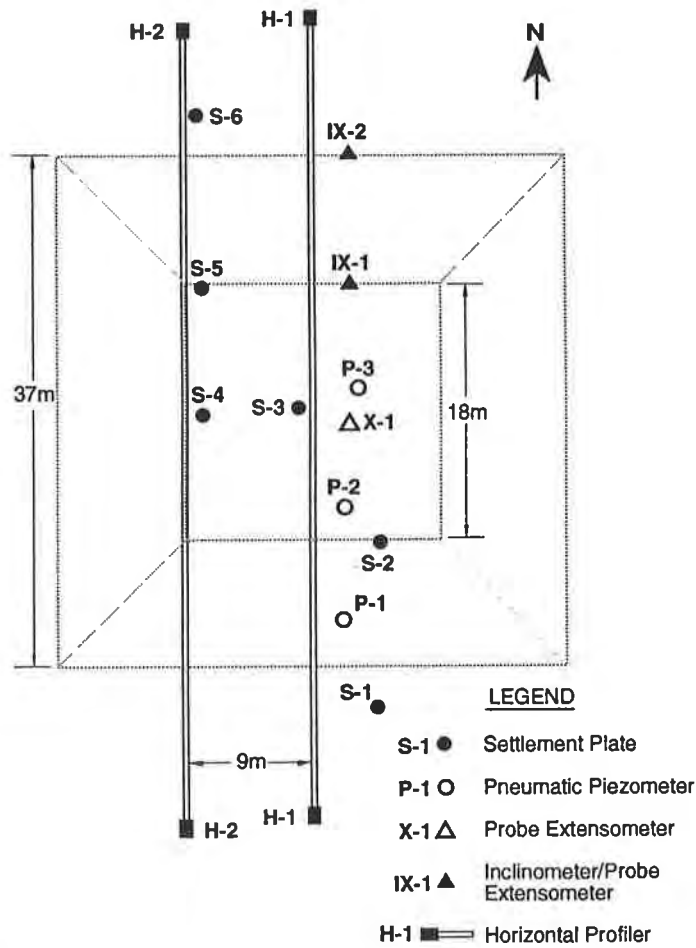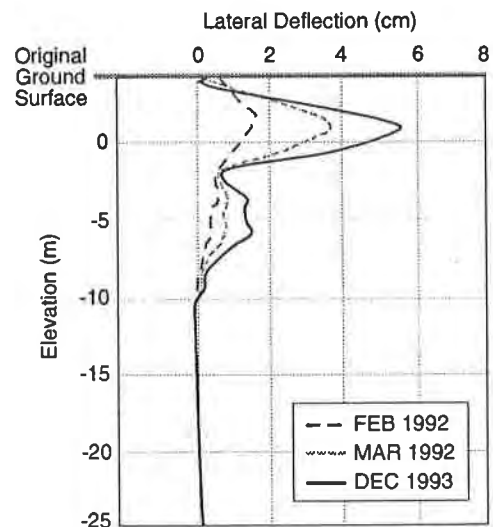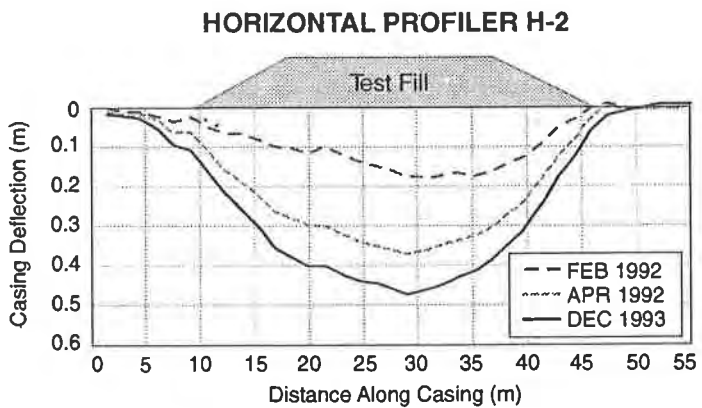
Figure 3. Test Fill Instrumentation Layout and Selected Results
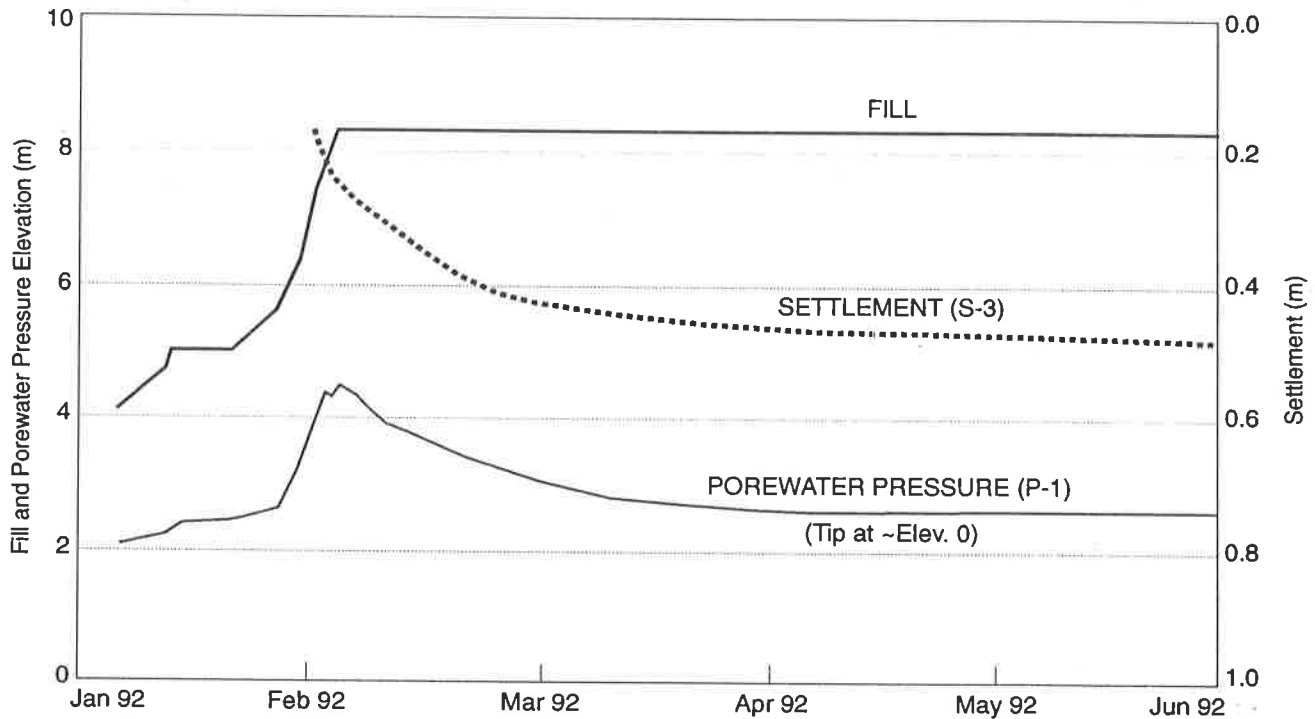
Figure 4. Test Fill Elevation, Porewater Pressure and Settlement vs. Time

lateral movement were measured. The fill operation was stopped immediately, and the rate of lateral movement stabilized within one day. As a result of this early incident, communication channels were improved during the rest of embankment construction. It was also discovered that the rate of embankment construction could safely exceed the rates recommended in design by at least 20 percent without resulting in failure of the foundation soils.

Embankment stability was primarily evaluated by comparing the rate of increase in porewater pressure and/or lateral movement to the incremental increase in fill height. As the ratio of rise in porewater pressure to the fill increment increased, projections could be made as to when a critical condition would develop. The projections were relayed to the contractor and the filling operation schedule was then optimized. On previous WSDOT projects, the ratio of the absolute magnitude of porewater pressure to the total fill height and the magnitude of lateral movement was often used as the controlling factor in determining the filling rate during staged construction. For the SR-509 embankments, however, these methods were found to be less meaningful and somewhat conservative indicators of stability.

EMBANKMENT PERFORMANCE

As indicated on Figure 2, the instrumentation for the embankment from Lincoln Ditch to Milwaukee Way was installed in groups at critical or representative locations. Each group included at least a settlement plate and two pneumatic piezometers. The instrument groups in more critical locations received an additional settlement plate and a horizontal profiler. Inclinometers and additional piezometers were added to selected groups.

A summary of results of the instrumentation is shown in Table 3. This table shows the maximum measured settlement from both the settlement plates and horizontal profilers for each of the instrument groups, and the maximum lateral deformation for the instrument groups that included inclinometers. The last column indicates those instrument groups that were installed in areas improved by stone columns. As expected, the larger settlements and lateral deformations occurred in the untreated areas. The differences in maximum settlements between the settlement plates and the horizontal profilers are believed to be due to the settlement of soil around the profiler casing and the settlement of the vaults.

Table 3. Instrumentation Summary

Instrument Group	Maximum Fill Height (m)	Maximum Settlement (Settlement Plate) (m)	Maximum Settlement (Horizontal Profiler) (m)	Maximum Lateral Movement (cm)	Stone Column Spacing (m)
1	12.8	1.2	0.8	11	2.7
2	12.5	1.7	1.2		
3	11.3	1.7		24	
4	10.1	1.6			
5	8.8	1.5	1.2	15	
6	7.3	1.1	0.8		2.7
7	8.5	0.7	0.4		2.7
8	8.2	0.8		9	2.7

Figure 5 shows an example of selected horizontal profiler and inclinometer data from instrument group 1. The shape of the vertical deformations across the embankment, shown in the plot of the horizontal profiler data, is similar to those observed in the test fill. The plot of the inclinometer shows the lateral deformation of the two distinct layers of soft, clayey silt.
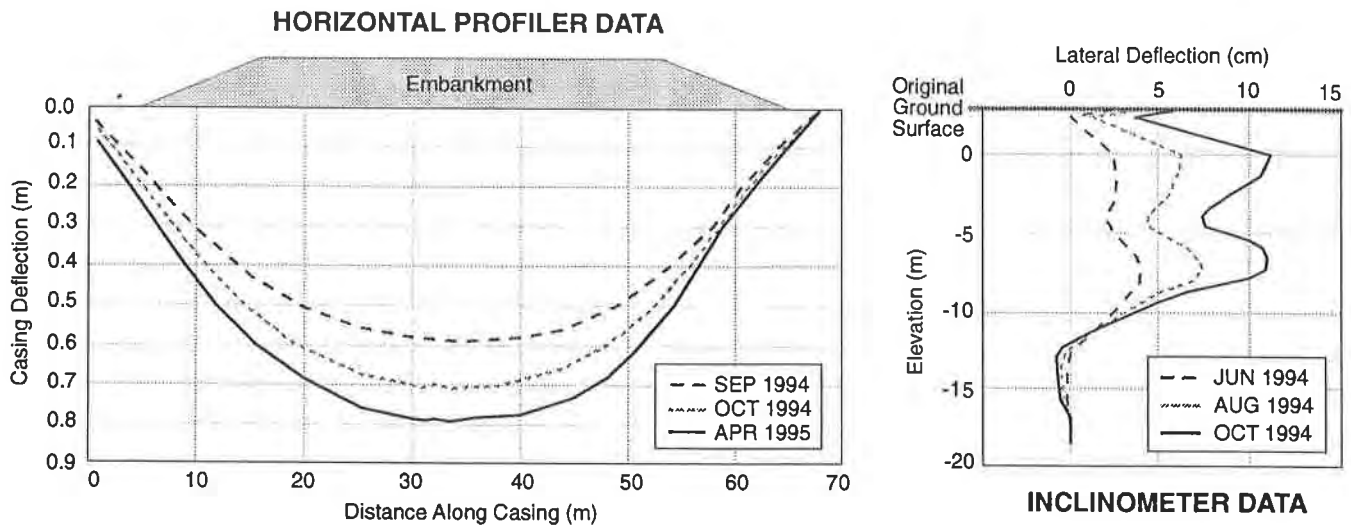
Figure 5. Horizontal Profiler and Inclinometer Data from Instrument Group 1
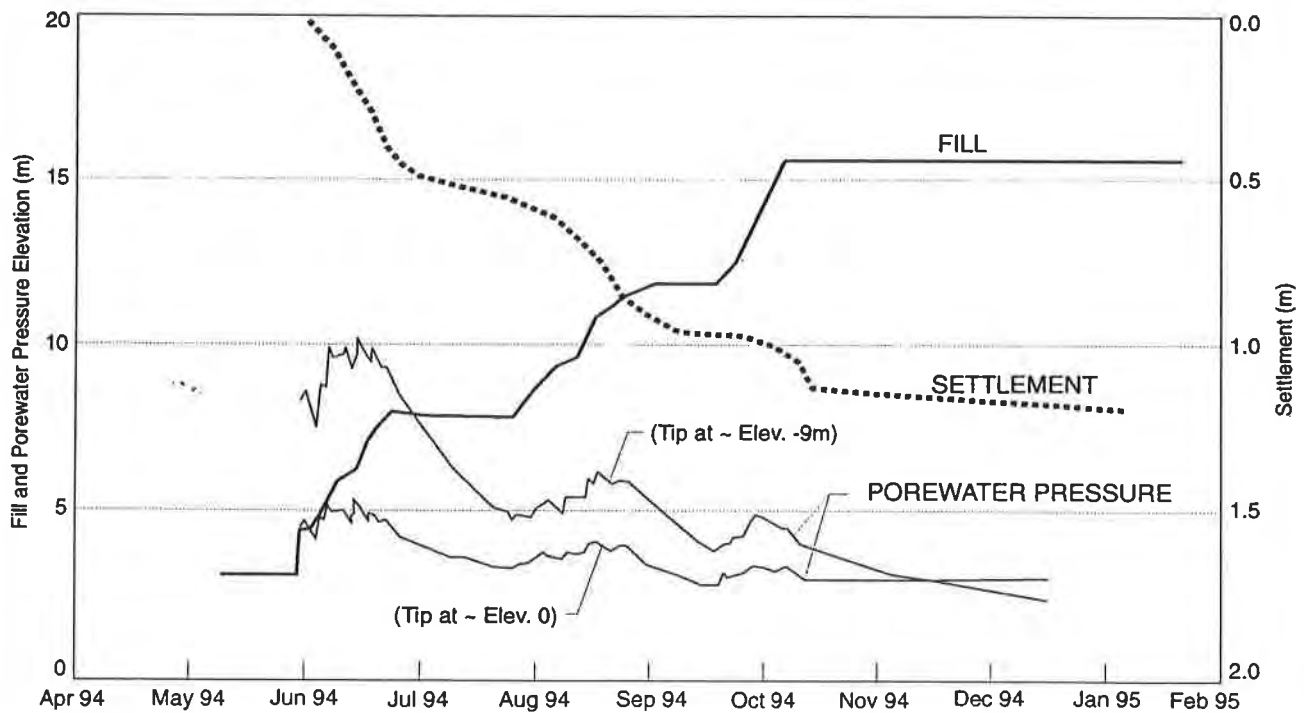
Figure 6. Fill Elevation, Porewater Pressure and Settlement vs. Time from Instrument Group 1

Figure 6 shows the relationship observed among the fill placement, the change in porewater pressure, and the increase in settlement over time from selected instruments from group 1. This plot illustrates the effect of the delay period in allowing the porewater pressure in the soft soils to dissipate, permitting these soils to consolidate and gain strength. The instrumentation allowed the embankment to be built in a little over four months (about a month less than predicted during design). In addition to using this data to monitor embankment stability and to determine adequate delay periods, it was also used to determine at what point the surcharge could be removed and the roadway paved.

CONCLUSIONS

Based on the design and results of the construction of the test fill and production embankments, several conclusions are apparent:

1. High-strength geotextile reinforcements were successfully used in conjunction with staged construction to economically build embankments over soft soils within the project schedule.

2. Unobtrusive instrumentation, such as pneumatic piezometers and horizontal profilers, were successfully used to control the rate of fill placement and embankment stability and to monitor embankment performance.

3. The test fill confirmed the feasibility of the production embankment design, provided an opportunity to evaluate the instrumentation performance, and aided in refining ground deformation predictions.

4. Settlements and lateral movements due to the soft, clayey silt were less in the areas improved by stone columns than in untreated areas.

REFERENCES

Christopher, B.R., and Holtz, R.D., 1988, Geotextile design and construction guidelines: Washington, D.C., Highway Institute Publication HI-89-050 (1989), prepared for the Federal Highway Administration by STS Consultants, Ltd., Northbrook, Illinois, October.

Mikkelsen, P.E., and Bestwick, L.K., 1976, Instrumentation and performance: urban arterial embankments on soft foundation soil: Engineering Geology and Soils Engineering Symposium, 14th Annual, Boise, Idaho, 1976, Proceedings, p. 1-18.

Rowe, R.K., Soderman, K.L., 1987, Stabilization of very soft soils using high strength geosynthetics: The role of finite element analyses: Geotextiles and Geomembranes, v. 6, no. 1, p. 53-80.

PHYSICAL OBSERVATIONS FROM SHALLOW-BURIED EXPLOSIVE EXPERIMENTS IN GEOGRID-REINFORCED EARTH

A. P. OHRT
USAE WATERWAYS EXPERIMENT STATION, USA

M. A. GABR
DEPT. OF CIVIL ENGINEERING
WEST VIRGINIA UNIVERSITY, USA

ABSTRACT

Numerous attack scenarios against military structures involve the detonation of an explosion in the soil backfill surrounding the targeted structure. Geosynthetic reinforcement could be employed in soil backfills around military targets to enhance the soil's mechanical properties and mitigate damaging blast effects. Mitigation of blast effects, including reduction of crater size, ejecta, and blast-induced soil displacements, could significantly enhance the survivability and functionality of protective structures. Six field experiments of shallow-buried explosive configuration were conducted to investigate the blast mitigating potential of high density polyethylene geogrids installed in a typical concrete sand. Two of the experiments were unreinforced, three of the experiments were reinforced with horizontally-oriented geogrids, and one experiment was reinforced with vertically-oriented geogrids. Results indicate that soils reinforced with horizontal geogrids displayed reduced crater dimensions and reduced permanent soil displacements. This paper describes the experimental program and presents physical observations (crater measurements, permanent soil displacements, etc.) obtained from the tests.

INTRODUCTION

Geosynthetically-reinforced soils have been successfully used in many earthen structures, such as retaining walls, embankments, reinforced slopes, etc. The reinforcement, typically consisting of horizontal layers of geotextile or geogrid, lends tensile strength and improved shear characteristics to the soil mass, often resulting in greater economy or higher performance. This same improvement in mechanical properties could prove useful for certain military applications as well. Several attack scenarios of interest involve detonations within a soil mass near the target of interest. The near-miss scenario of a buried structure (Figure 1a), the detonation of a munition beneath an airfield or road pavement (Figure 1b), and the artillery-type of attack on a field fortification are all examples where the detonation occurs in the soil surrounding the target and the blast loads propagate through the soil to load the structure. Of interest in this study is the

(a) REINFORCED BACKFILL AROUND
A BURIED STRUCTURE

(b) REINFORCEMENT OF
AIRFIELD SUBGRADE
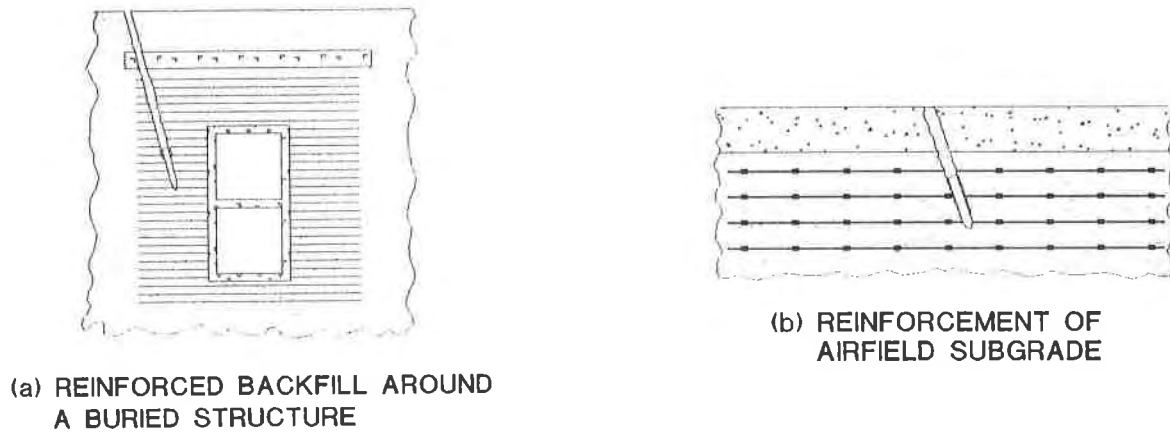
Figure 1. **Examples of potential military applications of geosynthetically-reinforced soils.**

possibility that blast loads acting upon the structure would be mitigated, or reduced, in some fashion by improving the mechanical properties of the soil backfill with geogrid reinforcement. If critical blast effects such as cratering and ejecta, soil displacements, or soil stresses could be reduced or altered in a favorable way, the survivability of certain military structures might be enhanced. Furthermore, the possibility of achieving greater economy in design and construction through the utilization of improved backfills is important in an era of declining budgets and changing threats.

While discussion of research pertinent to conventional geotechnical applications of reinforced soil is relatively abundant, the literature pertaining to blast loading of reinforced soil is rather sparse. Perhaps the most applicable research to date has been performed by the U.S. Air Force for the purpose of evaluating reinforced soil retaining walls for expedient construction. Available in the literature are the results of small-scale retaining wall experiments in a centrifuge (Bachus, et al, 1993), results of full-scale reinforced soil retaining walls loaded by bombs (Reid and Collin, 1995), and development of an analytical model for dynamic loading of reinforced soil retaining wall components (Tuan and Merkle, 1993). The configuration for all of the experiments and simulations involved the detonation of an explosion in the soil behind the reinforced soil retaining wall.

Most of the research to date on potential military applications of reinforced soil have been application specific (i.e., a design is conceptualized and then tested). Little research has been performed on the general mechanical response of the reinforced soil to the highly dynamic blast loads anticipated from a buried explosion. In this study, the dynamic response of a single geosynthetic reinforcement in a cohesionless soil was characterized through experiment and numerical simulation (not presented), with particular emphasis on identifying potentially useful blast mitigating effects. Six experiments were conducted that demonstrate and quantify the effects of geogrid reinforcement on crater size, soil stress, soil particle velocities, and soil particle displacements in a shallow-buried explosion configuration.

The discussions in this paper are limited to the physical observations obtained from the experiment series. These physical observations include physical measurements of the crater dimensions, measurements of the permanent, explosion-induced soil displacements from posttest excavation of sand columns, and observations of the failure locations in the reinforcement. It is intended that the results of active ground shock and ground motion instrumentation, as well as the results of the numerical modeling effort, be presented in future publications.

DESCRIPTION OF THE PHASE 1 AND PHASE 2 GEOGRID TESTS

A shallow-buried explosive configuration was selected for these experiments to maximize the ground motion and cratering response (in contrast to a surface or air burst) and to test with greater economy (in contrast to deeply buried configurations). Limitations in the scope of experimentation and parameter variation were established to achieve a reasonable test matrix. A typical concrete sand was used as the soil type for all of the tests. Geogrids of various style and strength were the only geosynthetic reinforcements used. The layer spacing of reinforcement was fixed at 15-cm for all of the reinforced soil experiments. This spacing was considered to be the minimum spacing likely to be used economically in practice. Hence, the parameters varied in the experiments were the mechanical properties of the reinforcement and its orientation.

The six experiments were conducted in two series, referred to as the Phase 1 and Phase 2 Geogrid Tests, respectively. Since little information was available on the blast mitigating characteristics of reinforced soil, the Phase 1 Geogrid Tests were conducted to evaluate the merit of the concept and to investigate whether a horizontal or vertical reinforcement orientation was clearly preferrable. The Phase 1 Geogrid Tests involved only posttest physical measurements of crater dimensions and permanent soil displacements, i.e., no active instrumentation was used. Given the clear evidence of blast mitigating effects from the Phase 1 experiments, the Phase 2 experiments were performed using ground shock and ground motion transducers to measure the radial soil stress and particle motion fields. Phase 2 experiments tested only the horizontal reinforcement orientation based upon the results of the Phase 1 experiments. Both experiment series included one comparable experiment in unreinforced soil to serve as a "control" test.

The features of each experiment are summarized in Table 1. Representative cross sections of an unreinforced experiment, a horizontally-reinforced experiment, and the vertically-reinforced experiment are shown in Figure 2.

Three test pits, each about 5-m square by 1.5-m deep, were excavated at the U.S. Army Engineer Waterways Experiment Station (WES) Big Black Test Site. A geotextile-lined gravel mattress with an outlet drain was constructed at the bottom of each test pit to create free-draining conditions within the compacted fill. The overall size and depth of the pit was selected to provide sufficient soil anchorage and to minimize edge effects upon measured quantities.

Table 1. Phase 1 and Phase 2 Geogrid Experiment Matrix.

Test Name	Geogrid Type	Geogrid Strength (kN/m)[1]	Geogrid Aperture Shape and Size (mm)	Geogrid Layer Orientation	Active Instrumentation?
Phase 1, Test 1	None	---	---	---	No
Phase 1, Test 2	Uniaxial	168	Elliptical (250 x 17)	Horizontal	No
Phase 1, Test 3	Uniaxial	168	Elliptical (250 x 17)	Vertical	No
Phase 2, Test 1	None	---	---	---	Yes
Phase 2, Test 2	Biaxial	39	Rect. (25 x 30)	Horizontal	Yes
Phase 2, Test 3	Uniaxial	103	Elliptical (250 x 17)	Horizontal	Yes

Note: [1] Geotechnical Fabrics Report, 1995 Specifiers Guide, 1994
--Uniaxial geogrid panels were comprised of two layers of uniaxial geogrid oriented perpendicular to each other and fastened with high-strength nylon cable ties.
--Geogrid layer spacing was constant at 15 cm.

Several important features of the experiments are evident on the cross sections of Figure 2. Four radials of five sand columns each were placed in each test. Sand columns are columns of dyed sand that are excavated posttest to reveal permanent soil displacements. Markers were placed at various surveyed positions within the column. These markers were then located during posttest excavation and surveyed to quantify permanent soil displacement. The colors of the sand column were alternated black and red to arrive at clearly visible deformation patterns that were convenient for photography. Sand columns were installed by pouring sand through forms installed in the backfill. The sand column form would be lifted about 6-cm and dyed sand poured into the cavity left beneath the lifted form. This sand would be tamped, the form lifted again, and the process repeated. When an elevation was reached for a marker, the number on the marker would be recorded and the marker dropped down the tube. The exact elevation of the marker would then be surveyed. This process was performed differently on the last horizontal test so as to avoid making cutouts in the horizontal geogrid panels for the sand column forms.

Geogrid panels were constructed outside of the test pit and installed when the proper elevation was reached in the pit during the backfill operation. For the axisymmetric stress and motion fields generated by explosions, biaxial geogrid products would have been preferrable. However, biaxial geogrid products are typically of lower tensile strength than uniaxial geogrid products. Consequently, uniaxial geogrid panels were constructed from two layers of uniaxial geogrid oriented perpendicular to each other and fastened together with high-strength nylon cable ties. This effectively simulated a high-strength biaxial geogrid layer better suited to the axisymmetric blast-induced loads. Cutouts in the horizontal geogrid panels were made to allow the panel to be placed over the sand column forms. Since these cutouts were found to influence the failure response of the geogrid panels, the last test was constructed is such a way as to avoid cutouts in the geogrid panels. Mechanical perimeter anchorage was provided at sixteen points
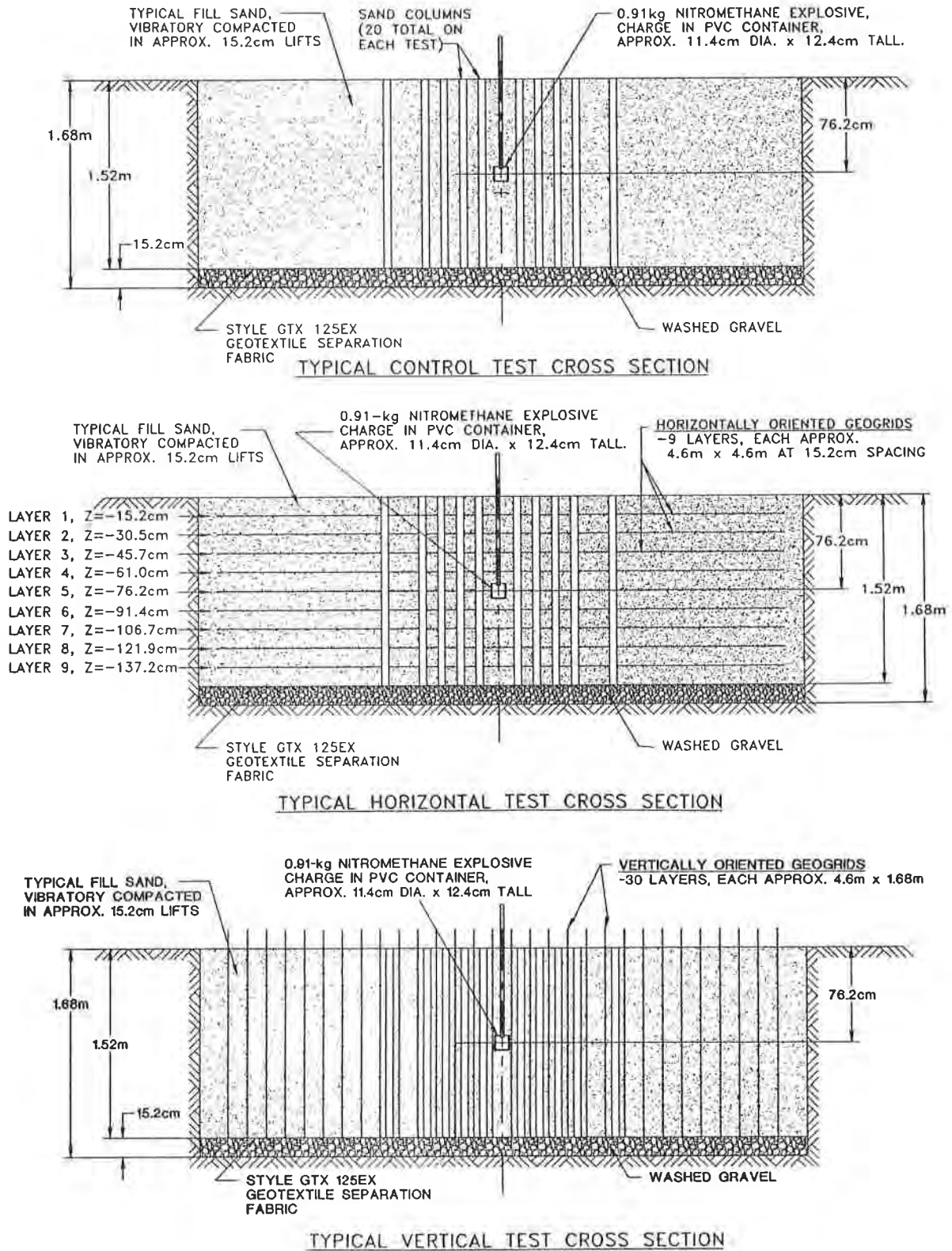
Figure 2. **Representative cross-sections of the control, horizontal, and vertical geogrid tests.**

around the perimeter of the test pit to enhance the soil anchorage of the finite-size test pit. Figure 3 shows a typical horizontal geogrid panel installation.

The explosive charge for each experiment was a 0.91-kg nitromethane charge with a commercial booster, primacord train, and electronic detonator. Nitromethane was selected because it was a reliable liquid explosive that could be poured into the buried charge container on the day of the test. The booster and primacord train were attached to a wooden dowel that was inserted into the charge container and positioned within the pool of nitromethane. The detonator was attached to the primacord train at the test bed surface and fired with an electronic firing unit.

Typical test construction was as follows (with the exception of the vertical test). An initial 15-cm lift of sand was placed within the test pit. Positions of sand columns were surveyed onto this lift and sand column forms (aluminum tubes) were positioned within this first lift and secured across the top of the test pit. Subsequent lifts of sand were carefully placed in 15-cm lifts around these sand column forms and compacted with a vibrating plate compactor. If the test involved horizontal reinforcement, the geogrid panel would be positioned after the lift had been compacted and secured at the points of perimeter anchorage around the test pit. If the test were instrumented, instruments might be placed prior to installing the geogrid panel. When the elevation of the explosive charge container was reached, a charge container made from standard PVC products was surveyed into position at the geometric center of the test pit. Backfill of the test pit continued in this fashion until the test pit surface was reached. The top surface of the pit was achieve an accurate surface and pretest elevations were surveyed for comparison to posttest crater profiles.

The vertical test required a special construction method. Here the geogrid panels were positioned within the empty pit and mechanically drawn taught (see Figure 4). An initial lift of sand about 0.7-m thick was hand shoveled between the vertical geogrid panels. The drain outlet from the pit was then closed and the test pit flooded. A concrete vibrator was then passed between the vertical geogrid panels. This method proved quite effective at compacting the sand for this difficult construction situation. Settling of the sand was visible upon passing the vibrator through a region of the test pit. The water was then drained and the pit allowed to dry. Subsequent lifts were placed by hand and compacted by walking between the rows. It is acknowledged that soil compaction in the Phase 1 Vertical Geogrid Test may have lacked consistency with depth. However, the flooding method was considered undesirable for the upper lifts out of concern that the charge container would settle to an unwanted elevation and that the test area would become saturated.

RESULTS OF THE EXPERIMENTS

The Phase 1 Geogrid Tests were completed in the spring of 1994 and the Phase 2 Geogrid Tests were completed in the fall of 1994. After each experiment the apparent crater (that is, the visible surface of the hole created by the explosion) was photographed and the crater profiles
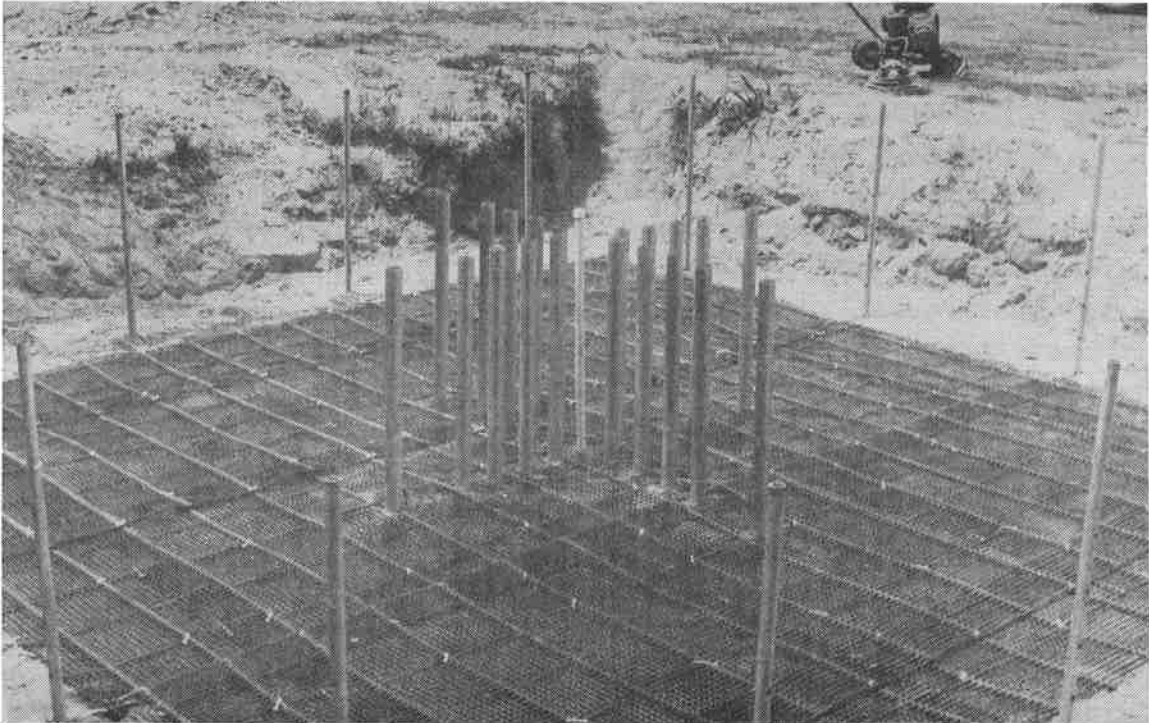
Figure 3. Photograph of a typical horizontal geogrid panel installation.
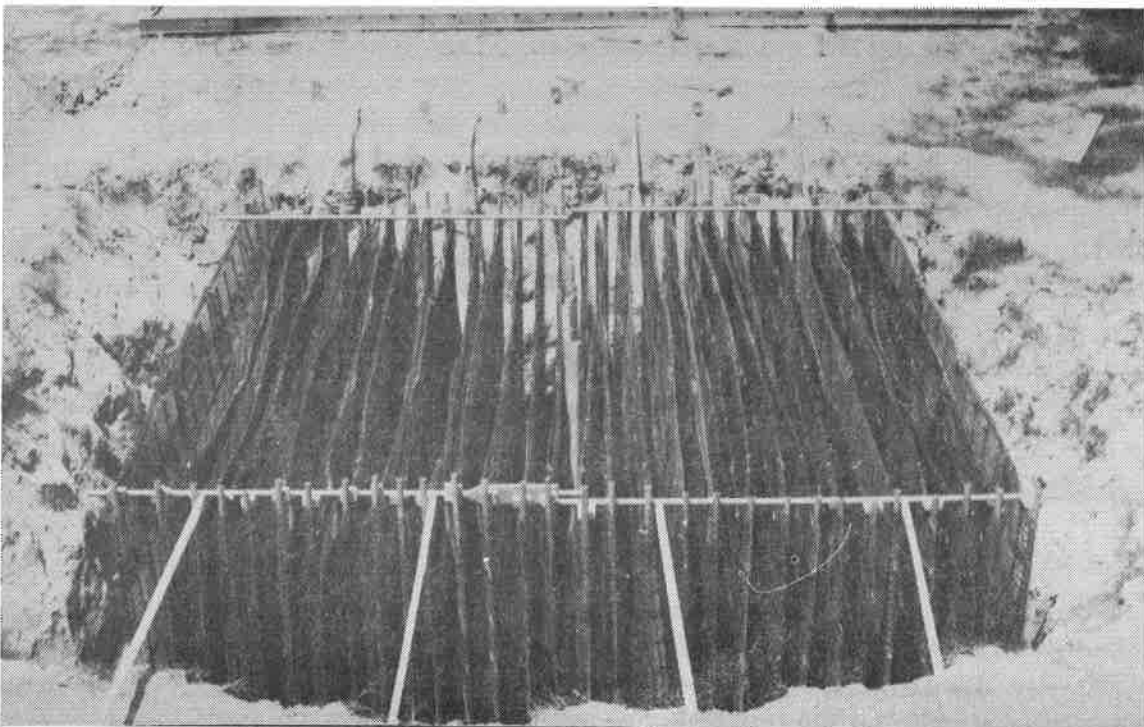
Figure 4. View of vertical geogrid panel installation prior to backfill.

surveyed. Once surface measurements were obtained, sand column excavation ensued. Throughout the test series the process of sand column excavation evolved to one of greater skill and utility. The most successful excavation approach involved the lift-by-lift excavation (by hand) of two opposite quadrants of the test pit. This would expose each of the four sand column radials. Typically, about 15cm of sand would be removed from the quadrant and the sand columns exposed. Photographs would be taken of the exposed columns and any markers that were located were surveyed and recorded. Then the geogrid panel would be carefully cut and removed, and the process repeated. Eventually, sand columns from upper layers would suffer slope failure and break away from the near vertical surface. On the Phase 2 test series successive photographs were taken from the same station with reference marks in the field of view to allow the "piecing together" of a composite view of the complete sand column radial.

Craters. Generally, the two control tests produced craters and sand column displacements that were consistent with those predicted by standard empirical methods (TM-855-1, 1986). The Phase 1 Horizontal Geogrid Test (Test 2) displayed a much smaller crater than the control test. The Phase 1 Vertical Geogrid (Test 3) produced an ellipsoidally-shaped crater that was larger than that of the horizontal geogrid test, yet smaller than the control test. Phase 1 experiment results are detailed in Ohrt, et al, 1994. Since the horizontal orientation proved more favorable in the Phase 1 experiment series, and also was more practical to utilize in practice, the Phase 2 experiment series tested horizontal geogrid orientations. The Phase 2, Test 2 (lower strength, biaxial geogrid) produced a crater nearly as large as that of the control test. It was also observed on this experiment that the geogrid had failed preferentially along the sand column radials where small cutouts of geogrid had been removed for test construction purposes. This prompted another look at the geogrid panels from the Phase 1 Horizontal Geogrid test and failures were noted along the sand column radials also, but to a lesser extent. Consequently, the sand column installation technique for the final test was modified, and an intermediate strength uniaxial geogrid was used. Sand columns were installed after the compaction of each lift with the aid of a wooden template that was surveyed into proper position within the test pit. The last Phase 2 experiment (Test 3) resulted in virtually no apparent crater. The seemingly anomalous result of the Phase 1, Test 2 crater (high strength uniaxial geogrid) being larger than that of the Phase 2, Test 3 crater (medium strength uniaxial geogrid) is explained by the effect of the sand column cutouts in the first two horizontal geogrid experiments. It is believed that if the Phase 1, Test 2 was repeated with the improved test construction method, the resulting crater would be very similar to that of the Phase 2, Test 3, with essentially no apparent crater. The basic differences in crater appearance between the control, horizontal, and vertical geogrid tests are illustrated in Figure 5.

With the final experiment being uninfluenced by cutouts in the geogrid panels, it is considered to be the most valid of the horizontally-reinforced tests. In Figure 6, its crater profile is plotted on the same graph as that of the control test (Phase 2, Test 1). As can be readily seen from this plot, the medium-strength reinforcement of Phase 2, Test 3 dramatically mitigated the cratering response from the shallow-buried explosion, essentially resulting in no apparent crater. Also on the plot are given the definitions of the parameters "apparent crater diameter" and
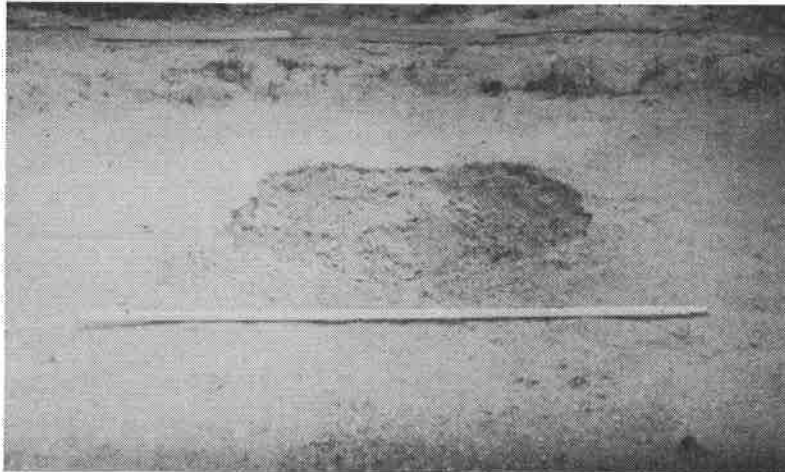
Control Test
(Phase 1, Test 1)
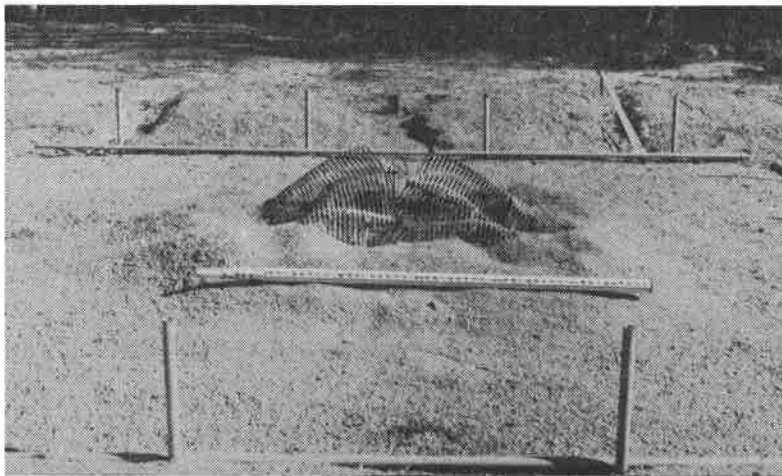
Horizontal Geogrid Test
(Phase 2, Test 3)
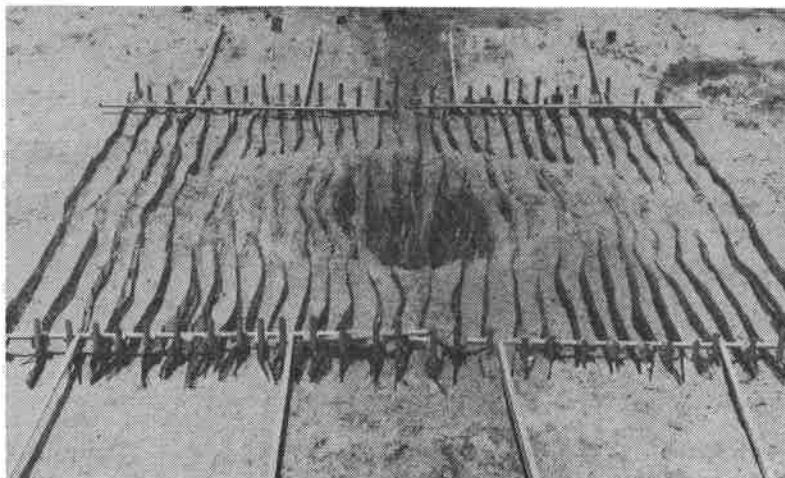
Vertical Geogrid Test
(Phase 1, Test 3)

Figure 5.   Photographs of apparent craters from a control test, a horizontal geogrid test, and the vertical geogrid test.

"apparent crater depth", making clear that customarily these measurements are taken from the pretest elevation, not the crater lip (TM-855-1, 1986). The apparent crater volume is that volume bounded by the pretest surface elevation and the surface of the apparent crater beneath it. The apparent crater dimensions for all six experiments are tabulated in Table 2.
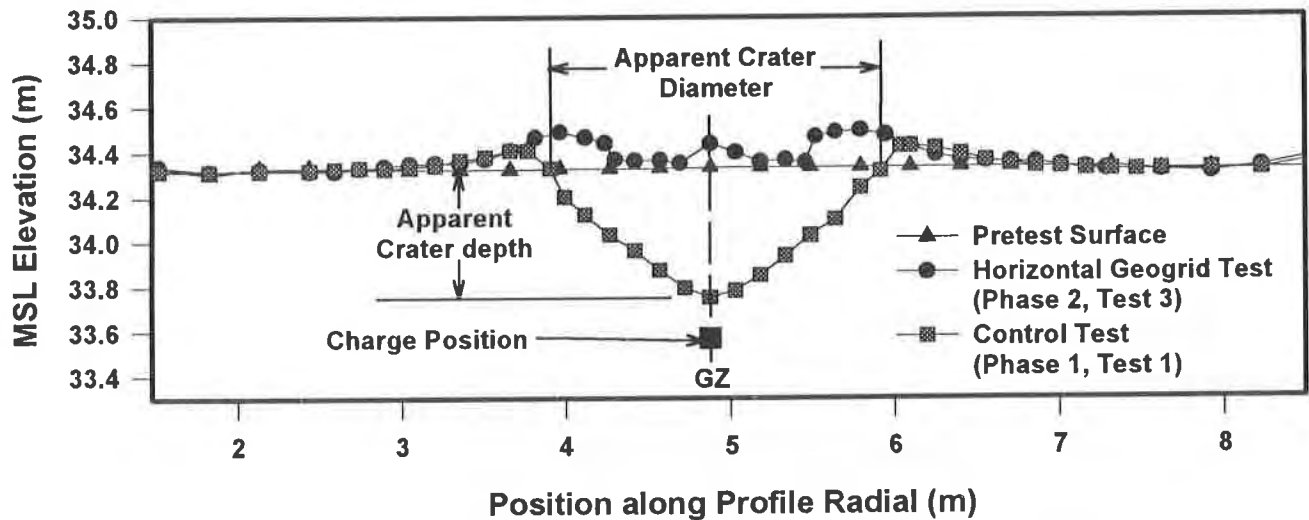
Figure 6. Apparent crater profiles from the final horizontal geogrid test and a control test.

Table 2. Crater dimensions from the Phase 1 and Phase 2 experiments.

EXPERIMENT	GEOGRID ORIENTATION	APP. CRATER DIAMETER (m)	APP. CRATER DEPTH (m)	APP. CRATER VOLUME (m³)
Phase 1, Test 1	None (Control Test)	2.12	0.63	0.86
Phase 1, Test 2	Horizontal	1.04 (50%)	0.22 (63%)	0.07 (91%)
Phase 1, Test 3	Vertical	1.92 (Major Axis) (6.8%) 1.43 (Minor Axis) (30%)	0.59 (1%)	0.84 (-4%)
Phase 2, Test 1	None (Control Test)	2.00	0.56	0.75
Phase 2, Test 2	Horizontal	1.77 (14%)	0.53 (11%)	0.60 (25%)
Phase 2, Test 3	Horizontal	0.00 (100%)	0.00 (100%)	0.00 (100%)
Note:	Numbers in parenthesis represent the percent reduction in the parameter from the <u>average</u> of the control tests, due to the presence of the soil reinforcement.			

Sand Column Displacements. Data obtained from the excavation of sand columns consists of the surveyed marker displacements and the visual record of the permanent displacement field along an excavated radial as typically obtained via photography or video footage. The permanent

displacements obtained from surveyed pretest and posttest marker positions tends to be quantitative in nature while the photographs of the excavated surface often give the analyst qualitative insight of the soil motions and related phenomena. For the Phase 2 tests, the systematic photographic approach resulted in quantitative data for the comparison of the last three experiments to each other.

Figure 7 is a close-up photograph of the excavated sand columns from the north radial of the first horizontal geogrid test (Phase 1, Test 2). The five sand columns and the cut layers of geogrid are plainly visible in the photograph. The explosive charge was located at the right edge of the photograph, centered on the geogrid layer nearest the center of the photograph. The heavily damaged geogrid in the upper righthand corner of the photograph is the region where the apparent crater had existed, but was cut into during excavation. An examination of sand column displacements in Figure 7 leads to a hypothesis regarding the response and motions of the reinforced soil layers. Of particular interest is a region of large radial displacements in the layer directly above the explosive charge position. The displacement of soil in this region is somewhat discontinuous in the sense that relatively undisturbed sand columns exist in layers above and below this layer. The proposed explanation for this finding is that the detonating explosive displaced the layers above the charge upward. As the upper geogrid/sand layers displaced upward, radial blast loads pushed soil beneath the displaced layers, resulting in the large radial displacements. Eventually the tensile strength of the upper layers of reinforced soil exceeded the applied blast loads, and the cratering action of the upper layers ceased. The remaining soil in the upper layers then subsided back into the crater. The sand columns in the upper region
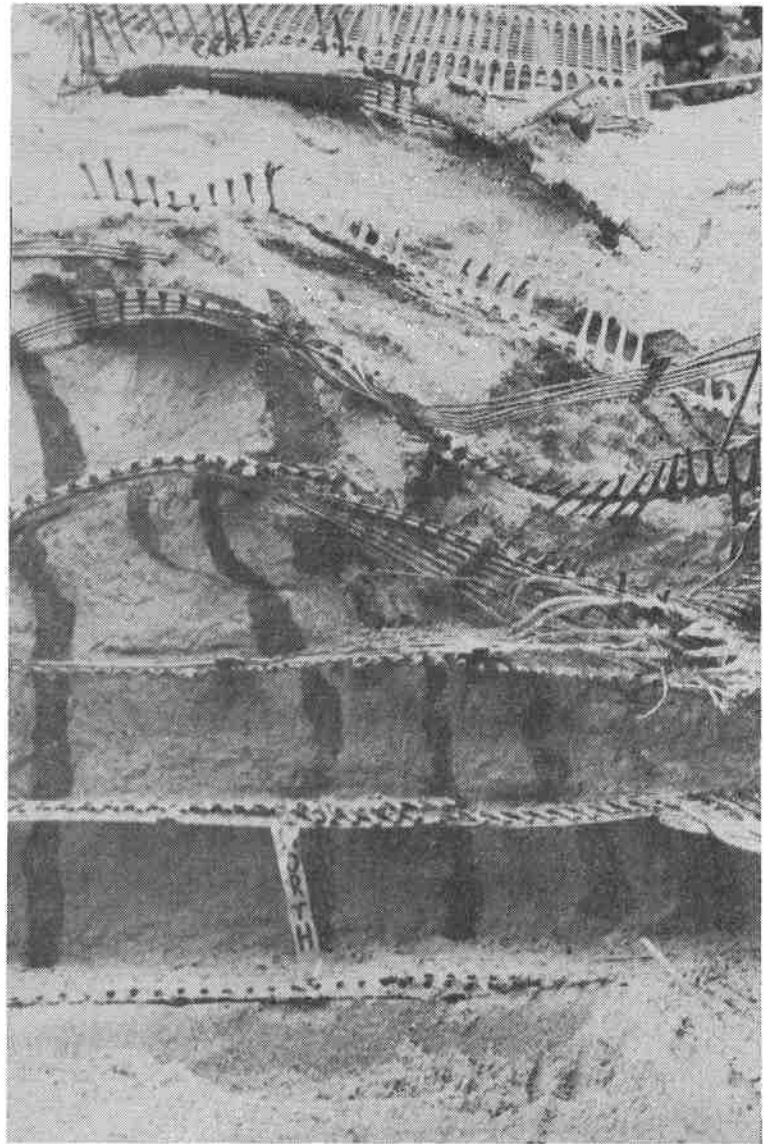
Figure 7.   Photograph of a sand column radial excavation from the Phase 1, Test 2.

of Figure 7 are actually displaced and tilted toward the explosive charge, characteristic of late-time subsidence into the crater. It is evident that layers beneath the explosive charge suffered little permanent displacement, especially at ranges distant from the charge. Much of this phenomena was captured by ground motion instrumentation in the Phase 2 experiment series.

Photographs taken during the various stages of sand column excavation of the Phase 2 tests were digitized and processed into the composite images of Figure 8. Since the photographs were taken from a fixed station outside the test pit looking into the excavation, some distortion due to visual perspective is present. Rather than attempt to correct for this, it is simply noted that the distortion for all of the Phase 2 experiments is similar (because camera stations were similar), and test-to-test comparisons can be made. Such a comparison is made in Figure 8 between the Phase 2, Test 1 (the control test) and Phase 2, Test 3. Also shown on the plot are the apparent crater profiles for the two experiments and the digitized geogrid panel positions for the Phase 2, Test 3. Significant differences in the soil deformation patterns from explosions in the unreinforced and reinforced media are obvious. The sand column displacements observed are typical of cratering behavior in sand. Here a clear zone is established where soil fails in shear and suffers large displacements. Most of the soil in this region is ejected, some subsides back into the cratered zone as is apparent from some sand columns "folding back" into the crater. With the addition of a medium to high-strength reinforcement, the soil displacement gradients are reduced, as is evidenced by the presence of relatively undisturbed sand columns in the region above the explosive charge. The reinforcement provides confinement to the soil grains, prompting a response resembling that of a layered media with tensile strength rather than the typical cohesionless soil. Note also that there is little or no evidence of sand columns (or even sand grains) migrating from one layer to the next. Consideration of the most distant sand column from the charge shows a distinct layered response, with sharp displacement gradients occurring at the layer interface. The mitigation of cratering, ejecta, and permanent soil deformation is clear from the deformation pattern plots of Figure 8.

CONCLUSIONS

Six shallow-buried explosive experiments were conducted to characterize the dynamic response and blast mitigating potential of geogrid-reinforced sand. Physical measurements of crater size, crater shape, and permanent soil displacements were taken. Measurements of ground shock and ground motion were obtained with active instrumentation. The physical observations were reported in this paper.

Geogrid-reinforced sand demonstrated a profound blast mitigating effect on the cratering response of a shallow-buried explosion. Medium-strength and high-strength geogrid-reinforced media had a substantially reduced crater dimension. Reductions in apparent crater diameter and depth was on the order of 50 to 100 percent (implying no apparent crater at all). Apparent crater volumes were reduced about 90 to 100 percent. Furthermore, the crater in the vertically-reinforced experiment was of ellipsoidal shape, indicating that presence of the reinforcement influenced cratering (otherwise the crater would have been axisymmetric). Horizontally-oriented geogrid
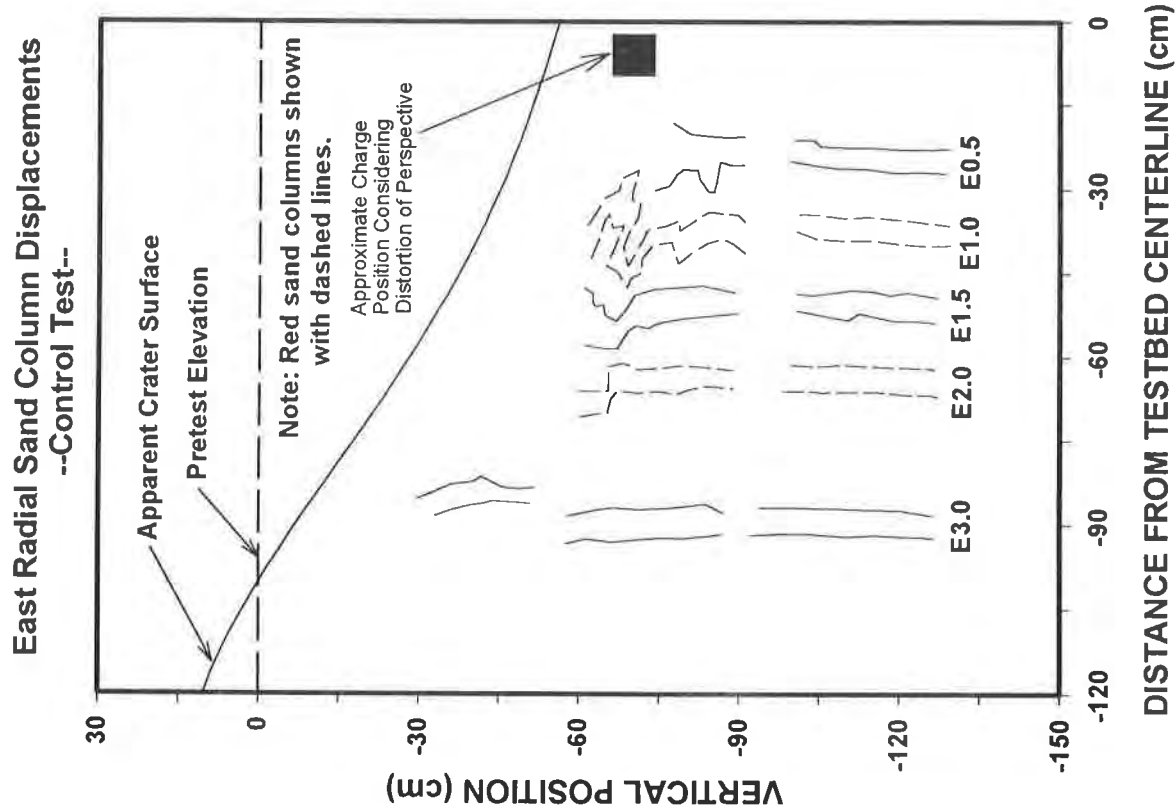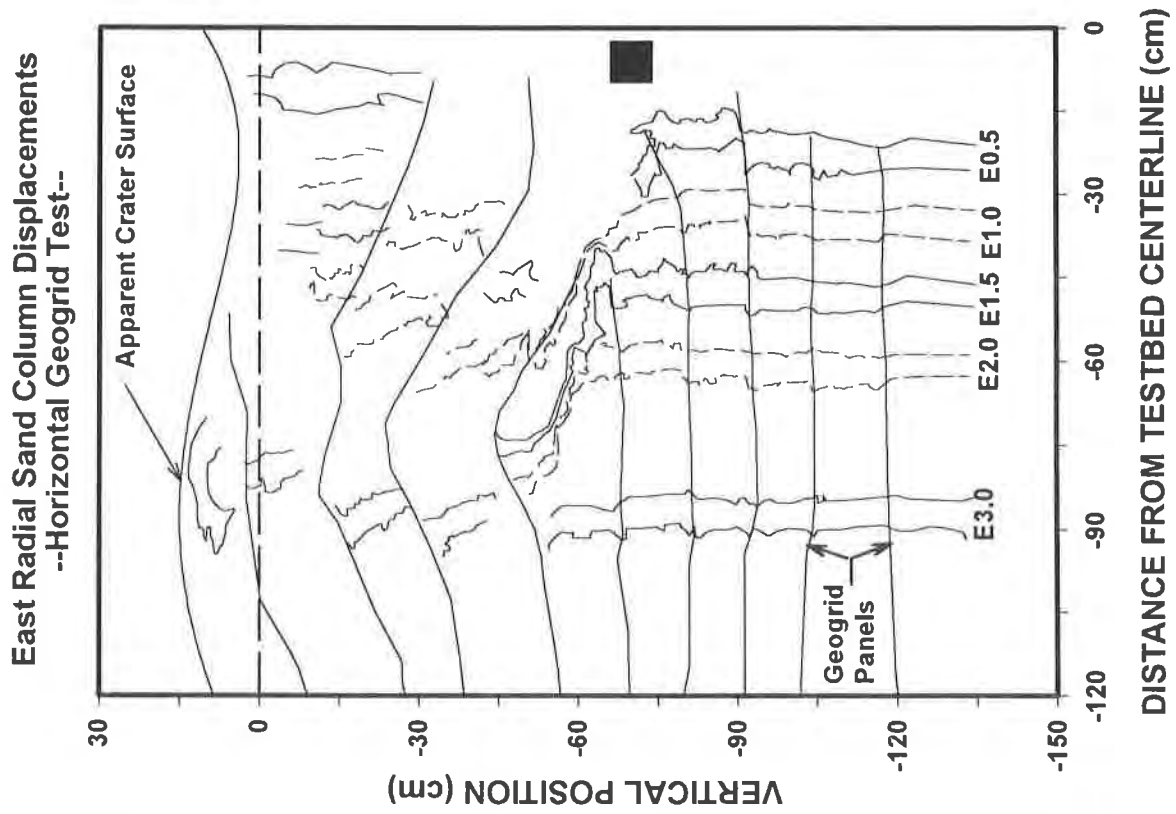
Figure 8. Comparison of sand column deformation patterns from the Phase 2, Test 1 (control test) and the Phase 2, Test 3 (horizontally-reinforced test).

reinforcement was more effective than the vertically-oriented geogrid reinforcement at mitigating cratering action, and was more practical to construct.

Cutouts in the geogrid panels to accomodate sand column forms were found to influence the experimental results by weakening certain regions of the geogrid panel. A change in sand column installation that did not require cutouts in the geogrid panels was employed in the final experiment with improved results. The apparently anomalous result of the first horizontally-reinforced experiment (with high-strength reinforcement) having a larger crater than the final horizontally-reinforced experiment (with medium-strength reinforcement) is most likely explained by the change in sand column installation.

Sand column deformation patterns revealed a zone of large radial displacements in the layer above the charge position for the horizontally-reinforced geogrid tests. The deformation pattern result from the layers above the explosion being displaced upward, and soil being pushed radially beneath them in the vacated space. The tensile strength in the reinforcement eventually exceeded the decaying blast loading and the upper layers cease to move upward, subsiding back into the cratered zone. Comparison of sand column deformations from the unreinforced experiments and the horizontally-reinforced experiments indicates that the geogrid reinforcement dramatically mitigates cratering, ejecta, and the permanent soil displacements in many regions of the explosive events. Displacement gradients from the horizontally-reinforced experiments are more characteristic of a layered media with tensile strength, rather than a cohesionless soil.

The blast mitigation qualities of geosynthetically-reinforced earth that were observed in this study could be beneficially applied to military structures or targets. The reduced crater dimensions expected in the reinforced soil could be useful in the design of subgrades in airfield or road pavements. Reinforced soil backfills might be placed around buried or earth-mounded structures to mitigate the displacement of soil toward the structure components. Tough and expedient field fortifications could conceivably be designed with geosynthetically-reinforced earth. Additional research is needed to understand the response of the geosynthetically-reinforced earth to the explosive loads from weapons that are larger, or perhaps more deeply buried. From a practical standpoint, economic analyses of specific applications should be performed, and attention given to operational considerations, e.g., repair and replacement after an attack.

ACKNOWLEDGEMENTS

REFERENCES

Bachus, R.C., Fragaszy, R.J., Jaber, M., Olen, K.L., Yuan, Z., and Jewell, R., (1993) "Dynamic Response of Reinforced Soil Systems Volume I: Report, Air Force Civil Engineering Support Agency, Technical Report ESL-TR-92-47.

Ohrt, A.P., Kiger, S.A., and Gabr, M.A., (1994) "Effect of Blast Loading on Geogrid-Reinforced Earth", 7th International Symposium on Interaction of the Effects of Munitions with Structures", Mannheim, Germany.

Reid, R.A. and Collin, J.G., (1995) "Response of Reinforced Soil Walls to Explosive Loading: Part II -- Full Scale Tests", Proceedings of the Geosynthetics '95 Conference, Nashville, TN, pp. 161-175.

TM 5-855-1, (1986) "Fundamentals of Protective Design for Conventional Weapons", Army Technical Manual, Headquarters, Department of the Army.

Tuan, C.Y. and Merkle, D. H., (1993) "Protective Shelter Construction With Reinforced Earth," Proceedings of the Geosynthetics '93 Conference, pp. 971-983.

FAILURE OF STEEP REINFORCED SOIL SLOPES

JORGE G. ZORNBERG
GEOSYNTEC CONSULTANTS, USA
NICHOLAS SITAR
UNIVERSITY OF CALIFORNIA AT BERKELEY, USA
JAMES K. MITCHELL
VIRGINIA TECH, USA

ABSTRACT

A centrifuge study was undertaken to investigate the failure mechanisms of geosynthetically reinforced steep soil slopes and to evaluate the assumptions in their design. The selected variables in the testing program were the reinforcement spacing, soil strength, and reinforcement strength. Failure in the models was characterized by well-defined shear surfaces through the toe of the slope. The moment of failure was defined by a sudden change in the rate of settlements at the crest of the slope, as monitored from transducers placed on top of the centrifuge models. Well-defined failure surfaces developed, which is in good agreement with current design methods for reinforced slopes based on limit equilibrium. Interpretation of the failure mechanisms in reinforced soil slopes also depends on the distribution of reinforcement forces with depth. However, in contrast to the current design assumptions that failure should initiate at the toe of the reinforced slopes, failure of all centrifuge slope models was observed to initiate at midheight of the slopes.

INTRODUCTION

Centrifuge testing provides a tool for geotechnical modeling in which prototype earth structures can be studied as scaled-down models while preserving prototype stress states. The principle of centrifuge testing is to raise the acceleration of the scaled model in order to reach prototype stress levels in the model. The combination of experimental centrifuge modeling results with analytic limit equilibrium predictions is a useful approach to investigate the performance of reinforced soil structures at failure. The investigation of the performance of geosynthetically reinforced soil slopes at failure is of particular interest because reinforced slopes are conventionally designed using a limit equilibrium approach.

Small-scale physical modeling of engineered earth structures has been used in the past to provide insight into failure mechanisms (e.g., Lee et al., 1973; Holtz and Broms, 1977; Juran and

Christopher, 1989). However, a limitation of scaled physical models is that the stress levels in the models are much smaller than in the full scale structures, thus leading to different soil properties and loading conditions. Finite element analyses have also been used to investigate failure mechanisms of reinforced soil structures (e.g., Hird et al., 1990; San et al., 1994). Standard finite element techniques are useful for analysis of structures under working stress conditions. However, modeling of failure in frictional materials requires special techniques to handle the localization of deformations, such as specific continuum formulations or the use of adaptive mesh refinement to capture slip discontinuities (Zienkiewicz and Taylor, 1991).

As part of a research program on the design, construction, and performance of high embankments, the California State Department of Transportation sponsored an extensive centrifuge study aiming at validating current design procedures for geosynthetically reinforced soil slopes (Zornberg, 1994; Zornberg et al., 1995). Limit equilibrium analysis methods have been traditionally used to analyze the stability of slopes with and without reinforcements. However, to date, limit equilibrium predictions of the performance of geosynthetically reinforced slopes have not been fully validated against monitored failures. This has led to uncertainty in their design. Consequently, an investigation was initiated to evaluate the assumptions and selection of parameters for the design of these structures. The results of the centrifuge tests provided an excellent opportunity to examine the validity of various assumptions typically made in the analysis and design of reinforced soil slopes. This paper presents a description of the failure observed in the different models tested as part of this investigation. Subsequent publications will present further evaluation of the failure mechanisms and implications of the results on the design of reinforced soil slopes.

CENTRIFUGE TESTING OF REINFORCED SOIL STRUCTURES

The stress dependent behavior of soils poses a problem when tests on small-scale geotechnical models are performed in the laboratory under a normal gravity field. In some cases, the use of appropriate surface loading can provide reasonable representation of the stresses created by body forces in a prototype structure. However, if body forces are to be properly represented in a model of the entire structure, it is necessary to turn to centrifuge testing.

Besides predicting the performance of prototype structures centrifuge testing can be performed for at least two other important purposes, both of which were of interest in this study:

- *The investigation of failure mechanisms*, in which the centrifuge is used as a tool to induce, in a model structure, levels of stress that are comparable to those usually found in prototypes. Such studies are often used to define new kinematically admissible collapse mechanisms and new statistically admissible stress distributions (Schofield, 1980; Mitchell et al., 1988); and

- *the validation of predictive tools*, in which the centrifuge is used to investigate the ability of numerical or analytical tools to predict the response of the small-scale model under prototype-like levels of stress (Shen et al., 1982; Liang et al., 1984). Simple geometries can be used in the models, and the analyses can incorporate the material properties, stress history, boundary loading conditions, and curved acceleration field that prevail in a centrifuge test.

As any experimental technique in geotechnical engineering, centrifuge testing does not reproduce exactly the conditions at which soil exists in an earth structure. This is due to the non-homogeneity and anisotropy of soil profiles, both in natural deposits and in man-made earth structures, and due to the limitations of the modeling tool. Some of the factors that cause differences between the behavior of model and prototype are: (i) the acceleration field in the centrifuge, which is directly proportional to the radius of rotation in a centrifuge model; (ii) the stress paths in the model, which are not necessarily identical to those of a structure built sequentially in the field; and (iii) the boundary effects, such as friction and adhesion between the walls of the model box and the soil, which can affect the results of the tests designed to represent plane strain conditions. Identification of these effects helps in the selection of model construction procedures that minimize their influence. More importantly, these effects can often be quantified and taken into account in the analytic tools used to evaluate the centrifuge test results.

The principle of centrifuge modeling is based upon the requirement of similarity between the model and the prototype. If a model of the prototype structure is built with dimensions reduced by a factor $1/N$, then an acceleration field of N times the acceleration of gravity, g, will generate stresses by self-weight in the model that are the same as those in the prototype structure. Additional scaling relationships can be determined either by analysis of governing differential equations or by dimensional analysis and the theory of models.

The scaling laws governing the problem under study (i.e. the behavior of cohesionless reinforced soil slopes at failure) were developed by assuming the validity of limit equilibrium. Specifically, similitude requirements which guarantee identical factors of safety in the model and the prototype structures lead to the conclusion that the same soil density and soil friction angle should be used in the model and in the prototype. These conditions can be satisfied by building the model using the same backfill soil used in the prototype structure. However, the scaling factor for the reinforcement tensile strength should be equal to $1/N$, where N is model scale. That is, an Nth-scale reinforced slope model should be built using a planar reinforcement N times weaker than the prototype reinforcement elements (Zornberg et al., 1995).

CHARACTERISTICS OF THE CENTRIFUGE MODELS

All reinforced slope models in this experimental testing program had the same geometry and were built within the same strong box. The models were subjected to a gradually increasing

centrifugal acceleration until failure occurred. The centrifuge tests were performed using a Schaevitz centrifuge at the University of California, Davis, designed to apply controlled centrifugal accelerations up to 175 g and with a limit of 4,500 g-kg at a nominal radius of 100 cm (39.4 in.). The payload of the testing package can be up to 45 kg (100 lb).

A strong box with inside dimensions of 419 mm x 203 mm in plan x 300 mm in height (16.5 in x 8 in x 11.75 in) was used to contain the model. A transparent Plexiglas plate on one side of the box enabled a side view of the model during testing. The other walls of the box were aluminum plates lined with Teflon to minimize side friction. The Plexiglas was lined with a mylar sheet overprinted with a square grid pattern, which provided a reference frame for monitoring displacements within the backfill. In order to prevent scratches and to minimize side friction, a second plain mylar sheet was used as a protection sheet. The box was sufficiently rigid to maintain plane strain conditions in the model.

The overall dimensions of the geotextile-reinforced slope models are given as shown in Figure 1 for the case of a model with nine reinforcement layers. The locations of displacement transducers are also indicated in the figure. All models were built with a total height of 254 mm (10 in). They consisted of 228 mm (9 in) high geotextile-reinforced slopes built on a 25 mm (1 in) thick foundation layer. The slope in all models was 1H:2V, and air dried Monterey No. 30 sand was used both as backfill material and foundation soil.
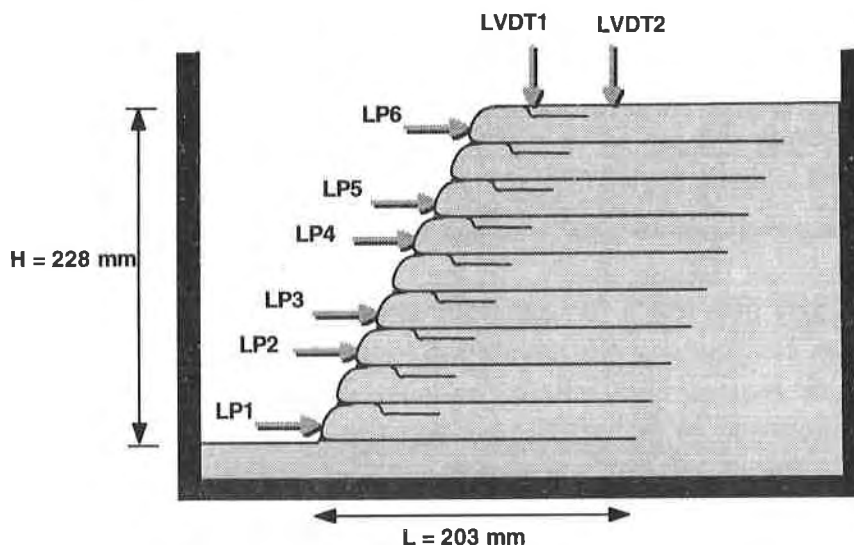
Figure 1 - Centrifuge model with 2.5 cm reinforcement spacing

The number of reinforcement layers in the models varied from six to eighteen, giving reinforcement spacings from 37.5 mm (1.5 in) to 12.5 mm (0.5 in). All models were built using the same reinforcement length of 203 mm (8 in). The use of a reasonably long reinforcement length was deliberate, since this study focused on the evaluation of internal stability against breakage of the geotextile reinforcements. By selecting long enough geotextile reinforcements,

external or compound failure surfaces were expected not to develop during testing. The geotextile layers were wrapped at the slope face in all models. Green colored sand was placed along the Plexiglas wall at each level of geotextile reinforcements in order to better identify the location of the potential failure surface. Black colored sand markers were placed at a regular horizontal spacing (25 mm) to monitor lateral displacements within the backfill material.

In order to guarantee consistent soil densities and placement conditions in the reinforced soil models, carefully controlled construction procedures were observed during model preparation. These procedures included sand pluviation through air under controlled discharge rate and discharge height to give uniform backfill relative densities of either 55% or 75%. A vacuum system was used to achieve the target backfill level. A detailed description of the construction procedures of the reinforced slope models is presented in Zornberg et al. (1995).

Six linear potentiometers were used to monitor the lateral displacements of the slope face. The linear potentiometers were supported by an aluminum plate and their location was adjusted for each model so that they were always placed at midheight between two reinforcement layers. Two linear variable displacement transducers (LVDTs) were used to monitor vertical settlement at the crest of the geotextile-reinforced models. Readings from these transducers proved very useful in accurately identifying the moment of failure. One electrical channel was additionally used to record directly the angular velocity (rpm) during centrifuge testing. A television camera, mounted at the center of the rotating structure of the centrifuge, and a video recording device were used as an additional monitoring system. This system provided not only a continuous and instantaneous monitoring of the tests while it was in progress, but also a permanent record of the model tests. A 45° mirror was used to view the model in-flight through the Plexiglas side wall. The recorded images were used to examine the initiation of failure and to identify the probable failure mechanisms.

After construction, the reinforced slope models were weighed and placed in the swing bucket of the centrifuge. Temporary support molds were removed, and both static and dynamic balancing of the rotating arm was performed. A mirror inclined at 45° was placed adjacent to the Plexiglas so that the model could be observed in-flight by the closed-circuit TV camera. Figure 2 shows the view of a model already placed in the swing bucket. The figure shows a top view of the model and its image through the slant mirror before placement of the displacement transducers. As the arm of the centrifuge spins, the buckets supported by hinged pins swings upward so that the top surface of the model is almost perpendicular to the plane of rotation. The models were subjected to a gradually increasing centrifugal acceleration until failure occurred.

The models were carefully disassembled after failure, and the backfill was vacuumed out and the geotextile reinforcements were retrieved. The retrieved geotextiles were used to evaluate the breakage pattern to locate the failure surface from the observed tears. The retrieved geotextile samples always showed breakage in a direction perpendicular to the direction of loading.
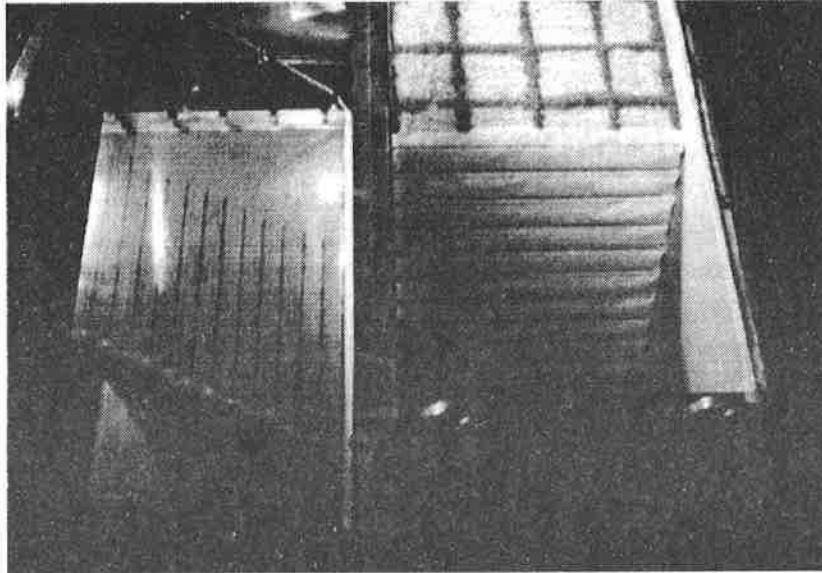
Figure 2 - Top view of Model B12, already placed in the swing bucket, and of its image through the slant mirror.

SCOPE OF THE TESTING PROGRAM

All variables in this testing program were selected so that they can be taken into account in a limit equilibrium analysis framework. Accordingly, the selected variables were:

- Vertical spacing of the geotextile reinforcements: four different reinforcement spacings were adopted;
- soil shear strength parameters: the same sand at two different relative densities was used; and
- ultimate tensile strength of the reinforcements: two geotextiles with different ultimate tensile strength were selected.

All models were built with the same slope and the same total height. The centrifuge tests performed as part of this study can be grouped into three test series, each aimed at investigating the effect of one of the variables:

- Baseline, B-series: performed to investigate the effect of reinforcement spacing. Centrifuge models with six, nine, twelve, and eighteen reinforcement layers were used in this series. Monterey No. 30 sand at 55% relative density and the weaker geotextile were used in all the models in this series.
- Denser soil, D-series: performed to investigate the effect of soil strength parameters on the stability of geotextile-reinforced slopes. A denser backfill (Monterey No. 30 sand at

75% relative density) than in the B-series was used. The geotextile used as reinforcement was the same as in the B-series.

- Stronger geotextile, S-series: performed to investigate the effect of geotextile ultimate tensile strength on the performance of reinforced slopes. These models were reinforced with a geotextile stronger than the one used in the other series. As in the B-series, Monterey No. 30 sand at 55% relative density was used as backfill material.

Each reinforced slope model in this study was named using a letter that identifies the test series (B, D, or S), followed by a numerical value that indicates the number of reinforcement layers used in the model. For example, Model B12 is the reinforced slope model from the B-series (Baseline), reinforced using twelve geotextile layers.

CHARACTERISTICS OF THE FAILURE SURFACES

Baseline B-series

All models in this series were tested using the same backfill density and the same geotextile fabric, but different reinforcement spacing. Typical results obtained after centrifuge testing of one of the models from the Baseline series (model B18) are presented in order to illustrate the type of data which was obtained throughout the study. The history of centrifugal acceleration during centrifuge testing of model B18 is shown in Figure 3. The acceleration was increased until sudden failure occurred after approximately 50 min of testing when the acceleration imparted to the model was 76.5 times the acceleration of gravity.
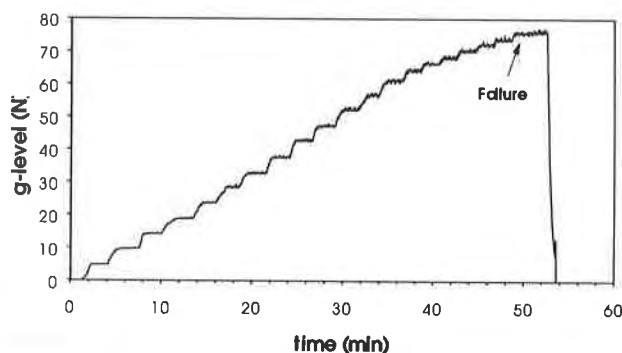
Figure 3 - G-level (N) versus time during centrifuge test of Model B18

Failure development in the reinforced slope could be identified from the TV images. However, settlements at the crest of the slope, monitored by LVDTs, proved to be invaluable to more accurately identify the moment of failure. The increasing settlements at the top of the reinforced slope during centrifuge testing was monitored at 12.5 mm (0.5 in.) and 62.5 mm (2.5 in.) from the crest of the slope. A sudden increase in the monitored settlements indicated the moment of failure when the reinforced active wedge slid along the failure surface. Recorded

images showing failure development of the models were an effective way of identifying the actual shape of the failure surface and the possible failure mechanisms. Figure 4 shows the failure surface that developed in model B18, as observed after unloading the model from the centrifuge bucket. As can be seen, the failure surface is clearly defined and goes through the toe of the reinforced slope.
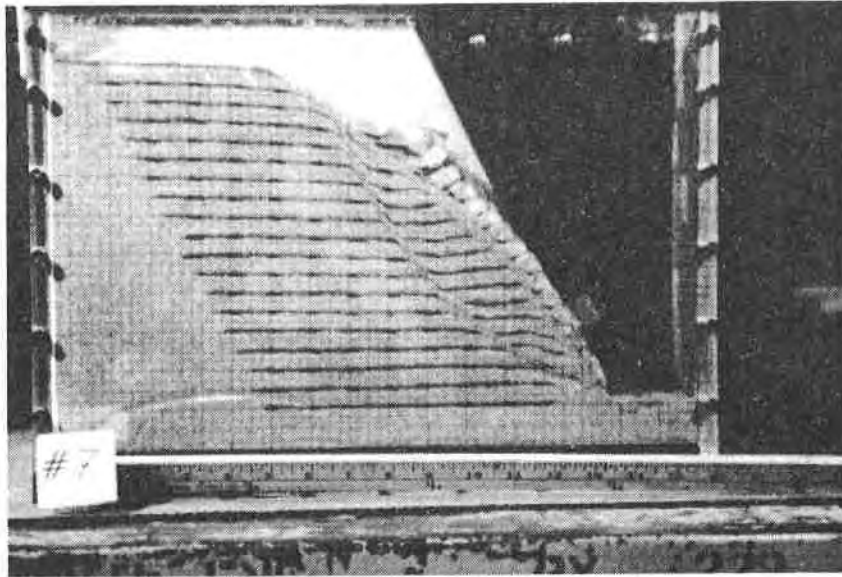
Figure 4 - View of model B18 after the centrifuge test

Figure 5 shows one of the geotextile layers retrieved from model B18 after centrifuge testing (fourth layer from the base of the slope). Since this particular layer was located towards the base of the slope, the failure surface intersected both the primary reinforcement layer and the overlapping length. Figure 6 shows the eighteen geotextiles retrieved after centrifuge testing of model B18. The geotextile shown at the top left corner of the figure is the reinforcement layer retrieved from the base of the reinforced slope model. The geotextile at the bottom right corner is the reinforcement retrieved from the top of the model. All retrieved geotextiles show clear breaks at the location of the failure surface. The pattern observed from the retrieved geotextiles shows that internal failure occurred when the reinforcements reached their tensile strength. The geotextile layers located towards the base of the slope model also showed breakage of the geotextile overlaps, which indicates that overlapping layers clearly contributed to the stability of the slope. No evidence of pullout was observed, even on the short overlapping layers.

The tears in the geotextile reinforcements were always perpendicular to the direction of loading, showing no evidence of edge effects caused by lateral friction between the model and the walls of the centrifuge box. If side friction had significant influence, the shape of the geotextile tears would have been expected to be curved. Additional evidence that edge effects were small was obtained by dissecting one of the models (model B6) after centrifuge testing. To

preserve the model, apparent cohesion was added to the initially dry sand by wetting the backfill after centrifuge testing. Dissection of the model was then performed in order to compare the pattern of displacements observed through the Plexiglas wall with those at the center of the model. Displacements observed within the model and at the interface with the Plexiglas wall were essentially identical.
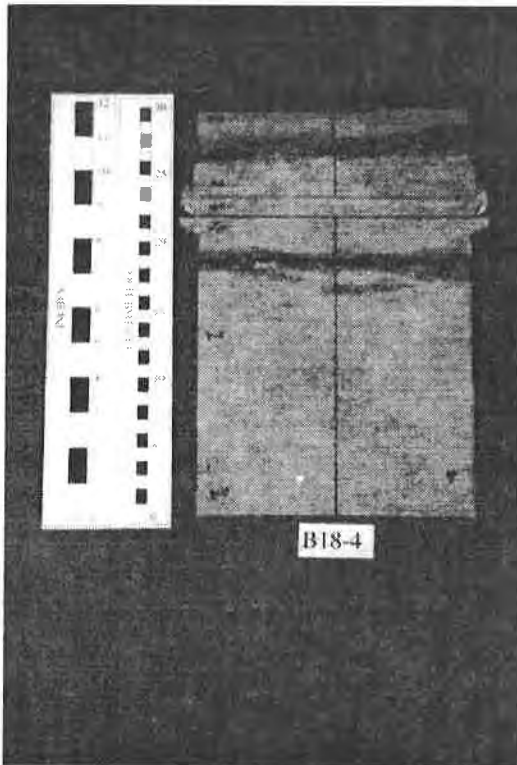
Figure 5 - Geotextile layer retrieved from model B18, showing tensile tears along the primary reinforcement and overlapping layers

The location of the failure surface could be determined after the test by measuring the location of the tears in the retrieved geotextile primary reinforcements and overlaps. Figure 7 shows the location of the failure surface for model B18, as measured from the retrieved geotextiles. The figure also shows the location of the failure as digitized from the video images recorded at the moment of failure during the test. The top layers of the models were outside the range of view of the images observed with the TV camera. There is a clear agreement between the two sets of experimental data used to estimate the location of the failure surface in the reinforced slope model. This good agreement is further evidence that edge effects during centrifuge testing were negligible.

Denser soil D-series

Models in this series had the same reinforcement layout and reinforcement tensile strength as the models in the B-series, but built using Monterey No. 30 sand at a higher relative density (75%). Figure 8 shows one of the models in this series, model D12, already placed in the centrifuge bucket and ready for testing. Catastrophic failure also occurred in this test. Figure 9 shows the failed model D12 after centrifuge testing. A clearly defined failure surface through the toe of the slope was also observed in all models from the D-series. Geotextile reinforcements were also retrieved from the models tested in the D-series. As was also the case for the models tested in the Baseline series, clear breakage of the reinforcements occurred in these models at the location of the failure surface, without any evidence of pullout.
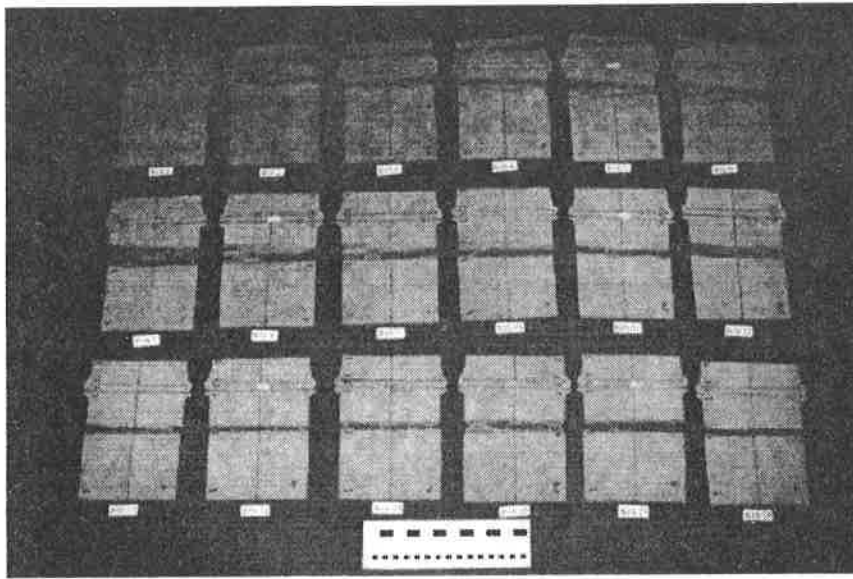
Figure 6 - View of model B18 after the centrifuge test
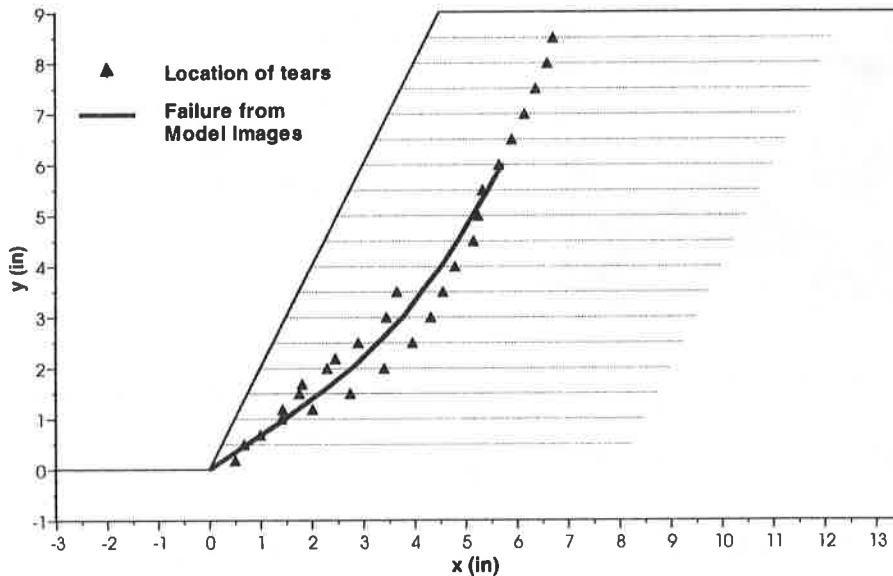
Figure 7 - Location of the failure surface for centrifuge model B18, as obtained from tears in the reinforcements and from images recorded through the Plexiglas wall

Denser soil D-series

Models in this series had the same reinforcement layout and reinforcement tensile strength as the models in the B-series, but built using Monterey No. 30 sand at a higher relative density (75%). Figure 8 shows one of the models in this series, model D12, already placed in the centrifuge bucket and ready for testing. Catastrophic failure also occurred in this test. Figure 9

shows the failed model D12 after centrifuge testing. A clearly defined failure surface through the toe of the slope was also observed in all models from the D-series. Geotextile reinforcements were also retrieved from the models tested in the D-series. As was also the case for the models tested in the Baseline series, clear breakage of the reinforcements occurred in these models at the location of the failure surface, without any evidence of pullout.

Figure 8 - Model D12 ready for testing
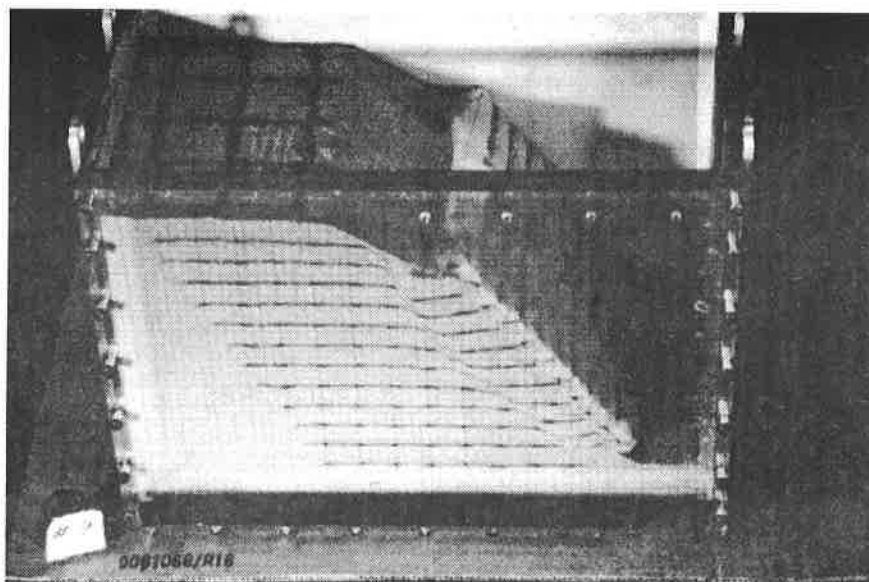
Figure 9 - Model D12 right after the test

The geometry, reinforcement layout, and backfill density in this series were identical to models in the B-series, but a geotextile with a higher tensile strength was used. Figure 10 shows the failure surface that developed in model S9 after testing. The photograph shows that the failure zone is slightly wider than the one observed in models built using the weaker geotextile. Although models reinforced using the stronger geotextile also failed along a clearly defined surface, they did not exhibit the sudden collapse observed in the failure of models built using the weaker fabric. This can be explained by results from tensile tests which show that the stronger geotextile reinforcement, differently than the weaker fabric, large strains after reaching the ultimate tensile strength.

The geotextile reinforcements retrieved after the tests showed severe straining at the location of the failure surface. However, complete separation breakage did not occur as in the models built using the weaker fabric. The tears and the magnitude of the permanent deformations in the geotextiles indicate that, also in this case, the reinforcements did reach their ultimate strength. Again, no evidence of pullout was observed and the overlaps towards the base of the models worked as additional reinforcements.
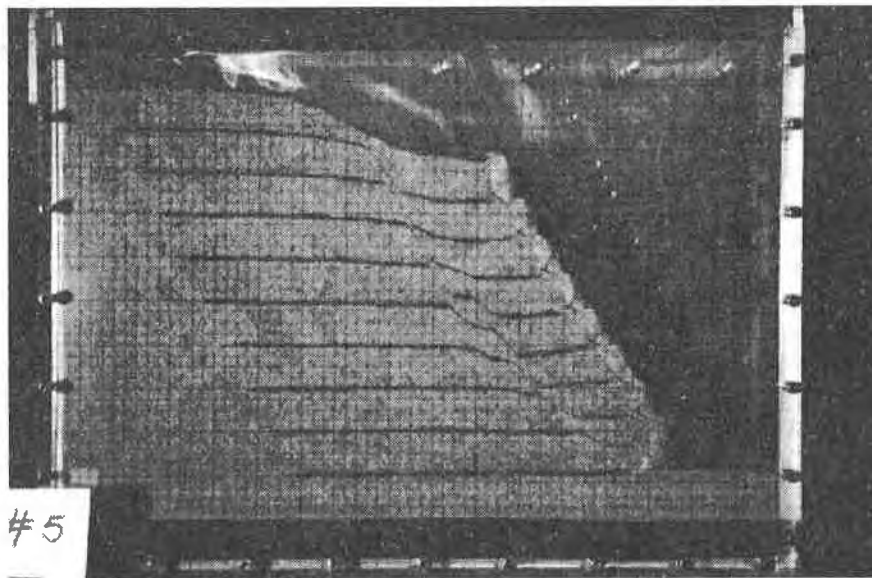
Figure 10 - Model S9 after testing

DEVELOPMENT OF THE FAILURE SURFACES

As already described, failure of all the models in this study was characterized by the development of a well-defined shear surface approximately through the toe of the slope. The

moment of failure, defined by a sudden change in the rate of settlements at the crest of the slope, was found to agree very well with the visual observation of the initiation of failure through the Plexiglas wall of the models.

Some differences in the development of failure were observed in the different test series. In the B-series, the time elapsed between initiation of failure and the final collapse of the model was relatively short. After initiation of failure, collapse generally occurred without an additional increase of the g-level. The time elapsed between initiation of failure and structure collapse appeared to be even shorter in the D-series tests. This may be attributed to a more rapid drop in strength in the denser backfill after it reaches peak strength. The time elapsed between initiation of failure and final structure collapse for the models built using a stronger geotextile (S-series) was greater than for the models in the other test series. Although the initiation of failure could be estimated with accuracy, and the failure surface was well defined, the moment of final structure collapse was more difficult to identify than in the other series. The post-failure performance may be attributed to the large displacements that the stronger fabric is able to sustain after reaching its ultimate tensile strength. This behavior was also observed in unconfined geotextile tensile tests, and is different from that of the weaker geotextiles, which shows a rapid drop in tensile strength after the peak. Thus, it appears that the post-failure behavior of the slope models until final structure collapse depends on the post-peak behavior of the backfill soil and, mainly, of the geotextile reinforcements.

Figure 11 shows the in-flight view of one of the models (model B12) at the moment of failure initiation during centrifuge testing. This image corresponds to the moment of failure defined by the transducers that monitored the settlements at the crest of the model. The image was recorded using the TV camera located inside the centrifuge. Careful study of the figure shows that the initiation of failure occurred approximately in the middle of the slope. This can be observed by kinks in the horizontal colored sand layers that were placed during construction at the levels of the reinforcements. The kinks initially appeared at approximately the midheight of the slope, and then failure rapidly extended to the reinforcement layers in the upper half of the model. The lower geotextile layers showed no evidence of kinking until the moment of ultimate structure collapse. The development of failure observed in the centrifuge slope models indicates that the lower reinforcement layers were not the ones to first reach failure. The same pattern of behavior was observed for the remaining reinforced soil models. Current design methodologies assume that the reinforcement tension distribution with depth is triangular with maximum tension at the base of the slope. This distribution implies that a progressive failure mechanism should start at the toe of the reinforced slope for uniformly spaced reinforcements of equal strength, which is inconsistent with the observed behavior.

Figure 12 shows the final collapse of model slope B12 as recorded in-flight during centrifuge testing. There is a very good agreement between the location of the failure surfaces obtained from the images on the Plexiglas wall and from the measurements of the geotextile reinforcement tears for all the tested models.
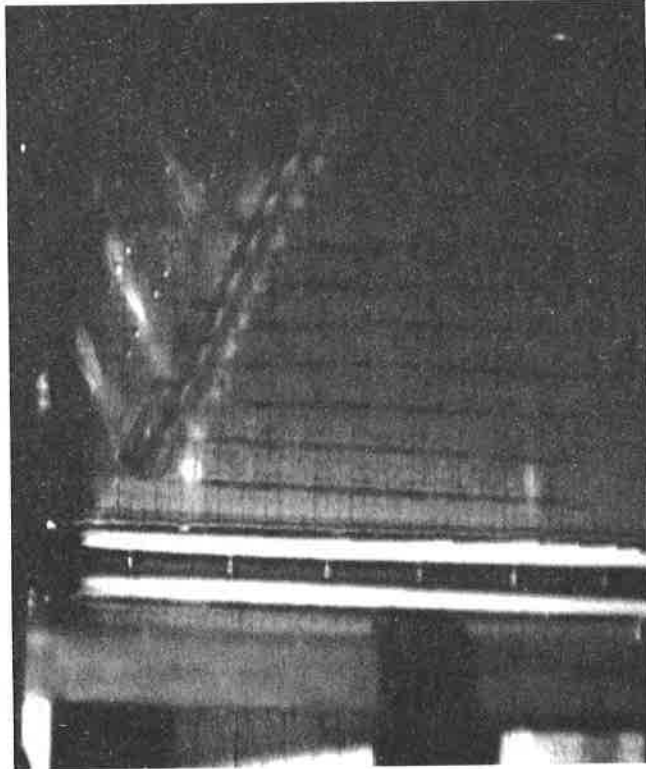
Figure 11 - Initiation of failure in Model B12
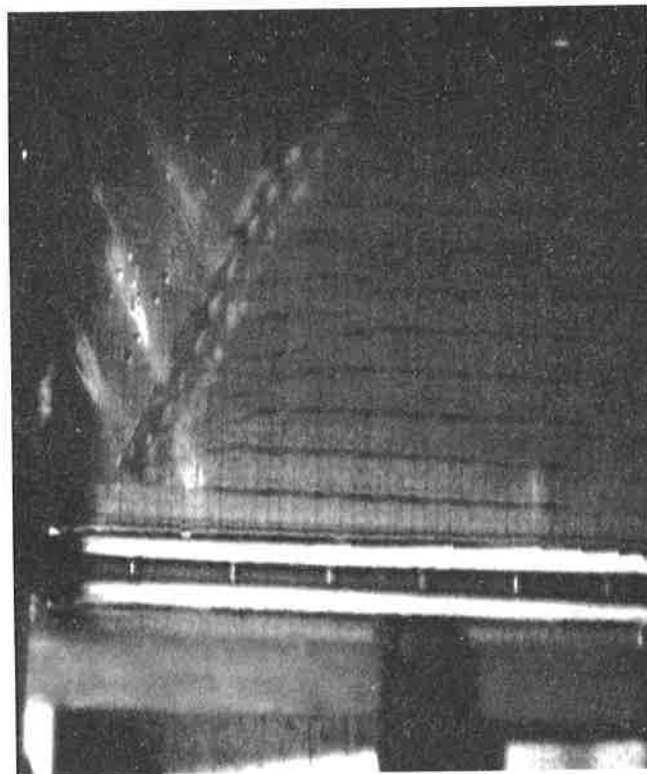
Figure 12 - Final collapse of Model B12

Because internal monitoring of the reinforcement strains was not possible due to the fragility of the geotextiles, direct observation was used instead. In order to verify the location of failure initiation, the testing progress for one of the centrifuge models (model D6) was stopped right after failure initiated, as monitored by the displacement transducers, but before final collapse. The common testing procedure, followed in all the other models, was to continue the test until collapse. Analysis of the retrieved geotextiles from model D6 confirmed that failure started at the middle of the slope height. While reinforcements in the upper half of the model showed the development of tears, the reinforcements in the lower half of the model showed only evidence of straining at the location of the failure surface. Straining was even difficult to identify in the lower geotextile layers. An additional piece of evidence that the reinforcement force distribution is not triangular, as commonly assumed in design, is the fact that the first geotextile layer (at the base of the slope) in all models did not show either tears or evidence of straining.

IMPLICATIONS FOR REINFORCED SLOPE DESIGN

The development of a well-defined failure surface is in good agreement with current design methods for reinforced slopes, which are based on limit equilibrium. The observed failure surfaces can be easily approximated by circular, log spiral, or bilinear surfaces which are conventionally used in the design of geosynthetically reinforced soil slopes.

Interpretation of the failure mechanisms in reinforced soil slopes also depends on a correct evaluation of the distribution of reinforcement forces with depth. From this distribution, the location of the first reinforcement that achieves its ultimate tensile strength can be identified. Current design methods for reinforced soil walls are based on assuming that reinforcement forces are proportional to the overburden pressure from the top of the wall. The rationale behind this assumption is that extensible reinforcements should resist the active earth pressure (Mitchell and Christopher, 1990). Although foundation stiffness has been found to affect the development of force in the lower reinforcement layers, field studies have shown that maximum tensile forces are well predicted by assuming a Rankine active condition in geosynthetically reinforced vertical walls.

In the case of reinforced soil slopes, which have their design based on limit equilibrium and not on working stress methodologies, the reinforcement force distribution with depth must also be assumed. By extending the observations gathered for the case of reinforced soil walls, triangular reinforcement tension distribution increasing proportionally with the depth below the slope crest has been assumed for reinforced soil slopes. This assumption is used in design charts that have been implemented based on limit equilibrium analysis of geosynthetically reinforced soil slopes (Schmertmann et al., 1987; Leshchinsky and Boedeker, 1989; Jewell, 1991). Current FHWA design method for reinforced soil slopes also recommends tensile forces distribution

directly proportional to depth below the slope crest for the case of slopes higher than 6 m (Christopher et al., 1990).

However, since failure of the models initiated at mid-height of the slope, the conventional triangular distribution of reinforcement forces with depth is not supported by the experimental results obtained in this study. This has major implications for design, since vertical spacing and ultimate strength of the reinforcements are currently selected considering the most critical zone is at the base of the structure.

The centrifuge test results indicate that failure does not start at the toe of the slope and, consequently, that the reinforcement with maximum tension is not located at the base of the slope. It appears that the maximum reinforcement tension with depth depends on the slope of the reinforced soil structure, and that for the 1H:2V centrifuge slope models the location of maximum reinforcement tension occurs at midheight of the slope. The distribution of maximum reinforcement tension with depth measured from well instrumented 1H:2V geogrid- and geotextile-reinforced slopes (Adib, 1988; Christopher et al., 1992) also indicate that the maximum reinforcement tension is not at the base of the slope, but approximately at midheight of the structure. A reassessment of the local equilibrium between reinforcement forces and working soil stresses may provide further insight into the possible reinforcement force distribution for reinforced soil slopes.

SUMMARY AND CONCLUSIONS

Limit equilibrium analysis methods have been traditionally used to analyze the stability of reinforced soil slopes. The accuracy of these methods depends on whether the assumed mode of failure adequately represents the conditions actually leading to the collapse of the structure. However, to date, limit equilibrium predictions of the performance of geosynthetically reinforced slopes have not been fully validated against monitored failures. Consequently, a centrifuge study was undertaken to investigate the performance of geosynthetically reinforced steep soil slopes at failure and to evaluate the assumptions in their design. This paper presents a description of the failure observed in the different models tested as part of this investigation.

Failure in the models was characterized by well-defined shear surfaces through the toe of the slope. The moment of failure was defined by a sudden change in the rate of settlements at the crest of the slope, as monitored from transducers placed on top of the centrifuge models. This moment of failure was found to agree very well with the visual observation of the initiation of failure in the models. The development of a well-defined failure surface is in good agreement with current design methods for reinforced slopes, which are based in limit equilibrium.

Interpretation of the failure mechanisms in reinforced soil slopes depends on the distribution of reinforcement forces with depth. From this distribution, the location of the first reinforcement that achieves its ultimate tensile strength can be identified. However, in contrast

to the current design assumptions that failure should develop from the toe of the reinforced slopes, failure of all centrifuge 1H:2V slope models was observed to initiate at midheight of the slopes. These results suggest that the reinforcement tension distribution with depth is not triangular with the maximum tension at the base of the slope. Instead, the test results suggest that the distribution of tension in the reinforcements with depth depends on the slope of the reinforced soil structure.

ACKNOWLEDGEMENTS

REFERENCES

Adib, M. E. (1988). Internal lateral earth pressure in earth walls, Thesis submitted in partial satisfaction of the requirements for the degree of Doctor of Philosophy. Department of Civil Engineering, University of California, Berkeley, California.

Christopher, B., C. Bonczkiewicz and R. Holtz. (1992). "Design, construction and monitoring of full scale test of reinforced soil walls and slopes." Recent case histories of permanent geosynthetic-reinforced soil retaining walls, F. Tatsuoka and D. Leshchinsky, eds. Tokyo, Japan: A.A. Balkema, 45-60.

Christopher, B. R., S. A. Gill, J. P. Giroud, I. Juran, J. Mitchell, F. Schlosser and J. Dunnicliff. (1990). Design and construction guidelines for reinforced soil structures - Volume I, Report No. FHWA-RD-89-043. Federal Highway Administration, U.S. Department of Transportation.

Hird, C. C., I. C. Pyrah and D. Russell. (1990). "Finite element analysis of the collapse of reinforced embankments on soft ground." Géotechnique 40(4), 633-640.

Holtz, R. and B. Broms. (1977). "Walls reinforced by fabrics - Results of model tests." Proc., International Conference on the Use of Fabrics in Geotechnics. Paris, 113-117.

Jewell, R. A. (1991). "Application of revised design charts for steep reinforced slopes." Geotextiles and Geomembranes 10, 203-233.

Juran, I. and B. R. Christopher. (1989). "Laboratory model study on geosynthetic reinforced soil retaining walls." Journal of the Geotechnical Engineering Division, ASCE 115(7), 905-926.

Lee, K. L., B. D. Adams and J. J. Vagneron. (1973). "Reinforced earth retaining walls." ASCE Journal of the Soil Mechanics Division 99(SM10), 745-764.

Leshchinsky, D. and E. Perry. (1987). "A design procedure for geotextile-reinforced walls." Geotechnical Fabrics Report 5(4), August, 21-27.

Liang, R.K., Tse, E.C., Kuhn, M.R. and Mitchell, J.K. (1984). "Evaluation of a constitutive model for soft clay using the centrifuge." Proc., Symposium on Recent Advances in Geotechnical Centrifuge Modeling, University of California at Davis, 55-70.

Mitchell, J. K. and B. R. Christopher. (1990). "North American Practice in Reinforced Soil Systems." Design and Performance of Earth Retaining Structures, Geotechnical Special Publication No.25, ASCE, June, 322-346.

Mitchell, J. K., M. Jaber, C. K. Shen and Z. K. Hua. (1988). "Behavior of reinforced soil walls in centrifuge model tests." Proc., Centrifuge 88. Paris, 259-271.

San, K., D. Leshchinsky and T. Matsui. (1994). "Geosynthetic reinforced slopes: Limit equilibrium and finite element analyses." Soils and Foundations 34(2), June, 79-85.

Schmertmann, G. R., V. E. Chouery-Curtis, R. D. Johnson and R. Bonaparte. (1987). "Design charts for geogrid-reinforced soil slopes." Proc., Geosynthetics '87 Conference. New Orleans, 108-120.

Schofield, A. (1980). "Cambridge Geotechnical Centrifuge Operations." Géotechnique 30(3), 227-268.

Shen, C., Y. Kim, S. Bang and J. Mitchell. (1982). "Centrifuge modeling of lateral earth support." Journal of Geotechnical Engineering, ASCE 108(GT9), September, 1150-1164.

Zienkiewicz, O.C. and R.L. Taylor. (1991). The Finite Element Method, Fourth Edition, Volume 2, McGraw-Hill, 807p.

Zornberg, J. G. (1994). Performance of Geotextile-Reinforced Soil Structures, Ph.D. dissertation, Department of Civil Engineering, University of California, Berkeley, California, 504 p.

Zornberg, J.G., Sitar, N. and Mitchell, J.K. (1995). Performance of Geotextile-Reinforced Soil Slopes at Failure: A Centrifuge Study, Geotechnical Research Report No. UCB/GT/95-01, April 1995, Department of Civil Engineering, University of California, Berkeley, California, 171 p.

THE BEHAVIOUR OF MODEL REINFORCED WALLS ON SOFT SOILS

E.M. PALMEIRA, PhD
L.M. MONTE, MSc.

UNIVERSIDADE DE BRASILIA, BRAZIL

ABSTRACT

This paper presents the results of tests with reinforced model walls built on a soft foundation soil. The walls were loaded to failure by a rigid footing located at different positions on the wall top. Internal and external displacements of the wall and footing stresses were assessed during the tests. Stiff and extensible reinforcements were used to reinforce the fill material of the wall. The results obtained showed a marked influence of the foundation soil on the deformability of the wall, failure mechanisms in the fill and strength of the system. The reinforcement stiffness and the location of the footing also affected the results obtained.

INTRODUCTION

Geosynthetics have been extensively used as reinforcement in retaining walls and steep embankment slopes. These types of reinforced structures are usually built on strong and stiff soil layers capable of resisting the mobilised stresses with minimum settlements. However, in pratical situations the foundation soil is compressible to some extent and the use of geosynthetic reinforced structures may be cost effective even on poor subgrades because of their flexibility and capability of withstanding large differential settlements. This flexibility may avoid the need for some expensive foundation solutions. When a soft foundation soil is present its strength and compressibility will be the controlling factors for the stability and deformability of the reinforced mass. The objective of the present work is to study the performance of reinforced model walls built on soft soil under the stresses caused by a rigid footing placed at different positions along the soil surface. This type of situation may occur in bridge abutments and other types of retaining structures built on soft subgrades. The details and results of this work are presented below.

EQUIPMENTS, METHODOLOGY AND MATERIALS USED IN THE TESTS

Experimentals: The model walls were built in a rigid steel box of 800 x 400 x 250 mm, as shown in Figure 1. The model reinforced walls were 200 mm high and covered the entire width of the box. The length and spacing between reinforcement layers were 125 mm and 40 mm, respectively. The frontal face of the box consisted of a perspex wall to allow for the observation of failure mechanisms and displacement of markers installed in the soils. A photographic technique was employed to obtain the position of the markers during testing. The failure mechanisms in the sand backfill were identified by thin layers of colored sand and the failure mechanisms in the soft foundation were detected by colored vertical layers of tooth paste. A localized stress was applied on the wall surface by a rigid metal footing 50 mm wide that covered the entire width of the box. A constant rate of vertical displacement of the footing of 1.5 mm/min was used to load the walls. The base of the model footing remained horizontal during all the test. Load and displacement transducers were employed to assess loads on the footing and horizontal and vertical displacements on the wall boundaries.

The borders of the box were sufficiently far from the footing and from the wall face in order to avoid boundary effects. The internal walls of the box were lubricated in order to minimize friction. Previous tests with the same equipment (Gomes, 1993) showed that this procedure was successful and the influence of side friction on the test results was negligible. Table 1 gives additional details on the geometry of the test setup.
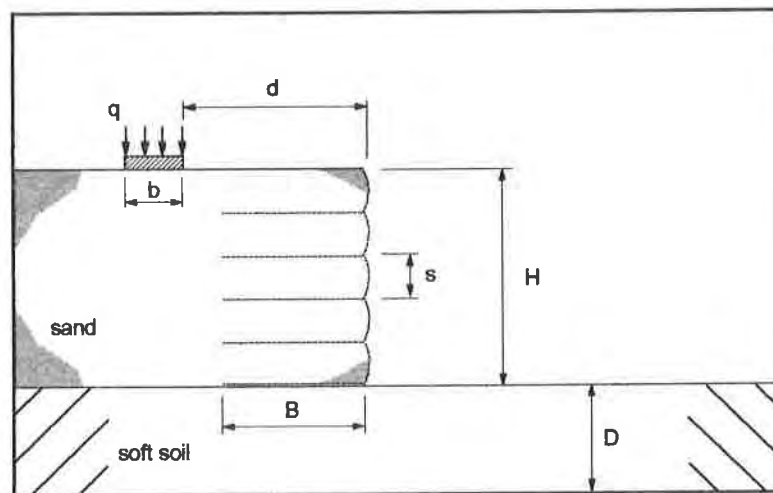
Figure 1. Schematic View of the Model Tests

Materials: The soil used in the models as fill material was an uniform medium sand and the soft foundation soil consisted of a kaolin layer. Table 2 summarises the main properties of the sand used. The soft layer was consolidated by self weight or by the

application of vertical stress on its surface before fill deposition to simulate typical scaled undrained strength and compressibility of foundation soil. The undrained strength of the soft soil was obtained by a special laboratory vane test apparatus. A typical variation of undrained strength with depth is presented in Figure 2. The ratio between shear modulus and undrained strength for the soft soil obtained from plate load tests was equal to 28. After the preparation of the soft subgrade the fill material was installed by pluviation to achieve an uniform and dense state. The technique use in the construction of the model walls was similar to what is done in the field. Firstly, the reinforcement layer was installed with one of its extremities resting on a mobile vertical plate covering the width of the box and fixed on the internal walls of the box. The sand was then pluviated up to the level where the reinforcement had to be folded to attend the specified spacing between reinforcement layers. The plate was then moved upwards and the process described above repeated for the next layers of reinforcement and sand.

Table 1. Geometrical Characteristics of the Model Tests

Symbol in Fig. 1	Value (mm)
H	200
B	125
s	40
b	50
d	25, 75 and 150
D	100

Two types of reinforcement materials were used to simulate stiff and extensible reinforcements. The stiff reinforcement was simulated by sheets of aluminium foil and the extensible reinforcement by sheets of pvc film. The main characteristics of these materials are presented in Table 3. The choice of materials was based on the necessity to adopt model materials that would simulate limits of stiffness for prototype reinforcement characteristics found in real reinforced structures

Table 2. Characteristics of the Fill Material

Total unit weight, kN/m^3	16
Specific gravity	2.63
Void ratio	0.60
Mean particle diameter, mm	1.27
Coefficient of uniformity	1.61
Friction angle (degrees) [1]	54-38 [2]

Notes:
(1) From direct shear test.
(2) Range of variation for normal stresses between 7 and 100 kPa.

Additional information on the equipment, testing methodology and materials can be found in Monte (1996).
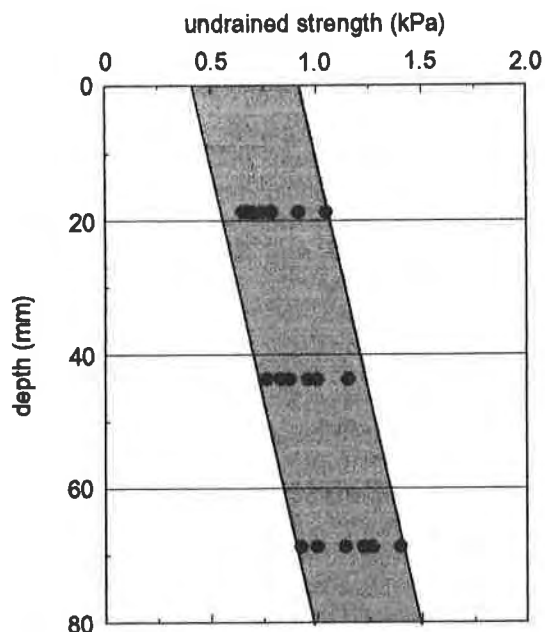
Figure 2. Typical Undrained Strength Profile with Depth for the foundation soil

Table 3. Reinforcement Characteristics

Reinforcement	Thickness (mm)	Mass per unit area (g/m^2)	$T^{(1)}$ (kN/m)	$J_{50}^{(2)}$ (kN/m)	$f^{(3)}$
pvc	0.02	20	0.10	0.16	0.51
aluminium	0.03	30	0.80	30.63	0.61

Notes: (1) Tensile strain (wide strip tests with 3%/min strain rate).
(2) Secant stiffness correspondent to 50% of the strain at failure.
(3) $f = \tan(\delta)/\tan(\phi)$, where δ = interface friction angle between sand and reinforcement and ϕ = sand friction angle.

RESULTS OBTAINED IN THE TESTS

Footing Bearing Pressures: Figures 3 and 4 present typical results of footing pressure (q) versus footing displacement (δ) for tests with aluminium and pvc reinforcements. Depending on the shape of the curves relating q and δ, footing pressures at failure were defined as the peak value of the curve or the value corresponding to its maximum

curvature, where a clear change of response in the test can be observed. For tests with the footing close to the wall face (d/B
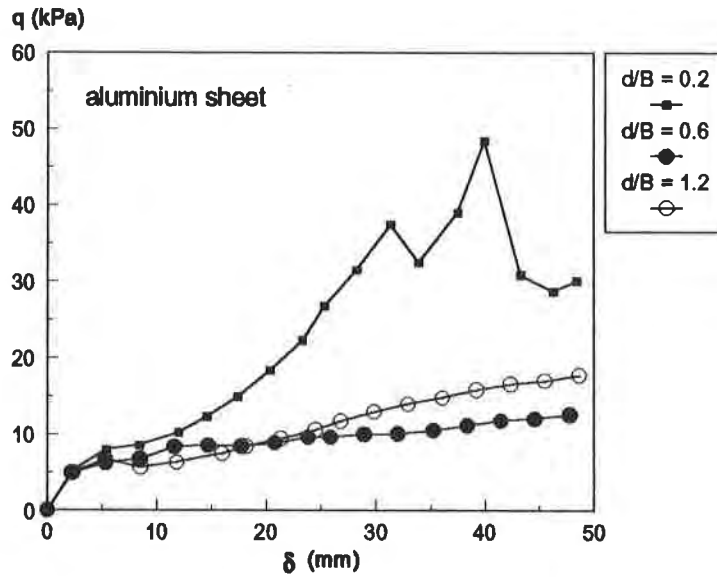
Figure 3. Pressure-Displacement Curves - Aluminium Sheet
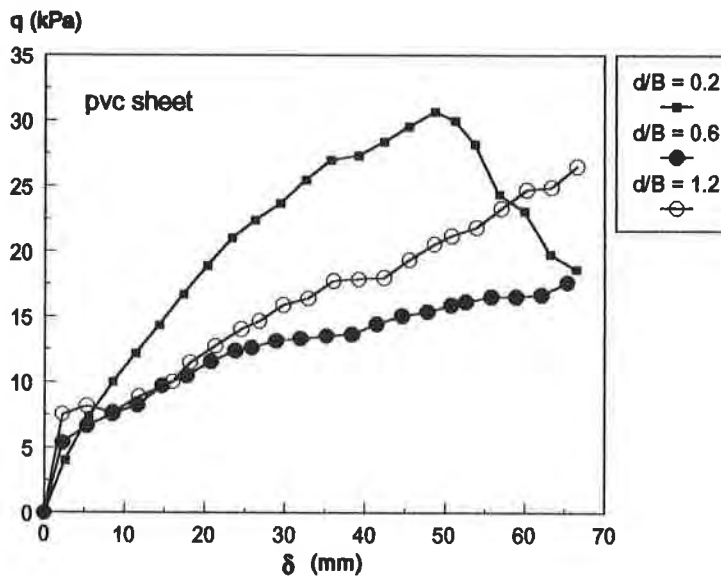
Figure 4. Pressure-Displacement Curves - PVC Film

= 0.2 , Fig. 1) there is a marked influence of the reinforcement type on the shape of the curve q x δ, which is not so clearly observed for footing locations far from the wall face. It can also be noted that for the extensible reinforcement (pvc) peak footing pressures were reached for much larger footing displacements for d/B equal to 0.2. A similar pattern

was also observed for the stiff reinforcement (aluminium) and d/B equal to 0.2, but in this case an earlier change on the curve shape can be observed for footing displacements below 10mm. It is believed that for both reinforcements the shape of the q x δ curve for d/B equal to 0.2 was affected by the failure mode of the soil-reinforcement system in this case, with the reinforced zone predominantly sinking in the soft subgrade as a rigid block. Higher footing pressures at failure were also observed for d/B equal to 0.2, particularly for the aluminium reinforcement. For values of d/B equal to 0.67 and 1.2 similar results were obtained for the stiff and extensible reinforcements.

Internal and External Displacements: Markers installed in the backfill and in the foundation allowed for the measurement of internal horizontal and vertical displacements during testing. Figures 5 (a) and (b) show displacement vectors of the markers at failure for tests with aluminium reinforcement and d/B = 0.2 and 1.2, respectively. For the footing on the reinforced mass the displacement of the markers is predominantly vertical. A rather different pattern is observed when the footing is located outside the reinforced mass, in which case the horizontal and vertical displacements are approximately the same. Similar results were also observed for the tests with the pvc film reinforcement. For the conditions of the tests in this work these results show that the reinforced zone behaved as a rigid block transferring the pressures to the underlying layer when the footing was on the reinforced mass.

Figures 6 (a) and (b) show contours of equal total horizontal displacements at failure for tests with d/B = 0.2 with the stiff and extensible reinforcements. It can be observed that the stiffness of the reinforcement causes a reduction on the magnitude of horizontal displacements in the reinforced zone. However, similar values of displacements and pattern of the curves were observed in the foundation soil for both cases with maximum displacements of approximately 3.5 to 4.0% of wall height.

Figures 7 (a) and (b) show contours of equal total vertical displacements at failure for tests with d/B = 0.2 with aluminium and pvc reinforcements. Larger vertical displacements can be observed for the extensible reinforcement. The reinforced mass behaved as a rigid block in the test with the stiff reinforcement. In both cases larger gradients of vertical displacements occurred in the region close to the rear of the reinforced zone.

Horizontal displacement profiles of the wall face at failure are presented in Figures 8 (a) to (c). The location of the footing and the reinforcement stiffness affect the horizontal displacements on the wall face. For values of d/B equal to 0.2 (Fig. 8a) the wall reinforced with the pvc film presented a non uniform displacement profile with larger displacements in the top half of the wall. Two

results for the wall reinforced with aluminium sheets are presented in Figure 8(a) for different values of footing displacement on the wall top (δ = 8mm and δ = 39mm), corresponding to different responses

(a) d/B = 0.2

(a) d/B = 1.2
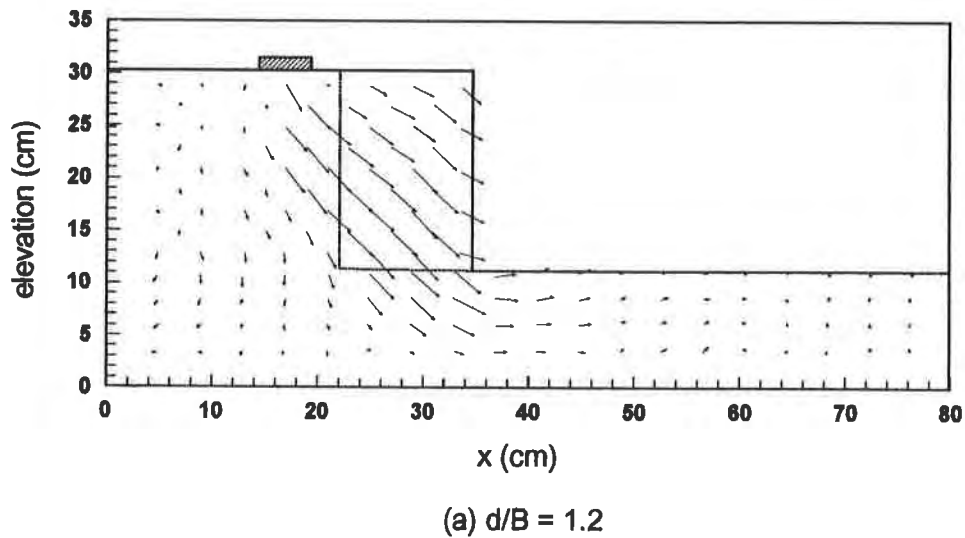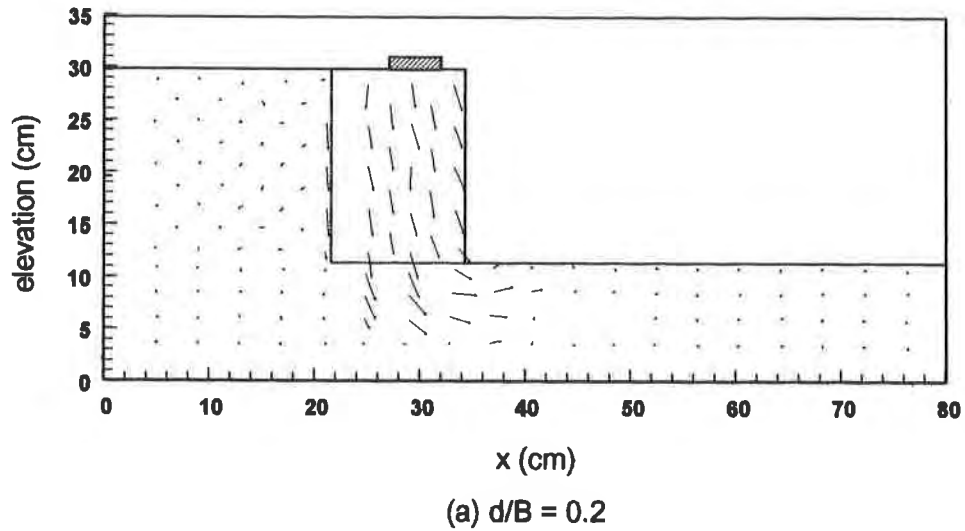
Figure 5. Displacement Vectors - Aluminium Sheet

of this wall for d/B equal to 0.2, as suggested by the results in Figure 3. For δ equal to 8mm larger horizontal displacements occurred at the wall toe. For δ = 39mm the horizontal displacement profile for the aluminium reinforcement was very uniform and almost vertical. For d/B equal to 0.6 a rotation of the wall face can be observed with considerably larger horizontal displacements at the toe of the wall for both reinforcements. Larger horizontal displacements in this region can be observed for the extensible reinforcement. This can be attributed to the higher values of reinforcement tensile forces in

that region (Chou and Wu, 1993). For d/B equal to 1.2 some rotation
of the wall face is still visible with greater horizontal
displacements at the lower half of the wall reinforced with the
extensible reinforcement. For d/B equal to 0.6 and 1.2 the profile of
horizontal displacements along the top half of the wall face was
affected little by the reinforcement type.
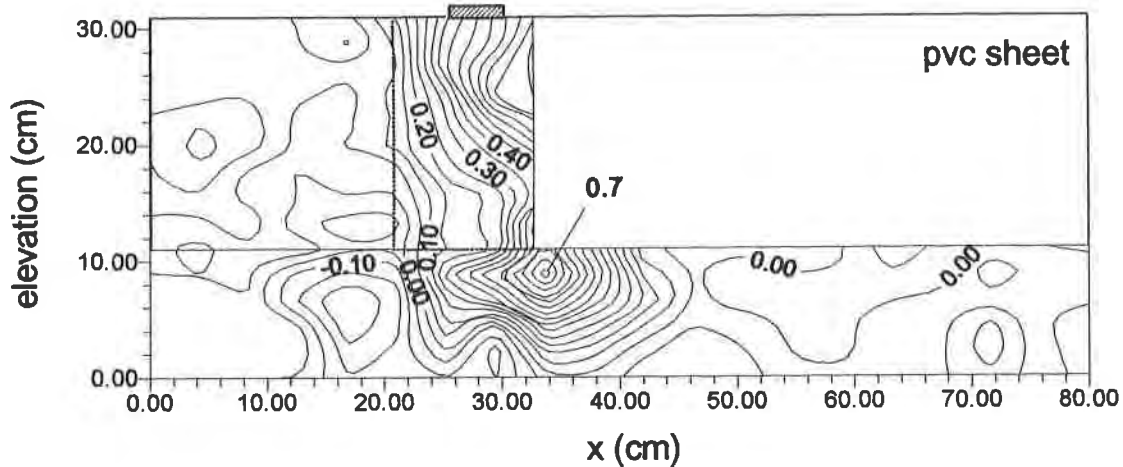
(a) pvc, d/B = 0.2
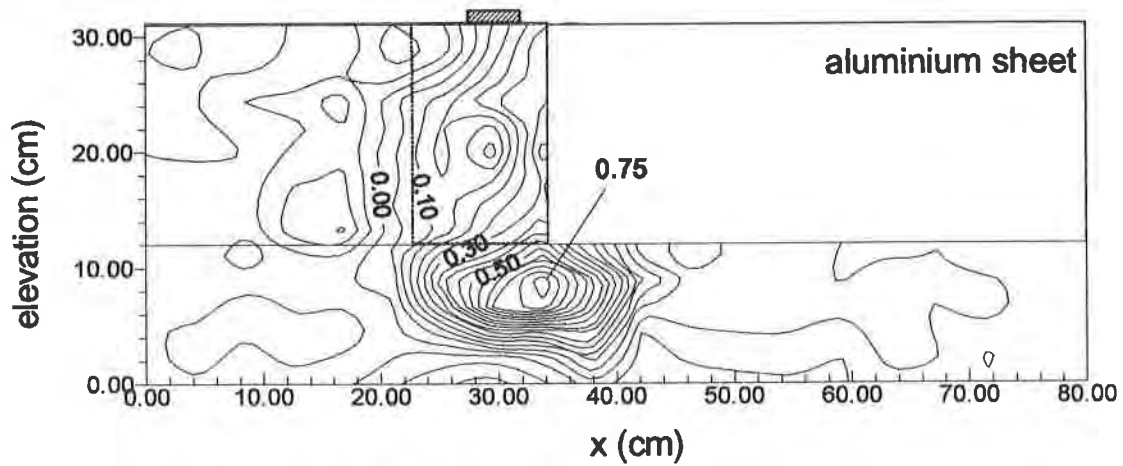
(a) aluminium, d/B = 0.2

Figure 6. Contours of Equal Horizontal Displacements (cm).

Results for similar model tests built on rigid foundation carried
out using the same sand and reinforcements (Gomes, 1993, and Gomes et
al, 1994) are also presented in Figures 8 (a) and (b). It can be
noted that the shape and magnitude of the horizontal displacement
profile is markedly affected by the characteristics of the foundation

soil. Similar results were obtained by Chou and Wu (1993) in a numerical analysis of reinforced walls on soft subgrade using the finite element method.
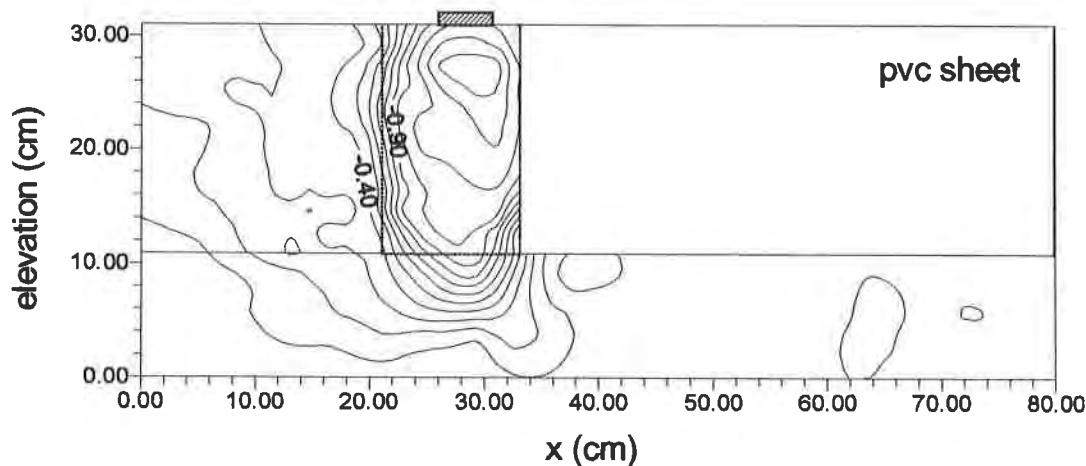
(a) pvc, d/B = 0.2
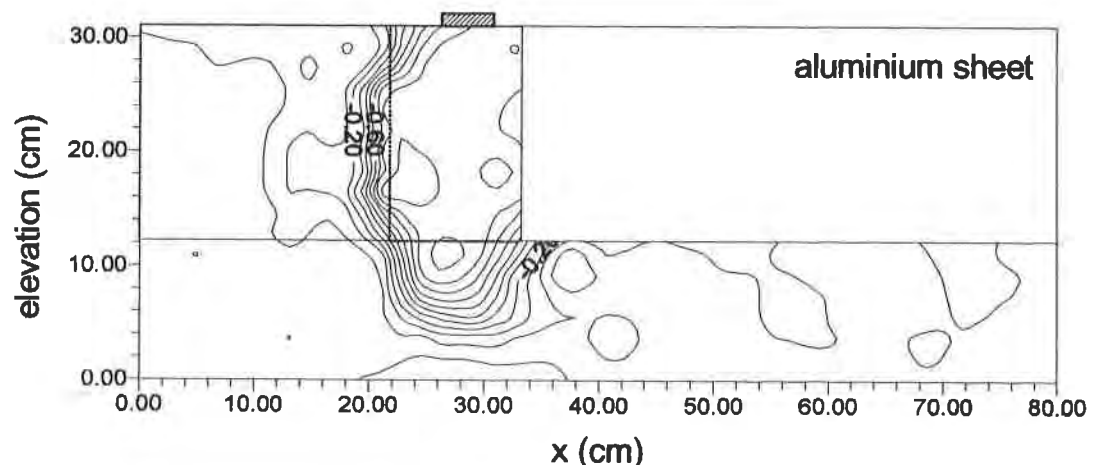
(a) aluminium, d/B = 0.2

Figure 7. Contours of Equal Vertical Displacements (cm).

Failure Mechanisms: Figures 9 (a) to (c) show the failure mechanisms observed in the model tests performed. For values of d/B equal to 0.2 or 0.67 the failure zone in the fill was very close to the rear face of the reinforced mass. For d/B equal to 1.2 a clear failure zone close to a straight line was observed in the fill material. Except for d/B equal to 0.2 the type of reinforcement had very little influence on the failure surface location in the soft subgrade. Deeper failure surfaces in the soft soil were observed for tests with

d/B equal to 0.2 and shallower failure surfaces were obtained for d/B equal to 1.2. In general, for the geometry and materials used in the tests the failure surface in the foundation reached a distance of 0.5 to 0.7H ahead of the wall face.
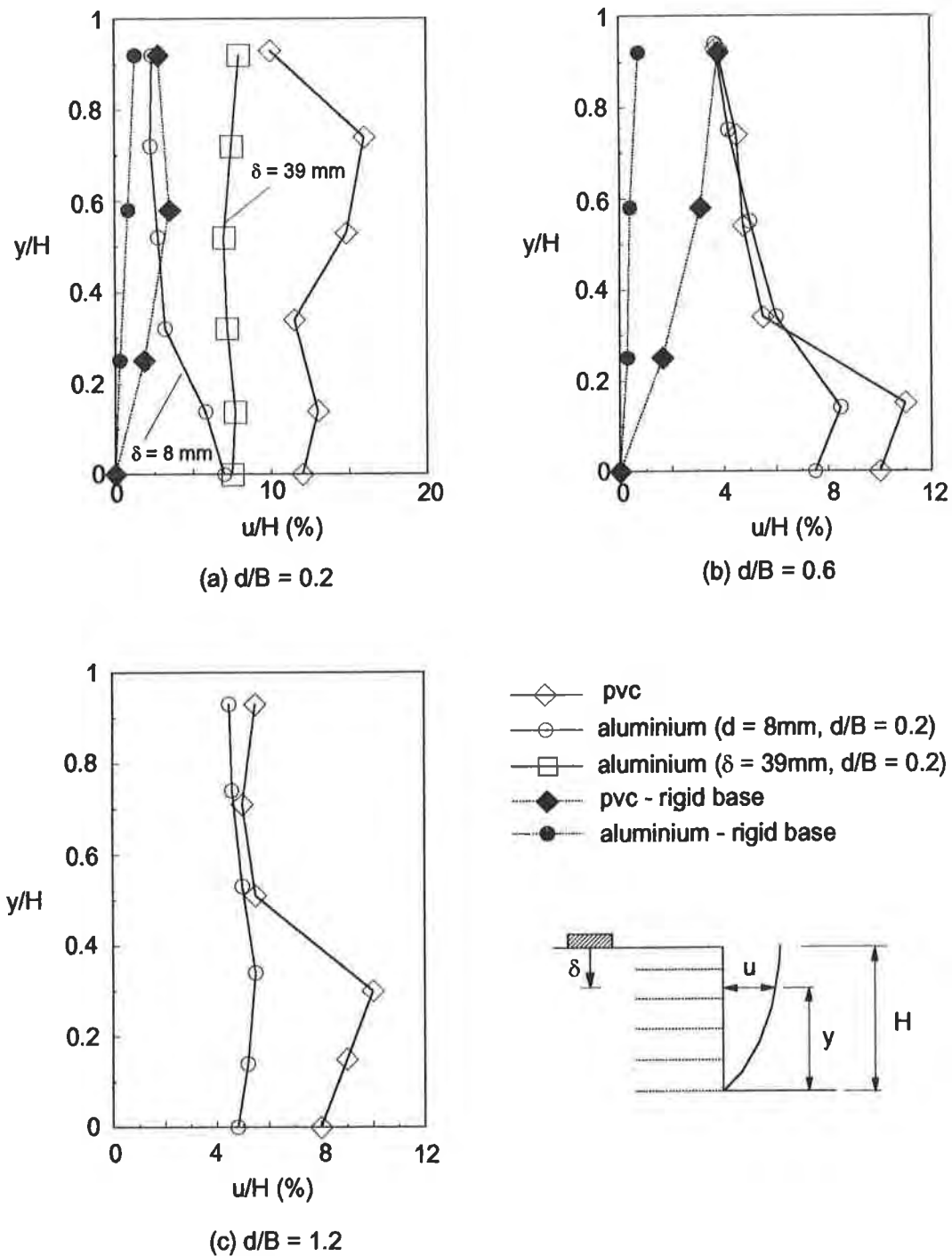
(a) d/B = 0.2

(b) d/B = 0.6

(c) d/B = 1.2

Figure 8. Horizontal Displacement Profiles on the Wall Face
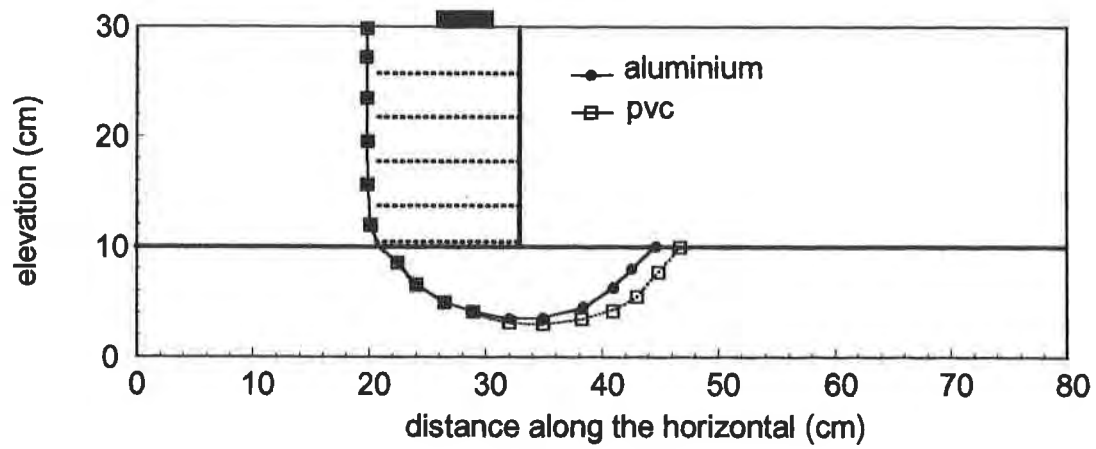
(a) d/B = 0.2
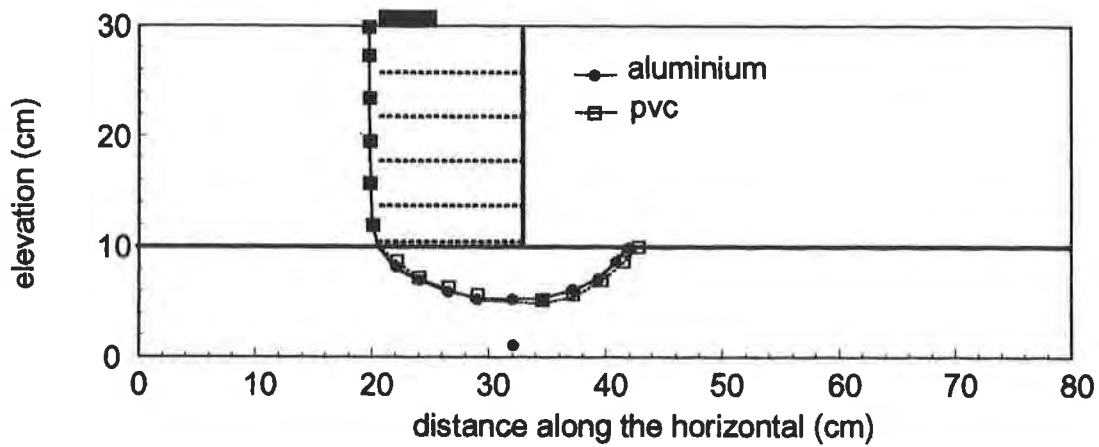
(b) d/B = 0.6
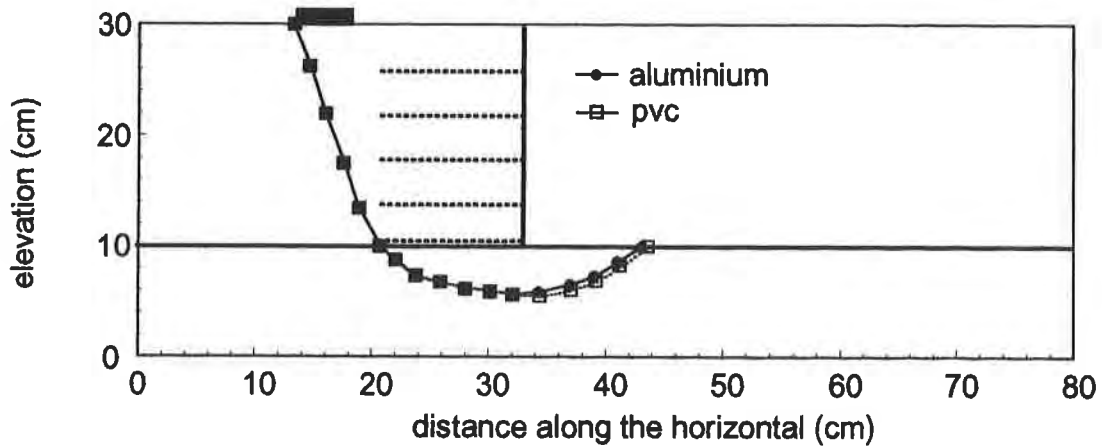
(c) d/B = 1.2

Figure 9. Failure Mechanisms

CONCLUSIONS

This work dealt with the behaviour of reinforced model walls built on soft soil and loading by a rigid footing on top. The main conclusions reached are summarised below.

The stiffness and strength of the foundation soil have a marked effect on the wall performance in terms of deformability and capacity of sustaining localized stresses on its top. The position of the footing on the wall top surface affects the magnitude and pattern of horizontal displacements on the wall face.

Walls on soft subgrades demonstrate a rearward rotation of the wall face with larger horizontal displacements at the wall toe. This contrasts with the behaviour of walls on rigid foundation, where maximum horizontal displacements occur at the wall top, demonstrating a forward rotation.

In general, for the conditions of the present test the reinforced mass behaved as a rigid block, particularly for the stiffer reinforcement. The location of the failure surface in the soft foundation was only slightly influenced by the reinforcement type.

REFERENCES

Chou, N.N.S. and Wu, J.T.H. (1993), "Effects of Foundations on the Performance of Geosynthetic-Reinforced Soil Walls", Proceedings of the Geosynthetics'93 Conference, NAGS-IFAI-IGS, Vancouver, Canada, Vol. 1, pp. 189-201.

Gomes, R.C. (1993), "Soil Reinforcement Interaction and Failure Mechanisms in Geotextile Reinforced Soils", DSc. Thesis, University of São Paulo, São Paulo, Brazil, 270 p. (in Portuguese).

Gomes, R.C., Palmeira, E.M. and Lanz, D. (1994), "Failure and Deformation Mechanisms in Model Reinforced Walls", Geosynthetics International, IFAI, Vol. 1, No. 1, pp. 45-65.

Monte, L.M. (1996), "A Study on the Behaviour of Model Reinforced Walls on Soft Soils", MSc Thesis, University of Brasilia, Brasilia, Brazil.

ANALYSIS OF THE COLLAPSE OF A 6.7 M HIGH GEOSYNTHETIC-REINFORCED WALL STRUCTURE

R.R. BERG
CONSULTANT, USA
M.S. MEYERS
U.S. ARMY CORPS OF ENGINEERS, USA

ABSTRACT

A 6.7 m high segmental block faced, geosynthetic-reinforced soil retaining wall collapsed suddenly seven weeks after construction. The project relationships between parties and engineering computations are summarized, analyzed and discussed within this paper to investigate the cause of failure. The contractual relationships of the various parties and their communications, or lack thereof, are detailed. The wall design and global stability analyses were separate design responsibilities on this project, which is typical practice with reinforced soil wall projects. Completion of the internal and external wall design, and global stability analyses by separate parties is diagnosed. Computations for global stability, compound stability, and bearing capacity are presented within. The computer modeling techniques, minimum acceptable safety factor, and quantification of soil parameters used in the global stability analyses are specifically addressed. The primary conclusion from this project is that the common practice of separating wall design and global stability responsibilities can lead to disastrous results. The lessons of this case history are germane to wall designers, geotechnical engineers, geosynthetic manufacturers and suppliers, and owners and developers.

INTRODUCTION

The failure of a 6.7 m high, segmental retaining wall (SRW) unit-faced, geosynthetic reinforced, mechanically stabilized earth wall (MSEW) is documented within. This structure was constructed to extend the backyard of a house on top of a steep bluff. The wall collapsed suddenly in August 1992, seven weeks after construction completion. The wall slid downslope approximately 13 m, with the SRW unit-faced reinforced mass remaining largely intact.

The purpose of this paper is to document the key findings of the authors' investigation of this failure. This paper is organized as follows: site description, subsurface investigations, contractual relationships, and project sequence of events are first summarized. The preliminary and final wall

structure configurations are described; and the details of the final design are reviewed. Wall failure, based upon first-hand observations by others and the authors' post-failure observations, is described. Investigation of the failure is then detailed, and probable causes of failure summarized. Conclusions and recommendations for future design and construction of MSEW structures are presented.

SITE DESCRIPTION

This project is located in the City of Eau Claire, in western Wisconsin as illustrated in Figure 1. The site is on a 32 m high bluff, about 550 m east of the Chippewa River. The retaining wall was constructed at the top of the bluff. This bluff slopes steeply to the southwest, at an angle of approximately 30°, and was covered with mature trees and grasses at the time of subsurface investigations. No slope distress was noticed during the investigations, with the exception of some surface sloughing and erosion at the crest of the slope. Some filling had been attempted at the crest of the slope based on the geotechnical consultant's report dated 1991.
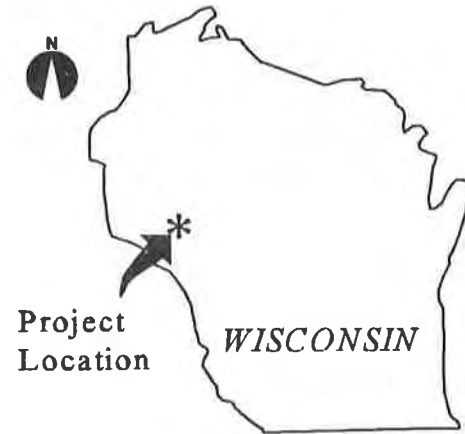
Figure 1. Site location.

Igneous and metamorphic rocks of Precambrian age underlie the area and form the bedrock surface. Glacial drift forms an almost continuous mantle, as much as 46 m in thickness, over the bedrock. Drift in the basin is composed of ground moraine, end moraine, and outwash. Drift is thickset in the preglacial and bedrock valleys and in areas of end moraine and outwash. Ground moraine, laid down by advancing glaciers, overlies most of the basin and has relatively low permeability, especially where it is composed of clays and silts. The project site consists of approximately 30 m of unpitted outwash soils overlying the ground moraine. This outwash was deposited by meltwater streams from stagnating glaciers (Young and Hindall, 1972).

A U.S. Department of Agriculture Soil Conservation Service near-surface soil survey was referenced in the geotechnical consultant's subsurface exploration reports. The hillside soil is described in this survey as a *Terrace Escarpment* feature, that are *moderately steep to very steep sandy escarpments along edges of stream terraces*. It was noted that few soil properties were given for this soil, in this survey, due to the highly variable nature of this soil on a county-wide basis.

SUBSURFACE INVESTIGATIONS

Two exploratory soil programs were conducted for the proposed wall. The initial program consisted of performing a moisture density test and hand boring at some (undefined) distance downslope of the proposed wall. A nuclear density testing apparatus was used to measure in situ density and moisture content at a depth of 0.3 m. A soil sample obtained from a depth of 3 m was used to conduct laboratory direct shear tests.

The field moisture-density test results gave a dry density of 15.9 kN/m³ and a moisture content of 2.8%. Direct shear testing was conducted, in accordance with ASTM D 3080. Three specimens recompacted to a density of 15.8 kN/m³ and moisture content of 2.4%, each, were sheared under normal stresses of 48, 96 and 144 kPa. The measured peak effective friction angle was 31.5°.

The second program consisted of two exploratory borings to further investigate subsurface conditions for the proposed retaining wall. Borings were taken at the toe of the slope and at the crest of the slope. The boring at the crest started at elevation 271.4 m and extended to a depth of 24.7 m. The boring at the slope toe started at elevation 238.9 m and extended down 15.5 m. As noted in the geotechnical consultant's report in 1991 - *The soil borings generally revealed predominately sands with some silt. The geologic origin of the sand appeared to be alluvium (water deposited). The boring at the crest of the hill appeared to contain up to 2 m of fill at the surface.* Water was encountered in the toe boring, at a depth of 4.7 m.

In situ soils consisted of sands, classified from field identification and four grain size analyses as SP and SP-SM, using the Unified Soil Classification System (USCS). The sand graded as fine or fine to medium size in the toe boring and to a depth of 14.3 m in the crest boring; and graded as fine to coarse size below a depth of 14.3 m in the crest boring. The 2 m depth of fill at the slope crest was identified as mostly silty sand, with some ashes, wood and metal.

Soil shear strengths through the depth of the borings were estimated by the geotechnical consultant. Reference information supporting the estimation of the shear strengths was not included in the subsurface investigation report. It appears that the estimates were based upon shear strength and moisture density testing, standard penetration test (SPT) values, visual classification, gradation testing, and experience. The shear strength estimates are summarized in Table 1.

Table 1. Shear strength estimates (by the geotechnical consultant in 1991).

	Depth (m)	ϕ'	c'
Crest Boring:	0 - 2.1 (fill)	25°	0
	2.1 - 4.6	30°	0
	4.6 - 15.2	35°	0
	15.2 - 24.7	40°	0
Toe Boring:	0 - 4.6	30°	0
	4.6 - 15.5	35°	0

CONTRACTUAL RELATIONSHIPS

Several parties were involved with this project. The parties were: owner; geosynthetic material supplier; geotechnical consultant; geogrid manufacturer; contractor; SRW unit supplier,

manufacturer, and licensor; and a civil engineering consultant. Relationships between these parties are illustrated in Figure 2, with contractual relations shown with a solid line and non-contractual relations (e.g., communications) shown in dashed lines.
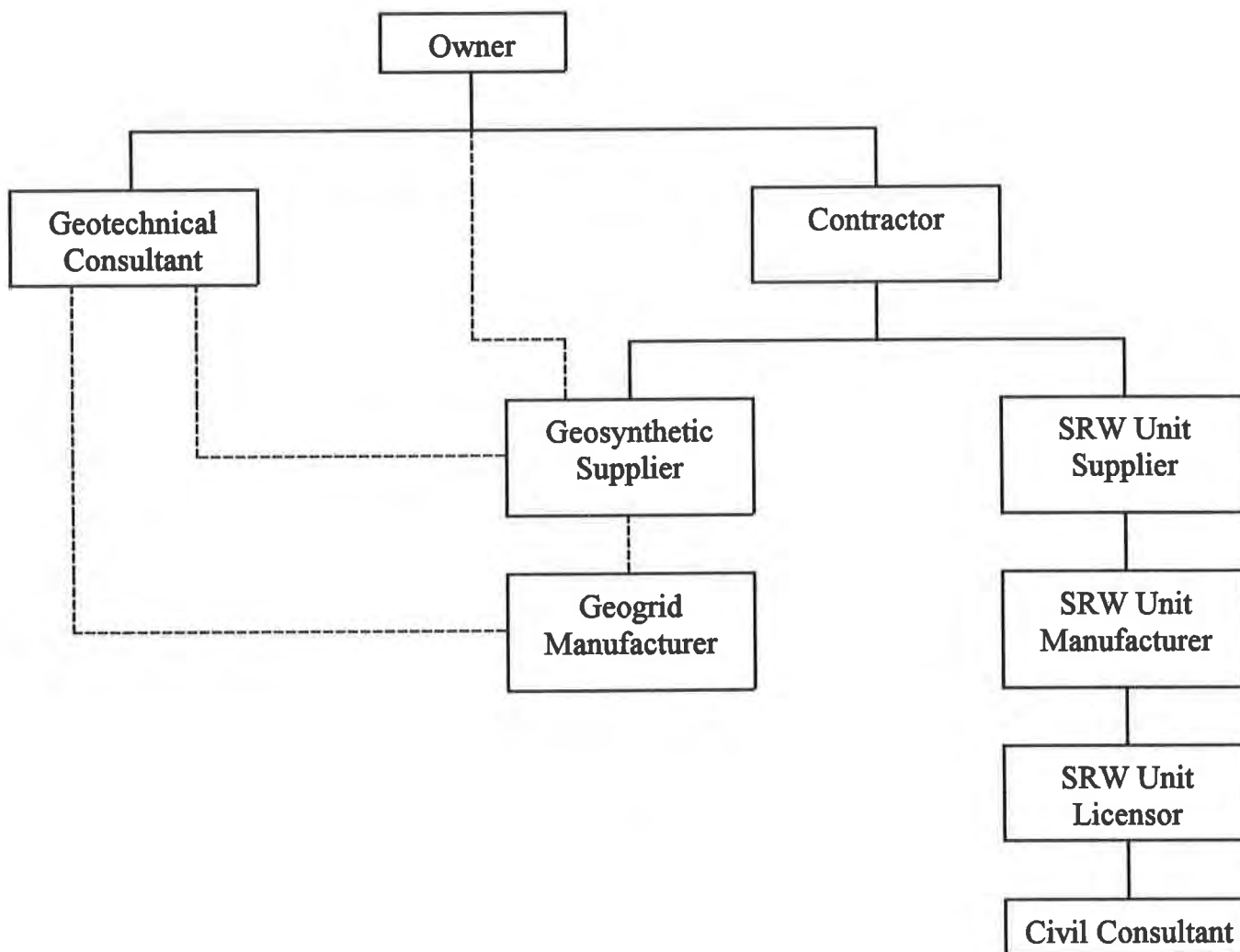
Figure 2. Relationships between parties.

Owner. The project owner is the couple that own the house, whose backyard was to be enlarged with the retaining wall. The owner had several discussions with the geosynthetic supplier and followed many of the supplier's recommendations. Subsequent to the failure and inability to reach an equitable settlement with the other parties, the owner filed a lawsuit. Named as defendants in the lawsuit were the contractor, geotechnical consultant, and civil consultant. The civil consultant was subsequently dropped from the lawsuit, and an out of court settlement was reached with the geotechnical consultant and contractor.

Geosynthetic Supplier. The geosynthetic supplier promoted the use of an engineered SRW, MSEW *package* to the owner. The *package* consisted of geogrid soil reinforcement, SRW facing units, and

construction plans prepared by a registered engineer. The geosynthetic supplier sold only the geogrid material to the contractor, after the contractor elected not to purchase the MSEW package.

Geotechnical Consultant. This local firm was retained by the owner to perform a preliminary site investigation, and subsequently, a detailed site investigation. Additionally, the geotechnical consultant was retained by the owner to prepare an engineering report with an estimate of overall slope stability safety factors, including methodologies and findings. The consultant's scope-of-work specifically excluded consideration of failure modes through the reinforced mass. The estimate of overall factor of safety was based upon the subsurface exploration reports, and slope and wall geometry information provided by the owner and geosynthetic supplier. The geotechnical consultant recommended that the preliminary wall design, furnished by the geogrid manufacturer, could be supported by the native soils. Furthermore, the geotechnical consultant recommended that qualified personnel be retained to provide on-site construction observations. The geotechnical consultant performed no additional design work and was not retained to provide any construction inspection services.

Geogrid Manufacturer. Feasibility of MSEW construction on this site was evaluated by the geogrid manufacturer, at the request of the geosynthetic supplier. A concern regarding global stability was raised by the geogrid manufacturer; this led to the second exploration program and a global stability analysis by the geotechnical consultant. A preliminary wall design, completed by the geogrid manufacturer, was used by the geotechnical consultant in the global stability computer model. The geogrid manufacturer had no further involvement in the engineering of this project as the MSEW package that included their design services was not purchased by the contractor.

SRW Unit Supplier. This local supplier sold the SRW units to the contractor. It is the authors' understanding that this supplier also sold the engineering design to the contractor.

SRW Unit Manufacturer. The manufacture furnished the SRW units to the supplier, and is a license holder for these proprietary SRW units.

SRW Unit Licensor. The civil consultant services were retained through the licensor. The licensor had a contract with the consultant to provide services on projects using their SRW units, on an as-needed basis.

Contractor. The contractor was retained by the owner to provide an engineered wall design and materials, and to construct the wall. This contractor is well experienced in construction of SRW-faced MSEW structures. The construction contractor, upon receiving approval to proceed with construction of the wall system separately procured materials and design services (i.e., they elected not to purchase the MSEW package). The civil engineering consultant was retained through the SRW block supplier to design the wall structure, assuming global stability was no longer a design concern.

Civil Consultant. Final design of the wall was prepared by the civil consultant. This consultant specializes in the design of SRW-faced MSEW structures. The civil consultant's scope-of-work specifically excluded global stability, which had been addressed by the geotechnical consultant. The geotechnical consultant's stability report prepared in 1992 was transmitted to the civil consultant. It is not known whether the preliminary wall design prepared by the geogrid manufacturer was transmitted to the civil consultant. The civil consultant was not retained to perform any inspection or testing during construction.

Project Sequence of Events. The sequence of events for this project and involvement of the various parties are listed in Table 2.

Table 2. Project sequence of events and party involvement.

Event	Party								
	O	GS	GM	GC	C	BS	BM	BL	CC
Initial field investigation	C	I		C					
Field investigation letter report	C	I		C					
Preliminary wall design	I	I	I						
2ND site investigation proposal	C	I		C					
Subsurface report	C		I	C					
Proposal for slope evaluation	C			C					
Slope evaluation report	C		I	C					I
Wall construction contract	C				C				
Wall design					C	C	C	C	C
Wall construction	C	I			C	I	I		
Crack in soil appeared	I								I
Wall failure	I								
Litigation	C			C	C				C

KEY: C - contractual responsibility I - non-contractual involvement in event
O - owner GS - geosynthetic supplier GM - geogrid manufacturer
GC - geotechnical consultant C - contractor BS - SRW unit supplier
BM - SRW unit manufacturer BL - SRW unit licensor CC - civil consultant

WALL STRUCTURE

Description. The design plan view and elevation are shown in Figures 3 and 4, respectively. This MSEW structure is 42.7 m long, has a maximum height of 6.7 m, and an average height of 5 m. It is composed of SRW facing units, geogrid soil reinforcement elements, and sand fill. The SRW units are approximately 150 mm high, 400 mm long, and 300 mm wide (toe to heel). The face of the units are straight, with a broken block finish. The SRW units are solid (i.e., no cavities to be filled with granular fill) and vertically connected with nylon/fiberglass pins. The SRW units are dry laid (i.e., no mortar) in a running bond configuration.
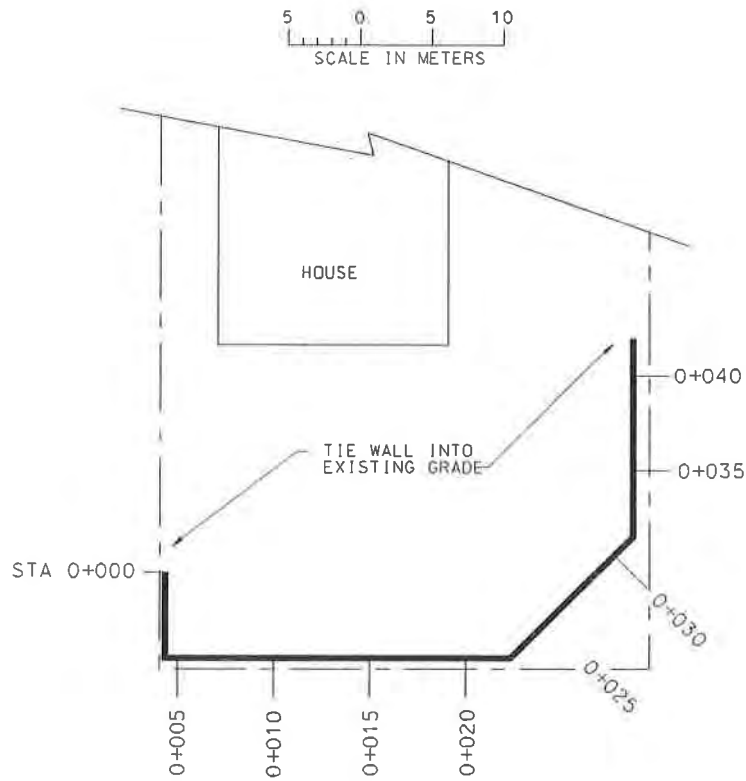
Figure 3. Design plan view.
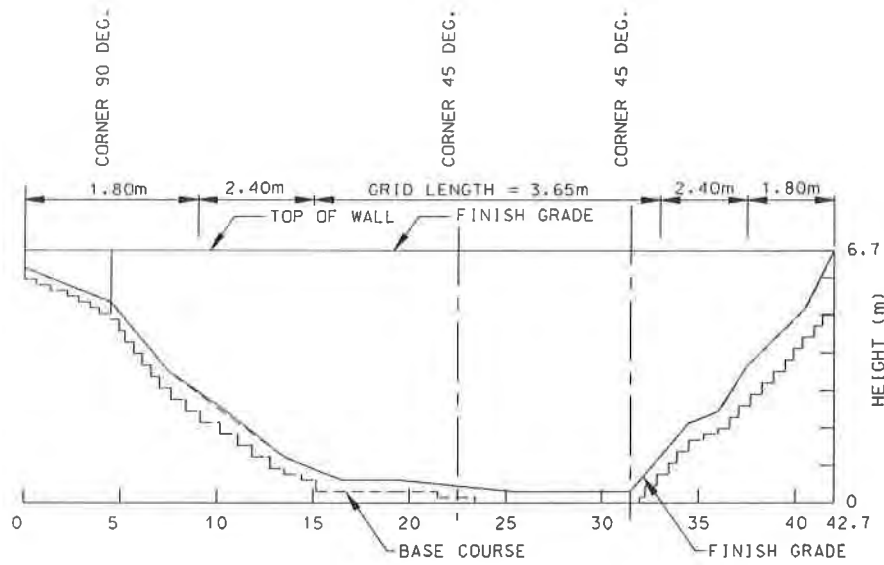
Figure 4. Design elevation view.

The soil reinforcement is an integrally formed, uniaxial, polyethylene geogrid. This geogrid has a long-term allowable strength of 17.7 kN/m, and soil shear and pullout interaction coefficients equal to 0.9, as reported by the manufacturer. The connection between the geogrids and SRW units is constructed by placing a transverse rib immediately in front of the SRW unit connection pins. Strength of the connection is primarily derived from friction.

The reinforced fill was a sand imported from offsite. Disposition of the existing silty sand fill at the crest of the slope was not determined in the authors' investigation. There was no vegetation established on top of the wall fill, prior to the failure.

Wall Design. The authors were not able to obtain a copy of the signed design drawings. All discussion regarding the wall design is taken from a set of drawings stamped *DRAFT*, which were provided to one of the authors during litigation of the wall failure.

It appears that the final wall design was completed with the aid of a computer program, developed by the geogrid manufacturer. Soil properties used in design were: wall fill and retained backfill unit weights of 18.8 kN/m^3 and $\phi' = 32°$; foundation soil $\phi' = 32°$; and foundation allowable bearing capacity equal to 239 kN/m^2. It was noted on the drawings that these values should be verified by the site soils engineer, and that the wall should be redesigned if the values were lower than stated. The specifics of internal design are not addressed within this paper as complete documentation was not available, and a review of internal design does not contribute to the discussion of this failure. A cross section of the wall at the maximum height is illustrated in Figure 5. Thirteen layers of geogrid reinforcement, 3.65 m long (from the front face of the SRW units) are used in this cross section.

The external stability analyses typically performed by a wall designer consists of determining factors of safety with respect to overturning, sliding and bearing capacity. An analysis, by the authors, of the wall structure at the maximum height section (i.e., 6.7 m), with soil parameters and software previously noted, yielded safety factors of 2.5 and 4.2 for potential sliding and overturning failures, respectively. A bearing pressure of 135 kN/m^2 was computed, which is less than the assumed allowable of 239 kN/m^2. Global slope stability of the structure was not analyzed by the civil consultant as it was specifically excluded from their scope-of-work. The wall was designed upon an understanding, or assumption, that an MSEW on this slope was globally stable.

Groundwater at the site is well below levels where they would be expected to influence the design of the wall system. A drainage system consisting of a zone of drainage fill material 300 mm wide immediately behind the SRW units was installed. A drainage collector system consisting of 100 mm diameter pipes was installed at the bottom of the drainage fill zone with outlets called for at 15 m intervals. The ground surface was to be graded to allow for positive drainage to a central collection ditch located away from the wall system. The drainage fill material zone was to be capped with impervious fill.

CAP UNIT

IMPERVIOUS FILL

REINFORCED
BACKFILL

152 mm

STRUCTURAL
GEOGRID
(SEE ELEVATION)

SRW
UNIT

RETAINED
BACKFILL

DRAINAGE FILL

6.7 m

APPROX.
EXCAVATION

GROUNDWATER
DRAINAGE

DRAINAGE TILE
100 mm DIA.
OUTLET EACH 15 m

LEVELING PAD
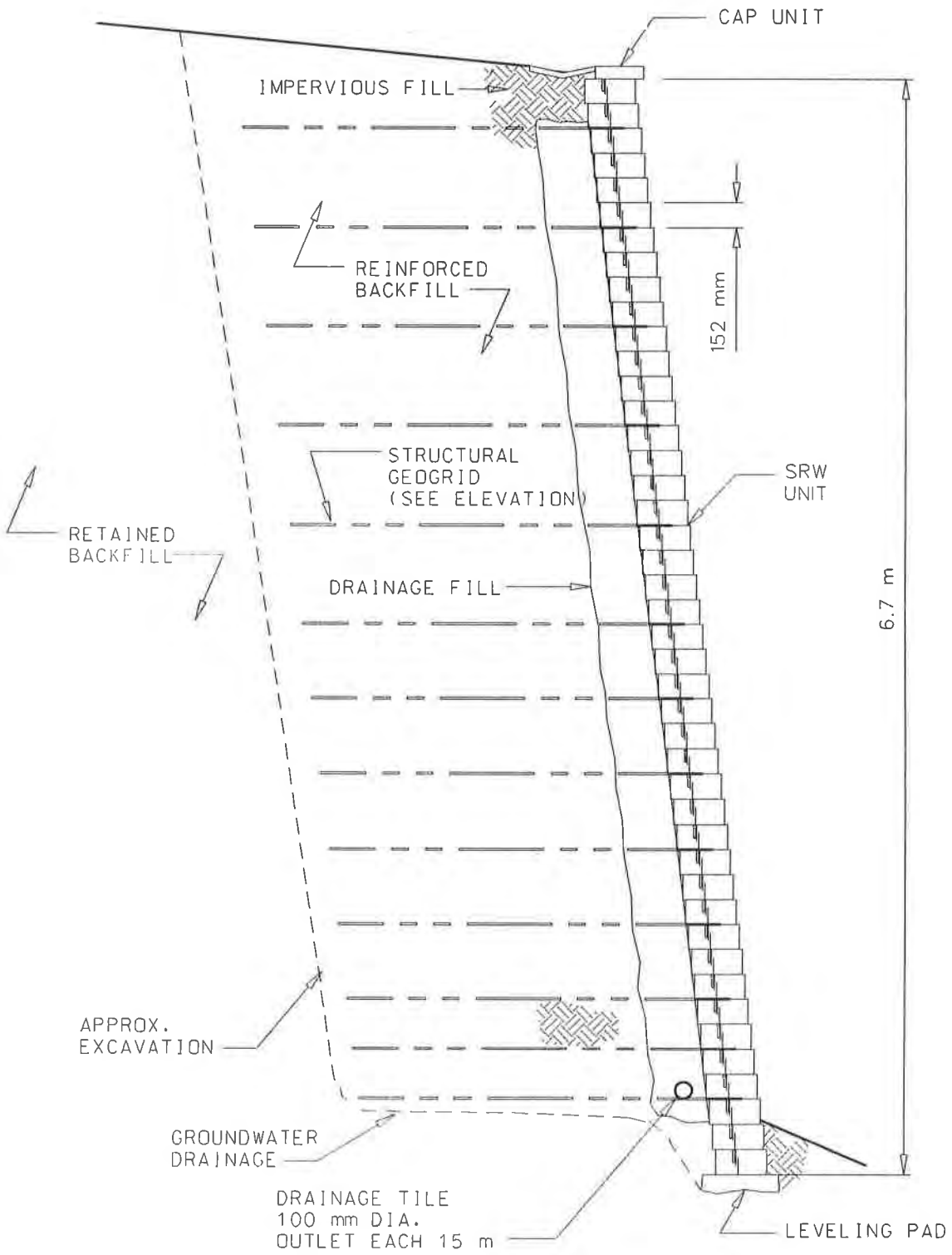
Figure 5. Design cross section at maximum height.

The geotechnical consultant's global stability model is shown in Figure 6. Soil stratigraphy, soil shear strengths, unit weights, and critical failure planes are listed. Note that the geotechnical consultant used an artificially high shear strength for the MSEW mass. This eliminated the need to model the geosynthetic reinforcement and also precluded a compound failure plane (i.e., plane passing behind, through and under the reinforced mass). The geogrid manufacturer's preliminary wall design was used in the analyses. The preliminary design used extended lengths of geogrids at the bottom of the MSEW (7 m long at the maximum wall height), presumably to prevent global failures, whereas the civil consultant's final design did not use extended lengths. A Janbu procedure with noncircular failure planes was used for the analyses. The geotechnical consultant stated in their report (1992) that *we are not authorized to evaluate the wall design, nor were we authorized to consider failure modes through reinforced portions of the proposed wall.* Thus, potential compound failure modes for the MSEW and slope were not evaluated by the geotechnical consultant. Nor were compound failure modes evaluated by the civil consultant.

FAILURE

The owner noticed a surface crack in the fill soil, at the back edge of the reinforced mass, within weeks of construction and contacted the civil consultant. The civil consultant informed the owner that such a crack was not unusual, and that the soil was likely settling. The owner called the civil consultant a second time stating that the crack seemed to be getting larger, and was again told that a crack was not uncommon.

On August 18, 1992, one of the owners and their four-year-old daughter were in the backyard when the retaining wall suddenly and catastrophically failed. The owner described the failure noise as a *loud rumbling*. The four-year-old was playing in the sand within a meter of the failure escarpment, as shown in Figure 7.

An upslope and a downslope view of the failed wall are presented in Figures 8 and 9, respectively. The ends of the wall remained in-place and the central portion of the wall slid downslope approximately 13 m. The central portion of the reinforced mass (SRW units, geogrid, and sand fill) remained relatively intact during this downslope translation.

INVESTIGATION OF FAILURE

The authors' investigation of this failure was limited. Construction of the MSEW was not reviewed. A cursory review of the internal stability calculations of the wall was performed, as this review did not uncover any details that would have contributed to the failure. Global stability, compound stability, and bearing capacity were thoroughly investigated, and are summarized below.
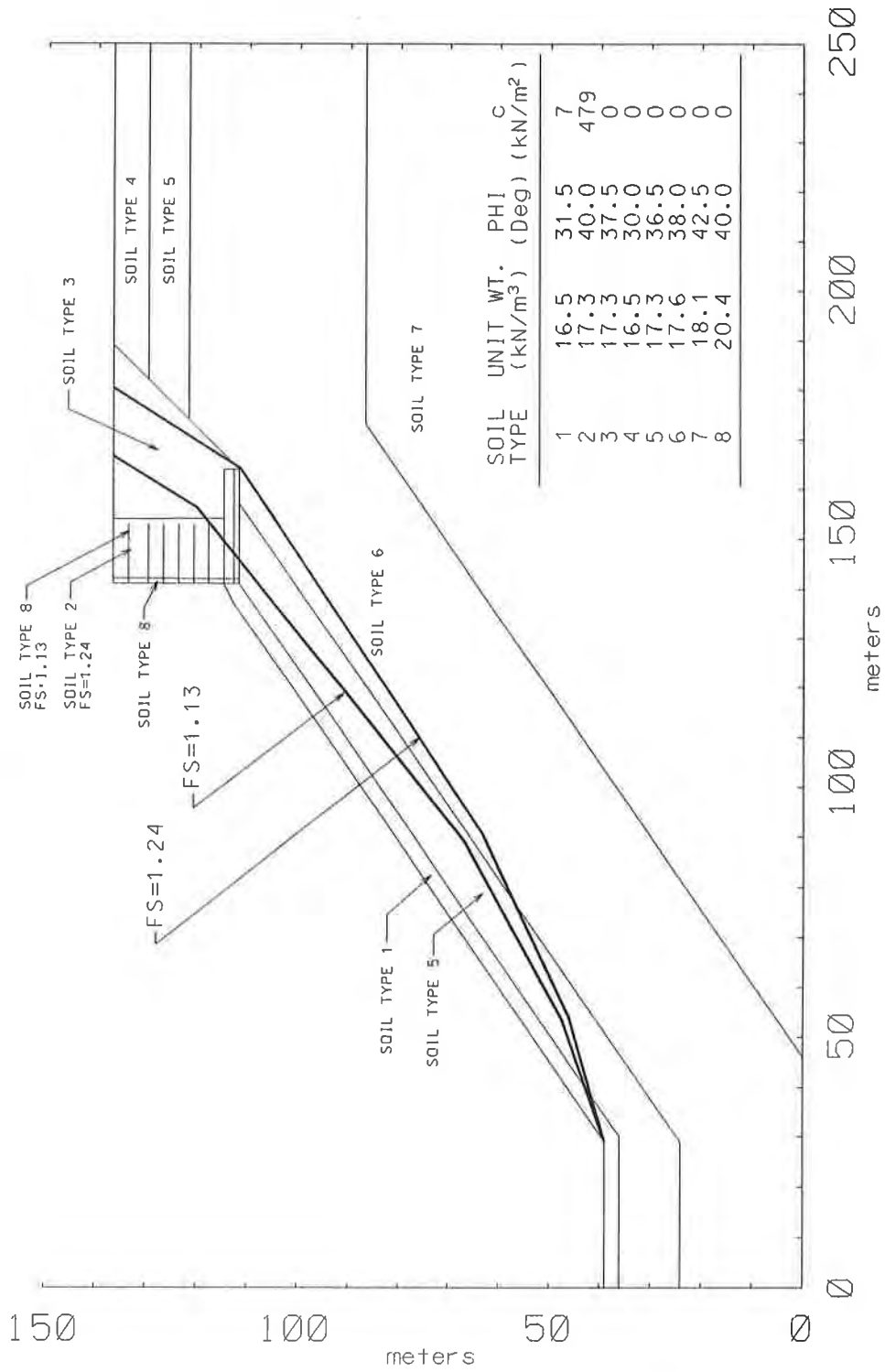
Figure 6. Geotechnical consultant's stability model with geotechnical consultant's critical global stability failure surface (FS = 1.24) and authors' compound stability failure surface (FS = 1.13).

Figure 7. View of the collapsed wall; the sand pail (see arrow) is where the owner's 4-year old daughter was playing when the wall collapsed.
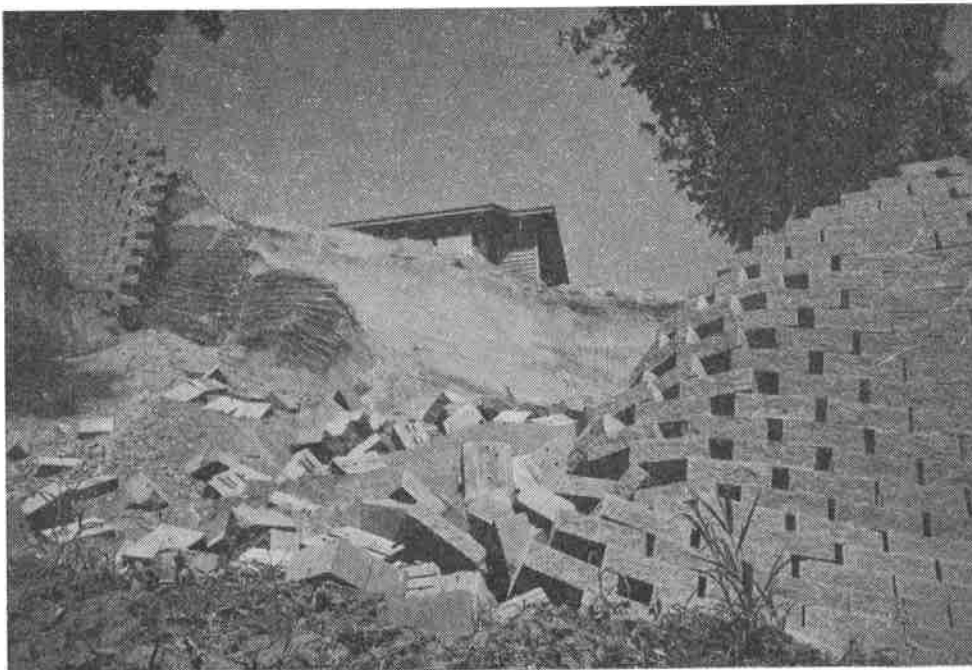
Figure 8. View of the collapsed wall, looking upslope.

Figure 9. View of the collapsed wall, looking downslope.

Global Stability. The geotechnical consultant's global stability analysis (Fig. 6) shows a critical failure surface behind the reinforced mass, with a factor of safety (FS) of 1.2. This result was checked by the authors with a different computer code using a Spencer's procedure with noncircular failure planes. The computed FS (Table 3) and failure surface location were similar.

The failure plane in the geotechnical consultant's analysis was primarily contained in soil types 5 and 6 (Fig. 6). The geotechnical consultant determined that soil types 5 and 6 had friction angles of 36.5° and 38°, and unit weights of 17.3 kN/m³ and 17.6 kN/m³ degrees, respectively. These friction angles are higher than the 30° and 35° noted in the subsurface investigation report (Table 1) for these zones. This difference was not specifically addressed in the stability report.

A new stratigraphic model of the site was developed by the second author, based upon his interpretation of the subsurface exploration results. This interpretation was based upon standard penetration test (SPT) values versus effective overburden pressure analysis. SPT values at their effective overburden pressure, and at the depth at which each SPT value was determined, was used to determine a relative density value for the soil at that depth (Figure 3, NAVFACS DM-7.1, 1982). The relative density value and the USCS classification for the soil at the depth of the SPT were then plotted (Figure 7, NAVFACS DM-7.1, 1982) to estimate friction angle, dry unit weight, void ratio, and porosity values for the soil at that depth. Moist unit weights were estimated by applying a typical moisture content, as indicated in the subsurface investigation reports.

Table 3. Summary of stability analyses.

Analysis By	Failure Mode	Analysis Procedure	Wall Design	Soil Profile	Factor of Safety
GC	Global	Janbu	GM	GC	1.19
Authors	Global	Spencer	GM	GC	1.24
Authors	Global	Spencer	GM	Authors	1.04
Authors	Global	Spencer	CC	GC	1.14
Authors	Global	Spencer	CC	Authors	1.00
Authors	Compound	Spencer	GM	GC	1.13
Authors	Compound	Spencer	GM	Authors	1.01
Authors	Compound	Spencer	CC	GC	1.12
Authors	Compound	Spencer	CC	Authors	0.99

KEY: GM - geogrid manufacturer   GC - geotechnical consultant   CC - civil consultant

When this information is plotted or tabulated with depth, similar SPT values and relative densities can be grouped to determine the approximate boundaries of stratigraphic units which have similar and consistent soil parameters. The authors' soil profile, presented in Figure 10, can be compared against the soil profile developed by the geotechnical consultant (Fig. 6). Overall, this interpretation led to lower shear strength friction angles.

Global slope stability was evaluated using the authors' stratigraphy and using a Spencer's procedure. A FS equal to 1.04 (Table 3) was computed for a failure plane passing behind the preliminary design MSEW (i.e., the reinforced mass modeled as shown in Fig. 6). The preliminary design generated by the geogrid manufacturer was 7.6 m high and used 7 m long geogrids in the lower portion of the MSE mass, and 3.6 m lengths in the upper portion. The constructed length of the reinforced mass, based on the civil consultant's design, was 3.7 m, as illustrated in Figure 10. Global stability analyses with this shorter reinforced mass yielded safety factors of 1.14 and 1.00 using the geotechnical consultant's stratigraphy and the authors' stratigraphy (Table 3), respectively.

Compound Stability. A compound stability failure plane for a reinforced soil system is defined as a plane which passes partially behind and partially through a reinforced mass (Berg et al., 1989). The global stability assessed by the geotechnical consultant (and by authors' as discussed in the preceding section) used an artificially high shear strength soil to model the reinforced mass. Thus, potential compound failure planes were prevented.

Compound failures were investigated by the authors using four models, having varying wall design and stratigraphy. The geogrid manufacturer's preliminary design and civil consultant's design wall models (Fig. 6 and 10, respectively) were modified by eliminating the artificially-high shear strength for the reinforced soil and inserting geogrid layers as designed and a reinforced soil shear strength of $\phi' = 32°$ and $c' = 0$. Compound failure planes with FS values equal to 1.13 and 1.12 for the preliminary and final wall designs, respectively, were determined using the geotechnical
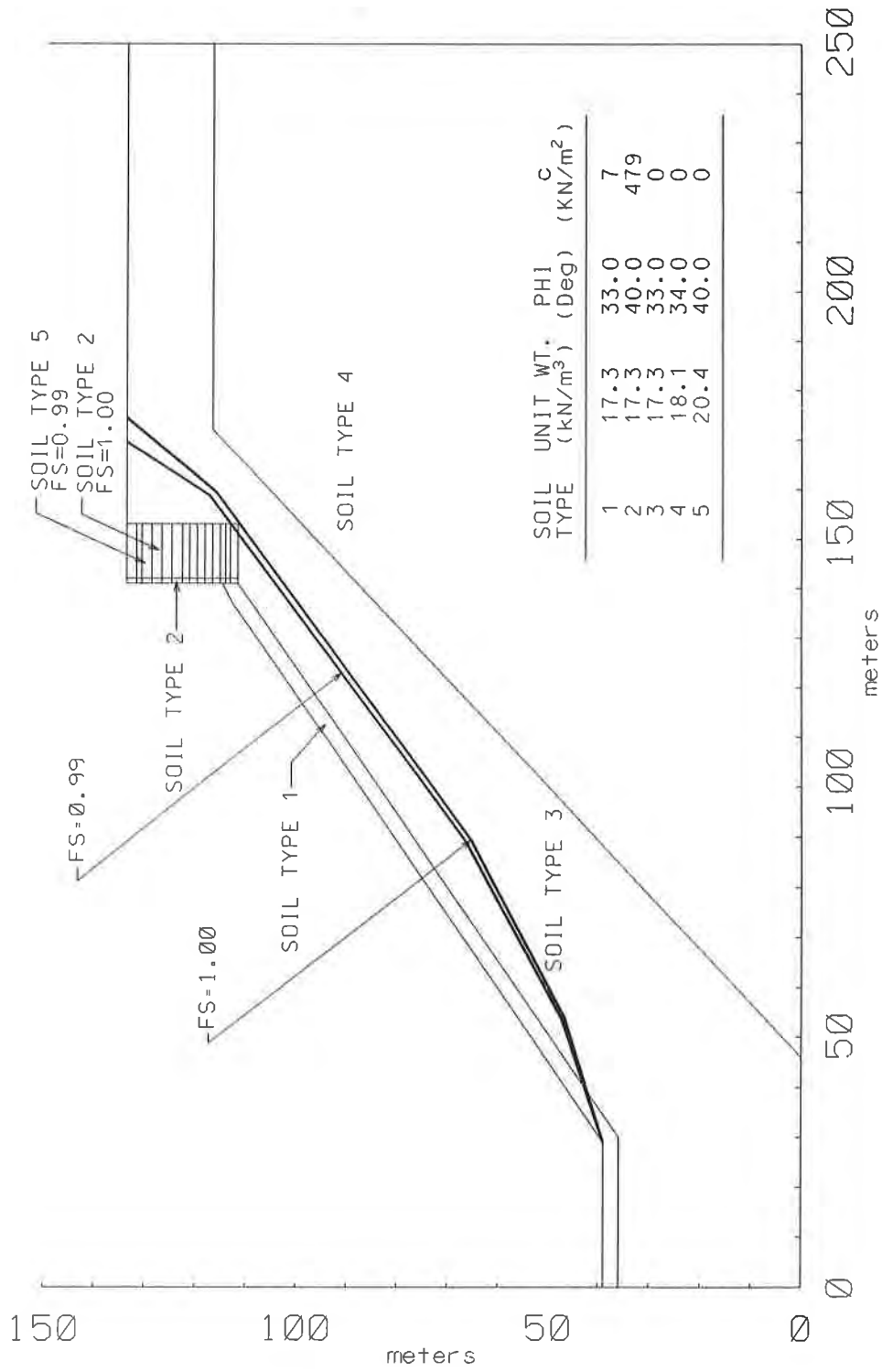
Figure 10. Authors' stability model with critical global stability failure surface (FS = 1.00) and critical compound failure surface (FS = 0.99).

consultant's stratigraphy model. Compound failure planes with FS values equal to 1.01 and 0.99 for the preliminary and final wall designs, respectively, were determined with the authors' stratigraphy model.

Bearing Capacity. The preliminary design provided by the geogrid manufacturer assumed an allowable bearing capacity of 239 kN/m^2. The civil consultant's final design was also based upon an allowable bearing capacity of 239 kN/m^2. This was an assumed value that reportedly was called out on the construction drawings to be verified in the field by the site soils engineer. A soils engineer was not retained for construction services. Thus, the assumed allowable bearing capacity was never verified.

A summary of ultimate and allowable bearing capacity values for several cases is presented in Table 4. The magnitudes of the decrease in ultimate bearing capacity (q_{ult}) due to the ground slope in front of the MSEW are noted. The allowable bearing capacity (q_{allow}) is computed using a factor of safety of 2. All values in Table 2 were calculated at the maximum height of the walls and a Meyerhof-type pressure distribution beneath the MSEW. Meyerhof depth and Hansen ground slope factors (Bowles, 1988) were used in the computations.

Table 4. Comparison of bearing capacity values.

Wall Design	Soil Profile	Bearing Capacity (kN/m^2)				% Reduction Due to Sloping Groundline
		Assumed Horizontal Groundline		With Sloping Groundline		
		q_{ult}	q_{allow}	q_{ult}	q_{allow}	
GM	GC	4,000	2,000	395	200	90 %
GM	Authors	2,440	1,220	315	160	87 %
CC	Authors	1,580	790	155	80	90 %

The geogrid manufacturer's wall design used reinforcement lengths of 7 m in the lower portion of the wall, and this design was 1 m higher than the constructed wall. The dimensions of the civil consultant's wall design gave a height of 6.7 m, grid lengths of 3.6 m, and a wall embedment depth of 0.3 m. A friction angle value of 36.5 degrees for the foundation and retained backfill materials was assumed using the geotechnical consultant's soil profile. The author's soil profile corresponded to a friction angle of 34° for the foundation and retained backfill materials.

The ultimate bearing capacity is reduced by approximately 90 percent due to the application of ground slope bearing capacity factors. The reduction of geogrid lengths from 7 m to 3.6 m results in a 50 percent reduction in allowable bearing capacity (with sloping groundline).

The authors analyzed the civil consultant's design and geogrid manufacturer's preliminary design using a vendor design program. A bearing pressure of 145 kN/m^2 was computed beneath the

geogrid manufacturer's preliminary wall design. This is below the computed allowable bearing capacity, calculated with either the geotechnical consultant's or authors' stratigraphy. A bearing pressure of 135 kN/m² was computed for the civil consultant's design. The authors computed an ultimate bearing capacity of 155 kN/m² using their stratigraphy that accounts for the ground slope; which results in allowable bearing capacity of 80 kN/m². Thus the bearing pressure significantly exceeds the computed allowable capacity.

REPLACEMENT WALL

The failed MSEW was replaced in 1995 with a combination MSEW and sheetpile wall. The new wall alignment was upslope of the first wall, and the exposed height of the MSEW is 2.4 m. Geogrids, 2 m long, were used to reinforce the soil. Salvaged integrally formed polyethylene geogrids and new polyester geogrids were used. Sheetpiles, 3⁺ m deep, were first driven in a continuous row about 1 m downslope of the new MSEW to increase stability of the soil retaining structure.

DISCUSSION

Project Responsibilities. Project responsibilities were documented in the Plaintiffs' Complaint. However, resolution of responsibilities and roles were never clearly defined as this lawsuit was settled out of court. The geotechnical consultant's role was limited, and excluded review of final design and construction inspection. Likewise, the civil consultant's role was limited, and excluded global stability assessment and construction inspection.

Communications on this project were lacking, as evidenced by the lack of documentation in the files reviewed by the authors and the resulting wall failure. The poor communications certainly contributed to the failure. The owner contracted separately with the geotechnical consultant and the contractor, and did not directly contract with the civil consultant. Therefore, the owner was responsible for communications between the geotechnical consultant and the contractor. The contractor was responsible for communications with the civil consultant, though contracting of the civil consultants services was through the SRW block supplier.

The two parties involved with design, the geotechnical consultant and civil consultant, are the furthest apart on the relationship chart (Fig. 2). Also, their services did not overlap within the project time frame (Table 2). Thus, their work was separated by both contractual relationships and time.

Soil Properties. The soil shear strength and unit weight values used in the geotechnical consultant's global stability model (Fig. 6) were optimistic, in the authors' opinion. This opinion is based upon the authors' experience, our interpretation and analysis of subsurface soil investigation data, and the benefit of post-failure analyses and hindsight. Unconservative soil properties result in low driving forces being resisted by high shear forces. This, in turn, results in the computation of an artificially high FS.

Hydrostatic Loads. It does not appear that hydrostatic loads contributed to failure of the MSEW. As noted in the geotechnical consultant's report in 1991, groundwater was at a level where it would not impact the wall system design or performance. Minimal rainfall occurred in the months of July and August, as documented in the Eau Claire area precipitation records (Personal Communication, 1996). One precipitation event with 65 mm of rain occurred in July. All other precipitation events were less than one-half inch, with most events recorded as a *trace*. Approximately 6 mm of precipitation was recorded within one week preceding the failure.

Wall Design. The wall constructed in accordance with the civil consultant's design and plans was markedly different from the preliminary wall design that was evaluated by the geotechnical consultant. The preliminary wall design used 7 m long geogrids in the lower portion of the wall, while the constructed wall geogrids were only 3.6 m long. This length reduction significantly impacts the computed FS for global stability, but, has only a minor impact on the compound failure FS. It was not readily apparent why the preliminary wall geometry was not used in the final design.

Global Stability. The recommendation made by the geotechnical consultant that the proposed wall system could be supported by the native soils was based upon the preliminary wall design and acceptance of a computed FS of 1.2. In the authors' opinion, this FS value is too low for a structure of this type. This opinion is based upon: accepted standards of practice; the authors' experience; criticality of the structure; interpretation of subsurface soil shear strengths; computer modeling techniques used; potential absence of consultant's involvement in final wall design and construction; and the benefit of post-failure analyses and hindsight. Global stability analyses with the authors' soil properties resulted in computed FS values of 1.04 and 1.00, which are indicative of impending failure.

Compound Stability. Compound failure planes should have been investigated during design of this MSEW. The geotechnical consultant clearly stated in their 1992 slope stability report that their scope of work did not include examination of failure planes passing through the reinforced mass. The civil consultant did not investigate compound failure modes as part of their design.

The practice of designing MSEW has grown from highway works, where it is common practice to divide the design responsibilities of global stability and wall design. This project followed this practice, and in doing so, compound failure planes were not investigated. Obviously, this is an oversight for MSEW structures constructed on slopes.

Had compound failure planes been investigated by the geotechnical consultant, using their soil profile and the geogrid manufacturer's preliminary wall design, a FS significantly lower (i.e., 1.1) than the global stability FS (i.e., 1.2) would have been computed. This should have led to a different conclusion regarding stability of the proposed wall structure, and to a redesign of the structure.

Bearing Capacity. It appears that bearing capacity for this project geometry and soil properties was not computed by either the geogrid manufacturer or the civil consultant, based upon our review. Rather, presumptive values were used in wall design. The authors' analysis clearly demonstrates that the MSEW would exceed a reasonable estimate of an allowable bearing pressure. Calculation

of an allowable capacity, even with assumed soil shear strength properties, in lieu of using assumed values should have led to questions regarding the stability of the proposed MSEW.

CONCLUSIONS

The primary conclusion of this investigation is that the common practice of separating wall design and global stability analysis for MSEW projects can lead or contribute to structural failure. Projects with sloping fills below, or above, the MSEW structure are of particular concern. On this project, the separation of design responsibilities resulted in:
- no communications between the civil and geotechnical consultants;
- an oversight of not investigating potential compound failure planes;
- no confirmation of allowable bearing capacity; and
- contributed, or led, to the catastrophic failure.

It is the authors' opinion that:
- more conservative soil shear strength friction angles and a higher acceptable safety factor should have been used in the global stability analysis;
- that compound failure planes should have been investigated; and
- that an allowable bearing capacity should have been calculated for the MSEW structure.
These opinions are based upon the authors' experience, and the benefit of post-failure analyses and hindsight on this project.

RECOMMENDATIONS

The authors make the following recommendations with respect to the design of SRW MSEW systems on sloping foundations, based upon this project and their experience:

1. Division of design responsibilities is not recommended. If such a division of work occurs, communication among all project parties should be maintained through final design and construction.

2. Compound stability, as well as global stability, must be analyzed to determine the minimum factor of safety with respect to slope stability.

3. The acceptable minimum factors of safety for global and compound stability should be independently considered for each site. There are numerous references in the literature discussing minimum allowable factors of safety for various site conditions, including critical versus non-critical structures, breadth of subsurface investigation, etc.

4. Allowable bearing capacity analyses must account for the ground slope in front of the MSEW. This factor can reduce the ultimate bearing capacity by 90 percent.

ACKNOWLEDGMENTS

REFERENCES

Berg, R.R., Chouery-Curtis, V.E., and Watson, C.H. (1989), Critical Failure Planes in Analysis of Reinforced Slopes, *Proceedings of Geosynthetics '89 Conference*, San Diego, California, February 21-23, pp. 269-278.

Bowles, J.E. (1988), *Foundation Analysis and Design*, Fourth Edition, McGraw-Hill Book Company, New York, 1004 p.

NAVFACS (1982), *Design Manual 7.1, Soil Mechanics*, Department of the Navy Facilities Engineering Command, Alexandria, Virginia.

Personal Communication (1996), Hydrology Section, U.S. Army Corps of Engineers, St. Paul District.

Young, H.L. and Hindall, S.M. (1972), *Water Resources of Wisconsin, Chippewa River Basin, Hydrologic Investigations Atlas HA-386*, United States Geological Survey, Washington, D.C.

DESIGN OF GABION-GEOSYNTHETIC RETAINING WALLS ON THE TELLICO PLAINS TO ROBBINSVILLE HIGHWAY

M.R. SIMAC
EARTH IMPROVEMENT TECHNOLOGIES, INC., USA
R.J. BATHURST
ROYAL MILITARY COLLEGE OF CANADA, CANADA
T.W. FENNESSEY
EASTERN FEDERAL LANDS DIVISION OF FEDERAL HIGHWAY
ADMINISTRATION, USA

ABSTRACT

During construction of the Tellico Plains to Robbinsville highway several MSE walls were built with hybrid wall system components, consisting of geogrid reinforcement and PVC coated gabion baskets. The selection of these materials was based primarily on the presence of a chemically active soil environment, availability of an economical fill source, aesthetic appearance, and overall cost. This paper summarizes the design procedures utilized to ensure wall stability along a mountainous highway alignment. It examines how the general MSE design guidelines presented in the project specifications can be augmented with currently accepted methods of analysis to provide a safe but economical wall design. Project and product-specific test results used in the engineering analysis of a 10m high MSE wall system that also functions as a toe buttress for a 30m high slope are presented.

INTRODUCTION

The highway between Tellico Plains, Tennessee and Robbinsville, North Carolina was opened to traffic in October 1996. It runs through the Cherokee National Forest in eastern Tennessee and the Nantahala National Forest in western North Carolina, and is a project of the U.S. Department of Agriculture, Forest Service (USFS). USFS utilizes the Eastern Federal Lands Division of the Federal Highway Administration (FHWA) for design and construction administration. An interactive design and construction procedure was dictated by extremely demanding site conditions, that required balancing the cost, constructability, material availability and visual impact of the highway as it skirts along the mountain tops and ridges. The key issues that controlled the highway design layout of each phase included:

- Maximum highway grades for passenger cars and truck traffic,
- Maximum side slope grades of 1.5H:1V for embankment fills,
- Minimize rock cut slopes and their visual impact,
- Minimize the number of bridges and retaining structures due to cost,
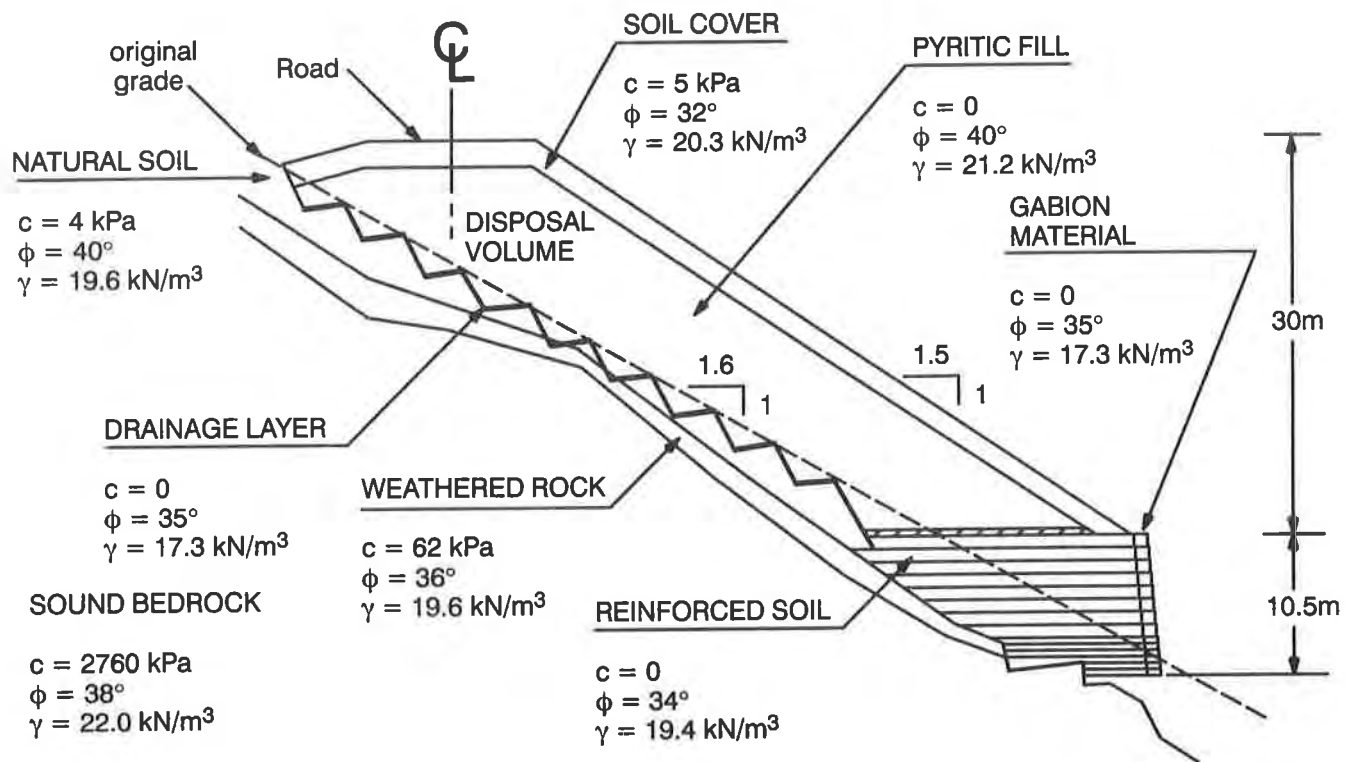
Figure 1. Project cross-section at maximum wall elevation.

- Quantity and availability of suitable earthwork fill materials, and
- Identification, handling and protection of pyritic rock materials.

This paper describes the design of geogrid reinforced retaining walls which were built in the summer of 1994 to meet demanding site grade requirements at two locations along the highway. The walls had maximum heights of 10 and 10.5m at the center and were 60m long. The walls tapered to minimum heights of about 2m at the ends. Both walls also retained steep (1.5H:1V) fill slopes which rose 30m above the top of wall to support the roadway traffic surface. A typical cross-section of the wall roadway is shown in Figure 1.

PROJECT DESIGN CONSTRAINTS

The decision to use retaining structures at these two locations was predicated on the existing natural side slope grades, which ranged from 2.5H:1V to 1.3H:1V. These existing grades would have required long and large volume sliver fills to accommodate the maximum proposed (1.5H:1V) embankment slope construction. However, this strategy would have resulted in the new fill chasing the existing slopes well down the mountain side to achieve adequate toe support. Selection of retaining walls allowed the designers to minimize fill volumes, as well as, construct the highway within the maximum 60m right-of-way established by the USFS to minimize destruction of trees and vegetation. This reduction of fill volume and visual environmental impact was balanced against the need to resolve another key design issue: How to utilize, but properly dispose of pyritic materials generated from the rock cuts? Early experience in the construction of this highway identified the conse-

quences of leaving pyritic materials susceptible to surface or groundwater flow. Pyritic rock materials decompose in the presence of water and oxygen to produce an extremely acidic leachate. Sulfuric acid leachate creates an environmental hazard for the wildlife and vegetation in the area, particularly for the fish that frequent the mountain spring water streams as a spawning area. The FHWA required that excavated pyritic rock materials be capped, and isolated from the foundation soil/rock and other embankment materials using a perimeter drainage system. The drainage system captures water before contact with the pyritic materials, thereby eliminating or at least minimizing the formation/release of acidic leachate. The retaining walls required for grade separation, also provided a toe buttress to support potentially large volumes of encapsulated pyritic rock. This design strategy allowed the pyritic rock materials from rock cuts to be used as fill material, easing concerns with fill availability, while minimizing a potential environmental hazard.

SELECTION OF GEOSYNTHETIC REINFORCED MSE WALLS

The selection of geosynthetic reinforced Mechanically Stabilized Earth (MSE) walls was based upon cost, performance, and service life factors as discussed below. The large change in grade (10.5m) at the wall locations eliminated the use of cast-in-place concrete wall configurations because of cost, projected to be as much as 50% more expensive. Other types of retaining walls were eliminated based on construction access and/or viability considerations. Consequently, the specifiers (FHWA) were left with a variety of MSE retaining structures from which to chose. Although used at one location along the alignment, traditional inextensible (steel) reinforced MSE structure with precast concrete facing panels had some major disadvantages: 1) The requirement of select fill for the reinforced soil volume would significantly increase the cost in this remote location; 2) The long-term durability (corrosion) of the inextensible (steel) reinforcement exposed to acidic leachate; and 3) The appearance of the facing system would not blend well with the natural environment, according to the USFS. Aesthetic considerations also eliminated segmental retaining walls using geosynthetic reinforcement. Geosynthetic reinforced steep slopes were eliminated because they greatly reduced the disposal volume for the pyritic rock material and the blasting operation would yield large particle sizes unsuitable for use with geosynthetic reinforcement. Ultimately, the specifiers selected a hybrid system that consisted of geosynthetic reinforcement and rock-filled gabion baskets. The gabion baskets were specified to be manufactured with PVC coated wire mesh. Additionally, the tie wire was PVC coated and any other mechanical fasteners required to close the baskets were specified to be made of stainless steel. The gabions were filled with locally available crushed rock. The facing system provided a natural stone finish that the USFS felt blended well with the environment and was visually consistent with other retaining structures used on the highway project. Geosynthetic reinforcement was specified because it could be used with the fine grain (silt size) soils available in the area for reinforced fill and was felt to be more durable because of its resistance to acidic soil conditions. Nevertheless, this was a departure from AASHTO specifications in effect at the time of the project design but was agreed to by USFS/FHWA because of project demands.

BIDDING AND SELECTION PROCESS

The FHWA prepared a performance-based specification to contract this hybrid gabion faced geo-

synthetic reinforced MSE wall system. This work item was bid at a unit cost per wall face area actually installed. The contract documents provided the location, finish grades, and lateral extent of the retaining walls. Material performance requirements and minimum properties for both the gabion basket and geosynthetic reinforcement were also specified. Because of the large number of possible material combinations, the specifications required the contractor to provide design submittals that were "stamped" or certified by a registered Professional Engineer. The required submittals consisted of the following:

- Material property testing on gabion and gabion fasteners,
- Material index property testing on geosynthetic reinforcement,
- Material design property testing on geosynthetic reinforcement,
- Facing connection strength testing between gabion and geosynthetic reinforcement,
- Soil compaction and strength property tests, and
- Design calculations and construction drawings with details.

The specifications outlined the method of analysis, required material property data, and the minimum safety factors for acceptable design. All these requirements followed those material evaluation and design procedures outlined in the AASHTO Task Force 27 (1990) report. Table 1 provides the minimum safety factors required for design. By specifying the design methodology, material properties and safety factors, the owner could be assured of receiving equivalent designs on a competitive basis. The owners also minimized their engineering costs for the structure by commissioning the project specifier to perform one review of the design - i.e. the design submitted by the successful "low bid" contractor. Generally, this approach encourages the wall designer to be more innovative, making the contractor more cost competitive. As with any contracting approach, there are some drawbacks. For complex projects, like this one, the "low bid" may be won by an incomplete design or optimistic interpretation of the specifications. This places a general or earthwork contractor in the uncomfortable position of relying on "preliminary" designs provided by vendors. Although it is customary for all material suppliers and bidders to honor their winning proposal this may create a financial hardship that could jeopardize quality of the completed structure, or an adversarial relationship with the owner's engineer that makes implementation of the specifications a difficult responsibility. It did neither on this project even though the "original" vendor design used to develop the bid price was significantly deficient in both quantity and strength of geosynthetic material required. The specifier can avoid this situation on complex projects, by convincing the owner to commission a knowledgeable designer to develop "generic" plans and specifications using a more traditional contracting approach. The FHWA has sample specifications that can be utilized for this purpose (Berg 1992; Elias and Christopher 1996).

SITE INVESTIGATION

The wall contractor was provided with results of a subsurface investigation performed by the FHWA. This report provided site specific information from exploration techniques which included; soil borings, rock coring, seismic refraction and electrical resistivity surveys, and shallow test pits. The site geometry and soil stratigraphy used in design are shown in Figure 1. The contractor per-

formed destructive soil borings for field verification of the natural site soils and depth to sound rock foundation material in the proposed wall area, prior to mass excavation. The shear strength parameters used for the design of the wall and the surrounding soil slope are provided in Table 2. The soil strength parameters used for the reinforced (infill) soil volume were verified by consolidated-undrained triaxial tests. The triaxial tests were run on reconstituted samples with a moisture content within –2% of optimum moisture content and a dry unit weight greater than 95% of standard proctor density (ASTM D–698).

TESTING AND EVALUATION OF WALL SYSTEM COMPONENTS

Gabion Baskets: The gabion baskets were supplied by the Maccaferri Gabion Corporation in two standard sizes of 915 and 457mm heights by 915mm deep and in lengths that varied from 1.8 to 3.6m. The PVC coated gabions were assembled on site and filled in three equal lifts with crushed rock about 100 to 200mm in maximum dimension. The gabions were closed, tied together using PVC coated tie wire or stainless steel "hog rings". The capacity of the hog rings was verified by tensile testing to ensure proper strength for closure of the baskets and revealed that two rings were required at each opening.

Geosynthetic Reinforcement: The type of geosynthetic reinforcement for this wall was selected by the general/wall contractor to be Miragrid™ geogrid reinforcement, as manufactured by Nicolon-Mirafi Group, Norcross, GA. The final selection of the specific geogrids to be used in the design was made by the wall designer, with approval of the FHWA. Information on the tensile strength, durability, construction site damage, direct sliding and pullout behavior of the reinforcement materials was supported by test data supplied by the geogrid manufacturer (Table 3). The calculated long-term design strengths for wall and slope stability analyses are also provided in Table 3.

Facing Connection Strength Testing: This unique hybrid MSE wall system required verification that the connection between the geogrid reinforcement and the gabion baskets was sufficient to meet project specifications. While the project specifications required a minimum of 100% of the applied tensile load at each reinforcement elevation to be carried by the connection, the senior writer's experience was that a minimum of 150% of the applied tensile load would account for larger variations in construction quality and loading conditions. The wall designer utilized this higher safety factor for the final design reinforcement spacing. The tests were carried out using the testing procedure developed by Bathurst and Simac (1993a) which has since became standardized as the NCMA test method SRWU–1, "Determination of Connection Strength between Geosynthetics and Segmental Concrete Units" found in the NCMA "Design Manual for Segmental Retaining Walls" (Simac et al. 1993). The test apparatus used to perform the tests is presented schematically in Figure 2. The test apparatus allows a maximum horizontal tensile load of up to 100kN to be applied to the geogrid while it is confined between two courses of gabion baskets. The gabion baskets were laterally restrained and surcharged vertically. A brief description of the test procedure follows: Full-scale facing connection models were constructed in the test apparatus. A half-meter wide sample of geogrid reinforcement was attached to the roller clamp. Initially the geogrid was not "hog ringed" to the lower basket as required by project specifications, in order to determine lower-bound connection strength envelopes. Subsequently, two tests on Type 1 geogrid were run with two hog rings attached
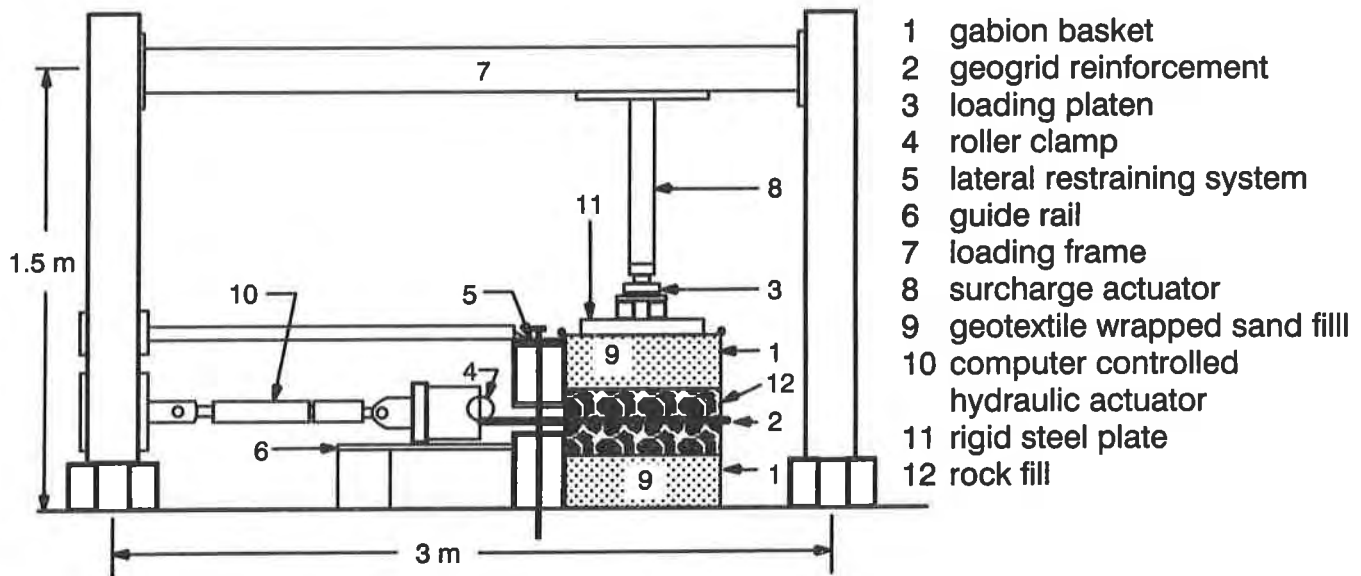
Figure 2. Connection test apparatus showing gabion basket and geogrid reinforcement.

to measure the improved connection strength. A second course of gabion baskets was placed over the reinforcement. Cobbles from the site were used to fill the baskets at the interface with the geogrid. A portion of the baskets was filled with a geotextile-wrapped sand to minimize the rock volume transported to the laboratory. Two wire-line LVDTs were connected to the geogrid where it exits the gabion baskets, to measure displacement of the geogrid at the back of the gabion basket. The test wall was then surcharged using the vertically oriented hydraulic jack shown in Figure 2. The only variable in a series of facing connection tests was the surcharge force, that simulated a range of wall heights above the connection. A computer-controlled horizontally mounted hydraulic actuator was utilized to apply a tensile force to the geogrid at a constant rate of displacement of 10% per minute (19mm per minute). The load and displacement of the hydraulic actuator were recorded continuously during testing with a computerized data acquisition system. A total of twenty-three (23) tests were performed by the two senior writers on wall heights varying between 2 and 9m (EIT 1995). A total of ten (10) and thirteen (13) tests were carried out using geogrid Type 1 and 2, respectively. Type 3 geogrid was tested previously as part of tests for a series of similar but lower height walls at the site and provided similar results (Simac et al. 1997). Plots of the peak connection strength versus the "required" capacity connection strength for design are provided in Figures 3a and 3b. Note that a safety factor of 1.5 was used for the required design capacity envelopes, as discussed above. The mechanical connections (hog rings) are only necessary for the Type 1 geogrid in combination with wall heights greater than 6m.

DESIGN AND ANALYSIS

The design of this hybrid retaining wall system required two different analyses; wall stability and global stability of the wall slope system. A general description of the analyses that were performed is provided below:
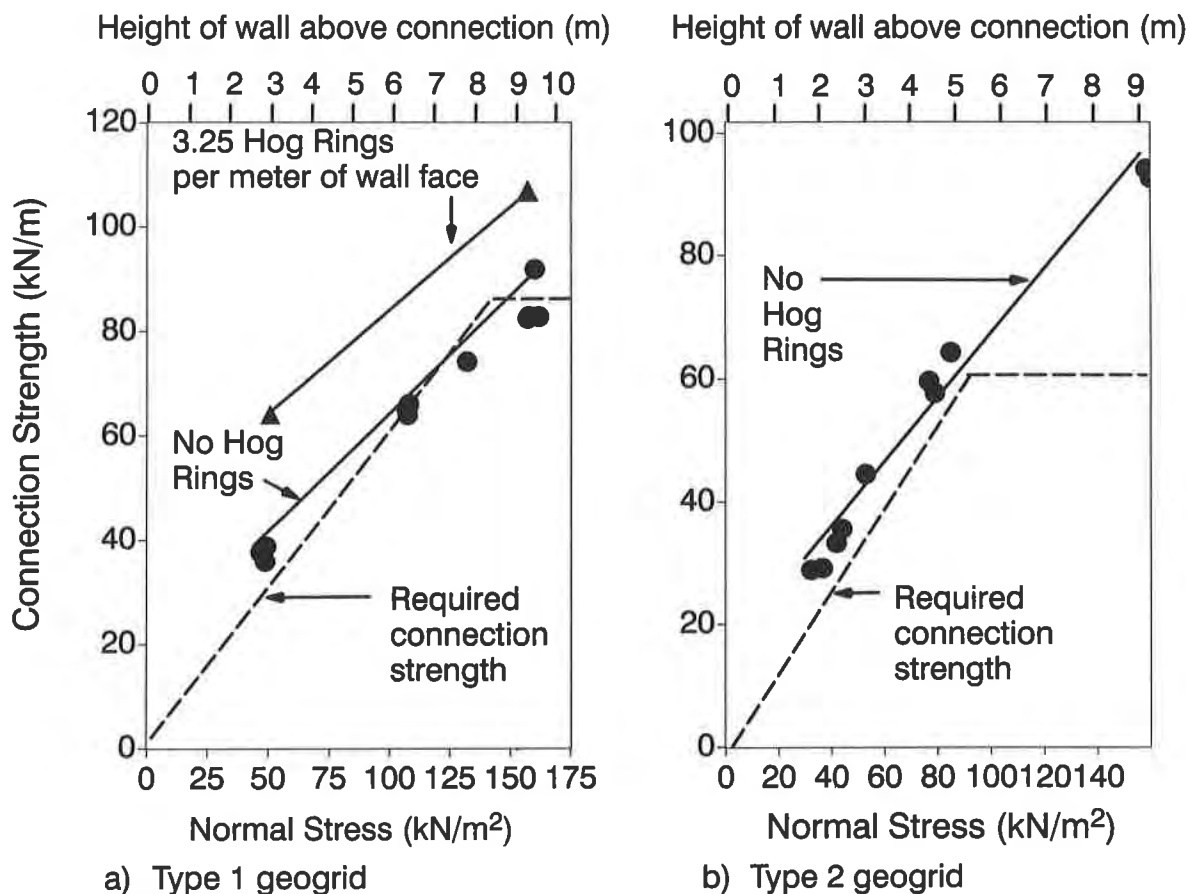
Figure 3. Connection strength test results and required connection strength for design.

Wall Stability: The geogrid reinforced MSE wall was designed to meet AASHTO Task Force 27 design guidelines (AASHTO 1990) in use at the time of the project and additional recommendations reported by Simac (1990). Computer programs developed by the lead writers (Bathurst and Simac 1993b) were used to calculate factors of safety for internal and external stability modes of failure. Potential modes of failure for modular wall systems are illustrated in Figure 4. Hand calculations were used to extend computer analysis results to evaluate internal sliding (Figure 4f) and local facing stability modes of failure (Figures 4g, 4h, 4i). Although developed for concrete units (Simac et al. 1993) this method of analysis is equally applicable to all reinforced soil structures comprised of modular components. Since the time of this project, a computer program for the generic design of modular facing systems has been developed by the NCMA (1995) and is described by Bathurst and Simac (1995). Wall stability analyses were performed for each incremental height module (gabion basket height 0.9m or 0.45m), up to the maximum wall height of 10.5m. The length, design strength (Table 3) and vertical spacing of the geosynthetic reinforcement were adjusted to meet all the minimum safety factors listed in Table 1 for the site conditions illustrated in Figure 1 and Table 2. The general layout of geogrid reinforcement to meet only wall stability requirements are shown in Figure 5. This geogrid reinforcement design is relatively non-standard due to the influence of the mixed (rock/soil) foundation conditions and the requirement that the wall function as a toe buttress for the 1.5H:1V slope above the top of wall. The bearing capacity analysis results from the computer programs had to be modified by hand to account for the sloping (2H:1V to 1.6H:1V) toe in front
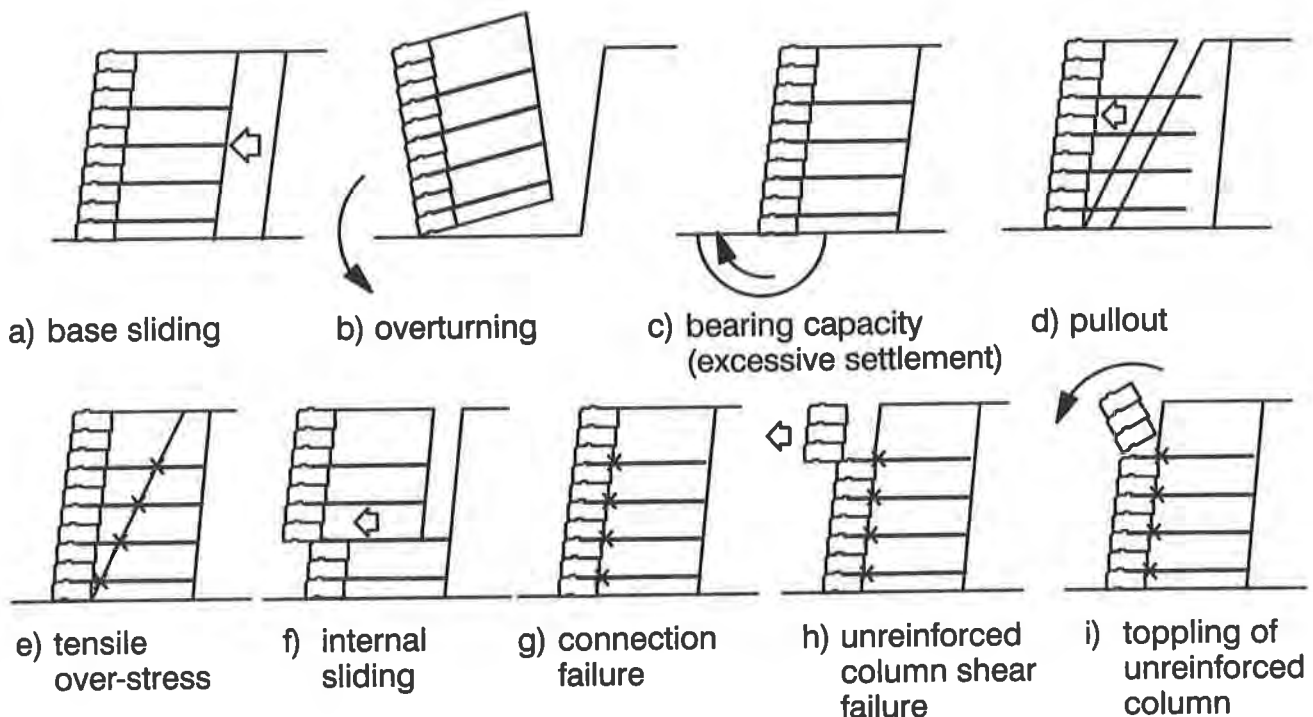
Figure 4. Modes of failure: External a), b), c); Internal d), e), f); Facing column; g), h), i) (adapted from Simac et al. 1993).

of the wall using the analytical technique proposed in NAVFAC (1982). The presence of the slope only slightly influenced (by 10 to15%) the magnitude of the bearing capacity safety factor, but all values were sufficiently above the minimum required value of 2.5 due to the long base reinforcement lengths required to satisfy base sliding. The influence of the rock foundation was significant in determining the minimum geogrid reinforcement length to prevent internal sliding along reinforcement layers. A design objective was to minimize rock excavation, yet ensure a stable structure even for the typical 3m benched rock cuts at this site. Simply stated, the design procedure was to perform an external stability analysis for a reduced height structure using the elevation of the rock cut benches as the preferred horizontal plane of sliding. The reduced height of structure required significantly longer reinforcement lengths to stabilize the fill slope (1.5H:1V) above the wall. Because of the random and unpredictable rock location, the reinforcement lengths could be terminated at a rock cut face, if encountered before reaching the minimum geogrid reinforcement length of 12m. There was also a practical limit of 6.1m used for the initial (base) rock cut bench width to provide sufficient room to operate equipment. The reinforcement spacing was dictated largely by the size of the gabion baskets selected for construction. The large vertical spacings dictated the use of very high strength reinforcement together with significant facing connection strength. Half-height (0.4m) baskets were utilized below 9m height to distribute the applied loads over a greater number of facing connections. The frictional shear capacity at each gabion elevation was calculated based upon the shear strength of the cobble fill. The available shear capacity was found to be sufficient to resist the applied shear forces that could distort or separate a course of gabion baskets from the courses above or below. Analyses for toppling failure indicated that the top 1.35m of the structures was stable for the 1.5H:1V slope terminating at the top of the uppermost basket.
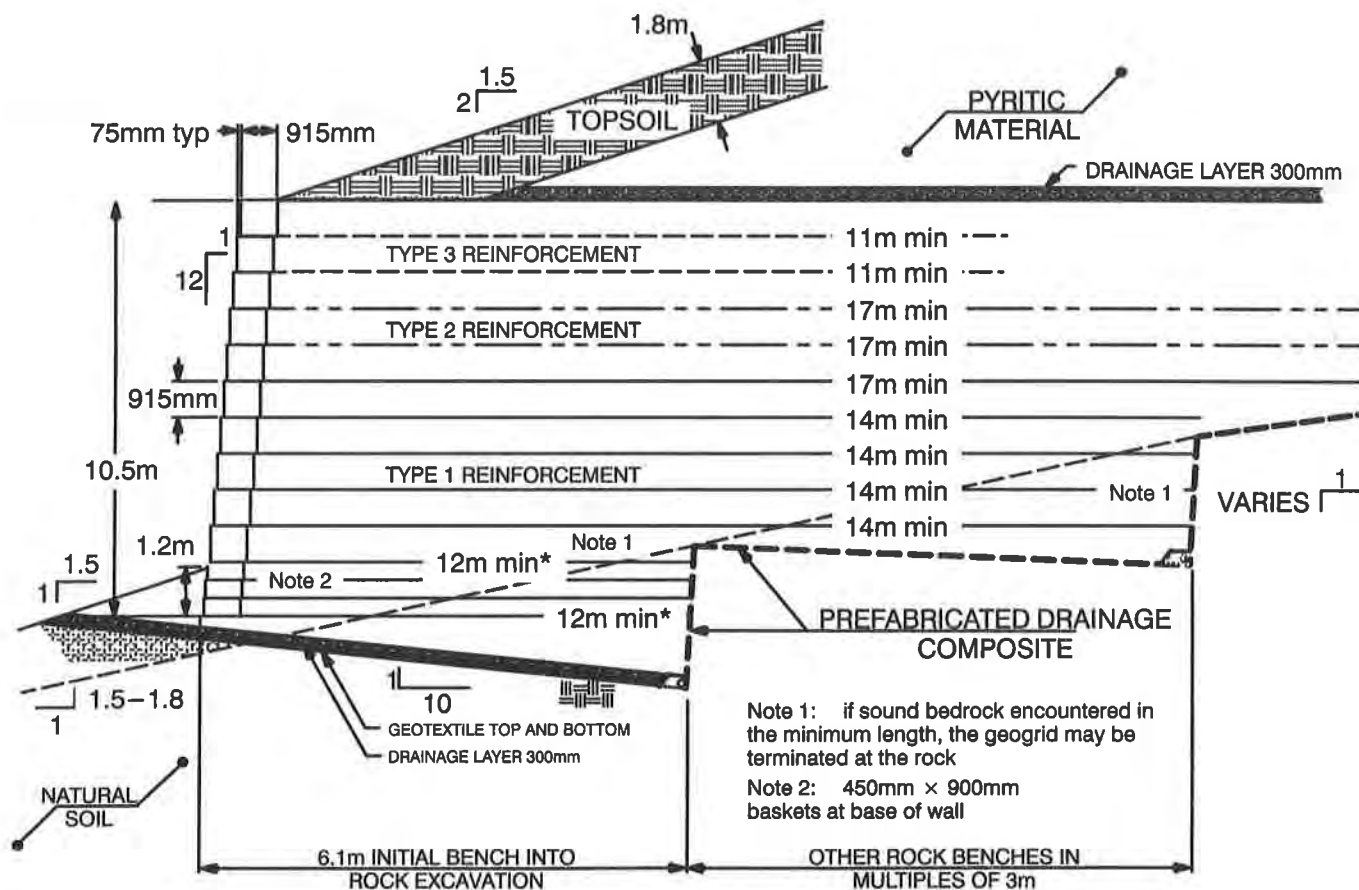
Figure 5. MSE section at maximum height of wall showing design based on (local) wall stability only.

Global Stability: The influence of the 30m tall 1.5H:1V slope supported by the geogrid reinforced MSE wall and the sloping (2.5H:1V to 1.6H:1V) toe below the wall was accounted for in the design. The suppliers of the "preliminary" design had originally hoped the relatively shallow (< 3m) bedrock at the site would be sufficiently excavated for external wall stability to ensure that the entire structure was stable on the side of the mountain. This eventually proved to be an unreliable assumption due to the natural slope, variable depth to rock formation, and excavation constraints. These conditions dictated that the geosynthetic reinforcement would contribute significantly to the stabilizing resistance of almost any toe buttressing scenario. Global stability analyses were performed using a commercially available computer program, STABGM (Duncan et al. 1985). The computer program utilizes a modified Bishop approach to the method of slices for analyzing circular slip surfaces through layered soil systems. It incorporates the stabilizing effects of the reinforcement as an additional restoring moment, calculated as the reinforcement force at its intersection with the base of a slice, multiplied by its moment arm. This program also permits modelling of the geogrid pullout resistance by varying the available reinforcement force along the entire geogrid length. Based on recommendations by Berg (1992) these analyses utilized a modified design reinforcement tension (see Table 3). Using the overall wall and slope geometry presented in Figure 1 and the soil parameters presented in Table 2, the geogrid reinforcement layout sufficient to satisfy wall stability (Figure 5) was analyzed for global (slope) stability. The results from these analyses indicated significantly

deficient safety factors (e.g. 1.13 to 1.20) with respect to the desired safety factor of 1.3 for global stability. The design strategy to overcome this initial deficiency focussed on increasing the length and number of reinforcement layers to improve the overall stability, which has been used successfully on other projects by the two senior writers (Simac et. al. 1991). Presented in Figure 6a are selected failure surfaces and corresponding safety factors for the final 10.5m high design section. A total of two layers of Type 1 geogrid were added in addition to those layers required for safe wall design only, and most of the geogrid layers were increased in length to achieve the required safety factor of 1.3. These differences are evident when comparing Figure 5 to Figure 6b. These figures also illustrate the sensitivity of the design to the location of the bedrock surface and the requirement that the geogrid reinforcement extend back far enough to intersect that surface. Therefore, the wall/slope geogrid reinforcement requirements increased significantly over that required for wall stability alone. The final geogrid reinforcement layout was communicated to the wall contractor using a complete set of construction drawings that were reviewed and approved by the FHWA.

SUMMARY

The Tellico Plains to Robbinsville highway was constructed using several walls made with hybrid MSE wall system components. The hybrid components were geogrid reinforcement and PVC coated gabion baskets. The selection of these materials was based primarily on the presence of a chemically active soil environment, availability of an economical fill source, aesthetic appearance, and cost. Based upon the writers' experience with this project the following observations and conclusions can be made:

1. Hybrid MSE systems can be successfully designed by implementing currently accepted methods of analysis for geosynthetic reinforced walls and slopes, using commercially available design and analysis software.

2. Product-specific facing connection testing is required for the design of modular faced retaining wall systems including the hybrid MSE system developed for this project.

3. The influence of sloping toe support on the global stability analysis of wall/slope systems may be significant. Standard wall design procedures, optimized to minimum design guidelines may be unsafe for walls placed on a slope.

4. Combining wall and slope reinforcement in the same design can be a cost-effective solution for geosynthetic reinforced wall design in steep slope applications.

5. Complex wall/slope designs may be beyond the reasonable scope of vendor-supplied design and contracting procedures. The owner may benefit more directly by utilizing conventional contracting procedures including a "generic" design in the contract documents to ensure a minimum long-term performance.

The walls described in this paper have been instrumented and the results of monitoring data will be presented in the future. Early data indicated some movement of the walls during construction of the upper fill slopes, but the deformations were within acceptable tolerances for this type of structure. However, since completion, these walls have performed as intended, without any visible manifestations of distress or unacceptable wall movements.
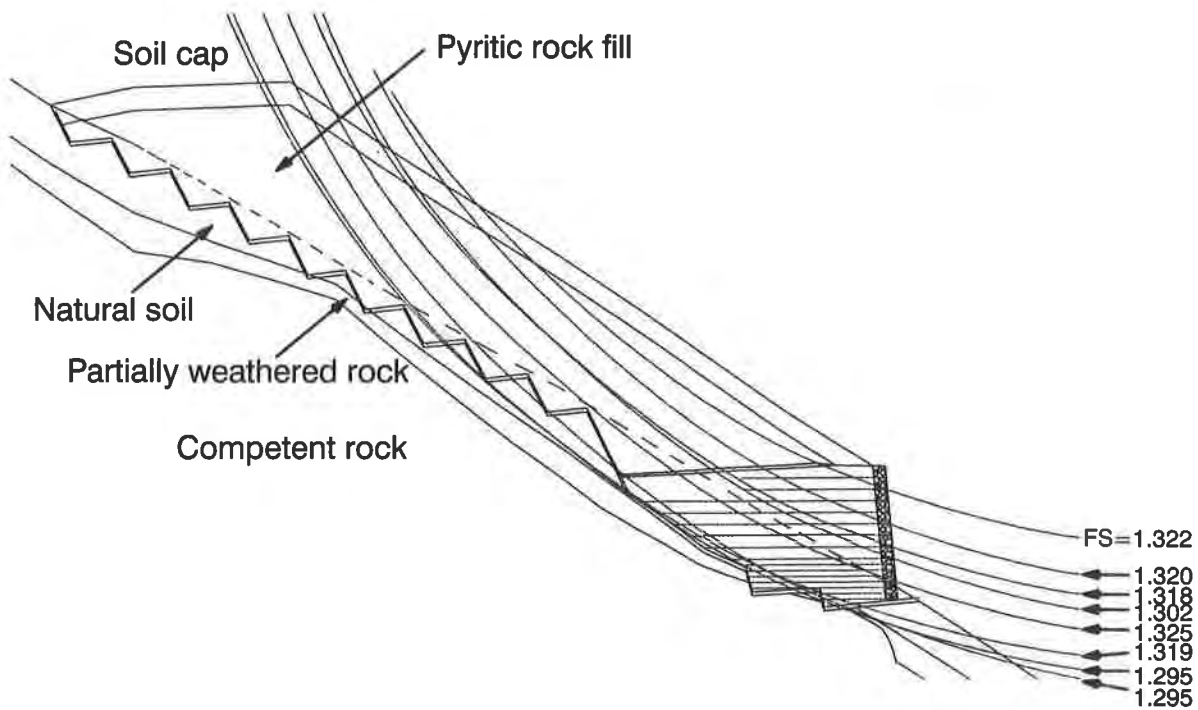
Figure 6a. Results of slope stability analyses leading to an increase in number and length of geogrid reinforcement layers.
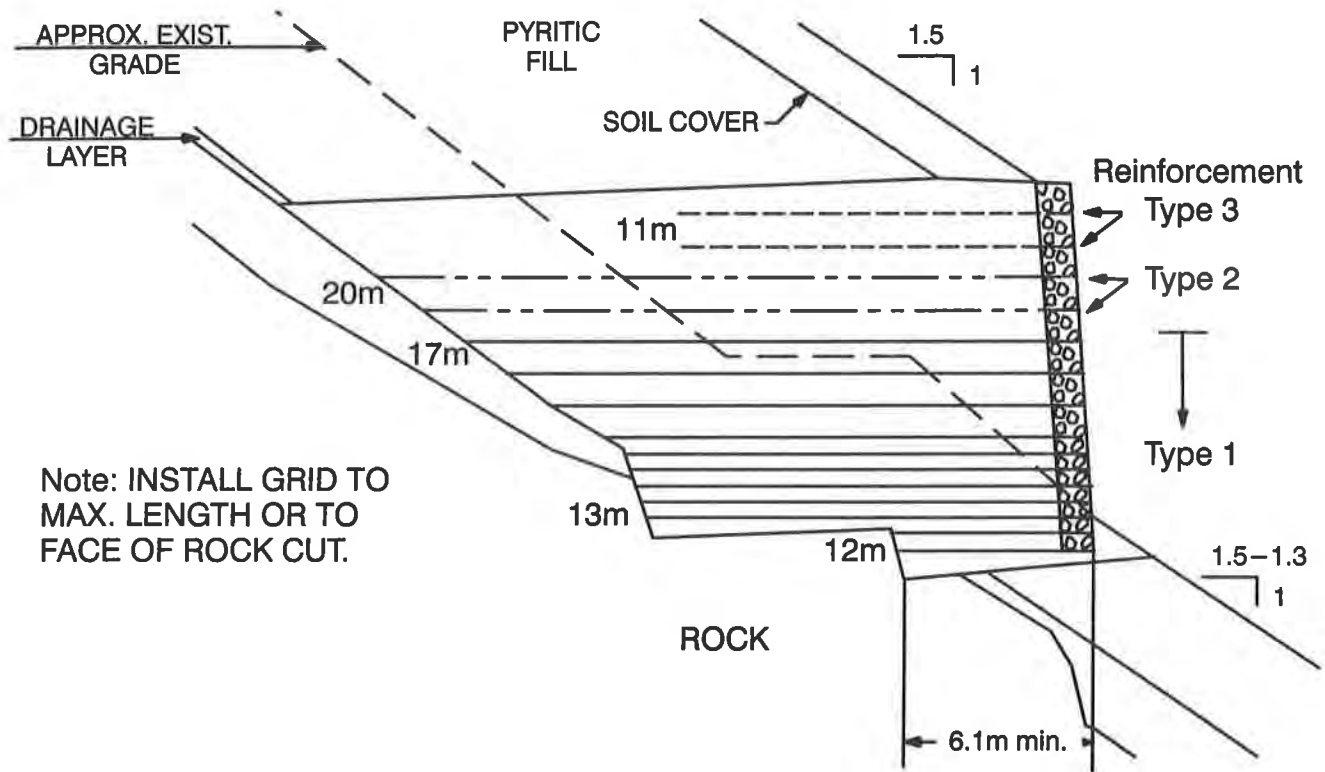
Figure 6b. Reinforcement arrangement to satisfy global stability only.

REFERENCES

AASHTO, 1990. Design Guidelines for Use of Extensible Reinforcements (Geosynthetic) for Mechanically Stabilized Earth Walls in Permanent Applications, *American Association of State Highway and Transportation Officials*, Task Force 27 Report, In-Situ Soil Improvement Techniques, Washington, DC, USA, August 1990, 38 p.

Bathurst, R.J. and Simac, M.R. 1993a. Laboratory Testing of Modular Unit-Geogrid Facing Connections, STP 1190, *Geosynthetic Soil Reinforcement Testing Procedures*, S.C.J. Cheng editor, American Society of Testing Materials, West Conshohocken, PA, pp. 32−48.

Bathurst, R.J. and Simac, M.R. 1993b. Two Computer Programs for the Design and Analysis of Geosynthetic-Reinforced Structures, *Geotextiles and Geomembranes*, Vol.12, No.5, pp.381–396.

Bathurst, R.J. and Simac, M.R. 1994. Geosynthetic Reinforced Segmental Retaining Wall Structures in North America, *5th International Conference on Geotextiles, Geomembranes and Related Products*, 6–9 September 1994, Singapore 24 p.

Bathurst, R.J. and Simac, M.R. 1995. Software for Segmental Retaining Walls, *Geotechnical Fabrics Report*, September 1995, pp. 20-21.

Berg, RR. 1993. Guidelines for the Design and Construction of Geosynthetic Mechanically Stabilized Earth Soil Slopes over Firm Foundations, *US Department of Transportation, FHWA*, Washington, DC, USA, 163 p.

Duncan, J.M., Low, B.K. and Schaeffer, V.R. 1985. STABGM: A Computer Program for Slope Stability Analysis of Reinforced Embankments, *Virginia Polytechnic Institute*, Department of Civil Engineering, Blacksburg, VA.

Earth Improvement Technologies, Inc., 1995. Report submitted to Robbinsville Contracting Company on *Facing Connection Test Results for Maccaferri PVC Coated Gabion Baskets and Miragrid 24XT and 22XT.*

Elias, V. and Christopher, B.R. 1996. Mechanically Stabilized Earth Walls and Reinforced Soil Slopes, Design and Construction Guidelines, Report No. FHWA–DP–82–1, Participant's Notebook for NHI Course, *Federal Highway Administration Office of Technology Applications.*

National Concrete Masonry Association, 1995. Design Software for Segmental Retaining Walls, *NCMA*, Herndon, VA.

NAVFAC, 1982. Design of Earth and Retaining Structures, Volume 7.2, 1981, pp 135–136.

Simac, M.R., Bathurst, R.J., Berg, R.R. and Lothspeich, S.E. 1993. National Concrete Masonry Association Segmental Retaining Wall Design Manual, *National Concrete Masonry Association* (NCMA), 2302 Horse Pen Road, Herndon, Virginia, USA, pp. 250.

Simac, M.R., Bathurst, R.J. and Fennessey, T.W. 1997. Case Study of a Hybrid Gabion Basket Geo-synthetic Reinforced Soil Wall, *Ground Improvement*, Vol. 1, No. 1, pp. 9–17.

Simac, M.R. 1990. Design Methodology for Miragrid Reinforced Soil Retaining Walls, *Mirafi Inc.*, Charlotte, NC.

Simac, M.R., Bathurst, R.J. and Goodrum, R.A. 1991. Design and Analysis of Three Reinforced Soil Retaining Walls, *Geosynthetics '91*, Atlanta, GA, Vol. 2, pp. 781–789.

TABLE 1: Specified minimum factors of safety for design of walls.

FAILURE MODE (see Figure 4)		
Base Sliding	FS_{sld}	1.5
Overturning	FS_{ot}	2.0
Bearing Capacity	FS_{bc}	2.5
Global (Slope) Stability	FS_{gl}	1.3
Reinforcement Tensile Over–stress	FS_{tos}	1.0
Reinforcement Pullout	FS_{po}	1.5
Gabion Interface Shear	FS_{sc}	1.5
Gabion-Reinforcement Connection	FS_{cs}	1.5

TABLE 2: Soil and rock properties used in analyses.

MATERIAL	c (kPa)	ϕ (deg)	γ (kN/m^3)
Gabion rock fill	0	35	17.3
Reinforced infill soil	0	34	19.4
Natural foundation and other soils	4	40	19.6
Partially weathered bedrock	62	36	19.6
Unweathered bedrock	2760	38	22.0
Pyritic rock fill	0	40	21.2
Slope soil cover (cap)	5	32	20.3

TABLE 3: Geogrid reinforcement and design properties.

Parameter		Type[5] 1	2	3
Tensile strength - MD (ASTM D-4595)		370	259	102 kN/m
Mass per unit Area (ASTM D-3776)		1288	1017	390 g/m^2
Creep Reduction Factor[3]	$(CRF)_{ls}$	0.58	0.58	0.55
	$(CRF)_{ss}$	0.35	0.35	0.30
Partial Safety Factors				
Polymer Durability[3]	(FD)	1.2	1.2	1.2
Construction Site Damage[3]	(FC)	1.25[4]	1.25[4]	1.25[4]
Overall Uncertainty[3]	(FS)	1.5	1.5	1.5
Coefficient of Interaction[3]	(C_i)	0.6	0.6	0.7
Coefficient of Direct Sliding[3]	(C_{ds})	0.9	0.9	0.95
Long Term Allowable Design Strength (wall design calculations)[1]	(T_{as})	86.5	60.5	20.4 kN/m
Long Term Allowable Design Strength (slope design calculations)[2]	(T_{als})	143.3	100.2	37.5 kN/m

Notes:

[1] Calculated according to recommendations found in AASHTO (1990) and project specifications, lesser of the two values:

$$T_{al} = \frac{T_{ult} \times (CRF)_{ls}}{FD \times FC \times FS} \qquad T_{as} = \frac{T_{ult} \times (CRF)_{ss}}{FD \times FC}$$

where T_{ult} is the wide width strip tensile strength (ASTM D-4595).

[2] Calculated according to (Berg 1992):

$$T_{als} = T_{al} \times 1.5$$

[3] From manufacturer's literature.

[4] FC = 1.25 is a default value even though in situ testing gave lower values.
[5] Polyester geogrid.

Marine

GEOSYNTHETICS 97

CONFERENCE

Long Beach, California USA

BEACH EROSION CONTROL STRUCTURE FOUNDATION ENHANCEMENT

ERIK J. OLSEN, P.E.
OLSEN ASSOCIATES, INC., USA
MARK H. WAYNE, PH.D.
TENSAR EARTH TECHNOLOGIES, INC., USA

ABSTRACT

In the spring of 1995, the southernmost shoreline of Tybee Island, Georgia was successfully stabilized through the construction of a groin field comprised of modular erosion control units supported by a geosynthetic marine mattress type foundation (Olsen, 1996). Simplistically, the goal of the project was threefold:

- To protect a failing seawall and eminently endangered adjacent residential properties,
- To construct a stabilized beach where the shoreline was lost due to an updrift federal terminal structure, and
- To expand the southerly limit of future beach restoration efforts on Tybee Island for purposes of maximizing recreational opportunities and shore protection.

LOCATION/SETTING

Tybee Island, the northernmost barrier island along the Atlantic coastline of the State of Georgia is located on the seaward periphery of the Holocene Savannah River delta. Tybee Island is bounded on the north by the Savannah River and separated from Little Tybee Island by Tybee Inlet to the south (Figure 1). The island has a length of 4.4 km and a maximum width, including high ground and marsh, of 4 km; elevations are generally less than 4.6 m above sea level. Historically, Tybee Island has been known as the City of Savannah's beach. However, as one of only three publicly accessible beaches located along the coastline of the State of Georgia, it serves as an important regional recreational amenity.

HISTORY OF SHORELINE CHANGE AND LOCAL EROSION CONTROL EFFORTS

Tybee Island has a long history of shoreline erosion and of numerous efforts to attempt some measure of control. Figure 2 shows a general chronology of the island's more modern morphology (1866 - 1982). Most of the early activities by local interests were originally directed toward protecting Fort Screven, located on the north end of the island. A detailed documentation of these attempts and the methods employed is provided by Taylor (1983).

EXPLANATION
...... 1866
---- 1913
—·— 1925
—— 1957
—— 1974
*** 1982

Figure 2 Tybee Island Shoreline Chronology

1 Mile

1 Kilometer

Figure 1 Project Location

It is hypothesized by Henry (1987) that while no quantitative data exist for comparative purposes, increased shoreline erosion based on historic records, tends to correlate with the significant increase in maintenance dredging of the adjacent Savannah River entrance and navigation channels. The history of dredging in the Savannah River indicates that only minor quantities of sediment were removed between 1872 and 1915; however, dredging activities increased rapidly after 1915. Modern dredging activities have averaged over 7 million cubic yards a year since 1970. Disposal sites are located in either upland diked impoundments adjacent to the river, or in an offshore area deeper than -30 ft. Large scale continuing deficits to the natural sand sharing system have been proffered by local interests as a probable significant factor in increasing shoreline erosion on Tybee Island beyond that resulting from natural causes.

Since the late 1800's, over 130 groins have been constructed island-wide and, while portions of them were moderately successful, maintenance and re-elevation were not carried out. By the 1970's, the vast majority had fallen into disrepair. According to Taylor (1983), bulkheads have been constructed or repaired on twelve occasions during the period 1907-1971. With the exception of the twice-repaired 1941 WPA concrete panel seawall, most have been destroyed or rendered ineffective. The South Beach Stabilization project was predicated on the need to protect development and infrastructure on the southern extremity of Tybee Island. The latter residential properties lay upland of the deteriorating WPA seawall which, in 1994, was essentially determined to be in eminent danger of failure due to both its condition and direct exposure to the dynamic environment of Tybee Inlet (see Figures 3 and 4).

FEDERAL BEACH EROSION CONTROL EFFORTS

The 1963 destruction of a 15 year old bulkhead in the vicinity of Fort Screven prompted the U.S. Army Corps of Engineers to initiate the formulation of a Federal Beach Erosion Control Project for most of the ocean shoreline of Tybee Island. Following congressional authorization, a contract was eventually awarded in September 1974 for the construction of a rubble mound terminal groin on the north end of the island. The groin extended 245 m seaward and 68 m landward from the 1912 seawall. Subsequent to groin construction, the initial beach restoration on Tybee began on 30 July, 1975 and consisted of the placement of 1.73 million meters of sand fill. The material was excavated by a hydraulic pipeline dredge from shoals approximately 610 m south of the south tip of the island, at the mouth of Tybee Creek. The beach fill extended from 18th Street on the south end of the island to the terminal groin on the north end along some 4,150 linear meters of shorefront.

As a direct result of the severe continuing erosion on the south end of the island where the principal concentration of commercial and recreational activities are located, a Task Force was initiated by the Georgia Department of Natural Resources to recommend to the Savannah District,

Figure 3   Pre-Project Seawall Conditions (Looking East)

Figure 4   Pre-project Seawall Conditions (Looking Northeast)

U.S. Army Corps of Engineers (COE), a new plan for long-term mitigation of beach erosion. The effort ultimately resulted in the construction of a singular southerly terminal rubble mound structure in 1986 at a location dictated by the District. In January, 1987, the first federally sponsored renourishment of Tybee Island was constructed. It consisted of the placement of approximately .76 M meters of sand on the beach at Tybee Island in two reaches; the south end from the southerly groin northward to about 14th Street, and the north end from the north terminal groin southward to about 6th Street.

During a 1994 deepening of the federally maintained Savannah River Navigation Project, the shoreline along the north end of Tybee Island was utilized as a one time beach disposal site for a portion of the material excavated from the adjacent channel cut. Although the Savannah District, COE intended to place some 1.5 M cubic meters of dredged material along the entirety of Tybee Island, a large percentage of the material was lost immediately since it was not beach compatible (i.e., mud, silts, clay and very fine sand). Consequently, the net benefit to the island's littoral system was substantially less than that predicted by the District. Beach widths were only improved between the north federal groin southward some 1,220 m to 2nd Street as a result of the disposal operation. Subsequently, much of the placed material was observed to move rapidly northward through the adjacent terminal groin which is low in elevation due to a lack of maintenance over the last decade.

SOUTH BEACH STABILIZATION PROJECT

In direct response to the substantially reduced success of the federal beach disposal project, and the fact that funding authorization for the Tybee Island Beach Erosion Control Project had been allowed to lapse by the Savannah District COE, the Georgia Ports Authority sought interim remedial assistance on behalf of the City of Tybee Island. With the concurrence of the Governor's Office and the State of Georgia Legislature, the G.P.A. was directed to make available some U.S. $4.9M of excess Bond revenue derived from the channel deepening project for purposes of erosion control on Tybee Island. Specifically, two (2) work items, and their respective priorities, to be addressed by this one time funding source were authorized as follows:

a.)　Stabilization of the south beach shoreline through the construction of a designed groin field with the coincident placement of 38,000 cubic meters of sand, and

b.)　Limited beach restoration, with the south beach immediately adjacent to and northward of the groin field designated as the highest priority fill site.

This Paper specifically addresses the design, permitting and construction of the groin field intended to stabilize the shoreline facing Tybee Inlet - between the south federal groin and Tybee Creek (i.e., Back River). Figure 5 graphically depicts the locations of previous federal shoreline

activities on Tybee Island and their relationship to the south beach stabilization project discussed herein.

DESIGN CONCEPT

Alternative actions considered to protect endangered upland development on the south end of Tybee Island included a large scale revetment or beach restoration stabilized by a terminal groin field. The latter was deemed by local interests to be the "preferred" alternative due to the recreational value of a restored beach. The coastal engineering firm of Olsen Associates, Inc. of Jacksonville, FL was retained by the City of Tybee Island to design and permit the project. The firm decided upon a series of suitably spaced radial groins constructed as either T's or an L (See Figure 6). The plan of improvement likewise called for the placement of a minimum of 38,000 cubic meters of fill within the groin field. The latter volume was considered sufficient to form a series of "crenulate" shaped beaches predicted to equilibrate between the structure T-heads.

The placement and length of the structure heads were determined by the desire to retain some minimum level protective beach between the structures at times when the adjacent nourishment project to the north was depleted. At other times, it was predicted that sand from the updrift restoration project would move into the groin field thereby increasing the effective beach widths of each cell. Once full, the groin field would effectively become "transparent" and material would subsequently move to the Back River shoreline or eventually be removed by tidal currents of Tybee Inlet.

The roots of the design premise and the prediction of the equilibrium planform within the groin field which would result from the design are similar to those implemented at Fisher Island, Florida (Bodge 1992). The concept is inspired by classic headland and spiral bay behavior and reinforced by descriptions of similar structures in eastern Europe.

Special Conditions included within the Georgia, DNR permits for the project required that the structures be designed to allow for "adjustability" in the future, if necessary. In order to meet this performance requirement, Olsen Associates, Inc. specified a precast concrete module known as the Campbell Erosion Control Unit. The design section for each groin called for the placement of a pyramid of three 12.7 ton modules with a stone core (see Figure 7). A Triton Marine ™ geogrid-type mattress system was specified in order to provide a stable foundation for the groins sufficient to protect against long-term settlement and the effects of local scour associated with the tidal currents and ocean waves typical of the site. Armor rock was added to the head of each groin to more completely dissipate energy and to minimize the probability of dislodgement of the precast concrete modules during low frequency storm events (i.e., tropical storms and hurricanes).
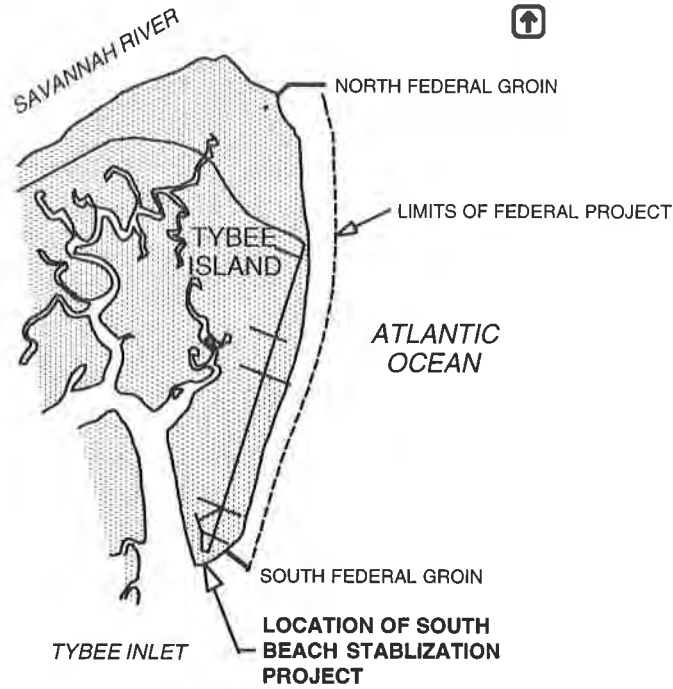
Figure 5 Locations of South Beach Stabilization Project and Previous Federal Activities
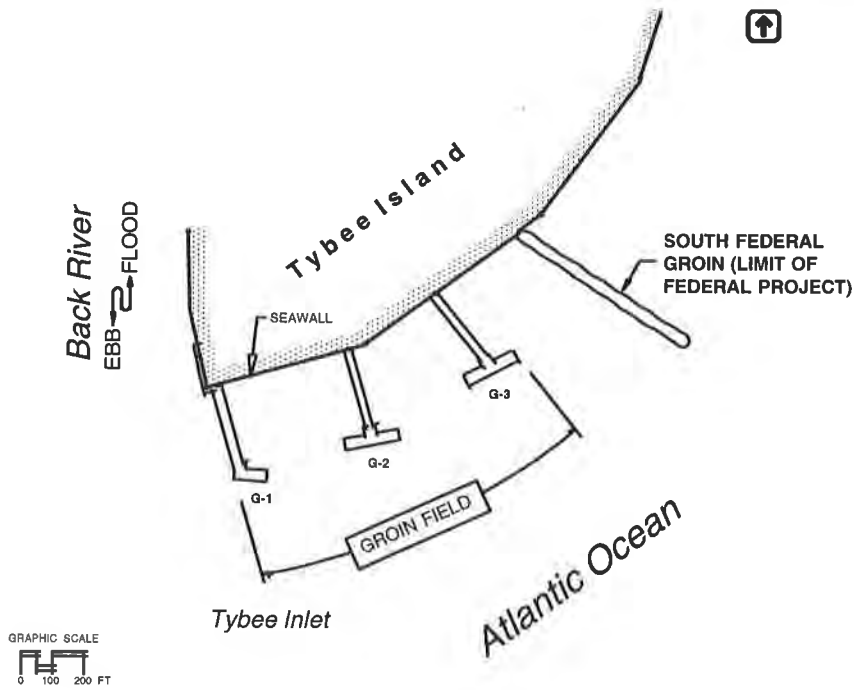
Figure 6 Location of Project Groin Field

An alternative initially considered for forming each groin was the conventional rubble mound construction method (See Figure 8). Alternately, the foundation for the Campbell units could theoretically have been designed with a geotextile separation and filtration layer. However, concerns about abrasion resistance would have necessitated use of a m 15 cm sand bedding layer. The latter type foundation would not have been possible to construct in the highly energetic tidally influenced environment associated with the project site which is located within the throat of a tidal inlet. For example, during flood tides, flow velocities across the site averaged 60 - 120 cm per sec. The intertidal nature of the site necessitated that the contractor perform groin component placement at low to mid-tide only. Construction was therefore intermittent during any 24 hour day and subject to delay by storms and/or periods of anomalous tidal conditions.

As depicted in Figure 8, use of a marine type mattress was ultimately specified for purposes of confining the foundation stone and allowing for successful deployment within the inlet flow field. Since the subgrade consisted of sand, a geotextile separator was not required below the mattress. Conversely, if the subgrade had consisted of any soil other than a clean sand, a geotextile would have been considered in the design process. Hence, gabion-type mattresses were specified by the Engineer due to their ability to confine the stone, allow for a relatively level surface necessary for erosion control module alignment and the minimization of settlement. It likewise allowed the entire foundation to act as a unit supporting the load generated by the groin mass (modules and rock). A geosynthetic geogrid mattress was selected due to the anticipated longevity of the material and the ability to construct large mattresses off site rather than in-place as necessitated by wire type gabions. Properties of the geogrid used to construct the gabion mattresses are presented in Table 1.
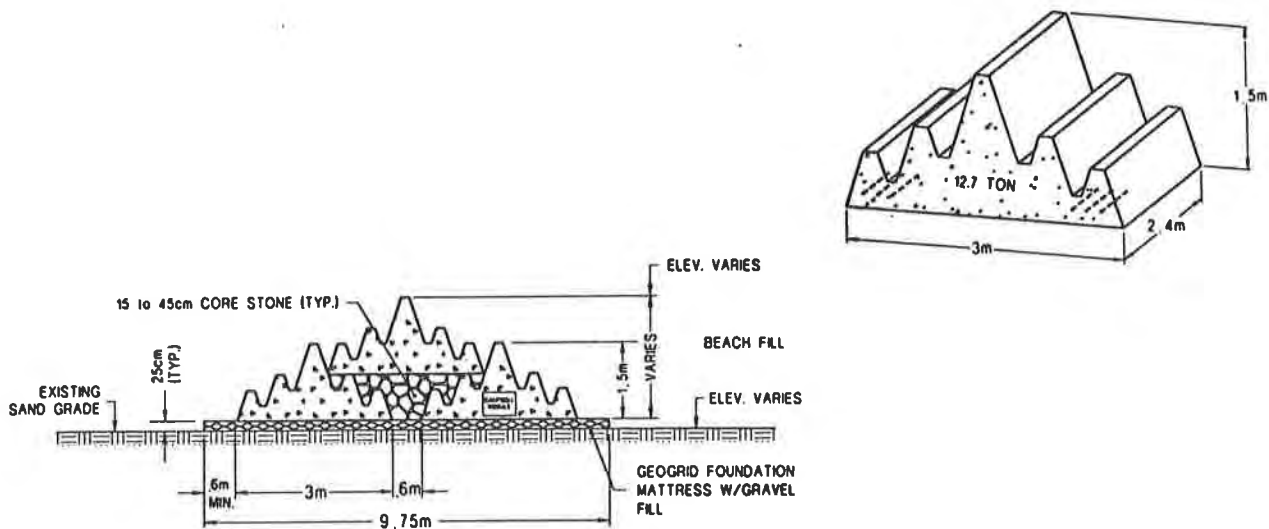
Figure 7   Typical Design Section And Campbell Module Detail

INITIAL CONDITION

FUTURE CONDITION

ARMOR

FOUNDATION STONE

SETTLEMENT
OF STRUCTURE

**CONVENTIONAL RUBBLE MOUND GROIN SUBSIDENCE
AND ASSOCIATED STRUCTURAL DETERIORATION**

INITIAL CONDITION

FUTURE CONDITION

MODULE (12.7T)

FOUNDATION STONE

**POTENTIAL MODULAR STRUCTURE DETERIORATION
DUE TO CONVENTIONAL FOUNDATION SUBSIDENCE**

VS.

GEOTEXTILE

6 in. SAND BEDDING LAYER REQUIRED
FOR ABRASION RESISTANCE

FOUNDATION STONE

GEOGRID MATTRESS

FOUNDATION ALTERNATIVES

FIGURE 8   DESIGN FOUNDATIONS CONSIDERED FOR
MODULAR GROIN CONSTRUCTION

Table 1 - Geogrid Properties

Property	Test Method	Units	Values For Upper & Lower Mattress Panels	Values For Mattress Diaphragms
Interlock				
Aperture Size	I.D. Calipered	mm		
- MD			137 (nominal)	137 (nominal)
- XD			16.8 (nominal)	16.8 (nominal)
Open Area	COE Method	%	60 (nominal)	60 (nominal)
Reinforcement				
Ultimate tensile strength (machine direction)	GRI GG1	kN/m	114 (minimum)	54 (minimum)
Initial Tensile Malulus	GRI GG1	kN/m	1898 (minimum)	730 (minimum)
Flexural Rigidity	ASTM D1388	mg-cm	6,600,000 (minimum)	670,000 (minimum)
Material				
High Density Polyethylene	ASTM D1248 Type III/Class A/ Grade 5	%	97	97
Carbon Black	ASTM D4218	%	2	2

CONSTRUCTION

The work was competitively bid by the Georgia Ports Authority, the project sponsor. The contractor selected for the project was Durocher Dock and Dredge, Inc. of Jacksonville, Florida. Their initial order of work included both the removal of seven existing derelict timber groins and casting the 12.7 ton concrete modules on the adjacent upland. The City of Tybee Island provided a 15 x 120 m Street and Right-of-Way adjacent to the site for purposes of mobilization and casting the 523 Campbell erosion control modules necessary to construct the three groins. Forms were fabricated by the Contractor sufficient to allow for the casting of 15 units per day. Most temporary stockpiling of the groin modules was accomplished on the intertidal beach.

The marine mattress segments were filled by placing the preassembled geogrid baskets into a metal frame on their 25 cm side. The frame was designed to vibrate while the mattresses were being filled with stone from a loader. The fixed vibration devices were placed at 2.4 m centers. They shook the stone down, increasing the density of the stone within the mattress. The stone for this project ranged in size from 4 cm minimum to 9 cm maximum. After a mattress had been filled, it was lowered 90^0 with the hinged portion of the vibratory frame. From this position, the mattress was picked up from one end by a crane with a single lifting bar and placed aside for future deployment. The ability to prefill all of the mattresses for rapid sequential installation at a later date was important to the staging of the project, once work on the beach had begun.

Groin G-1 was the first groin to be constructed and was oriented in a southerly direction. The other groins were constructed north of G-1 with gaps left in their stems so that transport equipment could move easily around the site (i.e., intertidal beach) during construction. Stone filled mattresses were stacked in the staging areas above an adjacent seawall to allow for rapid deployment. The tide range for the site is one of the highest for a southeast coast location (i.e., 2.1 m on average, 2.7 m spring). Hence, all construction materials were moved from the upland to a groin site for placement at mid or low tide. The mattresses were placed directly on grade without a geotextile; then Campbell modules were placed on the mattresses with the required core stone (See Figures 9 & 10). Once placement of the Campbell modules was completed, armor stone was placed on the structure heads to complete the groin construction.

Within three months of completion, the groin field was hydraulically filled with 38,000 cubic meters of sand during the construction of the adjacent small scale (i.e., 191,000 cubic meters) beach restoration project north of the south federal groin. The latter work was likewise sponsored by the Georgia Ports Authority. The stems of the groins were approximately 85 m in length. The outside length of the L-head portion of Groin G-1 was 32 m, whereas the T-heads of Groins G-2 and G-3 averaged about 54 m. The thickness of each mattress was 25 cm and the width was 1.4 m. The lengths of the mattresses ranged from 3 m to 8.5 m depending upon application. Some 8,400 tons of rock were placed as mattress, core or armor stone. Armor stone varied in weight between .9 and 2.7 tons.
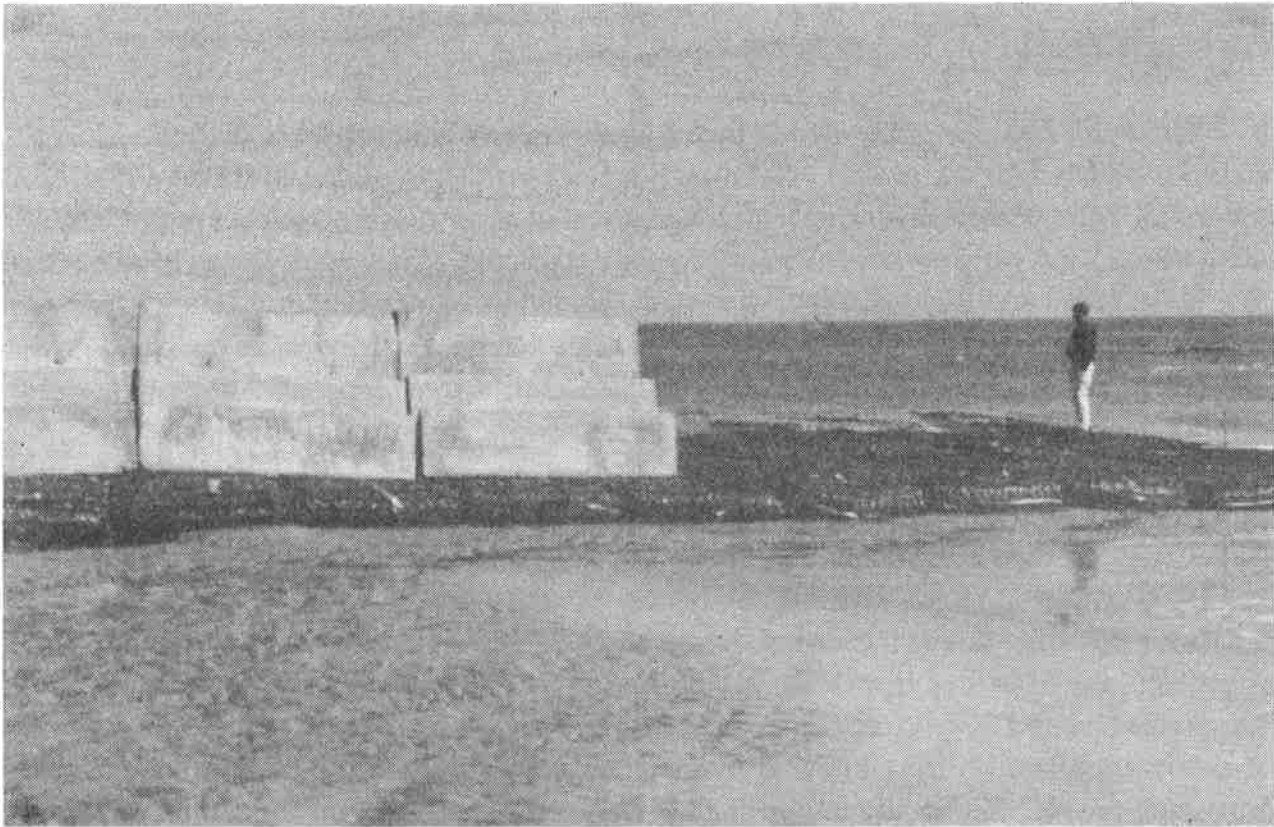
Figure 9   Mattress Placement On Grade (Low Tide)
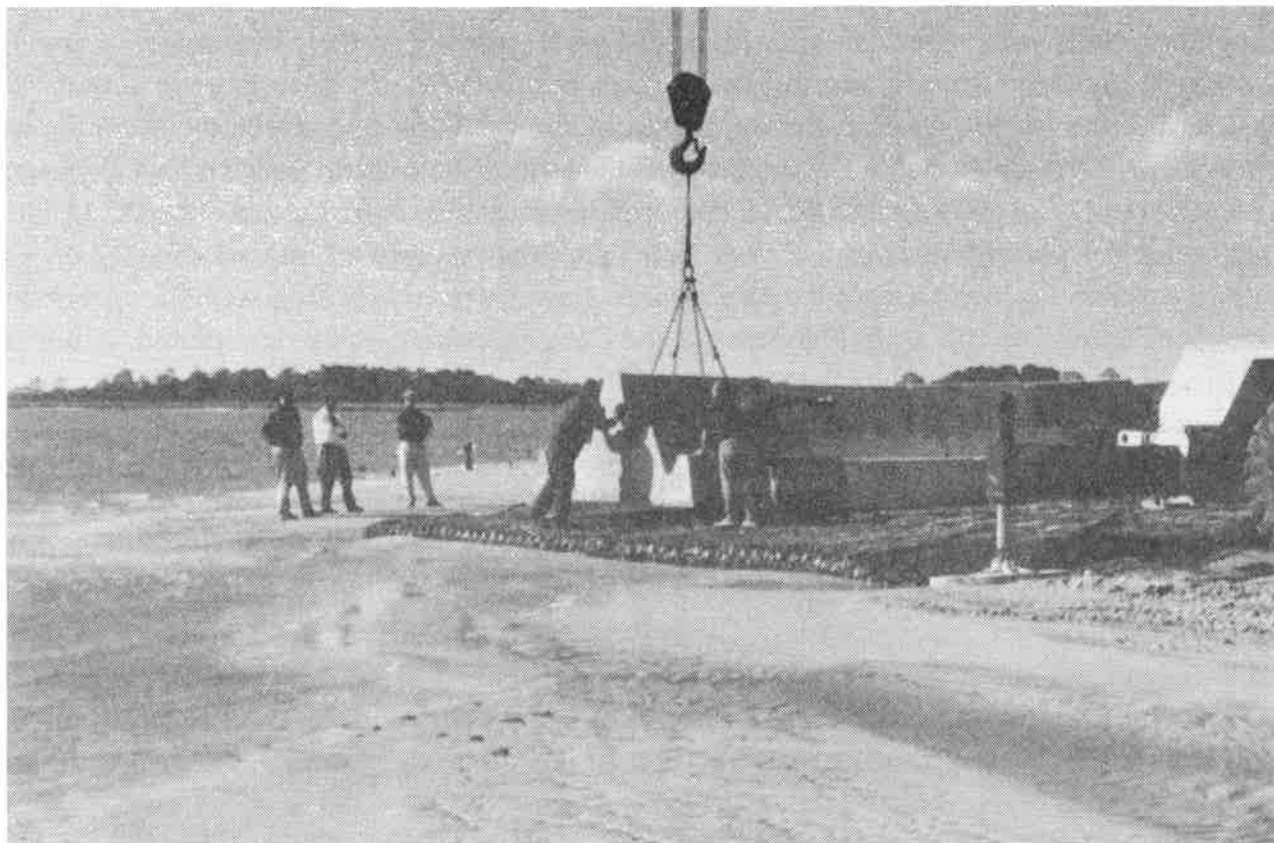
Figure 10   Module On Mattress (Low Tide) Placement

CONCLUSIONS

Both the project groin field as well as the entire insular shoreline is being monitored by survey for a minimum of 24 months pursuant to the Georgia, DNR Permit Conditions. Initial results indicate that the groinfield beach volume has increased substantially as a result of the entrainment of sand transported southward from the adjacent nourishment project. As of January, 1996 the structure field was essentially full and therefore capable of bypassing the net southerly transport.

The marine mattress system has functioned in accordance with the design intent of the engineer and should be considered primarily responsible for the structural integrity of the three groins to date. One year after placement, the groin modules continue to be well-aligned and show little to no visual indications of differential movement, dislodgement, or settlement resulting from tidal scour or wave impact. The terminal groin field presently successfully supports a wide protective beach seaward of the south end of Tybee Island (See Figures 11 & 12). Moreover its relative downdrift location appears to be improving the performance of the adjacent beach restoration project by reducing littoral gradients and corresponding sand losses through the porous rubble mound federal south groin.

REFERENCES

Bodge, Kevin R., 1992, "Aragonite Beach Fill At Fisher Island, Florida"; Shore & Beach, Vol 60, No.1, July 1992, University of California, Berkeley, California.

Griffin, M.N. and Henry, V.J., 1984, Historical changes in the mean high water shoreline of Georgia, 1857-1982, Georgia Department of Natural Resources, Geologic Survey Bulletin 98.

Henry, Vernon J., Dean, Robert G. and Olsen, Erik J., 1987, Short Course - "Coastal Engineering: Processes, Practices and Impacts", Assn. of Engineering Geologists, 3rd Annual Meeting, Atlanta, Georgia.

Olsen, Erik J., 1996 "Tybee Island South Beach Stabilization Project", Proceedings of the 1996 National Conference on Beach Preservation Technology, Florida Shore and Beach Preservation Association, St. Petersburg, Florida.

Taylor, L.A., 1984, "Final Report of the Tybee Island Technical Task Force", submitted to the Commissioner, Georgia Department of Natural Resources, Atlanta, Georgia.

Figure 11 Groin Field (Pre-Beach Fill)

Figure 12 Groin Field (Post-Beach Fill)

GEOTEXTILE CONTAINERS FOR EROSION CONTROL - A LITERATURE REVIEW

C. JOEL SPRAGUE, P.E.
SPRAGUE & SPRAGUE CONSULTING ENGINEERS
GREENVILLE, SC

ABSTRACT

Small geotextile containers, such as sandbags, have been used for decades primarily as temporary construction devices. Yet, more recently, the design and construction of very large geotextile containers has gained popularity because of their simple placement and construction, cost effectiveness and minimum impact on the environment. These containers are hydraulically or mechanically filled with a variety of material types, including concrete, gravel, sand, and, most recently, fine-grained materials to provide a beneficial use of dredged material having very high water content. This paper summarizes an international literature search on geotextile containers of various forms and serving various functions. An extensive list of references is provided to facilitate further study of the various forms or functions.

BACKGROUND

Woven and nonwoven synthetic fabrics, i.e. geotextiles, have been used for the past 30 years for various types of containers, such as small hand-filled sandbags, 3-dimensional fabric forms for concrete, large soil and aggregate filled bags, prefabricated hydraulically-filled tubes, site-fabricated mechanically-filled containers, and other innovative systems involving containment of soils using geotextiles.

Charlton (1984) and Koerner and Welsh (1980) and, most recently and comprehensively, Pilarczyk (1995) provide an overview of the many - primarily erosion control - applications using the various types of containers. Though construction of erosion control structures "in-the-dry" using dredged material filled geotextile containers is quite straight forward, underwater installation is often required and is thoroughly discussed by Groot and Door (1986) and Van Zanten (1986).

SMALL SANDBAGS

Hausemann (1990) provides an historical perspective on the versatile sandbag, especially in military applications such as field defenses, revetments for trenches and buildings, and emergency repairs. Peak annual usage in recent wars has ranged from 80 million during the Korean conflict to over 300 million in Vietnam. Sandbags typically measure 670mm x 370mm, hold up to 0.160 m^3 of soil, and weigh 20 to 25 kg.

Traditionally, sandbags were made from natural fibers which rotted when exposed to the weather. Bagdon (1971) reported on the added serviceability gained by using synthetic fibers such as PVC-coated fiberglass, polypropylene, high density polyethylene, and acrylic in the manufacture of sandbags. The most

durable bags, achieving up to 30 months of service, were made from acrylic fabrics.

Ressler (1979) and White (1980) have done research as a follow-up to German practices of using long tubular sandbags for overhead protection of fox holes.

Stephenson (1982) documented the common civilian use of small sandbags involving erosion control. Acrylic bags were used to protect an irrigation dam from the erosive forces of wind-generated waves. Significant protection was provided over the 18 month study period without significant deterioration. Kobayashi and Jacobs (1985a & 1985b) examined the stability of small sandbags under wave attack.

FABRIC FORMED CONCRETE

Sprague and Koutsourais (1992) recapped the evolution of fabric-formed concrete beginning with Norwegian, Johann Store's introduction in 1922 of the filling of large bags with concrete and placing them with a crane to build underwater structures such as breakwaters and piers. In 1965, according to Lamberton (1989), Dutch engineer H. F. J. Hillen attempted to take advantage of the low cost, durability, and high strength of modern synthetic fabrics to produce three-dimensional forms for casting concrete slabs by joining two layers of fabric into an envelope which, when injected with a very fluid fine-aggregate grout, sets up into a concrete mattress within minutes.

Since the 1960's, these high strength, water-permeable fabrics, woven of synthetic fibers, have been used as an in-place form for concrete or soil-cement in many erosion control applications as documented by Bates and Sprague (1991), Brandl (1994), Lamberton (undated,1969,1983a/b,1985), Lupton (1982), Porraz and Czerniak (1983), Porraz, et al (1977), Porraz and Solar (1986), Welsh and Dominske (1982) and Welsh and Koerner (1979). The intent of fabric formed concrete systems is to combine the durability of conventional rigid linings, such as cast-in-place concrete, asphaltic concrete, grouted riprap, stone masonry, and soil cement with more flexible and/or water-permeable protective rock systems such as riprap and gabions.

Additionally, fabric forms comprised of many long narrow tubes forming a mat have been filled with concrete while suspended by a crane and then placed on slopes to provide erosion control according to Ledeuil, et al (1986). Janis and Holmberg (1995) and Oertel (1995) describe the patented "Holmberg Technology" which involves concrete filled fabric forms. And, Kirschner and Kreit (1994) discussed the use of fabric formed concrete mats for geomembrane protection on side slopes.

Silvester (1986) provided a detailed description, including equations and a chart, of the theory associated with the pumped shape and resulting fabric stress of fabric formed concrete units.

LARGE SOIL AND AGGREGATE BAGS AND MATS

Not surprisingly, the forming of various shapes and sizes using fabric forms was found not to be confined to rigid structures made of concrete but could also be made of soils and aggregates. Very large sandbags for coastal, shoreline and river bank protection have been described by Anonymous (1990, 1992, 1996), Armstrong (1976), Bishop, et al (1994), Botzan, et al (1982), Chasten, et al (1993), Easley (1967), Gutman (1979), Harris (1987, 1989, and 1994), Mechemehl (1977), Ray (1977), Rogers (1994), USACOE (1981) and in sales literature [___(undated-b) and ___(1989)]. In more severe environments such as arctic conditions very large sand and gravel filled bags have been used to protect oil exploration islands according to Dorr and DeHann (1982), Gadd (1988 and 1994), and Liedersdorf, et al (1981).

Mats filled with granular material were described by Pilarczyk (1984), Nomes and Lupton (1984) and Tutuarima and van Wijk (1984). The mats were filled while

suspended by a crane and then placed on slopes to provide erosion control. Similarly, Levillain (1986) described the use of gravel filled fabric tubes sewn to filter fabric panels to ballast the filter fabric in place on a slope while riprap was placed on the fabric.

PREFABRICATED, HYDRAULICALLY FILLED TUBES

Still, a recurring effort to maximize the benefit of the soil containment capability of geotextiles is clear in the efforts to construct linear structures from hydraulically-filled geotextile tubes. Jakobsen and Nielsen (1970) reported on early efforts of the Danish to fill both permeable and impermeable fabric tubes with sand as far back as 1967.

Understandably, sand has been the fill material of choice for hydraulically filled geotextile tubes because of its ability to readily settle out inside the tube and to freely drain to create a stable structure. Consequently, until recently, nearly all of the reported uses of hydraulically filled tubes involve sand filling including, Bogossian, et al (1982), Brater (1979), Creed, et al (1994), de Bruin and Loos (1995), Jackson (1987), Ockels (1991), Olsen (1996), Perrier (1986), Richardson (1995) and in-house reports by Nicolon Corporation [___(1988c)] and by ACZ Marine [___(1990)]. Characteristically, sales literature from ACZ Marine [___(undated-a)] and Nicolon Corporation [___(undated-e)] only mentions sand filling.

Notable in the development of hydraulically-filled geotextile tubes is the development of a tube system using an impermeable fabric. The system is sold under the trade name Longard Tube. Longard Tubes have been evaluated in several actual installations as detailed by Armstrong (1976), Armstrong and Kureth (1979), Flick and Waldorf (1984), Sarti and Larsen (1983), and Shah (1982). The repair of a damaged tube was reported by Wagschal and Hoeckel (1992).

Yet, noticeably absent from the early development of hydraulically filled geotextile tubes is the use of alternative fill materials. Very recently, Bogossian, et al (1982), Fowler, et al (1994), Fowler and Sprague (1993 & 1995), Garbarino, et al (1994), Gill, et al (1995), Jorde & Haramis (1995), Landin, et al (1993 and 1994), Landin and Patin (1993), McLellan (1994), Sprague (1993), Sprague and Fowler (1994) and a Houston Power and Light in-house report [___(1991)] describe the use of non-sand fill. Most of these recent reports involve the use of fine-grained dredged sediments, while Bogossian, et al, looked at clay balls and shell, along with fine sand, and HP&L filled with fly ash. One of the most common applications is as an erosion resistant containment dike or breakwater for wetlands and shoreline reclamation as most recently described by Austin (1995).

Large diameter tube structures will require greater "engineered" certainty as to their filled shape and size if they are to be widely used as individual erosion control structures or containment dikes. Sprague, et al (1996) describe the current state of practice for tube design and construction. Also, a modest amount of investigation has been done by Carroll (1993, 1994a and 1994b), Kazimierowicz (1994), Liu (1981), and most recently Leshchinsky, et al (1996) into the theoretical determination of filled tube size and shape and the associated geotextile strength requirements. An additional consideration involves the ability of the geotextile to retain the fill material while allowing for drainage of free water. Juvonen (1984) demonstrated that fine-grained sediments may actually render a geotextile impermeable.

SITE FABRICATED, MECHANICALLY FILLED CONTAINERS

Only recently have large site-fabricated, mechanically-filled geotextile containers been attempted in the United States. Barnes (1994) and Fowler, et al (1995) describe an "experimental" installation involving hundreds of large containers dropped from a split-hull barge to redirect a river channel that was undertaken in early 1994. Fairweather (1995) and Risko (1995) reported on another demonstration project which disposed of contaminated materials at sea by encapsulating them in large geotextile containers and dropping them from a

split-hull barge. Yet, several similar installations have been undertaken previously in Europe, including an installation on the Old Meuse River in The Netherlands as described in an in-house report by the Rijkswaterstaat [___(1988b)]. Further, technical and sales literature by Nicolon Corporation [___(undated-d & 1988a)] provides additional details on the filling, fabrication, and installation of site-fabricated, barge-placed containers.

INNOVATIVE CONTAINMENT SYSTEMS

The future of geotextile containers may only be limited by the imagination. Some rather innovative containers documented in the literature include:

Fabric-confined wall structures.
  Fowler (1992)

Bags of railroad ballast attached to ties.
  Van Santvoort and Troost (1986)

Tubular gabions for erosion protection.
  Hall (1984)

Forms for mine back-filling.
  Dickson and Strydom (1990)
  Legge and Legge (1994)

Membrane Encapsulated Soil Layers (MESLs) / Pavement Sections (MEPSs).
  Lawson and Ingles (1982)
  Webster (1974)
  Webster and Andress (1976)

Water-filled fabric dams.
  Doty, et al (1984)
  ____ (1993)

Water-filled tube structures.
  Olheiser and Ragsdale (1995)
  Walke (1995)
  ____ (undated-c)
  ____ (1994)

Fabric-confined space structures.
  Harrison (1992)

Sand-filled fabric island.
  Dowse (1979)

Reusable fabric forms for reinforced concrete structures.
  Anonymous (1995)

CONCLUSIONS

A review of the sited references appears to validate that the use of geotextiles in containment of soils and other materials for the purpose of creating erosion resistant structures has been pursued for several decades, generally with much apparent success. The most recent references seem to indicate that there is currently a great deal of interest in the use of very large geotextile containers, especially hydraulically filled pre-fabricated tubes and mechanically filled site-fabricated containers. Perhaps these structures hold the greatest promise for large-scale, cost-effective installation of erosion resistant structures. This assumption remains to be confirmed or disputed in the literature. Other smaller geotextile containers, such as bags and fabric forms appear to be proven systems that have achieved significant acceptance and common usage and, therefore, their use is less likely to be considered "news worthy".

REFERENCES/BIBLIOGRAPHY

_____ (undated-a), "Ontwikkeling van zandwostsystemen", One page sales brochure, ACZ Marine Contractors BV, the Netherlands.

_____ (undated-b), "Support and Separation Mattress", One page sales brochure, ACZ Marine Contractors BV, the Netherlands.

_____ (undated-c), "Water Structures", 7-page sales brochure, Water Structures Unlimited.

_____ (undated-d),"Geocontainer the new system", In-house Report, Nicolon BV, the Netherlands.

_____ (undated-e),"Geotubes^R; Atlantic City Sand Dune Construction", Case Study, Nicolon Corp., Norcross, GA.

_____ (1988a), "Geosystems", 8-page sales brochure, Nicolon BV, the Netherlands.

_____ (1988b),"Bed Protection, Old Meuse, by Means of Geocontainers", In-house Report, Rijkswaterstaat, the Netherlands.

_____ (1988c),"Coastal Protection in the Leybucht, North Sea Coast, West Germany", In-house Report, Nicolon BV, the Netherlands.

_____ (1989 & 1994), "S.E.A.B.A.G.", Sales Brochure, Bulk Lift International, Carpentersville, IL.

_____ (1990), "Applications and Execution Aspects of Sand Tube Systems", In-house Report, ACZ Marine Contractors BV, the Netherlands.

_____ (1991),"Use of bottom ash as fill material for geo-tube dredge soil containment system", In-house Report, Houston Power & Light Company, Revenue Enhancement Department.

_____ (1993), "Sumigate Rubber Dams", Orange Peal Circular, Summer 1993, Rodney Hunt Company, Orange, MA.

_____ (1994), "Water Structures", Sales Brochure and attachments, Reef Industries, Inc., Houston, TX.

Anonymous (1990), Fighting Atlantic beach erosion, Land and Water, November/December, pp. 4-5.

Anonymous (1991), Cape Hatteras Light Weathers Storm . . . Nearby Bridge is Destroyed, Land and Water, January.

Anonymous (1995), Concrete walls display reusable formwork, Civil Engineering, May, p. 27.

Anonymous (1996), Seaworthy solution is turning the tide on beach erosion, Landscape Architect & Specifier News, February, pp. 46-48.

Armstrong, J.M. (1976), Low-cost shore protection on the great lakes: A demonstration/research program, Proceedings of the Fifteenth Coastal Engineering Conference, ASCE, Honolulu, pp. 2858-2887.

Armstrong, J.M. and Kureth, C.L. (1979), Some observations on the Longard Tube as a coastal erosion protection structure, Proceedings of Coastal Structures '79, ASCE, Alexandria, pp. 250-269.

Austin, T. (1995), A second life for dredged material, Civil Engineering, November, pp. 60-63.

Bagdon, V.J. (1971), Development of the long-life military sandbag, "Textile Research Journal", June, pp. 546-549.

Barnes, S. (1994), 'Red Eye Crossing' used as testing ground for new dike system, Louisiana Contractor, April, pp. 40-43.

Bates, J. and Sprague, C.J. (1991), Revetment system protects drift river wilderness, "Geotechnical Fabrics Report", Jan./Feb., pp. 20-23.

Bishop, D., Johanssen, K., and Kohlhase, S. (1994), Recent applications of modern geosynthetics for coastal, canal and river works, Proceedings of the 5th International Conference on Geotextiles, Geomembranes and Related Products, Singapore, pp. 545-548.

Bogossian, F., Smith, R.T., Vertimatti, J.C. and Yazbek, O. (1982), Continuous retaining dikes by means of geotextiles, Proceedings of the Second International Conference on Geotextiles, Las Vegas, pp. 211-216.

Botzan, D., Kellner, L., and Moisa, C. (1982), Construction elements for river bank defense structures using woven geotextiles, Proceedings of the Second International Conference on Geotextiles, Las Vegas, pp. 223-227.

Brandl, H. (1994), Geotextiles for underpinning river bridge piers, Proceedings of the 5th International Conference on Geotextiles, Geomembranes and Related Products, Singapore, pp. 783-786.

Brater, E.F. (1979), Observations on low-cost shore protection, Journal of the Port, Coastal and Ocean Div., ASCE, Vol. 105, No. WW4, November 1979, pp. 453-457.

Carroll, R.P. (1993), Theoretical analysis of inflated submerged fabric forms, Memorandum submitted to the J. Fowler, Corps of Engineers Waterways Experiment Station - with computer program.

Carroll, R.P. (1994a), The isotensile pancake: a unique submerged geotextile flexible form, Geotechnical Fabrics Report, September, pp. 12-19.

Carroll, R.P. (1994b), Submerged geotextile flexible forms using noncircular cylindrical shapes, Geotechnical Fabrics Report, October/November, pp. 4-15.

Carter, M., and S.P. Bently (1991), Correlations of Soil Properties, Pentech Press Limited, London, U.K., p. 4.

Charlton, F.G. (1984), Geotextiles for bank protection in relation to causes of erosion, Flexible Armoured Revetments, Thomas Telford Ltd., London, pp. 165-177.

Chasten, M.A., Rosati, J.D., McCormick, J.W., and Randall, R.E. (1993), Engineering design guidance for detached breakwaters as shoreline stabilization structures, U.S. Army Corps of Engineers, Technical Report CERC-93-19.

Creed, C.G., Olsen, E.J., and Bodge, K.R. (1994), The use of a sand-filled geotextile tube as an interim sand-tightening measure at an inlet jetty, Abstract submitted for cancelled C.O.E. workshop.

de Bruin, P. and Loos, C. (1995), The use of Geotubes[R] as an essential part of an 8.8 m high North Sea dike and embankment, Leybucht, Germany, Geosynthetics World, April/May, pp. 7-10.

Dickson, M.G. and Strydom, C.S. (1990), Geotextiles for backfilling on deep level mines, Proceedings of the Fourth International Conference on Geotextiles, Geomembranes and Related Products, The Hague, pp. 849-852.

Dorr, H.C. and DeHann, D.W. (1982), The Oosterschelde filter mattress and gravel bag, Proceedings of the Second International Conference on Geotextiles, Las Vegas, pp. 271-276.

Doty, C.W., Thayer, W.B. and Jessup, R.G. (1984), Automated fabric dam aids water research project, Proceedings of the International Conference on Geomembranes, Denver, pp. 127-132.

Dowse, B.E.W. (1979), Hydrostatically supported sand coastal structures, Proceedings of Coastal Structures '79, ASCE, Alexandria, pp. 405-421.

Easley, R.T. (1967), Sand-filled bags as dike material; Potamology Research Project 9, Potamolgy Investigations Report 21-1, US Army Waterways Experiment Station.

Fairweather, V. (1995), Dredging up the past, Civil Engineering, March, pp. 44-47.

Flick, R.E. and Waldorf, B.W. (1984), Performance documentation of the Longard Tube at Del Mar, California 1980-1983, Coastal Engineering, Vol. 8, No. 3, pp. 199-217.

Fowler, J. (1992), Geosynthetic reinforced barricades for ammunition storage, Safeload Program Technical Data Package, U.S. Army Corps of Engineers.

Fowler, J. and Sprague, C.J. (1993), Dredged material filled geotextile containers, Proceedings of Coastal Zone '93, ASCE,   pp. 2415-2428.

Fowler, J. and Sprague, C.J. (1995), Dredged material filled geotextile containers, Waterfowl habitat restoration, enhancement and management in the Atlantic Flyway, Third Ed., Environmental Management Committee, Atlantic Flyway Council, Technical Section, and Delaware Division of Fish and Wildlife, P.O. Box 1401, Dover, DE, pp. K83-K95.

Fowler, J., Sprague, C.J., and Toups, D. (1994), Dredged material-filled geotextile containers, U.S. Army Corps of Engineers, Environmental Effects of Dredging Technical Note, EEDP-05-01.

Fowler, J., Toups, D., Duarte, F., and Gilbert, P. (1995), Geotextile contained dredged material, Red Eye Crossing, Baton Rouge, LA, Proceedings of GLGGC '95, ASCE Cleveland Section, pp. 257 -   .

Gadd, P.E. (1988), Sand bag slope protection: design, construction, and performance, Arctic Coastal Processes and Slope Protection Design, ASCE, pp. 145-165.

Gadd, P.E. (1994), Geotextile failure in the marine environment: lessons learned in the arctic offshore, Abstract submitted for cancelled C.O.E. workshop.

Garbarino, S.D., Blama, R.N., Landin, M.C., Maynord, S.R., and Patin, T.R. (1994), Environmental restoration and enhancement using dredged material in Chesapeake Bay, Maryland, Proceedings of Dredging '94, ASCE, pp. 384-393.

Gill, J.W., McGowan, P., and Pitt, L. (1995), Beneficial Uses of Dredged Material for Habitat Restoration, Case Study: Eastern Neck Island National Wildlife Refuge wetland creation and erosion control project, Waterfowl habitat restoration, enhancement and management in the Atlantic Flyway, Third Ed., Environmental Management Committee, Atlantic Flyway Council, Technical Section, and Delaware Division of Fish and Wildlife, P.O. Box 1401, Dover, DE, pp. E65-E104.

Goldman, S.J., Jackson, K., and T.A. Bursztynsky (1986), Erosion & Sediment Control Handbook, McGraw-Hill, pp. 8.11.

Groot, J.M., and Dorr, J.C. (1986), Placing of geotextiles in deep water, Proceedings of the Third International Conference on Geotextiles, Vienna, pp. 489-494.

Gutman, A.L. (1979), Low-cost shoreline protection in Massachusetts, Proceedings of Coastal Structures '79, ASCE, Alexandria, pp. 373-387.

Hall, C.D. (1984), Tubular gabions, <u>Flexible Armoured Revetments</u>, Thomas Telford Ltd., London, pp. 157-164.

Harris, L.E. (1987), Evaluation of sand-filled containers for beach erosion control, an update of the technology, Proceedings of Coastal Zone '87, pp. 2479-2487.

Harris, L.E. (1989), Developments in sand-filled container systems for coastal erosion control in Florida, Proceedings of Coastal Zone '89, ASCE, pp. 2225-2233.

Harris, L.E. (1994), Dredged material used in sand-filled containers for scour and erosion control, Proceedings of Dredging '94, ASCE, pp. 537-546.

Harrison, R.A. (1992), Cylindrical fabric-confined soil structures, Proceedings of Third International Conference on Engineering, Construction and Operations in Space, ASCE, Denver, pp. 123-134.

Hausmann, M.R. (1990), <u>Engineering Principles of Ground Modification</u>, McGraw-Hill, pp. 573-578.

Jackson, L.A. (1987), Evaluation of sand filled geotextile groynes constructed on the Gold Coast, Australia, Proceedings of the 8th Australian Conference on Coastal & Ocean Engineering, Launceston, pp. 235-238.

Jakobsen, P.R. and Nielsen, A.H. (1970), Some experiments with sand-filled flexible tubes, Proceedings of the 12th Conference on Coastal Engineering, pp. 1513-1521.

Janis, W.A., and Holmberg, D.L. (1995), Holmberg technology, Proceedings of Conference XXVI, IECA, Atlanta, pp. 219-229.

Jorde, D.G. and Haramis, G.M. (1995), Water/dredge-filled tubes: a new level of flexibility for wetland managers, <u>Waterfowl habitat restoration, enhancement and management in the Atlantic Flyway</u>, Third Ed., Environmental Management Committee, Atlantic Flyway Council, Technical Section, and Delaware Division of Fish and Wildlife, P.O. Box 1401, Dover, DE, pp. K71-K82.

Juvonen, J. (1984), Experiences in the use of geotextiles in the water construction field in Finland, <u>Flexible Armoured Revetments</u>, Thomas Telford Ltd., London, pp. 285-288.

Kazimierowicz, K. (1994), Simple analysis of deformation of sand-sausages, Proceedings of the Fifth International Conference on Geotextiles, Geomembranes and Related Products, Singapore, pp. 775-778.

Kirschner, R. and Kreit, V. (1994), Innovative, protective mattresses for landfill geomembranes, Proceedings of the 5th International Conference on Geotextiles, Geomembranes and Related Products, Singapore, pp. 1015 - 1018.

Bishop, D., Johannssen, K., and Kohlhase, S. (1994), Recent applications of modern geosynthetics for coastal, canal and river works, Proceedings of the 5th International Conference on Geotextiles, Geomembranes and Related Products, Singapore, pp. 545-548.

Kobayashi, N. and Jacobs, B.K. (1985a), Experimental study on sandbag stability and runup, Proceedings of Coastal Zone '85, Baltimore, pp. 1612-1626.

Kobayashi, N. and Jacobs, B.K. (1985b), Stability of armor units on composite slopes, Journal of Waterway, Port, Coastal and Ocean Engineering, ASCE, Vol. 111, No. 5, pp. 880-894.

Koerner, R.M. and Welsh, J.P. (1980), <u>Construction and Geotechnical Engineering Using Synthetic Fabrics</u>, J. Wiley & Sons, pp. 160-229.

Lamberton, B.A. (undated), Fabric forms for concrete - a new technology with a long history, In-house report, Intrusion-Prepakt, Inc.

Lamberton, B.A. (1969), Revetment construction by fabriform process, Journal of the Construction Division, ASCE, July, pp. 49-54.

Lamberton, B.A. (1983a), Fabric forming for underwater concrete, Proceedings of Coastal Structures '83, ASCE, pp. 619-631.

Lamberton, B.A. (1983b), Fabric-formed revetment technology opens new engineering opportunities, "Geotechnical Fabrics Report", Summer, pp. 4-10.

Lamberton, B.A. (1985), Erosion-control objective: fabric-formed revetments protect shoreline, "Geotechnical Fabrics Report", July/August 1985, pp. 14-15.

Lamberton, B.A. (1989), Fabric forms for concrete, "Concrete International", December, pp. 58-67.

Landin, M.C., Patin, T.R. (1993), Innovative wetlands in urban settings using dredged material, Proceedings of Water Management in the '90s, ASCE, pp. 109-112.

Landin, M.C., Fowler, J., and Allen H.H. (1994), New applications and practices for beneficial uses of dredged material, Proceedings of Dredging '94, ASCE, pp. 526-536.

Lawson, C.R. and Ingles, O.G. (1982), Long term performance of MESL road sections in Australia, Proceedings of the Second International Conference on Geotextiles, Las Vegas, pp. 535-539.

Ledeuil, Gieulles, Mine and Richou (1986), River sills and water diverters made of concrete injected or reinforced cloth, Proceedings of the Third International Conference on Geotextiles, Vienna, pp. 1169-1174.

Legge, K.R. and Legge, W.C.S. (1994), Backfilling: A challenge for geotextiles, "Geosynthetics World", January, 1994, pp. 14-15,19.

Leidersdorf, C.B., Potter, R.E., and Goff, R.D. (1981), Slope protection for artificial exploration islands off Prudhoe Bay, Proceedings of the 13th Annual Offshore Technology Conference, Houston, pp. 437-447.

Leshchinsky, D., Leshchinsky, O., Ling, H.I., and Gilbert, P.A. (1996), Geosynthetic tubes for confining pressurized slurry: some design aspects, Journal of Geotechnical Engineering, ASCE, August, pp. 682-690.

Levillain, J.P., (1986), Geotextiles in bank protection: An experience of three years, Proceedings of the Third International Conference on Geotextiles, Vienna, pp. 1127-1129.

Liu, G.S. (1981), Design criteria of sand sausages for beach defences, Proceedings of the XIXth Congress IAHR, New Delhi, pp. 123-131.

Lupton, T.J. (1982), The advancing techniques in flexible forms, Proceedings of the Second International Conference on Geotextiles, Las Vegas, pp. 463-466.

McLellan, T.N. (1994), Beneficial uses of dredged material using geotextile tubes: case histories for the Galveston District, Abstract submitted for cancelled C.O.E. workshop.

Mechemehl, J.L. (1977), An engineering evaluation of low cost stabilization projects in Brunswick County, North Carolina, Proceedings of Coastal Sediments '77, ASCE, Charleston, pp. 696-715.

Nederlof, C. (1985), Verslag proef met 200m zandworst damvak Slaak, RWS, Directie S&S, Bouwbureau Stormvloedkering Oosterschelde, ONW-R-85075.

Nederlof, C. (1986), Verslag proeven met zandworsten, RWS, Directie S&S, Bouwbureau Stormvloedkering Oosterschelde, ONW-R-86007.

Nomes, J. and Lupton, T.J. (1984), Some recent developments in the field of flexible armoured revetments in the Benelux, Flexible Armoured Revetments, Thomas Telford Ltd., London, pp. 349-360.

Ockels, R. (1991), Innovative hydraulic engineering with geosynthetics, "Geosynthetics World", October, pp. 26-27.

Oertel, B. (1995), Nature builds the best beaches, Land and Water, September/October, pp. 42-45.

Olheiser, D. and Ragsdale, J.H. (1995), Waterfilled cofferdams for shore protection during remediation activities, Proceedings of Conference XXVI, IECA, Atlanta, pp. 89-92.

Olsen, E.J. (1996), Workshop on coastal erosion control and beach renourishment, Conference XXVII, Seattle, Int'l Erosion Control Assn.

Perrier, H., (1986), Use of soil-filled synthetic pillows for erosion protection, Proceedings of the Third International Conference on Geotextiles, Vienna, pp. 1115-1119.

Pilarczyk, K.W. (1985), Prototype tests of slope protection systems, Flexible Armoured Revetments, Thomas Telford Ltd., London, pp. 239-254.

Pilarczyk, K.W. (1995), Novel Systems in Coastal Engineering, Geotextile systems and other methods - an overview, In-house Report, Rijkswaterstaat, Road and Hydraulic Engineering Division, Delft, The Netherlands.

Porraz, J.L., Maza, J.A. and Munoz, M.L. (1977), Low cost structures using operational designs systems, Proceedings of Coastal Sediments '77, ASCE, Charleston, pp. 672-685.

Porraz, J.L. and M.T. Czerniak (1983), Applications of in-situ filled containers for arctic structures, Proceedings of Coastal Structures '83, ASCE, Arlington, pp. 601-609.

Porraz, J.L., and Solar, S.A. (1986), Geogrid-geotextile system to substitute mangrove fascines for breakwater construction, Proceedings of the Third International Conference on Geotextiles, Vienna, pp. 441-445.

Ray, R. (1977), A laboratory study of the stability of sand-filled nylon bag breakwater structures, Miscellaneous Report No. 77-4, US Army Corps of Engineers.

Ressler, S.J. (1979), Response of a tubular sandbag to thrust and moment loading, Miscellaneous Paper SL-79-9, US Army Engineer Waterways Experiment Station.

Richardson, G.N. (1995), Lessons learned from the failure of geotextile erosion control tubes, Geosynthetics: Lessons Learned from Failures, IFAI.

Risko, A.J. (1995), Memorandum for the Record, FY 95 Marina Del Rey Detailed Project Summary, US Army Engineer District, Los Angeles, Los Angeles, CA.

Rogers, S.M., Jr. (1994), Letter regarding cancelled C.O.E. workshop.

Sarti, G. and Larsen, J. (1983), Underwater filling of Longard Tubes, Proceedings of Coastal Structures '83, ASCE, Arlington, pp. 610-618.

Shah, V.K. (1982), Performance of sand-filled tube shore protection Tuktoyaktuk, North West Territories, Canada, Proceedings of Coastal Engineering '82, pp. 1901-1913.

Silvester, R. (1986), Use of grout-filled sausages in coastal structures, Journal of Waterway, Port, Coastal, and Ocean Engineering, ASCE, Vol. 112, No. 1, pp. 95-115.

Sprague, C.J. and Koutsourais, M.M. (1992), Fabric formed concrete revetment systems, Geotextiles and Geomembranes, Vol. 11, pp. 587-609.

Sprague, C.J. (1993), Dredged material filled geotextile tubes, Mobile District, Report to U.S.Army Engineer CEWES-CT.

Sprague, C.J. and Fowler, J. (1994), Dredged material-filled geotextile containers: case histories, research and upcoming workshop, Geotechnical Fabrics Report, October/November, pp 42-54.

Sprague, C.J., Goodrum, R.A., and Bradley, A.S. (1996), Dredged material-filled geotextile tubes: design and construction, Proceedings of Conference XXVII, Seattle, Int'l Erosion Control Assn., pp. 377-393.

Stephenson, R.W. (1982), A study of soil-filled synthetic fabric "pillows" for erosion protection, Proceedings of the Second International Conference on Geotextiles, Las Vegas, pp. 235-239.

Tutuarima, W.H. and van Wijk, W. (1984), ProFix mattresses – an alternative erosion control system, Flexible Armoured Revetments, Thomas Telford Ltd., London, pp. 335-348.

Van Santvoort, G.P.T.M. and Troost, G.H. (1986), Reinforced railway sleeperbed, Proceedings of the Third International Conference on Geotextiles, Vienna, pp. 159-164.

Van Zanten, R.V. (1986), Geotextiles and Geomembranes in Civil Engineering, John Wiley & Sons, pp. 318-320, 332-339.

US Army (1981), Low-cost shore protection, Final report on the shoreline erosion control demonstration program (Section 54), US Army Corps of Engineers. NTIS #ADA109379.

Wagschal, B. and Hoeckel, M. (1992), Workers repair Longard tube at south end beach, Boca Beacon, Boca Raton, FL, January 31.

Walke, R.H. (1995), Temporary water barriers: alternatives to conventional cofferdams, Proceedings of Conference XXVI, IECA, Atlanta, pp. 265-275.

Webster, S.L. (1974), Users' manual for membrane encapsulated pavement sections (MEPS), 74-2 Implementation Package, USAE Waterways Experiment Station, Soils and Pavements Laboratory.

Webster, S.L. and Andress, R.A. (1976), Investigation of fabrics and bituminous surfaces for use in MESL construction, Miscellaneous Paper S-76-14, USAE Waterways Experiment Station.

Welsh, J.P. and Dominske, D. (1982), Synthetic fabrics as a concrete forming device, Proceedings of the Second International Conference on Geotextiles, Las Vegas, pp. 457-461.

Welsh, J.P. and Koerner, R.M. (1979), Innovative uses of synthetic fabrics in coastal construction, Proceedings of Coastal Structures '79, ASCE, Alexandria, pp. 364-372.

White, R.W. (1980), Development of a tubular sandbag for overhead protection against small high-explosive superquick fuze rounds, Miscellaneous Paper SL-80-16, USAE Waterways Experiment Station.

APPLICATION AND DESIGN ASPECTS OF GEOCONTAINERS

KRYSTIAN W. PILARCZYK
RIJKSWATERSTAAT, ROAD AND HYDRAULIC ENGINEERING DIVISION
DELFT, THE NETHERLANDS

ABSTRACT

Geocontainers are relatively new engineering systems. The design is mainly based on experience. Some new preliminary design rules supported by analytical studies and some model and prototype tests are presented.

INTRODUCTION

Geocontainers hydraulically and/or mechanically filled with (dredged) materials have been successfully applied in hydraulic and coastal engineering in recent years (shore protection, breakwaters, etc.). They can also be used to store and isolate contaminated materials from harbor dredging, and/or to use these units as bunds for reclamation works (Fowler and Sprague, 1993, Pilarczyk, 1996). The first applications were based on the past experience with similar systems. Recently, new preliminary design rules supported by model and prototype tests, and some analytical calculations have been developed in the Netherlands. This new information is presented in this paper.

CONTAINER SYSTEMS

A geocontainer is a mechanically-filled geotextile and a "box" or" pillow" shaped unit made of a soil-tight geotextile. The containers are partially prefabricated by sawing mill widths of the appropriate length together and also at the ends to form an elongated "box". The "box" is then closed in the field, after filling, using a sewing machine and specially designed seams. Barge placement of the site-fabricated containers is accomplished using a specially configured barge-mounted crane or by bottom dump hoppers scows, or split barges. Thereafter containers are filled on a split barge and placed, when the barge is securely moored in the desired position. Positioning of such a barge for consistent placement - a critical element of constructing "stacked" underwater structures - is accomplished with the assistance of modern surveying technology. The volume of actually used geocontainers is from 100 to 1000 m^3.

The advantage of these large barge-placed containers include:

* Containers can be filled with locally available soil which may be available from simultaneous dredging activities.
* Containers can be relatively accurately placed regardless of weather conditions, current velocities, tides and water depths (the main advantages in comparison with other systems).
* Contained material is not subject to erosion during/after placement.
* Containers can provide a relatively quick system build-up.
* Containers are cost competitive, especially for larger projects.
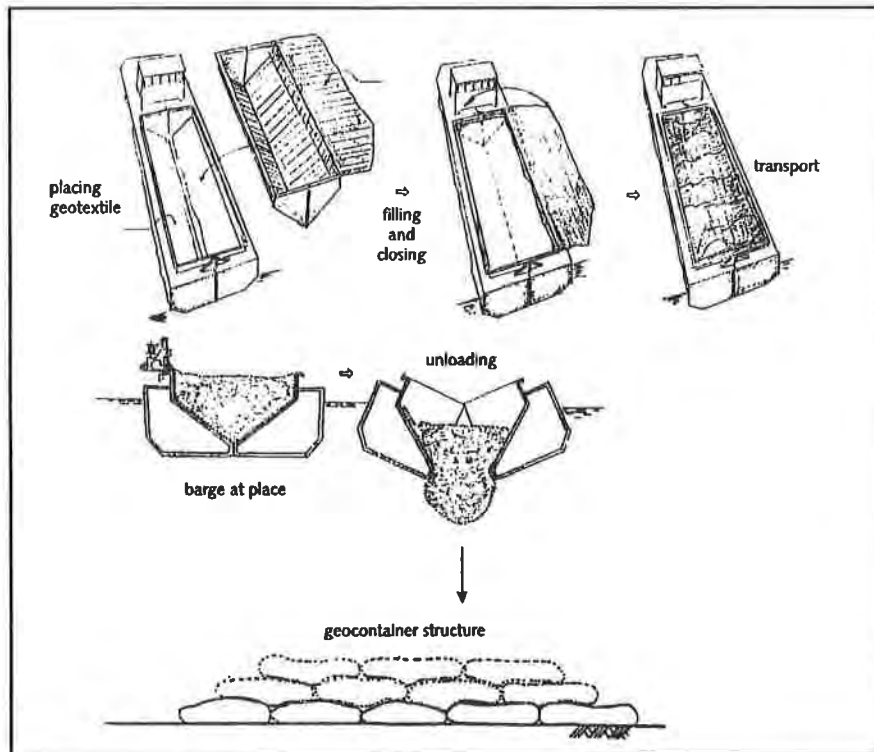
Figure 1 Filling and placing of a geocontainer

The major design considerations include sufficient geotextile and seam strength in order to resist pressures during filling and release, impact of the geocontainer on the bottom and compatibility between fabric and soil. Long-term U.V. resistance, resistance to abrasion, tearing and puncturing (including vandalism), and container flattening resulting from the consolidation of sediments within the container are additional design considerations (Leshchinsky, 1995, Adel, 1996).

Commonly, the filter geotextile (against scour) and a flat tube are fully deployed by floating and holding them in position prior to starting the filling operation. Geotubes are often used as a bottom protection for geocontainers. A sheet of geotextile is furnished with small geotubes at the edges. When these geotubes are filled with sand, they will keep the filter apron at place. This apron must also extend sideways of the geocontainer units, commonly 1-2 times the height of the entire structure.

SUMMARY OF DUMPING PROCESS AND PRACTICAL UNCERTAINTIES

A summary of various forces during the dumping and placement process is given in Figure 2.
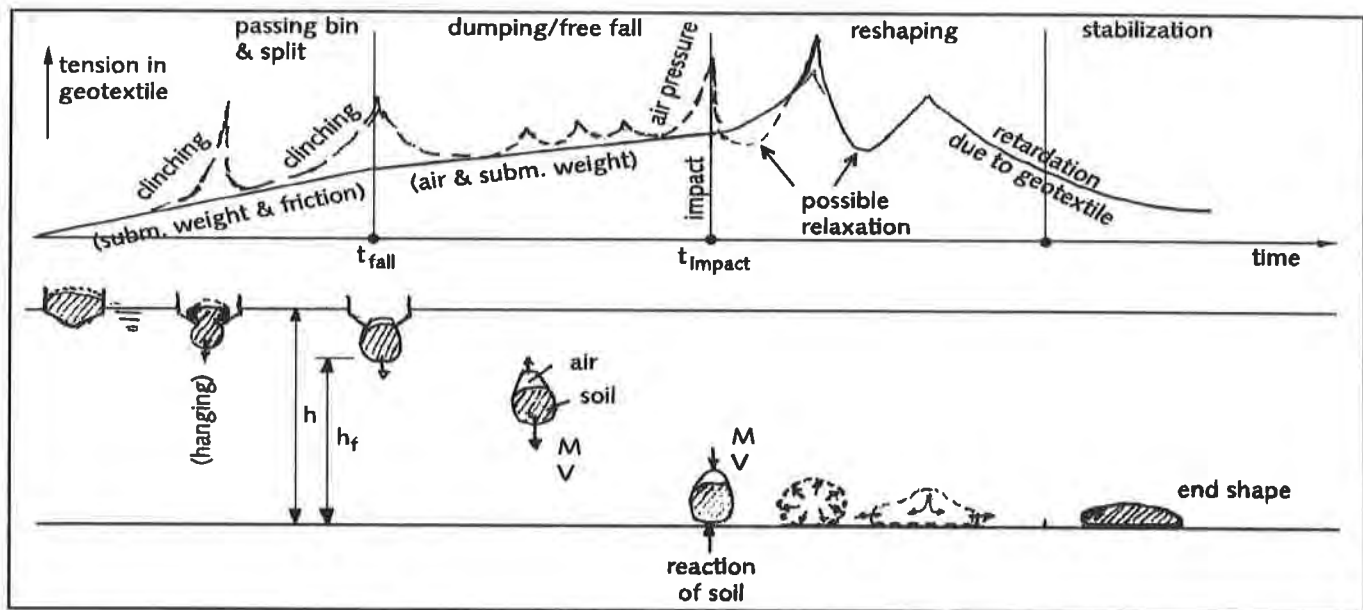
Figure 2 Development of forces during dumping process of geocontainers

1. After opening of the split of a barge the geocontainer is drawn down by the weight of the soil in the geocontainer whereas friction forces along the bin side resist this process. Due to these forces the tension in the geotextile develops mainly at the lower part of both sides of the geocontainer. The upper part is free of tension until the moment when the geocontainer is completely released.

2. A geocontainer will always contain a certain amount of air in the pores of soil and between the soil and the top of the geocontainer, where a surplus of geotextile is present. The air provides an additional buoyancy during sinking. The amount and location of air pockets depends on the consistency of the soil (dry, saturated) and uniformity of the dumping process. The air pockets will exert certain forces on the geotextile and will induce some strain in the geotextile. Analytical studies show that the influence of air is rather small.

3. The forces due to the impact at the bottom will be influenced by a number of factors:

*   The consistency of the soil inside the geocontainer such as the degree of saturation and its physical characteristics;
*   The amount of air;
*   The permeability or airtightness of the geotextile;
*   The strength characteristics of the geotextile;
*   The velocity at impact on the bottom; saturated soil in the geocontainer increases the velocity;
*   The shape and flow catching area of the geocontainer at impact;
*   The stiffness of the bottom. Sand, clay, soft soil, rock, soil covered with rockfill mattress or layers of previously placed containers react differently from each other.

During the impact the cross-sectional shape of geocontainer will be continuously reshaped; from a cone shape into a transitional cylindrical shape and after a certain amount of relaxation, into a semi-oval shape or flat triangular or rectangular shape, the latter being imposed by the soil type, the circumference of the geotextile, and its stress strain characteristics.

4. In the final situation the geocontainers may be either the core material of various protective structures or the geocontainers themselves are exposed to loading by currents and waves or other loadings such as ice, debris, ship collision, vandalism.

DESIGN CONSIDERATIONS

When applying geotubes or geocontainers the major design considerations are related to the integrity of the units during release and impact, the accuracy of placement on the bottom and the stability under current and wave attack. The following design aspects are of importance:

a) Forces during release of geocontainer from the bin;
b) Changes in shape of the units as a function of the perimeter of a unit, fill-grade, and opening of a split barge;
c) Dumping process and impact forces;
d) Dump velocity/equilibrium velocity, velocity at impact on the bottom;
e) Stresses in geotextile during impact and reshaping;
f) Hydraulic stability of the structure;
g) Resulting structural and operational requirements.

Some of these aspects are briefly discussed hereafter.

a) When passing the split opening, the geocontainer sheet must resist the clinching forces exerted at the split edges due to the weight of the already passed soil and the friction and jamming forces of the remaining upper part of soil (see Figure 3). The magnitude of such forces can be in order of the half weight of geocontainer per unit length. However, an uneven friction distribution during dumping (especially in the length direction) may increase these forces considerably. On the other hand, a sudden opening of the split barge up to the final width can effectively reduce these forces. Of course, the top of the geocontainer, which incorporates a large surplus of geotextile, will be tensioned only at the last moment of release of geocontainer. This surplus of geotextile sheet might be larger than needed for the release of the upper part of geocontainer. In such a case, the free space consists only of air and can function as a balloon during sinking.

A schematic representation of friction and tensile forces in geotextile during the release of container from the bin of the barge is given in Figure 4. For small geocontainers (and proper provisions inside the bin) these forces are usually lower than the impact forces. However, in the case of larger geocontainers and large friction factors these forces can be decisive for the proper choice of the strength of the geotextiles.
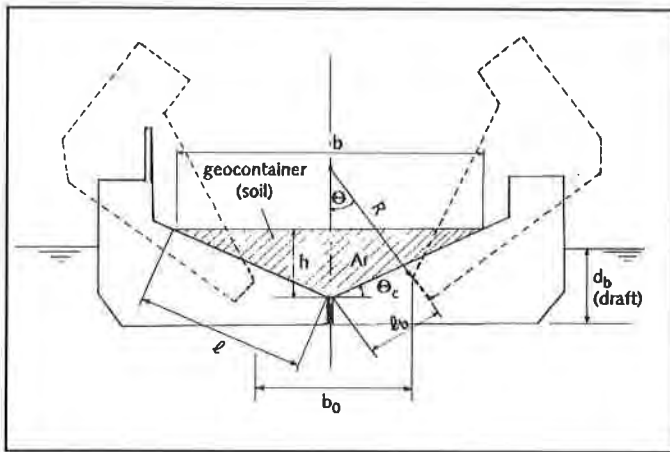
Capacity (volume) of the geocontainer: $V = 0.5 \ L \ b \ h$
where: L = total length of the geocontainer, b = top-width , and h = depth of soil.
The touch (side) length at the bottom 'l' is equal to:
$$l = \sqrt{h^2 + (0.5 \ b)^2}$$
and the split-opening width b_o as a function of the radius of rotation (R) and the angle of opening (θ) is given by: $b_o = 2 \ R \ \sin\theta$

Figure 3   The schematization of a bin for the calculation of forces
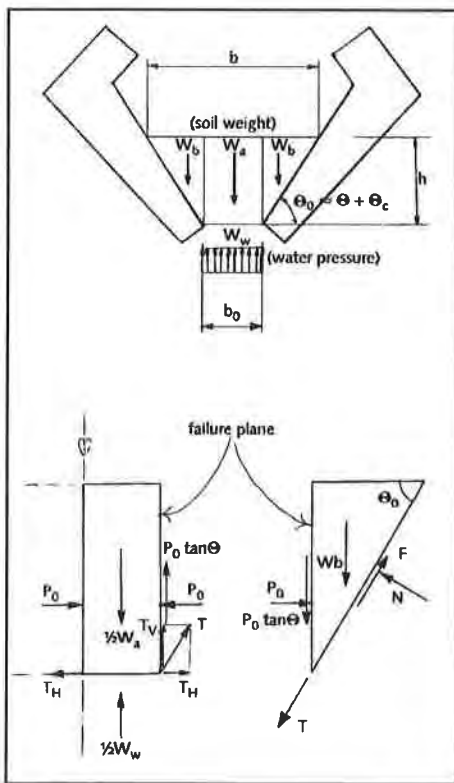
The weight of the middle and side parts of soil, and the cross-sectional area can be expressed as:

$$W_a = b_o \ h \ \gamma_s$$

$$W_b = 0.5 \ (b-b_o) \ h \ \gamma_s = 0.5 \ h^2 \ ctg\theta_o \ \gamma_s$$

$$h = 0.5 \ (b - b_o) \ tan\theta_o$$

$$A_f = V/L = 0.5 \ (b+b_o) \ h = 0.25 \ (b^2-b_o^2) \ tan\theta_o$$
or
$$b = \sqrt{4 \ A_f \ ctg\theta_o + b_o^2}$$

The equilibrium of the rectangular part in the vertical direction is:

$$T_v + P_o tan\phi = 0.5 \ (W_a - b_o w_w)$$
or
$$T_v = 0.5 \ (W_a - b_o w_w) - P_o tan\phi$$
and
$$T = \{0.5 \ (W_a - b_o w_w) - P_o tan\phi\} \ cosec\theta_o$$

Figure 4 Acting forces in the bin

The equilibrium of the triangle in the direction of the friction force F is:

$$F = W_b \ \sin\theta_o - P_o \ \cos\theta_o + P_o \ tan\phi \ \sin\theta_o + T$$

The equilibrium of the triangle in the direction of normal force N is:

$$N = W_b \ \cos\theta_o - P_o \ \sin\theta_o + P_o \ tan\phi \ \cos\theta_o$$

where P_o is the static earth pressure equal to: $P_o = 0.5 \, K \, \gamma_s \, h^2$, w_w is the water pressure in the function of loaded draft d_b, N is the normal force due to the soil pressure, F is the friction force, T is the tensile force in the geotextile, K = the coefficient of static earth pressure, and ϕ the angle of internal friction.

The criterion is that the friction force F cannot exceed μN in which μ is the friction coefficient between the geocontainer and the bin of barge. Thus,

$$F_{max} = \mu \, N$$

At the moment that F exceeds F_{max}, sliding along the barge starts and the maximum tensile force is reached.

After the hold of the split barge has begun to open, the underside of the geocontainer starts moving through the opening of the split barge. A part of the geocontainer is now hanging under the split barge. At a certain width of the split opening, the whole geocontainer falls through the opening and the falling speed increases rapidly. From this moment on the geocontainer is in a free fall. When the sand in the container is not uniformly distributed in longitudinal direction, the side of the container with the least load will usually drop first. Therefore, it is advised to fill the container with a little more sand at the both ends than in the middle. It will stimulate the horizontal sinking of the geocontainer.

The soil inside a container can be of various consistencies. As for hydraulic filling, it will be a fully-saturated soil (ρ_s = 2000 kg/m³). In the case of filling with relatively dry sand (with normal moisture), the main soil body will have a bulk density of about 1600 kg/m³. However, because there is always some leakage of water through the bottom split, the lower part of geocontainer soil will probably be saturated. The dumping process is of a short duration (a few seconds), therefore one may assume that this initial soil consistency remains nearly the same until at the moment of impact with the bottom.

In both cases, there will be a certain air pocket at the top of the geocontainer during the dumping process, that provides an additional buoyancy which may have an effect on the fall velocity and thus, on impact forces on the bottom.

This problem is much more serious in the case of filling with relatively dry sand. Then approximately 40 % of air is contained in the pores of the sand, and between the sand and the top fabric (i.e. a container with 200 m³ of dry sand may contain up to 80 m³ of air). During dumping, one or two large air pockets will be formed, which very often may cause the top seams to spring open. The reason for this is that the fabric, although sand-tight and water-permeable, is no longer able to release such a big quantity of air momentarily, and must therefore be regarded as relatively "airtight". It appeared to present major problems, particularly in the case of the thicker types of fabrics.

It is also possible that containers which remain intact during dumping may than collapse during impact with the bottom. The reason for this is also the large quantity of air that cannot be removed

immediately during the 'change of shape' which the container undergoes after impact.

Prototype observations showed that if the container had already collapsed during dumping (mostly on the sealing/closing seam), no further damage was found after impact. Where collapse occurred on the bed, damage was found on the seams at the ends and/or in the center; in most cases this damage was caused to the sealing seam. The possible collapse modes during dumping are illustrated in Figure 5.
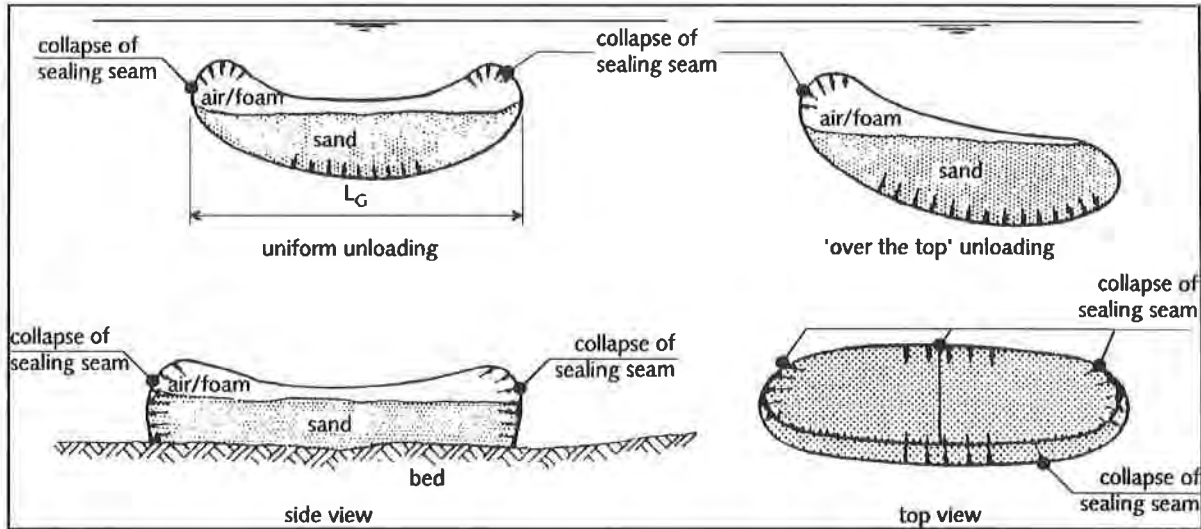
Figure 5   Possible collapse modes of geocontainers during dumping

To avoid such failures, the strong seams, special grills ("outlet valves/air vents" for air release at both ends of the geocontainer), and additional expansion seams with a proper capacity should be provided on the top of the geocontainer. It may also help to overcome the 'air problem' if the bin is placed under water after the container has been sealed. It may help to avoid air problems during dumping, and also to create conditions for more even placing. However, the replacement of air by water will increase the rate of sinking (fall velocity), and thus also the impact from landing on the bottom. In this case the high instantaneous impact pressure will be transmitted by the water into the geotextile which is too tight for the immediate release of this pressure.

The impact forces with the bottom are a function of the fall velocity (dump velocity) of a geocontainer. The derivation of the fall velocity is described hereafter.

b) The required perimeter of the geotextile enveloping the geocontainer, must be sufficiently long to resist the forces during the release of the geocontainer through a given split width b_o, at a fixed cross-sectional area of material in the geocontainer: A_f, Figures 6 and 7. The required perimeter of geotextile sheet, S_o, is given by:

$$S_0 \geq (2.5 \ to \ 4) \left(\frac{A_f}{b_0} + b_0 \right)$$

The real shape on the bottom (Fig. 7) will be more close to rectangular one for low filling grade (ϕ), while more close to the semi-oval shape for a high filling grade. Therefore the maximum height of geocontainer, a_b, in the final position will be:

$$\frac{S_0}{4}\left(1-\sqrt{1-16\,\varphi\,\phi}\right) < a_b < \frac{2\,S_0}{\pi}\left(1-\sqrt{1-14\,\varphi\,\phi}\right)$$

ϕ is the filling-grade ratio (≤ 1) and $\varphi = A_o/S_o^2$, where A_o is the maximum area of the cross-section of the split barge. These equations provide an estimation for the average number of geocontainers, required for a given structure.

c) When the geocontainer hits the bottom it reshapes. The originally vertically orientated cone transforms into a cylinder and finally reshapes into a horizontally orientated ellipse (Fig. 7).

d) The impact forces when the geocontainer hits the bottom are a function of the kinetic energy and thus the dump velocity of a geocontainer. Next to the accelerating gravity, flow resistance decelerates the geocontainer. When the gravitational force equals the flow resistance force, an equilibrium velocity is reached. This velocity (roughly 5 m/s), is:

$$V_{max} = \sqrt{\frac{2\ Vol\ (\rho_s - \rho_w)\ g}{A\ \rho_w\ C_d}}$$

Figure 6   Figure 7

with: V_{max} = equilibrium velocity [m/s], ρ_s = density of the material in the geocontainer [kg/m³], ρ_w = density of water [kg/m³], Vol = volume of geocontainer [m³], A = flow catching surface area of the geocontainer [m²], C_d=drag coefficient [-].

e) Just before touch down the geocontainer has maximum kinetic energy. This energy will be completely dissipated when the geocontainer is at rest. The main sources for energy dissipation are the work done by straining the geotextile, by reshaping the subsoil and by reshaping the material in the geocontainer.
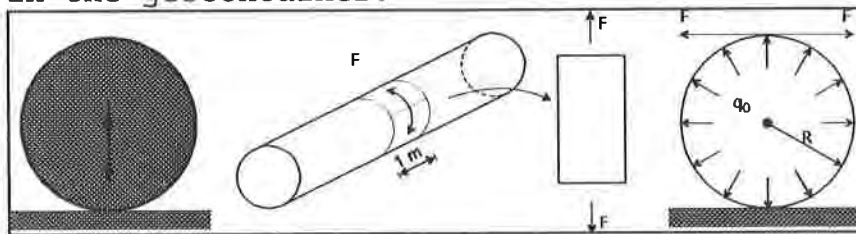
Figure 8 Schematization of impact forces
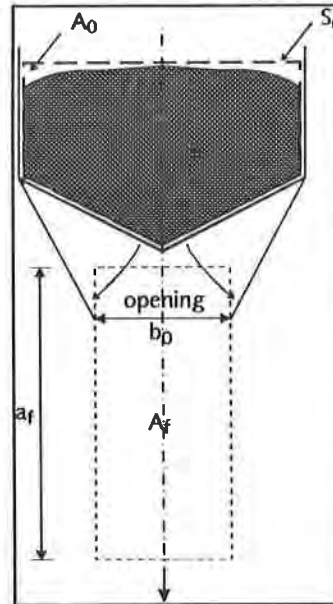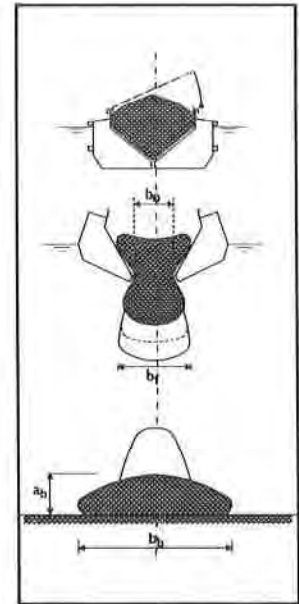
Assuming that a fraction K of the kinetic energy is dissipated by straining the geotextile, the pressure inside the geocontainer due to the impact, q_o, results in a tensile force, F, of the geotextile (Figure 8):

$$F = q_0 \, R \, L$$
$$q_0 = \sqrt{\frac{K \, Vol \, \rho_s \, v^2 \, E'}{S \, L \, R^2}}$$

with q_0 the overpressure inside the geocontainer [N/m²], Vol the volume of the material in the geocontainer [m³], ρ_s the density of the fill material [kg/m³] (ρ_s = 1600 for dry- and 2000 for saturated sand), v the velocity at touch down [m/s], E' = stiffness modulus of the geotextile [N/m], L = length of geocontainer [m], R = radius of geocontainer (=$S/2\pi$) [m], S = perimeter of geocontainer [m], and K = dissipation factor [-].

Other modes of failure due to the impact and reshaping and possible calculation methods can be found in den Adel (1996).

f) Stability tests for waves and currents have been carried out by the Delft Hydraulics using a linear scale (n_L) equal to 20 (DELFT HYDRAULICS/NICOLON, 1994). The structures tested consisted of several layers of parallelly oriented geotubes or geocontainers. These structures were meant to simulate a breakwater. A so-called 4-3-2 structure was applied: four containers or tubes in the bottom layer, three in the next layer and two in the top layer. For comparison with standard protection units the stability will be expressed in terms of the H_s/Δ D_{eq} parameter.

Based on these small-scale investigations and on literature, the following stability criteria for geotubes can be formulated (DELFT HYDRAULICS,1973, Wouters, 1995):

- tubes on the crest (at S.W.L. or submerged) lying parallel to the axis of a breakwater:

$$H_s/\Delta \, B = 1$$

where $\Delta = (\rho_s - \rho_w)/\rho_w$, B is the width (a measure of horizontal ovality) of a tube; one may roughly assume B = 1.1 D (D is the original diameter of a tube). Note: when the crest layer consists of two tubes, artificially connected to each other, the equivalent width is equal to 2B.
- when the tube is placed perpendicularly to the axis of a breakwater the stability can be approximated by

$$H_s/\Delta \, L = 1$$

where L is the length of a tube.

Notes: sand-filled units are applicable until H_s = 1.5 m. Waves up to H_s = 2 m are allowed if the structure is of a temporary nature. Due to the absence of reinforcement in mortar filled units it is very likely that for long tubes (say longer than 3D) cracks will occur as well;

some reinforcement should be recommended or an equivalent length should be taken equal to L < (3 to 4) D.

PROTOTYPE VERIFICATION

In order to verify the theoretical model for the dissipation of the kinetic energy in geocontainers during installation, prototype test have been performed in 1994 by Nicolon and Van Oord ACZ in the Netherlands.

Two geocontainers, filled with sand (170 and 130 m^3 respectively), were dumped at water depths of 18 and 13 m respectively). Each geocontainer had a theoretical volume (of 368 m^3) with the following dimensions: length approx. 24.5 m, width approx. 5.0 m, and height approx. 3.0 m; (A_o = 15 m^2). The maximum opening of the split barge was b_o = 2.5 m. The geocontainers were made of a polypropylene woven geotextile, Geolon¨ 120. This geotextile has the following characteristics: mass = 630 g/m^2, tensile strength (warp and weft direction) = 120 kN/m, Young's modulus of elasticity, E' = 1000 kN/m, characteristic opening size O_{90} = 170 μm, and permeability = 17 $1/m^2/s$.

The geocontainer was constructed of geotextile sheets, 5 m in width. The seams between adjacent sheets had a strength of 70% of the tensile strength of the geotextile. At the top of the geocontainer three reinforced air vents have been created to diminish the expected over pressures inside the geocontainer, which occur during the dump. At the front and rear end such air vents have been applied as well. Furthermore two longitudinal expansion seams were sewn at the top of the geocontainer with the intention to diminish excess tensile strain in the geotextile during the dump of the geocontainer. After being filled, the geocontainer is closed by means of a rope and a handstitch. The front end, the rear end and one longitudinal side are sewn together. Using ρ_s = 1600 kg/m^3 the K factor in

$$q_0 = \sqrt{\frac{K \; Vol \; \rho_s \; v^2 \; E'}{S \; L \; R^2}}$$

was determined.

For the first geocontainer K = 0.16 is found. This means that only 40% of the theoretical increase in pressure is observed. Furthermore it means that 84% of the kinetic energy is dissipated in other processes. The over pressure could escape because the geocontainer was ruptured before it reached the bottom. This is the main reason for the rather low value of K. For the second geocontainer a dissipation factor K = 1.37 is found, which is too high to be true: if the theoretical model is correct, the maximum value for K is 1.0. This means that the assumptions in the model are too rough.

The tensile forces in the geotextile are derived from the pressure inside the geocontainer as measured during these tests:

$$F = q_0 \; R \; L$$

where:
F   = tangential force in cylinder   [N/m]

q_o = pressure [N/m²]
R   = radius of cylinder [m]; (2.55 m)
S   = perimeter of geocontainer [m] (16 m)

For the first geocontainer (Volume = 170 m³ of sand) the observed overpressure of 17 kN/m² results in a tensile stress of 43 kN/m, for the second geocontainer (130 m³ of sand) an overpressure of 35 kN/m², results in a tensile stress of 89 kN/m. Inspection by divers revealed that geocontainer 1 failed at the front end during the impact on the sub soil. From the observations during the test it can be concluded that the geocontainer probably failed because of a reason which is not incorporated in the theoretical model. An uneven release of the geocontainer may have resulted in failure of one of the top seams. Geocontainer 2 did not fail.

The tensile strength of the seams of the geocontainer are approximately 70% of the tensile strength of the geotextile: 70% of 120 kN/m = 84 kN/m, whereas the tensile stress in geocontainer 2 is 89 kN/m. It has to be stated that these tensile stresses are caused by impact loads. The short term tensile strength of a geotextile is usually larger than the long term strength. Therefore, the tensile strength of the seams may be higher than 84 kN/m.

Theory predicts that the value of q_o is proportional to the volume of the material in the geocontainer. The fill volume of geocontainer 1 is larger than for number 2, 170 m³ and 130 m³ respectively, so a higher tensile stress in the geotextile around geocontainer 1 is to be expected compared to #2. This higher stress might have exceeded the tensile strength of the system, leading to partial rupture. Due to this rupture, the over pressure in the geocontainer can not build up, which leads to the observed over pressures for geocontainers 1 and 2: 17 kN/m and 35 kN/m respectively.

It should be stated that the theoretical models still are rough schematizations of the reality. These models can be used to give an indicative prediction only. They are merely a first step towards a more sophisticated model. Therefore, it is necessary to gain more insight in the physics of the dumping process and to perform more tests in order to assess the validity of the model. Possible reasons for the non-validity of the model could be:

- Non cylindrical shape of the geocontainer at maximum strain,
- The geocontainer is not equally filled over its length,
- The measured pressure is a local phenomenon, and
- The short term elasticity of the geotextile is larger than 1000 kN/m.

Practical note: prototype experiments indicate that geocontainers with a volume up to 200 m³ and dumped in water of which the depth exceeds 10 m, frequently have been damaged. Failure was caused by a collapse of the seams, when a geotextile with tensile strength less than 75 kN/m was applied, whereas nearly no damage was observed when a geotextile with a tensile strength equal or more than 150 kN/m was applied. This information can be of use for the first selection of geocontainers for a specific project.

APPLICATIONS

Nicolon BV has copyrighted the name for GeoTubes and GeoContainers. Geotubes are commonly used to assist in dike and groin construction whereas geocontainers are applied in the kernel of dikes. Both are either dumped from dump trucks or bottom dump (split) barges.

Geotubes have been used extensively on the northern shores of The Netherlands for dike construction where fine-grained dredged sands are pumped into a barrier dike for subsequent hydraulic filling behind this dike. Geocontainers have been used for construction of underwaterberms and scour protection.

Tubes filled with dredged material have been applied as containment dikes in Brazil and France and more recently in the Netherlands for river training structures on the rivers Waal, and Old Meuse (Rijkswaterstaat-Nicolon, 1988) and as shoreline protection at Leybucht on the North Sea in Germany. Application of these systems is illustrated in figure 9.

Recently several geotube and geocontainer projects have been designed and constructed in the U.S.A. (Fowler and Sprague, 1993), Malaysia, The Philippines and Japan; their performance is being documented so that improved design and construction methods can be recommended.

CONCLUSIONS

The following conclusions can be drawn based on the actual developments and experience.

- Geotubes and geocontainers offer the advantages of simplicity in placement and construction, cost effectiveness, and minimal impact on the environment.
- When applying geotubes and geocontainers the major design considerations/problems are related to the integrity of the units during release and impact, the accuracy of placement on the bottom (especially at large depths), and the hydraulic stability.
- When applying this technology the manufacturer's specifications should be followed. The installation needs an experienced contractor.
- Theoretical models to calculate the dump velocity and the impact forces of geocontainer on the subsoil have been developed and calibrated with the test results. However, the theoretical model to simulate the impact forces provides until now indicative results only.
- The technologies related to geotextile systems have been utilized extensively in Europe, Northern America, Mexico, Japan and Australia, producing often successful installations but only few technical details. Some manufacturers, contractors and research institutions are inclined to protect know-how to preserve market advantages. Therefore, to effectively commercialize these technologies it is necessary to uncover the technical details. Technically the methodologies have shown to be feasible but there are still many design and constructibility uncertainties that still must be addressed.

Therefore, further improvement of design methods and more practical experience at various loading conditions is still needed.
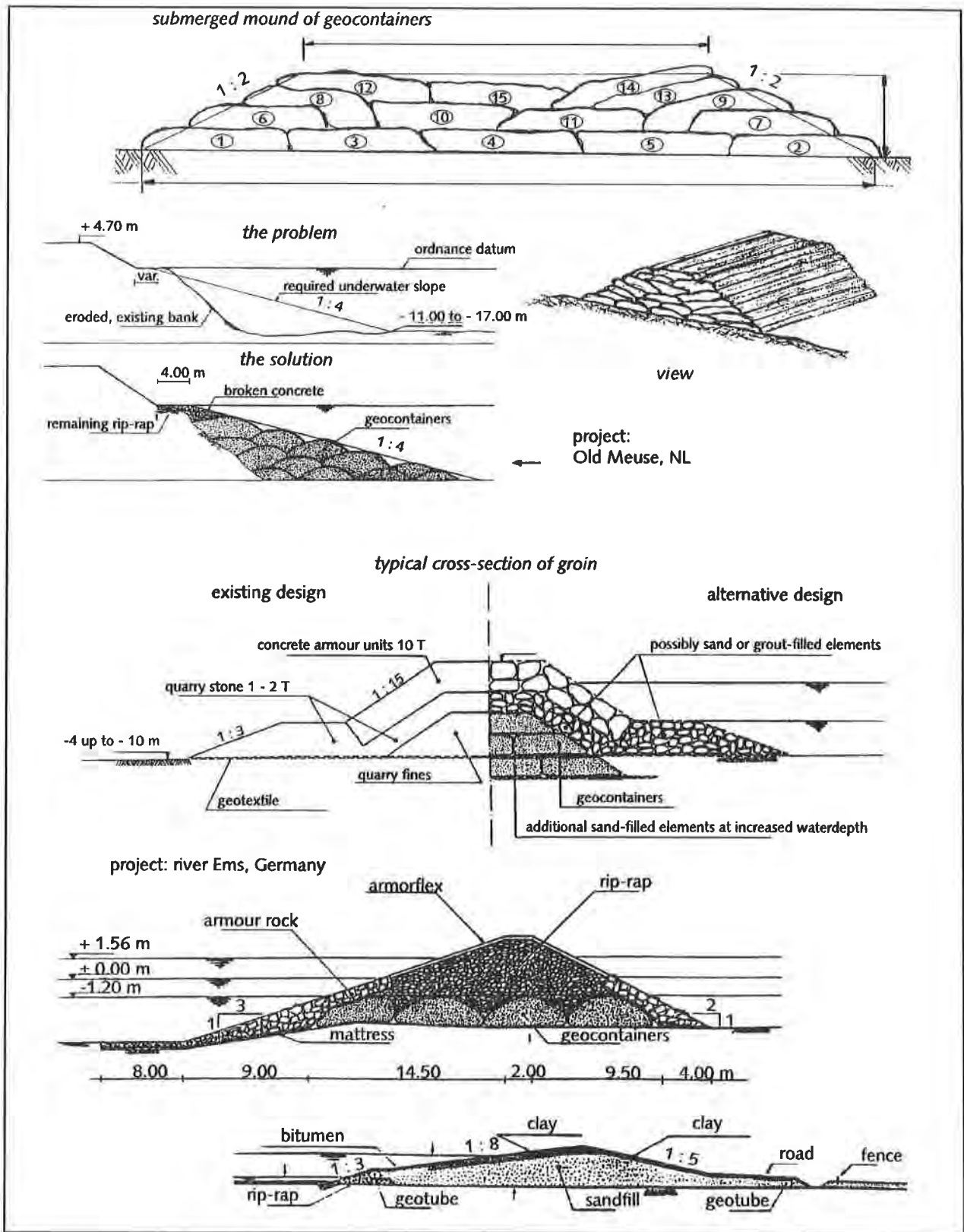
Figure 9 Examples of the placing and application of geocontainers

REFERENCES

Adel, H. den, 1996, Forces due to impact and deformation of geotubes (in Dutch), Delft Geotechnics, report CO-345040.

Adel, H. den, C.S.H. Hendrikse and K.W. Pilarczyk, 1996, Design and application of geotubes and geocontainers, Proceedings of the 1st European Geosynthetics Conference (EuroGeo), Maastricht, the Netherlands.

Delft Hydraulics Laboratory, 1973, Breakwater of concrete filled hoses, Report M 1085.

Delft Hydraulics/Nicolon, 1994, Stability of breakwaters constructed with Geotubes or Geocontainers, Two-dimensional model tests, Report on the model investigation, H2029.

Fowler, J. and C.J. Spraque, 1993, Dredged material filled geotextile containers, ASCE, Coastal Zone '93, New Orleans.

Leshchinsky, Dov and Leshchinsky, Ora, 1995, Geosynthetic Confined Pressurized Slurry (GeoCops): Supplement Notes for Version 1.0, May 1995 (Copyright Nicolon US).

Pilarczyk, K.W., 1995, "Novel systems in coastal engineering; geotextile systems and other methods", Rijkswaterstaat, Road and Hydraulic Engineering Division, the Netherlands.

Pilarczyk, K.W., 1996, Geosystems in hydraulic and coastal engineering - An overview, Proceedings of the 1st European Geosynthetics Conference (EuroGeo), Maastricht, the Netherlands.

Rijkswaterstaat - Nicolon, 1988, Bed protection, Old Meuse, by means of geocontainers, report VXT/HJ88.168, Publication of Nicolon B.V.

VAN OORD ACZ B,V., 1995, Test programme of geocontainers, Van Oord ACZ - Nicolon, the Netherlands.

Wouters, J., 1995, Stability of geosystems, Delft Hydraulics, report H1930/A2.95.40 (in Dutch)

Geosynthetics Durability

GEOSYNTHETICS 97 CONFERENCE
Long Beach, California USA

TEMPERATURE-DEPENDENT MULTI-AXIAL CREEP RESPONSE OF HDPE GEOMEMBRANES

S. M. MERRY
GeoSyntec Consultants, Walnut Creek, USA
J. D. BRAY
University of California, Berkeley, USA

ABSTRACT

Field-deployed geomembranes may be exposed to different temperature conditions over their design life. In this study, a multi-axial tension test apparatus, which is capable of performing constant stress creep tests, was used to evaluate temperature effects. This device subjects a test specimen to strain conditions that vary from plane strain at the clamped edges to balanced biaxial at the center. Thirty-six hour constant stress creep tests were performed on HDPE using a temperature range of 2°C to 53°C and stresses ranging from 2 MPa to 15 MPa. The experimental results indicate that at a given stress, the creep rate increases considerably at higher temperatures. Additionally, an adaptation of the Singh-Mitchell (1968) creep model, which is a rate process equation originally developed for soils, was found to characterize the observed stress-strain-time-temperature response from the constant stress creep tests over four logarithms of time.

INTRODUCTION

Geomembranes, unlike geogrids or geotextiles, are rarely designed as structural members which carry loads. Rather, the desired response for a geomembrane is to deform without failure. Hence, the ability of a geomembrane to elongate without failing is of paramount importance. However, the fact that geomembranes are not designed as structural members does not mean that once deployed, they may not be subjected to sustained loads. Numerous investigators have studied situations in which a geomembrane may be subjected to sustained loads (e.g., Giroud and Beech 1989; Koerner and Hwu, 1991; Bourdeau et al. 1993; and Merry et al. 1995). The response of a geomembrane to these loads is dependent on several factors, including stress-strain boundary conditions, rate of loading, chemical environment, and temperature.

Geomembranes deployed in field applications may be subjected to a variety of temperatures during their service life. Koerner and Koerner (1995) monitored the induced temperature of HDPE geomembranes at one municipal solid waste landfill. It was found that prior to being covered with soil, the temperature of a geomembrane may be significantly greater than the ambient temperature, particularly for a black geomembrane. However, following the first lift of waste (approximately 3 m), the geomembrane stabilized to an average temperature of 21° ± 2°C, independent of the ambient air temperature and further placement of waste. Hence, the use of a laboratory temperature of 21° ± 1°C would be appropriate for evaluating the long-term response of

HDPE for that particular case. As noted, their study was limited to one landfill. Other landfills, such as Azusa and Operating Industries, Inc. (OII), have different waste streams and consequently have been identified as having higher temperatures within the waste. While both of these landfills are currently unlined, a test liner has been constructed and is continually being monitored at Azusa. Additionally, both of these landfills, as well as other landfills, will likely have cover systems constructed in the future which may require geomembranes.

In this study, specimens of extruded HDPE from two manufacturers were subjected to constant stress creep tests using a multi-axial tension test system at temperatures ranging from 2°C to 53°C. The advantages of using a multi-axial tension test system compared to a uniaxial system have been discussed in previous studies (e.g., Koerner et al. 1990, Merry et al. 1995). To provide constant stress (as opposed to constant pressure), the computer-controlled loading algorithm was modified to systematically vary the pressure as the test specimen strains. While HDPE from only two manufacturers was used, it is felt that this study demonstrates the importance of evaluating the specific temperature conditions that a geomembrane will experience. Moreover, the testing methods and numerical modeling of the response of HDPE discussed in this study may be easily adapted to geomembranes from other manufacturers for project-specific material evaluation and design.

PREVIOUS TEMPERATURE EFFECTS STUDIES

Duvall (1993) performed constant pressure, multi-axial creep tests on 1.5 mm thick specimens of medium density polyethylene. These long-term (approximately 15,000 hour) creep tests were performed at temperatures of 23°C, 60°C, and 80°C using a 51 mm diameter apparatus. When performed at strains less than 57% (the point at which the centerline deflection is equal to the radius of the clamping ring), constant pressure multi-axial tension tests produce a condition of decreasing stress versus time; whereas a state of progressive failure due to increasing stress versus time is produced at strains greater than 57% under constant pressure conditions. Additionally, the ratio of the clamping ring diameter to specimen thickness was only 34. Nobert (1993) performed pressure controlled multi-axial burst tests using a 480 mm diameter apparatus over temperatures ranging from -25°C to 65°C. Merry (1995) performed strain controlled multi-axial tension tests using a 203 mm diameter clamping ring over temperatures ranging from about 13°C to 32°C. These studies found that both the initial secant modulus and the maximum stress decreased as the temperature increased.

MULTI-AXIAL TENSION TESTING

The testing system configuration used in this study is shown in Figure 1 (see Merry and Bray, 1995 for more details). A Sensotec (model MDLA15 ± 200 mm) linear variable differential transformer (LVDT) is used to measure the deflection of the geomembrane specimen at the center. The internal pressure is controlled with a pneumatic servo valve (DyVal model 10P) and is monitored with a pressure transducer (Validyne model DP15, 0-860 kPa). Process control and data acquisition during testing are controlled by an IBM-compatible PC operating Automated Testing System for Windows (ATS) software (Sousa and Chan, 1991) through a Metrabyte DAC02 and Computer Boards DAS16/330, respectively. While not shown in Figure 1, this research
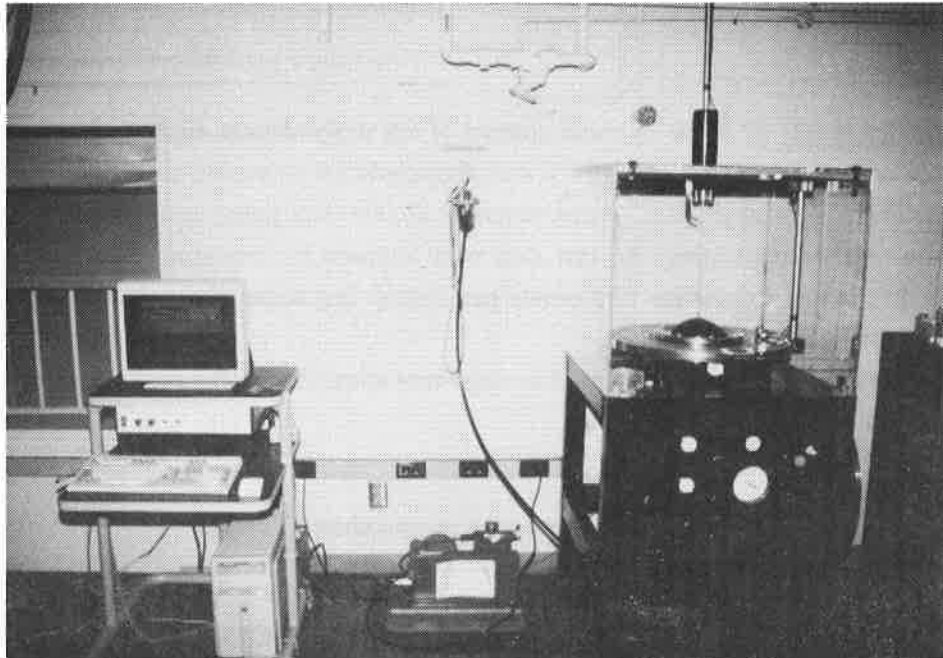
Figure 1 Multiaxial tension test system (after Merry and Bray, 1997)

was completed with the test apparatus in a temperature controlled room, which was maintained to within ±1° C and monitored with a 3-wire RTD temperature transducer.

Merry and Bray (1995) performed pressure and strain controlled multi-axial tension tests on 1.0 mm and 1.5 mm thick specimens of HDPE using clamping rings ranging in diameter from 102 mm to 508 mm at 21°C ± 1°C. It was shown that the stress-strain plots did not indicate any systematic variation as a result of the clamping ring diameter. Their study indicated that if the ratio of the diameter to the wall thickness is greater than 60 (L/t > 60), the multi-axial tension test results were indistinguishable from other test results satisfying this criteria. This study was conducted using a 203 mm diameter clamping ring with a maximum geomembrane thickness of 1.5 mm. Hence, the clamping ring diameter to material thickness ratio was at least 135, more than twice that recommended by Merry and Bray (1995).

Constant stress multi-axial tension tests were performed under controlled conditions (i.e., constant temperature during a particular test) on specimens of commercially available 1.0 mm (40 mil) and 1.5 mm (60 mil) thick smooth HDPE geomembrane. The HDPE geomembrane herein denoted as HDPE "A" is an extruded sheet, while the HDPE geomembrane herein denoted as HDPE "B" is a hybrid blown and extruded sheet. The laboratory temperature was varied for individual tests from about 2°C to 53°C, and the temperature for a particular test was maintained at ±1°C. A minimum of 24 hours of stabilization time preceded testing following a change of temperature. Approximately 15 m of air hose and a tank accumulator were used to ensure that the air supply temperature had equalized with the room temperature.

After specimen preparation (i.e., cutting out and punching of the bolt holes for the clamping ring), the test specimens were stored unrestrained in the temperature controlled room until needed. Although this condition subjected the specimens to a temperature cycle, no negative impact on the mechanical response of these specimens should be expected (Budiman and Mills, 1992). When starting a new test, a random specimen was installed on the base plate with the clamping ring on top during which time, a vacuum (<50 kPa vacuum) was applied through a vacuum port to keep the geomembrane free of wrinkles and prestressing. Clamping ring bolts

were torqued to approximately 61 N-m. A small amount of dry molybdenum disulfide (a nonreactive lubricant) was used at the contact point between the LVDT and geomembrane to ensure that shear stresses between the LVDT and geomembrane were negligible. Approximately 20,000 data points were taken from the initiation of the test until failure. Following testing, the raw data were reduced by averaging blocks of data to one point. Blocks sizes were determined to provide five points per quarter log scale of time. Constant stress tests were terminated after 36 hours.

An equation used to calculate the induced average true stress during the multi-axial tension test has been presented previously (Merry et al. 1993):

$$\sigma = \frac{(L^2 + 4\delta^2)^2 \ p}{16 \ \delta \ L^2 \ t} \qquad \text{for all } \delta \text{ and constant geomembrane volume} \qquad (1)$$

Koerner et al. (1990) presented Eq. (2) for calculation of the strain when $\delta < L/2$ and Merry et al. (1993) presented Eq. (3) for calculation of the strain when $\delta \geq L/2$.

$$\varepsilon(\%) = \left[\frac{\tan^{-1}\left(\frac{4L\delta}{L^2 - 4\delta^2}\right)\left(\frac{L^2 + 4\delta^2}{4\delta}\right) - L}{L} \right] \times 100\% \qquad \delta < L/2 \qquad (2)$$

$$\varepsilon(\%) = \left[\frac{\left(\frac{L^2 + 4\delta^2}{4\delta}\right)\left(\pi - \sin^{-1}\left(\frac{4L\delta}{L^2 + 4\delta^2}\right)\right) - L}{L} \right] \times 100\% \qquad \delta \geq L/2 \qquad (3)$$

where: σ is the in-plane stress, (kPa); p is the internal pressure, (kPa); L is the inside diameter of the clamping ring, (m); δ is the centerline deflection, (m); t is the geomembrane thickness prior to testing, (m); and ε is the strain with respect to the constrained diameter. Some of these terms are also shown in Figure 2.

Previous studies (e.g., Duvall, 1993; Merry et al. 1993) have suggested that polymeric materials such as HDPE and PVC are better represented as incompressible (constant volume) materials, and hence, Eq. (1) is appropriate for this study. It may be shown that Eqs. (2) and (3) provide identical results to equations presented by Giroud et al. (1990) and Giroud (1995) for the calculation of geomembrane strain assuming that the membrane deforms as a portion of a sphere (Merry 1995). These equations are based on the geomembrane deforming as a portion of a sphere, which is a reasonably appropriate assumption when properly designed clamping
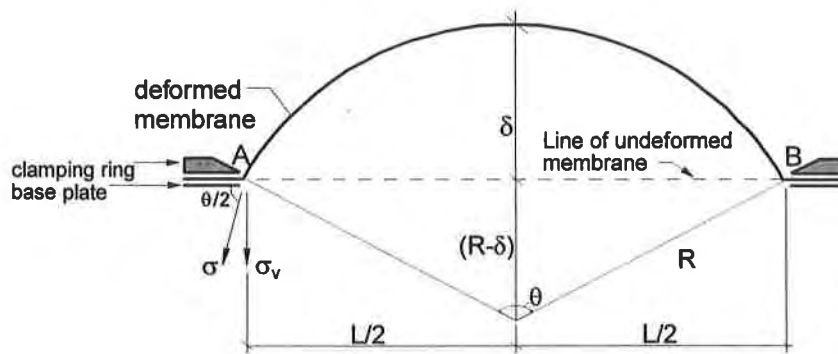
Figure 2 Multi-axial tension test boundary conditions and deformed geometry when $\delta < L/2$
(after Merry and Bray, 1997)

rings are used as described in Merry and Bray (1995). Hence, these equations are recommended for interpreting the data taken during the multi-axial tension test in lieu of those included in the current ASTM D 5617-94 standard test method which contains discrepancies as identified in Merry et al. (1993).

CONSTANT STRESS CREEP TESTING

HDPE specimens were subjected to 36 hour constant stress creep tests to evaluate the stress-dependent creep of HDPE geomembranes at different temperatures. To provide constant stress, the ATS software was modified so that the pressure would vary systematically as the deflection increased due to creep. Eq. (1) may be rearranged so that the internal pressure is expressed explicitly as a function of the desired constant stress as follows:

$$p = \frac{16\,L^2\,\delta\,t\,\sigma}{(L^2 + 4\delta^2)^2} \tag{4}$$

Values of the test constants (i.e., clamping ring diameter (L), material thickness (t) and the normal stress (σ)) are input prior to beginning of a particular test. After receiving closed-loop feedback from the LVDT for the current value of the centerline deflection (δ), Eq. (4) is evaluated by the process control system to update the target pressure required to maintain constant stress. Eq. (4) is evaluated throughout the test at a frequency of 2 Hz, although the software continually tries to obtain the current target pressure by sending an error signal to the servo valve at a frequency of 500 Hz. Figures 3-a through 3-f show the experimental stress-time relationships for several constant stress creep tests on HDPE "A" specimens. Because the DyVal servo valve was sensitive to temperature, lower gains had to be used at lower temperatures, which resulted in a slightly decreasing stress-time response. Nevertheless, using this control algorithm, the maximum standard deviation of stress for any single creep test was less than 0.25 MPa, and above 32°C, was less than 0.15 MPa.

As discussed previously, Duvall (1993) presented data from long-term creep tests on specimens of medium density polyethylene using constant pressure within the vessel.   Examination of Eq. (1) indicates that at
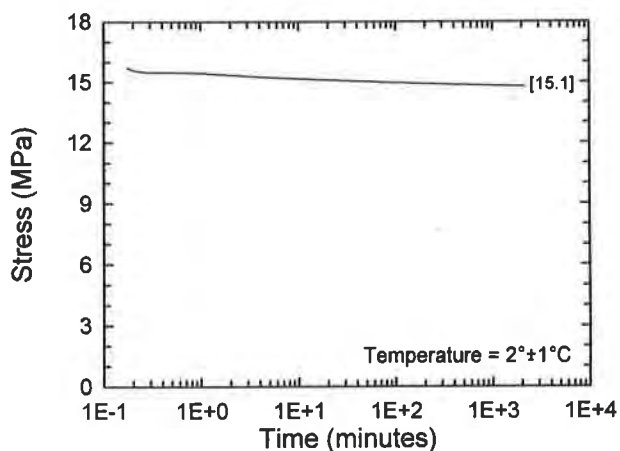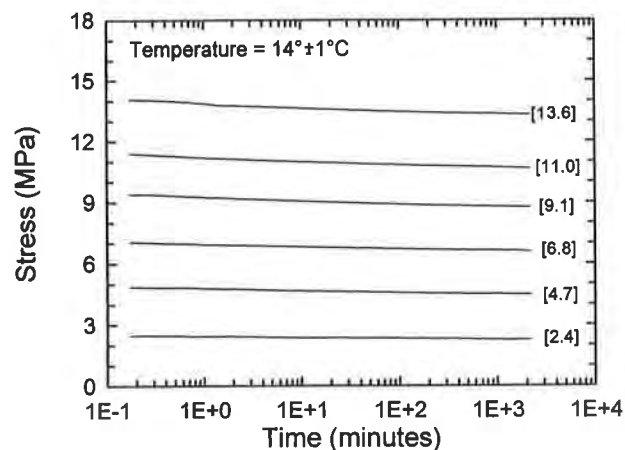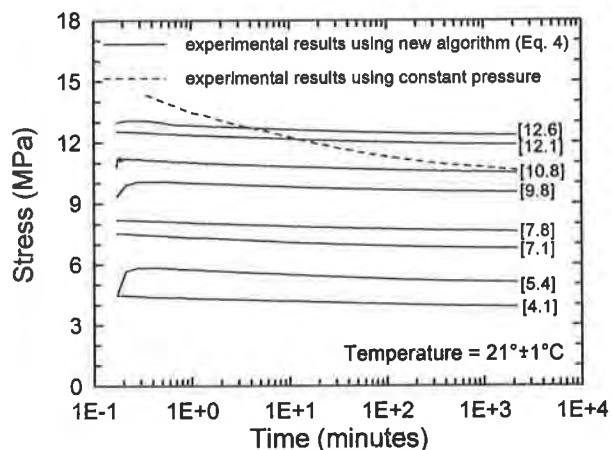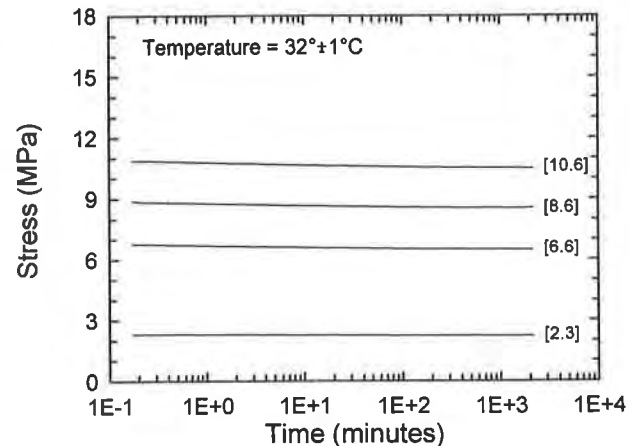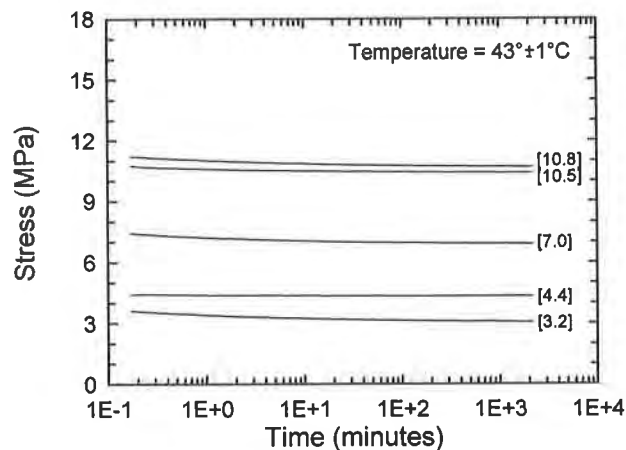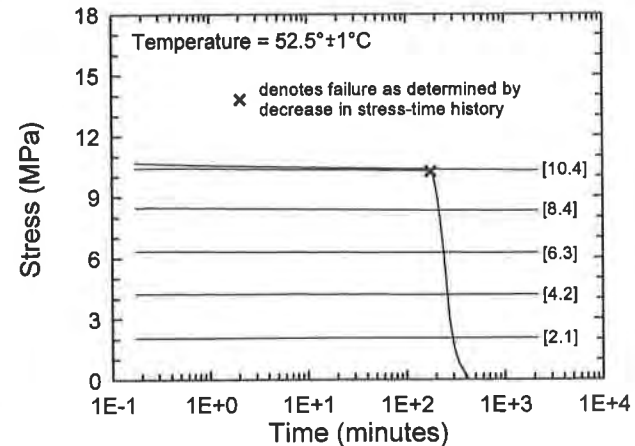
Figure 3 Experimental results of stress versus logarithm of time from multi-axial constant stress tests on HDPE "A" at (a) 2°C, (b) 14°C, (c) 21°C, (d) 32°C, (e) 43°C, (f) 52.5°C. Nominal stress during test shown in [ ].

constant pressure (p), the geomembrane stress (σ) decreases with increasing centerline deflection due to time-dependent creep. Figure 3-c also shows the stress-time history for a 36 hour constant pressure test. It is seen that the stress in the geomembrane continually decreases throughout the test, which results in underpredicting the creep strain with respect to the average stress during the test, which is an unconservative error. Berg and Bonaparte (1993) subsequently used Duvall's published results to establish guidelines for the allowable long-term performance of HDPE. Because these guidelines are based on an unconservative error, it is recommended that their findings be re-evaluated using results from long-term constant stress creep tests.

EXPERIMENTAL RESULTS

The results of accumulated strain versus logarithm of time at each temperature are shown as solid lines in Figures 4-a through 4-f. The dashed lines are numerical predictions of the experimental results which will be discussed later in this paper. From these results, several items are noteworthy. First, as the temperature is lowered, HDPE exhibits a stiffer response, which is consistent with the studies discussed previously. Third, Figure 4-a shows that a specimen induced to a stress of 15.1 MPa and a temperature of 2°C accumulated less than 8 percent strain and remained stable. Yet, a similar specimen induced to a stress of only 10.4 MPa at a temperature of 52.5°C (Figure 4-f) reached a strain of 20 percent and subsequently failed. Additionally, Figure 4-f demonstrates that a specimen that is subjected to a high enough stress level at a given temperature may accumulate sufficiently large creep strains to cause the creep rate to suddenly accelerate and consequently fail (see curves with induced stress equal to 10.4 MPa). This observation is also consistent with data from creep tests on geogrids presented by McGown et al. (1985).

It is also observed that the strain versus logarithm of time response for these thirty-six hour constant stress creep tests differs above and below about 30°C, with the strain versus logarithm of time decaying at temperatures above 30°C and accelerating at temperatures below 30°C. For the tests below 30°C , it is possible that the strain rate would decrease eventually decrease if left on test for sufficient time. However, it is also possible that the accelerating strain rate could continue, leading to failure. This could help explain why environmental stress cracking (ESC) of HDPE is so prevalent in cold weather applications. This observation is important and because it is not completely understood, further investigation is warranted.

Figure 4-f shows the results of five tests performed (4 HDPE "A" and 1 HDPE "B") at about the same stress (10.4 MPa) and the same temperature (52.5°C). Although these tests were subjected to the same stress and temperature, some differences are noteworthy. One of the test specimens failed after less than 200 minutes, three specimens continued to the end of the test without physical signs of distress, although the logarithmic creep rates for these tests were clearly increasing at the end of the test, and the last (HDPE "B") continued to the end of the test showing no signs of increased logarithmic strain rate. This slight difference is the first significant difference noted in the mechanical response of the geomembranes from these two manufacturers, as previous studies (e.g., Merry et al. 1995) found virtually no systematic difference in the stress-strain responses of these two geomembranes.

Many construction quality assurance specifications require that geomembrane deployment be stopped when the temperature reaches some value, typically 40°C. Figures 5-a and 5-b show the results of tests performed
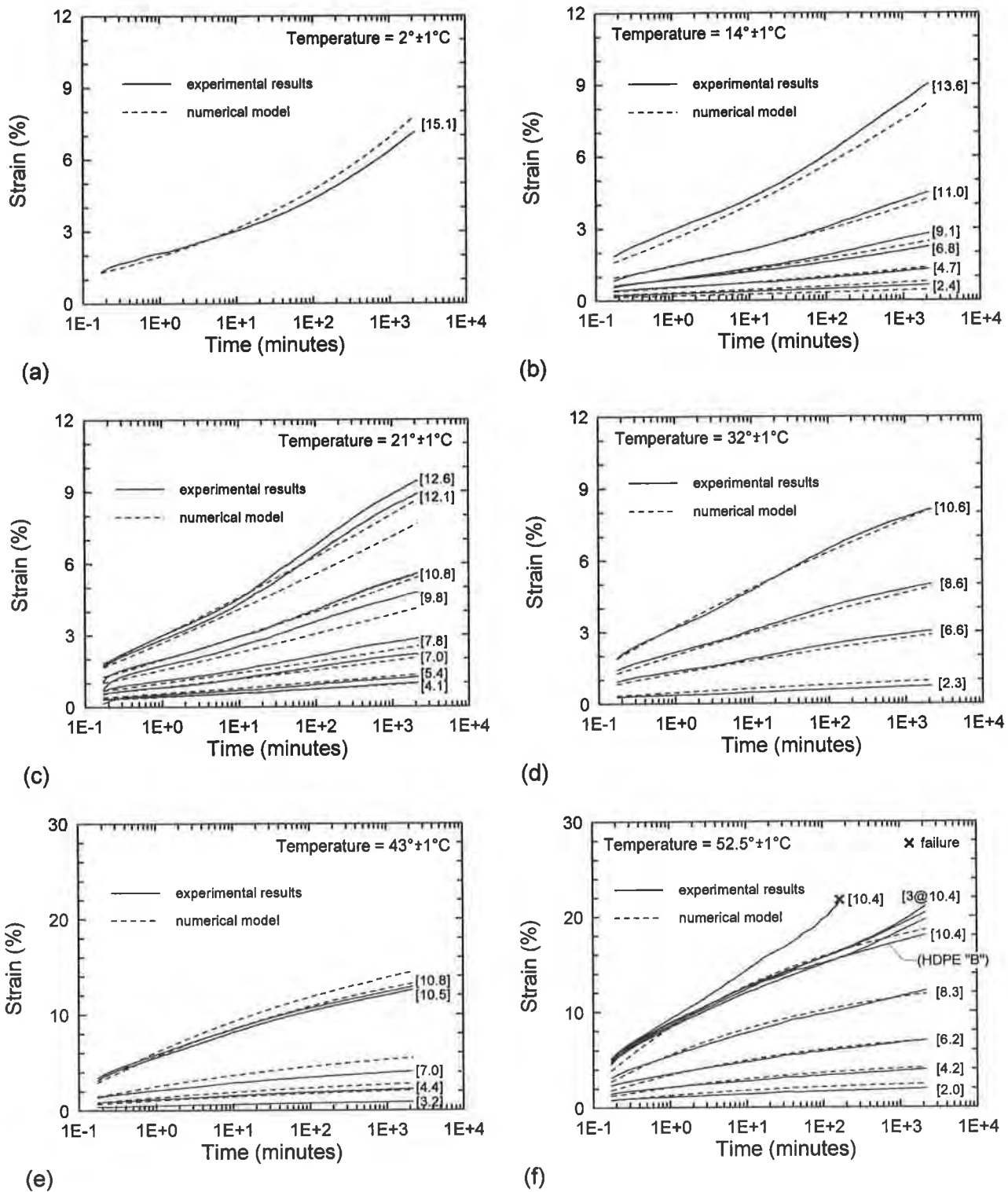
Figure 4 Experimental results of strain versus logarithm of time from multi-axial constant stress tests on HDPE "A" at (a) 2°C, (b) 14°C, (c) 21°C, (d) 32°C, (e) 43°C, (f) 52.5°C. Nominal stress during test shown in [ ].
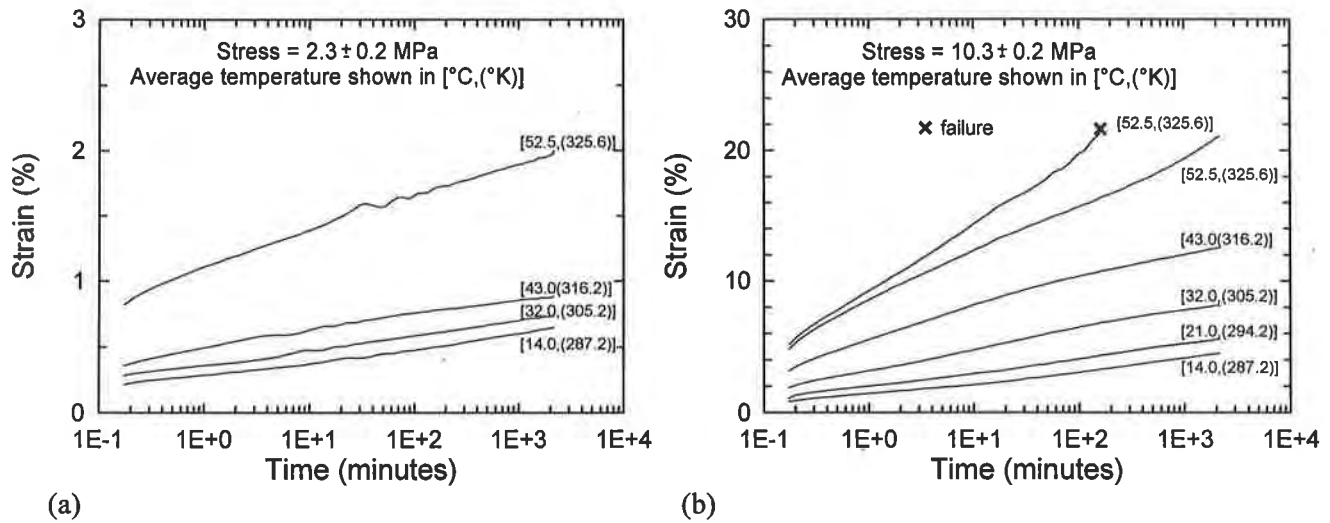
Figure 5 Strain versus logarithm of time from multi-axial constant stress tests at different temperatures on HDPE "A" at: (a) 2.3 MPa and (b) 10.3 MPa stress.

at a stresses of about 2.3 MPa and 10.4 MPa, respectively at different temperatures. These two figures support this specification and further emphasize the importance of evaluating the temperature conditions that will be expected both during installation and the active design life. For example, assuming a geomembrane thickness of 1.5 mm (60 mils), a crew pulling on the edge of a sheet during installation with a modest force of 20 lb/ft (292 N/m) will induce a stress of about 2.3 MPa. Now assume that the installation is performed in the heat of the day (temperature of the geomembrane is about 50°C) and it takes about 2 minutes to position the sheet. Under these conditions, it is possible that more than 1% strain could be induced (see Figure 5-a), which is about 20% of the total allowable strain if the desired strain limit in the field is 5%. As another example, a design engineer might calculate that a design is reasonable for an assumed temperature of 21°C and an induced stress of about 10 MPa. If the temperature in the field is significantly higher, the long-term performance of the liner system could be quite different, including the possibility of failure (see Figure 5-b).

NUMERICAL REPRESENTATION OF EXPERIMENTAL RESULTS

Singh and Mitchell (1968) presented the formulation of a mathematical equation for modeling the creep rate of soils. The three parameter mathematical model was derived as (Singh and Mitchell, 1968):

$$\varepsilon = \varepsilon_1(\sigma) + \frac{A}{1-m} e^{\alpha D} \left[t^{1-m} - 1 \right] \tag{5}$$

In this equation, the deviatoric stress (D) is the in-plane stress within a geomembrane during a multi-axial tension test, and ε_1 is the stress-dependent strain at time t=1 (in this case, 1 minute). For HDPE at constant temperature, the values of m, α, and A are constants. To find the parameters A, α, and m, the methods outlined by Singh and Mitchell (1968) were used as a first approximation followed by regression in a spreadsheet to refine the values

such that the overall error with respect to the observed experimental results was minimized. While a previous study (Merry and Bray, 1997) found that this equation captures the stress-dependent creep well over 4 logarithms of time, in this study, this equation was modified further to include the effects of temperature. Hence, Eq. (5) was modified by letting the parameters ε_1, m, α, and A become functions of the absolute temperature, (°K) as:

$$\varepsilon = \varepsilon_1(\sigma, {}^{\circ}K) + \frac{A({}^{\circ}K)}{1 - m({}^{\circ}K)} e^{\alpha({}^{\circ}K)D} \left[t^{1-m({}^{\circ}K)} - 1 \right] \tag{6}$$

Figure 6-a shows the relationship between the applied geomembrane stress and the value of the strain at 1 minute for HDPE "A" over the range of temperatures included in this study. While this plot shows some scatter and inconsistencies, particularly at lower stresses, the data do follow a systematic and distinct trend where the strain at minute (ε_1) increases with increasing stress or increasing temperature. Values of ε_1, m, α, and A were determined (as previously discussed) that best captured the results at each temperature. These values, which are

(a)

(b)

(c)

(d)
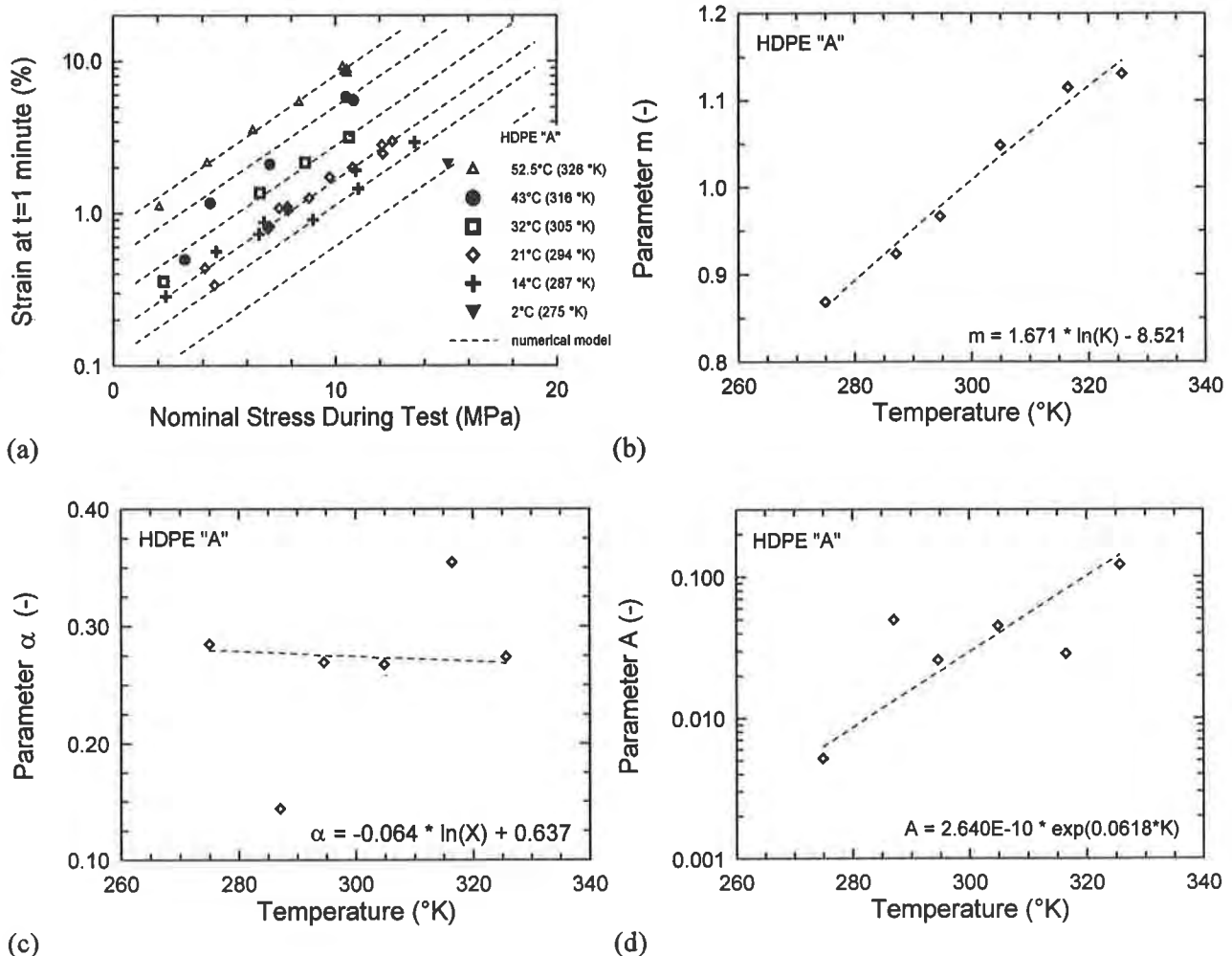
Figure 6 Temperature-dependent parameters for modified Singh-Mitchell creep model including: a) strain at time t=1, ε_1, b) parameter m, c) parameter α, and d) parameter A

presented in Table 1, were then plotted as a function of temperature and a best-fit line drawn through the data. These plots are shown in Figures 6-b through 6-d. The experimental data shown in Figures 4-b and 4-e show several test results that are inconsistent with each other and testing errors are suspected in some of the tests. Hence, the values of α and A from these two temperatures were omitted in determining the best-fit lines shown in Figures 6-c and 6-d.

The final best-fit equations for these parameters are presented in Table 2. The dotted lines shown in Figures 4-a through 4-f show the results of using Eq. (6) to represent the strain-time-temperature relationships that were obtained from the experimental creep tests for HDPE "A". Eq. (6) is seen to capture the observed results reasonably well over 4 logarithmic periods of time for stresses from 2 to 15 MPa, and at temperatures from 2°C to 15°C. Table 2 indicates that each of the parameters are temperature dependent. This provides further emphasis on the importance of evaluating the temperature conditions of where the geomembrane will ultimately be deployed if the long-term durability is to be reliably estimated. Additionally, if a more accurate fit is desired at a specific temperature, the values from Table 1 may be directly substituted in Eq. (5). Figures 7-a and 7-b show the generality of this numerical model by applying the parameters that were developed for HDPE "A" to model the experimental results obtained for HDPE "B". The quality of the fit is similar to that observed for HDPE "A" for over 4 logarithms of time.

Table 1. Singh-Mitchell model (Eq. 5) parameters used for HDPE geomembranes at each temperature

Temperature	Parameter		
(°C, °K)	m	α	A
1.7, 275	0.863	0.280	6.30E-03
13.9, 287	0.935	0.277	1.33E-02
21.4, 295	0.978	0.276	2.12E-02
31.7, 305	1.036	0.274	4.00E-02
43.3, 316	1.098	0.271	8.19E-02
52.5, 326	1.146	0.269	1.45E-01

Table 2. Equations used to predict modified Singh-Mitchell model (Eq. 6) parameters as a function of temperature and stress

Parameter	HDPE 'A'
A	$2.640E\text{-}10 \ \exp(0.0618 \ °K)$
α	$-0.064 \ \ln(°K) + 0.637$
m	$1.671 \ \ln(°K) - 8.521$
ε_1	$5.065 \exp(0.051 \ °K + 0.231 \ \sigma)$
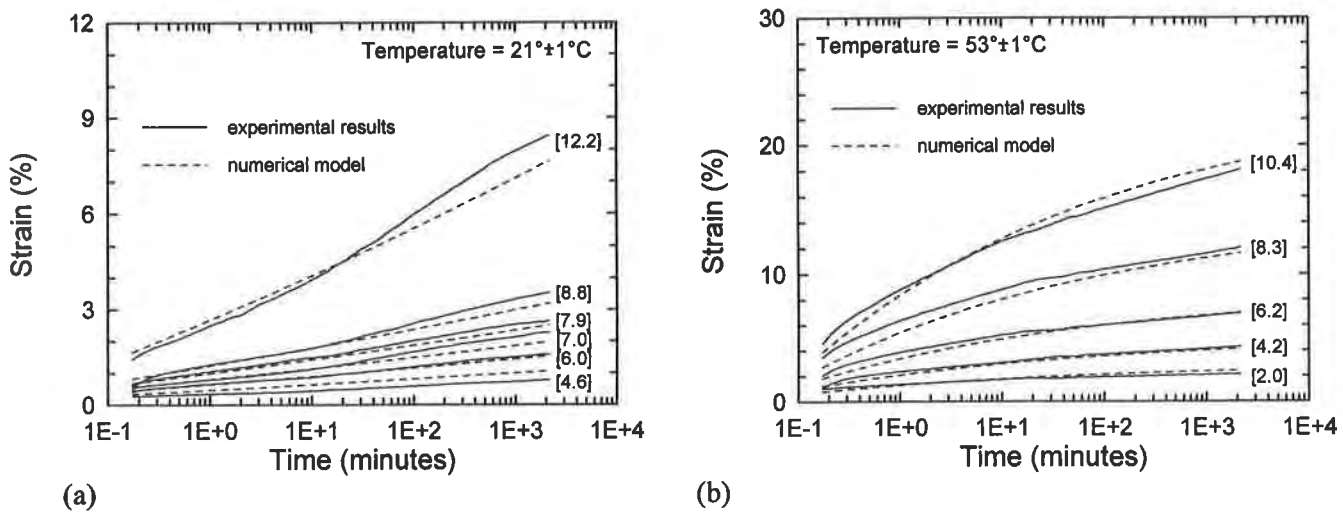
Figure 7 Multi-axial constant stress creep tests results for HDPE "B" at: (a) 21°C, (b) 53°C.
Nominal stress during test shown in [ ].

CONCLUSIONS

Geomembranes may be subjected to a range of temperature conditions over their design life. Installation, drag down on slopes, and differential settlement may induce stresses into these geomembranes. Hence, an understanding of the stress-strain-time-temperature response of geomembranes is an important design consideration. To evaluate the stress-dependent creep of HDPE, thirty-six hour duration constant stress multi-axial tension tests were performed on specimens of HDPE from two manufacturers under controlled temperature conditions. For these tests, the stress ranged from about 2 to 15 MPa, and the temperature ranged from 2°C to 53°C. The control software of the multi-axial system was modified so that the internal pressure was adjusted as the centerline deflection increased due to creep. This modification resulted in a constant stress-time relationship compared to creep tests performed previously at constant pressure in which the stress decays with time.

The results of these tests indicate that at as the temperature increases, the response of the geomembrane softens significantly. For these thirty-six hour constant stress creep tests, the strain versus logarithm of time response differs above and below about 30°C, with the strain versus logarithm of time decaying at temperatures above 30°C and accelerating at temperatures below 30°C. However, it is possible that below 30°C, an attenuating response would occur given sufficient time on test. Longer tests at temperatures below 30°C should be performed to investigate this as this has important implications on both the use of high temperature accelerated tests to investigate the durability of geomembranes and the observed phenomenon of cold-weather environmental stress cracking. At low temperatures, a geomembrane may appear to be stable at a given stress, however, at high temperatures and the same stress, creep rupture may occur even within 36 hours. Although the response of the two HDPE materials tested were quite similar, differences at high temperatures (53°C) and stress levels (10 MPa) were apparent, which suggests that project specific material evaluations are appropriate. In general, these results provide further evidence that for testing and design, stress-strain-time-temperature-chemical

compatibility should always be considered. Lastly, it was found that a modified Singh-Mitchell (1968) creep model, originally formulated for soils, captures the temperature-dependent creep of HDPE over a temperature range of 2°C to 53°C , a large range of stresses, and more than four log cycles of time. This model further emphasizes the importance of evaluating the temperature conditions that will be expected in the field as the four parameters used in this model are all temperature dependent. Additionally, a more accurate representation may be achieved through calibrating the parameters at the desired temperature.

ACKNOWLEDGMENTS

REFERENCES

American Society for Testing and Materials (ASTM), (1994). Standard Test Method for Multi-Axial Tension Test for Geosynthetics, D 5617-94, ASTM, Philadelphia, Pennsylvania.

Berg, R.R. and Bonaparte, R., (1993). "Long-Term Allowable Tensile Stresses for Polyethylene Geomembranes." *Geotextiles and Geomembranes*, 12(4), 287-306.

Budiman, J., and Mills, W.C., (1992). "Effects of Temperature Cycle on Embrittlement of Geomembrane." Environmental Geotechnology, Usmen and Acar, Y., editors, 237-241.

Bourdeau, P.L., Ludlow, S.J., and Simpson, B.E., (1993). "Stability of Soil-Covered Geosynthetic-Lined Slopes: A Parametric Study." in Proceedings, Vol. 3, *Geosynthetics '93*, Vancouver, B.C., Canada, IFAI, St. Paul, MN., 1511-1522.

Duvall, D. E., (1993). "Creep and Stress Rupture Testing of a Polyethylene Geomembrane Under Equal Biaxial Stress." in Proceedings, Vol. 2, *Geosynthetics '93*, Vancouver, B.C., Canada, IFAI, St. Paul, MN., 817-830.

Giroud, J.P., and Beech, J., (1989). "Stability of Soil Layers on Geosynthetic Lining Systems." in Proceedings, Vol. 1, *Geosynthetics '89*, San Diego, CA., USA, IFAI, St. Paul, MN., 35-46.

Giroud, J. P., Bonaparte, R., Beech, J. F., and Gross, B. A. (1990). "Design of Soil Layer-Geosynthetic Systems Overlying Voids," Journal of *Geotextiles and Geomembranes*, Vol. 9, Nos. 1, pp. 11-50.

Giroud, J. P. (1995). "Determination of Geosynthetic Strain Due to Deflection," Journal of *Geosynthetics International*, International Geosynthetics Society, Vol. 2, No. 3, pp. 635-641.

Koerner, G. R., and Koerner, R. M., (1995) "Temperature Behavior of Field Deployed HDPE Geomembranes," in Proceedings, Volume 3, *Geosynthetics '95*, Nashville, TN., USA, IFAI, St. Paul, MN., pp. 921-937.

Koerner, R. M., Koerner, G. R., and Hwu, B., (1990). "Three Dimensional Axisymmetric Geomembrane Tension Test." Geosynthetic Testing for Waste Containment Applications, ASTM STP 1081, Robert M. Koerner, editor, American Society for Testing and Materials, Philadelphia, PA, 170-184.

Koerner, R. M., and Hwu, B., (1991). "Stability and Tension Considerations Regarding Cover Soils on Geomembrane Lined Slopes." Journal of *Geotextiles and Geomembranes*, Vol. 10, Nos. 5-6, pp. 335-355.

Merry, S. M., Bray, J. D. and Bourdeau, P. L., (1993). "Axisymmetric Tension Testing of Geomembranes." ASTM, *Geotechnical Testing Journal*, GTJODJ, 16(3), Sept., 384-392.

Merry, S. M., Bray, J. D., and Bourdeau, P. L. (1995). "Stress-Strain Compatibility of Geomembranes Subjected to Out-of-Plane Subsidence." in Proceedings, Vol. 2, *Geosynthetics '95*, Nashville, TN., USA, IFAI, St. Paul, MN., Feb. 24-26, 799-812.

Merry, S. M., and Bray, J. D., (1995). "Size Effects for Axisymmetric Testing of Geomembranes." ASTM, *Geotechnical Testing Journal*, GTJODJ, 18(4), Dec., 441-449.

Merry, S. M., and Bray, J. D., (1997). "Time-Dependent Mechanical Response of HDPE Geomembranes." ASCE, *Journal of Geotechnical and Geoenvironmental Engineering*, Vol. 123, No. 1, Jan., 57-65.

Merry, S. M., (1995). "Mechanical Response and Properties of Geomembranes." Ph.D. Thesis, University of California, Berkeley, CA, 94720, 486 pages.

McGown, A., Andrawes, K.Z., Yeo, K.C., and DuBois, D., (1985). "The Load - Strain - Time Behaviour of Tensar Geogrids." Proceedings of the Symposium on Polymer Grid Reinforcement in Civil Engineering, Thomas Telford, editor, London, England, March, 11-17.

Nobert, J., (1993). "The Use of Multi-Axial Burst Test to Assess the Performance of Geomembranes." in Proceedings, Vol. 2, *Geosynthetics '93*, Vancouver, B.C., Canada, IFAI, St. Paul, MN., 685-702.

Singh, A. and Mitchell, J. K., (1968). "General Stress-Strain-Time Function for Soils." *J. of the Soil Mech. and Foun. Div.*, ASCE, 94(SM1), Jan., 21-46.

Shelton, W.S., and Bright, D.G., (1993). "Using the Arrhenius Equation and Rate Expressions to Predict the Long-Term Behavior of Geosynthetic Polymers." in Proceedings, Vol. 2, *Geosynthetics '93*, Vancouver, B.C., Canada, IFAI, St. Paul, MN., 789-802.

Sousa, J., and Chan, C. K. (1991). "Computer Applications in the Geotechnical Laboratories of the University of California, at Berkeley." in Proceedings, Vol. 1, ASCE Geotechnical Engineering Congress, Boulder, CO, 531-543.

LONG TERM RELATIONSHIP OF OUTDOOR EXPOSURE TO XENON-ARC TEST APPARATUS EXPOSURE

Thomas L. Baker, P.E.
Amoco Fabrics and Fibers Co.

ABSTRACT

The xenon-arc test apparatus (XWOM) exposure is a common accelerated test used to provide insight into the resistance of a geotextile to ultraviolet light degradation. This paper examines the long term effects of both outdoor and XWOM exposure on polypropylene, nonwoven geotextiles to develop a relationship between the two methods of exposure. Samples of three different weights of geotextile were exposed in both the xenon-arc test apparatus (XWOM) and outdoors at South Florida. The outdoor samples were exposed for incremental periods up to a year. A companion set of samples were exposed in an XWOM for periods up 3000 hours. The results of the exposures were evaluated and plotted based on the strength retained as a function of the ultraviolet radiant exposure. An examination was also made of the effect of temperature during the exposure. This was accomplished by exposing samples in an XWOM at temperatures above and below the standard temperature.

INTRODUCTION

A geotextile may be expected to survive a number of environmentally related challenges with regards to durability. One of these is its ability to withstand degradation due to sunlight, particularly the ultraviolet (UV) wavelengths in the sunlight. Because the effects of the sunlight can take an extended period to begin to be apparent in outdoor testing, an accelerated test method is desirable. Several methods of performing accelerated weathering of geotextiles are available. The period over which the geotextile will be exposed may also be uncontrolled during construction of a project. This paper focuses on the xenon-arc test apparatus (XWOM) as a method of accelerated weathering and its relationship to outdoor exposure over an extended period. The goal of this work is first to establish whether a correlation between xenon-arc test apparatus (XWOM) exposure and outdoor exposure exists and second to attempt to quantify that relationship.

Based on observations of performance of geotextiles, there appears to be an interaction between the UV exposure and temperature during exposure. The relationship of this interaction is not clearly defined. This work also made an attempt to examine the relationship between temperature and UV exposure.

The intensity of the light outdoors can vary through the year, from season to season. To perform the analysis for this study without being substantially affected by change in season it is necessary to normalize the exposure conditions. Therefore, this work is based on the light energy experienced by the geotextiles and not the time duration of exposure. The light energy is expressed as radiant exposure over a given span of wavelengths. For weathering of plastics the wavelengths of concern are usually the ultraviolet range (UV) generally taken as from 295 to 385 nanometers (nm). Radiant exposure is usually measured in mega Joules per square meter (MJ/m^2).

PROCEDURE

Geotextile Samples. To limit the number of potential variables, the work used only polypropylene, staple fiber, needle punched nonwoven geotextiles. The geotextiles included weight classes of 135 gm/m^2, 270 gm/m^2, and 406 gm/m^2 (4, 8, and 12 ounces per square yard). For each weight class there were six different subsets. The principal difference between the subsets was the source of the polypropylene resin. For each exposure period of a subset, four specimens were precut and mounted on a white cardboard backing. In each weight class subset four unexposed specimens were tested to determine a control strength.

To minimize variability, the unit weight of the specimens was carefully controlled. The unit weight of each of the four individual specimens for an exposure was within 10% of the target weight. The average unit weight of the four specimens for an exposure was less than 5% off of the target unit weight.

As mentioned, the main difference between the six subsets was the resin used to make the geotextile. All the resins contained a modest amount of hindered amine light stabilizer to which carbon black was added during production of the fiber. The fiber used in all of the fabrics was a 5 denier staple.

Outdoor Exposure. The outdoor samples were exposed by the South Florida Test Service at Miami, Florida from November 8, 1993 through November 8, 1994. South Florida is a frequently used reference for outdoor exposure in the textile industry. The conditions of exposure at South Florida are relatively harsh compared to most areas. A generalized relationship of radiant exposure for the world, adapted from Van Wijk and Stoerzer, compared to South Florida is shown in Figure 1. The figure does not take into account potential variations due to temperature or humidity. Based on Figure 1, South Florida exposure can be considered a relatively severe exposure condition for most of the world and the United States in particular.

The procedure used for the exposure included attaching precut 50 mm by 150 mm specimens to white blotter cardboard. The cardboard was, in turn, attached to frames pointed due south and at an angle of 45° to horizontal. The samples were exposed to the elements and not placed under glass. Sets of samples were returned and tested at intervals of 1, 2, 4, 6, and 12 months

The South Florida Test Service measured the exposure conditions during the study. Among other things they report the rainfall, temperature, total radiant exposure and total ultraviolet radiant exposure during the periods of exposure. The cumulative total ultraviolet radiant exposure between 295 nm and 385 nm, average monthly temperature, and cumulative rainfall measured for the periods of interest for this study are contained in Table 1.

GLOBAL COMAPRISON TO SOUTH FLORIDA IRRADIANCE

	< 80% Of South Florida
	80% to 120% Of South Florida
	> 120% Of South Florida
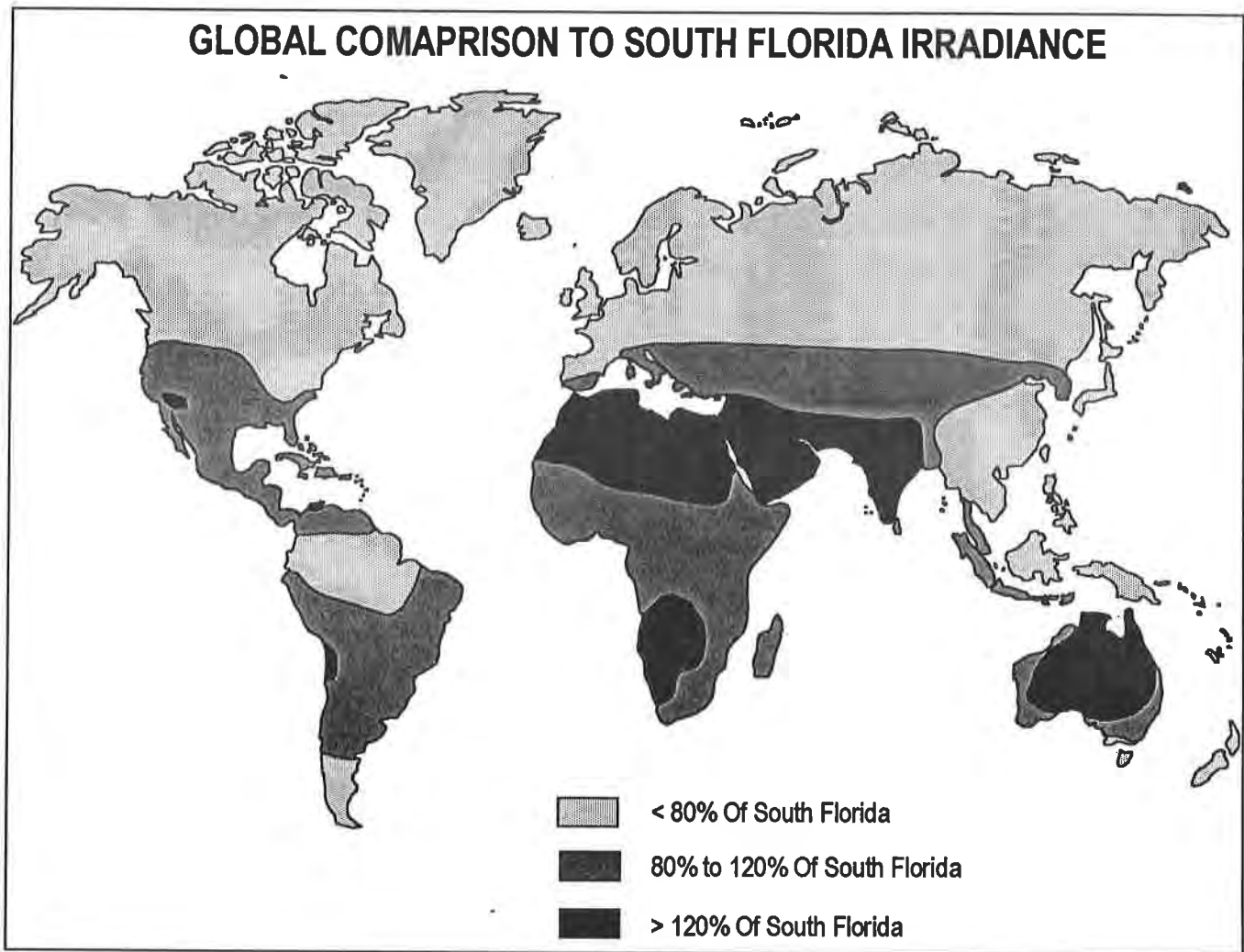
Figure 1 - Comparison of global radiant exposure to South Florida, adapted from Van Wijk and Stoerzer

TABLE 1 - OUTDOOR EXPOSURE CONDITIONS DURING STUDY					
	1 Month	2 Months	4 Months	6 Months	12 Months
Total (Cumulative) UV Radiant Exposure, MJ/m^2	20.23	38.45	77.46	128.34	256.95
Average Period Temperature, °C	24	21	21	22	24
Cumulative Rainfall, mm	2	3	80	199	1325

The conditions during this study have also been compared on a month by month basis in Figure 2. Figure 2 also presents the average and range in conditions measured by the South Florida Test Service for the eleven year period from 1985 through 1995. The moving 12 month average total UV radiant exposure at South Florida for the eleven year period, 1985 through 1995, is 302.8 MJ/m^2. The monthly average for the eleven year period was 25.3 MJ/m^2. From the plot of UV radiant exposure in Figure 2, the UV radiant exposure for the study period appears to be relatively low while the temperature and rainfall appear to be average or above. Further comparisons in this study are made on a UV radiant exposure basis so the impact of the relatively low radiant exposure during the period of this study is mitigated.

**VARIATION IN SOUTH FLORIDA CONDITIONS
FROM 1985 THROUGH 1995**

This Study, Nov 1993 to Nov 1994
Average, 1985 Through 1995
Shaded Area Range, 1985 Through 1995
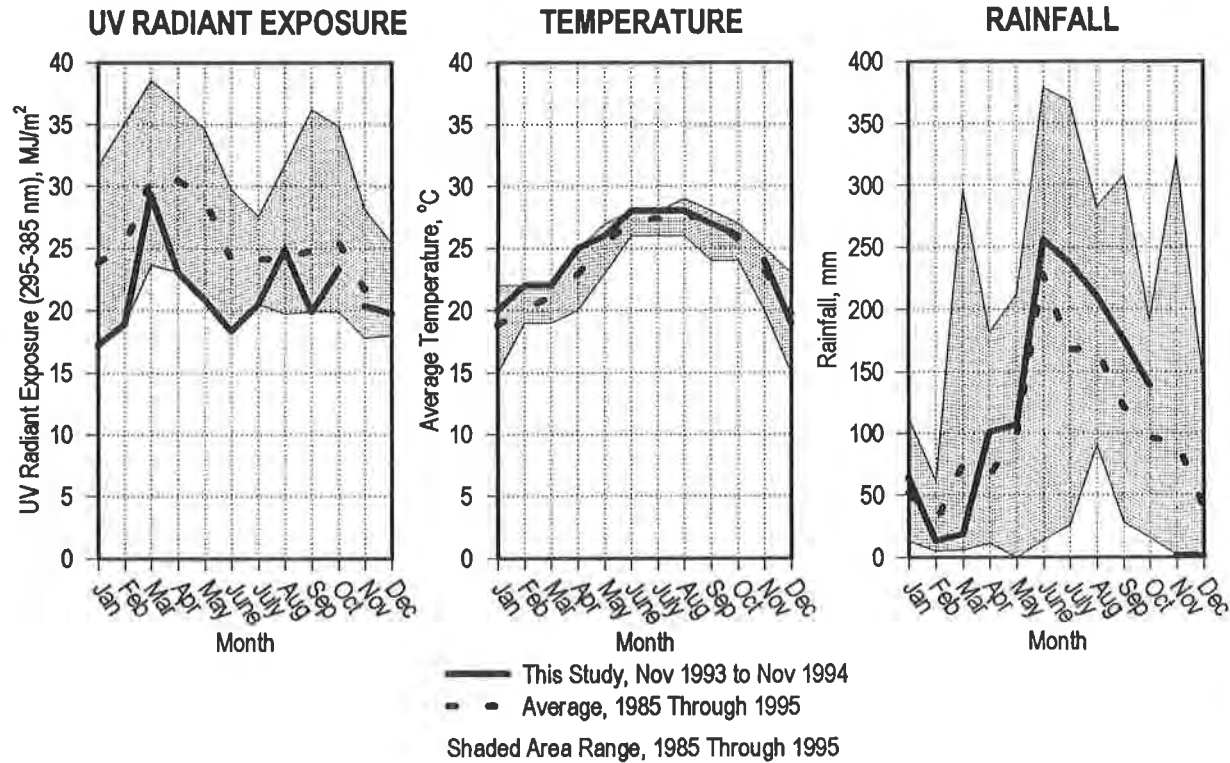
Figure 2 - Conditions during the outdoor exposure for this study compared to the conditions for the 11 year period, 1985 through 1995, adapted from data from South Florida Test Service.

<u>Xenon-Arc Test Apparatus (XWOM) Exposure.</u> The xenon-arc test apparatus (XWOM) was operated as required by ASTM D 4355-92 and G 26, Method A. An Atlas Ci65 Weather-Ometer® conforming to the requirements of a Type BH apparatus as described in ASTM G 26 was used. ASTM D 4355-92 uses a xenon-arc lamp with inner and outer borosilicate filter glass. Method A of ASTM G 26 calls for continuous exposure to light with an intermittent water spray. A type BH xenon-arc test apparatus (XWOM) has a water cooled lamp with a rotating sample rack and automatic humidity control. The XWOM is operated such that the samples are continuously exposed to the light in cycles of light only followed by light with a water spray. The cycles used were light only for 90 minutes followed by light and water spray for 30 minutes. ASTM D 4355-92 requires operating the XWOM at a temperature of $65°±5°$ C ($150°±10°$ F).

The XWOM was operated with an irradiance setpoint of 0.35 W/m²/nm at 340 nm. The lamps used may generally have a progressive drop in irradiance with use. The device has a sensor that monitors the light

irradiated by the lamp and adjusts the power to the lamp such that the irradiance is maintained at the set point, 0.35 W/m^2/nm band at 340 nm. The light sensors used were verified every thousand hours of operation.

Operated as described, the light from the XWOM closely simulates the light spectrum and energy observed in South Florida. Figure 3 shows a comparison of the light from the XWOM and South Florida in the UV wavelength range of 295 nm to 385 nm.
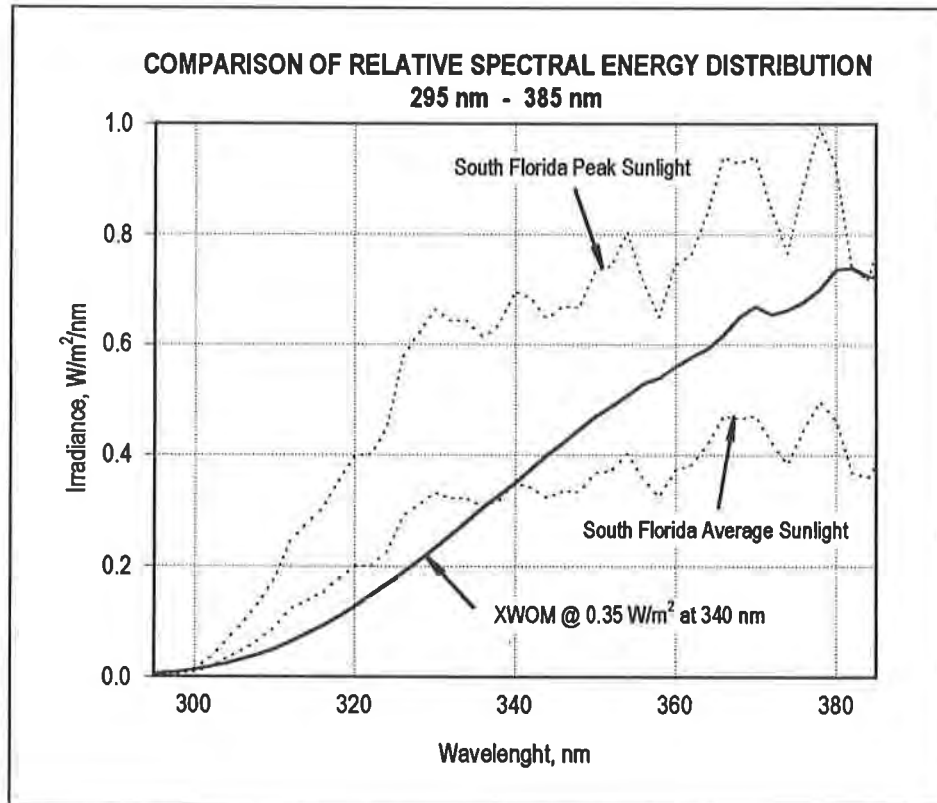
Figure 3 - Comparison of xenon-arc radiated energy to South Florida sunlight, courtesy of Atlas Electric Devices Co.

Samples were exposed in the XWOM for periods of 150, 300, 500, 1000 and 3000 hours. The radiant exposure in the UV range can be calculated by integrating the light energy for the wavelengths from 295 nm to 385 nm. For an XWOM operated as described, this works out to 28.9 W/m^2. The radiant exposure received in Joules/m^2 can be calculated by multiplying 28.9 W/m^2 by the length of exposure in seconds. For the periods of exposure used in this study the radiant exposure in the wavelength range of 295 nm to 385 nm is given in Table 2 in MJ/m^2 (1,000,000 Joules/m^2).

TABLE 2 - CALCULATED UV RADIANT EXPOSURE (295 NM - 385 NM) FOR STUDY XWOM EXPOSURE PERIODS						
XWOM Exposure, hours	150	300	500	1000	1500	3000
UV Radiant Exposure, MJ/m^2	15.6	31.2	52.0	104.0	156.1	312.1

To examine the effects of temperature on exposure, samples were also exposed in an XWOM operated at temperatures both above and below the standard, 65°C (150°F). To see if an elevated temperature can be used to further accelerate the XWOM test, a temperature of 85°C (185°F) was used. A lower temperature of 57°C (135°F) was also tried to see if the temperature induced shift was relatively uniform. The 57°C (135°F) lower limit temperature was as low as the XWOM could operate without special modification. Samples were exposed at each of the temperatures for 500 and 1000 hours or 52.0 and 104.0 MJ/m^2.

Oven Aging. As mentioned earlier, the standard XWOM is operated at a temperature of 65°C (150°F). This was the operating temperature used for most of the work for this study. Additional samples were exposed at temperatures of 85°C (185°F). Samples of the geotextile used were aged in a forced air oven to estimate what portion of the degradation of the geotextile might be related to the elevated temperatures in the XWOM. The forced air oven is considered a relatively severe way of checking oxidation of samples due to the constant flow of fresh air across the samples, which will not occur in actual use of a geotextile. However it is a close approximation of conditions in the XWOM. The samples were attached to a card and placed in the oven. Samples at 65°C (150°F) were in the oven for periods of 500, 800, and 3000 hours. From the results of the tests at 65°C (150°F) it did not appear that oven aging samples at 57°C (135°F) would result in any measurable degradation for the time durations investigated. In the oven aging performed at 85°C (185°F) the samples were aged for 500 and 1000 hours.

Testing. The exposed samples were all tested using a 50 mm (2 inch) strip tensile test as described in ASTM D 5035-90. The individual specimen unit weight, ultimate strength, and elongation at ultimate load were recorded. For each weight class subset, control specimens, which had not been exposed, were also tested. The average strength of each weight class subset of exposed specimens was divided by the average of the control specimens for the same subset to obtain a strength retained after exposure. The strength retained is used throughout this study.

RESULTS

The results are shown plotted as strength retained against radiant exposure in MJ/m^2. Figure 4 shows the results of the South Florida exposure and Figure 5 shows the results of the XWOM exposure. Plots are shown for each of the weight classes tested in this study, 135, 270 and 406 gm/m^2 (4, 8 and 12 ounces per square yard).

General Observations. The plots of the South Florida data shown in Figure 4 show a consistent trend of loss of strength with increasing radiant exposure. The strengths retained also show that as the weight increases the strength retained after exposure generally increases. The XWOM data also follows a distinct trend, although with more pronounced scatter. The XWOM data, in Figure 5, follows a similar trend for increasing strength retention with increasing unit weight for the same radiant exposure.

Another observation that can be made about the South Florida data and to a greater extent the XWOM data is the trend to have measured increases in strength retention at relatively short exposure periods. This trend can be observed for the 135 and 270 gm/m^2 geotextiles in particular out to one month (20.23 MJ/m^2) for the South Florida data and 150 hours (15.6 MJ/m^2) for the XWOM data. Increased strength after 150 hours of exposure has also often been noted during XWOM testing of production geotextiles. This may be due to secondary effects that offset the UV degradation. The exact cause is not known but may be due to; slight

SOUTH FLORIDA RATE OF DETERIORATION
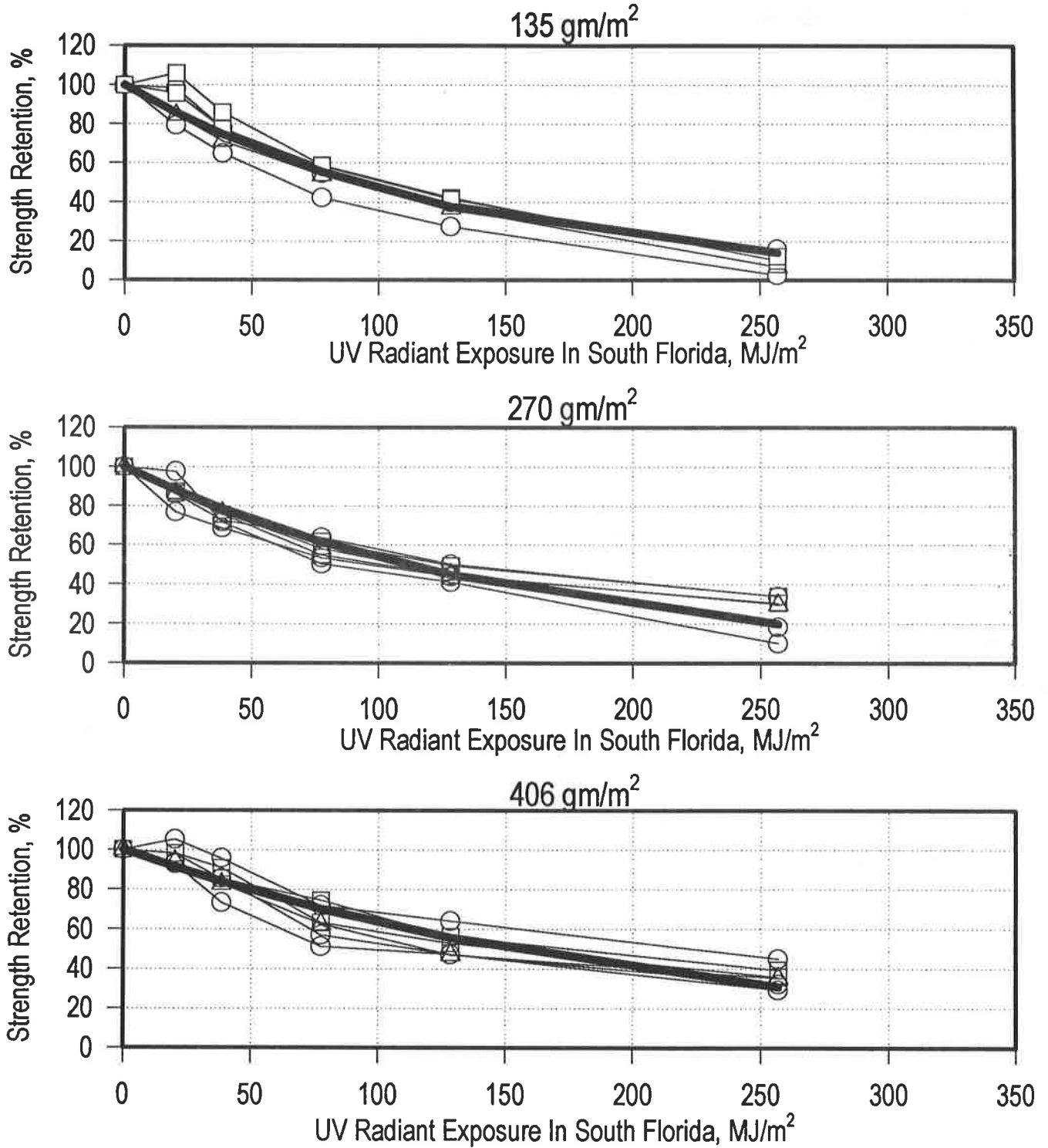
Figure 4 - Results of tests on samples from South Florida outdoor weathering. The best fit curve from the nolinear regression for each weight is shown as the bold line.

XWOM RATE OF DETERIORATION
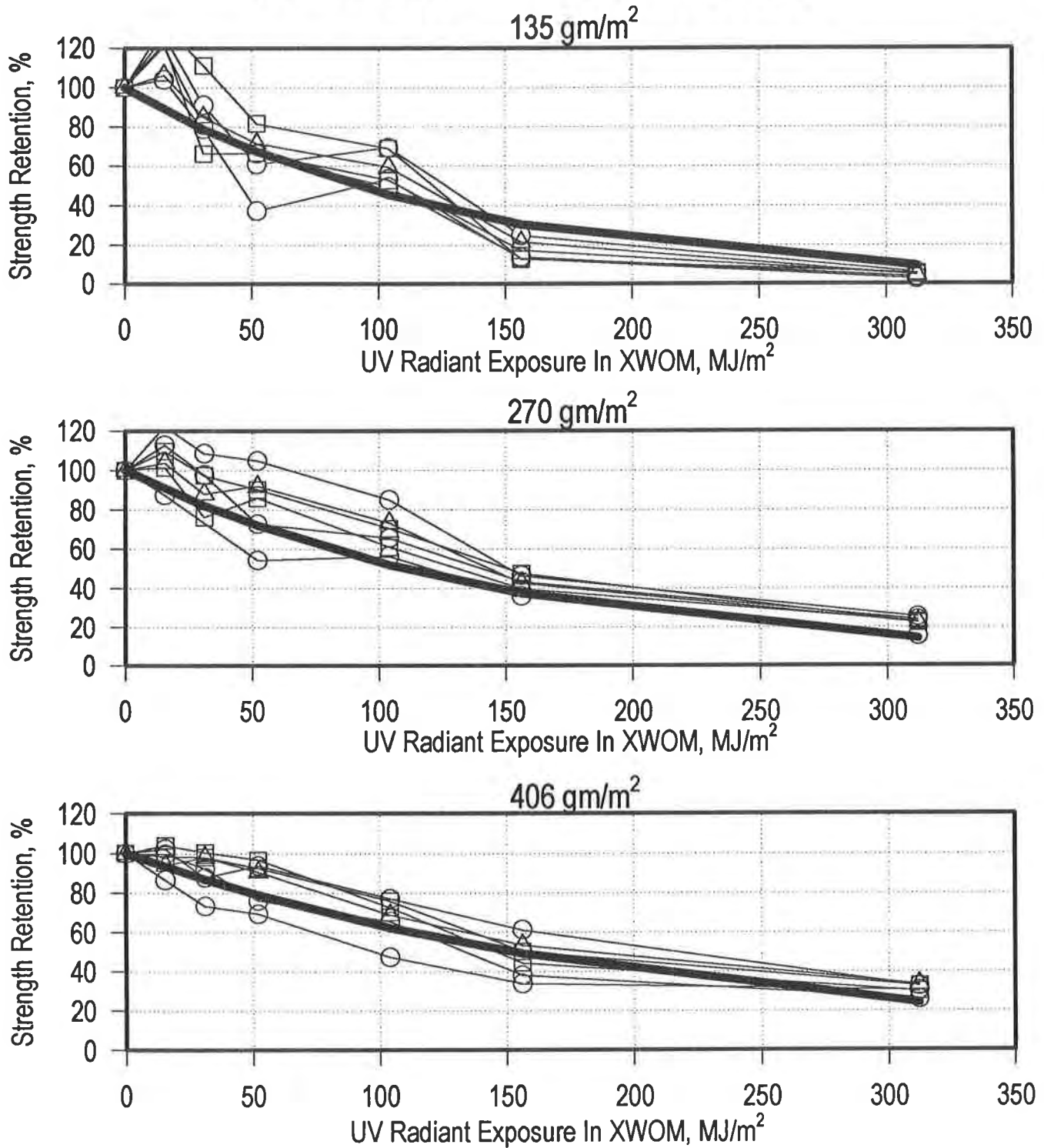
Figure 5 - Results of xenon-arc exposed samples. The best fit curve from the South Florida data for each weight shown as the bold line. Xenon-arc test apparatus (XWOM) operated at 65°C as given in ASTM D 4355-92

shrinkage that causes the fibers in the fabric to tighten, the removal of process finish from the fiber, or cross-linking of the polymer. The effect must be relatively minor because the trend seems to be less pronounced for the 270 gm/m^2 fabric than the 135 gm/m^2 and is not very apparent for the 406 gm/m^2 material.

Analysis of Results. It is desirable to quantitatively analyze the data to approximate an empirical model for the UV degradation of the geotextiles tested. To do this, a nonlinear regression analysis was performed on the South Florida data for each weight class. The analysis was performed using the curve fitting software in the SigmaPlot® program by Jandel Corporation. The computer software performs iterations based on an input equation to find constants that result in the smallest residuals or variances of the actual data from the calculated line.

A best fit line was calculated for the data for each weight class using an equation of the form:

$$SR = 100\ e^{-aI} \tag{1}$$

where:
SR = Strength Retained, %
e = base of the natural system of logarithms (2.718)
a = Constant
I = Radiant Exposure, 295 nm-385 nm, MJ/m^2

The decaying single exponential model chosen intuitively fits the conditions expected. The strength retained is 100% at 0 MJ/m^2 radiant exposure and decreases with increasing radiant exposure. Other models, including versions of polynomial and logarithmic equations, were also tried but resulted in much higher residuals and did not fit the boundary conditions well. For the South Florida data, the constant "a" calculated for each of the different weight classes are given in Table 3.

TABLE 3 - CALCULATED CONSTANTS	
Weight Class	"a"
135 gm/m^2 (4 osy)	0.00764
270 gm/m^2 (8 osy)	0.00632
406 gm/m^2 (12 osy)	0.00459

The next step was to take the curves established for the South Florida, outdoor, exposures and overlay them on the data for the XWOM exposed samples. This can be seen in Figure 5. The visual appearance of the outdoor best fit line to the XWOM data for each weight class is good. To test the fit, an analysis of the residuals was used. The residuals are defined as the difference between the individual data points and the best fit curve. The distribution for the residuals for the South Florida data were calculated for each weight class from their respective regression best fit line. Then the distribution of residuals of the XWOM data were calculated from the same outdoor line. The distribution of the residuals did not include the points at zero radiant exposure for either the South Florida data or the XWOM data, as this is somewhat artificial. The XWOM residual distribution did not include the points at 150 hours of exposure (15.6 MJ/m^2) because, as mentioned previously, there appears to be a secondary effect occurring at this exposure that has over-shadowed the effect of UV degradation at this point.
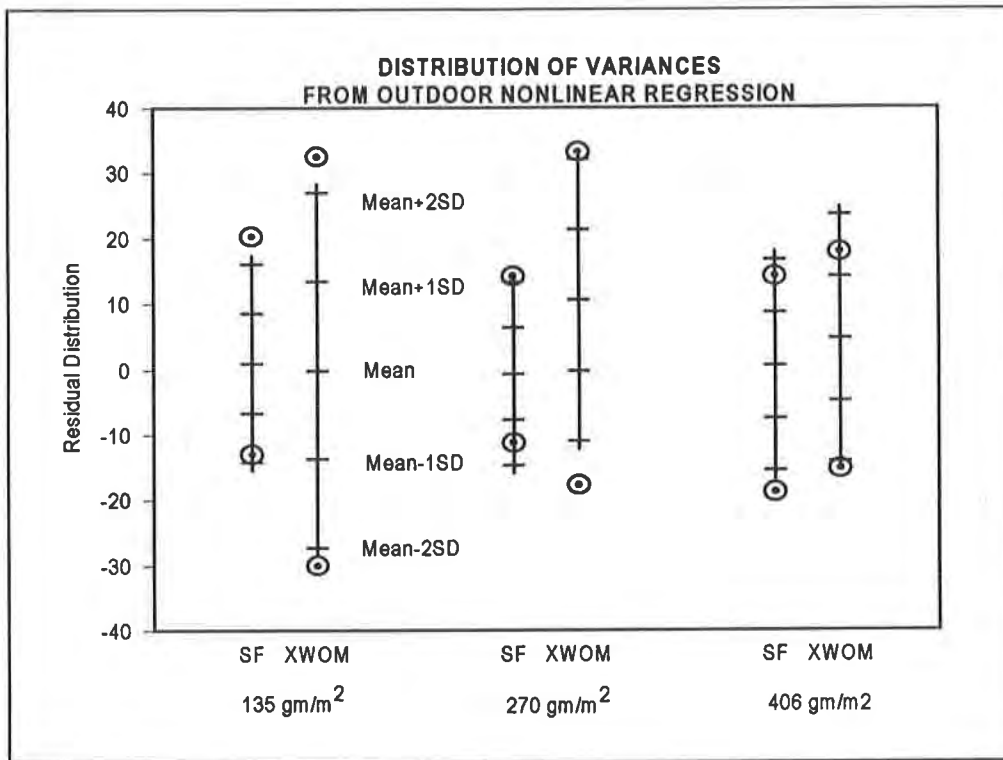
Figure 6 - Comparison of residuals of actual outdoor and xenon-arc exposed samples from South Florida. Circles indicate extreme range of data.

The distribution of the residuals is shown in Figure 6. The distributions show the mean of the residuals for each condition of exposure and weight along with the mean ± one and two standard deviations. In all of the cases, the mean of the XWOM residuals are within two standard deviations of the mean of the outdoor residuals. For the 135 gm/m² (4 ounces per square yard) and 406 gm/m² (12 ounces per square yard) data the XWOM mean is within less than one standard deviation of the South Florida residuals for the same weight. The XWOM residuals appear to have a slight bias to the positive, suggesting that the XWOM exposure, for the same radiant exposure, is slightly less harsh than South Florida exposure. There is a tendency for the XWOM data to have a somewhat greater scatter than the South Florida data. The XWOM uses a circulating fan to limit development of hot spots in the test apparatus. The constant turbulence caused by the fan may be the source of the greater scatter in the XWOM data.

Temperature Effects. The long periods of XWOM exposure subjected the samples to temperatures of 65°C (150°F). This created a potential for oxidation of the specimens to occur. In an effort to separate out some of

TABLE 4 - 65°C (150°F) OVEN AGED AVERAGE STRENGTH RETENTION			
Weight Class	500 Hours	800 Hours	3000 Hours
135 gm/m² (4 osy)	99.8	99.4	70.8
270 gm/m² (8 osy)	97.6	96.6	77.8
406 gm/m² (12 osy)	94.6	93.4	64.4

the effects of the elevated temperature on the samples, samples were aged in an oven at 65°C (150°F) for periods up to 3000 hours. The average strength retention of the six samples for each weight class after heat aging are shown in Table 4. The data indicates that up to at least 800 hours thermally induced oxidation has not occurred. By 3000 hours 30% to 50% of the degradation measured for the XWOM samples may be due to thermally induced oxidation

Effects of Variable Temperature During Exposure. To examine the effect of temperature on UV degradation sets of samples were exposed in an XWOM operated at temperatures of 57°C (135°F) and 85°C (185°F). Samples were exposed for periods of 500 hours and 1000 hours, which corresponds to 52.0 and 104.0 MJ/m^2 radiant exposure in the 295 nm to 385 nm, UV range. The results of these tests are shown in Figure 7. Decaying single exponential lines were plotted through each set of data. In these nonlinear regressions the exponents from the South Florida data were used and the strength retention at 0 MJ/m^2 was calculated to generate the best fit line through the data. Visual inspection of the data indicates a relatively good fit of the calculated curves to the data. In Table 5 are presented the calculated initial strength retention at 0 MJ/m^2 radiant exposure and constants "a" used in Equation 1.

Visual inspection of the data suggests that a shift in the effects of radiant exposure may be taking place. The XWOM is an accelerated test method and as would be expected the elevated temperature further accelerated the degradation. Likewise the tests run a lower temperature resulted in less degradation than at the standard XWOM temperature. Since the XWOM radiant exposure for a given length of time is the same regardless of temperature, the shift can also be considered a shift in exposure time.

TABLE 5 - CONSTANTS FROM VARIABLE TEMPERATURE TESTS			
Weight Class	"a"	Calculated Strength Retention at 0 MJ/m^2	
		57°C (135°F)	85°C (185°F)
135 gm/m^2 (4 osy)	0.00764	147.7	16.3
270 gm/m^2 (8 osy)	0.00632	138.3	48.4
406 gm/m^2 (12 osy)	0.00459	115.2	64.4

To calculate the estimated shift due to the temperature during XWOM exposure, the calculated initial strength retention at 0 MJ/m^2 from the variable temperature tests, shown in Table 5, was used as a reference point. Then, using the best fit curves from the South Florida outdoor data, the radiant exposure, "T" from Equation 1, necessary to produce the same initial strength retention in South Florida was calculated. The difference between the radiant exposure calculated from the South Florida data and the variable temperature tests was taken as the shift in radiant exposure to produce the same strength retention. Because of the close fit between the South Florida and XWOM data on a radiant exposure basis, an approximate experimental shift per degree C can be determined based on the 65°C temperature used in the standard XWOM exposure. These values are presented in Table 6.

With the exception of the 135 gm/m^2 (4 ounces per square yard) fabric data at 85°C (185°F), the absolute value of the radiant exposure shift is relatively uniform for both temperature conditions. The 135 gm/m^2 data at 85°C (185°F) was more degraded than the other samples. This may be the result of the fragile nature of these samples after exposure. The remaining samples exhibited a fairly uniform radiant exposure shift of about 5 MJ/m^2/°C difference from 65°C (150°F).

XWOM RATE OF DETERIORATION AT 57°C AND 85°C
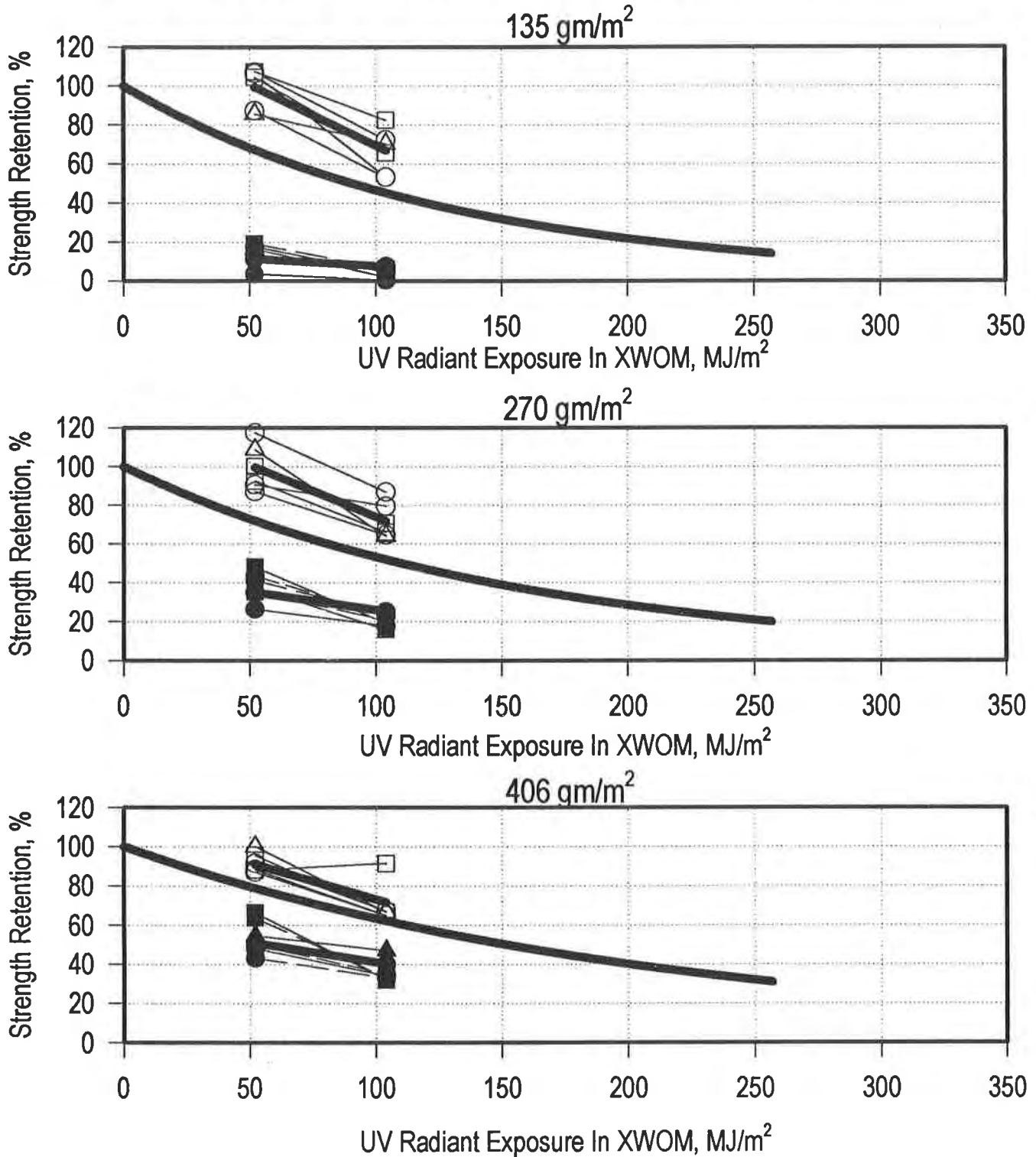
Figure 7 - Results of xenon-arc test apparatus (XWOM) tests at 57°C and 85°C. Solid symbols represent test results at 85°C. Open symbols represent test results at 57°C. The best fit curve for the South Florida outdoor data is plotted for reference.

TABLE 6 - CALCULATED SHIFT FROM SOUTH FLORIDA CURVE DUE TO TEMPERATURE				
Weight Class	Radiant Exposure Shift , MJ/m^2		Radiant Exposure Shift Per °C Variation from 65°C, MJ/m^2/°C	
	57°C (135°F)	85°C (185°F)	57°C (135°F)	85°C (185°F)
135 gm/m^2 (4 osy)	-51.0	237	-6.4	11.8
270 gm/m^2 (8 osy)	-51.3	115	-6.4	5.7
406 gm/m^2 (12 osy)	-30.8	96	-3.8	4.8

Oven aging of the samples was performed at 85°C (185°F). This was to estimate the portion of the degradation of the samples exposed in the XWOM at that temperature that was due to thermally induced oxidation. The results are presented in Table 7. Based on these results, 20% to 67% of the degradation at 500 hours and 44% to 80% of the degradation at 1000 hours in the XWOM at 85°C (185°F) is probably due to the operation temperature. Oven aging of samples at 65°C, which were given in Table 4, did not indicate significant thermally induced oxidation at times out to about 1000 hours. Therefore, oven aging was not performed at 57°C (135°F).

TABLE 7 - 85°C (185°F) OVEN AGED AVERAGE STRENGTH RETENTION		
Weight Class	500 Hours	1000 Hours
135 gm/m^2 (4 osy)	92.8	72.4
270 gm/m^2 (8 osy)	96.0	86.2
406 gm/m^2 (12 osy)	90.8	74.1

CONCLUSIONS

The work performed for this study has shown that a long term relationship can be developed between outdoor weathering and xenon-arc test apparatus (XWOM) exposure based on strength retention and UV radiant exposure. A decaying single exponential curve was fitted through the results of tests on samples exposed outdoor in South Florida. The same curve was then overlaid on the results of companion samples exposed in the XWOM. The variances of the actual data from the curves were compared for each of three weight classes of geotextile. The results of this comparison of the variances showed that the XWOM at the current ASTM D 4355-92 setting is slightly less damaging than the same amount of UV radiant exposure in South Florida. The relationship developed did fall within an acceptable range of scatter. This suggests that the results of the XWOM results could be used to approximate the long term outdoor performance of the geotextiles examined in this study.

The relationship developed in this study could be used in two possible ways. First the potential in-field exposure could be estimated and the XWOM could be used to expose samples to the same level of UV radiant exposure as is anticipated in the field but in a shorter time frame. For example, if it is anticipated that a geotextile will be exposed for the three month period of June through August, inclusive in Virginia. From Figures 1 and 2 an estimate of the UV radiant exposure could be made as follows. In south Florida for the

period in question a value of 27 MJ/m²/month or 81 MJ/m² for the three month period is a reasonable estimate. An estimate that Virginia would receive about 80% of the radiant energy of that received in South Florida or about 65 MJ/m², would be reasonable. An XWOM operated as given in ASTM D 4355-92 exposes the samples to about 0.104 MJ/m²/hour of operation. Thus a sample exposed in the XWOM for about 625 hours would receive about the same amount of radiant exposure as a sample exposed in Virginia for the three month period in question.

The second possible use of the relationships developed in this study, is to use the XWOM data to project an estimate of future results. For example, if results after 500 hours of XWOM exposure (52 MJ/m²) indicated a strength retained of 65%, Equation 1 could be solved for the constant "a" as:

$$SR = 100\ e^{-aI}$$
$$65 = 100\ e^{-52a}$$
$$a = 0.0083$$

Using this information a first estimate of the strength retained after the three month period in Virginia mentioned earlier (at 65 MJ/m²) could be made as:

$$SR \sim 100\ e^{-(0.0083)(65)}$$
$$SR \sim 58\%$$

So a first guess could be made that the material would have about 50% to 65% of its original strength after exposure for the three month period used in these examples. It should be realized that there are still several potential variables that are not defined in the relationship. These variables include temperature, moisture, and possibly elevation among others. All of these may be found to have a significant impact on the strength of a geotextile as further research is performed. The relationships developed in this study were based on work with polypropylene, staple fiber, needle punched nonwoven geotextiles with outdoor exposures in South Florida. Additional work should be performed including woven geotextiles and other locations for outdoor exposure to confirm the validity of these conclusions. Even without inclusion of these factors, the relationships developed in this study have value in making first estimates of possible field performance of geotextiles.

Results of tests on samples exposed in the XWOM at temperatures above and below the standard 65°C (150°F) indicated a relatively uniform shift in strength retention due to operation temperature. The shift measured from these tests indicated that by changing the temperature the same strength retention could be obtained at greater radiant exposures using lower temperatures and lower radiant exposures using higher temperatures. The shift due to temperature was on the order of 5 MJ/m²/°C. Understanding this transform may be useful in estimating geotextile performance in relatively hot environments from results in other locals. This conclusion is based on the results of tests at two temperatures and two exposures. Further testing should be performed at additional exposures to confirm the trend.

REFERENCE

Van Wijk, W. and Stoerzer, M., (1986), "UV Stability of Polypropylene", Third International Conference on Geotextiles, Vol. 3, pp 851-855.

INCREASING THE TEMPERATURE OF THE NOTCHED CONSTANT TENSILE LOAD ENVIRONMENTAL STRESS CRACK RESISTANCE TEST

R.W. THOMAS
TRI/ENVIRONMENTAL, INC.

J. SIEBKEN
NATIONAL SEAL COMPANY

ABSTRACT

The most useful test for evaluating the stress crack resistance of HDPE geomembranes is ASTM D5397, "Evaluation of Stress Crack Resistance of Polyolefin Geomembranes Using Notched Constant Tensile Load Test." This test involves placing a specimen with a controlled defect into a surfactant solution at an elevated temperature under a constant load and measuring the time it takes for the specimen to break. When tested at 50°C, geomembranes are generally considered acceptable if the time-to-failure under a load of 30% of the room temperature yield strength is greater than 200 hours. This length of time (>8 days) makes it difficult to use this test for QC/QA. The purpose of this project was to determine if the test temperature could be raised as a way to accelerate the test. Tests using six different loads were performed on two resins by two laboratories to select an appropriate load for tests at 80°C. Then, tests were performed on 12 geomembranes at 80°C under an applied load of 20% of the room temperature yield stress. The results of this study showed that brittle cracks can be produced at 80°C and that the required time can be reduced from 200 hrs to less than 24 hours.

INTRODUCTION

Brittle cracks were first observed in HDPE geomembrane seams 10 years ago by Peggs (1987). Since then, this subject has been extensively studied. There were two surveys, Geoservices (1989) and Koerner (1993), that helped identify the problem. Then, there were a number of papers that contributed to a better understanding of this phenomenon, including Peggs (1989, 1990), and Halse (1989, 1990a). And, finally, an appropriate test for evaluating the stress crack resistance of HDPE geomembranes was developed (Halse, 1990b, Hsuan, 1993a, 1993b, 1995).

The test is called the "Notched Constant Tensile Load Environmental Stress Crack Resistance Test" and is described in the American Society for Testing Materials (ASTM) standard test method D5397. The test involves placing a well defined notch into a small dumbbell shaped specimen, holding the specimen under a constant load in a surfactant solution (10% Igepal CO 630 in water) and waiting for a crack to grow from the notch all the way through the thickness of the specimen. The ASTM method describes a procedure for

performing the test at 10 different load levels and the generation of a master curve plotting log Load vs. log Failure Time. This curve will have a transition zone where the fractured surface changes from a mostly ductile appearing one to a mostly brittle appearing one. The transition time describes the stress crack resistance of the sample.

There is also an appendix to the standard method that describes a test at a single load (Hsuan, 1995). In this test, specimens are tested at a single load and their average failure time is a measure of the stress crack resistance. The generally accepted criteria for good stress crack resistance is 200 hours under a load equivalent to 30% of the geomembrane's yield strength at room temperature. The load was selected because it should be in the brittle region of the full curve for most geomembranes (Koerner, 1993). The time selected was based on test results generated on geomembranes that experienced field failures (Koerner, 1993).

This test has been directly responsible for a dramatic improvement in the quality of HDPE resins used for geomembranes. When it was first developed, there were a number of resins that were identified as having poor stress crack resistance. These resins have since been either improved or removed from the market place. The ultimate result of this test is that each year there are fewer and fewer problems with HDPE geomembrane cracks.

One of the limitations of this test is that it takes over 8 days of testing to reach 200 hours. This makes it hard to use as a QC/QA tool, where information is needed more quickly. Therefore, it would be desirable to accelerate this test. The most obvious ways to accelerate this test is by finding a more aggressive solution or increasing the temperature.

Increasing the temperature seems possible because stress crack tests have been done at 80°C for the last few years on samples of textured geomembranes and geomembrane seams, without notches (Thomas, 1993, 1994, 1995). Additionally, notched constant load tests have been reported at temperatures up to 75°C (Hsuan, 1995). Therefore, the purpose of this project was to explore the possibility of increasing the temperature of the notched constant load stress crack test to 80°C.

CONSIDERATIONS FOR ELEVATED TEMPERATURE TESTS

Effect of Temperature on HDPE. One of the factors one needs to consider before raising a test temperature is how the specimens might be affected. HDPE is a semi-crystalline thermoplastic which means that is will undergo dramatic morphological changes at temperatures near and above the crystalline melting point. These changes are displayed by the differential scanning calorimeter (DSC) thermal curve shown in Figure 1. This curve shows the amount of heat absorbed by the specimen as a function of increased temperature. It is essentially a melting profile of a HDPE sample. Notice that the curve begins to deviate from the extrapolated baseline at about 70°C. This is the very early stages of melting and involves poorly formed crystallites. Notice also that at 80°C, only a small amount of melting has occurred. This suggests that it may be appropriate to test HDPE at temperatures as high as 80°C although there is some changes that will occur in the microstructure of the polymer. There is no doubt that the test specimens will be softer and more flexible at 80°C.

The tensile strength of the HDPE sample is another property that will be affected by increasing the temperature. To determine how much, the tensile yield strengths of commercial geomembranes made from
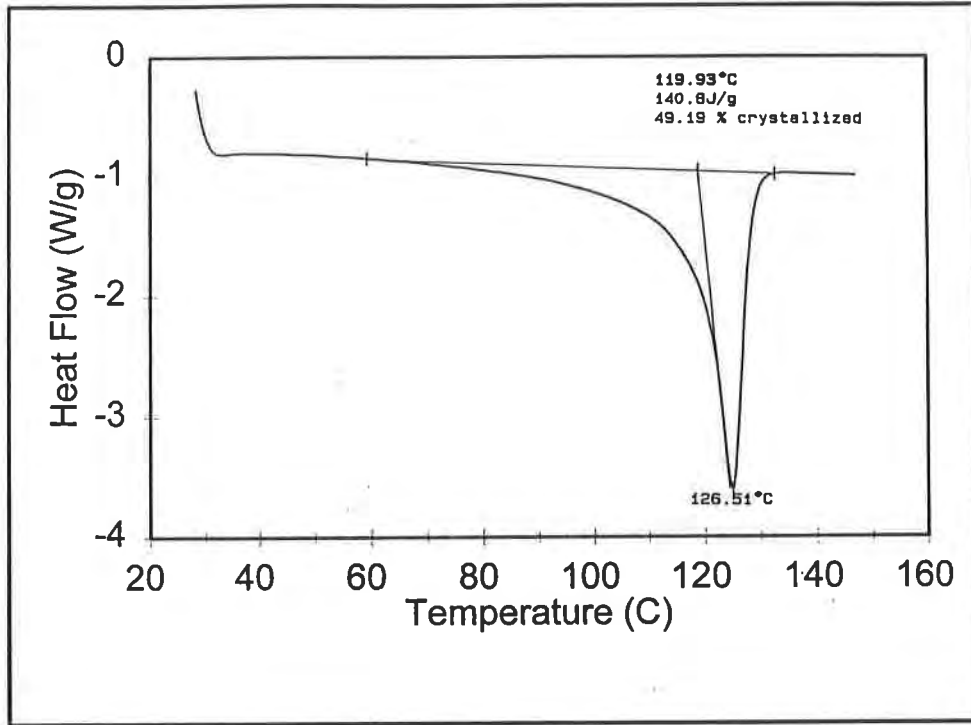
Figure 1. DSC Thermal Curve for a HDPE Geomembrane
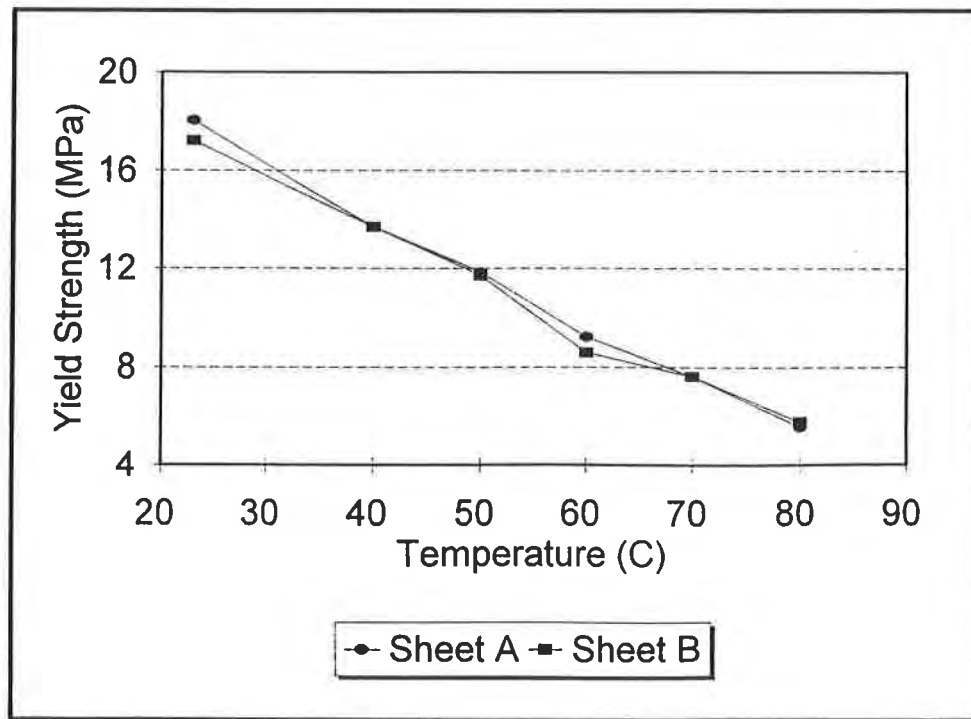
Figure 2. Effect of Temperature on Tensile Yield Strength

two different resins were measured in an environmental chamber at different temperatures. The results are shown in Figure 2. These are the cross machine direction data but similar curves were generated for machine direction samples.

Experiments on the two different geomembranes resulted in slopes and correlation coefficients that were nearly identical. At 60°C, the strength is about 50% of the room temperature strength and at 80°C, the strength is only about 30% of the room temperature strength. These results are very important if one is contemplating stress crack tests at 80°C.

Surfactant Selection. Most environmental stress crack tests that have been developed use a water-based solution of a non-ionic surfactant to accelerate the cracking process. The types of non-ionic surfactants that have been used for stress crack tests are from the general chemical family of ethoxylated alkyphenols. There is a variety of different ones available that vary by what kind of alkyl group is present and the number of ethoxyl repeating units are present in the main chain. One main property that is used to distinguish the different surfactants is the cloud point. These molecules contain both polar and non-polar groups, which means that part of the molecule is soluble in water and another part is not. The whole molecule is soluble in water at room temperature because the polar groups interact with water molecules through a weak molecular attraction called hydrogen bonding. However, as the temperature is increased, there will come a point where the heat will overcome the forces of hydrogen bonding and the surfactant will no longer be soluble. This temperature is called the cloud point and it is the point at which the surfactant in water turns from a clear liquid to a milky liquid. The surfactant essentially becomes insoluble, and therefore inactive, at temperatures above the cloud point.

The surfactant described in ASTM D5397 is Igepal CO-630. This is a branched ethoxylated nonylphenol with 9 ethoxyl repeating units in the main chain and a molecular weight of 616. Unfortunately, this surfactant cannot be used at 80°C because its cloud point is 55°C. Therefore, a different surfactant was required to perform the test at 80°C. The one used in this study was Igepal CA 720 at a concentration of 5% in water. This surfactant is a branched ethoxylated octylphenol with 12.5 repeating ethoxyl groups and a molecular weight of 756. It has more hydrogen bonding sites so it stays in solution to temperatures up to 85°C. The selection of surfactant and concentration was based on the fact that CA 720 is chemically identical to a surfactant already used in Germany for stress crack tests at 80°C called Marlophen 812N.

One of the interesting results of this study involved the stability of the surfactant solutions. ASTM D5397 allows for one to use tap water to make the surfactant solution. It also recommends that the bath be changed every two weeks because it has previously been believed that the Igepal is not stable and decomposes. The basis for this belief has been the change in the bath from a clear solution to a milky mixture. It is now believed that the cause for the bath "decomposition" is the use of tap water to make the solution. Salts disrupt hydrogen bonding and reduce the cloud point of the solution. This is shown graphically in Figures 3 and 4.

Notice that as the salt concentration is increased, the cloud point is decreased. So, what is happening in these baths is that water is evaporating, then as more tap water is added, the dissolved salts in the tap water are being concentrated. The final result is that the cloud point drops below the test temperature, which makes the bath turn milky. This fact is supported by the Igepal manufacturer who claims the solution should be stable and last for months, if not years.
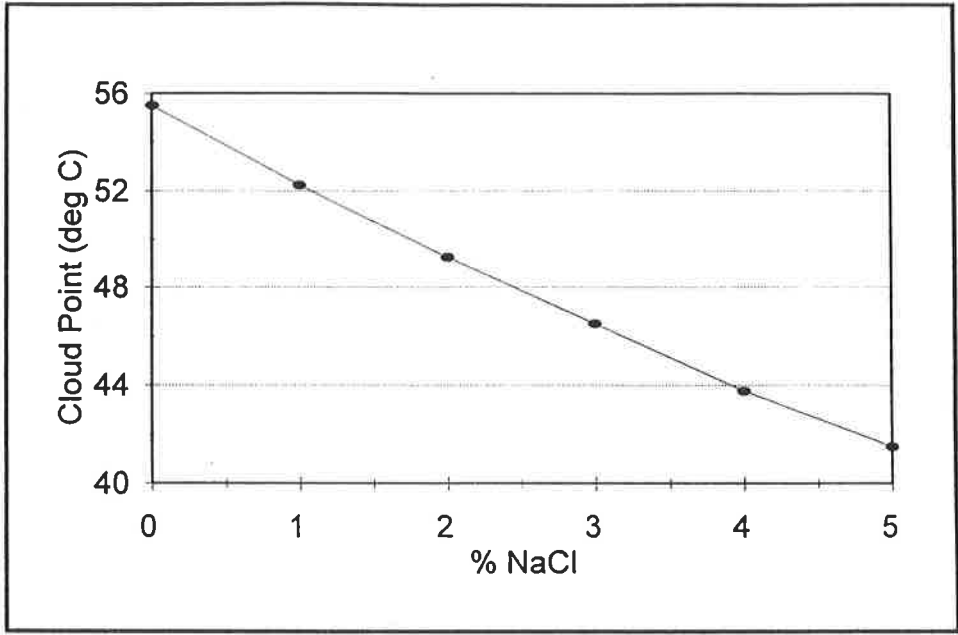
Figure 3. The Effect of Dissolved Salts on the
Cloud Point of 10% Igepal CO-630
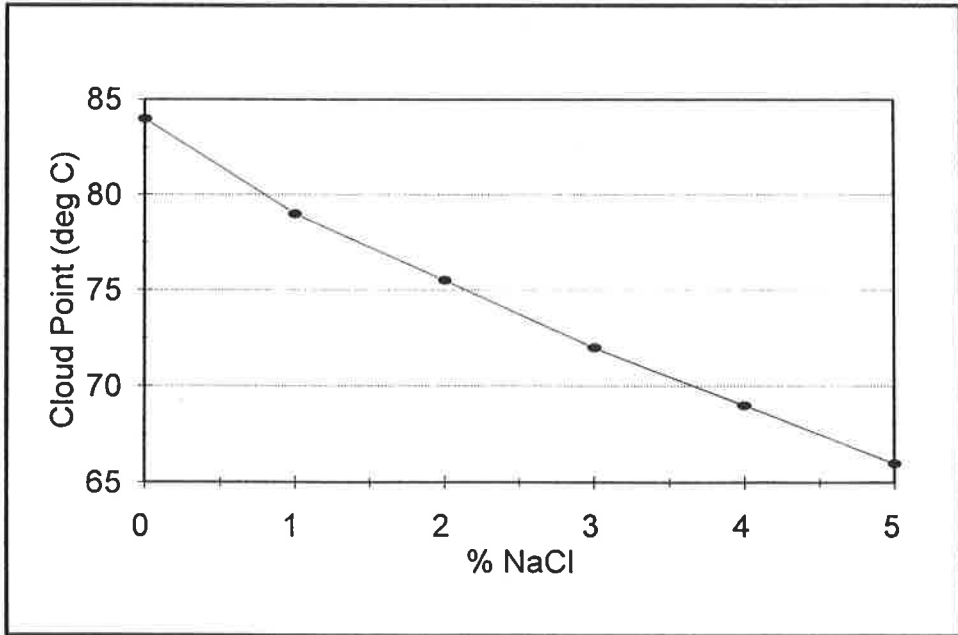
Figure 4. The Effect of Dissolved Salt on the
Cloud Point of 5% Igepal CA-720

Another very important issue is if the stress crack resistance is affected by the cloud point of the solution. It is known that a milky bath has lost its activity. However, it is not known if two solutions with different cloud points produce different results. This possibility was briefly investigated. Twenty specimens of a poor stress cracking geomembrane were tested in a solution made with deionized water. The failure time averaged 25.4 ± 3.5 hours. Then, 1% table salt was added and twenty more specimens tested. This time the average failure time was 24.0 ± 2.7 hours. Therefore, it doesn't look like the cloud point of the solution affects the stress crack resistance, although this should probably be confirmed with more experiments on other geomembranes. The main reason for using deionized or distilled water is to promote long bath life.

The bath life had a big effect on this study. Many early experiments were biased by the bath because the bath became cloudy during the experiment and this change was not noticed. In fact, this happened in both laboratories participating in this study. And, it happened in one laboratory more than once. The bath changing from clear to milky can be easily missed when plastic balls are used to cover the liquid to minimize evaporation. The problem is more evident in the baths at 80°C because water evaporates much more quickly and less dissolved salt is needed to drop the cloud point below the test temperature.

Applied Load Selection. Another one of the concerns with elevated temperature constant load tests is how one should select the magnitude of the applied load. Recall that for the single point constant load test at 50°C, a load equal to 30% of the room temperature yield strength is most often used. For Geomembrane A in Figure 2, 30% of its room temperature yield strength (18.1 N/mm^2, 2620 psi) is 5.42 N/mm^2 (786 psi). This would be the load for testing at 50°C. Notice though that the yield strength at 50°C is about 12.15 N/mm^2 (1760 psi). Therefore, the actual load the specimens would be under at the test temperature is 44.7% of the yield strength. If one were to use the same load to test at 80°C, the actual load would be about 95% of the yield strength. This certainly would not produce a brittle crack.

Another factor complicating the picture is that the force on the specimen changes as the crack grows. This is due the reduced cross-sectional area as the crack grows. By the time the crack grows half way through the sheet thickness, the force is nearly equivalent to the yield strength. This means that in this test, cracks may start brittle, but the ultimate failure will always be ductile because the force will exceed the yield strength of the specimen.

RESULTS AT VARIOUS LOADS

Tests were run at multiple loads to help determine the best load for a single load test at 80°C. The loads considered, along with the equivalent "at temperature" loads are shown in Table 2. Loads greater than 30% of the room temperature strength were not studied because the goal of this project was to grow brittle cracks. It was felt that the cracks formed above 30% would be mostly ductile.

Tests were performed by two different laboratories on geomembranes made from two different resins by the same geomembrane manufacturer. This part of the study was done during the period of questionable bath performance. Therefore, it is not appropriate to report the results. However, it was clear during the tests, that even though the failure times were questionable, the appearance of the fractured specimens provided valuable information. Therefore, from examining the failed specimens, it was determined that a load of 20% of the room temperature yield strength was an the highest load that would promote mostly brittle stress cracks. Loads higher than 20% produced more ductile appearing fractures.

Table 2. Loads Studied at 80°C

Load as a Percent of the Yield Strength at 23°C (18.1 N/mm² or 2620 psi)	Load as a Percent of the Yield Strength at 50°C (12.1 N/mm² or 1758 psi)	Load as a Percent of the Yield Strength at 80°C (5.74 N/mm² or 832 psi)
14.2	21.2	44.7
16.5	24.6	52.1
19.0	28.3	59.6
21.3	31.7	67.0
23.7	35.3	74.5
26.0	38.7	82.0
30.0	44.7	94.4

RESULTS AT A SINGLE LOAD

A single load of 20% of the yield strength at 23°C was chosen for the single point tests at 80°C. This load was selected because it was high enough to produce significant acceleration, but it was low enough to consistently produce a mostly brittle appearing fracture surface. It is also a value that should be easy to remember. Tests at this load were performed on 12 different geomembranes. The geomembranes were produced by 3 different manufacturers and represented 6 different HDPE resins. It is believed that this collection is fairly representative of geomembranes that have been used in this industry over the last 10 years.

In addition to the single point tests at 80°C in Igepal CA 720, tests were run at 50°C at a load of 30% of the room temperature yield strength in Igepal CO 630 to compare the results at the two temperatures. The results for the 12 different geomembranes are shown in Table 5. All of the tests at 50°C were run in solutions made with tap water and the tests at 80°C were run in solutions made with deionized water.

The sample codes indicate where different HDPE resins were used. So, in the case of Sample B, all six of the test samples were made from the same resin by the same manufacturer. Two results for the same thickness indicate where different batches of resins were used. Each letter corresponds to a different resin. Therefore, there are six resins represented that were made into geomembranes by three different manufacturers.

Figure 5 shows the correlation plot for these results. It is believed that there is sufficient agreement between the two temperatures to allow one to perform the test at 80°C. The results suggest that 200 hours at 50°C is equivalent to about 18 hours at 80°C. As a added factor of safety, one might use 24 hours as an acceptable time. This is an accelerating factor of 8.3, which is less than any measured during this study. The results of this study show that any resin that lasts 24 hours at 80°C will easily pass 200 hours at 50°C. This means that this test should be appropriate for use in QC/QA applications or for conformance testing. These results clearly showed that it is appropriate to perform this test at 80°C. The total accelerating factors measured were similar and agreed with those previously reported (Hsuan,1995). Hsuan reported accelerating factors of 3.4, 3.7, and 3.6 per 10°C for tests run on two geomembranes and a pressure pipe at temperatures from 40°C to 80°C. The average accelerating factor found in this study was 3.6 per 10°C.

Table 5. Single Point Stress Crack Test Results

Sample Code	Thickness (mm)	Failure Time at 50°C (Hrs)[1]	Failure Time at 80°C (Hrs)[2]	Accelerating Factor	
				Total	Per 10°C
A-80	2.0	265 ± 42	30.5 ± 1.4	8.7	2.9
A-60	1.5	173 ± 3	14.1 ± 1.0	12.3	4.1
B-100	2.5	146 ± 0	13.9 ± 0.5	10.5	3.5
B-80	2.0	182 ± 4	18.3 ± 0.6	9.9	3.3
B-80	2.0	155 ± 27	14.9 ± 1.0	10.4	3.5
B-60	1.5	180 ± 5	15.8 ± 1.6	11.4	3.8
B-60	1.5	161 ± 28	13.7 ± 1.3	11.7	3.9
B-40	1.0	362 ± 85	27.5 ± 1.4	13.2	4.4
C-80	2.0	82 ± 8.2	9.0 ± 1.3	9.2	3.1
D-60	1.5	65.3 ± 2.2	7.0 ± 0.4	9.3	3.1
E-60	1.5	11.2 ± 1.4	1.1 ± 0.1	10.2	3.4
F-60	1.5	822 ± 106	60.9 ± 11	13.5	4.5

1. 10% Igepal CO630 and load of 30% of room temperature yield strength.
2. 5% Igepal CA720 and load of 20% of room temperature yield strength.
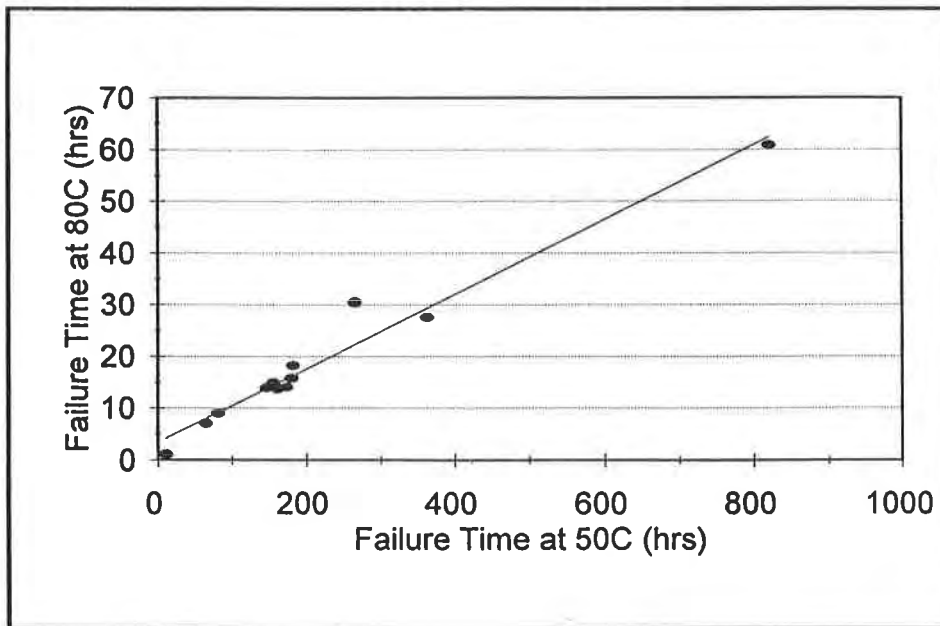
Figure 5. Correlation Between Results at 50°C/30% and 80°C/20%

SUMMARY AND CONCLUSIONS

The purpose of this study was to determine if the temperature of the notched constant load environmental stress crack resistance test could be raised from 50°C to 80°C in an effort to speed up the test. This paper first described different considerations for raising the temperature including the melting behavior of HDPE and the effect of temperature on the tensile yield strength.

Next, the effects of using tap water to make solutions of Igepal were also studied and results were presented which indicated that the baths become deactivated because of increased salt content, not because the Igepal is unstable. It was also shown that the presence of dissolved salts does not change the time-to-failure in stress crack tests on a geomembrane that breaks quickly. The use of distilled or deionized water is strongly suggested to dramatically increase the service life of the stress cracking solution.

Then, experiments were performed by two laboratories on two different geomembrane in an effort to determine the best load for performing single point tests at 80°C. The results from both laboratories suggested that a load equal to 20% of the room temperature yield strength produced fractured surfaces that appeared very similar to those found in tests at 50°C.

Finally, single point tests were performed by one laboratory at both 50°C and at 80°C on 12 different geomembranes and the results compared. The results showed excellent agreement between the geomembranes and with results reported previously in the literature. These results demonstrated that the notched constant load test can indeed be accelerated through an increase in temperature and a change in surfactant.

REFERENCES

Geoservices,Inc. (1989) "Preliminary Assessment of Stress Cracking of Polyethylene Liners" Draft report to USEPA, Task 6, Work Assignment 68-3, Under NUS Corp., 27 pages.

Halse, Y.H., Koerner, R.M., and Lord, A.E.,Jr. (1989) "Laboratory Evaluation of Stress Cracking in HDPE Geomembrane Seams", Durability and Aging of Geosynthetics, R.M. Koerner, Ed., Elsivier, London,pp. 177-194.

Halse, Y.H., Koerner, R.M., and Lord, A.E.,Jr. (1990) "Stress Cracking Morphology of Polyethylene (PE) Geomembrane Seams", Geosynthetics: Microstructure and Performance, ASTM STP 1076, I.D. Peggs,Ed., pp. 78-89.

Halse, Y.H., Lord, A.E., Jr., and Koerner, R.M. (1990) "Ductile-to-Brittle Transition Time in Polyethylene Geomembrane Sheet", Geosynthetic Testing for Waste Containment Applications, ASTM STP 1081, R.M.Koerner, Ed., pp. 95-109.

Hsuan, Y.G. and Koerner, R.M. (1995) "The Single Point-Notched Constant Tension Load Test: A Quality Control Test for Assessing Stress Crack Resistance", Geosynthetics International, Vol. 2, No. 5, pp. 831-843.

Hsuan, Y.G., Koerner, R.M. and Lord, A.E.,Jr. (1993a) "Stress Cracking resistance of HDPE Geomembranes", Journal of Geotechnical Engineering, ASCE, Vol 119,No.11, pp. 1840-1855.

Hsuan, Y.G., Koerner, R.M. and Lord, A.E.,Jr. (1993b) "Notched Constant Tensile Load (NCTL) Test for HDPE Geomembranes", ASTM Geotechnical Testing Journal, Vol. 16, No.4, pp. 450-457.

Koerner, R.M., Hsuan, Y.G. and Lord, A.E.,Jr. (1993) "Stress Cracking Behavior of HDPE Geomembranes and Its Prevention", Final Report to USEPA Contract CR-815692, available from NTIS as PB91-213660, Springfield, VA, 94 pages.

Peggs, I.D., (1987) "Evaluating Polyethylene Geomembrane Seams", Proceedings of the Geosynthetics '87 Conference, New Orleans, LA, pp. 505-518.

Peggs, I.D. and Carlson, D.S. (1989) "Stress Cracking of Polyethylene Geomembrane Seams: Field Experience", Durability and Aging of Geosynthetics, R.M. Koerner, Ed., Elsivier, London,pp. 195-211.

Peggs, I.D. and Carlson, D.S. (1990) "Brittle fracture in Polyethylene Geomembranes", Geosynthetics: Microstructure and Performance, ASTM STP 1076, I.D. Peggs,Ed., pp. 57-77.

Thomas, R.W., Kolbasuk, G.M., and Mlynarek, J., (1995) "Assessing the Quality of HDPE Double Track Fusion Seams", Proceedings of the Sardinia '95 Landfill Conference, pp.415-428.

Thomas, R.W. and Woods-DeSchepper,B., (1993) "Stress Crack Testing of Unnotched HDPE Geomembranes and Seams", Proceedings of the 7th GRI Seminar, Philadelphia,PA, pp. 116-125.

Thomas, R.W. and Woods-DeSchepper,B., (1994) "The Environmental Stress Crack Resistance of Coextruded Geomembranes and Their Fusion Seams", Proceedings of the 5th IGS Conference in Singapore, Vol. 3, pp. 945-948.

Effects of Freeze-Thaw Cycling on Geomembrane Sheets and Their Seams - Part II
Cold Temperature Tensile Behavior and Thermal Induced Cyclic Stress

Y.G. Hsuan, M.L. Sculli and Z.C. Guan,
GRI /Drexel University

A. I. Comer
US Bureau of Reclamation

ABSTRACT

Geomembranes are widely used as liquid barrier materials in rehabilitation of dams, canals, and waste containment facilities. In many locations such geomembranes are subjected to freeze-thaw cycling. However, the impact of the cyclic temperature effect on the long-term behavior of geomembranes is largely unknown. This study, sponsored by the Bureau of Reclamation and the Environmental Protection Agency evaluates the effects of cold temperature and freeze-thaw cycling on nineteen geomembrane sheets and 31 combinations of seams.

Regarding the effect of freeze-thaw cycling between +30°C and -20°C, after 200 cycles under unconstrained conditions, results showed no statistically significant changes in either geomembrane sheets or seams at tensile test temperatures of +20°C and -20°C. While under constrained conditions, test specimens were subjected to thermal induced cyclic stress as well as freeze-thaw action, the tensile behavior of geomembrane sheets and seams still remained unchanged even after 500 freeze-thaw cycles.

The cold temperature induced stress during the cold cycle of freeze-thaw cycles varied with polymer types. The magnitude of the stress is a factor of modulus and coefficient of thermal expansion of the material. Furthermore, the induced stress was the same for each freezing cycle and it remained unchanged until the temperature was increased. Regarding the initial stress caused by straining, it relaxed rapidly. The nonreinforced geomembranes exhibited a higher relaxation rate than the reinforced geomembranes.

For the effect of cold temperature on the tensile behavior of geomembrane sheets and seams, tensile strength increased and elongation decreased at the lower testing temperature. In addition, for each geomembrane, the shear strength responded differently than the peel strength. The majority of the hot wedge seams showed a lower increase in the peel strength than the corresponding shear strength.

INTRODUCTION

The effects of freeze-thaw cycling and cold temperature on mechanical behavior of any type of engineered barrier material should be a concern at locations where ground freezing conditions exist. Othman and Benson (1993) observed an approximately 9% increase in volume when the pore water within the compacted clay liner (CCL) froze. The expansion caused the formation of ice lenses which became channels for water to flow. Zimmie and La Plante (1990) found that CCL's become friable and experience an increase in their permeability after 10 to 15 freeze-thaw cycles. For this reason, CCLs are recommended to be placed beneath the depth of maximum frost penetration in areas where freezing conditions exist. Contrary, Hewitt and Daniel (1996) found that the hydraulic conductivity remained almost the same after three freeze-thaw cycles for three different geosynthetic clay liners (GCL). Regarding the overlapped seams, although one of the GCL seams showed a significant increase in the conductivity value after only one freeze-thaw cycle, the other two seams exhibited no changes.

Comparatively, for alternate barrier materials such as geomembranes, limited information is available regarding performance under freeze-thaw cycling. LaFleur et al. (1985) performed a freeze-thaw study on four different types of geomembrane seams which included solvent seamed ethylene propylene diene monomer (EPDM) rubber, solvent seamed isobutylene rubber, solvent seamed chlorosulfonated polyethylene (CSPE), and hot air seamed polyvinyl chloride (PVC). The seamed samples were strained to 10% strain and subjected to 150 freeze-thaw cycles. There was no change in the strength of any of the seamed geomembranes. For high density polyethylene (HDPE) geomembranes, Budiman (1994) conducted a freeze-thaw study on three geomembranes with thicknesses of 1.0, 1.5 and 2.0 mm. The test coupons were restrained in both the uniaxial direction and biaxial directions while subjected to freeze-thaw cycles between temperatures of 65°C and -20°C. After incubation, dumbbell shaped specimens were taken from coupons for the tensile test evaluation. No significant change in the tensile load-elongation characteristics were determined after 150 freeze-thaw cycles.

Another concern for geomembranes installed in areas where freezing conditions exist is the effect of cold temperature on their tensile behaviors. Many researchers (Rollin et al., 1984, LaFleur et al., 1985, Richards et al., 1985, Peggs et al., 1990, Giroud et al, 1993 and Budiman, 1994) found that as the temperature decreases, the strength (either the yield strength or the break strength) of geomembranes increases and break elongation decreases. This behavior was observed in geomembranes made from various types of polymers, including PVC, CSPE, and HDPE.

Although the above references studied the changes in tensile behavior of selected types of geomembrane sheets under freeze-thaw and cold temperature conditions, the behavior of many current geomembrane seam types were not included in these studies. Additionally, new types of geomembranes were not evaluated. Thus, the Bureau of Reclamation and the Environmental Protection Agency jointly initiated an extensive research study on a variety of geomembrane sheets and seams in September, 1993. The early results of this freeze-thaw study was presented in two papers, Hsuan et al., 1993 and Comer et al., 1995. A detailed final report of the study was published by the Bureau of Reclamation as R-96-3 (Reclamation, 1996). This paper presents a summary of all results of the study.

EXPERIMENTAL DESIGN

Geomembrane sheets and seams were cut into rectangular shaped specimens 25 mm wide by 150 mm long. Three specimens were included in each set for each designated test cycle.

The study consisted of four parts with a different experimental design for each. Parts I, II, and III involved subjecting test specimens to a series of freeze-thaw cycles under different strain conditions and testing conditions as shown in Table 1. Part IV was to investigate the induced tensile stress during the freeze cycle.

Table 1. Experimental design of different parts of study.

Part	Cyclic Temperature Range	No. of Cycles	Incubation Condition	Tensile Test Temperature
I	+20°C to -20°C	1, 5, 10, 20, 50, 100, 200	unconstrained	+20°C
II	+20°C to -20°C	1, 10, 50, 100, 200	unconstrained	-20°C
III	+30°C to -20°C	1, 10, 50, 100, 200, 500	constrained	+20°C
IV	+30°C to -20°C	2	constrained	+30°C to -20°C

In Parts I and II of the study, the freeze-thaw cycles were created by placing the specimens in a household freezer set at -20°C for approximately 16 hours, and then removed to room temperature conditions (approximately +20°C) for approximately 8 hours. All specimens were initially dry. However, condensation was observed on the surface of the specimens during the thaw portion of the cycles. Thus, the specimens experienced some amount of wet-dry cycling, but to an unknown and essentially uncontrolled amount.

In Part III of the study, all specimens, sheets and seams, were subjected to a constant tensile strain while being exposed to freeze-thaw cycling. The amount of strain corresponded to 25% of the sheet peak or yield load or seam shear peak load. The constrained specimens were enclosed within a temperature controlled chamber. The chamber was set to provide freeze-thaw cycles of -20°C for 16 hours and +30°C for 8 hours.

The purpose of Part IV of the study was to investigate the cold temperature induced tensile stress of constrained specimens during freeze-thaw cycles. The test specimen was elongated under a constant strain rate to the corresponding strain value used in Part III in an environmental chamber. Once the desired strain was reached, the specimen was locked into position. Simultaneously, the load and time were recorded until the test was terminated. The specimen was equilibrated at room temperature (about +20°C) for a half hour. It was then heated to 30°C for 12 hours. The chamber temperature was then cooled to -20°C for 2 hours and then was increased to +30°C for 2 hours. The -20°C and +30°C cycle was repeated a second time before the test was concluded.

TEST MATERIALS

This study involved nineteen different geomembranes and thirtyone combination of seams. All materials are commercially available and are used on various land and water remediation and environmental related projects.

Geomembrane Types. The nineteen geomembranes were made from seven different resin types. Geomembranes consisted of different thickness, surface texture and reinforcement. The type of geomembranes used in each part of the experiment is described in Table 2. Parts I and III included all nineteen geomembranes. Part II involved six of the nineteen geomembranes. Part IV included twelve different geomembranes.

Seam Types. The nineteen geomembranes were seamed using various seaming techniques. The seaming was performed by the geomembrane manufacturers or fabricators. Five seaming techniques were used in this study: chemical seams, hot wedge seams, fillet extrusion seams, hot air seams (thermal seams) and dielectric seams. Parts I and III included twentyseven different combinations of seams. Part II included thirteen seams, and Part IV included twelve seams. The seams types that are evaluated in each part of the experiment are listed in Table 2.

TENSILE TEST METHODS

The geomembrane sheet tensile tests for Parts I, II and III were evaluated using either 25 mm strip or dumbbell shaped test specimens. Uniform 25 mm strips were used for both seam shear and peel tensile tests. It should be noted that certain variations of current practice in sheet and seam testing were made. However, testing within a given material was consistent throughout, hence the resulting comparisons should be valid.

Tensile Tests for Geomembrane Sheets. Strip tensile tests and dumbbell tensile tests of nonreinforced geomembranes were performed according to ASTM D882 and ASTM D638 Type IV, respectively. PVC, CSPE, EIA and FCEA geomembranes were evaluated using strip tests. VLDPE, HDPE and fPP geomembranes were tested using dumbbell tensile tests. All scrim reinforced geomembrane sheet specimens were tested using a 25 mm strip test instead of the customary 100 mm grab tensile test.

Shear Tests for Geomembrane Seams. The shear tests for PVC, EIA and FCEA geomembrane seams were performed according to ASTM D3803. For HDPE, VLDPE and fPP geomembrane seams, ASTM D4437 test procedure was followed, but a strain rate of 8.5 mm/sec was used for testing VLDPE and fPP. For reinforced materials, the shear test followed the same procedure as the sheet test.

Peel Tests for Geomembrane Seams. The peel tests for HDPE, VLDPE and fPP were performed according to ASTM D4437; however, a strain rate of 8.5 mm/sec was used for testing VLDPE in Part I. All other geomembrane seams were tested according to ASTM D413. A 25 mm gage length was used throughout all peel tests.

RESULTS OF TENSILE TESTS ON THE FREEZE-THAW GEOMEMBRANE SHEETS AND SEAMS

The tensile test results of Parts I, II and III of the study are analyzed and presented. All parts focused on the effect of freeze-thaw cycling on the particular geomembrane sheets and seams stated earlier.

Data Analysis Approach. The potential effect of freeze-thaw cycling on various geomembrane sheet and seam specimens was evaluated based on the magnitude of percent change of the specific measured property from its corresponding initial value. In Part I, the initial values were

Table 2. Type of geomembrane sheets and seams.

Part(s) of Study	Sample No.	Geomembrane Type (i.e., Polymer)	Thickness (mm)	Style	Seam Type
I, II, III, IV	1(a)	PVC-R (cold temperature formula)	1.1	Scrim reinforced	Chemical
I, II, III	1(b)				Hot Wedge
I, III	2(a)	PVC	0.5	Smooth	Chemical
I, III, IV	2(b)				Hot Wedge
I, III	2(c)				Dielectric
I, II, III	3(a)	PVC	1.0	Smooth	Chemical
I, II, III, IV	3(b)				Hot Wedge
I, II, III	3(c)				Dielectric
I, II, III	4	VLDPE	1.0	Smooth	Hot Wedge
II, IV	4(a)				Fillet Extrusion
I, II, III	5	VLDPE	1.0	Textured	Hot Wedge
II	5(a)				Fillet Extrusion
I, III, IV	6	VLDPE	1.5	Smooth	Hot Wedge
I, III, IV	7	VLDPE	1.5	Textured	Hot Wedge
I, III	8	HDPE	1.0	Smooth	Hot Wedge
I, III	9	HDPE	1.0	Textured	Hot Wedge
I, II, III, IV	10	HDPE	1.5	Smooth	Hot Wedge
II	10(a)				Fillet Extrusion
I, II, III, IV	11	HDPE	1.5	Textured	Hot Wedge
II	11(a)				Fillet Extrusion
I, III, IV	12	fPP	1.0	Smooth	Thermal
I, III, IV	13	fPP-R	1.1	Scrim reinforced	Hot Wedge
I, III	14(a)	CSPE-R	0.9	Scrim reinforced	Chemical
I, III, IV	14(b)				Thermal
I, III, IV	15(a)	EIA	0.8	Smooth	Chemical
I, III	15(b)				Thermal
I, III	16(a)	EIA-R	0.9	Scrim reinforced	Chemical
I, III	16(b)				Thermal
I, III	17	FCEA	0.8	Smooth	Thermal
I, III	18	FCEA-R	0.8	Geotextile supported	Thermal
I, III	19	EIA-R	0.8	Scrim coated	Thermal

Key to Abbreviations:
PVC = polyvinyl chloride,   VLDPE = very low density polyethylene   t = textured
HDPE = high density polyethylene.   fPP = flexible polypropylene   R = scrim reinforced
CSPE = chlorosulfonated polyethylene,   EIA = ethylene interpolymer alloy
FCEA = fully crosslinked elastomeric alloy

the test results of non-incubated original sheet and seam specimens. In Part II, the initial values were data of non-incubated sheet and seam specimens that were obtained by testing at -20°C temperature. For Part III, the initial values were data of the first freeze-thaw cycle. These data were used because it was necessary to compare specimens that were also constrained.

For each material, the percent change from the baseline data was plotted against the logarithm of the number of incubated cycles. The tensile properties of geomembrane sheets evaluated were strength and elongation values at peak, yield or break, depending on the type of geomembrane. Only the strength values of the seamed samples were considered for the shear and peel tests. Since only three tests were performed at each cycle; a rigorous statistical analysis could not be carried out. Hence, the error limits for each property were arbitrarily developed as described in Hsuan et al. (1993). For each graph, two sources of variation were considered: internal and external variation. Internal variation resulted from differences within each set of three tests. External variation resulted from the variability between each set of tests. The summation of the two variations was considered to be the total error for that property. A change in any examined property is defined when a percent change value exceeded the total error.

Tensile Test Results. Based on the data analysis described above, the effect of freeze-thaw cycling for each tested geomembrane sheet and seam under different incubation and test conditions was evaluated. Due to the page limitation, only three selected percent change graphs are presented in this paper as examples. They can be seen in Figures 1 to 3. (All percent change graphs are included in the Reclamation report, 1996). In all three graphs, the individual error bar at each cycle falls within limits of the total error (i.e., the two horizontal lines) for that examined property.

Part I results. In this part of the experiment, the specimens were exposed to a maximum of 200 cycles in an unconstrained condition and then were tested at +20°C. The nineteen geomembrane sheets showed no changes in the examined tensile properties, i.e., neither the strength nor the elongation exceeded the error limits. Also the twenty-six combinations of seams exhibited no changes in either the shear strength or peel strength.

Part II results. In this part of the experiment, the specimens were exposed to a maximum of 200 cycles in an unconstrained condition and then were tested at -20°C. If defects were created in the incubated specimens due to freeze-thaw cycling, they probably would be more sensitive to cold temperature testing than the +20°C testing of Part I. For the six different geomembranes, no changes were observed in either the peak strength or peak elongation. Also the twelve combination of seams showed no change in both shear and peel strength.

Part III results. In this part of the experiment, the specimens were exposed to a maximum of 500 freeze-thaw cycles in a constrained condition and then were tested at +20°C. Even under these relatively severe incubation conditions, there was no change in any of the nineteen geomembranes. For the twenty-six combinations of seams, the results show no change in either the shear strength or peel strength.
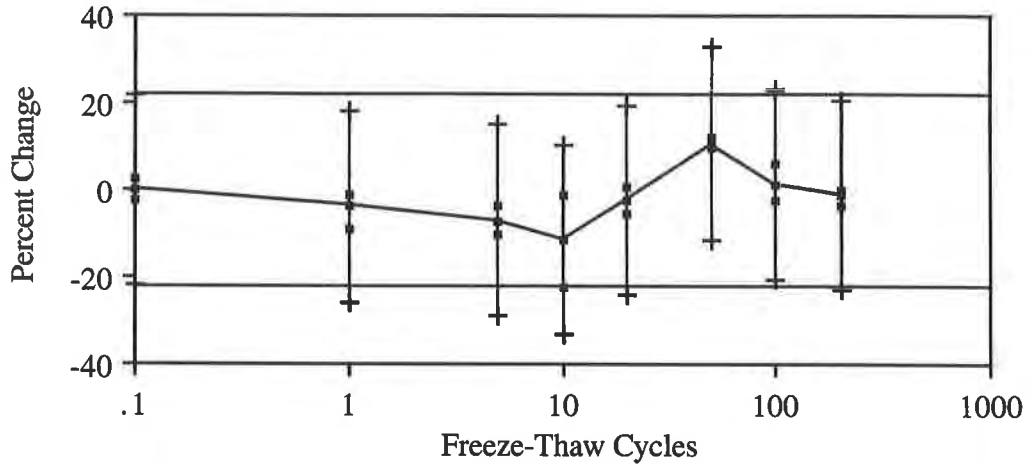
Figure 1. An example of Phase I result (1.0 mm HDPE-T sheet yield strength)
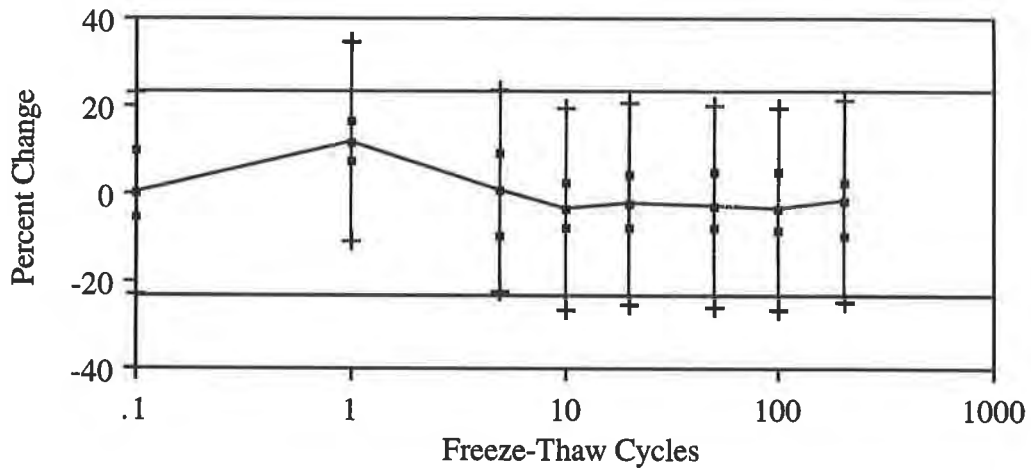
Figure 2. An example of Phase II result (1.0 mm PVC hot wedge peel seam strength)
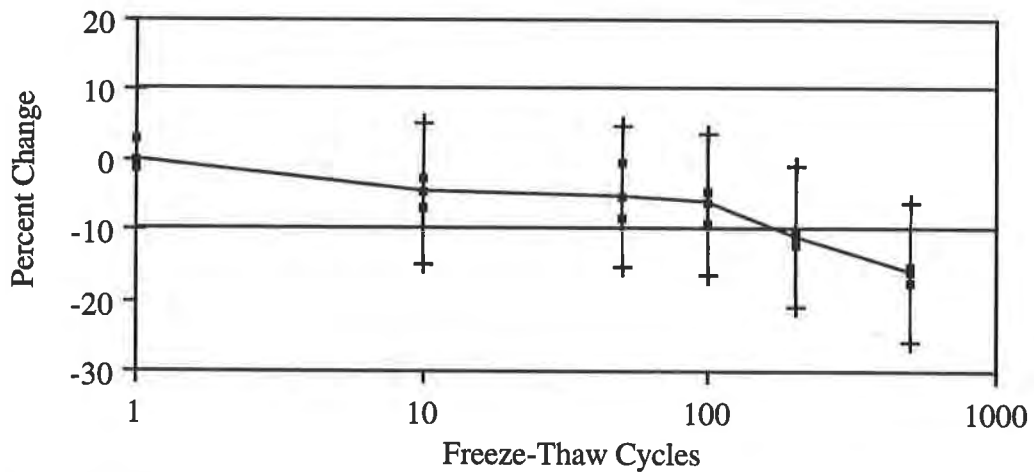
Figure 3. An example of Phase III result (1.1 mm PP-R hot wedge shear seam strength)

COLD TEMPERATURE INDUCED TENSILE STRESS IN CONSTRAINED GEOMEMBRANE SHEET AND SEAM SPECIMENS

This section presents the results of the Part IV study. The purpose of the Part IV study is to quantify the cold temperature induced cyclic tensile stress of constrained specimens in Part III of the study. Eight of the nineteen geomembrane sheets and eight of the twenty seven geomembrane seams used in Part III were evaluated. Tests were performed inside an environmental chamber in a tensile machine. The strain condition of test specimens was the same as that used in Part III of the study. All test specimens were strained and locked into values corresponding to 25% of maximum stress of the material. The load values were recorded with time. The chamber temperature changes were similar to the Part III study, heating from room temperature to +30°C and then cooling to -20°C. The only difference was the time duration at each temperature zone. The temperature was held constant at +30°C and -20°C for two hours instead of eight and sixteen hours, respectively. According to Lord, et al., (1995), the thermal induced stress would not relax as long as the temperature remained constant. It was found that two hour was a sufficient duration to establish equilibrium at each temperature so that the thermal induced stress could be evaluated.

The results were presented by plotting recorded load data against time for all tested geomembrane sheets and seams, as shown in Figure 4. Based on the resultant data, three issues were investigated and they are presented as follows:
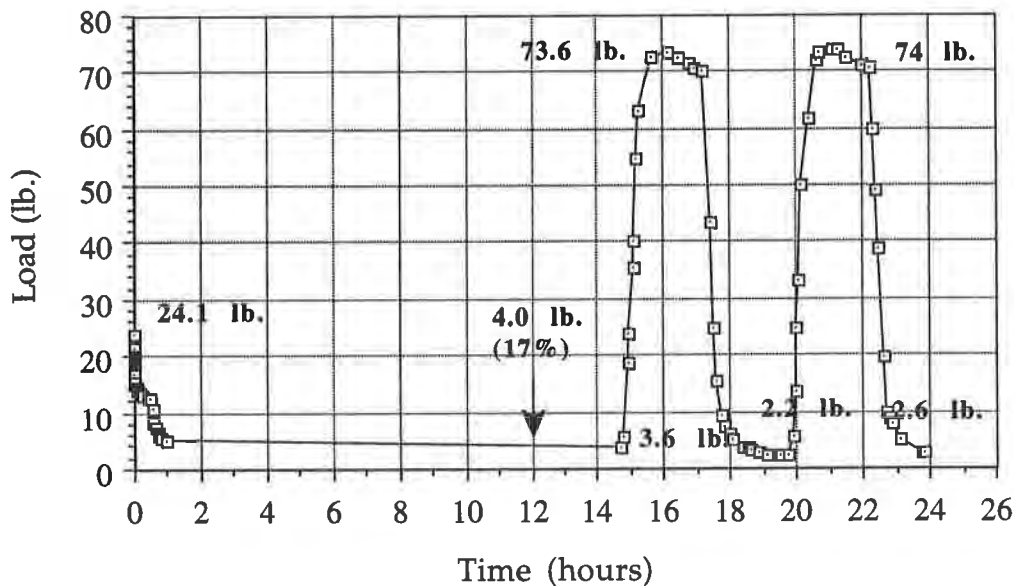
Figure 4. An example of load versus time plot (1.5 mm HDPE smooth sheet)

Stress Relaxation Within the First Twelve Hours. The initial induced stress due to straining relaxed rapidly within the first twelve hours. The stress relaxation behavior of different geomembrane sheets and seams was evaluated. For comparison purposes, the effects of variation in strain rate, gauge length, and strain value that were used in each individual test specimen were minimized by normalizing all stress data to the corresponding initial stress value (i.e., stress at time zero). The normalized stress data were then plotted against the logarithmic

of time as illustrated in Figure 5. (The normalized stress curves of all tested materials were presented in Reclamation report, 1996). Following are the observations made from the results:

1. In the first 12 hours of the test, specimens were exposed to room temperature for 30 minutes and then heated to +30°C for 12 hours. Both the geomembrane sheets and seams showed a significant amount of stress relaxation. For the non-reinforced geomembrane sheets and seams, 70 to 80 percent of the initial stress was relaxed, whereas a lower amount of relaxation was monitored in the reinforced materials, around 40 to 75 percent, as can be seen in Table 3. This is because the scrim in the reinforced materials has less relaxation tendency than the membrane component, thus restricts the total relaxation of the geomembrane.

2. The stress relaxation behavior of sheets and seams is very similar within each non-reinforced geomembrane type, as shown in Figure 6. In contrast, the seams of reinforced geomembranes exhibited a greater stress relaxation than the corresponding sheet materials, as indicated in Figure 7. This effect probably was due to the test configuration. In a seam shear test, the scrim in each of the two overlapping geomembranes is constrained on one side, whereas, in a sheet tensile test, the scrim is constrained on both sides. Consequently, a lesser restriction was imposed to the membrane component from the scrim in a shear seam test, allowing a greater stress relaxation.

Magnitude of Cold Temperature Induced Tensile Stress. As the temperature of the chamber decreased from +30°C to -20°C, a tensile load was induced in the test specimens. The magnitude of this induced load was calculated by subtracting the minimum load value at +30°C before onset of the cooling from the maximum load value at -20°C. The induced stress was obtained by dividing the load by the cross sectional area of the respective test specimens. Table 3 lists the induced stress values of all tested materials. Following are the observations made from the data:

1. For non-reinforced geomembranes, similar induced stresses were obtained in the same type of polymer, regardless of the variation in the thickness, surface finishing and seam types, for example:

   - the PVC group consists of an induced stress around 1720 kPa (250 psi)
   - the VLDPE group consists of an induced stress around 3800 kPa (550 psi)
   - the HDPE group consists of an induced stress around 8300 kPa (1200 psi)

2. For the seven polymer types involved in the test, HDPE exhibited the highest induced stress. This is due to its high linear thermal expansion coefficient and high tensile modulus. Based on Equation (1), a comparably high induced stress was expected.

$$\sigma = \alpha_{(t)} * \Delta T * E_{(t)} \qquad (1)$$

where: σ = induced stress
          $\alpha_{(t)}$ = coefficient of thermal expansion which is a function of temperature
          ΔT = temperature difference
          $E_{(t)}$ = tensile modulus which is a function of temperature
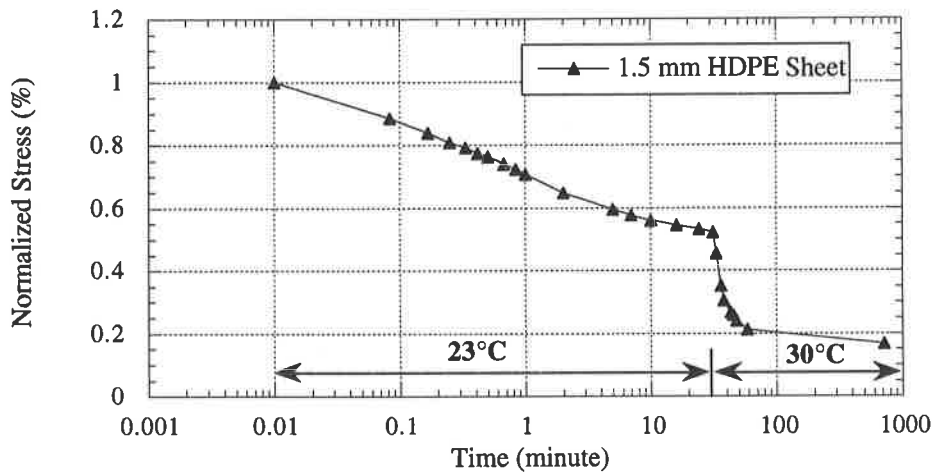
Figure 5. Stress relaxation behavior in first 12 hours of the test.
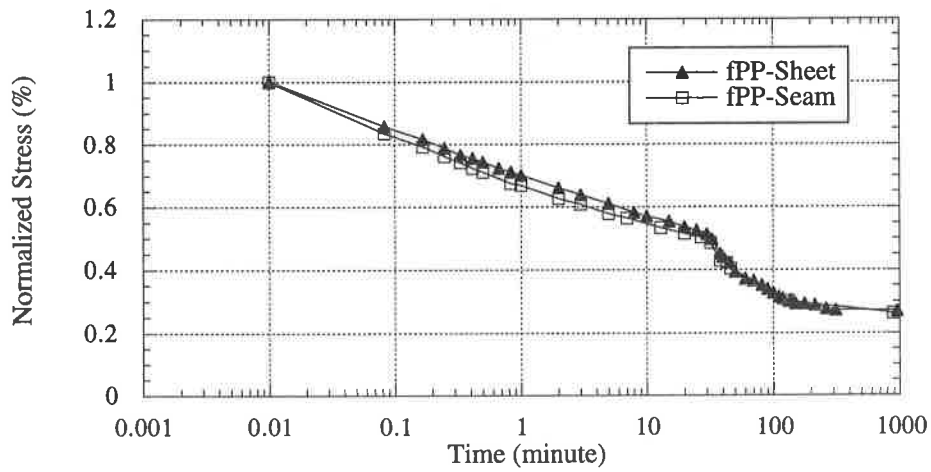
Figure 6. Stress relaxation behavior of non-reinforced geomembrane sheet and seam.
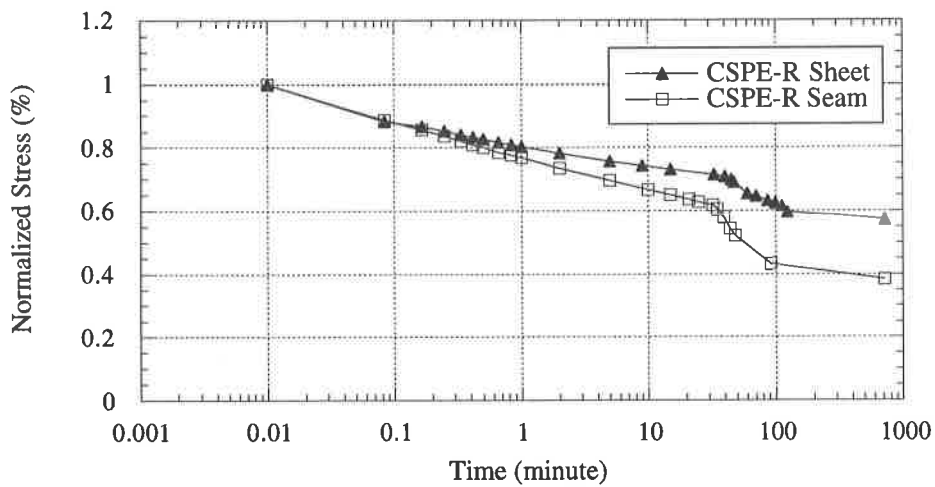
Figure 7. Stress relaxation behavior of reinforced geomembrane sheet and seam.

Table 3. Stress relaxation values and cold temperature
induced stress values for sheets and seams.

No.	Geomembrane	Thickness mm (mil)	Seam Type	% relaxation after 12 hrs.	Induced Stress (kPa)
1	PVC-R	1.1 (45)	Sheet	56	7030
1(a)			Chemical	70	8000
2	PVC	0.5 (20)	Sheet	75	2070
2(b)			Hot Wedge	71	1720
3	PVC	1.0 (40)	Sheet	76	1520
3(b)			Hot Wedge	81	1450
4	VLDPE	1.0 (40)	Sheet	77	3450
			Extrusion	83	3930
6	VLDPE	1.5 (60)	Sheet	82	3800
			Hot Wedge	80	3800
7	VLDPE-textured	1.5 (60)	Sheet	76	3860
			Hot Wedge	79	3800
10	HDPE	1.5 (60)	Sheet	83	8300
			Hot Wedge	83	8300
11	HDPE-textured	1.5 (60)	Sheet	84	8300
			Hot Wedge	89	9000
12	fPP	1.0 (40)	Sheet	73	2550
			Thermal	74	2000
13	fPP-R	1.1 (45)	Sheet	52	2760
			Hot Wedge	67	2620
14	CSPE-R	0.90 (36)	Sheet	43	3450
14(b)			Hot Air	62	3450
15	EIA	0.80 (30)	Sheet	87	2760
15(a)			Chemical	80	3450

Equation (1) also can be used to explain the low induced stress exhibited by the VLDPE materials. Although the VLDPE has a higher thermal expansion coefficient than the HDPE, it consists of a much lower tensile modulus.

In spite of the simplicity of Equation (1), accurately predicting the thermal induced stress is rather difficult due to the uncertainty as to what values of "α" and "E" should be used.

3. A four times higher induced stress was measured in the PVC-R than the PVC. Plasticizers have been added to the formulation of both geomembranes to increase their flexibility and lower their glass transition temperatures (T_g). The type of plasticizer used in each of the geomembranes is different. Subsequently, T_g values of both geomembranes are not the same. The higher induced stress in the PVC-R geomembrane is caused by its relatively high T_g value which is at -30°C, whereas the T_g of PVC is at -45°C. At a test temperature of -20°C, the PVC-R was approaching a glassy stage, thus the modulus of the material increased, resulting in a high induced stress.

Repeatability in the Magnitude of the Cold Temperature Induced Tensile Stress. The repeatability of the induced stress was investigated by repeating the cooling and heating cycle from +30°C to -20°C twice. From the load versus time graphs, such as the curve shown on Figure 4, the magnitude of the induced stresses in both cooling cycles was very similar for all tested materials. This suggests that the constrained specimens in Part III of the study were subjected to the same magnitude of cyclic stress during each of the 500 freeze-thaw cycles.

DISCUSSION OF FREEZE-THAW EFFECTS

In this section, the results of Parts I and III are separately discussed so that the effects of freeze-thaw cycling under different incubation conditions can be described.

Part I Study. After the nineteen geomembrane sheet and twenty seven geomembrane seam specimens were exposed to 200 freeze-thaw cycles in an unconstrained condition, no changes were detected in any of the sheet tensile behavior and seam shear and peel strengths. This suggests that freeze-thaw action does not affect the unconstrained geomembrane sheets and seams that can lead to change in their tensile behaviors.

Part II Study. Six geomembrane sheet and thirteen geomembrane seam specimens were exposed to 200 freeze-thaw cycles in an unconstrained condition, and then tested at -20°C. The low testing temperature was intended to emphasize any existing defects in the tested specimens which might be generated during the freeze-thaw cycles. However, no changes were observed in either the sheet or seam tensile behavior.

Part III Study. The same types of specimens used in Part I were exposed to 500 freeze-thaw cycles in a constrained condition. As indicated by the results of Part IV, a repeatable thermal induced stress was also imposed onto the constrained specimens during each freeze part of the cycles. The magnitude of the induced stresses depended on the type of the polymer. In addition, the induced stress remained in the specimen until the temperature of the specimen was changed. Thus, test specimens of this study were subjected to a much severer incubation

condition than those in Parts I and II. Even so, no changes were detected in any of the sheet tensile properties or seam shear and peel strengths. Additionally, it should noted that the test condition of Part III probably simulates most field situations in which the geomembrane is constrained by cover material, such as soil.

DISCUSSION OF THE EFFECT OF COLD TEMPERATURE TESTING

The effects of cold temperature testing can be evaluated by comparing data of Part II tests to data of Part I tests. The evaluation included strength and elongation of six geomembrane sheets and eight geomembrane seams.

Sheet Tensile Behavior. For all tested geomembranes, strength values at -20°C were higher than those at +20°C, but the corresponding elongation values were lower. The approximate percentage changes in the tensile strength and elongation are shown in Table 4. In both HDPE and HDPE-T geomembranes, their yield stress increased approximately 70% and yield elongation decreased approximately 15%. These values are rather different than those reported by Giroud et al., (1993). They found that the yield stress of the HDPE geomembrane increased 43% and yield strain decreased 26% between temperatures +20°C and -20°C.

The PVC-R geomembrane exhibited a different tensile behavior at -20°C in comparison to +20°C. At -20°C, a single breaking peak corresponding to the breakage of both membrane and scrim was detected. Comparatively, two peaks were monitored at +20°C which corresponded to the breakage of the scrim and subsequently the membrane failure. At -20°C, a single breaking peak was detected. The peak strength was 100% higher than that at +20°C. This change was probably attributable to the stiffening of the membrane component of the geomembrane. As the temperature decreased, the strength of the membrane increased. At -20°C, the membrane and the reinforced scrim acted as a single composite material, resulting a single breaking peak. Regarding the elongation, since the peak elongation at -20°C corresponded to the breaking of the entire geomembrane (i.e., both membrane and scrim), such value cannot be compared to the peak elongation at +20°C which respresented the breaking of the scrim alone.

For VLDPE geomembranes, both smooth and textured sheets, direct comparison was unable to be performed because of the different tensile behavior at -20°C and +20°C. A pronounced yielding was detected at -20°C testing which was not observed at +20°C. However, the breaking was not measured because of limited chamber height, thus this property can be used for comparison. Nevertheless, the overall tensile load at -20°C seems to be higher than that at +20°C over the evaluated elongation range.

Table 4. Approximate percent changes in the tensile properties
by decreasing testing temperatures from +20°C to -20°C

| No. | Materials | Sheet Tensile Test (% change) | | Seam Type | Seam Tensile Test (% change) | |
		Strength	Elongation		Shear strength	Peel strength
1	PVC-R	100% ↑	20% ↑	hot wedge	80% ↑	30% ↑
3	PVC	45% ↑	70% ↓	chemical	65% ↑	90% ↑
				hot wedge	70% ↑	20% ↑
				dielectric	10% ↑	50% ↑
4	VLDPE	n/a	n/a	hot wedge	n/a	60% ↑
5	VLDPE-T	n/a	n/a	hot wedge	n/a	65% ↑
10	HDPE	75% ↑	15% ↓	hot wedge	120% ↑	25% ↑
11	HDPE-T	70% ↑	17% ↓	hot wedge	120% ↑	10% ↑

note: n/a = non applicable

Seam Tensile Behavior. In the seam shear tests, all seams showed a higher strength at -20°C than at +20°C, as can be seen in Table 4. In all eight types of seams, the two HDPE geomembrane seams exhibited the greatest increase in the shear strength. Within the three different types of PVC seams, the dielectric seam had the least effect by the cold temperature testing. Regarding the two VLDPE geomembrane seams, the shear strength from Parts I and II could not be directly compared for the same reasons as explained in the sheet testing. However, a higher shear tensile load was measured at -20°C than at +20°C over the tested elongation range.

In seam peel tests, all geomembrane seams showed a higher strength at -20°C than at +20°C, as can be seen in Table 4. For PVC-R, PVC, HDPE and HDPE-T hot wedge seams, the peel strength showed a lesser increase than the corresponding shear strength. Contrary, the PVC chemical and dielectric seams showed a greater increase in the peel strength than the shear strength, indicating a greater stiffness being developed at the seam interface of these seam types.

CONCLUSIONS

The freeze-thaw effect on the tensile behavior of nineteen geomembrane sheets and thirty one combinations of seams was evaluated both a constrained and an unconstrained incubation condition. After 200 freeze-thaw cycles under the unconstrained incubation condition, the tensile properties of geomembrane sheets and seams showed no statistically significant change at both +20°C and -20°C testing temperatures.

For test specimens under the constrained condition, the cold temperature induced tensile stress during the cold cycle of the freeze-thaw cycling was investigated. It was found that the magnitude of the induced stress was the same for each polymer type regardless of the thickness, surface features and seam types. However, the stress value was dependent on the thermal expansion coefficient and modulus of each polymer. Also the induced stress was

reproducible in each cold cycle and remained in the specimens until the temperature was changed. Therefore, tested specimens in Part III were exposed to thermal induced cyclic stresses as well as freeze-thaw cycling. Even under these severe test conditions, the tensile performance of geomembrane sheets and seams was not affected in a statistically significant manner after 500 cycles.

The cold temperature testing led to an increase in strength and decrease in elongation of all tested sheet and seam specimens. The amount of changes for sheet materials varied between polymer types. In addition, for the same geomembrane, the shear strength responded differently than the peel strength. A higher percent increase was observed in the shear strength than the peel strength for all hot wedge seams. Contrary, the chemical and dielectric seams showed a greater increase in the peel strength than the shear strength.

The general conclusion of the various parts of this study is that currently available geomembranes and their respective seaming methods are not sensitive to freeze-thaw cycling under constrained and unconstrained conditions within the limits of this study. However, as anticipated, a gradual stiffening of the geomembrane materials will occur with decreasing temperature. Thus, the cold temperature tensile behavior will be evaluated if the material would be exposed to freezing conditions. Furthermore, the thermal induced contraction stress must be considered during the design.

ACKNOWLEDGMENTS

REFERENCES

Budiman, J., (1994), "Effects of Temperature on Physical Behavior of Geomembranes," Proceedings of the Fifth International Conference on Geotextiles, Geomembranes and Related Products, Singapore, 1093-1096.

Reclamation Report (1996), "Freeze-Thaw Cycling and Cold Temperature Effects on Geomembrane Sheets and Seams," Report Number R-96-03.

Comer, A.I., M.L., Sculli, and Y.G., Hsuan,(1995), "Effects of Freeze-Thaw Cycling on Geomembrane Sheets and Their Seams," Proceedings of Geosynthetics' 95, Nashville, TN, 853-866.

Giroud, J.P., K.L., Soderman, and M., Monroe,(1993), "Mechanical Design of Geomembrane Applications," Proceedings of Geosynthetics' 93, Vancouver, Canada, 1455-1468.

Hewitt, R.D., and Daniel, D.E., (1996), "Hydraulic Conductivity of Geosynthetic Clay Liners Subjected to Freeze-Thaw," to be published in ASCE Journal of Geotechnical Engineering.

Hsuan, Y.G., M.L., Sculli, and R.M., Koerner, (1993), "Effects of Freeze/Thaw Cycling on

Geomembranes and Their Seams; Part I - Strength Tests at +20°," Edited by Koerner, R.M and Wilson-Fahmy, R.F., Proceedings of the Seventh GRI Conference, Philadelphia, PA, USA, 209-224.

LaFleur, J., S.Z., Akber, Y., Hammamji, and M., Marcotte, (1985), "Tensile Strength of Bonded Geotextile-Geomembrane and Composites," Proceedings of the Second Canadian Symposium on Geotextiles and Geomembranes, Edmonton, Alberta, Canada, 219-224.

Lord, A.E.,Jr., T.Y., Soong, and R.M., Koerner, (1995), "Relaxation Behavior of Thermally-Induced Stress in HDPE Geomembranes", Geosynthetics International, Vol. 2, No. 3, 626-634.

Othman, M.A., Benson, C.H., Chamberlain, E.J., and Zimmie, T.F., (1993), "Laboratory Testing to Evaluated Changes in Hydraulic Conductivity of Compacted Clays Caused by Freeze-thaw: State-of-the-Art", Hydraulic Conductivity and Waste Contaminant Transport in Soils, ASTM STP 1142, D.E. Daniel and S.J. Trautwein, eds., ASTM, Philadelphia.

Peggs, I.D., D.S.,Carlson, and S.J., Peggs, (1990), "Understanding and Preventing 'Shattering' Failures of Polyethylene Geomembranes," Proceedings of the Fourth International Conference on Geotextiles, Geomembranes and Related Products, edited by G. Den Hoedt, The Hague, Netherlands, Vol. 2, 549-554.

Richards, E.A., J.D., Scott, and R.J., Chalaturnyk, (1985), "Cold Temperature Properties of Geomembranes," Proceedings of the Second Canadian Symposium on Geotextiles and Geomembranes, Edmonton, Alberta.

Rollin, A.L., J., Lafleur, M., Marcotte, O., Dascal, and Z., Akber, (1984), "Selection Criteria for the Use of Geomembranes in Dams and Dykes in Northern Climate," Proceedings of the International Conference on Geomembranes, Denver, Colorado, USA, 493-499.

Zimmie, T.F., and La Plante, C., (1990), "The Effects of Freeze/Thaw Cycles on the Permeability of a Fine-Grained Soil," Proceedings 22nd Mid-Atlantic Industry Waste Conference, Drexel University, Philadelphia.

DURABILITY OF GEOSYNTHETICS BASED ON ACCELERATED LABORATORY TESTING

A. Salman
Polytechnic University, USA
V. Elias
Earth Engineering & Sciences, Inc., USA
I. Juran
Polytechnic University, USA
S. Lu
PRI, Polytechnic University, USA
E. Pearce
PRI, Polytechnic University, USA

ABSTRACT

The use of geosynthetic products has been steadily increasing in construction of reinforced fills as retaining walls and steepened slopes and for landfills in containment of hazardous waste. An impediment to their full utilization has been a lack of methods to assess their durability in the environment that they may be placed. Therefore, to assess the durability of existing and improved geosynthetics, it becomes necessary to assess their durability within a very short time with respect to environmental parameters to which they will likely be subjected. This requires the development of accelerated laboratory tests at high temperature, permitting prediction of the behavior of the geosynthetics in actual use.

A Basic Autoxidation Scheme (BAS) for polyolefins has been adapted to develop a kinetic model for evaluating the mechanical degradation of polyolefin geosynthetic products. The model provides a satisfactory method to analyze the experimental laboratory data and estimates of strength loss caused by thermooxidation as a function of time.

For polyester based geosynthetics, which are subject to hydrolysis, analysis of experimental data indicates that molecular weight loss is a dominant mechanism leading to mechanical strength loss in acidic and neutral environments. Fiber surface erosion, as well as molecular weight degradation, are responsible for mechanical strength loss, when polyester based geosynthetics are immersed in alkaline media. An Arrhenius type kinetic model provides a satisfactory analysis model, and permits estimates of strength loss due to hydrolysis as a function of time.

RESEARCH OBJECTIVES

The scope of the research was limited to the laboratory investigation of thermooxidative and hydrolytic degradation in a few typical commercial product samples selected to represent

geosynthetic materials used in civil engineering projects. The full study tested 4 polyolefin based products and 3 polyester based products.

The overall objectives of the study are:

- to develop testing protocols for accelerated degradation techniques for polyolefin and polyester commercial geosynthetic products;

- to assess the rate of chemical and mechanical degradation of selected commercial geosynthetic products with potential estimate of their service life;

- to investigate effects of specific variables of material composition and environment on the degradation behavior of selected geosynthetics.

The scope of the study was by necessity limited in that:

- a small number of commercial geosynthetic products (and polymers) were considered;

- only "severe" conditions of treatment, as compared to the in-service conditions, are used to accelerate degradation to achieve measurable chemical and mechanical changes during 2 to 3 years of laboratory incubation time.

GEOSYNTHETIC MATERIALS TESTED

Results from two commercial geotextiles are reported in this study. They are: (i) polypropylene nonwoven geotextile, and (ii) polyester nonwoven geotextile. These materials are differentiated by the processes which cause their degradation. Polypropylene based materials are affected by oxidation in soil or by oxygen dissolved in soil water. Polyester products are subject to hydrolysis by different aqueous solutions present in soil.   The properties of geotextiles reported are shown on table 1.

ACCELERATED DEGRADATION OF POLYPROPYLENE GEOSYNTHETICS

It has been reported that polypropylene geosynthetics may oxidize resulting in polymeric molecular chain breaks. The reduction of the polymer chain length directly results in strength loss of a material. The available studies of polyolefins oxidation indicate that rates of oxidation are very low at ambient temperatures (Koerner, Lord and Hsuan, 1992; Wisse et al., 1982; 1990; Wisse, 1988; Horroks and D'Souza, 1992), however in the context of the lifetime of civil engineering applications, may not be negligible.

Comprehensive studies of polyolefin oxidation (Chien and Boss, 1967; Zolotova and Denisov, 1971) indicated that the rate of reaction depends on the oxygen partial pressure in the system as well on the temperature. It is further indicated in the literature (Reich and

Stivala, 1971; Kelen, 1982), that presence of transition metals or their salts in the system, may accelerate oxidation of polyolefins. However, consideration of these factors in the degradation performance of polypropylene geotextile PP-3 is beyond the scope of this reported investigation.

Table 1. Major characteristics of commercial geotextiles tested.

Product	Type	Antioxidant type	Mass per unit area, g/m² (oz/yd²)	Molecular weight, $\overline{M}_n \times 10^3$	CEG T_m^* °C, T_g^{**} °C	Wide width tensile strength, kN/m (lbs/in)
PP-3	Polypropylene nonwoven, needlepunched continuous filament	HALS	437 (13)	Unknown	CEG=N/A T_m=161.4°C	14.5 (83)
PET-5	Polyester nonwoven, spunbonded needlepunched continuous filament.	N/A	538 (16)	18.2	CEG=47 T_g=80.4°C	35.9 (205)

*T_m - Melting peak temperature; **T_g - Glass transition temperature.

Testing Procedures. The accelerated thermooxidative degradation test procedure used involves: (i) sample preparation; (ii) oven aging of prepared samples in forced draft ovens (iii) mechanical testing to determine tensile strength using a Wide Width Strip Test.

To perform accelerated thermodegradation of polyolefin geosynthetics in circulating air (21% O_2), forced-draft ovens with temperature uniformity of ±1 percent and substantial fresh air intake were used in a compliance with the ASTM D-3045 "Heat aging of plastics without load". The specimens of full "wide width" dimensions (200 mm x 200 mm) were suspended in the oven without pretension and without touching each other.

Geosynthetic specimens were retrieved at five consecutive time intervals. Duration of time interval is defined for each specific temperature of thermooxidation. If obtained data are insufficient for further interpretation, additional retrievals are scheduled. Retrieved specimens are tested for mechanical properties using Wide Width Strip Test Method (ASTM D4595). Each retrieval for all temperatures is represented by 5 specimens, retrieved at appropriated time intervals.

The samples of the nonwoven commercial geotextile PP-3 were exposed to five temperatures of 50°, 60°, 70°, 80° and 90°C. The strength loss versus time curves are shown on figure 1, indicate a non linear strength loss and the presence of an induction period. The induction period is defined as the initial period of oven aging, when no statistically significant changes of a tensile strength is observed. It appeared that the induction period increases as the temperature of the exposure decreases. The highest temperature of exposure of 90°C, appeared to be extremely severe for this product, which almost lost its total strength by the end of the 170-day long exposure. At lower temperatures, the strength loss versus time curves display a non-linear behavior after the induction period.

Neither shrinkage nor swelling have been observed over the period of exposure. SEM study of the fiber surface morphology indicated that there are no apparent changes on the fiber surface on a microlevel at a magnification of 3000x, for specimens aged at temperatures varying from 50° to 90°C. The monitoring of weight changes, indicated that there are no statistically significant variations in weight.
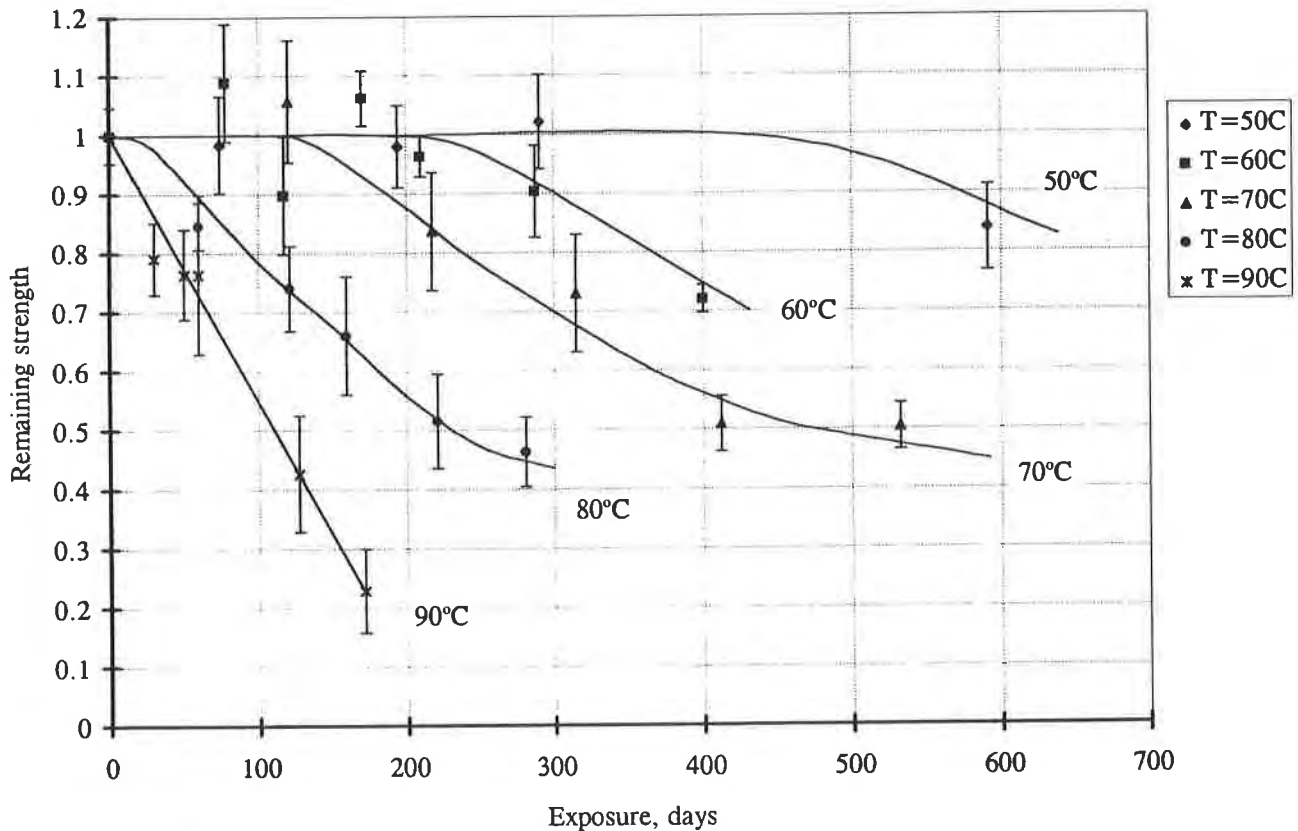
Figure 1. Tensile strength loss for PP-3 geotextile due to oven aging.

ANALYSIS OF EXPERIMENTAL RESULTS

The literature suggests that mechanical durability of polyolefin commercial geosynthetics can be evaluated using an Arrhenius type modeling. (Wisse and Birkenfeld, 1982; Allen 1991; Koerner, Lord and Hsuan, 1992;). The concept of Arrhenius modeling in accelerated degradation studies of polymeric materials is based on the well established concept that chemical reactions of many types proceed more rapidly at higher temperatures than at lower temperatures. It is therefore implied, that laboratory experimental results for mechanical properties of polymeric materials exposed to elevated temperatures could be used within the framework of an Arrhenius model to evaluate the life of geosynthetics at ambient temperatures. The Arrhenius equation widely used in the geosynthetic industry to predict a given strength loss of geosynthetics, is as follows:

$$K_r = Ae^{-(U_{act}/RT)} \tag{1}$$

where:

K$_r$ - is the reaction rate constant;
A - the pre-exponential factor, usually considered as a constant that is independent of temperature;
U$_{act}$ - the activation energy, which is also treated as a constant for each particular material and is independent of temperature;
R - the ideal gas constant; and
T - the temperature in °K.

The literature suggests that the values of apparent activation energy derived from experimental results by using the Arrhenius model, are not constant for the same material, within the range of applied temperatures. Wisse and Birkenfeld (1982) reported an U_{act} value of 93 kJ/mol for temperatures above 80°C and a value of 65 kJ/mol for temperature below 70°C. This appears to be inconsistent, as the activation energy of any polymeric material is a fundamental constant that does not depend on the temperature suggesting that the degradation process is more complex than modeled by a simple Arrhenius dependency.

The results of tensile strength losses during oven aging in circulating air (ASTM 3045) (figure 1), indicate that PP-3 at elevated temperatures up to 70°C exhibits a substantial period of time with no changes of mechanical strength followed by a nonlinear decay indicating that Arrhenius type modeling may be too simplistic to describe the degradation behavior of this geosynthetic product. Therefore, the basic chemical reactions of thermooxidation as well as their kinetics must be considered in formulating an appropriate numerical model.

Basic Autoxidation Scheme. Oxidation of polyolefins is a well known and studied process. The reaction of organic compounds initiated by the attack of molecular oxygen is

called autoxidation. The effect of auto-acceleration in the degradation of organic compounds caused by a reaction with oxygen had been well recognized in the literature. Studies on this phenomena led to the development of a basic autoxidation scheme (BAS) (Bolland, 1948; Kelen, 1982). This scheme includes all the important steps in oxidation and explains many features of the process. Recent theories of polymer oxidation are based on BAS with minor modifications and extensions (Reich and Stivala, 1971; Kelen, 1982).

The oxidative degradation of polymers is a free radical reaction and may be described by the following steps:

I. Initiation - formation of free radicals initiated by polymerization catalyst residues, heat or shear which initiate chain scission in the polymer generating free radicals:

$$polymer \xrightarrow{k_i, \ Energy, shear, heat} R \cdot \tag{2}$$

II. Radical conversion. The conversion of the hydrocarbon radical is an important step in which the majority of oxygen is absorbed by the polymer:

$$R \cdot + O_2 \xrightarrow{k_i} ROO \cdot \tag{3}$$

III. Chain propagation. At this stage oxygen centered radical species absorbs a hydrogen atom from the surrounding polymer to form hydroperioxide and create another free radical:

$$ROO \cdot + polymer \xrightarrow{k_i} R \cdot + ROOH \tag{4}$$

IV. Degenerate chain branching. i.e., the decomposition of hydroperoxides to radicals. This step is similar to the initiation step and therefore leads to auto-acceleration of the oxidation producing new portions of free radicals that can react with oxygen to continue the cycle:

$$ROOH \xrightarrow{k_i} RO \cdot + \cdot OH \tag{5}$$

V. Termination. Under most conditions, termination of free radicals in polymer oxidation occurs almost exclusively by participation of peroxy radicals:

$$ROO \cdot + ROO \cdot = products \tag{6}$$

Simplified Kinetics of Autoxidation of Polyolefins. The general scheme of polymer oxidation presented, is a simplified description of autoxidation of polyolefins and can be used for kinetic description of the main characteristics of the process. Such characteristics are the time dependence of oxygen absorption, temperature, pressure, and concentration dependence of oxidation rate. There are many other important parameters of polymer oxidation such as the change of molecular weight distribution, the formation of volatile products, and the change of polymer composition. A scheme which would allow the kinetic treatment of all processes would include many more steps than the simplified procedure, and the reactions would be chemically much more specific. Such an approach is, however, beyond the framework of this simplified analysis.

Assuming that the concentration of *RH*, i.e., the *C-H* bonds participating in the oxidation to be a constant, and that a steady state is reached very soon after the onset of the reaction, which is a usual and justified assumption of kinetics for chain reaction, the following expression for time dependence of hydroperoxide concentration was obtained (Reich and Stivala, 1971; Kelen, 1982) by solving the system of differential equations describing the BAS as shown in equations 2 through 6 :

$$[ROOH] = a(1 - e^{-bt}) \tag{7}$$

where a and b complex constants.

Equation (7) indicates that the reaction of thermooxidation, described in the BAS, is a first order reaction where the complex constant b may be treated as the apparent rate constant. Data reported in the literature (Zolotova, Denisov, 1971), clearly indicates the linear dependency of log kinetic constants plotted against the inverse of temperature, suggesting an Arrhenius type for the rate constant b in equation (7).

Thermooxidation results in polymer chain breaks and in the decrease of polymer molecular weight. The concentration of hydroperoxide, as a product of chain breaks, is proportional to the number of main chain breaks. The decrease in molecular weight, in turn, results in the decrease of tensile strength of the original polymer. Therefore, as a first approach, it can be assumed, that the degree of mechanical degradation defined as mechanical strength loss of a polymer due to thermooxidation, is proportional to the hydroperoxide concentration in a polymer mixture at any given time of oven aging. Considering that thermooxidation is a first order reaction (7), with an Arrhenius type rate constant, the normalized retained tensile strength F of a polymer can be expressed as:

$$F(t) = e^{-\bar{k}t}; \text{where } \bar{k} = A_1 e^{-U/RT} \text{ is an apparent rate constant} \tag{8}$$

Effect of Antioxidant Additives on the Kinetics of Autoxidation. Antioxidants used in polymer applications are generally classified by the mechanism in which they act as stabilizers during oxidation. Primary antioxidants provide stabilization by trapping or deactivating free radicals after they are formed. Secondary antioxidants decompose hydroperoxides into non-radical species therefore slowing the formation of free radicals. For each of these two categories, there are kinetic equations describing the consumption of antioxidants.

The most advanced mixtures of antioxidants provide almost complete protection against oxidation while their concentration in the polymer mixture is insignificant. After their consumption, the degradation of the polymer occurs in a manner similar to the process described by the Basic Autoxidation Scheme. The rate of consumption of antioxidants depends on the temperature in the reaction as well as on the oxygen partial pressure in the system. As a

first approach, it can be assumed, that the rate of antioxidant consumption in the polymer mixture could by described by an Arrhenius type temperature dependency when temperature is below the upper limit of antioxidant's working temperature.

The data reported in the literature (Karlsson, Smith and Gedde, 1992) indicate that there is an induction period during the mechanical degradation of medium density polyethylene (MDPE) oxidized at elevated temperatures. The reported results, indicate that the logarithm of the rate of consumption of antioxidant k_{ind}, is a linear function of the reciprocal temperature, which is similar to an Arrhenius type dependency. Therefore, an Arrhenius type functions could be used to extrapolate values of induction times observed at elevated temperatures to estimate anticipated induction time at ambient temperature for geosynthetics.

Interpretation Procedure. The kinetics of autoxidation for the general case of antioxidant presence, consist of two phases. The first phase (induction period) describes the consumption of antioxidants, with the rate of consumption defined by an Arrhenius-type dependency. During the second phase, the oxidation and corresponding mechanical degradation is described by the kinetics of the BAS resulting in equation (8).

The assumptions for autoxidation and corresponding first order kinetic equations for a constant oxygen concentration suggest a step-by-step procedure for the interpretation of laboratory aging data on mechanical degradation of polyolefin geosynthetic products, as follows:

1. The induction period t_{ind} is determined at each temperature of exposure, defined as the period of no statistically significant changes in mechanical strength. The rate of antioxidant consumption k_{cons} is defined as $1/t_{ind}$.

2. A linear regression analysis is conducted for the function $ln(k_{cons})$ versus the reciprocal temperature $(1/T °K)$. The obtained linear equation $ln(k_{cons}) = a(1/T) + b$ is used to find the value of the rate of antioxidant consumption and the value of induction period at any given temperature, $T_0 °K$:

$$k_{cons} = exp(a(1/T_0) + b); \quad t_{ind} = 1/k_{cons} \tag{9}$$

3. The exponent $f(t) = e^{-at}$ is used to fit experimental data for the observed progressive mechanical degradation, after the induction period for each temperature of aging. A semi-log chart may be used to plot $ln(F(t))$, where $F(t)$ is a retained strength, versus time t, and the slope of a linear trend a is a rate constant k at specific temperature of testing.

4. The obtained values of reaction constant are used to plot the logarithm of rate constant $ln(k)$ versus reciprocal temperature of aging (Arrhenius plot)

5. A linear regression analysis is used to find the equation for $ln(k)$ as a function of reciprocal temperature $1/T$, $ln(k) = a(1/T)+b$. The solution of this regression equation yields the value of rate constant k for the temperature of interest, T_0: $k(T_0) = exp(a(1/T_0)+b)$

6. The obtained rate constant value $k(T_0)$ in (10) is used to calculate retained strength $F(t)$ at a given time t or to calculate time t_i to reach certain level of strength F_i for a specific temperature $T_0 °K$:

$$F(t) = exp(-k(T_0)t); \quad t_i = (ln1/F_i)/k(T_0) \tag{10}$$

Kinetic Model Implementation for Experimental Data. Geosynthetic product PP-3 containing antioxidant additives exhibits an induction period from the degradation curves (see figure 1). The summarized data on induction period at elevated temperatures are shown in figure 2. Results for the consumption rate are shown in figure 3. It appears that a linear approximation satisfactory fits experimental data for consumption rate k_{cons} on an Arrhenius-type plot. The solution of the equation for linear regression of $ln(k_{cons})$ versus reciprocal temperature $1/T$ at 20°C or T=293°K, yields value of anticipated induction period $t_{ind} = 51$ years in which no strength loss is anticipated, under these testing conditions which do not consider potential antioxidant extraction in underwater regime.
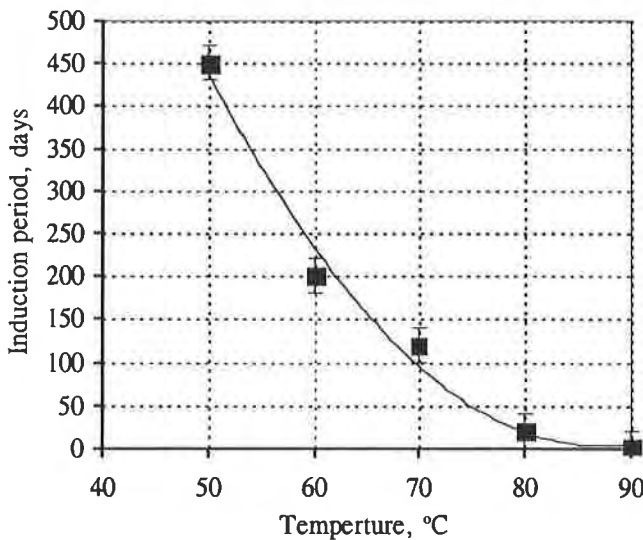
Figure 2. Induction period for PP-3.   Figure 3. Arrhenius plot for the consumption
rate k_{cons} for PP-3.
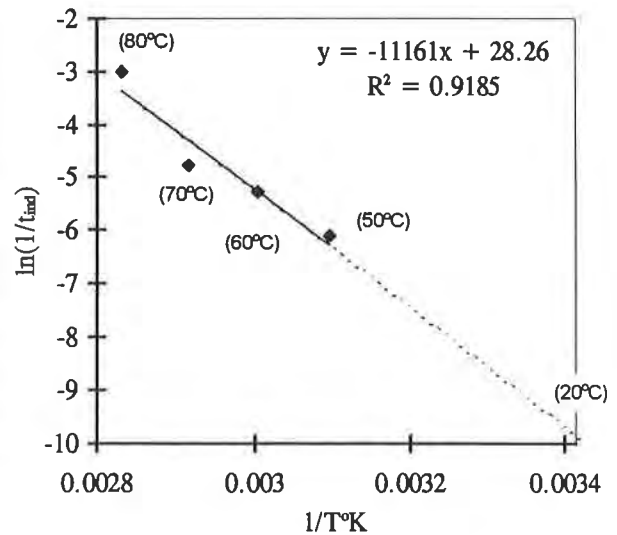
Interpretation of data for mechanical degradation observed after the induction period is conducted in accordance with the scheme for autoxidation previously described in steps 3 to 6. The exponential curve fitting is shown in figure 4. Figure 5 summarizes the result of the Arrhenius type modeling for the reaction rate.
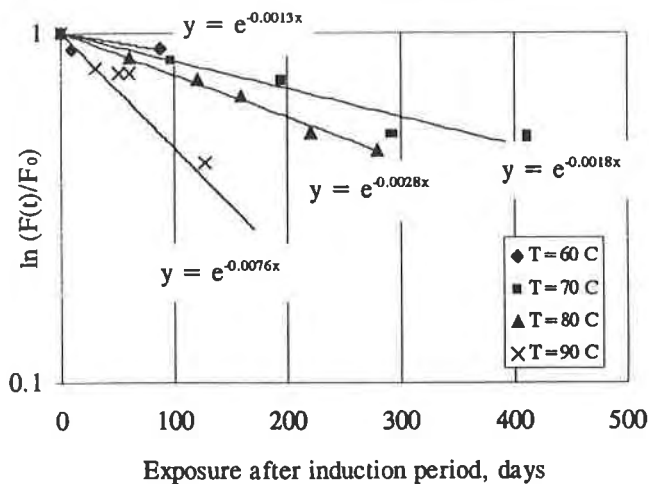
Figure 4. Exponential curve fitting for tensile strength degradation after induction period for PP-3.
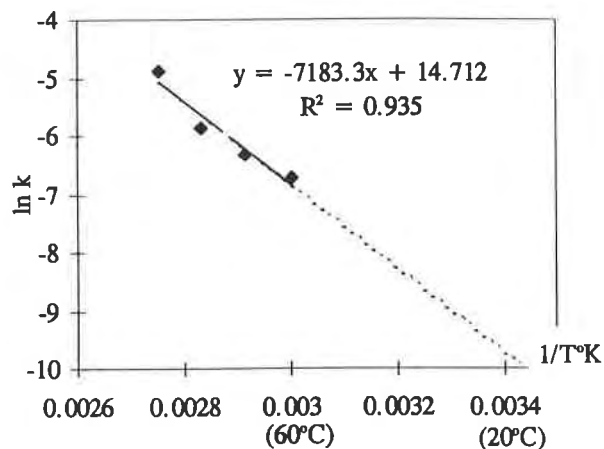
Figure 5. Arrhenius modeling for reaction rate of thermooxidative degradation for PP-3 after induction period.

The solution and sequential Arrhenius type modeling of the reaction rate yields an estimate of 50 percent strength loss at 20°C of 34.4 years after the induction period and provides an estimate of the value of apparent activation energy of 60 kJ/mol, giving a reasonable agreement with the value of 65 kJ/mol, reported by Wisse and Birkenfeld (1982) for PP geosynthetic with extracted antioxidants.

It appears, that the estimate for the induction period of 51 years with no strength loss, suggests that antioxidant consumption rate primarily determines the practical durability of this commercial product under conditions of testing.

According to BAS, it can be anticipated that lower oxygen concentration and stagnant atmosphere will result in an increase of the induction period and in a decrease of the degradation rate. Therefore, the obtained estimate of strength loss for the product is valid for severe environments which are not anticipated for in ground use above piezometric surface, and may be considered only as a very conservative upper limit estimate for the product performance in "in-service" conditions. Testing under conditions of reduced oxygen concentration is presently underway suggesting considerably longer useful life for the product tested.

ACCLERATED DEGRADATION OF POLYESTER BASED GEOSYNTHETICS

The literature indicates that polyester fibers will hydrolyze, with H^+ ions attacking the ester linkage and breaking the chain. This reduces the polymer chain length, with direct impact on the strength of the fiber. The comprehensive studies in the literature for polyester

hydrolysis indicated that rates of hydrolysis are low, but in the context of the lifetime of civil engineering applications, were not negligible.

Testing Conditions and Testing Procedures. The basic principles of hydrolysis indicate that environmental conditions have a strong impact on the hydrolytic degradation of PET materials leading to two different mechanisms of deterioration for tensile strength. In order to assess the influence of pH in the environment on the rate of mechanical degradation, the following conditions have been selected:

- Neutral environment of distilled water with pH=7
- Acidic environment of aqueous solution of H_2SO_4 at pH=1
- Alkaline media at pH=10 and pH=12 in aqueous solution of NaOH.

In order to achieve measurable changes of the tensile strength and molecular weight within a limited laboratory time, samples of materials are aged at elevated temperatures ranging from 40° to 80°C which are or below T_g for the PET tested. At least 5 consecutive retrievals over the period of exposure are used for each condition.

The accelerated hydrolytic degradation test procedure involves: (i) sample preparation; (ii) treatment of prepared samples in aqueous solutions of different pH; (iii) mechanical testing to determine tensile strength; (iv) chemical testing to determine average number molecular weight $\overline{M_n}$ by intrinsic viscosity η, and CEG measurements; and (v) analysis of surface morphology by SEM and/or optical microscopy.

The (200 mm x 200 mm) specimens were suspended on a frame without pretension and then submerged into the hydrolytic solution. The specially designed and manufactured reactor allows the placement of up to 40 specimens in the heated hydrolytic environment. Intensive stirring of the hydrolytic media is deployed, to maintain temperature uniformity of a solution at the level of ±1°C.

Experimental results of hydrolysis for PET-5 geotextile. The results indicate that there is a progressive tensile strength loss over the period of hydrolysis in distilled water. The experimental data on the tensile strength loss are shown in figure 6. Monitoring of weight loss indicates that there was no statistically significant changes of initial weight during hydrolysis in distilled water for the product tested. Further, there were no observed changes in the fiber diameter for the product tested in distilled water.

The degradation data in aqueous solution of H_2SO_4 at pH=1 appears to be similar to that obtained in distilled water at temperatures of 50°, 60° and 70°C. However, the degradation in this acidic media occurs faster than in distilled water.

The rate of mechanical degradation in alkaline media is significantly higher than observed at the same temperature in neutral media, as shown on figure 7. Hydrolysis in an alkaline media of pH=12 results in significant weight losses over the exposure period. This weight loss is accompanied by fiber surface erosion and fiber thinning observed on SEM microphotographs at a magnification of 3000x.
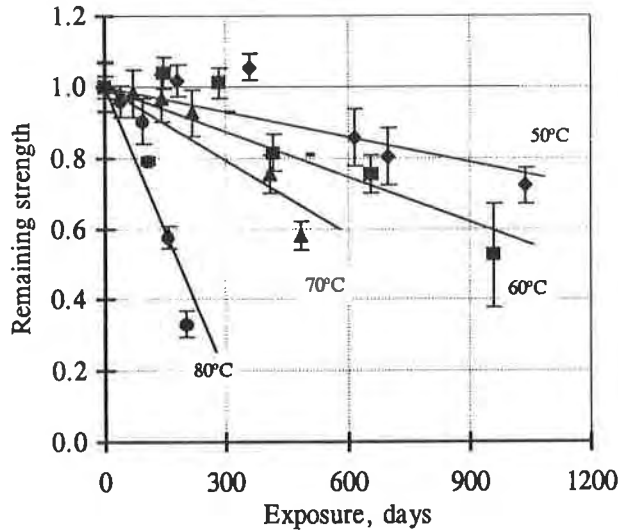
Figure 6. Tensile strength loss for PET-5 geotextile, in distilled water.
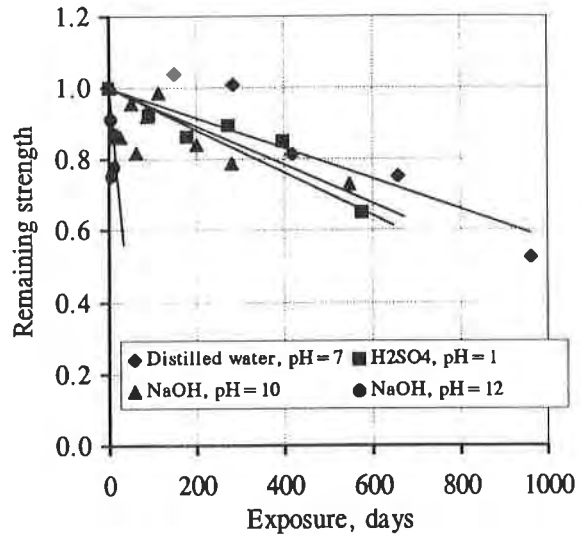
Figure 7. Effect of pH on the rate of mechanical degradation for PET-5 geotextile at 60°C.

Analysis of experimental results for hydrolytic degradation. Environmental variables such as a pH play a dominant role in determining the mechanism leading to the degradation of mechanical strength. There are two mechanisms responsible for the strength loss of PET which depend on the pH of the environment:

- viscosity degradation in aqueous solutions of different pH

- PET fiber surface erosion in alkaline media (pH > 7)

The experimental data developed has been analyzed for correlation between changes of tensile strength and viscosity and between tensile strength and fiber diameter during the process of hydrolysis. The degree of fiber surface erosion is characterized by a reduction of fiber diameter, where this information is available, or weight loss assuming that the latter is proportional to the change of fiber diameter caused by hydrolysis. Correlation coefficients $\rho_{x,y}$ are a measure of a linear relationship of X and Y, where X is tensile strength loss and Y is one of the following parameters: (i) viscosity, (ii) weight loss.

Using the developed test data correlation coefficients $\rho_{x,y}$ can be calculated and are shown in table 3.

Table 3. Correlation coefficients between tensile strength loss and weight loss, and between strength loss and viscosity changes for PET-5 geotextile.

Solution	pH	Temperature, °C	Correlation coefficient	
			Strength/weight	Strength/viscosity
H₂SO₄	1	70	0.36	0.86
Distilled water	7	70	-0.52	0.68
NaOH	10	70	0.96	0.87
NaOH	12	60	0.99	0.81

Significant correlation between strength loss and viscosity changes ($\rho_{x,y} \geq 0.67$) and absence of correlation between strength loss and weight changes strongly suggests that in neutral and acidic environment the chemical mechanism leading to viscosity degradation is responsible for mechanical strength losses. In alkaline media, hydrolysis results in both viscosity degradation and surface erosion manifested by weight loss.

Modeling of the degradation behavior for PET-5 geotextile. Hydrolytic reactions result in molecular weight degradation and surface erosion of PET fibers as observed in alkaline media, or both. Both of these mechanisms are the causes of a tensile strength deterioration. The tensile strength F, is a complex function of two variables M - molecular weight, and S - polymeric fiber cross section. The rate R of tensile strength loss can be defined as a time derivative of a complex function as follows:

$$R = \frac{\partial F}{\partial t} = \frac{\partial F}{\partial M}\frac{\partial M}{\partial t} + \frac{\partial F}{\partial S}\frac{\partial S}{\partial t} \tag{11}$$

The following assumptions can be made with regard to this process:

- Molecular weight degradation and fiber surface erosion are independent processes.
- The strength for a PET is proportional to both molecular weight M and fiber cross section S, therefore $\partial F/\partial M = C_M$ and $\partial F/\partial S = C_S$, where C_M and C_S are constants for the particular product. Results of this program and Schmidt et al. (1994) demonstrated that molecular weight/ tensile strength relationship appears to be a second degree polynomial which can be approximated within the range of measured values of molecular weight by a linear function, justifying the above assumption.

- The rate of molecular weight degradation according to mass action law (Adamson, 1973) is $\frac{\partial M}{\partial t} = k_M = Ae^{-U_M/RT} \times [C]^n$, where U_M is the apparent activation energy of hydrolysis, $[C]$ is a concentration of reactant, n is the order of the rate law ($n=0, 1, 2 ...$). Similarly, the rate of the surface erosion is presented as: $\frac{\partial S}{\partial t} = k_s = Ae^{-U_s/RT} \times [C]^m$, where U_s is apparent activation energy of surface erosion process.

Equation 11 could be rewritten according to the above assumptions as:

$$R = C_M Ae^{-(U_M/RT)} \times [C]^n + C_S Ae^{-(U_s/RT)} \times [C]^m \qquad (12)$$

If the activation energy of surface erosion is much greater than the activation energy of chain scission resulting in molecular weight loss, the deterioration will occur primarily due to polymer chain scission. When activation energy of chain scission is greater, the degradation will by determined by surface erosion process.

As discussed earlier, no surface erosion has been observed in distilled water and acidic solution of pH=1 for the PET tested. Therefore, only the first term in equation (12) should be used for numerical modeling. Experimental results of this program as well as the results reported in the literature (Burgoyne and Merii, 1993; Schmidt et al., 1994), suggest that the kinetics of hydrolysis may be described by a zero-order reaction law ($n=0$ in equation 12), therefore transforming equation (12) into:

$$R = k = C_M \times Ae^{-(U_M/RT)} \qquad (13)$$

Hydrolytic reaction in alkaline media results in some molecular weight degradation, similar to hydrolysis in neutral and acidic solutions, in addition to surface erosion of PET fibers. Both of these mechanisms are the causes of tensile strength deterioration. However, the apparent rate of surface erosion, observed in aqueous solution of NaOH at pH=12, is much higher than the rate of molecular weight degradation, therefore suggesting that the first term in equation (12) may be neglected. Data developed in this program suggests that zero order rate law, similar to (13), could be used in numerical modeling of the apparent surface erosion rate for PET product tested in NaOH at pH=12.

Results obtained in aqueous solution of NaOH at pH=10, indicate that the apparent rate of molecular weight degradation is comparable with the apparent rate of surface erosion suggesting that the apparent activation energies of both processes may have close values. Assuming that both reactions are of zero order, as discussed before, the kinetic equation (12) may be reduced to an expression similar to (13):

$$R = k = C \times e^{-(U/RT)}$$

(14)

where C is a complex constant, and U is an apparent activation energy.

In general, when the apparent activation energy of chain scission is not equal to the apparent activation energy of the surface erosion process, the apparent rates of both processes should be measured and kinetic modeling developed for each.

Kinetic equations 13 and 14, describing reactions of different mechanisms are of the same type. Therefore the same procedure has been used to analyze experimental data of tensile strength loss caused by hydrolysis in alkaline, acidic or neutral media for the PET product tested. Kinetic models for hydrolysis in neutral, acidic and alkaline solutions permit numerical estimates of anticipated time to 50 percent strength loss within the framework of an Arrhenius type modeling. The apparent activation energy for hydrolysis in distilled water appears to be of about 80 kJ/mol, for the PET tested. Summary of the developed models is presented in figure 8. Interpretation of test results for PET-5 geotextile yields estimates shown in figure 9.
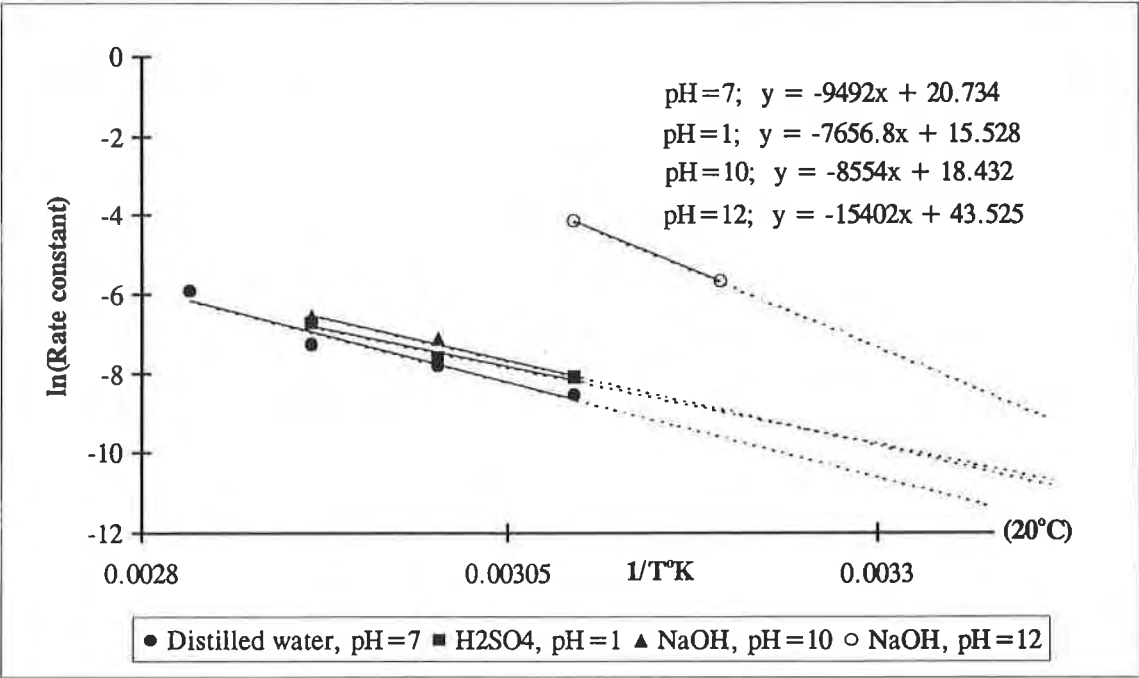
Figure 8. Summarized results of Arrhenius modeling for PET-5 product hydrolyzed in neutral, acidic and alkaline solutions.
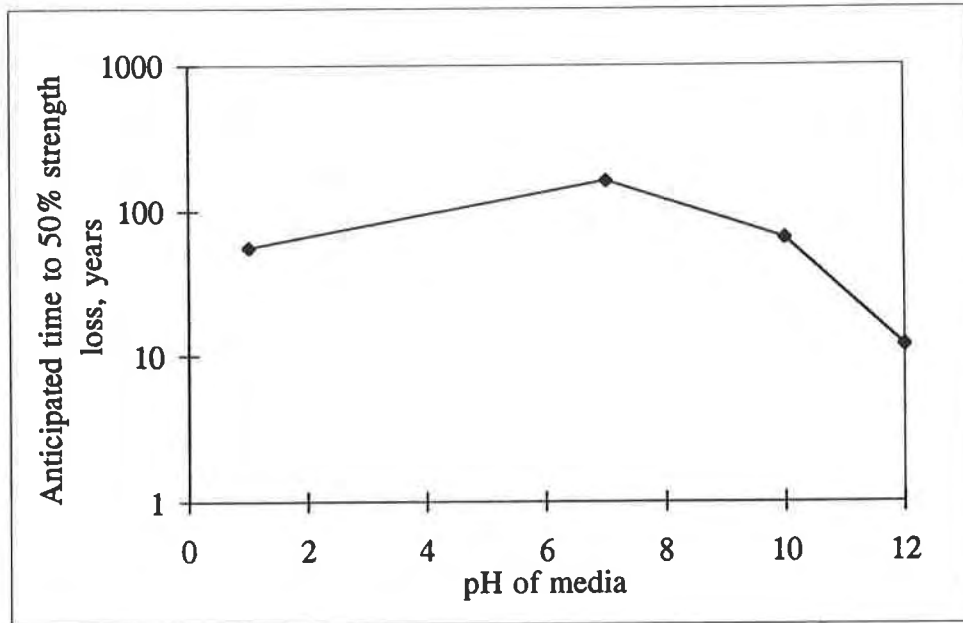
Figure 9. Estimates of anticipated time to 50 percent strength loss due to hydrolysis in solutions of different pH for PET-5 geotextile at 20°C.

CONCLUSIONS

Experimental data and interpretation of results for thermooxidation of polypropylene geotextile PP-3, suggest the following conclusions:

- Commonly used Arrhenius type of modeling appears to be too simplistic for interpreting the experimental laboratory aging data for thermodegradation for the product tested.

- Kinetic models developed within the framework of the Basic Autoxidation Scheme (BAS) appear to provide a satisfactory analysis of the observed experimental data and permit conservative estimates of time against strength loss at ambient temperature above piezometric level in ground, to be made for material studied.

- Products with effective antioxidants may exhibit significant induction times consistent with their useful life in civil engineering .

- Oven aging temperatures must be low enough and sampling frequent enough to permit a measurement of induction time.

The analysis of experimental data on hydrolysis for PET geosynthetic product PET-5, suggests the following conclusions:

- The dominant mechanism of hydrolytic reaction in neutral and acidic environment is molecular chain split, leading to molecular weight and tensile strength degradation.

- In the alkaline media the molecular weight degradation and fiber surface erosion (weight loss) are the key factors in determining the loss of a tensile strength.

- SEM studies indicate that in alkaline environment, hydrolysis of PET geosynthetic products results in fiber surface erosion and fiber diameter thinning.

- Kinetics of hydrolysis in solutions of different pH can satisfactory be described within the framework of an Arrhenius model. Application of an Arrhenius type modeling permits estimates of time against strength loss at ambient temperature in different media.

AKNOWLEDGEMENTS

REFERENCES

Adamson A.W.,(1973)"A textbook of physical chemistry", Academic Press, New York, 1079 p.

Allen T.M., (1991) "Determination of long-term tensile strength of geosynthetics: A state of the art review" Proceedings of Geosynthetics"91 Conference, Atlanta, GA, Feb. 26-28, 1991, Vol. 2, pp. 351-380.

ASTM D 4595, "Standard Test Method for Tensile Properties of Geotextiles by the Wide-Width Strip Method", American Society for Testing and Materials, Philadelphia, PA, USA.

ASTM D-3045, Heat aging of plastics without load", American Society for Testing and Materials, Philadelphia, PA, USA.

Bolland J.L., (1948) "Kinetic studies in the chemistry of rubber and related materials. VI. The benzoyl peroxide catalyzed oxidation of ethyl linoleate", Trans. Faraday Soc., Vol. 44, 669.

Chien J.C.W., Boss C.R., (1967) "Polymer reactions. V. Kinetics of autoxidation of polypropylene", Journal of Polymer Science: Part A-1, Vol. 5, 3091-3101.

Horrocks A.R., D'Souza J.A., (1992) "Degradation of Polymers in Geomembranes and Geotextiles" in "Handbook of Polymer Degradation" ed. by S. Halim Hamid, Mohamed B. Amin, Ali G. Maadhah, Marcel Dekker, Inc., New York, pp. 433-506.

Karlsson K., Smith G.D., Gedde V.W., (1992) "Molecular structure, morphology and antioxidant consumption in medium density PE pipes in hot water applications." Polymer Eng. Sci., Vol. 32, No. 10, pp. 649-657.

Kelen T., (1982) "Polymer degradation" Van Nostrand Reinhold Company, New York.

Koerner R.M., Lord A., Hsuan Y.H., (1992) "Arrhenius modeling to predict geosynthetic degradation", Geotextiles and Geomembranes, No 11, 151-183.

Reich L., Stivala S.S., (1971) "Elements of polymer degradation", McGrow-Hill, New York.

Schmidt H.M., te Pas F.W.T., Risseeuw P., Voskamp W., (1994) "The hydrolytic stability of PET yarns under medium alkaline conditions", Fifth International Conference on Geotextiles, Geomembranes and Related Products, Singapore, 5-9 September 1994, pp. 1153-1158.

Wisse J.D.M., (1988) "The role of thermo-oxidative aging in the long-term behavior of geotextiles", in Durability of geotextiles, RILEM, Chapmen and Hall, London, pp. 207-216.

Wisse J.D.M., Birkenfeld S., (1982) "The long term thermo-oxidative stability of polypropylene geotextiles in the Oosterschelde Project", Second International Conference on Geotextiles, Las Vegas, USA, 1982, Vol. 1, pp. 283-288.

Wisse J.D.M., Broos C.J.M., Boels W.H., (1990) "Evaluation of the life expectancy of polypropylene geotextiles used in bottom protection structures around the Ooster Schelde storm surge barrier". in Geotextiles, Geomembranes and Related Products. Edit. by Den Hoedt, Balkema, Rotterdam, pp. 697-702.

Zolotova N.V., Denisov E.T., (1971) "Mechanism of propagation and degenerate chain branching in the oxidation of polypropylene and polyethylene", Journal of Polymer Science: Part A-1, Vol. 9, 3311-3320.

GEOMEMBRANE INSTALLATION AND CONSTRUCTION SURVIVABILITY

JOHN L. GUGLIELMETTI
DUPONT ENVIRONMENTAL REMEDIATION SERVICES, USA
C. JOEL SPRAGUE
SPRAGUE & SPRAGUE CONSULTING ENGINEERS, USA
MICHAEL J. COYLE
DUPONT ENVIRONMENTAL REMEDIATION SERVICES, USA

ABSTRACT

This paper describes the results of an extensive field and laboratory study that evaluated the installation and construction survivability of geomembranes. The field investigation focused on modeling geomembranes used in landfill cap systems, while the laboratory testing complemented field observations to reveal how varying overburden and loading conditions affected the performance of seven geomembranes used in conjunction with different geosynthetic cushioning and drainage materials. Results indicate that all of the exhumed geomembrane panels were heavily damaged with holes and dimples. Flexible geomembranes performed better, but were damaged, which should result in the reconsideration of previously accepted design procedures for puncture resistance. In addition, damaged geomembrane panels retained a high percentage of their original strength and elongation properties, proving that current design practices for geomembrane strength parameters are appropriate. Interestingly, geomembrane panels were damaged during installation loading even though accepted installation practices were followed.

INTRODUCTION

The performance of landfill caps depends on their ability to minimize infiltration as well as restrict gas migration out of the waste mass. Technical developments over the past ten years has sparked debate over the ideal design of cap systems for Subtitle C and D facilities. Part of this debate includes available literature that suggests that efficient cap systems include a geomembrane (Landreth and Carson 1991; USEPA 1989a,b; and Koerner and Daniel 1992). Although the use of geomembranes in liner and cap applications is now commonplace, some knowledge gaps about their capabilities do still exist.

For instance, there is limited published information on installation damage and the construction survivability of geomembranes used in landfill caps. The limited available literature includes laboratory research (Wilson-Fahmy, et. al 1994; Hullings and Koerner 1991; and Carr and Gunkel 1984) and field studies (Carr and Gunkel 1984; Breitenbach 1992; Richardson 1996). If a stable geomembrane cap is constructed free of holes and dimples, then it should perform adequately over a long period of time. Thus, it is the authors' premise that installation stresses may be of greater significance than in-situ stresses.

This study is targeted at determining geomembrane damage and strength loss for geomembranes placed over severe subgrades. Note that if a geomembrane can survive installation stresses similar to that imparted during this study, then there should be little doubt that it will be able to perform well in actual field conditions. This assumes that the state of the practice for construction of a landfill cap with geomembranes includes a conscious effort made in regards to subgrade preparation and quality assurance.

PROJECT DESCRIPTION

The panel layout and typical cross section for this study appear in Figures 1 and 2, respectively. Coarse, angular stone was placed on firm subgrade with geomembrane panels over the stone (with and without geotextile cushioning materials of varying mass per unit area). A geosynthetic drainage layer consisting of a geonet and geotextile was placed directly over the geomembrane panels in the southern half of the test plot, simulating a cap with a drainage layer. The northern half of the test plot contained no geosynthetic drainage layer, simulating a cap without a drainage layer. Granular (gravelly sand) cover soil of uniformly varying thickness was either placed directly over the drainage layer (on the southern half of the test plot) or directly over the geomembrane panels (on the northern half of the test plot) with a low-ground pressure bulldozer. The geomembrane panels were loaded with a fully loaded dump truck to simulate construction traffic. Two panels of each geomembrane type did not receive dump truck loading, thereby serving as the control panels.

After loading, the geomembrane panels were exhumed and assessed both visually and mechanically for damage, and imperfections (i.e., dimples) and holes were counted. A large number of wide-width and multiaxial tensile strength tests were conducted and compared to the original as-received strengths to obtain percent strength retained. Results were evaluated to compare overall geomembrane performance and the effect of cover soil thickness, geotextile cushioning, and the geosynthetic drainage layer.
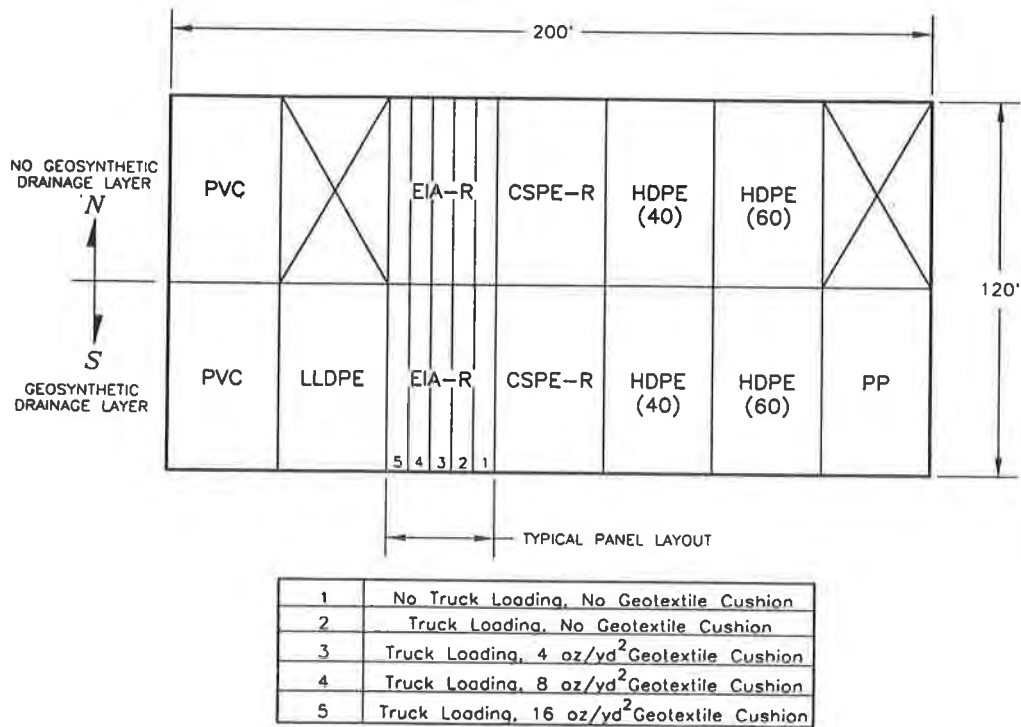
Figure 1. Geomembrane Panel Layout
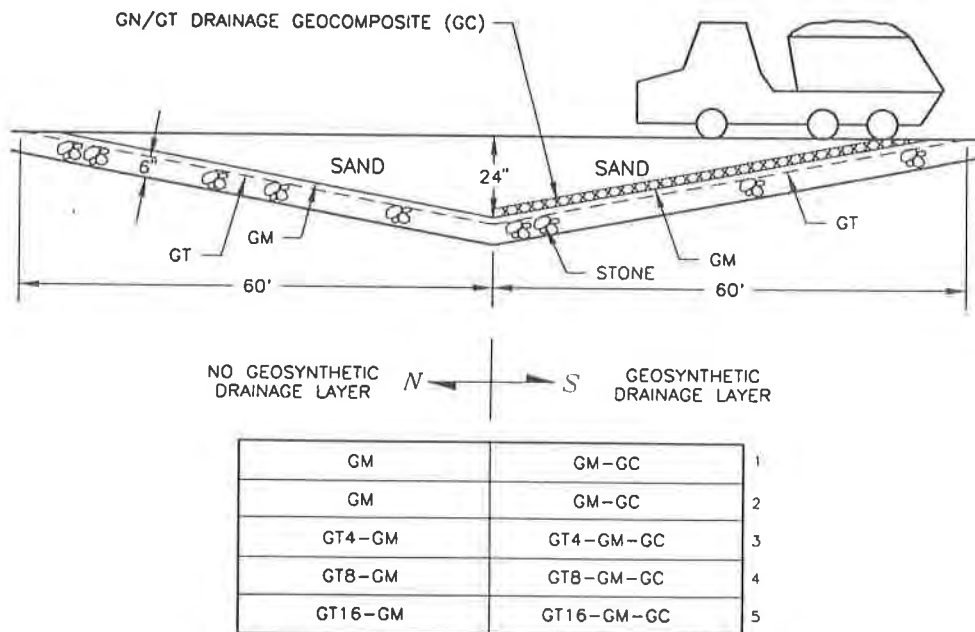
Figure 2. Typical Cross Section

Materials

The materials involved in this study are each described below and include geomembranes, geotextiles, geosynthetic drainage layer, stone base, and cover soil.

- Geomembranes
  Seven geomembranes (see Table 1) were evaluated for installation and construction survivability. The selected geomembranes are the most commonly used products for various physical containment applications.

Table 1. Geomembranes Evaluated

Geomembrane	Nominal Thickness ASTM D5199 mm (mil)
Polypropylene (PP)	1.0 (40)
High Density Polyethylene (HDPE)	1.5 (60) and 1.0 (40)
Chlorosulfanated Polyethylene-Reinforced (CSPE-R)	0.9 (36)
Ethylene Interpolymer Alloy-Reinforced (EIA-R)	0.9 (36)
Linear Low Density Polyethylene (LLDPE)	1.0 (40)
Polyvinyl Chloride (PVC)	0.75 (30)

Insufficient amounts of PP and LLDPE were available for both the northern and southern halves of the test plot (with and without a geosynthetic drainage layer). As a result, a comparison of geomembrane performance, with and without a geosynthetic drainage layer, could not be made for the PP and LLDPE geomembrane panels. The available material was placed on the southern half of the test plot with the geosynthetic drainage layer.

- Geotextiles
  Geotextile cushioning was placed directly over the stone subgrade and below the geomembrane panels. The cushioning materials were nonwoven, needle-punched, polyester geotextiles of varying mass per unit area (see Table 2).

Table 2. As-Received Geotextile Properties (per manufacturers' literature)

Geotextile Designation	Mass/Unit Area ASTM D5261 g/m^2 (oz/yd^2)	Puncture ASTM D4833 kN (lb)	Mullen Burst ASTM D3786 kPa (psi)	Trapezoid Tearing Strength ASTM D4533 kN (lb)	Grab Tensile/ Elongation ASTM D4632 kN (lb)/%
GT4	136 (4)	0.222 (50)	1311 (190)	0.178 (40)	0.489 (110)/60
GT8	271 (8)	0.444 (100)	2622 (380)	0.356 (80)	1.023 (230)/60
GT16	541 (16)	0.867 (195)	5382 (780)	0.667 (150)	2.224 (500)/70

- Geosynthetic Drainage Layer

A geonet and geotextile were placed directly over the geomembrane panels on the southern half of the test plot, simulating a drainage layer in a landfill cap. The geonet was made of HDPE with a 5.1 mm (0.20 in.) nominal thickness. A nonwoven, needle-punched, polyester geotextile with a mass per unit area of 541 g/m^2 (16 oz/yd^2) was placed over the geonet as a separation layer to prevent cover soil from filling geonet openings. The properties of this geotextile are described in Table 2.

- Stone Base and Cover Soil

A 150-mm (6-in.) layer of coarse, angular stone (AASHTO #3) was placed on a firm subgrade over the entire test plot. Gravelly sand cover soil (AASHTO #2A) of uniformly varying thickness was placed directly over the geosynthetic drainage layer. Table 3 shows the gradation characteristics for the stone base and cover soil.

Table 3. Stone Base and Cover Soil Particle Size Distribution per ASTM D422

Sieve Size	Percent Passing	
	Stone Base	Cover Soil
50.80 mm (2 in.)	100	100
25.40 mm (1 in.)	3	96
19.05 mm (0.75 in.)	1	93
12.70 mm (0.5 in.)	0	89
4.75 mm (#4)	—	84
2.00 (#10)	—	64
0.425 mm (#40)	—	40
0.250 mm (#60)	—	24
0.150 mm (#100)	—	19
0.075 mm (#200)	—	17

Field Test Plot

The field test plot was constructed and loaded as described below. After loading, the panels were exhumed, and the dimples and holes were mapped and logged. The activities associated with these procedures are described in detail below.

- Construction

The field test plot was constructed in a flat, open area at an existing construction site. The site was proof-rolled and contoured to allow a uniformly varying cover soil thickness ranging from 100 to 600 mm (4 to 24 in.). A uniform 150-mm (6-in.) layer of coarse, angular stone was placed over the entire prepared subgrade. Ten panels, 1.2 by 18.3 m (4 by 60 ft) of each geomembrane type were placed over the coarse stone with and without a geotextile cushioning layer. Each geomembrane panel was labeled to identify the geomembrane type, cushioning material, loading, and geosynthetic drainage layer. The geomembrane panels

were strategically spaced to allow the dump truck tires to pass directly over the centerline of each panel. Six geomembrane panels included a geotextile cushioning layer of 136, 271, and 541 g/m² (4, 8, and 16 oz/yd²) between the geomembrane and the stone. The remaining geomembrane panels did not receive a geotextile cushioning layer.

Once the stone, geomembrane panels, and geotextile cushioning layers were in place, the geosynthetic drainage layer was laid over the southern half of the test plot. A geonet was placed directly over the geomembrane panels and covered with a nonwoven, needle-punched, polyester geotextile with a mass per unit area of 541 g/m² (16 oz/yd²). The geosynthetic drainage layer was not placed over the northern half of the test plot. Granular cover soil was end-dumped off of the test plot and distributed over the geosynthetics with a 27-kPa (3.9-psi), low-ground pressure Komatsu D37P bulldozer. The bulldozer did not make any turns on the test plot. The cover soil thickness varied from 100 to 600 mm (4 to 24 in.) and was not compacted to any specific density. In fact, the only compaction the cover soil received was from the bulldozer during placement, which is typical of construction practices at most landfill cap construction sites.

- Loading
A loaded Moxy Model 6200S tandem dump truck with a ground contact pressure of 269 kPa (39 psi) made 20 passes (ten complete cycles) at a constant speed of 1.6 km/hr (1.0 mph) over the centerline of eight of the ten geomembrane panels. Two geomembrane panels without geotextile cushioning served as control panels and did not receive dump truck loading. The truck, without braking, traveled in a straight line and passed completely over the geomembrane panels and off of the test plot. As a result, a uniform rut depth of about 100 mm (4 in.) occurred directly under the tires.

- Exhuming Panels
After loading the geomembranes, each panel was exhumed. Initially, most of the cover soil, down to about 150 mm (6 in.), was removed with the same bulldozer used to place the cover soil. However, after one geomembrane panel was damaged by the bulldozer blade, this excavation method was modified. Subsequent to bulldozing, a Ford tired backhoe, located off of the geomembrane panels and equipped with an articulating bucket, excavated the majority of the cover soil. The remaining 150 mm (6 in.) of cover soil on the southern half of the test plot was removed by hand with shovels and/or water. The geosynthetic drainage layer prevented the shovels from damaging the geomembranes; however, the geomembrane panels on the northern half of the test plot (without a geosynthetic drainage layer) were easily damaged by hand shoveling, regardless of how careful the workers excavated. After the first few northern panels were damaged by shoveling, the exhuming process was modified and water was used to hose off the final 150 mm (6 in.) or less of cover soil. After removing the cover soil, the geomembrane panels were rolled and transported to a storage area for mapping/logging.

- Mapping/Logging
Each geomembrane panel was unrolled in a flat, grassy area. Generally, similar geomembrane types were laid side-by-side for the mapping/logging process. A square 300 by 300 mm (12 by 12 in.) was drawn every 3.0 m (10 ft) along the centerline of each geomembrane panel to count dimples and holes. The centerline received the highest pressure from the truck loading. Initially, dimples and holes within the square were marked, counted, and logged. However, after several geomembrane panels were logged, it became apparent that the number of holes counted by this method was not representative of the total number of holes for the entire panel. Therefore, the logging process was changed, and holes for the entire panel were marked, counted, and logged.

After logging the dimples and holes, the geomembrane panels were labeled for laboratory testing. A UPC bar code labeling system was used for ease of data entry in the laboratory. Prior to cutting the samples, the panels were photographed and videotaped for documentation. The samples were then cut, stacked, and delivered to the laboratory for testing.

Laboratory Testing

Wide-width and multiaxial tensile tests were performed to evaluate the effect of installation damage on geomembrane strength. Specifically, wide-width tensile tests were conducted to measure one-dimensional, in-plane geomembrane strength, and multiaxial tensile tests were conducted to measure three-dimensional, out-of-plane geomembrane strength. Five specimens of each as-received geomembrane type were subjected to both wide-width and multiaxial tests to obtain average conformance strength and elongation values.

All laboratory testing was performed by an accredited Geosynthetic Accreditation Institute (GAI) laboratory. Wide-width testing was conducted per ASTM Standard D4885, except that a strain rate of 10 mm (0.4 in.) per minute was used, versus 1.0 mm (0.04 in.) per minute. Three specimens were cut every 2.3 m (7.5 ft) along the centerline of each geomembrane panel. The three test values were averaged for comparison with the conformance test value. Because of the varying shape of the stress strain curves and the actual strength values used in design for the different geomembrane types, strengths were measured at different points for the different geomembrane types (see Table 4).

Table 4. Strengths Measured

Geomembrane	Strength Measured
PP	300% strain
HDPE, 1.5 mm (60 mil)	Yield and 100% strain
HDPE, 1.0 mm (40 mil)	Yield and 100% strain
CSPE-R	Scrim break
EIA-R	Scrim break
LLDPE	300% strain
PVC	Break

Multiaxial testing was conducted per ASTM Standard D5617. One specimen was cut every 2.3 m (7.5 ft) between wide-width specimen locations along the centerline of each geomembrane panel. Maximum stress and center deformation values were used for comparison with the conformance test values.

DISCUSSION OF RESULTS

The geomembrane panels were assessed for damage both visually and mechanically. Visual assessment included counting both the number of dimples per square every 3.0 m (10 ft) along the centerline of each panel and the total number of holes for each panel. Mechanical assessment included wide-width and multiaxial tensile laboratory testing. A discussion of results for each assessment is presented below. Note that the subgrade conditions used in this study are obviously far harsher than would be allowed under a geomembrane cap and thus, the comparisons of geomembrane performance are all relative.

Dimples

The total number of dimples per square was plotted versus the initial cover soil thickness, before tire rutting, for each geomembrane type. All five panels were included on the same plot to compare the effect of geotextile cushioning and loading. Separate plots were developed for panels with and without a geosynthetic drainage layer to assess the effect, if any, of a geosynthetic drainage layer. Figure 3 shows results for the PP panels, which are typical for the different geomembrane panels. Table 5 shows the average number of dimples per square per panel for each geomembrane. In general, fewer dimples were observed with increasing cover soil thickness and with higher mass per unit area geotextile cushioning. Similarly, the relative difference in number of dimples between loaded/unloaded and cushioned/uncushioned panels decreased with increased cover soil thickness, indicating that as cover soil thickness increases, geotextile cushioning is less significant. Extrapolating the data indicates that cover soil thicknesses greater than about 0.6 to 1.2 m (2 to 4 ft), depending on geomembrane type, results in the elimination of nearly all dimples.
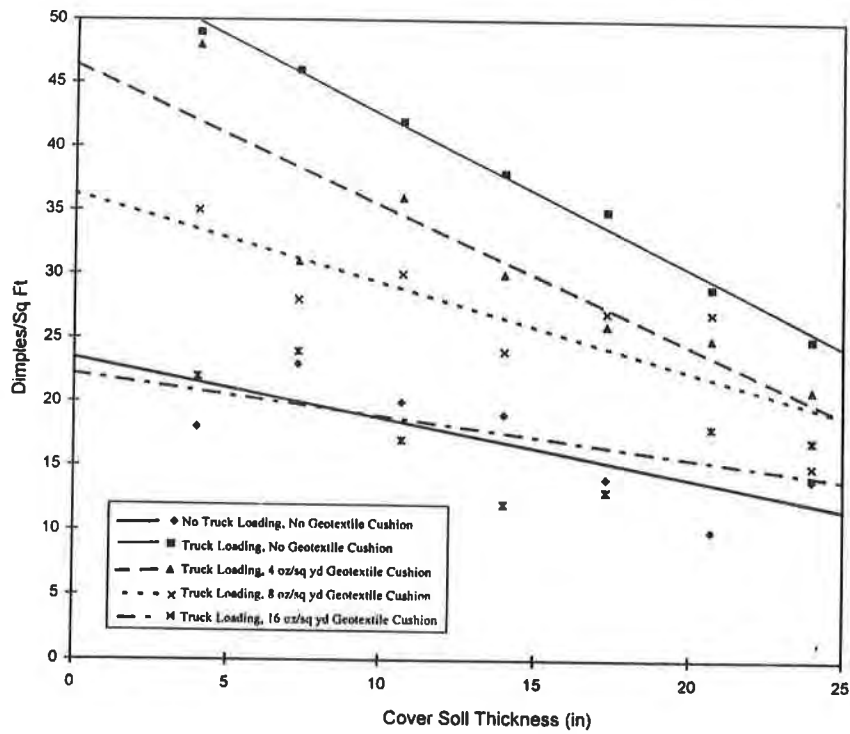
Figure 3. Dimples/sq ft, PP With Geosynthetic Drainage Layer
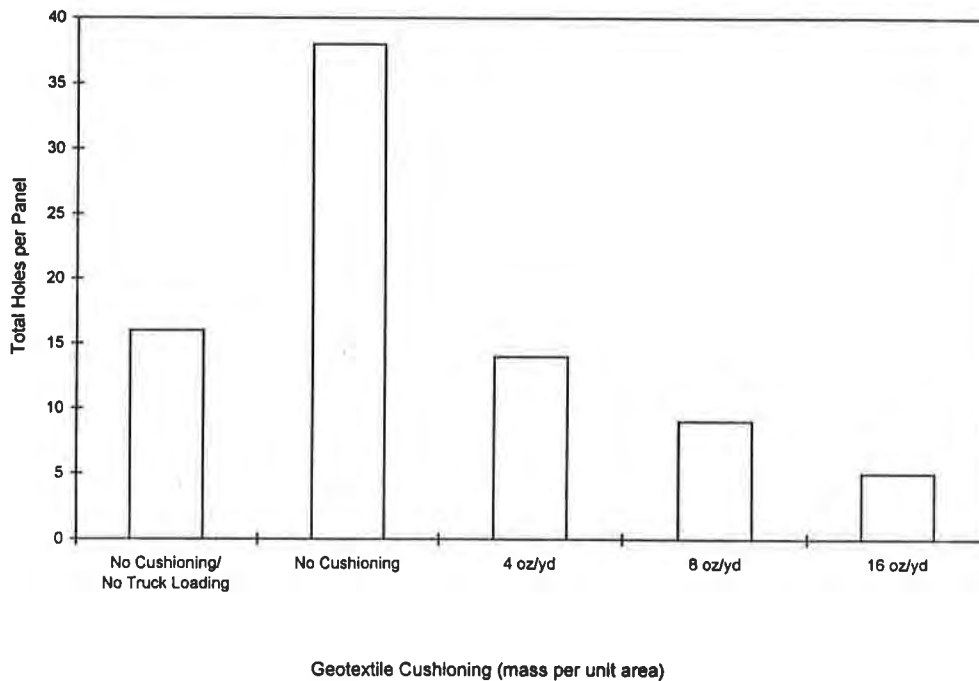
Figure 4. Holes/Panel, 1.0 mm (40 mil) HDPE Without Geosynthetic Drainage Layer

In all cases, and, as expected, the control panels (with no geotextile cushioning and no truck loading) had less dimples than the panels without geotextile cushioning that received truck loading. A comparison of the unloaded control panels with loaded panels reveals mixed results. Depending on geomembrane type, in some cases, geomembrane panels with 136, 271, or 541 g/m^2 (4, 8, or 16 oz/yd^2) geotextile cushioning with truck loading had the same approximate number of dimples as the unloaded control panel.

In all cases, the geomembrane panels with a geosynthetic drainage layer had fewer dimples than panels without the geosynthetic drainage layer. Reductions ranged from about 20 percent for the EIA-R panels to about 50 percent for the PVC panels, indicating that the geosynthetic drainage layer provided additional protection for the geomembrane panels. This additional protection may be the result of additional reinforcement or different stress distribution.

Holes

The total number of visible holes for each geomembrane panel were counted and plotted to compare the effect of different geotextile cushioning materials. Unfortunately, because of the initial mapping/logging process, there is insufficient data to make comparisons of all of the geomembranes. In addition, trends were not obvious regarding cover soil thickness. However, some general trends are apparent. Fewer holes were observed in the control panels than the panels without geotextile cushioning that received truck loading, indicating additional damage beyond installation damage. The flexible geomembranes (PP, PVC) had the least number of holes, and the stiffer HDPE geomembranes had the greatest number of holes. The number of holes in the reinforced CSPE-R geomembrane panels was between the flexible and HDPE geomembrane panels. Insufficient data was available for the EIA-R and LLDPE geomembrane panels to make meaningful comparisons.

As expected, geotextile cushioning reduced the total number of holes, with the higher mass per unit area geotextiles providing more protection. Reductions in the total number of holes with the heaviest geotextile, 541 g/m^2 (16 oz/yd^2), ranged between 50 and 90 percent. Because of the limited data, no apparent trend could be determined between geomembrane panels with and without a geosynthetic drainage layer. Table 6 shows the average number of holes per panel for each geomembrane.

Figure 4 shows the total number of holes for the 1.0-mm (40-mil) HDPE panels without a geosynthetic drainage layer. The plot shows the effect of truck loading without cushioning and demonstrated that more than twice as many holes were observed in the panel that received truck loading compared to the control panel. The geotextile cushioning materials also had a major impact on the total number of holes in the 1.0-mm (40-mil) HDPE panel. As

Table 5. Average Number of Dimples Per Square Per Panel

Geomembrane	No Load No Cushion	Truck Load No Cushion	Truck Load 136 g/m² (4 oz/yd²)	Truck Load 271 g/m² (8 oz/yd²)	Truck Load 541 g/m² (16 oz/yd²)
PP	17/-	38/-	31/-	27/-	18/-
HDPE-60	6/17*	13/22*	17/18*	15/14*	6/12*
HDPE-40	10/18*	21/32*	13/30*	17/30*	10/15*
CSPE-R	6/1*	5/25*	9/18*	6/9*	4/5*
EIA-R	4/11*	21/23*	14/16*	13/7*	8/3*
LLDPE	3/-	10/-	19/-	18/-	13/-
PVC	23/52*	43/73*	24/46*	19/34*	17/36*

* Without Geosynthetic Drainage Layer

Table 6. Average Number of Holes Per Panel

Geomembrane	No Load No Cushion	Truck Load No Cushion	Truck Load 136 g/m² (4 oz/yd²)	Truck Load 271 g/m² (8 oz/yd²)	Truck Load 541 g/m² (16 oz/yd²)
PP	16/-	79/-	60/-	100/-	47/-
HDPE-60	59/10*	28/13*	-/10*	-/1*	-/5*
HDPE-40	93/16*	97/38*	-/14*	-/9*	-/5*
CSPE-R	58/-	31/-	37/-	9/-	3/-
EIA-R	5/-	20/-	4/-	-/-	-/-
LLDPE	-/-	-/-	-/-	32/-	60/-
PVC	38/39*	102/59*	18/34*	51/22*	7/27*

* Without Geosynthetic Drainage Layer

shown, the cushioning reduced the number of holes by about 60 to 85 percent when compared to the panel without cushioning that received truck loading.

Holes were observed in every exhumed geomembrane, regardless of loading, cushioning, or cover soil thickness. Although the relative performance of the flexible, reinforced, and stiff geomembranes performed as expected, the large number of holes, particularly for the flexible geomembranes, was alarming. Based on puncture resistance research by Hullings and Koerner (1991), few, if any, holes were expected in the flexible geomembranes.

Wide-Width and Multiaxial Tensile Testing

Wide-width and multiaxial tensile tests were conducted to determine the percent strength retained of the exhumed geomembrane panels. Test results within two standard deviations of the average conformance values were considered within the expected limits of the test methods. Test values below two standard deviations were considered affected by the damage induced during installation and truck loading. In general, no significant reductions in strength were observed for any of the geomembrane panels; however, slight reductions were observed for several geomembrane panels under different conditions. Tables 7 and 8 show average wide-width and multiaxial test results, respectively, for every geomembrane panel.

- Wide-Width
  Yield strength for the 1.0- and 1.5-mm (40- and 60-mil) HDPE panels with or without a geosynthetic drainage layer were not affected. However, at 100 percent strain, strength reductions were noticeable, particularly for the 1.0-mm (40-mil) HDPE panels. Figures 5 and 6 show percent strength retained at yield and at 100 percent strain, respectively, for the 1.0 mm (40-mil) HDPE panels without a geosynthetic drainage layer. Clearly, the field-induced damage affected strength values at strains higher than yield. Additionally, the results indicate no strength loss at a cover soil thickness greater than 600 mm (24 in.). The 1.5-mm (60-mil) HDPE panels exhibited similar trends but with less loss of strength. These results differ from research conducted by Richardson (1996), which indicated yield strength reductions of damaged 1.5-mm (60-mil) HDPE geomembranes, but no significant strength loss at break.

  Results of the CSPE-R panels, the second strongest geomembrane panels tested, showed a consistent reduction in strength, regardless of cushioning and cover soil thickness. The tested strength of the CSPE-R panels averaged between 4 and 8 percent below the two standard deviation limit. However, the strain at scrim break for the exhumed panels was about 40 percent higher than the scrim break strain of the conformance tests.
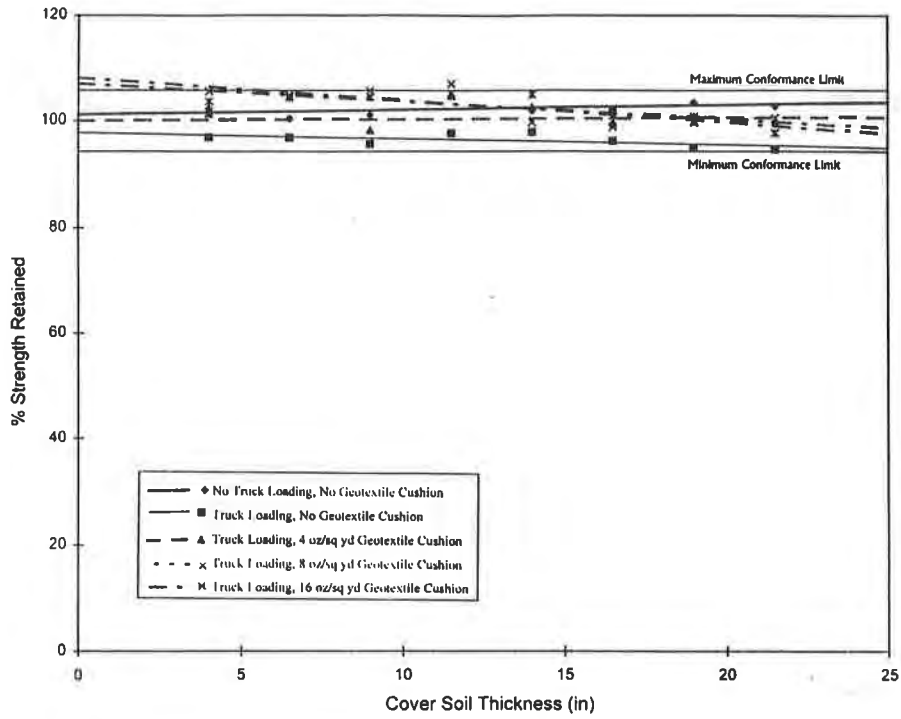
Figure 5. Wide-Width Tensile Test, Percent Strength Retained at Yield, 1.0 mm (40 mil) HDPE Without Geosynthetic Drainage Layer
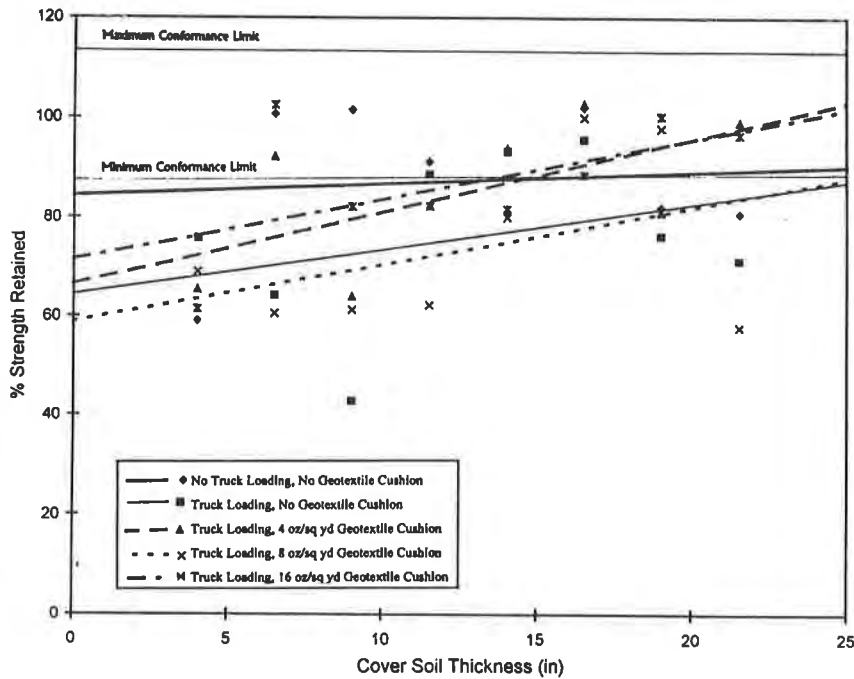
Figure 6. Wide-Width Tensile Test, Percent Strength Retained at 100% Strain, 1.0 mm (40 mil) HDPE Without Geosynthetic Drainage Layer

Table 7. Wide-Width Tensile Test: Percent Strength Retained Per Panel

Geomembrane	No Load No Cushion	Truck Load No Cushion	Truck Load 136 g/m² (4 oz/yd²)	Truck Load 271 g/m² (8 oz/yd²)	Truck Load 541 g/m² (16 oz/yd²)	Remarks
PP	92	99	99	98	102	
	—	—	—	—	—	
HDPE-60	100/87	105/104	102/100	100/98	99/91	Yield/100% Strain
	101/76*	103/96*	98/85*	98/96*	102/98*	
HDPE-40	102/80	95/68	101/88	97/75	99/89	Yield/100% Strain
	102*/87*	96*/76*	100*/85*	103*/74*	103*/87*	
CSPE-R	83	84	87	84	89	
	92*	86*	90*	88*	91*	
EIA-R	93	100	102	97	96	+ Panels Damaged During Exhuming
	99*+	85*+	85*+	101*+	100*+	
LLDPE	102	93	96	95	97	
PVC	88	79	92	95	105	
	91*	87*	86*	91*	93*	

* Without Geosynthetic Drainage Layer

Table 8. Multiaxial Tensile Test: Percent Strength/Elongation Retained Per Panel

Geomembrane	No Load No Cushion	Truck Load No Cushion	Truck Load 136 g/m² (4 oz/yd²)	Truck Load 271 g/m² (8 oz/yd²)	Truck Load 541 g/m² (16 oz/yd²)	Remarks
PP	98/97	—/—	99/96	98/105	97/94	
	—/—	—/—	—/—	—/—	—/—	
HDPE-60	97/86	101/96	98/96	—/—	102/91	
	99*/89*	104*/84	101*/87*	99*/87*	98*/86*	
HDPE-40	98/81	—/—	—/—	102/105	89/106	
	101*/98*	96*/91*	89*/86*	99*/92*	97*/95*	
CSPE-R	88/97	91/95	96/98	76/93	91/100	
	82*/100*	66*/75*	—/—	93*/98*	—/98*	
EIA-R	80/86	93/94	98/94	91/92	95/92	+ Panels Damaged During Exhuming
	64*/80*+	60*/80*+	71*/85*+	79*/88*+	77*/85*+	
LLDPE	90/92	93/98	92/100	106/95	103/103	
PVC	—/—	—/—	104/107	—/—	105/101	
	—/—	—/—	—/—	—/—	—/—	

* Without Geosynthetic Drainage Layer

The PVC geomembrane panel results also indicate some loss in strength. For the panels with a geosynthetic drainage layer, the greatest strength loss was found in those without geotextile cushioning. The uncushioned panel that received truck loading had a greater strength loss than the uncushioned panel without truck loading (79 versus 88 percent strength retained, respectively). Percent strength retained increased with heavier geotextile cushioning. Results for PVC panels without a geosynthetic drainage layer differed from those with a geosynthetic drainage layer. All panels exhibited some reduction in strength, but the largest reduction was observed in the panel without geotextile cushioning that had received truck loading.

There was no significant loss in strength, outside the two standard deviation range, in the PP, EIA-R, and LLDPE geomembrane panels.

- Multiaxial
  In the early phases of this study, the authors believed that the multiaxial test would provide the most meaningful strength results because of the large specimen size. However, because of the number of holes in the exhumed geomembrane panels, it was difficult to obtain specimens without holes. In some cases, holes were not visible until the test was in progress. Since holes, regardless of size, give inaccurate test results, the total number of data points is limited. Because of the limited number of data points and the wide range of results, trends were not easy to identify. Maximum elongation results showed less data spread and slightly more consistency. In general, except for a few geomembrane panels, three-dimensional strength and maximum elongation were minimally affected by damage induced during installation and loading.

CONCLUSIONS

Although a geomembrane liner would never be installed over a coarse, angular stone subgrade as in this study, meaningful results were produced for the relative performance of various geomembranes, cushioning geotextiles, and cover soil thicknesses. The following conclusions were made based on the study data:

- All of the exhumed geomembrane panels were heavily damaged with holes and dimples. Although the flexible geomembranes performed better (i.e., less holes) than the reinforced and stiffer geomembranes, they were damaged, which was unexpected. This conclusion may cause reconsideration of previously accepted design procedures for puncture resistance.
- Geotextile cushioning helps protect geomembranes from damage and, in some cases, significantly. However, even the heaviest geotextile did not prevent the puncturing of geomembranes, regardless of cover soil thickness or loading conditions.
- Thicker cover soils help protect geomembranes from damage under normal installation loads and heavier construction loads. Depending on geomembrane type, a minimum of 0.6 to 1.2 m (2 to 4 ft) of initial lift cover soil thickness is required to eliminate dimples.

- Clearly, a geosynthetic drainage layer over the geomembranes helped protect every geomembrane panel from damage. Reductions in dimples of 20 to 50 percent were observed for panels with a geosynthetic drainage layer. The authors cannot explain the phenomena, but the results are obvious. Many landfill caps are designed and constructed with geosynthetic drainage layers for drainage purposes, but also benefit from added geomembrane protection.
- Construction loading (truck loading) caused more damage to the geomembrane panels than installation loading (low-ground pressure bulldozer). However, the geomembrane panels were damaged even though accepted installation practices were followed, as with the control panels.
- Damaged geomembrane panels retained a high percentage of their original strength and elongation properties. Thus, current design practices for geomembrane strength parameters (i.e., partial factors of safety for installation damage) are appropriate.
- The wide-width tensile test is an appropriate test for measuring the in-plane strength of damaged geomembranes. Although the faster strain rate used may give slightly higher strength values, the relative strength retained values should be consistent.
- The multiaxial test is not appropriate for measuring the strength of geomembranes with holes without modifying the test procedure, such as using a very thin geomembrane of the same polymer in combination with the damaged geomembrane.

ACKNOWLEDGMENTS

REFERENCES

Breitenbach, A.J. (November 1992) "Geomembrane Liner Evaluation for Heap Leach Pads," Geotechnical Fabrics Report.

Carr, G.L., and Gunkel, R.C. (January 1984) "Laboratory Studies of Soil Bedding Requirements for Flexible Membrane Liners," EPA-600/2-84-021.

Hullings, D., and Koerner, R.M. (1991) "Puncture Resistance of Geomembranes Using a Truncated Cone Test," Geosynthetics '91 Conference, Atlanta, GA.

Koerner, R.M., and Daniel, D.E. (May 1992) "Better Cover-Ups," Civil Engineering, pp. 55-57.

Landreth, R.E., and Carson, D.A. (1991) "RCRA Cover Systems for Waste Management Facilities," Geotextiles and Geomembranes.

Richardson, G.N. (March 1996) "Field Evaluation of Geosynthetic Protection Cushions," Geotechnical Fabrics Report.

USEPA. (1989a) "Final Covers on Hazardous Waste Landfills and Surface Impoundments," Office of Solid Waste and Emergency Response Technical Guidance Document EPA530-SW-89-047.

USEPA. (1989b) "RCRA ARARs: Focus on Closure Requirements," Office of Solid Waste and Emergency Response Directive 9234.2-04FS.

Wilson-Fahmy, R.F., Narejo, D.B., and Koerner, R.M. (September 26, 1994) "A Design Methodology for the Puncture Protection of Geomembranes," Geosynthetic Research Institute Report #13.

EUROPEAN EXPERIMENTAL APPROACH TO THE TENSILE CREEP BEHAVIOUR OF HIGH-STRENGTH GEOSYNTHETICS

D. CAZZUFFI
ENEL Spa - CRIS, ITALY
A. GHINELLI
Florence University, ITALY
M. SACCHETTI
Florence University, ITALY
C. VILLA
ENEL Spa - CRIS, ITALY

ABSTRACT

As already well established the creep behaviour of geosynthetics depends on several factors, such as polymeric nature, manufacture process, creep load and temperature. Therefore, in order to investigate more specifically the long-term tensile creep of geosynthetics is necessary to know the effects of the single above mentioned factors over load-strain behaviour.

This paper describes the European experimental approach to evaluate the creep behaviour of high-strength reinforcement geosynthetics. After a first brief overview of the state of the art, particular attention is devoted to the description of the apparatus built at Florence University and of the test procedures adopted to evaluate the tensile creep behaviour of geosynthetics. A critical comparison between the tensile creep European standard and North American standard is also reported. Some tensile creep test results are finally illustrated.

INTRODUCTION

The most important problem using geosynthetics as reinforcement in civil geotechnical structures with a long design life (70-120 years) is directly connected with their long-term mechanical behaviour. In general terms, stability and serviceability of reinforced soil structures requires: (1) that the reinforcement does not attain its ultimate limit state of collapse (strength criterion) and (2) does not developing excessive strain over the design life of the structure (strain criterion). In order to provide the data needed to meet these requirements it is necessary to perform tensile creep tests.

To investigate more specifically the long-term tensile creep of some high-strength reinforcement geosynthetics an experimental research program has been carried out jointly by the Research Group on Special Materials of ENEL Spa - CRIS in Milano and the Civil Engineering Department of Florence University.

The main purposes of the research are:

1. define the most suitable test apparatus and procedures for evaluation of the tensile creep properties of high-strength geosynthetics;
2. evaluate the influence of polymer, structure type, geosynthetic structure, load level and ambient temperature on long-time mechanical behaviour of some reinforcement-geosynthetics;
3. develop a critical comparison between the tensile creep European standard (CEN prEN ISO 13431, 1995) and and North American standard (ASTM D5262, 1992).

STATE OF THE ART

As geosynthetics are generally manufactured from polymer materials they exhibit an elasto-viscoplastic behaviour, time, load and temperature dependent, under a sustained constant load. The creep behaviour of geosynthetics is generally presented as strain versus time or (log time) curves and strain rate versus time as shown in Figs.1a and 1b.

(a) Strain vs Time plot   (b) Strain Rate vs Time plot
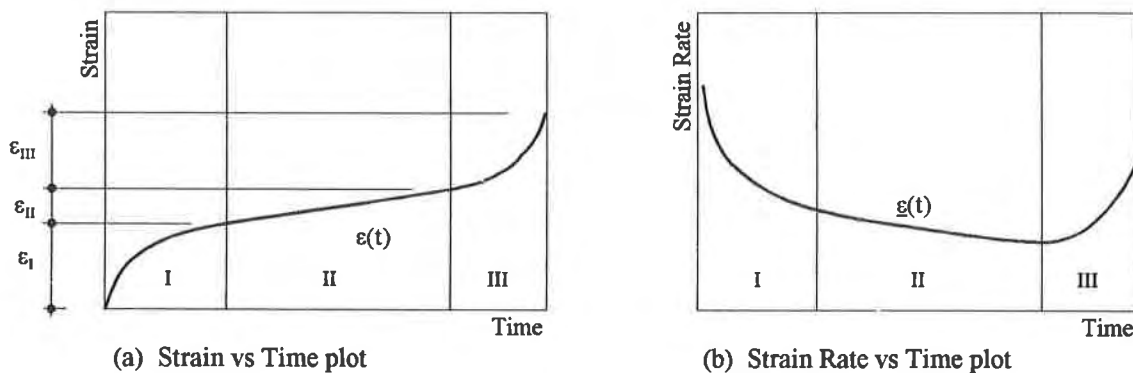
Fig. 1 Typical creep model

From these typical creep curves it is possible to identify 3 different creep stages, respectively named primary creep, secondary creep and tertiary creep. As general trend, the first stage where the strains develop very rapidly it followed by a transition period between primary and secondary creep where the strain rate is decreasing. At the secondary creep stage, the strain rate becomes a minimum before increasing again when tertiary creep is generated and failure reached.

At time t, the total strain $\varepsilon(t)$ can be expressed from the following equation:

$$\varepsilon(t) = \varepsilon_O + \varepsilon_I + \varepsilon_{II} + \varepsilon_{III}$$

where ε_O is the instantaneous strain and $\varepsilon_I, \varepsilon_{II}$, and ε_{III} are respectively the primary, secondary and tertiary creep strain. The ε_O is composed from both recoverable (elastic)

and irrecoverable (plastic) instantaneous strain. However the final sudden creep strain increase before rupture does not necessarily occur: it is typical for PE (polyethylene) and PP (polypropylene) not for PET (polyester) at standard load levels and temperatures (Müller-Rochholz and Koslowski, 1996).

On the basis of the dominant creep stage the are three type of creep generation: dominant primary creep, dominant secondary creep and dominant tertiary creep as shown in Fig.2.
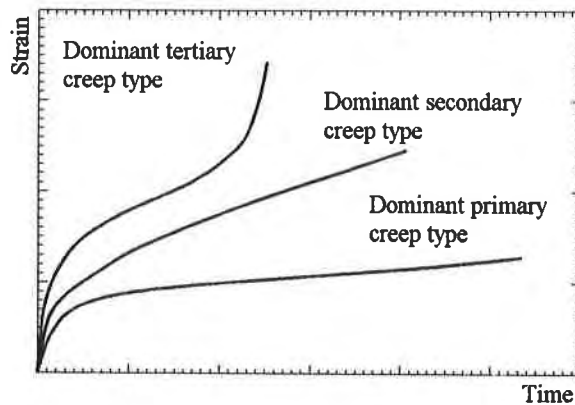
Fig. 2 Type of creep generation

As already very well known, the creep behaviour of geosynthetics depend from the following factors:

- polymer nature and polymer structure;
- geosynthetic structure;
- loading conditions;
- temperature conditions;
- soil environment.

Therefore, to investigate more specifically the long-term tensile creep of geosynthetics it is necessary to know the effects of each of the above mentioned factors on load-strain behaviour.

The most common polymers used to produce geosynthetics, such polyester (PET), polypropylene (PP) and polyethylene (PE), are all susceptible to creep. The creep sensitivity of polymers generally follows the following trend:

$$PET \Rightarrow PP \Rightarrow PE$$

Nevertheless, polymer structural parameters, such as molecular weight, molecular orientation, crystalline volume fraction, degree of branching and draw molecular ratio are also very important to evaluate creep sensivity of polymers (Ward, 1985; den Hoedt et

al., 1994).

Even the geosynthetic structure shows an important influence on the creep behaviour: for instance, in nonwoven geotextiles a realignment of polymer fibres, necking, crimps and elimination of wrinkles may produce an unpredictable, unrecoverable immediate strain. In general terms, these effects over the total creep strain follow the following trend:

NONWOVEN STRUCTURES ⇨ WOVEN STRUCTURES ⇨ INTEGRAL STRUCTURES

Typical strain-time curves at any temperature and various loads levels, expressed as a percentage of the tensile strength, are showed in Fig.3. A further method of presenting the test data is to plot the creep strain rate against the cumulative strain as illustrated in Fig.4, to obtain Sherby-Dorn curves. This plot clearly shows whether the material approaching failure or viceversa a state of stable equilibrium and can thus assist in the avoidance of long-term instability.
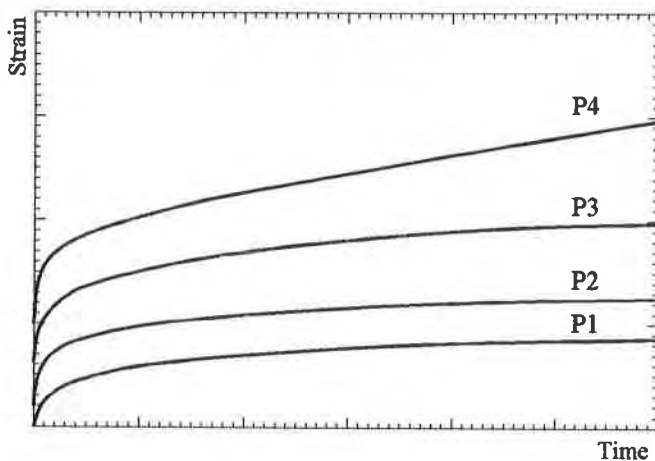
Fig. 3 Tensile creep plots at various load
        levels (P1, P2, P3 and P4)
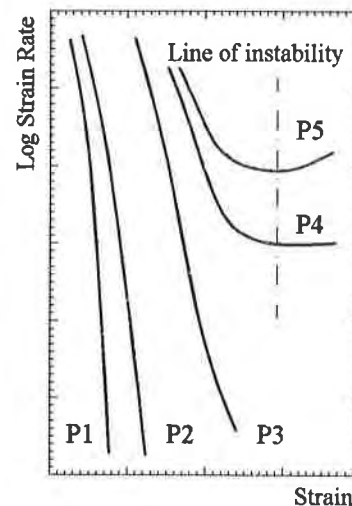
Fig. 4 Sherby-Dorn plots

The temperature effect over the tensile creep behaviour of reinforcement geosynthetics is directly influenced by polymer nature and polymer structure. The creep curves published from several autors (Müller-Rochholz and Reinhart, 1990; Rimoldi and Montanelli, 1993; den Hoedt et al., 1994) highlight the following considerations:

- a pronounced influence of temperature on strain-time behaviour for HDPE and PP geosynthetics; however, the temperature effect may be minimised for HDPE by increasing the molecular weight and molecular draw ratio as illustrated by Bush (1990);
- a negligible influence of temperature on strain-time behaviour for PET geosynthetics.

The effect of increasing temperature can be used to extend the long-term strength prediction of geosynthetics by time-temperature superposition techniques. However, for all polymer materials, the effect of load is many times greater than effect of temperature.

The soil environment has both chemical and mechanical influences on geosynthetics creep behaviour. The soil confines the reinforcement and restricts the freedom for lateral contraction under tensile load, hence altering the load-strain properties compared with 'unconfined' load-strain properties. However, several researchers (Levacher et al., 1994; Wu et Hong, 1994) highlighted a very small influence of the confining on tensile creep behaviour on geotextiles and moreover a negligible influence on geogrids.

TENSILE CREEP TEST APPARATUS

The tensile creep test apparatus designed and built at the Geotechnical Laboratory of Civil Engineering Department consist of the followings basic elements:

- a room with controlled constant temperature and humidity conditions;
- a rigid frame to support the loading;
- a device to grip the specimens;
- a loading system and a system to measure the change in gauge length with time.

A fenced box, made by thermally isolated panels, with external dimensions of 2,70 m × 4,90 m × 3,20 m (width × length × height) is shown in Fig.5.

Inside the box a rigid support frame built with steel elements is capable to hold in position twelve geosynthetic specimens as shown in Fig.6.
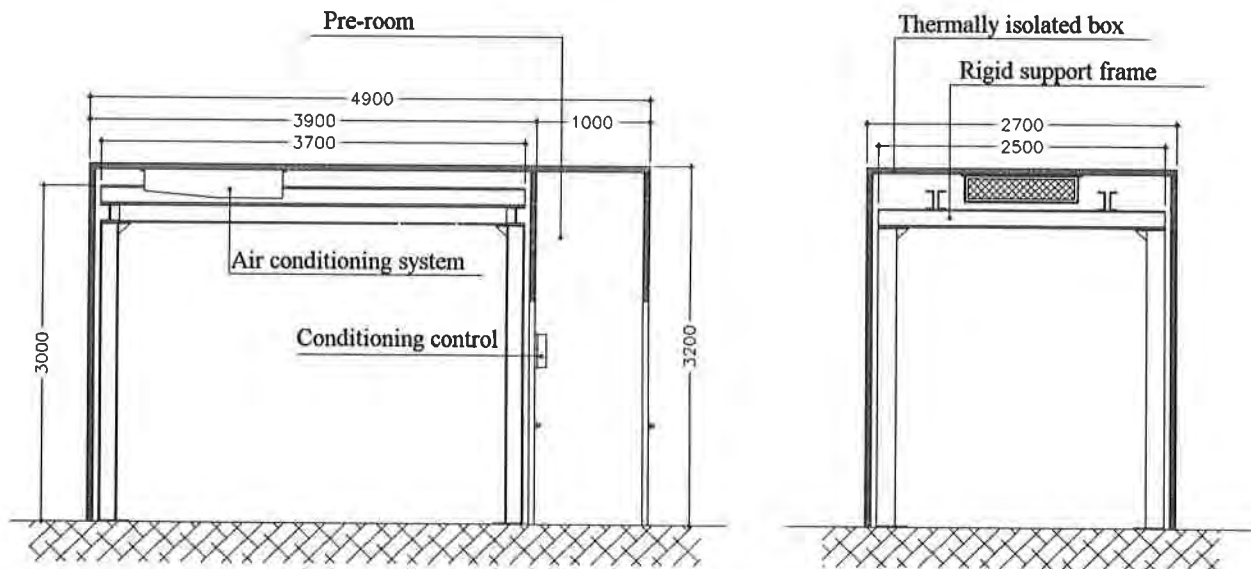
Fig. 5 Fenced box
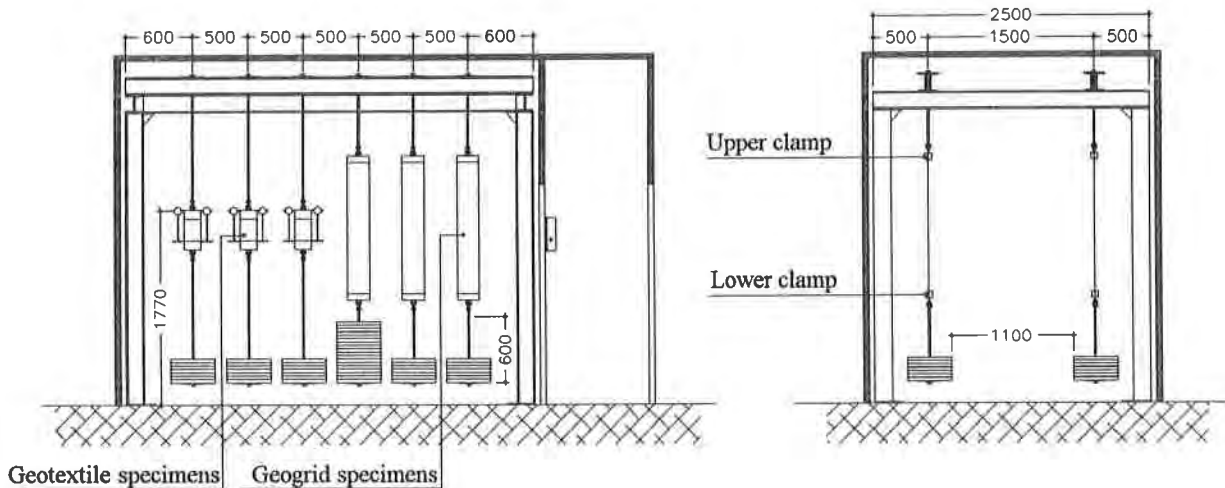
Fig. 6 Tensile creep apparatus

An industrial air conditioner installed in ceiling box is capable to generate a range of room temperature between +5°C and +60°C at relative humidity of 65% ±2%. An electronic device positioned outside the box is able to control the temperature and recording any its daily variations.

With reference to the grips device, very simple clamp types were built. The clamps were designed to hold the specimens firmly across the full width, without slippage and a way which does not cause any damage to the specimen.

As illustrated in Fig.7a the grips device for geogrids consisted of a precasting bar, made by a cold-setting polyester resin, at both the ends of the specimen (Rimoldi and Montanelli, 1993). A special mould was employed to obtain a bar in rectangular shape and to fix the specimen in a perfectly central and vertical position. After 24 hours of curing at ambient temperature the rectangular shaped blocks are ready to be inserted in the ending clamps. These was made by special tubular steel "C" shaped, 200 mm wide as shown in Fig.7b.

For geotextiles instead, the grips device consisted of two steel plate clamps as illustrated in Fig.8. To avoid possible specimens slipping from clamps these are reinforced at both grip ends by bi-component fast setting resin.
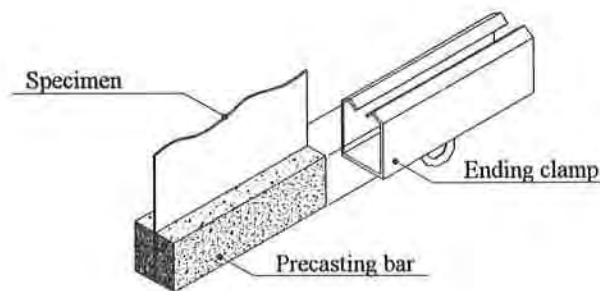
Fig. 7a Geogrids grip device
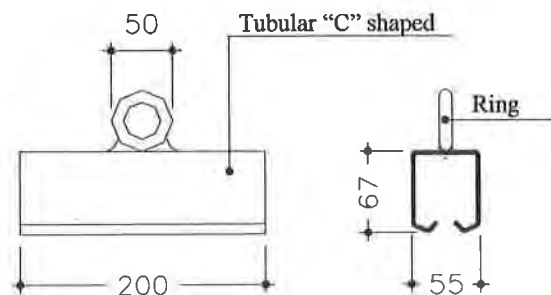
Fig. 7b Geogrids ending clamp
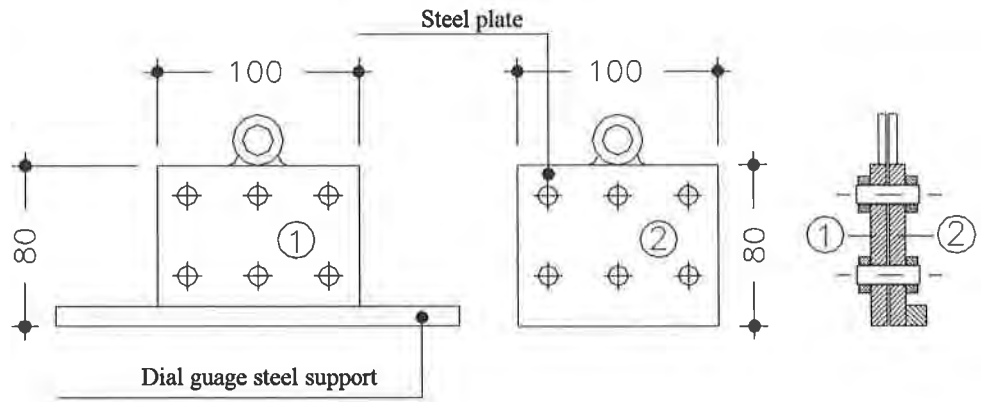
Fig. 8 Geotextiles ending clamp

The change in the length of the gauge length is measured between two parallel lines drawn across the full width of the specimen. The strain measuring apparatus adopted is able to measure the change with an accuracy of 0.1% of the gauge length, in accordance with the European standard.

For geogrids the total elongation was monitored by means of a direct reading graduated metallic ruler positioned directly on the specimen. The origin of the ruler was placed exactly at the top marked gauge line as illustrated in Fig.9.

As high-resistance geogrids are very unextensible, it is possible to adopt geogrid specimens with gauge length ≥ 1000 mm and thus to use a measurement apparatus with
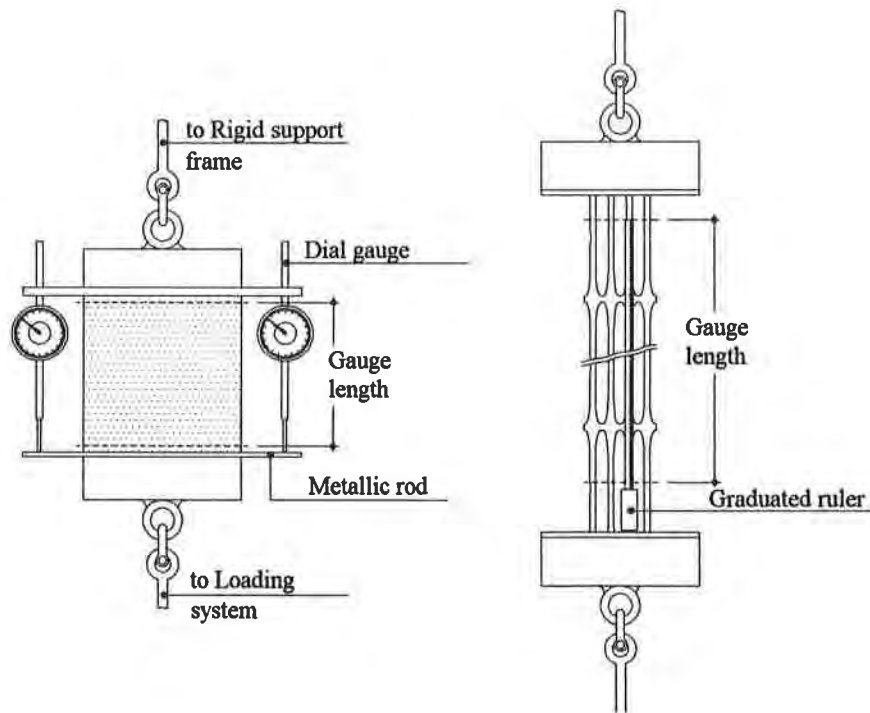
Fig. 9 Measurement system

absolute accuracy up to 1 mm to obtain a relative accuracy up to 0.1% in accordance with CEN standard. For geotextiles specimens instead, it is not possible to choose specimens with gauge length > 200 mm and thus the total elongation was monitored by the means of two dial gauge with absolute accuracy up to 0.001 mm, put at both end of the specimen and fixed at upper clamp by a metallic rod (see Fig.9), to obtain the relative accuracy request.

Calibrated steel discs with buttonhole, form a dead weight creep load system. Such a load system is very simple ed economic; moreover it is not necessary to ensure thet creep load remains constant during the test.

SPECIMEN SIZE

The size of the specimens is determined in accordance with European standard, in such way as to:

- to suit the accuracy of the measuring equipment being used;
- to comply with the technical representative width (TWR), defined as the smallest width that exhibits tensile strength/strain characteristics per unit length, within ±5% for tensile strength and ±10% for strain, at the maximum load;
- to allow the minimum gauge length to be established within the clamps such that there is a distance of not less than 20 mm between either end of the marked gauge length and the clamps.

The CEN standard prescribes that the minimum specimen gauge length shall be:

- not less than 200 mm;
- not less than two full meshes for geogrids;
- for all samples such length as will enable the measurement of the gauge length to an accuracy up to 0.1%.

Instead the minimum specimen width shall be:

- not less than the TRW;
- not less than two full ribs for all geogrids;
- for specimens which exhibit lateral contraction which is ≥ 10% not less than 200 mm; for all other materials not less 50 mm (see Fig.10).
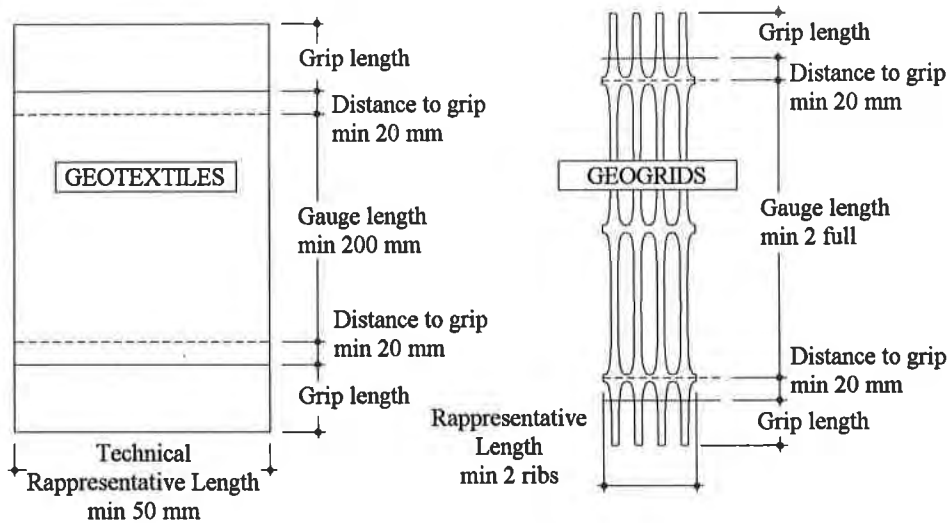
Fig. 10 Specimen dimensions

CEN and ASTM STANDARD COMPARISON

No substantial differences existing between European standard CEN prEN ISO 13431 and North American standard ASTM D 5262-92 with reference to the load system, strain measurement system and test procedures. However, other important parameters are very different and the most important are listed below.

About the accuracy of strain measurement , the ASTM standard prescribes an absolute accuracy up to ±0.003mm whereas CEN standard a relative accuracy up to ±0.1%. The ASTM standard does not allow the change in the gauge length of geogrids to be measured using the very simple and inexpensive graduate metallic ruler.

The European standard prescribes minimum sizes of the specimens (gauge length and width) following the procedures previously described, whereas the ASTM standard prescribes:

- for geotextiles, a minimum gauge length of 100 mm and a minimum width of 200 mm, which may be reduced to 100 mm for samples with tensile strength more than 100 kN/m;
- for geogrids, not less that one rib in the gauge length and not less than three longitudinal members in the across direction.

Finally, a different procedure concerns the loading time, i.e. the time necessary to apply the full creep load. In fact the CEN standard prescribe to apply the full load in not more than 60 seconds, whereas the ASTM standard prescribe to apply the full load rapidly, preferably at strain rate of 10 ±3%/min. This procedure is very difficult to follow in particular when using dead weights as loading system.

EXPERIMENTAL PROGRAM AND PRELIMINARY RESULTS

In the experimental program currently undertaken by the Research Group on Special Materials of ENEL Spa - CRIS in Milano and the Civil Engineering Department of Florence University, three geosynthetics are used: an HDPE extruded geogrid (M1), a PET woven geogrid (M2) and a PP/PET woven/nonwoven composite geotextile (M3). Each material is tested with tensile creep load of 20% (C1), 30% (C2) and 50% (C3) of wide-width tensile strength, and using room temperatures of 10°C (T1), 20°C (T2) and 40°C (T3).

The European standard procedures on tensile creep test indicate as first step to determine the wide-width tensile characteristics of the sample, including the strength and strain at peak, in accordance with EN ISO 10319. The most important results of wide-width tensile tests carried out at ENEL Spa - CRIS are summarised in Tab.1: the tests were performed using the apparatus and procedures described by Cazzuffi at al. (1994).

REF.	PRODUCT NAME	GEOSYNTHETIC TYPE	POLYMER TYPE	SPECIMEN SIZE		PEAK STRENGTH	STRAIN AT PEAK
				WIDTH [mm]	GAUGE LENGTH [mm]	[kN/m]	[%]
(M1)	TENAX TT 201 SAMP	EXTRUDED GEOGRID	HDPE	200	150	53.73	12.6
				3 rib	150	52.71	12.6
(M2)	FORTRAC 35/20-20	WOVEN GEOGRID	PET	200	150	53.13	11.3
				3 rib	150	48.86	11.3
(M3)	POLYFELT PEC 50/25	WOVEN\NWOVEN GEOTEXTILE	PP/PET	200	60	56.22	12.8
				100	60	53.66	12.8

Tab. 1 Product characteristics and wide-width tensile test results

The procedures to evaluate the tensile creep behaviour has been carried out in accordance with CEN standard; the following steps has been adopted:

1. on the specimen are marked the reference lines to give the required gauge length;
2. the specimen with their clamps is put into the apparatus device;
3. a preload equal to 1% of the selected creep load is applied and the initial gauge length is measured;
4. the full creep load is smoothly applied in not more than 60 seconds;
5. the change in the gauge length after the creep load has been applied, at the following times: 1, 2, 4, 8, 15, 60 minutes; 1,4 8, 24 hours; 3, 7 days, is recorded.

Some tensile creep test results are below reported. Typical tensile creep plots obtained (total strain vs. log time) for (M1) HDPE extruded geogrid, (M2) PET woven

geogrid and (M3) PP/PET woven/nonwoven composite geotextile at 20°C are showed respectively in Figs.11, 12 and 13.
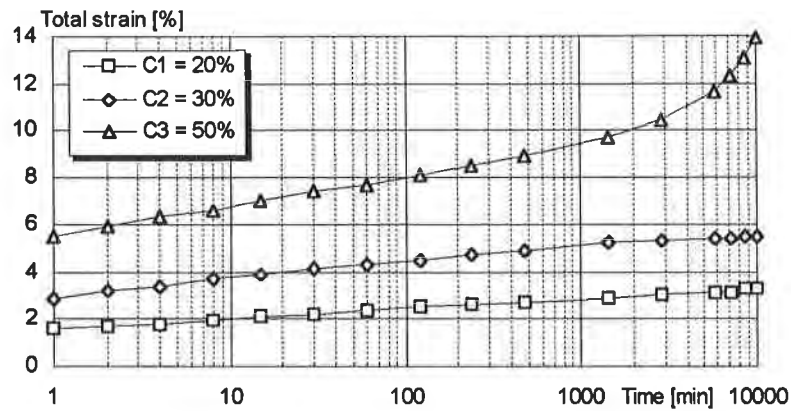
Fig. 11 Total strain vs log time curves for HDPE extruded geogrid (M1) at 20°C (T2)
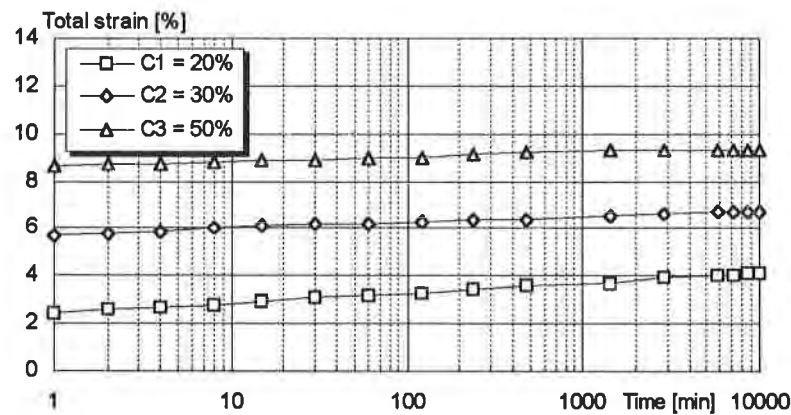
Fig. 12 Total strain vs log time curves for PET woven geogrid (M2) at 20°C (T2)
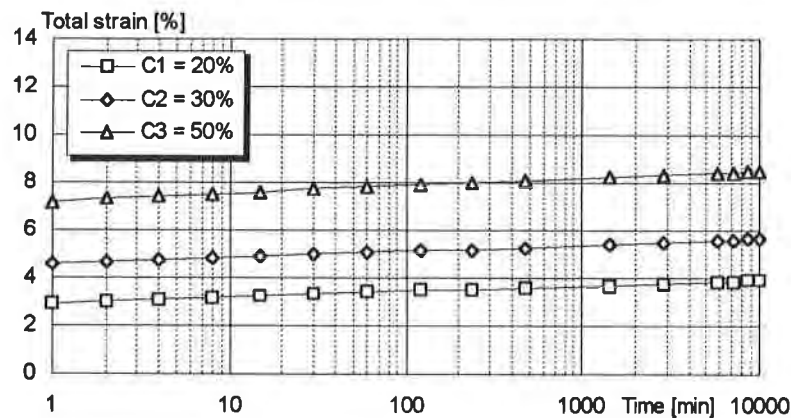
Fig. 13 Total strain vs log time curves for PP/PET woven/nonwoven geotextile (M3) at 20°C (T2)

Typical Sherby-Dorm plots obtained for the same above mentioned materials are illustrated in Figs. 14, 15 and 16.
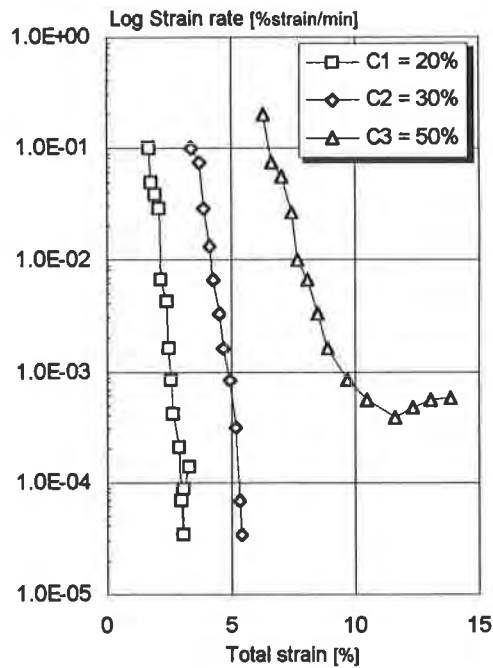
Fig. 14   Sherby-Dorm curves for HDPE
extruded geogrid (M1) at 20°C (T2)
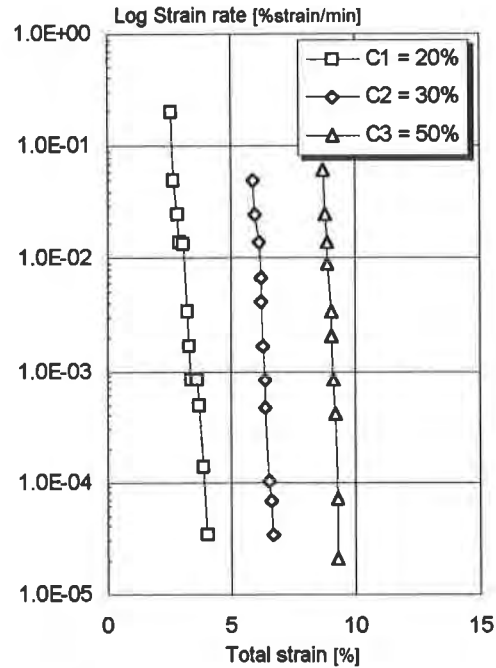
Fig. 15   Sherby-Dorm curves for PET woven
geogrid (M2) at 20°C (T2)
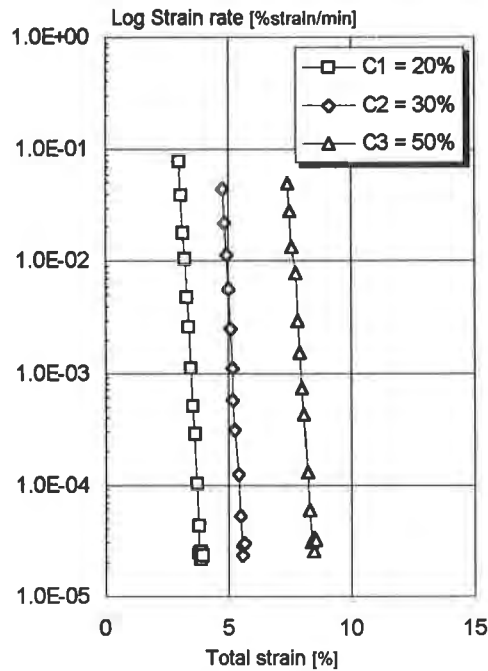
Fig. 16   Sherby-Dorm curves for PP/PET
w./nw. geotextile (M3) at 20°C (T2)

PRELIMINARY CONCLUSIONS

To investigate more specifically the tensile creep of some high-strength reinforcement geosynthetics an experimental program has undertaken jointly by ENEL Spa - CRIS in Milano and University of Florence. At the actual state of the research some preliminary conclusions can be drawn:

- the dead weight loading system appear to be the most easy, cheap and precise system to load the specimens. This system does not need to control that the creep load remains constant during the test and thus it is preferable than mechanical, hydraulic or pneumatic system;
- geogrids specimen with gauge length more than 1000 mm allows to use measurement system with absolute accuracy up to 1 mm, to obtain a relative accuracy up to 0.1% in accordance with prEN ISO 13431. This measurement system is very simple and economic;
- geotextiles with gauge length of 200 mm needed a measurement system with more absolute accuracy;
- the minimum width of the specimens shall be not less than two full ribs for geogrids, and not less than the TRW (technical representative width) for geotextile samples which exhibit lateral contraction less than 10%. In particular for PET/PP composite geotextile (M1) it has been possible to use 100 mm specimes width.;
- the preliminary short term results showed that the choice of equipment was correct and suitable to test high strength reinforcement geosynthetics. Hereafter the experimental results are in good agreement with other european tensile creep results.
- no significant difference are obtained between CEN and ASTM loading procedure;
- the preliminary short term results clearly showed that the HDPE extruded geogrid (M1) approaching to failure with load creep of 50% (C3) of wide-width tensile strength (see Fig.11 and Fig14).
- viceversa a state of stable equilibrium is reached for both other M1 load conditions (C1, C2) and for M2 and M3 materials (for all the three load conditions).

REFERENCES

ASTM D 5262 - 92, (1992) "Standard test method for evaluating the unconfined tension creep behavior of geosynthetics", Annual Book of ASTM Standards, ASTM, Philadelplhia, PA, USA.

Bush, D.I., (1990) "Variation of long term design strength of geosynthetics in temperatureup to 40°C", Proc. IV Int. Conf. On Geotextiles, Geomembranes an Related Products, pp. 673-676, The Hague, The Netherlands.

Cazzuffi, D., Ghinelli, A., Sacchetti, M., (1995) "Prove interlaboratorio per la valutazione delle proprietà meccaniche dei geosintetici con funzione di rinforzo", Atti del XIX Convegno Nazionale di Geotecnica, pp.295-304, Pavia, Italia.

CEN, prEN ISO 13431, (1995) "Geotextiles and geotextiles related products: determination of the tensile creep and creep rupture properties", Doc. CEN/TC 189/WG 3/N 31/Rev 1.

den Hoedt, G., Voskamp, W., Van den Heuvel, C.J.M., (1994) "Creep and time-to-rupture of polyester geogrids at elevated temperatures", Proc. V Int. Conf. On Geotextiles, Geomembranes an Related Products, pp. 1125-1130, Singapore.

Levacher, D., Blivet, J.C., Msouti, F., (1994) "Tensile and creep behaviour of geotextiles" Proc. V Int. Conf. On Geotextiles, Geomembranes an Related Products, pp. 1131-1134, Singapore.

McGown, A., Andrawes, K.Z., Yeo, K.C., DuBois, D., (1985) "The load-strain-time behaviour of Tensar geogrids", Polymer Grid Reinforcement, Thomas Telford, London.

Müller-Rochholz, J. and Koslowski, C., (1996) "Creep prediction", Proc. of The First European Geosynthetics Conference EUROGEO 1, pp. 1027-1030, Maastricht, The Netherland.

Müller-Rochholz, J., Reinhard, K., (1990) "Creep of geotextiles at different temperatures", Proc. IV Int. Conf. On Geotextiles, Geomembranes an Related Products, pp. 657-659, The Hague, The Netherlands.

Rimoldi, P., Montanelli, F., (1993) "Creep and accelerated creep testing for geogrids", Geosynthetics '93, pp. 773-787, Vancouver, Canada.

Ward, I.M., (1985) "The orientation of polymers to produce high performance materials", Polymer Grid Reinforcement, Thomas Telford, London.

Wu, C.S., Hong, Y.S., (1994) "Creep behaviour of geotextiles under confining stress", Proc. V Int. Conf. On Geotextiles, Geomembranes an Related Products, pp. 1135-1138, Singapore.

PREDICTION OF LONG-TERM STRAINS OF GEOSYNTHETICS FROM ACCELERATED-CREEP TESTS

Khalid Farrag
Louisiana Transportation Research Center, Baton Rouge, LA.
U.S.A.

ABSTRACT

The paper presents the results of accelerated-creep tests at elevated temperatures and discusses the applicability of the current procedures in extrapolating these results to longer time intervals.

Creep tests were performed on High Density Polyethylene (HDPE) geogrid typically used in soil reinforcement applications. These tests were conducted at various elevated temperatures and loading levels. The procedure for extrapolating creep strain-rates, utilizing the Arrhenius Equation, was evaluated. The results showed some limitations associated with the estimation of the activation energy and the corresponding predictions of strain-rates.

Another extrapolation procedure was also presented. It consisted of applying shift factors, a_T, on creep strain curves at elevated temperatures along the logarithm of time. This procedure was based on empirical formulation of the temperature dependancy of a_T, known as the WLF equation. The results of 1,000 hour tests at various temperatures were shifted to create 10,000 hour master strain curves. The established master curves were compared with the results of 10,000 hour creep tests at room temperature. The results showed that the analysis was applicable in predicting strains at longer times for the HDPE geogrid for loading levels below the creep loads where accelerated creep failure occurred.

INTRODUCTION

Long-term strength of geosynthteics is usually predicted from 10,000 hour extension creep tests [Allen (1996) and GRI (1991)]. It is a general practice that the results from these tests are extrapolated up to one order of time magnitude (i.e. up to 10 years) [Allen (1991) and Jewell (1988)]. Extension creep tests at elevated temperatures can accelerate testing durations to

reasonable time frames (1,000 hour) and their results can also be extrapolated to predict creep behavior at longer time intervals [Bush (1990), Müller and Kirschner (1990)].

The Strain-time-temperature relationship was evaluated for HDPE geogrid. This geogrid type had an average degree of crystallinity of about 60% , a glass-transition temperature of about -80°C (-112°F), and a melting temperature of about 120°C (220°F). The main reasons for selecting this type of polymer in the testing program were that it is typically used in soil reinforcement applications and it exhibits measurable changes in its creep response parameters with changes in temperature.

Creep tests at elevated temperatures were performed at various loads up to 40% of the maximum short-term strength of the geogrid, T_{max}. An estimation of the parameters associated with the application of the Arrhenius Equation is first presented. The applicability of applying this equation to predicting creep strain-rates at longer time intervals is assessed. A different approach for direct extrapolation of creep strains, rather that strain-rates, is also evaluated. This approach is based on applying time-shift factors a_T to shift temperature-creep curves to longer time intervals. The values of a_T were assessed experimentally and were compared with the empirical formulation of the temperature dependency of a_T known as the WLF equation [Aklonis (1983) and Ferry (1955)].

EVALUATION OF CREEP STRAIN-RATE USING ARRHENIUS EQUATION

The relation between temperature T and creep strain-rate $\dot{\varepsilon}$ can be expressed in the mathematical expression, the Arrhenius Equation, in the form [McCrum et al. (1988) and Shelton and Bright (1993)]:

$$\dot{\varepsilon} = A\, e^{-\frac{E}{RT}} \tag{1}$$

where, $\dot{\varepsilon}$ = creep strain-rate, t^{-1}
            A = a pre-exponential rate constant, t^{-1}
            E = experimental activation energy (cal/mol)
            R = universal gas constant (= 1.987 cal/mol-K)
and   T = absolute temperature ($^{\circ}$K).

Equation 1 shows that creep strain-rate increases with temperature and with the decrease in the activation energy, providing that all other factors affecting creep are kept constant. Equation 1 is usually used in predicting creep rates for longer time intervals. Although time t is not an explicit parameter in the equation, the ratio between $\dot{\varepsilon}_1$ at temperature T_1 and $\dot{\varepsilon}_2$ at temperature T_2 presents a multiplier coefficient of the kinetics μ that can be used in shifting strain-rates along the time axis. This relationship is expressed in the form [McCrum et al. (1988) and Segrestin (1988)]:

$$Ln \; \mu \; = \; Ln \; (\dot{\varepsilon}_1 \; / \; \dot{\varepsilon}_2) \; = \; \frac{E}{R} \; (\frac{1}{T_2} \; - \; \frac{1}{T_1}) \tag{2}$$

One of the inherit problems in the use of Arrhenius equation arises from the difficulty in determining the activation energy E from creep tests as the strain-rate is constantly changing during the test. However, a common and simple technique for the estimation of E consists of applying rapid change in temperature during creep under a constant load [Sherby and Dorn (1958)]. Creep strain rates $\dot{\varepsilon}_1$ and $\dot{\varepsilon}_2$ are measured before and after the change in temperature from T_1 to T_2, respectively, and E can be determined from equation 2.
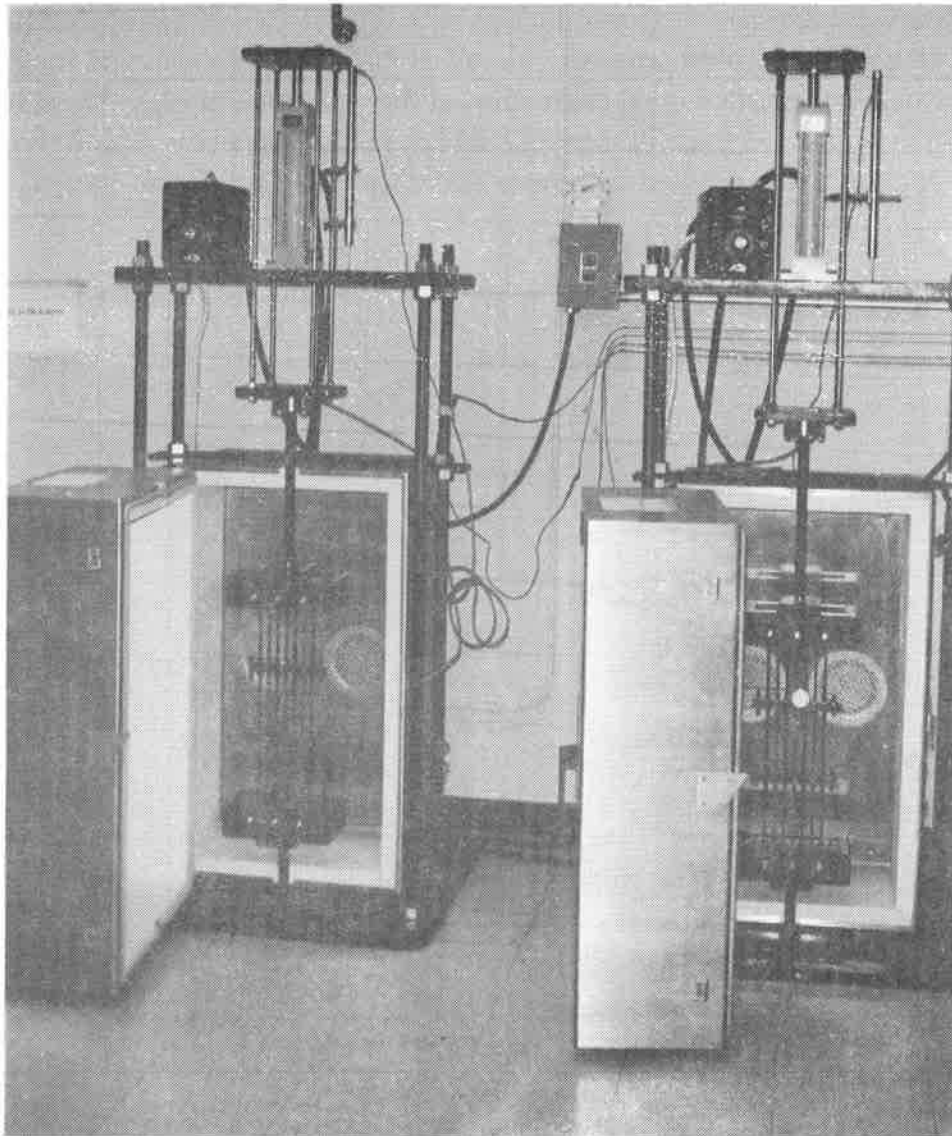
Figure 1. View of the temperature-creep testing equipment

The evaluation of the activation energy E at various creep loads was assessed through testing HDPE geogrid specimens of 6 in. (0.15 m) wide and about 19 in. (0.48 m) long at various elevated temperatures and loading levels. The equipment used in these tests consisted of two sets of creep testing frames (Figure 1).

The geogrid specimens were placed inside the test ovens and were tested at various temperatures ranging from $32^{\circ}C$ ($90^{\circ}F$) to $71^{\circ}C$ ($160^{\circ}F$). A hydraulic system applied creep loads ranging from about 18% to 40% of T_{max} . A detailed description of the equipment and testing program are presented elsewhere [Farrag, 1996].

The first set of tests on the geogrid consisted of increasing the temperature incrementally every 20 hours while maintaining the load constant. Typical results of these tests at an extension load of 1.5 Kips/ft (22 kN/m) are shown in Figure 2. The slopes of strains before and after the change in temperature represented creep strain rates at these temperatures and loading levels. The application of equation 2 resulted in an estimation of the activation energy for each loading level. Figure 3 shows the calculated activation energy at various loading levels. The figure shows that an increase in the applied loads resulted in a linear decrease in the activation energy.
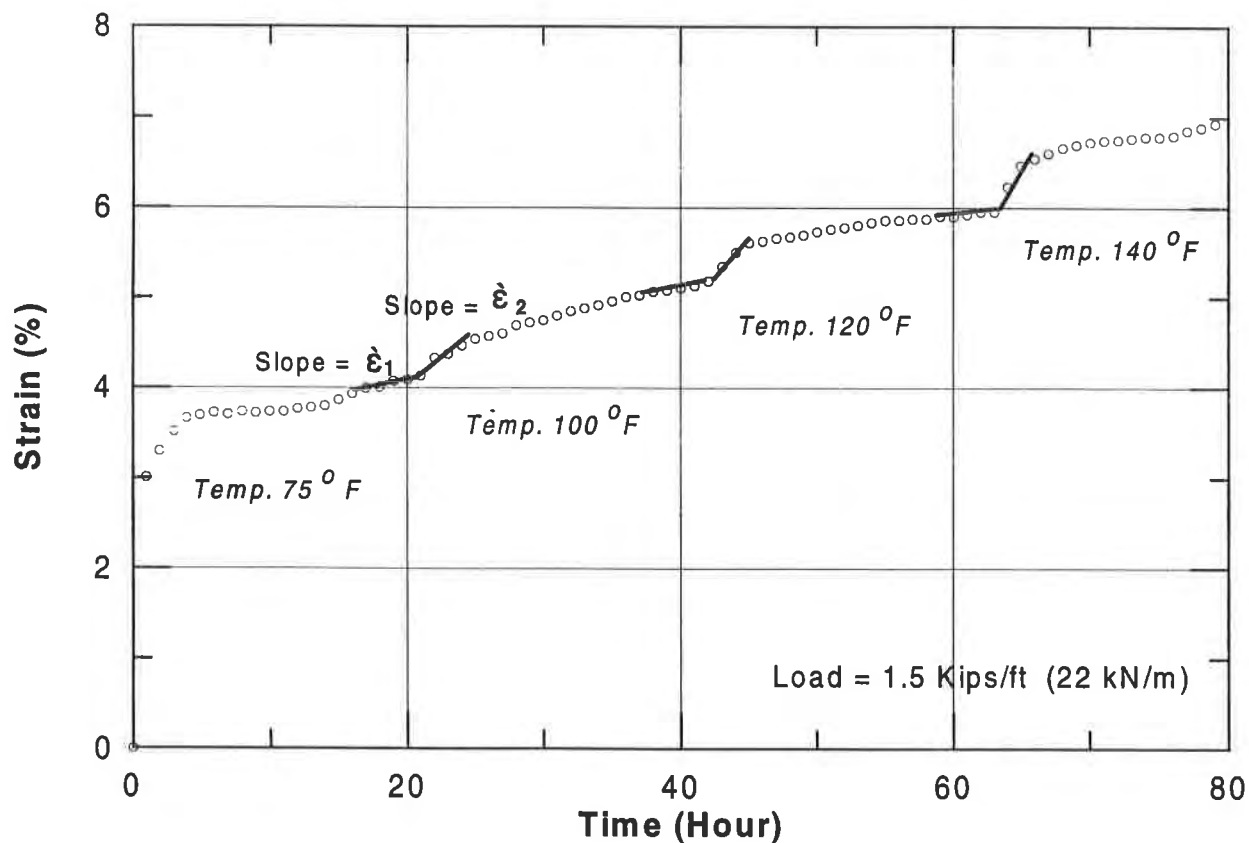
Figure 2. Change of creep strain-rates with temperature at constant load
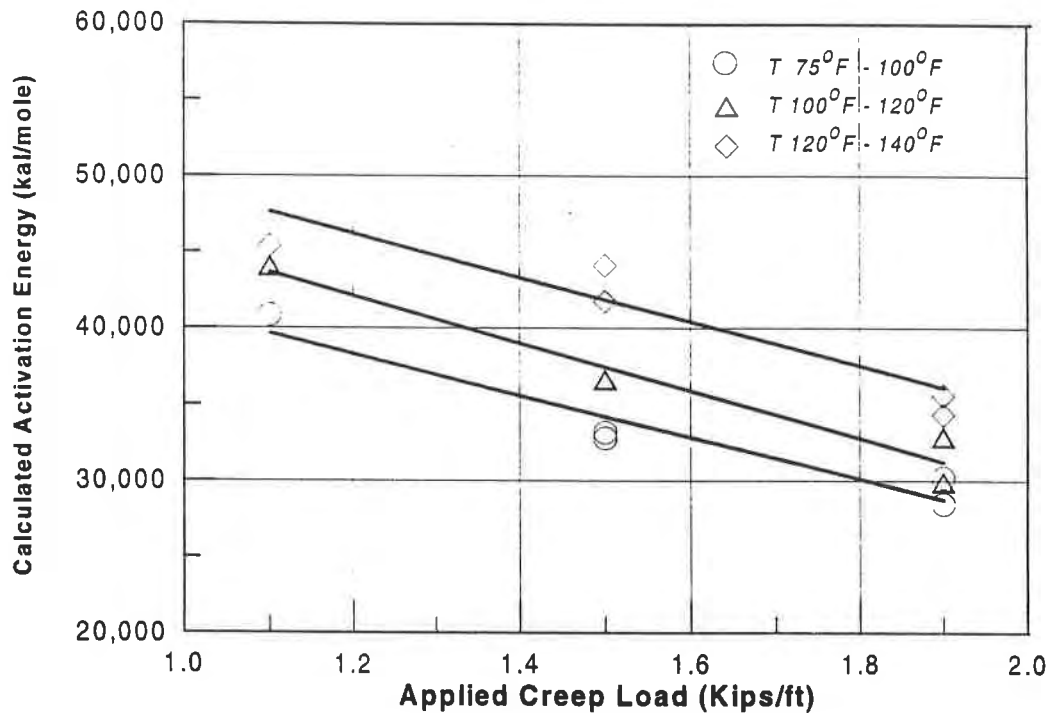
Figure 3. Change of the activation energy E with creep loads

The results in figure 3 also show that the activation energy was sensitive to the changes in temperature levels. Since E is assumed to remain constant over the time and temperature range for extrapolation of creep rates [Shelton and Bright (1993)], the application of equation 2 would only be valid within the temperature range where E is calculated.

The second set of tests consisted of running 1,000 hour extension tests on the geogrids at various temperatures and loading levels. Typical results of these tests at load 1.5 Kips/ft (22 kN/m) are shown in Figure 4 where strain rates are plotted versus time at various temperatures. The figure shows that the multiplier coefficient μ (defined in equation 2) does not provide a constant shift between the temperature ranges in the figure. The calculation of μ from equation 2 would require the correct estimation of E that corresponds to each temperature increase.

EVALUATION OF CREEP STRAINS USING THE WLF EQUATION

The results of 1,000 hour creep tests at creep load 1.5 kips/ft at various temperatures are plotted as log-strains versus log-time in Figure 5. When these curves are shifted along the time axis, a single curve, commonly known as the master curve, is established. This curve represents creep strains for longer time intervals. Creep strains for any time, t, can then be expressed as:
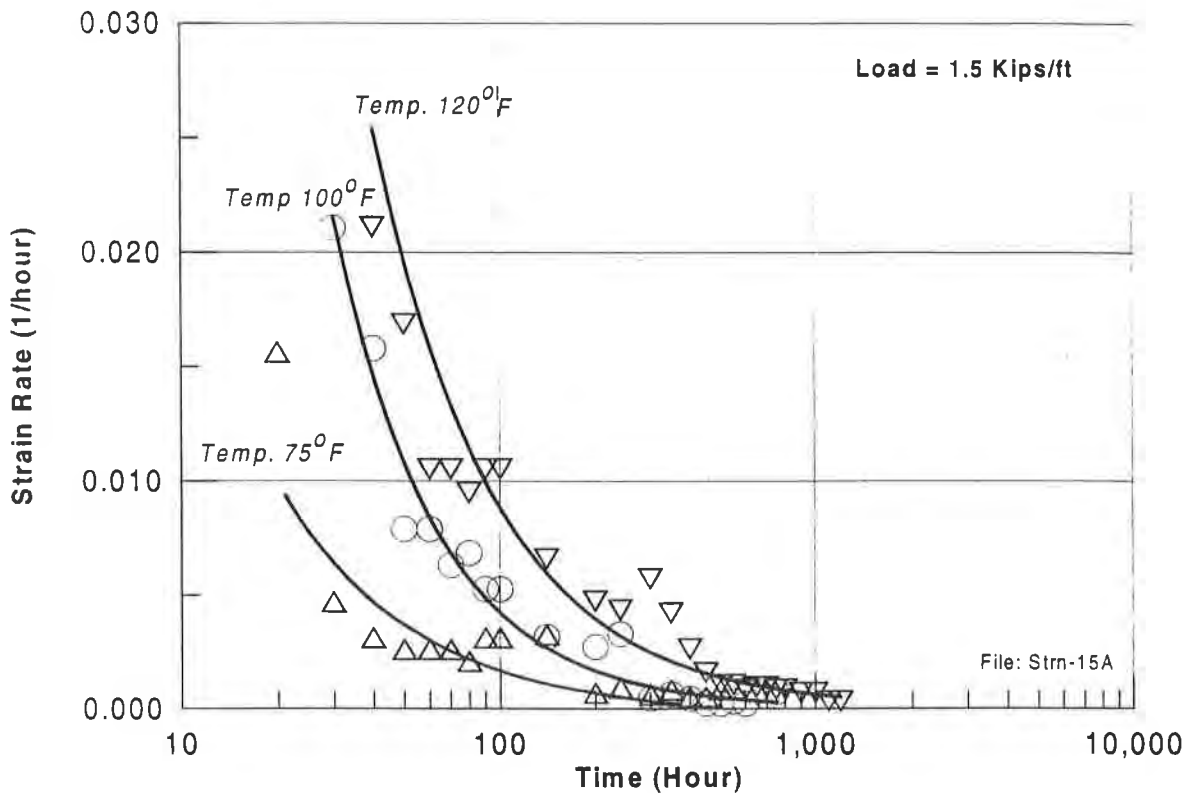
Figure 4. Change of creep strain rates in 1,000 hour tests at various temperatures
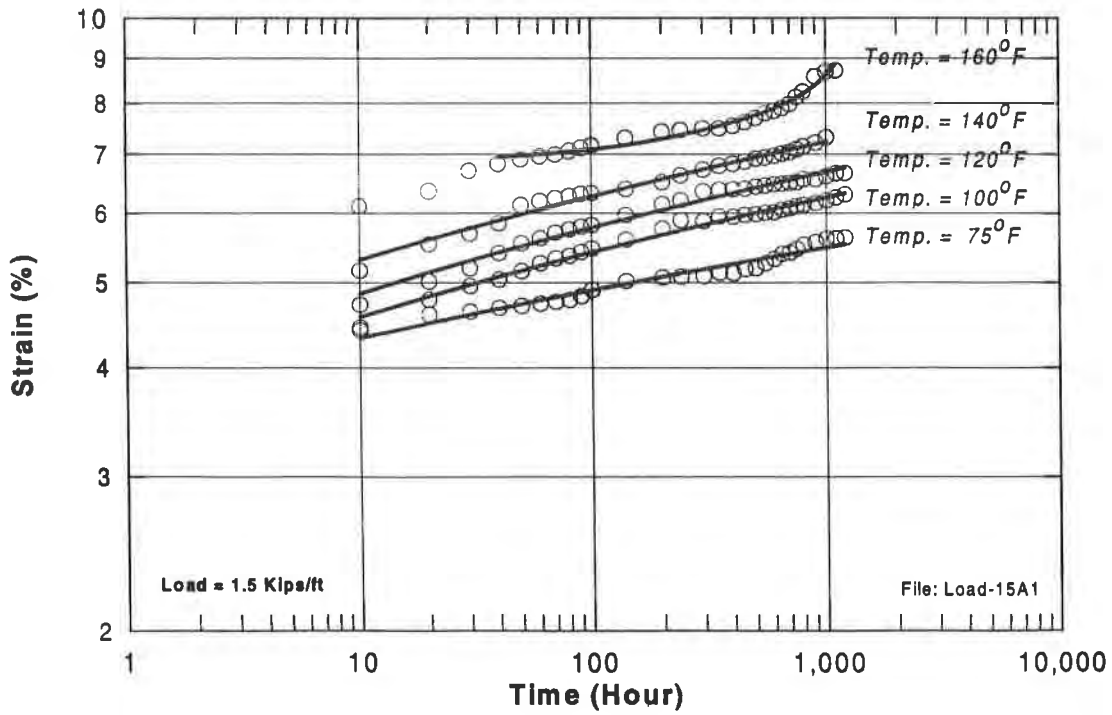
Figure 5. Results of 1,000 hour creep tests at elevated temperatures

$$E\ (T_o,t\ )\ =\ E\ (T,\frac{t}{a_T}) \tag{3}$$

where T_o is an arbitrary reference temperature, T is the elevated temperature, and the horizontal time shift is the logarithm of the shift factor a_T. The empirical value of the shift factor a_T (equation 3) was proposed by Williams, Landel and Ferry, the WLF equation, in the form [Ferry, 1955]:

$$Log\ a_T\ =\ \frac{-C_1\ (\ T-T_o\ )}{(\ C_2\ +\ T\ -\ T_o\ )} \tag{4}$$

where C_1 and C_2 are constants, and T_o is a reference temperature.

Applying the shift principal on the strain curves in figure 5, the adjacent strain curves at various temperatures were shifted to obtain one master curve. The shift factors were established graphically and regression analysis was conducted to obtain the best fit of a linear function of the master curve. This procedure was applied to the creep results at various loading levels. The logarithm of the horizontal shifts a_T from the experimental results are plotted versus temperature in Figure 6 for each creep load.
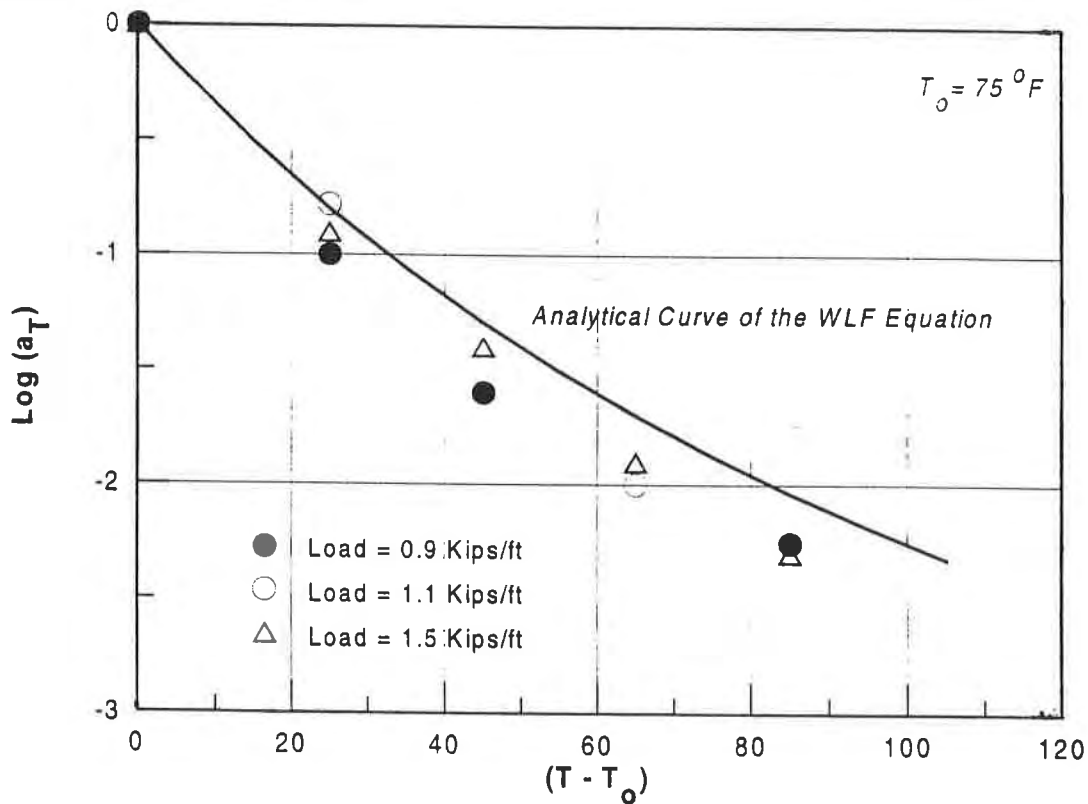
Figure 6. Analytical and experimental temperature shift factors a_T

The empirical values of a_T for the HDPE geogrid were calculated from equation 4 using typical values of the constants C_1 and C_2 as 17.4 and 51.6, respectively [Aklonis, 1983]. These values slightly change according to polymer type and they correspond to the glass-transition temperature, T_g, as a reference temperature. The analytical curve of the a_T function is plotted in the same figure. The figure shows that a_T did not change with the increase in creep loads and it compared well with the analytical curve.

In order to evaluate the established master curves, creep tests were performed for durations up to 10,000 hours at room temperature. The results of these tests were compared with the predicted strains from the master curves. Figure 7 shows the comparison between the 10,000 hour test results and the master curve for creep load 1.5 Kips/ft. The predicted strains from the master curve compared well with the experimental results at this loading level. It should be noted that the master curves compared well with the experimental results up to creep load of about 40% T_{max}. At this loading level creep failure occurred and the strain master curve did not compare with the accelerated creep strains.
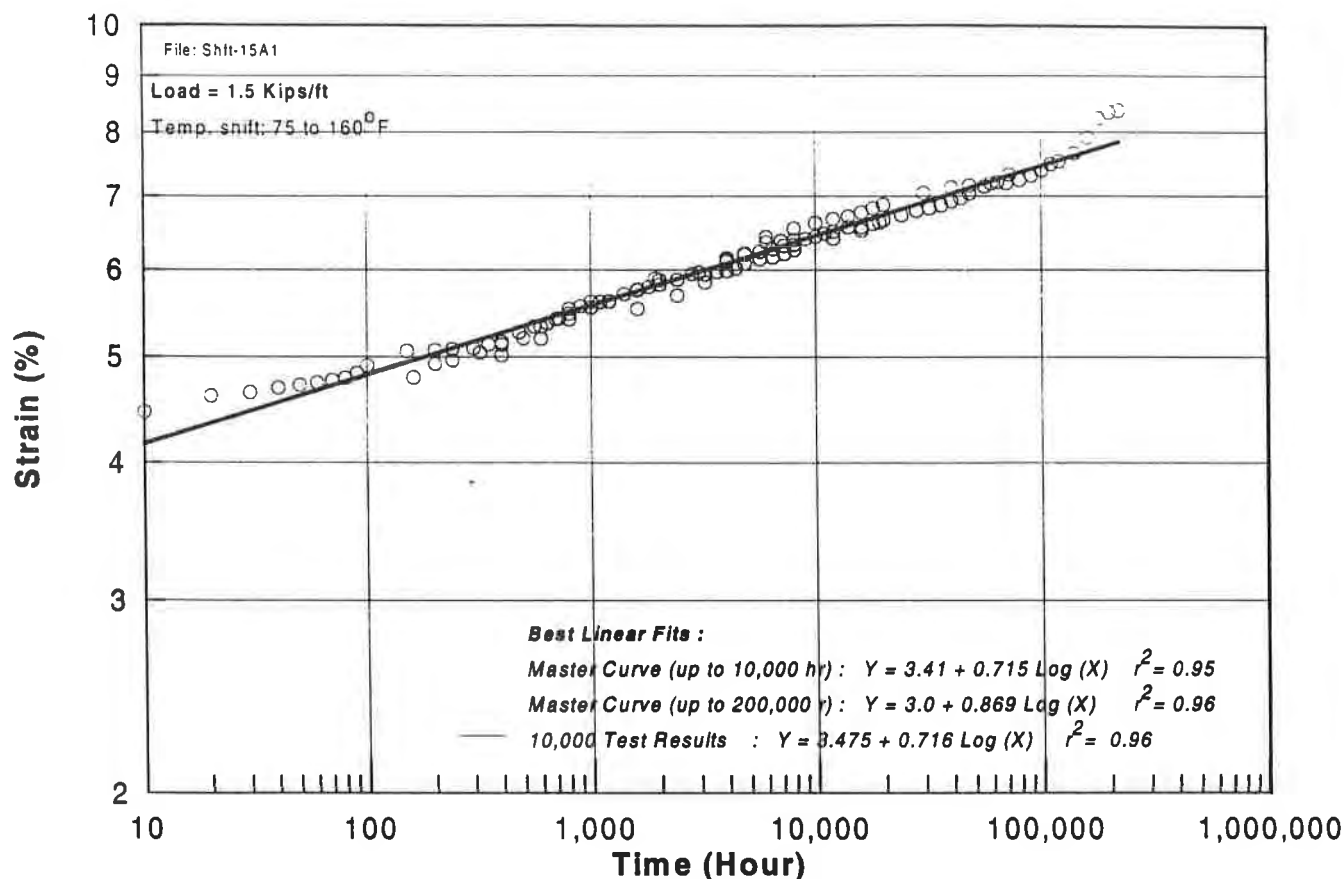
Figure 7. Comparison of the Master Curve and 10,000 hour experimental results

CONCLUSION

The application of the Arrhenius Equation in predicting strain-rates from temperature creep tests was presented. The evaluation of the procedure showed the sensitivity of the predicted values of the activation energy and the corresponding strain-rates to the variations in the input parameters. Test results demonstrated the necessity of properly estimating the activation energy E that corresponds to each creep load and temperature level.

The temperature-shift procedure, based on the WLF shift factors, was also presented. Temperature-shifts were established from 1,000 hour test results. The predictions were compared with 10,000 hour test results at room temperature. The comparison showed the applicability of the procedure for creep loads below accelerated creep failure.

Results from creep tests at temperatures up to 160 ^{O}F were utilized in predicting the 200,000 hour creep response. Application of higher temperatures and further shifts to longer time intervals should be verified and correlated with experimental results.

ACKNOWLEDGMENT

REFERENCES

Aklonis, J.J., and MacKnight, W.J., *Introduction to Polymer Viscoelasticity*, Jon Wiley and Sons, 2nd edition, 1983.

Allen, T.M., "Determination of the Long Term Tensile Strength of Geosynthetics: A State-of-the Art Review," *Geosynthetics'91*, Atlanta, 1991, pp. 351-379.

Bush, D.I., "Variation of Long Term Design Strength of Geosynthetics in Temperatures up to 40° C," *4th International Conference on Geotextiles, Geomembranes and Related Products*, The Hague, 1990, pp. 673-676.

Farrag, K., " Development of an Accelerated Creep Testing Procedure for Geosynthetics," in review, Geotechnical Testing Journal, ASTM.

Ferry, J.D., *Viscoelastic Properties of Polymers*, 3rd edition, John Wiley and Sons, 1955.

GRI-GG4 Standard Practice, *"Determination of the Long-Term Design Strength of Stiff Geogrids,"* Geosynthetics Research Institute, Drexel University, 1991.

Jewell, R.A., and Greenwood, J.H., "Long Term Strength and Safety in Steep Soil Slopes Reinforced by Polymer Materials," *Geotextiles and Geomembranes*, No.7, 1988, pp. 81-118.

McCrum, N.G., Buckley, C.P., and Bucknall, C.P., *"Principles of Polymer Engineering"*, 1988.

Müller-Rochholz, J., and Kirschner, R., "Creep of Geotextiles at Different Temperatures," *4th International Conference on Geotextiles, Geomembranes and Related Products*, The Hague, 1990, pp. 657-659.

Segrestin P. And Jailloux, J.M., " Temperature in Soils and its Effect on the Aging of Synthetic Materials", *Geotextiles and Geomembranes*, Vol. 7, 1988, pp. 51-69.

Shelton, W.S., and Bright, D.G., "Using the Arrhenius Equation and Rate Expressions to Predict the Long-Term Behavior of Geosynthetics Polymers," *Geosynthetics'93*, Vancouver, Canada, 1993, pp. 789-802.

Sherby, O.D., and Dorn , J.E., "Anelastic creep of Polymethyl Methacrylate", *Journal of Mechanics and Physics of Solids*, Vol. 6, 1958, pp. 145-162.

APPROACHES FOR THE PREDICTION OF LONG TERM VISCOELASTIC PROPERTIES OF GEOSYNTHETICS FROM SHORT TERM TESTS

J.S. THORNTON
TRI/ENVIRONMENTAL, INC.
S.R. ALLEN
TRI/ENVIRONMENTAL, INC.
R.W. THOMAS
TRI/ENVIRONMENTAL, INC.

ABSTRACT

Long term creep tests are often specified to predict the behavior of geogrids in reinforcement applications. These tests are expensive and are usually run for at least one year. This makes it difficult to test multiple replicates or to evaluate new and/or experimental products. Therefore, it would be desirable to make accurate long term predictions of viscoelastic behavior from the results of short term tests.

This internally funded research project was developed to explore different ways to speed up the prediction process. First, time-temperature superposition principles were used to shift wide-width creep results generated at $33°C$ to room temperature. This extended the creep curve from 8 months of actual data to more than 3 years of predicted results. Secondly, short-term creep and stress relaxation tests were performed on single ribs and these results compared to the longer term wide-width results. The results generated so far are encouraging, but limited. It does seem feasible, though, to produce a method for accurately predicting long term behavior from short term tests on well characterized materials like polyester geogrids. This method, while still under development, will rely heavily on time-temperature superposition and will probably involve short term tests on single rib specimens.

INTRODUCTION

The measurement and prediction of long term creep behavior of geosynthetics has been a required exercise during design for reinforcement applications. The traditional approach has involved determining tension creep behavior by applying a sustained load and measuring the total elongation of test specimens as a function of time while maintaining a specified temperature and humidity. A procedure has been developed for this approach and is now documented as ASTM D5262-92, *Standard Test Method for Evaluating the Unconfined Tension Creep Behavior of Geosynthetics.* The long-term nature of this test is burdensome. Most tests consume up to 10,000

hours requiring several dedicated test stations and a consistent, high quality environmental control system. This causes the test to be relatively expensive and inflexible. As materials change and alternative resins require investigation via comparison of creep properties, the requirement for long term testing precludes options in the context of fast-paced production schedules and limited financial resources.

The main objective of this project on the viscoelastic properties of geosynthetics is to reduce by an order of magnitude, or more, the amount of testing time needed to qualify a new geosynthetic product. Many new products are recombinations of well understood basic materials with viscoelastic properties that can be predicted with some accuracy. What is needed more than long term testing programs on a few replicates are more short term accelerated life tests on more statistically significant sample populations to provide design confidence intervals and to confirm or quantify long term trends. If this project is successful, burdensome testing costs to manufacturers can be relieved and artificial barriers to new product introductions can be lowered.

This paper represents a progress report on some of the initial efforts for this project. First, time-temperature superposition was used to generate longer term results more quickly from wide-width creep tests on flexible geogrids. Second, short-term creep and stress relaxation tests were performed on single ribs and the results compared to the wide width tests.

BACKGROUND

There are three important concepts that need to be understood in order to develop a reasonable approach for predicting long term behavior from short term tests. These are the principles of time-temperature superposition, the concept of power law behavior, and the distinctions between creep and stress relaxation. These concepts all may prove valuable during the pursuit of the stated project objective.

Time-Temperature Superposition. Polymer scientists have been using time-temperature superposition techniques for at least 4 decades to describe long term viscous or viscoelastic properties of polymers [see for example Ferry (1980)]. The fundamental notion is that elevating temperature accelerates the physical processes caused by mechanical load which result in various kinds of deformations of technological interest. The deformations we are interested in, such as creep strain, occur relatively rapidly when load is first applied, but the rate of increase decreases with time. Consequently, graphs produced with log time as the abscissa are indispensable for describing viscoelastic behavior. The precise way that increasing temperature accelerates these physical processes, or just how time dependent material response can be "shifted" along a log time scale has been studied extensively. An example of such a study on PETP will be introduced shortly. A temperature reduced time factor, a_T, relates the ratio of the time, t_T, for a viscoelastic process to proceed a given amount at an arbitrary temperature to the time t_R, for the same process at a reference temperature;

$$a_T = \frac{t_T}{t_R}$$ (1)

At temperatures greater than the reference temperature, a_T is less than 1. For this reason, some in the accelerated testing business refer to a_T, as an attenuation factor and A_T, defined as its reciprocal, as an acceleration factor.

According to the free volume theory [Ferry (1980)] the temperature dependence of a_T, is given by the well known Williams-Landell-Ferry (or simply WLF) equation. According to rate process theory [Krausz and Eyring (1975)] the temperature dependence of a_T, is given by an Arrhenius-type equation. The viscoelastic properties of many polymers obey WLF temperature dependence in the temperature range of the transition between glassy and rubbery behavior and Arrhenius temperature dependence at temperatures below the transition ranges. The purpose of these statements is not to confuse but to indicate that if one has some information about a polymer, well refined machinery exists to guide a disciplined effort to make long term predictions.

It's rather astonishing how far into the future viscoelastic properties have been predicted. As an example, Murayama et al (1968) examined stress relaxation of oriented PETP. Figure 1(A) displays the stress relaxation modulus as a function of log time at 14 temperatures from 22°C to 182° C. Note that the test time at each temperature is 10^4 seconds or about 3 hours. A reference temperature of 82° C was selected, and each of the modulus test segments were "shifted" horizontally along the time axis by an amount sufficient to obtain a smooth overlap of data at adjacent temperatures. The amount of horizontal shift for each of the non reference segments is by definition

$$\log a_{Ti} = \log t_{Ti} - \log t_R$$ (2)

where t_{Ti} is the time shift of the ith segment relative to, say, the fixed initial reference time of log t_R = 0 (1 sec). Figure 1(B) shows the time dependence of the relaxation modulus resulting form the superposition or shifting process and Figure 1(C) shows the temperature dependence of the attenuation factor a_T that defines the extent of each shift. The abscissa of Figure 1(B) ranges between 10^{-4} sec and slightly over 10^{16} sec for the reference temperature of 82°C. The uppermost time of 10^{16} sec is about 300 million years. This is quite a predictive accomplishment for fourteen 3 hour stress relaxation tests.

For most polymers, at low values of stress and strain (about 1% stress or strain or less) the isothermal viscoelastic response, or relationship between stress and strain depends only on time. Such a dependency is called linear viscoelastic behavior. At higher stresses, stress itself becomes an important factor and this complication is one element of non-linear viscoelastic behavior. Other complications in non-linear viscoelastic behavior include reversible effects of humidity. (Non

reversible effects of humidity and other chemical degradation processes are important considerations for accelerated life testing, but go beyond what we consider viscoelastic phenomena). Thus, in general, engineers interested in the viscoelastic properties of geosynthetic materials are faced with a rather complex situation where linear theory is helpful, but the governing relationships are empirical and yet to be discovered.

(A)

(B)

(C)
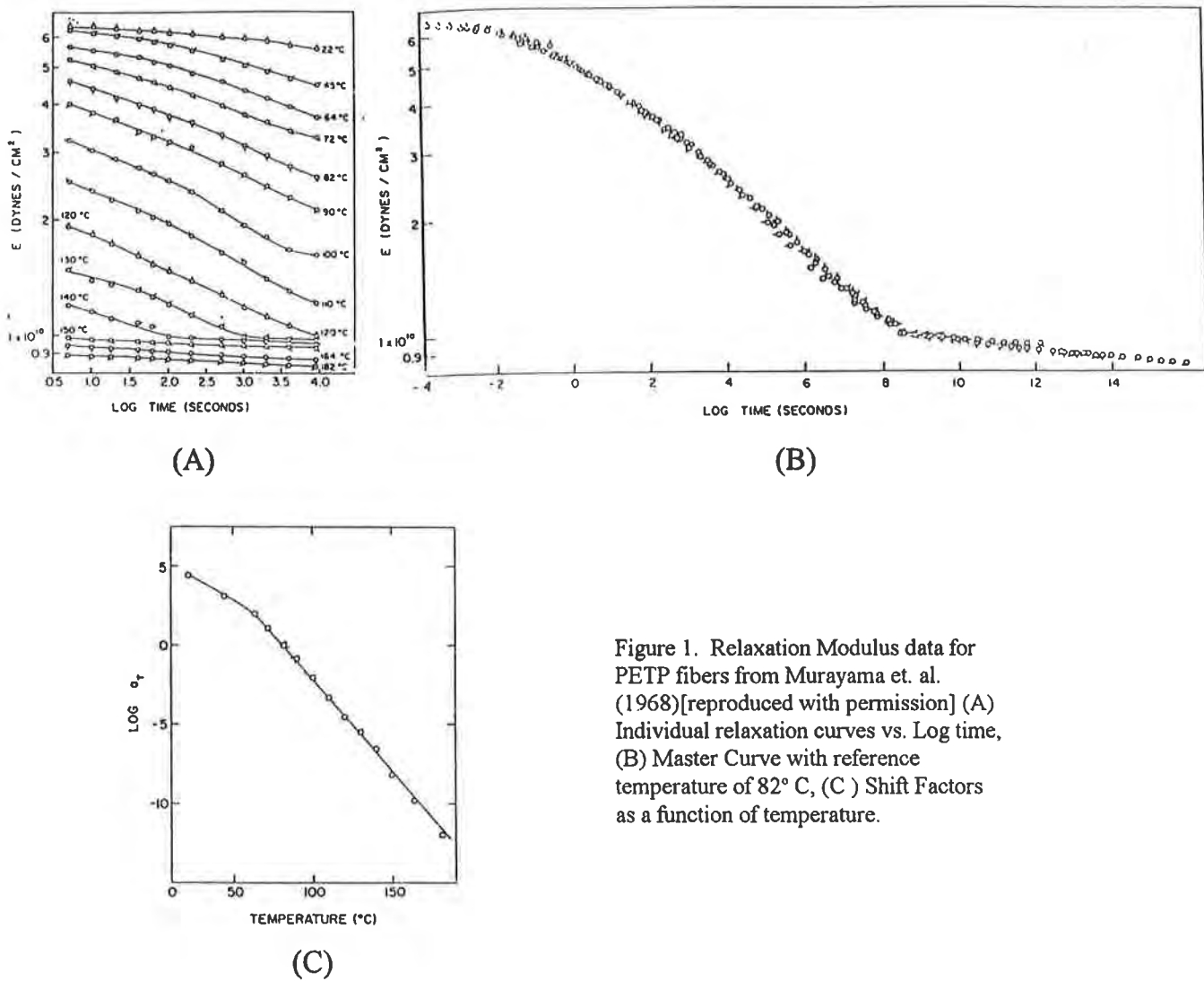
Figure 1. Relaxation Modulus data for PETP fibers from Murayama et. al. (1968)[reproduced with permission] (A) Individual relaxation curves vs. Log time, (B) Master Curve with reference temperature of 82° C, (C) Shift Factors as a function of temperature.

One interesting investigation of non-linear behavior of PETP films was by Titomanlio and Rizzo (1978) who measured stress relaxation and creep at loads above and below the yield stress and varied the ramp rate. The rates were varied over a 40 fold range. They found that all data obtained above the yield stress (at initial strains above about 1-2%) could be reduced to a single master curve by means of a simple time shift factor equal to the ratio of the ramp rate at a given rate to that for a reference rate. In contrast, linear viscoelastic theory states that within a factor of 3 to 10 of the ramp time, the creep or stress relaxation response of a polymer is independent of the ramp rate. These contrasting results suggest that the rate of strain application in the loading part of creep

experiments may be an important experimental consideration.

Power Law Materials. Referring to Figure 1B, there are two regions where the log of the relaxation modulus could be considered a linear function of log time. One is for nearly six orders of magnitude (between log time +2 and log time +8) and the other is for three orders of magnitude (between logtime -1 and log time +2). This leads to the form:

$$E_r(t)=E_o t^{-n} \tag{3}$$

where $E_r(t)$ is the relaxation modulus, E_o is a constant, t is time and -n is the slope of the relaxation curve (in log-log space) in the region of interest. This kind of behavior is exhibited by many materials that we call power law materials. Linear functions in log-log space are of great utility when, for example, we want to estimate behavior at times beyond our access to experimental data (e.g. 10 year predictions). Obviously, using the E_o and n in the -1 to +2 log time regime vs. the E_o and n for the +2 to +8 time regime would lead to serious differences in extrapolations to, say +9 log time. Thus, when doing log-linear extrapolations one needs considerably more than hope that the parameter of interest really follows a log-linear path. Regulatory agencies recognize this problem and usually limit extrapolations to one order of magnitude along a log time axis. This practice can be overly conservative in the many cases where supplementary historical data exists, such as the case for polyester fibers (e.g. Figure 1B). Since power law materials do not necessarily rigorously follow linear paths in log-log or semi-log space, we prefer "dead reckoning" extrapolations to ones based on linear regression analysis of all the data. Dead reckoning extrapolations emphasize the most recent decade of data to establish the most likely slope of future parameter movement.

The utility of the power law can be extended to obtain a reasonable representation over the time scale between glassy behavior and equilibrium behavior using the following broad band approximation:

$$E_r(t)=E_e+\frac{E_g-E_e}{(1+t/\tau)^n} \tag{4}$$

where E_e is the equilibrium relaxation modulus, E_g, is the glassy relaxation modulus, and τ is a characteristic relaxation time. We use non-linear regression analysis and obtain good fits to this equation for computer selected values for the four unknowns. This equation is useful to sense the onset of equilibrium from the shape of experimental relaxation curves, and we refer to it as the "equilibrium model." The equation is derived from a chi-squared distribution of relaxation times and is specific to a stress relaxation modulus. A simple form such as (4) has not been derived for the creep compliance, however we have found that (4) can be fit to creep modulus data just as well as relaxation data.

Stress Relaxation vs. Creep. Stress strain curves for rapid loading and equilibrium loading conditions are given in Figure 2. This is basically the difference between a dynamic tensile test and

a test where the strain rate was infinitesimally small. Two special paths from the rapid loading curve to the equilibrium curve are the horizontal one (constant stress, strain increases with time) for creep, and the vertical one (constant strain, stress decreases with time) for stress relaxation. We note that there are an infinite number of other paths between the two curves that are not restricted to constant stress or constant strain. Real engineering applications rarely provide constant stress or constant strain conditions, but the theories of linear viscoelasticity consider only the two special paths.
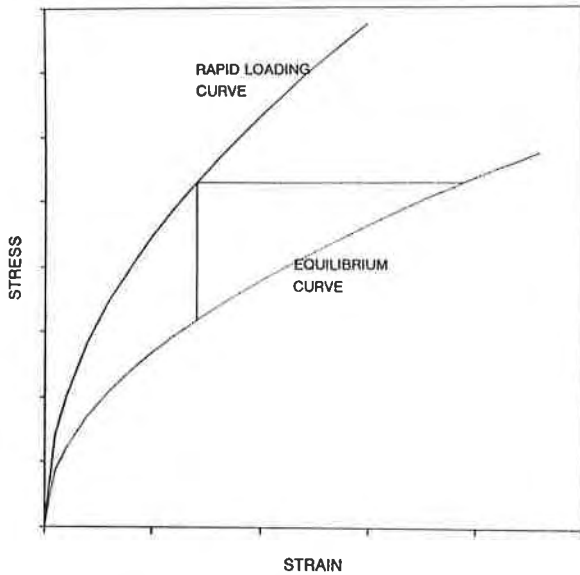
Figure 2. Rapid loading and equilibrium stress-strain curves showing the horizontal creep path and the vertical relaxation path to equilibrium.

For linear viscoelastic materials, there are exact relationships between creep compliance D(t) (or its reciprocal creep modulus, E_c (t)), defined as

$$D(t) = \frac{\epsilon(t)}{\sigma} = \frac{1}{E_c(t)} \qquad (5)$$

where $\epsilon(t)$ is time dependent strain and σ is constant stress, and stress relaxation modulus, defined as

$$E_r(t) = \frac{\sigma(t)}{\epsilon} \qquad (6)$$

where σ (t) is time dependent stress and ϵ is constant strain. The creep modulus and the relaxation modulus are not equal except under conditions where time dependent behavior is not an issue. Figure 3 displays the time dependence of the two moduli and illustrates their relative positions in the case of linear viscoelastic behavior. Thor Smith (1963) proved that for linear viscoelastic materials, the relaxation modulus was always less than the creep modulus in the transition region between glassy and rubbery (or equilibrium) behavior. He also proved that to achieve a given pair of stress-strain values, say σ^*, ϵ^* that a relaxation path starting at a fixed ϵ^* and a $\sigma > \sigma^*$ was faster than a path starting at σ^* and a $\epsilon < \epsilon^*$.

The relationship between E_r (t) and E_c (t) for a linear viscoelastic power law material can be shown to be [Williams (1980)]:

$$E_r(t) = \frac{\sin n\pi}{n\pi} E_c(t) \qquad (7)$$

where n, again is the power law exponent. Figure 4 shows a plot of this expression for three values of n with E_c @ t = 1 taken as unity. The vertical displacement between the two sets of curves is simply sin nπ/nπ. The horizontal displacement in decades can be shown to be log [sin nπ/nπ.]/n.

Table 1 gives values for the horizontal shift for the three values of n of Figure 4.
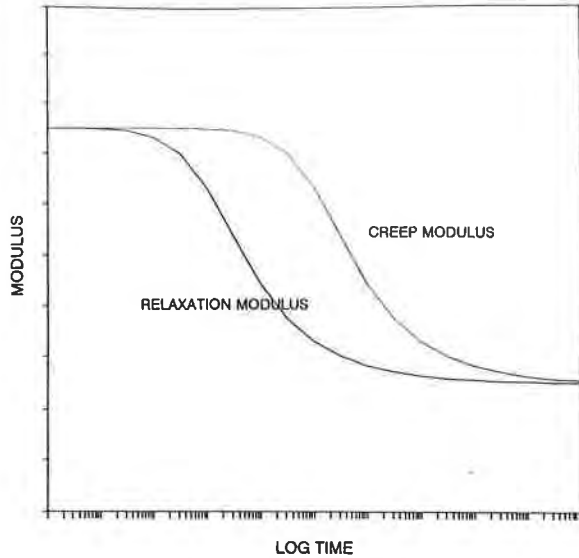
Figure 3. A comparison of the creep modulus and the relaxation modulus vs. log time for a linear viscoelastic material
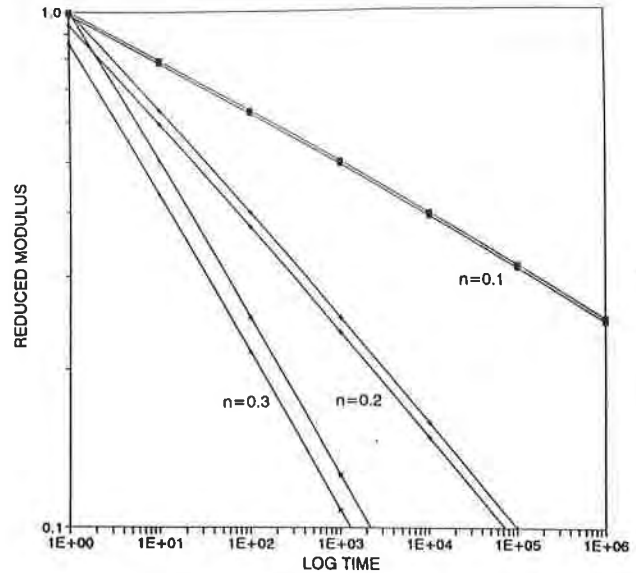
Figure 4. A comparison of the creep modulus (upper curve in each set) and the relaxation modulus (lower curve in each set) as a function of log time for a power law material and three values of the power law exponent

Table 1. Time Shift for Stress Relaxation
vs. Creep for a Power Law Material

n	log A (decades)	A (acceleration factor)
0.1	0.700	1.175
0.2	0.146	1.400
0.3	0.222	1.667

We have concluded that for a linear viscoelastic material the onset of equilibrium will be sensed sooner along a stress relaxation path than a creep path. We suspect that this is true as well for non linear materials and this is an active study area for us. This is an important concept because it suggests that more information can be generated from a stress relaxation experiment compared to a creep experiment over the same period of time.

EXPERIMENTAL

The material tested during this project was a medium strength (65 kN/m break strength) PVC coated polyester geogrid. The wide width ultimate tensile strength (UTL) of the grid was established by tests in accordance with ASTM D4595 using 10 cm diameter capstan grips.

The other tests performed included long term wide-width creep tests and short term single rib creep or stress relaxation tests. The long term wide-width creep tests were done in accordance with ASTM D5262-92 using 200 mm gage lengths and 400 mm spacing between grips at 21°C and 33°C and at 20% and 40% of UTL using bolted tapered grips. Slippage in the grips was not a problem at those load levels. Single rib specimens were tested at 33°C and at 20% and 40% of UTL in accordance with our standard laboratory practice.

For the wide-width creep tests, multi-station rigid lever action creep frames were designed and fabricated to provide a 10:1 mechanical advantage in the loading train. Ample space was provided to construct temperature controlled chambers around the test specimens. To achieve a temperature control of ± 0.2°C, which we considered necessary for this work (ASTM D5262-1992 calls for ± 2°C) we placed the creep frames and their environmental chambers in an isolated room that was controlled to 19 ± 1°C by cooling. Fine control to 21°C ± 0.2°C or 33°C ± 0.2°C was achieved by heating in the environmental enclosures. Since "room temperature" in Texas varies between 23 - 25°C, higher in the summer, it was not feasible to maintain either the mechanical testing lab at 21°C or to cool the chambers to 21°C and maintain low humidity therein.

Instron tests of creep and stress relaxation on single rib specimens using pneumatic grips were facilitated by the 4500 Advanced Function Panel of a Model 4505 Instron Testing Machine. A constant temperature of 33°C ± 1.0°C was provided by an Environmental Chamber.

Rates of loading in the creep frames were typically 30 to 45 seconds to peak load and in the Instron machine 4 to 6 seconds to peak load, an average ramp rate ratio of about 8. Creep strain was monitored manually for the creep tests in the frames using dial indicators magnetically attached to cross bars clamped to the samples to define the gage lengths. Creep strain output for the creep tests and feed back for strain control of the stress relaxation tests was provided by a clip-on extensometer with a 5 cm gage length. Load control for the creep tests and load monitoring for the relaxation tests was provided by a 10 kN capacity load cell from Instron.

RESULTS AND DISCUSSION

Long Term Creep Testing. Creep curves for four wide width samples are shown in Figure 5. The two samples labeled M20 and M40 were the first to be loaded in the creep frames at 21°C and at 20% and 40% respectively of the ultimate tensile load (UTL) for this lot of material. The other two samples labeled M20-NS and M40-NS were placed on test several months later in order to confirm the results being generated by the original samples. As of this writing, the M20 and M40 samples are still under test, but the 21°C portions of the M20-NS and M40-NS samples are complete as shown. Linear regression analyses using all of the M20 and M40 data was used to provide one of the extrapolations of the M20 and M40 curves to 10^6 hours (114 yrs). The other extrapolations, labeled "Dead Reckoning" also utilize linear regression analysis, but only on the last log time cycle of data. By the nature of the log time scale, 90% of the time under test is always in the last cycle of data. As readily observed, the dead reckoning extrapolations provide slightly lower estimates of

strain at 10^6 hours because dead reckoning begins to account for the tendency of the test samples to depart from semi log linear behavior as they approach equilibrium.

Two creep curves generated in creep frames at 33°C are plotted along with the previous 21°C data in Figure 6. The new curves are labeled M20-33C and M40-33C for the 20% and 40% UTL loads at this slightly elevated temperature. As this 33°C data was being generated we could see that time shifting of these data would not be possible without additional information, because they were falling within or below the 21°C data. Evidently, the two samples tested at 33°C are at the low end of the strain distribution for this lot of material. In order to obtain a direct estimate of the relative positions of 33°C and 21°C creep curves, we decided to change the temperature of the M20-NS and M40-NS samples, which were still under test at that time, from 21°C to 33°C. Figure 7A, which has two scales (left for the 20% UTL data and right for the 40% UTL data) shows the effects of this temperature change, and shows the relative positions of the curves for the M20-33 C and M40-33 C samples.
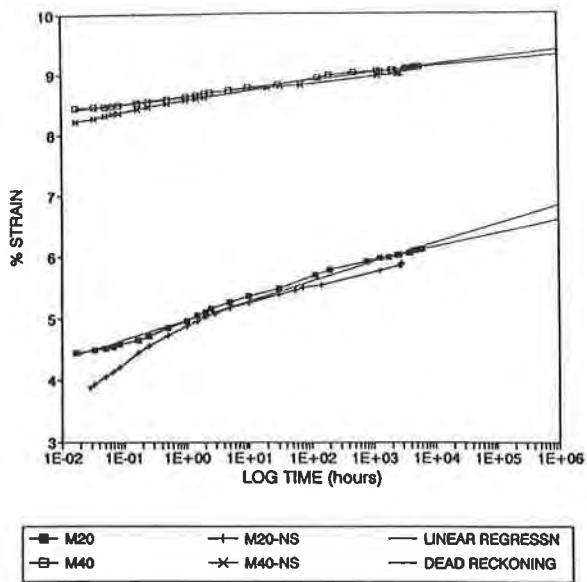
Figure 5. ASTM D5262 creep test results for medium strength geogrid samples at 20% (lower data set) and 40% (upper data set) of UTL at 21°C
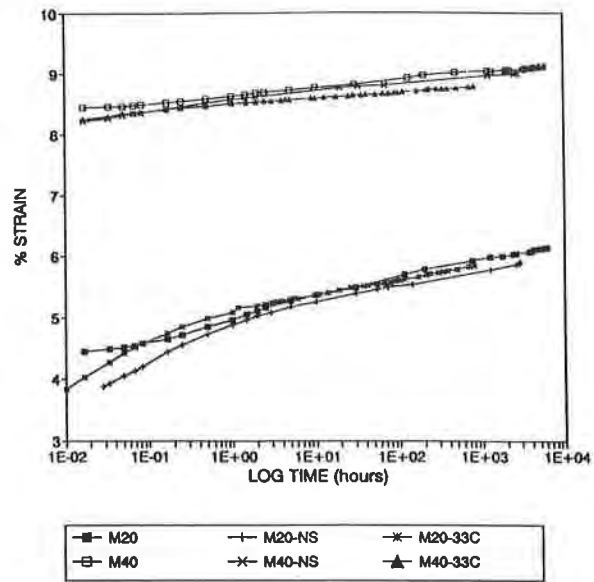
Figure 6. The results in Figure 5 plus creep test results at 33°C (note change of scale for the abscissa)

The process of rescaling and shifting the new 33°C data and the shifting of the prior 33°C data is illustrated in Figures 7B, 7C and 7D. The first step is rescaling, the result of which is shown in Figure 7B. Time, t', is subtracted (iteratively) from the original test time, t, accumulated on the M20-NS and M40-NS samples (beginning at 21°C) until the rescaled 33°C data are linear in semi-log space.

The rescaled data are nearly parallel to the prior 21°C and 33°C data, which confirms the validity of this approach. The break in the upper curves for the M40 -NS sample was due to an

interruption of that test caused by experimental difficulties. The second segment of the rescaled part is approximately parallel to the first segment, but not colinear. This is thought to be because the effective load had become very slightly higher.
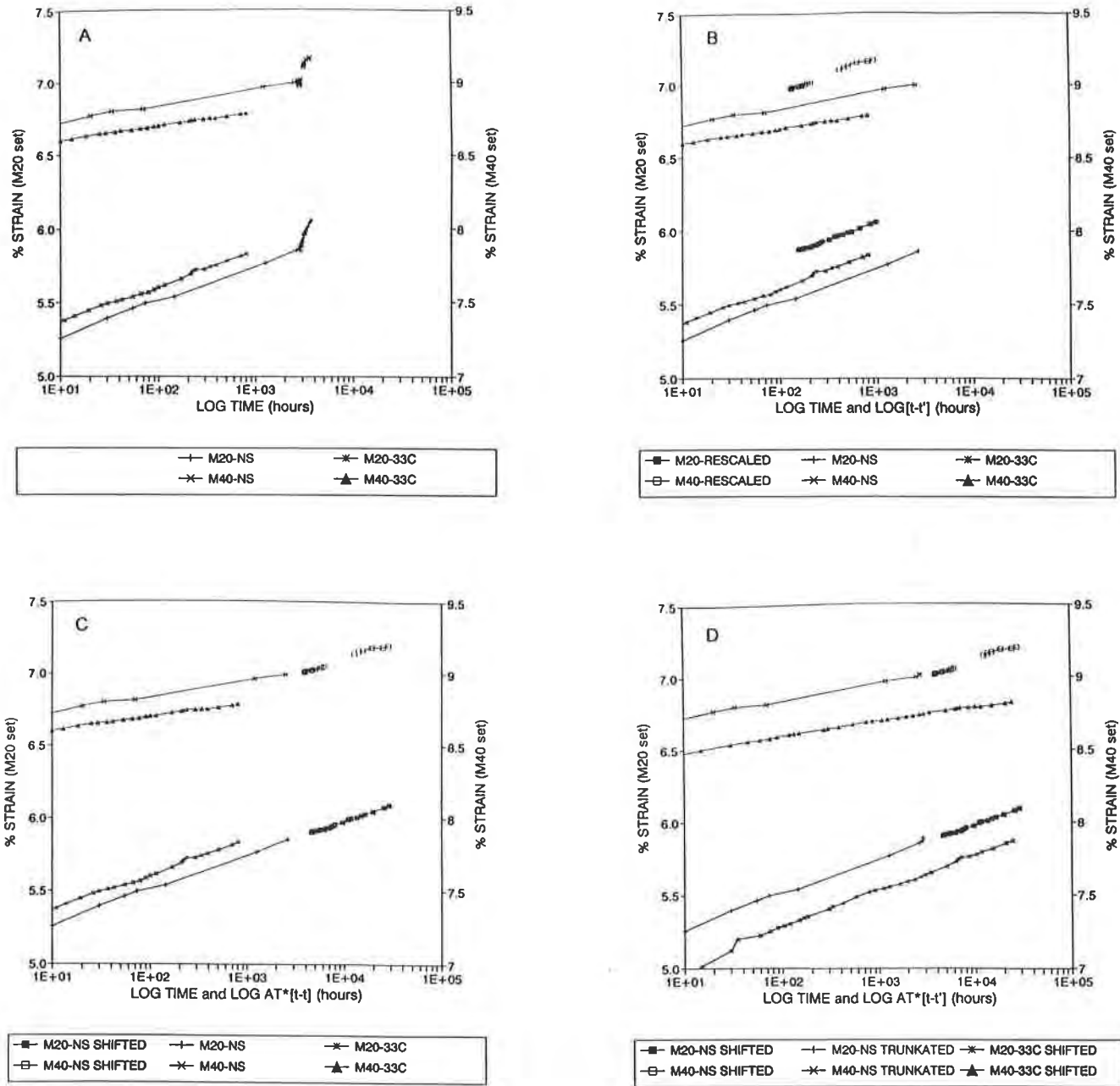
Figure 7. Creep Strain test data at 20% (scale left) and 40% (scale right) of UTL and 21° C and 33° C: (A) The temperature of samples M20-NS and M40-NS was changed to 33° C from 21° C at about 2500 hours causing abrupt change in slopes on the original or "old clock" time scale; (B) Rescaling the 33°C data by subtracting t' from each data point; (C) The rescaled data are shifted forward by a factor $A_T = 30$ to become colinear with the parent 21° C curves; (D) the curves for samples M20-33C and M40-33C are shifted forward by the same A_T factors as in C.

Next, as shown in Figure 7C, the rescaled data is shifted forward in log time by an amount log A_T (recognizing that log A_T * [t-t'] = log A_T + log [t-t']), until the shifted curves become colinear with the prior 21°C curves. In addition to the horizontal shift there is also a slight vertical shift applied to the rescaled data to account for a small net negative coefficient of thermal expansion of the specimen and measurement fixtures. Finally, as shown in Figure 7D the data for the M20-33C and M40-33C samples are shifted horizontally forward by the same log A_T established by the shift of the rescaled-NS data. Note that the shifted data now extend out to nearly 30,000 hours which is well over three years.

Figure 8 shows the data of Figure 7C combined with the data of Figure 5 with the addition of dead reckoning extrapolations of the shifted M20-33 C and M40-33 C curves. The combined data increase confidence in the slopes of the extrapolated curves and suggests that about a one-half percent strain uncertainty in extrapolated creep strain results may be expected.

Short Term Creep and Stress Relaxation Testing. Single rib results for M20 and M40 creep and stress relaxation as a function of log time in seconds are presented in Figures 9A through 9D. All the curves have similar appearances, but several features of these results are noteworthy:

- Triplicate samples were tested giving modulus spreads between 10 and 60 lb/rib/in, which is equivalent to 0.1 to 0.6% approximately strain spreads. With the exception of the relaxation curves for 20% UTL (Figure 9C), the spreads of the extrapolated results at 10^{10} sec are not significantly wider than the spreads of the data at 10^4 seconds.

- The creep modulus results are slightly more consistent than the stress relaxation results.

Figure 8. The data of 5 and 7C are combined to obtain this set of curves. The 33° C data having been shifted to 21° C extends the data range to over three years from about 8 months.

- The fit of the experimental data to the equilibrium modulus model is excellent. The RMS deviation per degree of fitting freedom ranged between 0.26 and 0.86 in the units of modulus (lb/rib/in/in). This is better than 0.1%.

- The extrapolated results at 10^{10} seconds are approaching, but have not yet achieved equilibrium.

- There is not a significant difference between results obtained in 3 hours and 24 hours.
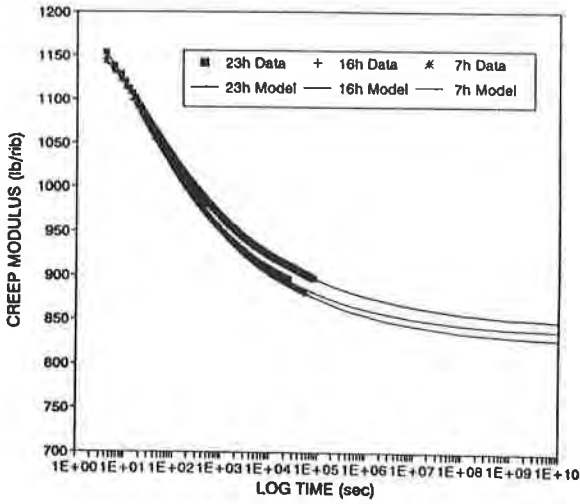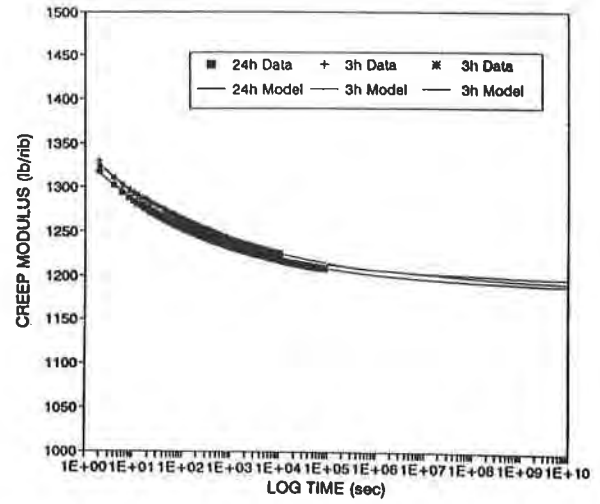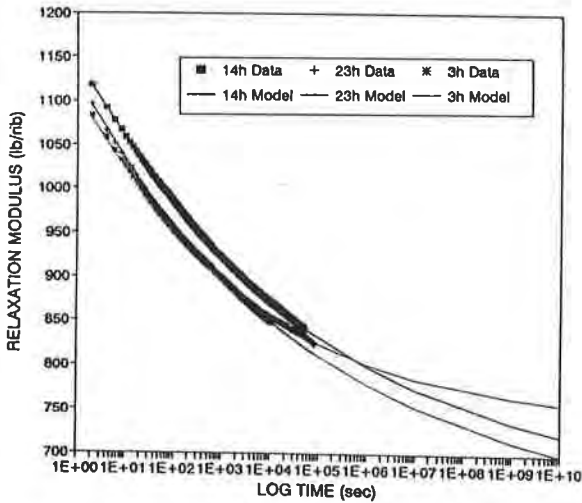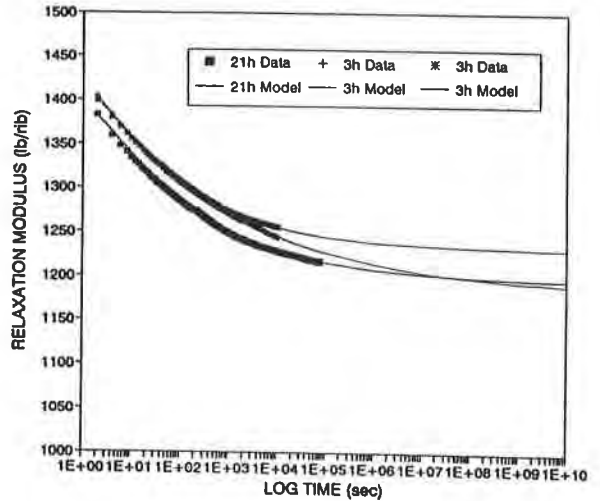
Figure 9. Single rib creep and relaxation test results at 33° fit to the equilibrium model: (A) Creep at 20% of UTL, (B) creep at 40% of UTL, (C) relaxation at 20% of UTL, (D) relaxation at 40% of UTL.

Stress Relaxation vs. Creep. Earlier we stated that for linear viscoelastic power law materials it is readily shown that for the same time, the stress relaxation modulus is always lower than the creep modulus. Here, we test the current short term results for the medium strength geogrid and find for the most part, the same answer. Because of the excellent fits of the data to the model curves, we felt there would not be a loss in generality by comparing the averages of the model fits instead of the averages of the data, and the former was easier to do. To facilitate the comparison, we

normalized the relaxation curves to the creep curves at one second. The results of this comparison are shown in Figure 10, and we see that indeed, the relaxation modulus is less than the creep modulus for all times. However, because of the shape of the 20% UTL creep curve at times less than 1000 seconds, a selection of normalization time between, say 10 and 100 seconds would have created a double cross over that would not have corrected itself until, say 10^4 to 10^5 seconds. Nevertheless, again for the most part we can conclude that for this non-linear material, the relaxation modulus is less than the creep modulus as a function of time.
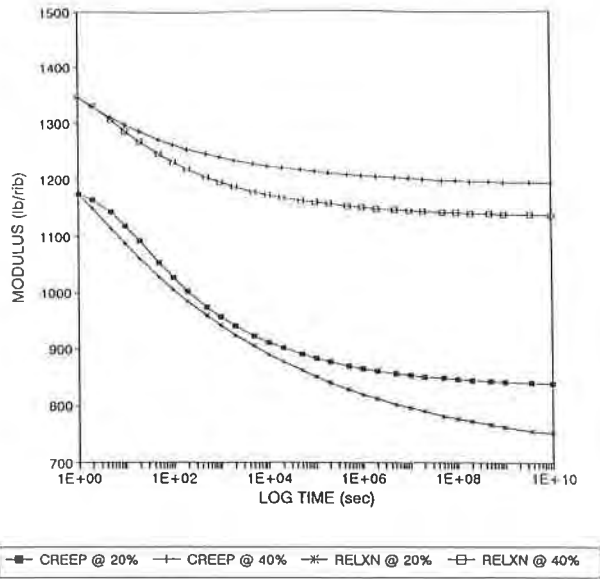
Figure 10. Creep and relaxation modulus equilibrium models at 20% and 40% of UTL and at 33° C and for 10 orders of magnitude in time. The relaxation modulus has been normalized to the creep modulus at 1 second.
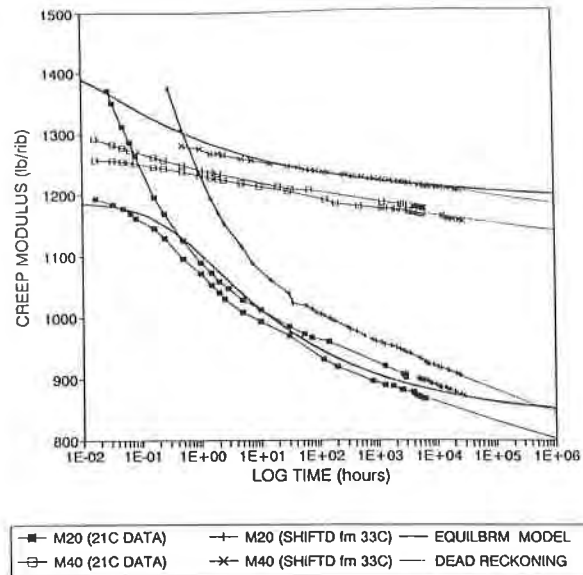
Figure 11. The data of Figure 8 expressed as creep modulus combined with shifted versions of the creep modulus models of Figure 10. The creep modulus models have been shifted to 21° C from 33° C, shifted for ramp rate, and the log time scale changed to hours from seconds.

Summary of Results. The 21°C and shifted 33°C creep strain results presented in Figure 8 are restated as creep modulus results and combined with the shifted 33°C average creep modulus model results of Figure 10 to give the presentation of Figure 11. Additionally, an acceleration factor for effect of ramp rate, A_R, was applied to the temperature shifted creep model curves utilizing the approach taught by Titomentio and Rizzo (1977). This second shift (@ A_R = 8), if really applicable, extends to nearly 6000 hours the shifted test times for the model results. Despite the vast differences in the testing protocols, the results are quite consistent. Probably as a consequence of the shorter test times used to construct the model curves, they display more curvature than the longer term creep results generated in the creep frames. Whether or not the ramp rate shift is applied, the 10^6 hour creep modulus estimates are not significantly affected. The extrapolated results from all the tests described are summarized in Table 2.

CONCLUSIONS AND FUTURE WORK

As a progress report on our efforts to improve methods for estimating long term viscoelastic properties of geosynthetic products, our conclusions are somewhat tentative. However, the following observations were made:

- Excellent temperature control (±0.1°C) is readily obtainable by the described method and we believe such control is essential to reduce variability of creep results.

- Single rib data appear indistinguishable from wide width results. This was expected because of decoupling of transverse from longitudinal modes of deformation in geogrids.

- There were little difference in the results of short term tests run in the Instron for 3 vs. 24 hours. Three hours appears sufficient to represent the time dependence of the moduli at 33°C.

- The controlled rapid loading available in Instron tests uncovers early time viscoelastic property data that is hidden by the slower loading process in traditional creep tests.

This paper represents the first output in a series of projects to develop accelerated test methods for determining the long term response and rupture properties of geosynthetic materials. The next efforts, currently underway, expand the use of the stepped isothermal method to include multiple temperature steps and higher loads to obtain creep-to-rupture data for several PET based geogrids. These efforts also include the generation of long term results for comparison with the accelerated test results.

REFERENCES

Ferry, J. D., (1980), Viscoelastic Properties of Polymers, 3rd Edition, John Wiley and Sons, N.Y.

Krausz, A. S. And Eyring, H., (1975), Deformation Kinetics, John Wiley and Sons, Inc., New York.

Murayama, T., Dumbleton, J. H., and Williams, M. L., (1968), "Viscoelasticity of Oriented Polyethylene Terephthalate," J. Appl. Polymer Sci., Vol. 6, pp 787-793.

Smith, T. L., (1963), "Ultimate Tensile Properties of Elastomers. I. Characterization by a Time and Temperature Independent Failure Envelope," J. Polymer Science: Part A, Vol. 1, pp 3597-3615.

Titomanlio, G., And Rizzo, G., (1977), "Master Curves of Viscoelastic Behavior in the Plastic Region of a Solid Polymer," J. Appl. Polymer Sci., Vol. 21, pp 2933-2941.

Williams, J. G., (1980), Stress Analysis of Polymers, 2nd Edition, Ellis Harwood Limited, Chinchester, England, pp 117-119.

Table 2. Extrapolated Values for Creep Strain, Creep Modulus
and Relaxation Modulus at 10^6 hours (3.6×10^9 seconds)

Parameter	Figure Nos.	Temp. (°C)	Specimen	Shifts	Extrapolation Type	Initial Load (% UTL)	Est. Strain (%)	Est. Modulus (lb/rib)
creep strain	1,4	21	M20 M20 M40 M40		linear regression dead reckoning linear regression dead reckoning	20 20 40 40	6.86 6.62 9.40 9.31	
creep strain	4	21	M20-33C M40-33C	from 33C	dead reckoning dead reckoning	20 40	6.29 8.97	
creep modulus	5	33	single rib 23 h 16 h 7 h		equilibrium model	20		851 829 838
creep modulus	6	33	single rib 24 h 3 h 7 h		equilibrium model	40		1190 1198 1194
relaxation modulus	7	33	single rib 14 h 23 h 3 h		equilibrium model	20		728 760 706
relaxation modulus	8	33	single rib 21 h 3 h 3 h		equilibrium model	40		1197 1193 1232
creep modulus	9	33	avg		equilibrium model	20 40		840 1194
relaxation modulus	9	33	avg		equilibrium model	20 40		755 1137
creep modulus	11	21	avg	from 33C ramp rate	equilibrium model	20 40		852 1200
creep modulus	11	21	M20 M40 M20-33 M40-33	from 33C	dead reckoning	20 40 20 40		843 1184 802 1140

Student papers

GEOSYNTHETICS 97

CONFERENCE

Long Beach, California USA

Migration of a contaminant through three landfill liner scenarios designs.

Fabienne C. Montgrain, ing. stag.
Département de génie civil, Université de Sherbroooke, Qué., Canada J1K 2R1

Abstract

This paper presents the results of an evaluation of three landfill liner designs proposed by the Ministry of Environment of Quebec for a new provincial solid waste regulation. The evaluation of the barrier designs was accomplished by studying the migration of Cl$^-$ with consideration of advective and diffusive processes. The computer models Pollute v6 and Migrate v9 were used. The basic soil parameters entered in the models were obtained in the laboratory. The three liners configurations considered are: (1) 6.0 meters of natural clay (K < 10^{-6} cm/s); (2) 3.0 meters of natural clay overlain by 1.2 meters of compacted clay; and 3) 3 meters of natural clay overlain by a composite liner consisting of a 1.5 mm (60 mils) HDPE geomembrane over 0.60 meters of compacted clay. The soil used in the laboratory studies is a non remolded clay typical of the formations found in the lowlands of the St-Lawrence valley (Champlain clays). The results show that the advance of the contamination front across the three different barrier designs depend on : (1) the efficiency of the leachate collection system during the post-closure phase ; and (2) the quality of the final cover . All three scenarios can be very effective in preventing the contamination of the soil and groundwater underneath the barrier by Cl$^-$, provided that high efficiency rates of the LCS and a good quality cover can be maintained throughout the post-closure period. The scenario involving the installation of a composite cover is quite effective, irrespective of the qualtiy control exerted during installation.

Key words: liners, migration, geomembrane, clays.

MIGRATION OF A CONTAMINANT THROUGH THREE LANDFILL LINER SCENARIOS DESIGNS

1. INTRODUCTION

Quebec's municipal solid waste regulation was issued in 1978. During the 1980's it was modified several times until a new regulatory text, incorporating modern concepts was proposed for consultation in 1992. Although some revisions have been made since then, the consultation period has not yet been completed. One of the main characteristics of the 1978 text refers to the acceptance of the principle that the leachate can be attenuate by the soil in contact with the wastes. In its new regulatory text (MEF, 1994), the Ministry of the Environment and Fauna of Quebec (MEF) proposed several landfill liner scenarios involving relatively impermeable protection liners. The hydraulic conductivity of the liner is the principal parameter by which the quality of the barrier is evaluated. No reference to diffusion- dispersion processes is made, although these processes can be of major significance in the transport of contaminant (Rowe et al., 1985, Quigley, M. R., 1994).

The main goal of this study is to evaluate the scenarios proposed, including the consideration of dispersive-diffusive transport. For such, several contaminant transport simulations were done using a tracer, Cl⁻ , normally present in high concentrations in sanitary landfill leachates. The results of the simulations allowed for a preliminary and limited evaluation of the potential impact of leachate migration through the proposed barriers. They show that the scenarios involving geomembranes perform quite well for all the initial conditions proposed including the consideration of diffusive processes and poor quality control (holes, poor contact between the geomembrane and the underlying compacted barrier). Other barrier designs may lead to critical contaminant levels under certain circumstances.

2. BACKGROUND

The three main mechanisms of contaminant transport, are advection, molecular diffusion, and dispersion. In many applications, as is the case of leachate migration through landfill barriers, the movement of contaminants will be primarily in one-direction, and can be predicted using the one-dimensional dispersion-advection equation for a layered deposit (Rowe et al., 1985):

$$n\frac{\partial C}{\partial t} = nD\frac{\partial^2 C}{\partial z^2} - nV\frac{\partial C}{\partial z} - \rho Kd\frac{\partial C}{\partial t} - \lambda c \qquad (1)$$

where, C = concentration of contaminant at depth z at time t;
D = coefficient of hydrodynamic dispersion at depth z;
V = groundwater seepage at depth z;
n = porosity of the soil at depth z;
ρ = dry density of the soil at depth z;
Kd = distribution (sorption) coefficient at depth z;
$V_A = nV =$ Darcy velocity;

λ = decay constant of the contaminate species

Once the contamination reaches the aquifer under the liner, the problem becomes bidimensional. The equation modelling the seepage can be written according to equation 2 (Rowe et al., 1996):

$$n\frac{\partial C}{\partial t} = nD_{xx}\frac{\partial^2 C}{\partial x^2} + nDzz\frac{\partial^2 C}{\partial z^2} - nVx\frac{\partial C}{\partial x} - nVz\frac{\partial C}{\partial z} - \rho Kd\frac{\partial C}{\partial t} - n\lambda c \qquad (2)$$

where, Dxx = hydrodynamic dispersion coefficient in the x direction at depth z;
Dzz = hydrodynamic dispersion coefficient in the z direction at depth z;
V_x and V_z = groundwater (seepage) velocity in the x and z directions;
Note : $nV_x = V_{Ax}$ = Darcy velocity in x direction $nV_z = V_{Az}$ = Darcy velocity in the z direction

1-D simulations were done using the Pollute v6 program (Rowe and al., 1994). This model allows for the calculation of the concentrations of a contaminant at user specified times and depths. 2-D simulations were realized with Migrate v9 program (Rowe and al., 1995).

3. MATERIALS AND METHODS

3.1 Selection of the contaminant

All the simulations were done using chloride Cl⁻ as contaminant because it is an excellent tracer, i.e., it is a conservative species (negligible sorption coefficient) (Shakelford C. D.,1991). Consequently, it will not be withdrawn from the mass flux of contaminants as the leachate migrate through the barrier. Also, according to Valiron, F. et al. (1994), a Cl⁻ concentration in excess of 250 mg/L becomes more dangerous for health as organic compounds containing chloride are formed. Chloride concentrations in a domestic leachate may reach up to 1881 mg/L (Shoiry, J.,1995).

3.2 Selection of the soil used

All simulations were executed with a non remolded Ste-Adelphe clay typical of the formations found in the lowlands of the St-Lawrence valley (Champlain clays).   This clay has a hydraulic conductivity in the order of 1×10^{-6} to 1×10^{-7} cm/s (unpublished results). Its characterization, made in the geoenvironment laboratory of the University of Sherbrooke, includes the determination of some parameters essential to model the contamination process, such as the diffusion coefficient of the Cl⁻. The value of $1,0$ cm²/ day obtained is in agreement with the results published in the technical literature for silty clays (Shakelford, 1991). The properties of the Ste-Adelphe clay are shown in table 1.

4. SIMULATIONS

The determination of Cl⁻ concentration was made for different depths underneath a typical landfill site occupying an area of 1 ha (330 m X 300 m) with side slopes of 1:2.5. All the simulations presented here take into account the scenarios proposed in the consultation document issued by the MEF (MEF, 1994). The first set of simulations evaluates the design whereby the landfill is built directly upon a 6.0 m thick natural soil. The second set studies the profile where one protection layer consisting of 1.2 m of compacted soil having a hydraulic conductivity, $K < 1 \times 10^{-7}$ cm/s is placed upon 3.0 m of natural soil having $K < 1 \times 10^{-6}$ cm/s. The last set evaluates the scenario where one protection layer is placed upon 3.0 m of natural soil ($K < 1 \times 10^{-6}$ cm/s). The protection layer consists of a 1.5 mm (60 mils) HDPE geomembrane laid upon 0.6 m of compacted soil having $K < 1 \times 10^{-7}$ cm/s . In all cases, the concentrations at the interface between the liner and the aquifer underneath were obtained.

Specific gravity	2.80
Dry density (g/cm^3)	1.01
Moisture content (%)	65.0
Saturation (%)	91
Soil porosity	0.67
pH	~ 7.00
Silt content (< 74 μm) (%)	34
Clay content (< 2μm) (%)	55
Mineralogy (non quantitative, in order of importance): Illite ; Chlorites ; Albite calcian, Anorthite, Microcline (Feldspar group) ; Hornblende (Amphibole) ; Quartz.	
Dissolved species (mg/L) Cl⁻ Na$^+$ K$^+$ Ca^{2+} Mg^{2+}	17.5 96.9 28.2 28.9 17.8
Exchangeable cations (meq/ 100 g dry wt.) Na$^+$ K$^+$ Ca^{2+} Mg^{2+}	1.29 2.04 8.56 5.89
Specific surface area (m^2/g)	68
Cation exchange capacity (meq/ 100g dry wt.)	17.77

Table 1. Properties of the Ste-Adelphe clay

5. BASIC HYPOTHESES

The simulations respect all the requirements of a functional leachate collection system (LCS). It is considered that an efficient rate of the LCS ranges from 100% to 80%. The advective flux is handled by the computer model by means of input data, such as the Darcy velocity, the amount of infiltration and the volume of leachate collected. The diffusion coefficient is given as input data.

It is assumed that the landfill is filled to capacity and that the final cover respects all the requirements described in the proposed regulation. Infiltration rates observed in certain landfills presently in operation in Québec range from 15% to 30% of the total annual precipitation (Théberge J., 1996). It was admitted an average infiltration rate of 20%, corresponding to a medium to poor cover.

It is also assumed that the concentration of Cl⁻ in the leachate decreases with time , as a result of waste degradation and infiltration. The initial source concentration was set to 1000 mg/L, corresponding to approximately the average of the normal interval of concentrations found in typical landfill leachates. It was also considered that Cl⁻ constitutes 0.2% of the total waste mass.

The simulations always considered the presence of a 3.0 m thick of aquifer underneath the liner. It was then assumed that there is sufficient dispersion/ mixing such that the concentration is uniform across the thickness of the aquifer.

All simulations were performed using a diffusion coefficient of chloride (D_{Cl^-}) which was obtained from single salt diffusion tests. It is acknowledged that the diffusion coefficient of chloride may vary in the presence of other compounds. Barone et al. (1988) found lower values of D_{Cl^-} for municipal solid waste leachate than for single salt solutions.

6. RESULTS

6.1 Simulations with scenario I landfill barriers

According to this scenario, solid wastes must be landfilled on land where a minimum of 6 meters of an homogeneous soil with a hydraulic conductivity equal or inferior to $1x10^{-6}$ cm/s can be found. A schematic of this scenario is presented in Figure 1.
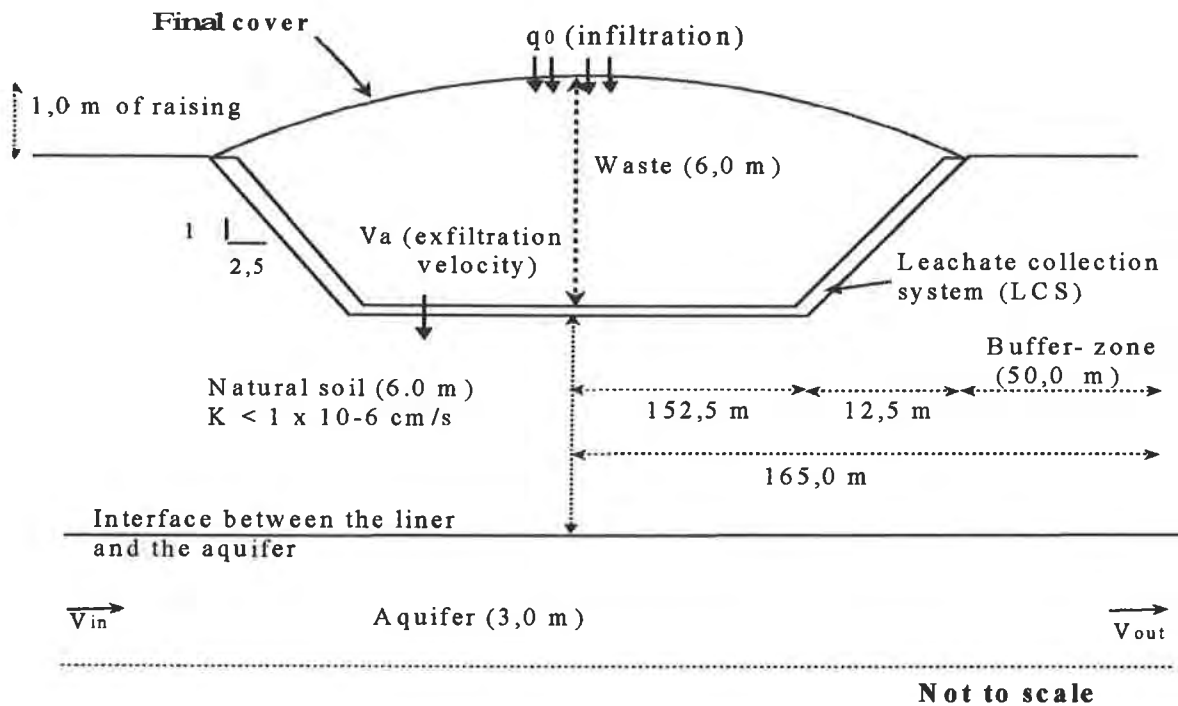
Figure 1. Schematic of a scenario I landfill

The objective here is to verify the efficiency of the clay liner against contaminant migration due to an accumulation of leachate (hydraulic gradient) and to a concentration gradient that induces molecular diffusion. The parameters commonly used for all the first set of simulations are summarized in Table 2.

PROPERTIES	VALUE	UNITS
Diffusion coefficient of Cl⁻, D_{cl-}	0.036	m^2/a
Distribution coefficient of Cl⁻, K_d	0.0	cm^3/g
Soil porosity, n	0.67	----
Dry density, ρs	1.01	g/cm^3
Natural barrier thickness, H	6.0	m
Source concentration, Co	1000	mg/L
Landfill length, L	300	m
Landfill width, W	330	m
Aquifer thickness, h	3.0	m
Aquifer porosity, n_b	0.30	----
Time of interest, t (from the closure of the landfill)	1,5,10,20,30,60 et 100	a

Table 2. Input parameters for the simulations with scenario 1 landfill barriers

6.1.1 Influence of the efficiency rate of the LCS

The chloride concentrations at 6.0 m down into the barrier at the interface between the liner and the aquifer are presented in Table 3. In these simulations, the upstream seepage velocity, v_{in} was set to 5 m/a, corresponding to a regional gradient of 0.05 and an aquifer having a hydraulic conductivity of approximately 1×10^{-3} cm/s, typical of gravelly soils of Québec (Landry, 1992). The results show that the concentration of Cl⁻ for all efficiency rates are below the 250 mg/L limit. The infiltration rate was set at 0.3 m/a, which corresponds to a poor cover system.

Depth	Efficiency rate of leachate collection system				
	100%	93%	90%	88%	80%
6.0 m	17.6 mg/L	41.3 mg/L	77.3 mg/L	101.6 mg/L	156.9 mg/L

Table 3. Concentration of Cl⁻ at the interface liner/ aquifer at the center of the site (t = 100 years)

6.1.2 Influence of the final cover quality

The quality of the cover has a direct influence on the production of leachate. In order to verify the influence of the infiltration rate, some simulations were done by varying it from 0.1 m/a to 0.3 m/a (poor cover). The efficiency rate of the L.C.S was set at 80%. Table 4 shows the chloride concentration at 5 and 6 meters in the barrier for various infiltration rates after 60 years of closure.

Depth in the liner (m)	Infiltration rate through the final cover			
	0.1 m/a	0.17 m/a	0.2 m/a	0.3 m/a
5.0	77.5	172.1	221.9	358.0
6.0	13.4	40.0	58.7	148.0

Table 4 - Concentrations of Cl⁻ (in mg/L) as a function of the quality of the final cover (t = 60 years)

The values in Table 4 shows that in the lower portion of the liner, the risk of contamination for a poor cover is relatively high. At 5 meters of depth, the chloride concentration is greater than the limit of 250 mg/L. In the hypothesis that a liner design corresponding to Figure 1 is accepted by the legislator, a good quality control (in this case a thorough hydrogeologic investigation) must then be exerted in order to ensure that the minimum thickness of 6.0 m actually exists throughout the landfill area.

6.1.3 Influence of the magnitude of the source concentration

In order to evaluate the influence of the source concentration on the contamination levels at the bottom of the barrier, another set of simulations was performed. There is strong evidence that higher concentrations than 1000 mg/L used in the simulations can be found in municipal solid waste leachate. The results are summarized in Table 5. They show that even if the source concentration is doubled, the

risk of contamination remains low, for a liner design involving a minimum of 6.0 m of natural soil ($K<1\times10^{-6}$ cm/s).

Depth	Source concentration of Cl⁻		
	1000 mg/L	1500 mg/L	2000 mg/L
6 m	6.2 mg/L	7.3 mg/L	7.9 mg/L

Table 5. Chloride concentration as a function of its source concentration at the interface between the liner and the aquifer (t = 100 years; LCS at 100% efficiency)

6.2 Simulations with scenario II landfill barriers

If a minimal thickness of a 6.0 meters of undisturbed soil with a hydraulic conductivity inferior or equal to 1×10^{-6} cm/s is not available, a supplementary level of protection is required. The supplementary level of protection must be placed on the bottom and along the walls of the landfill. This level of protection may be built following the two scenarios (a and b) presented below.

6.2.1 Simulations with scenario design II a landfill barriers

If at least 3.0 m of the natural soil mentioned above can be found, an impervious coating, made of clayey material, must be compacted to a minimum thickness of 120 cm and a hydraulic conductivity inferior or equal to 1×10^{-7} cm/s. The input parameters used in this 2nd set of simulations are summarized in Tables 6 and 7. The diffusion coefficient of Cl⁻ for the compacted clay was taken from the literature (Rowe, 1991-b). A schematic of scenario landfill IIa landfills is presented in Figure 2.
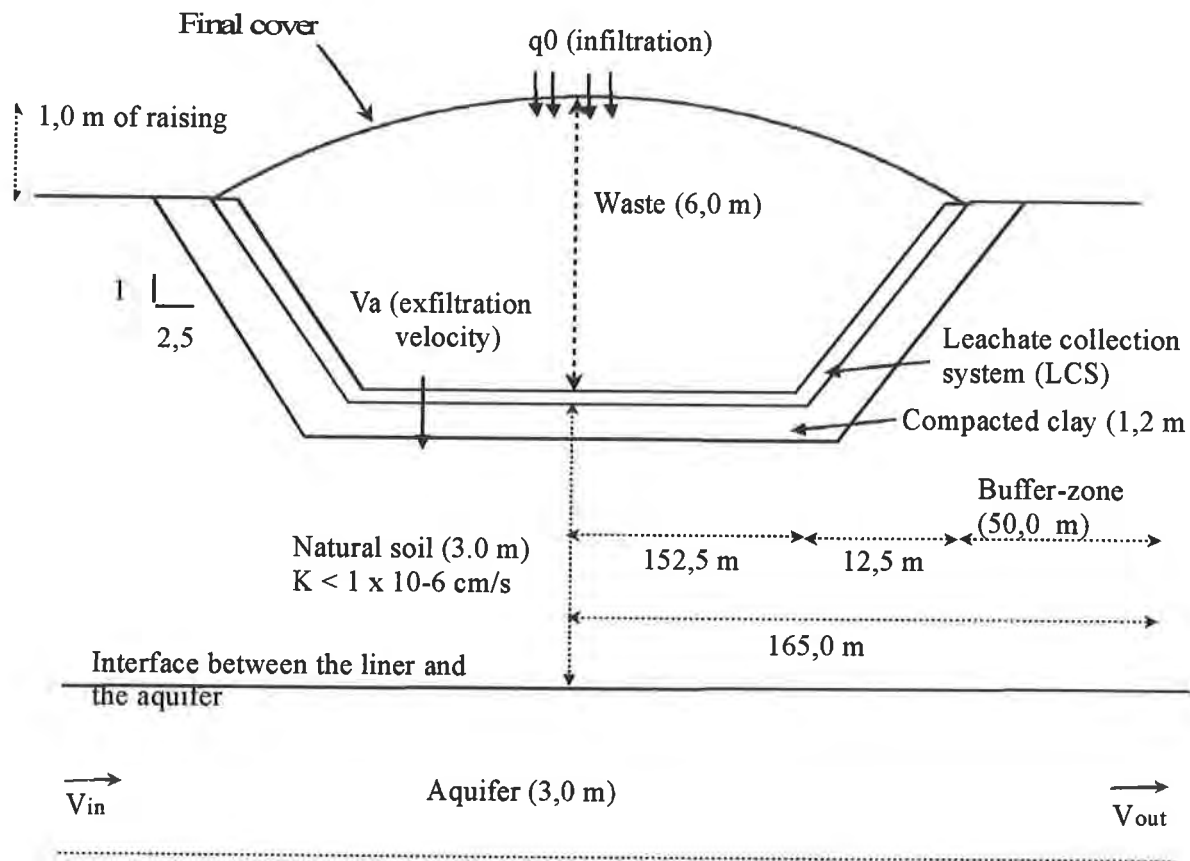
Figure 2 - Schematic of a scenario IIa landfill

PROPERTIES	VALUE	UNITS
Concentration source, Co	1000	mg/L
Reference height of leachate, Hr	8.4	m
Site length, L	300	m
Surface site width, Ws	330	m
Bottom site width, Wb	305	m
Thickness aquifer, h	3.0	m
Aquifer porosity, n_b	0.30	----
Times of interest, t	1, 5, 10, 20, 30, 60 et 100	a

Table 6- General input parameters for simulations with scenario IIa barriers

PROPERTIES	COMPACTED CLAY		SOIL UNDERNEATH	
	Value	Units	Value	Units
Diffusion coefficient Cl⁻, D_{cl-}	0.020	m^2/a	0.036	m^2/a
Distribution coefficient Cl⁻, K_d	0.0	cm^3/g	0.0	cm^3/g
Soil porosity, n	0.35	----	0.67	----
Dry density, ρs	1.90	g/cm^3	1.01	g/cm^3
Thickness of the layer, H	1.2	m	3.0	m

Table 7 - Specific input parameters for simulations with scenario IIa barriers

Chloride concentration profiles corresponding to a total thickness of 4,2 meters indicate that for the conditions imposed, the maximum allowed chloride concentration, 250 mg/L, is not reached when the leachate collection system has an efficacy rate of 88%. It can also be seen in Figure 3 that when the efficiency rate is set at 80%, the chloride migration after 60 years starts to become critical.
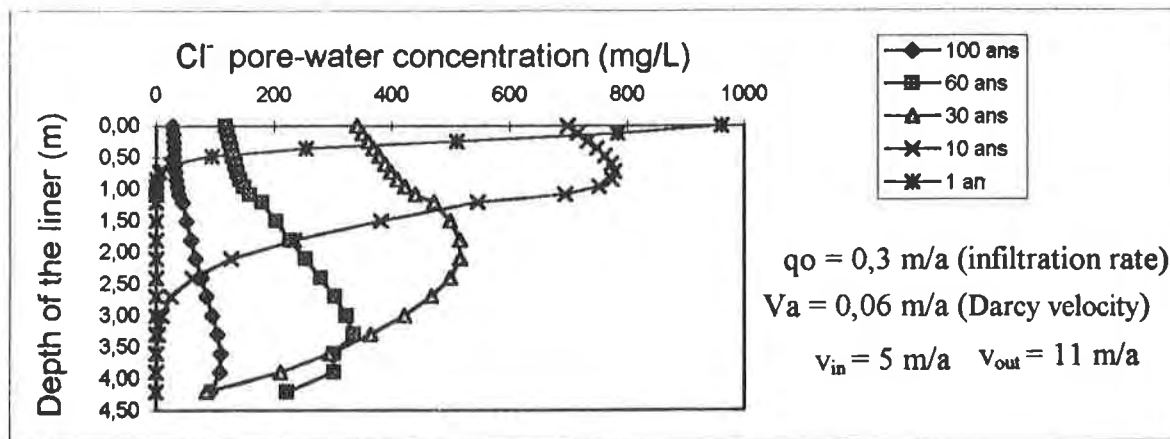
Figure 3. Chloride migration through scenario IIa barriers, (Efficiency rate = 80%)

Regarding this last remark, other simulations admitting a leachate collection system with a lower efficient rate of 50% were done. Such situation could happen if drains undergo a rapid clogging caused by salt precipitation (Quigley, 1994). Figure 4 shows that between 20 and 60 years, the Cl⁻ concentration directly under the site (in its center) will exceed 250 mg/L. Critical conditions at the limit of the buffer zone (50 meters away from the border of the landfill) will depend on the amount of mixing that occurs under the landfill. The level of contamination at the limit of the buffer-zone was also examined. Table 7 summarize the chloride concentrations at the interface between the liner and the aquifer at this point. It shows that the risk of contamination becomes critical when the leachate collection system is severally clogged. After 30 years, the chloride concentration is almost the double of the normal concentration allowed (Table 8).
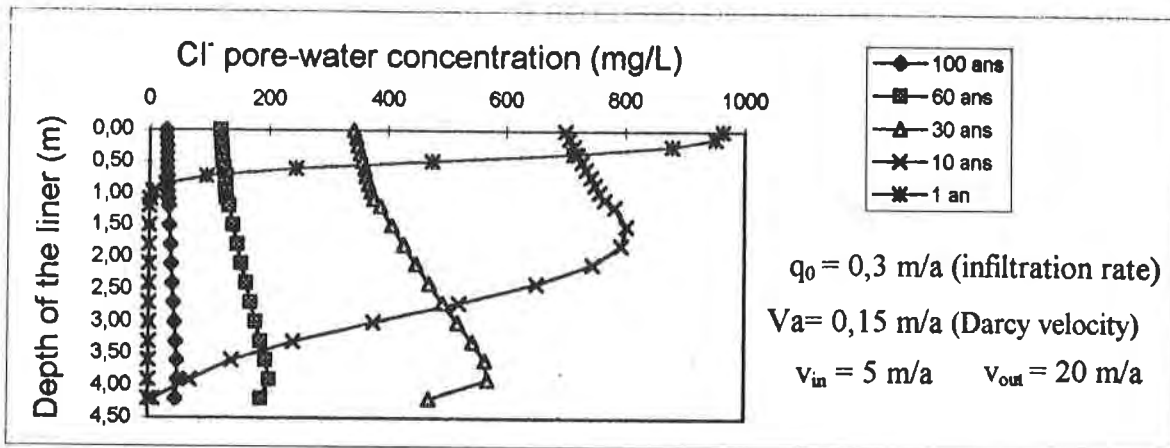
Figure 4. Chloride migration through scenario IIa barriers, (Efficacy rate= 50%)

Time (years)	Leachate collection system has an efficiency rate of 100%	Leachate collection system has an efficacy rate of 50%
30	0.4 mg/L	**486** mg/L
60	4.7 mg/L	243 mg/L
130	9.2 mg/L	**289** mg/L

Table 8. Concentration of Cl⁻ at the interface between the liner and the aquifer at the buffer-zone limit for various periods of time (scenario IIa barriers).

The last set of simulations for scenario IIa barriers aimed at verifying the influence of the source concentration on the contamination levels directly under the landfill (in its center). Table 9 summarize the values obtained. The results show that the risk of contamination at the interface between the liner and the aquifer (at 4.2 m depth) remains low even if the source concentration is set at higher values than 1000 mg/L.

Depth	Source concentration of Cl⁻		
	1000 mg/L	1500 mg/L	2000 mg/L
4.2 m	9.2 mg/L	10.1 mg/L	10.4 mg/L

Table 9. Chloride concentration as a function of its source concentration at the interface between the liner and the aquifer (t = 100 years; LCS at 100% efficiency)

6.2.2 Simulations with scenarios IIb landfill barriers

An alternative to scenario IIa is the construction of a composite liner composed of a 1.5 mm HDPE geomembrane laid upon 0.6 m of a compacted clay soil having a hydraulic conductivity equal or inferior to 1×10^{-7} cm/s after compaction (see Figure 5). For the needs of the simulations, it was necessary to determine an equivalent layer corresponding to the 60 cm of compacted soil $\qquad$ (K= 1×10^{-7} cm/s) and 300 cm of natural soil (K= 1×10^{-6} cm/s). The properties of this equivalent layer and the specific parameters used in the simulations are shown in Table 9. An efficiency rate 100% for the LCS was admitted for all scenario IIb simulations.
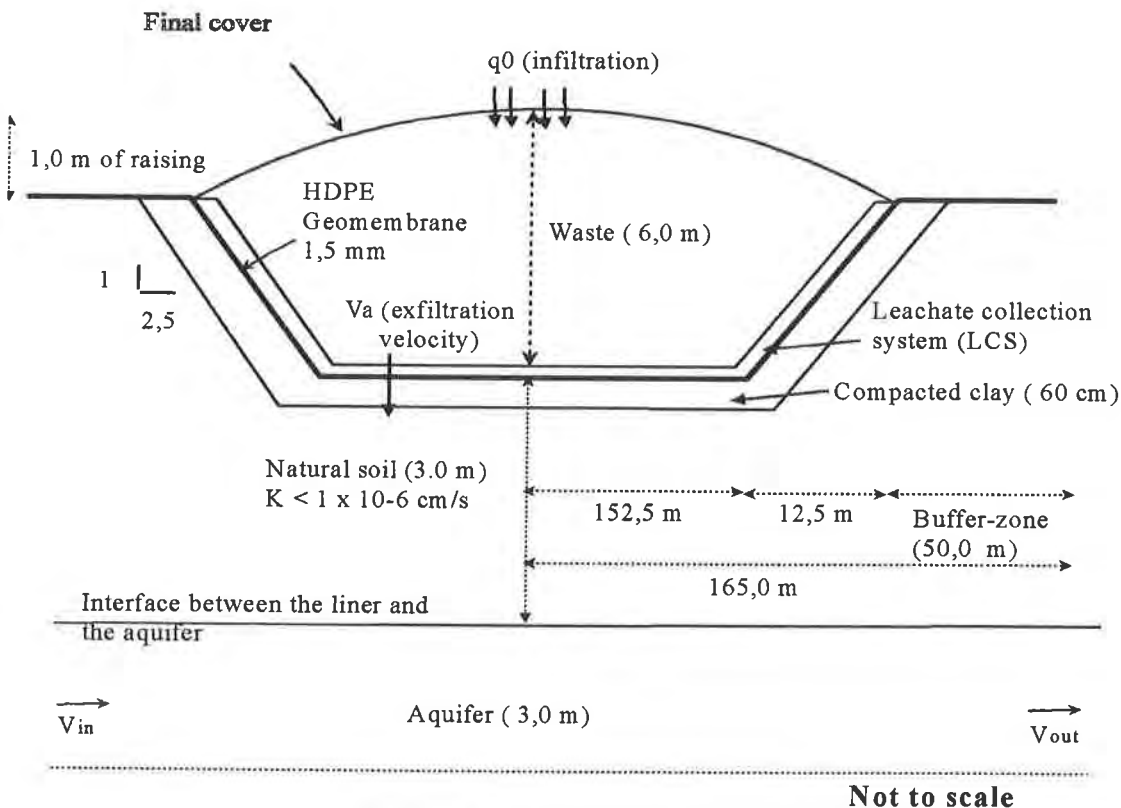
Figure 5. Schematic of a scenario IIb landfill barriers

PROPERTIES	GEOMEMBRANE		EQUIVALENT SOIL LAYER	
	Value	Units	Value	Units
Diffusion coefficient of Cl⁻, D_{cl-}	0.0003	m^2/a	0.033	m^2/a
Distribution coefficient of Cl⁻, K_d	0.0	cm^3/g	0.0	cm^3/g
Soil porosity, n	1.0	----	0.62	----
Hydraulic conductivity, K	2×10^{-15}	cm/s	4×10^{-7}	cm/s
Dry density, ρs	0.95	g/cm^3	1.16	g/cm^3
Thickness of the layer	0.015	m	3.60	m

Table 9. Specific input parameters

The hydraulic conductivity of the geomembrane is given directly by the model. The hydraulic conductivity of the equivalent layer is calculated as follows :

$$K_{equivalent} = \frac{360\ cm}{\left(\dfrac{60cm}{1X10^{-7}\ cm/s} + \dfrac{300cm}{1X10^{-6}cm/s}\right)} = 4X10^{-7}\ cm/s \qquad (3)$$

At first, the effect of increasing the number of circular holes in the geomembrane is examined. A default hole area of 1 cm^2 was used (Giroud and Bonaparte, 1989). By increasing the frequency of holes from 2.5/ hectare to 10/ hectare (very bad QA/QC), small changes were observed in the chloride concentration across the composite liner. Table 10 presents the chloride concentration as a function of the number of holes in the geomembrane, at the interface between the liner and the aquifer.

Depth	Frequency of holes in the geomembrane		
	2.5 holes/ hectare	5 holes/ hectare	10 holes/ hectare
3.6 m	6.8 mg/L	7.0 mg/L	7.3 mg/L

Table 10. Chloride concentration as a function of the number of holes in the geomembrane's holes at the interface between the liner and the aquifer (t = 100 years; A = 1 cm^2 ; LCS at 100% efficiency)

Complementary, simulations were made to verify the influence of the area of the holes. The results obtained are presented in Table 11. Again, the chloride concentrations obtained are low with correspondingly low risks of contamination.

Depth	Hole area		
	1 cm^2	5 cm^2	10 cm^2
3.6 m	7.5 mg/L	7.6 mg/L	7.7 mg/L

Table 11. Chloride concentration as a function of the hole area at the interface between the liner and the aquifer (t = 100 years; Frequency = 2.5 holes/ hectare; LCS at 100% efficiency)

Finally, another set of simulations allowed for an evaluating of the influence of the source concentration on the of contamination levels directly under the landfill. The results presented in Table 12 show that the risk of contamination remains low, even if the source concentration is set at higher values than 1000 mg/L.

Depth	Source concentration of Cl$^-$		
	1000 mg/L	1500 mg/L	2000 mg/L
3.6 m	7.5 mg/L	8.5 mg/L	8.9 mg/L

Table 12. Chloride concentration as a function of its source concentration at the interface between the liner and the aquifer (t = 100 years; LCS at 100% efficiency)

7. CONCLUSIONS

The results show that the advance of the contamination front across the three different barrier designs depend on : (1) the efficiency of the leachate collection system during the post-closure period ; and (2) the quality of the final cover . All three scenarios can be very effective in preventing the contamination of the soil and groundwater underneath the barrier by Cl⁻, provided that high efficiency rates of the LCS and a good quality cover can be maintained throughout the post-closure period. The scenario involving the installation of a composite cover is quite effective, irrespective of the quality control exerted during installation.

8. ACKNOWLEDGEMENTS

9. REFERENCES

Barone, S.F., Yanful, K. E., Quigley, M. R. et Rowe K. R., (1988), *Effect of multiple contaminant migration on diffusion and adsorption of some domestic waste contaminants in a natural caley soil.* Canadian Geotechnical Journal. Vol. 26, pp 189- 198.

Consultation document for a new solid waste regulation *(Projet de règlement sur les déchets solides)* (mars, 1994), technical version, Ministry of Environment and Fauna (MEF).

Giroud, J. P. et Bonaparte , R., (1989), *Leakage through liners constructed with geomembranes.* Part I. Geomembrane liners ; Part II. Composite liners. Geotextiles and Geomembranes (8) : 27-69; 71-112.

Landry, B. et Mercier, M., (1992), *Notions de géologie.* Third edition, Modulo Editor, 563 p.

Quigley, M. R.,(1994), *Municipal solid waste landfilling,* First Internatinal Congress on Environmental Geotechnics. July 10-15, Edmonton, Alberta, Bitech Publishers Ltd. pp 589-598.

Rowe, R. K., (1991b), *Some considerations in the design of barrier systems.* Proceedings of the 1st Canadian Conference on Environmental Geotechnics, Montréal, Canada. pp 157- 164.

Rowe, R. K. et Booker J. R., (1985), *1-D Pollutant Migration in Solid of Finite Depth,* Journal of Geotechnical Eng., Vol. 111, pp 479-499.

Rowe, R. K., Booker J. R. et Fraser M. J., (1996), *Migrate v9, version 9.0.7,* GAEA Environmental Engineering Ltd. ON., 307 p.

Rowe, R. K., Booker J. R. et Fraser M. J., (1994), *Pollutant v6, User's Guide.* GAEA Environmental Engineering Ltd. ON., 304 p.

Rowe, R. K., Caers C. J. et Barone F., (1988), *Laboratory determination of diffusion coefficients of contaminants using undisturbed clayey soil.* Canadian Geotechnical Journal, vol. 25, pp 108-118.

Shackelford, D. C. (1991), *Laboratory diffusion testing for waste disposal- A review.* Journal of Contaminant Hydrology, Elsevier Science Publishers B. V. Amsterdam, vol7, pp 177-217.

Shoiry, J. (1995), *Caractérisation des eaux de lixiviation des lieux d'enfouissement sanitaires et procédés de traitement applicables.* Proc. of the technological meeting., December 6, 1995, Laval, 30 p.

Théberge, J. (1996), *Gestion des eaux de lixiviation au L.E.S. Bestan inc.* Proceeding of a SAGEOS seminary on drainage in landfill sites., February 28, 1995, St-Hyacinthe, 20 p.

Valiron, F., Monod, J. et Coulomb R., (1994), *Mémento du Gestionnaire de l'Alimentation en eau et de l'Assainissement.* Tome 1, Eau dans la ville; Alimentation en eau. Lyonnaise des eaux, Paris, annexes de la deuxième partie.

A STRAIN-SOFTENING CONSTITUTIVE LAW FOR SMOOTH GEOMEMBRANE/SAND INTERFACES

JIE HAN
GRADUATE RESEARCH ASSISTANT
SCHOOL OF CIVIL AND ENVIRONMENTAL ENGINEERING
THE GEORGIA INSTITUTE OF TECHNOLOGY
ATLANTA, GA 30332
USA

ABSTRACT

Interfaces play an important role in many geotechnical engineering systems, including geomembrane/soil systems. Researchers have proposed a variety of constitutive laws for interfaces, most of which are based on the elastic-plastic stress-strain behavior. However, many experimental results show that smooth geomembrane/sand interfaces exhibit strain softening behavior. A new constitutive law based on the Mindlin contact theory and the state variable friction law is described in this paper. The constitutive law and experimental data both show that shear stiffness of interfaces calculated from direct shear tests is specimen size dependent. Evaluation of the stress-strain response computed with the model indicates good agreement with experimental data.

INTRODUCTION

The term "interface" is used to describe the region between two dissimilar materials where relative deformation may occur. Geomembrane/soil is an example of many interfaces commonly encountered in practice. The surfaces of geomembranes used in applications could be smooth or rough. It was recognized that surface roughness could play an important role in the mechanism of shear transfer (Uesugi, 1987). Smooth surfaces would promote sliding of sand particles, whereas rough surfaces would promote rolling of particles. Furthermore, for smooth surfaces only the particles very close to surface are involved in shear transfer, whereas for rough surfaces more particles in the sample are involved. Therefore, smooth and rough surfaces normally have different interface behavior. The study in this paper only focuses on the interfaces with a smooth geomembrane.

Based on experimental evidence, the stress-strain behavior at interfaces could be classified as one of four possible types as shown by the typical curves in Figure 1. According to the contact theory, the plastic response refers to the case where the contact area does not change as two surfaces slide relative to each other and the shear stress has reached a constant value. Strain softening or "slip weakening" (Dieterich, 1972; Ruina, 1983) occurs after a time dependent stabilizing during stationary contact. Alternatively, a friction force with a decreasing function of the instantaneous slip rate can result in slip weakening (during accelerating slip) and slip instabilities. Strain hardening is believed to be contributed by factors such as contact area growth and temperature change. Bowden and Leben (1938) found that metallic surfaces "stick" together until a sudden break occurs with a consequent very rapid "slip" as a result of the gradually increasing pull. The surfaces stick again and the process is repeated indefinitely. Since strain softening is the dominant behavior for smooth geomembrane/sand interfaces in experimental tests (Saxena et al., 1984; O'Rourke et al., 1989; Bemben et al., 1993 and Vaid et al., 1995), it is very important to develop a constitutive law which can model strain softening behavior appropriately. Details of the constitutive model are given in Han (1996) and are summarized below.

OVERVIEW

Existing Constitutive Models for Interfaces. A number of constitutive models for interfaces have been proposed for decades. The relationship between shear stress and strain (or displacement) was expressed as an exponential function by Kezdi (1957) or as a hyperbolic function by Clough and Duncan (1971) or as a quadratic curve by Zaman et al. (1984). In general, these models permit reasonable predictions for the specific cases for which they were developed, intuitively if the behavior is elastic-plastic. However, they are generally not useful in simulating the stress-strain relationship for interfaces where strain softening occurs. Using mathematical approaches based on the curve shape from his test results, Uesugi (1987) developed an empirical constitutive model, which could deal with the strain softening problem. However, there is no strong theoretical basis for the model. The constitutive model presented herein is based on the Mindlin contact solution (Mindlin, 1949) and the state variable friction law (Dieterich, 1979 and Ruina, 1983).

Mindlin Contact Theory. The solution for the problem of contact between two elastic spheres was first very successfully obtained by Hertz in 1882 (Mindlin, 1949). Mindlin (1949), Mindlin and Deresiewicz (1953) continued to study the cases of elastic spheres in contact under varying oblique forces. When the applied tangential force Q is less than the limiting friction force μP (P is the normal load and μ is the limiting friction coefficient), the equilibrium of two bodies in contact is undisturbed by the initiation of sliding. According to the Hertz theory, the tangential load would induce an infinite tangential traction at the boundary of the contact ellipse in the absence of slip. Thus some slip is inevitable at the edge of the contact area under the action of the smallest tangential force. With an increase of tangential force, the slip extends inward until the whole contact slides, at which stage $Q = \mu P$. Considering a circular Hertzian contact area, the relative tangential displacement δ between two contacting spheres under the action of a tangential force was derived by Mindlin (1949) as follows.

$$\delta = \frac{3\mu P}{16a}\left(\frac{2-\nu_1}{G_1}+\frac{2-\nu_2}{G_2}\right)\left[1-\left(1-\frac{Q}{\mu P}\right)^{\frac{2}{3}}\right] \qquad (1)$$
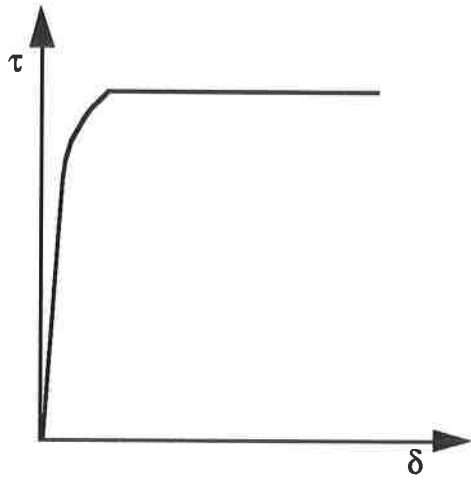
(a) Elastic-Plastic
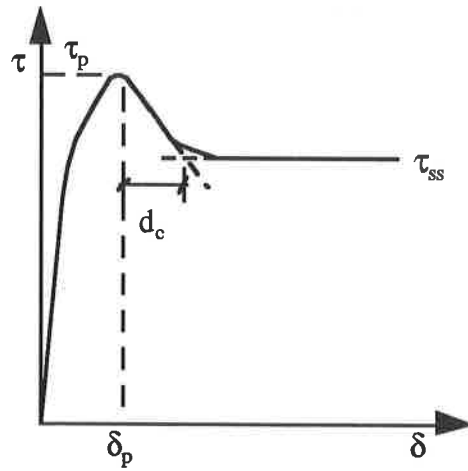
(b) Strain Softening
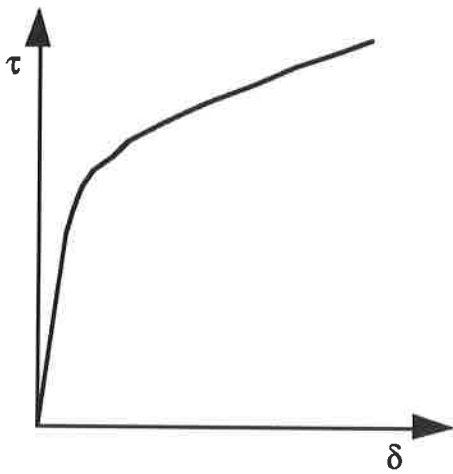
(c) Strain Hardening
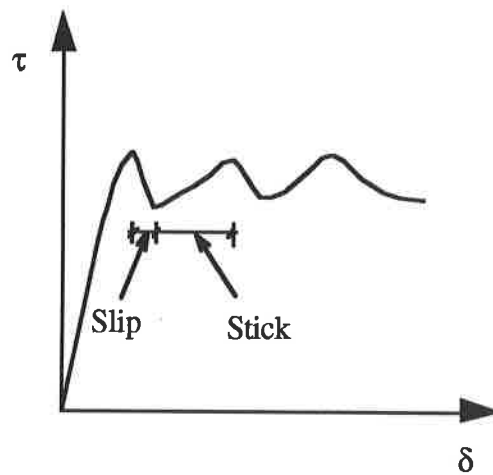
(d) Stick-Slip

Fig. 1 Typical Stress-Strain Behavior at Interfaces

where G_1 and G_2 are the shear moduli of two bodies, a is the radius of contact area, and v_1 and v_2 are their Poisson's ratios.

State Variable Friction Law. In order to explain the mechanism of crustal earthquakes caused by unstable fault slip, a lot of investigations have been made on history dependent frictional properties between rocks (Dieterich, 1979; Ruina, 1983; Dieterich and Kilgore, 1994). Byerlee (1970) proposed that instabilities as sliding proceeds are associated with decrease in the friction force from peak values. Based on several experimental observations, Ruina (1983) indicated that the shear stress τ depends on the slip rate V, the normal stress σ and the state θ. That is

$$\tau = f(\sigma, V, \theta) \tag{2}$$

The state of a given point on the surface is assumed to change with time continuously for finite slip rate V (or continuous slip displacement δ). The rate of change of state is attributed only to the instantaneous state at the point, the normal stress σ and the slip rate V:

$$\frac{d\theta}{dt} = g(\sigma, V, \theta) \tag{3}$$

After a series of mathematical work, Ruina (1983) proposed the following formula as a friction law:

$$\tau = \sigma\left[\mu_0 + \theta + A\ln(V/V_c)\right] \tag{4}$$

$$\frac{d\theta}{dt} = (-V/d_c)\left[\theta + B\ln(V/V_c)\right] \tag{5}$$

where V_c is a constant introduced for dimensional consistency, μ_0 is a constant which is related to friction coefficient, and d_c is termed as "characteristic distance", which is defined as the distance from the peak point to the transient point of steady state, as shown in Fig. 1 (b).

Dieterich and Kilgore (1994) indicated that d_c is approximately independent of slip speed and normal stress, but depends on surface conditions, and increase with surface roughness and size of contacting particles separating the sliding surface.

Failure Mechanism of Interface Shear Tests. It is common to study the shear behavior of interfaces between soil and some other material using a direct shear test or a simple shear test. The failure generally occurs along the preexisting interface surface, especially for relatively smooth surfaces. Based on the finite element analyses for the simple shear test, Duncan and Dunlop (1969) concluded a progressive failure started from near the ends of the specimen and the failure zones gradually increased towards the center. According to the experimental observations made using small hidden mirror viewers to watch the particle motion on the interface surface during the direct shear testing, a similar finding has been obtained by Yin et al. (1995). If the soil is placed in the upper shear box, which is subjected to a horizontal force on its right edge, the soil near the right edge tends to be compressed while the soil near the left

edge tends to expand. The overall stress-strain development may be divided into two phases. The first phase is referred to as "slip developing", in which the particle slip develops gradually from the exterior to the interior until full sliding occurs. This evidence is really similar to that for the Mindlin's problem as discussed earlier if the soil sample is assumed to behavior as an elastic solid. The second phase is referred to as " full sliding ", in which the particles tend to re-arrange in order to get the stable state during their sliding. It is also the similar problem related to the state change as Dieterich (1979) and Ruina (1983) dealt with. These phases are discussed in detail later.

CONSTITUTIVE LAW OF INTERFACES

Slip Developing. Based on the similarity of the slip mechanism between the direct shear test and Mindlin's problem, the Mindlin's solution may be utilized to simulate the shear stress-horizontal displacement relationship even though strictly speaking, it was not exactly Mindlin's problem. This is because the Mindlin's solution is based on the assumption of two smooth contacting spheres with a very small contact area compared with their sizes. It was treated as a half space problem.

It should be noted here that a and P in Eq.(1) represent the radius of the specimen and the total normal force, respectively. Considering geomembranes having a much higher shear modulus than soil mass, Eq.(1) can be modified as follows:

$$\tau = \tau_p \left\{ 1 - \left[1 - \frac{16G\ \delta}{3\pi\tau_p a(2-v)} \right]^{\frac{3}{2}} \right\} \tag{6}$$

where G is the shear modulus of soil mass and $\tau_p = \mu\sigma$.

The secant shear stiffness at peak K_p can be obtained by

$$K_p = \frac{\tau_p}{\delta_p} = \frac{16G}{3\pi(2-v)a} \tag{7}$$

where τ_p and δ_p are the shear stress and the horizontal displacement at peak.

If Poisson's ratio v is assumed to be 0.3 for sand mass, the above equation can be approximately simplified as:

$$K_p \approx \frac{G}{a} \tag{8}$$

Full Sliding. As discussed earlier, the state variable friction law can be utilized for this phase. By solving the differential equation in Eq. (5) and substituting θ into Eq. (4), it yields

$$\tau = \sigma \left[\mu_0 + C \exp\left(-\frac{V}{d_c}t\right) + D \ln\left(\frac{V}{V_c}\right) \right] \qquad (9)$$

where C and D are constants.

As illustrated in Fig. 1 (b), $Vt=\delta-\delta_p$ and $\tau=\tau_p$ when $\delta=\delta_p$, and $\tau=\tau_{ss}$ when $\delta\rightarrow+\infty$. By solving the constants C and D using these conditions, the final expression is given as

$$\tau = \tau_{ss} + \left(\tau_p - \tau_{ss}\right)\exp\left(-\frac{\delta-\delta_p}{d_c}\right) \qquad (10)$$

where τ_{ss} is the interface shear strength at the steady state.

The characteristic distance d_c can be determined from the shear stress-horizontal displacement curve as shown in Fig. 1 (b). The procedure is: (1) to draw a tangential line in the post-peak portion from the peak point and a horizontal line at $\tau=\tau_{ss}$, and (2) to find the displacement at the intersection of these two lines. The difference between the displacement at the intersection and the displacement at peak is the characteristic distance d_c. This procedure can also be verified from mathematical view of point.

PARAMETRIC STUDY

Interface Strength Test. In order to study the parameters adopted in the new model, several interface strength tests were performed by using direct shear apparatus. The direct shear apparatus consisted of a 63.5mm diameter shear box. HDPE geomembrane specimens were glued onto a plywood substrate used as a base platen. The tests were conducted at normal stresses ranging from 50 to 300 kPa and soil relative densities ranging from 42 to 93 percent. The average surface roughness R_s of the geomembrane specimens is 1.07 (Dove et al., 1997) and they are classified as smooth geomembranes. Two Ottawa sands (20/30 and F-70) were selected, which have rounded to subrounded grains. The mean grain size D_{50} for Ottawa 20/30 is 0.6 mm and that for Ottawa F-70 is 0.2.

In order to investigate the specimen size effect, other experimental data were collected from the literature (Vaid et al., 1995; Bemben et al., 1993; O'Rourke et al., 1989; Saxena et al., 1984).

Shear Strength. Fig. 2 shows the peak interface shear strength and the strength at the steady state plotted as a function of normal stress for tests of sand on HDPE geomembrane. There is a linear relationship between interface shear strength and normal stress. The peak interface friction angle is approximately 21.2^0 and the friction angle at the steady state is 17.3^0. The size of specimen has insignificant influence on the interface shear strength.

Shear Stiffness and Shear Modulus. The shear stiffness parameter is commonly used for the interface element in the finite element method, which could be determined from the shear stress-horizontal displacement curve of direct shear tests (Desai et al., 1984 and Clough and Duncan, 1981). It was normally thought that the shear stiffness was specimen size independent. However, Eq. (7) shows that the shear stiffness from direct shear tests has a function of the size
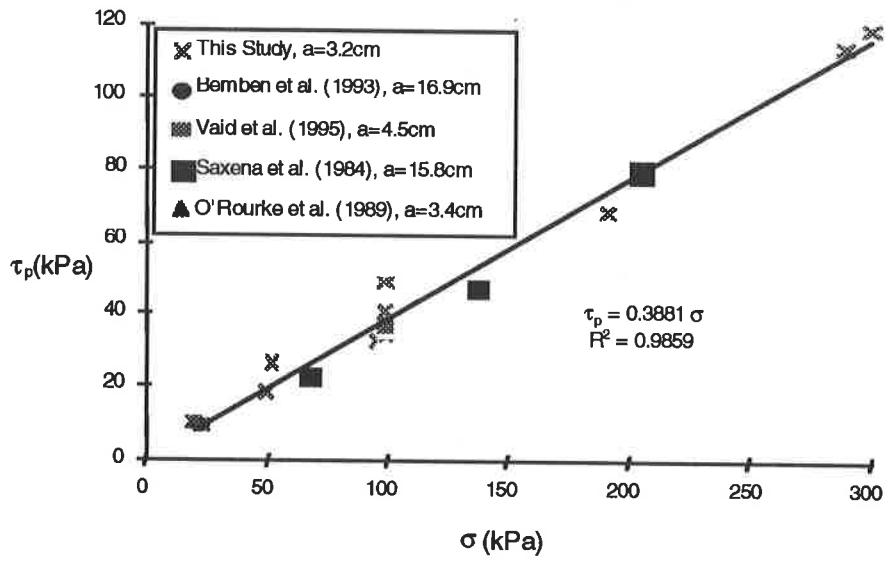
(a)
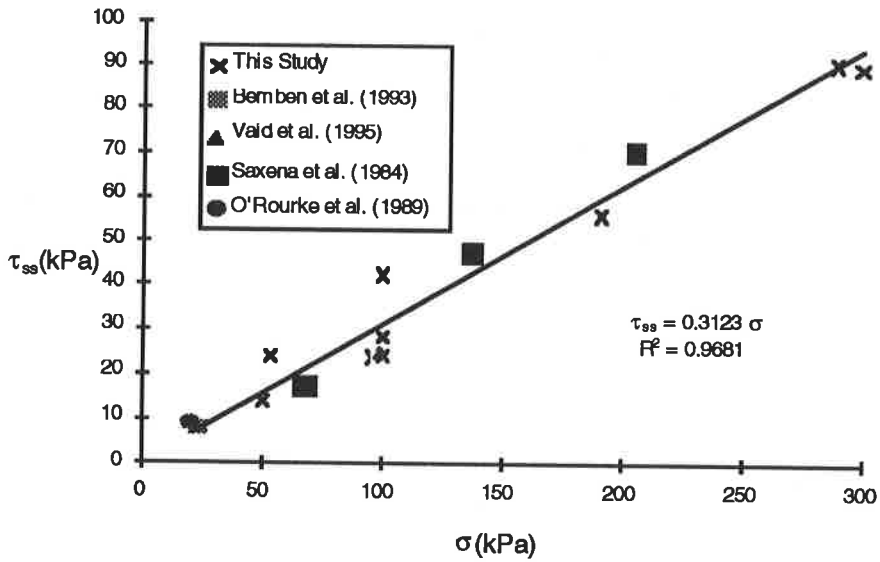
(b)

Fig. 2 Shear Stress versus Normal Stress for Direct Shear Tests of
Ottawa Sand on HDPE Geomembrane
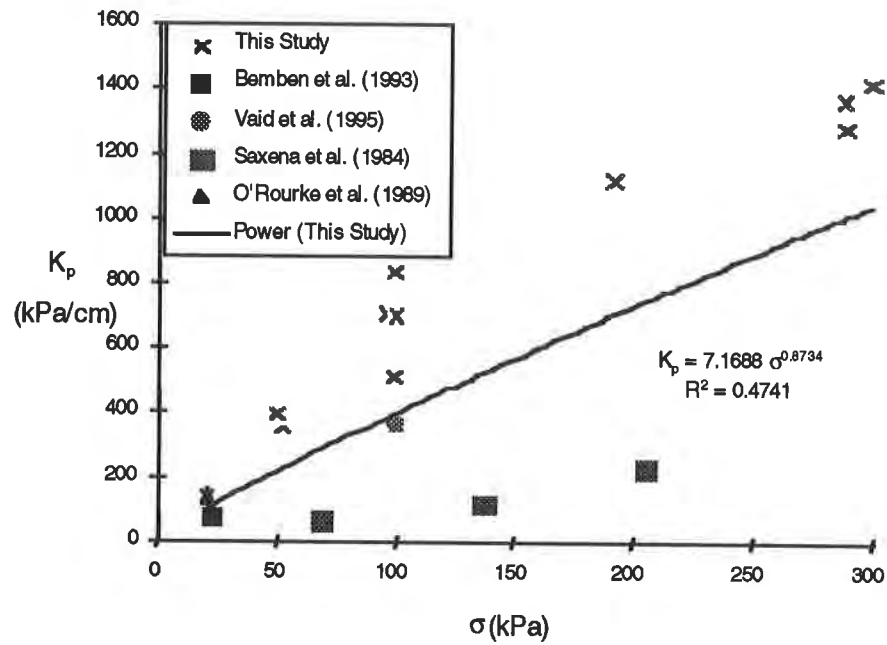
(a)
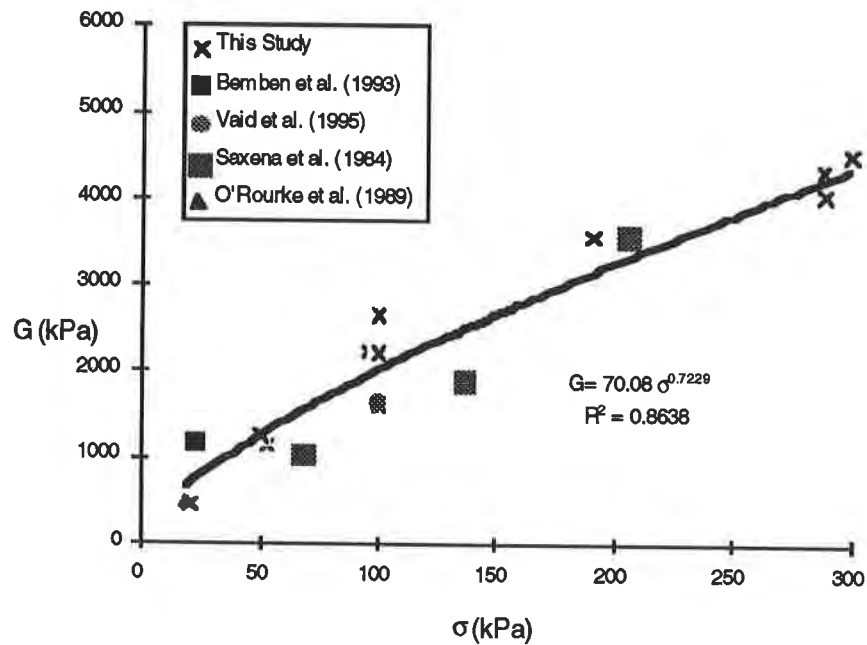
(b)

Fig. 3   Shear Stiffness or Modulus versus Normal Stress for Direct Shear Tests of Sand on HDPE Geomembrane

of specimen. This is also the reason why the data from different references as shown in Fig. 3(a) are so scatter, in which different specimen sizes were adopted for tests. If the shear stiffness is multiplied by the radius of specimen as expressed in Eq. (8), the shear modulus has a good relationship with the normal stress as shown in Fig. 3(b). The data scatter may be attributed to other factors such as the density of soil mass.

Characteristic Distance: As shown in Fig. 4, the characteristic distance seems to have a relationship with the size of specimen. Since large specimens have more particles, they need more displacement for particles to re-arrangement and to achieve the steady state. The characteristic distance may also be affected by other factors such as surface roughness of geomembrane, particle size of sand, density of soil mass, etc. Even though smooth geomembranes were referred to in all the references, their surface roughness parameters may not be same. The term "smooth" or "rough" was normally used based on a relative sense. Due to lacking in enough data at this stage, the relationship between the characteristic distance and other factors needs investigating further in the future.
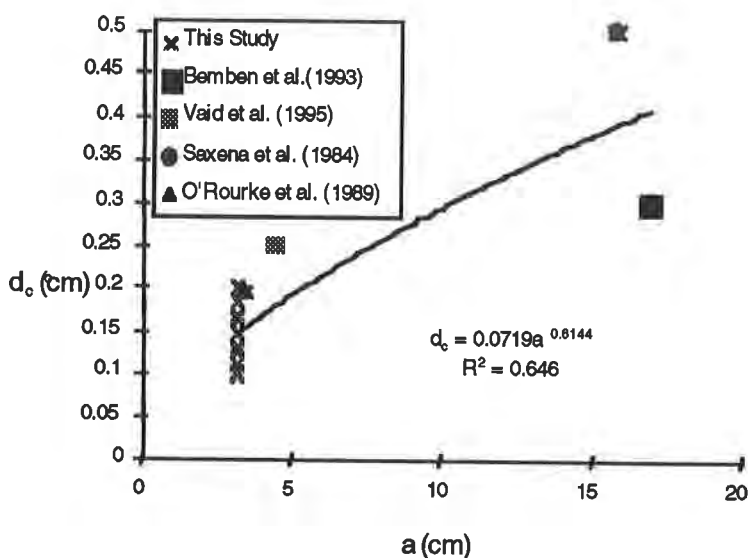
Fig. 4 Characteristic Distance versus Specimen Size

COMPARISON BETWEEN EXPERIMENTAL DATA AND MODEL SIMULATION

As shown in Fig. 5, the model could simulate the shear stress-horizontal displacement behavior from tests very well. Once the correlations discussed in the parametric study are well established, the model can also be used to predict interface shear behavior. It is found that the shear mudulus at a low normal stress in Fig. 5(b) is higher than that at a high normal stress in Fig. 5(a). This may be because the soil used in Bemben et al. (1993) has a higher relative density.
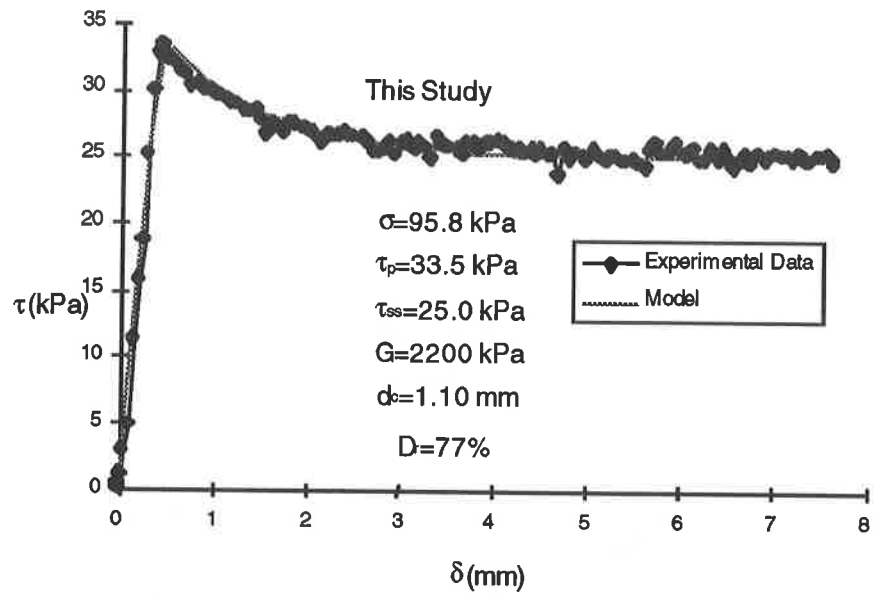
(a)
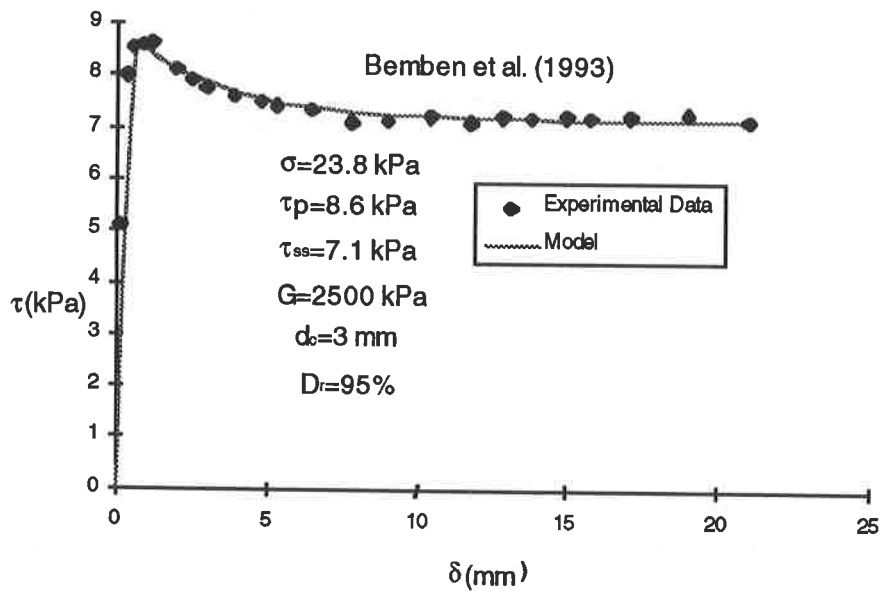
(b)

Fig. 5 Comparison between Experimental Data and Model Simulation

CONCLUSIONS

The constitutive model of interfaces discussed in this paper, which is based on the Mindlin contact theory and the state variable friction law, could successfully simulate the strain softening behavior for smooth geomembrane/sand interfaces. The theory and the parametric study show that the shear stiffness of interfaces from direct shear tests is specimen size dependent. Shear modulus is independent of specimen size but has a function of normal stress. Based on the experimental data in this study, the specimen size has insignificant influence on the shear strengths.

ACKNOWLEDGMENT

Dr. J. David Frost, the author's advisor at the Georgia Institute of Technology is gratefully acknowledged for his advice and support.

REFERENCES

Bemben, S. M. and Schulze, D. A. (1993). "The influence of selected testing procedures on soil/geomembrane shear strength measurements." Geosynthetics'93, Vancouver, Canada, pp. 619-631.

Bowden, F. P. and Leben, L. (1938). " The nature of sliding and the analysis of friction." Proceedings of the Royal Society of London, Series A, 169, pp. 371-391.

Byerlee, J. H. (1970). " The mechanics of stick-slip." Tectonophysics, No. 9, pp. 475-486.

Clough, G. W. and Duncan, J. M. (1971). " Finite Element analysis of retaining wall behavior." Journal of Soil Mechanics and Foundations Division, Vol. 97, No. SM 12, pp. 1657-1674.

Desai, C. S., Zaman, M. M., Lightner, G. G. and Siriwardane, H. J. (1984). "Thin layer element for interfaces and joints." International Journal for Numerical and Analytical Methods in Geomechanics, Vol. 8, pp. 19-43.

Dieterich, J. H. (1972). " Time-dependent friction in rocks." Journal of Geophysical Research, Vol. 77, pp. 3690-3697.

Dieterich, J. H. (1979). " Modeling of rock friction 1. Experimental results and constitutive equations." Journal of Geophysical Research, Vol. 84, No. B5, pp. 2161-2168.

Dieterich, J. H. and Kilgore, B. D. (1994). " Direct observation of frictional contacts: new insights for state-dependent properties." Pure and Applied Geophysics, Vol. 143, No. 1/2/3, pp. 283-302.

Dove, J. E., Frost, J. D., Han, J. and Bachus, R. C. (1997). "The influence of geomembrane surface roughness on interface strength." Geosynthetics'97.

Duncan, J. M. and Acres, H. G. (1969). "Behavior of soils in simple shear tests." Proc. 7th Int. Conf. on Soil Mechanical Foundation Engineering, Vol. 1, pp. 101-109.

Han, J. (1996). "Mechanical behavior of fiber-reinforced polymeric piles in sand." In preparation for Ph. D dissertation, The Georgia Institute of Technology.

Kezdi, A. (1957). "Bearing capacity of piles and pile groups." Proc. of 5th ICSMFE, Vol. 2, London, pp. 46-51.

Mindlin, R. D. (1949). " Compliance of elastic bodies in contact." Journal of Applied Mechanics, September, pp. 259-268.

Mindlin, R. D. and Deresiewicz, H. (1953). " Elastic spheres in contact under varying oblique forces." Journal of Applied Mechanics, Vol. 75, September, pp. 327-344.

O'Rourke, T. D., Druschel, S. J., and Netravali, A. N. (1989). "Shear strength characteristics of sand-polymer interfaces." Journal of Geotechnical Engineering, Vol. 116, No. 3, pp. 451-469.

Ruina, A. (1983). " Slip instability and state variable friction laws." Journal of Geophysical Research, Vol. 88, No. B12, pp. 10359-10370.

Saxena, S. K. and Wong, Y. T. (1984). "Friction characteristics of a geomembrane." Proc. Int. Conf. on Geomembranes, Industrial Fabrics Association International, pp. 187-190.

Uesugi, M. (1987). " Friction between dry sand and construction materials." Ph.D thesis, Tokyo Institute of Technology, pp. 306.

Vaid, Y. P. and Rinne, N. (1995). "Geomembrane coefficients of interface friction." Geosynthetics International, Vol. 2, No. 1, pp. 309-325.

Yin, Z. Z., Zhu, H. and Xu, G. H. (1995). " A study of deformation in the interface between soil and concrete." Computers and Geotechnics 17, pp. 75-92.

Zaman, M. M., Desai, C. S. and Drumm, E. C. (1984). "Interface model for dynamic soil-structure interaction." Journal of Geotechnical Engineering, Vol. 110, No. 9, pp. 1257-1273.

NUMERICAL ANALYSIS OF INSTRUMENTATION OF A GEOSYNTHETIC REINFORCED WALL

WEI F. LEE
UNIVERSITY OF WASHINGTON, U.S.A

ABSTRACT

In order to develop more economical and practical design tools of geosynthetic reinforced soil (GRS) retaining structures, a two-phase research project has been conducted by the University of Washington to obtain the knowledge of the stress and strain levels occurring in GRS structures. The first phase included carrying out an extensive instrumentation program of the Interstate-90 Rainer Avenue GRS wall and performing series of laboratory tests using newly developed unit cell device. The second phase included conducting analytical modeling in order to reproduce the results of both laboratory tests and filed instrumentation. It was found that by using the composite element concept, numerical models can successfully simulate the instrumentation results of the Interstate-90 Rainer Avenue GRS wall. Moreover, information on working stresses inside the GRS retaining walls was obtained from the modeling study. Both the framework and the primary results of the numerical modeling study are described in this paper.

INTRODUCTION

The present design procedures of geosynthetic reinforced soil (GRS) retaining walls are known to be very conservative (Bell et al., 1983). Many GRS retaining structures designed in North America were designed by using the conventional tie-back wedge technique (Steward et al., 1977, Christopher and Holtz, 1985), which is known to severely overestimate the stress and strain levels within the GRS retaining structures (Yako and Christopher, 1987). In order to define the actual stress and strain distribution occurring in the GRS wall, a two-phase research project has been conducted by the University of Washington. The project includes an extensive instrumentation program on a GRS wall, a laboratory test program using a newly developed plane strain device, and finally, numerical modeling using results of instrumentation and laboratory tests.

The test wall was constructed in Seattle, Washington, USA. It had maximum height of 12.6 meters and supported a 6 meter high surcharge fill (Fig. 1) and was the highest GRS wall built at that time (Allen, 1992). The Washington State Department of Transportation designed and supervised the construction. The wall was extensively instrumented and monitored during and after construction to evaluate its deflections and stress and strain levels occurring in it (Christopher, et al., 1990). Results of the instrumentation have been reported by Holtz, et al., (1990), and Allen et al., (1991).

A load control, plane strain, unit cell device (UCD) was designed and fabricated at the University of Washington to aid in the prediction of the working stresses and deformations within GRS structures (Boyle, 1995). The UCD, which tests a reinforced soil specimen in the laboratory, is used to directly measure the deformation and major principal stress of the composite specimen, and the tension of the geosynthetic reinforcement (Fig. 2). The results of the UCD tests are used to define composite properties of soil/geosynthetic system.

Finally, numerical models of Rainer Avenue wall have been created using UCD composite elements. The results of the analytical modeling and its application in the development of working stress and strain levels occurring in GRS retaining structures are presented in the following sections.

COMPUTER PROGRAM

The commercial computer program, "Fast Lagrangian Analysis of Continua" (FLAC) is used in this research. FLAC is a two-dimensional explicit finite difference program. In FLAC, materials are represented by elements that form a grid to fit the shape of the modeling object. It is able to simulate the in-soil behavior such as elastic material, groundwater flow, or special constitutive models defined by the user (Itasca Consulting Group, 1993). All FLAC model analyses are performed on IBM-compatible computers.

MATERIAL PROPERTIES

Backfill Soil. A relatively clean subrounded to subangular gravelly sand (D_{60}=0.61mm, Cu=4.1, and Cc=1.0) was selected for the retaining wall backfill and preload fill. The soil had an average moist density of 2082.4 kg/m^3 and moisture content of 7.5%. Triaxial testing indicated that the triaxial friction angle of this backfill soil ranges from 43 to 47 degrees under four different confining pressures (Allen et al., 1992).

Foundation Soil. Soil properties of moist density 2002.3 kg/m^3, friction angle 35 degrees, and Young's modulus 29,800 kN/m^2 were assigned for the foundation soil.

Geosynthetics. Four kinds of geosynthetics were used in the wall. Table 1 provides a summary of their general characteristics (after Allen et al., 1992, and Boyle, 1995).

Table 1. Geosynthetics characteristics.

Distance from Top of Wall (m)	Geosynthetics Type [1]	Density (kg/m^3)	Wide Width Tensile Strength (kN/m)[ii]	Elongation at Peak Tension (%)	Secant Modulus at 5% Strain (kN/m)[iii]
0-3	PP-W-SF	22.6	31	21	198
3-6	PP-W-SB/2-SF	45.2	62	16	453
6-9	PP-W-SB/3-SF	67.8	92	17	662
9-12	PET-W-MF	226	186	18	1068

[i] PP = polypropylene, PET = polyester, W = woven, SB/n = stitch-bonded n layers, SF = slit film, MF= multi-filament.
[ii] Wide width tensile tests (ASTM D-4595) from Allen, et al. (1992)
[iii] From Boyle, (1995)

RESEARCH PROGRAM

The concept of the analytical modeling is to develop the composite elements using results from UCD tests. The composite elements are then used to form the test wall models (Fig. 3 and Fig. 4). Because of the difficulty and high cost of performing the UCD test, efforts also are being conducted to determine the relationship between conventional properties and composite properties. Both complex and simplified models are being developed for this study. Complex models include: elastic material representing the geosynthetic reinforcement, Mohr-Coulomb material representing the soil, and the soil/geosynthetic interfaces. Simplified models include only the Mohr-Coulomb material.

Modeling UCD Test Results. Two kinds of models were created to reproduce UCD test results and study the composite properties. The complex model, Model UCD-C (Fig. 3), includes one elastic element, two Mohr-Coulomb elements, and two interfaces. The elastic material element represents the geosynthetic within the UCD specimen. Two Mohr-Coulomb elements represent the confining soil above and below the geosynthetics. Two zero thickness interfaces are inserted between the soil and the geosynthetic reinforcement. Model UCD-S (Fig. 4) is the simplified model which includes only Mohr-Coulomb elements. Table 2 summarizes

the composite properties used in the analytical models as obtained from UCD tests. A total of 23 UCD test results were reproduced in both the complex and simplified models[1].

Table 2. Composite properties.

Confining Pressure (kPa)	Geosynthetics Type	Soil Density (kg/m³)	Soil Friction Angle (degrees)		Young's Modulus (kN/m²)
			Triaxial	Composite	
12.5	PP-W-SF	2082.4	50	76	2.30E+04
20			48	67	3.00E+04
12.5	PP-W-SB/2-SF	2082.4	50	77	2.5E+04
20			49	75	3.0E+04
25			48	72	3.5E+04
12.5	PP-W-SB/3-SF	2082.4	50	78	3.0E+04
20			49	75	3.3E+04
25			48	72	4.0E+04
12.5	PET-W-MF	2082.4	50	78	4.0E+04
20			49	74	5.0E+04
25			48	73	5.5E+04
50			47	67	6.0E+04

Defining The Composite Element. A UCD specimen which consists of geosynthetic reinforcement and confining soil is defined as a composite element. Composite elements composed of different reinforcements under varying confining pressures can represent the elements within the GRS retaining structures. Therefore, stress and strain levels within the GRS retaining structures can be studied by observing the numerical models assembled by composite elements. Studies of the UCD test results have shown that the composite element has the following features (Boyle and Holtz, 1994, Boyle, 1995):

a) The geosynthetic reinforcement increases the plane strain friction angle of soil. The ratio of the composite plane strain friction angle to that obtained from triaxial tests ranges from 1.40 to 1.56 for different geosynthetics under different confining pressures.

b) The modulus of woven geosynthetics decreases due to very low strain rates and in-soil confinement. As the strain rate decreases, the modulus deduction increases. Modulus deduction is also influenced by the type of synthetic polymer.

---

[1] 23 UCD tests include specimens which are made by four different geosynthetic reinforcements under varied confining pressures.

c) According to the findings, relationship between composite strength properties and strength properties obtained from conventional tests can be represented by the following equations:

$$\phi_c = a*\phi_{tri} + b \quad \text{(Eq. 1)}$$

ϕ_c = GRS composite plane strain friction angle of, in degrees,
ϕ_{tri} = friction angle obtained from conventional triaxial test, in degrees,
a, b = coefficients.

$$M_c = k*M_{wwt} \quad \text{(Eq. 2)}$$

M_c = GRS composite geosynthetic modulus,
M_{wwt} = geosynthetic modulus obtained from in-isolation wide width test,
k = deduction coefficient.

Coefficients a, b, and k should be determined by the UCD test or a similar device which can measure the composite strength properties. However, because of the difficulty and high cost associated with such tests, the following values can be used for estimation[2].

a = 1.5, b = 0,

k = 0.45 for polypropylene geosynthetic reinforcement,
0.80 for polyester geosynthetic reinforcement.

<u>Modeling Test Wall Performance.</u> As in the UCD models, two kinds of test wall models are used in this study. Model WALL-C is the complex model which consists of the UCD-C elements. It includes the elastic material elements, Mohr-Coulomb material elements, and interfaces. Model WALL-S is the simplified model which is composed of the UCD-S elements. Both complex and simplified models use extra Mohr-Coulomb elements with plane strain strength properties[3] to represent the foundation soil and unreinforced backfill. In the WALL-S models, less reinforced zones represented by plane strain elements are inserted between the reinforced layers. A total of 14 wall models have been created for this study so far. Among these, model WALL-C11 (Fig. 3) and WALL-S12 (Fig. 4) are the latest and most developed models. Table 3 summarizes the features of model WALL-C11 and WALL-S12. At present, both models only model the stage from the beginning to the end of construction. The preload stage will be modeled in the further study. Results of models WALL-C11 and WALL-S12 are presented in the following section.

---

[2] Based on data of 32 UCD tests performed by Boyle (1995)
[3] $\phi_{ps}=1.5\phi_{tri} - 17°$ (Holtz and Kovacs, 1981)

Table 3. Features of test wall models WALL-C11 and WALL-S12.

	WALL-C11	WALL-S12
Number of Elastic Elements (represent geosynthetics)	1024	0
Number of Mohr-Coulomb Elements I (represent GRS composite zone)	1024	1024
Number of Mohr-Coulomb Elements II (represent foundation soil and unreinforced backfill [a])	928	1952
Number of Interfaces	64	0
Iteration Time[b] (hours)	48	2.3

[a] Plane strain strength properties were assigned to these elements.
[b] Iteration time using IBM-compatible computer with 486DX_66 CPU and 20MB memory.

RESULTS AND DISCUSSIONS

1. Because a small strain range (less than 2%) is modeled in this study, all UCD test results approach a linear stress-strain relationship in the modeling strain range. Figure 5 shows a typical result of modeling UCD tests. Both the UCD-C complex model and the UCD-S simplified model show a linear behavior in the modeled strain range and have good agreement to the test results.

2. Figure 6 shows the vertical displacement contours of models WALL-C11 and WALL-S12 (contour interval 40mm). Figure 7 shows the horizontal displacement contours of models WALL-C11 and WALL-S12 (contour interval 30mm).

3. Because of the huge increase of iteration time and small affect on the stress-strain levels within the test wall, both WALL-C11 and WALL-S12 didn't model the surface wrapping of the test wall. Therefore, large displacements were found along the surfaces of both models. This is the reason for the high density of displacement contours occur along the surfaces of plots in Figures 6 and 7.

4. In Figure 6, except the "surface falling effect", explained in item 3 above, the average vertical displacement (settlement) along the base of test wall is 43mm for WALL-C11 and 45mm for WALL-S12. Both models show good agreement to the consolidation settlement computed with the assumed foundation soil properties.

5. In Figure 7, failure angles for both models are found to be in the range of 65 to 75 degrees. This range has a good agreement to the location of maximum stress-strain zone observed

from the instrumentation (Fig. 8). Model WALL-C11 shows a curved failure surface and a wider maximum stress-strain zone which is considered to be close to the real situation. Model WALL-S12 shows a narrower maximum stress-strain zone and a straight-line Rankine failure surface because only Mohr-Coulomb material was used in this model.

6. Figure 9 compares the wall face deflections obtained from modeling result to those measured in the field. As shown in the figure, model WALL-C11 overestimates the deflection. However, its result is close to the maximum measured displacement and envelopes the possible range of displacement. Though model WALL-S12 underestimate the deflection results, it predicted a more reasonable wall performance.

7. Figure 10 compares the deflections obtained from modeling to those obtained by inclinometer measurements. Model WALL-C11 overestimates the deflection by a average factor of 2.5. Model WALL-S12 shows a better agreement to the field measurement though it underestimates the deflection.

CONCLUSION

1. Both complex and simplified models acceptably predict the deflection and stress-strain levels of the test wall.

2. The complex model WALL-C11 has advantages of predicting a more accurate failure surface shape, a higher deflection, and soil/geosynthetic interaction. However, its long iteration time is not economic for practical design work.

3. The simplified model WALL-S12 predicts the wall performance in a reasonable range with a much lower iteration time. Its disadvantage is the lack of information on interaction between soil and geosynthetic reinforcement. Though it underestimates the deflection of the test wall, with a good choice of factor of safety, it would be a more economical and practical model for design work.

4. Results of both models prove that the composite element concept is feasible in the design of GRS retaining structures. The composite element approach to GRS retaining structure design can lead to much more economical and efficient designs than those obtained using the conventional tie-back wedge method.

5. Equations 1 and 2 in the proceeding section offer simple and direct estimate of the composite properties. More UCD tests and numerical modeling results are expected in the future to support the feasibility of these relations. Moreover, the design of GRS retaining structures is expected to improve as more information on composite properties is developed.

ACKNOWLEDGEMENT

REFERENCES

Allen, T.M., Christopher, B.R., and Holtz, R.D., (1992), "Performance of a 12.6 m high geotextile wall in Seattle, Washington", Geosynthetic-Reinforced Soil Retaining Walls, Int. Symp. on Geosynthetic-Reinforced Soil Retaining Walls. Balkema Pulb., pp. 81-100.

Bell , J.R., Barrett, R.K., and Ruckman, A.C. (1983), "Geotextile Earth-Reinforced Retaining Wall Tests: Glenwood Canyon, Colorado", Transportation Research Record, 916. pp. 59-69.

Boyle, S.R., (1995), "Deformation Prediction of Geosynthetic Reinforced Soil Retaining Walls", PhD. Dissertation, University of Washington, Seattle, 391p

Boyle, S.R., and Holtz, R.D., (1994), "Deformation Christeristics of Geosynthetic-Reinforced Soil", 5th International Conference on Geotextiles and Geomembranes and related products, Singapore. Vol.1 pp. 361-364.

Christopher, B.R., and Holtz, R.D. (1985), "Geotextile Engineering Manual", Report No. FHWA-TS-86/203, Federal Highway Administration, Washington, D.C., March 1985, 1044p.

Christopher, B.R., Holtz, R.D., and Allen, T.M. (1990), "Instrumentation for a 12.6 m high geotextile-reinforced wall", Performance of Reinforced Soil Structures, British Geotechnical Society Conference, Glasgow. pp. 73-78.

Holtz, R.D., Allen, T.M., and Christopher, B.R., (1991), "Displacement of a 12.6 m high geotextile-reinforced wall", Proc. Tenth European Conference on Soil Mechanics and Foundation Engineering, Florence. pp. 725-728.

Holtz, R.D., and Kovacs, W.D., (1981), "An Introduction to Geotechnical Engineering", Prentice-Hall, Inc., Englewood Cliffs, NJ, 733p

Itasca Consulting Group, (1993), "Fast Lagrangian Analysis of Continua Version 3.2", Itasca Consulting Group, Inc., Minneapolis, MN, Vol. I, II, III,

Steward, J., Willamson, R.J., ans Mohney, J., "Guidelines for Use of Fabrics in Construction and Maintenance of Low-Volume Roads", USDA, Forest Service, Portland, OR, 1977.
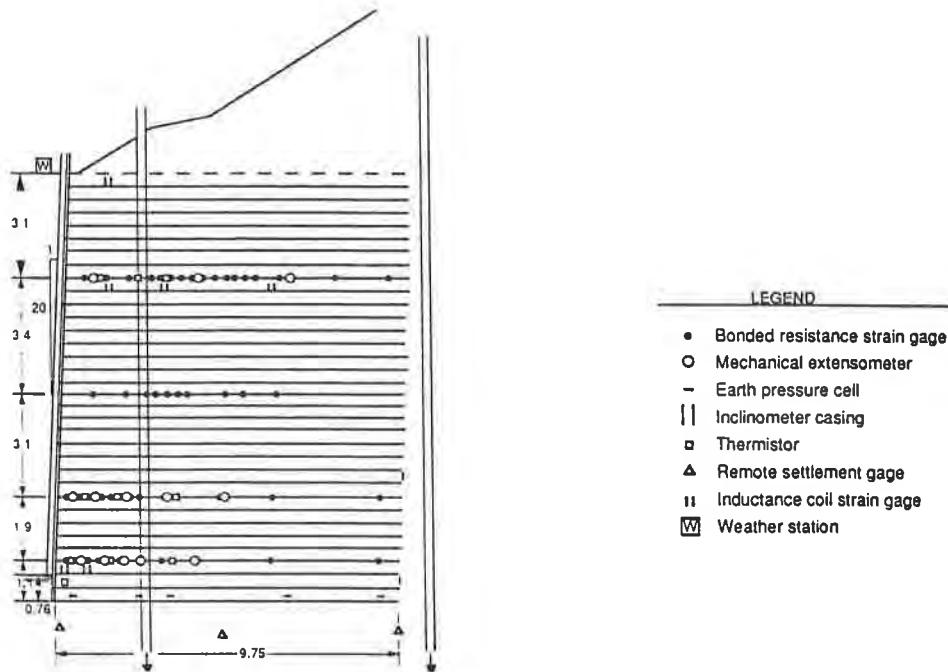
Figure 1. Instrumented wall section (Allen et al. 1992).
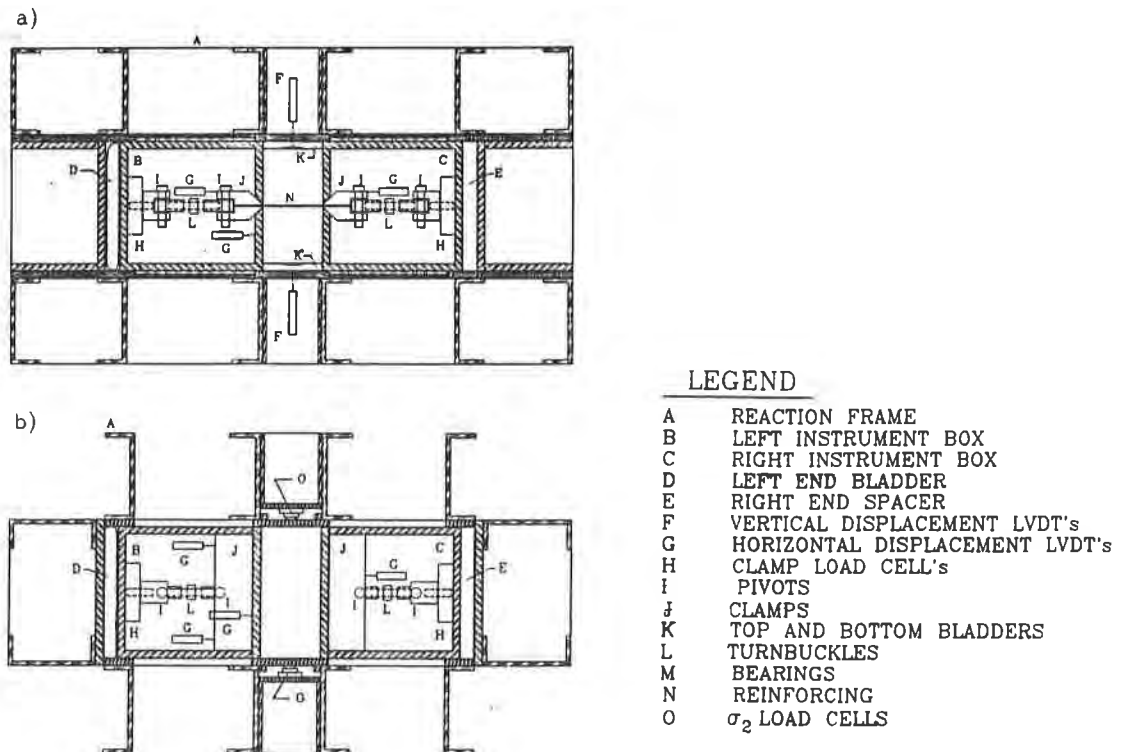
Figure 2. Schematic of Unit Cell Device a) profile cross section b) plan view cross section (Boyle, 1995).

UCD-C model
composite elastic element

composite Mohr-Coulomb element
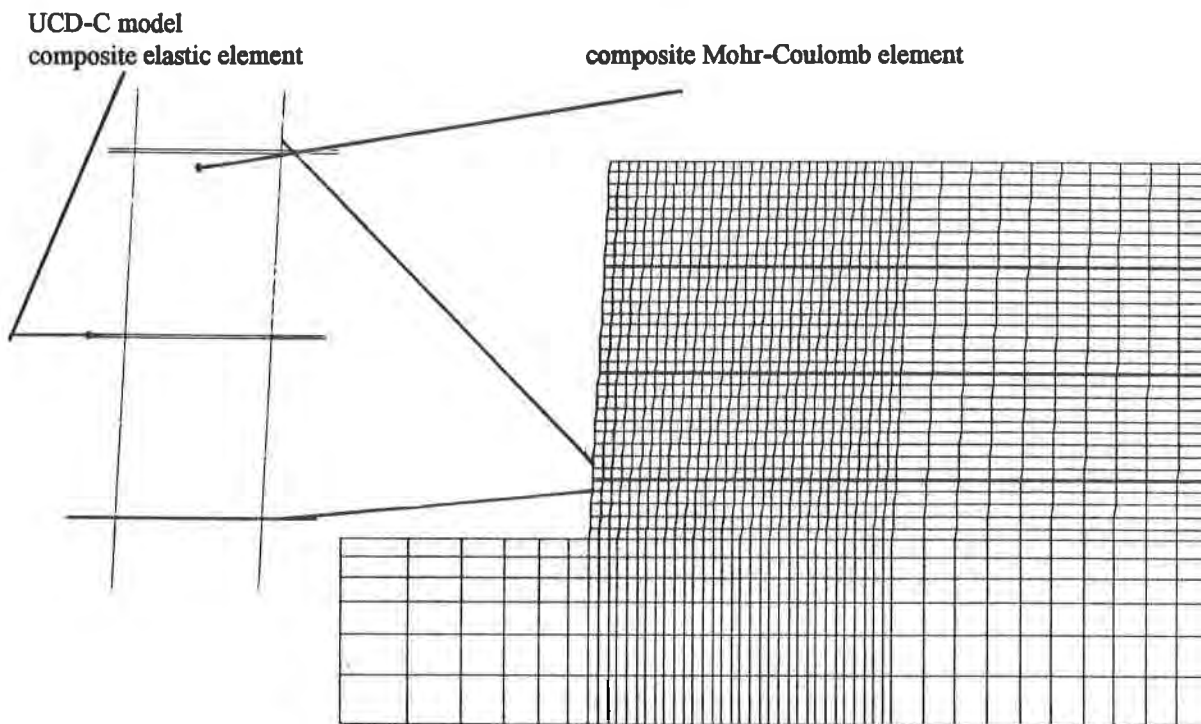
Figure 3. Grids plot of UCD-C model and WALL-C11 model.

UCD-S model
plane strain Mohr-Coulomb element

composite Mohr-Coulomb element
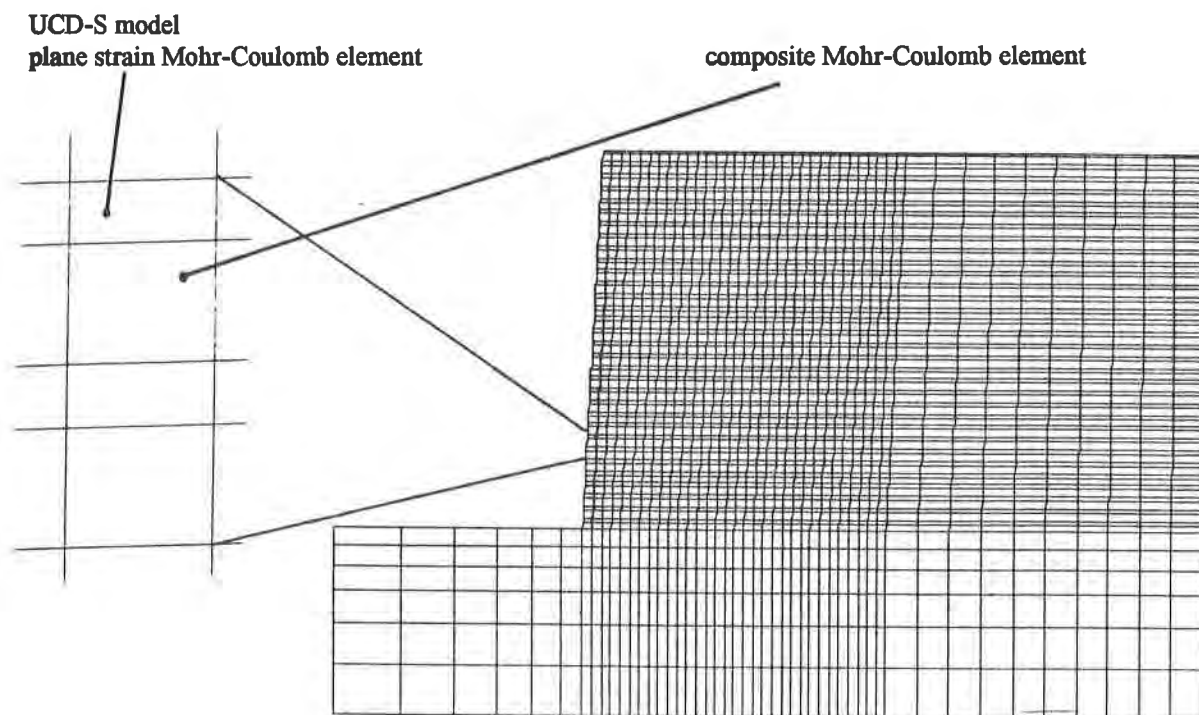
Figure 4. Grids plot of UCD-S model and WALL-S12 model.
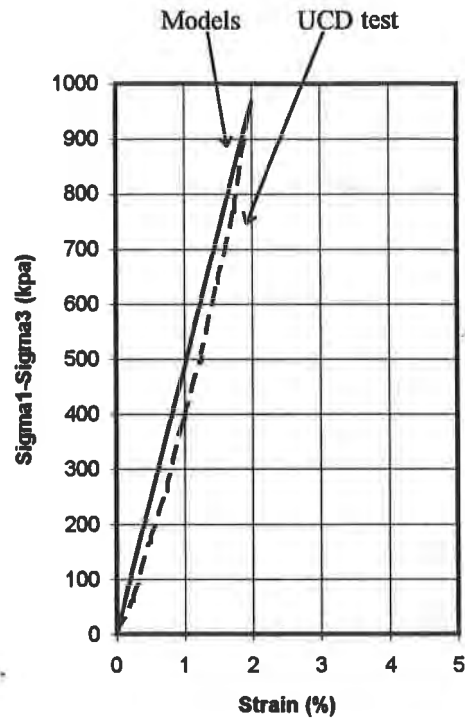
Figure 5. Typical results of UCD test modeling (backfill soil with geosynthetics PET under confining pressure of 12.5 kPa, after Boyle, 1995).
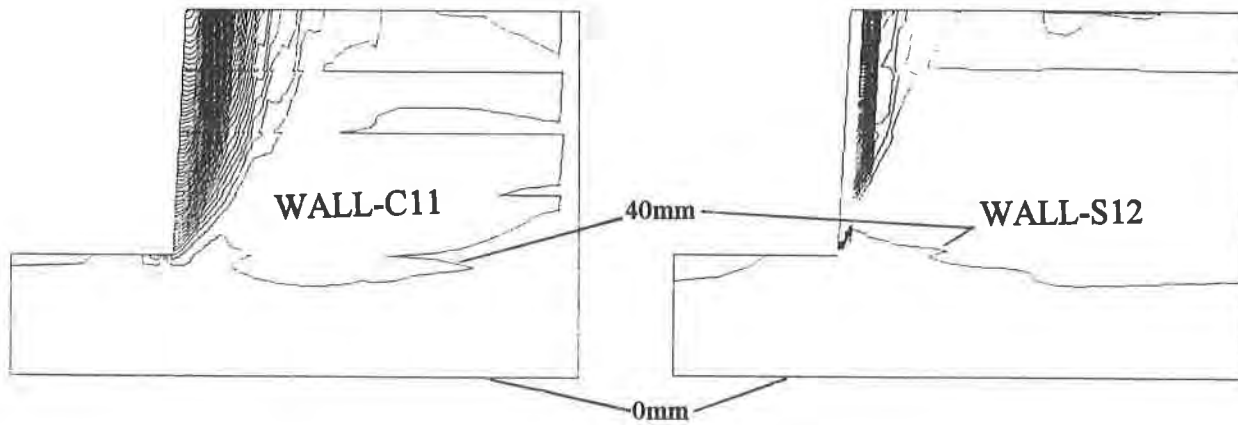
Figure 6. Vertical displacement contours plots of wall models WALL-C11 and WALL-S12.
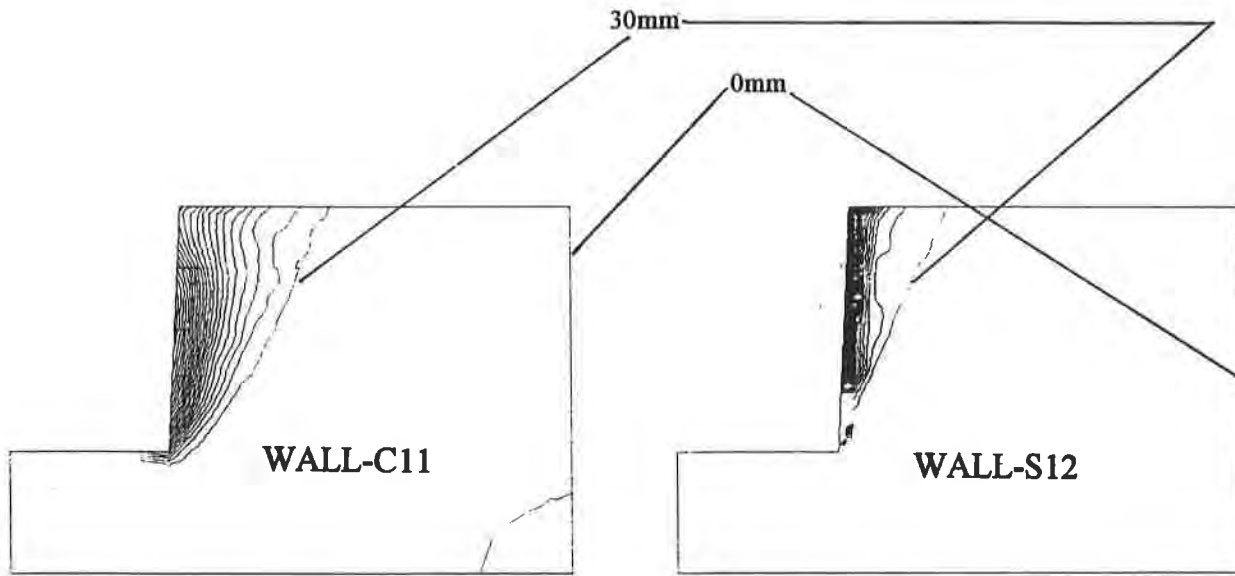
Figure 7. Horizontal displacement contours plots of wall models WALL-C11 and WALL-S12.

Horizontal distance from toe of the wall (m)
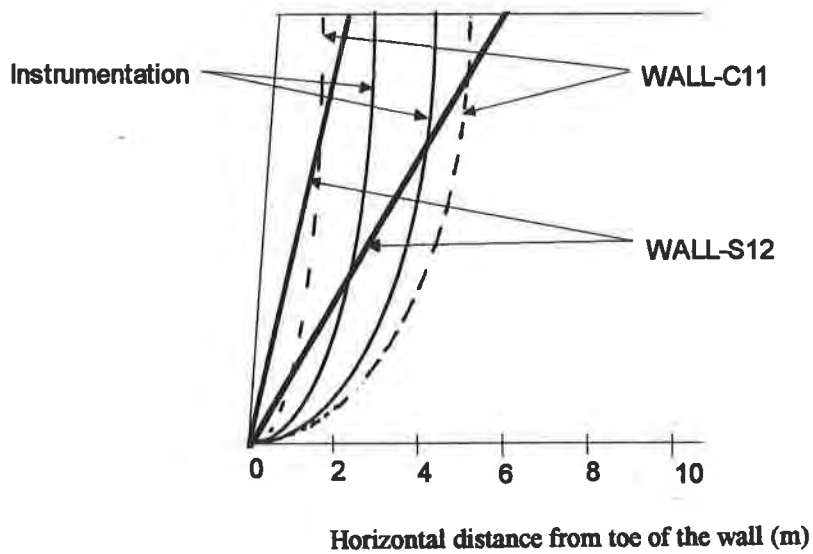
Figure 8. Locations of maximum stress-strain zone from modeling and instrumentation results (after Allen et al., 1992).
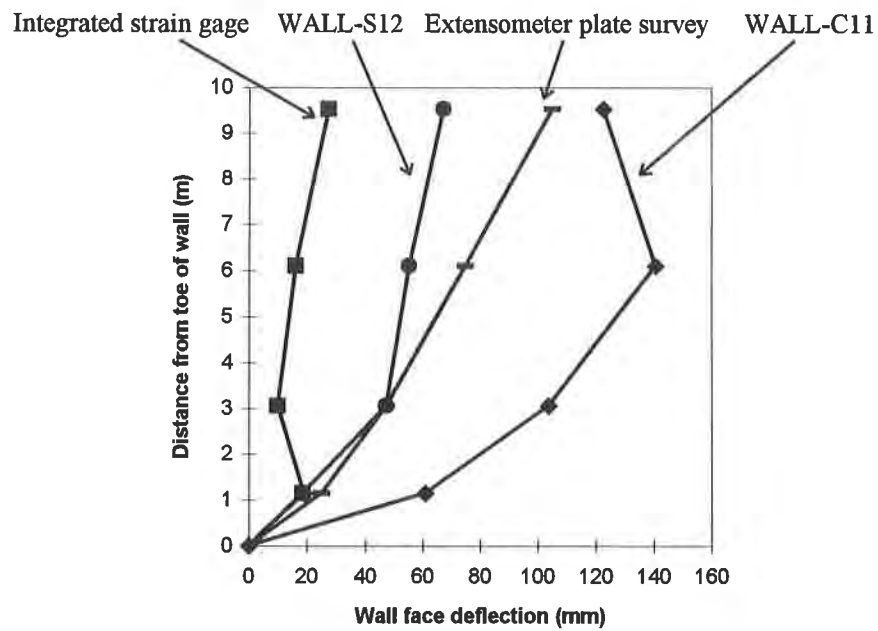
Figure 9. Result of wall face deflection during construction as determined from wall models and various instrumentation methods (after Allen et al., 1992).
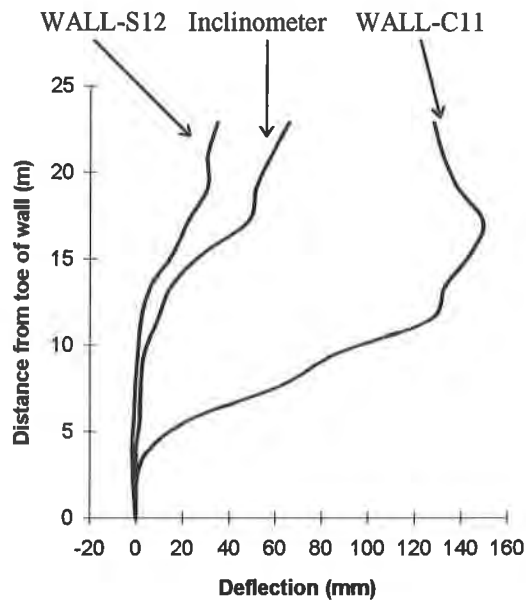
Figure 10. Results of deflection perpendicular to the wall face from modeling result and inclinometer in the middle of the reinforced backfill (after Allen et al., 1992).

HOOP COMPRESSION TESTING OF HDPE LEACHATE COLLECTION PIPE

RICHARD W.I. BRACHMAN
Graduate Student
Geotechnical Research Centre • the University of Western Ontario
London, Ontario • N6A 5B9 • Canada

ABSTRACT

The results from hoop compression tests conducted on leachate collection pipes buried in sand and stone backfills are presented. The comparisons of pipe response for sand and stone backfill indicate that leachate collections pipes experience adverse service conditions when deeply buried in a waste containment facility. Nonuniform deformations and surface strains were measured for the thick high density polyethylene pipe.

INTRODUCTION

High density polyethylene (HDPE) drainage pipes are an important geosynthetic component of the leachate collection system in modern waste containment facilities. They serve the vital role of collecting, transporting and removing contaminants from the facility. Ensuring their structural stability is an important issue during design for the leachate collection system.

Design measures intended to minimize the potential of particulate, chemical and biological clogging of the leachate collection system (see Rowe et al., 1995) can lead to adverse service conditions for the pipe that are not experienced in typical buried pipe applications. For example, stone is often specified as the backfill material surrounding the pipe. The large open void space and small surface area provided by the stone help to minimize biological clogging. However, the use of coarse stone may be detrimental to the pipe performance because of the discontinuous support provided to the pipe. The pipe is supported at discrete points around the circumference by the stone rather than the more continuous support provided by other backfill materials (eg. sand, well graded gravel). Stress concentrations arising from the discontinuous support may significantly affect the performance of the drainage pipes. Thicker polyethylene pipes are typically specified for use in landfill applications as a result of this adverse service condition.

The performance of these geosynthetic materials is a function of both the soil backfill and the pipe. Previous studies (eg. Moore, 1993) have demonstrated that polyethylene pipes behave different than conventional piping materials like steel, aluminum, polyvinyl chloride or fibreglass. These latter materials are stiff in the hoop direction and do not experience circumferential shortening like thin polyethylene pipes. The response of a thick polyethylene pipe is also likely to be different to that of a thin pipe. Laboratory testing of thick high density polyethylene pipes is warranted to identify how these geosynthetic materials perform when deeply buried in a landfill.

Laboratory testing of HDPE drainage pipes (320 mm outside diameter, DR 11) surrounded by two different backfill materials under hoop compression is reported in this paper. The nature of the loading and the details of the test facility are briefly discussed. The materials involved in the tests are summarized. The instrumentation used to measure deformations and surface strains of the pipe are described. Results of the tests conducted with different backfill materials are presented to examine the performance of HDPE drainage pipes under axisymmetric hoop compression.

HOOP COMPRESSION LOADING

Figure 1a isolates the vertical σ_v and horizontal σ_h stresses that develop some distance away from the pipe when deeply buried in a waste containment facility. This loading acting on the soil pipe system may be considered as the sum of a mean component (Figure 1b) and a deviatoric component of loading (Figure 1c) where $\sigma_m = \frac{1}{2}(\sigma_v + \sigma_h)$ and $\sigma_d = \frac{1}{2}(\sigma_v - \sigma_h)$, respectively. The mean component leads to axisymmetric soil and pipe behaviour in response to the mean stress σ_m acting on the soil pipe system. Compressive hoop stresses develop in the pipe when subjected to this load. The deviatoric component of loading features the deviator stress σ_d acting on the soil pipe system. This leads to pipe ovalling with both compressive and tensile hoop stresses in the pipe.
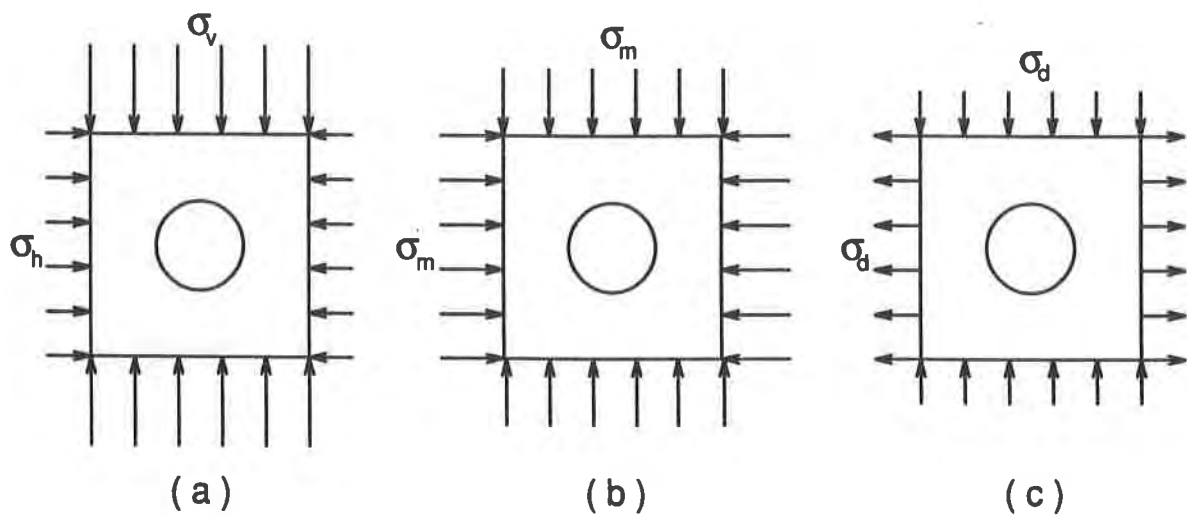
Figure 1. Loading under deep burial (a), mean (b) and deviatoric (c) components

Ideally, any laboratory investigation of buried pipe response would attempt to closely model the biaxial stress state expected under deep burial; such facilities do exist (eg. Brachman et al., 1996). However, it is often advantageous to examine the soil and pipe response subject to the mean (or hoop compression) component of loading only. Hoop compression tests involve simple boundary conditions, require a small volume of soil, and provide results that are relatively straightforward to model and interpret.

The particular details of the hoop compression test cell used to obtain the laboratory results for this paper have been reported elsewhere by Moore et al. (1996). Figure 2 shows plan and elevation sections of the test cell. Figure 3 is a photograph showing a plan view of the pipe, coarse stone backfill, bladder and steel test cell. Essentially, a test specimen of pipe 1.4 m long was placed inside a 0.9 m diameter cylindrical steel test cell with the longitudinal axis of the pipe oriented in the vertical plane. The pipe was surrounded by the backfill soil. Once the lid of the cell was placed, a pressurized air bladder was used to apply a radial stress (p) to the soil pipe system. The bladder pressure p is close to the free field uniform stress σ_m (the soil zone absent beyond the air bladder has a small effect on the stress condition). The pipe response (deformations and surface strains) were recorded as the bladder pressure was applied.
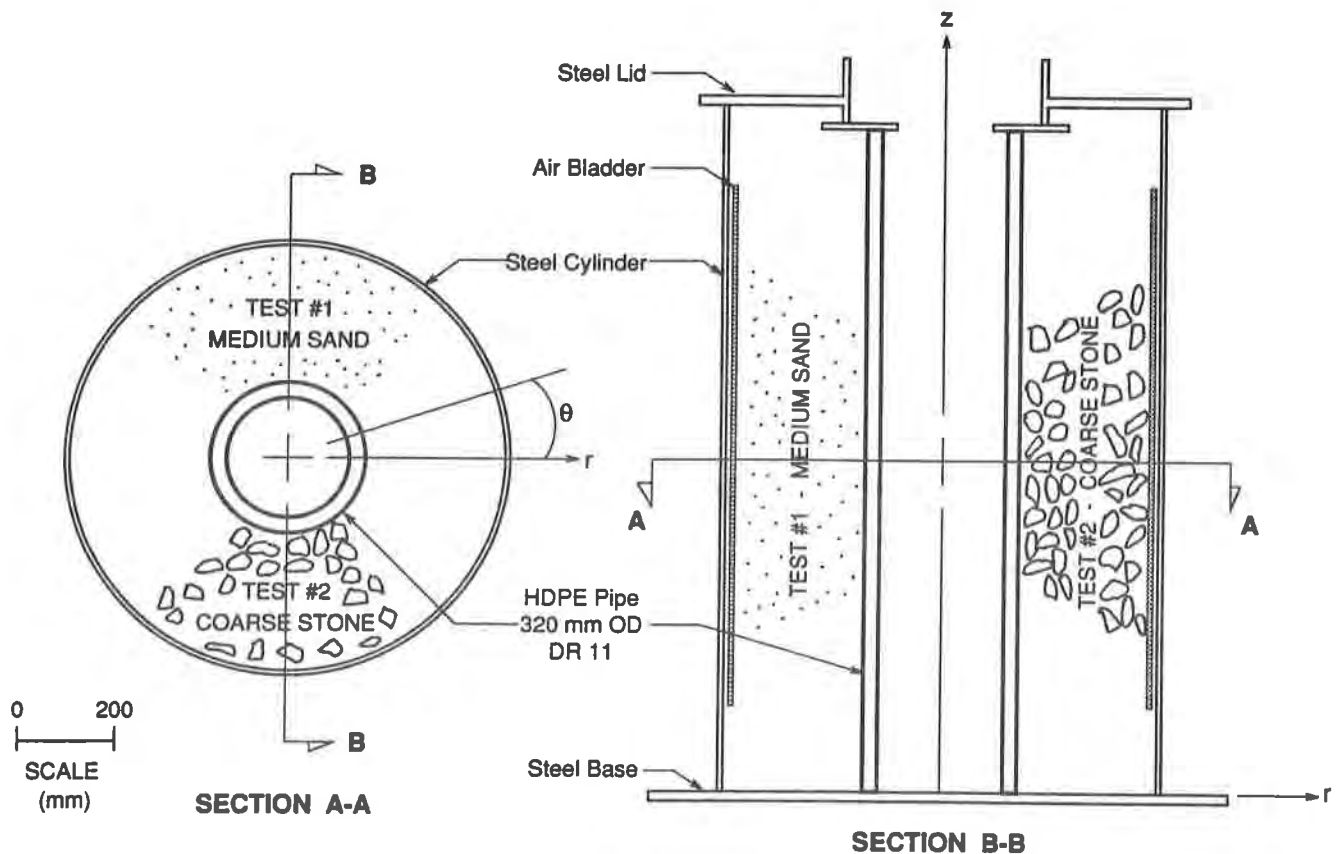
Figure 2. Plan and elevation views of hoop compression testing

Figure 3. Plan view of test cell showing pipe, stone backfill and bladder

BACKFILL MATERIALS

Two different backfill materials were used in the testing. The grain size distribution curves for these two materials are shown in Figure 4. The first material was a poorly graded medium sand (SP) while the second was a poorly graded 50 mm coarse gravel (GP). The 50 mm stone is commonly specified as the drainage medium for leachate collection systems. The two different backfill materials represent different loading conditions for the pipe. The support provided by the sand backfill will tend to be more uniform (the small sand particles provide almost continuous support around the pipe circumference), whereas the coarse stone will provide nonuniform support (discontinuous support from finite number of contact points randomly distributed around the circumference). Figures 3 and 5 show the point loading conditions arising from the coarse stone backfill.

Backfilling procedures were selected to obtain uniform densities within the sand. The material was dumped in place, with the height of the fall constant for each lift. The material was placed in 150 mm thick lifts and was compacted imparting the same energy to each lift (dropping a 7 kg plunger a distance of 300 mm with three passes around the circumference). The densities were measured with a nuclear density meter that was calibrated with sand cone density tests to compensate for the close proximity of the steel and polyethylene. The sand was placed at an average bulk density of 1790 kg/m³, and an average water content of 3.4%. The
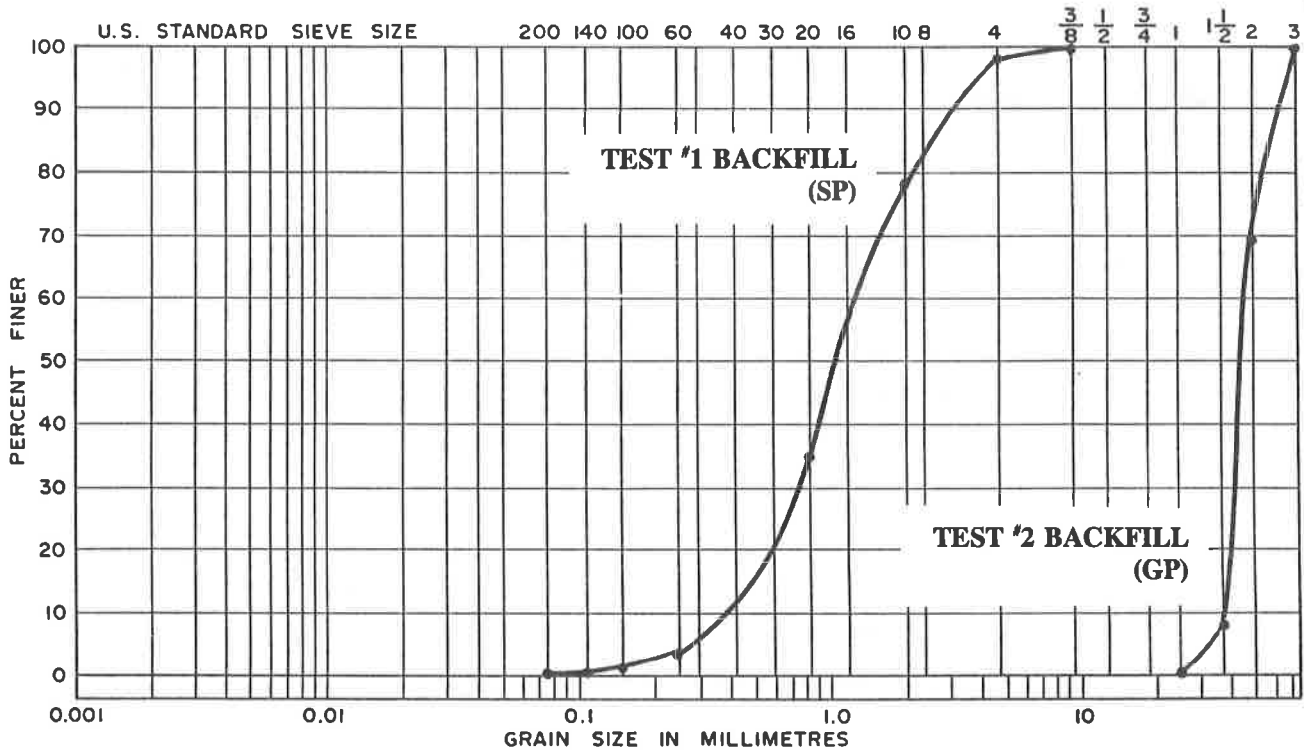
Figure 4. Grain size distribution curves for sand (SP) and stone (GP) backfill

Figure 5. Discontinuous support provided to pipe by 50 mm stone

stone was also dumped into the cell, however, no effort was made to compact the stone. The stone was placed at an average bulk density of 1410 kg/m³. This was obtaining by determining the net weight of the stone in the cell and estimating the volume occupied by the stone.

INSTRUMENTATION

Pipe Deflections. The deflections of the pipe were measured using a laser analog sensor. The laser was mounted on a linear motion block and rail system capable of translating in the vertical (z) direction. Rotation in the circumferential (θ) direction of the entire assembly was achieved using two flange bearings located at the lid and base of the cell. This arrangement allowed the deflection to be measured at any point inside the pipe. The error associated with the laser and repeatability between readings has an estimated tolerance of ± 0.15 mm.

Pipe Strains. The surface strains of the pipe were measured using electrical foil strain gauges. Stacked rosettes with a gauge length of 2 mm were selected to provide a measure of strain over a small region (important when investigating the effect of coarse stone backfill). Strain gauging the interior of a small diameter pipe was not a trivial task. The gauges were applied as specified by the manufacturer.

The layout of gauges for Test #1 was selected to measure the variation of strain in the pipe when uniform backfill support is provided. Four rosettes were placed on the inside surface around the circumference at $\theta = 0°$, 90°, 180° and 270°, and two were placed on the outside at $\theta = 0°$ and 270°, where z= 845 mm. Two single gauges (also 2 mm gauge length) were oriented in the circumferential direction at $\theta = 225°$ and 315° at this section.

The objective of Test #2 was to observe the effect of the coarse stone backfill on surface strains of the pipe. A grid of rosettes located on a small portion of the inside surface of the pipe was selected to monitor the variation of strains beneath one stone contact point. Figure 6 shows the gauge layout. The centre of the grid corresponds to the location $\theta = 270°$ and z = 845 mm, where a stone was placed on the outside of the pipe. A grid marking the location of the gauges was used to position the stone contacts in this region (Figure 5). Carbon paper placed on the outside surface of the pipe was used for recording the location and spacing of the contact points. The rosettes were placed at 22.5 mm centre to centre spacings in the z direction (locations A, B, C, D and E) and at 18 mm spacing in the θ direction (locations F, G, C, H and I). This grid allowed the variations in circumferential and axial strains to be observed both in the z and θ directions beneath one stone contact point. Two rosettes were also located at opposite points B and D on the outside surface of the pipe.

The potential that the strain readings can be affected by the presence of the gauge itself is acknowledged (eg. Beatty and Chewning, 1979). This arises as the stiffness of the gauge (metal foil, polymer backing and glue) is similar to that of the polyethylene. Comparisons between measured strains (using strain gauges) and calculated strains (based on measured deflections) will be made to observe the stiffening effect of local strain readings.
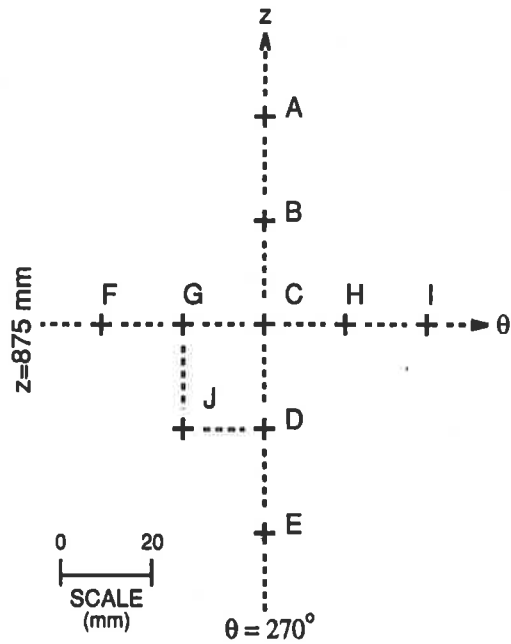
Figure 6. Location of strain gauges for Test #2

TEST #1 RESULTS - SAND BACKFILL

The load path followed for Test #1 is shown in Figure 7, plotting the bladder pressure p against the elapsed time of the test. The 50 kPa increments of pressure were rapidly applied and kept constant for a 10 minute duration. The maximum pressure of 500 kPa corresponds to overburden loading of 50 m of waste, assuming γ_{waste} = 10 kN/m^3. Pipe deformations, surface strains, and gauge stiffening results from Test #1 are examined.
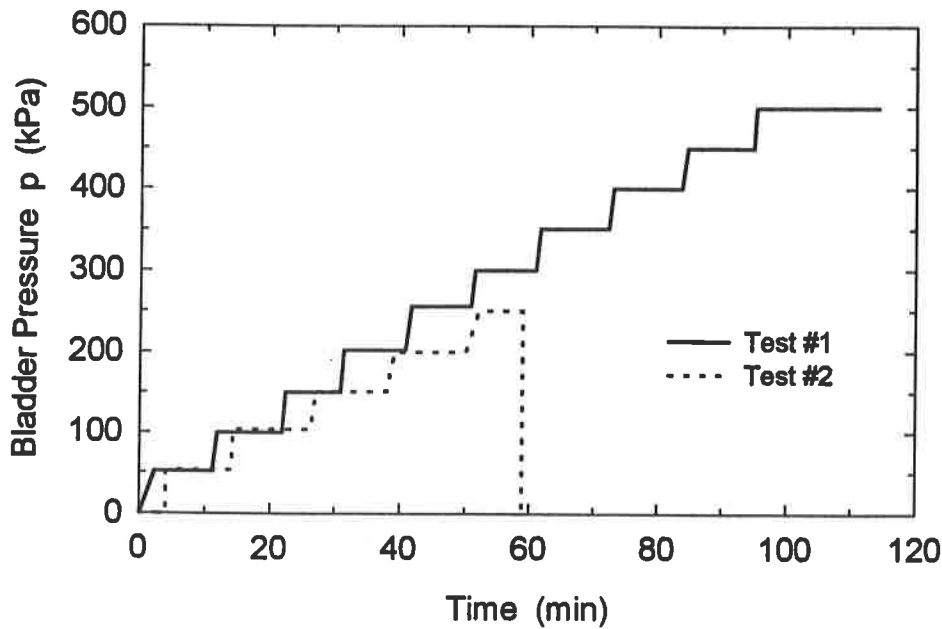
Figure 7. Load paths for Test #1 and #2

Pipe Deformations. The deflected shape of the pipe when tested in the sand backfill is plotted in Figure 8a for the central section (z = 700 mm). Values are shown for applied bladder pressures of p = 0 (initial shape), 250 and 500 kPa, and are magnified by a factor of twenty. These plots are presented to observe the mode of deformation of the pipe when subjected to hoop compression loading. The diameter decreases as pressure is applied. There appears to be a shift in the position of the pipe as it translates down and to the right. Excluding the rigid body translation, axisymmetric deformations were experienced by the pipe. At an applied pressure of 500 kPa, the average diameter change (ΔD) is -1.49 mm, with a 15% difference between the largest (-1.6 mm) and smallest (-1.35) measured values across diameters 0° - 180° and 90° - 270°, respectively.
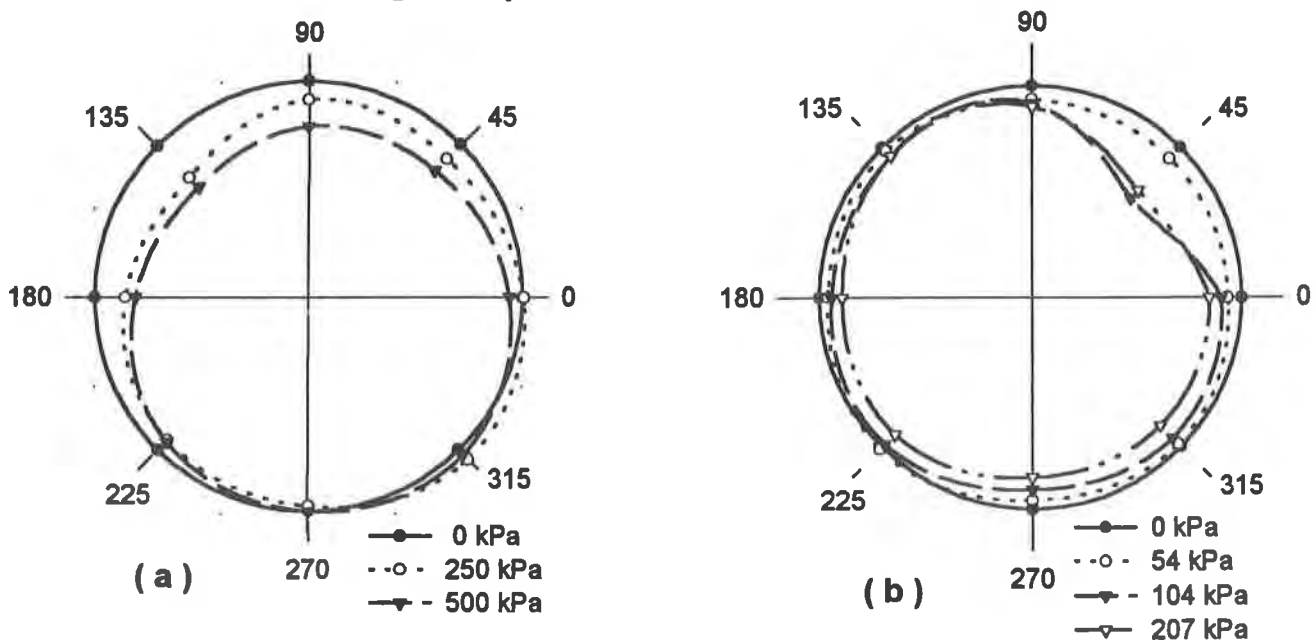
Figure 8. Deflected shape (x 20) at central section for Test #1 (a) and Test #2 (b)

Surface Strains. The circumferential (ϵ_θ) and axial (ϵ_z) surface strains of the pipe are now examined. The strain values are plotted against time, with compressive strains negative. Strain values are expressed as micro-strain ($\mu\epsilon$), where 1000 $\mu\epsilon$ is 0.1% strain.

Figure 9 plots the measured circumferential strains on the inside surface of the pipe for Test #1 at z=810 mm. Values are shown for ϵ_θ measured at four circumferential positions (θ= 0°, 90°, 225°, and 270°). The circumferential gauges located at θ=180 and 315° did not provide readings (damaged lead wire connections). The strain rapidly increased when the bladder pressure was applied followed by a creep component of strain for the remainder of each increment. The measured values of ϵ_θ became increasingly negative under hoop compression loading, and reached an average value of ϵ_θ = -4360 $\mu\epsilon$ at a time of 112.4 minutes (p = 500 kPa). A 4% difference was observed between the maximum value (ϵ_θ = -4450 $\mu\epsilon$) measured at 270° and the minimum value (ϵ_θ = -4260 $\mu\epsilon$) recorded at 90° for this load level. Overall the strain readings in the circumferential direction were uniform.
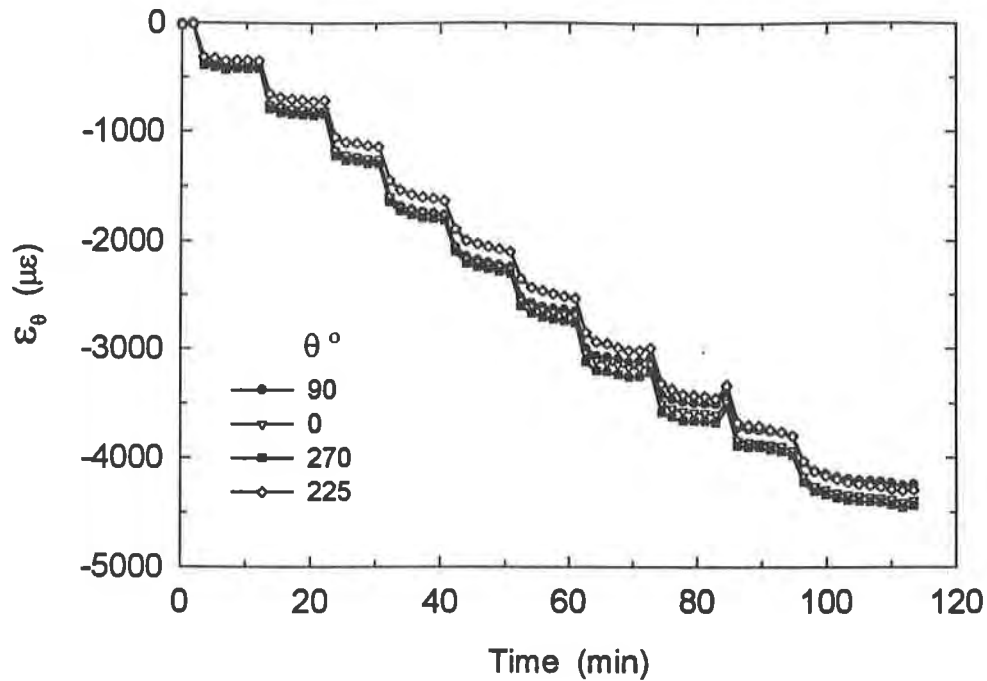
Figure 9. Measured circumferential strains (ϵ_θ) for Test #1

The effect of the gauge stiffness upon the local strain readings may be observed by comparing circumferential strain values measured using strain gauges with values calculated based on measured deflections. For axisymmetric conditions where there is no variation of circumferential deflections in the circumferential direction (ie. $\partial \rho_\theta / \partial \theta = 0$), the strains on the inside surface of the pipe can be expressed as $\epsilon_\theta = \Delta D / D_i$, where D_i is the inside diameter of the pipe. Figure 10 shows that the average strain measured with the strain gauges ($\epsilon_{\theta \, avg}$) is consistently smaller in magnitude than the strain computed from the average diameter change ($\Delta D_{avg}/D_i$). Apart from some scatter of the values based on deflections at pressures of 150 kPa and 450 kPa, the two curves exhibit similar trends. At an applied bladder pressure of 500 kPa the strain gauges detect only 73% of the circumferential strain calculated based on deflections. The strain gauge readings are consistently smaller because of a reinforcing effect provided by the gauge itself. The stiffness of the gauge is similar to that of the polyethylene, resulting in a local perturbation in the strain field beneath the gauge. Surface strain readings on polyethylene obtained from conventional strain gauges should be corrected for this stiffening effect. For the remainder of this paper, comparisons are made based on measured (uncorrected) strain values.

The axial strains measured on the inside surface at this section (z = 810 mm) are presented in Figure 11. Values of ϵ_z are shown for locations $\theta = 0°$, 90°, 180°, and 270°. The axial strains feature a similar pattern as ϵ_θ, with a rapid increase in strain followed by a creep component. The measured ϵ_z values increase to an average value of 2890 $\mu\epsilon$ at 112.4 minutes (p = 500 kPa). These strains are positive implying extension of the inner surface of the pipe in the axial direction.
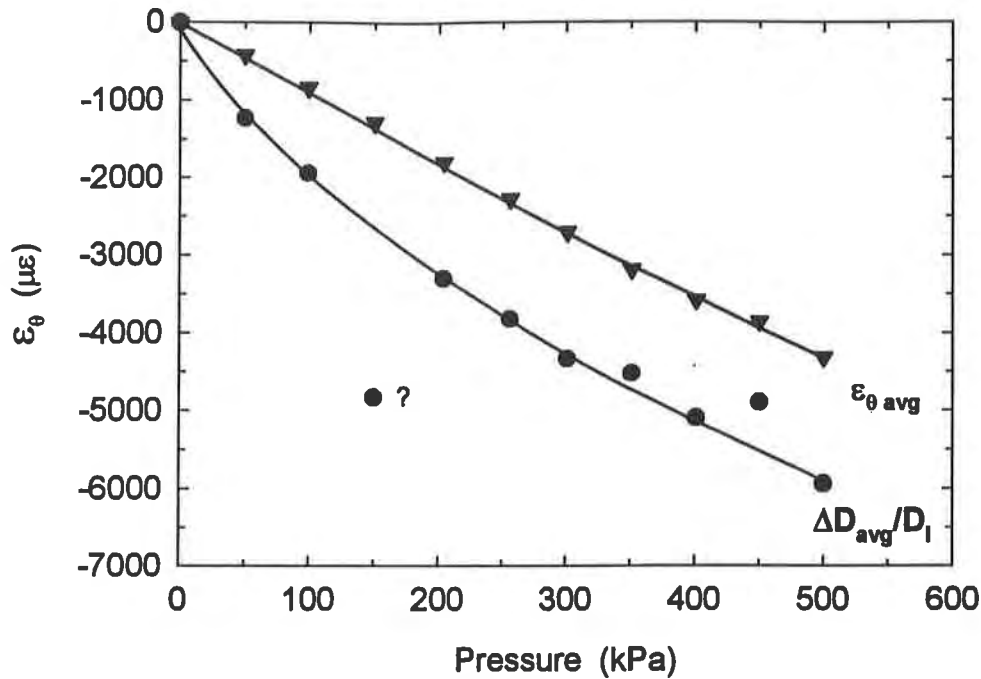
Figure 10. Stiffening effect for strain gauges on polyethylene surface

The positive axial strains measured in this test result from lack of confinement in the axial direction. The deflection of the lid of the cell was estimated to be 3 mm when the bladder was at a pressure of 500 kPa, which corresponds to an axial strain of roughly 2100 $\mu\epsilon$. The hoop compression cell was originally designed for testing large diameter profiled wall polyethylene pipes which feature a small cross-sectional area. However, for thick pipes that feature a large cross-sectional area, coupled with the high Poisson ratio for polyethylene ($\nu=0.46$), large axial forces are generated during testing. The stiffness of the steel lid and insert plate were not sufficiently high to obtain the plane strain conditions ($\epsilon_z = 0$) that are expected to prevail in the field. The end restraint conditions for this test are probably closer to plane stress conditions ($\sigma_z = 0$) which are also relevant for the leachate collection pipe problem (eg. pipe leading into manhole). Another component of the observed axial strains arises from longitudinal bending of the pipe because the load is not applied across the entire pipe length.

The axial strains vary more than the circumferential strains. There is a 20% difference between ϵ_z values measured at $\theta = 0°$ and 90°. This variation arises because of bending in the axial direction that tends to reduce the axial strains at $\theta = 0°$ and 270° and increase the values at $\theta = 90°$ and 180°. This bending is consistent with the deformations depicted in Figure 8.

TEST #2 RESULTS - STONE BACKFILL

The load path followed for Test #2 (Figure 7) was similar to that for Test #1. The maximum pressure obtained in Test #2 was 250 kPa, limited because the bladder failed at this load level. A pressure of 250 kPa is equivalent to an overburden stress of 25 m of waste ($\gamma_{waste} = 10$ kN/m³). The deformations and surface strains for Test #2 are now presented.
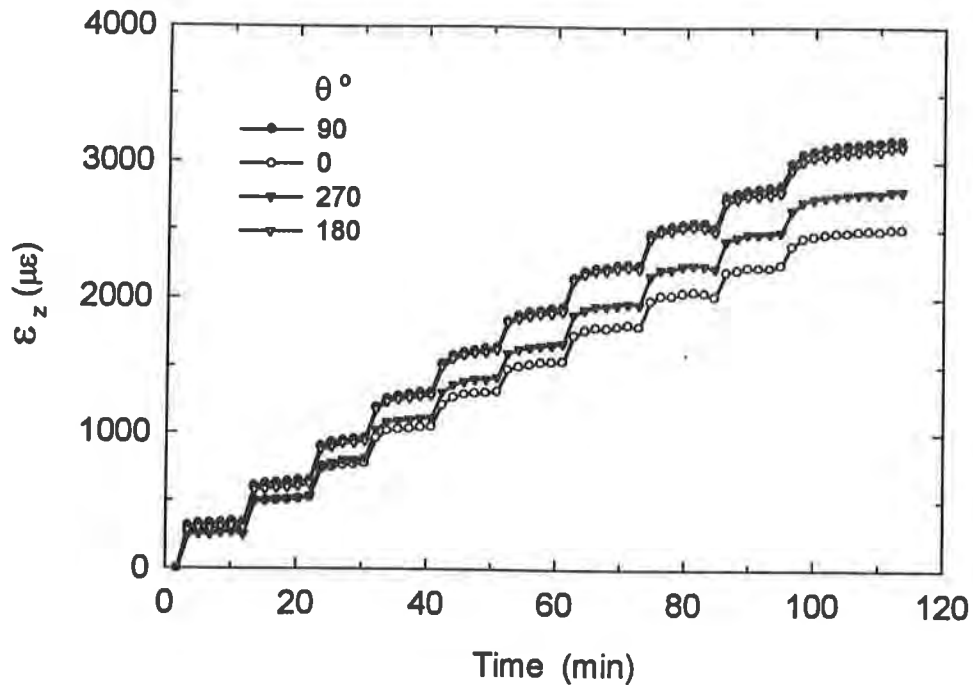
Figure 11. Measured axial strains (ϵ_z) for Test #1

Pipe Deformations. The deflected shape of the pipe when tested with the 50 mm stone backfill is plotted in Figure 8b for four load levels (0, 54, 104 and 207 kPa), and again, the deformations are magnified by a factor of 20. The deflected shape is roughly circular for the first load increment 54 kPa. For the next and all subsequent load levels, the deflected shape is nonuniform with a large deflection observed at $\theta = 45°$. At a pressure of 207 kPa, the diameter change is -2.25 mm across the 45° - 225° diameter, while it is equal to -1.6, -1.5 and -1.2 for diameter lines 0° - 180°, 90° - 270°, and 135° - 315°, respectively. It is challenging to physically account for the large deflection observed at 45°. The possibility that this is a result of a laser error was ruled out because of the consistency of deflection readings at this point for all load levels in this test. Similar nonuniform deflections were observed at other sections in this and another test. Therefore, the nonuniform deflections are directly attributed to the discontinuous support provided to the pipe from the coarse stone backfill.

Surface Strains. The variations of surface strains are examined to determine the effect of the discontinuous support provided by the coarse stone backfill. First, variations of circumferential strain are examined. The variation of ϵ_θ in the circumferential direction is plotted in Figure 12 showing strain measured at points F, G, C, H, and I of the strain gauge grid (Figure 6). The strains increase to a maximum average value of -1970 $\mu\epsilon$ at 58 minutes (p = 250 kPa). The sudden decrease in strain at 58.7 minutes corresponded to the failure of the bladder. There is 38% difference in ϵ_θ between points G and I at a time of 58 minutes. The maximum value at this pressure was measured at point G (ϵ_θ = -2380 $\mu\epsilon$) and the minimum value at point I (ϵ_θ = -1490 $\mu\epsilon$). Variation of ϵ_θ in the axial direction is plotted in Figure 13 for points A, B, C, D, and E of the grid (Figure 6). At the same load level (p = 250 kPa), there

is a 27% difference between the measured maximum (ϵ_θ = -2120 $\mu\epsilon$) and minimum (ϵ_θ = -1540 $\mu\epsilon$) values at points B and E, respectively.

The circumferential strain readings from the sand test were used to demonstrate that consistent strain readings could be reproduced under axisymmetric conditions. Therefore, the observed variation in circumferential strain for Test #2 is attributed to the point loading conditions imposed by the 50 mm stone backfill. The following observations can be made regarding the variation of circumferential strain on the inner surface of the pipe:

- the maximum ϵ_θ values were measured in between closely spaced contacts (Points B, F, and G),
- the next highest values were measured at points directly beneath stone contacts (Points C and A),
- the lowest values measured were at points between widely spaced contacts.
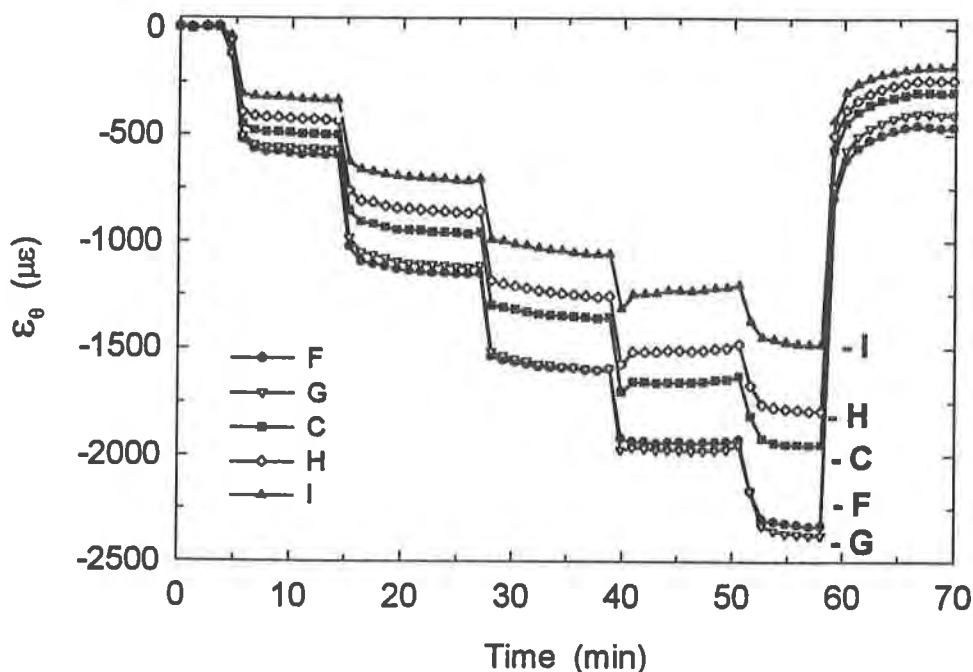
Figure 12. Variation of ϵ_θ in the circumferential direction for Test #2

The variation of axial strains in the circumferential direction are examined in Figure 14 for points F, G, C, H, and I of the strain gauge grid (Figure 6). There is a 43% variation in ϵ_z between points C and F at 250 kPa. These variations are also attributed to the point loading of the coarse stone on the pipe, as they occurs over a small section of the pipe interior.

Strain variations of the order of 40% have been measured on the inside surface of the pipe. These variations occur because of the discontinuous support provided to the pipe from the coarse drainage stone. The stress concentrations resulting from the point contact loading are of practical interest to the engineering community. Computation of stresses from measured values

of surface strain is not a trivial exercise. Issues such as the strain gauge stiffening effect, selection of a modulus value for polyethylene, and thick pipe response complicate the computations of stress from values of surface strain. It is likely that the stresses within the pipe vary in a similar manner to those observed for the surface strains. Further work is required to characterise the stress distribution in the pipe beneath the stone contacts.
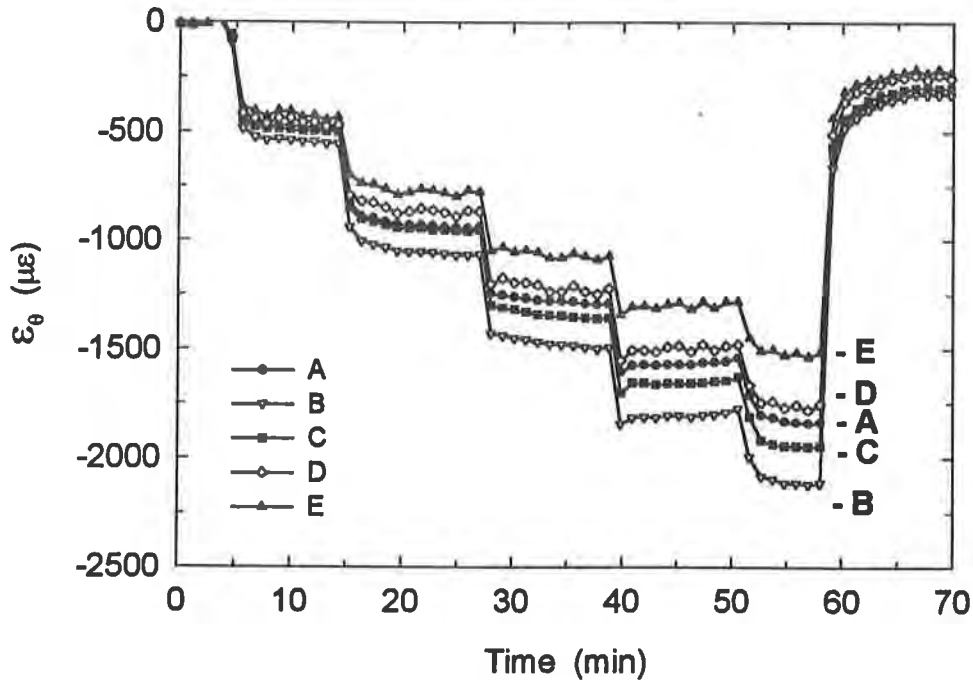
Figure 13. Variation of ϵ_θ in the axial direction for Test #2
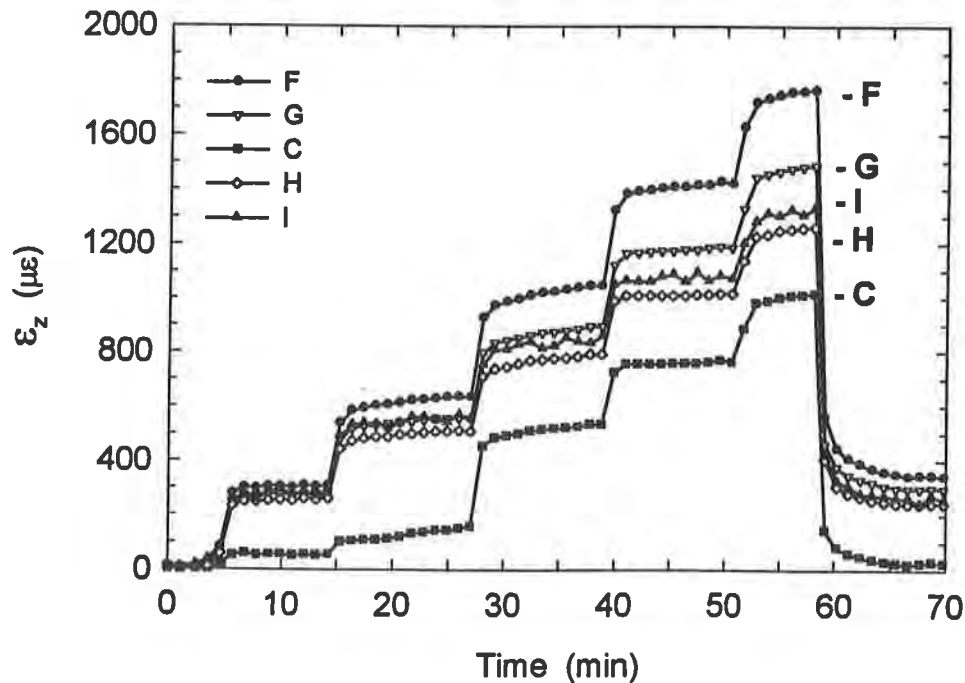
Figure 14. Variation of ϵ_z in the circumferential direction for Test #2

SUMMARY

The results of hoop compression tests for 320 mm diameter, DR 11 HDPE drainage pipes tested with medium sand and coarse stone backfill materials were presented. The loading conditions, test cell features and instrumentation were described. When tested with the sand backfill the thick polyethylene pipe response was largely axisymmetric. The measured diameter changes of the pipe were uniform, although some translation was observed. The measured circumferential strains closely matched each other demonstrating that consistent reading could be obtained. Axial restraint was closer to plane stress conditions. A stiffening effect of strain readings using electrical foil strain gauges was observed. The results of the test conducted with coarse stone backfill demonstrated that nonuniform pipe deflections occur because of the discontinuous nature of support provided to the pipe by the stone. Circumferential and axial strains on the inside surface of the pipe varied over 40% beneath one stone contact. Comparison of tests with medium sand and coarse stone backfill materials demonstrated the adverse conditions a leachate collection pipe experiences when deeply buried in a leachate collection system. Further research is warranted to better characterize the thick polyethylene pipe response under these loading conditions.

ACKNOWLEDGEMENTS

REFERENCES

Beatty, M.F., and Chewning, S.W. 1979. Numerical analysis of the reinforcement effect of a strain gauge applied to a soft material, Int. J. of Eng. Sci., Vol. 17, pp. 907 - 915.

Brachman, R.W.I., Moore, I.D., and Rowe, R.K. 1996. A new laboratory facility for evaluating the performance of small diameter buried pipes, 1996 Annual Conference of the Canadian Society for Civil Engineering, May 29 to June 1, Edmonton, pp. 72 - 83.

Moore, I.D., Laidlaw, T.C., and Brachman, R.W.I. 1996. Test cells for static pipe response under deep burial, 49th Canadian Geotechnical Conference of the Canadian Geotechnical Society, September 23 to 25, St. John's Newfoundland, Canada, pp. 737 - 744.

Moore, I.D. 1993. Structural design of profiled polyethylene pipe - Part I - Deep burial, Geotechnical Research Centre Report GEOT-8-93, University of Western Ontario.

Rowe, R. K., Quigley, R.M., and Booker, J.R. 1995. Clayey Barrier Systems for Waste Disposal Facilities, E & FN Spon (Chapman & Hall), London.

EVALUATION OF NEEDLE PUNCHED GEOSYNTHETIC CLAY LINERS' INTERNAL FRICTION

J.F. Berard, Ecole Polytechnique de Montreal, Canada

The goal of this research program was to evaluate in laboratory the internal shear stress resistance parameters for needle-punched GCLs.

The testing program was performed with a 305 by 305 mm direct shear box on 6 (six) different needle-punched GCLs. Shear rates of 1.0, 0.1 and 0.01 mm per minute, as well as normal stresses of 25, 50 and 100 kPa were used at different moisture contents of the bentonite to simulate various conditions.

It has been observed that changing the moisture content of the bentonite or the shear rate affects the internal shear resistance of a needle-punched GCL. It is imperative that these parameters be fixed in order to develop a standard test procedure to determine the internal shear resistance of this material.

INTRODUCTION

Since the mid 1980's various types of geosynthetic clay liners, also known as geoclay liners (GCLs), have been used either as impervious barriers, separators or protective layers. Their ability to withstand internal shear forces can be a key factor, especially where GCLs are installed on a slope and when a vertical load is applied (a landfill would be a good example).

According to ASTM D4439, a GCL is a factory manufactured, hydraulic barrier typically consisting of bentonite clay or other very low permeable material, supported by geotextiles and/or geomembranes which are held together by needling, stitching or chemical adhesives.

The goal of this research program was to evaluate in laboratory the internal shear stress resistance parameters for needle-punched GCLs. Testing under various conditions enabled the isolation of different variables each having an effect on the peak internal shear strength of the GCLs studied. The direct shear testing was performed in general accordance with the ASTM standard test method D 5321-92, "Determining the Coefficient of Soil and Geosynthetic or Geosynthetic and Geosynthetic Friction by the Direct Shear Method".

EXPERIMENTAL PROGRAM

Materials. The needle punched GCLs used consisted of powdered sodium bentonite confined between a woven and non-woven geotextiles. The manufacturing process, by which the needle punched reinforcement is achieved, consists of pushing needles through the top non-woven geotextile, the full thickness of the bentonite and the bottom woven geotextile, allowing the fibers from the first geotextile to anchor themselves into the second geotextile. The two geotextiles are then said to be needle punched together, securing the bentonite in place and reinforcing the layer of clay (bentonite) over the entire surface of the GCL. A density of approximately 2.5 million fibers per square meter is achieve, creating a quasi continuous bonding between the two geotextiles.

Bentonite is a clay mineral consisting mostly of the mineral montmorillonite, with low permeability, expansive characteristics and high absorption capacity. Sodium bentonite has a greater water absorption capacity then calcium bentonite and is generally preferred in the making of GCLs. An extensive description of various clay minerals was done by Mitchell (1993).

Six different needle punched samples were tested under various conditions. The difference between the samples consisted mostly in the use of different woven geotextiles. Prior to performing any shear resistance test, each sample was characterized by the mean of a peel test, performed in general accordance with ASTM D4437. Peel tests results are presented in Table 1 below. This standard is generally used to peel apart two sections of geomembrane connected together by a welded seam. The result indicates what is the necessary force in Newton in order to separate or peel the two sections if the width of the weld were equal to 10 cm. The test is

performed at a speed of 50 mm per minute. The thickness and mass per unit area for each GCL are also given in Table 1.

Table 1. Various Properties of the GCLs

GCL Number	Peel Resistance (N/10cm)	Thickness (mm)	Mass per Unit Area (kg/m^2)
1	55	7.2	5.0
2	78	7.6	5.8
3	183	7.9	5.0
4	40	7.2	5.0
5	71	7.6	5.8
6	131	7.9	5.0

There is no standard for peel tests applied to GCLs. Nevertheless, using the method previously described seemed to be applicable to GCLs, considering that the end result between a peel test and a shear test is very similar, that is the rupture of all bonds between the two geotextiles. The major difference is the fact that the bentonite in the GCL does not contribute in the peel test, whereas in the shear test a small portion of the shear resistance can be attributed to the bentonite.

Experimental Set-Up. The testing program was performed with a 300 by 300 direct shear box, and the following parameters were used:

- 6 different GCL samples
- 3 shear rates: 1, 0.1 and 0.01 mm per minute
- Various degrees of hydration: dry (ambient conditions), partially and fully hydrated
- 3 normal stresses: 25, 50 and 100 kPa

The GCL samples were soaked under various loads for different periods of time, ranging from 2 hours to over 14 days. The samples were always hydrated with distilled water. The appropriate normal stress (25, 50 or 100 kPa) was applied prior to the soaking, in a separate apparatus which allowed to prepare up to four samples at the time. Normal stresses were applied using four separate pneumatic bellows, on an area of 300 by 300 mm, corresponding to the area where the fiber reinforcement was kept intact prior to shearing the GCL. Also, a thin geomesh similar to a window screen was placed against the two geotextiles, in order to bring water to the center of the sample and therefore allow the hydration process to be more uniform over the area to be sheared.

The upper and lower boxes of the shearing device have been filled with concrete, and a layer of abrasive sand (St-Canut sand, No. 10) was glued with epoxy on both faces in contact with the GCL. The sand provided a good adhesion between the boxes and the two geotextiles of the GCL, therefore mobilizing the full length of the sample during the shear test. Clamping

devices located on each box were used to fix the geotextiles to the appropriate box. A pneumatic bellow was used to apply the normal load. The stationary section was the upper box (300 by 300 mm) and the traveling section was the lower one (300 by 500 mm). The lower box was allowed to move for at least 50 mm during the shear test.

In each test, the two geotextiles of a new GCL sample were attached to the upper and lower shear box with compression clamps to confine failure to the needle punched bentonite interface. Oversized samples (in length) were used in order to keep a constant area while shearing. Each sample had an initial area of 300 by 300 mm kept intact while the needle punched fibers outside that area were cut, shortly before shearing, either by gently peeling the GCL by hand or by carefully cutting them with a knife.

The use of a loading and soaking device separated from the shear box required that each sample be unloaded, moved and installed on the shearing device before the normal stress could be reapplied. The period of time required to complete the operation was critical because while unloaded the bentonite was free to swell, therefore it had to be kept to a minimum. A period of about 15 to 20 minutes was required to complete the sample transfer from one apparatus to the other, and to reapply the normal stress.

Bentonite samples were taken for water content evaluation from the GCLs after shearing, and visual inspection of the sheared surfaces was also done.

RESULTS AND DISCUSSION

Laboratory Test Results. A total of 132 GCL samples were sheared in undrained conditions due to the relatively high shear speeds used. A typical set of results is presented in Figure 1a). These results are from the GCL No. 2 sheared at 0.1 mm per minute after being hydrated for more than 14 days. Each normal load (25, 50 and 100 kPa) will yield a different maximum shear resistance. Figure 1b) shows the relation between normal load and maximum shear resistance, from which it is possible to measure the Mohr-Coulomb parameters C (cohesion or adhesion) and ϕ (angle of internal friction).
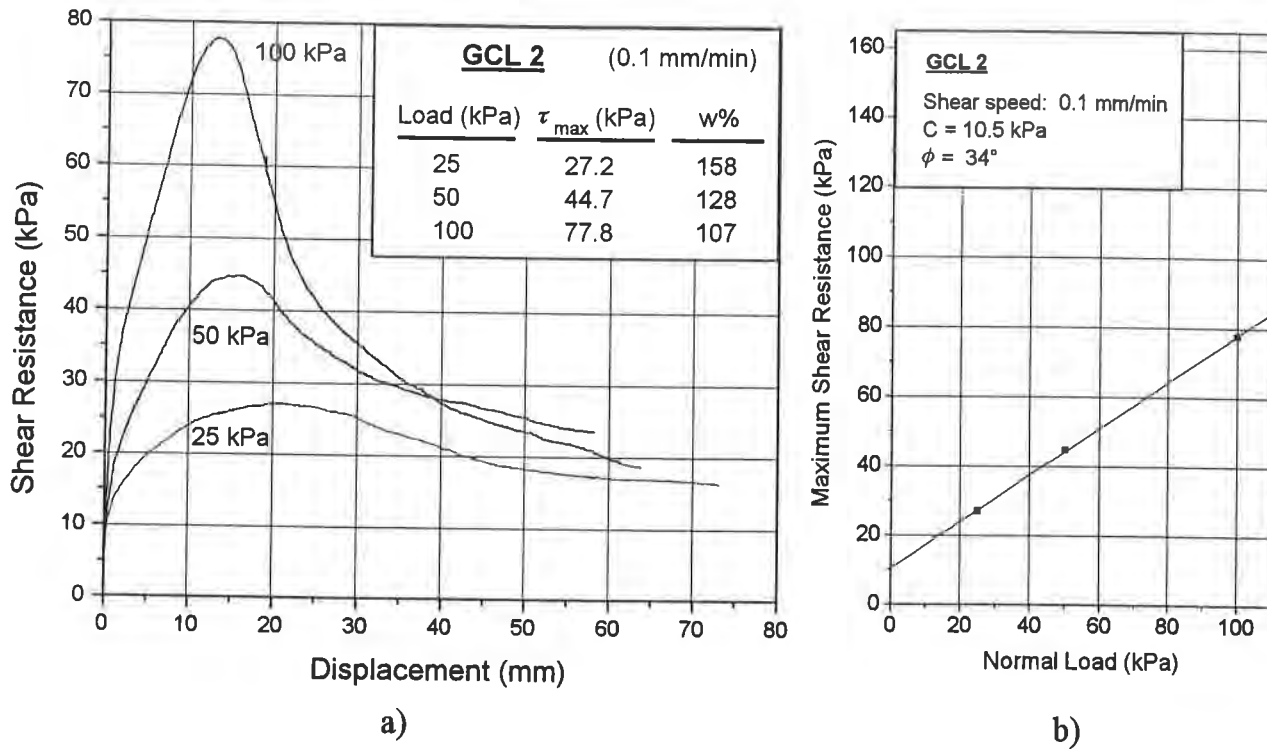
Figure 1. Typical Shear Test Results and Associated Mohr-Coulomb Failure Envelope

Influence of Shear Speed. The laboratory test results mentionned in the previous section are summarized in Table 2 presented below. The values presented correspond to an average of the tests performed with a specific GCL and at a given shear speed (N=3 or 4 tests at 1 mm/min, N=2 at 0.1 mm/min and N=1 at 0.01 mm/min). The results from the dry GCL samples as well as from some samples hydrated without a normal load being applied were not included, as these results are influenced by other factors which have a significant impact on the GCLs' behavior. These factors will be discussed later.

The average values of the shear resistance (τ in kPa) presented in Table 2 are used to isolate the influence of the shear speed over the shear resistance. The tendency is expressed as a percentage of increase (or decrease) between two shear resistance values, for a difference in shear speed of one order of magnitude (1 and 0.1 or 0.1 and 0.01 mm/min), or two order of magnitude (1 and 0.01 mm/min).

An increase of shear resistance was expected to follow an increase of shear speed, and this tendency was confirmed by the overall average of the test results. Increasing the shear speed from 0.1 to 1 mm/min resulted in an average increase of 19% of the shear resistance, and similarly a speed increase from 0.01 to 1 mm/min yielded an average increase of 41% of the shear resistance. Those values correspond to a general tendency observed while the tests were

performed, but do not represent individual results, considering that in Table 2 alone variations ranging from -2% to +71% were observed, regardless of the speed difference.

Table 2. Average Shear Resistance and Average Moisture Content According to the GCL Type, Normal Load Applied and Shear Speed

GCL No.	Shear Speed (mm/min)	0.01			0.1			1		
	Load (kPa)	25	50	100	25	50	100	25	50	100
1	τ_{avg} (kPa)				28.0	49.3	64.2	35.4	50.0	71.1
	$w\%_{avg}$ (%)				127	108	95	129	119	88
	τ increase 1 order							+26%	+1%	+11%
2	τ_{avg} (kPa)				28.5	51.4	83.0	35.1	50.5	91.1
	$w\%_{avg}$ (%)				128	99	85	117	94	73
	τ increase 1 order							+23%	-2%	+10%
3	τ_{avg} (kPa)			101.9	35.9	51.6	109.3	40.5	62.8	111.4
	$w\%_{avg}$ (%)			108	106	108	99	126	128	92
	τ increase 1 order						+7%	+13%	+22%	+2%
	τ increase 2 order									+9%
4	τ_{avg} (kPa)	20.2	32.6	57.3	26.7	41.1	63.4	34.6	48.0	84.0
	$w\%_{avg}$ (%)	136	113	94	111	105	80	103	94	84
	τ increase 1 order				+32%	+26%	+11%	+30%	+17%	+32%
	τ increase 2 order							+71%	+47%	+47%
5	τ_{avg} (kPa)	26.3	41.2	66.8	29.5	44.7	81.2	35.3	59.3	101.8
	$w\%_{avg}$ (%)	109	95	83	102	90	78	86	81	75
	τ increase 1 order				+12%	+8%	+22%	+20%	+33%	+25%
	τ increase 2 order							+34%	+44%	+52%
6	τ_{avg} (kPa)	27.6	54.6	82.4	31.5	54.3	84.1	42.3	59.0	112.7
	$w\%_{avg}$ (%)	155	130	110	155	121	109	121	113	97
	τ increase 1 order				+14%	-1%	+2%	+34%	+9%	+34%
	τ increase 2 order							+53%	+8%	+37%
Avg 1	τ increase 1 order				+19%	+11%	+11%	+24%	+13%	+19%
	τ increase 2 order							+53%	+33%	+36%
Avg 2	τ increase 1 order					+14%			+19%	
	τ increase 2 order								+41%	

The standard ASTM D 5321-92 requires that a shear speed of 1.0 mm/min be used to perform the shear test. In light of the results presented in Table 2 and considering the shear speed of 1 mm/min as a reference, reducing the speed from 1 to 0.1 mm/min will result in an average reduction of 16% of the shear resistance, and the average reduction will be of 30% for a speed decrease from 1 to 0.01 mm/min.

Influence of Moisture Content. The influence of the moisture content over the internal shear strength can be observed in Figure 2 below, representing the tests performed at 1 mm per minute with GCL No. 2. The test results are divided into categories of normal loads, and any comparison of water content should be done within a given category and not with all the data available.
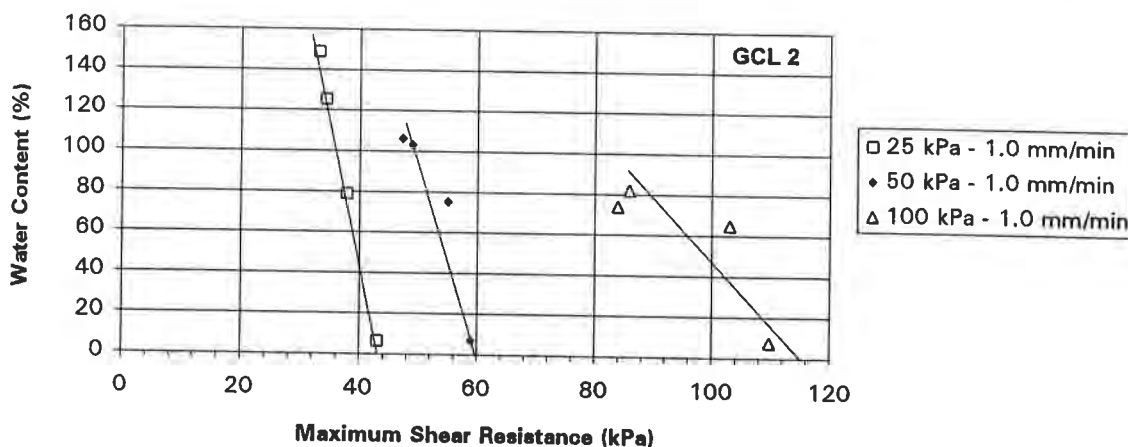
Figure 2. Relation Between Shear Resistance and Moisture Content for GCL No. 2

It has been observed, for a given normal load, that a decrease of the shear resistance corresponds to an increase of the water content. This fact can be explained by the reduced amount of inter-particular contacts when more water is present around the clay particles. There is also an interaction between the clay particles and the fibers running through the bentonite layer, and although it may be difficult to evaluate, this interaction is probably governed in a similar fashion as the clay particles are, therefore an increase of moisture content will reduce the amount of clay particles and fibers interactions.

GCL No. 2 was also tested in dry or ambient conditions. The dry bentonite exposed to ambient air will always have some moisture in it, in this case the moisture contents ranged between 6 and 8%. The quasi absence of water around the clay particles will have an important positive effect on the shear resistance, but this condition is not representative of a full scale application, because the water content will normally have the time to increase before an important load is applied.

Computation of the variation of the shear resistance (in %) for GCL No. 2, according to a variation of the moisture content, can be found in Figure 3. Each point corresponds to a

variation calculated for two points that are part of the same category (all data points in a category have the same shear speed and the same normal load applied). In general, an increase in moisture content of 10% will result in a decrease of the shear resistance by about 3%. Other GCLs show very similar variations, and the same increase in moisture content for all 6 GCLs tested results in an average decrease of the shear resistance by about 4%.
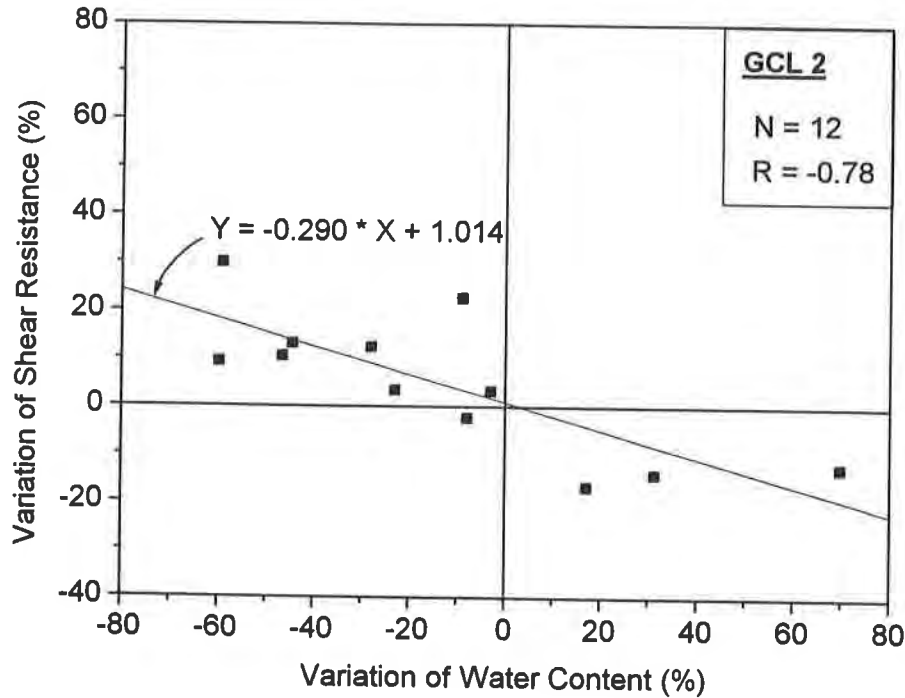
Figure 3. Relation Between the Variation of Moisture Content and the Variation of Shear Resistance for GCL No. 2

Angle of Internal Friction. The angles of internal friction are directly related to the values of maximum shear resistance obtained. The values indicated in Table 3 are the result of three tests performed at three different normal loads.

A variation of a few kPa for the tests performed at 25 and 100 kPa are immediately noticed by a variation of the angle of friction. It has also been noticed from the peel tests results that a spatial variability in the needle punched samples exists and may be more noticeable when single results are used instead of the average of many tests.

Table 3. Angle of Internal Friction for Each Test Category

Speed (mm/min)	Hydration Time	GCL 1 Peel: 55	GCL 2 Peel: 78	GCL 3 Peel: 183	GCL 4 Peel: 40	GCL 5 Peel: 71	GCL 6 Peel: 131
1	dry Ambient	42°	46°	53°			
	2 H				38°	42°	42°
	14 H	26°	41°	39°	29°	43°	46°
	14 H Submerged				39°	41°	46°
	48 H	23°	34°	45°			
	>14 D	26°	35°	45°	28°	40°	48°
	>14 D Free Swell				5°	13°	35°
0.1	14 H	26°	37°	45°	26°	29°	37°
	>14 D	19°	34°	-	26°	40°	33°
0.01	>14 D				26°	28°	35°

Relation Between Peel Test Value and Angle of Friction. The relation between the peel test value and the angle of friction is presented in Figure 4. Peel tests have been performed many times for each GCL, as required by the appropriate ASTM standard. Variability in the test results is greater for some GCLs than others, showing coefficients of variation ranging from 1% to 50%, but with most of the values below 20%, indicating that spatial variation in the needle punched reinforcement exists to various degree depending on the GCL.

Figure 4 shows that for a given peel value, the angle of friction will vary with the moisture content of the bentonite, which is directly related to the hydration time. Therefore, it is not possible to determine a value of internal angle of friction based only on a peel test result.

The results obtained are also in general concordance with the article from Heerten & Al. (1994) on the long-term shear behaviour of GCLs. Nevertheless, the relations presented are valid only if the variation between peel test results for a given GCL are kept within acceptable limits (to be defined), and the GCL sample is loaded during the hydration, which was not the case in the article, for reasons presented in the following section.
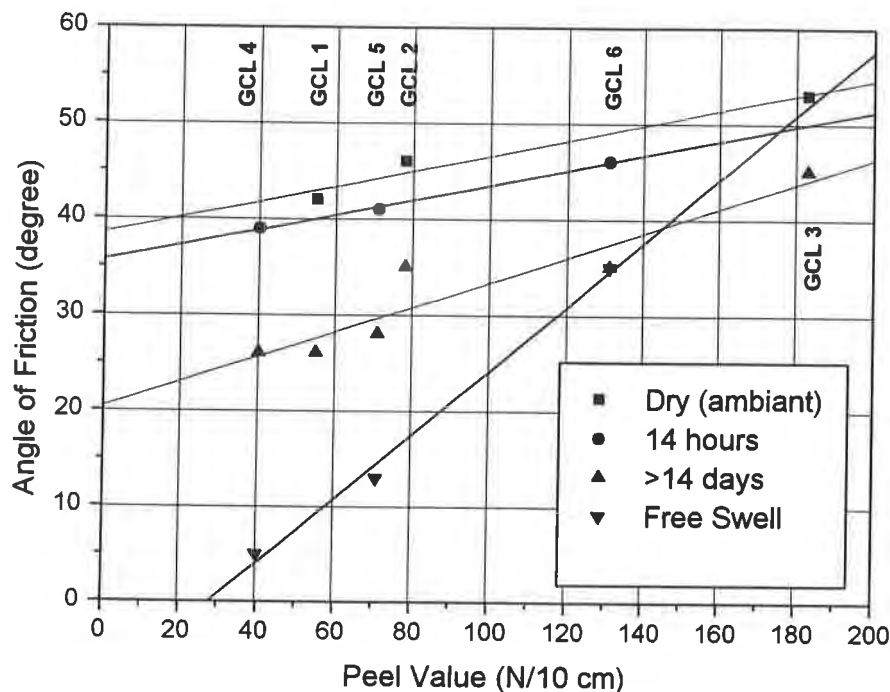
Figure 4. Relation Between the Peel Test Value and the Angle of Internal Friction

<u>Influence of Free Hydration on the Internal Shear Resistance</u>. Nine samples were hydrated without being submitted to a normal load; therefore, they were free to swell, limited only be the available space between the two geotextiles. The shear resistance of these samples were usually lower than the shear resistance of the sample having a normal load applied at all time. Two different factors may explain why the internal shear resistance of a GCL is lower when it is allowed to hydrate in an unconfined state.

It was observed that the bentonite in an unconfined GCL had a water content, after shearing, 2 to 3 times greater than the bentonite hydrated under a normal load. The increase in water content will generate positive pore pressures when the normal load is applied for the shear test, therefore reducing the interaction between the clay particles.

Most importantly, the pressure generated by the bentonite during the unconfined hydration can be high enough to damage the needle punched bonding holding the two geotextiles together. It has been determined by Shan in 1990 that the required pressure, applied to a sodium bentonite sample submerged in tap water in order to have zero vertical displacement, is in the order of 135 kPa. The pressure applied by the bentonite inside the GCL sample should always be inferior to this value, considering the fact that the bentonite is allow to have a limited volume gain during the free hydration. Nevertheless, it may be high enough to cause irreversible damage to the GCL.

Figure 5 is similar to Figure 1 but GCL No. 5 is showed this time. Three points with relatively high moisture content values can be found on the figure, and for two of these three data points the shear strength is clearly too low (50 and 100 kPa). This can be explained by the fact that during the free swell the GCL sample has been damaged by the swelling pressure of the bentonite, therefore reducing the strength of the needle punched fiber reinforcement.
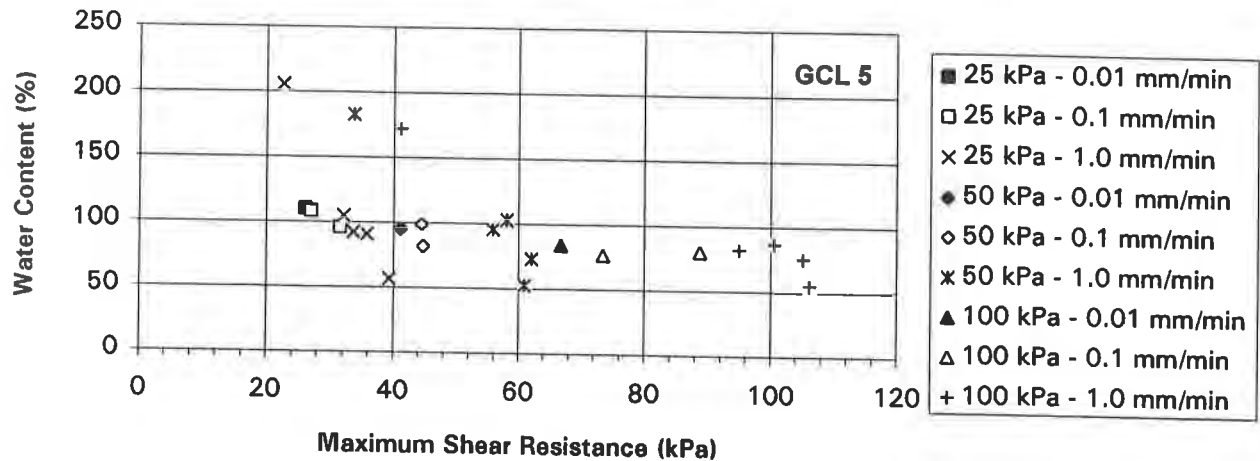
Figure 5. Relation Between Shear Resistance and Moisture Content for GCL No. 5

CONCLUSIONS

It has been observed that changing the moisture content of the bentonite or the shear rate affects the internal shear resistance of a needle-punched GCL. The ASTM standard test method D5321-92 asks for a shear speed of 1.0 mm per minute, but such a speed yields a much higher shear resistance than if a speed of 0.01 mm per minute is used. A slower speed is also more representative of a long term type of application and will result in a lower angle of internal friction. It would be a safer practice to use the reduced values for full scale application of GCLs.

No standard test at the present time is tailored to the specific characteristics of GCLs. Nevertheless, the shear speed of 1.0 mm per minute is very practical considering that it can be easily performed by most laboratories and it is less time consuming than other shear speeds (over 3 days for 0.01 mm/min compared to 1 hour for 1.0 mm/min). Therefore, it is recommended that a speed of 1.0 mm per minute be used, and a factor of 0.7 be tentatively applied to the maximum shear resistance in order to reduce the value by 30%, which is the average difference between shear speeds of 1.0 and 0.01 mm per minute. The suggested factor of 0.7 should be revised when more data is available, especially from slower shear speeds or long term applications of GCLs.

Also, in defining a standard test method for GCLs the hydration process should be specified, in order to have a better control over the moisture content of the GCLs being tested. Normal loads should always be applied during hydration, otherwise damage to the GCL caused by the pressures developped by the swelling bentonite may alter the shear test results.

Special care should be taken during full scale application of GCLs in order to prevent its hydration prior to the application of a normal load. Even a moderate shower on an uncovered GCL may be sufficient to reduce a comfortable factor of safety against instability to a fragile equilibrium between resistance and failure.

It is not possible to determine a GCL's internal angle of friction based only on a peel test result, considering that the value of the angle will vary with the moisture content of the bentonite, and the peel test does not take into account the influence of the bentonite on the internal shear resistance.

ACKNOWLEDGEMENTS

REFERENCES

Heerten, G., Saathoff, F., Scheun, C., Von Maubeuge, K. (1994). On the Long-Term Shear Behaviour of Geosynthetic Clay Liners (GCLs) in Capping Sealing Systems, International GCL Symposium, Nürnberg.

Mitchell, K. J. (1993). Fundamentals of Soil Behavior, John Wiley and Sons, Inc., 437 p.

Shan, H.-Y. (1990). Laboratory Tests on a Bentonite Blanket, MSCE Thesis, University of Texas in Austin.

Remediation and Containment

SPRAY POLYUREA COATINGS FOR PRIMARY AND SECONDARY CONTAINMENT

J. Winn Darden, Willamette Valley Company, Eugene, OR USA
Rob Loomis, Willamette Valley Company, Eugene, OR USA
F. T. Roehm, Willamette Valley Company, Escondido, CA USA

ABSTRACT

This paper describes the use of a spray polyurea coating systems as barrier coatings in two projects: The first, in which a spray-on liner consisting of a polyurea coating applied on a spun-bonded, polyester geotextile was used as a pond liner (primary containment), and the second, where polyurea was sprayed on a non-woven, polypropylene textile and used as a secondary containment barrier. Polyurea coatings have application and performance characteristics which make them useful as impermeable barrier membranes in primary and secondary containment in a variety of industries.

REASONS FOR PRIMARY AND SECONDARY CONTAINMENT

The use of primary and secondary containment is driven primarily by two factors: government regulations and economic considerations.

Secondary containment in areas where hazardous waste is handled has been required by the Federal Government for many years. It has been only in the last several years that secondary containment has also been required in areas where certain other chemical products are stored. Examples of regulated materials include gasoline, jet fuel, heating oil, fertilizers, and pesticides. Individual states implementing these regulations include Alaska, New York, Ohio, Wisconsin, New Jersey, and Florida. In many cases, these states have developed secondary containment regulations which are more stringent and more specific than those required by the Federal Government. In Florida, for example, synthetic liners used for secondary containment must be puncture resistant, have a permeability to the stored product of less than 1×10^{-9} m/second (m/s), be chemically compatible with

the stored liquid for at least 30 days, and be approved by the state Department of Environmental Protection.

There are also economic factors driving installation of primary and secondary containment. In many instances, an accidental spill requires costly cleanup. Spills or leaks which continue over a long period of time may contaminate soil and ground water, which will need to be remediated, again a costly undertaking. Primary containment may also be necessary where loss of a material from a storage area is considered undesirable. In arid areas, water may be continually reused in many facilities due to its scarcity. A leak in a holding pond which results in water loss can be costly. "Zero discharge" targets for industrial facilities lead to requirements for impermeable containment of waste streams.

PROJECT SITE HISTORIES

Coal/Water Slurry Storage Pond. The first project in this paper was done at a coal-fired power plant in the southwestern U. S. At this site, coal was delivered in the form of a coal/water slurry via pipeline from mines in New Mexico and Arizona. During the late 1970's, eight storage ponds, each about 16,000 m^2 (175,000 ft.^{2}), were constructed to insure a constant supply of slurry to feed the boilers. One of the ponds was chosen by the utility to be coated for this project.

The surfaces of the storage ponds consisted of an asphalt layer on a sand base. The native soil in the area was a silty, sandy alluvial material which appeared to be free draining. The pond was resurfaced with asphalt in 1990. When in use, the pond was kept 80-90% full of the coal/water slurry. If idle, the pond was 30-40% full This pond was emptied about once a year, cleaned, and repaired. Foot traffic and light vehicle traffic were common in the pond when empty or idle. Occasional heavy truck and construction vehicle (e.g. front end loaders) traffic was expected during shut down. The coal/water slurry was moved from the pond to the plant via a pipe bridge, which was supported by concrete columns coated with an epoxy mortar.

The asphalt surface had deteriorated. Pavement cracks ranging in size from small hairline cracks (less than 2 mm) to fairly large(greater than 10 mm) had occurred, and were anticipated to continue to occur as water percolated into the subgrade. The cracks formed due to substrate movement, and to the extremes in temperature and UV exposure found in the desert. A number of large asphalt patches were present, some of which have partially sloughed down the slope of the pond, again most likely due to climatic conditions. Some large areas appeared to have been damaged by construction equipment.
Problems arose for the utility because cracks in the asphalt allowed water to move from the pond into the sandy soil of the subgrade, resulting in substantial water loss. Due to the scarcity of water in this region, this facility discharged little or no water from its operations; rather, water was reused where possible. In addition, the water in the pond leached water soluble chemicals from the coal,

which were transported into the subgrade by the water, causing possible environmental concerns. Finally, the asphalt currently in use required replacement after short periods of time, leading to excessive downtime during pond maintenance.

The problem faced by the utility was to find a cost-competitive impermeable lining which could be installed in a short period of time to reduce the loss of water from the pond. The chosen product had to be traffic resistant, and needed to withstand a variety of environments, including constant exposure to water, and the temperature extremes in the desert when the pond was drained for maintenance. It had to withstand exposure to UV radiation, almost constantly at the edges of the pond, and in the whole pond during maintenance periods. Finally, the lining chosen had to be repairable by the personnel at the plant site.

Oil Product Pipeline Pumping Station. The second project was the installation of secondary containment at a pumping station for an oil products pipeline company. The site, in the Pacific Northwest, has been in use for over 40 years. The base of the pumping station was a combination of native soil with gravel, and some areas of concrete. There were over 150 penetrations in the 200 m area, including tower feet, pipes, and conduits. Some of the pipes were no more than 0.5 meters off the ground. The area was surrounded by a 0.15 m asphalt curb.

The pipeline company had recently experienced some small spills and leaks in several pumping stations. Although no environmental damage occurred, the company instituted a program to place impermeable liners in its pumping stations, with the primary goal of eliminating soil and water contamination by small leaks which may occur over long periods of time from pipe joints, valves, and other areas.

The pumping station could not be out of service for long periods of time, therefore the chosen method for secondary containment could not be time consuming. The large number of penetrations presented the problem of insuring that secondary containment was leak-proof around each one. In addition, the project was to be done in the fall in the Northwest, when temperatures fall to freezing or below, and rain is always a possibility. As in the first project, resistance to UV radiation, and to foot and light vehicle traffic were important as well.

ALTERNATIVE MATERIALS OF CONSTRUCTION

Many alternative products can be used for primary and secondary containment, some of which were considered for use in these two projects. The first were concrete and asphalt. can be used. Concrete can be expensive to install, and may require long cure times, especially in cold weather, which may lead to excessive facility downtime. In addition, concrete may crack and spall over time, or with substrate movement, reducing its effectiveness as a long-term

containment barrier.   Asphalt will be dissolved by many petrochemicals, requiring regular use of special topcoats. Asphalt may have a relatively short life span, especially under severe environmental conditions. Both concrete and asphalt are difficult to seal around penetrations, and installation may be impossible in areas where space is limited, such as underneath pipe racks.

Traditionally, high-density polyethylene (HDPE) geomembranes, or geosynthetic clay liners (GCLs) have been widely used in primary and secondary containment. HDPE has excellent chemical resistance, and is relatively easy to install. However, HDPE can be difficult to seal around penetrations, and may require the use of a soil cover since it tends to wrinkle when exposed to light and ambient temperature changes. GCLs are easier to fit around penetrations, but may also require the use of a soil cover.

Many types of coatings are also used in primary and secondary containment.   Many chemically resistant coatings are rigid and inflexible which can lead to cracking as the substrate moves. Many coatings require long cure times, sometimes as long as seven days, before traffic can be allowed. This problem also limits the use of some coatings in cold weather. Many products cannot be used where humidity or substrate moisture is high.   Some coatings have poor traffic resistance, and require special construction techniques to be used in high traffic areas. Finally, many coatings contain solvents, which may be hazardous to workers, and which are regulated under some local air pollution control statutes.

SPRAY POLYUREA COATINGS

Spray polyurea coatings were developed by Texaco Chemical Company (now Huntsman Corp.) in the late 1980's. Polyurea was originally used in a process called reaction injection molding (RIM) to make automobile parts.   Slight modifications in the chemistry of the systems allowed the products to be spray applied as coatings.

Polyurea coatings belong to the family of polyurethanes, with differences in the reactants which leads to some important differences in application and performance. Polyurea coatings are formed when an isocyanate pre-polymer (called the "A" or "iso" component) is mixed with polyfunctional amines (called the "B" or "resin" component), rather than with polyols. No catalyst is required. Additives such as UV stabilizers and pigments or dyes are added to the resin component.

The iso and resin components, both liquids, are usually formulated at a ratio of 1:1 by volume. The components are mixed in special plural component metering equipment at elevated temperature and high pressure. After mixing, polyurea coatings have gel times (the time required for initial setting to occur) of two seconds to one minutes, and tack-free times (the time required for the coating to lose its "stickiness") of as little as five seconds.

Characteristics of Polyurea Coatings. Polyurea spray-on liners have some characteristics in common with other spray-on liners, which have been discussed in a previous paper. Installation with spray-on liners is relatively easy, since the coating is sprayed in place at the project site. The liner can easily be molded to fit at penetrations. Spray-on liners can be applied directly onto properly prepared surfaces such as concrete tank rings, pipes, and conduits, which reduces installation time. Once the liner is sprayed in place, it forms a continuous barrier film which contains no seams. These liners offer good resistance to degradation by UV light, allowing them to be placed with no soil cover. Finally, the polyurea liners can be repaired easily with urethane patch kits.

Polyurea coatings also have characteristics which are unique. Because of the rapid reaction between the isocyanate and the polyamines which make up the polyurea system, cure times for polyurea coatings are extremely fast, often as little as two seconds. The coatings cure to a "tack-free" state, where foot traffic can be tolerated, within 20 seconds of application. Facility downtime can be reduced. Second, because of the speed of these chemical reactions, they can be used under conditions where moisture is present; that is, in hot, humid weather, or in cool, damp weather with little or no effect on the properties of the finished coating. Third, polyurea coatings are formed by processes which vary little in reaction time with temperature. Thus, the tack-free times for polyurea coatings are short even at low temperatures. These characteristics mean that polyurea coatings can be used under adverse field conditions with little effect on their performance. These properties also reduce the potential for improper application in the field.

The iso and resin components of polyurea systems are 100% solids; that is, they contain no solvents. This eliminates any potential conflict with local air quality regulations which may limit the use of certain solvents. The finished coatings are tough, offer excellent puncture resistance, and retain their flexibility at temperatures as low as -51° C. Combined with excellent abrasion resistance, this enables these films to stand up well to traffic. Polyurea coatings have good chemical resistance to a variety of petrochemicals. Other chemical products, such as fertilizers and dilute acids and bases, have little effect on the coatings. The coatings meet most regulatory requirements for permeability and compatibility as discussed earlier.

Typical Physical Properties of Polyurea Coatings. Table 1 records a number of typical physical properties for polyurea coatings at a film thickness of 0.75 mm. The data in Table 1 illustrates the properties discussed above. Table 2 gives permeability and compatibility date for polyurea coatings with a variety of chemical products, also at thicknesses of 0.75 mm.

Table 1. Performance Data for Polyurea Coatings

Physical Property	Test Results	Test Methods

Tensile Strength, MPa (psi)	22.3 (3,229)	ASTM D412
Elongation, %	312	ASTM D412
100% Modulus,MPa (psi)	13.3 (1,926)	ASTM D412
200% Modulus,MPa (psi)	18.7 (2,712)	ASTM D412
Die C Tear Strength, N/m (pli)	92.3 (527)	ASTM D624
Taber Abrasion, mg wt. Loss (1000g, 1000 revolutions, H18 wheel	180	ASTM D1630
Puncture Resistance, N (lb.)	1,560 (351)	ASTM D4833
Mandrel Bend, -60°F, 1" Mandrel	Pass; no cracking	ASTM G11
Hydrostatic Resistance, MPa (psi)	526	ASTM D751
Soil Burial Test	Pass	ASTM D3083
Adhesion to Concrete, MPa (psi) (pressure washed at 4,000 psi)	2.4 (350) (failure in concrete)	ASTM D4541
Q-UV Weather-o-meter, 313 UV Bulb, 7,100 hr.	No surface cracking	ASTM G53

Table 2. Permeability and Compatibility of Polyurea Coatings with Chemical Products

Chemical Product	Permeability, m/second (ASTM E96)	Compatibility, % Change in Coating Thickness[1]
Water	9.30×10^{-11}	+1.3
Chemical Product	**Permeability, m/second (ASTM E96)**	**Compatibility, % Change in Coating Thickness[1]**
Diesel Fuel	1.17×10^{-10}	+3.1
Motor Oil	9.90×10^{-11}	+0.4
Jet A Fuel	7.80×10^{-11}	+1.7
Fuel Oil #2	2.90×10^{-11}	+2.0

[1] Compatibility is measured by taking the % difference in thickness of the sample before and after the test.

Disadvantages of Polyurea Coatings. Polyurea suffers from some of the same problems as other spray-on liners. First, test standards for polyurea coatings are not necessarily the same as those applied to geomembranes. Quality control for field applied liners is extremely difficult, since samples must be sprayed in the field, then sent back to a laboratory for testing. This limits the usefulness of field testing to insure compliance with specifications. Monitoring the thickness of the polyurea coating during application is also difficult, often requiring destructive testing (cutting the liner). The fast cure time of polyurea elastomers precludes the use of thickness gauges.

One major disadvantage of polyurea coatings is the necessity of using plural component application equipment to spray the liners. This equipment is expensive, and can be difficult to operate and maintain. Experienced applicators are crucial to successful installation of the systems.

APPLICATION EQUIPMENT

Polyurea coatings are applied using plural component application equipment capable of achieving pressures of at least 13.8 MPa (2,000 psi) and maintaining a minimum temperature of 66° C (150° F).

The two liquid components are removed from their containers using 2:1 drum pumps. In cold weather, drum heaters may be needed to insure that the components are removed from the drums at the proper ratio. They are fed into the spray unit, where the system pressure is increased to the operating pressures given above. In-line heaters increase the temperature of the liquid materials. The separate components are metered in a 1:1 by volume ratio. Then, they enter hoses heated by trace lines to maintain minimum temperatures, and are fed to the spray gun.

The components are mixed by a process called impingement mixing. In this process, the two components are mixed at the gun in a small mixing chamber Gellation of the resulting mixed stream occurs in seconds. High temperatures and pressures are required to insure complete mixing of the two components, which will lead to optimum physical properties for the finished coating.

PROJECTS USING POLYUREA COATINGS AS CONTAINMENT LINERS

Two projects using polyurea as a containment liner are detailed: One in which the polyurea coating/geotextile system was used for primary containment as a pond liner, and the other where the system was used in secondary containment in an oil products pipeline pumping station.

Polyurea Coatings as Primary Containment Liners. A spray polyurea coating was specified by the utility to line the large holding pond described above. Polyurea was selected over other materials because of its rapid cure time, its minimal expansion and contraction over a wide temperature range, its UV resistance, its seamless construction, its traffic resistance, and its impermeability to water.

The major design problem at the holding pond was that its asphalt substrate moved to a much greater extent than concrete or other substrates. Given the wide range of environmental conditions found in the desert over the course of a year, this potential for substrate movement was even greater. Direct application of the coating to the asphalt was thus precluded. A method had to be found which would effectively bond the polyurea coating to the pond's surface, but would

not adversely affect the integrity of the coating. Another problem with the surface was the large number of cracks found in the asphalt. Filling the cracks with polyurea or some other material was feasible, but would increase material costs and application time significantly.

These issues were addressed by the use of a 0.18 mm thick, 25 g/m², spun-bonded, polyester geotextile as a surface on which to apply the polyurea coating. The geotextile was lightly bonded to the asphalt surface using a very thin film of the polyurea coating as a bonding or primer coat. This surface was then coated with an average of 1.25 mm (50 mils) of the polyurea coating.

Some repair and preparation of the asphalt surface was necessary prior to placement of the textile. Large voids were filled with asphalt or Portland cement. All rocks, sticks, and other objects which might penetrate the coating from below were removed from the substrate. Metal and concrete surfaces were brush blasted to provide good adhesion for the polyurea coating.

The polyurea coating used in this project met the following specifications:

Table 3. Specifications for Polyurea Coating as a Pond Liner

Physical Property	Specification
Hardness, Shore D	50 ± 5
Tensile Strength, MPa (psi)	17.2 (2,500) minimum
Elongation, %	400 ± 50

The geotextile was bonded to the asphalt surface of the pond by applying a light coat, or tack coat, of less than 0.25 mm onto the asphalt, then unrolling the textile into the still tacky coating. When applied in films of greater than 0.5 mm, the specified polyurea coating has a gel time of 2-3 seconds, and a "tack-free" time of 20 seconds. However, when applied in a thinner film, this tack-free time is extended to 45-60 seconds. This enabled the contractor to apply the tack coat to the asphalt substrate, and still have time to unroll the textile onto the tack coat. The textile was then smoothed with a broom to minimize "fish eyes" and wrinkles. The coating applicator developed a mechanical roller where the 1 m wide rolls of geotextile were placed to ease the task of unrolling the textile. Each width of geotextile was overlapped onto the adjacent piece a minimum of 0.1 m (4 inches) to insure that a seam-free membrane was formed after the topcoat was applied. Foot and vehicle traffic on the geotextile were minimized until the tack coat had completely cured. This was necessary to insure that the surface of the geotextile remained as smooth as possible.

Bonding the geotextile to the pond's surface took six days, approximately 72 hours. Approximately 720 man-hours were used during

this phase of the liner installation. A photograph of the process is shown below.
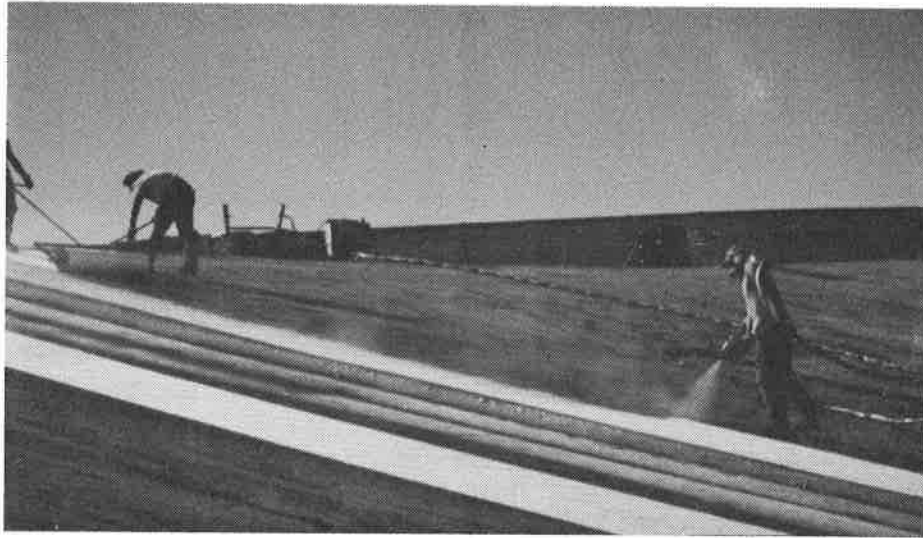
Figure 1.   Bonding the Geotextile to the Asphalt Surface

During the project, most of the geotextile was bonded to the asphalt surface of the pond prior to the application of the topcoat, with the exception of the bottom of the pond. The polyurea topcoat was applied to the geotextile at an approximate thickness of 1.25 mm (50 mils). Two plural component spray units were used, each with a crew of three: One man sprayed the coating, another moved hoses and spelled the spray man, and one monitored pressure and temperature on the spray unit, moved drums, and other miscellaneous tasks.

If more than 8 hours had elapsed during topcoat application (for example, when the crews quit for the night), cleaning was necessary to insure a good, continuous bond between previously applied topcoat and new topcoat. The applied coating was cleaned of dust and particulates, then swabbed with acetone, which slightly softens the surface of the coating. At start-up, the new coating was overlapped 0.1 m onto the old coating to insure that a seam-free membrane was being installed.

The geotextile was placed approximately 0.3 m onto the concrete columns supporting the pipeline bridge. The textile was bonded to the columns using the polyurea coating as an adhesive. Then the textile was covered with about 1.25 mm of the coating. The coating was applied to a point about 0.3 m above the textile.

Application of the polyurea topcoat lasted 5 days, or 60 hours. A total of 360 man-hours were used in the application of the topcoat. The photograph below shows an example of topcoat installation.

Figure 2.   Application of the Polyurea Topcoat

Many factors can affect the quality of the installed liner system.   Temperature, relative humidity, mix temperature and pressure, and wear and tear of equipment parts are all factors which must be considered.   During the course of the pond lining project, temperature and humidity were monitored using appropriate gauges.   Component mix temperature and pressure were monitored regularly by the applicator. A regular maintenance schedule for the equipment was defined and maintained throughout the project.

During the course of the project, physical properties were monitored by spraying a thin film of polyurea onto a sheet of polyethylene, to which the polyurea will not bond.   These samples were returned to the lab for analysis.   The pond was divided into four sectors for sampling purposes.   Five coating samples were obtained from each sector, and the physical property results averaged.   They are reported in Table 4 below.

Table 4.   Physical Property Test Results for Polyurea Coating

POND SECTION

Physical Property	A	B	C	D	Mean	Std. Dev.
Tensile Strength, MPa	25.3	23.1	22.9	22.3	23.4	1.3
Elongation %	437	383	417	421	414	19.7
Tear Strength, N/m	56.0	51.5	57.1	52.5	54.3	2.7
Hardness, Shore D	47	52	52	50	---	---

These results show that the variation about the mean for each of the physical properties tested is relatively small. The consistently high test results indicate that optimum pressure and temperature were maintained throughout the project.   Of the time spent in topcoat application, only 10-15 man-hours were spent monitoring equipment processing parameters.   Thus, the factors which have the most effect on physical properties of the polyurea coating can be monitored regularly at a relatively small cost.

This method of monitoring physical properties has one major drawback: It is not possible to use this method to monitor properties of the coating as it is being applied. In essence, it is imperative that the applicator closely monitor temperature, pressure and other parameters during the application. An experienced hand on a spray unit is also essential.

To monitor the thickness of the topcoat, destructive testing (that is, cutting into and measuring the topcoat) was performed at intervals during the application of the topcoat. Again, the pond was divided into four quadrants, and the average of five thickness measurements in each quadrant was recorded. Results are shown below in Table 5 below.

Table 5. Polyurea Coating Thickness

POND SECTION

Property	A	B	C	D	Mean	Std. Dev.
Thick-ness, mm	1.45	1.09	1.52	1.32	1.34	0.19

While the results in the table indicate that the thickness of the applied coatings was only slightly above the mean (1.34 mm vs. 1.27 theoretical mm), there appears to be a substantial variation in the results from each quadrant. Unfortunately, the coating thickness was not monitored on an ongoing basis, so it could not be determined if the contractor got closer to the specified coating thickness as the project proceeded. While there are other methods of monitoring coating thickness available (for example, using a counter in the spray unit to determine the amount of product applied per count), often during field application they are time-consuming to use, and therefore realistically will probably not be used by the contractor.

Approximately one year after the installation of the polyurea coating in the holding pond, a visit was made to the utility to determine the condition of the liner. There was some damage around the top of the pond, apparently due to bulldozer traffic. The interior of the pond, while discolored, was intact. Samples taken from the rim of the pond were tested, and gave results similar to those given in Table 4.

Polyurea Coating as a Secondary Containment Liner in a Pumping Station. In this project, polyurea was chosen due to its ability to cure at low temperatures, its ability to develop excellent physical properties despite damp conditions, its UV resistance, and speed of cure. Due to the presence of over 150 penetrations, the ease of attachment of polyurea coatings to pipes, concrete, and plastic was a major consideration leading to its selection.

At the pumping station, a 170 g/m^2, 1.75 mm thick, non-woven polypropylene geotextile was used as the substrate on which the

polyurea coatings was applied. The polyurea coating used as the secondary containment barrier film had the following properties:

Table 6. Specifications for Polyurea Coating for Pumping Station

Physical Property	Specification
Hardness, Shore D	50 ± 5
Tensile Strength, MPa (psi)	15.2 (2,500) minimum
Tear Strength, N/m (pli)	15.8 (90)minimum
Elongation, %	200 ± 30

The geotextile was cut to fit the layout of the pumping station. Care was taken to insure that geotextile pieces near penetrations allowed for adequate application thickness to insure a leak-proof membrane. Each piece of geotextile was overlapped onto the adjacent piece a minimum of 0.1 m. As in the previous project, this was done to insure that the finished coatings was seam-free. The geotextile was laid up and over the 0.15 m high asphalt curb.

The polyurea coating was first applied to the area of overlap between the pieces of geotextile. Approximately 0.25 mm of the product was used to "glue" the separate pieces of geotextile together. Because of the light weight of the textile, if individual pieces were sprayed, the textile would be blown around by the force of the spray stream. When bonded together, the textile laid flat, reducing the difficulty of the application.

The polyurea coating was applied at an average of 2.3 mm (90 mils). The first pass with the polyurea coating was applied at approximately 0.25 mm (10 mils). This was necessary to minimize loss of the polyurea coating caused by soaking into the fabric. In open areas of the containment area, the product was used at approximately 1.5 mm (60 mils). At areas around penetrations, the coating was applied at variable thickness, depending on the workmanship of the applicator. The more snug the seal made around a penetration with the geotextile, the less material had to be used to seal the penetration. Up to 6.5 mm (250 mils) of polyurea were used at some penetrations.

During this project, the geotextile was laid out on the first day. A light rain fell during the night, wetting the fabric. In addition, the temperature was approximately 2° C (36° F) on the morning that the application of the coating began. The coating was applied to damp areas of the geotextile fabric, with no apparent effect on the finished coating. The gel time of the product at project start was 25-30 seconds, with a tack free time of 60-75 seconds at 2° C. In the afternoon, when the temperature had risen to 20° C (68° F), the gel time was 3-5 seconds, with a tack free time of 25-30 seconds.

Due to the highly variable nature of coating thicknesses required in this project, thickness measurements were not taken. The project was completed in two days. A photograph of the nearly completed project is shown below. Note the large number of penetrations.
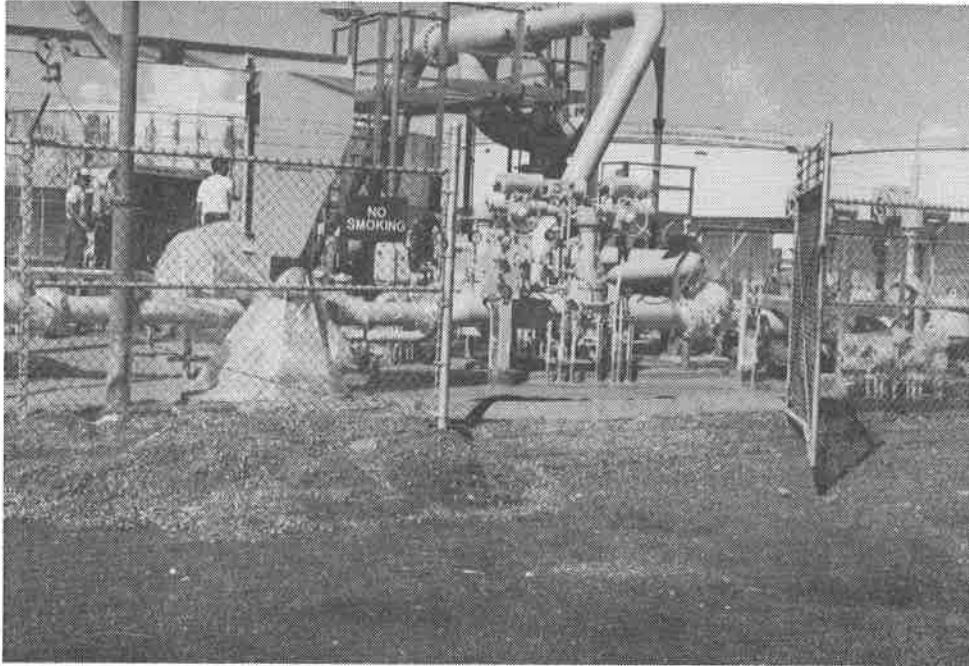
Figure 3. Polyurea Coating in the Pumping Station

SUMMARY

Polyurea spray-on liners provide a cost-effective method of primary and secondary containment, with a number of advantages over other technologies. They do, however, have a number of drawbacks which should be taken into consideration before they are used in the field. With proper design and installation, these liners can be used successfully on both small and large projects, and offer real advantages in installation in areas with large numbers of penetrations.

REFERENCES

Druschel, S. J., et. Al.; "Using a Spray-On Liner for Secondary Containment at an Oil Tank Field." Geosynthetics '93, Vancouver, B. C., Canada, pp. 1027-1037.

Texaco Chemical Company, Technical Bulletin, "Spray Polyurea Coatings," 1989.

EVALUATION AND REMEDIATION OF A FIRE DAMAGED GEOSYNTHETIC LINER SYSTEM

F.T. Adams
Golder Construction Services, Inc., USA
L.K. Overmann
Golder Construction Services, Inc., USA
R.L. Cotton
General Electric Company, USA

ABSTRACT

A fire in a hazardous waste landfill damaged the liner system consisting of compacted clay, geomembranes, geonets, geotextiles, and granular soils. Following waste excavation, the visibly damaged liner system materials were removed and samples of each component were obtained from the perimeter of the visibly undamaged area. Geomembrane samples were tested for tensile characteristics and index properties; geonet samples were tested for grab tensile properties and thickness. Test results were compared to the original specifications, manufacturers' quality control data, quality assurance conformance test results, and baseline sample data from an unaffected part of the landfill. Geomembrane baseline results exceeded the original specifications, and the specifications were used as the basis of acceptance of the perimeter samples. Geonet baseline results were inconclusive, with grab elongation consistently below the original specifications. A statistical approach was used to delineate the limit of affected geonet using the baseline sample data. The liner system was reconstructed to the limits defined by this testing program and returned to service following acceptance by the regulatory agencies.

INTRODUCTION

In September 1993, a fire was discovered within the waste of an active hazardous waste landfill containing industrial waste sludges and other chemical manufacturing by-products. Based on measurements taken from thermocouples installed in the vicinity of the fire, the temperature near the liner system may have approached 800 degrees Celsius (°C). Extensive efforts were made to first contain, and then extinguish the fire through late 1993 and into the summer of 1994. The fire was finally extinguished in August 1994.

In order to determine if the liner system was damaged as a result of the fire, the owner excavated waste from the affected portion of the landfill. The area of waste removal was approximately 560 square meters (m^2) (6,000 square feet (ft^2)). Following waste excavation,

visible damage to the liner system was observed over an area of approximately 300 m^2 (3,200 ft^2). The damaged area was limited to the side slope of the bottom liner system near the landfill perimeter, which has a slope of approximately three horizontal to one vertical (33 percent). A photograph of the affected area following removal of the most visibly damaged materials is presented as Figure 1.

The liner system on the side slope consists of the following components (from top to bottom):

- An ultraviolet resistant filter polypropylene (PP) geotextile;

- A 0.3-m (12-in.) thick sand protective layer;

- Two nonwoven filter polyester (PET) geotextiles (Primary Geotextiles);

- A high density polyethylene (HDPE) geonet drainage layer (Primary Geonet);

- A 2-mm (80-mil) thick HDPE geomembrane liner (Primary Geomembrane);

- Two nonwoven filter PET geotextiles (Secondary Geotextiles);

- An HDPE geonet drainage layer (Secondary Geonet);

- A 2-mm (80-mil) thick HDPE geomembrane liner (Secondary Geomembrane); and

Figure 1 Photograph of Affected Area

• A 0.9-m (36-in) thick layer of compacted clay having a hydraulic conductivity of less than or equal to 1×10^{-7} centimeters per second (cm/sec) (Secondary Clay Liner).

Damage to the geosynthetic components of the liner system in the immediate vicinity of the fire ranged from complete disintegration; to melting and fusing of the various components together further from the center; to rippling and stretching of the materials along the perimeter of the visibly damaged area. In several areas, evidence of melted geosynthetic materials was observed in desiccation cracks in the secondary clay liner.

Each of the liner system components listed above, except for the ultraviolet resistant filter geotextile, was subjected to evaluation testing and subsequently repaired as described herein.

EVALUATION OF LINER SYSTEM DAMAGE

A work plan was first prepared to describe the methods of evaluating and defining the extent of the damaged liner system. These methods consisted of a two-phased approach which included initial delineation of the extent of damage by visual observation, followed by a sampling and testing program for each liner system component around the perimeter of the damaged area. The test results from this program would be used confirm that sufficient materials had been removed to allow the various components to function as intended. All of the liner system components listed above were sampled and tested, except for the protective sand layer and the uppermost ultraviolet resistant geotextile. However, sampling and testing of only the geomembrane and geonet components are the subject of this paper.

Selection of Test Methods. In order to define the extent of the testing program, several geosynthetic tests were considered and evaluated. Many chemical tests are available which can be used to assess damage at the molecular level (Koerner, 1994). These include Differential Scanning Calrimetry (DSC), to determine the oxidative induction time (OIT) for assessing the amount of antioxidant is the polymer, and Gel Permeation Chromatography (GPC), which determines the distribution of molecular weight of the polymer chains. Damage to the polymers may be indicated by a change in the loss of antioxidant during the OIT test or a shift in the distribution curve of molecular weight from that of a newly manufactured geomembrane.

Polyethylene, polyester, and polypropylene, which are the polymers used to manufacture the geosynthetic materials installed in the subject liner system, are all thermoplastic polymers, i.e. the material can be repeatedly heated to its softening point, shaped or worked as desired, and cooled to preserve the remolded shape. Intense heating of the material above the melting point will result in obvious visible damage. Heating of the material to a temperature close to, but below, the melting point may result in some softening, but should not damage the material at the molecular level depending upon the time that the material is subject to temperatures in this range. Therefore,

testing of material at the macroscopic level, such as for strength or index physical properties, is more appropriate for assessing damage to the materials in areas where visual damage is not evident.

Following an evaluation of these and other more common test methods, it was concluded that the simplest approach for assessing damage to the geosynthetic materials was to measure select physical/mechanical properties such as thickness and tensile strength, and tensile elongation characteristics. Physical property tests are much less expensive and quicker to perform than the more sophisticated tests such as DSC and GPC described above. In addition, the results are much less subjective and, therefore, easier to interpret. They also allow for comparison to the original specifications, to the manufacturer's quality control (QC) data, and to the quality assurance (QA) conformance test results obtained prior to initial installation of the liner system in 1989. Tensile characteristics at break are a very good indicator of damage and the test provides the stress-strain relationship of the material. Of particular importance, especially for the geomembranes, is the elongation at break, which is more sensitive to material degradation than the elongation at yield. In addition to tensile characteristics, other tests performed included thickness, density, and melt flow index for the geomembranes, and thickness for the geonets.

Establishment of Minimum Standards. Minimum standards had to be established for comparison of test results to determine if the physical properties of the liner system components had been affected by the fire. These standards could be established by either: (1) using the minimum value listed in the original specifications for the particular property; (2) using the manufacturer's QC data; (3) using QA conformance tests performed prior to material installation; (4) performing comparison testing of geosynthetic materials from the landfill base liner outside of the area affected by the fire; or (5) performing tests on archive samples of the materials, if available. Use of (2), (3), (4), (5), or a combination of these, would allow establishment of the minimum standards using statistical methods.

Following consultation with the owner and regulatory agencies, it was decided that samples of each geosynthetic component of the liner system would be obtained at two locations far enough away from the damaged area so as to have a reasonably negligible probability of having been affected by the fire. These samples are hereafter referred to as the "baseline samples." The locations chosen were approximately 50 m (160 ft) east of the fire damaged area. The baseline samples were obtained at two locations along the length of side slope at similar distances from the crest as the limits of the fire damaged area, so as to account for possible affects of stress within the landfill at depth.

Samples were also obtained from around the edge of the fire damaged area and are referred to as the "perimeter samples." It was agreed that the original specifications would be used as the minimum standards to determine acceptability of the perimeter samples if the baseline sample test results were above these specifications. If the baseline results were below the original

specifications, a new minimum standard would be developed using the baseline sample data to determine acceptability of the perimeter samples.

SAMPLING

Perimeter Samples. As waste was removed and the liner system components were cleaned as best as possible, sample locations were identified around the perimeter of the damaged area. The first perimeter sample was obtained near the top of the slope above the fire damaged area and is labeled as Location 1 on Figure 2. Although the fire damaged area was located on the landfill side slope approximately 10 m (30 ft) from the crest, it was agreed that all of the geosynthetic materials from the damaged area up the slope to the anchor trench would be removed to avoid tie-in seams along the slope. Perimeter samples obtained at Location 1 were initially proposed as baseline samples. However, it was decided not to use these results for establishment of the baseline since the location was too close to the fire damaged area.
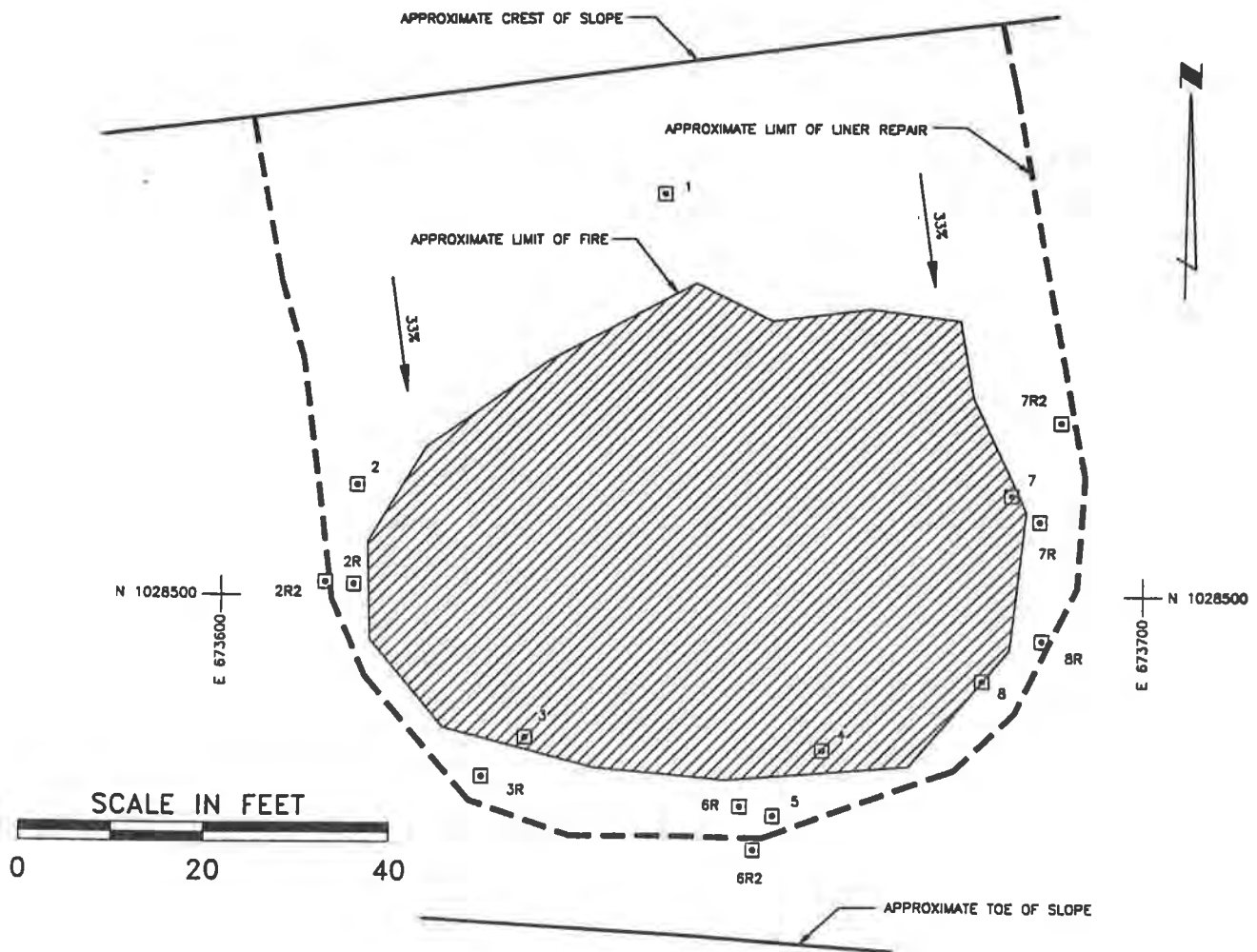
Figure 2 Sample Location Plan

Additional samples of the various geosynthetic layers were obtained at Locations 2, 3, and 4. Upon removal of samples at Location 4 near the bottom of the exposed slope, visible damage to the upper secondary geotextiles was noted. As a result, all geosynthetic samples obtained at Location 4 were abandoned and not tested, and additional waste had to be excavated to expose a larger area of the liner system. After approximately 3 m (10 ft) of additional liner system was exposed at the bottom of the excavation, samples were obtained at Locations 6, 7, and 8. Locations 2, 3, 4, 6, 7, and 8 are shown on Figure 2.

Results on some of the samples taken from Locations 2, 3, 6, 7, and 8 did not meet the original specifications, and additional samples were obtained adjacent to these locations but further from the center of the fire damaged area. The approximate locations of the second group of samples are shown as 2R, 3R, 6R, 7R, and 8R on Figure 2. Due to additional failures of some of the samples obtained at Locations 2R, 6R (primary geomembrane liner only), and 7R, a third set of samples was required. The approximate locations of this third group of samples are shown as 2R2, 6R2, and 7R2 on Figure 2.

Baseline Samples. Baseline samples of the geosynthetic liner system components were taken from two locations approximately 50 m (160 ft) east of the fire damaged area. These samples were obtained from Locations 5 and 9, which are not depicted on Figure 2 due to scale restrictions.

It should be noted that unexposed archive samples of 80-mil HDPE geomembrane from the original 1989 installation were also tested. These samples are designated GMBLP-3 (Archive 6P) in Table 1 and GMBLS-3 (Archive 9) in Table 2.

GEOMEMBRANE TEST RESULTS

Test Methods. Laboratory tests were performed in accordance with appropriate American Society for Testing and Materials (ASTM) test methods. Test conducted on the geomembrane included thickness (ASTM Method D751), melt flow index (ASTM Method D1238), density (ASTM Method D792), and tensile properties (ASTM Method D638). Standard United States (US) units of measure are used herein since the original specifications, quality control and quality assurance test data, and the test results presented in this paper were all reported using these units.

Primary Geomembrane. Test results obtained on samples of primary geomembrane liner are summarized in Table 1. Primary geomembrane samples taken around the perimeter of the damaged area are designated as GMP-1 through GMP-3 and GMP-6 through GMP-8 in Table 1, and correspond to Locations 1 through 3, and 6 through 8, respectively, of Figure 2. A second set of samples obtained adjacent to Locations 6, 7, and 8 are given the suffix "R", while a third set taken near Locations 6 and 7 are designated by the suffix "R2." For simplicity, only the results of tests on the three baseline samples and final samples taken at each perimeter location (Samples GMP-1 through GMP-3, GMP-6R2, GMP-7R2, and GMP-8R) are shown in Table 1.

Table 1. Primary Geomembrane Test Results

Sample No.	Thickness (mils)	Density (g/cm^3)	Melt Flow Index (g/10min)	Tensile Strength at Break MD*(ppi)	Tensile Strength at Break TD*(ppi)	Tensile Elong. at Break MD*(%)	Tensile Elong. at Break TD*(%)
Min. Spec.	80.0	0.940	0.02	320.0	320.0	700	700
GMBLP-1	80.4	0.951	0.14	390.4	396.1	1054	1082
GMBLP-2	77.9	0.954	0.13	387.3	386.0	874	897
GMBLP-3	88.5	0.954	0.19	430.0	387.2	894	829
GMP-1	95.4	0.953	0.19	379.4	326.2	783	721
GMP-2	88.7	0.956	0.20	372.7	397.4	804	841
GMP-3	85.5	0.957	0.20	363.2	387.3	988	1041
GMP-6R2	88.9	0.957	0.19	391.5	387.7	817	827
GMP-7R2	85.2	0.956	0.15	395.0	401.3	818	842
GMP-8R	90.6	0.956	0.16	422.6	379.8	807	790

*MD = Machine Direction
 TD = Transverse Direction

Table 2. Secondary Geomembrane Test Results

Sample No.	Thickness (mils)	Density (g/cm^3)	Melt Flow Index (g/10min)	Tensile Strength at Break MD(ppi)	Tensile Strength at Break TD(ppi)	Tensile Elong. at Break MD(%)	Tensile Elong. at Break TD(%)
Min. Spec.	80.0	0.940	0.02	320.0	320.0	700	700
GMBLS-1	87.9	0.954	0.17	401.6	400.0	829	846
GMBLS-2	85.4	0.956	0.18	365.7	372.0	764	798
GMBLS-3	84.1	0.954	0.19	299.4	300.5	666	662
GMS-1	84.4	0.955	0.19	361.1	382.1	815	863
GMS-2R2	91.2	0.956	0.15	421.8	372.6	843	774
GMS-3R	85.9	0.955	0.15	393.0	401.5	802	818
GMS-6R	84.2	0.956	0.19	368.0	372.1	833	828
GMS-7R2	87.7	0.955	0.18	394.1	356.7	812	801
GMS-8R	89.9	0.955	0.19	394.6	340.1	831	713

As discussed above, the original specifications were to be used to establish the minimum standards on which to base acceptance of the perimeter samples, as long as the baseline samples test results were also consistently above these values. As this was generally the case for the primary geomembrane, the original specifications were used, and these minimum values for thickness, melt flow index, density, and tensile properties are listed in Table 1. The only exception to this was a low thickness measurement of 77.9 mils on Baseline Sample GMBLP-2. However, since the measured thickness values on the remainder of the baseline and perimeter samples all exceeded the 80-mil minimum listed in the specifications, no alteration of the minimum value for geomembrane thickness was deemed necessary.

The test results presented in Table 1 indicate that all perimeter samples of primary geomembrane met or exceeded the original specifications for thickness, density, melt flow index, tensile strength at yield, and tensile elongation at yield.

All of the baseline samples, as well as perimeter samples GMP-1 through GMP-3 met or exceeded the minimum specified values for tensile strength and elongation at break. The initial test results for tensile strength and/or elongation at break failed in one or both (machine and transverse) directions for Sample Nos. GMP-1, GMP-6, GMP-7, and GMP-8. The results of Sample No. GMP-1 were discarded since the geomembrane at this location was to be removed as part of the liner system repair. Subsequent sampling and testing of the primary geomembrane liner was required adjacent to Locations 6, 7, and 8 until Sample Nos. GMP-6R2, GMP-7R2, and GMP-8R passed the minimum criteria for tensile strength and elongation at break.

Based on the evaluation testing, the edge of the damage to the primary geomembrane liner was defined by Sample Nos. GMP-2, GMP-3, GMP-6R2, GMP-7R2, and GMP-8R. These locations are shown on Figure 2.

It is interesting to note that retesting of Sample Nos. GMP-6R2 and GMP-8R was required to achieve the minimum specified values for tensile strength and elongation at break without further excavation of waste or additional field sampling. Initial testing of these samples failed to meet one or more of the specified criteria based on the average of five or more specimens selected at random across the sample. Upon detailed review of the test results, a significant variation was noted between the data for individual specimens. The retesting was performed on specimens selected from the side of the sample which was furthest from the fire in an attempt to establish a pattern of variability within the sample. The results of this retesting indicated that much higher values of tensile strength and elongation at break were obtained from specimens taken furthest from the fire than from specimens selected randomly across the sample. Since the size of the samples was generally only 0.3 m (1 ft) by 1 m (3 ft), these findings appear to indicate a relatively abrupt increase in tensile properties of the primary geomembrane away from the fire. While a rigorous testing program to confirm this observation was not performed, the data obtained from the secondary geomembrane liner, as discussed below, also supports this conclusion.

<u>Secondary Geomembrane Liner.</u> Test results obtained on samples of secondary geomembrane liner are summarized in Table 2. Secondary geomembrane samples taken around the perimeter of the damaged area are designated as GMS-1 through GMS-3 and GMS-6 through GMS-8 in Table 2, and correspond to Locations 1 through 3, and 6 through 8, respectively, of Figure 2. A second set of samples obtained adjacent to Locations 2, 3, 6, 7, and 8 are given the suffix "R", while a third set taken near Locations 2 and 7 are designated by the suffix "R2." For simplicity, only the results of tests on the three baseline samples and final samples taken at each perimeter location (Samples GMS-1, GMS-2R2, GMS-3R, GMS-6R, GMS-7R2, and GMS-8R) are shown in Table 2.

Since the two baseline samples (GMBLS-1 and GMBLS-2) obtained from within the landfill exceeded the original specifications for geomembrane, these specifications were used to establish the minimum values for thickness, melt flow index, density, and tensile properties, which are listed in Table 2. It should be noted that the test results for tensile strength and elongation at break in both the machine and transverse directions for Baseline Sample GMBLS-3 were below the minimum specified values of 320 pounds per inch (ppi) and 700 percent, respectively. GMBLS-3 consisted of an archive sample of geomembrane which was stored at the site following installation of the liner system in 1989. While these test results indicated a possible degradation of tensile properties with time, the baseline samples obtained from within the landfill did not support this conclusion, so the original specifications were maintained as the minimum standards for geomembrane.

The test results presented in Table 2 indicate that all perimeter samples of secondary geomembrane met or exceeded the original specifications for thickness, density, melt flow index, tensile strength at yield, and tensile elongation at yield.

Of the initial set of perimeter samples tested, only GMS-1 met or exceeded the minimum specified values for tensile strength and elongation at break. The initial test results for tensile strength and/or elongation at break failed in one or both (machine and transverse) directions for Sample Nos. GMS-2, GMS-3, GMS-6, GMS-7, and GMS-8. Subsequent sampling and testing of the primary geomembrane liner was required adjacent to Locations 2, 3, 6, 7, and 8 until Sample Nos. GMS-2R2, GMS-3R, GMS-6R, GMS-7R2, and GMS-8R passed the minimum criteria for tensile strength and elongation at break.

Based on the evaluation testing, the edge of the damage to the secondary geomembrane liner was defined by Sample Nos. GMS-2R2, GMS-3R, GMS-6R, GMS-7R2, and GMS-8R. These locations are shown on Figure 2. Similar to the observations described above for two samples of the primary geomembrane liner, retesting of Sample Nos. GMS-6R and GMS-8R indicated that much higher values of tensile strength and elongation at break were obtained from specimens taken furthest from the fire than from specimens selected randomly across the sample.

GEONET TEST RESULTS

Test Methods. Tests conducted on geonet included thickness (ASTM Method D1777) and grab tensile strength and elongation. Grab tensile strength and elongation testing was performed in accordance with ASTM Method D1632 using a strain rate of 5 cm (2 in) per minute and a gauge length of 6.4 cm (2.5 in). Although Method D1682 has been discontinued by ASTM and replaced with Method D5035, ASTM D1682 was utilized, with the modifications noted, to be consistent with the original specifications and to reflect the procedures utilized by the geonet manufacturer in 1989.

It should be noted that the strand structure of geonet materials, and the non-homogenous strength and elongation of the strand elements, cause the load-displacement (stress-strain) curves to be somewhat erratic and therefore subject to interpretation. As a result, "break" was defined for the purpose of this evaluation as the point (both strength and corresponding elongation) beyond yield of the material at which the first geonet strand ruptures.

Primary Geonet. The results of testing performed on samples of primary geonet are summarized in Table 3. Primary geonet samples obtained around the perimeter of the damaged area are designated as GNP-1 through GNP-3 and GNP-6 through GNP-8 in Table 3, and correspond to Locations 1 through 3, and 6 through 8, respectively, of Figure 2. A second set of samples obtained adjacent to Locations 2, 3, 6, 7, and 8 are given the suffix "R", while a third set taken near Locations 2 and 7 are designated by the suffix "R2." For simplicity, only the results of tests on the two baseline samples and final samples taken at each perimeter location (Samples GNP-1, GNP-2R2, GNP-3R, GNP-6R, GNP-7R2, and GNP-8R) are shown in Table 3.

The test results presented in Table 3 indicate that all baseline and perimeter samples of primary geonet exceeded the original specification for thickness and grab tensile strength in the machine direction. The results of grab tensile strength in the transverse direction were all consistently below the original minimum specification of 50 pounds per inch of width (ppi) for both the baseline and perimeter samples. The orientation of the sample (machine or transverse direction) was not stipulated in the original specifications. Since geonet rolls are, with only rare exception, placed such that the machine direction is along the line of maximum slope (down slope rather than cross slope), it was assumed that the original specification refers to the strength of the geonet in the machine direction only. This conclusion was supported by an examination of the original quality control data which presented grab tensile strength results below 50 ppi in the transverse direction. Furthermore, the manufacturer's own specification for grab tensile strength at break in the transverse direction was 30 ppi at the time the geonet was manufactured (1989), although this value was not specifically listed in the original specifications for the project. Since the results of grab elongation in the transverse direction for both the baseline and perimeter samples were comparable, this property was not considered in the evaluation of the acceptability of the perimeter samples.

Table 3. Primary Geonet Test Results

Sample No.	Thickness (mils)	Grab Tensile Strength at Break MD(ppi)	Grab Tensile Strength at Break TD(ppi)	Grab Tensile Elongation at Break MD(%)	Grab Tensile Elongation at Break TD(%)
Min. Spec.	200.0	50.0	--	200	100
GNBLP-1	276.6	56.9	41.8	102	143
GNBLP-2	285.3	60.5	37.9	85	143
GNP-1	277.7	71.3	36.3	34	188
GNP-2R2	272.0	69.8	42.4	49	140
GNP-3R	279.7	68.0	43.8	403	163
GNP-6R	268.4	64.6	40.3	64	170
GNP-7R2	290.6	62.8	36.2	67	178
GNP-8R	272.7	67.2	40.2	97	424

Table 4. Secondary Geonet Test Results

Sample No.	Thickness (mils)	Grab Tensile Strength at Break MD(ppi)	Grab Tensile Strength at Break TD(ppi)	Grab Tensile Elongation at Break MD(%)	Grab Tensile Elongation at Break TD(%)
Min. Spec.	200.0	50.0	--	200	100
GNBLS-1	273.8	60.6	41.8	71	286
GNBLS-2	275.4	60.9	38.2	53	196
GNS-1	278.1	66.1	42.0	76	165
GNS-2R2	276.1	53.8	39.8	72	131
GNS-3R	266.1	52.3	37.0	178	258
GNS-6R	254.6	61.1	40.0	58	134
GNS-7R2	283.0	71.6	42.0	255	201
GNS-8R	275.6	59.9	42.9	125	359

The results of grab tensile elongation at break in the machine direction for all primary geonet samples were below the original minimum specification of 200 percent. The results of grab tensile elongation at break in the transverse direction for all samples exceeded the original minimum specification of 100 percent, except for Samples GNP-6 and GNP-8. Subsequent testing of Samples GNP-6R and GNP-8R exceeded the 100 percent for grab elongation in the transverse direction.

Two of the primary geonet material samples (GNP-3R and GNP-8R) exceeded the lowest baseline values for tensile elongation at break in the machine direction (85 percent). The remaining three samples (GNP-2R2, GNP-6R and GNP-7R2) were less than the lowest baseline value. As a result, a statistical evaluation of this property was performed.

For the purpose of this statistical evaluation, the baseline samples from both geonet layers were considered representative of the primary geonet. This assumption improves the level of confidence of the results of the analysis by expanding the baseline data base, and is considered valid because all of the geonet material was produced by the same manufacturer, to the same specifications, and installed through random selection of the rolls from an on-site stockpile. Furthermore, this assumption can be considered conservative because, once installed, the secondary geonet was not subject to the same exposure conditions as the primary geonet and, therefore, would be expected to be of equal or better quality at the time the baseline samples were obtained.

The statistical analysis was performed by comparing test results from the five final perimeter samples of primary geonet (GNP-2R2, GNP-3R, GNP-6R, GNP-7R2, and GNP-8R) and data obtained from the four baseline samples of primary and secondary geonet (GNBLP-1, GNBLP-2, GNBLS-1, and GNBLS-2) to see if the samples were of equal quality. Two assumptions were required to conduct the statistical analysis. The first is that the data is normally distributed. The natural logarithm (ln) of elongation (ε) is normally distributed based on a normal probability plot and the Kolmogorov-Smirnov test. Secondly, the data should be statistically independent. Specimen results within a given sample are not independent based on an analysis of variance; hence average values of $\ln(\varepsilon)$ for the samples were analyzed, giving nine independent test results (four baseline and five perimeter samples). The mean $\ln(\varepsilon)$ for the perimeter samples was compared to that of the baseline samples using a t-test. This analysis indicated that the mean $\ln(\varepsilon)$ for the perimeter samples is greater than or equal to that for the baseline samples at the 5 percent significance level (i.e., a 95 percent confidence level). It was then concluded that the perimeter samples have a quality that is at least equal to that of the baseline samples. A plot of the $\ln(\varepsilon)$ of each specimen, as well as the mean, from each of the baseline and perimeter samples of the primary geonet is presented on Figure 3.

Another approach to the analysis is to compare individual specimen results from the perimeter samples to the individual specimen results from the baseline samples. If it is assumed that $\ln(\varepsilon)$ is normally distributed, the lower 95 percentile value from the 20 baseline samples is 3.51 ln(%). A comparison of this lower bound to the results of the 25 individual perimeter specimens indicates that none of these 25 perimeter specimens has a $\ln(\varepsilon)$ value less than 3.51 ln(%). Based on this analysis, each of the primary geonet samples is acceptable as defining the limit of the area damaged by the fire based on this property.
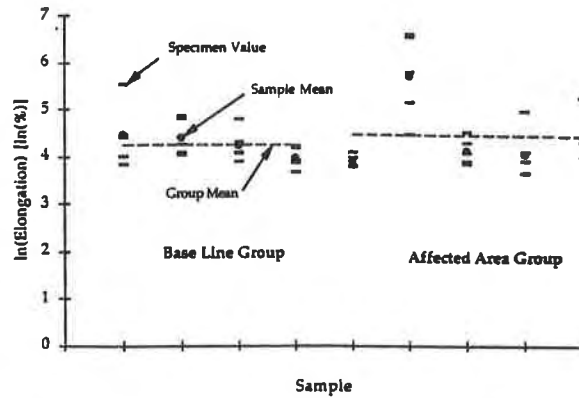
Figure 3 Plot of ln(ε) for Primary Geonet and Baseline Samples

Based on this evaluation, the primary geonet samples (GMP-2 R2, GNP-3R, GNP-6R, GNP-7R2, and GNP-8R) were deemed to be of equal or greater quality than the baseline samples within appropriate statistical significance. Therefore, these five samples sufficiently defined the limits of the fire-damaged area for this material and established, at a minimum, the perimeter of the area to be repaired.

Secondary Geonet. The results of testing performed on samples of secondary geonet are summarized in Table 4. Secondary geonet samples obtained around the perimeter of the damaged area are designated as GNS-1 through GNS-3 and GNS-6 through GNS-8 in Table 4, and correspond to Locations 1 through 3, and 6 through 8, respectively, of Figure 2. A second set of samples obtained adjacent to Locations 2, 3, 6, 7, and 8 are given the suffix "R", while a third set taken near Locations 2 and 7 are designated by the suffix "R2." For simplicity, only the results of tests on the two baseline samples and final samples taken at each perimeter location (Samples GNS-1, GNS-2R2, GNS-3R, GNS-6R, GNS-7R2, and GNS-8R) are shown in Table 4.

The test results presented in Table 4 indicate that all baseline and perimeter samples of secondary geonet exceeded the original specification for thickness and grab tensile strength in the machine direction. As with the primary geonet, the original minimum specification of 50 pounds per inch of width (ppi) was interpreted as not being applicable to grab tensile strength in the transverse direction. Since the results of grab elongation in the transverse direction for both the baseline and perimeter samples were comparable, this property was not considered in the evaluation of the acceptability of the perimeter samples.

The results of grab tensile elongation at break in the machine direction for all secondary geonet samples were below the original minimum specification of 200 percent. However, all perimeter sample test results for this property exceeded the lowest baseline result of 53 percent, and all but GNS-6R exceeded the highest baseline result of 71 percent. Based on this comparison, the perimeter samples were considered to be statistically equivalent to the baseline samples without further analysis.

The results of grab tensile elongation at break in the transverse direction for all samples exceeded the original minimum specification of 100 percent, except for Sample GNS-7. Subsequent testing of Sample GNS-7R2 exceeded the 100 percent minimum specification for grab elongation in the transverse direction.

Based on this evaluation, the secondary geonet layer material meets or exceeds the original material specifications and/or the baseline sample test results. Therefore, the five final samples of geonet sufficiently define the limits of the fire-damaged area for this material and establish, at a minimum, the perimeter of the area to be repaired.

SUMMARY AND CONCLUSIONS

A fire in a hazardous waste landfill was found to have damaged the bottom liner system. Following removal of waste and visibly damaged liner system components, a testing program was conducted to confirm that a sufficient area of material had been removed. Testing performed on HDPE geomembrane and geonet included tensile characteristics and index physical properties. Subsequent resampling was required at some locations around the perimeter of the visibly damaged area until test results met or exceeded the original specifications. This approach was successful for the geomembranes and the geonets with the exception of grab tensile elongation at break in the machine direction for the geonets. Acceptance of these layers required that a statistical analysis be performed on this property using baseline sample data collected from another part of the landfill unaffected by the fire. This analysis demonstrated that the primary geonet samples were statistically equivalent to the baseline samples within a 95 percent confidence level. This testing program was used to define the limits of damaged material requiring repair. The practical approach taken for this evaluation allowed for comparison of simple physical/mechanical properties obtained during the testing program with the original specifications and QA/QC test results documented prior to material installation. The statistical analysis provided a rational basis of acceptance of materials without unnecessary additional waste removal and delay in repair of the damaged liner system of an active hazardous waste landfill, which minimized the potential for harm to public health and the environment.

ACKNOWLEDGMENTS

REFERENCES

Koerner, Robert M. (1994) "Designing with Geosynthetics", Third Edition, Prentice-Hall, Inc., Englewood Cliffs, New Jersey, 704 pp.

GEONET LEAKAGE DETECTION SYSTEM FLOW PATTERNS FOR ZERO LEAKAGE ESTIMATION OF LANDFILL DOUBLE LINER SYSTEMS

M. SHIVASHANKAR,
ECKLER ENGINEERING, CORAL SPRINGS, FLORIDA, USA
J. E. FLUET, JR.,
J&G ASSOCIATES, EAST WAKEFIELD, NEW HAMPSHIRE, USA
D. V. REDDY,
DEPARTMENT OF OCEAN ENGINEERING, FAU, BOCA RATON, FLORIDA, USA.

ABSTRACT

Many modern landfills are constructed with double liner systems. Leachate leakage rates through double liner systems are calculated using recently developed formulations which are theoretically correct for leakage detection system (LDS) materials that have unrestricted lateral flow properties. But their applicability to geonets, the most commonly used LDS material, has yet to be determined. In double liner systems, the leakage through the primary liner, the properties of the LDS material, and the slope of the LDS determine the flow patterns in the LDS. These flow patterns are then used to determine the amount of leachate, if any, which leaks through the bottom liner into the ground.

This paper reports the experimental determination of the flow patterns in geonets, and their relationships to established design formulations. It also proposes new and more accurate design formulations.

1. INTRODUCTION

Double liner systems are being used to contain leachate in many modern municipal and all hazardous landfills and surface impoundments. These double liner systems typically have geomembrane or composite top and composite bottom liners with a leakage detection system (LDS), sometimes called a secondary leachate collection system, between the two liners. In the case of landfills the double liner system also includes a leachate collection system (LCS) above the top liner. The types of liners and drainage materials significantly influence the flow patterns and the flow rates in the leakage detection layer. Figure 1 schematically illustrates a double liner system.
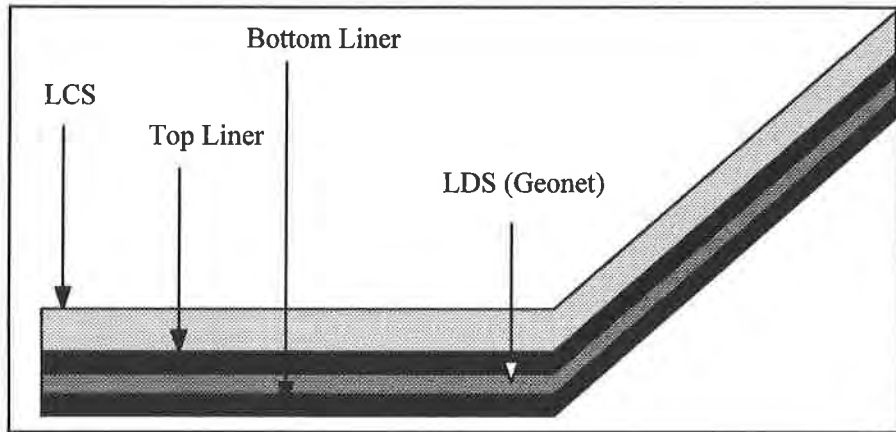
Figure 1 Cross-section of a double liner system

1.1 Technical Background   Giroud, Bonaparte and others have developed analytically and empirically-based liner system equations which have become the industry standard [1,4,5,6,7]. Liner system calculations typically begin with determination of the quantity of leachate generated and the rate at which it enters the LCS. The resulting flow patterns in the LCS are then determined and used to calculate leachate leakage through the top liner into the LDS. The LDS flow patterns are then determined and used to assess: the impact of top liner leakage, action leakage rates (ALR) for hazardous sites, leak detection time, the probability of zero leakage through the bottom liner, and leachate leakage, if any, through the bottom liner.

1.2 Probability of Zero Leakage   All of the above LDS flow pattern-related calculations have been discussed elsewhere [1,2,9], except for the probability of zero leakage. In any double liner system, there is a probability that a hole in any given area of the bottom liner will not be aligned "downstream" of the leakage through a hole in the overlying top liner. If the hole in the bottom liner is not in the wetted area created by the flow from the leakage through the top liner, Figure 2, there will be no leakage through the bottom liner.

In the case where there is one hole in each of the top and bottom liners the probability of the bottom liner hole not being in the LDS "wetted area" due to the top liner leak may be determined by calculating the area of the LDS flow path, and comparing that to the area considered.

The following equation for the width of the LDS flow path has been developed by Giroud[4],

$$B = \{2(Q_l/k)^{0.5}/\sin\alpha\}\ \{1+[2 \times \sin\alpha\ /(Q_l/k)^{0.5}]\}^{0.5} \dots\dots\dots\dots\dots\dots (1)$$

where:
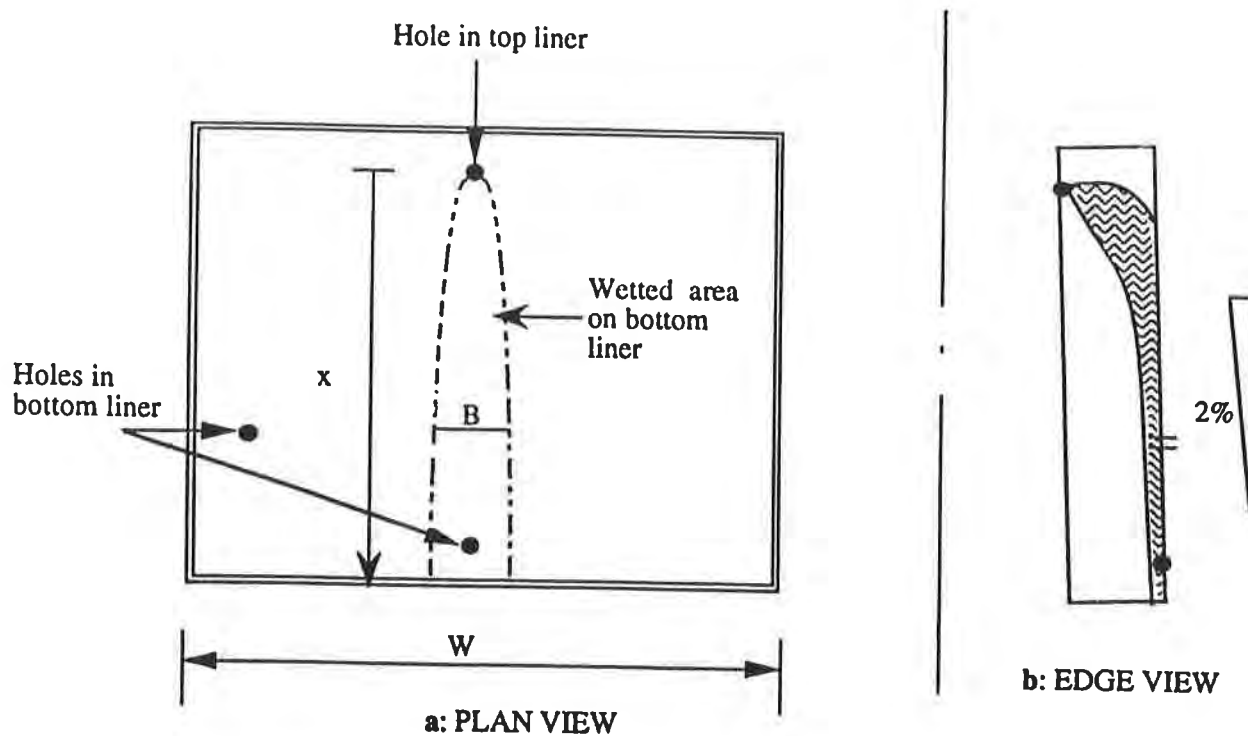
Figure 2. Alignment of holes in top and bottom liners

B = width of the LDS flow path (m);
Q_l = leakage through hole in top liner (m³/s);
k = hydraulic conductivity of the LDS (m/s);
α = slope of the LDS (deg);
x = distance downstream from the hole in the top liner (m).

When the distance, x, is maximum, i.e., x_{max}, then the equation determines the maximum width of the flow path, B_{max}. Similarly, use of the average distance, x_{ave}, will produce the average width, B_{ave}.

Equation 1 is theoretically correct, but does not consider the variation in LDS flow patterns which might be generated by geonets as opposed to, say, gravel. Unlike gravel or other equally non-laterally flow restrictive materials, geonets (the most popular choice for LDS materials) somewhat restrict the lateral flow.

Assuming 1 hole in each of the top and bottom liners, a conservative estimate of the percentage probability of the hole in the bottom liner not being in the wetted area due the leakage through the top hole (i.e., the probability of zero leakage into the ground) was given by Fluet [3] as follows:

$$P = \{1 - B_{max}/W\} \times 100. \quad\dots\dots\dots\dots\dots\dots\dots\dots\dots\dots\dots\dots\dots\dots\dots\dots\dots (2)$$

where:

P = percentage probability of zero leakage through the bottom liner (%);

B_{max} = width of the flow path at the maximum possible distance x_{max} from the hole in the top liner obtained from Equation 1 (m);

W = width available for flow (m).

This expression may also be stated as:

$$P = \{1-A_w/A_t\} \times 100. \qquad\qquad\qquad (3)$$

where:

A_w = the maximum wetted area in the LDS (m^2);

A_t = the LDS area available for flow, (m^2).

A_t, the area available for flow, is the area that corresponds to one leakage hole. For example, for a high degree of quality assurance, one may expect one hole per 4047m^2 (suggested practice for designers [1], when the design standard is one hole per acre), and A_t would be 4047m^2. With lesser quality assurance, one might expect one hole per 1350m^2 (when the design standard is three holes per acre), and A_t would be 1350m^2.

This formulation quite conservatively assumes that the shape of the flow path is rectangular with a width equal to the widest point of the actual shape. It underestimates the actual probability of zero leakage, since it assumes a rectangular flow area which envelops the actual parabolic area.

2.0 SCOPE OF THE STUDY

The study included two objectives:

1. Design and fabrication of a test setup to determine the flow patterns in geonets, and
2. Development of improved design formulations for prediction of the probability of zero leakage into the ground.

The first objective was achieved by constructing a tilt-table supporting a large box in which the different layers of geosynthetics were placed to simulate a typical landfill double liner system, and monitoring the actual flow patterns in geonets resulting from a leak hole in the overlying primary liner. The second objective was achieved by analytically and empirically improving Equations 1 and 3 and developing new formulations.

3.0 EXPERIMENTAL PROCEDURE

The study was conducted in a box measuring, 2.44 m x 2.44 m x 15 cm., and mounted on a Tilt-Table. The table is hinged on the downstream side and rests on a screw jack on the

upstream side, allowing a tilt up to 20^0. A small tank fitted with a float to maintain a constant head provides the input flow, and another tank across the downstream width of the table, collects the flow. A schematic of the tilt-table is shown in Figure 3, and a cross-section of the simulated liner system is shown in Figure 4.
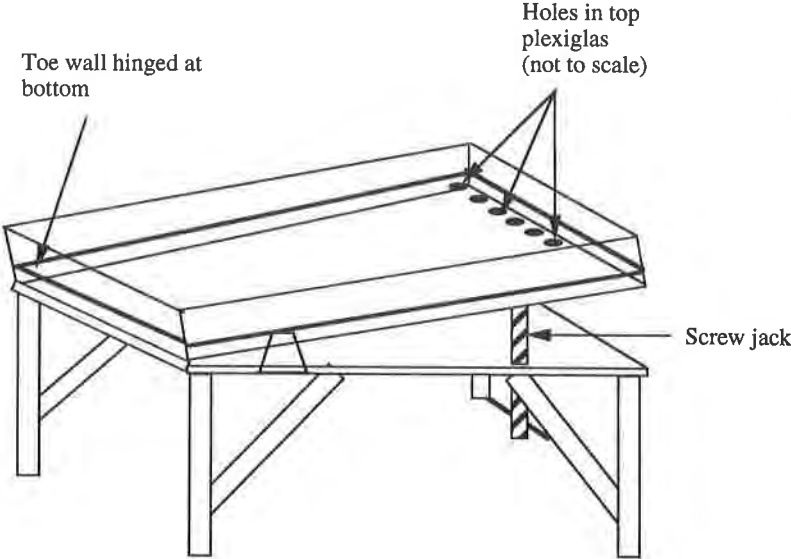
Figure 3   Schematic of the tilt-table

a: Side view

b: Elevation view
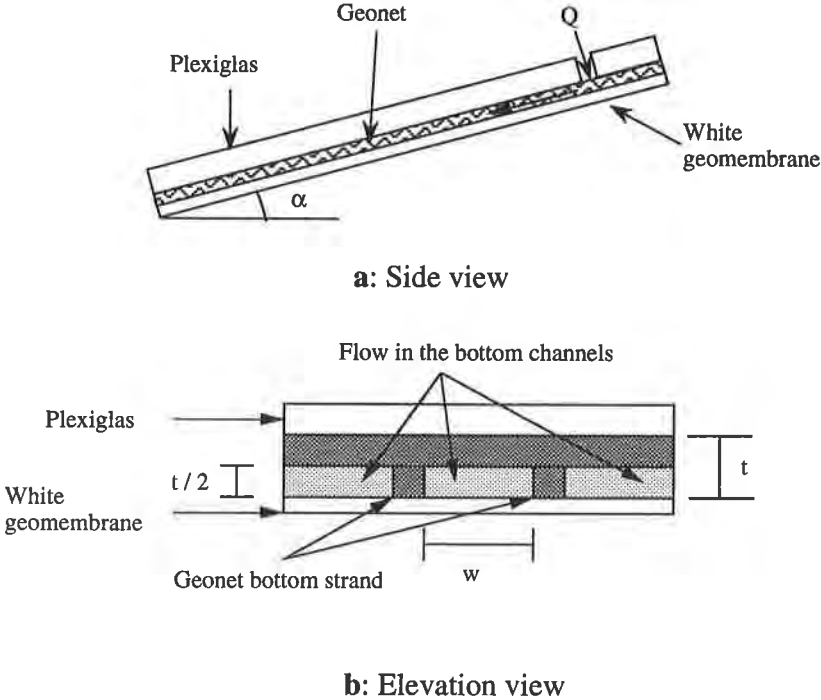
Figure 4   Cross-section of the simulated liner system

A 5.5 mm thick geonet, with a published hydraulic transmissivity of 2×10^{-3} m^2/s, was used for the testing. A white geomembrane was used as the bottom liner in order to better observe the flow patterns. The geonet was placed on the white geomembrane and was then overlaid by a 12 mm thick plexiglas sheet which acted as the top liner. Flow into the geonet LDS was introduced through 1cm^2 holes in the plexiglas. To further enhance the monitoring, the flow water was mixed with a fluorescent dye. Steel plates were placed on the plexiglas to produce a total confining stress of 0.15 kPa on the geonet. This is comparable to the lowest stress seen in the field.

The study was conducted at six different slopes: 1°, 2°, 5°, 8°, 11°, and 14° to observe the variation in the flow patterns.

Five different input flow rates were used:
- 1.702 x 10-4 m^3/s
- 1.223 x 10-4 m^3/s
- 1.032 x 10-4 m^3/s
- 8.333 x 10-5 m^3/s
- 6.333 x 10-5 m^3/s

The upper limit of the flow rates approximates the maximum flow through a 1cm^2 hole in a permitted liner system, and the lower limit is the lowest flow/slope combination which produced coherent flow channels. Flow rates below this level result in several discrete flow channels.

3.1 Observations. The bottom channels of the geonet clearly have a major influence on the flow patterns, Figure 5. In terms of the physical characteristics the geonet can also be identified by the number of channels per unit width (N_w). This is a key characteristic since geonets allow only channel flow. For the geonet sample used in this study, there were 86 channels per meter of the geonet width with each channel being 8mm wide (internal dimension).
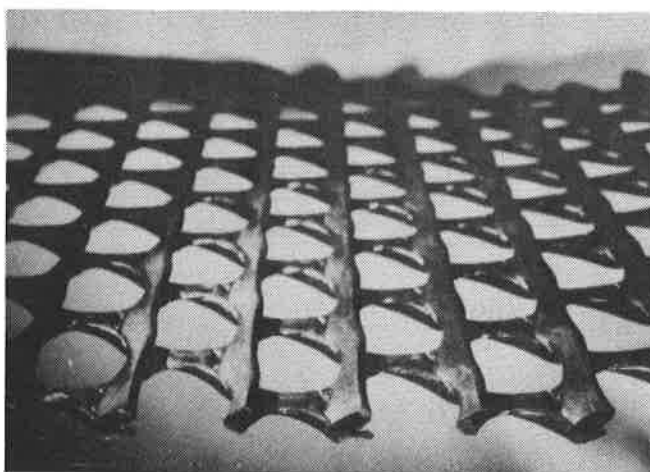
Figure 5   3-D picture of a typical geonet

The dyed water spread laterally as the flow depth exceeded the thickness of each bottom geonet strand. In other words, the water spread to the adjacent channels as it exceeded the capacity of each channel. This reached a location where the number and total volume of the bottom geonet channels was adequate to contain the flow. Beyond this point, the dyed water flowed in the same number of geonet bottom channels without any further spreading. This width, where the water flows in a fixed number of channels, is referred to in the study as the "stabilized width", and the location where the stabilized width begins is called as "transition point." The area prior to the transition point is called the "initial flow region". The initial flow region was observed to be approximately triangular. This phenomenon is observed whenever the confining stress is adequate to cause full contact between the bottom geonet strands and the underlying geomembrane. However, when the confining stresses are very low, the flow could spread by escaping through the spaces between the bottom geonet strands and the underlying geomembrane. This could result in flow patterns which differ from the one described above. It is noteworthy that the study was done at a very low confining stress($\approx$ 0.15 kPa); and virtually no flow was observed beneath the bottom geonet strands. It may, therefore, be concluded that, as a practical matter, no flow will occur beneath the lower geonet strands under field conditions.

3.2 Measurements. The widths of the flow paths were measured transverse to the direction of flow from the leak hole to the downstream end, for all the different combinations of flow rates and bottom slopes, at regular intervals. The width measurement was possible up to a downstream distance of approximately 2.25m.

4.0 ANALYSIS

4.1 Initial flow region. The initial flow region of the geonet LDS flow path was investigated for various bottom slopes and discharges. The actual widths measured were plotted against the distance downstream and compared with the calculated values using Equation 1 for the same set of variables. The procedure was followed for all the different sets of acquired data. For slopes steeper than 5 degrees, the widths estimated by Equation 1 are very close to the observed values, although Equation 1 describes a parabolic flow path, and the shape of the actual initial flow path is more triangular than parabolic. For slopes flatter than 5 degrees, Equation 1 overestimates the actual flow widths. For such shallow slopes, the following empirically derived modification to Equation 1 better fits the observed data:

$$B = \{1.5(Q_l/k)^{0.5}/\sin\alpha\} \{0.5+[2 \times \sin\alpha /(Q_l/k)^{0.5}]\}^{0.5} \quad \dots \dots \dots \dots \dots \quad (4)$$

where:
B   =   width of the LDS flow path (m);
Q_l =   leakage through hole in top liner (m³/s);
k   =   hydraulic conductivity of the LDS (m/s);
α =   slope of the LDS (deg);
x   =   distance downstream from the hole in the top liner (m).

Equation 4 is henceforth referred to as the "modified Giroud Equation". The actual widths of the flows at shallow slopes, the flow width estimations using Giroud's equation and the flow width estimations using modified Giroud's equation are shown graphically in Figures 6.
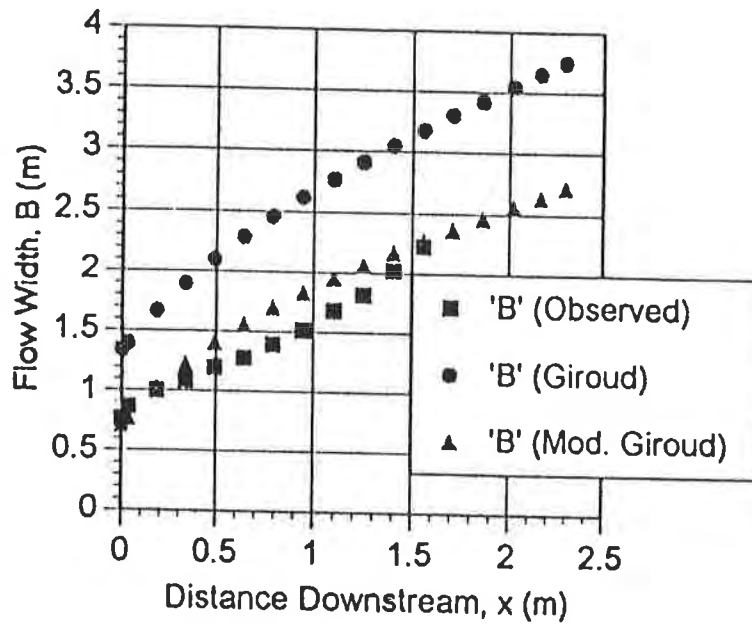
$\alpha = 1.15° \ \& \ Q = 6.33E\text{-}5 \ m^3/s$
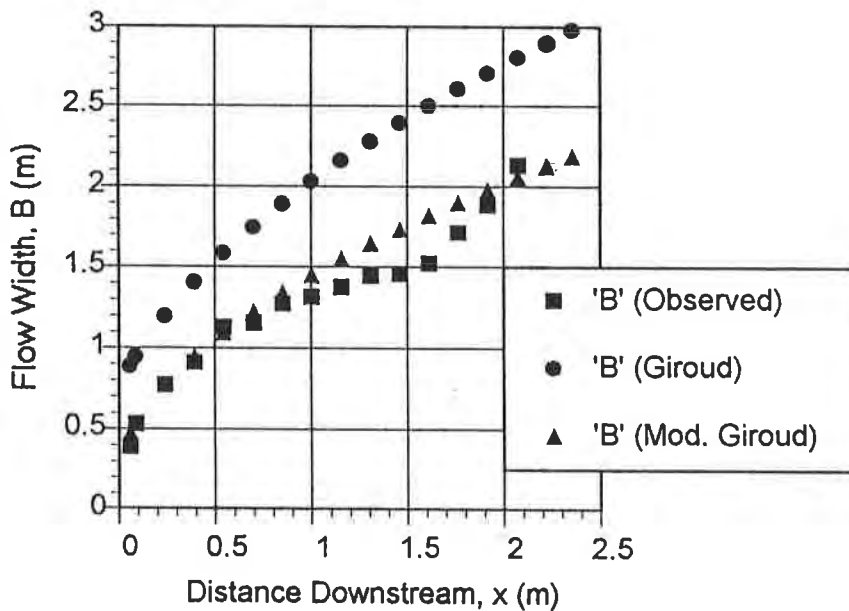
$\alpha = 2° \ and \ Q = 8.33E\text{-}5 \ m^3/s$

Figure 6 Comparison graphs

4.2 Stabilized flow width. Due to the limitations of the apparatus used in this study, it was not possible to experimentally determine the transition point for all conditions studied. However, recognizing that the transition point is needed to determine the stabilized flow widths of the flow patterns and the wetted areas in the geonet LDS, an analytical expression was derived. This analytical expression is based on the concept of channel flow in the geonet. Specifically, if the confining stress is adequate, the geonet bottom strands are firmly in contact with the underlying geomembrane, and flow will spread only by overflowing the geonet bottom channels. The transition point is, therefore, the point at which a given number of geonet bottom channels carry all of the flow. The total width of the those "wetted" channels is the stabilized flow width.

To determine the stabilized flow width, one must first determine the flow velocity. Manning's formula can be used to determine the flow velocity. The mean velocity of flow, V, is given by,

$$V = (1/n) R^{2/3} S^{1/2} \dots\dots\dots (5)$$

where:

n = Manning's roughness coefficient which depends on the nature of the channel materials (for polymeric materials it is approximately 0.012);

R = the hydraulic radius (m);

S = slope of the hydraulic gradient (deg.).

Since the flow is not pressurized, the hydraulic gradient is approximately parallel to the bottom slope. Therefore,

$$S = \tan\alpha \dots\dots\dots (6)$$

where:

α = bottom slope (deg.).

Considering that the liquid flows full in the geonet channel, the wetted perimeter of the channel, P, can be estimated as

$$P = (t/2 + t/2 + w) = (t + w) \dots\dots\dots (7)$$

where:

t = thickness of the geonet (m);

w = the interior width of one geonet channel (m).

The hydraulic radius, R, can then be estimated as

$$R = A_c/P, (m).$$
$$= A_c/(t + w) \dots\dots\dots (8)$$

where:

A_c = cross sectional area of a geonet channel (m²).

Since, also

$$A_c = (t/2)(w) \ldots \ldots (9)$$

then,

$$R = (1/2 \ tw)/(t+w) \ldots \ldots (10)$$

Therefore, combining Equations 5, 6, and 10,

$$V = \{1/n\} \ \{(1/2 \ tw)/(t+w)\}^{2/3} \ \{\tan\alpha\}^{1/2} \ldots \ldots (11)$$

By continuity, we know that the flow rate is the same at all the cross sections of the flow.

$$Q = V \ A \ldots \ldots (12)$$

where:

V   =   flow velocity, Equation 11;
A   =   cross sectional area of flow (m^2),

Also,

$$A = A_c \ N \ldots \ldots (13)$$

where:

A_c =   cross-sectional area of a given geonet channel, Equation 9;
N   =   the number of geonet channels in which the liquid flows.

Now, by combining Equations 11, 12, and 13,

$$A_c = [n \ Q] / [N \ \{(1/2 \ tw)/(t+w)\}^{2/3} \ \{\tan\alpha\}^{1/2}] \ldots \ldots (14)$$

where:

$$Q = Q_1 = \text{leakage through hole in top liner (m3/s)};$$

Then, combining Equations 9 and 14, and solving for N,

$$N = [2 \ n \ Q_1] / [t \ w \ \{(1/2 \ tw)/(t+w)\}^{2/3} \ \{\tan\alpha\}^{1/2}] \ldots \ldots (15)$$

Finally, the overall stabilized flow width is given by

$$B_s = N / N_w \ldots \ldots (16)$$

where:

B_s =   stabilized flow width (m);
N   =   the number of geonet channels in which the liquid flows;
N_w =   the number of channels per unit width of of geonet (m^{-1}).

Or, stated in a more usable form,

$$B_s = [2 \, n \, Q_1] \, / \, [N_w \, t \, w \, \{(1/2 \; tw)/(t + w)\}^{2/3} \; \{\tan\alpha\}^{1/2}] \dots \dots \dots \dots \dots (17)$$

This width (B_s) includes the bottom of the geonet strands which are in contact with the bottom geomembrane. Since this contact surface is not wetted, the widths of the bottom geonet strands must be excluded from leakage calculations. Therefore, for leakage calculations, the width of the bottom geomembrane which is wetted by the channel flow is given by:

$$B_w = N \, w \dots \dots \dots \dots \dots \dots \dots \dots \dots \dots \dots \dots \dots \dots \dots \dots (18)$$

where:
B_w = the wetted width (m);
N = the number of geonet channels in which the liquid flows;
w = the interior width of one geonet channel (m);

Or, stated in a more usable form,

$$B_w = [2 \, n \, w \, Q_1] \, / \, [\, t \, w \, \{(1/2 \; tw)/(t + w)\}^{2/3} \; \{\tan\alpha\}^{1/2}] \dots \dots \dots \dots \dots (19)$$

4.3 Probability of zero leakage into the ground. The actual wetted area of the LDS, prior to the stabilization of the flow width, may be determined by integrating Equation 1, with respect to the distance downstream (x). The resulting equation is:

$$A_{wl} = \frac{2Q_1}{3k(\sin\alpha)^2} \left\{ 1 + \frac{2x\sin\alpha}{\sqrt{\dfrac{Q_1}{k}}} \right\}^{\frac{3}{2}} \tag{20}$$

where:
A_{wl} = wetted area in the LDS (m²);
x = length of LDS flow path (m);
Q_1 = leakage through top liner (m³/s);
k = hydraulic conductivity of the LDS (m/s);
α = slope of the LDS (deg);

In the case of geonet restricted lateral flow, the maximum wetted area can be closely approximated by:

$$A_{w2} = B_w \, x_{max} \dots \dots \dots \dots \dots \dots \dots \dots \dots \dots \dots \dots \dots \dots \dots \dots \dots (21)$$

where:
A_{w2} = maximum wetted area in the LDS (m²);

B_w = the stabilized width (m);

X_{max} = maximum distance downstream, of LDS flow path (m).

This conservatively assumes the entire area is rectangular, whereas the initial width prior to the transition point is actually triangular. Nonetheless, since the initial width area is relatively small, the rectangular assumption is valid.

Therefore, by combining Equations 3, 20, and 21, the percentage probability of a hole in the bottom liner not being in the wetted area due to the leakage through the top hole is given by:

$$P = \{1 - A_{wo}/A_t\} \, 100 \quad \dots\dots\dots\dots\dots\dots\dots\dots\dots\dots\dots \quad (22)$$

where:

P = probability of zero leakage (%);

A_{wo} = A_{w1} or A_{w2} (Equations 20,21) as appropriate (m²)

A_t = the LDS area available for flow, (m²).

This modified version (using A_{w1} or A_{w2}) of Fluet's original equation is more accurate and should, therefore, be used henceforth.

5. CONCLUSIONS

The modified methodology predicts more accurate values to calculate the wetted area in the geonet LDS due to the top liner leak, and to determine the probability of zero leakage into the ground.

The study results clearly demonstrate that the analysis of geonet lateral flow differs from that of gravel. Specifically, the study concludes that the Giroud equation for flow widths has only limited application to geonet flow and must be applied or modified as follows:

- For slopes greater than 5 degrees, the Giroud equation is valid in the initial flow region only.

- In the initial flow region, for slopes less than 5 degrees, the Giroud equation must be empirically modified as follows:

$$B = \{1.5(Q_i/k)^{0.5}/\sin\alpha\} \, \{0.5+[2 \text{ x } \sin\alpha \, /(Q_i/k)^{0.5}]\}^{0.5}$$

- For the stabilized flow width, the following analytically derived equation must be used:

$$B_w = [2 \text{ n w } Q_i] / [\text{ t w } \{(1/2 \text{ tw})/(t + w)\}^{2/3} \, \{\tan\alpha\}^{1/2}]$$

The study also concludes that the Fluet equation for probability of zero leakage calculations should be modified as follows:

$$P = \{1 - A_{wo}/A_c\}\,100$$

where A_{wo} is:

- For unrestricted lateral flow,

$$A_{wl} = \frac{2Q_1}{3k(\sin\alpha)^2}\left\{1 + \frac{2x\sin\alpha}{\sqrt{\dfrac{Q_1}{k}}}\right\}^{\frac{3}{2}}$$

- For geonet flow,

$$A_{w2} = [2\,n\,w\,Q_1\,x_{max}]\,/\,[\,t\,w\,\{(1/2\;tw)/(t+w)\}^{2/3}\,\{\tan\alpha\}^{1/2}]$$

where:
A_{w2} = maximum wetted area in the LDS (m^2);
B_w = the stabilized width as shown above (m);

6. ACKNOWLEDGEMENTS

7. REFERENCES

1.   Bonaparte, R., Giroud, J. P., and Gross, B. A., "Rates of Leakage Through Landfill Liners", Proceedings of Geosynthetics '89, San Diego, CA, IFAI, St. Paul, MN, Vol. 1, 1989, pp. 18-28.

2.   Fluet, J. E., and Reddi V. J.,"The Role of Monitoring Wells in Modern Landfill Designs", Report to the Florida Center For Solid and Hazardous Waste Management, 1994.

3. Fluet, J. E., Jr., "A Comparison of Florida Landfill Liner System Standards to Federal Standards," Report submitted to FDER, Rev 16, July 1993.

4. Giroud, J. P., Gross, B. A., and Durasse, J., "Flow in Leachate Collection Layers", in Design and Performance of Geosynthetic Lining Systems for Waste Containment, IFAI Publishers, St. Paul, MN, 1993.

5. Giroud, J. P., and Bonaparte, R., "Leakage Through Liners Constructed with Geomembranes, Part I: Geomembrane Liners", Geotextiles and Geomembranes, Vol. 8, No. 1, 1989, pp. 27-67.

6. Giroud, J. P., and Bonaparte, R., "Leakage Through Liners Constructed with Geomembranes, Part II: Geomembrane Liners", Geotextiles and Geomembranes, Vol. 8, No. 2, 1989, pp. 71-111.

7. Giroud, J. P., Khatami, A., and Badu-Twenaboah, K., "Evaluation of the Rate of Leakage Through Composite Liners", Geotextiles and Geomembranes, Vol. 8, No. 4, 1989, pp. 337-340.

8. Giroud, J. P., and Fluet, J. E., Jr., "Quality Assurance of Geosynthetic Lining Systems", Geotextiles and Geomembranes, Vol. 3, No. 4, 1986, pp. 249-287.

9. USEPA Document #EPA 530-R-92-004, "Action Leakage Rates for Leak Detection Systems", 69p.

LOCATING GEOMEMBRANE LINER LEAKS UNDER WASTE IN A LANDFILL

D. L. Laine
Leak Location Services, Inc., U.S.A.
A.M. Binley, Ph.D.
Lancaster University, U.K.
G.T. Darilek, P.E.
Leak Location Services, Inc., U.S.A.

ABSTRACT

An Electrical Leak Imaging and Monitoring (ELIM [SM]) survey was used to locate leaks under 2.5 meters of stabilized waste in an active geomembrane-lined landfill. The landfill is lined with two 2-mm thick HDPE geomembranes that are separated by a geonet drainage layer. The primary liner is covered with 600 mm of drainage sand and 2.5 meters of stabilized waste for a total cover thickness of more than 3 meters. The principle of the ELIM method is to apply a voltage across the geomembrane liner and then to measure the resultant electrical potentials at widely spaced points. The data is processed using specialized mathematical inversion algorithms to image the locations of the leaks. The processed data indicated a leak near the center edge of the landfill cell. The suspect area was excavated to reveal two 80-mm long cuts in the primary liner.

INTRODUCTION

A high-voltage electrical leak location survey method has been used to locate leaks at more than 400 geomembrane-lined facilities world-wide (Laine and Darilek, 1993; Colucci et al., 1996). This commercial, field-proven technology has located many leaks that were not previously detected using other test methods and inspections, or that were caused during the placement of the protective soil cover. The method and equipment can locate leaks after the protective soil cover is placed over the liner and is a very cost-effective way to check liner installation quality or quickly solve a leakage problem. However, these commercial surveys are conducted using closely-spaced measurements on the soil with less than 1 meter of soil and no waste on the liner. The ELIM method is an advanced extension of this basic method that was developed to allow leaks to be detected under a much deeper soil and waste cover. In addition, the ELIM method allows for collection of data on a much wider spacing, or around the perimeter of a landfill cell, eliminating the need to place numerous data collection electrodes in the landfill cell. The ELIM method can also be used as a monitoring system.

ELIM METHOD

The ELIM method detects electrical paths through an electrically insulating geomembrane liner caused by water or moisture in holes through the geomembrane liner. Electrical current is induced through the leaks by connecting a current source to one electrode placed in the soil covering the liner and a second current sink electrode placed in the leak detection zone for double-lined systems or in earth ground for single-lined systems. Electrical current flowing through the leaks in the liner produces current sources at the leaks. These points are located by making potential measurements around the perimeter of the landfill or with a widely-spaced grid of electrodes on the floor of the landfill. The data is then processed using specialized inversion algorithms to locate leaks in the geomembrane liner that are associated with the high current sources at the leaks. The inversion algorithms determine the distribution of current density that best reproduces the observed voltage data. This is achieved through a non-linear least squares fit to the data. The validity of the ELIM method was verified using a medium scale physical model of a geomembrane lined facility.

The Electrical Leak Imaging and Monitoring system can be used as a permanent monitoring system or to investigate active landfill cells. A major advantage of the method is the ability to collect data around the perimeter of the landfill cell without placing electrodes on the floor area. This allows the method to locate leaks in active landfills after waste has been placed on the floor area. The use of the method as a permanent monitoring method would enable landfill operators to evaluate long term performance of the landfill liner system. This is especially important for subtitle D landfills that have a single synthetic geomembrane liner. If a leak develops the ELIM system would alert the landfill operator of a leak and determine the location. A United States patent is pending for the ELIM survey method.

ELIM LANDFILL SURVEY

Landfill Description. This application of the ELIM method was at an active hazardous waste landfill for stabilized residue from a recycling operation and stabilized contaminated soil. The landfill had a known leakage problem that could not be solved using conventional test methods. The landfill has a depth of 18 meters with a surface area of approximately 4.4 hectares and a floor area of approximately 1 hectare. Figure 1 shows a cross section of the lining system for the landfill. The cell has two 2-mm thick HDPE geomembrane liners separated by a geonet drainage layer. The primary liner was covered with 300 mm of a clean drainage gravel. An additional 300 mm of a protective sand was placed over the gravel. The two drainage materials are separated by a thick geotextile. The stabilized soil waste was placed on the protective sand.

Survey Procedure. The ELIM survey was conducted in an area where 2.5 m of stabilized waste was placed in the landfill cell. Other areas of the landfill cell had as much as 5 m of waste covering the floor area. The top layer of waste was very solid so 20 mm diameter holes were drilled about 100 mm deep to support the measurement electrodes.

300 mm SAND
GEOTEXTILE
300 mm GRAVEL
2 mm GEOMEMBRANE
GEOGRID
2 mm GEOMEMBRANE
600 mm COMPACTED
CLAY
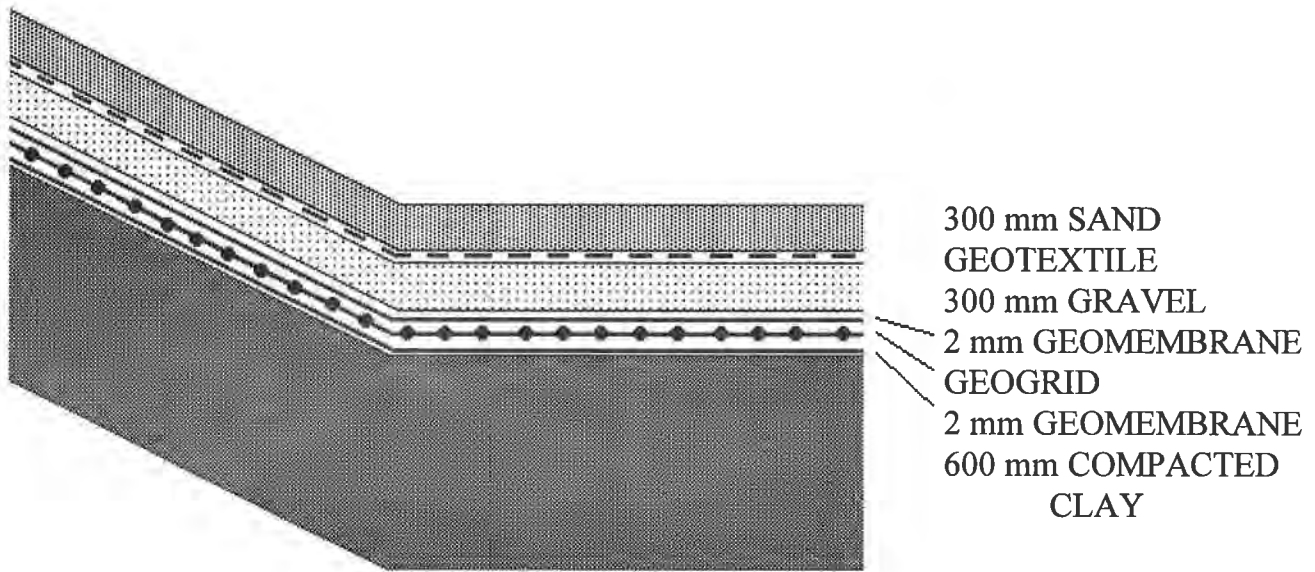
Figure 1. Cross Section of the Liner System

Figure 2 shows the survey layout. To create electrical flow through the liner, a low-frequency alternating current source was connected to one electrode placed in the leak detection layer with a current sink connected to a second electrode placed in the waste material covering the liner. The current source can provide up to 400 volts and 500 mA, depending on the load. A potential reference electrode was installed in a region of the landfill away from the area of suspected leakage. The location of the remote electrode is quite arbitrary, its purpose being to provide a common reference point for all of the potential measurements. As an alternative, the electrode can be put at some remote location away from the landfill. A synchronous voltage measurement meter with signal averaging capabilities was used to make potential measurements relative to this reference electrode on a 5 m by 5 m spacing over the part of the floor area that was covered with 2.5 m of waste. Data was collected over an area of 4,000 square meters. One-hundred sixty-eight data measurements were made.

Survey Results. Figure 3 is a shaded surface display of the processed data. To remove any effects of variations in the current magnitude that may occur with such measurements, the data is shown as transfer resistances, which are the ratios of measured potentials to the magnitude of the injected current. The data clearly indicates a distinct anomaly located at grid position 60 meters east and 10 meters north. The broad nature of the anomaly is a result of the waste thickness smearing the effect of the leak current source at the measurement points on the surface of the waste. This effect was confirmed by performing simulation trials using a three-dimensional finite element solution of the governing equations for this potential equation problem. For shallower waste the effect of the leak would be much more pronounced.
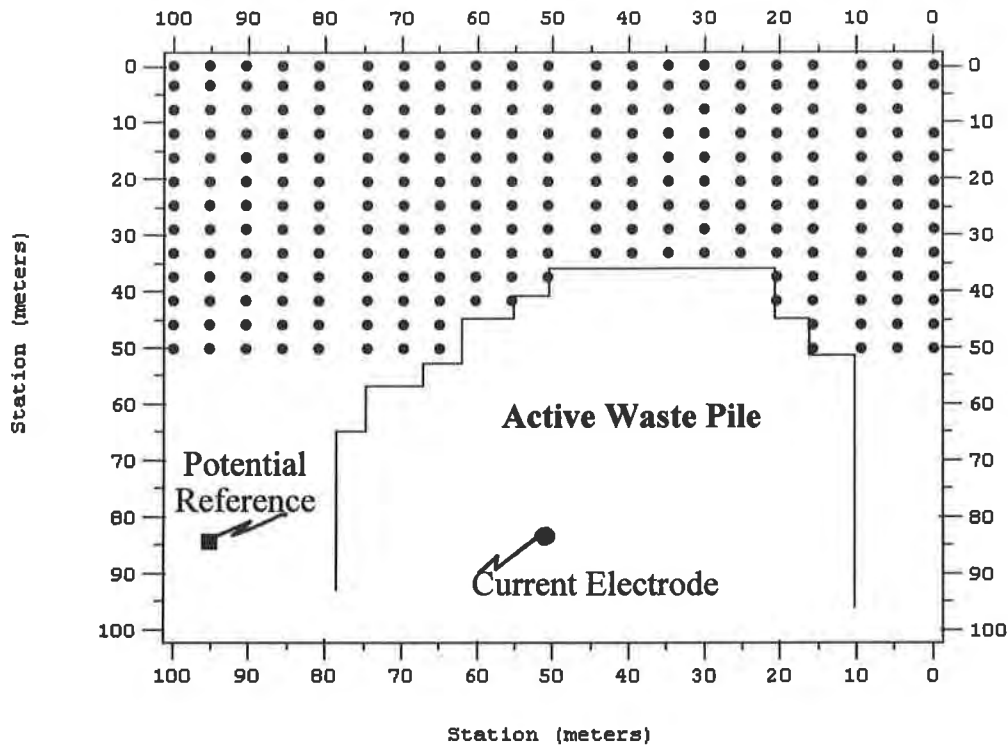
Figure 2. Survey Grid Showing Position of Current Electrode, Potential Reference Electrode, and Measured Potential Electrodes (black dots). The Second Current Electrode was Placed in the Leak Detection Layer.
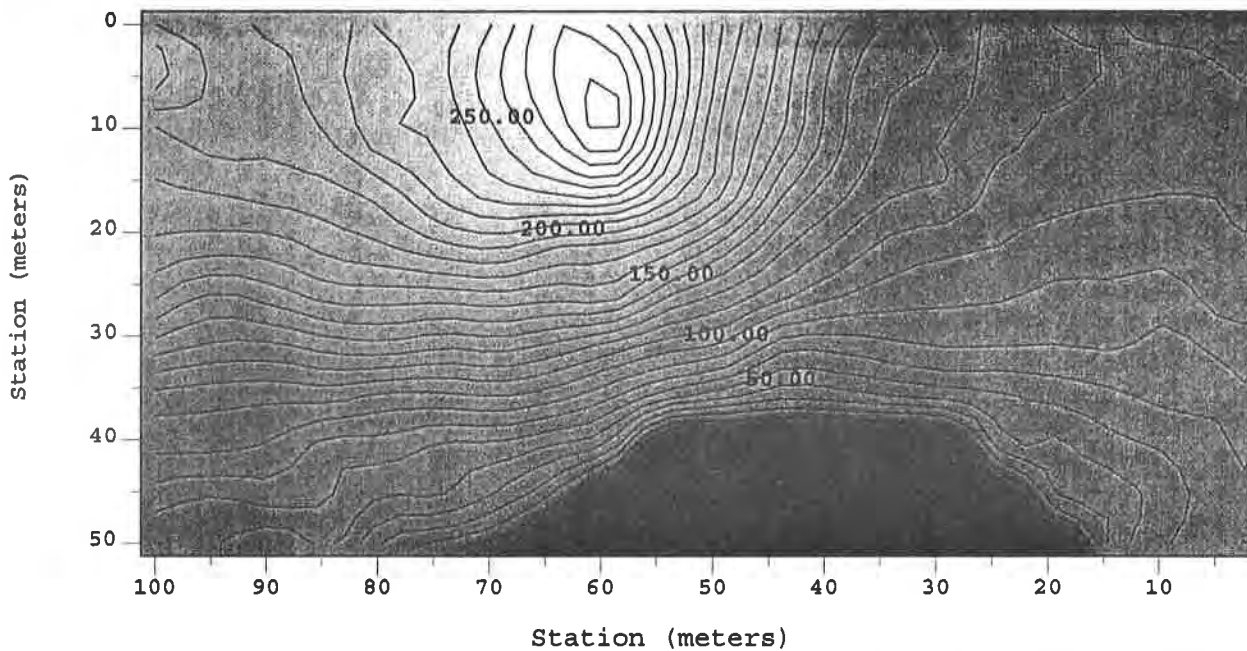
Figure 3. Contour Plot of Processed ELIM Data Collected Over Three Meters of Waste High Contour Value Indicates Leak Position

Based on the results of the ELIM survey, recommendations were made to the landfill operators to excavate the area of the imaged anomaly to identify the source of the signal. The feature was excavated to expose two closely-spaced cuts approximately 80 mm in length.

SUMMARY AND CONCLUSIONS

An ELIM survey was used to accurately locate two small leaks under 3 m of waste in a geomembrane lined landfill cell. This was the first application of the technique in an active landfill. Measurements were collected on the waste using a widely-spaced electrode grid. This allowed fewer data points to be collected, which saved time and money in identifying the leakage problem. The technique described does not rely on measurements on a regular grid, or in fact within the landfill cell. By using appropriate numerical inversion algorithms we are able to determine leak signals in a tomographic fashion, although sensitivity is reduced in comparison with using data collected within the cell.

REFERENCES

Laine, D.L., Darilek, G.T., (1993) "Locating Leaks in Geomembrane Liners of Landfills Covered With a Protective Soil," Geosynthetics '93 Conference Proceedings, Vol 3, pp. 1403-1412.

Colucci, P., Crozier, F., and Laine, D.L., (1996) "Geomembrane Liner testing using the GLLS®: A high-voltage electrical leak location system," Proceedings of the First European Geosynthetics Conference, pp. 749-750.

PERFORMANCE OF GEOTEXTILES IN LANDFILL COVERS

L.J. REITZ
David J. Newton Associates, Inc. USA

R.D. HOLTZ
University of Washington, USA

ABSTRACT

As part of the research into the performance of geotextiles in landfill covers, 14 test pits were excavated in five landfill covers constructed between 1988 and 1992 in Washington State. Materials used in the drainage system were examined and documented. Specimens of geotextiles (all 8 oz/yd^2, needle punched nonwovens) as well as samples of the vegetative and sand drainage soils, were obtained for laboratory analyses.

Laboratory tests indicated that the geotextiles satisfactorily performed their intended filtration function. No apparent migration of fines into the drainage layer was detected. The degree of clogging was evaluated by performing permittivity tests on specimens of the exhumed geotextiles, as retrieved and after washing. Washing typically resulted in permittivity increases on the order of 30 to 90 percent.

INTRODUCTION

The final closure of a modern solid waste landfill requires that the landfill be covered. The purpose of the cover system is several fold; it provides a barrier to keep man and other animals out of the waste, it reduces the amount of precipitation that can infiltrate into the waste thus reducing leachate production, and it helps to prevent odor and gases produced by the waste from spreading into the neighboring properties. During the past ten years, geosynthetic materials have been widely used in the construction of landfill covers.

The basic cover utilizing geosynthetics consist of the following layers in order from the waste up (Figure 1): a foundation layer consisting of fill soil, a geomembrane bedding layer, the geomembrane, a 30 to 45 cm thick drainage layer, a geotextile, a vegetative soil layer, and finally a topsoil layer. The drainage layer could be replaced with a geocomposite.
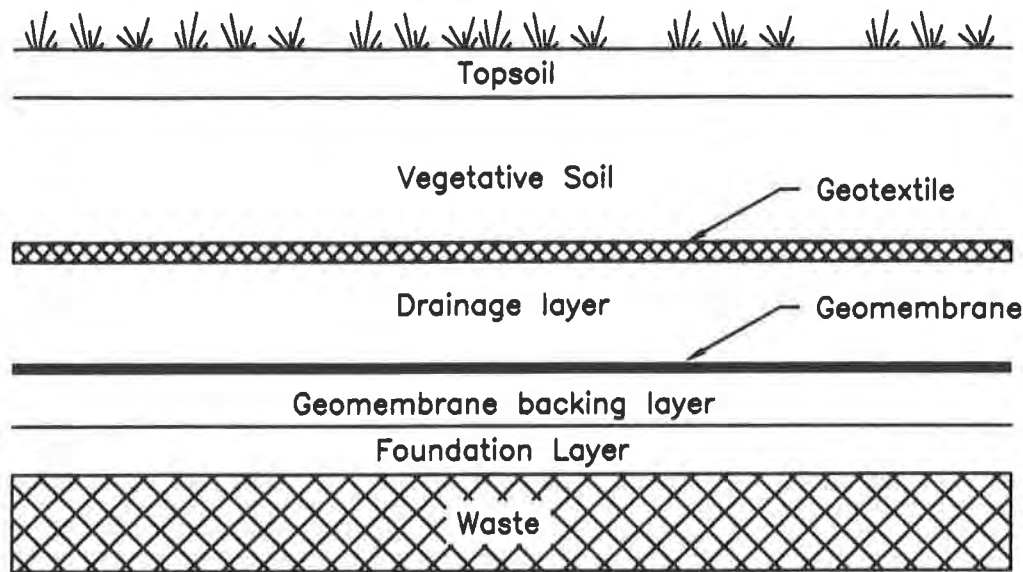
Figure 1 - Typical landfill cover section

The geomembrane is the impermeable barrier that prevents moisture from infiltrating into the waste. The drainage layer drains moisture away from the membrane and helps to prevent water from building up above the geomembrane. The geotextile acts as a filter to prevent fines in the vegetative soil from piping into and clogging the drainage layer. The vegetative layer and topsoil allows the growth of vegetation which reduces erosion and infiltration by evapotranspiration.

Special design issues for landfill covers using geosynthetics are cover slope stability, settlement (total and differential), and drainage. Drainage and slope stability are an interrelated topic, as an improperly functioning drainage system can reduce the overall stability of the slope.

Surprisingly, there has been little research to evaluate the long-term field performance of cover drainage systems. This paper summarizes the results of investigation on the performance of geotextiles in landfill cover drainage systems to determine if clogging or migration of fines had occurred since construction.

SITE CHARACTERISTICS

The investigations were conducted at a landfill located in the Puget Sound region of Washington State, approximately 30 km southeast of Seattle. The landfill is approximately 372 ha in size, and at the time this research was done, six separate covers had been constructed between 1988 and 1992. Access to five of these covers was allowed for this research.
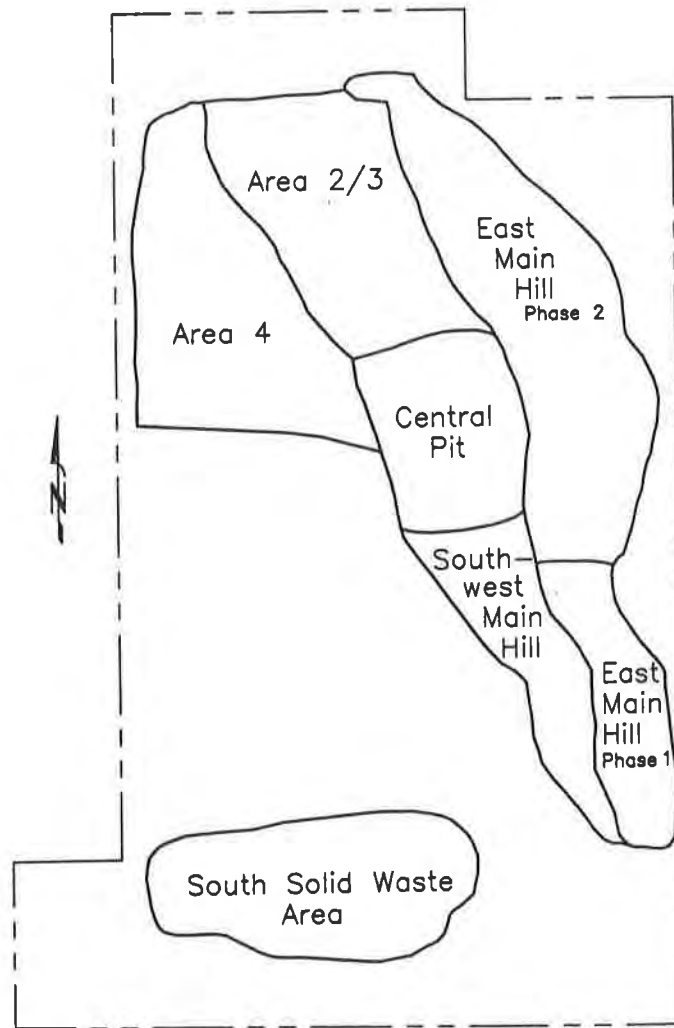
Figure 2 - Site Plan

The soils at the site consist of glacial till and glacial outwash deposits which extend more than 100 m below the ground surface. The site is situated at an elevation of approximately 107 m to 244 m above mean sea level. The climate at the site is typical for the Puget Sound area. The average annual precipitation for the area is on the order of 1500 mm, while the average annual temperatures range from 3° C to 17° C.

Landfilling began at the site in 1963. Three areas (Figure 2), the South Solid Waste Area, the Main Hill Phase I, and the Main Hill Phase II, have been closed. Final cover systems have been constructed on these areas. Two areas, the Central Pit and the Southwest Main Hill, are not receiving waste at this time and have had interim covers constructed. Areas 2 and 3 have had both an interim and a final cover constructed. Only Area 4 is currently receiving waste. Eventually, the Central Pit, Southwest Main Hill, and Areas 2 and 3 will receive additional waste. It is estimated that the landfill will reach capacity in the year 2016.

This study investigated the conditions of the three final covers and the two interim covers. Areas 2 and 3 were not investigated. Similar construction procedures were used for all of these five areas. General earthfill from on-site sources was placed to bring the waste mound to the design grades and to provide a firm base for the geomembrane. Imported sands were used for the drainage layer while on-site glacial till soils were used for the vegetative and topsoil. In some areas, sewage treatment sludge was used as topsoil. The drainage layer material, vegetative soil, and topsoil were placed in single lifts. Only low ground pressure equipment was used to spread the fill materials on the geomembrane and the geotextile.

FIELD PROCEDURES

The site investigation procedures consisted of excavating approximately two to three test pits per cover section. An additional three test pits were excavated in an area that was observed to have experienced differential settlement. A total of 14 test pits were excavated.

During the excavation process the condition of the vegetation, soil, and geosynthetics were visually observed and documented by making field notes and taking photographs. In situ testing, including sand cone densities and torvane shear tests, was conducted on selected samples to determine the density and shear strength of the soils. A sample of the vegetative soil was taken within approximately 10 cm of the geotextile. Approximately 30 cm diameter samples of the geotextiles were then cut out and placed in plastic bags. Samples of the drainage layer sand were taken from immediately below the geotextile and immediately above the geomembrane. Soil and geotextile samples were taken from the test pits for later laboratory testing. Details of the field procedure can be found in Reitz (1995).

Prior to backfilling, the condition of the geomembrane, where exposed, was noted. No attempt was made to retrieve specimens of the geomembrane.

LABORATORY ANALYSES

The objective of the laboratory analyses was to evaluate the drainage and filtration properties of the retrieved soils and geotextile samples.

Water Content Tests. Natural water content tests were conducted on all soil samples from each test pit in order to determine the general soil-moisture profile. The water content tests were conducted in accordance with ASTM D 2216.

Grain Size Distribution Analysis. Grain size distribution tests were conducted on all vegetative and drainage layer samples obtained from the test pits in order to classify the soils. The test results were also used to determine if clogging of the drainage layer had occurred by comparing the distributions to the original specifications and using correlations to hydraulic conductivity.

The grain size distributions were also used for evaluating filter design. The tests were conducted in general accordance with ASTM D 422.

Permittivity Tests. Permittivity tests were performed on the geotextile samples in the same condition as they were when removed from the landfill cover. The samples were then washed to remove soil particles and retested. A comparison of the permittivity from the "as is" condition and the after-washed condition was made. The permittivity tests were conducted in general accordance with ASTM D 4491. A description of the equipment and testing procedures can be found in Metcalfe, et al. (1995).

OBSERVATIONS AND TEST RESULTS

Site Investigations. The field investigations took place between December 2 and 16, 1994, typically one of the wetter times of the year in the region. The vegetative soils generally consisted of glacial till derived soils which were gravelly, silty sands. The in situ dry densities of the vegetative soils ranged from 15.7 to 21.2 kN/m^3, while the moisture contents of the soils ranged from 7.9 to 20.9 percent.

The drainage layer materials consisted of clean, coarse sands. The in-situ dry densities of the sands ranged from 15.0 to 17.0 kN/m^3, while the moisture contents ranged from 4.3 to 16 percent.

The layer thickness and grain size distributions of the soils in the covers were generally as specified. However, it was not uncommon to encounter cobbles and boulders in the vegetative soils, sometimes placed directly on the geotextiles. The largest boulders encountered were about 46 cm in diameter. The specifications for the cover soils typically required that the maximum particle size be no greater than 15 to 20 cm. In one test pit located in the Central Pit/Southwest Main Hill Cover, rutting on the order of 5 cm deep was observed in the geotextile. Even where boulders had been placed directly on the geotextile and where rutting had occurred, no apparent damage to the geotextiles was observed.

The geotextiles were all needle punched nonwovens, 8 oz/yd^2. Most of the geotextiles were continuous filament polypropylene or polyester, although the geotextile used in the East Main Hill Phase I cover was a staple fiber polypropylene.

The geomembrane was exposed in eight of the 14 test pits excavated. In only one area was potential damage to the geomembrane observed. In this test pit, several bumps approximately 1 cm in height were measured. It appeared that these bumps may have been the result of the geomembrane being placed directly on gravel size particles.

Even though the field investigation was conducted during a wet time of the year, very little standing water on the surface or water in the drainage layer was observed. Soggy ground surface conditions and standing water were observed in some areas of the South Solid Waste Area. This cover is near level in many areas making surface water runoff problematic and the vegetative soils in the cover had been densely compacted making the soil nearly impermeable.

Water was observed flowing in the drainage layer in only two test pits. In Test Pit 1, located in the East Main Hill Phase II cover, water was encountered when the geotextile was first exposed. The water level increased to a level approximately 10 cm above the geotextile, which is much greater than the 30 cm drainage layer thickness assumed for design (Thiel and Stewart, 1993). Approximately 5 cm of water was observed in the drainage layer in one test pit in the Southwest Main Hill cover.

Drainage Layer Clogging. Clogging of the drainage layer will occur if fine soil particles from the vegetative soil are allowed to penetrate into the drainage layer. An increase of fine material in the drainage layer will lead to a decrease in the hydraulic conductivity and a resulting increase in the pore pressure in the drainage layer. An increased pore pressure will cause an increase in the infiltration through the geomembrane and a decrease in the slope stability of the landfill cover.

The amount of clogging that the sand drainage layer potentially experienced was determined by three different methods. In each of the test pits in which the drainage layer was exposed, samples of the sand were taken from just under the geotextile and just above the geomembrane (only one sample was taken from Test Pit 1 due to the flowing sands). Grain size distribution tests were conducted on each of the retrieved sand samples. The results of these grain size distributions were used by all three methods to determine if clogging had taken place in the drainage layer.

The first method just compared the grain size distributions (GSD) of the samples retrieved from the top and bottom of the drainage layer. If the distributions of the two drainage layer samples were similar, then the drainage layer was either clogged equally, or it was in the same condition as installed. The second method compared the measured GSDs to the specifications. If the sand drainage material was still within specifications, then the sand was not significantly clogged. The specifications for the drainage layer in the East Main Hill Phase I cover were changed during construction and only the original specifications were available for this report. Therefore, the drainage layer from this cover cannot be checked for clogging using this second method.

The final method was to use a correlation of the grain size to the hydraulic conductivity such as the one proposed by Hazen. If the hydraulic conductivity is within the specifications, then the drainage layer was considered to be not clogged enough to negatively effect its performance.

A summary of the results of the three methods used to evaluate the potential clogging of the sand drainage layer are shown in Table 1; the results indicate that no significant clogging occurred. In all cases, the most important criteria, hydraulic conductivity, had been met. In one case, the GSDs from the top and bottom of the drainage layer did not compare because one sample was coarser than the specifications. However, this does not indicate clogging by fine particles.

In five instances the drainage sands did not meet the GSD specifications. Four of these cases were the result of the percent passing the No. 200 sieve being slightly higher (1% to 2%) than the specifications. However, the conformance testing at the time of construction also indicated that some of the material used in construction exceeded the specifications for the amount of fines passing the No. 200 sieve. Therefore, this lack of conformance with the specifications does not appear to be the result of clogging

Geotextile Clogging. The amount of clogging that the geotextiles may have experienced since installation was determined by conducting permittivity tests on retrieved and washed samples. Four test specimens were cut from the geotextile sample retrieved from each test pit, except Test Pits 1 and 2, where only one test specimen was cut from the retrieved sample because these samples were small. The permittivity test procedure followed is outlined in Metcalfe, et al. (1995).

Each test specimen was subjected to five successive test runs in as close as possible to an undisturbed condition. With each subsequent run on the unwashed sample, the permittivity would increase as the specimen tended to cleanse itself. The specimens were then carefully washed and subjected to another five successive test runs. Although, it was impossible to remove all the soil particles that were embedded into the fibers of the geotextile, the washed specimens simulated the permittivity of the geotextile when it was installed. The estimated degree of clogging was based upon a comparison of the permittivity in the unwashed condition to the washed permittivity.

The unwashed permittivity tests are only an estimate of the undisturbed permittivity. Some disturbance was experienced when the sample was removed from the test pit and placed in a plastic bag. When the test specimen was cut from the retrieved sample, additional disturbance probably occurred. The test procedure required that the test specimen be soaked in water for a period of 24 hr prior to testing. The soaking permitted some dislodging of fine soil particles from the geotextile. Therefore the results of the unwashed permittivity tests should not be considered as representative of the minimum field permittivity of the geotextiles.

Table 1 – Summary of drainage layer clogging criteria

Landfill Cover	Test Pit	Depth (m)	Comparable Gradations	Gradation Meets Specifications	Hydraulic Conductivity k (cm/sec)	k Meets Specifications	Comments
East Main Hill	1	0.51 to 0.30	*	yes	9.61×10^{-2}	yes	1 sample obtained
Phase II	2	0.91 to 1.07	yes	yes	9.00×10^{-2}	yes	
	2	1.37 to 1.52	yes	yes	9.00×10^{-2}	yes	
	3	0.91 to 1.07	no	yes	9.00×10^{-2}	yes	
	3	1.32 to 1.42	no	no	3.03×10^{-1}	yes	coarser than specifications
	4	0.61 to 0.76	yes	no	7.84×10^{-2}	yes	exceeds -No. 200 by 0.3%
	4	0.91	yes	no	7.84×10^{-2}	yes	exceeds -No. 200 by 0.3%
	13	0.76 to 0.91	yes	yes	6.76×10^{-2}	yes	
	13	1.17 to 1.22	yes	yes	1.23×10^{-1}	yes	
East Main Hill	5	0.61 to 0.76	yes	*	6.25×10^{-2}	yes	specifications changed
	5	1.01	yes	*	6.25×10^{-2}	yes	specifications changed
Phase I	12	0.51 to 0.66	yes	*	6.25×10^{-2}	yes	specifications changed
	12	1.01	yes	*	6.25×10^{-2}	yes	specifications changed
Central Pit/ Southwest	6	0.61 to 0.76	yes	yes	7.84×10^{-2}	yes	
	6	0.86 to 0.89	yes	yes	7.84×10^{-2}	yes	
Main Hill	7	0.51 to 0.66	yes	no	6.25×10^{-2}	yes	exceeds -No. 200 by 0.3%
	7	0.74	yes	yes	6.25×10^{-2}	yes	
	8	0.61 to 0.76	yes	no	4.00×10^{-2}	yes	exceeds -No. 200 by 0.9%
	8	0.91	yes	yes	4.84×10^{-2}	yes	
South Solid	10	0.61 to 0.76	yes	*	1.60×10^{-1}	yes	specifications not available
	10	0.81	yes	*	1.60×10^{-1}	yes	specifications not available

The results of the permittivity tests are summarized Figure 3 which is a plot of the average permittivity increase from the unwashed to washed condition for each of the four landfill cover areas.
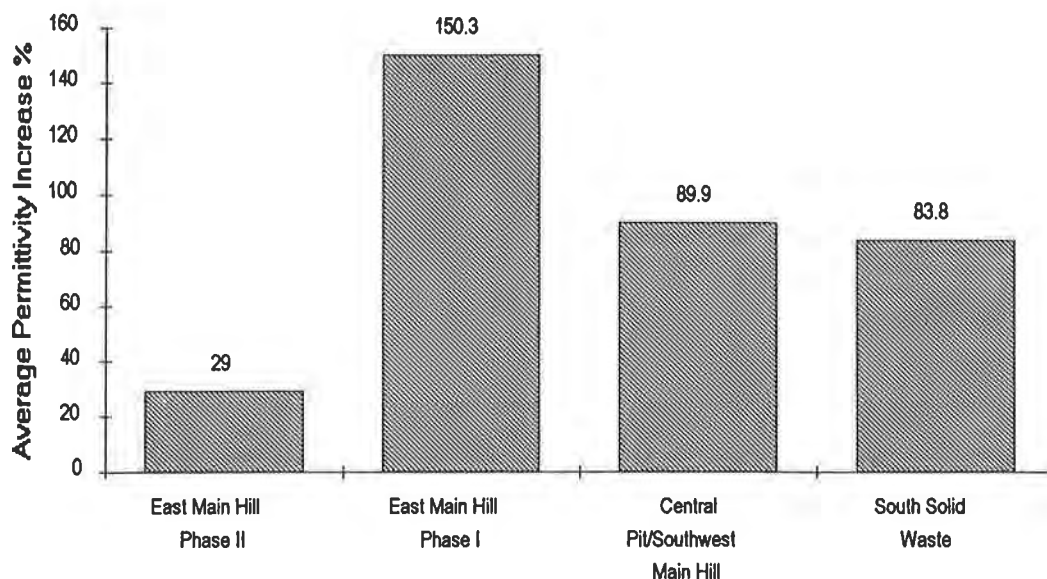
Figure 3 - Average permittivity increase for each landfill cover.

As Figure 3 shows, the average permittivity increase was generally less than 100 %. Only two test pits were excavated in the East Main Hill Phase I cover. The average permittivity increase in one of these two test pits was less than 10 % while the other test pit had an average permittivity increase of over 300 %.

Granular Filter Design Analysis. The GSDs of the soil samples taken from the vegetative soil and drainage layer were evaluated to determine their acceptability as granular filters. The granular filter criteria for the samples closest to the geotextiles are summarized in Table 2. In order to meet granular filter criteria (Cedergren, 1987), the $D_{15,filter}/d_{85,soil}$ should be less than or equal to 4 to 5, and the $D_{15,filter}/d_{15,soil}$ needs to be greater than or equal to 4 to ensure that the hydraulic conductivity of the filter is significantly greater than that of the soil.

The results indicate that the soils used in the construction of the vegetative soil and drainage layer generally met the criteria for granular filters. The gradation requirement to prevent migration of soil particles into the filter material was met in all the test pits. The soils in two test pits, however, did not meet the requirement to ensure that the hydraulic conductivity of the filter media was significantly greater than the soil. In these two cases, the gradation of the vegetative soil was relatively coarse.

Table 2 - Applicability of granular filter criteria

Landfill Cover Area	Test Pit	$D_{15filter}/D_{85soil}$	$D_{15filter}/D_{15soil}$	Meets Requirements
East Main Hill Phase II	1	0.03	>6	yes
	2	0.03	>5.5	yes
	3	0.25	>5.1	yes
	4	0.45	>5.1	yes
	13	0.7	>4.7	yes
East Main Hill Phase II	5	0.01	3	no
	12	0.02	>4.1	yes
Central Pit / Southwest Main Hill	6	0.03	4.7	yes
	7	0.02	4.3	yes
	8	0.03	>4.0	yes
South Solid Waste	10	0.02	3.1	no

Because the soils used in the vegetative and drainage layers met the requirements for a granular filter, it is unlikely that the drainage layer would experience clogging by fines even if the geotextile was damaged.

Geotextile Filter Design Analysis. The permittivity test results show that some areas have experienced greater clogging of the geotextile than others. In order to help determine potential reasons for the differences in clogging, the soil GSDs and geotextile apparent opening size (AOS) were evaluated using the criteria for geotextile filter design presented in Christopher and Holtz (1988). The results of this evaluation are presented in Table 3.

The GSD of the vegetative soil sample taken closest to the geotextile was used. The AOS of the geotextile is the manufacturer's specification for the geotextiles believed to be used in the construction of the covers. The AOS from conformance testing at the time of construction was not reported.

The geotextile samples that generally experienced the greatest increase in permittivity between the unwashed and washed conditions were those in which the criteria for clogging was not met. Christopher and Holtz (1988) recommend that the AOS be greater than three times the D_{15} of the soil. Most of the geotextile samples generally met this requirement; however, the samples from the Central Pit/Southwest Main Hill and South Solid Waste Area did not.

Table 3 – Applicability of geotextile filter criteria

Landfill Cover	Test Pit	B	BD85soil (mm)	D15soil (mm)	3D15soil (mm)	AOS (mm)	Meets Criteria ?
East Main Hill Phase II	1	1	15	<0.075	<0.23	0.21	yes
	2	1	15	<0.075	<0.23	0.21	yes
	3	1.8	2.7	<0.075	<0.23	0.21	yes
	4	1	0.85	<0.075	<0.23	0.21	yes
	13	1.8	0.9	<0.075	<0.23	0.21	yes
East Main Hill Phase I	5	1	40	0.1	0.3	0.212	no
	12	1	16	0.075	0.23	0.212	yes
Central Pit/ Southwest Main Hill	6	1	12	0.075	0.23	0.180	no
	7	1	18	0.075	0.23	0.180	no
	8	1	12	<0.075	<0.23	0.180	no
South Solid Waste	10	1	16	0.075	0.23	0.180	no

CONCLUSIONS

- The geotextiles in this study survived both boulders being placed directly on them, and rutting.

- All of the geotextiles in this study performed their function of filtration well, with no apparent migration of fines into the drainage layer and only minor clogging.

- With the careful consideration and testing of the soils used in landfill construction, more effective and economical use of geotextiles could be made.

ACKNOWLEDGMENTS

REFERENCES

Christopher, B.R. and Holtz, R.D. (1988) "Geotextile Design and Construction Guidelines", FHWA, Report No. FHWA-HI-90-001, 297pp.

Cedergren, H.R. (1987) "Seepage Control in Earth Dams", Embankment-Dam Engineering, Casagrande Volume, p. 23.

Metcalfe, R.C., Holtz, R.D., and Allen, T.M. (1995) "Field Investigations to Evaluate the Long-Term Separation and Drainage Performance of Geotextile Separators", Proceedings Geosynthetics '95, Nashville, Vol. 3, pp. 951-962.

Reitz, L.J. (1995) "Performance of Geosynthetics in Landfill Covers", M.S.C.E. Project Report, 133pp.

Thiel, R.S. and Stewart, M.G. (1995) "Geosynthetic Landfill Design Methodology and Construction Experience in the Pacific Northwest", Proceedings Geosynthetics '93 Vancouver, Vol. 3, pp.1131-1143.

EVALUATING THE PERFORMANCE OF FLORIDA DOUBLE-LINED LANDFILLS

RICHARD B. TEDDER
FLORIDA DEPARTMENT OF ENVIRONMENTAL PROTECTION, USA

ABSTRACT

A study was conducted on field performance of active double-lined landfills in Florida. Actual leachate flow data were compiled for 24 cells from these facilities. Using reasonable assumptions, theoretical leakage rates through the primary liner into the Leak Detection System (LDS) for each cell were calculated and compared with actual flow data. The theoretical leakage rates generally resulted in conservative estimates of actual LDS flow rates indicating the landfills were performing at acceptable levels. However, landfills designed with a geonet above and below the primary geomembrane liner had higher LDS flow rates than other liner designs. These landfills also had leachate sumps located inside the landfill. In one case, the elevated LDS flow rates appeared to be related to higher heads in the sump. Thus, liner designs can affect LDS flow rates and design engineers should consider additional protection for leachate sumps located inside the landfill.

INTRODUCTION

The Florida Department of Environmental Protection (DEP) Solid Waste Management Facilities Rule, Chapter 62-701, Florida Administrative Code (F.A.C.), allows landfills to be constructed with a composite liner design or a double liner design. These liner designs were developed by the DEP with the assistance of a Technical Advisory Group (TAG), consisting of landfill design engineers from Florida, and are believed to be sufficient minimum design standards to protect Florida's ground water. The double liner design became effective in Florida on August 1, 1990, and currently consists of at least the following components (from top down): a 61 cm (24 in) thick layer of drainage sand designed to limit the head on the primary liner to no more than 30.4 cm (12 in); a 1.5 mm (60-mil) thick HDPE geomembrane primary liner; a leak detection layer with a minimum hydraulic conductivity of 10 cm/sec designed to prevent flooding and to have a head no greater than 2.5 cm (1 in) on the secondary liner; a 1.5 mm (60-mil) thick HDPE geomembrane secondary liner; a 15 cm (6 in) thick subbase with a maximum hydraulic conductivity of 1×10^{-5} cm/sec.

The double liner design was criticized as not being protective of Florida's fragile ground water supply. Medley Expansion Landfill in Dade County reported

actual flow rates in the Leak Detection System (LDS) which were much higher than estimated flow rates using reasonable design assumptions recommended by the TAG. The TAG estimated that leakage into the LDS for a typical double-lined landfill in Florida would be approximately 83.2 liters/1000 m^2/day (89 gpad). Actual LDS flow rates in Cell 1 of the Medley Expansion Landfill were reported as high as 633 liters/1000 m^2/day (677 gpad).

To estimate leakage into the LDS, the TAG assumed: a design consisting of the minimum liner components required by the rule; a geonet for the LDS; drainage sand hydraulic conductivity of $1x10^{-3}$ cm/sec; constant head on the primary liner at the maximum allowed value by rule of 30.5 cm (12 in); and liner defects at a frequency of 1 per 4,000 m^2 (1 per acre) with an area of 1 cm^2 per defect. The leakage into the LDS was then estimated using the following equation proposed by Bonaparte et. al. (1989) for leakage through a geomembrane resting on a high-permeability material and overlain by a drainage layer:

$$Q = 3a^{0.75}h^{0.75}k_d^{0.5} \hspace{5cm} (1)$$

where:
Q = steady-state rate of leakage through one geomembrane hole, m^3/s;
a = area of hole in geomembrane, m^2;
h = head of liquid on top of the geomembrane, m;
k_d = hydraulic conductivity of the drainage layer overlying the geomembrane, m/s.

Since the actual LDS flow rates at Medley Expansion Landfill were much higher than that predicted using the TAG assumptions, questions were raised about these assumptions. In particular, the assumptions on liner defect area and frequency were challenged. In response to these concerns, in March 1995 the DEP initiated a study of all the active double-lined landfills in Florida to determine how their field performance compared with earlier predictions made by the TAG. This paper presents the results of that study.

LEACHATE FLOW RATE DATA

Florida has 9 active double-lined landfills which collectively include a total of 24 landfill cells. These cells range in size from 18,212 m^2 (4.5 acres) to 80,940 m^2 (20 acres). The DEP obtained leachate flow rate data either from information already contained in the Department files or by direct contact with the landfill owner/operators. The time periods of flow data for each cell ranged from 3 to 64 months depending on the age of the cell or the time when accurate leachate flow measurements became available. A list of the Florida double-lined landfills used in this paper with their corresponding areas and dates of available leachate flow date are given in Table 1.

The DEP obtained data for both the Leachate Collection System (LCS) on top of the primary liner and the LDS between the primary and secondary liner for each double-lined landfill. The leachate flow rates were reported as monthly totals for each cell. Using the corresponding cell areas and the number of days for each month, the total values were converted into unitized daily flow rates. Because of the landfill designs, the LCS flow rates for the Broward Interim Contingency Landfill and the Site 7 Landfill were not available for the individual cells and were reported as one total flow for all the cells in each landfill. Also, LCS flow data were not reported for the West Pasco Landfill. With the exception of Berman Road Landfill, the DEP also obtained total rainfall amounts for the reporting periods of each cell.

Table 1. Florida active double-lined landfills.

County	Landfill	Cell Name	Cell Area, acres	Dates For Flow Data, Mo/Yr	Months Of Flow Data
Broward	Central Disposal	Stage I	4.50	11/94 to 03/95	5
Broward	Central Disposal	Stage II	6.01	11/94 to 03/95	5
Broward	Central Disposal	Stage III	5.58	11/94 to 03/95	5
Broward	Broward Interim Contigency	Cell 1-A	11.25	01/90 to 04/95	64
Broward	Broward Interim Contigency	Cell 1-B	11.25	01/90 to 04/95	64
Broward	Broward Interim Contigency	Cell 3 (A+B)	11.50	01/94 to 04/95	16
Columbia	Winfield Landfill	Cell 1	7.30	08/92 to 04/95	33
Dade	Medley - Expansion	Cell 1	18.50	03/94 to 04/95	14
Dade	Medley - Expansion	Cell 2	10.00	03/94 to 04/95	14
Dade	Medley - Expansion	Cell 3	16.60	03/94 to 04/95	14
Duval	Trail Ridge Landfill	Cell A	20.00	01/94 to 03/95	15
Duval	Trail Ridge Landfill	Cell B	18.00	01/94 to 03/95	15
Duval	Trail Ridge Landfill	Cell C	18.00	01/95 to 03/95	3
Marion	Baseline Landfill	Cell III-A	10.92	01/93 to 03/95	27
Marion	Baseline Landfill	Cell III-B	15.47	01/93 to 03/95	27
Okeechobee	Berman Road Landfill	Cell 3	7.60	10/94 to 03/95	6
Okeechobee	Berman Road Landfill	Cell 7	4.80	06/94 to 03/95	10
Palm Beach	Site 7 Landfill	Cell A-A	10.38	03/94 to 04/95	14
Palm Beach	Site 7 Landfill	Cell A-B	9.68	03/94 to 04/95	14
Palm Beach	Site 7 Landfill	Cell A-C	9.78	03/94 to 04/95	14
Palm Beach	Site 7 Landfill	Cell A-D	9.26	03/94 to 04/95	14
Palm Beach	Site 7 Landfill	Cell A-E	8.13	03/94 to 04/95	14
Pasco	West Pasco Landfill	Cell A-1	10.00	09/91 to 03/95	43
Pasco	West Pasco Landfill	Cell SW-1	10.00	09/91 to 03/95	43

NOTE: 1 acre = 4,047 m^2

The reported rainfall amounts, and a summary of the LCS and LDS flow rates for each cell are given in Table 2. The minimum and maximum monthly flows and the total average flow for the reporting periods are presented as unitized daily leakage rates for each cell. The total average LCS flow rates for all the cells ranged from 110 liters/1000 m^2/day (118 gpad) to 9,081 liters/1000 m^2/day (9,712 gpad). These large daily LCS flow rates reflect the fact that on the average Florida receives between 1.2 meters (48 inches) to 1.5 meters (60 inches) of rain per year. The total average LDS flow rates for all the cells ranged from 0.56 liters/1000 m^2/day (0.6 gpad) to 428 liters/1000 m^2/day (458 gpad). The maximum monthly LDS flow rates ranged from 3.3 liters/1000 m^2/day (3.5 gpad) to 633 liters/1000 m^2/day (677 gpad).

The areas for the three Medley Expansion Landfill cells presented in Table 1 are the total areas for the cells which include both the base and side slope areas. The actual base areas for Cells 1, 2 and 3 are 9,713 m^2 (2.4 acres), 19,021 m^2 (4.7 acres) and 25,090 m^2 (6.2 acres), respectively. As will be explained later in this paper, only the base areas of these cells were double-lined. Consequently, the base areas, not the total areas, were used to calculate the unitized daily leachate flow rates contained in Table 2 for Medley Expansion Landfill. In all the remaining cells, the total areas were used.

DOUBLE-LINED LANDFILL DESIGNS

Information for the double-lined landfill designs used in this paper was obtained either from Department files or directly from the landfill owner/operators and their consultants. A summary of the liner components, including the LCS and LDS designs, for all 24 cells is contained in Table 3.

In evaluating the designs for the nine landfills, it was determined that 13 of the 24 cells had designs that achieved or exceeded the current double liner design standards contained in Chapter 62-701, F.A.C. The remaining cells that were not constructed according to this design standard included Baseline Landfill, Cell III-A; Broward Interim Contingency Landfill, Cells 1A, 1B, 3(A+B); Site 7 Landfill, Cells A-A to A-D; West Pasco Landfill, Cells A-1, SW-1; and Medley Expansion Landfill, Cell 1. All of these cells, except Cell 1 of Medley Expansion Landfill were permitted and constructed before August 1, 1990, the effective date for the current double liner requirements. These cells were constructed with some variation of the current double liner design while only a single clay or single geomembrane liner was required and so exceeded the minimum landfill design requirements at the time they were permitted.

Medley Expansion Landfill, Cell 1 was also permitted before August 1, 1990 and not designed strictly in accordance with current DEP double lined standards. This landfill was constructed in the valley between two existing landfills, and the double liner was placed on the base of each cell while a single geomembrane was extended up the side slopes. Due to shallow side slopes in Cell 1, the existing DEP liner rules would require the double liner extend all the way up the side slope.

Even though some of the landfills were constructed before the DEP had double liner requirements in place, it is believed all of the double-lined cells were constructed with reasonably good Construction Quality Assurance (CQA). Florida began requiring landfill liners in 1985 and has always included CQA requirements during liner installations.

Table 2. Leachate flow rate summary.

Landfill - Cell	Total Period Rain, Inches	Leachate Collection System (LCS)			Leachate Detection System (LDS)		
		Minimum Monthly Flow, GPAD	Maximum Monthly Flow, GPAD	Total Average Flow, GPAD	Minimum Monthly Flow, GPAD	Maximum Monthly Flow, GPAD	Total Average Flow, GPAD
Central Disposal - Stage I	34.50	910	4,876	2,155	9.5	276.0	77.0
Central Disposal - Stage II	34.50	683	1,313	958	32.4	130.0	90.0
Central Disposal - Stage III	34.50	604	6,462	2,634	21.8	340.0	127.0
Broward Interim Cont.- Cell 1-A	313.50	-	-	-	0.0	75.4	7.7
Broward Interim Cont.- Cell 1-B	313.50	-	-	-	0.0	66.4	11.0
Broward Interim Cont.- Cell 3 (A+B)	92.40	-	-	-	11.8	82.1	28.6
Broward Interim Cont.- All Cells	313.50	26	1,814	788	-	-	1.5
Winfield Landfill - Cell 1	109.20	112	11,875	9,712	0.0	38.9	1.5
Medley Expansion - Cell 1	83.00	707	1,421	812	133.2	677.0	458.0
Medley Expansion - Cell 2	83.00	179	440	259	52.6	95.5	76.5
Medley Expansion - Cell 3	83.00	306	539	355	58.3	150.8	113.4
Trail Ridge Landfill - Cell A	71.40	55	224	118	0.0	4.7	2.2
Trail Ridge Landfill - Cell B	71.40	107	1,126	429	0.4	130.2	18.2
Trail Ridge Landfill - Cell C	12.60	230	450	314	54.6	82.3	66.3
Baseline Landfill - Cell III-A	124.50	59	1,882	201	1.1	37.9	14.0
Baseline Landfill - Cell III-B	124.50	107	778	378	0.3	113.2	24.5
Berman Road Landfill - Cell 3	-	864	3,429	1,838	0.0	19.3	3.4
Berman Road Landfill - Cell 7	-	373	1,926	789	0.0	5.7	0.6
Site 7 Landfill - Cell A-A	96.00	-	-	-	1.7	8.2	3.8
Site 7 Landfill - Cell A-B	96.00	-	-	-	2.7	3.6	3.1
Site 7 Landfill - Cell A-C	96.00	-	-	-	3.8	6.2	4.9
Site 7 Landfill - Cell A-D	96.00	-	-	-	6.0	10.7	7.8
Site 7 Landfill - Cell A-E	96.00	-	-	-	3.3	34.0	10.5
Site 7 Landfill - All Cells	96.00	423	2,505	1,254	-	-	-
West Pasco Landfill - Cell A-1	132.80	-	-	-	1.6	12.3	6.3
West Pasco Landfill - Cell SW-1	132.80	-	-	-	2.1	11.1	5.7

NOTE: 1 GPAD = 0.935 liter/1000 m^2/day
1 inch = 2.54 cm

Table 3. Summary of double-lined landfill designs.

Landfill	Liner Group	LCS Type	Primary Liner	LDS Type	Secondary Liner
Medley Expansion Cells 1,2,3	I	24 in. sand+geonet $k_{sand}=1\times10^{-3}$ cm/s	HDPE 60 mil	geonet	HDPE + 6 in. soil $k_{soil}=1\times10^{-5}$ cm/s
Central Disposal Stages I,I,III	I	24 in. sand+geonet $k_{sand}=1\times10^{-3}$ cm/s	HDPE 60 mil	geonet	HDPE + GCL $k_{GCL}=2\times10^{-9}$ cm/s
Trail Ridge Landfill Cells A,B,C	I	24 in. sand+geonet $k_{sand}=1\times10^{-3}$ cm/s	HDPE 60 mil	geonet	HDPE + GCL $k_{GCL}=2\times10^{-9}$ cm/s
Baseline Landfill Cell III-A	II	24 in. sand $k_{sand}=1\times10^{-3}$ cm/s	HDPE 100 mil	geonet	12 in. Clay $k_{clay}=1\times10^{-8}$ cm/s
Baseline Landfill Cell III-B	II	24 in. sand $k_{sand}=1\times10^{-3}$ cm/s	HDPE 60 mil	geonet	HPDE + 12 in. clay $k_{clay}=5\times10^{-8}$ cm/s
Winfield Landfill	II	24 in. sand $k_{sand}=1\times10^{-3}$ cm/s	HDPE 60 mil	geonet	HDPE + 6 in. soil $k_{soil}=1\times10^{-5}$ cm/s
Site 7 Landfill Cells A-A to A-D	III	24 in. sand+geonet $k_{sand}=3.8\times10^{-3}$ cm/s	HDPE 60 mil	12 in. sand+geonet $k_{sand}=3.8\times10^{-3}$ cm/s	HDPE + 6 in. sand $k_{sand}=3.8\times10^{-3}$ cm/s
Site 7 Landfill Cell A-E	III	24 in. sand+geonet $k_{sand}=3.8\times10^{-3}$ cm/s	HDPE 60 mil	12 in. sand+geonet $k_{sand}=3.8\times10^{-3}$ cm/s	HDPE + 6 in. soil $k_{soil}=1\times10^{-5}$ cm/s
Broward Interim Cont. Cells 1A,1B,3 (A+B)	IV	24 in. sand $k_{sand}=1\times10^{-2}$ cm/s	HDPE 60 mil	12 in. sand+geonet $k_{sand}=1\times10^{-4}$ cm/s	HDPE + 6 in. sand $k_{sand}=1\times10^{-4}$ cm/s
West Pasco Landfill Cells A-1,SW-1	IV	24 in. sand $k_{sand}=1\times10^{-2}$ cm/s	HDPE 60 mil	12 in. sand $k_{sand}=1\times10^{-2}$ cm/s	HDPE + 6 in. soil $k_{soil}=5\times10^{-5}$ cm/s
Berman Road Landfill Cells 3,7	V	24 in. sand+geonet $k_{sand}=1\times10^{-3}$ cm/s	HDPE + GCL $k_{GCL}=2\times10^{-9}$ cm/s HDPE=60 mil	geonet	HDPE + GCL $k_{GCL}=2\times10^{-9}$ cm/s

NOTE: 1 inch = 2.54 cm
60 mil = 1.5 mm

In order to clarify the various double liner designs and their impacts on LDS flow rates, each design was placed into one of five general groups which are shown in Figure 1. The groups were defined by the liner components directly above and below the primary geomembrane liner. In some cells, additional liner components other than those shown in Figure 1 are in the LDS or subbase designs. While these additional components affect leakage estimates through the secondary liner, they do not affect leakage into the LDS and were not shown on Figure 1.

Group I included all cells which had a geonet above and below the primary geomembrane. Group II had sand above and a geonet below. Group III had a geonet above and sand below. Group IV had sand both above and below the primary geomembrane. Finally, Group V cells used a double composite liner system where the soil component of the composite liners consisted of a geosynthetic clay liner (GCL). This group had a geonet above the primary liner and a GCL below it. The group names for each cell are also shown in Table 3. Using this classification method, 9 of the 24 cells were in Group I, 3 were in Group II, 5 were in each of Groups III and IV, and 2 were in Group V. The double-lined landfill design assumed by the TAG corresponded to the Group II cells as shown in Figure 1b.

It should also be noted that the Group I and Group V landfills had both the
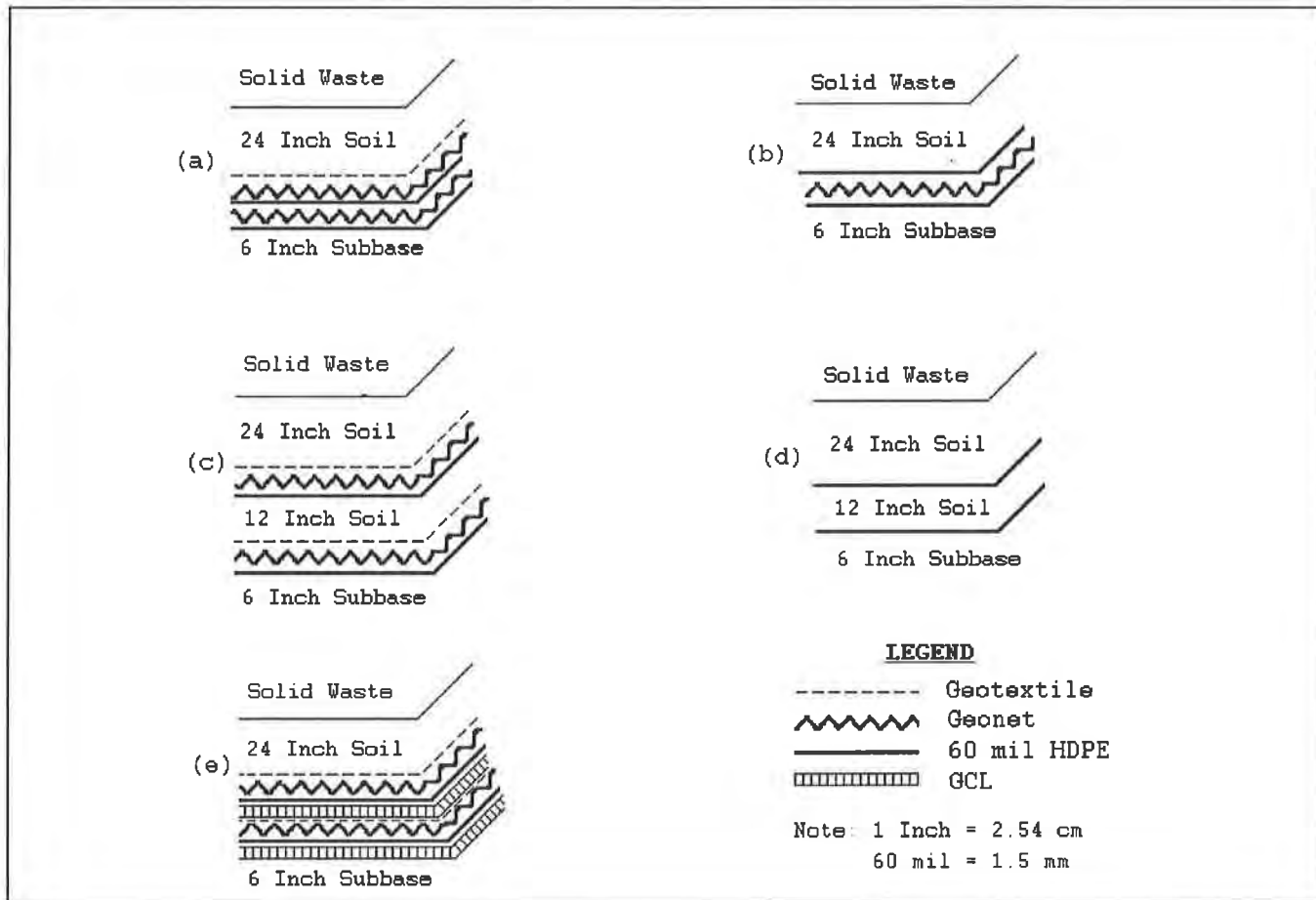
Figure 1. General groups of double-lined landfills: (a) Group I;
(b) Group II; (c) Group III; (d) Group IV; (e) Group V.

LCS and LDS leachate sumps located within the lined area of the landfill. This is a common design practice which has the advantage of eliminating liner penetrations. Leachate is accumulated in shallow sumps inside the landfill and pumped out through riser pipes over the liner side slopes rather than flowing by gravity through a liner penetration to a wetwell located outside the landfill. Group II, III and IV landfills collected the leachate in wetwells located outside the landfill.

ESTIMATION OF LANDFILL LEAKAGE RATES

In order to evaluate the field performance of the double-lined landfills, calculations of theoretical leakage rates into the LDS were needed. If the assumptions used by the TAG to estimate leakage were flawed, then many of Florida's double-lined landfills should have LDS flow rates higher than theoretically predicted flow rates. As noted above, however, many of the double-lined landfill designs were different from the design assumed by the TAG when developing the solid waste rule. It was decided to use the TAG assumptions along with each specific double-lined landfill design to estimate leakage into the LDS and then through the secondary liner. The theoretical leakage rates into the LDS could then be compared to actual field data.

The TAG assumptions used to estimate leakage were: constant head on the primary liner at the maximum allowed value by rule; a liner slope of 2 percent; a maximum drainage length of 45.7 m (150 ft); average contact between the geomembrane and low-permeability soil components for a composite liner; defects in the primary liner align with defects in the secondary liner; and liner defects at a frequency of 1 per 4000 m^2 (1 per acre) with an area of 1 cm^2 per defect. In addition to Equation 1, other equations were used to estimate leakage either into the LDS or through the secondary liner. These additional equations will now be described.

To estimate leakage through geomembranes overlain and underlain by high permeability materials such as a geonet above and below a geomembrane, Bonaparte et. al. (1989) recommend the use of Bernoulli's equation for free flow through an orifice in the following form:

$$Q = C_B a (2gh)^{0.5} \qquad (2)$$

where:
Q = steady-state rate of leakage through one geomembrane hole, m^3/s;
C_B = dimensionless coefficient assumed to be 0.6 for geomembrane holes;
a = area of hole in geomembrane, m^2;
g = acceleration of gravity, 9.8 m^2/s;
h = head of liquid on top of the geomembrane, m.

To estimate leakage through a composite liner with average contact between the geomembrane and the soil component of the liner, the following equation was used:

$$Q = 0.6a^{0.1}h^{0.9}k_s^{0.74} \qquad (3)$$

where:
Q = steady-state rate of leakage through one geomembrane hole, m^3/s;
a = area of hole in geomembrane, m^2;
h = head of liquid on top of the geomembrane, m;
k_s = hydraulic conductivity of the soil underlying the geomembrane, m/s.

Equation 3 is identical to the good contact and poor contact equations recommended by Bonaparte et. al. (1989) for estimating leakage through composite liners but uses a coefficient with a value of 0.6. This coefficient is an average of the coefficients from the good and poor contact equations. The TAG recommended this modification to approximate leakage through composite liners with average contact conditions.

To estimate the liquid depth on the secondary liner, the following equations were used:

$$X_{ave} = X_{max}/2 \qquad (4)$$

where:
X_{ave} = average distance downstream from a hole in the primary geomembrane, m;
X_{max} = maximum drainage length along secondary liner, m.

$$B_{ave} = [2(Q/k_d)^{0.5}/\sin\alpha][1 + (2X_{ave}\sin\alpha)/(Q/k_d)^{0.5}]^{0.5} \qquad (5)$$

where:
B_{ave} = average flow width in drainage layer, m;
Q = leakage rate into drainage layer, m^3/s;
k_d = hydraulic conductivity of drainage layer, m/s;
$\sin\alpha$ = slope of drainage layer, dimensionless;
X_{ave} = average distance downstream from a hole in the primary geomembrane, m.

$$D = Q/(B_{ave}k_d\sin\alpha) \qquad (6)$$

where:
D = Depth of liquid in drainage layer, m;
Q = leakage rate into drainage layer, m^3/s;
B_{ave} = average flow width in drainage layer, m;
k_d = hydraulic conductivity of drainage layer, m/s;
$\sin\alpha$ = slope of drainage layer, dimensionless.

Equation 4 was recommended by the TAG as a reasonable location downstream of a defect in the primary liner to calculate leakage through a defect in the secondary liner. Equations 5 and 6 were recommended by EPA (1992) for estimating the width and depth of the liquid layer on the secondary liner at the average distance downstream from the defect in the primary liner.

In addition to the above equations, basic design information about each landfill cell was obtained from DEP files or from the landfill owner/operators and their consultants. The hydraulic conductivity of the drainage media and subbase soils used for each cell is included in Table 3. The hydraulic conductivity of the GCL material, when used in a design, was assumed to be 2×10^{-11} m/s. Also, information used for the design head over the primary liner, the liner slope, hydraulic conductivity of the geonet, if used in the design, and the maximum drainage length along the secondary liner are given in Table 4.

Since many of the double-lined landfill designs were different than that proposed by the TAG, three additional assumptions had to be made in order to estimate liner leakage. First, for landfills with a geonet in the LCS overlaying the primary geomembrane, i.e., Group I, III and V landfills, the maximum head on the

Table 4. Select landfill design parameters.

LANDFILL	DESIGN HEAD, INCHES	BOTTOM SLOPE, %	GEONET Kd, M/SEC	Xmax, M
TAG Report Design	12.00	2	0.25	45.70
Central Disposal	0.16	2	0.15	45.70
Broward Interim Cont.	12.00	2	0.20	10.70
Winfield Landfill	12.00	2	0.20	14.20
Medley Landfill - Cell 1	0.16	2	0.15	30.40
Medley Landfill - Cell 2	0.16	2	0.15	39.60
Medley Landfill - Cell 3	0.16	2	0.15	36.60
Trail Ridge Landfill	0.20	2	0.20	54.90
Baseline Landfill	12.00	2	0.20	15.20
Berman Road Landfill	0.20	2	0.20	100.60
Site 7 Landfill	0.20	4	0.20	9.10
West Pasco Landfill	12.00	2	NA	15.20

NOTE: 1 inch = 2.54 cm

primary geomembrane used for leakage calculations was the estimated thickness of the geonet under maximum compression forces expected in the landfill, rather than 30.5 cm (12 in) assumed by the TAG. This is consistent with the TAG approach of using the maximum head allowed by rule. If a geonet is used as the primary component in the LDS, the DEP solid waste rule requires that the leachate head not exceed the thickness of this drainage layer. It was assumed this same constraint should apply if the geonet was used as the primary component of the LCS.

Second, if drainage sand was placed both over and below a geomembrane liner and if both soil layers had similar hydraulic conductivities, i.e., within the same order of magnitude, it was assumed that Equation 1 could be used to estimate leakage through the liner. This occurred with the design of the West Pasco Landfill where the drainage sands had a hydraulic conductivity of 1×10^{-2} cm/s. In using Equation 1, it was assumed that sand above the geomembrane had better contact with a liner defect than sand below the liner. Since the hydraulic conductivities were similar, leakage out the bottom of the defect would be faster than leakage into it from the top and Equation 1 should still apply.

Third, the liner components used in the Site 7 Landfill resulted in a quasi-composite liner design. Quasi-composite liners are similar to composite liners, but the soil component of the liner has a hydraulic conductivity greater than 1×10^{-6} m/s which, according to Bonaparte et. al. (1989), is the upper bound limit for the use of Equation 3. There are no design equations currently available for estimating leakage from these liners. Rather, leakage estimates were obtained using an extrapolation method recommended by Giroud et. al. (1994). This method involved a graphical interpolation on log/log paper between the endpoint for the average contact composite equation, Equation 3, and the maximum value obtained using Bernoulli's equation, Equation 2. Using this interpolation method, leakage through the quasi-composite liners could be estimated.

Using the above equations, assumptions and specific design information, estimated leakage rates through the primary and secondary liner for each landfill cell were obtained and are given in Table 5. Due to the major differences in the

Table 5. Comparison of estimated and actual liner leakage rates.

Landfill - Cell	Liner Group	Estimated Leakage Through Primary Liner to LDS, GPAD	Actual Average Leakage Through Primary Liner to LDS, GPAD	Actual Maximum Leakage Through Primary Liner to LDS, GPAD	Estimated Leakage Through Secondary Liner Based on Actual Average LDS Flow, GPAD
Central Disposal - Stage I	I	3.88E+02	7.70E+01	2.76E+02	2.60E-05
Central Disposal - Stage II	I	3.88E+02	9.00E+01	1.31E+02	2.90E-05
Central Disposal - Stage III	I	3.88E+02	1.27E+02	3.40E+02	3.70E-05
Broward Interim Cont.- Cell 1-A	IV	6.80E+01	7.67E+00	7.50E+01	2.70E-02
Broward Interim Cont.- Cell 1-B	IV	6.80E+01	1.10E+01	6.60E+01	3.40E-02
Broward Interim Cont.- Cell 3 (A+B)	IV	6.80E+01	2.86E+01	8.20E+01	6.50E-02
Winfield Landfill - Cell 1	II	8.90E+01	1.47E+00	4.80E+00	1.40E-03
Medley Expansion - Cell 1	I	3.88E+02	4.58E+02	6.77E+02	5.80E-02
Medley Expansion - Cell 2	I	3.88E+02	7.70E+01	9.60E+01	1.60E-02
Medley Expansion - Cell 3	I	3.88E+02	1.13E+02	1.51E+02	2.10E-02
Trail Ridge Landfill - Cell A	I	4.29E+02	2.20E+00	4.70E+00	1.80E-06
Trail Ridge Landfill - Cell B	I	4.29E+02	1.82E+01	1.30E+02	7.70E-06
Trail Ridge Landfill - Cell C	I	4.29E+02	6.63E+01	8.20E+01	1.80E-05
Baseline Landfill - Cell III-A	II	8.90E+01	1.40E+01	3.80E+01	2.70E-02
Baseline Landfill - Cell III-B	II	8.90E+01	2.45E+01	1.13E+02	1.80E-04
Berman Road Landfill - Cell 3	V	5.70E-04	1.60E-01	4.00E-02	2.40E-07
Berman Road Landfill - Cell 4	V	5.70E-04	2.00E-03	1.30E-02	1.30E-08
Site 7 Landfill - Cell A-A	III	2.50E+01	3.80E+00	8.00E+00	2.10E-01
Site 7 Landfill - Cell A-B	III	2.50E+01	3.10E+00	3.60E+00	2.00E-01
Site 7 Landfill - Cell A-C	III	2.50E+01	4.90E+00	6.00E+00	2.30E-01
Site 7 Landfill - Cell A-D	III	2.50E+01	7.80E+00	1.07E+01	2.80E-01
Site 7 Landfill - Cell A-E	III	2.50E+01	1.05E+01	3.40E+01	4.80E-03
West Pasco Landfill - Cell A-1	IV	2.81E+02	6.30E+00	1.20E+01	1.90E+00
West Pasco Landfill - Cell SW-1	IV	2.81E+02	5.70E+00	1.10E+01	1.80E+00

NOTE: 1 GPAD = 0.935 liter/1000 m^2/day

various double liner designs, there were significant differences in the estimated leakage rates through those systems. Theoretical leakage rates into the LDS ranged from 5.0×10^{-4} liters/1000 m^2/day (5.7×10^{-4} gpad) for the Group V cells to 401 liters/1000 m^2/day (429 gpad) for the Group I cells. Estimated leakage rates through the secondary liner ranged from 1.2×10^{-8} liters/1000 m^2/day (1.3×10^{-8} gpad) to 1.8 liters/1000 m^2/day (1.9 gpad).

The estimated leakage rate into the LDS for the Group I landfills averaged 374 liters/1000 m^2/day (400 gpad) which was much greater than the 83.2 liters/1000 m^2/day (89 gpad) assumed by the TAG. This average leakage rate was also much greater than the action leakage rate into the LDS of 93.5 liters/1000 m^2/day (100 gpad) recommended by EPA (1992). However, both the TAG and EPA used the Group II liner design to derive their LDS leakage rate estimates. The estimated LDS leakage rates for Group II through V landfills were at or below the estimated values by the TAG and EPA.

RESULTS

Evaluation of Landfill Leakage Rates. Estimated leakage rates to the LDS for each cell are compared with actual average leakage rates and actual maximum monthly leakage rates in Table 5. A comparison of the estimated with actual average LDS flow rates for all the cells is shown in Figure 2. Points below the 45 degree reference line in Figure 2 indicate that the actual LDS flow rates for the cells represented by those points were less than their corresponding estimated values.

The actual average LDS flow rates were well below the estimated LDS flow rates for all cells with the exception of Cell 1 of the Medley Expansion Landfill and the two cells at the Berman Road Landfill. Even though the actual leakage rates into the LDS exceeded theoretical leakage rates for Berman Road Landfill, the leakage rates were very low as would be expected with a double composite liner design, and the elevated leakage rates were believed related to construction water pumped out during start-up of the cells.

The actual maximum LDS flow rates were below estimated flow rates for 17 of the 24 cells. In addition to Cell 1 of the Medley Expansion Landfill and the two
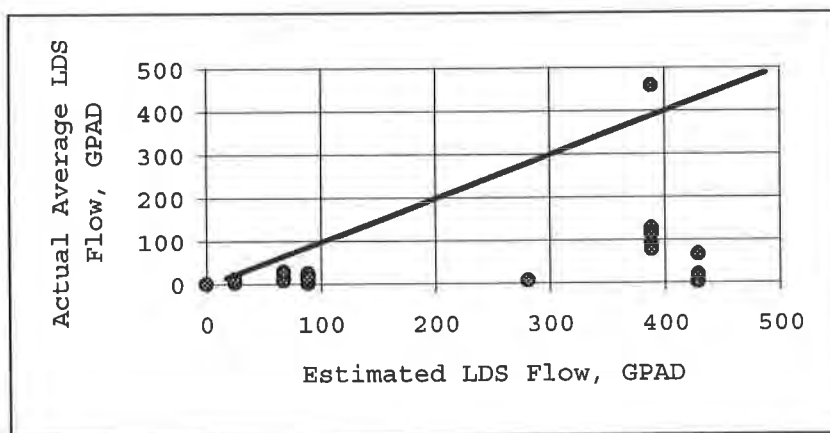
Figure 2. Estimated LDS flow rates compared to actual average LDS flow rates. For points below the 45 degree reference line, the actual average LDS flow rate was less than the estimated flow rate.
Note: 1 GPAD = 0.935 liters/1000 m^2/day.

cells from Berman Road Landfill, the remaining cells which had higher maximum LDS flow rates were Broward Interim Contingency Landfill, Cells 1-A and 3(A+B); Baseline Landfill, Cell III-A; and Site 7 Landfill, Cell A-E. Excluding Cell 1 of Medley Expansion Landfill, the elevated maximum LDS flow rates were reported to be related to construction water accumulated in the LDS prior to operation of the cell, compression water expelled from the LDS during increasing overburden pressures and accidental or deliberate discharges of stormwater directly into the LDS. These explanations by the landfill owner/operators were reasonable since the actual average LDS flow rates for these cells were well below the estimated LDS flow rates. Also, there was no evidence of a chronic leakage problem to the LDS in these cells as would be expected if significant flaws existed in the primary liner.

Impacts of Liner Design on Actual LDS Leakage Rates. During this study, it was noticed that the highest actual average LDS flow rates occurred in the Group I landfills which were constructed with a geonet above and below the primary geomembrane. In addition, these landfills had double-lined leachate sumps located inside the landfill. With these designs, the Group I landfill cells averaged 107 liters/1000 m^2/day (114 gpad) of flow into the LDS which was an order of magnitude higher than all the other cells. Since Equation 2 is the governing equation for estimating leakage through the primary geomembrane in these cases, it is clear that small heads over liner defects for these designs can result in large leakage rates through the primary liner.

Based on this study, it appeared that only Cell 1 of the Medley Expansion Landfill had LDS flow rates which indicated a liner leakage problem was occurring through the primary liner. This landfill cell was in Group I and had the leachate sump located inside the landfill. To investigate this problem, the owner/operator began to experiment with the leachate head levels in the sump. This testing occurred over a 60 day period. Sump heads could be lowered by lowering the "pump-on" set point. Normal operations had the pump-on set point at the maximum level of 61 cm (24 inches) which corresponded to a LDS flow rate of approximately 467.5 liters/1000 m^2/day (500 gpad). When the head in the primary sump was lowered to 25 cm (10 inches), the LDS flow rates dropped to approximately 121.6 liters/1000 m^2/day (130 gpad). The results of this test are shown in Figure 3.

CONCLUSIONS AND RECOMMENDATIONS

As a result of the data collected and evaluated for this paper, the following conclusions were reached:

1. Using available equations and reasonable assumptions about liner leakage for double-lined landfills which also have good liner Construction Quality Assurance, it is possible to make reasonable predictions of actual LDS leakage rates.

2. The assumptions used for leakage calculations in this paper tended to over predict actual leakage rates into the LDS for Florida double-lined landfills and indicated that the landfills were performing within expectations.

3. While many factors can affect liner leakage rates, it also appears that the design of the liner system can affect leachate flow rates into the LDS. This was most apparent in the Group I landfills where the primary liner was designed with a geonet above and below the primary geomembrane. The high hydraulic transmissivity of geonets has the
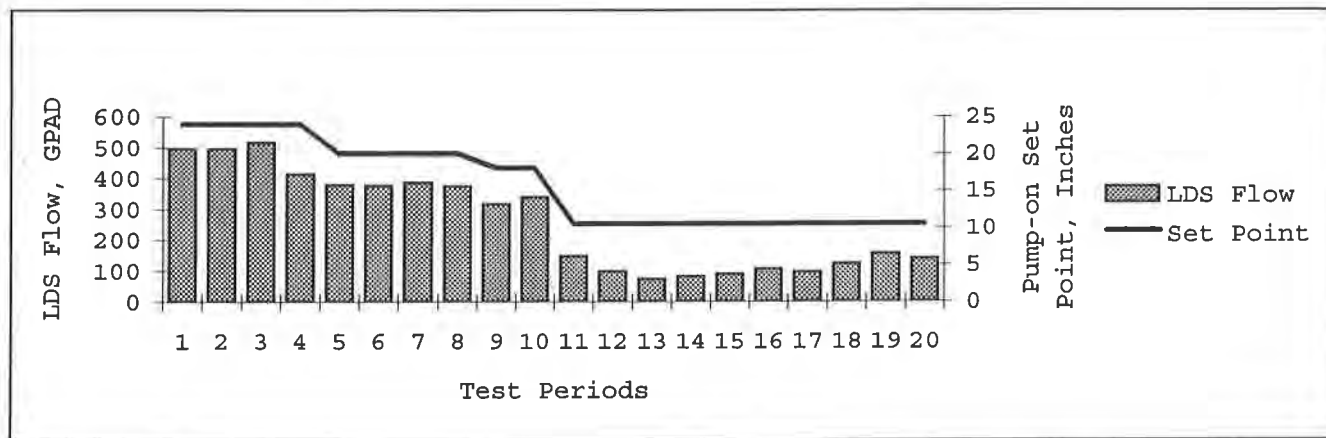
Figure 3. Medley Expansion Landfill LDS flow rates relative to sump head.
Note: 1 GPAD = 0.935 liters/1000 m^2/day

       advantage of quickly removing leachate from the landfill. However, this property also results in a lower resistance to leachate flow which may increase leakage through liner defects for Group I designs. These design impacts should be considered when the performance of a double-lined landfill is being evaluated.

4. The action leakage rate for the LDS of 93.5 liters/1000 m^2/day (100 gpad) proposed by EPA (1992) is appropriate when the LCS design consists of drainage sand over the primary geomembrane. However, if the liner design includes a single geonet layer both above and below the primary geomembrane, then the estimated and actual LDS flow rates presented in this paper for Group I double-lined landfills in Florida suggest that an action leakage rate of approximately 374 liters/1000 m^2/day (400 gpad) is more appropriate for these facilities.

5. While sumps located inside the landfill have the advantage of eliminating liner penetrations, they also may contribute to increased LDS flow rates due to the higher heads inherent in these sumps. Liner systems in sumps with a geonet above and below the primary geomembrane liner may be especially vulnerable to these increased LDS leakage rates. Engineers should consider this when designing double-lined landfill sumps and should include additional layers of protection in the sumps or reduce the number of liner seams present in the sump areas.

REFERENCES

Bonaparte, R., Giroud, J.P., and Gross, B.A., (1989) "Rates of Leakage Through Landfill Liners", Proceedings of Geosynthetics '89, Vol. 1, San Diego, California, pp. 18-29.

Giroud, J.P., Badu-Tweneboah, K., and Soderman, K.L., (1994) "Evaluation of Landfill Liners", Proceedings of the Fifth International Conference on Geotextiles, Geomembranes and Related Products, Singapore, pp. 981-986.

USEPA, "Action Leakage Rates For Leak Detection Systems", (1992) EPA/530-12-92-004, 22 p.

TEMPERATURE CORRECTED TENSILE STRENGTHS FOR GEOMEMBRANE FIELD SEAMS

J. A. MILLS
LAYFIELD PLASTICS (1978) LTD.

J. R. STANG
LAYFIELD PLASTICS (1978) LTD.

ABSTRACT

Tensile testing of geomembrane seams is a fundamental aspect of the Quality Assurance plan on many installation projects. Qualification welds and cut-out coupons are sampled and tested in peel and shear modes on portable tensile testing machines (tensiometers) in a variety of weather conditions. Field testing is often performed at ambient temperatures with little or no conditioning prior to the test. Temperature correction charts are currently not available for the testing methods and geomembrane materials currently in use. Since thermoplastic geomembrane materials show a dramatic change in tensile properties with temperature, field test results can often appear to fall below project requirements. This study investigates temperature/tensile behaviour of commonly used geomembrane materials. Using both laboratory and field tests, a correction factor was found to adjust tensile strengths at break from ambient test temperature to standard test temperature. This correction factor can be used to calculate an immediate temperature corrected tensile strength at break, which can be used to estimate specification compliance of properly conditioned samples.

INTRODUCTION

In the last ten years the testing and Quality Control (QC) procedures used on geomembranes have undergone fundamental changes. Moving from strictly visual techniques to more quantifiable methods, one of the most dramatic changes has been the use of tensiometers in the field. Portable tensiometers are now relatively inexpensive, readily available, and are standard equipment with most geomembrane installers.

Portable tensiometers are used in the field by the installation contractor to rapidly estimate if the seam strengths prepared will meet the required project specifications. The results

provided by an on-site portable field tensiometer allow the contractor to proceed with installation immediately without having to wait for specification conformance testing from an off-site laboratory. Using the results given by the field tensiometer, the contractor predicts whether the off-site conformance testing will be successful, and proceeds with installation based on this prediction. It is vital that the contractor accurately estimates whether the seam samples sent off-site will meet the job specifications so that costly seam cut-outs and repairs are avoided.

A fundamental problem with using portable tensiometers in the field is that it is difficult to maintain an accurate test temperature. There are different ways that contractors have attempted to control test temperature including climate controlled trailers, moving the tensiometer out of direct sunlight, using buildings or other site facilities, and even performing testing at the hotel where the crews are billeted. Generally, the larger the job, the easier it is to include facilities to control testing temperature. On some projects, however, the testing must take place at temperatures far from the ideal of +23°C. On these projects the contractor needs some way to compensate the observed test value to +23°C so that a prediction of specification conformance can be reached.

There are two situations when the accuracy of the portable tensiometer is most suspect. The first situation is in very hot weather. In elevated temperatures the tensile strength of the material decreases and minimum seam strengths may not be met on field equipment. Elevated test temperatures also increase the elongation of the material, often exceeding the stroke of the tensiometer. Low test results on warm days usually lead to the installer replacing seams that apparently do not meet specification. The second situation where accuracy may be compromised is in cold weather when material being tested may not meet a minimum tensile elongation requirement. Other cold weather problems that may contribute to an inaccurate result are; exceeding the tensile capacity of the load cell, and freezing the electronics of the tensiometer.

This paper investigates the feasibility of a temperature correction factor that may be applied by contractors to accurately predict the results of off-site specification conformance testing of field seams when field testing was performed at temperatures other than +23°C. This paper does not recommend the use of field testing performed at temperatures other than +23°C for final specification acceptance testing. Further testing would also be required to confirm whether the portable field tensiometers retain their accuracy at varying temperatures.

SCOPE

This study looked at the problems associated with variations in testing temperature when testing geomembranes with portable tensiometers. The goal of this study was to determine if there was a regular relationship between the tensile strengths at break of geomembrane materials and temperature, and to determine a "correction factor" that would allow extrapolation of field testing results to an approximation of standard laboratory temperature. The study took place in

three phases. The first phase tested a number of materials to select candidates for further testing and to determine the testing limits of the available apparatus. The second phase of the study looked at three thicknesses each of PVC and HDPE and checked temperature vs. tensile strength at break for material and seam samples. The third and final phase of the study involved taking a portable tensiometer into a temperature controlled room and testing material and seam samples at extreme ambient conditions.

The tensile performance of thermoplastic materials has been well understood for many years. Simply put, as the temperature increases the tensile strength decreases. There is also a corresponding increase in tensile elongation as temperature increases. For most thermoplastic unsupported geomembrane materials the relationship between temperature and tensile strength is linear throughout the expected service temperatures. In a series of 500 tests on HDPE Giroud et al (1993) showed that the temperature versus tensile performance was a linear relationship between -20°C and +70°C. Richards et al (1985) showed that for PVC and HDPE the temperature versus tensile performance was linear between +23°C and -26°C.

The purpose of this study was to look at tensile strength at break under field testing conditions that varied in temperature and to see if a correction factor could be prepared that accurately predicted values at standard test temperature.

PHASE ONE TESTS

The first phase of testing was used to determine the capacities and testing capabilities of an available apparatus. Using a temperature conditioning chamber attached to a lab tensiometer, a series of tests were performed on HDPE, PVC, PP, and a proprietary PVC alloy material trade named Arctic Liner™. Table 1 lists the materials that were tested. All materials tested were unsupported thermoplastics. Figure 1 shows the general arrangement of the conditioning chamber. Solid and liquid CO_2 were used to reduce the temperature in the chamber while integral heaters were used for elevated temperature testing. The Instron conditioning chamber was mounted on an Instron Model 1123 tensiometer and all tests were recorded on chart paper. The apparatus had a restricted stroke of 450 mm (18") due to the size of the conditioning chamber which reduced available crosshead travel.

Phase one testing used a specimen width of 12 mm (0.5") in a "dog-bone" type specimen and tested in accordance with the American Society for Testing and Materials (ASTM) standard D638. A grip separation of 100 mm (4") was used. A temperature range of +60°C to -14°C was chosen based on the capabilities of the apparatus. Three specimens were tested of each sample.

Material	Thickness	Supplier
Flexible Polyvinyl Chloride (PVC)	0.5 mm, 0.75 mm, 1.0 mm	Nanya Plastics
High Density Polyethylene (HDPE)	1.0 mm, 1.5 mm, 2.0 mm	Columbia Geosystems
Flexible Polypropylene Alloy (PP)	0.5 mm, 0.75 mm, 1.0 mm	Layfield Plastics
PVC-Nitrile alloy (Arctic Liner™)	0.75 mm	Canadian General Tower

Table 1. Material Descriptions.

Figure 1. View of test apparatus showing conditioning chamber.

Figure 2 shows the tensile strength at break results from the first testing phase for 1.5 mm (60 mil) HDPE, 1.0 mm (40 mil) PVC and 0.75 mm (30 mil) Arctic Liner™ materials. Each of the materials shows a roughly linear relationship between tensile strength at break and temperature. Figure 3 shows the relationship between elongation and temperature for phase one. The restricted elongation available with the apparatus limited testing on a number of materials. Testing of PP was not successful due to the limited stroke of the apparatus which prevented testing to break.
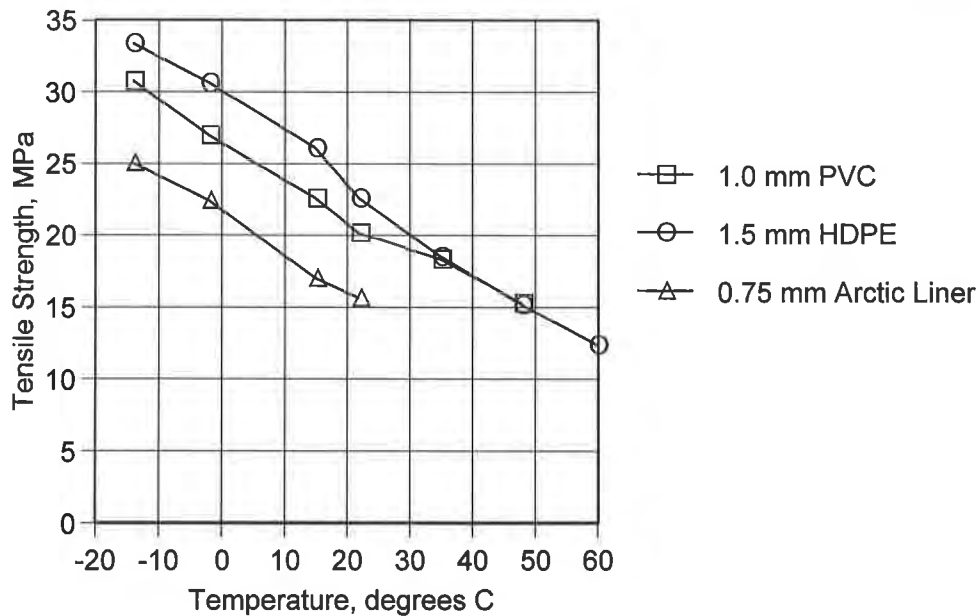
Figure 2. Phase 1 - Tensile Strength at Break vs. Temperature
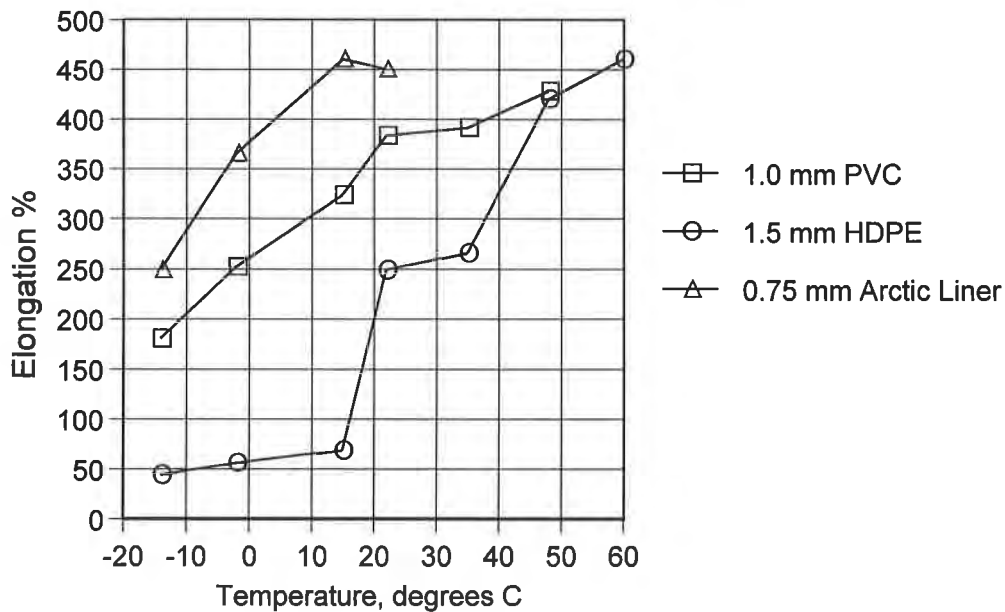
Figure 3. Phase 1 - Elongation at Break vs. Temperature

The results of the first phase showed that the temperature/tensile strength at break relationship for the geomembrane materials was approximately linear over the range of temperatures tested. Tensile test results appeared to be relatively consistent. Elongation test results appeared to have a strong trend towards linearity, however variation in the small sample size precluded direct conclusions on elongation properties. A more complete listing of the observations of this phase is contained in the unpublished student paper "Effects of Temperature on Tensile Properties of Liner Materials" by Jason Stang.

The first phase of testing showed that the limited stroke of the apparatus would not support testing of the highly flexible materials such as PP and Arctic Liner™, and that PVC and HDPE materials could not be tested at temperatures above +48°C. The first phase test also showed that a maximum gauge length of 100 mm (4") would be required to allow testing at elevated temperatures. For the next phase of testing the upper test temperature was limited to +48°C and the testing was restricted to PVC and HDPE with a gauge length of 100 mm (4").

PHASE TWO TESTS

The purpose of phase two was to see if there was a direct correlation between the temperature vs. tensile strength at break of parent material and field seams. Phase two testing began with an investigation into a suitable field testing method. PVC tensile strength is specified according to National Sanitation Foundation Standard 54 for Flexible Membrane Liners (NSF 54). NSF 54 specifies that PVC parent material strength is tested with ASTM D882, in a 25 mm (1") strip tensile test. Bonded seam strength is specified using ASTM D3083 with a 25 mm (1") wide specimen and a grip separation of 100 mm (4") plus the width of the seam.

The PVC seams prepared for this test had a width of approximately 32 mm (1.25"). This would have led to a grip separation of approximately 132 mm (5.2"). In phase one testing it was seen that a grip separation of more than 100 mm (4") would exceed the available elongation of the apparatus when testing PVC. Because of this limitation the grip separation for seam testing was set at 100 mm (4"). The strain rate for PVC testing was set at 500 mm/min (20"/min).

HDPE parent material tensile strength is normally specified based on the test method ASTM D638 (a "dogbone" style test with the waisted section about 12 mm wide). HDPE tests of bonded seam strength in the field use a 25 mm (1") strip tensile test (ASTM D4437). In field applications it is common practice to compare HDPE parent material strength to seam strength by testing 25 mm (1") wide strip specimens. In this phase of testing 25 mm (1") wide strip samples were used for all specimens to more closely reflect field testing.

Gauge length for HDPE testing is complicated by the width of the seam which can reach 50 mm (2") wide. To follow the requirements of NSF 54 requires a grip separation of 100mm ± 50 mm or 150 mm (6"). However, phase one testing showed that a gauge length over 100 mm (4") would not be possible to test on the available apparatus. For this phase of testing a 100 mm (4") grip separation was used for both parent material and seam specimens. An informal survey of HDPE installers in North America revealed that a 100 mm (4") gauge length is commonly used in seam testing in the field with portable tensiometers.

The last point of discussion was the strain rate. The strain rate for HDPE testing is normally specified at 50 mm/minute (2"/min), however field operations may increase the strain rate to 500 mm/minute to speed testing. Initially all samples had been tested at a strain rate of

500 mm/min (20"/min) and this strain rate was maintained throughout all testing phases for all materials. Although this is different from the normally specified strain rate of 50 mm/min (2"/min) the faster strain rate gives similar results for HDPE in tensile strength at break. Under certain conditions a contractor may use the faster strain rate for estimating seam compliance. All testing in this study was conducted at the same strain rate of 500 mm/min (20"/min).

Phase two of the study modeled field testing using the laboratory tensiometer and conditioning chamber to see if a temperature correction factor could be obtained for PVC and HDPE materials. Three temperatures were chosen for phase two testing; +48°C, +23°C , and -14°C. This met the range of field conditions that would be expected while keeping within the limitations of the test apparatus. Three thicknesses of PVC and three thicknesses of HDPE were tested. Each material was tested for parent material strength and seam strength using a 25 mm (1") wide specimen and a grip separation (with and without seam) of 100 mm (4"). A special testing grip was manufactured for the lab tensiometer to fit within the temperature conditioning chamber and to test 25 mm (1") wide specimens.

Three specimens of each material were tested at each of the three temperatures. Parent material specimens were die cut from sheet goods so that the testing was oriented in the cross machine direction (the normal seaming testing direction). Seam specimens were prepared using field wedge welding equipment in 0.5 mm (20 mil) PVC, 0.75 mm (30 mil) PVC, 1.0 mm (40 mil) PVC, 1.0 mm (40 mil) HDPE, 1.5 mm (60 mil) HDPE, and 2.0 mm (80 mil) HDPE. The seam specimens were prepared such that the tensile tests were in the typical cross machine direction. All seam samples for test phases two and three were prepared at the same time with the same lot number of material. Three replicate specimens were tested for each thickness of material.

Specimens were conditioned for a minimum of one hour prior to testing. Each specimen was briefly handled with gloves while being loaded into the testing grips, and the testing chamber was allowed to return to its set temperature before each test. Figure 4 shows the results of the PVC tensile testing while Figure 5 shows the results of the HDPE testing.

The results showed a number of interesting points. First, the linearity of the relationship between temperature and tensile strength appears to be strong. Regardless of the original tensile strength of the material, the variation with temperature appears to be consistent. Tensile strengths were plotted using the units of pressure (MPa) which minimizes variation due to thickness differences between specimens. Using pressure units (MPa) the slopes of the lines remain consistent independent of the material thickness and tensile strength. A "best fit" line was calculated for each set of specimens tested and an average of the slopes of the best fit lines was calculated for each of the test materials. The PVC material had an average slope of -0.21 MPa per degree C, while HDPE showed an average slope of -0.25 MPa per degree C.

Figure 4. Phase 2 - PVC Tensile Strength at Break vs. Temperature
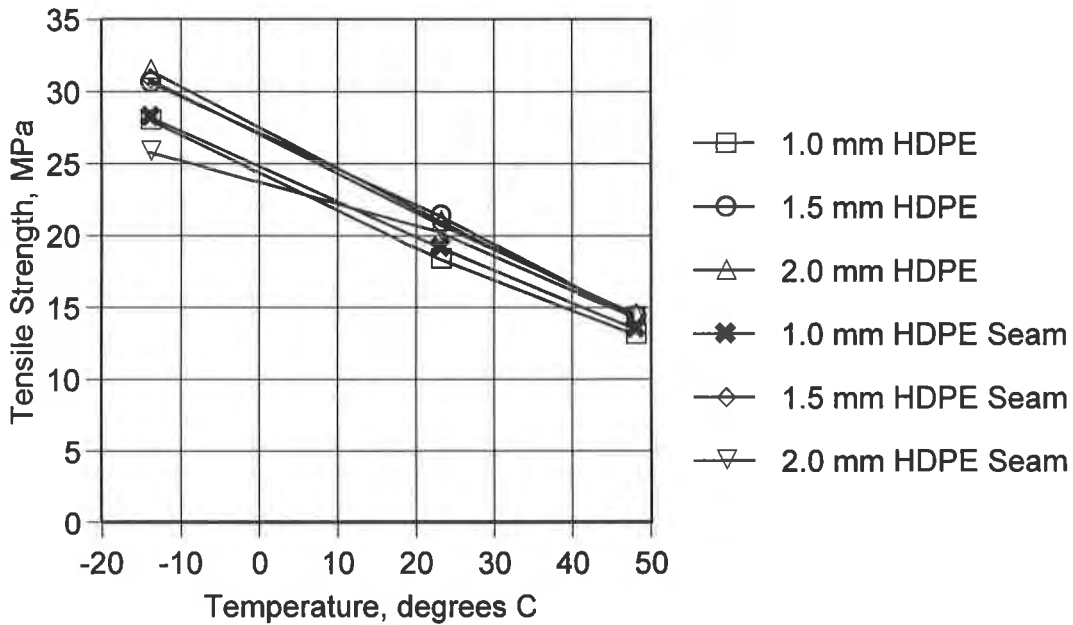
Figure 5. Phase 2 - HDPE Tensile Strength at Break vs. Temperature

Figure 6 shows the relationship between the elongation of the PVC samples and temperature. An average of the slopes of the best fit lines for PVC elongation shows an average slope of 3.3% elongation per degree C. The HDPE elongation data in Figure 7 shows significant departures from consistency and a quantifiable result was not possible. Additional testing would be required to clearly determine the relationship between HDPE elongation at break and temperature.
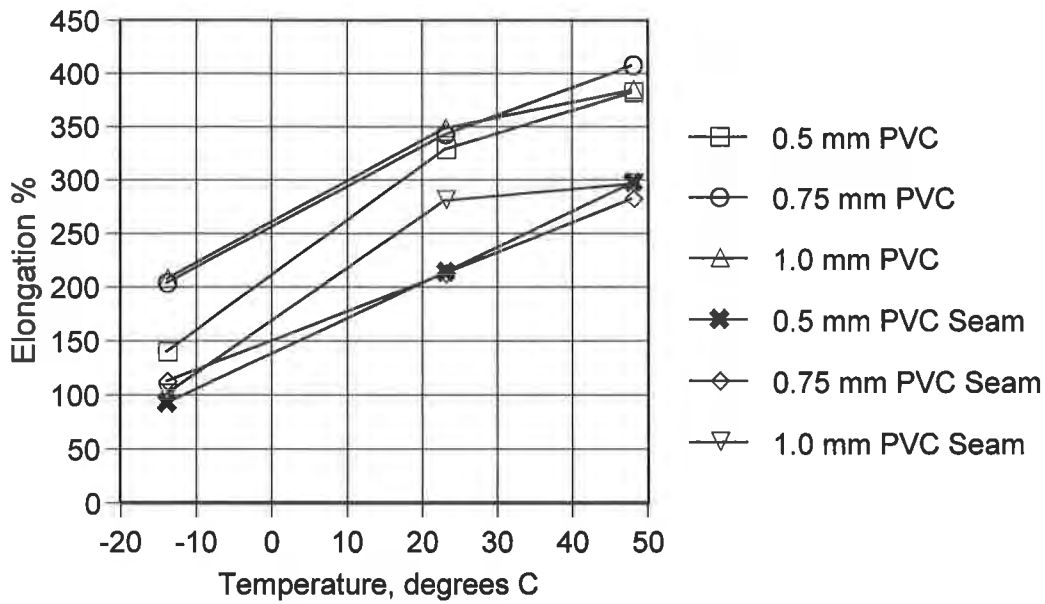
Figure 6. Phase 2 - PVC Elongation at Break vs. Temperature
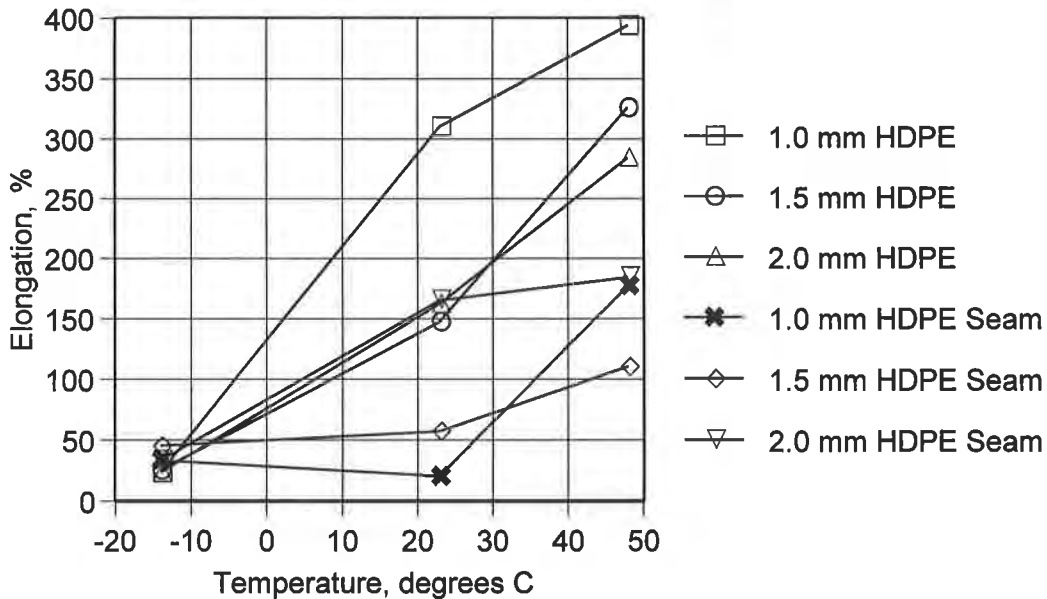
Figure 7. Phase 2 - HDPE Elongation at Break vs. Temperature

PHASE THREE TESTS

The third and final phase of the study attempted to model actual in-field conditions during testing. Using a Columbine "Accura Lite" portable tensiometer samples were tested at elevated and reduced temperatures. For the cold temperature testing a temperature controlled room was used. This room was maintained at a constant temperature of -14°C for 24 hours prior to the commencement of testing. Samples were placed within the chamber 15 hours prior to the test. The portable tensiometer was placed in the room one hour prior to testing to allow it to stabilize at the lower temperature. All samples were tested in the chamber in one session.

The elevated temperature testing was carried out in a heated room. The room had a set temperature of +62°C and was turned on two hours prior to the test. Samples were placed in the heated room 45 minutes prior to the testing. The portable tensiometer was placed within the heated room and allowed to stabilize at temperature for ½ hour. Testing proceeded from the thin gauge samples to the thicker gauges to allow the thicker materials more conditioning time. A thermometer was placed at the tensiometer grips and the temperature was recorded for each set of specimens tested. The temperature rose slowly over the course of the tests from +61 to +66°C.

A final check was made by performing tests on all samples at room temperature with the portable tensiometer. These tests were performed in our plant QC lab using the same portable tensiometer used for the elevated and reduced temperature testing. Samples were placed in the lab 24 hours prior to testing. Elongation measurements were not taken for phase three testing.

Although the portable tensiometer used had been calibrated seven days prior to this testing the calibration was not checked at each test temperature. This would be typical of a field tensiometer where it would be used in a range of temperatures without additional calibration. In this testing the results of the tests were compared with the laboratory tests to see if the test values were consistent. Phase three tests used specimens that were prepared at the same time as the samples tested in phase two. This allowed a direct comparison of results.

Figure 8 shows the PVC test results from phase three testing. The graph is strongly linear and shows a good fit with the testing performed in phase two. The average of the best fit line slopes for phase three testing for PVC shows a result of -0.18 MPa per degree C. Figure 9 shows the results for HDPE materials. The average slope of the best fit lines for the HDPE testing shows a result of -0.22 MPa per degree C. Elongations were not measured for phase three testing. Seam samples were not tested for 1.0 mm and 1.5 mm HDPE during phase three testing.

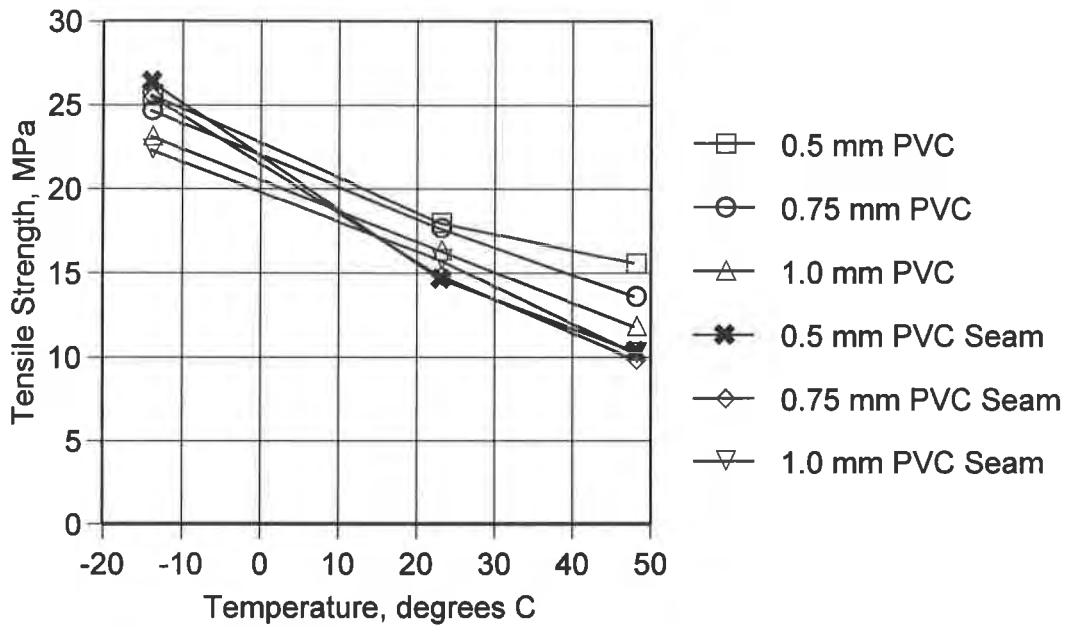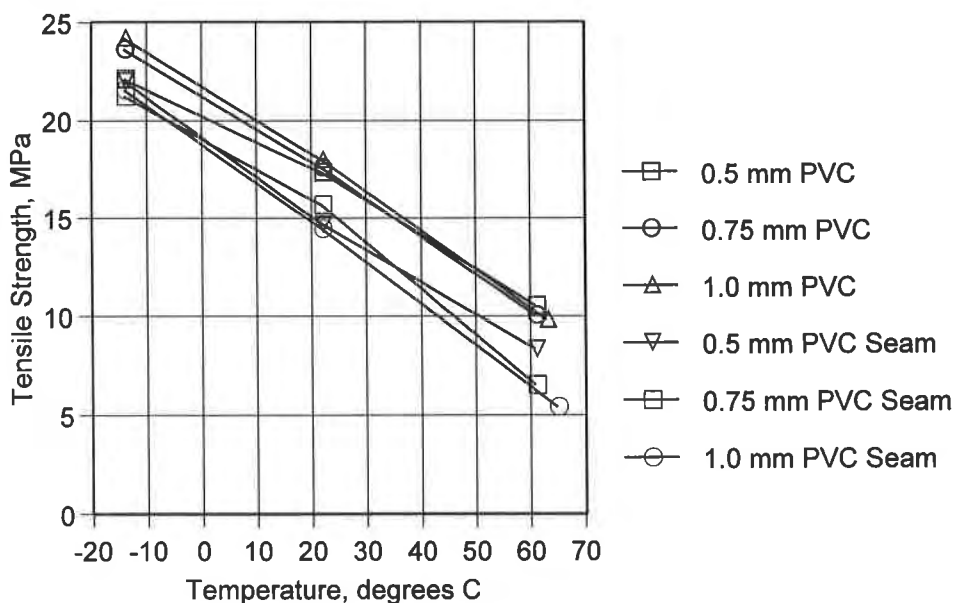

Figure 8. Phase 3 - PVC Tensile Strength at Break vs. Temperature
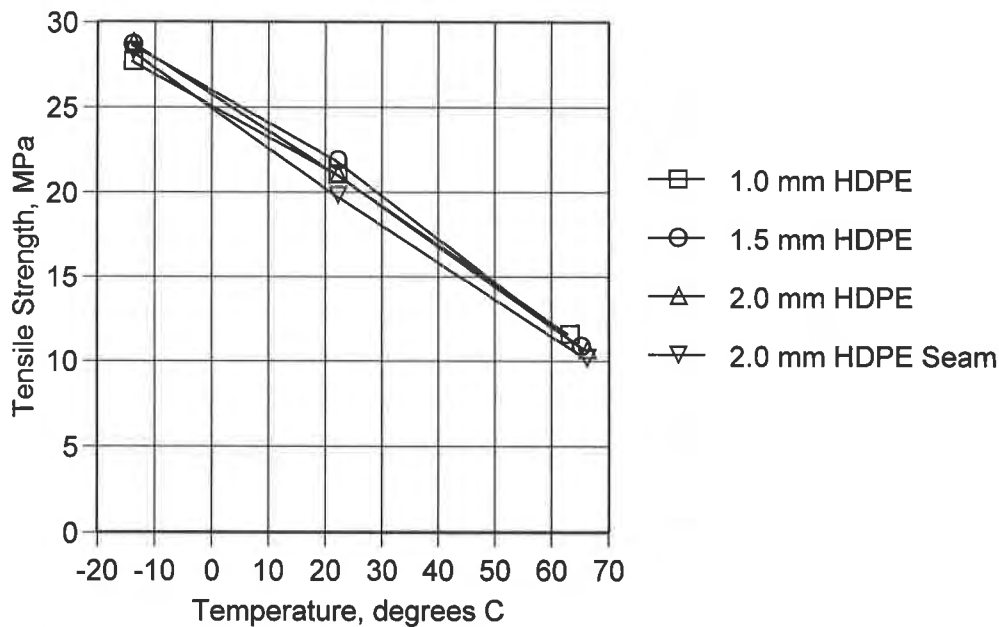
Figure 9. Phase 3 - HDPE Tensile Strength at Break vs. Temperature

TEMPERATURE CORRECTION FACTORS

This study found that a temperature correction factor can be calculated so that samples tested in the field can be adjusted to standard test temperature. This factor was independent of the thickness and initial strength of the materials tested. Although the sample size in this testing program was small, a correction factor was calculated for both PVC and HDPE tensile strength at break and for PVC elongation. The correction factor for PVC was found to be between -0.18 and -0.21 MPa per degree C (phase two and three respectively). The overall average for PVC (average of all slopes from phase two and three testing) was a tensile correction factor of -0.20 MPa per degree C. The elongation correction factor for PVC was 3.3% elongation per degree C. The overall tensile strength at break correction factor for HDPE was -0.24 MPa per degree C (for testing performed at 500 mm/minute).

ACCURACY AND COMPLIANCE PREDICTION

The purpose of the correction factors is to allow an installation contractor to accurately estimate whether compliance testing will be successful when field tests are performed at other than standard temperatures. In order for this estimate to be useful the error in the method needs to be determined. Fortunately, most field seam testing occurs at, or near +23°C. It is only as the testing temperature moves further away from +23°C that the accuracy of these correction factors decrease. Given the example of the two correction factors for PVC of -0.18 and -0.21 MPa per degree C, a line calculated for each slope offers the results as graphed in Figure 10. This graph shows how the accuracy of the correction factor at temperatures near +23°C is a very close approximation, however at the extremes of testing temperature the accuracy diminishes. At

+48°C the variation in the correction factors amounts to 0.75 MPa or about 7%. As the testing temperature moves closer to +23°C the error in these correction factors decreases. For testing temperatures between 0 and +40°C these factors will give a reasonably accurate prediction of compliance performance for seam strengths performed on portable tensiometer equipment.
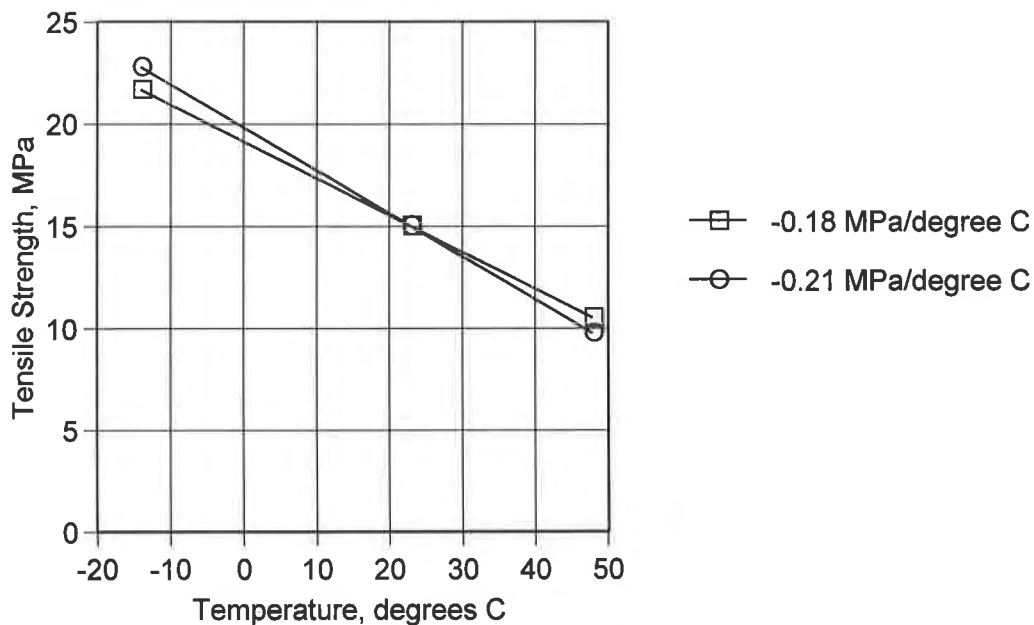
Figure 10. Temperature Correction Factors for PVC Tensile Strength at Break

CONCLUSIONS AND RECOMMENDATIONS

A temperature correction factor was found for each of PVC and HDPE materials that can be used to normalise field seam test results for tensile strength at break to +23°C. These correction factors allow the contractor to predict the specification conformance of seams tested at other than standard test temperature. The correction factors are most accurate at test temperatures close to +23°C and retain reasonable accuracy to the full range of expected testing environments.

For conformance testing, however, our recommendation is that all compliance testing be performed with properly conditioned samples in a temperature controlled laboratory environment. Although this technique of temperature correction will serve the installation contractor well, it will not serve as a replacement for correctly conditioned testing in a laboratory. This testing also shows that the use of portable tensiometers in the field to determine specification compliance by third party QC must consider climate control when performing testing. If temperatures cannot be accurately maintained during conformance testing the validity of the test results cannot be guaranteed.

PVC Correction Chart			
Temp degree C	Add to mPa	Add to psi	Temp degree F
0	4.6	667	32
1	4.4	638	33.8
2	4.2	609	35.6
3	4	580	37.4
4	3.8	551	39.2
5	3.6	522	41
6	3.4	493	42.8
7	3.2	464	44.6
8	3	435	46.4
9	2.8	406	48.2
10	2.6	377	50
11	2.4	348	51.8
12	2.2	319	53.6
13	2	290	55.4
14	1.8	261	57.2
15	1.6	232	59
16	1.4	203	60.8
17	1.2	174	62.6
18	1	145	64.4
19	0.8	116	66.2
20	0.6	87	68
21	0.4	58	69.8
22	0.2	29	71.6
23	0	0	73.4
24	-0.2	-29	75.2
25	-0.4	-58	77
26	-0.6	-87	78.8
27	-0.8	-116	80.6
28	-1	-145	82.4
29	-1.2	-174	84.2
30	-1.4	-203	86
31	-1.6	-232	87.8
32	-1.8	-261	89.6
33	-2	-290	91.4
34	-2.2	-319	93.2
35	-2.4	-348	95
36	-2.6	-377	96.8
37	-2.8	-406	98.6
38	-3	-435	100.4
39	-3.2	-464	102.2
40	-3.4	-493	104

HDPE Correction Chart			
Temp degree C	Add to mPa	Add to psi	Temp degree F
0	5.52	801	32
1	5.28	766	33.8
2	5.04	731	35.6
3	4.8	696	37.4
4	4.56	661	39.2
5	4.32	627	41
6	4.08	592	42.8
7	3.84	557	44.6
8	3.6	522	46.4
9	3.36	487	48.2
10	3.12	453	50
11	2.88	418	51.8
12	2.64	383	53.6
13	2.4	348	55.4
14	2.16	313	57.2
15	1.92	278	59
16	1.68	244	60.8
17	1.44	209	62.6
18	1.2	174	64.4
19	0.96	139	66.2
20	0.72	104	68
21	0.48	70	69.8
22	0.24	35	71.6
23	0	0	73.4
24	-0.24	-35	75.2
25	-0.48	-70	77
26	-0.72	-104	78.8
27	-0.96	-139	80.6
28	-1.2	-174	82.4
29	-1.44	-209	84.2
30	-1.68	-244	86
31	-1.92	-278	87.8
32	-2.16	-313	89.6
33	-2.4	-348	91.4
34	-2.64	-383	93.2
35	-2.88	-418	95
36	-3.12	-453	96.8
37	-3.36	-487	98.6
38	-3.6	-522	100.4
39	-3.84	-557	102.2
40	-4.08	-592	104

Table 2. Temperature Correction Factors for Tensile Strength at Break.

As a final calculation, a simplified temperature correction table for PVC and HDPE has been prepared as Table 2. This table allows the correction for temperature to be made simply by adding the corresponding adjustment factor to the test value measured in MPa or psi. This table covers most installation temperatures from 0 to +40°C.

ACKNOWLEDGEMENTS

REFERENCES

American Society for Testing and Materials, "ASTM D638 Standard Test Method for Tensile Properties of Plastics."

American Society for Testing and Materials, "ASTM D882 Standard Test Methods for Tensile Properties of Thin Plastic Sheeting."

American Society for Testing and Materials, "ASTM D3083 Standard Specification for Flexible Poly(Vinyl Chloride) Plastic Sheeting for Pond, Canal, and Reservoir Lining."

American Society for Testing and Materials, "ASTM D4437 Standard Practice for Determining the Integrity of Field Seams Used in Joining Flexible Polymeric Sheet Geomembranes."

Giroud, J.P., Soderman, K.L., and Monroe, M., (1993) "Mechanical Design of Geomembrane Applications", Proceedings, Geosynthetics '93 Conference, Vancouver, B.C.

National Sanitation Foundation (NSF), (1993) "Flexible Membrane Liners", NSF Standard 54, 30p. plus appendices.

Richards, E.A., Scott, J.D., and Chalaturnyk, R.J., (1985) "Cold Temperature Properties of Geomembranes", Proceedings, Second Canadian Symposium on Geotextiles and Geomembranes, Edmonton, Alberta.

Stang, J. R. (1996) "Effects of Temperature on Tensile Properties of Liner Materials", student paper, unpublished.

ANCHORAGE STRENGTH AND SLOPE STABILITY OF A LANDFILL LINER

P. VILLARD, J.P. GOURC, N. FEKI
IRIGM-Lgm, GRENOBLE UNIVERSITY, FRANCE

ABSTRACT

In order to determine reliable dimensions of an anchorage system and satisfactory operation of the watertight liner in a waste landfill, it is essential to make an accurate assessment of the tensions acting on the geosynthetics on the top of the slope. Experimental and theoretical studies have been carried out in parallel. The former concern a full-scale experiment undertaken in Montreuil sur Barse on a waste storage site with instrumented slope. The latter concern anchorage tests performed on a scale model for different anchorage geometries.

INTRODUCTION

To ensure proper safeguards for the environment, waste landfill centres must be built with watertight linings even when elongation occur to prevent any contamination of the underlying ground. The problems occasionally encountered on site (Seed 1990) have already highlighted the inadequacies of existing design methods whether for the determination of anchorage capacities or for estimating the forces acting on the various components of the lining system.

To obtain a clearer picture of geosynthetic head tensile forces a full-scale experimental programme was carried out on an instrumented site at Montreuil sur Barse (France) as part of a collaboration agreement between various state-run and private laboratories (ADEME, government agency for the environment, CEMAGREF at Antony, IRIGM at the University of Grenoble, LRPC, Ponts et Chaussées in Nancy).

The anchorage strength for several anchorage geometries (linear anchorage and trench anchorage) was determined by scale model tests in a two-dimensional medium comprising small diameter rollers (Schneebeli rollers). A comparison between numerical results and experimental results is given for the linear anchorage geometry.

MONTREUIL SUR BARSE EXPERIMENTAL PROGRAMME

Experimental set-up. A full-scale experiment (Tanays 1995 and Le Tellier 1993) was carried out at the Montreuil sur Barse waste storage centre (France), based on an instrumented test plot with lining system comprising a support soil of compacted clay, a geomembrane PEHD of 2 mm thick (GM), a non woven geotextile BIDIM666 (GT) and a 30 cm thick layer of granular material (cf. figure 1). Relatively steep slopes (Base/Height = 2/1)) were selected to allow significant measurements of tensile forces and displacements.
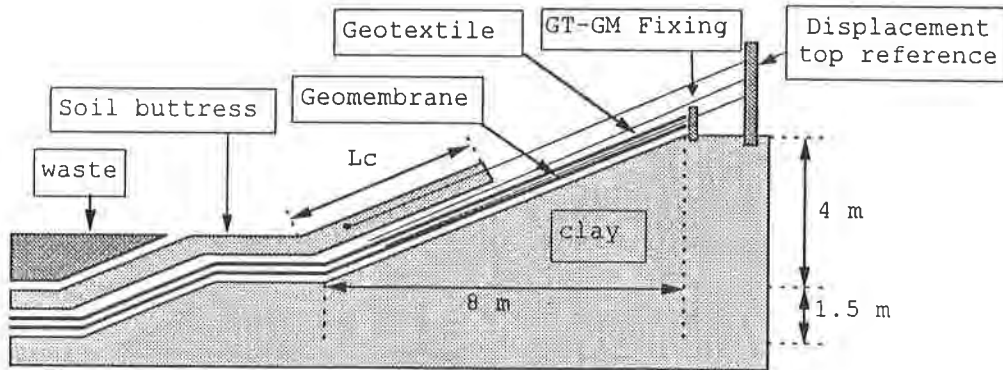
Figure 1. Montreuil sur Barse experimental system

Displacements of the lining system components are measured by fine, sheathed metal cables fixed to the sheets or to metal T-sections planted in the soil, and linked to a measurement terminal. Top tensile forces are measured by electronic sensors placed between the sheet clamp and the fixing post.

The granular soil layer was loaded metre by metre on the slope until a loading length Lc of 6 m was obtained. Figures 2 and 3 illustrate the displacements in the granular material, and in the geotextile and the geomembrane during loading of the protective soil layer as a function of the position on the slope L.
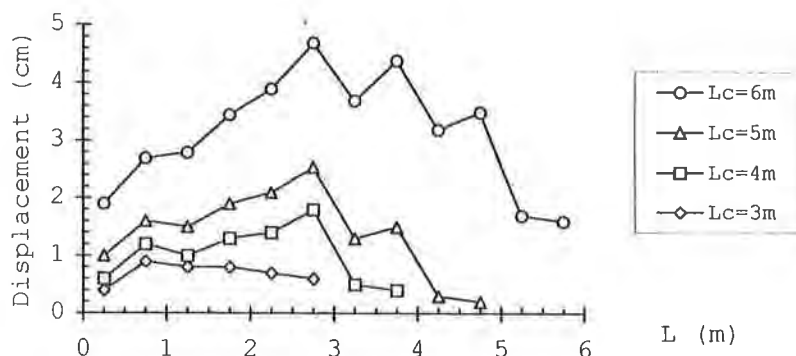
Figure 2. Displacement in the granular material
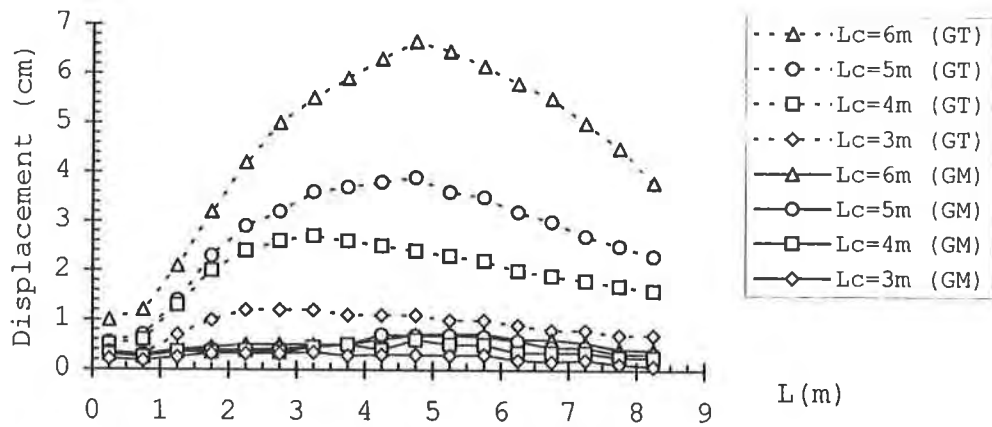
Figure 3. Displacement in the geosynthetics
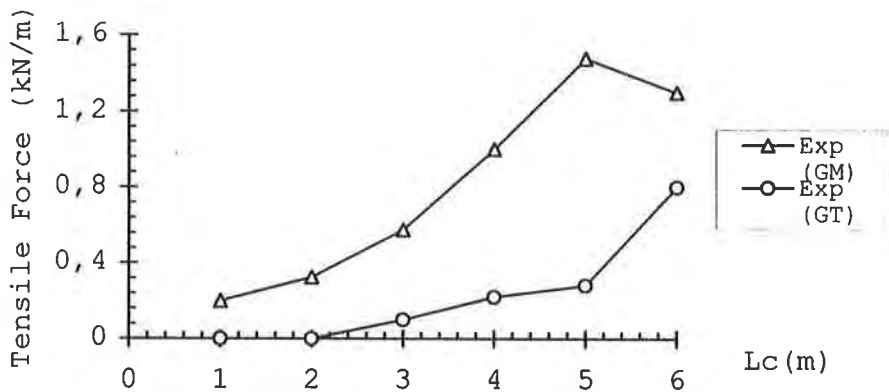
Figure 4. Top displacement in the geosynthetics

Figure 3 shows that the displacements in the geotextile are greater than those in the geomembrane. The relative downward displacement between geotextile and geomembrane induces a frictional force towards the bottom of the geomembrane. The top displacements in the geotextile are due to tilting of the fastening post under the effect of tensile forces.

Figure 4 presents the tensile forces acting on the geomembrane and geotextile sheets on the top of the slope. The tensile forces in the geomembrane result from the frictional forces on either side of the sheet: driving force of the geotextile, resisting force of the underlying clay. These surface interactions determine the tensile force level in the geomembrane. Note that a good liner design will produce a minimum amount of tensile force in the geomembrane sheet which plays an essentially containment role and is not a tensile component.

From the displacements shown in figure 3, the strains occurring in the geosynthetics can be deduced (cf. figure 5). Strains in the geomembrane are very small. The geotextile is strained at the top and

compressed at the bottom of the slope, probably corresponding to the formation of folds. The tensile modulus of the geomembrane is much higher than that of the geotextile and, as a result, despite the much smaller strains compared to the geotextile, the tensile force in the geomembrane is much higher.
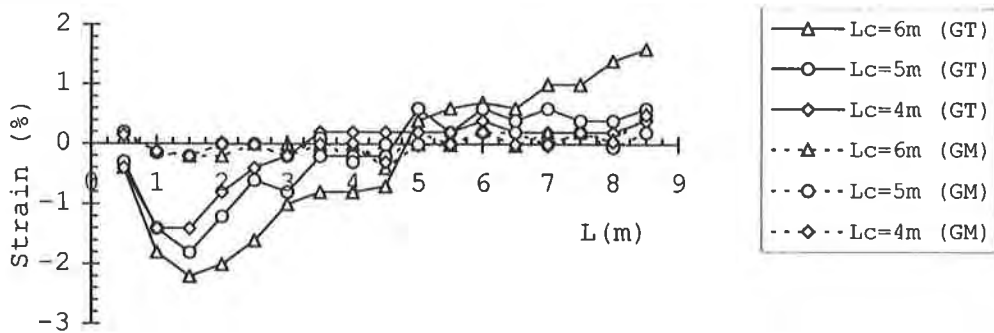
Figure 5. Strain in the geosynthetics

Estimate of the tensile force on the top of the slope in the different geosynthetic sheets was analytically defined by means of a limit equilibrium method (Giroud 1989 and Koerner 1991). The comparative results are given on figure 11, and discussed below, with the F.E.M. results.

Numerical modelling. The mechanical properties of the materials and their interfaces were determined in the laboratory (Feki 1996). The tensile stiffness values of the geotextile and geomembrane are 65 kN/m and 458 kN/m. Their behaviour under compression is assumed to give values 20 to 10 times lower respectively in order to allow for the formation of folds in the geosynthetics observed at the toe of the slope. The granular material (volumic weight of 18 kN/m^3) is assumed to be elastic (E = 1200 kPa and v 0.3). The frictional effect at the interface is modelled on figure 6. For a given normal force, σn, the maximum frictional force, τm, that can develop at the interface is: $\tau m = \sigma n . \tan \phi g$. Up is the relative displacement value at which the force τm is reached. The friction characteristics measured in laboratory are presented in table 1.
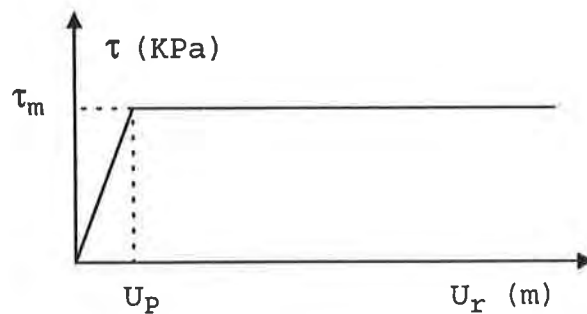
Figure 6. Interface behaviour law

Table 1. Friction characteristics

Nature of friction	φg	Up (mm)
Granular soil/GT	29°	2
GT/GM	12°	2
GM/clay	9°	2

A finite-element numerical analysis was made based on a computation code specific to this type of structure, notably integrating large strains at interface level (Villard 1996). The geosynthetic sheets have a non-linear behaviour with the membrane effect being taken into account. The soil elements are assumed to be subject to high strain. The parameters of the interface laws are defined in terms of normal force, relative displacements and force trajectory followed at the interface.

The meshing considered to model the Montreuil sur Barse experimental programme is presented in figure 7. The interface includes 4 lines of nodes belonging respectively to the supporting ground, the geomembrane, the geotextile and the gravel layer. Loading of the granular soil was modelled metre by metre by progressive loading of the elements on the slope.
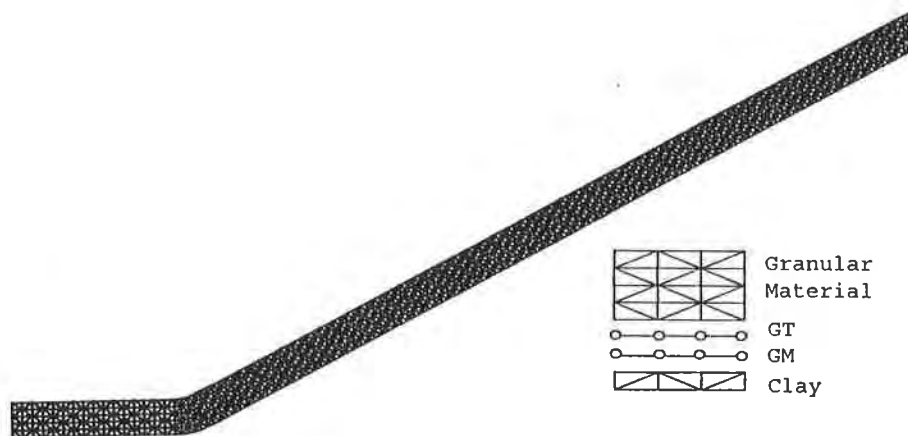
Figure 7. Modelling of the experimental programme

The graphs in figures 8 and 9 give a comparison of the experimental and the theoretical displacements in the granular materials and geotextile for loading lengths Lc of 3, 4, 5 and 6 m. Figure 10 presents the tensile forces obtained at the head of the geosynthetic components as a function of loading length Lc.

The correspondence between the F.E.M. results is perfectly acceptable taking into account the uncertainties related to any full-scale experiment.
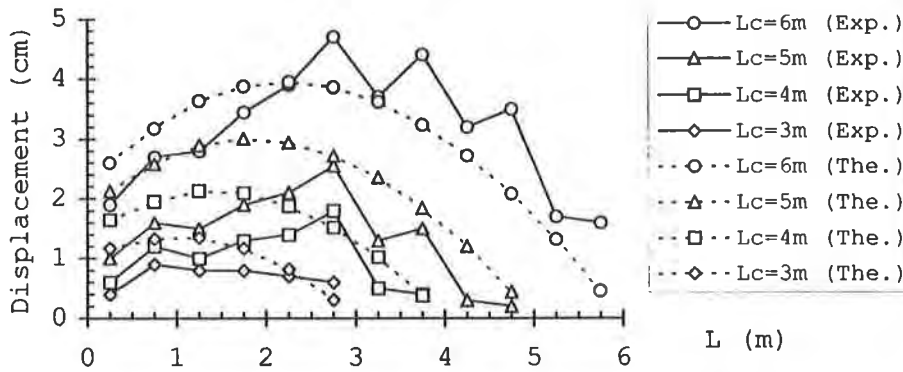
Figure 8. Displacement in the granular material – Comparison with FEM
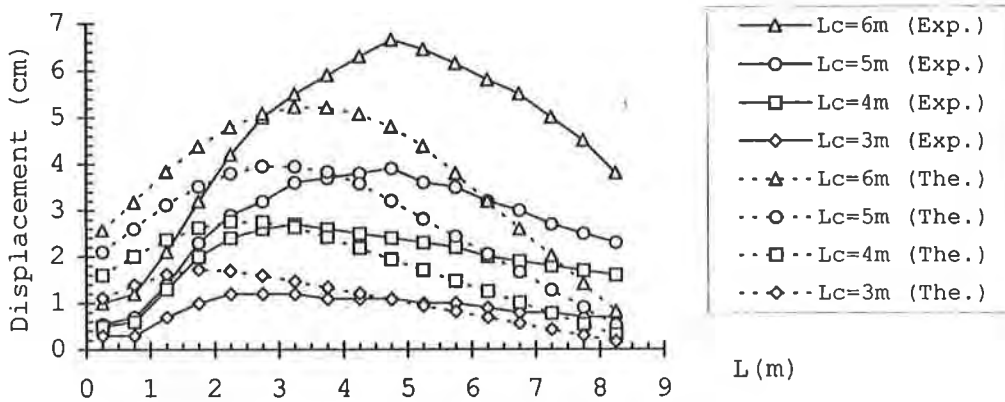
Figure 9. Displacement in the geosynthetic – Comparison with FEM
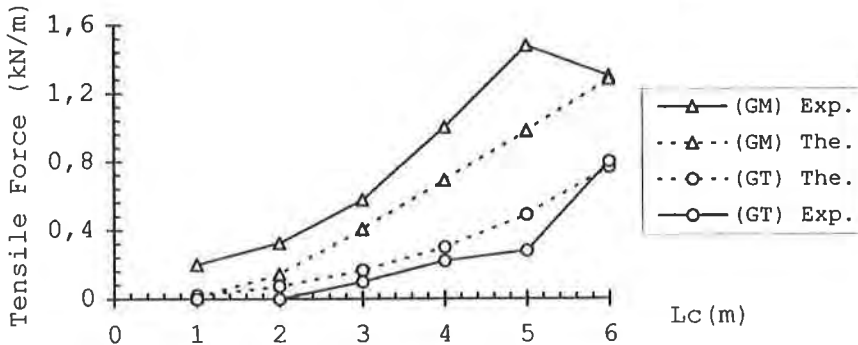
Figure 10. Geosynthetic top tensile force – Comparison with FEM

On the other hand, comparison with analytical solutions (Giroud 1989 and Koerner 1991) (cf. figure 11), exhibits satisfactory results for the tensile force in the geomembrane (lower sheet) and poor results for the tensile force in the geotextile (upper sheet). This significant discrepancy is correlated to the actual compressive state of the geotextile sheet in the lower part of the slope (figure 5), resulting of the construction process when the analytical methods consider a tensile state for the whole geotextile length.
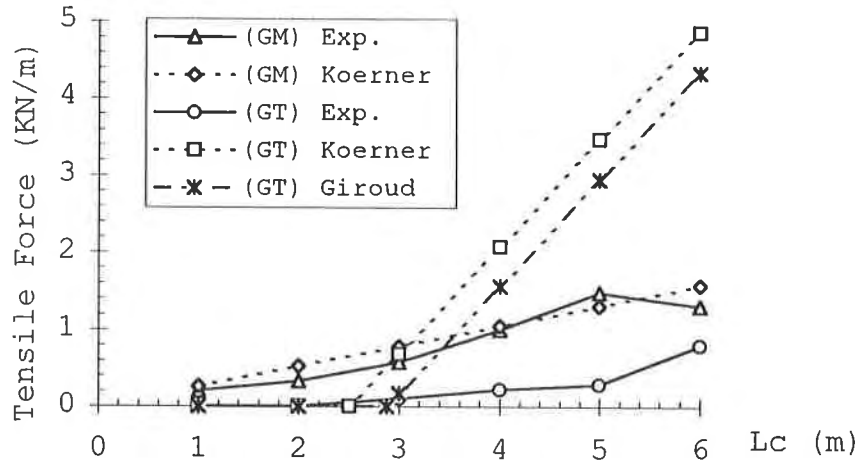
Figure 11. Geosynthetic top tensile force – Comparison with analitycal methods

This shows the complexity of the tensile force development phenomenon in geosynthetics along the slope. If the geosynthetic head clamping device, in this instance a fastening post used only to measure the forces involved, is replaced by a ground anchorage system, the behaviour would be even more complex. In the following section the behaviour of different anchorage systems is examined.

DETERMINATION OF ANCHORAGE STRENGTH

Experimental device. Sheet anchorage tests are carried out on a scale model (cf. .figure 12) in a two-dimensional medium comprising 3 to 5 mm diameter Duralumin rollers (Schneebeli rollers). The geotextile sheet (non woven thin sheet), preceded by a metallic guard sheet, is gradually extracted from the rollers at a rate of about 1.5 mm/minute. The tensile forces and displacements measured at the head are recorded by a central data logging unit every 20 seconds. Reference points are fixed on the sheet and on the adjacent rollers. By taking photographs at regular intervals, the displacement of the sheet and the rollers during extraction can be monitored thanks to the stereophotogrammetric technique (Desrue 1983).

In order to quantify the influence of sheet geometry on the anchorage strength, several series of tests were performed with respectively linear anchorages (sheet length of 30 cm and 40 cm), L-shaped anchorages (sheet length of 30 cm) and U-shaped anchorages (sheet length of 40 cm). In each test case, the height of the soil cover is 15 cm thick for the rollers. The metallic guard sheet is 20 cm long.
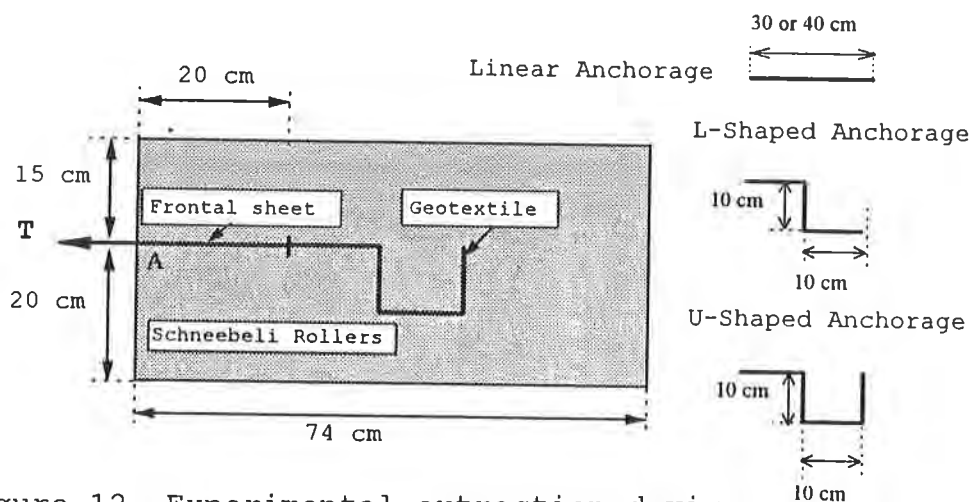
Figure 12. Experimental extraction device

Experimental results. The tensile forces measured at the head of the metallic sheet (point A) are presented for the different anchorage geometries on figure 13.
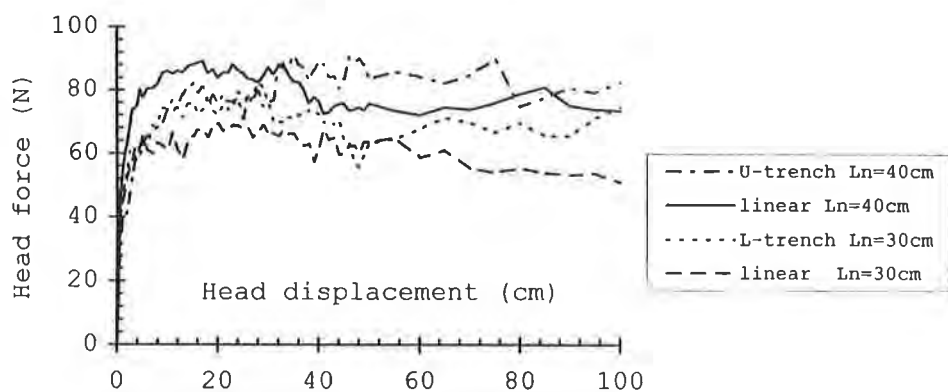
Figure 13. Variation in tensile force at the sheet head

It is worth noting that, for the same sheet length, the anchorage geometry has little effect on the maximum head force. It should be stressed, however, that the maximum tensile force in trench anchorages tends to be reached for relatively greater displacement values compared to linear anchorage (influence of the deformability of sheet bends in trench anchorage, increasing radius of curvature during extraction).

The displacements measured at various points of the sheet are presented for each type of anchorage on figures 14 to 16. Figure 14 shows that the maximum tensile force is reached in the sheet for head displacements greater than one centimetre. For trench anchorage systems (cf. figures 15 and 16), there is a break in the curve at the sheet bends leading to a delay in reaching maximum tensile force in the various sections of the anchorage zone(cf. figure 17).
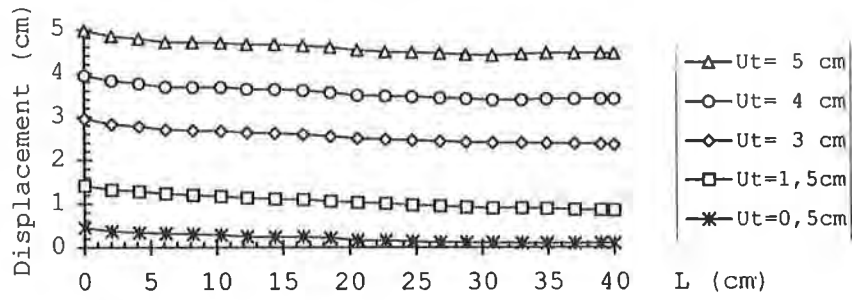
Figure 14. Displacement in the sheet for linear anchorage
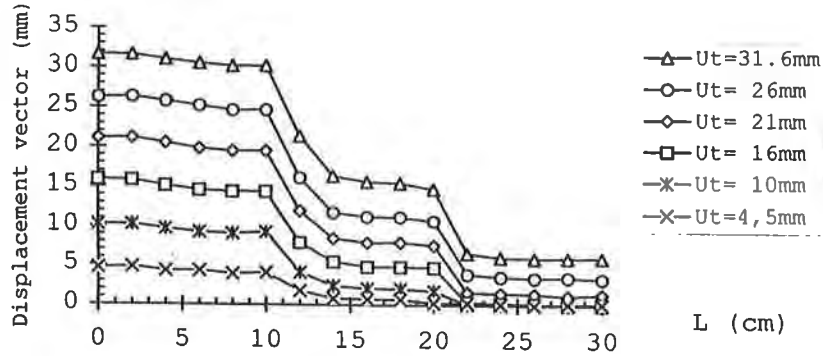
Figure 15. Displacement in the sheet for L-shaped anchorage
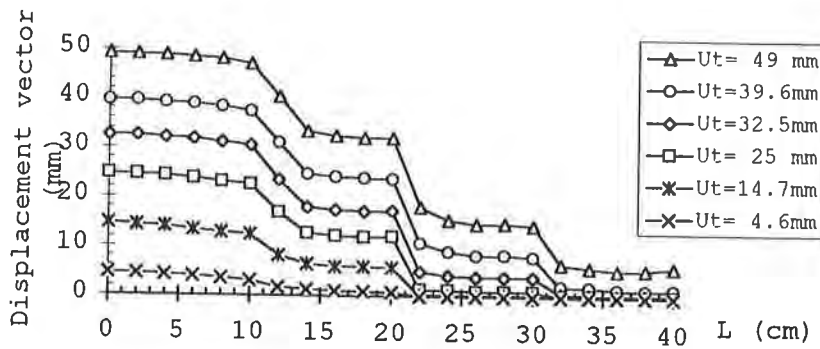
Figure 16. Displacement in the sheet for U-shaped anchorage
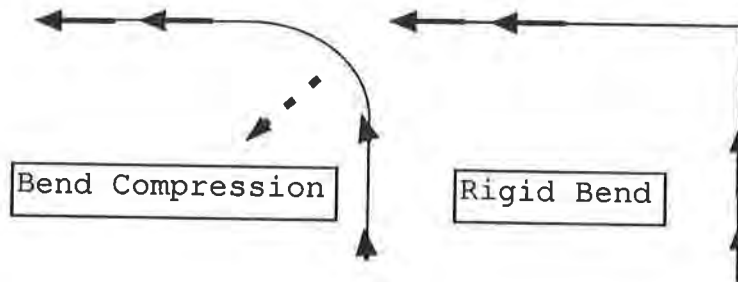
Figure 17. Influence of sheet fold compression

To highlight the mechanisms involved during extraction, figures 18 to 20 illustrate the displacement fields obtained in the rollers by stereophotogrammetry.
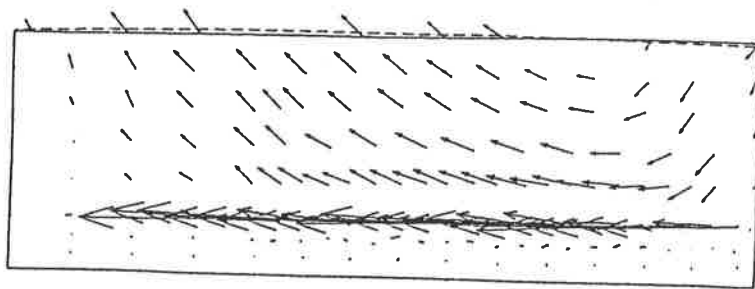
Figure 18. Displacement fields in the rollers (linear anchorage)
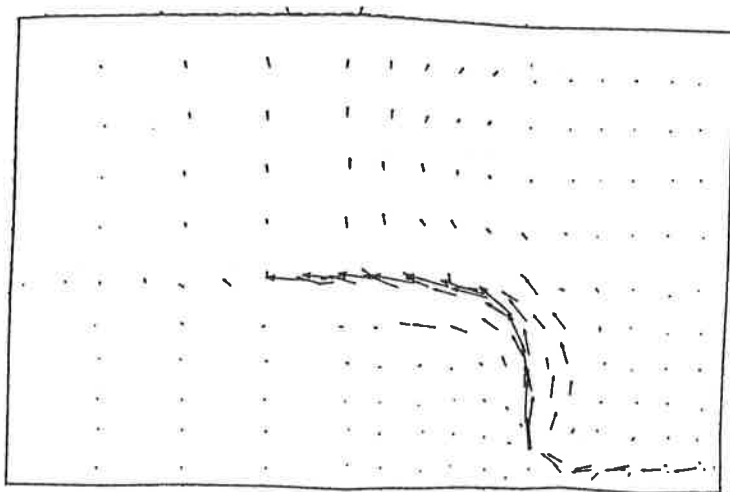
Figure 19.. Displacement fields in the rollers (L-shaped anchorage)
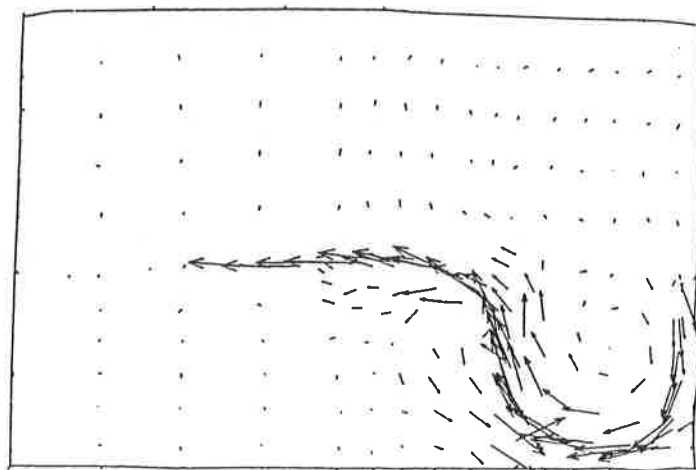
Figure 20. Displacement fields in the rollers (U-shaped anchorage)

Estimate of the pull-out strength for trench-anchorage was the purpose of very few research studies. An analytical approach was proposed (Daniel 1988), considering the thrust of soil at rest for the vertical elements of the geosynthetic sheet and no specific effect of the anchorage bend.

Finite-element modelling of linear anchorage. The computation parameters were obtained by means of additional tests carried out in the laboratory. The characteristic curves of the materials and their interface are presented on figures 21, 22 and 23. The results for the geotextile/Schneebeli rollers interface were obtained by using sheets with a metal plate bonded on both sides. The behaviour of the Schneebeli rollers is modelled according to a Drucker-Prager type elasto-plastic law ($C = 1$ kPa, $\phi = 22°$, $\psi = 17°$, $E = 6000$ kPa and $\nu = 0.35$). The metal plate behaves in a linear plastic manner ($E = 7 \times 10^7$ kPa).
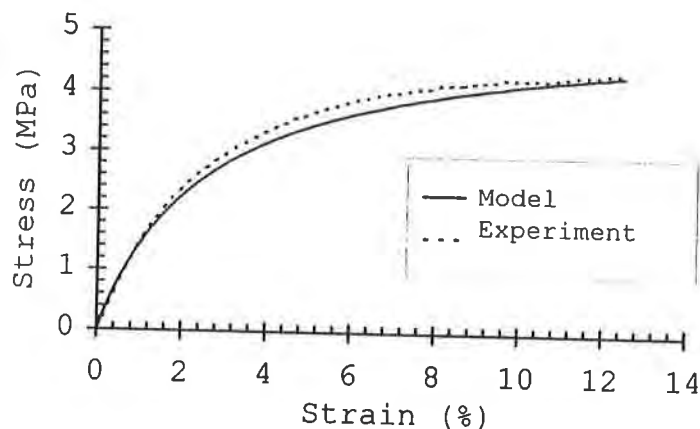
Figure 21. Behaviour of the geotextile
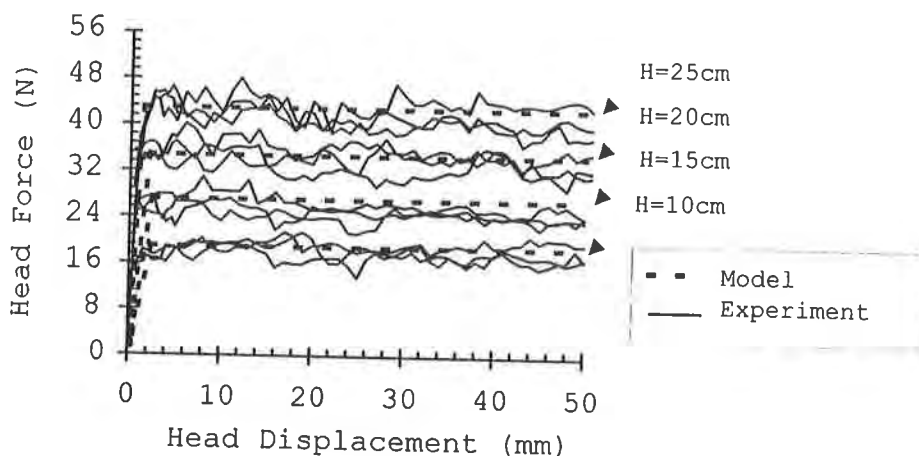
Figure 22. Behaviour of the plate/roller interface
(Plate of 20 cm X 6 cm)
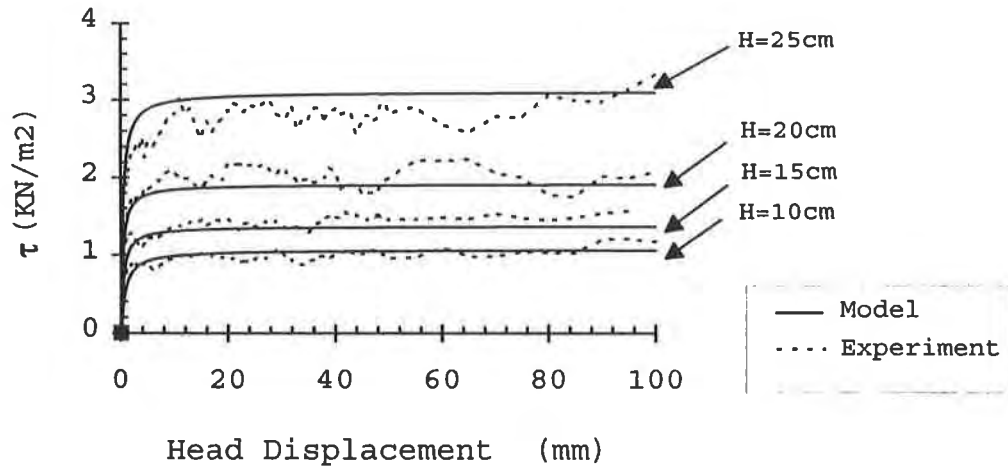
Figure 23. Behaviour of the geotextile/roller interface

The meshing used to model the linear anchorage system is presented on figure 24. The soil is discretised into 1332 three-node triangular elements, the sheet and the plate into 31 two-node bars. The interface is characterised by three lines of nodes belonging respectively to the underlying soil, the geotextile sheet and the overlying soil.
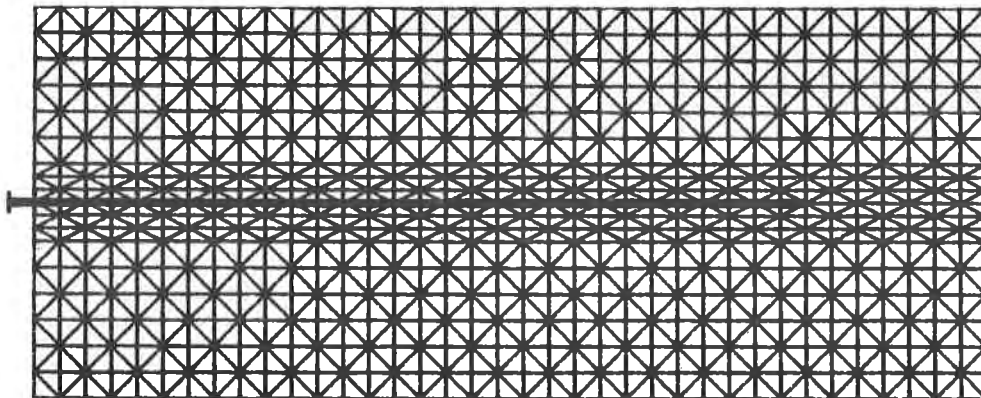
Figure 24. Modelling the linear anchorage system

The results were obtained by gradual extraction of the sheet until a head displacement of 12 mm was reached. 20 to 30 iterations are required for convergence of each computation step. The results obtained are compared with the experimental results on the graphs in figures 25 and 26.
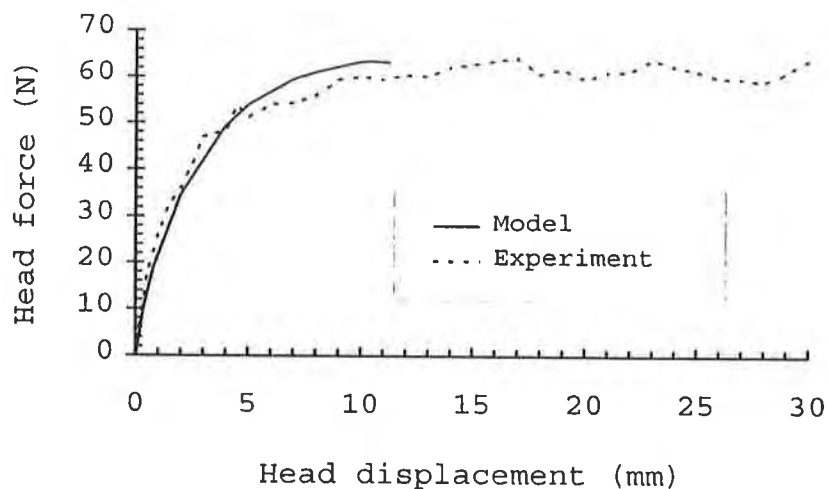
Figure 25. Comparison of sheet head forces
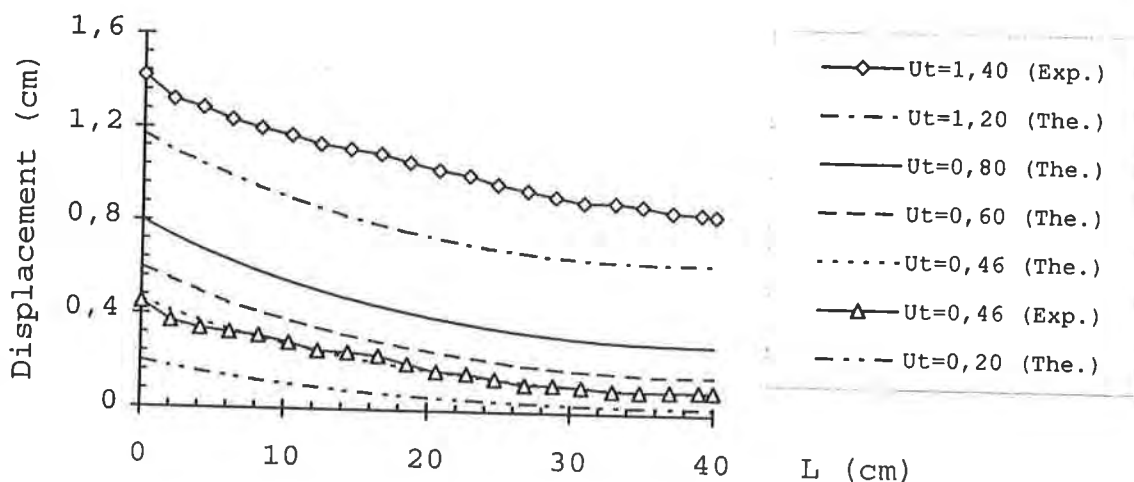
Figure 26. Comparison of head displacements

There is a good correlation between the theoretical and experimental results for both the assessment of head tensile forces and for determination of displacements in the sheet.

CONCLUSIONS

- The analytical methods proposed to estimate the behavior of geosynthetics along the slope and as anchorage prove sometimes inadequate, due to the complex kinematics

- The finite element method results are acceptable as a whole and open up interesting possibilities in terms of geosynthetic sheet dimensioning and anchorage systems. The model study of the Montreuil sur Barse test required a computation methodology and a choice of relatively sophisticated behaviour laws which was not always very

easy, given the difficulties encountered in determining the parameters. It was possible to model the linear anchorage test by developing a specific computation code which, in particular, enabled sheet pullout to be simulated. The method can easily be adapted to the case of curved anchorages and the model of the trench anchorage system is currently being established.

ACKNOWLEDGEMENTS

REFERENCES

Daniel, D.E., (1988), University of Texas, Austin, TX, Personal communication, from Koerner, R.M., Designing with geosynthetics, Prentice hall, 1990.

Desrue, J., (1983) "About the application of Stereophotogrammetry in measuring finite strains", Revue Française de Mécanique, vol 3.

Feki, N., (1996) "Modèles physique et numérique de la stabilité des couvertures géosynthétiques sur pente. Application aux centres de stockage des déchets", Thèse de Doctorat de l'Université de Grenoble (France), IRIGM-Lgm.

Giroud, J.P., and Beech, J.F., (1989) "Stability of soil layers on geosynthetic lining system", Geosynthetic 89, San Diego USA.

Koerner, R., and HWU, B.L.,(1991) "Stability and tension considerations regarding cover soils on geomembrane lined slopes", Geotextiles and Geomembranes, vol. 10, pp 335-355.

Seed, R.B., Mitchell, J.K. and Seed, H.B.,(1990) "Kettleman hills waste landfill slope failure II : Stability analyses", Journal of Geotechnical Engineering, vol. 116, N° 4, April 1990.

Le Tellier, I., Bernhard, C., Gourc, J.P., and Matichard, Y., (1993) "An experimentation on municipal landfill lining systems at Montreuil sur Barse", Geoconfine 93, Montpellier (France), Vol 1, pp 225-230.

Tanays, E., Feki, N., and Berroir, G. , (1995) "Stabilité sur pente d'un dispositif d'étanchéité par géomembrane : Expérience en vraie grandeur", Géotextile Géomembranes Rencontre 95, vol 2, pp. 56-63.

Villard, P., (1996) "Modelling of interface problems by the Finite Element Method with considerable Displacements", Computers and Geotechnics, vol. 19, N° 1, pp 23-45.

DEVELOPMENT AND INSTALLATION OF AN INNOVATIVE VERTICAL CONTAINMENT SYSTEM

BELINDA BURSON
GSE LINING TECHNOLOGY, INC., USA
ARTHUR C. BAKER, P.E.
EARTH TECH, INC., USA
BARBARA JONES
REMEDIATION TECHNOLOGIES INC., USA
JOHN SHAILER
COLUMBIA GAS COMPANIES, USA

ABSTRACT

In recent years it was discovered that coal tar was leaching from a former gas manufacturing plant into an adjacent creek. was coal tar. The coal tar was a major by-product of the gas manufacturing process and, although most of it was re-sold, some was stored on-site in underground tanks which permitted the coal tar to leach into the soil.

As part of an approved remediation plan for this site, a barrier wall comprised of High Density Polyethylene (HDPE) sheets and jet grouting was utilized together to eliminate the migration of coal tar. The jet grouting was used for the first time to eliminate leakage at the HDPE/bedrock interface. This trenchless technology also provided for a flexible construction method for dealing with site constraints, ongoing activities, geologic conditions and subsurface obstructions. Following barrier wall construction, recovery wells were installed to manage groundwater on the upgradient side of the impermeable barrier wall.

SITE HISTORY

From the mid 1880's until the early 1950's, gas for consumer use in York, Pennsylvania was manufactured from coal at The York Gas Company plant on the banks of the Codorus Creek. The York plant was built in 1885. Originally the plant was designed as a dry coal gasification process. By the turn of the century, a major improvement in manufactured gas was installed at the plant. The new process was called the water gas or blue gas process, after the distinctive color of the flame produced by the burning of the product. Blue gas was generated by injecting steam into the hot coal generated gas stream to further crack low molecular weight hydrocarbons from the coal. This process is still in use today in the chemical process industries, and generates what is known as Producer's Gas.

The York facility soon became one of the largest manufactured gas plants (MGP) along the east coast of the United States. Its growth can be charted by the addition of gas holders. The original gas holder, an in-ground holder, was built when the plant was originally constructed. Gas holders were large vertical, cylindrical structures which stored the manufactured gas at pressure for smooth delivery into the gas distribution system at night or during times of peak usage. The holders were necessary because the manufacturing process was a batch process while the need for gas was a smooth and continuous process. Holder number one had a capacity of 4,246.5 cubic meters (150,000 cubic feet) of storage. By 1927, three holders had been added bringing the plants working capacity to over 84,950.5 cubic meters (3,000,000 cubic feet).

During the manufacture of gas, tar was driven off the coal, much like the process for making coke from coal in the metal refining business. Initially, because of the high temperatures involved in the process, the tar was in the vapor phase. As the gas cooled during purification and storage, the tar would condense. Coal tar was created as a by-product of this process in large quantities. Coal tar was, and still is, a valuable by-product. Thus, much of the coal tar that was generated at the York site was sold to the pharmaceutical, chemical and asphalt business. However, some of the coal tar remained at this site (a typical situation at former MGP's).

SITE CHARACTERIZATION

This five-acre site is currently the location of an active gas utility service center now owned by Columbia Gas of Pennsylvania. Codorus Creek borders the site to the east for a distance of approximately 305 meters (1,000 feet) (See Figure 1). Residential areas surround the site to the north and northwest, and commercial and residential areas bound the property to south and southwest. Two sets of railroad tracks traverse the site from east to west and divide it into three sections. The site is underlain by fill (average of 1.5 - 3.0 meters (5 - 10 feet) thick), native silts and clays, with occasional sand and gravel (average thickness 3.0 - 7.6 meters (10 - 25 feet)), and bedrock. The bedrock consists of limestone in the northern portion of the site, fractured dolomite in the southern portion, with weathered sandstone, shale, and mudstone in the central portion. There are two groundwater zones, the shallow unconsolidated zone in the soils overlying bedrock, and the bedrock aquifer. Shallow unconsolidated zone groundwater is encountered at an average of 4.6 - 6.1 meters (15 - 20 feet) below ground surface. Both the bedrock and unconsolidated zone groundwater flow east toward Codorus Creek. There is no residential groundwater usage in the vicinity of site.

During many years of operation and the subsequent closure of the MGP, some process residuals migrated to subsurface soils and groundwater. Over time, the presence of coal tar-like material in the form of dense non-aqueous phase liquid (DNAPL), was observed seeping from the bank of the Codorus Creek. DNAPL was also noted in some monitoring wells on site. The DNAPL was found to be slightly more dense than water, with a specific gravity of 1.04. There appeared to be two horizontal zones of migration of the DNAPL toward the creek, at the bedrock contact, and to a lesser extent, at the interface between the fill and native soil.

Figure 1. Looking south along Codorus Creek with railroad track transecting the site.

STATE AND LOCAL INVOLVEMENT

In a project of this sort, the public utility company must deal with the state Public Utility Commission and Department of Environmental Protection (DEP). After discovering the seepage at the York site, an extensive and costly investigation was conducted by Columbia, with reports being submitted to the DEP. This investigation characterized the horizontal and vertical extent of contamination. The results of that investigation led to the remediation plan developed for Columbia by its consulting engineer.

Clear guidance was received from the DEP as to the issues to be addressed in its remediation work plan. Following submittal, DEP environmental cleanup program managers quickly identified those portions of the program which they approved, and also those portions of the program which required further definition. For example, the underlying geology of the site created very specific concerns about the ability to fully intercept the flowing coal tar and contaminated groundwater. However, the geotechnical and remediation contractors selected were able to provide demonstrative evidence of the ability of their products and services to achieve the required results. This information was jointly presented to the Pennsylvania DEP and its concurrence in the remediation approach was promptly received. Construction could literally begin within a few months.

There were also local concerns. Only a few years ago, local residents had reason to complain about subterranean vibrations caused by the installation of a new sanitary sewer system through the bedrock underlying their homes. Due to the proposed construction method, concerns about repeating those kinds of problems, as well as general environmental concerns by residents of York had to be addressed in a proactive manner. The public utility company met with the Mayor, his staff, and local members of the Pennsylvania legislature in order to explain the project and provide a timetable. The city and the company cooperated in the development of press releases and public meetings, at which the project was again explained and all questions responded to. Further, the company provided a special phone number that could be called should any concerns or questions arise. It was the company's position that public concerns are usually a result of a lack of understanding. By fairly and fully explaining the entire project at an early stage, and providing the opportunity to be continually updated, the company was able to keep the public and its customers fully informed.

Additionally, during the course of construction itself, various members of the press visited the site and were shown everything that was going on. The DEP also visited the site frequently with their suggestions or recommendations being incorporated into the project on an immediate and ongoing basis. An example of this flexibility came when the Senior Program Manager for the South Central Region, upon observing the construction of a section of the cutoff wall near a railroad track, suggested that the wall be extended further toward the railroad track in order to intercept additional potential sources of seepage. The wall was moved as the construction proceeded and while the DEP manager was present.

A truly collaborative effort between the Pennsylvania DEP, the consulting engineer, and the company itself resulted in the rapid approval of an innovative method of interception and management of coal tar and coal tar contaminated groundwaters.

SELECTION CRITERIA FOR THE CUTOFF WALL

During the process of remedial planning, seepage of DNAPL along the bank of the Codorus Creek was regarded as the highest priority. Several scenarios were evaluated. The primary purpose of the system would be to intercept the tar-like material. Groundwater would also be intercepted although modeling had shown that the potential for groundwater from the unconsolidated zone to affect the water quality of Codorus Creek would be low. Several barrier system types and configurations were evaluated before selecting the jet grout/HDPE wall system with recovery wells.

Two locations were considered for the installation of the barrier, along the property boundary at an average elevation of 7.6 - 9.1 meters (25 - 30 feet) above the bedrock/soil interface, or at the creek bank, within a few feet of the bedrock interface. The higher location was chosen because of accessibility, site control, and long-term maintenance considerations (See Figure 2).

Codorus Creek floods periodically, and system components installed at the creek bank would have been susceptible to flood damage.
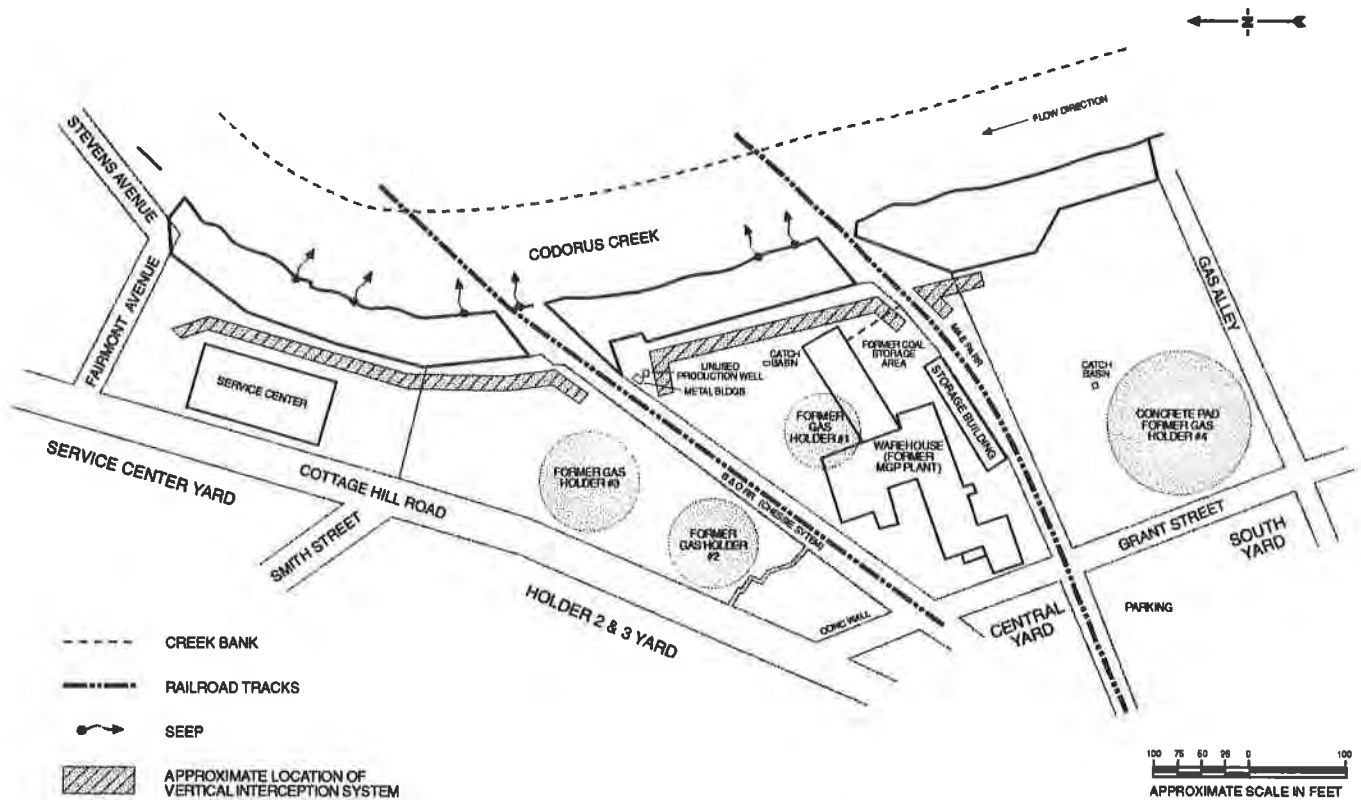
Figure 2. Site plan.
(Reprinted by permission of Columbia Gas Companies, 1995)

Slurry Wall Technology. In the United States, the most widely used cutoff wall has been the soil-bentonite slurry wall. The typical permeability of the slurry mix being 10^{-7} cm/sec to water, with the in-place wall permeability potentially varying due to contamination and competence of the contractor. Recent studies have shown that solutions of hydrocarbons can seriously affect the impermeability of clays. The mechanism in this case is dissolution of the soil binding agents in the clay followed by movement of the clay particles out of the barrier. Laboratory permeabilities do not take into account field conditions. During construction, slough from the side walls of the trench can cause what is known as "windows" or areas of higher permeability. Other issues of concern are performance life, trench stability and handling and disposal costs of spoils. At the York site, the barrier wall was placed only 3 meters (10 feet) from the edge of the bank of the Codorus Creek and thus the potential for slurry loss into the creek was high. Working space was limited and was a narrow as 9 meters (30 feet).

HDPE Vertical Barrier System. Since 1980, interlocking HDPE barrier systems have become increasingly utilized especially in areas of limited access, high disposal costs, depths where performance of a slurry wall is questionable, high concentrations of saline and/or chemicals, and

where a containment and collection system is desired in one trench. HDPE, as the US EPA's material of choice for containment, has proven to have a low permeability (2.7×10^{-13} cm/sec to water), high chemical resistance and a long service life. "Recent estimates of 1000-year lifetime for HDPE are not beyond reach. Indeed the time to subsequent half-life of the engineering properties of a properly formulated HDPE geomembrane is many centuries and eminently suited for the containment of waste sites." (Koerner, 1996)

Although many EPA 9090 compatibility tests have been performed on HDPE using a variety of chemicals without any failures, some hydrocarbons (aromatic or chlorinated) can reduce the tensile strength of HDPE. This "softening" of the material is reversible and does not increase the permeability of the product. Therefore, in most vertical applications the loss of tensile strength is irrelevant. Another phenomenon which can occur during exposure to hydrocarbons is the loss of some stabilizers. Again, this is irrelevant in vertical applications because the need for stabilizers is minimal when the product is buried.

The particular HDPE barrier wall selected had been installed to depths exceeding 100 feet, on over 25 sites in the US alone, and is comprised of 2.03 mm (80 mil) geomembrane, patented HDPE interlocks and a hydrophilic seal. Unlike other systems, the interlock consists of two profiles - a male and female (Figure 3). This allows for the vibratory, trenchless installation. The interlocks are extruded and vacuum sized to create exceptional quality and consistency with tolerances less than .025 cm (1/100 inch). These interlocks are then joined to panels of HDPE geomembrane through fusion welding. The dual-wedge welding system allows for an air channel to be created and used to test the integrity of the weld. The panels are fabricated to site specific requirements in a factory-controlled environment as another quality control step. Panels are then shipped on flat bed trucks to the jobsite. Most panels can be off-loaded by hand.
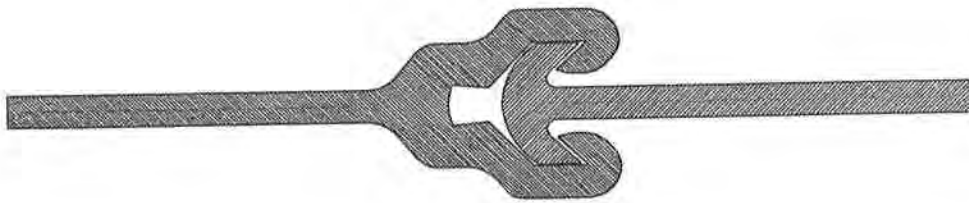
Figure 3. Interlock profile used to join sheet of HDPE geomembrane.

Sealing of the interlocks is achieved with a chloroprene-based, hydrophilic seal. The seal is an extruded profile which is 8 mm (.3 inches) in diameter. When exposed to water, it can expand up to 8 times its original volume. The hydrophilic cord is inserted in a 6 mm (.23 inches) groove in the female profile which therefore creates a positive seal even before expansion takes place. Unlike grouts or other types of sealants, continuity can be ensured because the seal is an extruded profile. As part of the construction quality assurance program,

this seal is monitored for continuity in the field. If the seal is broken during installation, the panel can be withdrawn and the seal restarted.

The design of this system along with the elongation properties of HDPE allow for substantial soil deformation without affecting the integrity of the barrier wall. This particular system is designed such that the interlock has a greater strength than the adjoining geomembrane. Therefore, if a stress is applied to the system, the geomembrane would elongate before the potential failure of the interlock.

Jet Grouting. Conceptually, jet grouting is the high pressure injection of a cement and bentonite slurry, horizontally into a granular or alluvial soil strata to produce an improved "Soil-Crete". The injection pressures of grout slurry material range from 351.5 - 421.8 kg/sq. meter (5,000 - 6,000 psi). The Single Phase Jet Grout method relies on the high velocity of the jet stream to cut, remove and mix the in-situ soil with the bentonite/cement slurry. Excess material is typically ejected from the column being developed through the borehole. One major advantage of the jet grouting process is that large diameter columns 0.9 - 1.5 meter (3 - 5 feet) can be created from a small diameter drill hole (7.6 cm (3 inch)) and subsurface obstructions or utilities can be by-passed or avoided. The columns are then interconnected, by overlapping, to create a containment wall system.

The Composite Jet Grout/HDPE Barrier Wall. Constructability issues combined with the performance of a slurry wall led the consulting engineer to a trenchless installation of interlocking HDPE panels combined with jet grouting. This combination was also considered for application with an integrated collection trench, but was not selected because of the potential for long-term clogging of the collection trench and maintenance difficulties over the life of the system.

The combination HDPE/jet grout with recovery wells was chosen because it met the following criteria:

- HDPE had been documented to be chemically compatible with coal tar and coal tar constituents

- The jet grout process would provide a seal to control DNAPL migration between the bottom of the HDPE panels and the irregular bedrock contact

- The installation process would result in minimal generation of spoils, compared to a conventional slurry wall approach

- The combination system would allow for flexibility in working around subsurface obstructions such as drainage pipes, where jet grout could be used to the surface in lieu of HDPE panels

- The installation process would result in minimal disturbance of service center or neighborhood activities, compared to more invasive approaches such as slurry wall installation or soil excavation
- The installation was cost competitive

PRELIMINARY ENGINEERING

The York site subsurface has been extensively characterized during several environmental investigations. More than 100 soil and rock borings and 22 monitoring wells have been installed. This extensive characterization base was used for the preliminary engineering review of the feasibility of using an HDPE/jet grout installation. In addition, laboratory tests were performed on grout mixes combined with clean, moderately tar-contaminated, and heavily tar-contaminated site soils. The presence of tar did not substantially affect the set of the grout mixes in the laboratory.

The preliminary engineering review determined that there were two practical concerns with the proposed system. These were:

- The inability to construct the barrier system under the railroad tracks in two locations
- The potentially impacted zone between the HDPE/jet grout barrier and the creek bank that would not be "captured" by the system

The barrier system could not be constructed under the railroad tracks because appropriate easement terms could not be negotiated between the railroad company and the utility company. The solution was to construct barrier "wing walls" on both sides of the railroad tracks and then install pumping wells at the wing walls to control groundwater flow and collect DNAPL, where present. The Pennsylvania DEP accepted this modification to the plan.

It was recognized that the installation of the barrier system from the site elevation, above the creek bank, was the only practical approach considering the limited access and flood-prone nature of the creek bank. This would thus result in a potentially impacted zone outside of the barrier system. However, the system has intercepted the major flow path of the MGP residuals form the site and is predicted to result in continuing and long-term improvement to environmental quality of the Codorus Creek.

CONSTRUCTION

Jet Grouting. From the overall site layout drawings (illustrated in Figure 2) the exact containment wall layout was developed by the geotechnical contractor into a set of plan and profile drawings with each injection point identified. The project consisted of a total of 379 injection points (one hole every 76 cm (30 inches)) to develop a containment wall 285.7 meters (940 feet) in length. The soils along the alignment of the barrier wall consisted of granular, non-

cohesive fills with large amounts of cinder material. Also mixed into the fill were varying amounts of rubble and debris such as bricks and concrete. These highly permeable soils were underlain by competent bedrock which varied greatly in depth throughout the entire length of the wall. The plan and profile drawings were used throughout the project to monitor progress, record the depth of each point and establish the top of the jet grout area, as well as to document the limits of the HDPE vertical barrier. Figure 4 shows the "as built drawing of the center portion of the project which highlights the irregular surface of the bedrock confining layer as well as the extent of the jet grouted area . Note the overlap between the HDPE panels and the jet grouted area to create a minimum 45.7 centimeter (18 inch) interlocking key.

The holes were pre-drilled down to competent bedrock with conventional air-track equipment to expedite the jet grouting process. Next the drill rod and jet grout lance were inserted to design depth using a truck mounted drill rig (See Figure 5). The grout was then injected into the soil matrix horizontally by the carbide nozzles located on the sides of the jet grout lance. As the lance was pressurized with the grout slurry and then rotated at a fixed rate of one revolution per minute, the grout dispersed radially out into the in-situ soils to produce a cylindrical shaped column. By continuing this process in an upward progression of 45.7 cm (18 inch) lifts, the columns were constructed to design heights.

The grout slurry was supplied to the lance by a positive displacement piston pump capable of delivering pressures of up to 703.1 kg/sq. cm (10,000 psi). The pump operator continuously monitored the pressure and flow rate of the grout slurry. The mix tank and pump were trailer mounted (See Figure 6) to be easily transported on site. The slurry was batch produced in a high speed shear mixer to properly blend the water, cement and bentonite and provide a homogeneous mixture to the pumping system. Quality control of the grout slurry was maintained throughout the project by viscosity (via Marsh Funnel) and unit weight testing twice per day. Also, a total of six (6) samples of the grout spoil were collected and tested for permeability.

Areas that were to receive the HDPE vertical barrier panels were drilled to bedrock and jet grouted upwards to an elevation approximately 6 meters (20 feet) below the ground surface.

Areas that did not receive the HDPE barrier (i.e., utility and railroad crossings, sub-surface obstructions, etc.) were jet grouted upwards to ground surface. These full height columns were constructed in a primary/secondary pattern throughout each workday. This pattern allowed for the column to stabilize before the adjacent column was constructed. It was noted that during the secondary column construction, grout spoil would discharge from adjacent and nearby completed columns. This provided sufficient evidence that the columns we interlocking and that there was good communication between the holes. These columns produced a spoil return of 10% - 15% of injected material volume. Due to the coal tar contamination of the soils, all spills materials were placed in lined roll-off containers and transported to a hazardous waste disposal facility. The appearance of the spoil material was a well blended mixture of in-situ soil and the
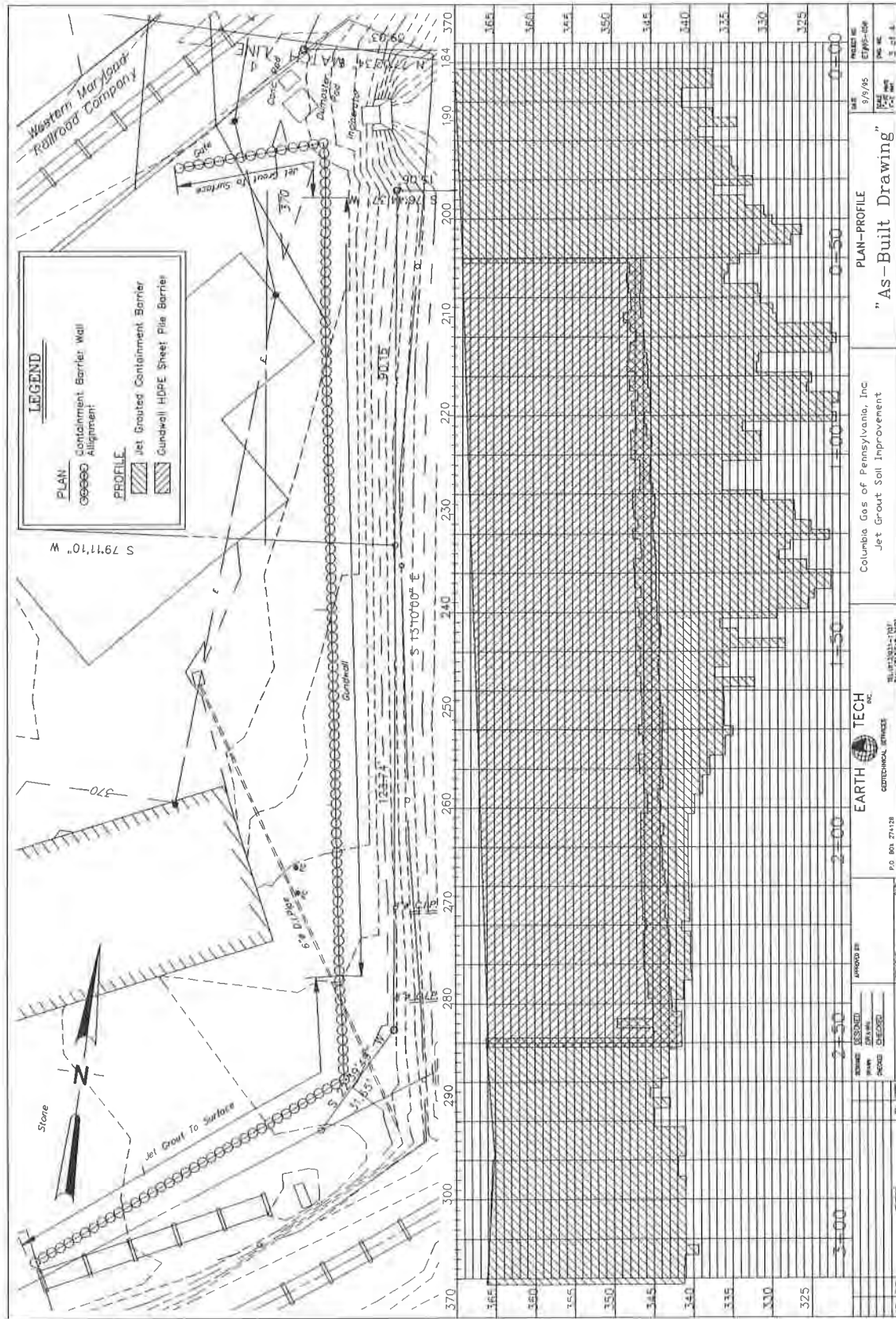
Figure 4. "As-Built" plan and profile depicting containment wall

Figure 5. Truck mounted drill rig with mast extended. Barrier wall alignment in foreground.

grout slurry. The consistency of the spoil was a viscous paste which after several hours (allowing cement activation) would become a plastic material, easily handled with shovels or excavating equipment.

HDPE Vertical Barrier System. HDPE panels were installed without the development of a trench, thus reducing the amount of contaminated spoils to be disposed. Immediately following the jet grouting procedure, panels were driven to a depth of 7.3 m (24 feet) or until refusal. This keyed the panels into the "constructed" clay layer.

Installation of HDPE panels was achieved with conventional vibratory pile driving equipment. The equipment was sized such that access could be granted in areas of a narrow working space and to minimize impact of ongoing site activities. A 65 ton rubber tire crane held an ICE 612 hydraulic, vibratory hammer. The hammer weight of 6,214 kg (13,700 pounds) combined with an eccentric moment of 4,000 in-lbs made for quick insertion of each panel. Panels can be driven as quickly as 53.3 cm (1.75 feet) per second. A steel insertion plate is used as a template to drive the flexible HDPE panels. This plate is designed and built to job specific requirements by the HDPE manufacturer/installer (See Figure 7).

Figure 6. Trailer mounted pump and mixer.

Some amount of cinder and debris was expected to be encountered. However the jet grouting operations consisting of a hole every 76 cm (30 inches) combined with probing ahead of panel installation using the insertion plate, it was possible to identify areas which would not be suitable for HDPE panel installation. At these areas the grout column was extended up to the surface in replacement of an HDPE panel. This technique was also utilized around existing utilities, rather than temporarily removing or relocating them. At each intersection with a utility, the grouted area was extended laterally to allow for the HDPE panels to be keyed laterally and vertically.

Panels were 91 cm (3 feet) wide and were constructed of 2.03 mm (80 mil) HDPE geomembrane. The thickness of the geomembrane was selected based upon chemical exposure and subsurface conditions. It has been shown through research and development that the 2.03 mm (80 mil) thickness offers flexibility while maintaining durability when driven through 1.9 cm (3/4 inch) gravel. The panels were attached to the steel insertion plate at the bottom of each panel. An anchoring device was attached to the panels during factory fabrication. For installation, the bottom of the insertion plate engaged the anchoring device and allowed the HDPE panel to be "pulled" into the subsurface. When design depth or refusal was reached, the insertion plate was withdrawn and the HDPE panel remained in place. This process was repeated, interlocking the panels, to create the HDPE barrier wall (See Figure 8).

Figure 7. Installation of HDPE barrier wall utilizing conventional pile driving equipment.

The sealing of the interlocks was accomplished using a chloroprene-based, hydrophilic cord. This 8 mm (.3 inch) cord was inserted into the 6 mm (.23 inch) groove of the female profile. As the panel moved into the subsurface the seal was monitored to ensure that it was moving into the interlock at approximately the same rate. If the seal stopped moving, indicating that it had broken, the panel was removed and the seal restarted. This quality control step ensured that all interlocks were sealed.

Recovery Wells. A groundwater recovery system consisting of eight recovery wells installed into the top of bedrock (average depth of 7.6 meters (25 feet)) was completed once the barrier was in place. The purpose of the groundwater recovery system was to maintain the original groundwater elevation on the upgradient side of the wall, and to control the flow of groundwater at the barrier wing walls. The recovered groundwater is pretreated in an on-site system consisting of an oil/water separator and granular activated carbon. The pretreated groundwater is discharged to the City of York Wastewater Treatment Plant under an industrial discharge permit.

IN-PLACE PERFORMANCE

Since its installation in the fall of 1995, the HDPE/jet grout barrier system with recovery wells appears to be performing satisfactorily. The groundwater recovery system of seven wells operates at an average pumping rate of 900 gallons per day. The recovered water is pretreated on site and disposed of through the local wastewater treatment facility. At this time (summer, 1996), hydrocarbon-like seepage has not been observed at the fill/native soil or soil/bedrock interfaces. A continued reduction in hydrocarbon-like seepage is predicted over the next two to three seasons.
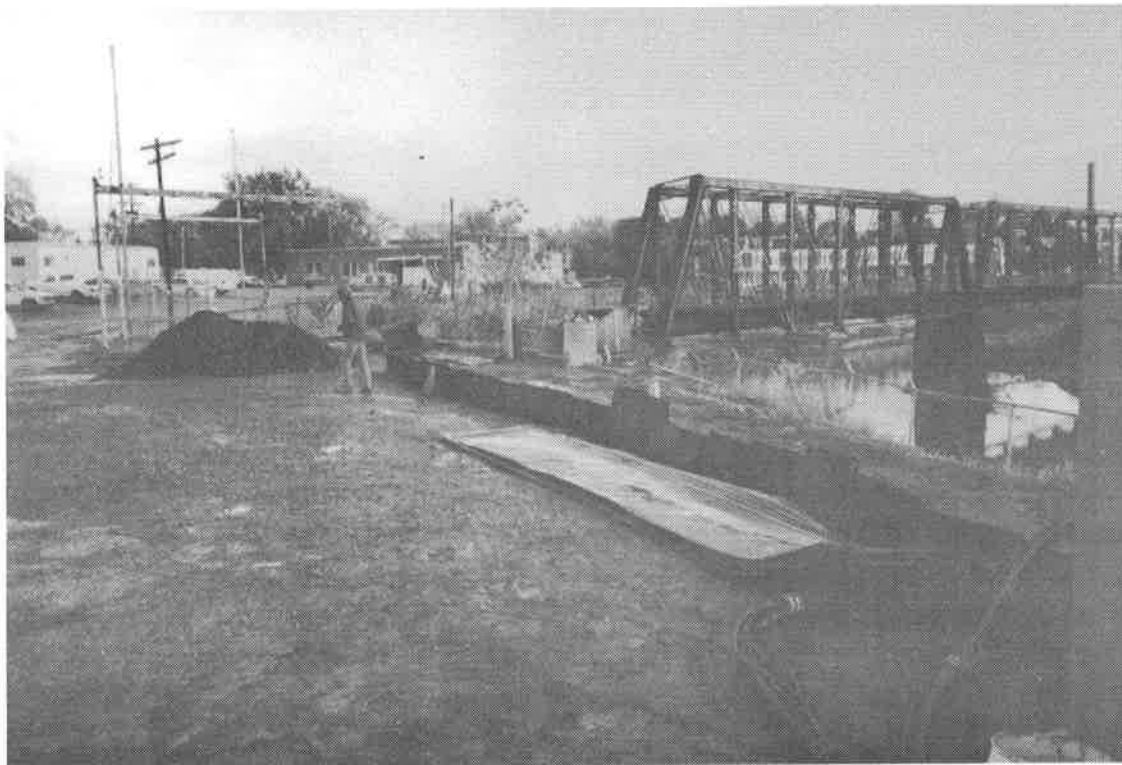
Figure 8. Installed section of HDPE barrier wall.

REFERENCES

Koerner, R.M., (1996) "Remediation vs. Containment of Solid/Liquid Waste Sites.", Geosynthetics World, Vol. 6, No. 1, pp. 6-7.

Ruff, A.C., (1995) "Protecting the Environment. CPA Digs in with Remediation Project at York.", Horizons Magazine, December, 1995, pp. 4-7.

WHAT IS AN APPROPRIATE FACTOR OF SAFETY FOR LANDFILL COVER SLOPES?

C.N. LIU
THE UNIVERSITY OF TEXAS AT AUSTIN, USA
R.B. GILBERT
THE UNIVERSITY OF TEXAS AT AUSTIN, USA
R.S. THIEL
THIEL ENGINEERING, USA
S.G. WRIGHT
THE UNIVERSITY OF TEXAS AT AUSTIN, USA

ABSTRACT

Factors of safety used for the design of embankment dams are not necessarily appropriate for the design of landfill covers. The level of uncertainty in the design of cover slopes may be greater than for embankment dams due to the lack of project-specific strength testing and the effect that small changes in water and gas pressures can have on stability. Laboratory shear tests are presented to illustrate the sources of uncertainty in interface strength for cover slopes. Sensitivity analyses are performed to highlight the importance of fluid pressure on the factor of safety. Finally, a simplified methodology is presented for selecting the appropriate factor of safety by considering design uncertainty and balancing costs and benefits.

INTRODUCTION

Landfill cover systems typically consist of a barrier layer overlain by a drainage layer, cover soil and vegetation and sometimes underlain by a gas collection or drainage layer. The individual components in the system include both soil and geosynthetic materials. Interfaces between individual components form potential sliding surfaces in the cover system (Fig. 1).

A limit equilibrium model is commonly used in practice to evaluate the stability of cover slopes. The factor of safety for static conditions is defined as the ratio of the available strength divided by the strength required for stability, which for an infinite slope is expressed by

$$FS = \frac{c' + (\gamma z \cos\alpha - u)\tan\phi'}{\gamma z \sin\alpha} \qquad (1)$$

where
FS = factor of safety
γ = unit weight of material in slope
u = fluid pressure in slope at interface of slippage
c' = effective stress failure envelope intercept for interface
ϕ' = effective stress failure envelope slope for interface
α = slope angle
z = depth below the ground surface for interface

Note that the effects of toe buttressing and tensile reinforcement are not included in Eq. (1). In the authors' experience, an infinite slope analysis is a common, and appropriate, type of analysis for many landfill cover systems. However, the probabilistic approach outlined in this paper for infinite slopes could readily be adapted to cover systems where toe buttressing is significant (generally only applicable for relatively short slopes) or where geosynthetic reinforcement elements are explicitly included in the design.
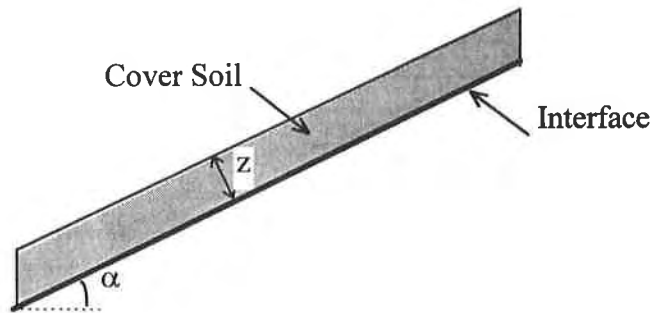
Fig. 1 Geometry of cover slope

A factor of safety of about 1.5 is commonly used for the design of slopes in landfill cover systems. This factor of safety has been adopted from the design of embankment dams. Experience over the past 50 years has indicated that this safety factor provides a reasonable balance between cost and performance for embankment dams. However, landfill cover slopes are not embankment dams. The magnitudes of uncertainty in design and the consequences of failure are different. In this paper, we will highlight and discuss the importance of these differences. We will also present a simplified methodology to obtain an appropriate factor of safety for a cover slope by (1) explicitly accounting for uncertainty in the performance and (2) considering the cost of failure.

INTERFACE SHEAR STRENGTH

An important difference between landfill cover slopes and embankment dams is the amount of strength testing used in design. For a typical embankment dam, many project-specific strength tests are conducted. Conversely, it often happens that very little, if any, project-specific interface strength testing is performed in the design of a cover slope. The apparent rationale for the lack of testing with cover slopes is the perception that there is negligible uncertainty in interface strengths for geosynthetic materials because they are man-made. However, there are many sources of uncertainty in geosynthetic interface strengths, including (1) material variability, (2) accuracy of test methods, (3) the effects of moisture, and (4) post-peak strength reductions with displacement.

Variability in Geosynthetics. In order to study material variability for geosynthetics, the interface between a polyvinyl chloride (PVC) geomembrane and a woven geotextile was tested using a tilt table device. The geomembrane was a 40-mil thick PVC geomembrane manufactured by Watersaver Company, Inc. The smooth geomembrane had a faille finish, a fine patterned surface much like that of a very fine file, on one side. The non-faille side was placed against the geotextile. The woven geotextile was the upper component in the needle-punched geosynthetic clay liner (GCL) product manufactured by

Bentomat®. Test specimens were 133 mm x 133 mm in size. The 600-mm long tilt table was raised at a rate of about 2° per minute. The angle at which observable sliding occurred was used to estimate the interface strength. Five tests each were performed at three normal stresses ranging from 5 to 17 kPa. For both the geotextile and the geomembrane, the individual test specimens were obtained from the same batch of material. The test results are shown on Fig. 2.

Variability in the interface strength tends to increase with increasing normal stress. A useful measure of this variability is the coefficient of variation (c.o.v.), which is equal to the standard deviation divided by the mean value at a given normal stress. The c.o.v. values are essentially constant with normal stress, and range from 1 to 2 percent.

Test results for a different batch of the woven geotextile at an approximate normal stress of 15 kPa are shown on Fig. 3. The variability between batches is more significant than the variability within a batch. The difference of the average-strength-to-normal-stress ratios between batches is about 5 percent. This result indicates that conducting repeated tests on material from a single batch will not capture fully the magnitude of material variability.

Including both intra- and inter-batch variability, the variability in the strength of this geosynthetic interface is still relatively small. For example, typical c.o.v. values for the strength of soils range from 10 to 30 percent. However, the variability of the geosynthetic interface strength cannot be neglected if only one specimen is tested at a single normal stress (a common practice for cover slopes). This single strength measurement, which would be used to design the slope, could easily be more than 5 percent different from the average measured strength for the interface.
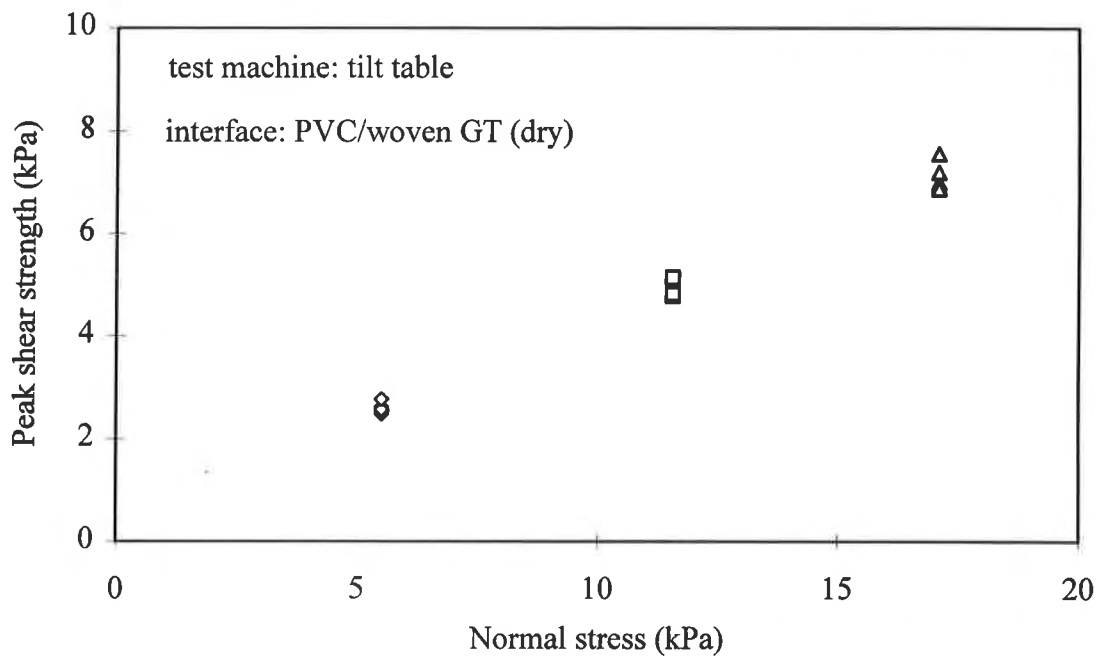
Fig. 2 Variability in peak interface strength
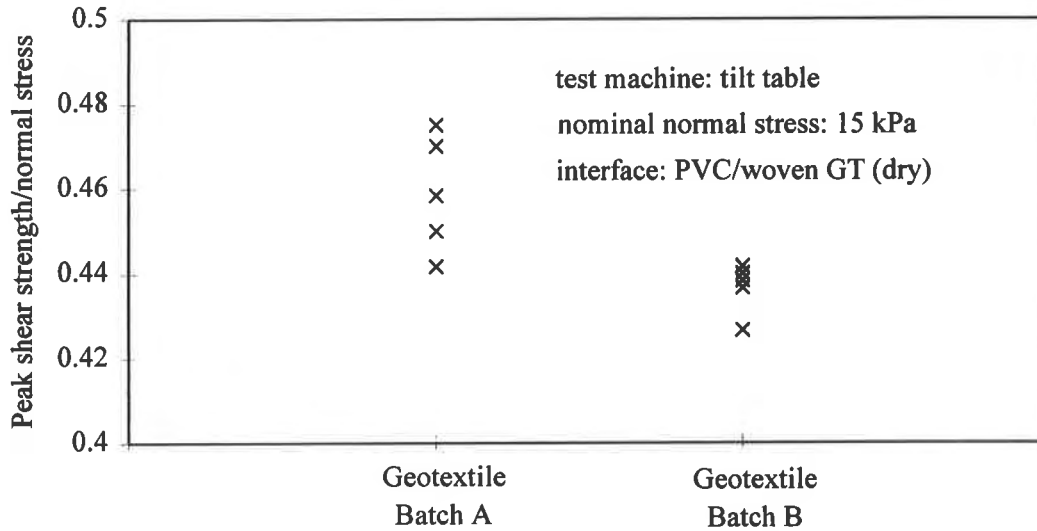
Fig. 3 Variability in peak interface strength between batches

Accuracy of Shear Strength Test Methods. Shear strength tests were performed on the woven geotextile/PVC geomembrane interface using four different devices: a direct shear box with a circular specimen 64 mm in diameter (Direct Shear #1); a direct shear box with a circular specimen 60 mm in diameter (Direct Shear #2); a double interface shear device (Gilbert, et al. 1995) with a square specimen 102 mm on a side (Double Interface Shear); and the tilt table with a 133 mm square specimen. In all cases except the tilt table tests, a 0.5-mm/min shear rate was used. A comparable shear rate was applied in the tilt table tests by rising the table at 2° per minute. Since the strength measured with the tilt table corresponds to the peak strength, the measured peak strengths from the other devices are used for comparison. From five to ten tests were conducted with each device to account for inter-device (or material) variability.

The test results are shown on Fig. 4. The variability between devices is significant. Surprisingly, there is a large discrepancy in results from the two direct shear boxes with similar specimen sizes; the average ratio of strength to normal stress from Direct Shear #2 was 87 percent of that for Direct Shear #1. Other than the small difference in specimen size, there is no other apparent difference in these two direct shear devices that could account for this discrepancy in results. The results from the double interface and tilt table devices were closer together than those from the direct shear boxes. In fact, the double interface shear device and the tilt table produced results that are comparable to the average result for the two direct shear boxes.

In order to further investigate the differences between different test methods, tests were performed at normal stresses ranging from 5 to 18 kPa for each test method. A linear failure envelope was fit through the test data using a least squares regression analysis, and the results are summarized in Table 1. The failure envelopes for the double interface and tilt table devices are similar, while that from the direct shear box is flatter. For these failure envelopes, the difference in strength at a given normal stress is as large as 10 percent. For example, the strengths at a normal stress of 5 kPa range from 2.19 to 2.39 kPa.

Fig. 4 Variability in peak interface shear strength between test devices

Table 1 Comparison of failure envelopes for different test devices

Test Method	Number of Tests	Intercept c' (kPa)	Slope ϕ' (°)	r^2
Direct Shear #1	15	0.45	21.2	0.99
Double Interface Shear	9	0.07	24.0	0.99
Tilt Table	15	0.08	22.9	1.00

Moisture Conditions. Moisture can lower the effective stress failure envelope for interfaces with geosynthetics. Tilt table tests were performed on specimens of the PVC geomembrane/woven geotextile interfaces that were submerged in a bath of water. An approximate shear rate of 0.5 mm/min was used to ensure complete drainage of the geotextile based on its permittivity. The test results, shown on Fig. 5, indicate that the submerged interface strength is more than 15 percent smaller than the dry interface strength. It is important to emphasize that this strength reduction is not related to water pressure at the interface because the geotextile was drained.

Moisture can also reduce the effective stress strength parameters for the interface between a PVC geomembrane and the woven geotextile of a geosynthetic clay liner (GCL) because hydrated bentonite from the GCL can extrude into the interface (Gilbert, et al. 1996). To investigate the effect of bentonite on the drained interface strength, tilt table tests were conducted on submerged interfaces in which bentonite was smeared on the woven geotextile at an areal density of 0.0002 g dry bentonite per mm^2. The rate used to raise the tilt table, about 1° per minute, was slow enough to ensure drained conditions for this thin layer of bentonite. The test results are shown on Fig. 5. Upper and lower bounds for the

effective stress failure envelope are also given. The upper bound roughly corresponds to the dry, clean interface while the lower bound corresponds to the submerged, smeared interface. The lower bound strength is about 50 percent of the upper bound strength.
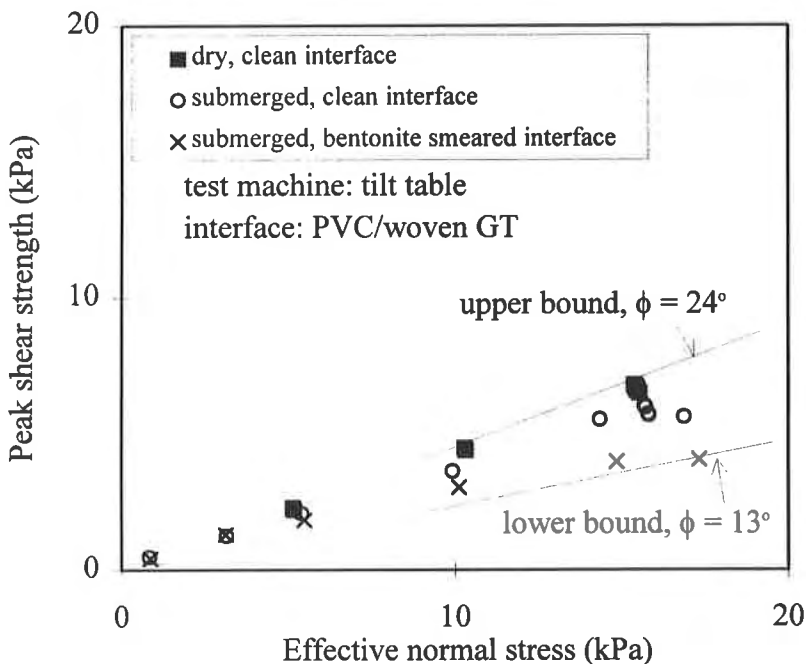
Fig. 5 Effect of moisture on effective stress failure envelope

Post-Peak Strength Reductions. Many interfaces with geosynthetics exhibit post-peak reductions in strength with displacement. A peak strength is mobilized at a small displacement (typically much less than 10 mm); the strength then decreases with further displacement, eventually approaching a residual value. For example, a plot of stress versus displacement for the submerged PVC geomembrane/woven geotextile interface with smeared bentonite is shown on Fig. 6. The bentonite was smeared on the woven geotextile at an areal density of 0.0002 g dry bentonite per mm^2. The test was performed using the double interface shear device, and the interface was sheared at a drained shear rate. The strength after large displacement is about 80 percent of the peak strength. Gilbert and Byrne (1996) and Stark et al. (1996) present data demonstrating that the residual strength for some geosynthetic interfaces is as small as 30 percent of the peak strength.

The ability to measure accurately the large-displacement or residual strength is affected by the test method and specimen size (Gilbert, et al. 1995). However, even if the peak and residual strengths for an interface are well established, uncertainty in the available strength in a cover slope (peak or residual) is a significant source of uncertainty in cover slope performance. Displacements during construction may be large enough to induce post-peak strength reductions. For example, displacements in a cover soil during construction were measured in thirteen, 10-m high cover slopes for a field test project (Scranton 1996). The measured displacements were greater than 25 mm on average. These displacements during

construction are far greater than those required to mobilize peak strengths (typically less than 10 mm). In addition, long-term deformation and creep may lead to strain softening of shear strength.
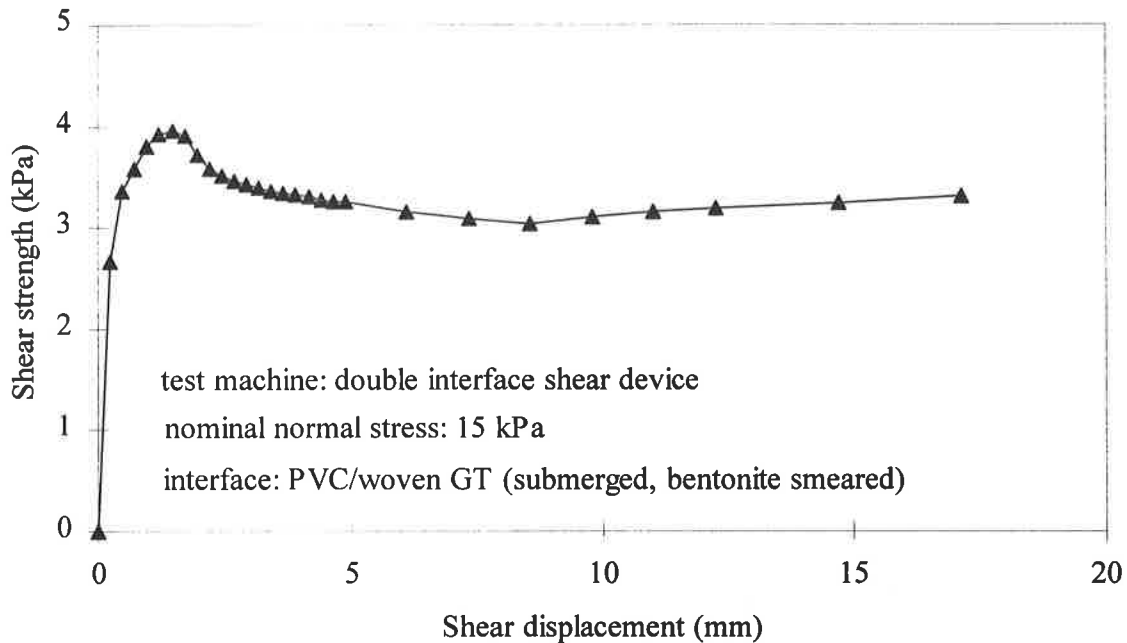
Fig. 6 Shear stress-displacement curve showing strain softening for a drained test

FLUID PRESSURE

Another difference between cover slopes and embankment dams is the effect that small changes in fluid pressure can have on the factor of safety. Because the overburden pressure on an interface in a cover system is typically small compared to that on the critical slip surface in an embankment dam, the factor of safety for a cover slope is more sensitive to a small change in fluid pressure. In order to demonstrate this sensitivity, the derivative of the factor of safety (Eq. (1)) with respect to fluid pressure is given as follows

$$\frac{dFS}{du} = \frac{-\tan\phi'}{\gamma z \sin\alpha} \tag{2}$$

As the overburden pressure on the interface decreases (that is, as the depth of the interface, z, decreases), the factor of safety becomes more sensitive to fluid pressure (that is, the magnitude of the derivative dFS/du increases).

It is widely acknowledged that water pressures at interfaces above barrier layers in covers will be affected by infiltration. For example, Thiel and Stewart (1993), Giroud et al (1995) and Soong and Koerner (1995) discuss the fluid pressures that may develop above barrier layers from infiltration and seepage. However, there are also sources of fluid pressure on interfaces below barrier layers that are not

related directly to infiltration, for example gas pressures and pore water pressures due to rapid changes in the total stress. While these sources of fluid pressure are typically neglected because they are small, they can have a large impact on stability for a cover slope, as demonstrated in the following example.

The effect of small changes in fluid pressure on the stability will be analyzed for the cover slope shown on Fig. 7. The interface of concern is that between the PVC geomembrane and the woven geotextile of the GCL. Test data for the strength of this interface are shown on Figs. 5 and 6. Two sources of fluid pressure will be examined for this case: (1) gas pressure from the underlying waste and (2) pore water pressure due to a rapid change in the unit weight of the overlying cover soil if it becomes saturated during a rain storm.
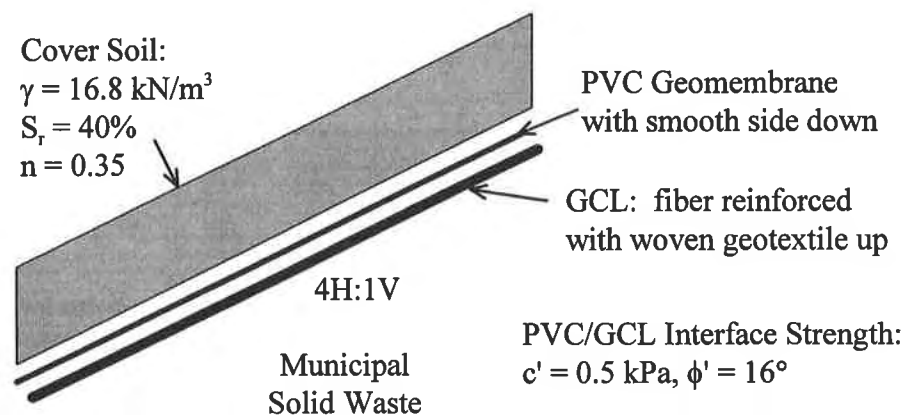
Fig. 7 Example cover slope used for stability analyses

The magnitude of gas pressure at the base of a landfill cover is site specific, depending on a number of factors such as the waste composition and age, the moisture content of the waste, and the type and effectiveness of gas extraction systems. Average, ambient gas pressures for typical municipal solid waste landfills have been reported to be on the order of 1 kPa (Findikakis and Leckie 1979), while one of the authors (Thiel) has measured values ranging from 0 to 4 kPa below cover systems. The factor of safety for this slope, calculated using Eq. (1), is summarized in Table 2 for different gas pressure conditions. Two geometries are included: a temporary configuration during construction when a 0.3-m thick drainage layer is placed over the geomembrane and the final configuration when there is 0.9-m of cover soil over the geomembrane.

The results in Table 2 demonstrate two important points. First, a small increase in fluid pressure can have a large impact on the factor of safety. For both configurations, a 4 kPa gas pressure leads to a factor of safety less than one. For reference, a 4 kPa gas pressure corresponds to an equivalent water head of 0.4 m. Second, the factor of safety is more sensitive to fluid pressure for smaller overburden stresses. The factor of safety decreases from 1.56 to 0.62 for a 0.3-m thick cover due to a 4-kPa increase in gas pressure, while it only decreases from 1.29 to 0.97 for a 0.9-m thick cover.

Another potential source of fluid pressure at the interface is a rapid increase in the unit weight of the cover soil from rainfall infiltration. This increase in total normal stress at the interface will initially be

carried by water pressure if the interface is saturated. Since the bentonite layer in the GCL will limit drainage below the woven geotextile, it may take days for this excess water pressure to dissipate; therefore, the effective normal stress and, thus, the strength, at the interface will not change during a storm event. However, the shear stress applied to the interface increases due to the increase in the weight of the cover soil. Hence, the factor of safety will temporarily decrease until the excess water pressure at the interface dissipates. The effect of a rapid increase in the unit weight of the cover soil, assuming that cover soil saturation increases from 40 to 100%, is demonstrated in Table 2. The factor of safety decreases from 1.29 to 1.15 for the 0.9-m thick cover.

Table 2 Effect of fluid pressure on the factor of safety

Case	γ (kN/m³)	u (kPa)	FS for 0.3-m Cover (construction)	FS for 0.9-m Cover (post-construction)
No Fluid Pressure	16.8	0	1.56	1.29
Typical Gas Pressure	16.8	1	1.32	1.21
High Transient Gas Pressure	16.8	4	0.62	0.97
Rapid Increase in Cover Soil γ	18.8	0.6 (0.3-m cover) 1.7 (0.9-m cover)	1.39	1.15

SO WHAT IS AN APPROPRIATE FACTOR OF SAFETY?

The intent of a factor of safety is to account for uncertainty in design. The actual factor of safety for a cover slope interface is not known due to uncertainty in the interface strength, the fluid pressure, the unit weight of soil above the interface and the constructed slope angle. By estimating values for these variables and then applying a factor of safety of about 1.5, designers intend that there is only a small chance that the actual factor of safety is less than one. However, there is a danger in blindly applying a safety factor of 1.5 without considering the probability of a slope failure. First, the probability may be unacceptably large, leading to unintended risk. Second, the probability may be unnecessarily small, leading to excessive cost. The objective of this section is to provide and demonstrate tools for evaluating the amount of uncertainty in the factor of safety, estimating the probability of a slope failure, and determining an appropriate factor of safety considering costs and benefits.

Uncertainty in the Factor of Safety. Uncertainty in the factor of safety for an interface arises from uncertainty in the individual design variables. The contribution of an individual variable to the overall uncertainty in the factor of safety depends on the (1) magnitude of uncertainty in the variable and (2) sensitivity of the factor of safety to the variable. Appendix A provides a simple tool for quantifying uncertainty in the factor of safety. Equations are given to estimate the mean factor of safety and the standard deviation in the factor of safety as a function of the means and coefficients of variation (c.o.v.) for all the variables in Eq. (1).

As an example, further analyses for the cover slope shown on Fig. 7 and analyzed in Table 2 (post-construction case with 0.9-m of cover soil) are presented in Table 3. Estimates of the c.o.v. for each

variable are provided, and the partial derivatives of FS with respect to each variable are calculated (Appendix A). The soil unit weight and the fluid pressure at the interface are assumed to be positively correlated since transient increases in γ may induce excess water pressure below the geomembrane. In addition, c' and tanϕ' are assumed to be negatively correlated from the linear regression analysis (that is, a larger slope on an envelope fit through the data would be associated with a smaller intercept).

The estimated mean factor of safety, μ_{FS}, is 1.21 from Eq. (A.1), while the estimated standard deviation in the factor of safety, σ_{FS}, is 0.22 from Eq. (A.2). In addition, a measure of the contribution of each variable to the overall uncertainty in the factor of safety is presented in Table 3. This uncertainty contribution factor is defined as follows

$$\text{Uncertainty Contribution Factor for X} = \frac{\sigma_{FS} - \sigma_{FS(\Omega_x=0)}}{\sigma_{FS}} \quad (3)$$

where X is a design variable and $\sigma_{FS(\Omega_x=0)}$ is the standard deviation of the factor of safety if there were no uncertainty in that particular variable. If a variable contributes little to the overall uncertainty in the factor of safety, then its uncertainty contribution factor will be near zero. Conversely, this factor will be near one for variables that contribute significantly to uncertainty in the factor of safety. The results in Table 3 show that uncertainty in the fluid pressure and failure envelope slope contribute most to uncertainty in the factor of safety. The failure envelope's slope (tanϕ') contributes because its c.o.v. is relatively large <u>and</u> the factor of safety is sensitive to this variable (its partial derivative is large). The fluid pressure contributes primarily because its c.o.v. is very large. While the slope angle's sensitivity is large, it makes a negligible contribution to uncertainty in the factor of safety because its c.o.v. is very small. It is interesting that uncertainty in the failure envelope's cohesion intercept contributes little to uncertainty in the factor of safety. This result is due to two factors in this example. First, since the mean value for c' is small, the factor of safety is not very sensitive to changes in c' relative to the other variables. Second, the negative correlation between c' and tanϕ' dampens the effect of uncertainty in c' because smaller values of c' tend to be associated with larger values of tanϕ'. However, as the mean value of c' increasing, its contribution to the overall uncertainty will increase.

Table 3 Calculations to estimate uncertainty in the factor of safety

Variable X	Mean Value μ_X	c.o.v. Ω_X	$\dfrac{\partial FS}{(\partial X / \mu_X)}$	Uncertainty Contribution Factor
γ^*	16.8 kN/m³	0.05	-0.06	0.0
$(c')^{**}$	0.5 kPa	0.20	0.14	0.0
u^*	1 kPa	1.0	-0.08	0.1
$\tan(\phi')^{**}$	tan16°	0.20	1.07	0.6
α	14°	0.03	-1.25	0.0

$^*\rho_{\gamma,u} = 0.5$; $^{**}\rho_{c',\tan(\phi')} = -0.5$

Reliability. The reliability of the interface is defined as the probability that the factor of safety will be greater than 1.0. Once μ_{FS} and σ_{FS} are calculated for a particular case, the reliability can be approximated as follows

$$\text{Reliability} = \text{Probability that FS} > 1 \cong \Phi\left(\frac{\mu_{FS} - 1}{\sigma_{FS}}\right) \qquad (4)$$

where Φ is the standard normal function, which is tabulated in many statistics textbooks and available in most spreadsheet packages. In the previous example with $\mu_{FS} = 1.21$ and $\sigma_{FS} = 0.22$, the reliability is approximated by $\Phi[(1.21-1)/0.22] = 0.83$. This reliability provides a useful measure of how confident we are that the interface will be stable: a reliability of 0 means we are certain that it will not be stable while a reliability of 1 means we are certain that it will be stable. Alternatively, the probability that the interface is not stable in this case is equal to 1-0.83, or 0.17.

In most design situations, multiple cases are analyzed. For example, four possible cases were analyzed for this interface in Table 2. The previous reliability calculations correspond to the case denoted "Typical Gas Pressures." Since each of the four cases could occur and there is a chance of instability associated with each case, the overall probability for the interface should account for all of these possibilities. The overall or total failure probability for an interface can be obtained as follows

$$\text{Total Failure Probability} = \sum_{\text{all cases}} (\text{Failure Probability for Each Case}) \times (\text{Likelihood of Case}) \qquad (5)$$

As an example, Table 4 summarizes calculations of the total failure probability for this cover slope interface. The total failure probability, 0.18, is dominated by the failure probability for the typical gas pressure case since this is the most likely (or the most frequent) condition over the design life of the cover.

Table 4 Calculation of total failure probability for interface

Case	Failure Probability	Likelihood over Design Life	Total Failure Probability
No Fluid Pressure	0.10	0.2	0.10×0.2
Typical Gas Pressure	0.17	0.7	0.17×0.7
High Transient Gas Pressure	0.53	0.05	0.53×0.05
Rapid Increase in Cover Soil γ	0.26	0.05	0.26×0.05

$$\Sigma = 0.18$$

Finally, there are multiple interfaces in most typical cover systems. Since slippage may occur along any of these interfaces, the reliability for the slope must account for all of the potential interfaces of sliding. A simple and conservative approximation for the probability of instability in the slope is to add the individual probabilities of failure for each interface

$$\text{Failure Probability for Slope} \cong \sum_{\text{all interfaces}} \text{Failure Probability for each Interface} \qquad (6)$$

For example, there are three interfaces of concern in the cover system shown on Fig. 7: cover soil/PVC; PVC/GCL; and GCL/subgrade. If the total failure probabilities for the interfaces are 0.01, 0.18 and 0.05 respectively, then the probability of failure for this slope is $0.01 + 0.18 + 0.05 = 0.24$. As the number of interfaces increases, the probability of slope failure will tend to increase. Also, interfaces with relatively small failure probabilities may have a negligible effect on the overall failure probability for the slope.

Appropriate Factor of Safety. An "appropriate" factor of safety is defined as one that provides an optimal balance of costs and benefits. For both embankment dams and cover slopes, the primary cost associated with a smaller factor of safety is a greater probability of slope failure. A simple model to capture the impact of this cost is the expected cost of failure

$$\text{Expected Cost of Failure} = C_F p_F \qquad (7)$$

where C_F is the cost of a slope failure and p_F is the probability of a slope failure. As the mean factor of safety decreases, the probability of failure and, thus, the expected cost of failure increases.

In order to relate the mean factor of safety to the expected cost of failure, a "contour" plot of the failure probability versus the mean and standard deviation for the factor of safety is shown on Fig. 8. This plot corresponds to a single interface under a single design condition. Fig. 8 can be used to determine an appropriate factor of safety in several ways, as discussed in the following paragraphs.

First, if a level of reliability is desired for a landfill cover system that is comparable to that for other civil engineering systems such as embankment dams, then the required mean factor of safety can be determined from Fig. 8. For example, typical lifetime failure probabilities for embankment dams are on the order of 0.0001 to 0.001. Given a standard deviation in the factor of safety equal to 0.22 obtained for the PVC/GCL interface (Fig. 7), the required factor of safety is between 1.6 and 1.7 to achieve this reliability (Fig. 8). This required factor of safety is larger than that used in embankment dams because there is more uncertainty in the design of a typical cover slope due to a lack of strength testing and the sensitivity to small changes in fluid pressure. For example, Christian et al. (1994) obtained a standard deviation of 0.14 in the factor of safety for an embankment slope. Note that this standard deviation is consistent with a mean factor of safety of about 1.5 for an embankment dam. Therefore, a factor of safety greater than 1.5 would be appropriate for cover slopes if a failure probability of 0.0001 to 0.001 is desired

Second, it is possible to reduce the uncertainty in the factor of safety for cover slopes by performing project-specific strength tests. If the target probability of failure is 0.0001 to 0.001, then the mean factor of safety could be as small as 1.2 for a standard deviation of 0.05 in the factor of safety (Fig. 8).

Finally, the cost of failure is also important in defining an appropriate factor of safety. It may not be reasonable to achieve the same level of reliability in a landfill cover system as for an embankment dam because the cost of failure is usually smaller. The expected cost of failure, Eq. (7), incorporates information about both the probability and cost of failure. The cost of failure could range widely from

repairing a small slump to replacing an entire cover, and can be significantly affected by litigation costs. Consider as an example two cover slopes with costs of failure of $100,000 and $1,000,000, respectively. If they are both designed with a factor of safety of 1.7 (i.e. failure probability of 0.001 for standard deviation of the factor of safety equal to 0.22), then the expected costs of failure are extremely small ($100 and $1,000), respectively. To achieve an acceptable expected cost of failure, say $10,000, the slopes should be designed with factors of safety ranging from 1.25 for the $100,000 failure cost to 1.5 for the $1,000,000 failure cost. This simple example demonstrates that the appropriate factor of safety for a cover slope depends on the amount of uncertainty and the cost of failure, and therefore, is project-specific.
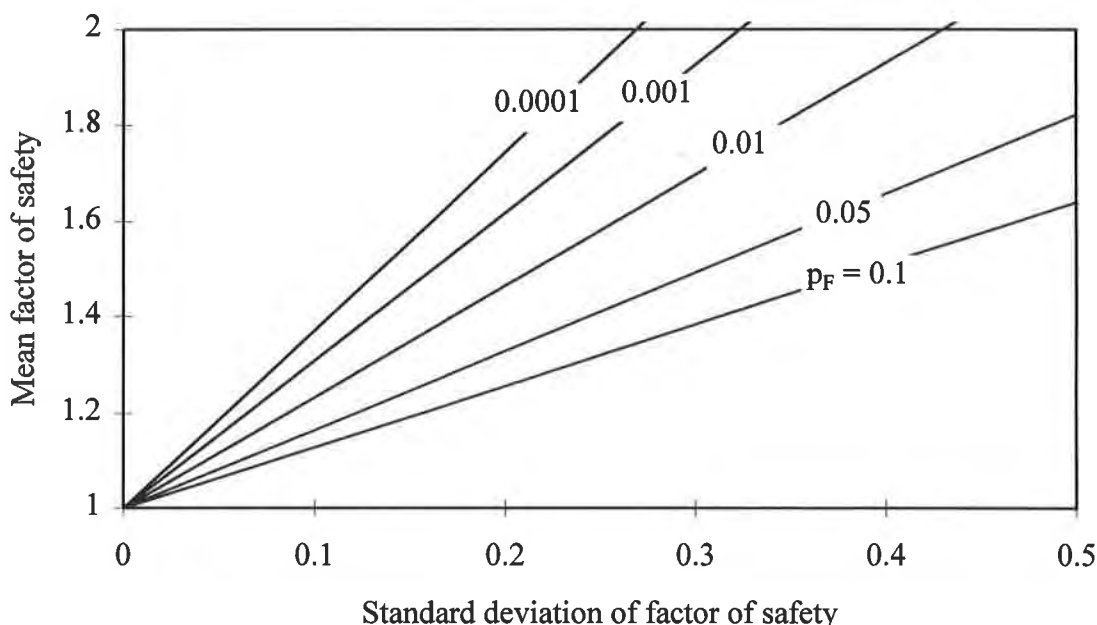
Fig. 8 Failure probability contours versus the mean and standard deviation of the factor of safety

CONCLUSIONS

In summary, selection of an appropriate factor of safety needs to be evaluated on a project-specific basis. Blind application of a factor of safety equal to 1.5 is not appropriate. An appropriate factor of safety for a cover slope could range from as small as 1.1 to greater than 1.5 depending on the amount of uncertainty and the cost of failure. The major factors affecting uncertainty in the performance of a cover slope are interface shear strengths and fluid pressures. Interface shear strengths contribute significant uncertainty if little project-specific testing is performed in design. We have demonstrated that the interface strength for geosynthetic materials can vary within and between batches, that test methods and test conditions can bias the results, and that the available strength depends on displacement due to strain softening. Fluid pressures contribute significant uncertainty because small changes in fluid pressure can have a significant effect on stability. Also, fluid pressures acting on cover system interfaces can include both water and gas pressures. Finally, we have provided a set of practical tools for quantifying

uncertainty in the factor of safety, estimating the reliability of a cover slope, and ultimately selecting an appropriate factor of safety for design.

Although these tools help in developing an optimal design, there is ample room for improvement with future work. The cost of a slope failure is related to the scale of the failure, the time when the failure occurs, and the number of failures over the design life. None of this information is conveyed adequately in a single factor of safety or reliability value.

REFERENCES

Christian, J.T., Ladd, C.C., and Baecher, G.B., (1994) "Reliability applied to slope stability analysis", Journal of Geotechnical Engineering, ASCE, Vol. 120, No. 12, pp. 2180-2207.

Findikakis, A.N. and Leckie, J.O., (1979) "Numerical simulation of gas flow in sanitary landfills", Division of Environmental Engineering, ASCE, Vol. 105, No. 5, pp. 927-945.

Gilbert, R.B. and Byrne, R.J., (1996) "Strain-softening behavior of waste containment system interfaces", Geosynthetics International, Vol. 3, No. 2, pp. 2-23.

Gilbert, R.B., Fernandez, F.F. and Horsfield, D.W., (1996) "Shear strength of a reinforced geosynthetic clay liner", Journal of Geotechnical Engineering, ASCE, Vol. 122, No. 4, pp. 259-266.

Gilbert, R.B., Liu, C.N., Wright, S.G. and Trautwein, S.J., (1995) "A double shear test method for measuring interface strength", Geosynthetics '95 Conference Proceedings, Vol. 3, pp. 1017-1029.

Giroud, J.P., Bachus, R.C., and Bonaparte, R., (1995) "Influence of water flow on the stability of geosynthetic-soil layered systems in slopes", Geosynthetics International, IFAI, Vol. 2, No. 6, pp. 1149-1180.

Scranton, H.B., (1996) "Field performance of sloping test plots containing geosynthetic clay liners", Master Thesis, University of Texas at Austin, 206p.

Soong T.Y. and Koerner, R.M., (1995) "Seepage induced slope instability", Proceedings of the 9th GRI Conference, pp. 235-255.

Stark, T.D., Williamson, T.A., and Eid, H.T., (1996) "HDPE geomembrane/geotextile interface shear strength", Journal of Geotechnical Engineering, ASCE, Vol. 122, No. 3, pp. 197-203.

Thiel, R.S. and Steward, M.G., (1993) "Geosynthetic landfill cover design methodology and construction experience in the Pacific Northwest", Geosynthetics '93 Conference Proceedings, Vol. 3, pp. 1131-1144.

APPENDIX A. FIRST-ORDER APPROXIMATIONS FOR THE MEAN AND STANDARD DEVIATION OF THE FACTOR OF SAFETY

The mean or expected factor of safety can be estimated as follows

$$\mu_{FS} \cong \frac{\left[\mu_\gamma z \cos(\mu_\alpha) - \mu_u\right]\mu_{\tan\phi'} + \mu_{c'}}{\mu_\gamma z \sin(\mu_\alpha)} \qquad (A.1)$$

where μ indicates the mean (or "best guess") value for a parameter. Therefore, the mean value for FS is simply estimated from Eq. (1) by using the mean value for each parameter. Likewise, the standard deviation in FS can be estimated as follows

$$\sigma_{FS}^2 \cong \left(\frac{\partial FS}{\partial \gamma / \mu_\gamma}\right)^2 \Omega_\gamma^2 + \left(\frac{\partial FS}{\partial c' / \mu_{c'}}\right)^2 \Omega_{c'}^2 + \left(\frac{\partial FS}{\partial u / \mu_u}\right)^2 \Omega_u^2 + \left(\frac{\partial FS}{\partial \tan(\phi') / \mu_{\tan(\phi')}}\right)^2 \Omega_{\tan(\phi')}^2$$

$$+ \left(\frac{\partial FS}{\partial \alpha / \mu_\alpha}\right)^2 \Omega_\alpha^2 + 2\left(\frac{\partial FS}{\partial \gamma / \mu_\gamma}\right)\left(\frac{\partial FS}{\partial u / \mu_u}\right)\rho_{\gamma,u}\Omega_\gamma\Omega_u \qquad (A.2)$$

$$+ 2\left(\frac{\partial FS}{\partial c' / \mu_{c'}}\right)\left(\frac{\partial FS}{\partial \tan(\phi') / \mu_{\tan(\phi')}}\right)\rho_{c',\tan(\phi')}\Omega_{c'}\Omega_{\tan(\phi')}$$

where σ_{FS} is the standard deviation for FS, Ω indicates the coefficient of variation for a parameter (the standard deviation divided by the mean), ρ is the correlation coefficient between two parameters ($\rho_{\gamma,u}$ will tend to be positive since an increase in infiltration will increase both the unit weight and the pore water pressure, while $\rho_{c',\tan(\phi')}$ will tend to be negative since c' and tan(ϕ') are negatively correlated in a conventional regression analysis), and the partial derivatives of FS with respect to each parameter are evaluated at the mean values as follows

$$\frac{\partial FS}{\partial \gamma / \mu_\gamma} = \frac{1}{z \sin(\mu_\alpha)}\left(\frac{\mu_u}{\mu_\gamma}\mu_{\tan(\phi')} - \frac{\mu_{c'}}{\mu_\gamma}\right)$$

$$\frac{\partial FS}{\partial c' / \mu_{c'}} = \frac{\mu_{c'}}{\mu_\gamma z \sin(\mu_\alpha)}$$

$$\frac{\partial FS}{\partial u / \mu_u} = \frac{-\mu_u \mu_{\tan(\phi')}}{\mu_\gamma z \sin(\mu_\alpha)} \qquad (A.3)$$

$$\frac{\partial FS}{\partial \tan(\phi') / \mu_{\tan(\phi')}} = \frac{\left[\mu_\gamma z \cos(\mu_\alpha) - \mu_u\right]\mu_{\tan(\phi')}}{\mu_\gamma z \sin(\mu_\alpha)}$$

$$\frac{\partial FS}{\partial \alpha / \mu_\alpha} = \frac{\mu_\alpha}{\mu_\gamma z \sin(\mu_\alpha)} \left[\frac{-\mu_\gamma z \mu_{\tan(\phi')} + \mu_u \mu_{\tan(\phi')} \cos(\mu_\alpha) - \mu_{c'} \cos(\mu_\alpha)}{\sin(\mu_\alpha)} \right]$$

These derivatives indicate the change in FS for a percentage change in a parameter about its mean value. Therefore, they are useful measures of the sensitivity of FS to the various parameters.

GEOMEMBRANES AS AN INTERIM MEASURE TO CONTROL WATER INFILTRATION AT A LOW-LEVEL RADIOACTIVE WASTE DISPOSAL AREA

M.R. WEISHAN
NEW YORK STATE ENERGY RESEARCH AND DEVELOPMENT AUTHORITY,USA
T.L. SONNTAG
NEW YORK STATE ENERGY RESEARCH AND DEVELOPMENT AUTHORITY,USA
W.D. SHEHANE
SEAMAN CORPORATION, USA

ABSTRACT

Using an exposed geomembrane an an interim measure to cover a closed, Low-Level Radioactive Waste Disposal Area requires unique design and construction considerations.

In response to a Resource Conservation and Recovery Act Administrative Consent Order, the New York State Energy Research and Development Authority (NYSERDA) used very low-density polyethylene (VLDPE) geomembrane as an interim measure to cover two soil-capped, grass-covered waste trenches to address a rapid increase in water accumulation in the trenches. Two years later, NYSERDA covered the remaining grass-covered trench caps with a reinforced ethylene interpolymer alloy (EIA-R) geomembrane to reduce water accumulation in these trenches.

This paper addresses the differences in geomembrane materials and discusses the lessons learned during design, construction, and operation since installation of the covers. Discussed are the successes and obstacles regarding the use of both geomembrane materials as an exposed cover, selecting the geomembrane materials, anchoring the geomembrane from wind uplift, and mitigating the increased surface water runoff from the geomembrane covered area.

INTRODUCTION

The New York State Energy Research and Development Authority (NYSERDA) has management responsibility for monitoring and maintaining the shut-down, commercial, Low-Level Radioactive Waste (LLRW), State-Licensed Disposal Area (SDA) at the Western New York Nuclear Service Center (Center), located in southwestern New York State. At the SDA, packaged LLRW was placed in trenches excavated in the native silty-clay soil. The waste was covered with the excavated soil and vegetated with grass.

The wet climate, combined with the relatively impermeable underlying soil, resulted in the gradual accumulation of the water infiltrating into the trenches. As an interim action, NYSERDA installed an exposed geomembrane cover over the vegetated soil caps to minimize water accumulation in the trenches.

BACKGROUND

The SDA occupies approximately 6.07×10^4 square meters of the 1.35×10^7 square-meter Center, site of the world's first commercial nuclear fuel reprocessing plant. Currently, NYSERDA holds title to and maintains the Center on behalf of the people of New York State, with the exception of approximately 8.09×10^5 square meters containing the shut-down nuclear facility. The United States Department of Energy (DOE) is currently using the majority of the shut-down nuclear facility to perform the West Valley Demonstration Project (WVDP). The primary purpose of the WVDP is to solidify the liquid high-level radioactive waste and to decontaminate and decommission the facilities used in the WVDP.

From 1963 to 1975, the SDA operator placed approximately 6.8×10^4 cubic meters of packaged, commercial, LLRW in two sets of parallel trenches referred to as the north and south areas; each containing seven trenches, numbered 1 through 7 and 8 through 14, respectively (Figure 1). Typically, the trenches are approximately 170-meters long, 6-meters deep, and vary in width from 6 meters at the bottom to 11 meters at the top. Each trench has a mounded cover with a drainage swale between adjacent trenches.

The trenches are constructed in Lavery till, described as a silty-clay or clayey-silt, pebble-cobble till. This area was used for disposal trenches because the high clay content and high degree of over-consolidation of the Lavery till make it virtually impermeable at depth, having a hydraulic conductivity of about 1×10^{-8} centimeters per second (cm/sec). However, the upper till and soil caps are fractured as a result of weathering, making it generally more permeable than the unweathered till beneath.

Because of the amount of precipitation and the very low permeability of the unweathered till in the lower part of the trenches, water enters the trenches by permeating through the upper weathered till or the trench covers and tends to accumulate in the trenches. Water that enters the trenches and contacts the disposed wastes mobilizes the radionuclides and other contaminants in the wastes. Even though current water infiltration rates through the grass-covered, silty-clay caps are quite low, water that enters the trenches will accumulate and increase the potential for an uncontrolled release.

Covering the trenches with an exposed geomembrane was performed as an interim measure until closure or long-term management is initiated for the SDA. NYSERDA is currently reviewing options for closure or long-term management of all facilities at the Center including the SDA. Because all closure and long-term management alternatives for the SDA trenches require treatment or solidification of the leachate, this interim measure is consistent with long-term management goals and closure options. Leachate removed from trenches will have to be managed and treated as LLRW and possibly as RCRA mixed waste due to the potential applicability of a RCRA hazardous waste designation. Covering the trenches is also consistent with regulatory and best management philosophies due to reducing the potential for a release of leachate and the generation of waste.

PROJECT SCOPE

This project was conducted in two phases and involved the installation of approximately 5.26×10^4 square meters of exposed geomembrane over closed trenches used for the disposal of dry LLRW. NYSERDA decided to use a geomembrane cover because past efforts to improve the soil trench caps had only limited success.

Initial Phase. The initial project involved installation of a soil-bentonite slurry wall along the upgradient side of Trench 14, along with a geomembrane cover over two trenches. Very low-density polyethylene (VLDPE) was selected for the 1.21×10^4 square meters of cover. This project was initiated to halt a sudden, rapid rise in the leachate levels in these two trenches.
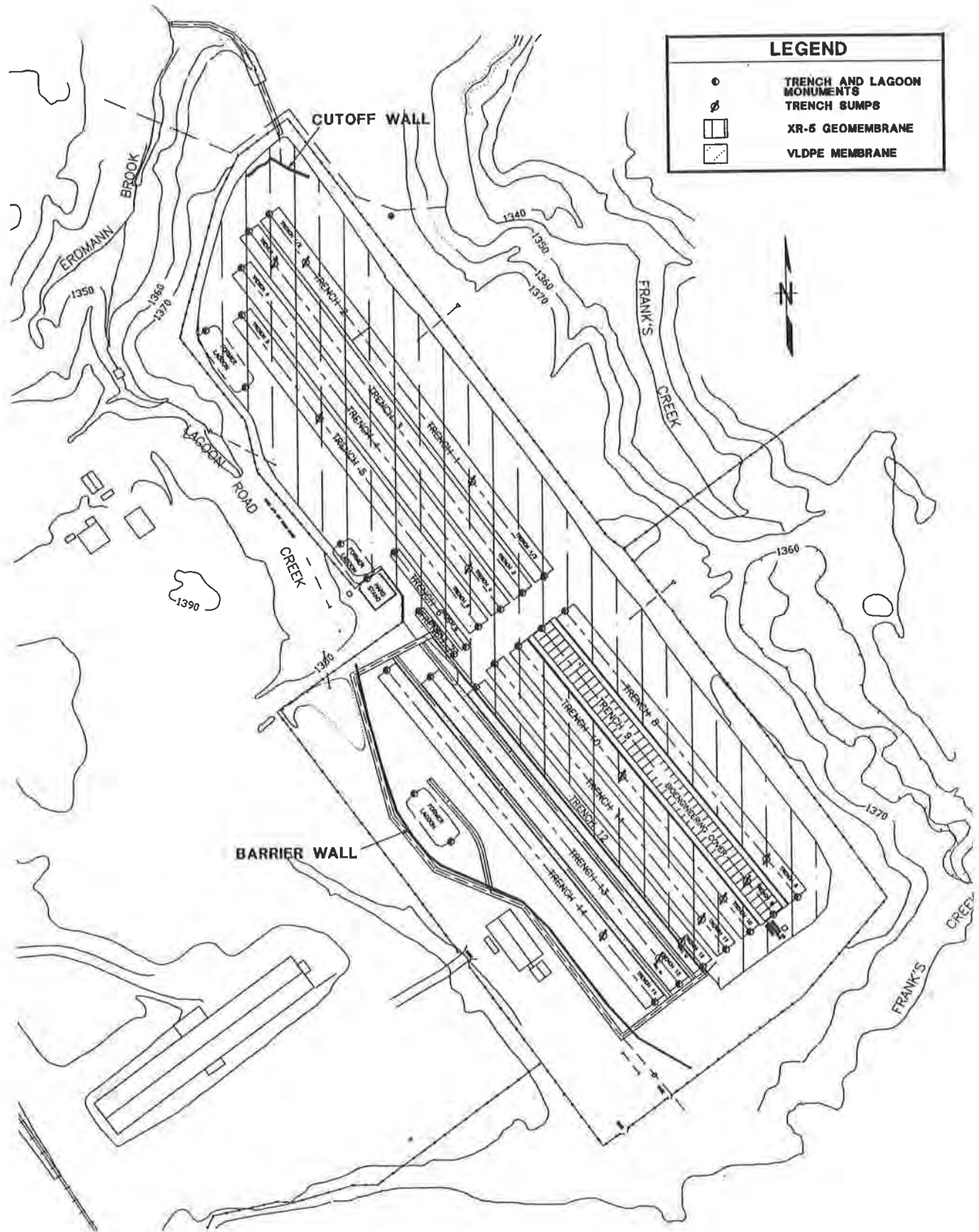
Figure 1. Map of Project Site

Because NYSERDA was not able to determine whether water was entering the trenches by infiltrating through the trench caps or via shallow groundwater flow through fractures or permeable soil lenses in the upper weathered till, the slurry wall and geomembrane cover represented a combined solution. The slurry wall was installed first, followed by installation of the VLDPE trench cover. The VLDPE cover extends from the center line (high point) of Trench 12 across Trenches 13 and 14 and over the slurry wall, terminating in a perimeter drainage collection/anchor trench (Figure 2). Additional vee-shaped wind anchors were installed in the drainage swales between trench caps. Surface preparation prior to installation of the geomembrane cover included stripping the grass from the trench caps, regrading areas to accommodate cover installation, and excavating the perimeter trench for the VLDPE. The perimeter anchor trench is filled with stone and perforated pipe that serves as a collection channel conveying precipitation runoff away from the trenches. The perforations limit the amount of runoff entering the drainage pipe and serve to limit the peak runoff.

After completion of the slurry wall in September 1992, there was an immediate decrease in the accumulation of leachate in Trenches 13 and 14. Trench levels stabilized after installation of the geomembrane cover in May 1993.

Additional Phase. Based upon the success of the initial phase and the fact that leachate levels continued to rise .05 to 0.1 meters per year in the other trenches, regulatory agencies requested that NYSERDA propose an additional interim measure(s) for the remaining trenches. Building upon the success of the initial project, NYSERDA proposed covering the remaining trenches with a geomembrane cover. A review of hydrogeologic reports and the groundwater monitoring program did not support installation of a slurry wall as part of this phase.
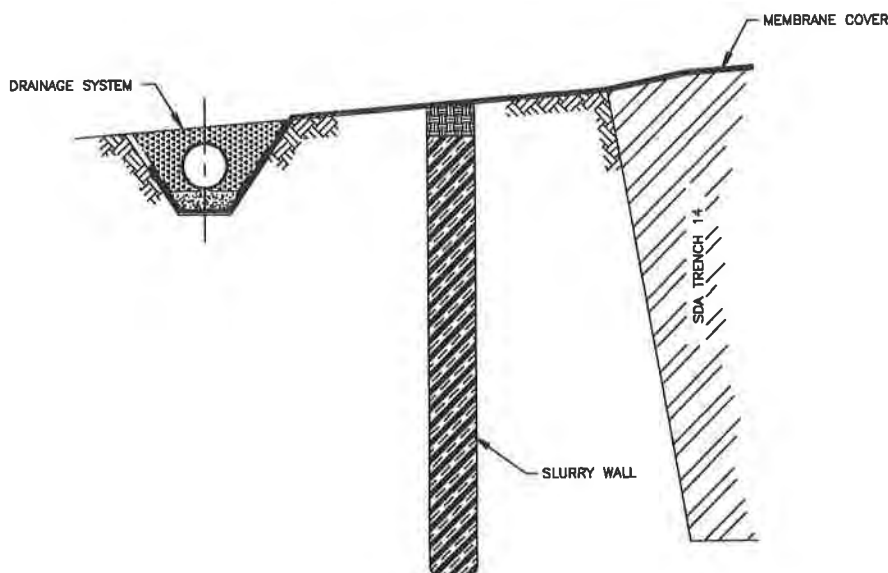
Figure 2. Cross Section Slurry Wall, Geomembrane Cover, and Drainage Collection/Anchor Trench

A design report (Reference 1) was prepared for this project. The report included a review of the materials and design features of the initial phase, with particular emphasis on reducing the amount of excavation. Although the upper soils are generally free of contamination, NYSERDA had, on occasion, encountered low levels of contamination from past operations when excavating in the SDA. Reducing excavation minimized the potential for having to manage contaminated soil, expedited construction, and decreased construction costs.

INITIAL PHASE DESIGN FOCUS

The geomembrane cover project is an interim measure to maintain the SDA in a safe condition while NYSERDA selects and initiates long-term closure or management plans. NYSERDA determined that a ten-year design life would allow sufficient time. By electing to use a single layer geomembrane exposed to the environment, unlike a standard landfill or RCRA cover, the design considerations were somewhat unique. Particular attention was given to material exposure, ways to anchor the geomembrane from wind uplift, and ways to manage the increased runoff.

Geomembrane Material Selection. VLDPE was selected over other geomembrane materials for its combined characteristics of flexibility, resistance to cold stress, resistance to tearing or stress cracking, and relative cost. It was believed that VLDPE could best survive the conditions of settlement and subsidence that can occur on the trenches. At that time, VLDPE was considered to have suitable resistance to ultraviolet light (UV). Although High Density Polyethylene (HDPE) has more UV resistance, it has a higher coefficient of expansion, more sensitivity to stress cracking, less elasticity, and a slipperier surface than VLDPE (NYSERDA staff must routinely walk across the cover to gather environmental data and inspect the surface). Polyvinyl Chloride (PVC) was rejected principally because of its poor weathering characteristics. Chlorinated polyethylene (CPE) was eliminated because potential abrasion from foot traffic could result in loss of strength, and delamination could occur as a result of temperature changes. Reinforced Ethylene Interpolymer Alloy (EIA-R) was also eliminated because it is less flexible and more expensive than VLDPE.

Wind Anchorage. The perimeter of the geomembrane cover could be secured using standard anchor trenches. Because the cover would remain exposed, additional anchorage was needed to prevent wind uplift. Sand bags or similar ballast such as tires were initially considered. Sand bags were eliminated because they were expected to deteriorate before the ten-year design life of the cover. Tires were eliminated due to aesthetic and environmental concerns such as visual appearance, potential breeding area for mosquitos, and potential disposal problems when they were no longer needed. A unique design was needed to provide required anchorage. It was solved using vee-shaped anchor trenches (Figure 3) excavated in the low areas between the trenches. After the cover was installed, sand was placed in the trenches to prevent wind uplift (Photo). The sand was covered with a piece of geomembrane to prevent erosion.
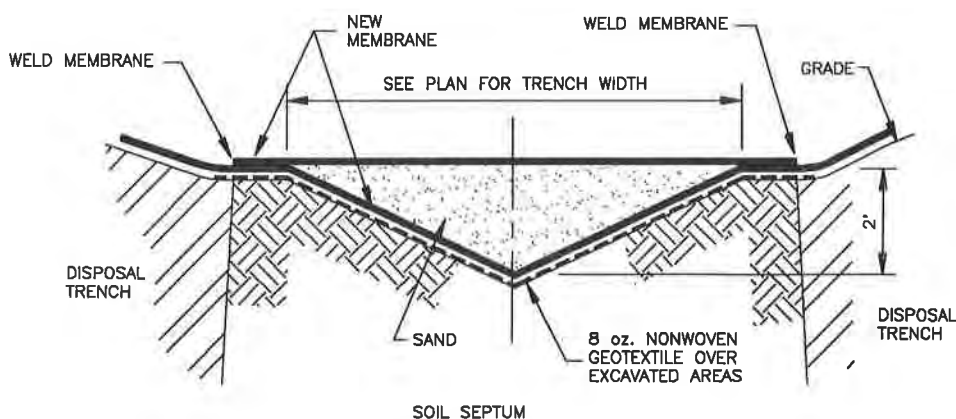
Figure 3. Vee-shaped Wind Uplift Anchor Trench Detail

Precipitation Runoff. Since covering the trenches with a geomembrane would increase the amount of surface water runoff, consideration had to be given to collecting and managing the runoff. Another consideration was to provide a cutoff trench to keep the ground or surface water from overtopping the slurry wall. To accomplish both objectives, the geomembrane perimeter anchor trench was designed as a combination anchor/runoff collection trench on three sides. The trench was designed to include a perforated pipe backfilled with stone to collect the water, instead of backfilling with excavated material. All runoff discharges through a single pipe into an adjacent stream.

REVIEW OF INITIAL PHASE

Design features and performance of the initial phase were reviewed during design of the additional phase. The initial performance of the VLDPE material, the effectiveness of the runoff collection system, and the performance of the vee-shaped wind anchor were the key features reviewed. These were evaluated with particular emphasis on NYSERDA's expectation that minimizing removal of grass and excavation of soil would limit the potential to uncover and manage contaminated soil, reduce construction time, and limit the amount of soil exposed to erosion.

Cover Performance. After completion of the initial phase, the leachate levels in the affected trenches immediately stabilized. Monthly inspections did not reveal any holes, signs of damage, and degradation for the two-year period after installation of the VLDPE. Two concerns arose during these monthly inspections and routine monitoring of the wells. Expansion and contraction of the cover significantly stressed the booted protrusions through the cover and broke two, four-inch PVC monitoring wells. Also, the smooth VLDPE surface is slippery when wet, frosty, or snow covered, resulting in a worker safety concern.

In addition, the VLDPE material was evaluated against original material specifications through a laboratory testing program. Five samples of the two-year old cover were collected and tested for stress, strain, and puncture resistance. Each sample was tested five times for each parameter and an average value was calculated. Test results (Table 1) of the VLDPE installed during the initial phase exceeded new material specifications in all cases.

Table 1. Average Values of Test Results for VLDPE After Two Years of Exposure

PROPERTY TESTED (ASTM METHOD)	AVERAGE VALUE TWO-YEAR EXPOSURE	NEW MATERIAL SPECIFICATION
Tensile Strength at Break (ASTM D638)	351/358 Newtons/centimeter (N/cm) (Machine/Transverse Dir.)	174 N/cm
Elongation at Break (ASTM D638)	977/979 % (Machine/Transverse Dir.)	780 %
Tear Resistance (ASTM D1004)	107/107 Newton (N) (Machine/Transverse Dir.)	71 N
Puncture Resistance (ASTM D4833)	356 N	267 N

Runoff Collection System. The runoff collection system was examined at irregular intervals during and following storms. Water effectively runs off the cover without any notable ponding. The depth of flow in the runoff collection and discharge pipes was observed to be less than ten percent of the diameter. Rip-rap treatment at the outfall has prevented any notable erosion. Thus, the system functions well below its design capacity.

<u>Wind Anchor Trenches.</u> The vee-shaped wind anchor trenches were observed during periods of locally high winds (30-50 miles per hour). While there was some lifting of the geomembrane over the sand in the vee-shaped wind anchors, no lifting or flapping of the VLDPE cover was observed. The wind anchor trenches functioned effectively. The challenges with these wind anchors are placing the sand during construction due to the confined working area and access when the wind anchor is surrounded by geomembrane, and the inability to use a wedge welder to make the long welds along the sides of the cover over the sand.

<u>Other Observations.</u> Surface preparation for the initial phase included stripping the trenches of grass and topsoil so that the geomembrane could be placed directly upon the bare silty-clay soil. After the trenches were stripped, wet, cold weather developed and installation of the geomembrane had to be delayed until suitable spring weather arrived. Precipitation on the cover during the fall and winter exposed an abundance of small, sharp shale-fragments. As a result, it was determined that a geofabric should be placed beneath the VLDPE to reduce the chances of a puncture.

Another element considered during design of the initial phase was gas generation from decomposition of LLRW in the trenches and whether venting would be needed. Based upon historical knowledge, it was decided that gas vents were not needed; however, flap vents could easily be added at a future time if a problem developed. No buildup of gas has been observed beneath the cover.

<u>Conclusions and Recommendations.</u> Based upon the performance of the exposed VLDPE cover and the experience gained, the following conclusions and recommendations were developed for design and installation of the additional phase:

1. Thermal expansion needs to be considered when selecting the cover material.
2. Suitability for walking needs further consideration when selecting the cover material and/or designing the cover.
3. The vee-shaped wind anchor trench design is effective.
4. The runoff collection system design parameters need additional consideration due to the increased area being covered.
5. Gas generation beneath the VLDPE has not been a problem.

ADDITIONAL GEOMEMBRANE COVER PROJECT DESIGN

Following the success of the initial phase, the regulatory agencies concurred with NYSERDA's recommendation to install a geomembrane cover on the trenches that still had a grass surface. The area to be covered by this phase was over three times the area of the initial phase. Thus, additional considerations and objectives were established, primarily to limit peak runoff and to minimize the amount of excavation.

<u>Limiting Excavation.</u> As part of the design for the additional cover, NYSERDA required that excavation be minimized and that surface preparation be limited. The reasons for limiting excavation were to:

- Minimize the potential for uncovering and managing contaminated soil;
- Make the trench covers less vulnerable to weather during construction;
- Limit the preparation effort and the amount of sod and topsoil to be disposed of; and
- Reduce the overall project cost.

As a result, NYSERDA decided to place the geomembrane directly on top of the grass. However, placing the geomembrane directly on the grass required reconsideration of the geomembrane material selection (see section on Geomembrane Material Selection).

Placing the geomembrane directly on the grass reduced the potential for excavating and managing contaminated soil. Project construction was expedited by limiting the area of soil and sod to be checked for contamination. An overland radiation survey was conducted in advance of construction to identify areas of surface or near-surface contamination. This allowed design changes to avoid contaminated areas prior to construction, thereby saving time and negotiations during construction. Minimizing the earthwork area reduced the expanse that had to be surveyed for radiation during construction, which would slow progress. Minimizing excavation also eliminated the need to find a location to dispose of all the soil and sod.

In the initial project, excavation was necessary for the wind anchors and the drainage collection system. Considering the objective of minimizing the amount of excavation in the SDA, these two areas were examined for ways to minimize the amount of excavation in the SDA.

Following evaluation of the wind anchors, the standard rectangular perimeter anchors were retained. It was also decided to use the same vee-shaped trench design used between the trenches in the initial phase to anchor the geomembrane from wind uplift. To provide additional anchorage needed to prevent wind uplift in other low areas, sand was piled in a mound on the liner, then covered with a strip of geomembrane similar to the vee-anchors. Mounding the sand meant no excavation would be required.

The runoff collection system for the initial project required substantial excavation. To minimize excavation for the additional cover, earthen berms were constructed to form five, above grade, runoff detention areas adjacent to the trenches. Each detention area discharges to a location that existed prior to construction of the detention areas. The geomembrane cover would be extended through the detention areas to act as a liner, virtually eliminating the possibility of water in the detention areas infiltrating into the adjacent trenches.

Limiting Peak Runoff. A key part of the design was to establish a drainage and erosion plan that would limit peak runoff rates at or below those prior to installation of the cover. Also, erosion control measures at the five discharge points (especially in the northeast corner of the site) were required since active erosion existed at nearly all of the locations where water discharged from the trenches.

Since the cover has a design life of ten years, a conservative, 25-year, 24-hour storm was used for the design rainfall. A comparison of design discharges from the grass-covered trenches with those from the geomembrane, with and without the detention areas, is shown below in Table 2.

Table 2. Detention Area/Peak Runoff (Cubic Meters per Second)

Detention Area/Condition	Grass	Geomembrane (No Detention)	Geomembrane With Detention
1) S. End Trench 10	6.8	15.1	6.8
2) E. Side Trench 8	13.6	34.1	12.1
3) E. Side Trenches 1/2	3.4	6.8	2.6
4) NE Corner Trench 2	8.5	17.0	8.3
5) W. Side Trench 5	8.5	17.0	6.0
Totals	40.8	90.0	35.8

While the initial phase drainage collection system worked very well at reducing peak flow rates, minimizing excavation was the overriding factor in the decision to construct runoff detention basins as described above.

Design of the detention basins included a smaller three- or four-inch pipe in the bottom of the basin to limit discharges from smaller, more frequent storms, and a larger overflow pipe to drain the less frequent, but more severe storms after detention requirements were met (Figure 4 and Photograph 1).
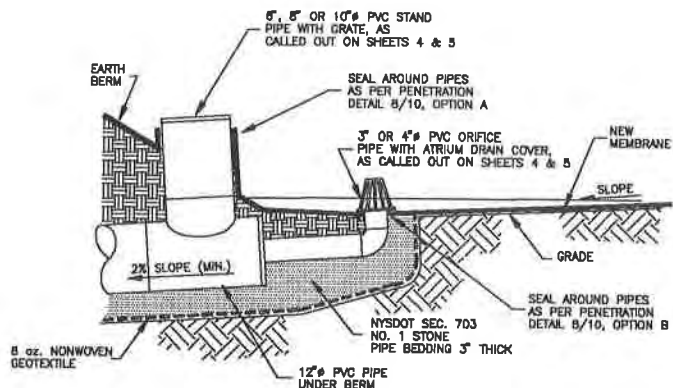
Figure 4 and Photograph 1. Detention Basin Discharge System

Geomembrane Material Selection. After the review of the initial phase, it was necessary to reconsider geomembrane materials. Placing the geomembrane on the grass would require a geofabric beneath the geomembrane, or the material must have a high puncture resistance. Geosunthetic materials were evaluated for:

1. UV resistance - Anticipated life span (ten-year minimum)
2. Puncture resistance
3. Coefficient of thermal expansion
4. Safety and maintenance
5. Compatibility (for welding to VLDPE)
6. Constructability - Additional requirements
7. Cost

Eight different geosynthetics were considered. The list included VLDPE, high density polyethylene (HDPE), linear low density polyethylene (LLDPE), coex seal (core of VLDPE sandwiched by HDPE), chlorosulfonated polyethylene (CSPE), reinforced polypropylene (R-PP), reinforced ethylene interpolymer alloy (EIA-R), and a geosynthetic clay liner (GCL).

After gathering information from the various manufacturers, suppliers and installers, an initial screening process eliminated some of the alternatives considered. Although VLDPE had initially proven to be effective in the initial phase, it was eliminated from further consideration because the resin used to produce this material had been taken off the market. Likewise, coex seal was eliminated because the resin for the VLDPE core was no longer available. CSPE and LLDPE were also eliminated due to their low resistance to UV exposure.

The remaining geomembranes (HDPE, R-PP, EIA, and GCL's) were evaluated in more detail. GCL's need to be installed under a soil cover (preferably several feet) to preserve their permeability properties, since there is a loss of permeability in the dried or desiccated clay. If covered, UV resistance is not a factor in their long-term effectiveness. If punctured, GCL's are somewhat self-sealing, depending on the amount of confining stress placed on the clay. The self-sealing capability is also dependent on the moisture content. GCL's could lose the ability to provide the desired impermeable barrier if the clay desiccates during dry summer months.

By planting grass on the soil cover, GCL's would have the least slippery surface of the materials being considered, other than textured HDPE. GCL's would also have only a physical bond to the VLDPE. Although wind anchors are not required, the requirement to cover the GCL with soil and grass significantly affects the cost of the project. In addition, this project is an interim measure. Installing a GCL with a soil and grass cover could be perceived by the public as a permanent closure, bypassing their input to the closure process. GCL's were not selected because of the cost to cover the geotextile with soil, our inability to inspect the integrity of the cover, and the likely perception that this would become a permanent cover.

HDPE has a high resistance to UV, a relatively low puncture resistance (Figure 5), and a high coefficient of thermal expansion of 6.7 x 10 E-4. Although HDPE is slippery, a textured surface is available at an added cost. HDPE could be welded to VLDPE, but HDPE is quite stiff, lacking the elasticity to conform to the topography (i.e., vee-shaped wind anchors) without a special approach.
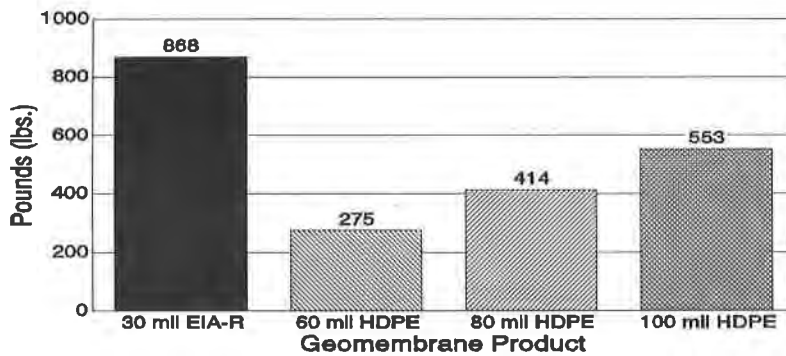
Figure 5. Puncture Resistance (lbs.) of EIA-R Versus HDPE (ASTM D751:Ball Tip)

R-PP is a laminate with a very high UV resistance, a very high puncture resistance, and a low thermal expansion coefficient of 7.2 x 10 E-5. The material is less slippery than HDPE because there is some texture created by the reinforcement. R-PP cannot be bonded to VLDPE, other than physically.

EIA-R is a coated fabric with a very high UV resistance, the highest puncture resistance, and a very low thermal expansion coefficient of 8 x 10 E-6 (Figure 6). EIA-R is similar to R-PP in slipperiness, gaining some texture from the embedded fibers. EIA-R cannot be bonded to VLDPE, other than physically.
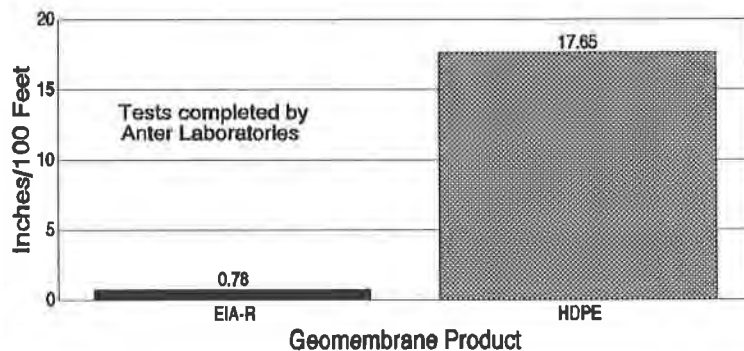
Figure 6. Thermal Expansion (Inches/100 Feet/150 °F Change) of EIA-R Versus HDPE (ASTM E228)

Although the properties of EIA-R met our criteria better and EIA-R has been in service for over 20 years, (as opposed to the four years R-PP has been used as a geomembrane), both EIA-R and R-PP were specified as acceptable alternatives for the geomembrane cover material. The R-PP was included to enhance competition and encourage a better price.

CONSTRUCTION EXPERIENCE

The contractor selected to construct the additional geomembrane cover elected to use EIA-R (8130 XR-5) manufactured by Seaman Corporation. Specifications required that the geomembrane be fabricated in large panels to minimize the number of field seams. This was particularly important because the construction schedule showed that panel installation would occur in the fall when wet, cold weather can hamper field work. Construction started in August 1995.

The XR-5 material was fusion-welded in the factory to make 29 panels, which varied in width from 10 meters to 17 meters and in length from 20 meters to 110 meters. Over half of the panels were 17 meters wide and all but two were over 93 meters long. The panels arrived folded on pallets and were deployed using a track-mounted hydraulic backhoe. The contractor had difficulty getting the geomembrane to uniformly conform to the bottom of the vee-shaped wind anchors. As sand was placed on the geomembrane in the vee-shaped depressions, some shifting of geomembrane occurred, and in some areas the geomembrane bridges a depressed area.

Placing sand in the vee-shaped wind anchors, which are located in the middle of the cover, remains a logistical problem. Without operating equipment on top of the geomembrane, there is no easy way to move the sand to the wind anchors when they do not extend to the edge of the geomembrane. One method that worked to minimize this situation, when the wind anchor trenches were perpendicular to the panel seams, was to leave the end panels until last. However, when the panels were placed perpendicular to the wind anchor trenches, they extended across more than one vee-shaped wind anchor. As sand was placed in one wind anchor trench the panel shifted, making it difficult to keep the geomembrane conforming to the ground surface, as described in the previous paragraph.

Several different methods for hauling the sand were tried. Skid steer loaders were used, driving on the previously placed sand. Although this was a slow process, it was fairly successful when the sand was moist. But, when the sand dried out, it became impractical. A rubber-tired, front-end loader with a side dump bucket was also used, driving alongside the wind anchor trench on several layers of geofabric cushioning (Photograph 2). This seemed to work relatively well without noticeable damage to the geomembrane beneath.

Where only minor amounts of sand were needed, six-wheel all-terrain vehicles (ATV's) with dump backs were used to move sand to these locations. They operated directly on the geomembrane. Where a particular route was used many times, sand from the tires and spillage caused some noticeable wear on the surface of the XR-5.

Generally, the mounded wind anchors were left until the end. Thus, sand bags used during geomembrane installation were available and stacked to form the mounded wind anchor. This created a neater looking wind anchor versus dumped sand, which was difficult to handle.

A problem with installing the wind anchor covers in the middle of the geomembrane was attaching the cover to the geomembrane. The attachment required two bonds, which cannot be made using a wedge welder. XR-5 had to be bonded using a leister while the VLDPE had to be extrusion welded, which slowed production.

Photograph 2. Loader Placing Sand in Vee-Shaped Wind Uplift Anchor

Where the XR-5 met the VLDPE, it was lapped over the VLDPE and a mound of sand was placed approximately four feet in from the edge. Instead of welding a separate panel over the sand (like the other mounded wind anchors), the edge of the XR-5 panel was folded over the sand to form a teardrop-shaped wind anchor and leistered to itself (Figure 7).

Figure 7. Teardrop Anchor Along XR-5/VLDPE Interface

To boot the flush bottom drain in the runoff detention areas, an inverted boot was developed. The drain line was installed, backfilled with sand, and was left protruding slightly above grade until the geomembrane panel was installed. Then a boot was made and attached to a coupling (Photograph 3). The sand around the vertical drain was excavated and the pipe was cut off at the appropriate depth. Then the coupling was attached to the pipe with the boot facing down. The area around the coupling and boot was backfilled with sand, and the boot was welded to the geomembrane, forming a neat, flush junction (Photograph 1).

Photograph 3. Underside of Inverted Boot Attached to Coupling

CONCLUSIONS

Using exposed geomembrane as an interim cover over radioactive waste disposal trenches required unique design and construction considerations. Particular attention was paid to selecting the geomembrane materials, anchoring the geomembrane from wind uplift, and managing the increased runoff from urbanizing the area. However, the result is that the geomembrane covers have significantly reduced leachate accumulation in the disposal trenches while requiring minimum maintenance.

Areas where additional improvement could be made are in the design and construction of wind anchors in low areas in the middle of the geomembrane and in providing a better walking surface in frosty or snow-covered conditions.

REFERENCES

Dames & Moore, (1995) "Design Report, Installation of Additional Geomembrane Covers, State-Licensed disposal Area, Western New York Nuclear Service Center, West Valley, New York."

INSTALLATION OF GEOSYNTHETIC CLAY LINERS AT CALIFORNIA MSW LANDFILLS

MICHAEL SNOW
GEOSYNTEC CONSULTANTS, USA
KRZYSZTOF S. JESIONEK
GEOSYNTEC CONSULTANTS, USA
EDWARD KAVAZANJIAN JR.
GEOSYNTEC CONSULTANTS, USA
R. JEFFREY DUNN
GEOSYNTEC CONSULTANTS, USA

ABSTRACT

The California regulations for liner systems at municipal solid waste (MSW) landfills require that alternatives to the prescriptive federal Subtitle D liner system have a containment capability greater than that of the prescriptive system. Regulators may also require a demonstration that use of the prescriptive system is burdensome prior to approval of an alternative liner design. This paper presents seven case histories of the design and installation of geosynthetic clay liners (GCL) as an alternative to the low-permeability soil component of the prescriptive Subtitle D composite liner system at MSW landfills in California. These case histories cover GCLs from different manufacturers and landfill sites with a wide range of conditions including canyon landfills with slopes as steep as 1H:1V.

INTRODUCTION

Geosynthetic clay liners (GCLs) are now widely used as an alternative to traditional compacted clay liners (CCLs) in both liner and cover systems. There are two types of GCLs currently available on the market: (i) geotextile-backed GCLs; and (ii) geomembrane-backed GCLs. The primary advantages of the use of GCLs over CCLs in liner systems include: (i) availability; (ii) resistance to desiccation; (iii) rapid and safe construction, particularly on steep slopes; and (iv) increased uniformity of material quality. Secondary advantages of the use of GCLs include: (i) reduced construction impacts (e.g., dust, noise); (ii) increased airspace; and (iii) reduced production of consolidation water (of particular importance in double liner systems).

The application of GCLs at landfills in California has identified several issues related to the permitting, design, and construction of GCL liner systems. These include:

- On what basis should the containment capability of a GCL be compared to a CCL?
- What shear strength should be used for the GCL in stability analyses?

- What quality assurance/quality control conformance testing and monitoring should be performed?

After a brief review of the regulatory requirements for MSW liner systems in California and of the issues identified above, this paper reviews seven GCL case histories from California, and discusses current practice with respect GCL permitting, design, and construction.

CALIFORNIA REGULATIONS

Federal criteria for liner systems at MSW landfills are contained in Part 258 of Title 40 of the Code of Federal Regulations (referred to hereafter as Subtitle D) which became effective on October 1993. In these federal regulations, two types of liner system designs are allowed: (i) a site-specific design that meets a performance standard; or (ii) a prescriptive minimum standard. The prescriptive minimum standard includes a 0.6-m thick CCL overlain by a geomembrane. The CCL is required to have a hydraulic conductivity no greater than 1×10^{-9} m/s. The geomembrane is to be overlain by a leachate collection and removal system (LCRS) which controls liquid head to a value no greater than 0.3 m.

The State of California amended existing liner system regulations for MSW landfills to reflect the Subtitle D requirements. These amendments further addressed the federal "site-specific" alternative design provisions by allowing the use of alternative liner system designs "...where the performance of the alternative composite liner's components, in combination, equal or exceed the waste containment capability of the prescriptive design."

CASE HISTORIES

Lopez Canyon Sanitary Landfill Area "C"

The Lopez Canyon Sanitary Landfill is located about 80 km northwest of Los Angeles, California. The construction of the Disposal Area "C" liner system was divided into two phases, Phases I and II. The lined area of Disposal Area "C" is approximately 12.3 ha in plan, with about 5.3 ha on the base and about 7.0 ha on the side-slope. The site is a canyon landfill with side slopes as steep as 1H:1V (Figure 1) which are over 90-m high (Snow et. al; 1994b). Construction for Phase I began on December 1992 and construction of the Phase II liner system was completed in June 1994. An alternative GCL composite liner was approved by state regulators for the side-slopes based on a demonstration of its superior liquid containment capability (Snow et al., 1994a) in comparison to the Subtitle D prescriptive composite liner.

Construction of the Phase I side-slope liner system included (top to bottom): (i) Trevira 1145, 410 g/m^2 nonwoven geotextile; (ii) Gundle (Gundnet), 5-mm thick geonet; (iii) National Seal Company "Friction Seal," 2.0-mm thick smooth/textured high density polyethylene

(HDPE) geomembrane; and (iv) James Clem Corporation Claymax "Shear Pro" geosynthetic clay liner.

Figure 1 - Lopez Canyon Sanitary Landfill Area "C" side-slope GCL installation

The "Shear Pro" GCL includes two 108 g/m^2 woven geotextiles stitched together with a layer of bentonite in between. Construction of the Phase II side-slope liner system included (top to bottom): (i) Synthetic Industries "T1201," 410 g/m^2 nonwoven geotextile; (ii) SLT North America "Hypernet," 5-mm thick geonet; (iii) SLT North America "Hyper-Flex," 2.0-mm thick smooth/textured HDPE geomembrane; and (iv) Colloid Environmental Technologies Company "Bentomat SS," geosynthetic clay liner. The "Bentomat SS" GCL includes a 112 g/m^2 slit film woven geotextile and a 203 g/m^2 needlepunched nonwoven geotextile. Both geotextiles are needlepunched together with a layer of bentonite in between. In both phases, the GCL was underlain by a shotcrete veneer to provide an even surface for support of the GCL.

Approximately 20,970 m^2 of "Shear Pro" and 71,940 m^2 of "Bentomat SS" were delivered to the site. Twenty-nine samples of GCL were collected for conformance testing. A conformance test series consisted of dry mass per unit area (ASTM D 3776) and hydraulic conductivity (ASTM D 5084, modified). Twenty-two of the GCL samples had hydraulic conductivities between 1.0 x 10^{-11} and 2.5 x 10^{-11} m/s. The hydraulic conductivity was measured under confining pressures ranging from 36 to 360 kPa and hydraulic gradients ranging from 9 to 330. The dry mass of bentonite per unit area varied from 3,812 to 4,301 g/m^2 for Phase I and

from 4,301 to 5,572 g/m^2 for Phase II. The lower Phase I dry mass per unit area values results were reflected in higher hydraulic conductivity values for five (5) samples which failed to meet the specified maximum value of 5 x 10^{-11} m/s.

Eight interface shear conformance tests (ASTM D 5321) were performed for Phase II with the GCL hydrated and the woven geotextile component in contact with the textured geomembrane. The tests were performed at a displacement rate of 1 mm/min. and included all components of the liner system in a "sandwich". The use of a sandwich allowed shear to occur along the weakest plane bieng either along an interface or internally within the GCL. In each test the failure occurred at the geonet/smooth geomembrane interface. This indicates that the peak internal shear strength of the GCL and the GCL/textured geomembrane interface peak shear strength were higher than those measured for the geonet/smooth geomembrane interface. Peak shear strength friction angles ranged from 10 to 12 degrees and residual strength friction angles ranged from 10 to 11 degrees. A similar test for the Phase I materials resulted in a peak friction value of 7 degrees with a residual friction value of 5 degrees. Apparent adhesions for all tests ranged between 0 and 15 kPa. A site inspection performed following the January 1994 Northridge earthquake indicated that the composite liner system performed well with no apparent damage from the earthquake (Kavazanjian, 1994).

Shafter-Wasco Landfill Module 2

The Shafter-Wasco Landfill is located approximately 4.4 km west of the City of Shafter, California. The Shafter-Wasco Landfill is an "area fill" landfill with 3H:1V side slopes about 6-m high. The lined area of Module 2 is approximately 8.9 ha in plan, with about 7.1 ha on the base and 2.2 ha on the side slope. Geosynthetics installation began in April 1995 and was completed in June 1995. Construction of Module 2 included a GCL composite liner on the base and side slopes comprised of (top to bottom): (i) Synthetic Industries "1001," 340 g/m^2 nonwoven geotextile; (ii) Synthetic Industries "601," nonwoven 205 g/m^2 geotextile on the side-slopes only; (iii) Poly-Net "3000" geonet; (iv) National Seal Company "Friction Seal" 1.5-mm thick smooth/textured HDPE geomembrane; (v) Albarrie Naue, Ltd. "Bentofix NS Enhanced" geosynthetic clay liner; and (vi) 0.45-m thick select subgrade layer with a maximum hydraulic conductivity of 1.0 x 10^{-7} m/s. The "Bentofix NS Enhanced" GCL consisted of a 270 g/m^2 needlepunched nonwoven geotextile and a 110 g/m^2 woven geotextile needlepunched together with a layer of bentonite in between. The use of an alternative GCL composite liner system on the base of the landfill was approved by the regulators contingent on the presence of the underlying select subgrade layer. The select subgrade layer had specified grain size requirements, including at least 20 percent by weight finer than the No. 200 sieve, to protect against bentonite migration from the GCL into the subgrade.

Approximately 96,350 m^2 of "NS Enhanced" GCL was delivered to the site. In all, 21 samples of GCL were collected for thickness (ASTM D 1777), dry mass per unit area (ASTM D 3776), hydraulic conductivity (ASTM D 5084, modified), and interface shear

(ASTM D 5321) conformance testing. The dry mass of bentonite per unit area ranged from 3,813 to 5,279 g/m^2, thickness ranged from 5.8 to 7.9 mm, and hydraulic conductivity ranged from 5.1 x 10^{-12} to 4.7 x 10^{-11} m/s at a confining pressure of 36 kPa. The average hydraulic conductivity was 1.5 x 10^{-11} m/s.

Twenty-five interface shear conformance tests were performed with the GCL hydrated and sheared at normal stresses ranging from 36 to 144 kPa. For each test, geosynthetics were obtained from different rolls on-site. The first two tests were performed at different displacement rates, 1 and 0.0025 mm/min., with the nonwoven geotextile side of the GCL against the silty sand select subgrade. The slower test gave a higher peak friction angle (30 versus 23 degrees) but a similar residual friction angle (21 degrees) in comparison to the faster test. Two additional (2) tests were then performed at the same displacement rates with the woven geotextile side of the GCL in contact with the textured geomembrane. In this case both tests had similar interface shear strengths with a peak friction angle of 23 degrees and residual friction angles of 16 and 18 degrees. The reduction from peak to residual strength at the GCL/textured geomembrane interface is consistent with previous observations (Byrne, 1994).

The remaining tests were divided into two groups. In both groups, the woven geotextile side of the GCL was placed in contact with textured geomembrane. The first group consisted of twelve (12) tests with the select subgrade, GCL, and smooth/textured geomembrane. The range of shear strengths obtained is presented on Figure 2. For all tests, the initial failure occurred at the GCL/select subgrade interface with peak friction angles ranging from 16 to 22 degrees. However, as the sample was sheared, the failure plane (the plane along which displacement was occurring) transitioned to the GCL/textured geomembrane interface, with residual friction angles ranging from 12 to 16 degrees. The second group of nine (9) tests included all components of the liner system in a "sandwich" (i.e., select subgrade/GCL/geomembrane/geonet/340 g/m^2 geotextile). In these tests, failure occurred at the geonet/smooth geomembrane interface with peak and residual friction values ranging from 11 to 14 degrees.

Puente Hills Landfill Phase 1B

The Puente Hills Landfill is located in Whittier, California. Phase 1B is comprised of a canyon with a long narrow floor and side slopes on three sides. The lined area of Phase 1B is approximately 6.9 ha in plan, with about 1.7 ha on the base and about 5.2 ha on the side-slopes. The lined side-slopes vary from 3.25H:1V to 1.5H:1V with heights up to 60 m (Figure 3). Geosynthetics installation began in March 1996 and was completed in June 1996.

The components of the Phase 1B side-slope liner system include (from top to bottom): (i) Amoco 4512, 410 g/m^2 nonwoven geotextile on the 1.5H:1V slopes; (ii) JDR Enterprises, Inc. (JDR) J-D Rain 200 N, 5-mm thick geonet on the 1.5H:1V slopes; (iii) JDR Enterprises, Inc. J-D Rain 200 FNF, 410 g/m^2 geotextile / 5-mm thick geonet / 270 g/m^2 geotextile - geocomposite on the 3.25H:1V slopes; (iv) Serrot Corporation HST S/S 2-mm thick
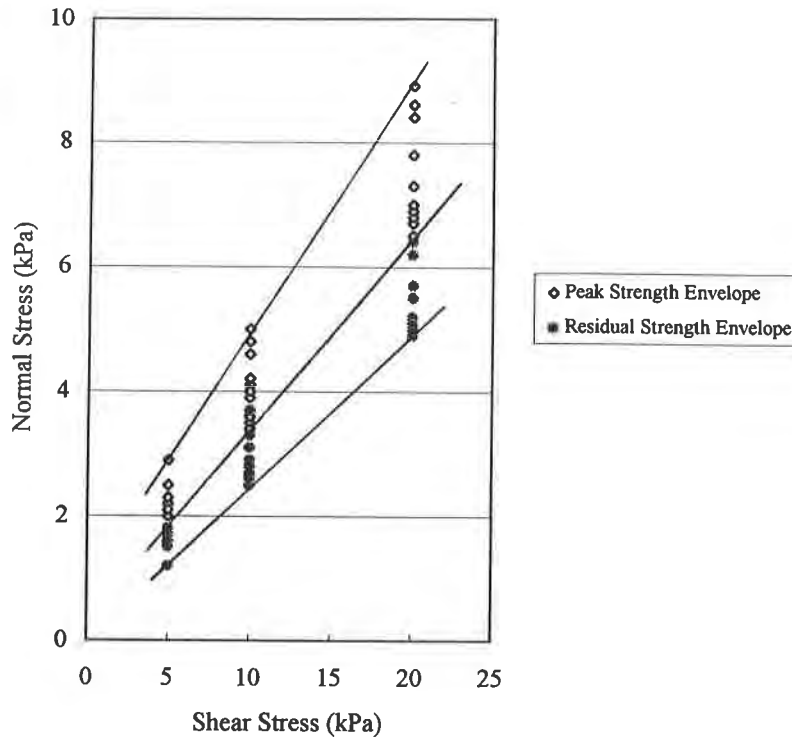
Figure 2 - Shafter-Wasco Landfill Module 2 GCL interface shear strengths

smooth/textured HDPE geomembrane on the 1.5H:1V slopes; (v) National Seal Company 2-mm thick textured/textured HDPE geomembrane on 3.25H:1V slopes; (vi) Colloid Environmental Technologies Company (CETCO) "Bentomat DN" geosynthetic clay liner; and (vii) Polyflex, 0.75- to 1.0-mm thick textured/textured HDPE geomembrane moisture barrier. The moisture barrier was used to control potential hydration of the GCL thereby ensuring that higher shear strengths could be mobilized for the GCL. The "Bentomat DN" included two 203 g/m^2 needlepunched nonwoven geotextiles. The GCL geotextiles were needlepunched together with a layer of bentonite in between.

Approximately 66,980 m^2 of the "Bentomat DN" was installed in Phase 1B. Thirty-two (32) samples of GCL were collected for conformance testing. The GCL was tested for dry mass per unit area (ASTM D 3776) and hydraulic conductivity (ASTM D 5084, modified). The dry mass of bentonite per unit area ranged from 4,300 to 5,130 g/m^2 while the hydraulic conductivity ranged from 6.1 x 10^{-12} to 5 x 10^{-11} m/s at a confining pressure of 144 kPa.

Three interface shear conformance tests were performed under dry conditions and sheared at a displacement rate of 1 mm/min. at normal stresses ranging from 200 to 805 kPa. These tests included the moisture barrier/GCL/2-mm thick Serrot geomembrane in a "sandwich". The nonwoven geotextile component of the GCL was in contact with the textured side of the 2-mm thick Serrot geomembrane. Peak and residual failure occurred along the GCL/2-mm thick Serrot

geomembrane interface. Peak friction ranged from 21 to 26 degrees with peak apoparent adhesions ranging from 20 to 39 kPa. Residual friction ranged from 21 to 22 degrees with residual apparent adhesions ranging from 1.8 to 21 kPa.
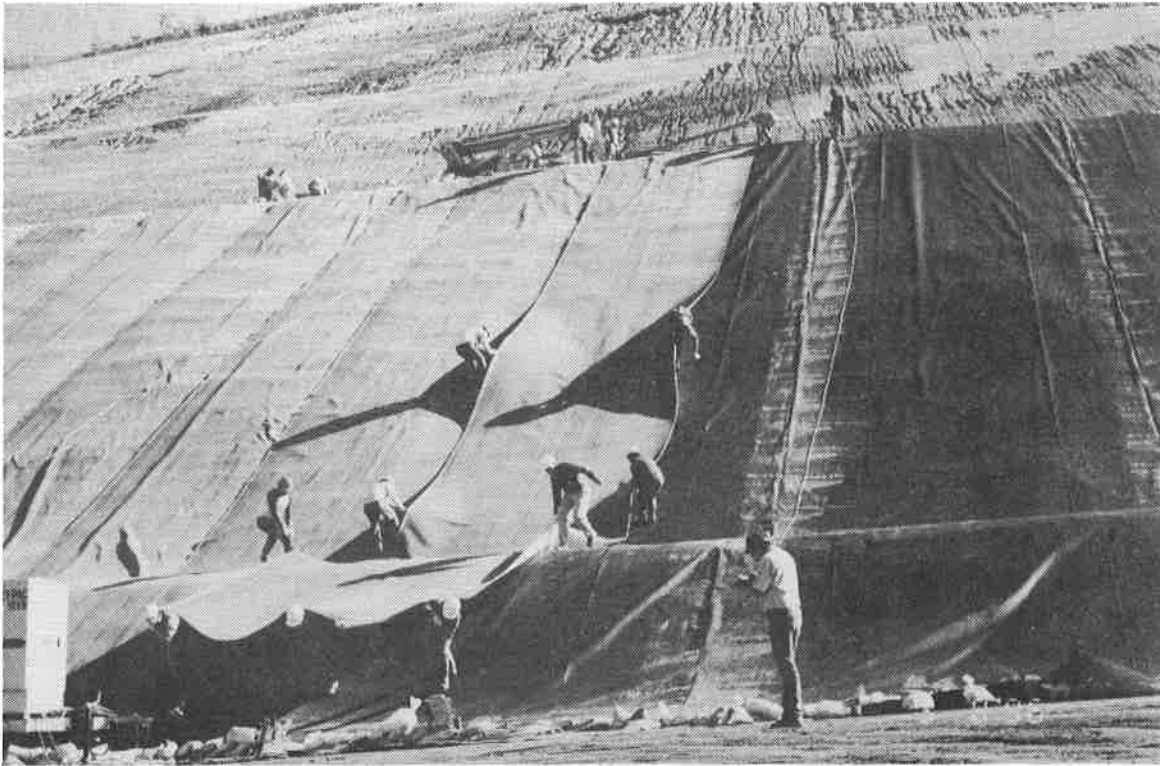
Figure 3 - Puente Hills Landfill Phase 1B GCL installation.

Sunshine Canyon Landfill County Extension Phase I Stage 1

The Sunshine Canyon Landfill spans the border between the City and County of Los Angeles at the northern end of the San Fernando Valley. The Phase I of the County Extension lies entirely within Los Angeles County. Phase I is divided into two stages and is characterized by narrow canyons with side slopes of 1.5H:1V lined to heights of over 20 m (see Figure 4). The site is in an active seismic region and presented several slope stability challenges during the design stage. The lined area of Stage 1 includes about 1.7 ha on the base and about 2.0 ha on the side slopes. Construction of the Stage 1 composite liner began in May 1996 and was completed in July 1996. The Stage 1 side-slope composite liner system included (top tobottom): (i) Synthetic Industries 1701, 340 g/m^2 of nonwoven geotextile; (ii) GSE Lining Technology, Inc. (GSE) "Gundnet," 5-mm thick geonet; (iii) GSE "Hyperflex FF," 1.5-mm thick smooth/textured HDPE geomembrane; and (iv) GSE "Gundseal" geosynthetic clay liner with 1.5-mm thick HDPE geomembrane backing placed against the subgrade.

Approximately 37,065 m^2 of "Gundseal" were installed in Stage 1. Eight (8) GCL samples were collected for conformance testing. The GCL was tested for dry mass per unit area (ASTM D 3776), hydraulic conductivity (ASTM D 5084, modified), free swell (USP/NF/XVII), and puncture strength (ASTM D 4833). The dry mass of bentonite per unit area ranged from 4,843 to 7,355 g/m^2 while the hydraulic conductivities ranged from 1.45 x 10^{-12} to 3.24 x 10^{-12} m/s at a confining pressure of 36 kPa. The hydraulic conductivity tests were performed by placing controlled slits in the geomembrane backing to isolate the bentonite component of the GCL.

Figure 4 - Sunshine Canyon Landfill Phase I Stage 1 GCL installation

In addition, two interface shear conformance tests were performed under partially hydrated conditions at a displacement rate of 1 mm/min in accordance with ASTM D 5321. Partial hydration was obtained by creating a defect in the GCL geomembrane backing and saturating the sample for 24 hours. The use of partial hydration addressed the potential hydration of the bentonite through defects in the geomembrane backing. The tests were performed with the GCL, geomembrane, and geonet in a "sandwich." In both tests, the failure occurred at the geonet/smooth geomembrane interface. Peak friction of 11 and 14 degrees was obtained with apparent adhesions of 3 and 7 kPa, respectively. Residual friction of 10 and 11 degrees was obtained with apparent adhesions of 2 and 8 kPa, respectively

Vasco Road Sanitary Landfill Disposal Unit 6

The Vasco Road Sanitary Landfill, a canyon landfill located in Alameda County, California, is a few kilometers from an active Holocene fault. Disposal Unit 6 (DU-6) at the site is a 10 ha area of the landfill characterized by 2H:1V side-slopes (Figure 5). Due to varying hydrogeologic and subgrade conditions, within the area two different liner systems were installed utilizing GCLs with both geotextile carrier and HDPE geomembrane backing.

In 1994, the side-slope portion of a 3 ha portion of the DU-6 area was lined as follows (top to bottom): (i) Tensar "DC610589" single-sided geocomposite LCRS; (ii) Gundle 2-mm thick HDPE geomembrane (textured on bottom, smooth on top); (iii) CETCO "Bentomat ST" GCL with geotextile carrier; and (iv) Polyfelt "TS800" 410 g/m^2 nonwoven geotextile. A total of approximately 23,000 m^2 of "Bentomat ST" GCL was installed in DU-6 in 1994.
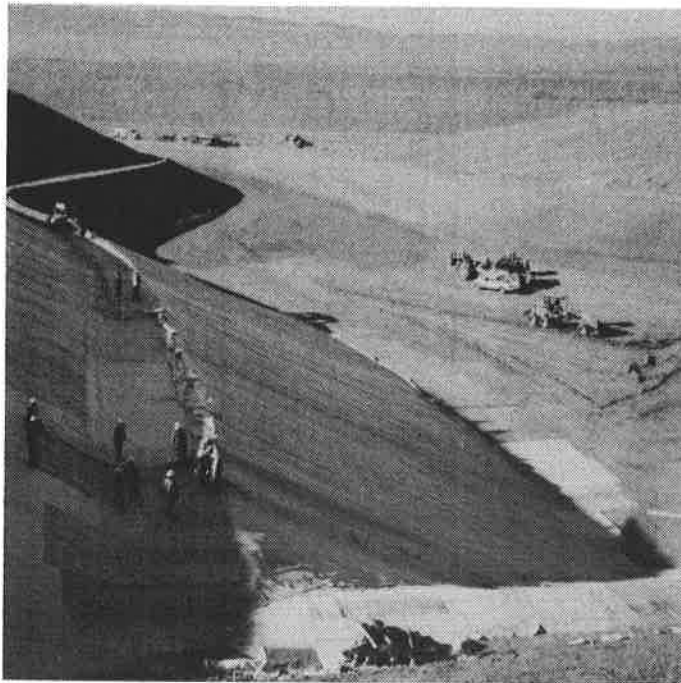
Figure 5 - Vasco Road Sanitary Landfill DU-6 side-slope GCL installation

In 1995 and 1996, a liner system incorporating an HDPE geomembrane-backed GCL was installed on the side-slopes in the remaining 7 ha portion of DU-6. The liner system consisted of (top to bottom): (i) Tensar "DC410500" single-sided geocomposite LCRS; (ii) Gundle Lining Systems, Inc. (Gundle), 2-mm thick HDPE geomembrane liner; (iii) Gundle "Gundseal" GCL, with a 0.75-mm thick HDPE geomembrane carrier placed against the underdrain; and (iv) Tensar

"DC420541" double-sided geocomposite underdrain. The HDPE geomembrane-backed GCL was used to reduce potential hydration of the GCL from the presence of ground-water seeps observed on the side-slopes, which were collected by a geocomposite underdrain layer. Approximately 30,700 m^2 of the "Gundseal" GCL were installed in DU-6 in 1995.

As part of liner design, interface shear tests were conducted to obtain the shear strength parameters. The tests were performed under both dry and hydrated conditions on the entire liner system "sandwich" at a displacement rate of 5 mm/min. Both geotextile and HDPE geomembrane carrier type GCLs were used in the tests. The test results indicated failure at the geonet/smooth geomembrane interface with a peak friction of 12 and 13 degrees and apparent adhesion of 9.6 and 8.4 kPa for unhydrated and hydrated conditions, respectively. Corresponding residual friction of 12 and 13 degrees and apparent adhesion of 7.9 and 8.4 kPa for unhydrated and hydrated conditions, respectively, was also measured during the test.

Three conformance tests performed on the "Bentomat ST" GCL samples indicated unit weights (ASTM D 3776) between 5,206 and 5,594 g/m^2, puncture strengths (ASTM D 4833) of 0.54 to 0.68 kN, ultimate strengths (ASTM D 4595) of 9.63 to 18.57 kN/m, moisture contents (ASTM D 2216) of 13.7 to 15.4 percent, and hydraulic conductivity (ASTM D 5084, modified) of 1.45 x 10^{-11} to 6.9 x 10^{-12} m/s at a confining pressure of 36 kPa.

Four (4) conformance samples of the "Gundseal" GCL were tested. The bentonite portion of the GCL was tested for unit weight (ASTM D 3776) and moisture content (ASTM D 2216). The results indicated unit weights of bentonite ranging from 4,972 to 5,263 g/m^2 and moisture contents from 17.7 to 22.5 percent. The HDPE geomembrane portion of the GCL was tested for specific gravity (ASTM D 792), thickness (ASTM D 751), yield and break tension (ASTM D638), carbon content (ASTM D 1603), and carbon black dispersion (ASTM D 2663).

B&J Drop Box Sanitary Landfill Disposal Module 2.2

The B&J Drop Box Sanitary Landfill is located in Solano Country, California The site is characterized by moderate seismic activity and high ground-water conditions. Due to the hydrogeologic conditions, the HDPE geomembrane-backed GCL was selected as an alternative to the prescriptive Subtitle D CCL composite liner. Disposal Module 2.2 (DM-2.2) of the landfill expansion, constructed in 1995 and 1996, is approximately 5 ha. The liner system configurations used in the base and side-slope are depicted on Figure 6.

An interface shear testing program was performed during the design phase in accordance with ASTM D 5321. Three tests with hydrated GCLs were performed, including: (i) CETCO "Bentomat ST" GCL with woven geotextile against 1.5-mm thick GSE "Hyperflex Frictionflex" HDPE geomembrane; (ii) CCL against the 0.375-mm thick smooth HDPE geomembrane-backed GSE "Gundseal" GCL; and (iii) CCL against the 0.75-mm thick textured HDPE geomembrane-backed "Gundseal" GCL. All three tests were performed at a constant

shear displacement rate of 1 mm/min. The test results indicated a peak friction of 13 degrees for cases (i) and (iii) and 10 degrees for case (ii). Peak apparent adhesions for cases (i), (ii), and (iii) were 22, 3, and 19 kPa, respectively. Residual friction of 7 degrees was obtained for cases (i) and (ii) and 13 degrees was obtained for case (iii). Corresponding residual apparent adhesions were 10, 5, and 19 kPa for cases (i), (ii), and (iii), respectively.
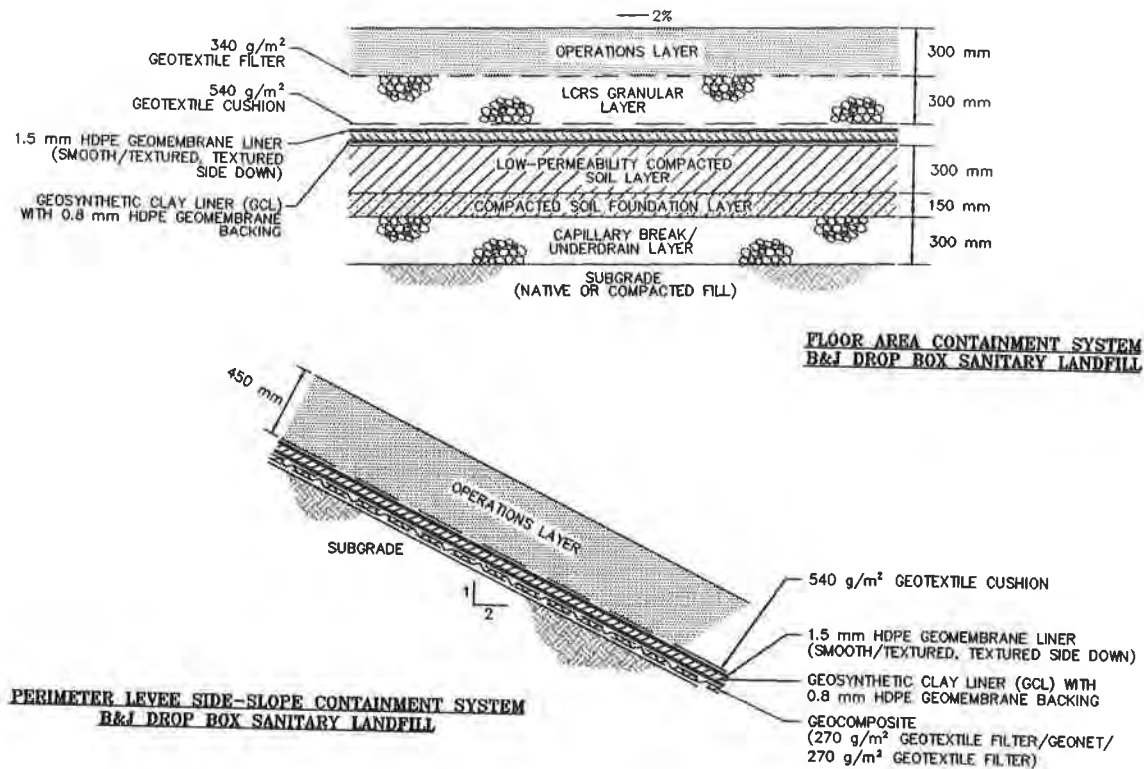
Figure 6 - B&J Landfill DM 2.2 base and side-slope GCL liner configurations

Three conformance samples of the "Gundseal" GCL were obtained during the 1995 construction of the liner system. The bentonite portion of the GCL was tested for bentonite content (ASTM D 3776) and moisture content (ASTM D 2216). The results indicate bentonite contents ranging from 5,172 to 5,335 g/m² and moisture contents ranging from 17.2 to 18.4 percent. The HDPE geomembrane portion of the GCL was tested for specific gravity (ASTM D 792), thickness (ASTM D 751), yield and break tension (ASTM D 638), carbon content (ASTM D 1603), and carbon black dispersion (ASTM D 2663).

Cummings Road Sanitary Landfill

The Cummings Road Sanitary Landfill is located near Eureka, California. The site is in an active seismic zone. A 2 ha expansion of the landfill with 1.5H:1V side-slopes was designed in 1994 and constructed in 1995 (Figure 7). An alternative to a CCL composite liner for the side-slopes

was approved by the state regulators based on a demonstration of equivalent liquid containment capability. The GCL side-slope composite liner system consisted of the following (top to bottom): (i) Nicolon "S1000" 340 g/m^2 nonwoven geotextile; (ii) Tensar "NS140551" geonet; (ii) GSE 1.5-mm thick textured/textured HDPE geomembrane; (iii) GSE 0.75-mm thick textured HDPE geomembrane-backed "Gundseal" GCL with the geomembrane backing against the underdrain; and (iv) Tensar "NS140551" geonet sandwiched between two layers of Nicolon "S1000" 340 g/m^2 nonwoven geotextile as a geocomposite underdrain installed in "wet" areas only.

Figure 7 - Cummings Road Landfill side-slope GCL installation

Based on GeoSyntec's analysis, the critical interface surface was between the geonet and HDPE geomembrane. Two conformance samples of the GCL were tested indicating dry bentonite unit weights (ASTM D 3776) of bentonite of 5,091 and 5,386 g/m^2 and moisture contents (ASTM D 2216) of 19.5 and 20.3 percent. Hydraulic conductivity tests (ASTM D 5084, modified) of the "Gundseal" GCL, including the geomembrane backing, indicated values of 7.4 x 10^{-13} and 7.2 x 10^{-13} m/s. Additionally, the geomembrane portion of the GCL was tested for yield and break tension (ASTM D 638) and puncture strength (FTMS 101/2065).

CURRENT TRENDS

The preceding case histories are summarized in Table 1 and illustrate some current trends in the permitting, design, and construction of GCL composite liners at MSW landfills. The liquid containment capability of GCLs is now being accepted by state regulators as equal to or superior to that of Subtitle D CCLs. However, in evaluating the waste containment capability of an alternative liner system it is important to recognize the contribution of the LCRS to the containment capability of a liner *system*. An LCRS can be designed to reduce the hydraulic head to less than the Subtitle D prescriptive head of 0.3 m, thereby increasing the liquid containment capability of an alternative composite liner system in comparison to the Subtitle D prescriptive composite liner system. Including consideration of the effectiveness of the LCRS provides a more realistic comparison of the containment capability of alternative and prescriptive composite liner system designs.

GCLs are also gaining acceptance as both base and side-slope alternative liner components. In some base liner systems, GCLs are being combined with CCLs where the CCL has a hydraulic conductivity higher than 1×10^{-9} m/s. The hydraulic conductivity of GCLs has been found to relatively consistent, with most values less than 5×10^{-11} m/s. Given the consistency of GCL hydraulic conductivity, designers may consider the use of lower conformance testing frequencies for hydraulic conductivity where dry mass of bentonite per unit area conformance testing is already included in the QA/QC program.

The shear strength of GCLs used in liner system applications is an issue which continues to generate significant discussion among designers and regulators. GCL shear strength is an important parameter in slope stability evaluations, as failure within a liner system component or along an interface may be the critical failure mechanism for an MSW landfill (Mitchell et al., 1990). The actual shear strength of a GCL will depend on site specific conditions including: (i) degree of hydration of the bentonite; (ii) confining pressure; (iii) stress path; (iv) effectiveness of internal reinforcement mechanisms; (v) nature of the interface materials; (vi) allowable strain; (vii) nature of the hydrating liquids; and (viii) structure of the GCL.

Shear strength data obtained during the design phase provides the designer valuable information for stability analyses and grading design. Both interim stability of the cover materials and overall waste mass stability must be evaluated. For several of the steep slope applications presented herein, cover material stability was obtained by progressively placing the cover materials in a wedge configuration to a limiting height as waste disposal operations proceed.

However, the shear strength of the actual GCL materials delivered to the site for installation may vary from those tested during design. Variability in the manufacturing of GCLs (and other geosynthetics) and the use of different GCLs (and other geosynthetics) from those tested during design can impact the shear strength of the GCL. Interface shear test results presented for the

Table 1 - Summary of GCL Case Histories

Site/Project	Application	GCL	Geomembrane	LCRS Design
Lopez Canyon Phase I, Area C	1H:1V slope composite liner	James Clem "Claymax ShearPro"	National Seal "Friction Seal" smooth/textured	geonet on smooth side of geomembrane
Lopez Canyon Phase II, Area C	1H:1V slope composite liner	CETCO "Bentomat SS"	SLT "Hyper-Flex" smooth/textured	geonet on smooth side of geomembrane
Shafter-Wasco Module 2	bottom and 3H:1V slope composite liner	Albarrie Naue "Bentofix NS Enhanced"	National Seal "Friction Seal" smooth/textured	geonet on smooth side of geomembrane
Puente Hills Phase 1B	1.5H:1V and 3.25H:1V slope composite liner	CETCO "Bentomat DN" w/ geomembrane moisture barrier beneath	Serrot HST S/S on 1.5H:1V slope and National Seal "Friction Seal" on 3.25H:1V slope, textured/textured	geonet on smooth side of geomembrane on 1.5H:1V slope and two-sided geocomposite on textured geomembrane on 3.25H:1V slope
Sunshine Canyon Phase I, Stage 1	1.5H:1V slope composite liner	GSE "Gundseal" w/ geomembrane down	GSE "Hyperflex" smooth/textured	geonet on smooth side of geomembrane
Vasco Road DU-6 (1994)	2H:1V slope composite liner	CETCO "Bentomat ST"	Gundle HDPE geomembrane smooth/textured	geonet of one-sided geocomposite on smooth side of geomembrane
Vasco Road DU-6(1995/96)	2H:1V slope composite liner	Gundle "Gundseal" w/ geomembrane down	Gundle HDPE geomembrane smooth/textured	geonet of one-sided geocomposite on smooth side of geomembrane
B&J Drop Box DM-2.2	bottom and 2H:1V slope composite liner	GSE "Gundseal" w/ geomembrane down	GSE "Hyperflex Frictionflex" smooth/ textured	operations layer on slope and drainage gravel on bottom, both over smooth side of geomembrane
Cummings Road	1.5H:1V slope composite liner	GSE "Gundseal" w/ geomembrane down	GSE HDPE geomembrane textured/textured	geonet on textured side of geomembrane

Shafter-Wasco Landfill indicate that, significant variations in GCL interface shear strength values can be expected. As a result, it appears warranted to incorporate GCL interface shear testing as part of the QA/QC program. The frequency of testing should reflect the importance that the shear strength has in the design of the project. The hydration of the GCL can significantly impact the shear strength. Where potential hydration of the GCL results in unacceptable shear strengths, the use of moisture barriers or geomembrane-backed GCLs can be used to control potential hydration.

There appear to be few MSW landfill liner applications where the installation of a GCL is not easier than a CCL. In steep side slope applications, GCLs may be the only viable and economical alternative where a composite liner system is specified. The controlled quality and ease of installation of GCLs often result in a lower cost of construction and QA/QC as well as an expedited construction. The primary construction issue related to deployment of GCLs is the potential for hydration. Hydration of a GCL prior to completion of the liner can result in stability problems during construction and/or waste placement due to observed decreases in the GCL shear strength (Daniel et al., 1993). Specifications typically require the removal and replacement of any prematurely hydrated GCL. Many specifications will further require the contractor to cover all GCL at the end of each day's work with geomembrane to avoid possible hydration.

QA/QC monitoring and testing procedures are becoming well established. However, QA/QC conformance testing requirements can vary significantly amongst projects and should be carefully reviewed on a project-specific basis. Factors to consider in evaluating the need for a conformance test include: (i) is the test reflective of a design consideration; (ii) is the test indicative of variations in the manufactured product; (iii) does the cost of the test warrant the benefit of the information obtained; (iv) is the parameter being measured known to be highly variable; and (v) does the turnaround time needed to make the test compatible with a QA/QC program and construction schedule; and (vi) are there overlaps in the conformance testing program (i.e., there is no need to measure mass per unit area and hydraulic conductivity at the same frequency since they provide complimentary information applicable to the same property).

ACKNOWLEDGMENTS

REFERENCES

Byrne, R.J. (1994), "Design Issues with Strain Softening Interfaces in Landfill Liners," Proceedings, WasTech '94, January, 26 p.

Daniel, D.E., Shan, H.Y., and Andersen, J.D. (1993), "Effects of Partial Wetting on the Performance of the Bentonite Component of a Geosynthetic Clay Liner," Proceedings, Geosynthetics '93, March, pp. 1483-1496.

Kavazanjian, E., Jr. (1994), "Performance of a Geosynthetic Landfill Liner System in the 1994 Northridge Earthquake, An Interview", Geotechnical Fabrics Report, March, pp. 18-24.

Mitchell, J.K., Seed, R.B., and Seed, H.B. (1990), "Stability Considerations in the Design and Construction of Lined Waste Depositories," Geotechnics of Waste Fills - Theory and Practice, American Society of Testing and Materials, ASTM STP 1070, pp. 207-224.

Snow, M.S., Bonaparte, R., and Kavazanjian, Jr., E. (1994a), "Leachate Containment Capability of an Alternative Composite Liner System," Proceedings, WasTech '94, January.

Snow, M.S., Kavazanjian, Jr., E., and Sanglerat, T.R. (1994b), "Geosynthetic Composite Liner System for Steep Canyon Landfill Side Slopes," Proceedings, Fifth International Conference on Geotextiles, Geomembranes, and Related Products, Sept.

MANAGING DESICCATION CRACKING IN COMPACTED CLAY LINERS BENEATH GEOMEMBRANES

J. J. BOWDERS, D. E. DANIEL
The University of Texas - Austin, Texas
J. WELLINGTON
The City of Garland, Garland Texas
V. HOUSSIDAS
The University of Texas - Austin, Texas

ABSTRACT

Thermal gradients pose a significant driving force for desiccation of the soil component of composite barriers. In this study, black and white-surfaced geomembranes were placed over two compacted clay soils in large-scale laboratory test cells. Soil A was from an actual landfill liner and was highly plastic (PI = 42-48%). Soil B was a moderately plastic clay (PI = 28%). The clays were monitored as the exposed geomembranes were subjected to daily temperature cycles typical of field conditions. Peak temperature on the upper surface of the black geomembrane was 66°C to 68°C and for the white-surfaced geomembrane was 60°C. Soil temperatures were the same beneath both the black and white-surfaced geomembranes but the moisture contents were different. The soil beneath the black geomembrane desiccated faster and to a greater degree than that beneath the white-surfaced geomembrane. A greater rate of heat transfer into the soil beneath the black geomembrane, and the much greater wrinkling that was observed for the black geomembrane, were the causes. Engineers should consider providing a construction specification that designates a safe exposure time for an uncovered geomembrane overlying a compacted clay liner. Use of white-surfaced geomembranes may extend by a few weeks or more the safe operating period during which no significant damage occurs to the underlying clay liner, but field data are needed to document actual desiccation in clay liners.

INTRODUCTION

Composite barriers consist of a geomembrane and an underlying layer of low-permeability compacted clay acting in unison to limit either infiltration in the case of covers, or leakage in the case of liners. The composite action of a barrier is only effective when the soil component maintains a low hydraulic conductivity. Several mechanisms can act to compromise the low hydraulic conductivity of the compacted clay component - chemical attack, differential movements, freeze-thaw and desiccation. In this study we focused on desiccation of the clay liner as a result of heating of an uncovered geomembrane resting directly on compacted clay and subjected to daily heating-cooling cycles. This condition can exist in the field for days, weeks, or months, depending on how long the geomembrane is exposed.

When a composite liner is exposed to the direct sunlight, a black geomembrane can heat to temperatures up to about 70°C (Koerner and Koerner 1995, Cadwallader et al 1993, Basnett and Bruner 1993). A thermal gradient is then established in the underlying compacted clay, which is cooler than the geomembrane. Thermal gradients can pose a significant driving force for the movement of moisture especially within unsaturated soils (Mitchell, 1993). Movement of moisture may then lead to desiccation of the soil component of composite barriers (Terzaghi and Peck 1967, Doll 1996, Vielhaber, et al. 1994). Surface temperatures on white-surfaced geomembranes have been reported between 43°C and 57°C . These temperatures are somewhat less that those for black geomembranes and may reduce the significance of thermally driven desiccation of the underlying clay liner.

The objective of this study was to develop quantitative data under controlled conditions to determine the extent to which black and white-surfaced HDPE geomembranes limit desiccation of underlying compacted clay liners. It was expected that there would be less heating and desiccation of the clay beneath the white-surfaced geomembrane, and we sought to quantify the effect of the surface color of the geomembrane in carefully controlled tests.

EXPERIMENTAL PROGRAM

Soils were compacted into two test cells each measuring approximately 1 m by 1 m in plan (Figure 1). Tests were performed for two soils. Soil "A" was obtained from an actual landfill liner and was a highly plastic clay (PI = 42 to 48%). Soil "B" was a moderately plastic clay (PI = 28%). The geotechnical index properties for these soils are given in Table 1.
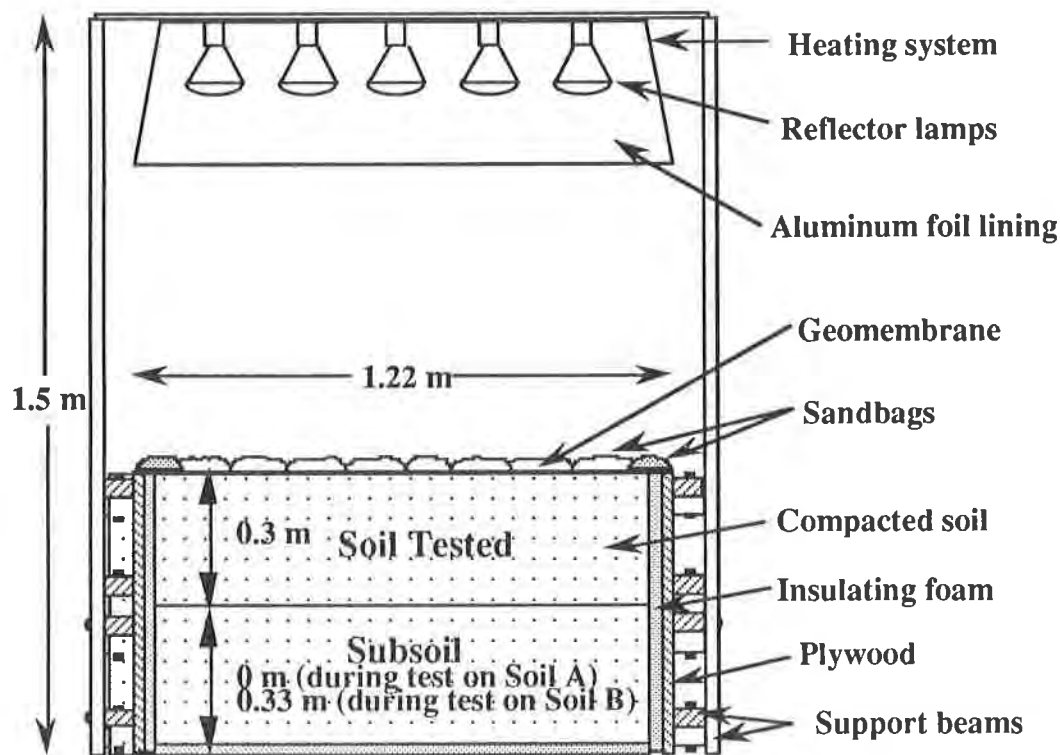

Figure 1 - Elevation view of a typical test cell used in this study. Note: Soil A was tested at a thickness of 0.33 m. Soil B was tested at a thickness of 0.3 m but was placed atop soil A.

Soil A was tested first. It was compacted (molding water content 30%) in 11-cm lifts for a total height of 0.33 m in each test cell. No subsoil was used beneath it. The soil was instrumented with thermocouples (Figure 2). The thermocouples were embedded in the soil at depths of 6 cm, 13 cm and 20 cm. Each test cell also contained ten 10-cm diameter Proctor molds embedded in the compacted soil. The Proctor molds contained soil compacted to the same water content and density as the test soil. The intent was to periodically extract the samples from the molds and measure the hydraulic conductivity directly in the Proctor molds. The molds did not work very well because the soil shrank away from the molds. The molds were not used for Soil B.

One test cell was covered with a smooth, black HDPE geomembrane and the other with a smooth, white-surfaced HDPE geomembrane. Thermocouples were also affixed to the upper and lower surface of the geomembranes.

Table 1 - Geotechnical index properties of the soils used in this study.

Soil Property	Test Method	Soil A	Soil B
As-Received Moisture Content (%)	ASTM D4945	15-21	21
Specific Gravity of Solids	ASTM D854	2.75-2.85	2.68
Liquid Limit (%)	ASTM D4318	64-66	43
Plasticity Index (%)	ASTM D4318	42-50	28
Percent Passing No. 200 Sieve (<0.074 mm)	ASTM D1140	70	30
Max Dry Density (kN/m^3) (pcf)	ASTM D698	15.2 (97)	18.4 (117)
Optimum Moisture Content (%)	ASTM D698	25	16

Soil B was compacted (molding water content 21%) in three 10-cm lifts on top of a 0.33 m prepared soil base. A soil base was used because the heating extended deeper than expected in the test on Soil A, and the soil base minimized boundary effects in the test on Soil B. This made a total thickness of soil barrier of about 0.6 m. Thermocouples were embedded in the soil at depths of 10 cm, 20 cm and 30 cm. Testing conditions for Soil B were the same as those for Soil A, with the exception of no Proctor molds in the compacted liner. Two cells (one for a white-surfaced geomembrane and the other for the black geomembrane) were again used.

Each cell was heated for 10-12 hours with heat lamps, and then the heat lamps were turned off for the rest of the day. The heating systems were calibrated to yield a 30°C increase above ambient temperature on the upper surface of a black geomembrane. This increase is typical of those recorded for field cases of smooth, black geomembranes by Basnett and Bruner (1993) and Cadwallader et al (1993). The same thermal energy was delivered to cells containing the black geomembrane and white-surfaced geomembrane. The heating - cooling cycles were repeated for 60 or more days.
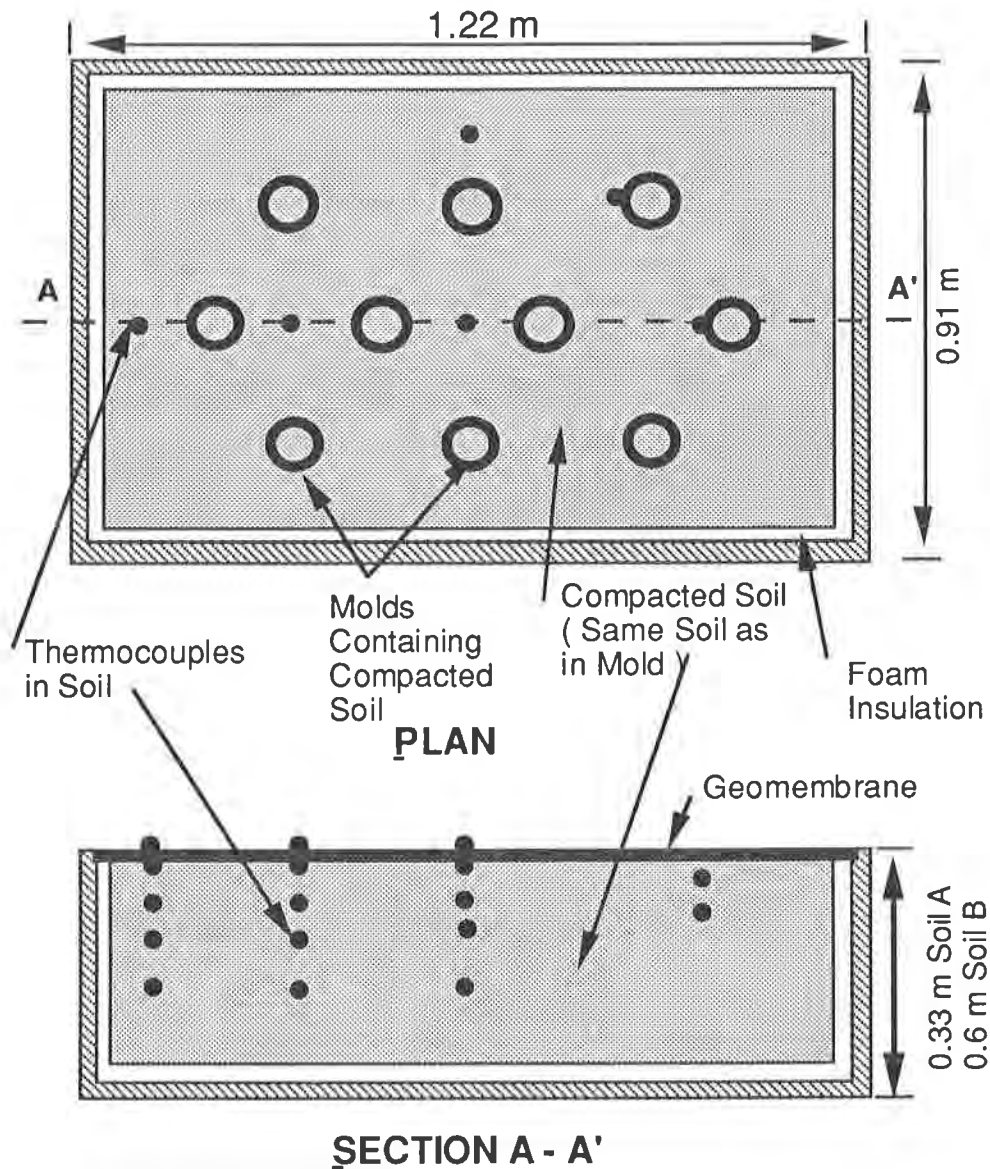
Figure 2 - Plan and elevation view of the instrumented compacted clay showing location of the thermocouples (Soils A and B) and the locations of hydraulic conductivity samples (Soil A only).

Parameters monitored included temperature on the geomembrane and within the soil mass (monitored with thermocouples), water content of the soil mass (determined by periodically sampling the soil), hydraulic conductivity (Soil A only, determined by permeating the soils inside Proctor models), and soil crack dimensions and patterns (determined by periodic observation and measurement). The frequency of monitoring varied slightly between Soil A and Soil B tests; but in general, soil temperatures were measured daily until a thermal equilibrium was established. Moisture contents were determined at pre-selected intervals, i.e., after 1, 3, 7, 14, ... heating cycles (one heating cycle per day).

RESULTS AND DISCUSSION

Temperatures. A typical temperature versus time response is shown in Figure 3. While all of the test cells showed a similar response, the absolute temperatures varied between the soils and between the black or white-surfaced geomembranes (Table 2). Ambient temperature for all of the tests was 21°C (70°F). Note that the peak temperatures (steady-state) for all depths (even at 30 cm) were reached after about 7 days of heating-cooling cycles.

There was a maximum temperature difference of 5°C to 9°C between the surfaces of the black and white-surfaced geomembranes for the two soils. This is less than 18°C to 24°C difference reported by Cadwallader et al (1993) but closer to the 13°C reported by Koerner and Koerner (1995). Differences in surface temperatures between black and white-surfaced geomembranes can be attributed to several factors including color of the geomembrane (although labeled white, geomembranes can vary from white to translucent, and the "white" geomembrane tested in this study could be described as very light gray), moisture conditions of the underlying soil, intimacy of the geomembrane/soil contact, boundary sealing and the method of thermocouple contact to the surface of the geomembrane. While every effort was taken to make the laboratory test cells and procedures representative of field conditions, there were some variations. The most significant variation from field conditions may have been the boundary sealing conditions. Sandbags were placed intermittently around the edges of the geomembranes. This allowed vapor vent channels between the sandbags.

Table 2 - Average peak temperatures (°C) for the duration of the tests.
(GM = Geomembrane)

Location	Soil A		Soil B	
	Black GM	White GM	Black GM	White GM
GM (top)	68	59	64	59
GM (bottom)	***	***	65	60
d = 10 cm	39	39	39	39
d = 20 cm	37	36	34	34
d = 30 cm	***	***	32	32

Another important finding regarding temperatures is the depth of heating and steadiness of temperature at depth. In about 7 days (7 heating-cooling cycles) the soil temperatures at a depth of up to 30 cm rose to 32°C (Soil B) and remained there throughout the cooling cycle (Table 3). For Soil A, the temperatures at 20 cm rose to 36°C and became steady. Thus, there was no cooling of the soil at a depth of 20 to 30 cm during the 12 to 14 hour period when no heat was applied to the surface of the geomembrane. At depths nearer the surface, the soil temperatures decreased during the cooling periods; however, the temperature remained well above ambient (21°C) even for depths as shallow as 10 cm.
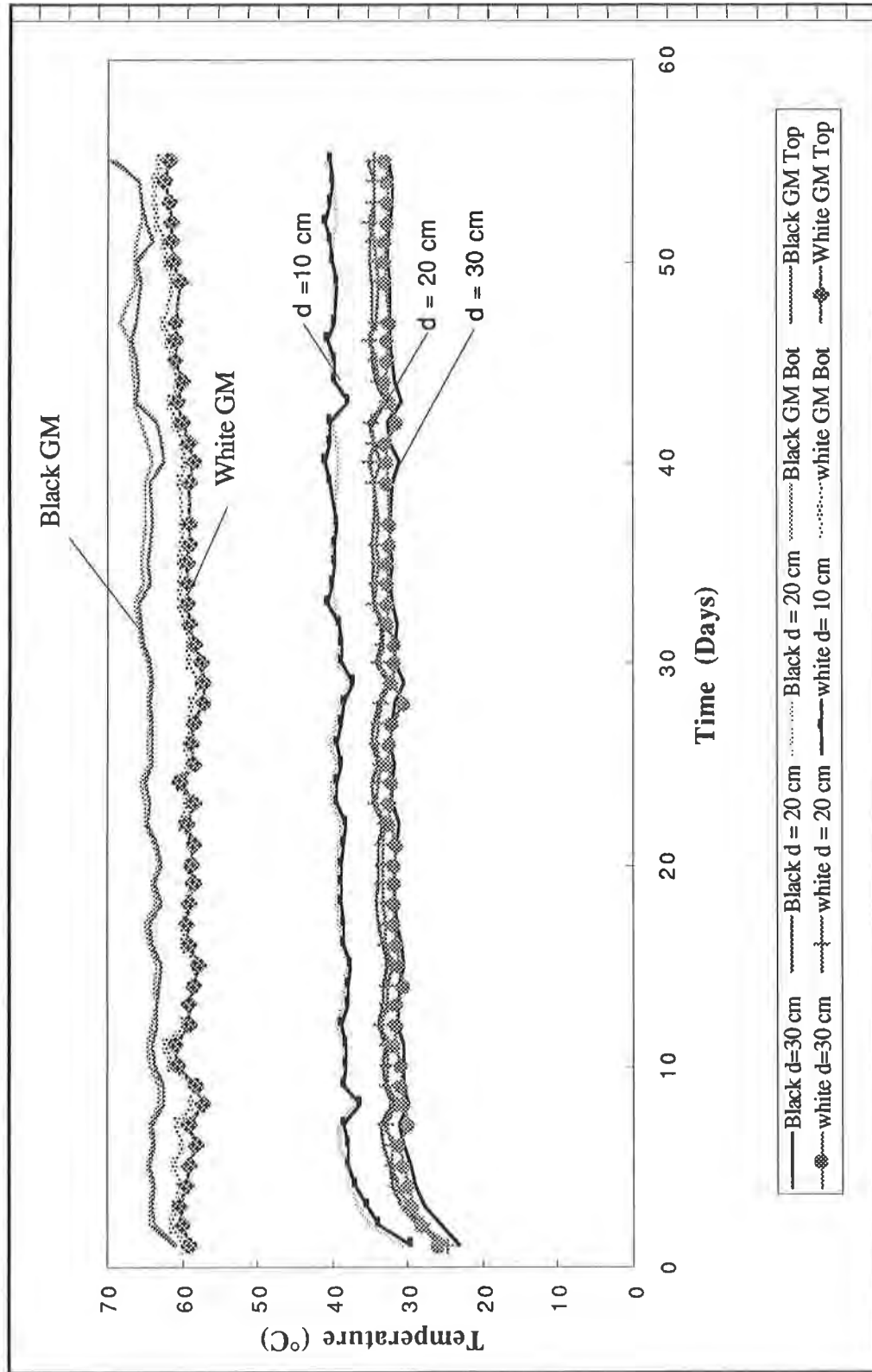
Figure 3 - Fluctuations of the maximum temperature for the black and white geomembrane on Soil B.

Table 3 - Average maximum and minimum temperatures (°C) in the soil and on the geomembrane after 7 heating-cooling cycles.

	Black		White	
	Maximum	Minimum	Maximum	Minimum
Soil A				
GM (top)	68	26	59	29
d = 10 cm	39	36	39	34
d = 20 cm	37	36	36	35
Soil B				
GM (top)	64	27	60	27
GM (bottom)	65	27	61	28
d = 10 cm	40	31	40	31
d = 20 cm	24	32	34	32
d = 30 cm	32	32	32	32

Moisture escaped from the heated zone by two processes. The first process is that of thermally driven flow due to the temperature gradient. Moisture always migrates down a gradient in energy, i.e., toward cooler regions of the clay liner or the boundaries of the test cells. The second process of moisture loss is through evaporation and vapor transmission. As the temperature of the air in the soil pores rises, the air is capable of carrying a greater amount of water vapor. Some of the pore air escapes from the compacted layer and can move laterally beneath the geomembrane. In the test cells, sand bags were placed on the perimeter of the geomembrane, but vapor could escape between the sand bags. In this process, the compacted clay loses additional moisture. Basnett and Bruner (1993) noted such movement of water beneath geomembranes in the field.

Water Contents. While the temperature profiles indicate thermal gradients existed in the compacted clay, they did not in themselves indicate whether or not the soil had desiccated. The temperature profiles under the black and white-surfaced geomembranes were similar; however, the moisture profiles were very different.

As the soil pores become dewatered, either by liquid moisture migration or by evaporation, the pore water pressures become negative, thus increasing the effective stress (but not the total stress) in the soil. The negative pore water pressure acts in all directions and results in a tendency for cracking of the soil mass (Fredlund and Rahardjo 1993). Thus, monitoring of the soil moisture profiles, and not the temperatures, is key to assessing the integrity of the compacted clay liner.

Soil A. Soil moisture profiles for Soil A are shown in Figures 4a and 4b. The profiles were taken at the center of the test cell (plan view) and show the change in moisture content versus depth after 30 heating cycles (Fig 4a) and after 60 heating cycles (Fig 4b). The molding water content for Soil A was 30 percent (about 4 % above optimum water content). After 30 heating cycles, the soil moisture content beneath the black geomembrane decreased from 30% to about 10% over the upper 15 cm of the soil layer. At a moisture content of 10%, the soil was dry, hard, and severely cracked. Fifteen centimeters (6 inches) is the typical thickness of a compacted lift of soil. Although there are no guidelines concerning how much desiccation is

too much, loss of a full lift (15 cm) of soil to desiccation would almost certainly be considered unacceptable. The soil moisture content beneath the white-surfaced geomembrane decreased from 30% to an average of 26% over the upper 15 cm of the soil layer over the same 30 day period. A 4 percentage point drop in moisture content is much less severe than the 20 percentage point decrease observed beneath the black geomembrane. Beneath the white-surfaced geomembrane, the soil moisture did not change below a depth of about 15 cm during the first 30 heating cycles.

The soil moisture profiles after 60 heating cycles are shown in Figure 4b. Beneath the black geomembrane the moisture content decreased to below 10% in the upper 15 cm. The moisture content decreased to 25% at a depth of more than 20 cm. Beneath the white-surfaced geomembrane, the moisture content decreased to about 15% (from the original 30%) over the upper 7 cm. Below about 7 cm, the soil moisture was >26% and was unchanged from the molding moisture content below a depth of 20 cm. From the results of the tests using Soil A, there is clearly a significant difference in the soil moisture response beneath the black and white-surfaced geomembranes.

Cracking patterns were observed for Soil A in both test cells. Surface crack patterns were similar, but the depth of the cracking was much different. Cracks in Soil A penetrated the full depth of the clay liner (30 cm) beneath the black geomembrane after 60 heating cycles. Beneath the white-surfaced geomembrane, cracks penetrated from 4 to 6 cm after 60 heating cycles for Soil A (Wellington 1995).

The black geomembrane was also observed to contain more and larger wrinkles than the white-surfaced geomembrane. Using the thermal expansion coefficient for HDPE (8E-05/°F) and the measured geomembrane temperatures, the black geomembrane should have elongated 8.6 mm and the white geomembrane only 6.3 mm. While the calculated difference seems small, our visual observations showed that the black geomembrane had larger wrinkles (2.1 cm max height) compared to the white geomembrane, which had a maximum height of wrinkles of 1.6 cm.

Soil B. Soil moisture profiles for Soil B were determined over 5-cm intervals for the upper 30 cm of compacted clay layer (Soil B was underlain by 30 cm of subsoil). The measured soil moisture contents were averaged for (a) the upper 15 cm of the layer and (b) for the upper 30 cm of the layer. The results are shown in Figure 5.

The normalized volume of water remaining in the soil versus time is shown in Figure 6. Soil B was compacted to a dry density of 16.3 kN/m^3 at a molding water content of 21 percent. The initial volume of water in the soil was calculated. The volume of water remaining in the soil was determined based on the periodically measured moisture contents. This value was normalized by dividing by the original volume of water in the soil.

The responses in Figures 5 and 6 show that the rate of drying was fairly constant during the first 8 weeks in both test cells. The rate of drying in the top 15 cm of Soil B beneath the black geomembrane was about 50% higher than the rate of drying beneath the white-surfaced geomembrane. If the top 30 cm of Soil B are considered, the rate of moisture loss under the black geomembrane was approximately 30 to 40% higher than that under the white-surfaced geomembrane. Between weeks 8 and 12, it appears that the soil was drying slightly faster under the white-surfaced geomembrane. During the last 4 weeks of the test, the soil beneath

the black geomembrane ceased to dry, while the soil beneath the white-surfaced geomembrane continued to dry but at a slower rate than before. There is an indication that the moisture content beneath the black geomembrane increased slightly during this period, probably because some moisture from the lower compacted clay layer was migrating into the upper layer.
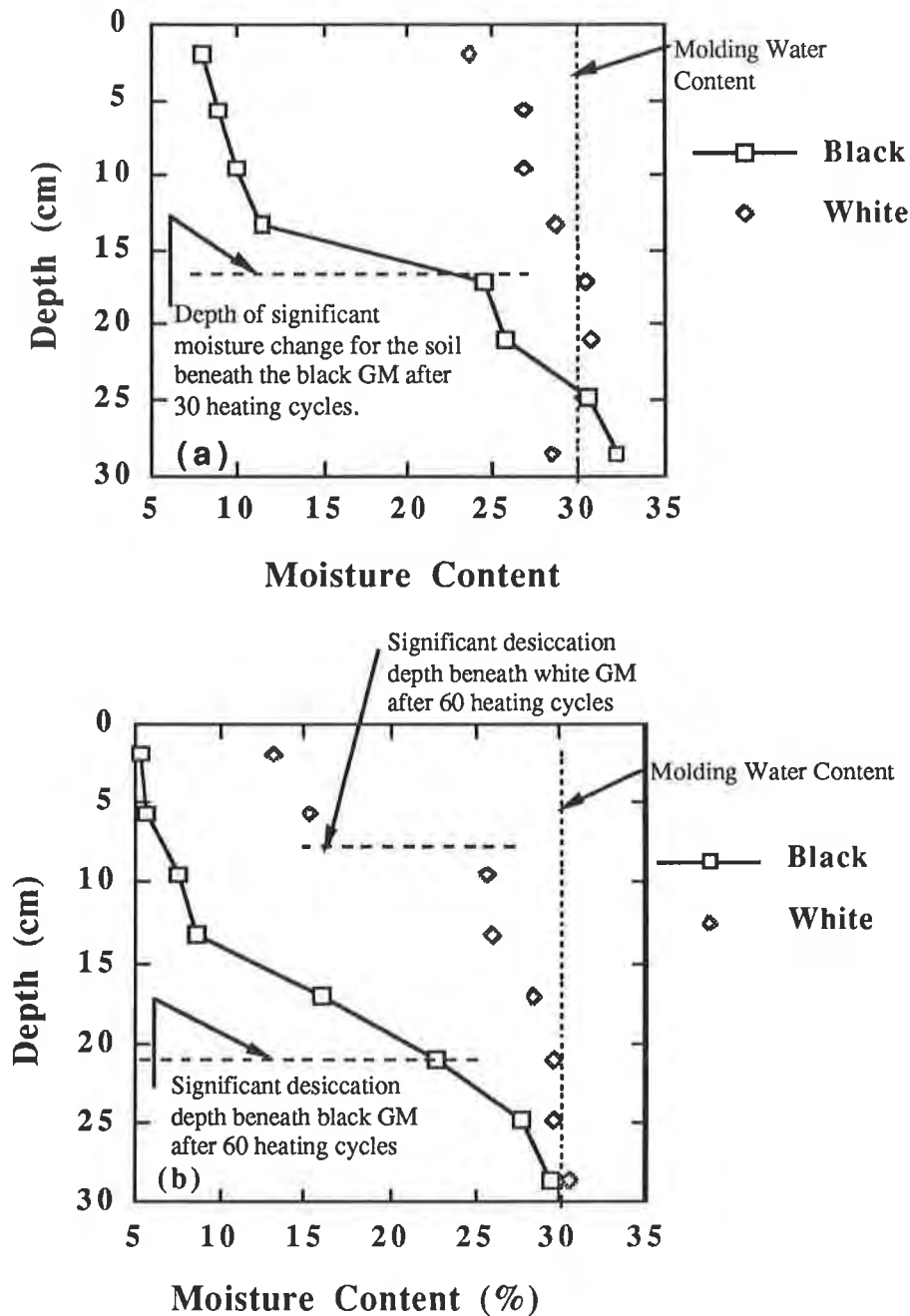

Figure 4 - Water content versus depth for Soil A beneath the black- and white-surfaced geomembrane (a) after 30 days and (b) after 60 days.
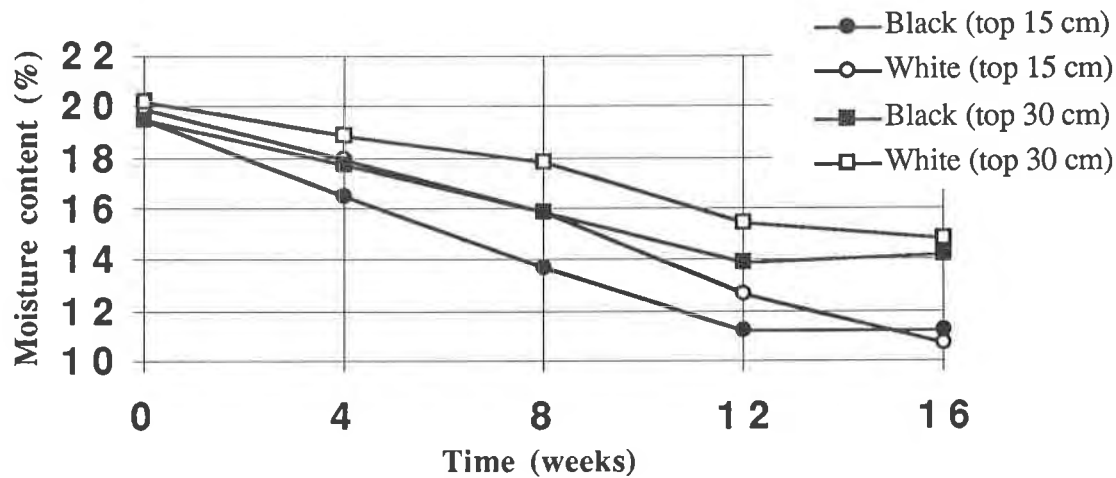
Figure 5 - Average water contents in the top 15 cm and top 30 cm of Soil B beneath the black- and white-surfaced geomembrane for 0 to 16 weeks of heating-cooling cycles.

These data indicate that the volume of water lost from the soil over the entire testing period was about 25 liters and was the same for both test cells. However, when the soil was excavated to study cracking after the test, the soil beneath the white-surfaced geomembrane was found to be noticeably softer than that beneath the black geomembrane at depths exceeding 10 to 15 cm. This would logically follow from the moisture contents as shown in Figure 4(b) – higher moisture, softer soil.

Examination of the cracking in Soil B showed that the soil beneath the black geomembrane had more cracks than beneath the white-surfaced geomembrane. At the conclusion of the test, the soils in both test cells were excavated to expose a vertical profile. Soil B beneath the black geomembrane was severely cracked to a depth of 10 cm. Several hairline cracks extended to 20 cm and three cracks of 1 to 2 mm width extended the full depth of the layer (30 cm). Beneath the white-surfaced geomembrane, Soil B contained numerous cracks to 10 cm and a few cracks to 20 cm. Two cracks extended the full thickness of the layer (30 cm).

The pattern and size of wrinkles for the black and white-surfaced geomembranes on Soil B were assessed. While the patterns were different, the maximum height of the wrinkles was about the same (2.2 cm)
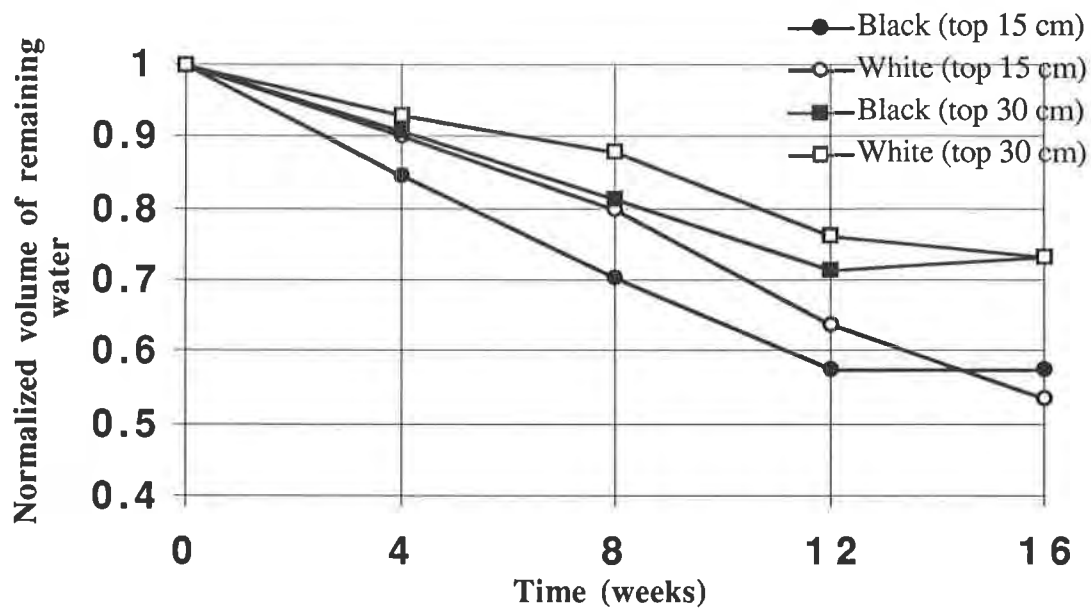
Figure 6 - Normalized volume of water remaining in Soil B beneath the black- and white-surfaced geomembranes for 0 to 16 weeks of heating-cooling cycles.

Discussion. Both soils exhibited greater loss of moisture beneath the black geomembrane than beneath the white-surfaced geomembrane (Table 4). Considering only the upper 15 cm of soil in the test cells, after eight weeks of heating cycles, Soil A lost almost 70% of its original moisture from beneath the black geomembrane and only 30% beneath the white-surfaced geomembrane. Soil B lost 30% of its original moisture beneath the black geomembrane and 20% beneath the white.

Table 4 Percentage of water remaining in the upper 15 cm of the compacted clay layer after 8 weeks of heating cycles

SOIL	Plasticity Index	% Water Remaining in the Upper 15 cm After 8 Weeks of Heating Cycles	
		Black GM	White GM
A	42-50	23	67
B	28	70	80

The rate of moisture loss was more rapid for the soils beneath the black geomembrane (Table 5). In just 14 to 28 heating cycles, Soil A lost one-third of its initial moisture when it was placed below the black geomembrane. Eight weeks of heating cycles were required to remove a similar amount of moisture from Soil A beneath the white-surfaced geomembrane. Soil B had a slower rate of moisture loss beneath both the black and the white-surfaced geomembranes than that for Soil A. However, for Soil B there remained about a 4 week lag for the soil moisture content beneath the white-surfaced geomembrane to remove one-third of its original value.

Table 5 - Time required for the upper 15 cm of compacted clay to loose 33% of the initial moisture.

	Time to Loose 33% of Initial Moisture from the Upper 15 cm of Soil (Weeks)	
SOIL	Black GM	White GM
A	2 to 4	8
B	8	12

An analysis was performed of heat transfer to conduct a heat balance. Results are discussed for Soil A. The soils beneath the black and white-surfaced geomembranes were essentially identical at the beginning of the cyclic heating process. The mass of dry soil in both boxes was approximately 240 kg, and the initial mass of water contained within the soil was approximately 72 kg in both cells. The initial water content in the soils was 30%. The final average water content at the end of 60 days of heating was 19% and 26% in the soil beneath the black and white-surfaced geomembranes, respectively. The computed mass of water remaining in the soil after 60 days of heating was 45 kg and 63 kg for soil beneath the black and white-surfaced geomembranes, respectively. Thus, 9 kg of water were evaporated from the soil beneath the white geomembrane, while 3 times as much water (27 kg) was evaporated from the soil beneath the black-surfaced geomembrane.

The heat of vaporization of water is 2.26 MJ/kg (Mitchell, 1993). Thus, the energy required to evaporate the above-mentioned amounts of water from the soil beneath the black and white-surfaced geomembranes was 20 and 60 MJ, respectively. Since there was 3 times as much water evaporated from the soil beneath the black geomembrane, there was 3 times as much energy consumed in evaporating the water.

The significance of the energy required to evaporate water may be evaluated by comparing the heat of vaporization with the calculated amount of energy required to heat the soil. The soil was initially at approximately 21°C, and after 60 days of heating, the temperature below a depth of a few centimeters was approximately 38°C. Thus, the temperature rise at depth was about 17°C. Based on the heat capacity values reported by Mitchell (1993) for water and soil minerals, and the known initial water content of the soil, the heat capacity of the compacted soil is estimated to be 1.51 kJ/kg-°C. The calculated amount of energy required to raise the temperature of the soil 1°C is 0.47 MJ. The calculated amount of energy stored by the soil when it was heated from 21°C to 38°C is therefore 8 MJ. This amount of energy is much less than the amount of energy needed to vaporize water from the soil, which was estimated to be 20 MJ for the soil beneath the white-surfaced geomembrane and 60 MJ for soil beneath the black geomembrane.

This analysis of heat stored and heat required to vaporize water demonstrates that the temperature of the soil is only one small indicator of where heat goes in the system. The white-surfaced geomembrane reflects more heat than the black geomembrane. Thus, more energy is transferred to the soil beneath the black geomembrane. Heat transfer through the geomembrane results in an increase in temperature within the soil. The heating immediately begins to evaporate water from the soil, and a significant amount of heat is used in evaporating water. In a sense, the process of water evaporation tends to keep the soil cool. Thus, even

though the temperatures in the soils beneath the black and white-surfaced geomembranes were about the same, the amount of thermal energy transferred to the soil beneath the black geomembrane was far greater than the amount of thermal energy transferred to the soil beneath the white-surfaced geomembrane. Temperature alone is not a very good indicator of the complex heat transfer process.

PRACTICAL IMPLICATIONS

The test results presented in this paper clearly show that compacted clay will dry out and crack beneath a geomembrane. Although the test conditions do not exactly replicate field conditions (especially the short distance that water vapor had to travel to leave the laboratory test cells), there is ample evidence from the field that clay liners can desiccate beneath exposed geomembranes. There is also clear evidence of water vapor migration and condensation, e.g., at the toe of slopes. I would also appear that soils of increasing plasticity are likely to undergo greater desiccation for a given temperature regime. The analogy is similar to that of swelling soils (Holtz and Kovacs, 1981).

The main question is: how long can a geomembrane liner be left uncovered (exposed) without risking significant damage to the underlying compacted clay? To answer this question, one must first develop criteria for defining significant damage to a clay liner. Such criteria are beyond the scope of this paper. As a starting point, major drying of an entire lift of soil ($\cong$ 15 cm) is considered significant. Soil A underwent major drying after 2 to 4 weeks beneath the black geomembrane and after about 8+ weeks beneath the white-surfaced geomembrane. Soil B underwent major drying after 4 to 8 weeks beneath the white-surfaced geomembrane. Under field conditions, drying could be faster or slower. However, these laboratory results indicate: (1) major desiccation occurs within 2 to 8 weeks beneath a black geomembrane; and (2) use of a white-surfaced geomembrane prolongs the safe exposure period by about 2 to 6 weeks (nominally, about one month),

More work clearly needs to be performed to document desiccation in the field, particularly for geomembranes that are left uncovered for more than a few weeks.

CONCLUSIONS

Laboratory tests indicate that temperatures in the soils beneath both black and white-surfaced geomembrane liners that are exposed to daily heating cycles will increase, reach equilibrium in about a week, and will be similar to one another. The difference in temperatures provided by the two geomembrane surfaces does not account for the differences in the desiccation of the underlying soil. The much greater rate of heat transfer into the soil beneath the black geomembrane, and the much greater wrinkling that was observed in the black geomembrane, were the causes for greater drying beneath the black geomembrane.

An observation based on the findings of this work is that temperature-induced damage to compacted clay liners occurs beneath both black and white-surfaced geomembranes. The rate of desiccation was significantly larger beneath the black geomembrane. Engineers should consider providing a construction specification that designates a safe exposure time for an uncovered geomembrane overlying a compacted clay liner. Use of white-surfaced geomembranes may extend by a few weeks or more the safe operating period during which no significant damage occurs to the underlying clay liner. However, data from the field are lacking, and perhaps the most important conclusion from this work is that data need to be

collected from the field to document the degree of desiccation in compacted clay liners that are covered by exposed geomembranes for periods of a few weeks or more.

ACKNOWLEDGMENTS

REFERENCES

Basnett C and Bruner RJ (1993) "Clay desiccation of a single-composite liner system," Proceedings Geosynthetics '93, Vancouver BC, pp 1329-1340.

Cadwallader MW, Cranston M and Peggs ID (1993) "White-Surfaced HDPE Geomembranes: Assessing Their Significance to Liner Design and Installation," Proceedings Geosynthetics '93, Vancouver BC, pp 1065-1079.

Döll P (1996) Modeling Moisture Movement Under the Influence of Temperature Gradient: Desiccation of Mineral Liners Below Landfills, PhD Dissertation, Institute für Okologie, Technical University of Berlin, Germany, pp 251.

Fredlund DG and Rahardjo H (1993) Soil Mechanics for Unsaturated Soils, Wiley, NY 517p.

Holtz RD and Kovacs WD (1981) An Introduction to Geotechnical Engineering, Prentice Hall, Englewood Cliffs, NJ, 733p.

Houssiadas V (1995) "Desiccation cracking of compacted clay barriers overlain by geomembranes," MS Thesis, Department of Civil Engineering, Geotechnical Engineering Center, University of Texas at Austin, December, 76p.

Koerner GR and Koerner RM (1995) "Temperature Behavior of Field Deployed HDPE Geomembranes," Proceedings Geosynthetics '95, Nashville, TN, v3, pp921-937.

Mitchell JK (1993) Fundamentals of Soil Behavior, Second Edition, John Wiley and Sons, New York, 437p.

Terzaghi K and Peck RB (1967) Soil Mechanics in Engineering Practice, Wiley, NY, 729p.

Vielhaber B, Melchoir S, Berger K, and Miehlich G (1994) "Field Studies on the Thermally Induced Desiccation Risk of Cohesive Soil Liners Below Geomembranes in Landfill Covers," Proceedings 33rd Hanford Symposium on Health & Environment, In-Situ Remediation: Scientific Basis for Current and Future Technologies, Eds Gee and Wing, Pt 1, pp663-674.

Wellington J (1995) "Desiccation of compacted clay covered with white- and black-surfaced geomembranes," MS Thesis, Department of Civil Engineering, Geotechnical Engineering Center, University of Texas at Austin, May, 68p.

Design of GCL Barrier for Final Cover Side Slope Applications

Gregory N. Richardson, Ph.D., P.E.
G.N. Richardson & Associates, USA

Abstract

During the middle to late 80's, geosynthetic clay liners (GCL) were used as barrier layers on CERCLA covers to limit long term infiltration. This usage is increasing due to further regulatory driven need to limit infiltration on all waste containment systems and concerns about long-term dessication of compacted clay barriers. The addition of the GCL to a final cover system on a side slope creates the potential for failure of the slope caused by pore water pressure buildup immediately above the GCL and internal shearing of the GCL. This paper presents guidelines for (1) estimating the surface water infiltration rate above the GCL, (2) evaluate the shear stress in the GCL, (3) evaluating the acceptable level of pore water pressures above the GCL, and (4) estimating the actual leakage through the GCL. The ratio of the percentage of water infiltrating through the GCL to the total surface water infiltrating the cover system is termed the GCL efficiency. Laboratory data relating GCL efficiency to slope angle, infiltration rate, and pore pressure relief layer properties are presented.

Introduction

Geosynthetic Clay Liners (GCL) have been used in the USA and Europe since the late 80s to limit surface water infiltration at environmental restoration sites. Their uniformity as a manufactured product, speed of construction, relative insensitivity to freeze-thaw, and economy have led to an increasing use in the closure of both new lined landfills and in final cover systems over environmental restoration projects. The simplest GCL final cover system for side slopes is shown on Figure 1. The primary components of this system include (1) an erosion resistant vegetative layer that commonly includes a top soil layer and a vegetative support layer, (2) a pore water pressure relief layer, (3) the GCL infiltration barrier, and (4) a structural fill layer. The most important design parameter is the maximum rate of water infiltration through the vegetative layer to the pore water pressure relief layer. The final design must provide a minimum static factor of safety against sliding failure greater than 1.5, and provide an acceptable level of infiltration through the GCL. Each of these design consideration is presented in this paper.

Evaluation of Infiltration Rate

The maximum rate that surface water infiltrates to the pore water pressure relief layer on the side slope cab be estimated using either of the two following methods:
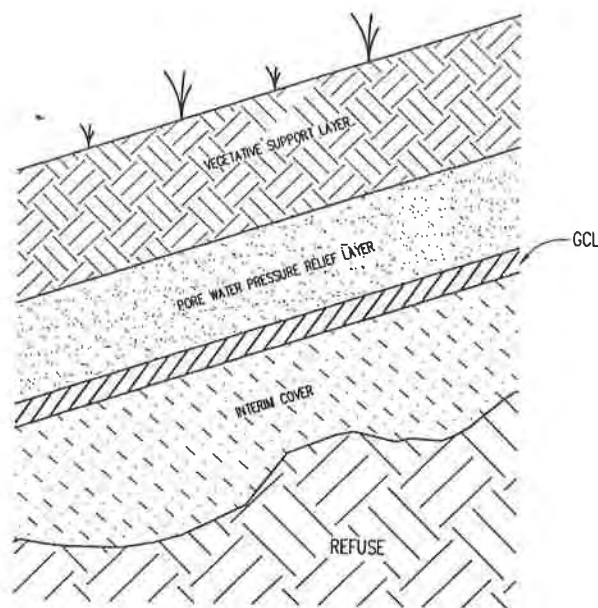
Figure 1. Typical GCL Final Cover System on Side Slope

<u>Method One - HELP3 Analysis</u> ---- In the latest version of HELP, Schroeder [1] has incorporated the research of Woolhiser, et al[2], to allow a conservative estimate of the rate and quantity of water infiltration through the side slopes. This method modifies the SCS runoff coefficient, CN, based on the following equation:

$$CN_{II} = 100 - (100 - CN_{IIo}) \cdot (\frac{L^{*2}}{S^*})^{CN_{IIo}^{-0.81}}$$

(1)

where L^* is a standardized dimensionless length, (L/500 ft), S^* is a standardized dimensionless slope, (S/0.04), and CN_{IIo} is the runoff coefficient for a mild slope under average soil moisture conditions. The peak daily rate of water infiltration through the vegetative layer can quickly be determined using the HELP model. HELP analyses performed in the southeast, assuming a good grass stand, predicted peak monthly infiltration through the vegetative layer ranging from 4 to 7 inches. This corresponds to equivalent infiltration velocities from 4 to 7×10^{-6} cm/sec. Note that the HELP based impingement rates are orders of magnitude less than predicted based on unit gradient method recommended by Thiel and Steward [3] for the Pacific Northwest. The difference with unit gradient assumption becomes less with good quality vegetation and increased permeability of the vegetative support layer. Vegetative cover layers that are not loams, e.g., sandy soils common to coastal regions, may approach the unit gradient condition.

<u>Method 2 - Unit Gradient</u> ---- Thiel and Steward [3] showed a vertical unit flow gradient exists for landfills in the northwest that are observed to have a vegetative layer that saturates during

the winter months. Under the unit gradient, the apparent vertical rate of infiltration, v, is given by Darcy's Law as follows:

$$Q = v \cdot A = K \cdot I \cdot A = K \cdot A \rightarrow v = K \quad (2)$$

Thus for the 4H:1V slope previously evaluated using the HELP model the infiltration rate would be equal to the permeability of the vegetative layer, or 1×10^{-4} cm/sec. Comparing the infiltration rates predicted by Method 1 and Method 2 clearly shows that the unit gradient assumption is very conservative when saturation of the final cover surface layers does not occur.

Evaluation of Maximum Allowable Pore Water Pressure

The stability of the soil veneers above the GCL can be evaluated by the following general equations for the stability of an infinite slope by Matasović[4]:

$$FS = \frac{c/(\gamma \cdot z \cdot \cos^2\beta) + \tan\phi\left[1 - \gamma_w(z-d_w)/(\gamma \cdot z)\right] - k_s \cdot \tan\beta \cdot \tan\phi}{k_s + \tan\beta} \quad (3)$$

where FS = factor of safety, k_s = seismic coefficient, γ = unit weight of slope material(s), γ_w = unit weight of water, c = cohesion, ϕ = angle of internal friction of the assumed failure interface or surface, z = depth to the assumed failure interface or surface, and d_w = depth to the water table (assumed parallel to the slope). The above equations yield the factor of safety explicitly for both cohesive (c $\neq$ 0) and cohesionless soils (c = 0). If there is no surface water infiltration, the depth to the water table, d_w, is set equal to the depth to the assumed failure plane, z.

Setting the seismic coefficient and cohesion equal to zero, and defining the pore water pressure, p_w, as $\gamma_w(z-d_w)$, Equation 3 reduces to the following expression:

$$FS = \frac{\tan\phi\left[1 - p_w/(\gamma \cdot z)\right]}{\tan\beta} \quad (4)$$

The allowable pore water pressures for a minimum slope stability factor of safety of 1.5 are shown on Figure 2 as a function of slope angle, β, and the interface friction angle, ϕ. For typical applications of a GCL on a side slope, e.g., $\beta = 14°$ and $\phi = 22°$, the allowable pore water pressure is only 30 psf or approximately 0.2 psi.

Internal Shear on GCL Barrier

The maximum shear stress, τ, acting on the GCL can be calculated[5] as follows:
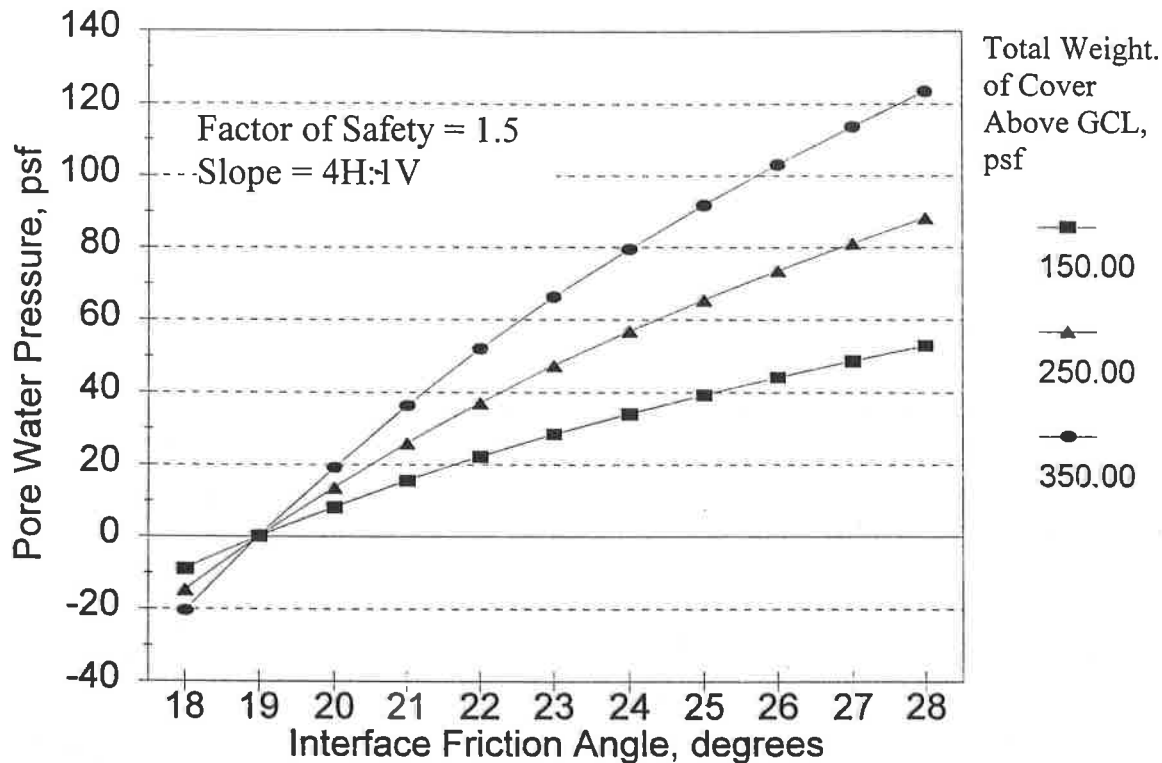
$$\tau = W_T \sin\beta \quad (5)$$

Figure 2. Allowable Pore Water Pressure on Side Slopes

where W_T is the total weight of the cover system over a unit area of the GCL and β is the slope angle. This relationship is shown on Figure 3 for a range of typical slope angles and cover unit weights. Use of a reinforced GCL having a post-hydration shear strength of 500 psf satisfies most typical cover applications. The use of an unreinforced GCL is not recommended since the possibility for full hydration and resulting loss of shear strength of the GCL exists.

Transmissivity of Pore Water Pressure Relief System

Thiel[3] showed that the minimum permeability, K_{pwr}, of the pore water relief layer is given by the following:

$$K_{pwr} = (v \cdot L) / D \cdot \sin \beta \tag{5}$$

where L is the slope distance between drainage outlets on the pore pressure relief system and D is the maximum head acting on the barrier. For pore water relief layers constructed with sand, the maximum head acting on the system is controlled by slope stability considerations and is found by dividing the allowable pore water pressure determined from Figure 2 by the density of water, γ_w. For pore water relief layers constructed with geonets, the minimum acceptable transmissivity of the geonet is given by the product of $K_{pwr} \cdot D$. The actual transmissivity of the geonet is commonly an order of magnitude greater than the minimum requirement.
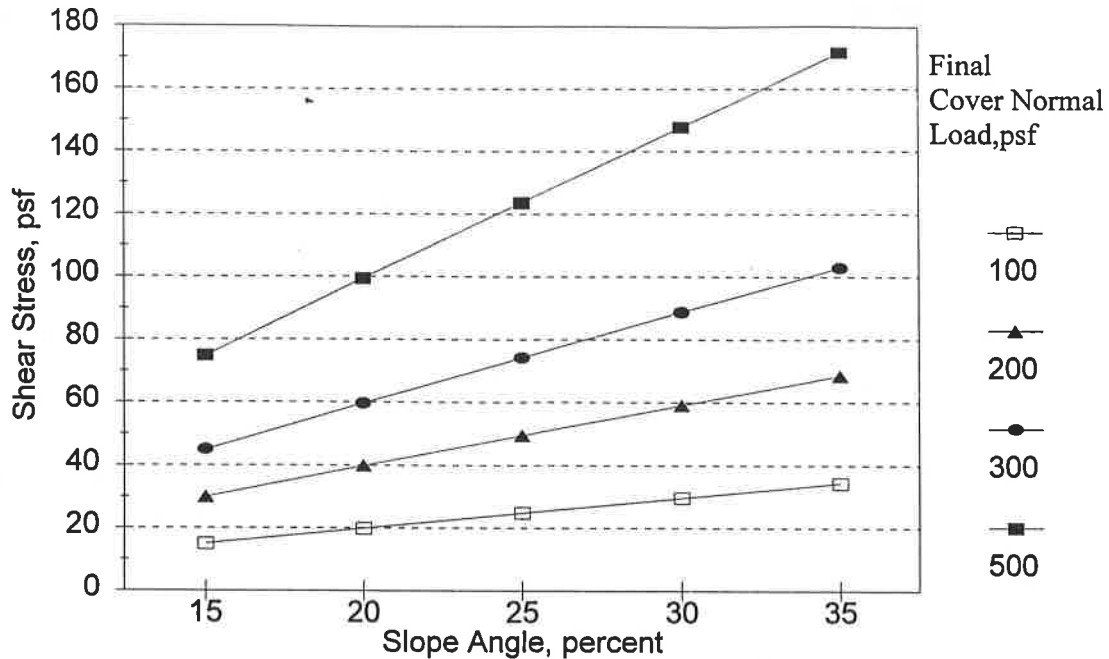
Figure 3. Shear Stress Acting on GCL on Side Slopes

Infiltration Through GCL

The maximum head acting on the GCL can be obtained from Figure 3. The average head acting on the GCL will be approximately half of the maximum head since the pore water pressure will be approximately zero at the drainage outlets at the top and bottom of the slope. The average flow gradient, $I = \Delta H/\Delta L$ acting across the GCL will then be given by $I = D/2t_{GCL}$, where t_{GCL} is the thickness of the GCL. Using Darcy's Law, the flow through the GCL, Q_{GCL}, can be expressed as follows:

$$Q_{GCL} = K_{GCL} \cdot \frac{D}{2 \cdot t_{GCL}} \cdot L \cdot 1 = \frac{K_{GCL} \cdot D \cdot L}{2 t_{GCL}} \tag{7}$$

By substituting Equation 5 into Equation 6, we can produce a general expression for the flow through a GCL side slope barrier as follows:

$$Q_{GCL} = \frac{K_{GCL} \cdot v \cdot L^2}{K_{PWR} \cdot 2 \cdot t_{GCL} \cdot \sin\beta} \tag{8}$$

The percentage of side slope infiltration water that actually penetrates the GCL, referred to as barrier efficiency, E, by the author, can be calculated by comparing Q_{GCL} to the total infiltration, $v \cdot L \cdot 1$. The efficiency of the GCL, E_{GCL} can be given as

$$E_{GCL} = [1 - \frac{K_{GCL} \cdot L}{K_{PWR} \cdot 2 \cdot t_{GCL} \cdot \sin\beta}] \cdot 100\% \qquad (9)$$

The GCL efficiency based on Equation 8 is presented on Figure 5 for a range of typical side slope conditions. For the majority of common side slope conditions, the GCL barrier clearly limit infiltration to less than 1% of the actual total side slope infiltration using clean sands or a geonet in the pore water pressure relief layer. For most of the southeast, the side slope infiltration represents less than 25% of the total precipitation. Thus the maximum infiltration anticipated through the side slope GCL is less than .25% of the total annual precipitation.
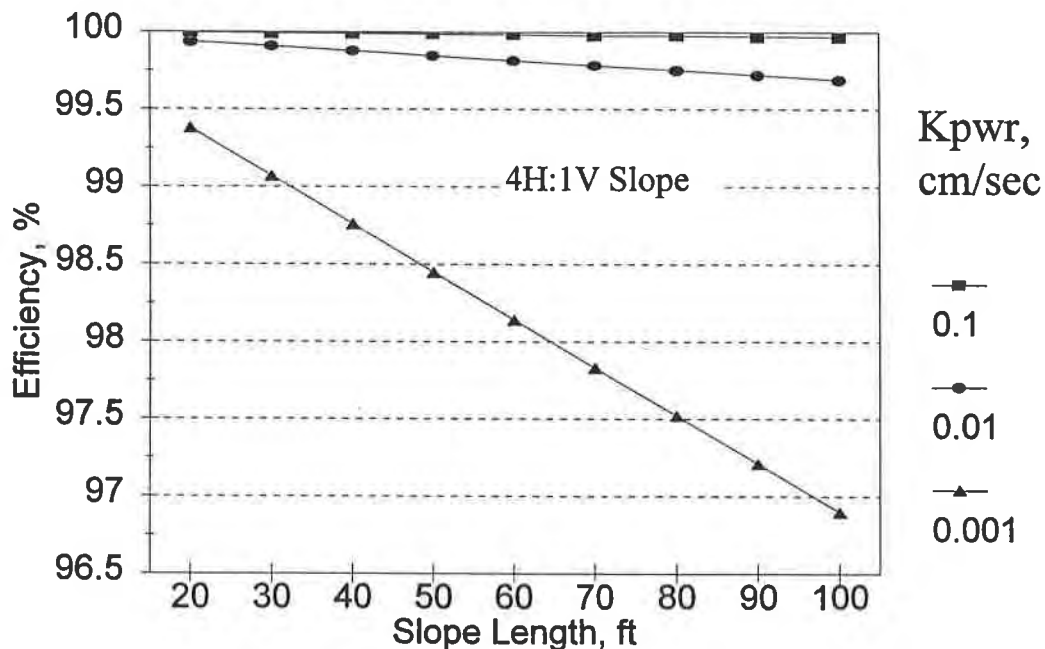

Figure 4. GCL Side Slope Infiltration Efficiency

Laboratory Evaluation of GCL Efficiency

A limited series of laboratory tests were performed to verify the relative magnitude of both leakage through the GCL and actual GCL efficiency as predicted by the above equations. These tests were performed in small (90x60 cm) flow boxes. Details of the flow boxes are shown on Figure 5. The flow boxes were mounted so that the slopes could vary from
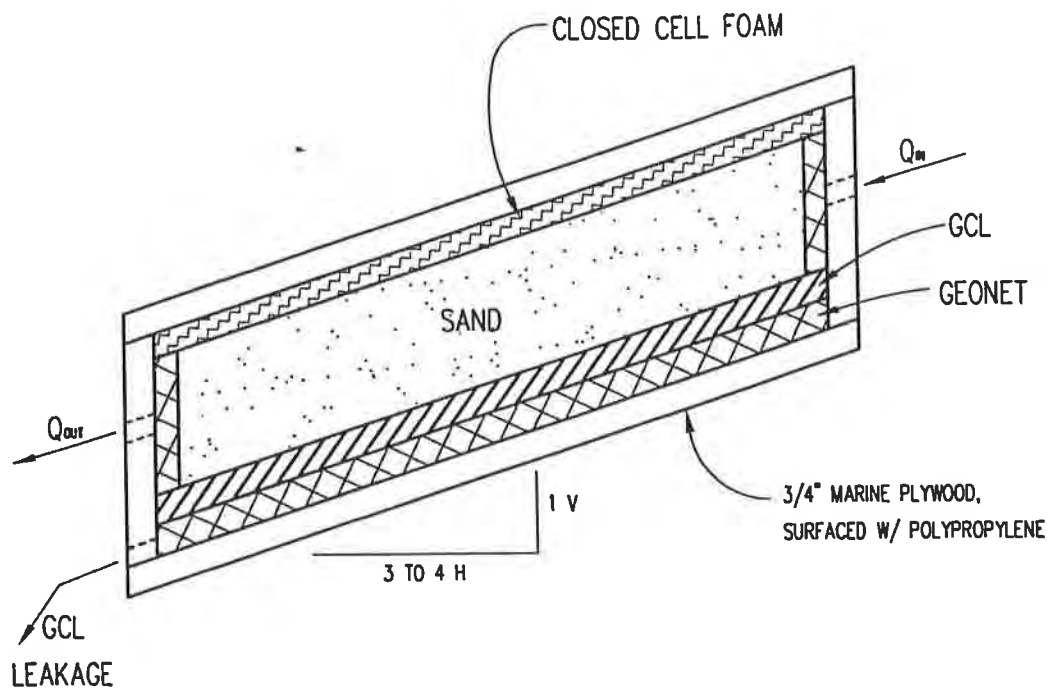
Figure 5. Laboratory GCL Efficiency Test Cell

4H:1V(14.0°) to 3H:1V(18.4°). Water was pumped into the flow boxes at a rate ranging from 0.6 to 1.5 gallons per minute. The sand is a clean, relatively uniform sand commonly used for construction of water well sand filters. The sand has a D_{10} grain size of 0.10 cm. Based on Hazen's formula, $k(cm/sec) = 100\ D_{10}^2$, the sand has a permeability of ≈ 1.0 cm/sec.

The GCL efficiency can be calculated from Equation 9 assuming the permeability of the GCL is 5×10^{-9} cm/sec and that the thickness of the GCL is 0.5 inch. The GCL thickness was measured as samples of the as-tested GCL was removed from the flow boxes and average 12 mm. The GCL efficiency predicted based on Equation 9 is equal to approximately 100%, i.e., no infiltration. Test data from the flow boxes is given on Table 1 for several measured flow rates. The quantity of water infiltrating through the GCL is so small that it had to be captured in a sealed bottle to prevent evaporative loss from destroying it.

It should be noted that minor infiltration through the GCL did occur for the initial 24-hours of each test. This was the time required for the bentonite granules to hydrate sufficiently that such that the GCL sealed. The GCL efficiency predicted based on Equation 8 is equal to approximately 99.99%. The measured efficiency for these tests ranged from 98.4 to 100%, but could not be quantified to the accuracy of Equation 9. The majority of GCL samples tested had no measurable infiltration through the GCL after the initial 24 hour wetting cycle. What infiltration that did occur is thought to be due to difficulties in sealing the GCL edges during the tests.

Table 1 Laboratory GCL Efficiency Test Data

Slope	Series Description, (Box 1 or 2 - Series)	Supply Rate, liter/min	Leakage Rate cc/min	Efficiency %
4H:1V	Coarse Sand-1-A	2.3	38	98.4
	Coarse Sand-2-A	3.0	0	100
	Coarse Sand-1-B	5.7	12	99.8
	Coarse Sand-2-B	5.7	0	100
	Fine Sand-1-A	.25	0	100
	Fine Sand-1-B	.25	5	98.0
3H:1V	Coarse Sand-1-A	2.3	14	99.4
	Coarse Sand-2-A	2.3	0	100
	Coarse Sand-1-B	5.7	0	100
	Coarse Sand-2-B	5.7	0	100

Unfortunately, the GCL's are inherently so efficient that longer slope lengths are required to collect measurable flow through the GCL. The tests were repeated using a finer sand having a permeability of approximately .01 cm/sec. Under the same circumstances, the finer sand produced no discernable increase in leakage through the GCL even though the head acting on the GCL was increased.

Example Application

Design a GCL side slope barrier cover for a landfill located near Raleigh, North Carolina. Assume a 4H:1V side slope, a minimum interface friction value between the GCL and the sand pore water relief system of 22 degrees, a sand drain layer permeability of 1×10^{-2} cm/sec, and that the cover section includes a 24-inch thick vegetative support layer and a 9-inch thick sand pore water relief layer over the GCL.

- Evaluation of Infiltration Rate : The design infiltration rate is obtained based on HELP analysis as 6.1×10^{-6} cm/sec.

- Evaluation of Maximum Allowable Pore Water Pressure : The unit weight of the soil overlying the GCL is approximately 100x(24+9)/12= 366 psf. Using an interface friction of 22° and a unit weight of ≈350 psf, the maximum allowable pore water pressure is obtained from Figure 2 as 52 psf or approximately 10 inches of water.

- Evaluate the Actual Pore Water Pressure : The actual head acting on the GCL can be calculated from Equation 5 by assuming a drainage length, L. For most covers in the East, it is common to place side slope swales every 20 foot vertical which results in a maximum drainage length of approximately 82.5 feet. Equation 5 can be modified as follows:

$$D = v \cdot L / (K_{pwr} \cdot \sin \beta) \tag{10}$$

Substituting site values into Equation 5, the calculated maximum head acting on the GCL is ranges from 2 feet for a 1×10^{-3} cm/sec sand to 0.2 feet for a 1×10^{-2} cm/sec sand in the pore water pressure relief system. Obviously, the head of water must be less than the thickness of the pore water pressure relief layer. For this example, we will assume a 1×10^{-2} cm/sec sand is available such that the maximum head acting on the GCL is 0.2 feet.

- Calculate Infiltration Through GCL : The leakage through the GCL can be found using Equation 7 with $K_{GCL} = 5 \times 10^{-9}$ cm/sec, $D_{AVE} = 0.2/2 = 0.1$ feet, L = 82.5 feet, and the thickness of the GCL, t_{GCL}, assumed equal to 12 mm. The resulting flux is equal to 6.8×10^{-8} ft^3/sec or 0.00053 gal/ft^2/day.

- Calculate the GCL Efficiency: The efficiency of the GCL can be calculated from Equation 9 with $K_{GCL} = 5 \times 10^{-9}$ cm/sec, $K_{PWR} = 1 \times 10^{-2}$ cm/sec, L = 82.5 feet, and the thickness of the GCL, t_{GCL}, equal to 12 mm. Substituting these values predicts an efficiency of 99.78%.

Summary

This paper presents a general methodology for the design of GCL barriers on side slope applications. The design procedure accounts for slope stability and infiltration considerations and can be adapted for side slopes of varying steepness. Additionally, the result of the numerical analysis and limited laboratory test program indicate that the use of a GCL barrier in such systems is capable of limiting infiltration through the cover to less than 1% of the surface infiltration. Since less than 25 % of the site precipitation typically infiltrates such slopes the total infiltration may be less than 0.25% of site precipitation. Thus in most applications, the use of a GCL barrier alone will provide adequate control of infiltration and eliminate stability problems associated with the use of composite barriers on side slopes.

References

1. Schroeder, P.R., et al (1994), "The Hydrologic Evaluation of Landfill Performance Model," EPA/600/R-94/168b, Environmental Protection Agency, Office of Research and Development, Washington, DC.

2. Woolhiser, D.A., Smith, R.E., and Goodrich, D.C. (1990), "KINEROS, A Kinematic Runoff and Erosion Model: Documentation and User Manual," ARS-77, US Department of Agriculture, Agricultural Research Service.

3. Thiel, R.S., and Steward, M.G. (1993), "Geosynthetic Landfill Cover Design Methodology and Construction Experience in the Pacific Northwest," Proc. *Geosynthetics '93*, IFAI, St. Paul, MN.

4. Matasović, N. (1991), "Selection of Method for Seismic Slope Stability Analysis," Proc. *2nd International Conference on Recent Advances in Geotechnical Earthquake Engineering and Soil Dynamics*, St. Louis, Missouri, Vol. 2, pp. 1057-1062.

5. T. William Lambe and Robert V. Whitman, 1968. Soil Mechanics, John Wiley & Sons, New York, pp 355.

SI Conversions

1 inch = 2.54 cm
1 psf = 0.04788 kilonewtons/square meter
1 pcf = 5.787 kilonewtons/cubic meter
1 gallon = 0.00037854 cubic meter

Geosynthetics in a Salinity-Gradient Solar Pond Environment

M.A. Lichtwardt
Bureau of Reclamation, USA

A.I. Comer
Bureau of Reclamation, USA

ABSTRACT

This paper describes the latest in salinity-gradient solar pond lining systems. The high-temperature, high-salinity environment unique to a salinity-gradient solar pond resulted in failure of the geomembrane liner at the El Paso Solar Pond Test Facility after only eight years of operation. Research involved in pond reconstruction led to the selection of a lining system consisting of a flexible polypropylene (PP) geomembrane for the sidewalls and a specially formulated geosynthetic clay liner (GCL) on the bottom of the pond. The two liners have been installed and a comprehensive test program is being conducted to measure their performance.

The environment encountered in a salinity-gradient solar pond will be discussed as well as material selection criteria and the design of the two liners. Preliminary results of the GCL performance monitoring will also be presented.

INTRODUCTION

In the spring of 1992, a leak was detected in the primary geomembrane liner in the main pond at the El Paso Solar Pond Test Facility. Strength testing indicated that the liner had become brittle and in some areas its strength was as low as 10% of its original value. This failure demonstrated the need for liners capable of withstanding the harsh environment of a salinity-gradient solar pond which typically includes high temperatures, high salinity, and low pH. In 1994 the pond was reconstructed with 15° sideslopes, and a new lining system was designed specifically for this application. The new lining system consisted of a flexible polypropylene (PP) geomembrane on the sidewalls and a geosynthetic clay liner (GCL) on the bottom of the pond. It was designed in such a way as to allow monitoring and testing of two geosynthetic materials. The lining system was installed in 1994. A test program has been developed, and data is currently being collected to measure the performance of both the geomembrane and the GCL in this environment.

HOW A SALINITY-GRADIENT SOLAR POND WORKS

Fluids such as water and air rise when heated. Salinity-gradient solar ponds stop this process when large quantities of salt are dissolved in the hot bottom layer of the pond, making it too dense to rise to the surface and cool.

Salinity-gradient solar ponds consist of three layers. The top layer, called the upper convective zone, is cold and has little salt content. The bottom layer, called the storage zone, is hot and very salty. Separating these two layers is the gradient zone in which the salt content increases with depth. Water in the gradient cannot rise or fall because the water above it has less salt content and is therefore lighter, and the water below it has a higher salt content and is heavier. The stable gradient zone acts as a transparent insulator, permitting sunlight to be trapped in the storage zone. The El Paso Solar Pond has a surface area of approximately 4000 m^2 (1 acre) with the water depth averaging 3.2 meters. The storage zone is about 1 m deep and typically operates at temperatures of 70-93°C (160-200°F). This thermal energy is used for industrial process heat, to generate electricity, and to desalinate water.

XR-5 LINER FAILURE

The primary liner that failed in 1992 at the El Paso Solar Pond Test Facility was XR-5 8130 (SP), an ethylene interpolymer alloy (EIA) coated polyester fabric. It was installed in 1984 over an existing Hypalon (chlorosulphonated polyethylene) liner. At the time of installation, the estimated life of the XR-5 was 20 years and a 10-year warranty was provided by the manufacturer. A failure analysis indicated that the XR-5 liner had become brittle, and the strength of the material near the bottom of the pond was as low as 10% of its original value. The material installed near the top of the pond indicated 90% of original strength.

A total of 102 holes were found in the liner with 91 of these in the storage zone and 11 in the gradient zone (Robbins, 1994). The largest hole was located at the top of the storage zone and was 1.04 meters (41 inches) long. In many areas, the subgrade had shifted, causing additional stress and failure of the liner. The conclusion was that the XR-5 had deteriorated beyond repair and would have to be replaced.

The unique environment of a salinity-gradient solar pond includes high temperature, high salinity, and low pH. Over a period of many years, a solar pond liner is also subjected to temperature cycling which can have an adverse effect on the mechanical properties of a geomembrane. During the eight years of operation at the El Paso Solar Pond, the liner in the storage zone was exposed to a saturated brine (NaCl) solution at temperatures up to 93°C (200°F), with ions of free chlorine, copper, aluminum, iron, and sulfate present (Lu, 1996). The pH ranged from 4 to 7. Chemicals such as copper sulfate and hydrochloric acid were occasionally added to the pond to prevent algae growth and to provide clarity control. Investigations are ongoing to

determine what caused the loss of strength in the liner, but it appears that the high temperature, high salinity, and low pH all contributed to the failure.

LINER SELECTION

There are five different environments in a salinity-gradient solar pond that must be considered in determining the parameters for liner selection - the anchor trench, the area exposed to ambient conditions, and the upper convective, gradient, and storage zones. These are shown in Figure 1.
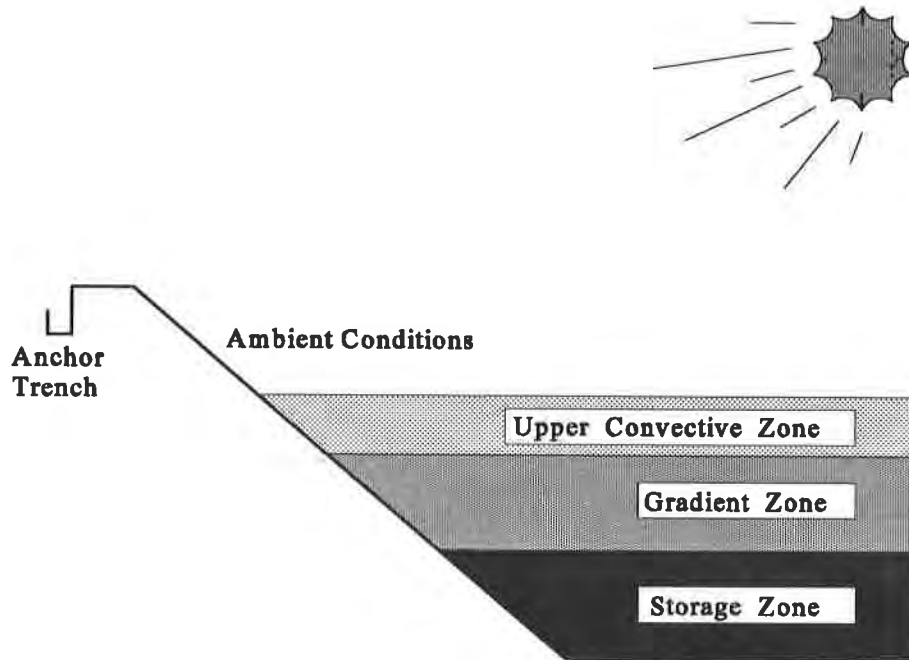

Fig. 1. Solar Pond Cross-Section

Each of these has its own unique environmental elements. The storage zone has the harshest environment with the following conditions:

$$\text{Maximum Temperature} = 93°C \ (200°F)$$
$$\text{Specific Gravity} = 1.2$$
$$\text{pH} = 4 \text{ to } 7$$

Conditions from each zone were considered in determining the best possible lining system design.

The first liner design to be investigated was a compacted clay/plastic lining system. This type of liner was installed in the 250,000 m² (60-acre) solar pond at Beit Ha'arava, Israel with promising results. A compacted clay/plastic liner offers many advantages including low cost and

puncture resistance, however, finding a suitable clay locally for such a liner is often difficult. In El Paso, five local clays were tested to determine optimum compaction, hydraulic conductivity, and mineralogical composition. When none of the five clays proved acceptable for use in a solar pond environment, attention turned to a flexible geomembrane liner and a GCL which uses a thin layer of bentonite clay to achieve low permeability without requiring field seaming.

Geomembrane Liner

A suitable geomembrane liner for a salinity-gradient solar pond application would ideally have the following qualities:

- Low cost (materials and installation)
- Long life
- High-temperature resistance
- Corrosion resistance
- UV resistance
- Good puncture resistance
- Good tensile properties
- Low coefficient of thermal expansion
- Low weight

After extensive research into the properties and characteristics of various materials, the decision was made to use a flexible polypropylene liner. Polypropylene has excellent high-temperature and chemical resistance properties, a low coefficient of thermal expansion, and good mechanical properties.

The new flexible polypropylene liner was manufactured by GSE Lining Technology, Inc. (formerly Gundle Lining Systems) using resin provided by Montell Polyolefins (formerly Himont USA). Material testing was conducted on the polypropylene liner by GSE. These tests showed that the material has good temperature resistance, chemical resistance, and elongation properties.

Geosynthetic Clay Liner

There are several advantages to using a GCL in a solar pond rather than a conventional geomembrane or compacted clay/plastic liner. A GCL can be overlapped and does not require seaming which makes the installation much easier and less expensive.

The GCL manufactured for the El Paso Solar Pond is a modified version of Gundseal®, a product of GSE Lining Technology, Inc. The GCL for the El Paso installation has a 30-mil flexible polypropylene geomembrane backing with 0.5 cm (0.2 inches) of bentonite clay bonded to one side. The bentonite was obtained from the Bentonite Corporation.

The hydraulic conductivity of the bentonite is determined by the type of bentonite used, the type and strength of the permeant liquid, and whether or not it is hydrated with fresh water prior to permeation (Daniel, 1994). The bentonite selected for the El Paso solar pond has a 92% montmorillonite content and is formulated to resist the effects of contamination from salt water. It has a free swell of 31 ml per 2 g of dry material. The GCL was hydrated with fresh water to maximize its performance and to simulate what would occur in a real world application.

LINER INSTALLATION

The installation of the two liners and all necessary instrumentation at the El Paso Solar Pond Test Facility was completed in 1994, and the 4000 m^2 (1 acre) main pond was back in operation by April 1995. Figure 2 shows the design of the two lining systems.

The sidewall liner is 40-mil polypropylene installed over a 30-mil polypropylene secondary containment liner. These two liners are separated by a 340 g/m^2 (10 oz/yd^2) geotextile, and the lining system is equipped with a leak detection system.

The GCL was installed on the bottom of the pond with the clay side down to minimize contact between the bentonite and the sodium chloride brine. The drainage system installed underneath the GCL was designed to duplicate a real-world installation while monitoring the leakage rate. The seams were overlapped 30-50 cm (12-20 inches) and an overburden greater than 1.44 kPa (30 lb/ft^2) was installed as recommended by the manufacturer.

PERFORMANCE TESTING

A test program has been established to measure the performance of the two liners and to study the aging and durability characteristics of the flexible polypropylene geomembrane in a solar pond environment.

Flexible Polypropylene Geomembrane

Several test coupons were fabricated, instrumented with type-T thermocouples, and installed on the south-facing slope of the solar pond. These coupons extend from the anchor trench to the bottom of the pond so that material from all zones of the pond can be analyzed. The physical and mechanical properties of the exposed material are tested periodically, and the results compared to those obtained from unexposed samples of the original material. In addition, the surface morphology of the exposed material is observed using a scanning electron microscope.

Parallel to the field-aging study, samples of the polypropylene are evaluated in the laboratory under controlled accelerated aging tests. To simulate sunlight aging, the geomembrane is exposed to UV in a UV-fluorescent weatherometer and examined at regular intervals. The laboratory
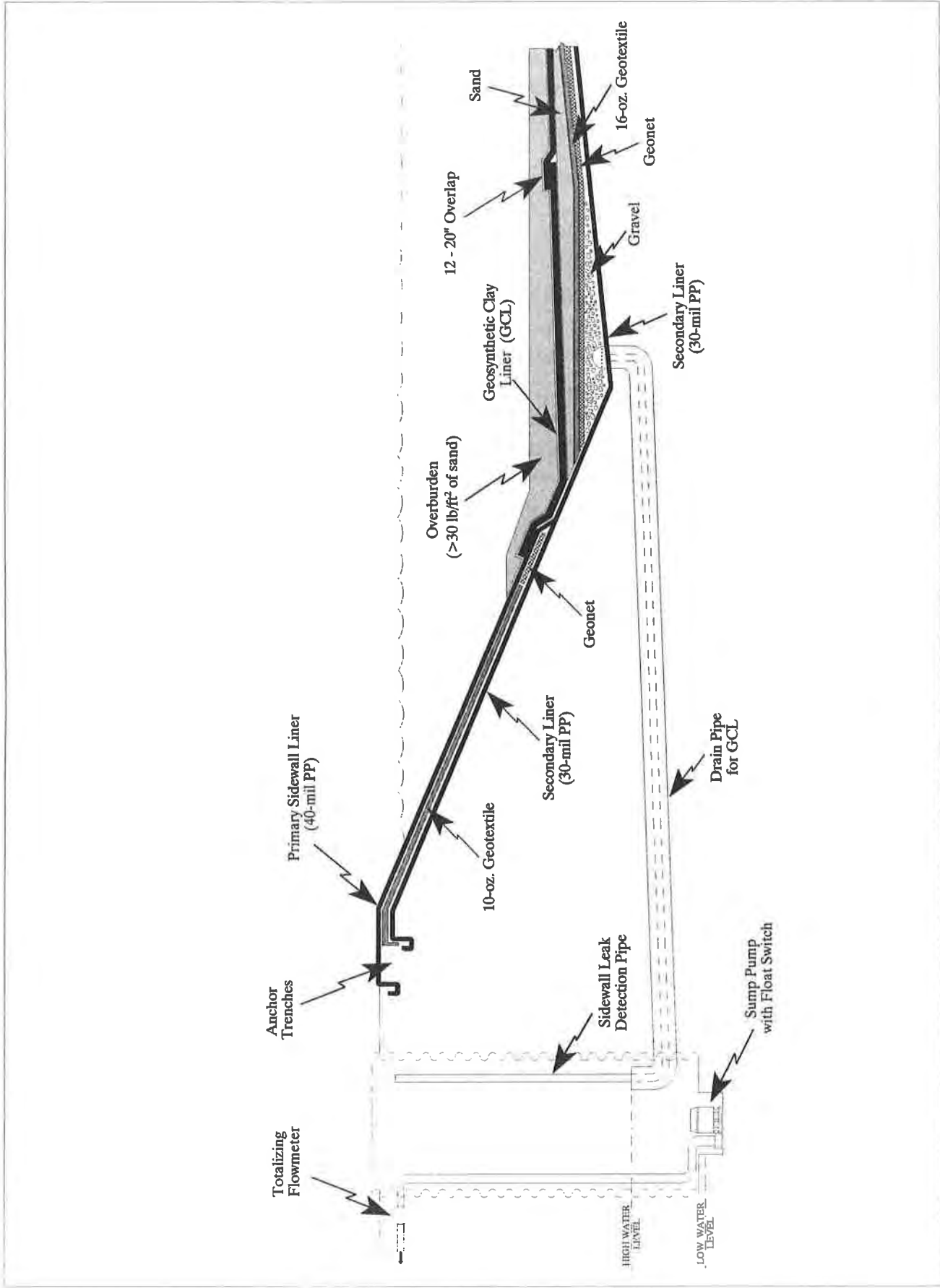
Figure 2: Composite Liner Design and Monitoring System at the El Paso Solar Pond Test Facility

experiment will continue until 50% reduction in mechanical properties is observed. The results will be reported in future work.

All laboratory testing of the flexible polypropylene geomembrane is being conducted by the Geosynthetic Research Institute at Drexel University. The first coupon sample was retrieved in December 1995, and the second sample was retrieved for analysis in July 1996.

GCL Monitoring

The hydraulic conductivity of a GCL can be determined by measuring flow through the liner as a function of time. As illustrated in Figure 2, any water that permeates the GCL is collected in a sump and intermittently pumped out through a totalizing flow meter. The data is recorded on a regular basis to determine if the permeability is acceptable and to determine what effects the high-temperature, high-salinity, low pH environment has on the GCL.

Figure 3 shows the temperatures that were measured in the storage zone at the beginning of the heating season in the Spring of 1996. The sharp decreases in temperature coincide with periods
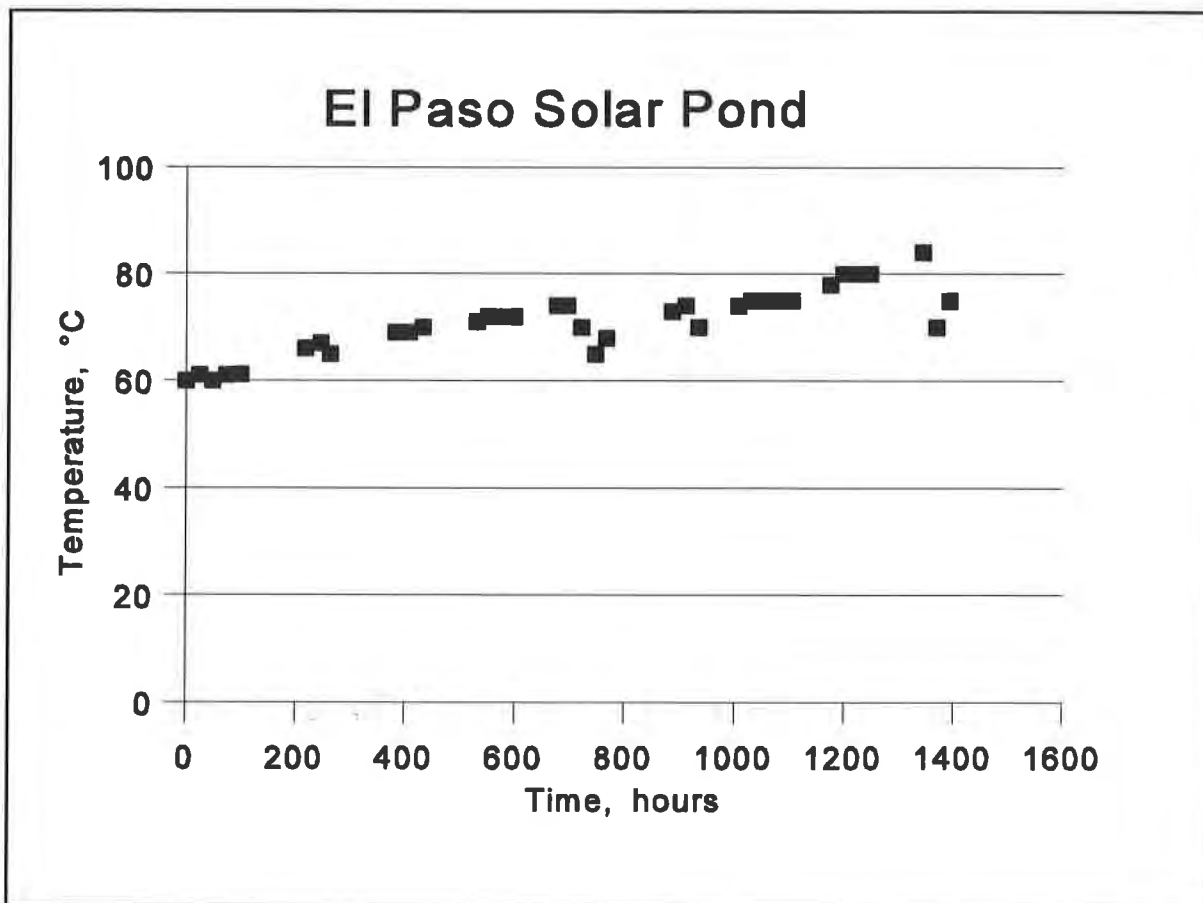

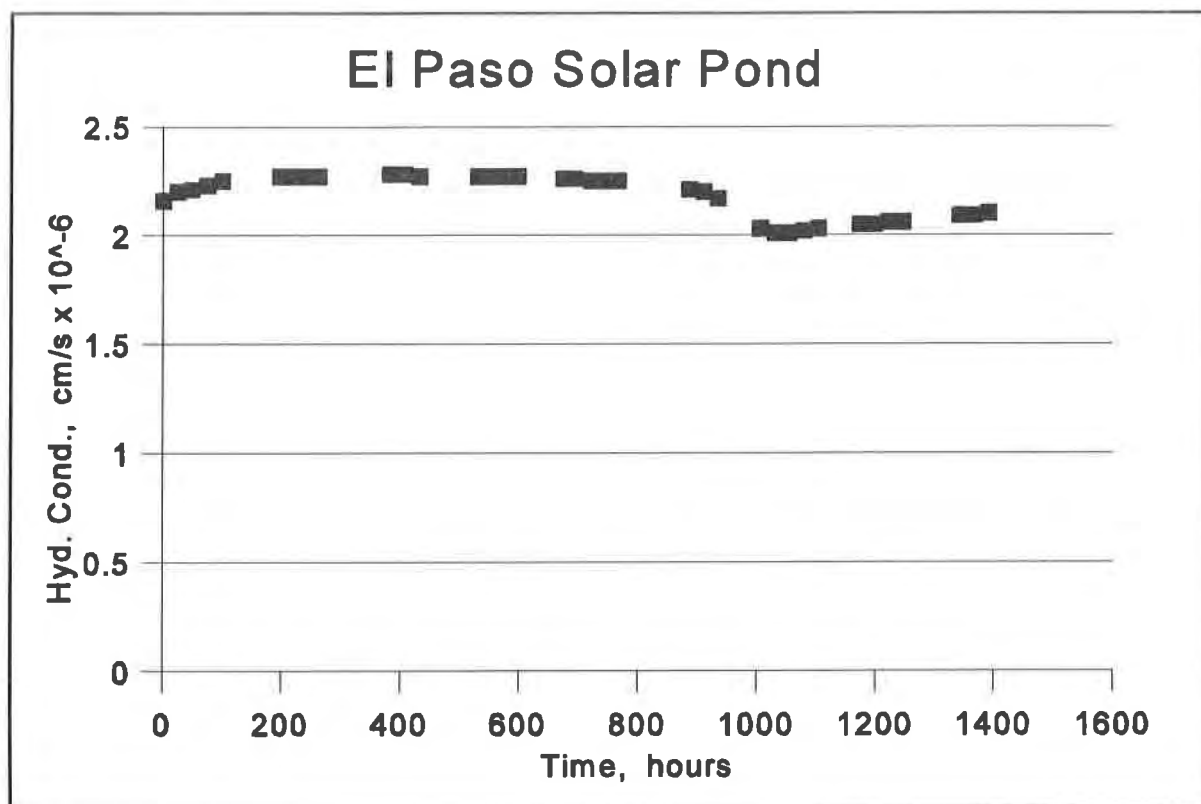**Figure 3:** Storage Zone Temperature vs. Time

Figure 4: Hydraulic Conductivity of the GCL vs. Time

when thermal energy was being withdrawn from the storage zone. Figure 4 shows the hydraulic conductivity of the GCL over the same nine-week period. Currently, the hydraulic conductivity is about 2×10^{-6} cm/sec. It appears that the hydraulic conductivity may improve with increasing temperature, but more data is needed before any definitive conclusions can be made.

The preliminary hydraulic conductivity data also indicates that the permeability of the bentonite has increased since the initial start-up of the pond in 1995. At that time values on the order of 1×10^{-6} cm/sec were measured. This increase may be due to the effect the sodium chloride has had on the bentonite.

CONCLUSIONS

The current hydraulic conductivity of the GCL is 2×10^{-6} cm/sec. This is higher than expected for a GCL, but satisfactory for a salinity-gradient solar pond. This value may be higher due to the high salinity and low pH experienced in the storage zone of the solar pond. However, the hydraulic conductivity of the GCL at the El Paso Solar Pond is comparable to that of the compacted clay/plastic lining system used in Israel, which consisted of three 20 cm (8 inch) layers of compacted clay, each separated by a geomembrane. The preliminary data indicates that the

permeability of the GCL may improve with increasing temperature, but more data is required before definitive conclusions can be drawn.

The PP geomembrane has also performed well in the high-temperature, high-salinity, and low pH environment. However, as predicted by the performance testing, the primary liner above the water line has experienced premature failure due to UV degradation. Further investigation revealed that the polypropylene resin was improperly stabilized. A new primary liner with the proper stabilizers will be installed in February of 1997.

ACKNOWLEDGMENTS

REFERENCES

Daniel, D.E., and J.L. Ruhl, "Effects of Leachate on the Hydraulic Conductivity of Bentonite and Contaminant-Resistant Bentonite in Gundseal®," University of Texas at Austin, Austin TX, 1994.

Lu, H., and A.H.P. Swift, "Reconstruction and Operation of the El Paso Solar Pond with a Geosynthetic Clay Liner System," *Solar Engineering - 1996*, ASME Press, New York NY, 1996.

Robbins, M.C., and A.H.P. Swift, "Liner Selection for the El Paso Solar Pond," University of Texas at El Paso, El Paso TX, 1994.

Erosion Control

GEOSYNTHETICS 97

CONFERENCE

Long Beach, California USA

GEOTEXTILE REINFORCED VEGETATED SPILLWAYS

F. GASPER, P.E.
USDA - NATURAL RESOURCES CONSERVATION SERVICE, USA
D. W. BURGDORF
USDA - NATURAL RESOURCES CONSERVATION SERVICE, USA

ABSTRACT

The United States Department of Agriculture-Natural Resources Conservation Service (Formerly the Soil Conservation Service) in Michigan has developed a concentrated flow area protection system using nonwoven geotextiles in combination with vegetation. The system incorporates a 135 g/m² (4 oz./yd.²) nonwoven geotextile and selected plant species to provide permanent erosion control for concentrated flow situations. This system has been installed as reinforced vegetated spillways for channels and dams, and as repair for eroded areas in new and existing waterways. This system was developed to provide a natural looking, low cost, hydraulically efficient, alternative to hard structures such as rock chutes, concrete chutes, and pipe spillways. The use of nonwoven geotextiles for permanent erosion control has been under development since 1989.

Current design and installation techniques are based on experience with 500 installations, Construction Industry Research and Information Association Report 116[1], and tests on turf reinforcement mats. The design flows for chute spillways have been up to 3.4 m³/sec (120 ft.³/sec.) The overfalls controlled by chute spillways have been up to 5 m (17 ft.) high. A 50% to 80% reduction in design and installation costs compared to traditional erosion control structures has been documented.

INTRODUCTION

Grass is commonly used as a low cost means of protecting the soil surface against the erosive forces of flowing water. The major drawback of using vegetation as the sole protection medium is that high flow velocities tend to dislodge both soil and vegetative growth. By incorporating a non-woven geotextile as a reinforcing material, soil erosion and vegetative detachment are greatly reduced. The geotextile provides additional shear strength to the vegetative and soil structures, allowing relatively high flow velocities.

Thousands of small gully erosion sites at the edges of streams and lakes, and in waterways need treatment, but cost and complexity of solutions, as well as, restricted access for construction equipment and material limits the installation of needed erosion control structures. United States Department of Agriculture-Natural Resources Conservation Service (NRCS) (Formerly the Soil Conservation Service) in Michigan has developed a method of erosion control using lightweight non-woven geotextile fabric for soil reinforcement and filtering to maintain soil beneath the geotextile. The design, installation and monitoring of 500 geotextile spillways has provided information for reliable design, construction and maintenance. This method of turf reinforcement may also be applied to auxiliary spillways for dams.

HISTORY

The original installations in Michigan were installed in 1988 by NRCS District Conservationist, James Vosburgh with help from Agrimat representatives from B&B Marketing of Madison, Wisconsin (a geotextile fabric supplier) without professional engineering or plant materials specialist input. These were reviewed in the field by the authors in the spring of 1990. Standard construction drawings were developed and eight trial geotextile spillways were constructed in Shiawassee County, Michigan. A paper on these original eight spillways was presented to the American Society of Agricultural Engineers in 1992[2]. Additional information was obtained from the Construction Industry Research and Information Association-Report 116[1] and United States Department of Transportation Hydraulic Engineering Circular 15[3].

Evaluations were made on several sites per year since initial installations were made. The success rate is over 95%. Success is defined as 80% cover and no indications of erosion from under the geotextile. A NRCS report was completed in September of 1994 that provided recommendations for changes in the standard design,

construction techniques, allowable flow velocities and vertical drop limits. The 1994 report involves detailed study of the eight Shiawassee County installations plus 35 other spillways.

DESIGN

Location. Appropriate location is where soil and climate conditions can provide a vigorous growth of the vegetation. The geotextile spillway is designed for concentrated flow conditions where vegetation alone is not a stable solution. This technique has been used in the midwestern United States, primarily in Michigan.

Soils. The recommended soils have a minimum of 20 per cent of material passing the #200 sieve. The best soils to construct in are loamy lower plasticity soils. These soils have clods that are relatively easy to break, good moisture holding capacity, and adequate strength for slope stability. Spillways in sandy soils have not been successful due to erosion of the material from below the geotextile and difficulty in establishing vegetation. Good soil-geotextile contact is difficult to obtain in heavy soils due to clods. Spillways have been placed on organic soils successfully.

Geotextile Materials. The geotextile weight criteria is set to provide strength while allowing root penetration requirements. Heat bonding is allowed on one side of the material. The smoother fabric surface created by heat bonding increases the likelihood of the seed mixture rolling or sliding off the geotextile material. As a result, any heat bonded face is placed in direct contact with the soil. The geotextile specified below serves three purposes:

1) It provides an erosion resistant barrier until the vegetation becomes established. In the initial stages of grass growth, an unprotected soil surface is highly susceptible to erosion.

2) The soil, geotextile and vegetation work together to provide a more stable channel than vegetation alone. Non-reinforced vegetated areas are more likely to have individual plants dislodged due to flowing water than reinforced vegetated water courses (Hewlett, 1987). The vegetation in conjunction with the geotextile function as a single unit instead of individual plants.

3) The geotextile acts as a filter to limit soil movement through the geotextile.

Property	Test Method	
Weight		100 to 160 gm/m² (3.5 to 5.5 oz./yd.²)
Tensile Strength	ASTM D 4632	0.5 kN min. (100 lbs. min.) 1/
Mullen Burst Strength	ASTM D 3786	1450 kPa min. (210 psi min.) 1/
Elongation	ASTM D 4632	100% max. 1/
Puncture	ASTM D 4833	0.2kN min. (50 lb. min. 1/)
Ultraviolet Light Resistance	ASTM D 4355 150 hr. exposure	70% min. tensile strength retained
Apparent Opening Size (AOS)	ASTM D 4751	Less than or equal to 0.212 mm (70#)2/
Permittivity	ASTM D 4491	0.70 sec.-1 1/

1/ Minimum roll value (weakest principal direction): average minus two standard deviations (only 2-1/2 percent will be lower).

2/ U.S. standard sieve size.

Vegetation. The vegetation has functions of shading the geotextile to reduce ultraviolet light degradation and permanently anchoring the geotextile to the soil. A seeding rate of approximately 450 kg/ha (400 lb./acre) has been used. This amounts to less than 0.9 kg (2 lb.) of seed per spillway since the average surface area of geotextile spillways has been only (200 to 300 ft.²). The seed recommended includes perennial rye, tall fescue, smooth brome, and creeping red fescue. Several other seed blends have been used and more study could be done on appropriate mixtures. A dormant seeding (seeding in early winter) was used on a three structures and was successful. Observation in the field indicates that legumes such as Birdsfoot Trefoil can grow successfully.

Hydrology. The spillways in this study have been designed to safely handle the runoff from a 10-year 24 hour rainfall. The maximum design flow has been 3.4 m³/sec (120 ft.³/sec.) The geotextile spillway has not been used for continuous flow situations. This is due to the difficulty in maintaining vegetation in saturated soil conditions.

<u>Hydraulics.</u>   The flow velocities for the spillways have been calculated using Manning's equation using "n" values obtained from retardance curves[4].   By observation of vegetation, appropriate retardance values for design are "B" for capacity and "C" for velocity for slopes that are 3H:1V or flatter Slopes steeper than 3H:1V have been designed using retardance curve "D" for velocity design.   The maximum design velocities have been 3 m/sec (10 ft./sec.) for short duration storms.   The duration of the storm is limited by the maximum spillway capacity and through not allowing continuous flow situations. Newly installed geotextile spillways have not been damaged by velocities of 4.3 m/s (14 ft./sec.)   Newly constructed geotextile spillways have failed under flow velocities of 5.5 m/s (18 ft./sec.). Allowable shear stress was not calculated.

Drawings.   A Michigan NRCS standard drawing has been developed and included with this paper.

INSTALLATION

<u>Site Preparation.</u>

1) The surface is shaped as a spillway with a slope of 2H:1V to 7H:1V. The soil is fertilized and limed as needed.
2) The upstream and downstream ends of the spillway are trenched.
3) The area of the spillway that will be in contact with the geotextile is smoothed and clods and rocks greater than 1.3 cm (1/2 in.) diameter are removed.
4) The geotextile is cut and placed on the slope and into the trenches.
5) The geotextile is stapled at top and bottom near trench locations.
6) The geotextile is wetted and seed is spread at the specified rate.
7) Straw and erosion control blanket are placed over the geotextile.
8) The trenches are filled, anchoring the ends of the geotextile and erosion control blanket.
9) The geotextile is stapled 0.6 m (2 ft.) on center. Additional staples are placed as needed to insure geotextile contact with the soil.
10) Watering the geotextile spillway a few times a week for 2 to 3 weeks improves the early germination and growth.
11) The geotextile spillway is revisited in about a month to staple and reseed as necessary.

<u>Seams.</u> Three methods of seaming two pieces of geotextile together have been tested:

1) Laying the geotextile across the slope with the seam perpendicular to flow. Only lower geotextile section is placed in an anchor trench.
2) Laying the geotextile across the slope with the seam perpendicular to flow. Both upper and lower geotextile placed in an anchor trench.
3) Geotextile placed with an overlap of about 0.3 m (12 in.) at the middle of the spillway, with the geotextile running the full spillway length.

All three have been successful. The preferred method is placing the seam parallel to the flow for two reasons. 1) Construction is easier because only two anchor trenches are needed. 2) Not disturbing the soil in the spillway by building anchor trenches provides less chance for settlement problems. The seed did not have significant problems growing through two layers of fabric.

PERFORMANCE

The geotextile spillways installed to date have a success rate of greater than 95%. Success is defined as 80% cover by vegetation and no erosion below the geotextile after 1 year. Root penetration has been excellent where soil-geotextile contact has been maintained.

Most problems have been in the establishment of vegetation. These are directly related to poor soil-geotextile contact, use of heavier than specified geotextile, herbicide contaminated soil or runoff, or drought. The fix for the soil-geotextile contact problem is more staples and seed. Degradation of the geotextile material has not been obvious after 6 months or more of exposure.

Problems other than vegetation establishment have occurred with 7 of the more than 500 geotextile spillways installed in Michigan. Two spillways had slope failures in very sandy soils. One spillway installed near a city was damaged when used for sledding by children.

Geotextile spillways have not failed due to lack of vegetation or failure of the geotextile material by high velocities.

Some of the geotextile spillways have shown evidence of sedimentation at both the upstream and downstream edges. This sediment may need to be removed if the vegetation becomes buried. If the

accumulated sediment does not interfere with the performance of the geotextile spillway, it may be left in place as it blocks ultraviolet light. This helps maintain the long term integrity of the geotextile. Adequate upstream protection from high sediment laden runoff is recommended.

Work by Hewlett, 1987, has shown that root penetration through the geotextile layer reduces as the thickness of overlying soil is increased. For these geotextile spillways, the grass mixture was sown directly on the geotextile material. No soil was placed over the seed.

A typical cost for a 9 m (30 ft.) long by 4 m (12.5 ft.) wide spillway is about $200, including labor and materials. This is less than 1/2 the price of a typical pipe drop erosion control (side inlet) structures and less than 1/5 the cost of wood weir drop structures built in Michigan. The inspection time is also reduced because the total installation time required averages 1 1/2 hours.

SUMMARY

The installation of geotextile spillways in Michigan have proven successful. The success of over 500 geotextile reinforced spillways have shown that vegetation used in conjunction with geotextiles can serve as an effective spillway alternative. Major advantages of the geotextile spillways are low installation costs, performance of new construction, and aesthetically pleasing appearance.

REFERENCES

1.   Hewlett, H.W.M., Boorman, L.A. and Bramley, M.A., (1987) Design of Reinforced Grass Waterways, Construction Industry Research and Information Association - Report 116.
2.   Jeffrey P. Porter, Fred Gasper, James C. Dickie, and James R. Vosburgh, (1992) Use of Non-woven Geotextile Reinforced Vegetated Chutes as Cost Effective Grade Stabilization Structures, American Society of Agricultural Engineers.
3.   United States Department of Transportation, Federal Highway Administration, (1988) Hydraulic Engineering Circular No. 15.
4.   United States Department of Agriculture-Agricultural Research Service, (1987) Stability Design of Grass Lined Channels, Agriculture Handbook Number 667.

ISOMETRIC VIEW

EARTHFILL

FLOW

GEOTEXTILE

CHANNEL SIDE SLOPE

RIPRAP

DESIGN: Q = _____ cfs (80 max.), S = _____ :1
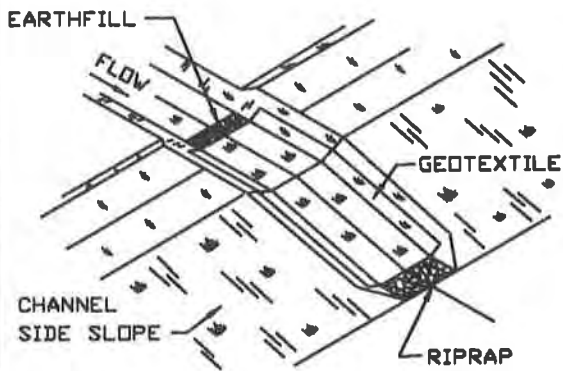
Unit Capacity (CFS/ft. width) q	Slope (H:V) S	Entrance Depth (ft.) D	Chute Depth (ft.) d
2	2:1 to 7:1	1.0	0.5
2.5	2.5:1 to 7:1	1.0	0.5
3.5	3:1 to 7:1	1.25	0.7
4	4:1 to 7:1	1.5	0.8
5	6:1 to 7:1	1.75	1.0

Minimum Chute Width "W" = Q/q = _____ ft.

ESTIMATE OF QUANTITIES

RIPRAP (D_{50} = 6 IN.) _____ TONS
GEOTEXTILE   W=___ FT.x L=___ FT.
EROSION CONTROL BLANKET _____ SQ.YDS.
STAPLES OR STAKES   _____ EACH
SEEDING & MULCHING   _____ SQ.FT.

SECTION ON CENTERLINE

ELEV. _____
as built _____

TOP OF FILL ELEV._____
as built _____

CHANNEL SIDE SLOPE

ECB or (ECN & STRAW MULCH)

D = __ ft.

EARTHFILL

1 ft.

1
S= _____
(2 min.)

d
D

ELEV._____
as built_____

(10' max.)

1 ft.

GEOTEXTILE
(shall be one piece or joined as shown below)

5 ft.min.
ENTRANCE APRON LENGTH

L_c = _____ as built= _____
SLOPE LENGTH

2 ft.
RIPRAP LENGTH

1 ft.

BOTTOM OF CHANNEL

RIPRAP
D_{50} = 6 in.

TYPICAL CROSS SECTION

ECB or (ECN & STRAW MULCH)

d= __ ft.

1
2 or flatter

GEOTEXTILE
(Lap 12" at center of chute for two piece installation.)

W = _____ (20 ft. max.)

DRAWING SO-A-0740 MEETS REQUIREMENTS OF STANDARD AND SPECIFICATION 410, GRADE STABILIZATION STRUCTURE.

ENGINEERING JOB CLASS _____

COOPERATOR _____
_____ COUNTY, MICHIGAN
LOCATION _____

GEOTEXTILE REINFORCED VEGETATED CHUTE (WITHOUT TAILWATER)
(SHEET 1 OF 3)

U.S. DEPARTMENT OF AGRICULTURE
NATURAL RESOURCES CONSERVATION SERVICE
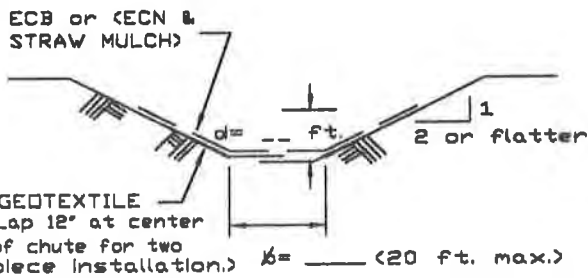
Standard Drawings shall NOT be altered without State Conservation Engineer approval.

MICHIGAN ENGINEERING STANDARD DRAWING		NOT TO SCALE
Approved By	S.C.E.	
	Date 4-17-91	
Drawing No. SO-A-0740	Sheet 1 of 3	REV. 2-17-95

Designed _____
Drawn _____
Traced _____
Checked _____
Approved By _____
Title _____
Title _____
Drawing No. SO-A-0740

CAD DRAWING SOA0740

MAINTENANCE REREQUIREMENTS

A maintenance program shall be established by the land user to maintain capacity and vegetative cover. Items to consider are as follows:

1. Protect structure from damage by livestock, herbicide runoff, farm equipment and vehicles.

2. Maintain inlet and outlet areas free of any obstructions.

3. Repair structure as soon as possible after damage is noted.

4. Reestablish vegetative cover immediately where erosion has removed established seeding. Staple, seed and mulch areas where grass is not growing.

5. Mow and fertilize annually to maintain vigorous growth.

MATERIAL REQUIREMENTS

Geotextile:

The geotextile shall meet the requirements of Construction Specification MI-165, Nonwoven Geotextile, Class III. The geotextile material shall be 3.5 to 5.5 oz./sq.yd. The geotextile shall be one or two pieces. A single piece is prefered.

Erosion Control Netting (ECN) and Straw Mulch:

The netting shall be extruded oriented polypropylene netting. The mesh openings shall be 1/2 inch to 1.0 inch in each direction. The weight shall be approximately 3 lbs. per 1,000 sq. ft. Straw mulch shall be spread 1 inch to 2 inches thick before the netting is placed.

Erosion Control Blanket (ECB):

The erosion control blanket shall use straw or straw/coconut mulch at the rate of approximately 0.5 lb. per sq. yd. Additional straw may be placed between the geotextile and ECB to provide for better seed germination.

Riprap:

The riprap shall meet the requirements of Construction Specification MI-164, Loose Rock Riprap.

RIPRAP GRADATION
(D_{50} = 6 inches)

SIZE (INCHES)	(POUNDS)	% SMALLER BY WEIGHT
12	125	100
9	50	60-100
6	16	30-50
1.5	0.2	5-25

CONSTRUCTION NOTES

1. Construction operations shall be carried out in such a manner and sequence that erosion and air and water pollution will be minimized and held within acceptable limits.

2. The completed job shall present an appearance of good workmanship and shall conform to the lines, grades, and elevations shown on the drawings or as staked in the field.

3. All operations shall be carried out in a safe and skillful manner. Safety and health regulations shall be observed and appropriate safety measures used.

COOPERATOR _____
_____ COUNTY, MICHIGAN
LOCATION _____

GEOTEXTILE REINFORCED VEGETATED CHUTE (WITHOUT TAILWATER)
(SHEET 2 OF 3)

U.S. DEPARTMENT OF AGRICULTURE
NATURAL RESOURCES CONSERVATION SERVICE

Designed				Approved By			
Drawn				Title			
Traced				Title			
Checked				Sheet	Drawing No. SD-A-0740

REV. 2-17-95

CONSTRUCTION SEQUENCE

1. Excavate to finished grade of required section and slope.

2. Dig trenches on upstream end and downstream toe.

3. Hand rake grade to prepare seedbed. If seedbed is difficult to rake, topsoil may be added. DO NOT use herbicide contaminated topsoil. Remove all rocks, clods, and clumps larger than 1/2 inch diameter. Spread fertilizer and lime and rake into seedbed. Fertilize according to soil tests or at a minimum rate of 2 lbs. of 12-12-12 fertilizer (or its equivalent) per 100 sq. ft.

4. Place geotextile on prepared grade. Extend geotextile into trenches for anchorage at upstream and downstream ends as shown on sheet 1 of 3. Staple geotextile at one to two foot intervals across the entrance apron and along overlap of geotextile pieces.

5. Seed onto geotextile at the following rates: (the geotextile may be wetted prior to seeding to reduce seed movement during ECB placement and stapling.

SEED	RATE (lbs/100 sq.ft.)
Perenial Rye	0.25
Tall Fescue	0.5
Smooth Brome	0.5
Creeping Red Fescue	0.5

6. Place Erosion Control Blanket (ECB) over seed. Straw mulch and Erosion Control Netting (ECN) may be used in lieu of ECB. The ECB or ECN shall extend into both trenches as shown on sheet 1 of 3.

7. Staple netting and geotextile at 2 ft. intervals starting at the centerline of the channel and working out toward each side. Additional staples shall be placed where the geotextile does not contact the soil.

8. Fill upstream trench with earth. Fill downstream trench with riprap. Geotextile shall have consistent soil contact. Stretch the geotextile as little as possible.

CONSTRUCTION TOLERANCES

Depth at Centerline: Grade to plus or minus 0.1 ft.

Width: 0 to 1 ft. wider

Side Slopes: plus or minus 0.5 ft./ft. but not steeper than 2:1

FINISH AND CLEANUP

The site area and the designated spoil areas will be finished in a relatively smooth condition ready for seeding. All rocks 3 inches in diameter or larger and roots shall be removed from the disturbed areas adjacent to the geotextile reinforced waterway. All disturbed areas shall be smoothed, fertilized and seeded at the same rates as the geotextile reinforced vegetated chute.

COOPERATOR _____

_____ COUNTY, MICHIGAN

LOCATION _____

GEOTEXTILE REINFORCED
VEGETATED CHUTE
(WITHOUT TAILWATER)
(SHEET 3 OF 3)

U.S. DEPARTMENT OF AGRICULTURE
NATURAL RESOURCES CONSERVATION SERVICE

Designed	___ ___ ___	Approved By ___ ___ ___
		Title ___ ___ ___
Drawn	___ ___ ___	Title ___ ___ ___
Traced	___ ___ ___	Sheet / Drawing No.
Checked	___ ___ ___	__ of __ SD-A-0740

REV. 2-17-95

FLEXIBLE CHANNEL LINER STUDY AT THE TxDOT/TTI HYDRAULICS AND EROSION CONTROL FIELD LABORATORY

Jett A. McFalls
Texas Transportation Institute

ABSTRACT

Texas Transportation Institute's (TTI) Environmental Management Program is currently operating a full-scale, outdoor evaluation facility for the performance testing of selected erosion control materials. The overall purpose of the facility is to produce and maintain a defensible "Approved Products List" to be used on all Texas Department Of Transportation (TxDOT) construction and maintenance activities. TTI's goal was to construct a facility which would simulate the highway environment to the greatest degree possible while providing the capability of collecting data on the critical performance factors of roll-type erosion control products. To achieve this goal the Hydraulics and Erosion Control Field Laboratory was constructed. The facility has the capability to conduct performance tests on erosion control products for embankment protection and for flexible channel liners.

INTRODUCTION

The erosion control industry and the Federal Highway Administration (FHWA) recognize a wide variety of generic materials that may be used as erosion control protection. Erosion-control blankets that met the Texas Department of Transportation's standard specifications for the past twenty years consisted of two products. Technically, products that did not meet the material-based specification were excluded from the specification and bidding process. In response to this practice, TxDOT searched for alternatives that would provide a fair system of selecting and specifying erosion control products based upon their performance. TxDOT and TTI initiated a cooperative research study in 1989 to help further this initiative.

Once TTI determined TxDOT's needs and reviewed the current state-of-practice in erosion control, it recommended evaluating erosion control materials based upon their field performance rather than traditional laboratory testing. Since the textile industry developed erosion-control blankets and mats, a variety of laboratory tests were developed to describe physical properties such as tensile and shear strength, heat resistance, etc. However, these tests do not adequately describe or test field performance. Laboratory tests and field observations suggest there is great variation in strength, durability, soil-blanket interaction, and vegetation response between generic material classifications and between manufactured brands of similar materials. Soil-fabric interaction, vegetation establishment, and installation methods are critical factors to consider in determining field performance characteristics.

TTI developed evaluation methodologies for the Department's most pressing needs: erosion-control blankets in varying slope applications and flexible channel liners in varying shear stresses. A state-of-the-art facility was designed and constructed during a two year period to accommodate these application areas and more. Today, the facility is a nine hectare site that includes approximately three hundred linear meters by six vertical meters of fill embankment, ten at-grade channels, two reservoirs, pumping stations, rainfall simulators, and various instrumentation.

Since 1991, an annual evaluation of erosion control products have been studied at the Hydraulics and Erosion Control Laboratory. Data on specific field performance characteristics such as apparent vegetation coverage and sediment loss are collected and analyzed. Vegetation coverage is collected and analyzed by a video/image capture, an interactive, color analysis process. Artificial rainfall simulations provide the researchers with sediment loss ratios. TxDOT uses the data to support their Annual List of Approved Materials and develop standard installation detail sheets as construction document inserts. Private industry, TxDOT, and TTI cooperatively work to further this important area of environmental research and development. This cooperation led to a timely and fair program through which manufacturers' erosion control related materials are evaluated for use in TxDOT's construction and maintenance activities. The research objectives set forth include the following:

- Determine the acceptable performance level in fostering the establishment of vegetative cover and sediment retention for slope and channel application areas within highway rights-of-way.

FLEXIBLE CHANNEL LINER STUDY

The flexible channel liner testing facility consists of ten, at-grade channels (six with a 7% centerline gradient, and four with a 3% centerline gradient). Each open channel has a trapezoidal cross section that includes a 0.30 meter (1 foot) flat bottom, 1:1 side slopes, and a typical 0.91 meter (3 feet) depth beginning 4.5 meters (15 foot) downstream of the channel release gate. The total length of each test channel is 26 meters (85 feet). Water for the channels is supplied by an industrial grade, high-volume, low-head, axial-flow, pump capable of producing over 136,260 liters per minute (36,000 gallons per minute).

Channel treatment begins with the installation of the flexible channel liner and the application of the TxDOT rural area, warm-season seed mixture for the District. Fertilizer is applied integrally with the seed mixture at the rate of 102.15 kg per 0.405 ha (225 lbs./acre). Experimental control consists of one channel receiving the same vegetative treatment with no erosion-control material in place. Treatment plots are analyzed for their sediment retention performances (channel deformation) and apparent vegetative density coverage with respect to shear stress capacity range.

Sediment retention criteria are as follows:
- Acceptable flexible channel liners should reduce the sediment loss and channel degradation from the protected treatment area significantly greater than from bare ground (Control).

- Flexible channel liners should effectively protect the seed bed from a short duration flow that produces less than 95.76 Pa (2 lbs/ft^2)shear stress on the channel bottom within the first 90 days after installation.

Vegetation density coverage criteria are as follows:
- Acceptable flexible channel liners should promote significantly greater vegetative cover on the protected treatment area as compared to bare ground (Control).

- Acceptable flexible channel liners should promote a vegetative cover within the first six months after installation by protecting the seed bed from the impacts of shear stress from water flow and rain splash from raindrop velocity.

- In cohesive soils (clay), vegetation density should reach and maintain a minimum coverage of 70% during the first six months after installation.

Shear Stress Data

In straight line channels, the maximum tractive force occurs on the bottom and near the center of the channel. The force generated at this point is a function of Y, the unit weight of water; d, the depth of flow; and S, the average slope of the channel bottom (energy gradient). This relationship allows one to estimate the maximum permissible tractive force with a single calculation as follows:

$$\tau_d = YdS$$

Manning's "n" value for Flexible Channel Liner Research

For the flexible channel liner study, the researchers determined Manning's "n" value to simulate flows of equal shear stress upon the liner's bottom. To determine Manning's "n" or roughness coefficient for each flexible channel liner, researchers used an indoor flume facility located at the College of Ocean Engineering, Texas A&M University. Physical dimensions of the box-shaped flume are approximately 0.46 m (18 in) in width, 1.22 m (4 ft) in height, and 21 m

(70 ft) in length. The energy gradient is 2% longitudinally along the flume bottom. Researchers view the flows through the plexiglass sides of the flume.

The researchers attached the product to the plywood flume bottom with carriage bolts and washers placed 0.46 m (18 in) on center. At a predetermined rate of flow (Q), the researchers simulated a series of flows to collect velocity and depth measurements. Using a digital flow meter, the researchers recorded velocity at six different location in a single cross-section, to calculate the average velocity during uniform flow. The researchers used a point-gauge instrument to calculate depth of flow. Flow duration was for twenty minutes with data recorded every four minutes. Manning's "n" may be determined since rate of flow (Q), channel geometry and slope, measured resultant mean water velocity and depth of flow, are known. With this data, the research team figured a minimum, normal, and maximum Manning's "n" for each product prior to any flow simulations in the field.

Channel Degradation (Sediment) Data for Flexible Channel Liners

Following installation, each product is given a 90-day resting period to promote the initial growth of vegetation prior to initiating a series of increasing, shear-stress flows. After the 90-day rest period, a series of simulated flows begin. Prior to each flow, channels are pre-wetted to moisten the channel surface. Based upon the determined Manning's "n", and the known geometry of the channel, the depth of the water is controlled to initiate a series of increasing flows on 48 Pa (1 lb/ft^2) increments. Each flow is repeated twice, each flow being twenty (20) minutes after uniform flow has been achieved. During the test flows, measurements are taken approximately every two minutes to determine the water velocity. Further, data is collected regarding product movement (loss of intimate contact with the soil). To determine channel deformation, cross sections are taken before and after each test flow. Using a point gauge at four different stations along the channel, seven readings are taken at each station as shown in figure one. This procedure enables the researchers to quantify sediment retention and sediment bed load migration.
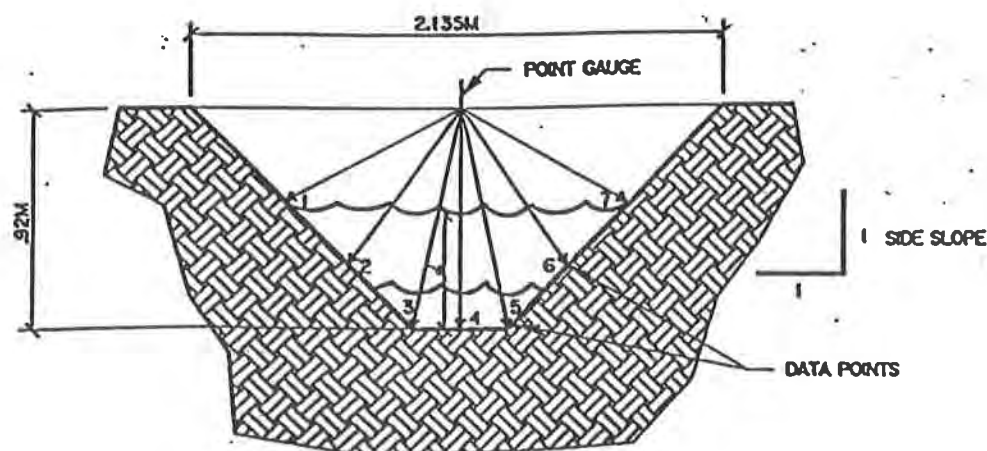
Figure 1: Channel cross section showing location of measurements

The average soil displacement exhibited within the channel is compared to the adopted maximum soil displacement standard to determine acceptance or rejection. All channels are also sampled to determine the growth of vegetation. Each channel is initially sampled at the end of the 90-day resting period for vegetation production. The final density sample is normally taken during November. The vegetation density achieved within the channel by the final sampling is compared to the adopted minimum vegetation density standard to determine acceptance or rejection.

Shear Stress (Material Performance) Data for Flexible Channel Liners

Before and after flow simulation, researchers visually inspected each treatment channel for any damage or undermining of the material. Significant rips, tears, pulling away at the seams or loss of material, etc., were recorded on a channel diagram and photographed. Since the researchers incrementally increase the shear stresses placed upon the flexible channel liners, these visual inspections help to determine if the liner should receive the next level of shear stress.

If a flexible liner has reached its maximum permissible tractive force capability, it has reached its "failure" point. "Failure" in this context refers to the amount of bare ground exposed due to the failure of the material to withstand the shear stresses generated upon them. One obvious failure point is the material physically pulls away from the surface and is transported downstream, thereby no longer providing protection to the channel surface. Minor migration of material components within the flexible channel liner, such as excelsior or straw materials, would not constitute a failure as described here. No repairs were made to the flexible channel liners when damage resulted from a simulated flow event.

CONCLUSIONS AND TEST RESULTS

The research work accomplished at TTI continues the Federal Highway Administration's work cited in the FHWA Hydraulic Engineering Circular 15. While HEC 15 establishes that the maximum tractive force occurs at the bottom center of the channel floor (point 4 in the following figure), the TTI sediment loss data does not support this as the location of the maximum amount of soil deformation or movement. The location which actually exhibit the most soil loss is at points 3 and 5. Furthermore, the data also indicates that point 4 actually exhibits the least amount of soil deformation in 75% of the shear stress test flows performed. This seems to indicate that shear stress in not necessarily related to soil displacement. It seems to suggest that the flow turbulence at these edges is possibly more significant than the shear stress.
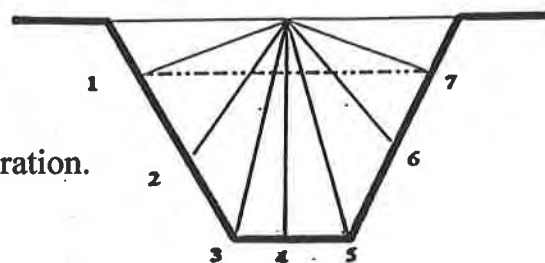
Channel Sampling Points

Figure 2: Typical channel configuration.

Failure appeared to be equally due to material failure as well as erosion failure. While most of the material damage seemed to occur early during the twenty minute test flows, erosion occurred throughout the entire twenty minute tests. Very little material damage took place at staple points even though some of the materials had a tendency to float. Stapling pattern did not seem to affect the erosion. However, the more staples, the less material damage.

In HEC 15, the maximum recommended shear stress values in an unvegetated condition for flexible channel liners range from 7.18 to 95.76 Pa (.15 - 2 lbs/ft²). In a vegetated condition (Class C) it was 100.49 (2.1 lbs/ft²). When tested in a vegetated condition at TTI, three flexible channel liners protected the channels during test flows in excess of 383 Pa (8 lbs/ft²). The following table presents the levels at which each of the test materials were tested.

SUMMARY OF DATA

Class 2 - 1996 Flexible Channel Liner Performance Test Results								
Conditions	0-96 Pa (2 lbs/ft²)		0 - 192Pa (4 lbs/ft²)		0 - 287Pa (6 lbs/ft²)		0 - 383 Pa (8 lbs/ft²)	
Minimum Standards	Sediment (cm of channel deformation)	Density (% cover final round)	Sediment (cm of channel deformation)	Density (% cover final round)	Sediment (cm of channel deformation)	Density (% cover final round)	Sediment (cm of channel deformation)	Density (% cover final round)
	1.15	70%	1.00	70%	1.00	70%	0.80	70%
Product A	0.5611	78.116	0.7554	78.116	0.7516	78.11	0.6931	78.116
Product B	0.3541	79.982	0.4646	79.982	0.6154	79.982	0.6293	79.982
Product C	0.5666	92.853	0.853	92.853	0.5930	92.853	0.59214	92.853
Product D	0.8648	71.830	0.7565	71.830	0.8296	71.830	0.9994	71.830
Product E	0.6784	86.574	0.7871	86.574	1.0169	86.574	1.0642	86.574
Product F	0.7866	54.664	1.1029	54.664	not tested		not tested	
Product G	0.9736	82.394	1.0861	82.394	1.2780	82.394	1.32551	82.394
Product H	1.1487	56.954	1.0671	56.954	1.0950	56.954	not tested	
Product I	0.4974	59.490	0.6113	59.490	not tested		not tested	

NOTE: Shaded cells represent unsuccessful performance levels
KEY: Product A: Dense, three-dimensional web of green Polyolefin fibers
          oriented and mechanically bonded between two nets.
          Product B: 100% coconut fiber stitch bonded between a heavy duty
          UV stabilized bottom net, and a heavy duty UV stabilized middle
          netting overlaid with a heavy duty UV stabilized top net.
          Product C: UV stabilized, three dimensional, multi-layered structure
          of polyethylene netting.

Product D: Dense web of extra-thick PVC monofilament thermally welded together.

Product E: UV stabilized, three dimensional, polypropylene.

Product F: Machine produced mat of curled wood excelsior with a photo degradable extruded plastic mesh on both sides.

Product G: Three dimensional matrix of heavy nylon monofilaments fused at intersections.

Product H: Biodegradable, Aspen wood fiber with a permanent UV stabilizing netting underlaid with a non-woven textile fabric

Product I: Woven, undyed jute

REFERENCES

1. Chow, Ven Te. 1959. OPEN-CHANNEL HYDRAULICS. McGraw-Hill Book Company, New York.

2. Chen, Y. H., Cotton, G. K. 1986. DESIGN OF ROADSIDE CHANNELS WITH FLEXIBLE LININGS. HYDRAULIC ENGINEERING CIRCULAR NO. 15. Federal Highway Administration, FHWA-IP-87-7

3. S.H. Godfrey, H.C. Landphair, J.A. McFalls. 1993. THE PERFORMANCE OF FLEXIBLE EROSION CONTROL MATERIALS. Research Report 1914-1. Texas Transportation Institute, Environmental Management Program.

4. S.H. Godfrey, H.C. Landphair, J.A. McFalls. 1994. THE PERFORMANCE OF FLEXIBLE EROSION CONTROL MATERIALS AND HYDRAULIC MULCHES. Research Report 1914-2. Texas Transportation Institute, Environmental Management Program.

SEEPAGE CONSIDERATIONS AND STABILITY OF SANDY SLOPES REINFORCED BY ANCHORED GEOSYNTHETICS

HOSSEIN GHIASSIAN, TARBIAT MODARRES UNIVERSITY, IRAN
DONALD H. GRAY, UNIVERSITY OF MICHIGAN, USA
ROMAN D. HRYCIW, UNIVERSITY OF MICHIGAN, USA

ABSTRACT

Stability against shallow mass sliding as well as surface erosion and piping in sandy slopes depends on the flow direction, particularly near the ground surface. The flow regime near the surface is very important in anchored slopes because an anchored net or fabric fastened to the slope causes undulations or irregularities on the surface which in turn affect the flow pattern and stability of the slope. This influence of an undulating surface was investigated by analyzing slopes with different surface topographies, boundary configurations (or shapes), and internal drainage conditions. Numerical solutions show that the flow direction near undulating surfaces can adversely affect stability. The solutions appeared to be in good agreement with experimental observations. Flow net analyses also suggest that adverse seepage conditions near undulating surfaces can be corrected by inserting drains at anchor locations.

INTRODUCTION

In environmentally sensitive areas such as coastal sand dunes, anchored geosynthetic systems offer a non-intrusive alternative to traditionally armoring methods such as rip rap, for protecting sandy slopes against internal and external water forces (Hryciw et al., 1995; Ghiassian, 1995). Water can cause instability by generating seepage forces within the slope and erosive tractive forces at the surface of the slope. In coastal slopes, a common mode of mass failure is shallow sliding or sloughing, often triggered or accompanied by surficial erosion. These failures may be caused by wave action, exfiltrating water, or water flowing over (parallel to) the slope. Surficial failure in sandy slopes can be arrested or prevented by imparting a confining stress to the slope surface by means of a fabric or net, usually made of synthetic material, that is stretched over and pulled down tightly on the ground surface by means of anchors (Koerner, 1984; Koerner and Robins, 1986). The anchors are inserted through and fastened to the fabric. For the anchored system to be effective, the ground surface must have, or develop, a curvilinear shape so that the tension created in the fabric imparts compressive stresses over the surface. This imparted or induced confining stress is directly proportional to the tension in the fabric and inversely proportional to the radius of curvature of the surface.

Because of this requirement for a curvilinear surface, the flow regime in an anchored slope will differ from that of a flat slope near the surface. This flow regime in turn will influence the

near-surface stability of a slope significantly. In fact, stability analyses show a direct relationship between the factor of safety and the flow direction with respect to the surface. The direction of seepage vectors can vary substantially along an irregular or undulating surface. Therefore, seepage analyses are necessary to characterize the flow regime in such slopes and to identify critical zones where seepage conditions could adversely affect stability.

This paper presents several examples of seepage analyses for slopes with curvilinear surfaces, different boundary configurations (or shapes), and internal drainage conditions. Drains such as planar geopipes can be inserted along anchors to divert emerging flow directions to more favorable directions as shown in these examples. The analyses are based on numerical techniques since closed form solutions are not available for these cases.

STABILITY OF ANCHORED SLOPES

The stability of sandy slopes against shallow sloughing and surficial erosion can be increased greatly using an Anchored Geosynthetic System, AGS (Hryciw and Haji-Ahmad 1992; Gray and Hryciw 1993; Hryciw et al. 1994). This technique was initially suggested by Koerner and Robins (1986) and Koerner (1984). The method provides additional confining pressures to the slope through a system of tensioned fabric and anchor rods, therefore, increasing the shear strength of the soil and stability of slope. A study has been conducted at the University of Michigan on the use of AGS for stabilizing cohesionless slopes with parallel or emerging seepage. A view of an experimental slope stabilized by an anchored geosynthetic system is shown in Fig. 1. A detailed description of the experimental system is beyond the scope of this paper, and has been presented by Ghiassian et al. (1995).
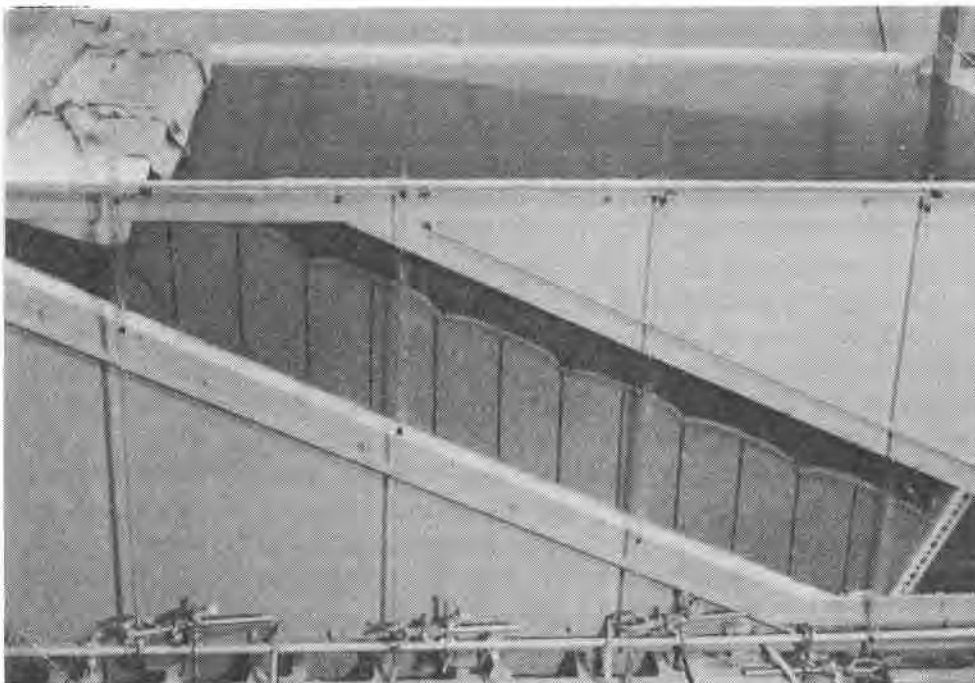
Fig. 1. Apparatus for testing effectiveness of anchored gesynthetics for stabilizing saturated sand slopes subjected to combined seepage and surface runoff

A force-equilibrium analysis can be used to examine the influence of external and internal forces on the stability of an infinite slope. Fig. 2 shows a schematic of an element in an infinite slope under gravity, anchored geosynthetic, and seepage forces. To mitigate surficial erosion problems due to overslope water runoff, Hryciw (1990) suggested installation of anchors in pre-plowed furrows running along a slope's contours. By this technique, fabric curvature develops only in the cross-sectional plane shown in Fig. 2 and therefore the problem may be considered as 2-dimensional. In Fig. 2, T_o represents the resultant force exerted by the geosynthetic per slope area ($b \times 1$) where b is the spacing between rows of anchors. In general, the direction of T_o may be assumed to coincide with the anchor orientation. The factor of safety against Coulomb sliding for this element can be written as (Ghiassian, 1995):

$$F.S. = \frac{\cos \beta + \xi_b \cos \theta - A_b \cos \lambda}{\sin \beta - \xi_b \sin \theta + A_b \sin \lambda} \tan \varphi \tag{1}$$

where (referring to Fig. 2):

$$A_b = i \frac{\gamma_w}{\gamma_b} \qquad \text{(the buoyant seepage coefficient)} \tag{2}$$

$$i = \frac{\sin \beta}{\sin \lambda} \qquad \text{(the seepage gradient)} \tag{3}$$

$$\xi_b = \frac{T_o}{zb \cos \beta \gamma_b} \qquad \text{(a dimensionless buoyant AGS load coefficient)} \tag{4}$$

β	=	slope angle,
θ	=	anchor orientation with respect to the normal to the slope,
λ	=	seepage direction with respect to the normal to the slope ($0<\lambda<180°-\beta$),
γ_b and γ_w =		buoyant unit weight of soil and unit weight of water respectively,
b	=	spacing between anchor rows,
T_o	=	load from AGS per row spacing per unit width of slope,
z	=	depth to the failure surface (or equivalent thickness of the sliding mass, see Ghiassian, 1995),
ϕ'	=	soil effective friction angle.

A dry sandy slope will remain stable provided its inclination does not exceed the friction angle or repose angle of the sand. However, water seeping or percolating through a slope can affect the stability of a slope dramatically. It can be seen from equation 1 that as λ becomes smaller, FS will decrease. This contribution of seepage to the stability can also be observed in Fig. 3. Here, the ratio of safety factor of an unreinforced or plain slope with seepage (FS) to that of a dry slope (FS_{dry}) is shown versus λ. One can see that, the stability of a previously dry slope drops by approximately one-half when water seeps parallel to the slope ($\lambda = 90°$). The stability is decreased even more when the seepage emerges from the slope ($\lambda < 90°$), and when $\lambda = \beta$ the slope looses its strength completely and liquefies. On the other hand, the stability is equivalent to that of a dry slope when the water flows vertically downward ($\lambda = 180°-\beta$). In situations where water flows over the slope surface or emerges from the surface, surface erosion or piping can occur and accompany or trigger shallow mass failure.
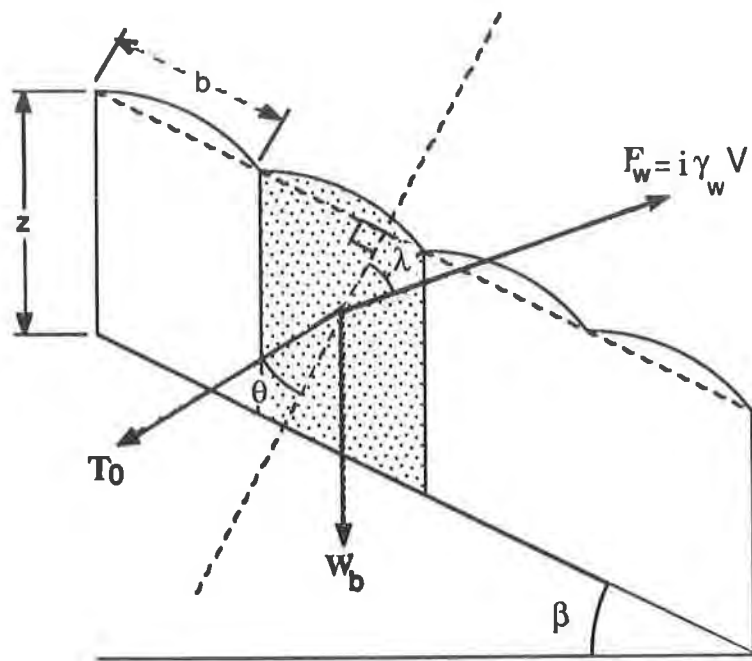
Fig. 2. Schematic representation of body force (W_b), external anchor force (T_o), and seepage force (F_w) in an infinite slope with seepage acting in a variable direction ($0 < \lambda < 180° - \beta$)
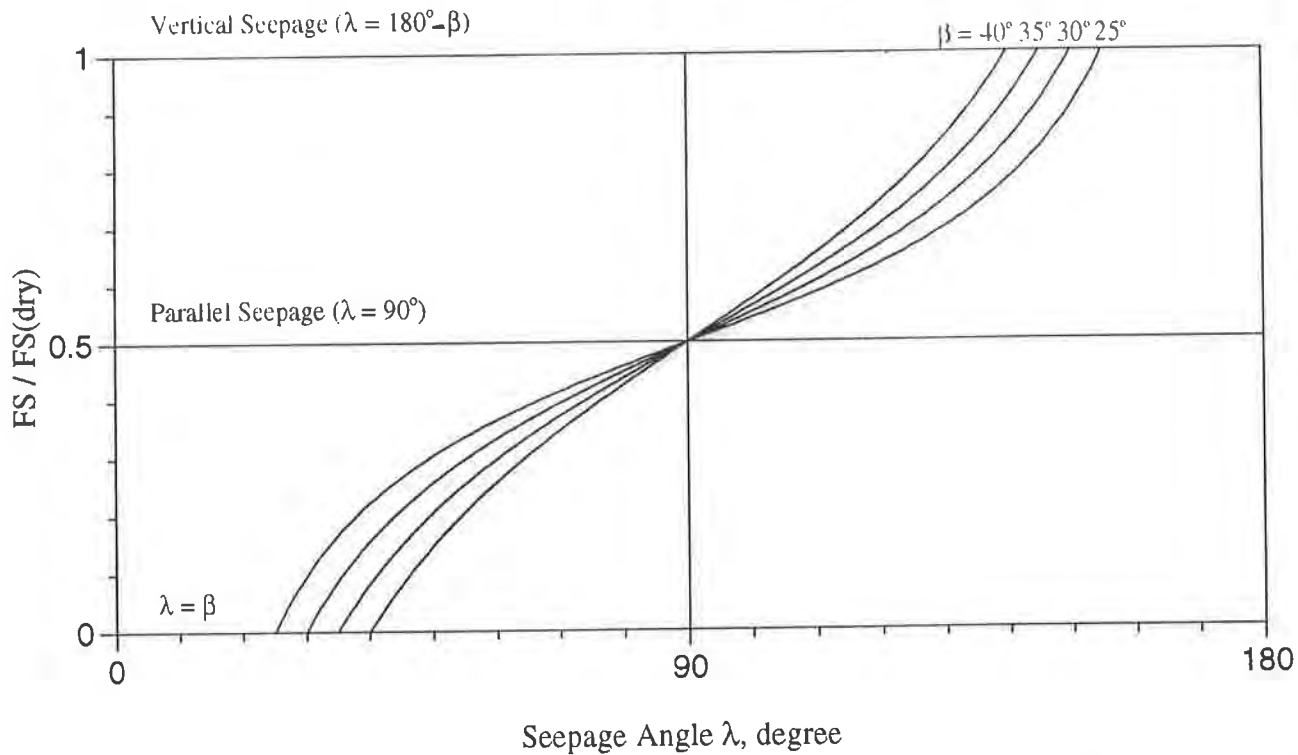

Fig. 3: Influence of seepage on the stability of sandy slopes as a function of slope angle (β) and seepage direction (λ)

SEEPAGE ANALYSES

Slopes stabilized by anchored geosynthetics have an irregular, curved or undulating surface. A curved surface shape creates some confining stress on the slope when a fabric or geonet is placed and tensioned over the slope. This confining stress increases the mass stability as well as erosion resistance of the slope. The generated normal stress (σ_n) through the stretched fabric with tension (T) is inversely dependent on the radius of curvature of the surface (R) as:

$$\sigma_n = \frac{T}{R} \tag{5}$$

Ideally, the shape of the slope surface should be such that it optimizes stress distribution while minimizing the unfavorable influences of surface irregularity on the flow. The following seepage analyses will illustrate some of these important considerations.

For a slope with curvilinear undulations there is no exact analytical seepage solution. Toth (1963) presented an approximate solution for a two-dimensional, homogeneous, isotropic medium with impervious base, top and bottom boundaries, and a sinusoidal surface. Similar to the "flat surface" solution, he approximated the actual flow regime by a rectangle where the heads along the sinusoidal surface have been used for the upper side of the rectangle. In a similar approximation, Freeze and Witherspoon (1966) presented a mathematical model for a two-dimensional, homogenous and isotropic or horizontally layered medium with simple water-table configurations. Unfortunately, when the top and bottom boundaries are pervious, these approximations do not provide an analytical solution to the problem, and therefore, it is necessary to resort to numerical techniques.

Numerical methods can solve many complex flow problems for irregular regions, boundary conditions, and geohydrologic settings. An iterative finite difference technique can be used to solve (or satisfy) the Laplace equation. This iterative technique is based on a "relaxation process" that simultaneously calculates hydraulic heads at various node points in a network (Shaw and Southwell, 1941; Freeze and Witherspoon, 1966, 1967). The iteration continues until the difference between two consecutively computed heads at all points become very small. The technique is simple and efficient for solving a set of finite-difference equations. Numerical methods are also capable of treating general, nonhomogeneous, anisotropic, and three-dimensional problems (Southwell, 1946; Freeze and Witherspoon, 1966, 1967). Electronic spreadsheets have recently been used successfully to solve finite difference problems by the relaxation technique (Das, 1983; Kleiner, 1985). Many finite difference problems which previously required fairly sophisticated programming, can be solved with relative ease and accuracy on a spreadsheet. The numerical solutions presented herein are all based on a spreadsheet solution. Calculated values of the hydraulic heads at nodal points were used to plot contours of equipotential lines.

1. Circular Arc Surface. Conceptually, the simplest curvilinear surface is a circular arc as shown in Fig. 4. In this example, the slope had a maximum thickness of 22.5 cm and arc-relief of 1.875 cm. The arcs have a chord-spacing of 12.5 cm. The slope angle is 25°. A finer 0.625 cm x 0.625 cm mesh was used in order to more accurately approximate the slope topography. Only 1/4 of the total 150 cm slope length was analyzed, using the same boundary conditions, i.e. pervious top and bottom ends, and an impervious base. Results for the full 150 cm length
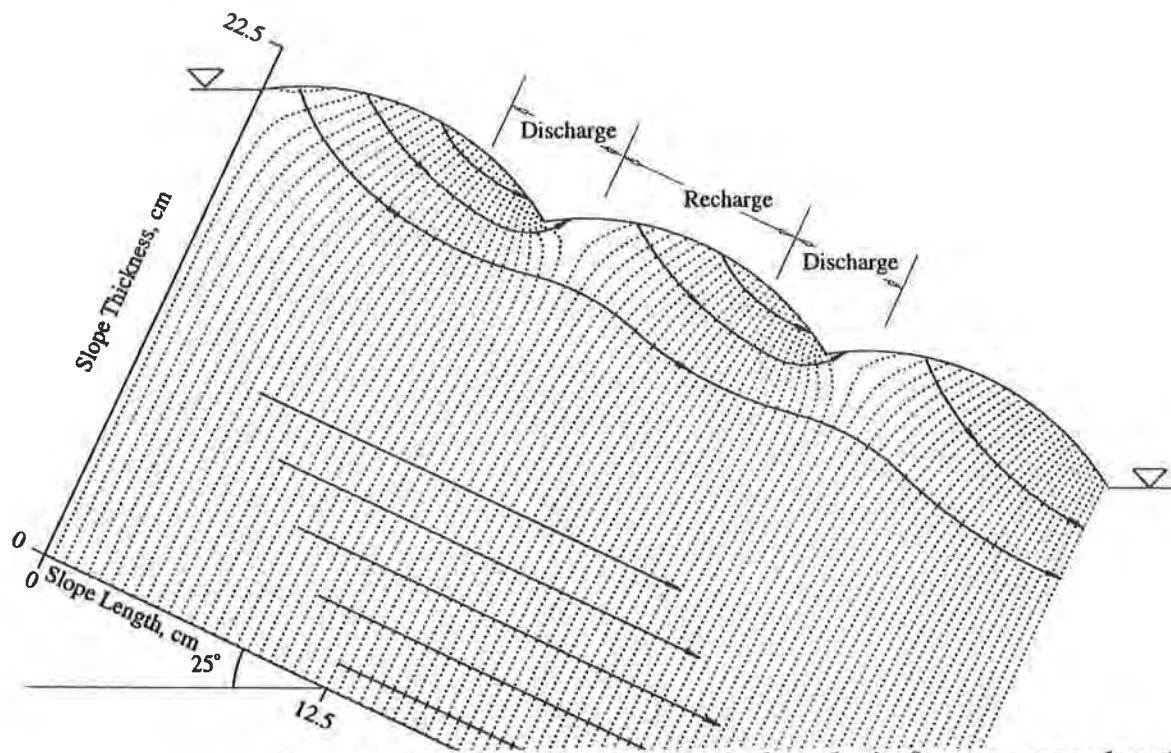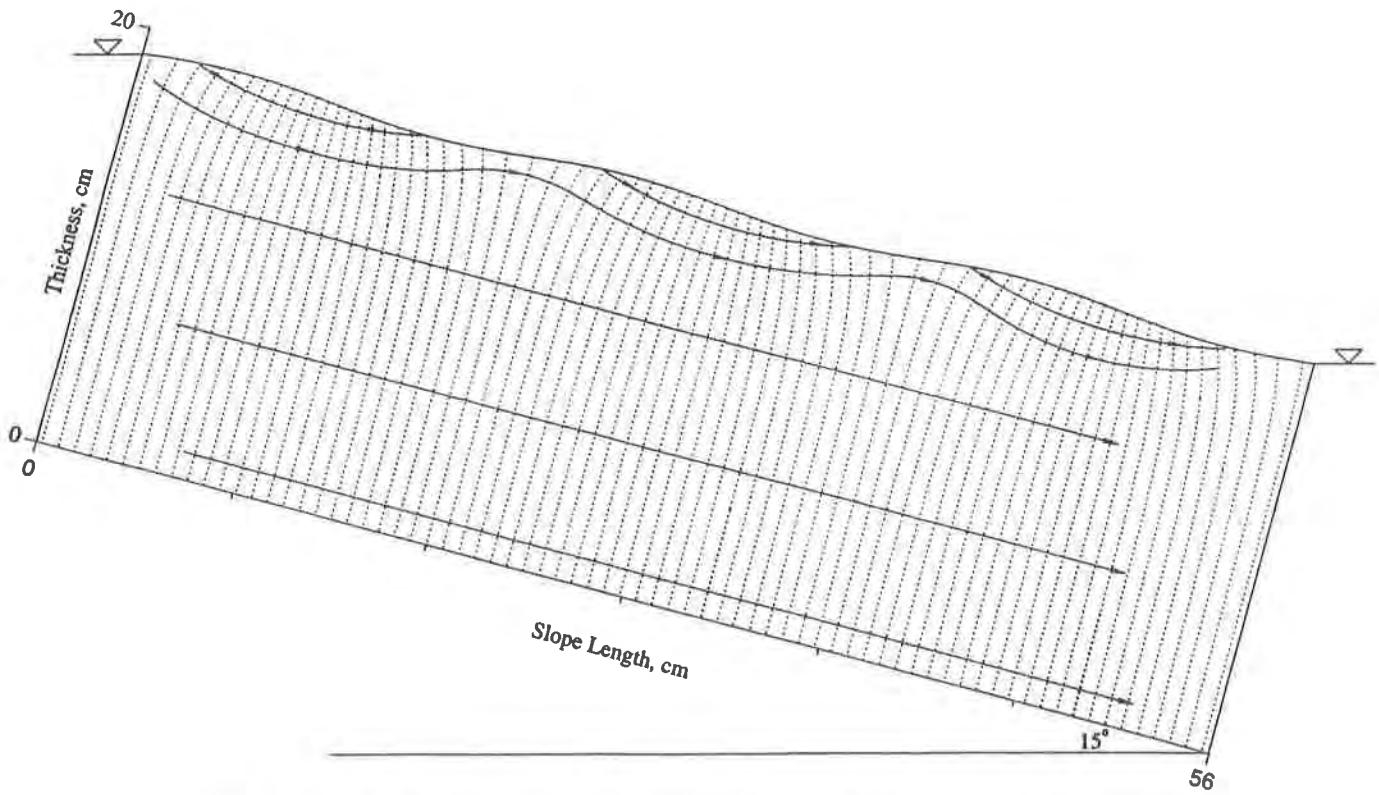
Fig. 4. Equipotential lines (contours) obtained by a numerical analysis for a rectangular slope prism with a circular arc surface. The upper sloping surface is pervious; bottom sloping surface, impervious. The top and bottom end boundaries are perpendicular to the base.

slope were found to be very similar and the end boundaries were found to have negligible effect on the flow regime, particularly near the surface. As shown in Fig. 4, the flow regime in hummocky surfaces is controlled mainly by surface topography rather than slope length and end boundaries.

There are two types of flow zones created at the surface, namely recharge zones and discharge zones. The recharge zones are concentrated at topographic highs whereas the discharge zones are concentrated at topographic lows. Since the discharge zones exhibit a smaller projected area, they are subject to more intense flow. In-situ, the discharge zones are also generally smaller than recharge zones as reported by Freeze and Witherspoon (1967). As shown in Fig. 4, the influence of topography on the flow field diminishes with depth such that the equipotential lines become fairly uniform and parallel deeper in the slope. These findings are consistent with the results of studies on ground water basins reported by Toth (1963), and Freeze and Witherspoon (1966, 1967).

These seepage variations near the surface always tend to occur whenever undulations or irregularities are introduced into the final shape of the slope face. For example, in conventional "face wrapped" geogrid/geotextile reinforced embankments or buttress fills, each soil layer is wrapped by a geosynthetic fabric, tensioned slightly, and staked at the top of the layer such that a curvilinear surface is created at the slope face as shown in Fig. 5. Thus, an undesirable seepage pattern can develop on the downslope side of each layer which can cause piping problem and instability in the slope. An advantage of an AGS system in this regard is that it creates sufficient normal stresses beneath the fabric to resist piping and particle instability. In all these techniques, however, the fabric must be fine enough to act also as a filter unless other filtering methods such as vegetation and bioengineering are also provided.
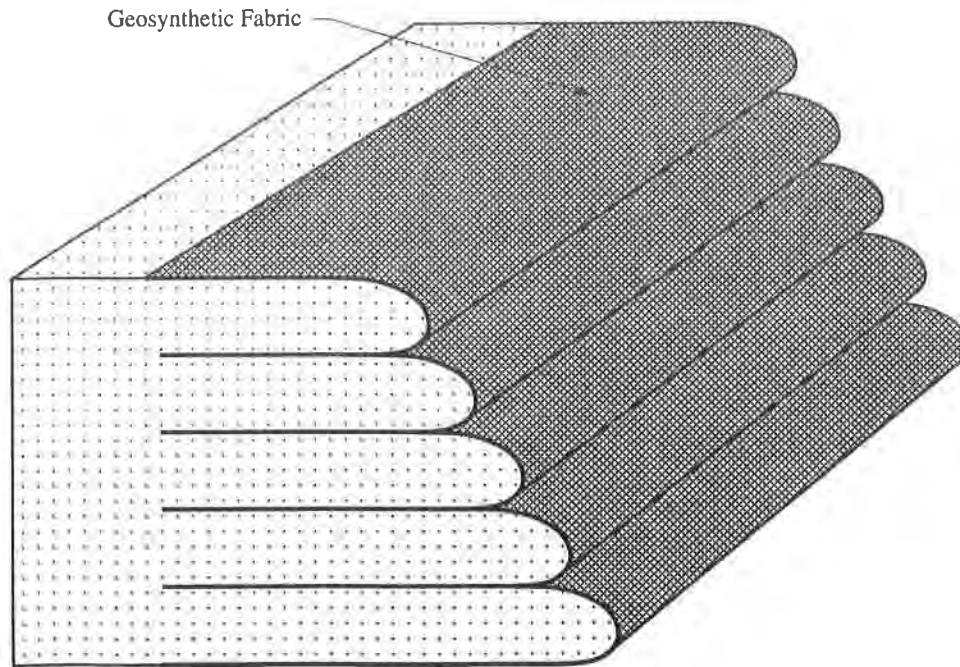
Fig. 5. Schematic of a "face wrapped" geogrid/geotextile reinforced embankment

2. Undulating Surface. Iverson and Major (1986) presented an example of a numerical solution for flow within a saturated slope with a hummocky or sinusoidal surface. Their slope has similar boundary conditions as the one considered by Toth (1963), i.e. impervious top, bottom, and base. Toth has presented an analytical solution to this problem as well by approximating the region as a rectangle.

Two example problems solved by numerical analysis are presented here, for the case of a slope with pervious and perpendicular top and bottom boundaries. The first example is shown in Fig. 6. The slope has a length of 56.25 cm, a thickness of 18.75 cm, and a slope angle of 15°. The hummocks or undulations have a wave length of 18.75 cm and a wavelength-to-amplitude ratio of 60. The mesh size is 0.3125 cm x 0.3125 cm. The second example (Fig. 7) has a hummocky surface with a larger amplitude (three times the one in the first example) to show the effect of larger variation in surface topography. The slope dimension and mesh size for this example are similar to those of the previous example. It should be noted that the slope surface, i.e. the hummocky boundaries are assumed to coincide with the phreatic line. In other words, the slope is assumed to be fully saturated under the flow from the top reservoir. The possibility of ponding water in valleys is avoided by assuming that the discharge water in the valleys can drain in the z direction (along the valley), as commonly occurs in the field. Both examples show the strong asymmetrical influence of topography on seepage directions near the hummocky ground surface. This effect, however, is more pronounced in Fig. 7 due to the higher amplitude-length-ratio of the hummocks. Distinct recharge and discharge zones occur in these examples too. The recharge is concentrated at the crest of the hummocks and the discharge is concentrated at the trough. The influence of topography decreases with depth in both examples. A general conclusion, attributed to Toth (1963), about the influence of hummocks on flow in a homogenous, isotropic slope can be summarized as:

- The influence increases as the amplitude of the hummocks increases,
- The influence increases as the depth to the impermeable layer decreases.

Fig. 6. Equipotential lines (contours) obtained by a numerical analysis for a rectangular slope prism with a sinusoidal surface and wave length to amplitude ratio of 60.
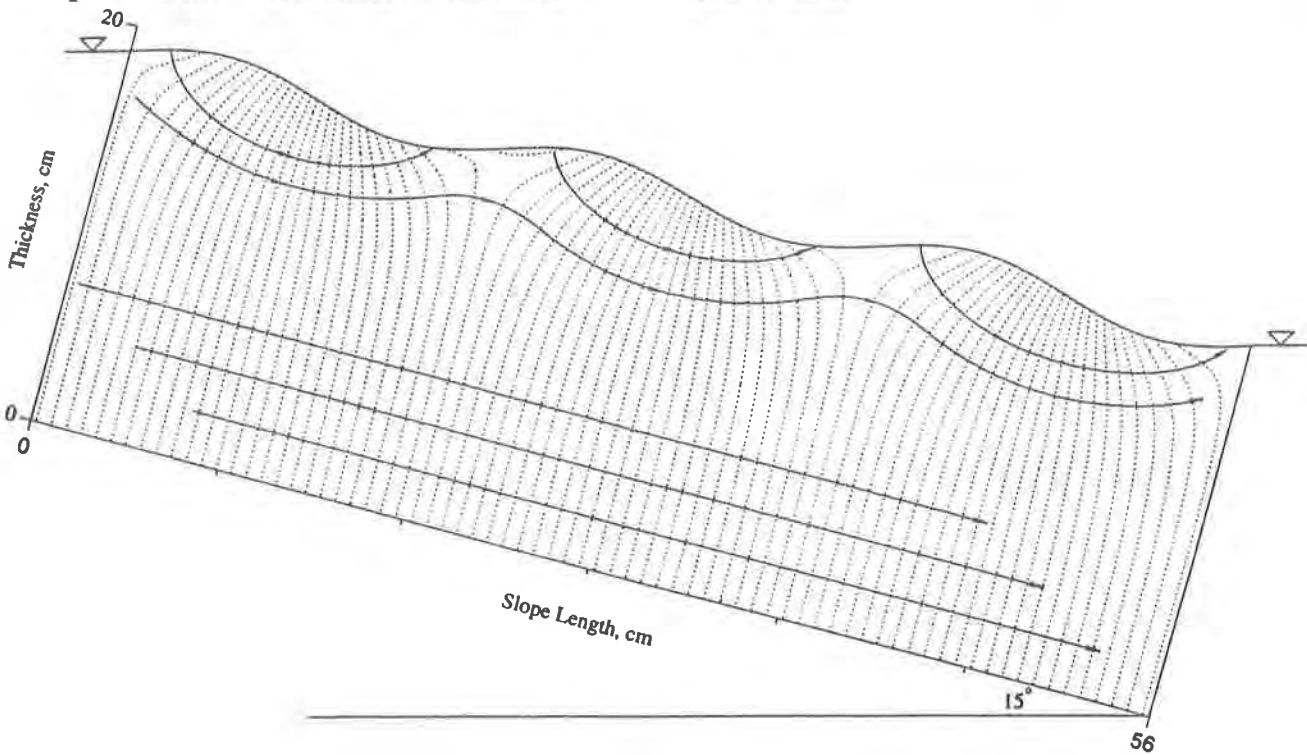
Fig. 7. Equipotential lines obtained by a numerical analysis for a rectangular slope prism with a sinusoidal surface and wave length to amplitude ratio of 20.

3. Curvilinear Surfaces with Drainage. The preceding examples show that the surface topography can influence the near surface flow field significantly. The flow field in turn can affect the surficial stability of a sandy slope. The mass stability decreases as the seepage direction (λ) becomes smaller and flow starts emerging from the slope as shown in Fig. 3. The resistance to piping is also dependent on the seepage angle at the exit points. At small seepage angles, seepage forces exceed intergranular stresses or forces of cohesion, and cause the detachment and movement of soil particles. Once a pipe forms, it enlarges quickly because of further concentration of flow lines in this critical area. Therefore, the most vulnerable portion of a slope for surficial instability is where water is emerging from the slope, i.e. the discharge area. In the three previous examples of slopes with curvilinear surfaces, it was observed that the discharge is concentrated in the "valleys". In all of these examples the minimum exit angle of flow, or in other words, the most severe seepage condition, occurs at the downstream side of the valleys. In a slope reinforced by an anchored system, this zone is located just downhill of each anchor. This region is most susceptible to piping and surface erosion. One solution to this discharge problem is to divert the seepage and change the direction of flow by incorporating a drainage system at the discharge zone (see Hryciw et al., 1994). The effectiveness of this solution can be investigated by analyzing flow patterns for different surface topography and drain configurations. Three examples are presented here for purpose of illustration. The first example is a slope with an undulating, curved surface (represented by a polynomial expression) and no drain (Fig. 8). The second example has the same slope shape or prism but with a drain oriented normal to the surface (Fig. 9). The third example is the same slope but with a drain inclined at a 45° angle (Fig. 10).

In all three examples, the slope undulations are at 12.5 cm spacing and the arc-relief is 1.875 cm. The slope angle is 25°, with the same dimensions as used in the example of Fig. 4. The mesh size is 0.625 cm x 0.625 cm. The finite difference analysis in all three cases was performed for the entire slope region but only the portion of the region near the drain is used to show the flow pattern. The results of flow analysis on the slope with no drain (Fig. 8) are consistent with those found for sinusoidal or circular surfaces. The discharge zone, as before, is concentrated at the valley. Very good agreement was observed for the flow pattern between the numerical predictions and experimental results, where a dye was used to reveal the flow lines (Fig. 11). Figures 9 and 10 show the results of the numerical analyses for slopes with normal and inclined drains respectively. The drain length is 2.5 cm in the first case, and 5 cm in the second case. The influence of drainage in changing the flow pattern near the surface can be seen in both figures. This influence, however, is more pronounced in Fig. 10 where the drain is at 45° to the slope. As a result of the drainage, the emergent flow from the discharge zone has been eliminated. Some portion of the collected water comes to the surface through the drain where it once again becomes beneficial recharge. This latter drain orientation is fortuitous because it is oriented approximately in the same direction as the "optimal" anchor orientation in anchored slopes (see Hryciw, 1991; Ghiassian, 1995). Accordingly, a combined "anchor-drain" system would be highly beneficial to stabilization of sandy slopes by anchored geosynthetics.

CONCLUSIONS

The stability of cohesionless slopes such as coastal dunes can significantly decrease due to internal seepage and external tractive stresses from wave action and runoff. In situations where emerging flow or exfiltration occurs, piping can result and accompany or trigger shallow mass failure. The key parameter in affecting stability is the flow direction. In slopes reinforced by Anchored Geosynthetics, the problem is more pronounced because of curvilinear surfaces,
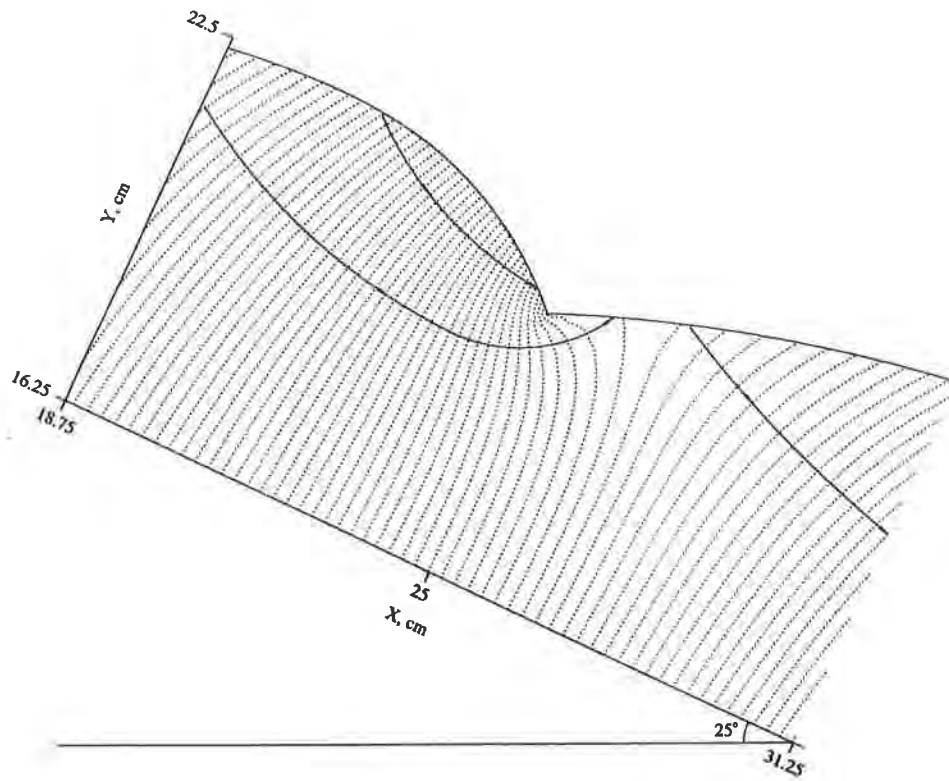
Fig. 8. Equipotential lines (contours) obtained by a numerical analysis for a rectangular slope prism with a curvilinear surface, 25° slope angle, and no drain
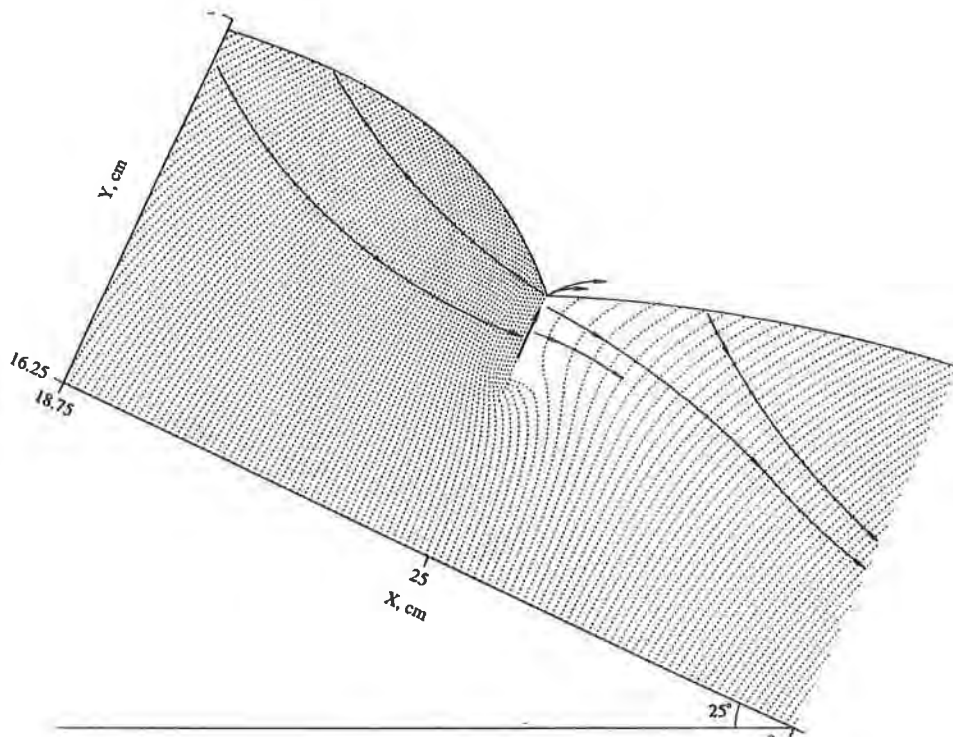

Fig. 9. Equipotential lines obtained by a numerical analysis for a rectangular slope prism with a curvilinear surface, 25° slope angle, and a drain oriented normal to the slope.
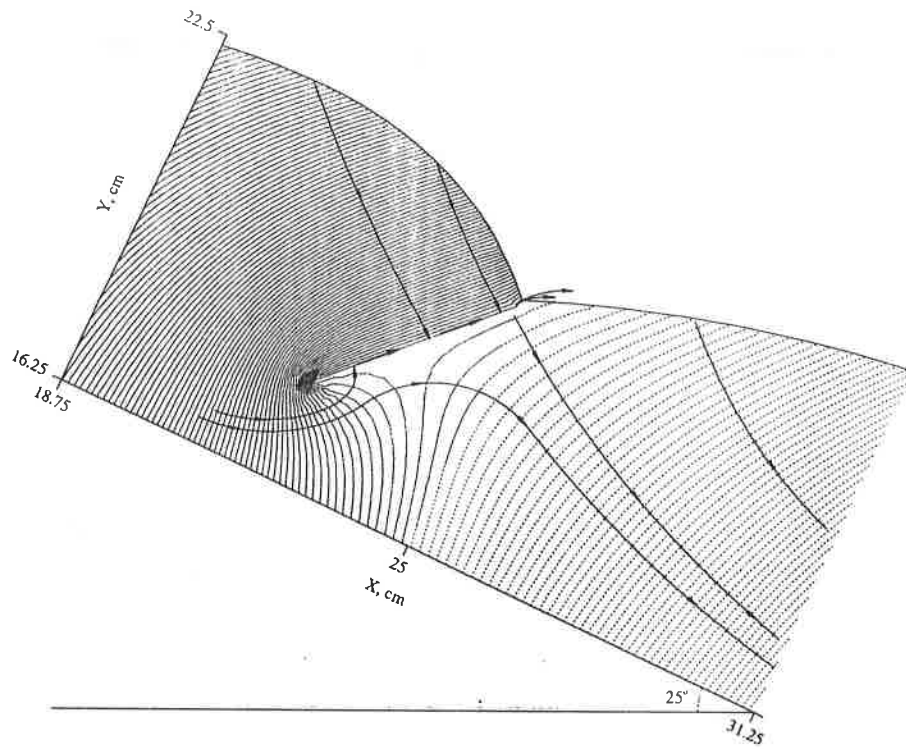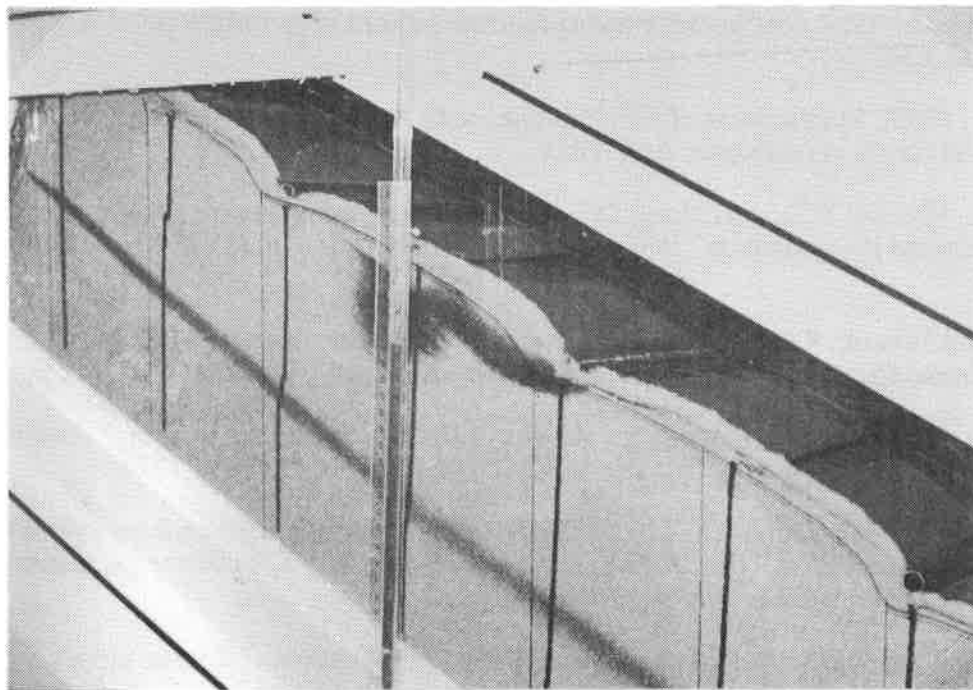
Fig. 10. Equipotential lines obtained by a numerical analysis for a rectangular slope prism with a curvilinear surface, 25° slope angle, and a drain oriented 45° to the slope.

Fig. 11. Flow pattern observed in laboratory testing of anchored geosynthetic slopes with seepage

and consequently, greater variation of flow patterns near the ground surface. This has been demonstrated through seepage analyses of several slope prisms with different shapes, surface topography, and boundary conditions. These results show the strong asymmetrical influence of topography on seepage directions near the ground surface. The results for hummocky surfaces indicate that more flow variation occurs as the amplitude of the hummocks increases.

The importance of near surface drainage in diverting emerging flow and converting it to a more favorable flow pattern was demonstrated by numerical analyses. Insertion of relatively short drains into slopes with an undulating surface at topographic lows or troughs can improve the shallow mass stability and piping resistance considerably by preventing seepage water from exiting the slope at points beneath the anchored geosynthetic. These drains will be most effective if they are incorporated into the anchorage system for the geosynthetics.

ACKNOWLEDGMENT

REFERENCES

Das, B. M. (1983). Advanced soil mechanics. McGraw-Hill Book Co., New York, N.Y.

Freeze, R. A., and Witherspoon, P. A. (1966). "Theoretical analysis of regional groundwater flow: 1. Analytical and numerical solutions to the mathematical model." *Water Resources Res.*, 2, pp. 641-656.

Freeze, R. A., and Witherspoon, P. A. (1967). "Theoretical analysis of regional groundwater flow: 2. Effect of water-table configuration and subsurface permeability variation." *Water Resources Res.*, 3, pp. 623-634.

Ghiassian H. (1995). Stabilization of Sandy Slopes with Anchored Geosynthetic Systems, Ph.D. thesis, The University of Michigan, Ann Arbor.

Ghiassian, H., Hryciw, R.D., and Gray, D.H. (1995). "Laboratory testing apparatus for slopes stabilized by anchored geosynthetics." Paper accepted for publication in *ASTM Geotech. Testing Journal*, in press.

Gray, D.H. and Hryciw, R.D. (1993). Biotechnical stabilization of coastal landforms. *Proceedings*, International Riprap Workshop, Colorado State University, Vol. 1, July 12-16, pp. 341-356.

Hryciw, R. D. (1991). "Anchor design for slope stabilization by surface loading," *Journal of the Geotechnical Engineering Division*, ASCE, Vol. 117, No. 8, 1260-1274.

Hryciw, R. D., and Haji-Ahmad, K. (1992). "Slope stabilization by anchored geosynthetic systems: anchorage optimization." *Proceedings of the ASCE Specialty Conference on Slopes and Embankments*, Berkeley, CA, , July pp. 1464-1480.

Hryciw, R. D., Gray H. D., and Ghiassian H. (1995). "Stabilization of coastal slopes by anchored geosynthetics," *Proceedings of U.S./Taiwan Geotechnical Engineering Collaboration Workshop*, Jan. 9-11, Taipei, Taiwan.

Iverson, R. M., and Major, J. J. (1986). "Groundwater Seepage Vectors and the Potential for Hillslope Failure and Debris Flow Mobilization." *Water Resources Research*, Vol. 22, NO. 11, Oct., pp. 1543-1548.

Kleiner, D. E. (1985). "Engineering with spreadsheets." Civil Engr. , ASCE, Vol. 55, No. 10, pp. 55-57.

Koerner, R. M. (1984). "In-Situ soil stabilization using anchored nets." *Proc. Conf. on Low Cost and Energy Saving Construction Methods*, Rio DeJaniero, Brazil, pp. 465-478.

Koerner, R. M., and Robins, J. C. (1986). "In-Situ stabilization of soil slopes using nailed geosynthetics." *Proc. of the 3rd Int. Conference on Geotextiles* , IFAI, 395-400.

Shaw, F. S., and Southwell, R. V. (1941). "Relaxation methods applied to engineering problems, VII.." *Proc. Roy. Soc. Lond.*, A178, pp. 1-17.

Southwell, R. V. (1946). "Relaxation methods in theoretical physics." *Oxford University Press.*, pp. 248.

Toth, J. (1962). "A theory of groundwater motion in small drainage basins in central Alberta, Canada." *J. Geophys. Res.*, Vol. 67, No. 11, pp. 4375-4387.

Toth, J. (1963). "A theoretical analysis of groundwater flow in small drainage basins." *J. Geophys. Res.*, Vol. 68, No. 16, pp. 4795-4812.

USE OF GEOSYNTHETICS TO VEGETATE STEEP SLOPES - CASE HISTORIES

L. E. WARD
AKZO NOBEL GEOSYNTHETICS, USA
J. LUNA
AKZO NOBEL GEOSYNTHETICS, USA

ABSTRACT

One of the first uses of a geosynthetic material for a permanent erosion control application was on the dikes of Holland around 1973. Since then millions of square meters of geosynthetic mats have been used successfully to reinforce vegetation on steep slopes, channels, stream banks, etc. These Turf Reinforcement Mats* (TRM) work with the root system of the vegetation to protect the soil from the erosive forces of rain, wind and wave action far above the ability of a vegetative layer alone.

This paper will provide case histories of three permanent erosion control installations. Before and after descriptions as well as installation techniques will be discussed. Design considerations will be presented when available. The installations include a 1/2 : 1 cut slope, a cut slope with a loose rocky face and a steep slope with surface erosion as well as sloughing problems.

Definitions:
* Turf Reinforcement Mats (TRM'S): A three dimensional matrix made of long term non-degradable polymers having sufficient open area to allow for soil and root interaction with the filaments. The matrix allows the vegetation to withstand much higher velocities and shear stresses than a vegetative layer alone.

INTRODUCTION

The design of erosion control solutions is often empirical due to the lack of generally accepted design criteria. Several manufacturers of permanent erosion control mats are working together within the Erosion Control Technology Council (ECTC) to determine valid performance parameters for these products. Unfortunately this

work will take considerable time, and until these methods are tested and proven, experience of the designer will often dictate product specifications. Therefore, case histories of proven performance in various applications are of great benefit to the designer.

CASE HISTORIES

Protection of a weathered rock slope in Germany. The problem in this case was the steep weathered rock face was next to a heavily traveled highway Figure 1). The cut slope posed a dangerous hazard when the rock would break loose and fall onto the roadway. This project being in Germany and installed may years ago made it difficult to locate the designer and contractor.
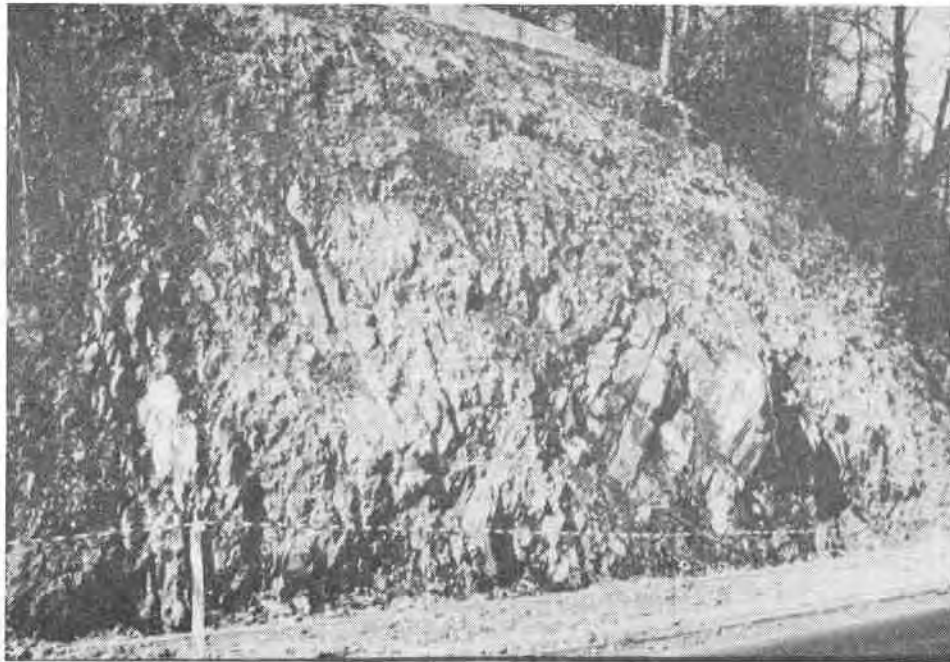
Figure 1: Weathered rock face

To alleviate the potential hazard a geosynthetic TRM was installed over the face of the slope to reinforce the soil vegetative root system much to save the loss of soil holding the rock on the face of the slope. The geosynthetic was then covered by a steel netting to hold the loose rock in place prior to the establishing of vegetation (see Figure 2).

In order to anchor the steel netting and geosynthetic to the face long rebar tee shaped pins where placed at the necessary rate to obtain intimate contact with what soil was available (see figure 3). The face of the slope was then hydraulically

seeded using a mixture of water, seed, fiber, soil stabilizer, fertilizer and soil
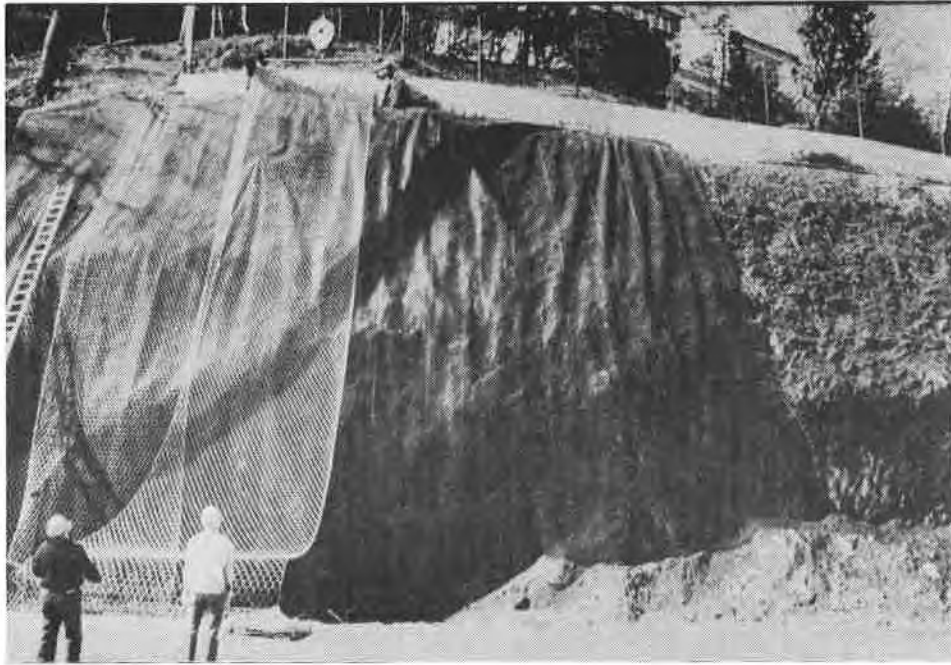
Figure 2: Installing Geosynthetic and steel netting

Figure 3: Rebar tee shaped anchor pins

Figure 4: Hydroseeding slope face

The slope was hydraulically seeded twice in order to fill the geosynthetic and steel material. It is important to choose a geosynthetic which is open enough to allow the mulch to pass through the material and have good contact with the soil. After a few months the potentially hazardous weathered rock face was permanently stabilized with the turf reinforcement matrix.
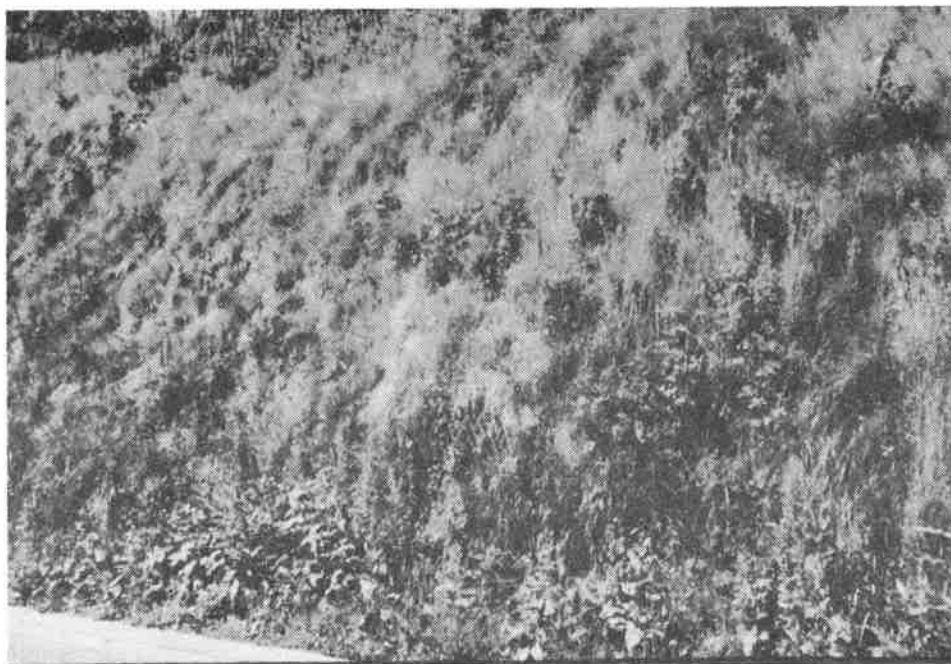
Figure 5:

Figure 5: Stabilized rock face

Turf reinforcement on 1/2:1 cut slope. Engineers designing a $60 million addition to a northwestern United States manufacturing facility had only one direction to expand -- into a hill. The resulting excavation project required the removal of more than 400,000 cubic yards of dirt and the stabilization of slopes as steep as 1/2:1. Five terraces were cut in the hill to provide a drainage system. Each terrace is about 4.6 meters (15 feet) wide and each slope is approximately 7.6 meters (25 feet) high.

The geosynthetic was laid in strips over the slopes with 1 meter (3.28 feet) extending onto the terrace for anchorage (see Figure 1). The geosynthetic was fastened to the slope using .305 meter (1 foot) long nails with washers. The slopes were so steep the installers had to use ladders in order to nail the matting properly. The nails used were approximately 15.24 cm (6") long X .95 cm (3/8") diameter with a 3.81 cm (1-1/2") washer. (see figures 2 and 3).

The hill was hydroseeded after the geosynthetic material was installed. A mixture of perennial rye grass, fescue, clover and bent grass assured a well-entrenched vegetated cover. The area was then irrigated with a sprinkling system to ensure a quick good stand of vegetation.

The results within a couple of months were better that expected. The slopes are protected from surface erosion with the root system intertwined in the nylon matrix of the geosynthetic (see Figure 4).
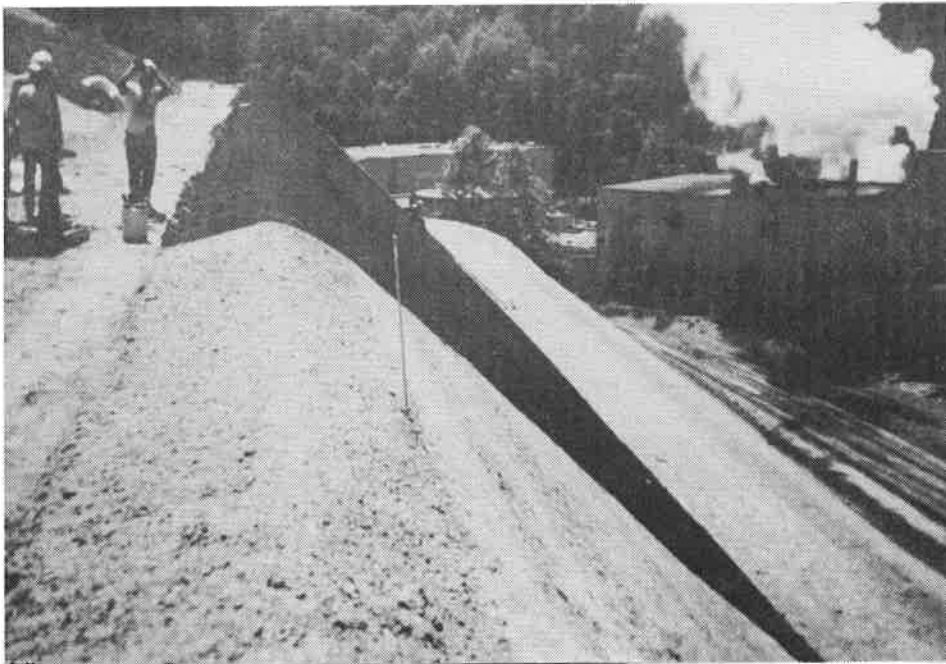
Figure 6: Start of Installation
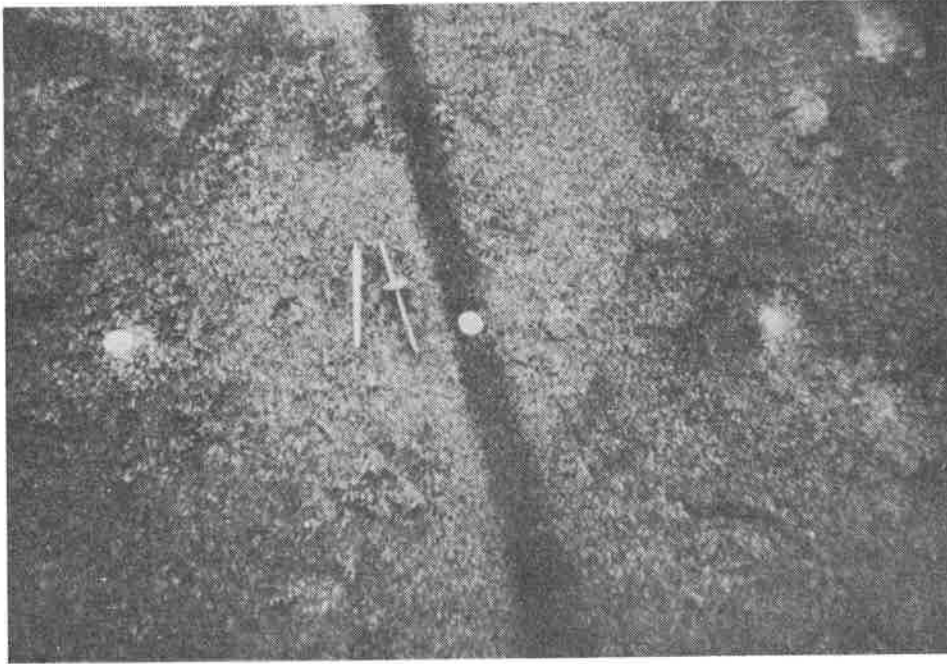
Figure 7: Nails used to anchor mat
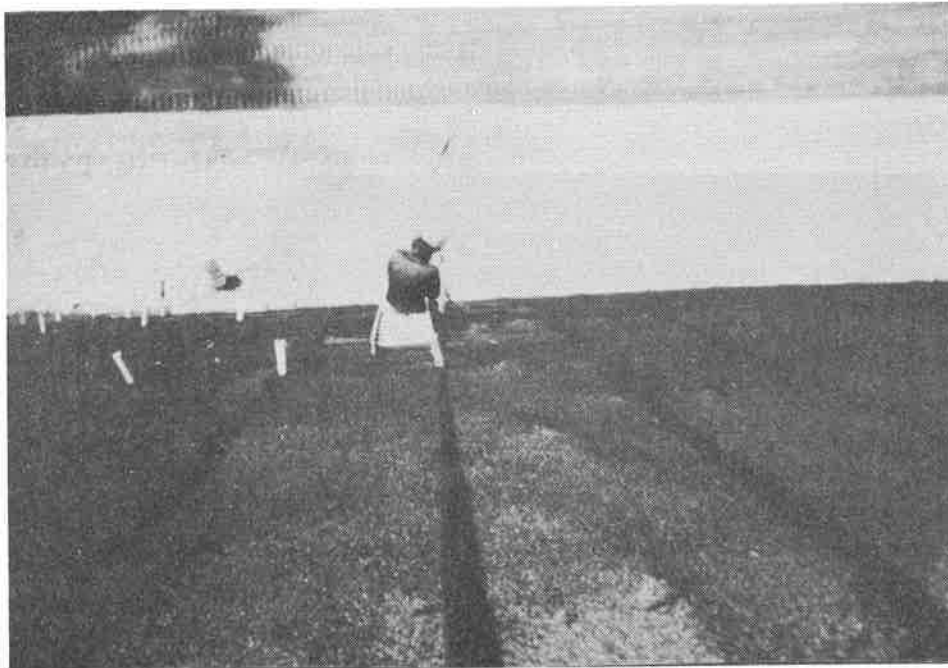
Figure 8: Use of ladders for installation
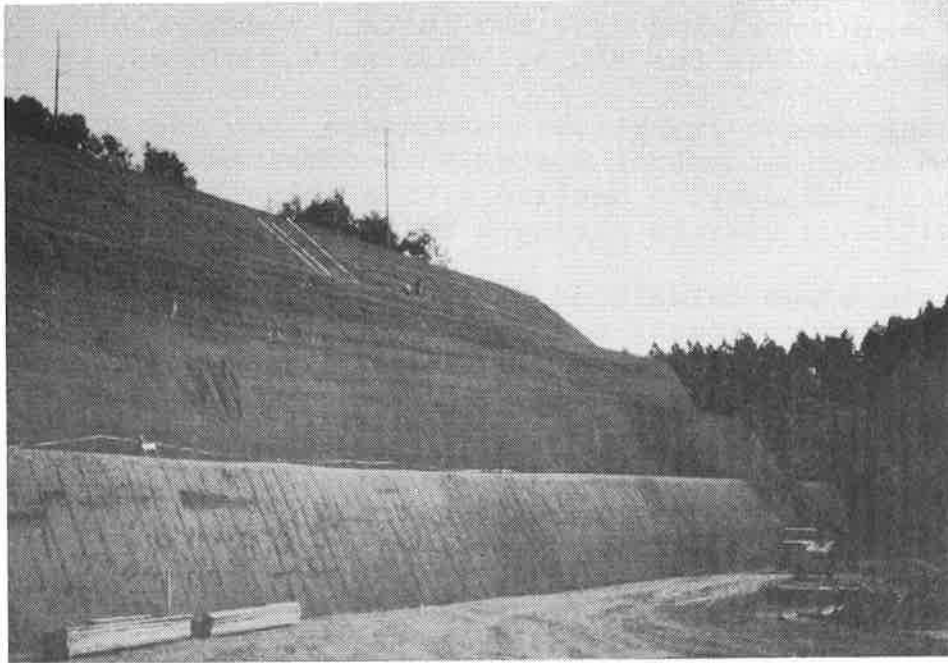
Figure 9: After two months growth

Erosion protection on a steep slope with a shallow slip plane. When contractors cut too far into a hill to expand a luxury car lot on Long Island, New York. The resulting slope was unstable, steep and threatened to crumble under an electrical transmission tower.
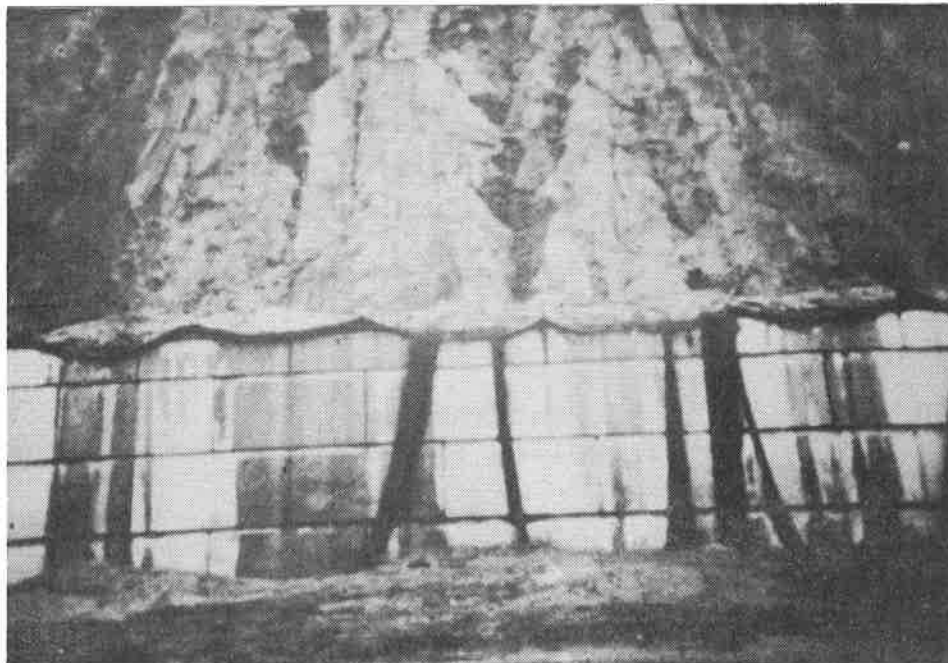

Figure 10:

Figure 10: Initial erosion control methods did not work. The first attempt to stabilize the slope was to construct a 6 meter (20 foot) high retaining wall and install a degradable erosion control blanket over the slope. This method did not work.

As a permanent stabilization measure, the engineers chose a new reinforced erosion control system that combines the three-dimensionally of a nylon matting with a polyester PVC-coated geogrid. With an ultimate tensile strength of 1500 lbs/ft.

The slope was calculated to be from 1.25 to 1.5:1 and had to be hand groomed as equipment could not be placed on the slope. The geosynthetic mat was anchored in a trench at the crest of the slope and rolled down to the retaining wall.
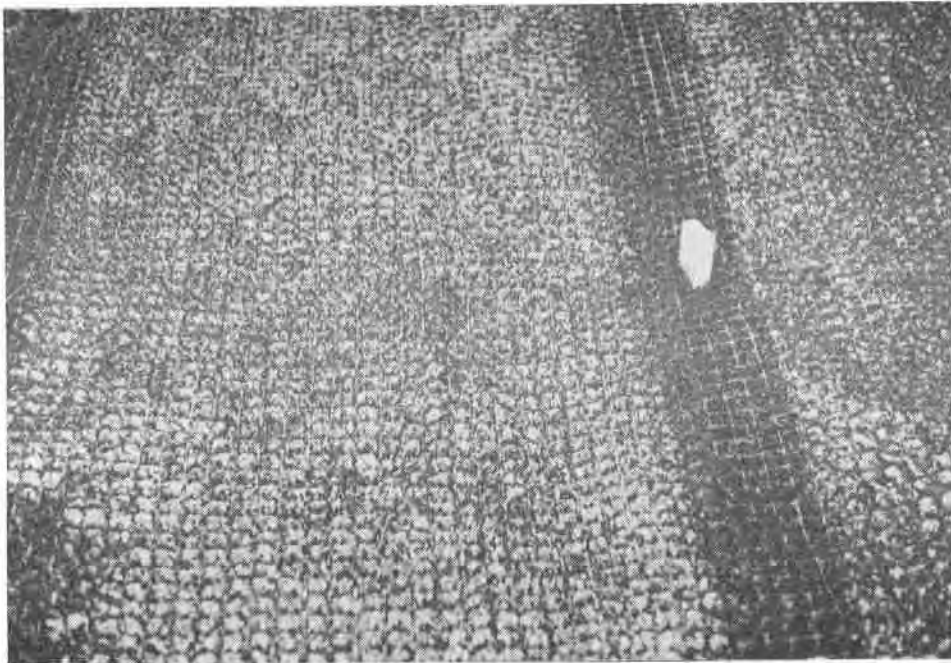
Figure 11: Rolling out and anchoring the matting

To anchor the matting 102 mm x .76 meter (4" x 2 1/2') tapered wooden stakes were used to connect the overlaps and to intercept the shallow slip plane (see figure 11).

About a week after the matting was installed and the slope, using a hand broadcaster applied rye mixture, heavy rains fell in the area.

There was no loss of soil or vegetation. The area is no longer an eye-sore for those walking or driving around the car lot. Any

potential danger to the foundation of the electrical tower has been eliminated.
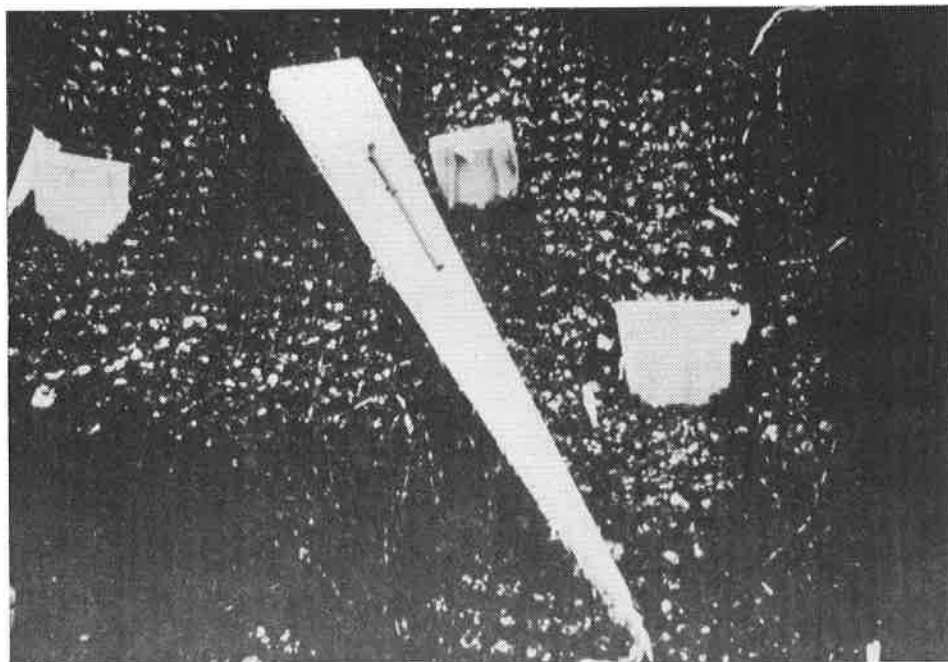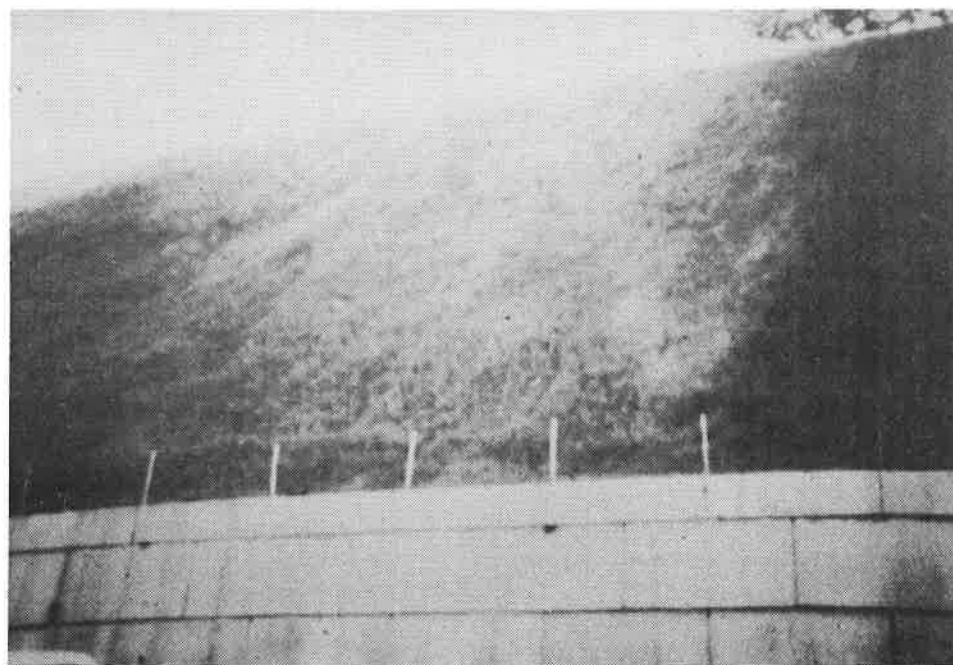

Figure 12: wooden stakes for anchoring

Figure 13: Completed project

Conclusions

These and other case studies demonstrate the use of TRM'S are a viable solution for erosion protection on a variety of steep slope applications.

Notes

HIGH STRENGTH EROSION CONTROL MAT SUPPORTS VEGETATION ON A CUT ROCK SLOPE

BILL TROLINGER, P.E.
TENNESSEE DEPARTMENT OF TRANSPORTATION (USA)

DERON N. AUSTIN, E.I.T.
SYNTHETIC INDUSTRIES, INC. (USA)

ABSTRACT

During the widening of U.S. Highway 25E from Clinch Mountain to U.S. Highway 11W in Grainger County (USA), the Tennessee Department of Transportation (TNDOT) was faced with the challenge of cutting a 0.5H:1V rock slope and preventing fragile limestone, sandstone and shale deposits from falling near passing motorists. Although hard armor solutions such as retaining structures and shotcrete were considered, concern over the aesthetics of highway expansion and costs associated with 7.5 km of potential hazards forced TNDOT to create an innovative vegetative solution. These 42.5 meter tall rock slopes were hydraulically seeded, anchored with wire mesh and rock bolts and stabilized with a unique three-dimensional woven geotextile erosion control mat.

Presented herein is a detailed case history of a unique application of a high strength permanent erosion control mat on a challenging project. This project summary documents the feasibility study, design parameters, specification and contract document preparation, supply and installation of specially-fabricated 3.6 meter wide rolls. Also included are cost comparisons and construction techniques for future users. A series of installation photographs accompanies this paper to create a practical technical reference for all involved in geosynthetics.

INTRODUCTION

Geosynthetic erosion control materials have been used to reinforce vegetation on disturbed, newly-seeded soil slopes for over 20 years. Turf reinforcement mats were first utilized on dikes in Holland in 1973 and on soil slopes adjacent to the Blue Ridge Parkway near Asheville, North Carolina (USA) in the summer of 1978. The success of these early applications for slope erosion control and dike protection, combined with product research and development, led to the use of geosynthetic erosion control materials in more challenging civil engineering applications. As a result, the initial performance limits for geosynthetic erosion control materials have been extended to include flexible channel lining systems, shoreline protection and near vertical soil and rock slopes.

When properly installed with appropriate seed mixes and fertilizers, geosynthetic erosion control materials provide a method to enhance the long-term performance of vegetative cover. The most common types of geosynthetic erosion control materials have been classified as turf reinforcement mats (TRMs). These lofty, three-dimensional matrices retain seed, hold soil, stimulate and accelerate germination and entangle with plant roots, stems, stolons and rhizomes. Historically, TRMs have been composed of mechanically or melt-bonded polypropylene, polyethylene, polyvinyl chloride or nylon nettings, monofilament yarns or fibers entangled to create a lofty and dimensionally-stable matrix. Although traditional TRMs exhibit tensile strengths up to 3,500 N/m, documented use on disturbed soil or rock slopes steeper than 1H:1V is rare.

As a result, engineers desiring turf reinforcement on near vertical slopes should consider permanent erosion and reinforcement matrixes (PERMs). The design features of these materials include a very resilient structure, excellent soil retention capacity, increased hydraulic performance limits and tensile strengths of up to 40,000 N/m. Although the TNDOT specified a traditional TRM on this project, a PERM was chosen as the most appropriate method to vegetate and stabilize the 0.5H:1V rock cut slopes. This product was selected due to its superior strength, durability, abrasion resistance, puncture strength and frictional characteristics.

BACKGROUND

The TNDOT has been widening sections of US 25E (SR-32) between Cumberland Gap, Tennessee, south of Middlesboro, Kentucky, and Interstate 40 for the past 20 years. This 85-km section of roadway serves as a major connector between Eastern Tennessee and Southeastern Kentucky. However, dramatic traffic increases, coupled with environmental concerns and a difficult geological setting, have slowed progress of these improvements. Upgrade of the 7.5-km section from the 4-lane south of Bean Station northwest to the 4-lane near Miller Hollow Road was delayed for several years due to a combination of these factors. The existing roadway is nestled between the backwaters of Cherokee Lake and steep terrain composed of geological formations which may produce acid leachates (Miller 1994).

GEOTECHNICAL INVESTIGATION

An extensive geotechnical report, boring logs and laboratory analysis was completed by the TNDOT in July 1992. The investigation revealed the presence of competent soil and rock for the roadway subgrade but combinations of fragile limestone, shale, siltstone and sandstone layers along the proposed alignment (Figure 1). Although these geological formations have the potential for producing acid leachates when exposed, much of the statigraphy can be seen along the existing roadway cuts along U.S. Highway 25E adjacent to the proposed alignment.

A total of twelve (12) borings were drilled between Station 978+50 and 1022+00, which is where the majority of rock on the project would be blasted and excavated. Specific rock strata from Station 978+50 to the end of the project were identified as Pumpkin Valley Shale, Rome Formation (thin-bedded to medium-bedded shale, siltstone, sandstone, and argillaceous limestone), Grainger Formation (siltstone and sandstone) and Chattanooga Shale (Trolinger 1993). These rock layers typically have a southeastern dip and a strike perpendicular to the proposed roadway. Furthermore, a fault is situated between the Rome and Grainger formations which could make the cut slope area susceptible to excessive weathering, spalling and potential rock falls.
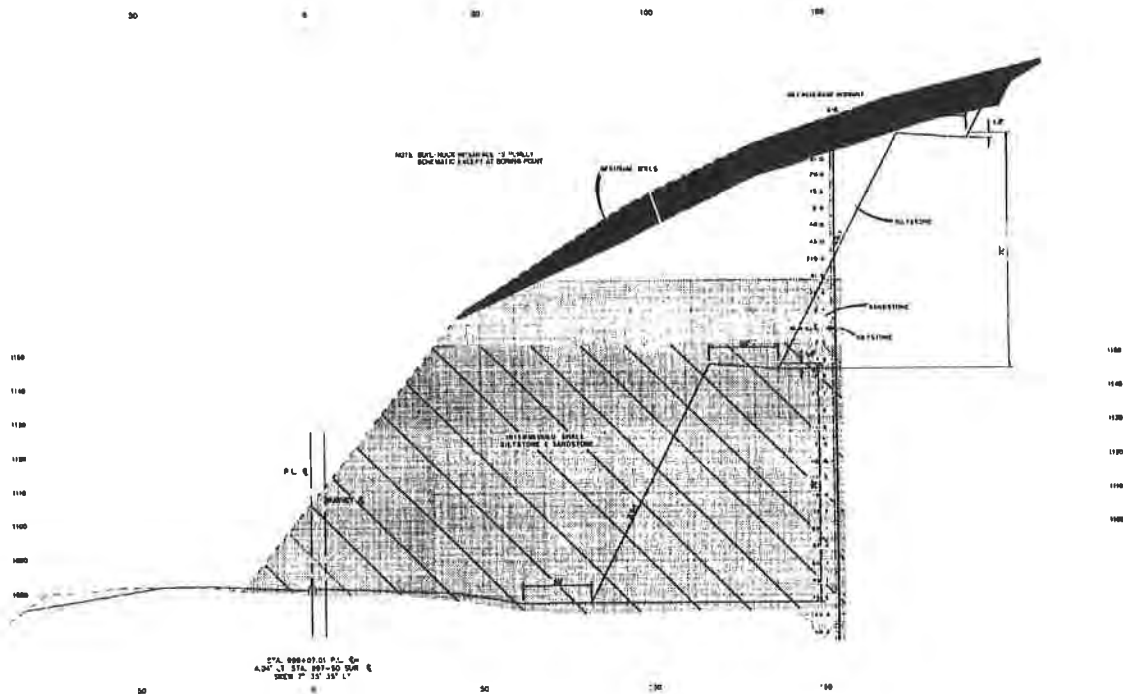
Figure 1. Cross-Section of Typical Soil & Rock Borings

THE DESIGN

Although the TNDOT determined the finished grade of the cut rock slope would need to be nearly vertical in order to meet the proposed roadway alignment, several design alternatives were analyzed during the initial feasibility study: (1) incorporate the steep cut rock slopes needed for alignment and provide for rockfall protection and runoff control; or (2) utilize flatter, more stable slopes but realign the roadway and insulate the acid producing materials from runoff. Since flatter slopes would drive excavation quantities up by 8 to 10 fold, the utilization of 1.5H:1V slopes was eliminated due to the excess excavation that would become necessary. With over 50,000 square meters of mandatory rock splitting already estimated, the cut slopes would need to be as steep as possible in order to minimize the costs of excavation. Furthermore, reducing the amount of excavation would not only lower treatment costs but also produce a smaller area of cut rock face with acid-producing potential. This excess excavation cost, combined with subsequent treatment procedures, would have more than tripled the estimated project cost. These factors led the engineers to work with 0.5H:1V bottom slopes and varying top slopes from 0.5H:1V to 2H:1V.

Since the use of very steep cut slopes would minimize excavation quantities and cut face area exposed to runoff, the TNDOT had to then analyze several options for rockfall protection and runoff control including: (1) the establishment of vegetation on the slope itself coupled with benches; (2) covering the cut faces with shotcrete; or (3) building retaining structures for even steeper (vertical) slopes. Since the cost of a retaining structure for the cut rock slope was estimated at $13.5 million (US) and global stability analyses of the 0.5H:1V slopes indicated acceptable safety factors, retaining structures were not necessary and a more economical solution was available. Although shotcrete would eliminate rockfall and insulate the exposed surface from runoff, poor aesthetics and a cost of $9 million (US) led to a detailed examination of wire mesh, a solution previously used by the TNDOT to control rockfall. TNDOT also realized that a turf reinforcement mat used in conjunction with the wire mesh would help to establish vegetation and control runoff. The estimates of this system ranged from $1.5 to $3 million (US), 67% less than the shotcrete system considered.

Each cut slope along this section of the alignment would require 21.3-meter high slopes constructed with 6.1-meter maintenance benches sloped at a grade of 15 percent to the horizontal (Figure 2). These benches were designed to reduce slope lengths and help establish a vegetated shelf to capture runoff and slaked slope material. A protective cover of vegetation would establish to help reduce the formation of an acid runoff from the steep slopes. Based upon the feasibility study and the design analysis, TNDOT selected a combination of wire mesh and permanent erosion and reinforcement matrix, designated as "Erosion Control Blanket - Type II", to be used on all exposed rock cut slopes from Station 978+50 to Station 1029+50 (see Table 1). This "rock slope wire meshing" would help stabilize the face, initiate development of vegetation, prevent rockfall from endangering motorists and provide superior long-term

aesthetics (Figure 3). In addition a "wire mesh vegetation mattress" was to be placed on each bench. This mattress consisted of the wire mesh, the Erosion Control Blanket - Type II and a temporary degradable straw blanket wrapped around a 600 mm thick core of top soil mix (Figure 4). This mattress would serve as a bed for vegetation growth on the benches.
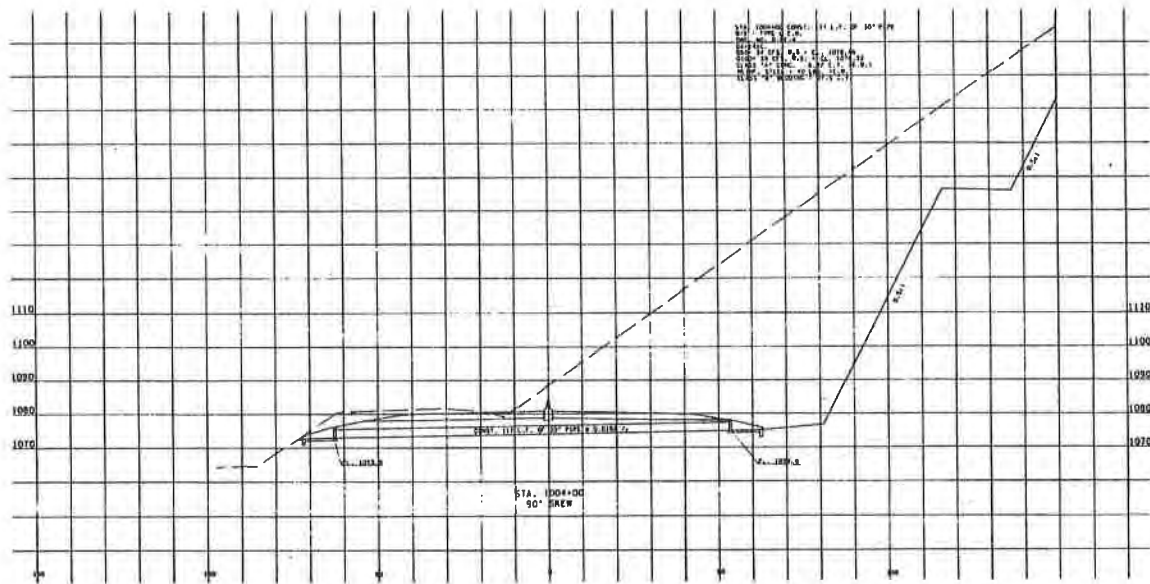

Figure 2. Typical Cross-Section for Station 978+50 to 1029+50

Table 1. Recommended Rock Cut Slope Batters

STATION	BOTTOM SLOPE	TOP SLOPE
978+50 to 998+50	0.5H:1V	2H:1V
998+50 to 1006+00	0.5H:1V	1H:1V
1006+00 to 1009+50	0.5H:1V	2H:1V
1009+50 to 1019+00	0.5H:1V	0.5H:1V
1019+00 to 1022+00	0.5H:1V	1H:1V
1022+00 to 1029+50	0.5H:1V	0
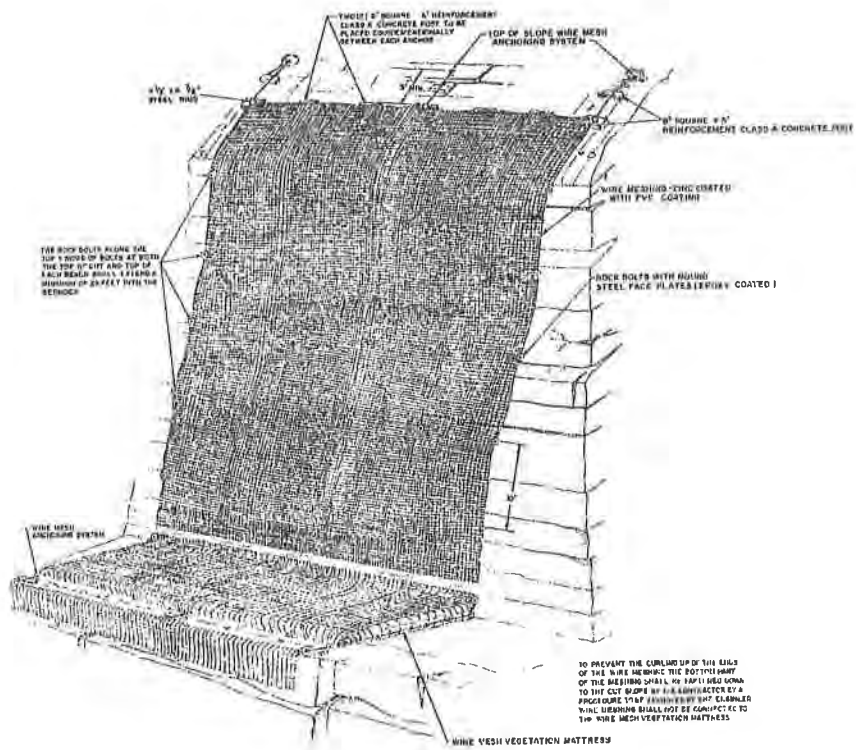
Figure 3. Rock Slope Wire Meshing Detail
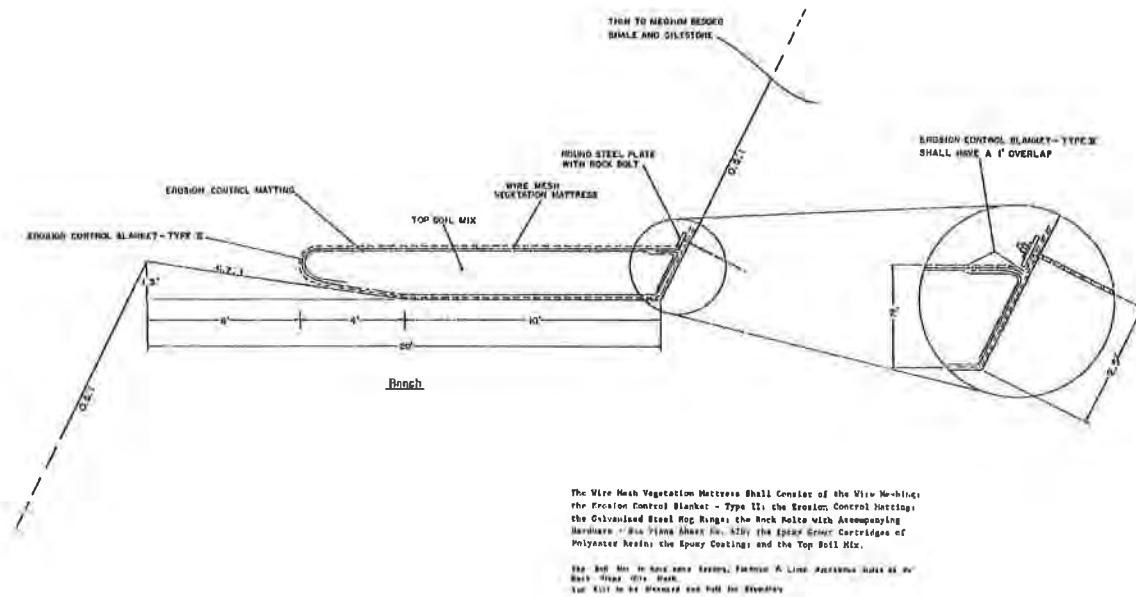
Figure 4. Wire Mesh Vegetation Mattress

ROCK SLOPE WIRE MESHING

The rock slope wire meshing selected by the TNDOT consisted of wire mesh and the Erosion Control Blanket - Type II. The specified wire mesh was to be hexagonal, double-twisted, PVC-coated galvanized steel wire with an approximate diameter of 2.7 mm (without coating), a minimum tensile strength of 413.4 MPa and a maximum opening dimension of 100 mm. The Erosion Control Blanket - Type II specified was a synthetic three-dimensional crush resistant, pliable, resilient structure highly resistant to chemicals and environmental degradation (Trolinger 1993). This component of the rock slope wire meshing was designed to provide soil and seed anchorage for seed development (Table 2).

Table 2. Specification Requirements for Erosion Control Blanket - Type II

PROPERTY	SPECIFICATION	SUPPLIED MATERIAL
Filament Diameter	0.3 mm	0.5 mm
Mass Per Unit Area	400 gr/m^2	475 gr/m^2
Thickness	19 mm	12.7 mm
Color	Black	Black
Tensile Strength	3360 N/m x 3070 N/m	4430 N/m x 3250 N/m
Tensile Elongation	50 x 30 %	50% (max)
Maximum Shear Stress	40 N/m^2	480 N/m^2
Resiliency (3 cycles, 690 kPa)	80 %	80%
Soil Holding Capacity	0.017 m^3/m^2	n/a

INSTALLATION TRIALS

In order to confirm the proposed products' holding and reinforcement capabilities, a test section was installed on June 27, 1995. Elmo Greer & Sons, Inc. and Mills Landscaping installed the seed, mulch and it fully penetrated the proposed product, PYRAMAT® permanent erosion and reinforcement matrix manufactured by Synthetic Industries. The installation also verified the drapability of the product and demonstrated that a rock bolt spacing of 3.0 to 3.6 meters was adequate to secure the wire mesh vegetation mattress.

CONTRUCTION

Prior to installation of the rock slope wire meshing and wire mesh vegetation mattress, the excavated cut rock slope was treated with dry lime applied at the rate of 1,100 kg/ha and one-half of the specified 10-10-10 pelletized fertilizer of 165 kg/ha. The first of two

applications of seed and mulch was also applied. This seed mix consisted of 9.2 kg/ha annual rye, 18.4 kg/ha of Kentucky 31 fescue and 550 gr/ha of weeping lovegrass. The mulch consisted of 260 kg/ha of printers scrap paper and wood cellulose, applied at a maximum moisture content of 8 percent (Trolinger 1993).

The permanent erosion and reinforcement matrix and the wire mesh was anchored at the top of the slope and unrolled down the cut rock slope face (Figure 5). The contractor had the initial shipment of material pre-fabricated into 3.6 x 45.7 meter rolls in an effort to facilitate installation. However, subsequent shipments of the permanent erosion and reinforcement matrix and the wire mesh were installed separately in order to maintain intimate contact with the surface of the cut slope. Stainless steel hog rings and 18 mm wire rope were fastened on 300 mm centers to the wire mesh. The wire rope was anchored at the top of the slope using 150 mm x 150 mm x 450 mm reinforced concrete anchor blocks spaced at 6.7 meter intervals. Epoxy-coated rock bolts were placed into the slope at intervals of 3.4 meters horizontally and 2.8 meters vertically and embedded 1.5 to 7.5 meters deep into the rock strata. These rock bolts featured a tensile strength at 2 percent strain of 85 percent of the ultimate strength of 760 MPa. Round steel plates measuring 165 mm in diameter and 9.5 mm thick were then placed over the rock bolts and secured with epoxy, polyester resin or Portland cement grout (see Figure 6). The grout displayed a cured compressive strength of 110 MPa, a tensile strength of 17.2 MPa and a shear strength of 51.7 MPa (Trolinger 1993).
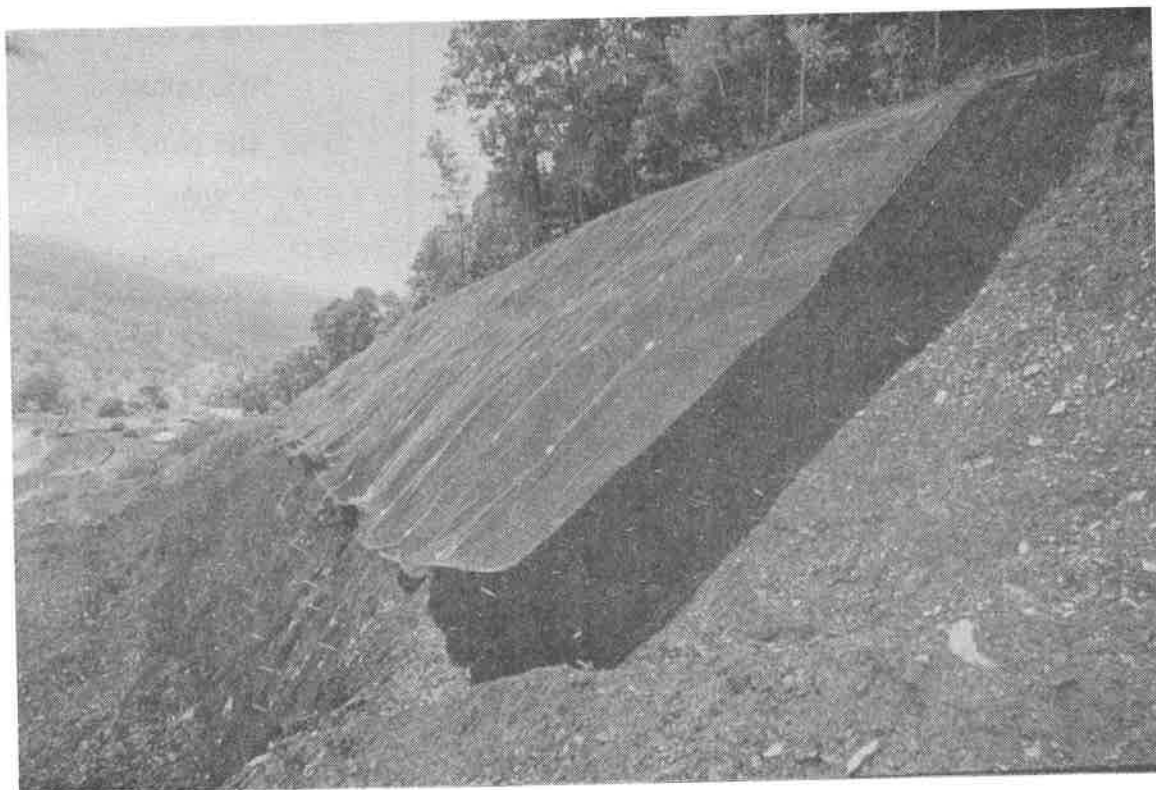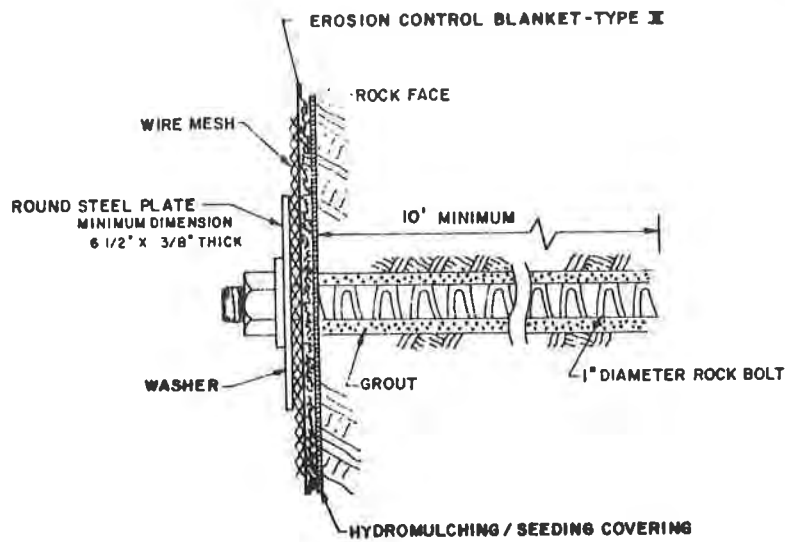

Figure 5. Installation of Rock Slope Wire Meshing

ROCK BOLT SPACING FOR WIRE MESHING

Rock bolts used to secure wire meshing are to be installed in horizontal rows which shall be 10' apart starting at the top of the slope; with individual rock bolts being spaced at 10' intervals along the horizontal row (see diagram).

Figure 6. Rock Bolt Detail

After the successful installation of the rock slope wire meshing, the other half of the 10-10-10 pelletized fertilizer, seed and mulch was applied. Again, the specified seed mix consisted of 9.2 kg/ha annual rye, 18.4 kg/ha of Kentucky 31 fescue and 550 gr/ha of weeping lovegrass. The mulch consisted of 260 kg/ha printers scrap paper containing wood cellulose at a maximum moisture content of 8 percent.

OBSERVATIONS & CONCLUSIONS

Although it is too early to measure the long-term performance of this innovative use for geosynthetic erosion control materials, initial observations made by field personnel over the first growing season indicate emergence of vegetation in the upper sections of the rock slope wire meshing on the top slopes. The initial concern with rock fall during and after construction has been eliminated and the rock slope wire meshing did prove to be the most economical option from a materials and construction cost perspective. The only concern expressed by the engineer and the contractor was the initial lack of small rock fragments and soil for seedling development. However, the contractor did recognize that a two-step installation of the permanent erosion and reinforcement matrix and wire mesh does improve intimate contact which accelerates vegetative growth and maximizes erosion control. Recognizing the intensity of the summer sun and rock

weathering that would occur during the first season, there have been discussions regarding possible re-seeding if necessary.

The permanent erosion and reinforcement matrix chosen by the contractor withstood the stresses of installation, conformed well to the irregular rock cut slope surface and retained mulch and seed to guarantee maximum growth potential. The permanent erosion and reinforcement matrix used was necessary due to its three-dimensional crush resistant structure, yet it was pliable, resilient and highly resistant to ultraviolet, chemical and environmental degradation. The permanent erosion and reinforcement matrix successfully provided adequate soil and seed anchorage for seed development. Since there is much confidence that this system will perform as originally designed, the TNDOT anticipates using this vegetated rock slope wire meshing system on other cut rock slopes around the state.

Figure 7. Partially Vegetated Slopes Three Months After Installation

CLOSING

Due to the challenges on this project and the innovative use of geosynthetic erosion control materials on a rock cut slope, interested parties will continue to monitor the performance of the permanent erosion and reinforcement matrix. The authors envision a technical paper at a future geosynthetic conference that reports the observed durability and performance over a longer period of time. Furthermore, the uniqueness and use of the permanent erosion and reinforcement matrix won the 1996 Industrial Fabrics Association International, International Achievement Award - Geosynthetic Products for this project.

ACKNOWLEDGEMENTS

REFERENCES

Trolinger, B., "Geologic Report - Project No. 29002-1223-04, U.S. 11W (S.R. 1) and U.S. 25E (S.R. 32) from 4-Lane South of Bean Station Northwest to 4-Lane near Miller Hollow Road, Grainger County", TNDOT, Nashville, TN, August 4, 1993.

Miller, D.T., "Roadway Plans - U.S. 11W (S.R. 1) and U.S. 25E (S.R. 32) from 4-Lane South of Bean Station Northwest to 4-Lane near Miller Hollow Road, Grainger County", prepared for the TNDOT by H.W. Lochner, Inc., December 23, 1994.

Geosynthetics '97 Conference Proceedings

Volume 1
High-Strength Reinforcement
Marine
Geosynthetics Durability
Student Session
Remediation and Containment
Erosion Control

Volume 2
Pavement Systems
Economics
Interface Friction Testing
Seismic Design and Construction
Mining
Filtration

GEOSYNTHETICS 97 CONFERENCE
Long Beach, California USA

Geosynthetics '97

Conference Proceedings

Volume 2

Pavement Systems
Economics
Interface Friction Testing
Seismic Design and Construction
Mining
Filtration

GEOSYNTHETICS
97
CONFERENCE
Long Beach, California USA

SOLMAX

Geosynthetics '97
Conference Proceedings

Volume 2
Pavement Systems
Economics
Interface Friction Testing
Seismic Design and Construction
Mining
Filtration

GEOSYNTHETICS
CONFERENCE
Long Beach, California USA

Geosynthetics '97 *Conference Proceedings*

Conference Organizers

The Industrial Fabrics Association International (IFAI) is extensively involved in the
geosynthetics industry, and serves its membership by facilitating the worldwide
development, application and proper utilization of products manufactured by the
geosynthetics industry.

The North American Geosynthetics Society (NAGS) is a professional society dedicated to
advancing the use of geosynthetics as engineering materials, and providing forums to
facilitate communication among geosynthetics-related interests.

The International Geosynthetics Society (IGS) is the international professional society that
brings together individuals and organizations involved with geosynthetics. The IGS has
members in 58 countries.

Notice and Disclaimer
The opinion expressed and the technical data provided herein are those of the author(s) and do not necessarily represent the
opinion of the geosynthetics industry, the Industrial Fabrics Association International, the North American Geosynthetics Society
or the International Geosynthetics Society . The above organizations make no representations or warranty, either express or
implied, as to (1) the fitness for any particular purpose of any of the information , design or standards contained in this book or
any products manufactured or constructed in accordance there with; or (2) the merchantbility of any such information , designs,
standards or products. The use by any individual or entity of any of such information , designs, standards or products constitutes
and acknowledgement and agreement by such individual or entity that the Industrial Fabrics Association International, The
North American Geosynthetics Society and the International Geosynthetics made no representation or warranty with respect to
the fitness, merchantability, or quality of such information, designs, standards or products.

GEOSYNTHETICS '97 CONFERENCE
Long Beach, California USA

Foreword

The contributions and success of the previous geosynthetics conferences presented the Geosynthetics '97 Organizing Committee with outstanding precedents to meet. The technical papers published in past proceedings from the geosynthetics conference series have proven to be valuable reference documents for the industry. The 76 papers published in these proceedings provide up-to-date contributions to that heritage. The papers that were accepted to this conference were eligible for the Awards of Excellence sponsored by NAGS and industry partners. This program was initiated to recognize excellence in the state-of-the-art and state-of the-practice of geosynthetics in North America.

The papers in these proceedings were selected from 167 abstracts received by the Organizing Committee in response to an international call for papers in 1995. The Technical Review Committee that reviewed the abstracts was composed of prominent members of the geosynthetics community representing academia, manufacturers, design and construction consultants, government, and a testing laboratory. Ten topic leaders in the Technical Review Committee were engaged to run eleven topics, which were presented in 17 sessions at the conference. The selected papers were reviewed by a minimum of two qualified individuals under the direction of the technical session leaders.

The Geosynthetics '97 challenge was to continue the tradition of disseminating the most current state of knowledge and practice in the geosynthetics industry, in the form of focused topics. Topics such as durability, filtration, interface friction, soil reinforcement and pavement systems continue to be of great value as advances are made in design approaches, laboratory studies, and documented case histories. Specialty topics on economics, marine, mining, and seismic design are fresh to the geosynthetics conference series, and were included to provide new focus areas for this venue.

We are pleased to continue the Student Paper Competition that was started at Geosynthetics '95. Under the leadership of Dr. Andre Rollin, a panel of industry, academic and government professionals selected five student papers which were presented at the conference and are published in these proceedings. IFAI and NAGS provided expense-paid trips to the students to participate in the conference as part of their efforts to support the future of our industry.

We must recognize the individuals comprising the Technical Review Committee, session leaders, paper reviewers, and advisors who donated their time to maintain the high standard of technical contribution provided in geosynthetics conference series. The dedication, cooperation, and quality efforts from these individuals is not only invaluable to the benefit of these proceedings, but is symptomatic of the actual and potential value and importance that geosynthetics play in the basic infrastructure of our society.

Larry Well
Co-Chairman, Technical Committee
Geosynthetics '97

Richard Thiel
Co-Chairman, Technical Committee
Geosynthetics '97

Geosynthetics '97
Organizing Committee

Organizing Committee Chairman
John N. Paulson
Strata Systems Inc.
Cumming, Georgia USA

Technical Committee Co-chairman
Larry W. Well
CH2M Hill
Portland, Oregon USA

Technical Committee Co-chairman
Richard S. Thiel
Thiel Engineering
Oregon House, California USA

Advisor
Richard J. Bathurst
Royal Military College Of Canada
Kingston, Ontario Canada

Advisor
Y. Grace Hsuan
Geosynthetic Research Institute
Drexel University
Philadelphia, Pennsylvania USA

Panel Session Chairman
Rick Thomas
TRI/Environmental Inc.
Austin, Texas USA

Secretary General
Danette R. Fettig
Industrial Fabrics Association International
St. Paul, Minnesota USA

Geosynthetics '97
Technical Review Committee

Technical Committee Chairman
Larry W. Well
CH2M Hill
Portland, Oregon USA

Technical Committee Chairman
Richard Thiel
Thiel Engineering
Oregon House, California USA

High-Strength Reinforcement
Barry Christopher
Roswell, Georgia USA

Mining
Brian Simpson
Golder Associates
Lakewood, Colorado USA

Remediation & Containment
Gregory Richardson
G.N. Richardson & Associates
Raleigh, North Carolina USA

Seismic Design and Construction
Edward Kavazanjian, Jr.
GeoSyntec Consultants
Huntington Beach, California USA

Interface Friction Testing
Allen Marr
GeoTesting Express
Acton, Massachusetts USA

Pavement Systems
Mark Marienfeld
Amoco Fabrics & Fibers Co.
Atlanta, Georgia USA

Economics
Alice Comer
Bureau of Reclamation
Materials Engineering
& Research Lab
Denver, Colorado USA

Erosion Control & Marine
Marc Theisen
Synthetic Industries Inc.
Chatanooga, Tennessee USA

Durability
Donald Bright
The Tensar Corp.
Morrow, Georgia USA

Filtration
Shobha K. Bhatia
Syracuse University
Syracuse, New York USA

Table of Contents: Volume 1

HIGH-STRENGTH REINFORCEMENT

MARINE

Table of Contents: Volume 1

GEOSYNTHETICS DURABILITY

STUDENT SESSION

Table of Contents: Volume 1

REMEDIATION AND CONTAINMENT

Table of Contents: Volume 1

Table of Contents: Volume 2

PAVEMENT SYSTEMS

ECONOMICS

Table of Contents: Volume 2

Table of Contents: Volume 2

MINING

FILTRATION

Pavement Systems

GEOSYNTHETIC-REINFORCED PAVEMENT SYSTEM : TESTING & DESIGN

FILIPPO MONTANELLI
TENAX SPA, ITALY
AIGEN ZHAO
TENAX CORPORATION, USA
PIETRO RIMOLDI
TENAX SPA, ITALY

ABSTRACT

A large scale experimental program was presented in this paper, aimed at the improvement of the understanding, and evaluation of the structural contribution of geosynthetic reinforcement to pavement systems. The structural contribution of a geogrid was quantified by the increase in the layer coefficient of the base course material. Design parameters derived from the laboratory testing were analyzed and presented. A design method for geosynthetic reinforced pavement system was developed. A design example and design charts are provided. A cost benefit analysis is also conducted.

INTRODUCTION

Geosynthetics, as applied to flexible pavement systems, have been widely used in recent years. The benefits of geosynthetics in flexible pavement systems were presented by Barksdale, et al. (1989). Geosynthetic reinforcement is typically placed in the interface between the aggregate base course and the subgrade. Although many projects of this kind have been successfully installed, there is still a lack of understanding about the behaviour of the composite system, especially rigorously quantifying the structural contribution by geosynthetic reinforcement and incorporating it into a design methodology.

A large scale experimental program was presented in this paper, aimed at the improvement of the understanding, and evaluation of the structural contribution of a geogrid to pavement systems. Laboratory tests were performed to study flexible pavement systems under simulated traffic loading conditions. Asphalt layer, aggregate base course and subgrade soil were included in the pavement sections. Pavement sections with different subgrade strength were tested.

Number of dynamic loading cycles along with the pavement deformation were recorded. Flexible pavement testing with different geosynthetic reinforcement was conducted in conjunction with University of Milan as reported by Cancelli et al. (1996).

Existing design methods for flexible pavements include empirical methods, limiting shear failure methods, limiting deflection methods, regression methods, and mechanistic-empirical methods. AASHTO method is a regression method based on the results of road tests. AASHTO published the interim guide for design of pavement structures in 1972, a revised version in 1981. Reliability concept is used in the current AASHTO design method, however, design method in accordance with the interim guide are still being used due to its simplicity and familiarity to design engineers. In this paper, design parameters derived from the laboratory testing were analyzed and presented. A modified AASHTO design method (based on the interim guide) for geosynthetic reinforced pavement system, capable of determining the required aggregate thickness (when the asphalt thickness is given) or the required asphalt thickness (when the aggregate thickness is given), was developed. The structural contribution of a geogrid reinforcement on flexible pavements is quantified by the increase in the structural layer coefficient of the aggregate base course. A design example and design charts are provided. Cost benefit analysis is also presented.

TESTING PROGRAM

The typical cross-section of testing set-up is shown in Figure 1. A geosynthetic layer was placed only in one half of the box section, while the other half was left unreinforced to be used for comparison purposes. This technique allows a greater precision in determining reinforcement effects since the properties of the soils in the two halves were the same because the two parts of the box were filled at the same time using the same soil handling procedures. The geogrid reinforcement layer was placed flat above the layer of loose soil and then folded at 90° at the box sides. The geogrid was folded to the metal box sides to model the anchorage effect in a typical wide road base. In this way the pullout failure of geogrid is prevented due to the relatively small dimensions of the testing box. Similar concept was utilized by Gregory and Bang (1994).

Up to 300,000 sinusoidal loading cycles have been applied through a circular loading plate having 300 mm diameter. The tests have been performed at a frequency of either 5 or 10 Hz and the load was ranging from 0 to 40 kN with an equivalent maximum applied pressure of 570 kPa. The vertical settlements (ruts) have been recorded as a function of number of cycles together with the permanent deformation in the road section.

The sinusoidal cycle loading has been applied through a servohydraulic actuator controlled by an Instron 8580 digital multi-axis closed-loop controller and the rut depths were measured by a transducer inside the piston. The settlements and the elastic rebounds of the asphalt layers have been measured during the tests, under the loading plate, every 100 cycles. The distribution of the permanent deformation on the aggregate was recorded during the tests by measuring the

displacements of the asphalt surface in several locations, and of the asphalt/aggregate and aggregate/subgrade interfaces at the end of each test.
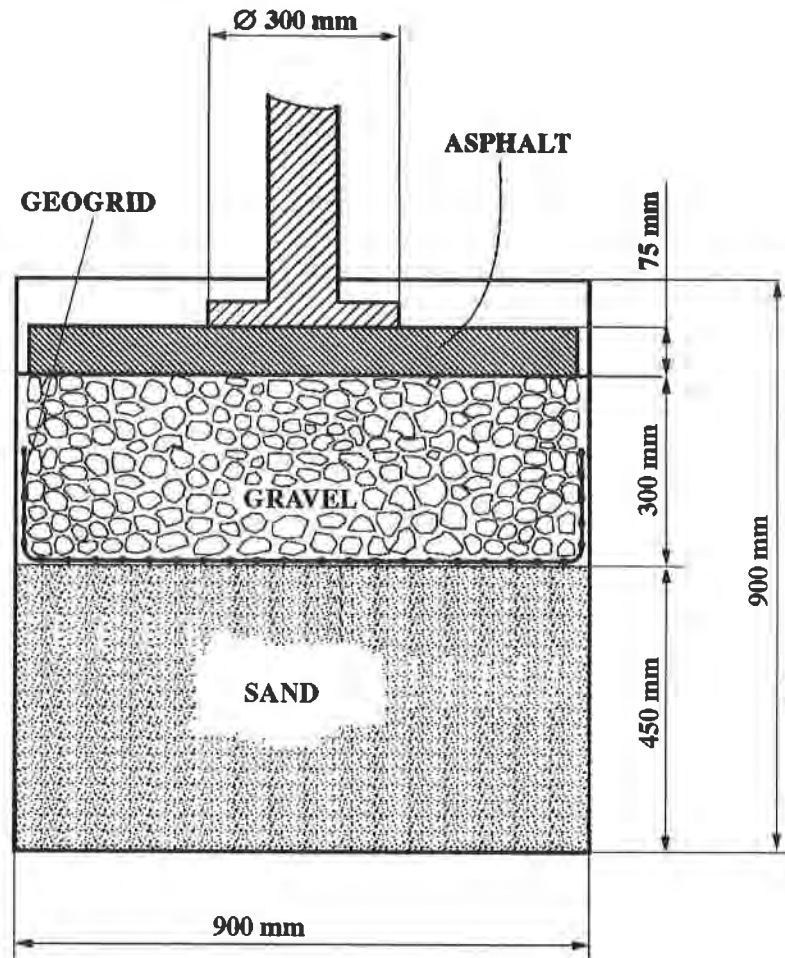
Figure 1. Pavement testing set-up

The thickness of the asphalt layers has been kept constant and equal to 75 mm. The asphalt specifications were in accordance to the Italian highway department requirements. Crushed limestone produced from oversize quarried aggregate was selected as the base course material. This material is typically used for paved roads. The maximum particle size of the aggregate was 30 mm. The gravel aggregate was placed in 300 mm thickness and compacted to achieve a density of about 17.50 kN/m^3. The soft and compressible subgrade was simulated by means of about 450 mm of loose uniform sand having a uniformity coefficient U»2, dry density γ=19.00 kN/m^3 and an optimum moisture content w = 15%. This sand is called Ticino siliceous sand since it is dredged from the Ticino river. A constant moisture content of 10% for the sand was selected. Several subgrade shear strengths with CBR value ranging from 1% up to 18% (ASTM D1883) have been used in the tests by changing sand density. The gradation curve for asphalt, crushed stone, and the subgrade sand are shown in Figure 2 as per ASTM D136.
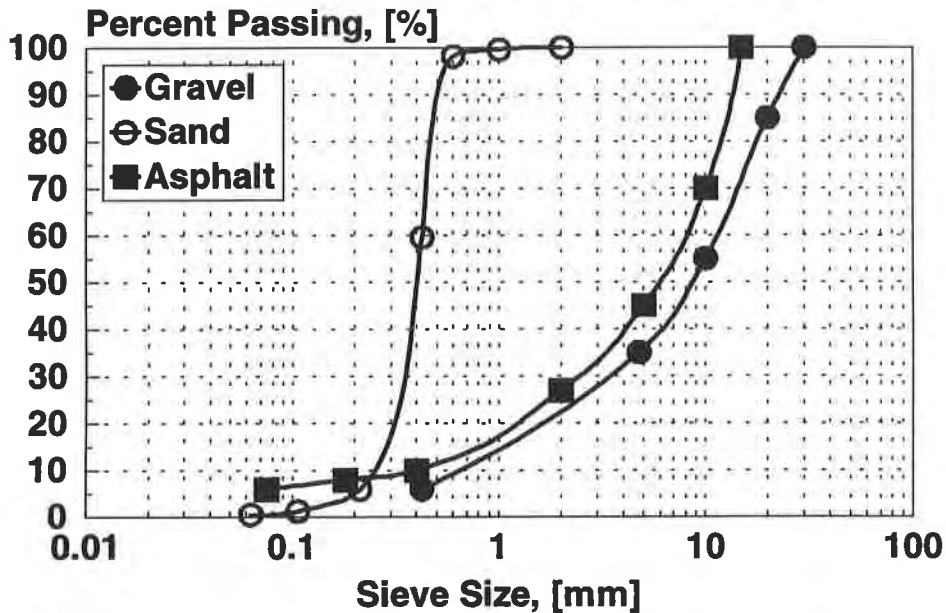
Figure 2. Gradation curves for crushed limestone, sand and asphalt.

A multilayer biaxially oriented polypropylene geogrid, Tenax MS220, manufactured by continuous extrusion and orientation processing is used as reinforcement in the tests. Its main properties are listed in Table 1.

Table 1. Properties of the multilayer geogrid used in the tests

		Machine Direction	Cross Machine Direction
Unit weight	g/m2	220	
Aperture size	mm	21	25
Peak tensile strength	kN/m	13.5	20.5
Tensile modulus @2% strain	kN/m	205	300
Yield point strain	%	12	11
Junction strength	kN/m	12.2	18.5

TEST RESULTS AND ANALYSIS

Figure 3 shows the comparisons of vertical settlement between reinforced and unreinforced sections. Ruts geometry for reinforced and unreinforced sections have been analyzed to determine differences in depth and shape of the deformed sections.
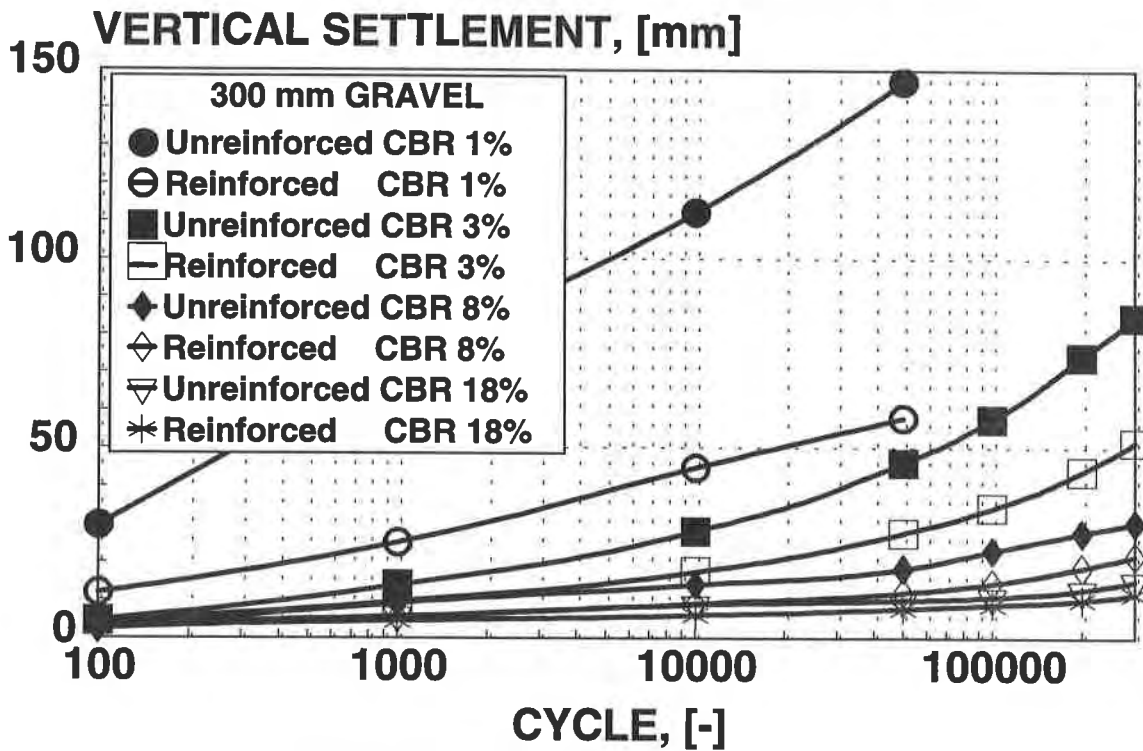
Figure 3. Comparisons between unreinforced and reinforced sections.

Typical permanent rut geometry for CBR =1% and 18% are presented in Figure 4. As it can be noticed by analysing Figure 4, the deformation curves are very sharp in proximity of the loading plate area. In fact, the failure type for all the performed tests has been a puncture failure by shearing the asphalt layer not sufficiently supported by the layer underneath. This type of failure is essentially due to the type of subgrade used during the tests. In fact the soft sand has a very high compressive behaviour and largely reduces its volume when compressed. Moreover the rigid loading plate generated high shear stresses on the asphalt at its edges.

The influence of different aggregate base thickness on the pavement performance is presented in Figure 5. Reinforced section with one layer of geogrid reinforcement performed significantly better than unreinforced sections with thicker base course. Due to the limitation in the depth of the testing box, the unreinforced section with base thickness of 500 mm has only 300 mm thick sand subgrade, which contributed to smaller settlement as shown in the figure.
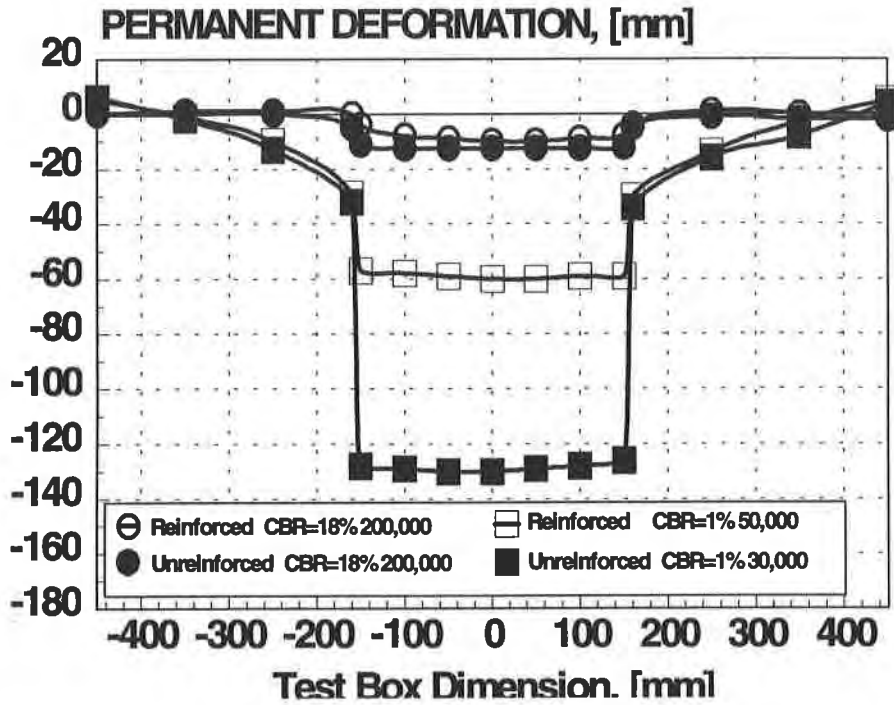
Figure 4. Typical ruts geometry for unreinforced and reinforced sections with different CBR values.
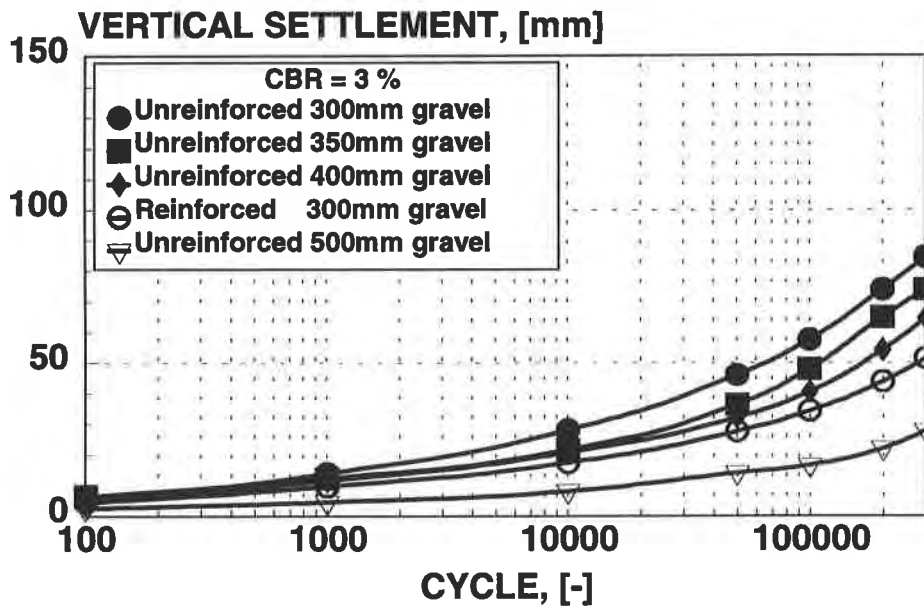
Figure 5. Comparisons between unreinforced and reinforced sections for several base thickness.

The deformed shape of the asphalt - aggregate and aggregate-subgrade interfaces, at the end of a test, are shown in Figure 6 and Figure 7. It is interesting to note that the maximum settlement, both at the asphalt-aggregate and at the aggregate - subgrade interfaces, is much lower for the geogrid reinforced sections than for the unreinforced ones. Figures 6 and 7 also show that 2 layers of geogrids, one at the base and one at the mid thickness of the aggregate layer, are able to provide more stiffening to the base layer than 1 geogrid only: in fact with 2 geogrids, the deformation is much more uniform and the maximum settlement is lower.

PERMANENT DEFORMATION, [mm]
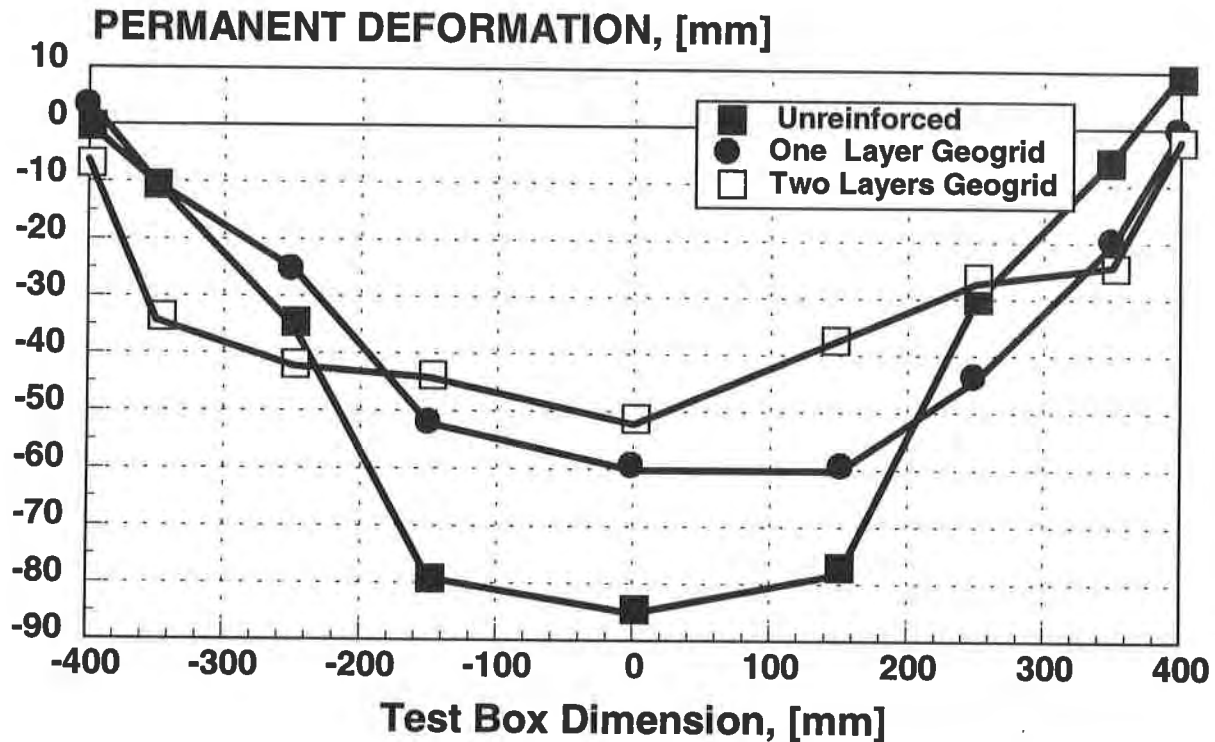
Figure 6. Typical deformed shape of the asphalt-aggregate interface
at the end of a test.

Function of the subgrade CBR versus number of cycles is presented in Figure 8 based upon data presented in Figure 3. Figure 9 shows the traffic improvement factor (the ratio of the number of load cycles for the reinforced section to that of unreinforced section at a given rut depth). Figure 9 is simply obtained from the ratios of the related points in Figure 8. The chart in Figure 8 allows to evaluate the increase of design life (in terms of increased number of vehicles passing) which can be achieved by placing a geogrid in a given road section. As indicated in Figure 8, the structural contribution of a geogrid reinforcement is nearly constant when the subgrade CBR value larger than 3% for both 12.5 mm and 25 mm rut depth; while for relatively

weak subgrade with CBR value equal to 1%, the structural contribution of a geogrid under 25 mm rut depth is significantly larger than rut depth of 12.5 mm.
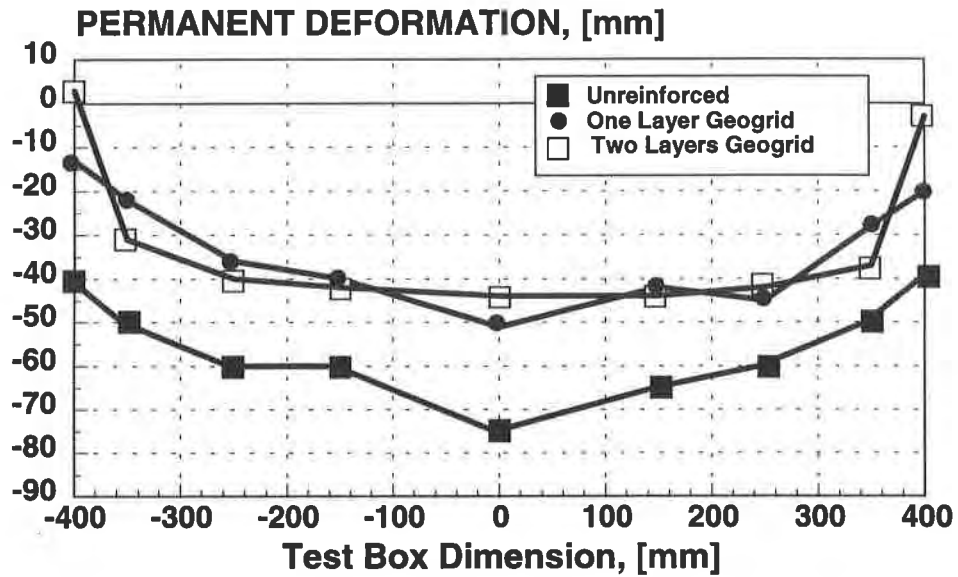
Figure 7. Typical deformed shape of the aggregate-subgrade interface at the end of a test.
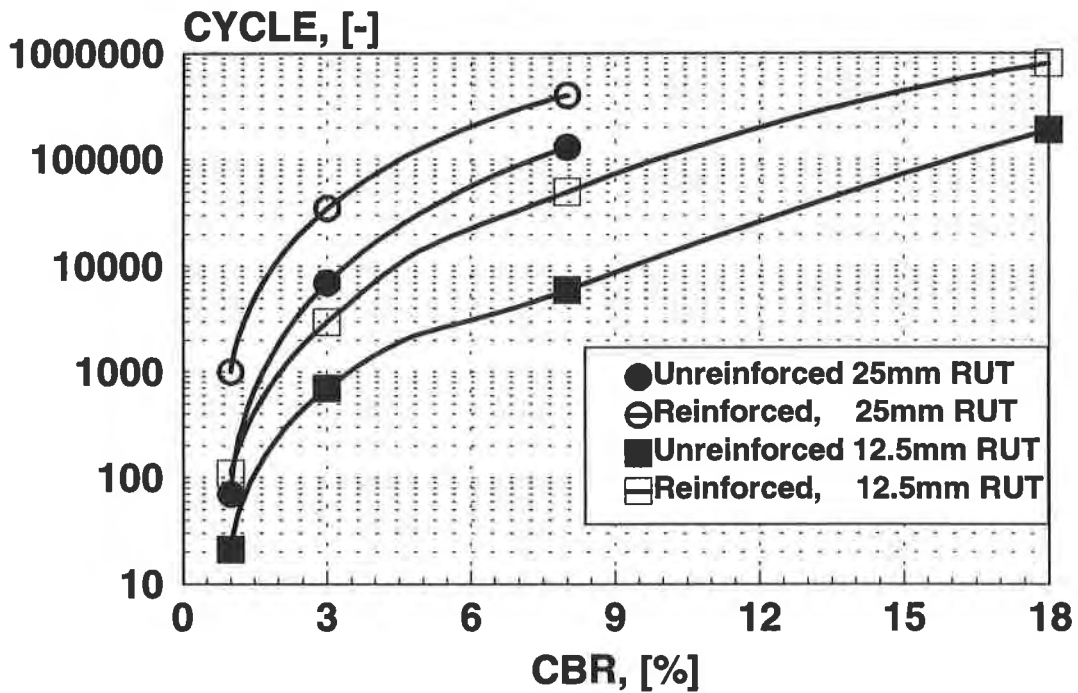
Figure 8. CBR vs. cycle number for reinforced and unreinforced sections at given rut depth.

Traffic Improvment Factor, [-]
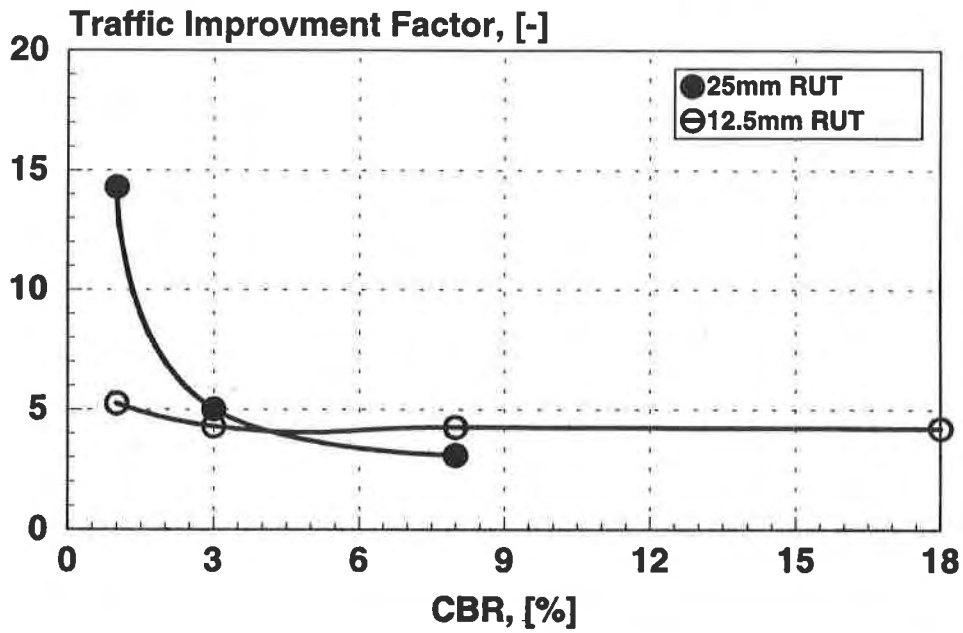
Figure 9. Traffic improvement factor vs. CBR for two rut depth.

AASHTO DESIGN METHOD FOR FLEXIBLE PAVEMENTS

The AASHTO method utilizes an index named "structural number" (SN) to indicate the necessary combined structural capacity of all pavement layers overlying the subgrade. SN is a function of subgrade strength, expected traffic intensities, pavement life, and climatic conditions.

For unreinforced pavement sections, a simple design equation is used in AASHTO method (based on AASHTO interim guide, 1981).

$$SN = a_1 \cdot d_1 + a_2 \cdot d_2 + a_3 \cdot d_3 \tag{1}$$

where the subscripts 1, 2 and 3 refer to the asphalt wearing course, aggregate base course and subbase course (if applicable), and a_1 a_2 a_3 are the layer coefficient used to characterise the structural capacity of different layers in the pavement system, d_1, d_2 and d_3 are their thickness. The better the course material, the higher the layer coefficient. The structural number is directly proportional to the layer coefficients and their thickness.

Design details based on design charts are straight forward and outlined in the AASHTO interim guide. The input design parameters are the average subgrade CBR value, design terminal serviceability index P_t the regional factor R, and the total equivalent 80 kN (18-kip) single axle loads (EAL) throughout the design life. Based on these design values, the required structural number can then be calculated. After the layer coefficients of asphalt wearing course, base course

and subbase course are determined, the required thickness of the base course (or asphalt layer) can be calculated.

MODIFIED AASHTO METHOD WITH GEOGRID REINFORCEMENT

In the modified AASHTO method the structural contribution of geosynthetics on flexible pavements is quantified by the increase in the structural layer coefficient of the aggregate base course. Equation (1) now becomes

$$SN = a_1 * d_1 + a_2 * (\alpha_r / \alpha_u) * d_2 \qquad (2)$$

where a_r/a_u is the layer coefficient ratio (greater than 1). a_r/a_u can be determined by results obtained from empirical tests on flexible pavement system with and without a geogrid reinforcement.

$$\alpha_r / \alpha_u = \frac{(SN_r - a_1 * d_1)d_u}{(SN_u - a_1 * d_1)d_r} \qquad (3)$$

where SN_r and SN_u are the structural numbers for reinforced and unreinforced pavement systems respectively, d_r and d_u are the thickness of the aggregate base course. The asphalt thickness was kept constant for all reinforced and unreinforced sections. The influence of the asphalt layer to the layer coefficient ratio is neglected in the calculations. This assumption eliminates the need to assume a layer coefficient for the asphalt for the calculation of the layer coefficient ratio. Then equation (3) becomes

$$\alpha_r / \alpha_u = \frac{SN_r * d_u}{SN_u * d_r} \qquad (4)$$

Figure 10 presents the layer coefficient ratio based on empirical pavement testing with and without a geogrid reinforcement (serviceability index $P_t = 2$, regional factor $R = 1$).
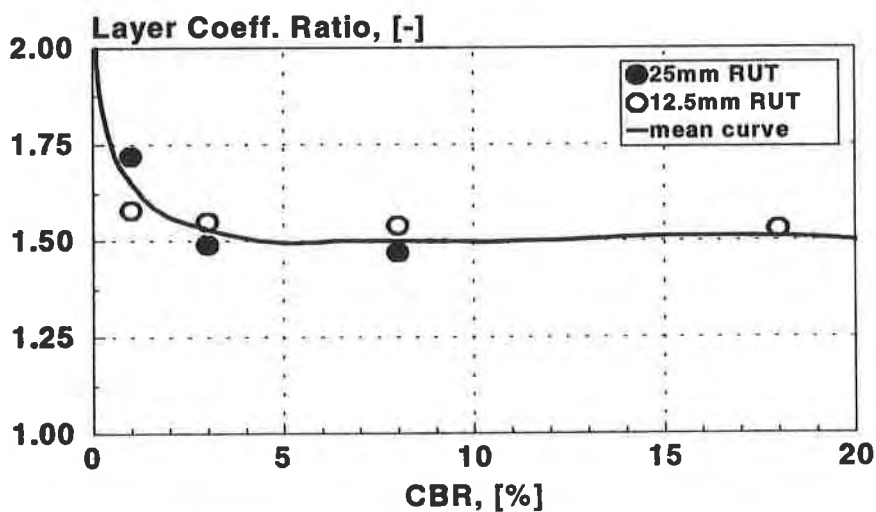
Figure 10. Layer coefficient ratio vs subgrade CBR

As a result, a reduction in aggregate thickness can be achieved by equation (2)

$$d_2 = \frac{SN - a_1 * d_1}{(\alpha_r / \alpha_u) * a_2}$$ (5)

or instead, the asphalt thickness can be reduced

$$d_1 = \frac{SN - (\alpha_r / \alpha_u) * a_2 * d_2}{a_1}$$ (6)

DESIGN EXAMPLE AND DESIGN CHARTS

Design Parameters:
Average subgrade CBR = 5%
total 80 kN (18 kip) equivalent single axle load application: 1,500,000
design terminal serviceability index $P_t = 2$
regional factor R = 1.5
layer coefficient for asphalt surface = 0.44
layer coefficient for the aggregate base course = 0.15
maximum permissible rut depth =12.5 mm

The layer coefficient ratio is taken 1.5 (based on Figure 10)
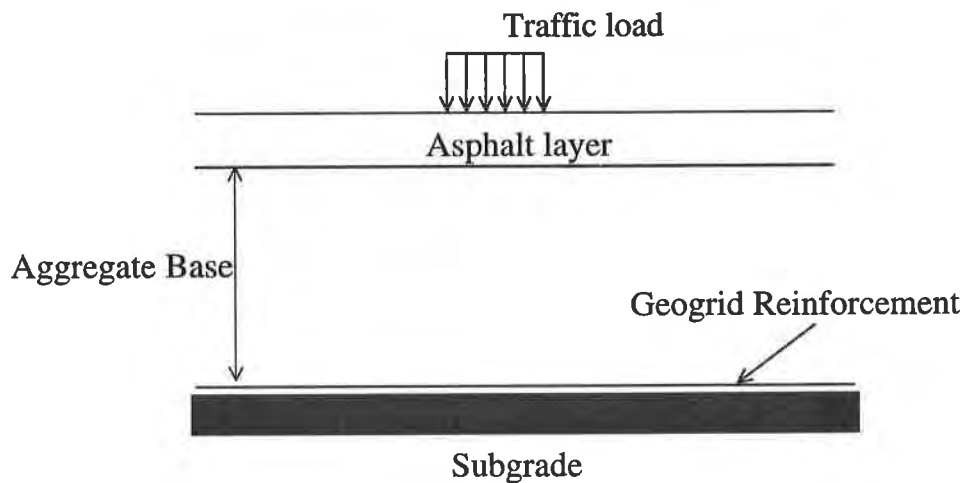
Figure 11. Geosynthetic reinforcement in base reinforcement application.

Calculation Results:

The aggregate thickness without geogrid is equal to 42.52 cm (16.74 in); the aggregate thickness with the geogrid = 28.35 cm (11.16 in). A saving of 14.17 cm (5.58 inches) of aggregate is achieved when using a geogrid reinforcement in this example.

Figure 12 is a design chart demonstrating the required fill thickness in pavement system with and without a geogrid reinforcement. The data used in this chart: asphalt thickness is 6.35 cm (2.5"), the regional factor is 1.5, the service index is 2.5, and three total equivalent standard axle loads. Figure 13 is the design chart for pavements with serviceability index equal to 2.
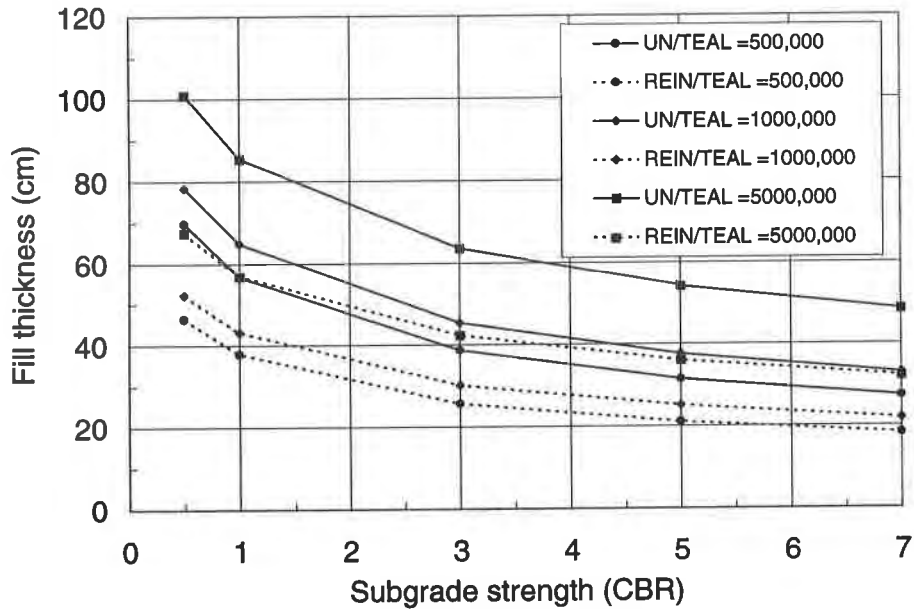
Figure 12. Aggregate fill thickness vs. subgrade strength ($P_t = 2.5$)
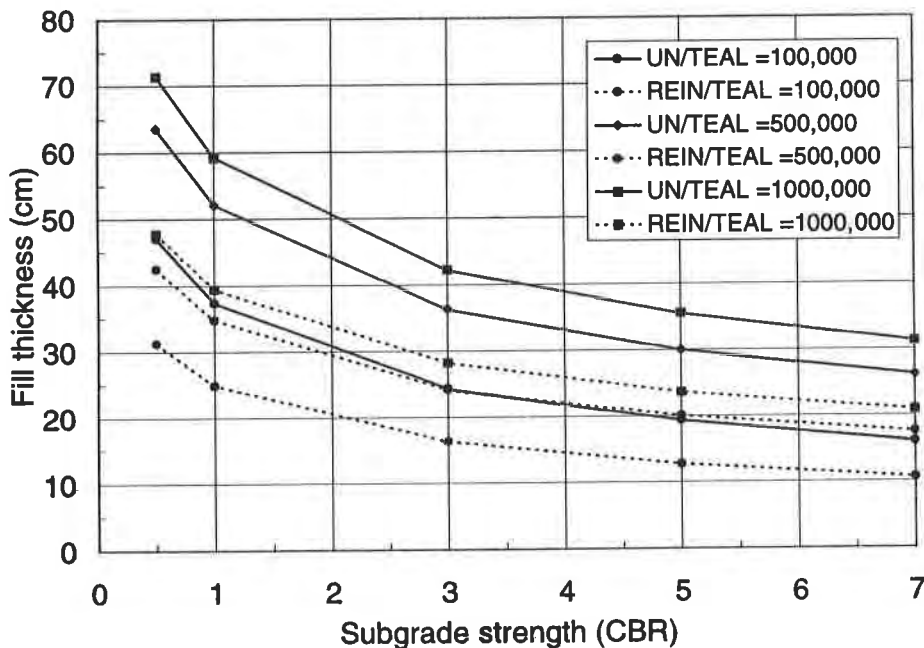
Figure 13. Aggregate fill thickness vs. subgrade strength ($P_t = 2.0$)

COST SAVING ANALYSIS

Cost savings when using a geogrid reinforcement in a pavement system will vary by project. Using the design calculation from the above example, it can be demonstrated as follows: Using an average cost of $32.7/m^3 ($25/yd^3) for graded aggregate base (GAB) in place, and a cost of $1.7/m^2 ($1.4/yd^2) for geogrid in place, the net savings for utilizing a geogrid reinforcement in this example is $2.93 /m^2. The cost saving per square meter for various traffic, subgrade strength, and serviceability index is presented in Figure 14, and 15.
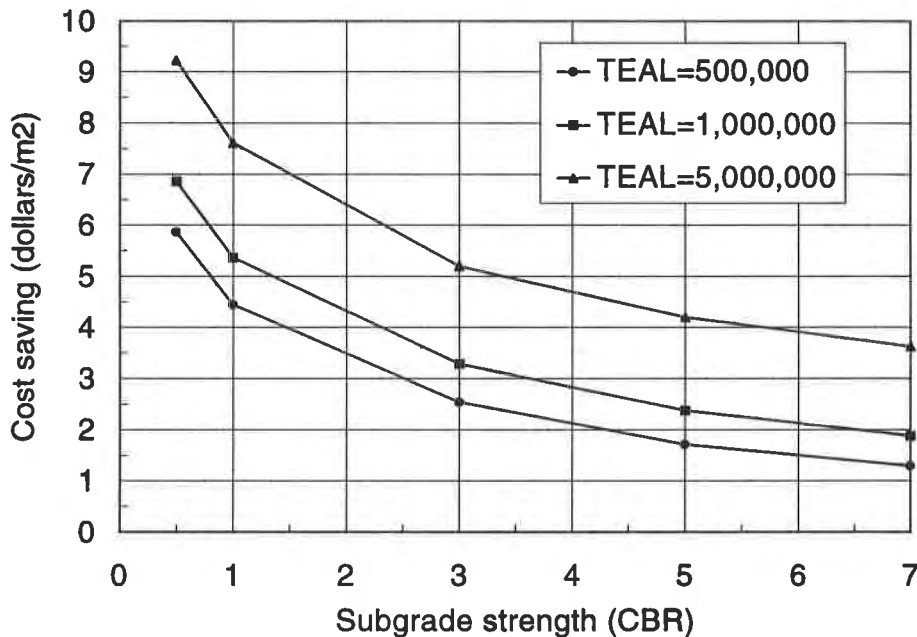
Figure 14. Cost savings in pavement with a geogrid reinforcement $(P_t = 2.5)$

CONCLUSIONS

The testing results obtained from this experimental research program demonstrated that a geogrid reinforcement placed at the subbase/aggregate interface effectively increases the service life of a paved road. Geogrid reinforcement provides a more uniform load distribution and a deduction in the maximum settlement both at the asphalt-aggregate and aggregate-subgrade interfaces.

A modified AASHTO design method capable of incorporating the effect of geogrid reinforcement is developed. The contribution of geogrid reinforcement to pavement system is quantified by the increase in the structural layer coefficient of the aggregate. The layer coefficient ratio was found to be between 2 to 1.5, depending mainly on the subgrade CBR. Design example is provided. Design charts are developed to facilitate preliminary design. Cost

analysis is conducted comparing geogrid reinforced pavement to conventional unreinforced pavement. Figures 14 and 15 demonstrate that geogrid reinforcement is a cost effective solution to flexible pavement system.
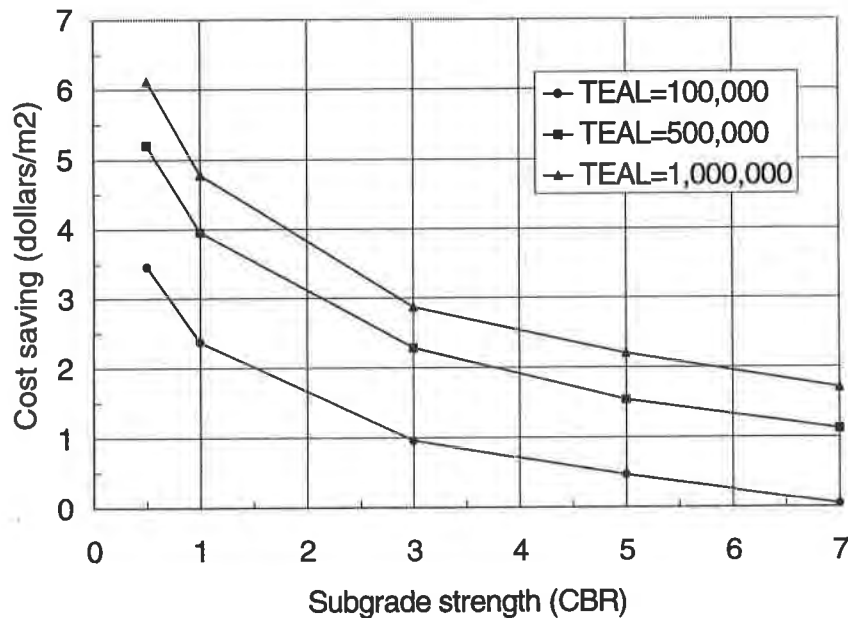
Figure 15. Cost savings in pavement with geogrid reinforcement (P_t= 2.0)

REFERENCES

American Association of State Highway and Transportation Officials, (1981), "AASHTO interim guide for design of pavement structures".

ASTM D-136 - 94, (1994), "Standard test method for sieve analysis of fine and coarse aggregates", *ASTM Volume 04.02*, Philadelphia.

ASTM D-1883 - 94, (1994), "Standard test method for the CBR (California Bearing Ratio) of laboratory-compacted soil", *ASTM Volume 04.08*, Philadelphia.

Barksdale, R.D., Brown, S.F. and Chan, F., (1989)."Potential benefits of geosynthetics in flexible pavement systems", *National Cooperative Highway Research Program Report*.

Cancelli A., Montanelli, F. and Rimoldi, P., Zhao, A. (1996), "Full scale laboratory testing on geosynthetics reinforced paved roads", *Proc. Int. Sym. on Earth Reinforcement, 573-578*.

Gregory G.H. and Bang S., (1994), "Design of flexible pavement subgrades with geosynthetics", *Proc. of 30th Sym. Eng. Geology and Geotechnical Eng., 569-582*.

LABORATORY MODEL TESTS TO EVALUATE GEOTEXTILE SEPARATORS IN-SERVICE

WEN-SEN TSAI
MOH AND ASSOCIATES, INC., TAIWAN ROC
ROBERT D. HOLTZ
UNIVERSITY OF WASHINGTON, USA

ABSTRACT

The paper summarizes the results of cyclic plate load tests on three different thicknesses of base aggregate, various types and weights of separator geotextiles, and two soft subgrade soils (CBR ranging from 0.5 to 7). Separators investigated included heatbonded nonwovens (140 and 200 g/m^2), needlepunched nonwovens (140 and 280 g/m^2), and a woven slit-film (140 g/m^2), a "perfect" (graded granular) filter, and a "perfect" (geomembrane) separator. Geotextile survivability, rut depths, pore water pressures developed in the subgrade during cyclic loading, and potential fines migration through the geotextile and into the base course were all carefully monitored.

It was found that if they survived installation and dynamic stresses, the geotextiles performed their intended separation function quite well. Pore water pressures in the subgrade increased initially and then decreased as the number of loading cycles increased. Peak pore pressures depended on aggregate thickness, subgrade soil type, and CBR, but appeared to be independent of geotextile type and weight. Some geotextile clogging was observed, but it did not cause any signifcant increase in generated subgrade pore pressures; fines migration was insignificant.

INTRODUCTION

Although the primary function of a geotextile in roadway applications is separation, the system may also be influenced by secondary functions such as filtration, drainage, and reinforcement. Additional issues associated with geotextiles are survivability, soil contamination, clogging, blinding and degradation.

In order to improve our understanding of the behavior of geotextile separators, an experimental study was conducted to investigate their performance under various loading conditions. Laboratory model tests were conducted to simulate repeated vehicle loading on different subgrade soil-geotextile-aggregate systems, and geotextile and subgrade performance was monitored after various numbers of cyclic load applications.

Preliminary results of this study were presented by Tsai and Holtz (1994) at the Singapore Conference. The objective was to experimentally assess separation geotextiles for their (1) in-service survivability, (2) ability to retard fines migration, and (3) influence on subgrade pore pressure dissipation. The study is now complete and this paper summarizes the remainder of the experimental results.

EXPERIMENTAL SETUP, SOILS, AND TEST PROCEDURES

Experimental Setup and Loading Conditions. A 0.416 m³ (110 gal) steel drum, shown in Figure 1, was used to contain the layers of aggregate and soft soil used to simulate a common roadway section. The separator was installed between the aggregate base and subgrade. Miniature pressure transducers were buried within the subgrade to monitor changes in pore pressures during loading, and a procedure was developed to observe potential fines migration through the separator from the subgrade during cyclic loading. Details of the instrumentation and monitoring systems are given in Tsai (1995).

In order for the laboratory model tests to represent in-service field loading conditions, the test apparatus had to satisfy two requirements: 1. The stress levels applied to the geotextile due to the dynamic load at the aggregate surface in the test should be the same as in the field. 2. The boundary of the test apparatus should not interfere with the failure zone in the subgrade, if the subgrade fails in shear under dynamic loading.

For the stress level experienced by the geotextile in the test to be the same as in the field, the ratio of the thickness of the base course and the diameter of the loaded area in the model tests was the same as it would be in the field under "standard" loading conditions. An 80 kN (18 kip) single axle load, called the equivalent single axle load (ESAL), is the standard in the common AASHTO pavement design procedure, and a tire pressure of 620 kPa (90 psi) is common for loaded dump trucks. Thus the contact area between the tire and pavement for this loading, expressed as a ratio of wheel load to tire pressure, was 0.0645 m² (100 in²) on dual tires The equivalent diameter of the tire print in the field was 280mm.
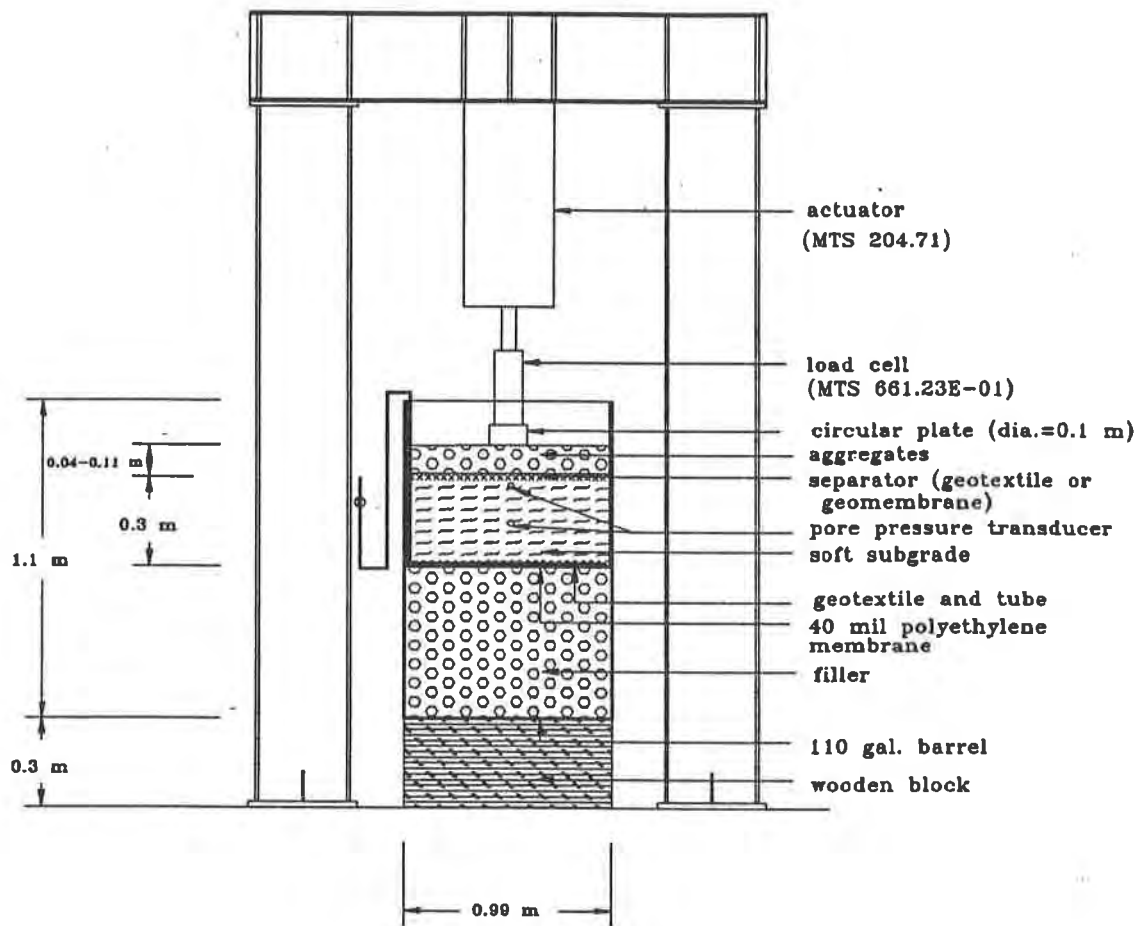
Figure 1 Schematic diagram of experimental set-up.

In order to ensure that the test container boundary did not interfere with the potential failure zone in the subgrade, the maximum diameter of the loaded area in the model was limited to 100 mm. Since the tire print was scaled to 100 mm from 280 mm, the applied force was also scaled to 4.9 kN from 80 kN to obtain the same vertical stress (620 kPa) on the aggregate surface. A simple calculation using a linear elastic computer program ELSYM5 was done to verify that the vertical stresses at the top of the subgrade in the laboratory tests were within 87% of the stresses in the field with the three different aggregate thicknesses utilized. Thus, it was felt that the two conditions given above were satisfied in the model tests. See Tsai (1995) for additional details of these calculations.

Loading frequency used in this study was one Hz.

Soils. Two different soils, a silty (ML) soil and a clayey (CL) soil, were used to model the subgrades in the study. The silty soil was a tailing material obtained from a quarry crusher washing operations. The clayey soil was obtained by mixing 5% bentonite by weight into the silty soil. Table 1 shows the basic classification properties of these two materials.

Table 1. Basic properties of the subgrade soils and base course aggregate.

Property	Silty Soil	Clayey Soil	Crushed Stone
% passing US No. 200 sieve	81	82	0
Coefficient of Uniformity	25	NA	3.6
Coefficient of Curvature	1	NA	1.3
Plastic Limit, %	27	24	NA
Liquid Limit, %	38	46	NA
Unified Soil Classification System	ML	CL	GP
Permeability, cm/sec	1.2×10^{-7}	2.9×10^{-8}	NA
Maximum Dry Density, kg/m^3	1580	1622	1922
Optimum Moisture Content, %	20.5	20.3	NA[a]

a. The proctor compaction curve was flat and did not show a peak.

The crushed stone aggregate was similar to the base material used by WSDOT for pavements. Its basic properties are shown in Table 1. The aggregate was classified as GP.

Testing Procedure. The testing procedure reported by Tsai and Holtz(1994) and Tsai (1995) was followed in all tests reported in this paper.

TEST PARAMETERS AND GEOTEXTILE PROPERTIES

Table 2 shows the parameters of the 19 tests reported in this paper. Three different aggregate base thicknesses, six separators, two different subgrade soils and four subgrade strengths were used. The granular filter separator (GF) was designed based on the U.S.B.R. (1974) criteria. The impervious (MEM) separator consisted of one piece of 0.36 mm (14 mil) polyethylene sheet protected by a 530 g/m^2 needlepunched nonwoven geotextile. The granular filter and the impervious separators were considered to be the two extreme conditions for separators. The granular filter separator was a perfect separator in terms of filtration, but had no tensile strength. On the other hand, the geomembrane simulated a perfect separator or a completely clogged geotextile.

Table 2. Test parameters.

Test No.	Thickness of Aggregate Course (mm)	Separator	Subgrade Soil Type	Subgrade Strength (CBR)
110-HB4-Silt-2	110	HB4	Silt	2
110-NP4-Silt-2	110	NP4	Silt	2
110-SF4-Silt-2	110	SF4	Silt	2
110-Null-Silt-7	110	Null	Silt	7
110-Null-Silt-2	110	Null	Silt	2
110-Null-Silt-1	110	Null	Silt	1
55-HB4-Silt-2	55	HB4	Silt	2
40-GF-Silt-2	40	GF	Silt	2
40-MEM-Silt-2	40	MEM	Silt	2
40-HB4-Silt-2	40	HB4	Silt	2
40-HB4-Clay-2	40	HB4	Clay	2
40-HB6-Silt-2	40	HB6	Silt	2
40-NP4-Silt-2-a	40	NP4	Silt	2
40-NP4-Silt-2-b	40	NP4	Silt	2
40-NP4-Clay-2	40	NP4	Clay	2
40-NP4-Silt-1	40	NP4	Silt	1
40-NP4-Silt-0.5	40	NP4	Silt	0.5
40-NP8-Silt-2	40	NP8	Silt	2
40-SF4-Silt-2	40	SF4	Silt	2

Most of the tests were conducted on a silty subgrade. The tests with clayey subgrade needed about one month for complete consolidation due to the low permeability of the clayey soil. Since this was very time-consuming and because the results of the tests with the clayey soil were similar to those with the silty soil, only two tests with a clayey subgrade were conducted.

In Table 2, a symbol of form A-B-C-D-E identifies each test conducted:

A is the thickness of the base course in mm, and B represents the type of separator used in the test. If it was a geotextile, then its mass per unit area in oz/yd^2 is also given. NP represents a needlepunched nonwoven geotextile, HB is a heatbonded nonwoven, and SF represents a slit-film woven geotextile. GF represents a granular filter separator. MEM represents an impervious

plastic membrane. Null means that no geotextile used. The properties of the geotextiles can be found in Table 3.

Subgrade soil type is indicated by C, while D is the subgrade strength in CBR; E represents the sequence of a test, if the test is repeated.

Table 3. Nominal physical and mechanical properties of geotextiles used in the study. Data is based n 1992 Specifier's Guide and telephone conversations with the manufacturers.

Geotextiles	Structure	Polymer Type	Thickness ASTM D 1777 mm (mil)	Mass per Unit Area ASTM D 3776 g/m² (oz/yd²)	Grab Strength ASTM D 4632 kN (lb)%	Puncture Resistance ASTM D 4833 kN (lb)	Tear Strength ASTM D 4533 kN (lb)	Apparent Opening Size ASTM D 4751 mm (US Standard Sieve Size)	Permittivity ASTM D 4491 sec⁻¹
NP4	Nonwoven	PP	1.3 (50)	142(4.2)	0.511(115)50	0.267(60)	0.222(50)	0.30(50)	2.3
NP6	Nonwoven	PP	1.8(70)	204(6.0)	0.711(160)50	0.355(75)	0.311(70)	0.25(60)	1.8
NP8	Nonwoven	PP	2.3(90)	268(7.9)	0.933(210) 50	0.445(100)	0.380(85)	0.21(70)	1.3
HB4	Nonwoven	PP	0.4(17)	132(3.9)	0.578(130)100	0.178(40)	0.267(60)	0.212(70)	0.7
HB6	Nonwoven	PP	0.5(19)	197(5.8)	1.000(225)90	0.289(65)	0.400(90)	0.106(140)	0.1
SF4	Woven	PP	NA	136(4.0)	0.801(180)15	0.334(75)	0.311(70)	0.595(30)	0.03

RESULTS AND DISCUSSION

Rut Depth. Ruts are one of the most important indicators of roadway performance. Hence, the influence of geotextiles on ruts can be used to evaluate the behavior of geotextile separators. In the model tests, the rut depths were determined based on the readings of a built-in LVDT in the MTS actuator.

Figure 2 shows a typical development of rut depth on the aggregate surface in a test where the geotextile was found to have survived. From this figure, we can see that the rate of rut depth development was high initially, and then decreased with the number of cycles.
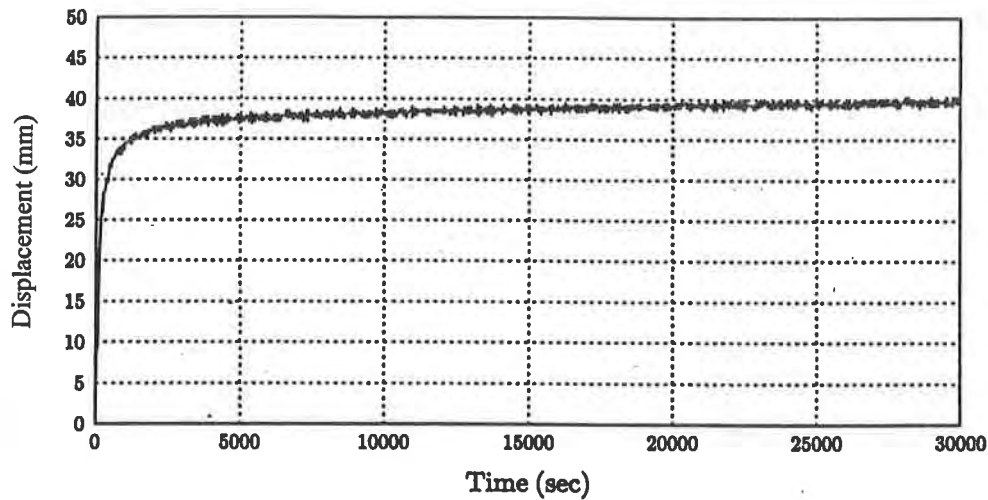
Figure 2 Typical development of rut depth on aggregate surface

A summary of the measured ruts obtained in the tests are shown in Table 4. Among the tests, some subgrades experienced local shear failure, especially the softer ones (40-NP4-Silt-0.5, 40-NP4-Silt-1, etc.). These tests generally had large ruts, some as deep as 147 mm. It was also found that the presence of geotextiles increased the bearing capacity of subgrades if the geotextiles survived construction and repeated loading. For instance, 40-GF-Silt-2 had a local subgrade shear failure, while 40-NP4-Silt-2a had satisfactory performance, even though both had the same aggregate thickness and subgrade strength. The tests in which geotextiles were found to have failed also showed deeper ruts (e.g. 40-HB4-Silt-2 and 55-HB4-Silt-2) compared with the tests where geotextiles were found to have survived (e.g. 40-NP4-Silt-2 and 40-HB6-Silt-2).

As expected, the tests with 110 mm thick aggregate bases had much smaller ruts than the tests with thinner bases (40 mm) at the same subgrade strength. The rut depth in the control test (110-Null-Silt-2) was large--49 mm--which is greater than twice the rut depths from all the tests with geotextiles (Figure 3). It is also interesting to find that tests with geotextiles over soft subgrades (e.g. 110-HB4-Silt-2, etc.) resulted in similar or smaller ruts than the test on a much stronger subgrade (110-Null-Silt-7). Hence, even nonwoven geotextiles appeared to provide some reinforcing effect. However, the results show no significant difference in ruts among the tests with different geotextiles. Therefore, the influence of the modulus of the geotextile on rutting is apparently not significant, at least for these tests.

Table 4. Summary of Test Results.

Test	Rut Depth (mm)	Peak Pore Pressure at top (kPa)	Peak Pore Pressure at middle (kPa)
110-HB4-Silt-2	18	31	14
110-NP4-Silt-2	20	34	10
110-SF4-Silt-2	18	30	5
110-Null-Silt-7	20	30	41
110-Null-Silt-2	49	25	12
110-Null-Silt-1[a]	154	39	62
55-HB4-Silt-2	130	60	80
40-GF-Silt-2	118	64	103
40-MEM- Silt-2	50	89	20
40-HB4-Silt-2	94	48	29
40-HB4-Clay-2	70	58	35
40-HB6-Silt-2	42	41	29
40-NP4-Silt-2a	45	50	21
40-NP4-Silt-2b	46	50	21
40-NP4-Clay-2	63	62	32
40-NP4-Silt-1	97	54	37
40-NP4-Silt-0.5	147	12	39
40-NP8-Silt-2	41	36	15
40-SF4-Silt-2	46	44	

a. The shaded rows indicate the tests where either the subgrades or the geotextiles were found to have failed

Figure 4 shows the ruts obtained from the tests with 40 mm thick aggregate bases. The ruts ranged from 41 mm to 63 mm except the test with a subgrade of CBR = 1, which had ruts of 97 mm. The ruts from the 40 mm thick aggregate tests were about 20 to 40 mm greater than the tests with a 110 mm thick aggregate base. Similar to the results from the tests with 110 mm thick aggregate base (Figure 3), the influence of moduli of geotextiles on ruts is not significant (Figure 4).
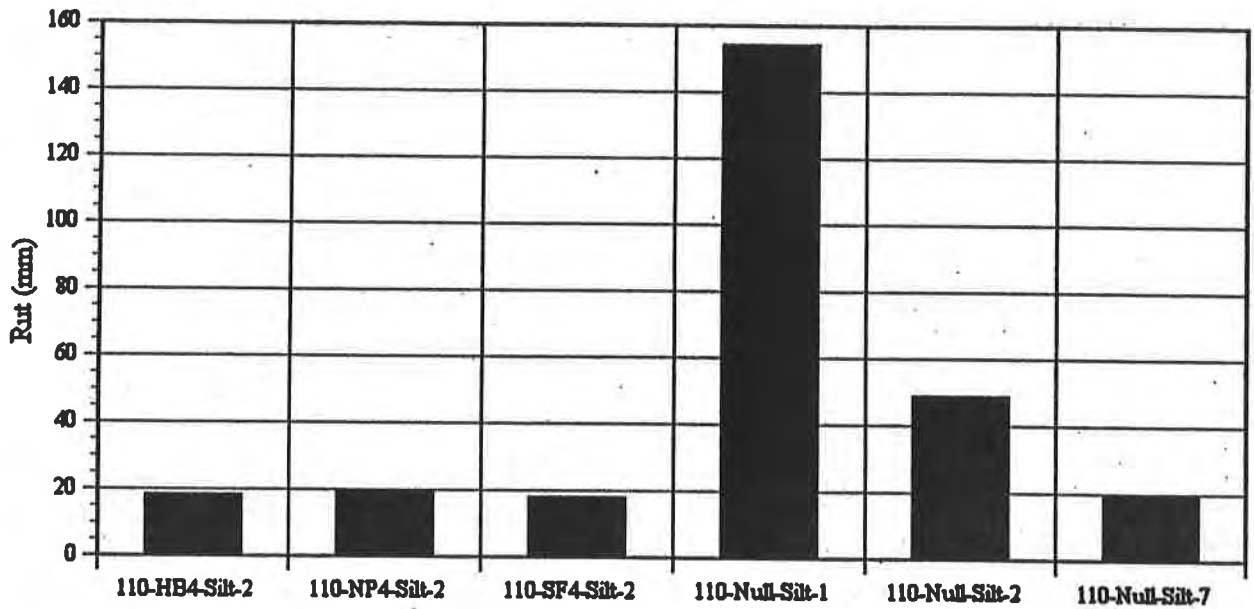
Figure 3 Final ruts from the tests with 110 mm thick base course.
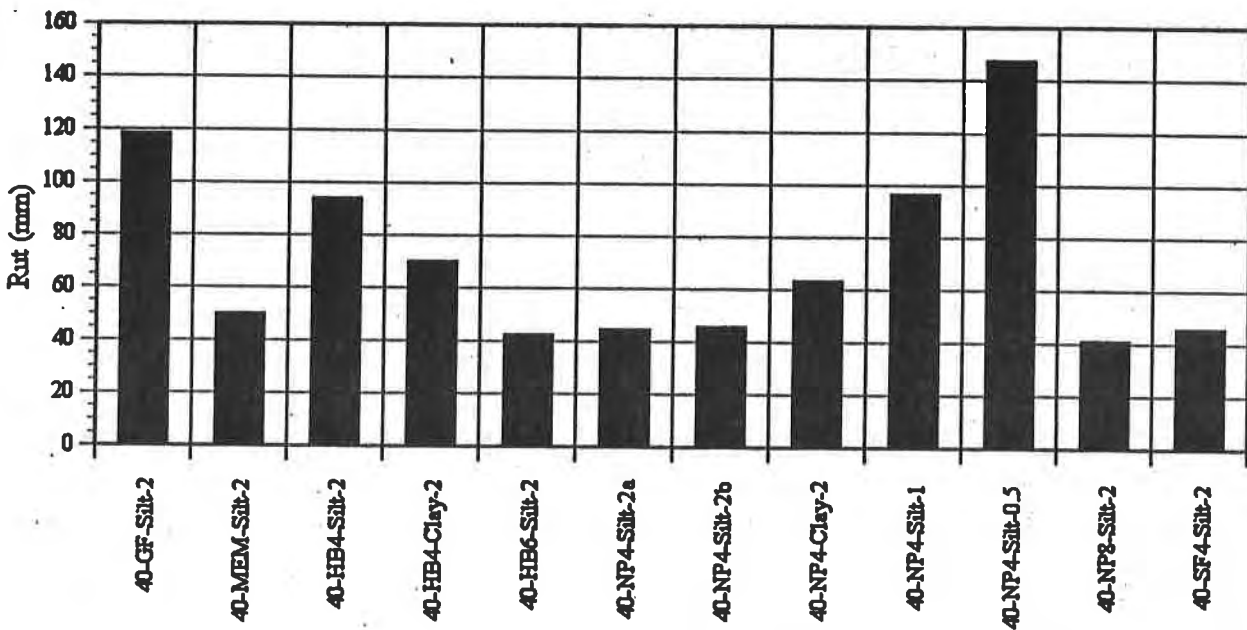
Figure 4 Final ruts from the tests with 40mm thick base course

When the ruts measured in Test 110-Null-Silt-2, which had thicker aggregate (110 mm) but no geotextile, are compared with those from the tests with thinner aggregate and geotextiles (e.g. Tests 40-NP4-Silt-2 and 40-SF4-Silt-2), the tests with thinner aggregate and with a geotextile other than HB4 had the same or smaller (Table 4). This implies that, if the geotextiles

survive placement and dynamic loading, geotextiles may replace up to a 70 mm aggregate layer at the laboratory model scale, which corresponds to 190 mm in full scale.

Note that the rut depth of Test 40-MEM-Silt-2 was greater than rut depths in tests with separators of lower moduli, e.g. 40-HB6-Silt-2, 40-NP4-Silt-2, 40-NP8-Silt-2. Similarly, the test with the clayey subgrade (Test 40-NP4-Clay-2) had a deeper rut (63 mm) than Test 40-NP4-Silt-2 (45 mm) which had the same experimental parameters except subgrade soil type. This can be explained by the long-persisting high pore pressures in the clay, as discussed in the following section. This pore pressure reduced the modulus of the subgrade, and thus higher plastic subgrade deformation occurred.

The ruts discussed in this section are not equivalent to the ruts that would occur in the field, since the results are determined from scale model tests. Since a fixed wheel path is simulated in these tests, the ruts obtained in laboratory tests are probably greater than in the field.

Pore Water Pressure. Dynamic loads from wheel loads could induce excess pore pressures within the subgrade, especially on soft subgrades, which could lead to a significant reduction in bearing capacity as well as subgrade modulus. The presence of a geotextile may provide drainage and promote dissipation of excess pore pressures, as long as the base layer is not contaminated with fines and its permeability is not too low to easily drain.

The changes in pore pressure induced within the subgrade in the laboratory model tests were monitored using two pore pressure transducers at the locations shown in Figure 1. Figure 5 shows a typical development of pore pressures within the subgrade at two different vertical locations (referred to as top, t, and middle, m). Figure 5 illustrates that the pore pressure at the top of the subgrade dissipates faster than at the middle. This seems reasonable, since the drainage path at the top is shorter than at the middle. Based on Boussinesq theory, we know that the subgrade at the top experiences higher stress than at the middle. Therefore, as shown in Table 4, the pore pressure at the top was greater than at the middle except for the tests which either had local shear failures in the subgrade or had no geotextile separators. Those tests which had local shear failures caused large depressions on the subgrade surface. The top pore pressure transducer in these subgrades could not accommodate such large depressions, and they were found to have been significantly displaced from their initial locations. Since some tests failed after only a few cycles and the initial locations of pore pressure transducers at the top of the subgrades could not be maintained (i.e. directly below the center of the loaded area), it is not rational to evaluate the effect of the separators on the pore pressure dissipation in these tests. In all tests, pore pressures increased initially and then decreased with time. Similar pore pressure development was also obtained from the partially drained dynamic triaxial tests conducted by Hyodo et al. (1992) and from the laboratory model tests conducted by Nishida and Nishigata (1994).
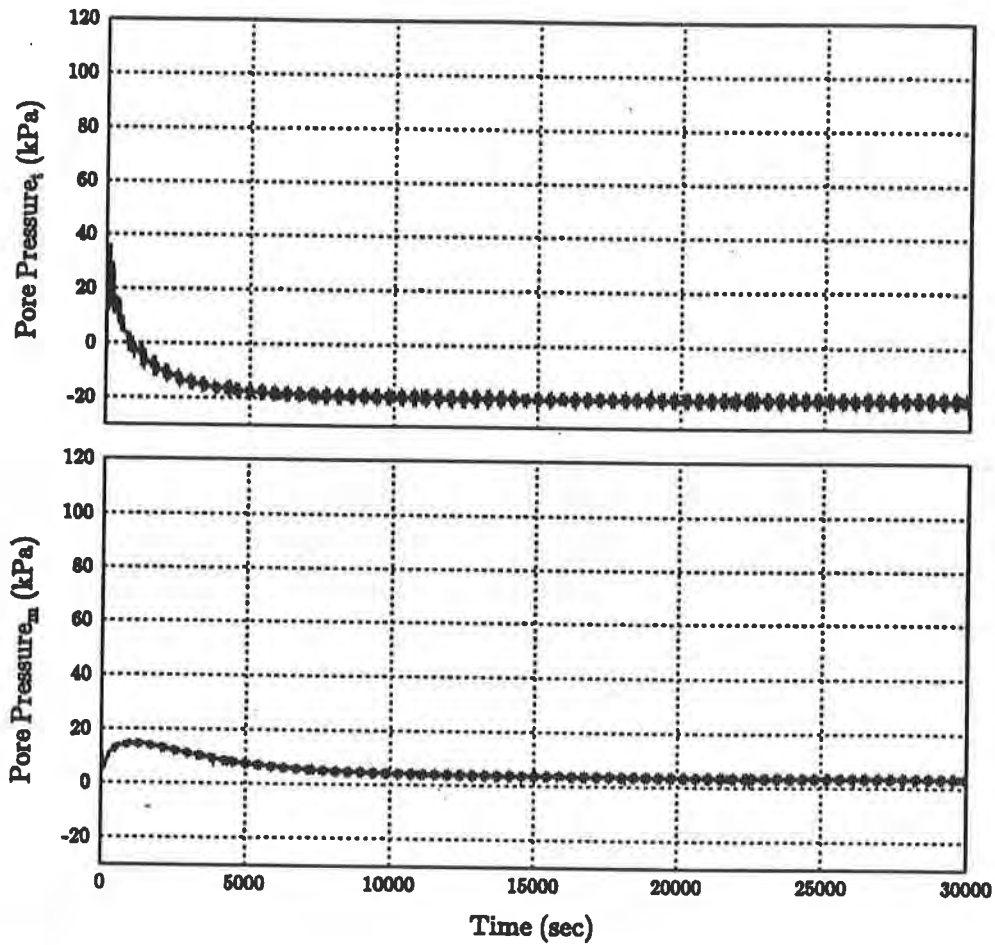
Figure 5   Typical pore pressures developed with number of loading cycles.

Figures 6 and 7 show the peak pore pressures from the tests with 110 mm and 40 mm thick aggregate bases, respectively. Among the tests with the 110 mm thick aggregate base and the same subgrade strength (CBR), peak pore pressures at the top of the subgrade were in the range of 30 to 34 kPa with geotextiles, while the control test (without geotextile) had the lowest peak pore pressure, 25 kPa.
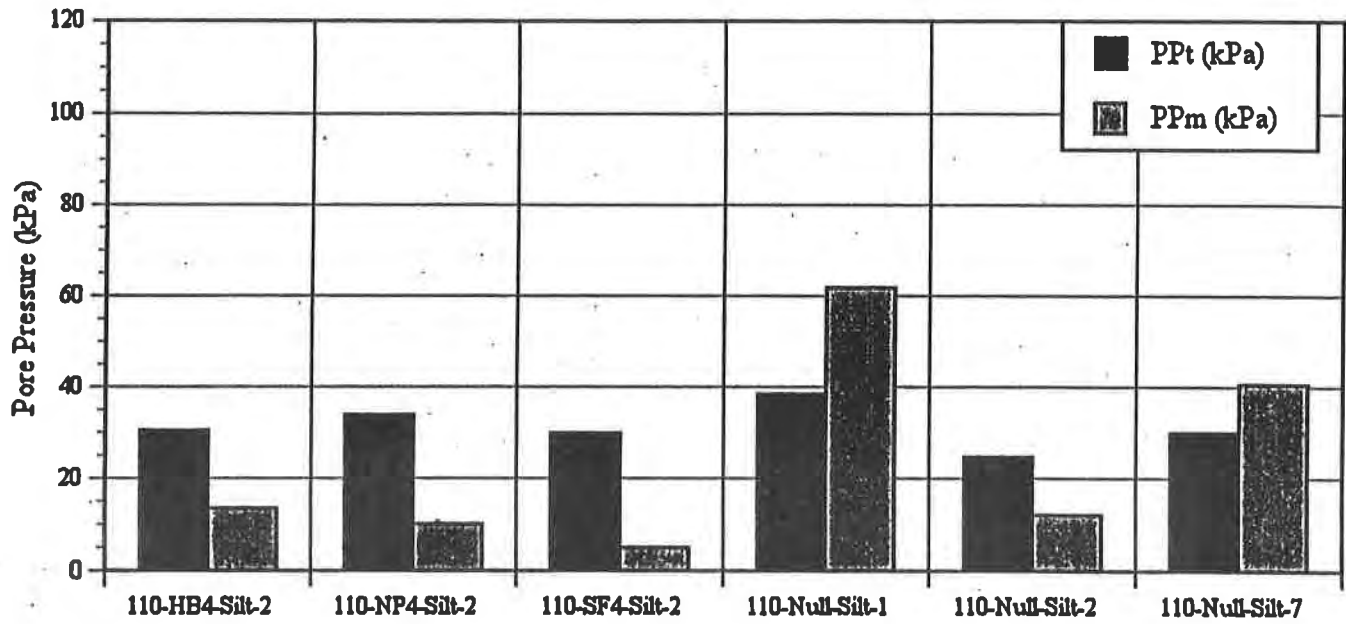
Figure 6 Peak pore pressures from the tests with a 110 mm thick base course.
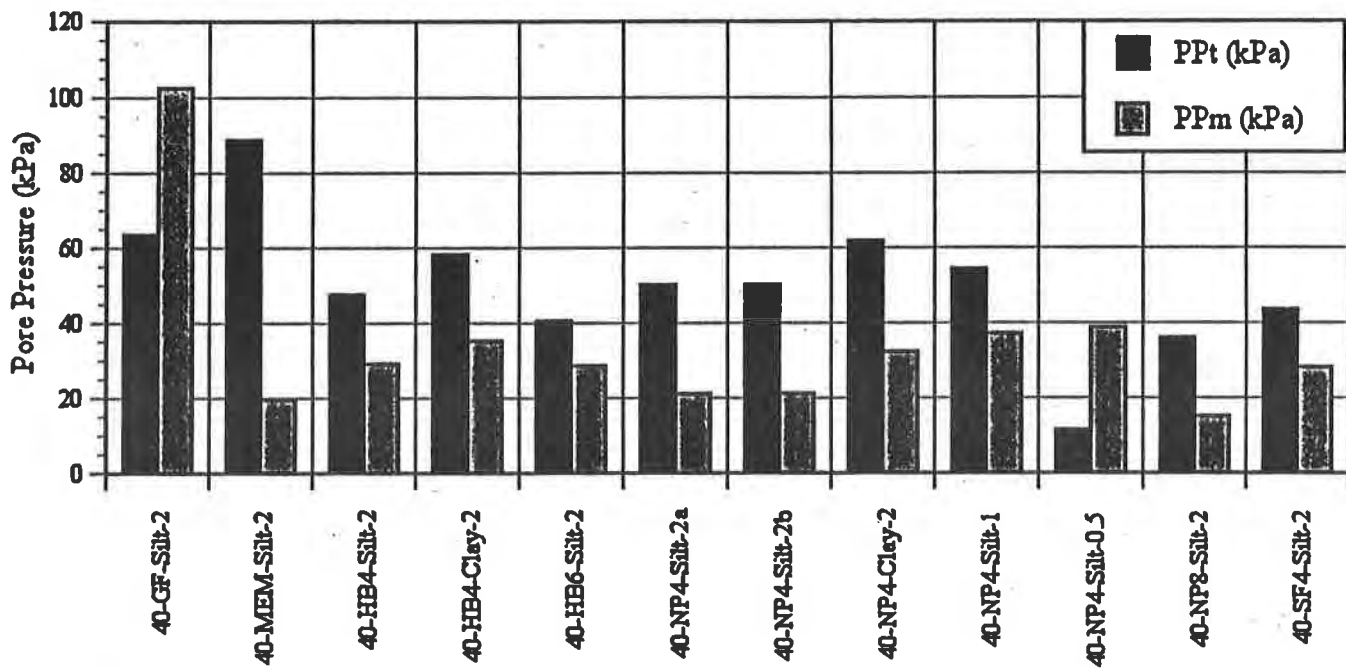
Figure 7   Peak pore pressures from the tests with a 40 mm thick base course.

The tests with the thinner (40 mm thick) aggregate base had higher peak pore pressure at the top of the subgrade. This is reasonable since the stress on the subgrade under a thinner base is higher than under a thicker base (Boussinesq theory). The peak pore pressures at the top of the subgrades in the tests with the 40 mm thick aggregate layer and silty subgrades with CBR 2 were in the range of 36 to 54 kPa; the only exception was the test with a membrane as a separator. In this test, the peak pore pressure at the top of the subgrade was extremely high, 89 kPa, and the pore pressure took a longer time to dissipate than for any other test. This high and long-persisting pore pressure can be explained by the impermeable nature of the membrane. The test with a clayey subgrade had the second highest peak pore pressure, 62 kPa. This pore pressure was 10 kPa higher than that from the tests with the same aggregate, separator and subgrade strength but on a silty subgrade. Similar to the test with a membrane separator (40-MEM-Silt-2), this test also had long-persisting pore pressures.

The test with the lower subgrade strength (CBR 1) had a slightly higher peak pore pressure than the tests with stronger subgrade (CBR 2).

In general, among the tests with various geotextiles, if they had the same aggregate thickness, subgrade soil and strength, pore pressures did not appear very different. Therefore, there appears to be no relationship between the induced peak pore pressures and hydraulic properties of the geotextiles. Similar findings were also found by Nishida and Nishigata (1994).

Soil Contamination and Clogging. To evaluate the ability of a geotextile to retard fines migration, the entire crushed stone aggregate base was weighed before as well as after the dynamic loading. The weights of crushed stone decreased slightly after dynamic loading in most tests (Tsai, 1995), probably because some fine particles from the aggregate above migrated into and then became embedded in the openings of the geotextiles during dynamic loading.

After dynamic loading, the geotextiles were exhumed and inspected to examine their pores for clogging. It was found that some minor clogging occurred, but it did not seem to cause any problems. The measurements from the pore pressure transducers also showed that pore pressures still dissipated. As the results from the membrane test (110-MEM-Silt-2) imply, clogging may not cause a serious problem, because excess pore water pressure can dissipate in all directions, not only upward through geotextile separators.

CONCLUSIONS

If they survive construction and service life, a geotextile appears to increase the bearing capacity of subgrade. Rut depth was significantly affected by aggregate base thickness, subgrade soil type, subgrade strength and the presence of a geotextile, but not geotextile type and weight. Hence, the use of separators with different moduli does not appear to influence the different final ruts. Deeper ruts were caused by long-persisting high pore pressures, which were

caused by the low permeability of the subgrade or "completely clogged" separators (modeled by a perfect geomembrane separator).

Based on the results from pore pressure measurements in the subgrade, peak pore pressure was influenced by aggregate base thickness, subgrade soil type and subgrade strength, but not geotextile type and weight. The impervious separator in Test 40-MEM-Silt-2 had the highest pore pressure. All separators had good performance in retarding fines migration, provided they survived the dynamic loading. Some clogging in geotextiles was observed but did not cause a significant increase in pore pressure, since even partially clogged geotextiles always had a permeability greater than the underlying subgrade

REFERENCES

Hyodo, M., Yasuhara, K., and Hirao, K. (1992) "Prediction of Clay Behaviour in Undrained and Partially Drained Cyclic Triaxial Tests". Soils and Foundation, Vol. 32, No. 4, 117-127.

Nishida, K., and Nishigata, T. (1994) The Evaluation of Separation Function for Geotextiles", Proceedings 5th International Conference on Geotextiles, Geomembranes and Related Products, Singapore, Vol. 1, pp. 139-142.

Task Force 25. (1989) "Guide Specification for Geotextiles in Separation Applications," AASHTO-AGC-ARBTA Joint Committee.

Tsai, W.-S. (1995) Evaluation of Geotextiles as Separators in Roadways, Ph. D. Thesis, University of Washington, Seattle, 173 pp.

Tsai, W.-S., and Holtz, R. D. (1994) "Performance of Geotextile Separators in Laboratory Model Tests", Fifth International Conference on Geotextiles, Geomembranes, and Related Products, Singapore, Vol. 2, pp. 663--666.

U. S. Bureau of Reclamation. (1984) Earth Manual, 2nd Ed., Denver, 810 pp.

GEOSYNTHETIC STABILIZED FLEXIBLE PAVEMENTS

Imad L. Al-Qadi, Thomas L. Brandon, and Salman A. Bhutta
Virginia Tech, USA

ABSTRACT

The performance of geosynthetic stabilized flexible pavement systems is under investigation. Laboratory test sections were constructed and dynamically loaded to simulate a typical secondary road. The laboratory study demonstrated that geotextiles offer substantial improvement to the performance of pavements constructed over weak and moderate subgrade. This improvement was attributed to the separation capabilities of the geotextiles and their ability to prevent the development of a transition layer (intermixing layer). To verify the laboratory results, nine instrumented full-scale field test sections were constructed as a part of a secondary road. Three groups, each group consisting of geotextile and geogrid stabilized and non-stabilized test sections, were constructed. The base course thickness varied between the three groups. Monitoring of the field test sections is currently in progress. This paper presents a summary of the laboratory results and describes the construction, monitoring, testing, and preliminary results of the field study. Preliminary field results support the separation mechanism theory and the development of a transition layer when a separator is absent.

INTRODUCTION

Secondary roads are the most commonly encountered flexible pavement systems in the United States. The vehicles that utilize these roadways are usually the same type and weight as those traveling the nation's interstate highways, but at lower volume. The common failure of secondary roads with such traffic load is premature rutting. Also, subgrade fines migrate into the base course layer, or aggregate from the base course penetrates into a soft subgrade, jeopardizing the structural capacities and compromising the drainage capabilities of the pavement system, hence accelerating the rutting failure mode. This leads to a reduction in the pavement service life.

There are several ways to increase the stability of secondary road systems, among them the use of geosynthetics. Most of the research carried out to determine the potential benefits of geosynthetic stabilization has been limited to laboratory-based research. The use of geosynthetics in the field has been based on trial and error or on past experience. Since limited comprehensive laboratory or field experiments have been conducted to document the

performance of geosynthetic stabilization, it is difficult to determine accurately how much geosynthetic stabilization may increase a pavement's structural capacity, or the cost effectiveness of the use of these materials for stabilization.

The research presented in this paper is intended to characterize the improvements obtained by using geosynthetic stabilization in a flexible pavement. Improvement is interpreted as an increase in the structural capacity of the pavement. Laboratory flexible pavement test sections were constructed, dynamically loaded to a predetermined pavement rut depth, and excavated; the resulting data was analyzed to identify test section performance. Full-scale field test sections were constructed and their performance under typical traffic loading is currently being monitored.

LABORATORY FLEXIBLE PAVEMENT TEST SECTIONS

A total of eighteen flexible pavement test sections were designed, constructed, and dynamically loaded over the course of the laboratory research program. The subgrade soil and base course aggregate were reused for the construction of each test section to eliminate variability in construction materials between tests. Results for each test section were analyzed and their performances were compared.

Testing Facility and Construction Materials. Eighteen flexible pavement sections (the first two were for fine tuning the experiment) were constructed and tested within an instrumented retaining wall pit built by Sehn and Duncan (1990). The test pit has two opposing rectangular side walls, 3.1 m (10.0 ft) long by 2.1 m (7.0 ft) high, and a back wall, 1.8 m (6.0 ft) wide by 2.1 m (7.0 ft) high. The test pit floor, side walls, back wall, and entrance ramp were constructed of reinforced concrete. An I-beam, crossing over the test pit, provided the reaction for the pavement loading system.

The subgrade soil (of the pavement system) consisted of Yatesville silty sand (YSS). The soil was excavated from alluvial deposits at the foundation of Yatesville Lake Dam in Lawrence County, Kentucky. It is a silty sand in accordance with the Unified Soil Classification System (USCS) and an A-4 in accordance with AASHTO. It has approximately 40% non-plastic fines, and has a specific gravity of 2.67. The subgrade material was placed at California Bearing Ration (CBR) values of approximately 2% and 4%.

Two types of woven polypropylene fabric geotextiles and a geogrid were utilized in the laboratory study. Geotextile "A" is a Class 3 separation geotextile as defined by AASHTO and geotextile "B" is a Class 1 woven stabilization geotextile as defined by AASHTO (AASHTO, 1995). The geogrid has an aperture size (MD/XD) of 25/33 mm and an ultimate wide width tensile strength of 1172 kg/m. Geosynthetics for all stabilized test sections were placed on the subgrade surface at the subgrade-base course interface.

The base course was a granite aggregate classified as 21-A by the Virginia Department of Transportation (VDOT). Modified Proctor compaction tests (ASTM D 1557-91) yielded a maximum dry density for the base course aggregate of 22.9 kN/m³ (146 pcf) at a moisture content of 5.8%. The specific gravity and absorption (ASTM C 97-90) of the aggregate were 2.81 and 0.4%, respectively. The compacted base course thicknesses were approximately 15 cm (6 in) and 20 cm (8 in); the 20 cm (8 in) layer was constructed in two lifts. The aggregate was compacted to a minimum of 95% of the maximum dry density determined by ASTM D 1557, within ± 0.5% of the optimum moisture content.

The hot-mix asphalt (HMA) layer was a VDOT classified SM-2AL with unpolished limestone aggregate. The final target thickness for the HMA layer was 7.0 cm (2.8 in). The surface elevation of each lift of the construction materials was surveyed to determine each layer thickness. In addition, quality control tests were conducted, including dry density and moisture content of the subgrade and base course layers, and density of the HMA layer. Hot-mix asphalt core samples were also obtained for creep compliance and resilient modulus measurements. Smith *et al.* (1995) provide details on the job mix formula (JMF) and quality control results. The layer thicknesses and subgrade CBR values are presented in Table 1.

Table 1. Test section properties.

Section No.	Stabilization Type	Subgrade CBR (%)	HMA Layer (cm)	Base Course (cm)
3	Geotextile A	4.5	7.1	13.5
4	Geogrid	5.7	7.9	13.5
5	None	5.4	7.9	11.4
6	None	4.4	7.4	14.7
7	Geotextile B	4.2	7.1	14.7
9	None	5.4	8.4	21.1
10	None	4.3	7.1	14.0
11	Geotextile A	4.4	7.4	15.0
12	Geogrid	4.6	7.9	14.2
13	None	4.2	6.1	19.6
14	Geotextile A	4.5	7.9	22.4
15	None	2.0	7.4	13.2
16	Geotextile A	2.2	9.4	12.2
17	Geotextile A	2.0	7.4	13.2
18	Geogrid	2.0	7.4	13.2

Pavement Loading, Instrumentation, And Data Acquisition. The loading system for the laboratory test sections was designed to simulate a dual tire load from an 80 kN (18 kips) axle with a tire pressure of 550 kPa (80 psi). The designed 40 kN (9 kips) force load was transmitted to the pavement surface through a 30 cm (12 in) diameter and 1.9 cm (0.75 in) thick steel plate at a frequency of 0.5 Hz. The 40 kN (9 kips) load on the steel plate resulted from a 17.8 kN (4 kips) applied by a Bellofram air cylinder to a lever arm (used to increase the force). A 44.5 kN (10 kips) load cell was placed directly on top of the load plate to monitor the applied forces.

The pavement surface displacement was monitored using an isolated horizontal array of eight Linear Variable Displacement Transformers (LVDTs). Two LVDTs were positioned on the steel loading plate top surface, each at 2.5 cm (1.0 in) from the outside edge. The remaining six LVDTs were spaced evenly, 15 cm (6 in) apart, along the centerline of the pavement surface.

The pavement loading was applied on 200 consecutive load cycles (load sequence). After each load sequence, the lever arm of the loading apparatus was adjusted to accommodate any permanent deformation occurring in the pavement system. It was determined that any recoverable deformation of the pavement system would occur within five minutes of ceasing the loading cycles. The LVDTs were read before each test sequence and five minutes after each load sequence was terminated. Failure of the pavement was defined as an average surface permanent deformation of 2.5 cm (1.0 in) measured at the loading plate.

Six Kulite type 034 total stress earth pressure cells were installed in four test sections to determine the change in total earth pressures within the subgrade due to dynamic loading conditions. The cells were placed at 0.3 m (1.0 ft) and 0.9 cm (3.0 ft) from subgrade surface at the cross-section centerline. Two were placed directly underneath the loading plate, and the other four were placed at 0.5 m (1.5 ft) from the centerline; two on each side.

Excavation of Test Sections. The layers of each flexible pavement test section were excavated after failure. The primary objective of the excavation was to measure physically the amount of deformation in each of the layers, and to examine visually the mechanisms of failure. The front half of the test section was excavated to a depth of approximately 0.9 m (3.0 ft). The pavement layer deformations and thicknesses were measured from a straight edge placed across the upper surface of the HMA layer. Photographs of the exposed excavation were taken. Any evidence of migration of the subgrade fines or of penetration of the base course aggregate in a test section was recorded.

Results of The Laboratory Test Program. The pavement surface deformations considered were those attained after the full rebound of the pavement surface. Most of the sections tested underwent a significant portion of the total deformation in the first 25 load cycles. This compression is similar to what is experienced in the field during the first few months of normal traffic loading. The pavement surface displacement during the initial 25 load cycles was considered "seating deformation." A typical result is shown in Figures 1 and 2 for a CBR of approximately 4% and 2%, respectively. Smith *et al.* (1995) give detailed results on this part of the research.

Another way to compare performance is to evaluate the surface deformation at a specific number of cycles. Due to variation in loading pressure, the applied load was normalized and converted to equivalent single axle load (ESAL) to account for load variation between cycles and for the effect of the rigid plate and frequency (presented under Service Life Prediction). A typical deformation at layer interfaces (after failure) is presented in Figure 3.
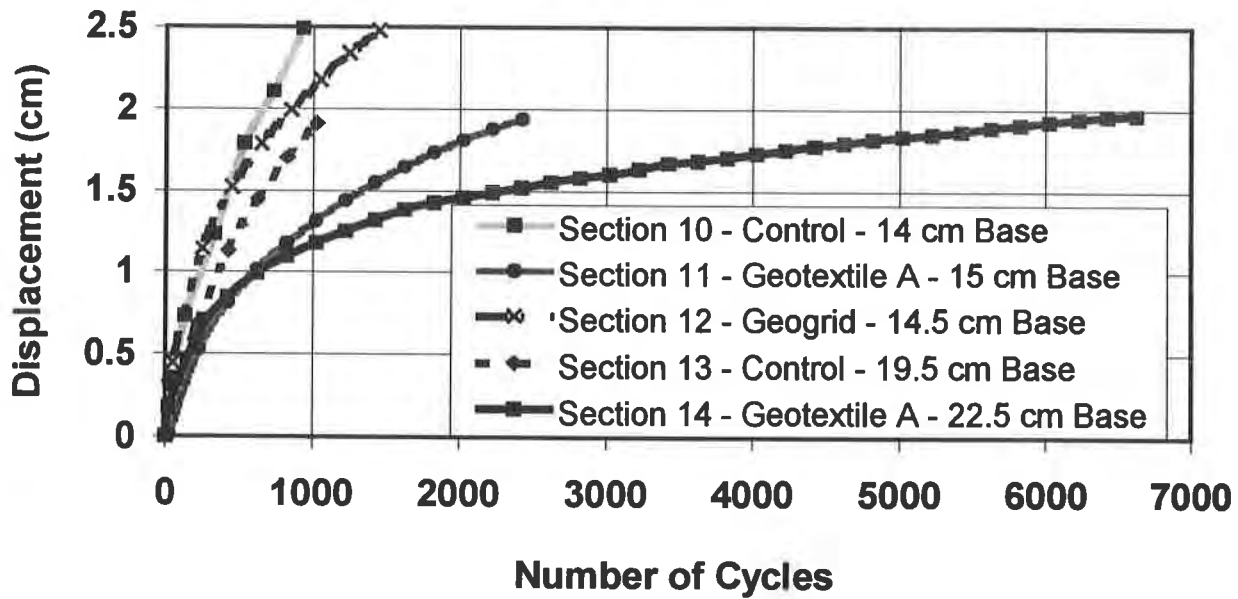
Figure 1 Deformation of the pavement surface as a function of the number of applied load cycles (CBR ≈ 4%).
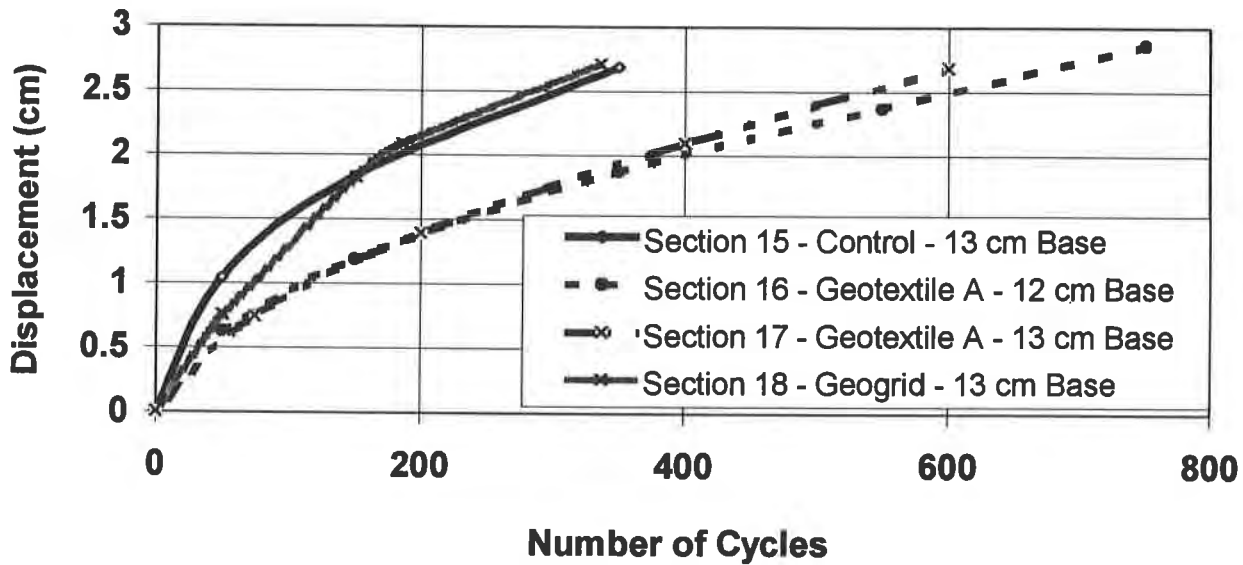
Figure 2 Example of deformation of the pavement surface as a function of the number of applied load cycles (CBR ≈ 2%).

Reaction of Flexible Pavement to Dynamic Loading. The reaction of a test section to dynamic loading was determined at approximately 25 cycles from the end of each load series. The averaged slope of the hysteresis loops taken for three consecutive load cycles was determined to be the reaction of the test section at that point and termed "stiffness." The pavement surface

deformation measured in the analysis was the deflection of the steel load plate during dynamic loading.

The change in the stiffness of a section during testing may give some indication of the effectiveness of geosynthetic stabilization as pavement deformation increases. The initial values of stiffness can be characterized by the initial thicknesses of the pavement layers and the moduli of the compacted materials. As testing proceeds, the relative stiffness of a section is dependent on the changing pavement layers moduli. The stiffness analyses for sections 3 through 9 generally showed an increase in stiffness for the stabilized sections during testing. The exception was test section 7, stabilized with geotextile B. The response of this section was similar to that of the test section (No. 9) constructed with an additional 5 cm (2 in) of base course aggregate. The stiffness analyses for sections 10 through 14 showed an initial decrease in stiffness for all of the test sections. Both of the geotextile-stabilized test sections exhibited an increase in stiffness towards the end of their testing periods. The control test sections showed a stiffness decrease with no stiffness recovery as displacement increased. For sections 15 through 18 (subgrade CBR is approximately 2%), the two geotextile-stabilized sections showed a definite increase in stiffness as deformation increased. In general, the test sections stabilized with geotextile showed an increase in stiffness during dynamic loading as pavement surface deformation increased.
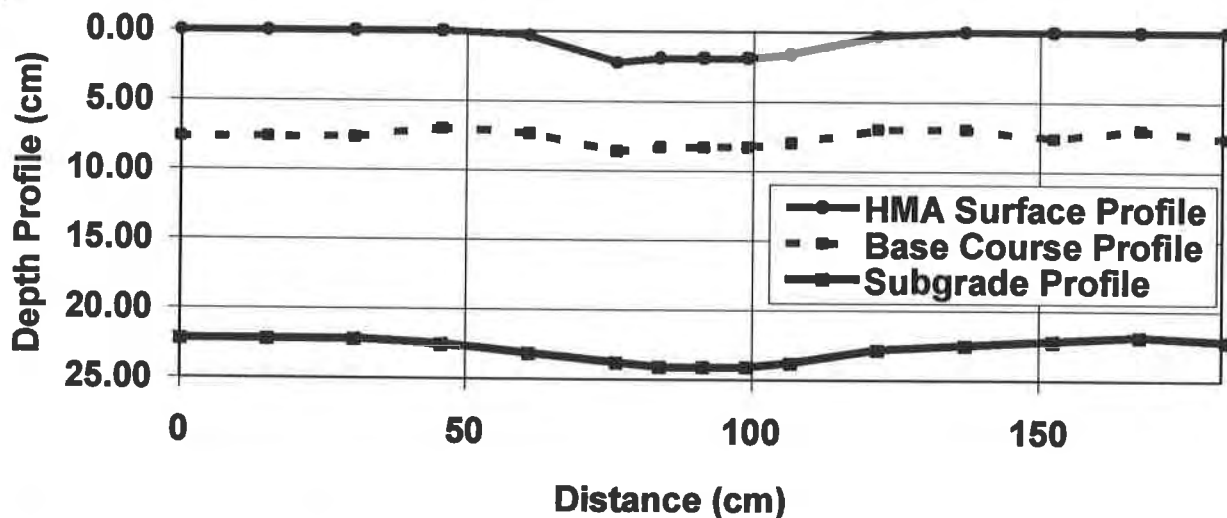
Figure 3 A typical deformation profile at the HMA surface and layer interfaces.

Total earth pressures that developed in the subgrade in four test sections during dynamic loading were analyzed. The test sections utilizing geosynthetics exhibited less of an increase in pressures within the pavement system subgrade than did the control sections constructed with the same base course thickness. Lacina (1995) provides details on stiffness and pressure analyses. The pressure trends for the geosynthetic stabilized test sections support the test section excavation findings. The researchers attributed this behavior to the creation of a

transition layer (intermixing layer) which has a lower resilient modulus than the base course. That layer was also evident during excavation when a geotextile was not used. Thus, the structural capacity of the base course layer is compromised, causing the pressures measured in the subgrade layer to increase.

Service Life Prediction. The dynamic loading system used on the test sections did not always impart the same magnitude of load to the pavement surface, and the load frequency was lower than the frequency imparted by normal vehicle speeds. To compare the performances of each of the test sections, it was necessary to apply conversions to the recorded data to normalize the results with respect to an equivalent dual tire dynamic load and with respect to appropriate vehicle speeds (Al-Qadi *et al.*, 1994). The AASHTO pavement design procedure was used as the basis for converting the applied loads (after being corrected for frequency and rigid plate effects) to ESAL.

Table 2. Predicted number of ESALs to cause failure in the field, and service life prediction for 3750 ESALs per year at an average speed of 64 km/hr (40 mph).

Sect. No.	Total No. of Applied ESALs for 2.5 cm Displacement	Allowable Number of ESALs to Failure *AASHTO*	Allowable Number of ESALs to Failure *Kenlayer*	Predicted Number of ESALs to Failure *Kenlayer*	Service Life Based on Allowable ESALs (years) *Kenlayer*	Service Life Based on Predicted Service Life (years) *Kenlayer*
3	17615	40147	20390	42527	5.2	10.3
4	8823	151512	63116	63116*	14.7	14.7**
7	20091	42930	19284	48504	4.9	11.6
11	37117	56455	25929	89609	6.5	19.7
12	15631	68178	35362	37737	8.7	9.3
14	73486	251775	87921	182188	19.4	34.3
17	2368	3783	2002	5717	0.5	1.5
18	593	6638	2547	2547*	0.7	0.7**

* Predicted ESAL repetitions less than allowable ESAL repetitions.
+ Control and duplicate sections are not included (control sections were used as references).
** Service life based on predicted ESALs is less than service life based on allowable ESALs.

An 80 kN (18 kips) dual wheel axle load with a contact pressure of 550 kPa (80 psi) was used as the design applied load. The *KENLAYER* computer program, developed by Huang (1993), was used to determine the conversion factors for the frequency of the applied load. Thus, predicted ESALs to failure were calculated and presented for a speed of 64 km/hr (40 mph) as shown in Table 2. These values represent the number of ESAL repetitions to fail a test section based on a rutting criterion of 2.5 cm (1.0 in) under field loading conditions. The service life prediction for a typical secondary road with 3750 ESAL per year and an average speed of 64 km/hr (40 mph) is also shown in Table 2. These estimates are valid due to consistency of materials in all sections and the similarity between the soil classification and

strength of the ASSHO Road Test (on which ASSHTO Guide for Design of Pavement Structures is based) and the soil used in this study. Although Table 2 provides a reasonable comparison between each of the test sections, results may differ in the field.

Based on the above findings, Figure 4 may be used to evaluate the benefits of using geotextiles in flexible pavements. It may be used to reduce the total thickness of a flexible pavement or to increase its service life (which is preferred). The two curves presented in Figure 4 are based on all laboratory data for control and geotextile-stabilized sections. Both curves passed t and F statistical tests and had an R^2 greater than 98%. To reduce the total pavement thickness, one may use the design ESAL (without the reliability effect) and find the corresponding value when a geotextile is used (both curves should have the same "Applied ESAL," as shown by the dotted line in Figure 4. The new ESAL value is corrected for reliability and then used to determine the structure capacity of the pavement. If increasing the service life is desired, the design ESAL (without reliability effect) is used to obtain the "Applied ESAL" from the "Geotextile" curve. Determine the value corresponding to the same "Applied ESAL" using the "Control" curve, as shown by the solid line. Correct the obtained ESAL for reliability and that will be the ESAL that the pavement will sustain with the current design if a geotextile is incorporated. Discussion of the details of this method is beyond the scope of this paper; forthcoming publication will develop this method in depth.
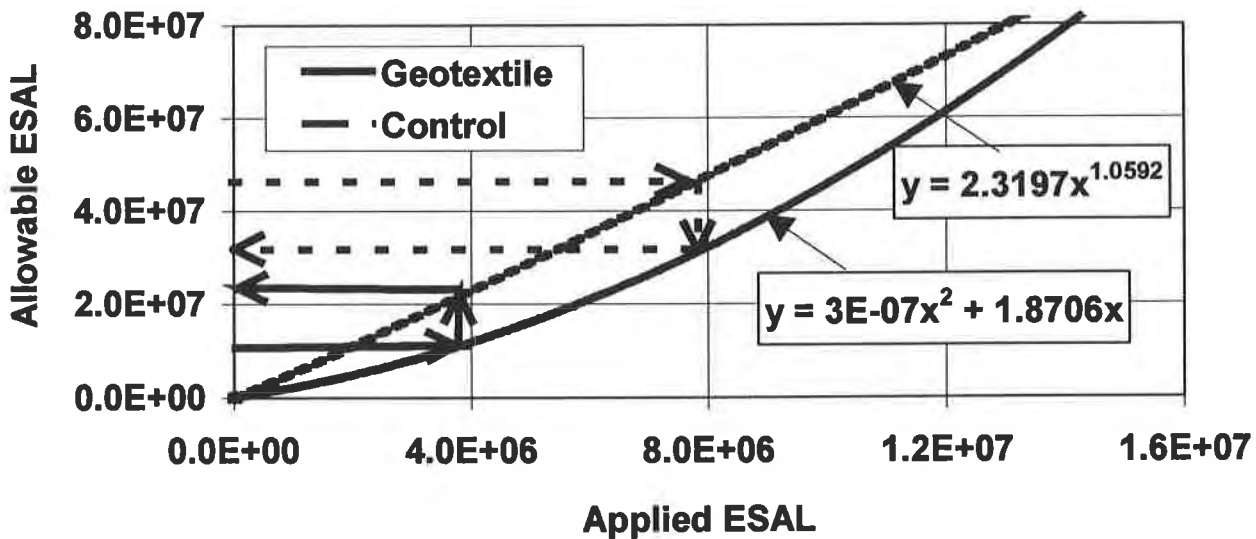
Figure 4 Correction curves for incorporating geosynthetics in flexible pavements

It is obvious that the use of geosynthetic stabilization has improved the performance of flexible pavement sections with respect to permanent deformation. Geotextile stabilized test sections sustained from 1.7 to over 3 times the number of load repetitions that control sections experienced to cause a permanent deformation of 2.5 cm (1.0 in). From the research results, the authors conclude that stabilizing flexible pavement with a geotextile can increase its service life more than 50%, especially in the field, where environmental effects may accelerate the base

course contamination and aggregate penetration into subgrade and thus increase the thickness of the transition layer.

FULL-SCALE FIELD FLEXIBLE PAVEMENT TEST SECTIONS

In order to evaluate geosynthetically stabilized flexible pavements in the field, nine heavily instrumented test sections were constructed as part of the realignment of Routes 757 and 616 located in Bedford County, Virginia. Each test section was 15 m (50 ft) long. Three test sections were constructed using a geogrid (sections 3, 6, and 9), three with a geotextile (sections 2, 5, and 8), and three non-stabilized (sections 1, 4, and 7). Geosynthetic stabilization was placed on top of the subgrade layer. The constructed base course thicknesses were 10 cm (4 in) for sections 1-3, 15 cm (6 in) for sections 4-6, and 20 cm (8 in) for sections 7-9. The HMA thickness averaged 8.9 cm (3.5 in). The thicknesses of the pavement layers were determined by surveying during construction and core sampling after construction. The same types of geosynthetics tested in the laboratory study were used; the geotextile was type A. The influence of stabilization type and base course thickness were the principal variables considered.

The pavement test sections were instrumented with earth pressure cells, HMA and soil strain gauges, soil moisture blocks, and thermocouples. The geotextiles and geogrids were also instrumented with strain gauges. All instrumentation, cabling, and data acquisition facilities were located underground. The data acquisition system is triggered by truck traffic passing over piezoelectric sensors and operates remotely. The corresponding data is transferred to Virginia Tech via a modem for processing. Monitoring was initiated in Fall 1994, and it is planned to continue for a minimum of three years.

Construction Materials and Instrumentation. The native soil was excavated to a depth of roughly 1 to 6 m (3 to 20 ft) from the existing surface elevation to expose the proposed subgrade surface. The upper 60 cm (2 ft) of the subgrade was then scarified and compacted. The subgrade material was classified as an ML and CH by the USCS soil classification method, and as an A-7-6 by the AASHTO classification method. Moisture contents for the subgrade ranged from 24 to 31% with corresponding dry densities of 12.3 and 14.0 kN/m^3 (78.6 and 89.1 pcf), respectively. These values were determined from nuclear density tests on the subgrade surface. The average saturated CBR value for the subgrade soil was approximately 5%.

The base course material was a VDOT class 21-B limestone aggregate. The aggregate was carefully pushed over the test sections with a front-end loader and bladed over the instrumented sections using a motor-grader to avoid damage to the geosynthetics and instrumentation. The average dry density (using a nuclear gauge) of the base course layer was 22.4 kN/m^3 (143 pcf). Moisture contents ranged from 2.0% - 3.2%, with an average of 2.6%.

A chip seal layer with a maximum aggregate size of 1.3 cm (0.5 in) was placed on the base course prior to the HMA wearing surface and was compacted using a vibratory roller. Two HMA layers (SM-2AL) were then placed and compacted with a vibratory roller to a thickness of

7.6 cm (3.0 in). The roadway was surveyed to determine the thickness of the HMA layer after completion of layer construction. In addition, core samples were taken from most sections. The core samples were used to determine layer thicknesses and HMA resilient modulus, creep compliance, and MDF.

More than 150 instruments were installed in the test sections. Earth pressure cells were installed 2.5 cm (1.0 in) below the surfaces of the subgrade and base course layers in all test sections. Strain gauges were installed at the bottom of the HMA layer in all of the test sections, roughly 2.5 cm (1.0 in) below the surface of the subgrade in the non-stabilized test sections, and on the underside of the stabilization layer in the stabilized test sections. Thermocouples were installed in the subgrade, base course, and HMA layer of selected test sections to monitor temperature variations. Gypsum block soil moisture sensors were installed in the subgrade and base course layers of selected test sections. Piezoelectric polymer traffic sensors were installed at the surface of the HMA wearing surface to trigger the data acquisition system and monitor vehicle speeds across the test sections. Once the system is triggered, the instrumentation is continuously sampled at a frequency of 200 Hz for a period of either 12 or 10 seconds. The length of time used for sampling is dependent on where a vehicle enters the test section. Twelve seconds are used to read the instruments in all the test sections, while 10 seconds are used to read those instruments in sections 7 through 9 (when vehicles enter from the intersection). The majority of the instruments were placed in the right wheel path of the inside lane of the test sections. A typical response of the piezoelectric sensor to different axle loads at different vehicular speeds is shown in Figure 5. Al-Qadi *et al.* (1996) provides details of each instrument and the instrumentation process.
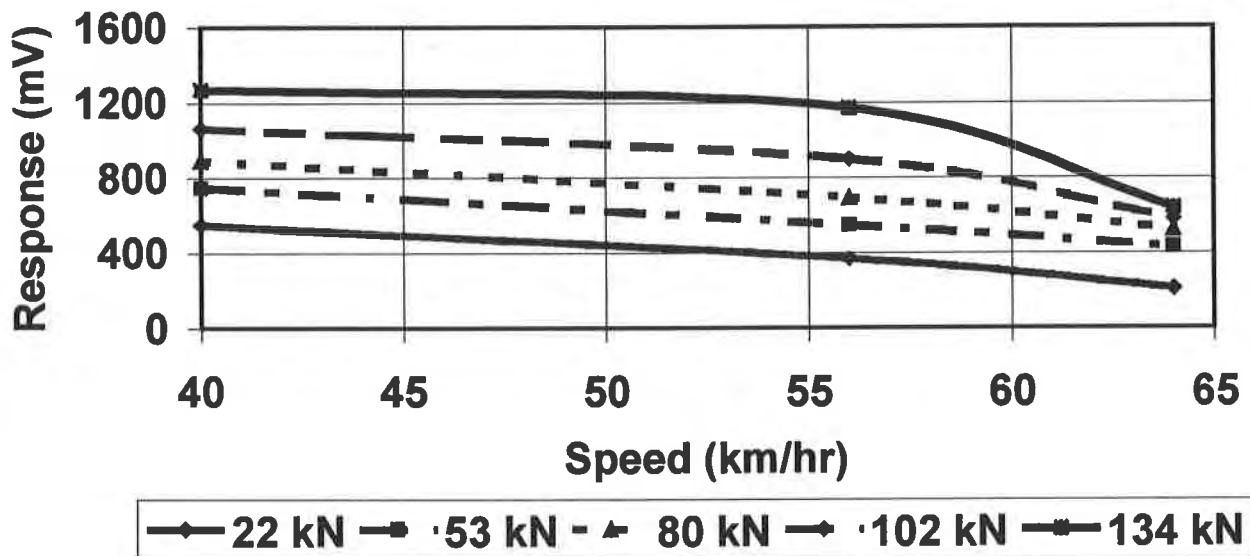
Figure 5 Piezoelectric response to axle loads at different speeds (tire pressure = 420 kPa).

Performance of the Test Sections. Frequent rut depth measurements, falling weight deflectometer (FWD) tests, and instrument calibrations were performed at the site, in addition to the instrument responses to loading and environment changes. These tests were done to monitor the performance of the test sections over time.

Instrument Calibrations. A single axle flat-bed truck with specified load configurations, tire pressures, and traveling at specific speeds has been used to measure accurately test section instrumentation responses. Three calibrations have been performed. In each calibration, single axle loads of 22, 53, 80, and 102 kN (5, 12, 18, and 23 kips), tire pressures of 420, 490, 560, 630, and 700 kPa (60, 70, 80, 90, and 100 psi), and vehicle speeds of 40, 56, and 64 km/hr (25, 35, and 40 mph) have been used. The data acquisition system is triggered manually during the calibration process to ensure complete instrument readings. Figure 6 shows the response of earth pressure cells installed in the subgrade. The reduction in pressure with increasing vehicle speed is expected. It is also known that as a vehicle's speed increases, the pressure and damage to a pavement system decrease, provided that the road surface is not rough. In addition, as the tire pressures and wheel loads increase, the damage to the pavement system increases.

Measured stresses and strains were checked using a pavement analysis program. The program was used to develop horizontal stress and strain profiles for a single axle. The exact wheel paths of traveling vehicles can thus be identified; instruments are distributed in the expected wander area. In general, lower pressure in the subgrade was measured in the geosynthetic-stabilized sections compared to unstabilized sections (as shown in Figure 6). This may be attributed to the development of a transition layer where stabilization was not used.
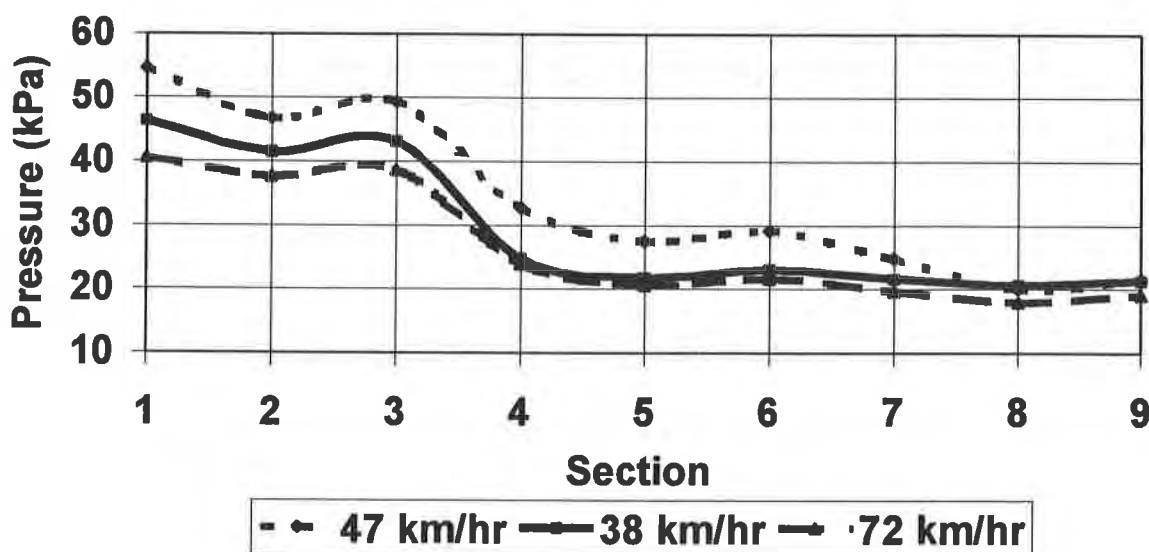
Figure 6 A typical subgrade pressure cell gauge response.

Falling Weight Deflectometer Tests. A VDOT FWD has been used on the test sections. Six separate test groups (each test was conducted over a wide range of loads) have been performed

since the test section was in service. The data were analyzed using the *MODULUS* computer program to back calculate subgrade layer moduli from the test data. The FWD test results for the subgrade are given in Figure 7. Temperature was recorded during the FWD testing to correct for in-situ HMA resilient modulus. The HMA and base course resilient moduli used in the program and were based on extensive testing of HMA and base course materials in the laboratory (Al-Qadi *et al.*, 1996). The variation in the moisture content was minimal over the past two years (with the exception of periods following high snowfall). From the analysis of the FWD results, it was concluded that sections stabilized with geotextiles enhanced the apparent contribution of the subgrade to the overall pavement performance by at least 20%. The observed apparent subgrade enhancement is independent of seasonal changes in subgrade condition and the thickness of the granular base layer.
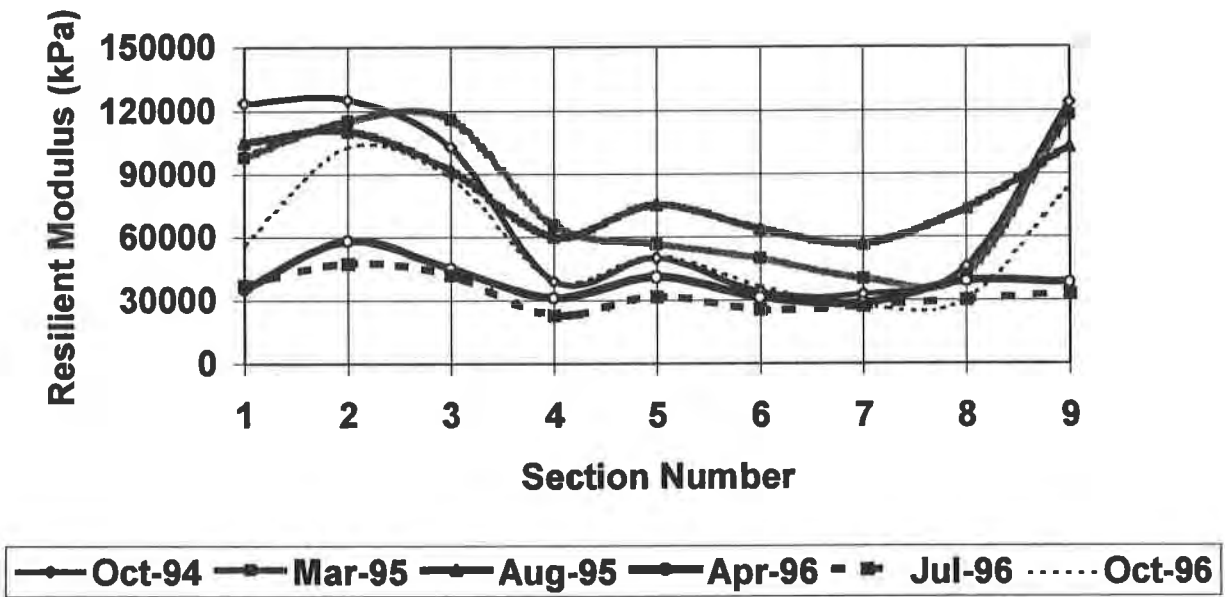
Figure 7 Subgrade resilient modulus results from FWD tests.

Test Section Pavement Surface Rut Depths And Ground Penetration Radar Exploration. The rut depth of the pavement surface has been recorded monthly since the third month the road was in service. The rut depths in the inner and outer wheel paths were measured using a straight edge. The results shown in Figure 8 are the averaged rut depths measured on the surface of the field test sections 1 though 3 (the weakest sections). As shown in Figure 8, the unstabilzed section has already failed. Heavy loading traffic was applied in September 1996 which accelerates the rut depth development. The effect on unstabilized section was very significant..

Ground penetration radar (GPR) was used at 900 MHz to detect any variations at base course-subgrade interface. In Figure 9, the lighter the area, the higher the reflection of electromagnetic waves. In the indicated areas (base course-subgrade interface), the higher reflection may occur because of higher moisture or subgrade soil migration into the base course. Due to the fact that moisture is the same in the three sections, soil migration is a reasonable

assumptions. Also, the base layer (above the indicated areas) appears to be the smallest section, followed by section 3.
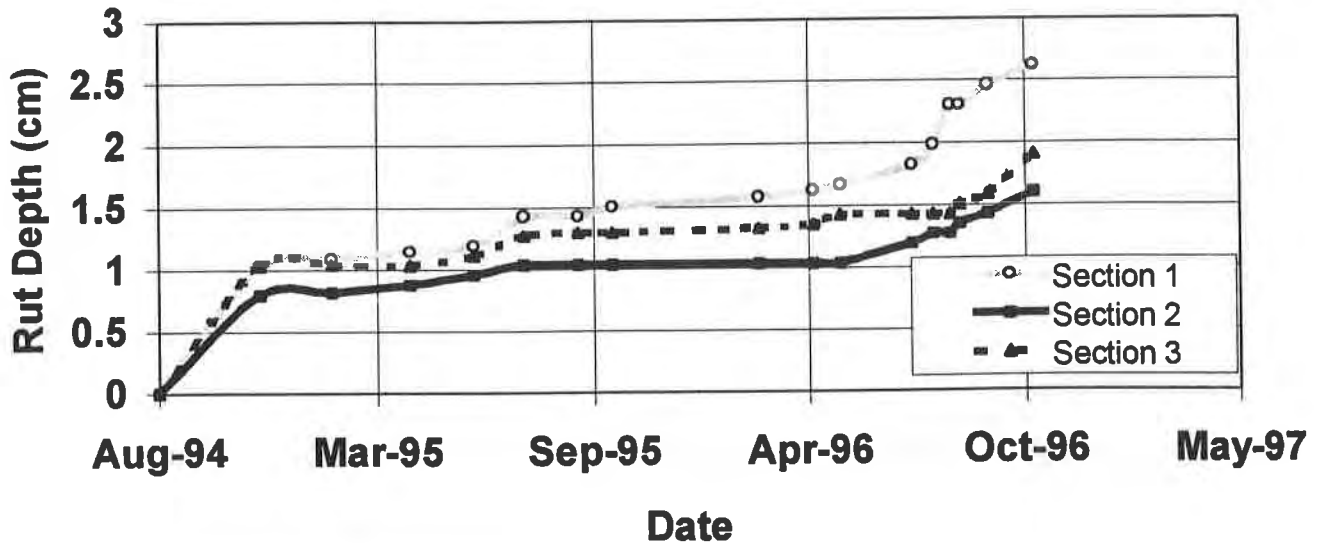
Figure 8 Measured rut depth for sections 1 through 3.
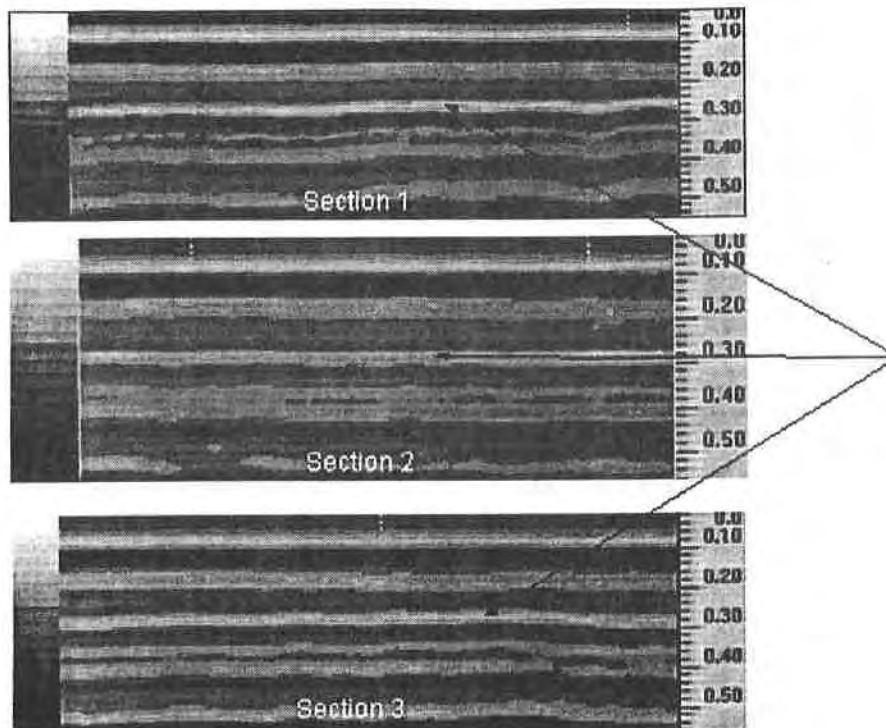
Figure 9 Transition layer by ground penetration radar (sections 1, 2, and 3).

SUMMARY AND FINDINGS

It is the authors' opinion (based on this research) that in order for the geosynthetic's tensile strength to effectively come into play, substantial rutting must occur in the pavement subgrade. If the rutting is significant, it can cause damage to the pavement system and rehabilitation may become necessary before the tensile strength of geosynthetics become a significant factor. This research suggests that whereas the tensile strength of geosynthetics is not a primary rationale for the use geosynthetics at the subgrade-aggregate layer interface, the separation function provided by geosynthetics is an important mechanism to improve the performance of flexible pavement systems. Without separating the untreated base course layer and subgrade, a transition layer (intermixing layer) would form and its thickness would increase with time and traffic. The formation of such a layer would jeopardize the structural capacity of the pavement system. When a geotextile is placed at the interface between the base course and a soft subgrade, the contamination is avoided and a transition layer may not be formed. Hence, geotextile aids in maintaining the structural integrity of the pavement system.

Considering the results of the laboratory testing program and the preliminary results from the field investigation, the following conclusions are made:

- Geotextile stabilization increases the service life of flexible pavements. This conclusion is based on a rutting criterion of 2.5 cm (1.0 in) or less. For a laboratory test section, roughly two to three times more load repetitions were required to failure when a geotextile was used as a separator than were required for unstabilized pavement.
- The benefit of geotextile stabilization is evident in the increase in the pavement system stiffness as pavement surface displacement increases (compared to unsatabilized pavement).
- A transition layer may develop in flexible pavements where no stabilization is used. This layer is an intermixing of the base course and subgrade and it is weaker than the base course layer.
- Use of geotextile stabilization offers improvement to the performance of a pavement section constructed on a weak subgrade. Separation provided by geotextiles is an effective method to improve flexible pavement performance and increase its service life.
- Preliminary results from the field sections support the importance of the separation theory, the development of a transition layer, and the increase in pavement service life due to goesynthetic stabilization.

REFERENCES

AASHTO, (1995) "Draft Standard Specification for Geotextiles," AASHTO Designation: M288-96 DRAFT, Proposed for Publication in <u>AASHTO Standard Specification for Materials, Part 1</u>, 18th Edition, pending December 1995 ballot, AASHTO, Washington, DC

Al-Qadi, I. L., Brandon, T. L., Valentine, R. J., Lacina, B. A., Smith, T. E. (1994) "How Do Geosynthetics Improve Pavement's Performance," Infrastructure: New Materials and Methods for Repair Conference, ASCE, San Diego, California, November, 1994, pp. 606-616.

Al-Qadi, I. L., Brandon, T. L., Bhutta, S. A., Lacina, B. A., and Appea, A. (1996) Field Testing of Geosynthetically Stabilized Pavement Sections, 2nd Progress Report, The Via Department of Civil Engineering, Virginia Tech, Blacksburg, VA.

AASHTO (1993). AASHTO Guide for Design of Pavement Structures, Washington, DC

Brandon, T. L., Al-Qadi, I. L., Lacina, B. A., and Bhutta, S. A. (1996), "Construction and Instrumentation of Geosynthetically Stabilized Secondary Road Test Sections," *Transportation Research Board,* 75th Annual Meetings, Washington, DC

Huang, Y. H. (1993). Pavement Analysis and Design, Prentice Hall, Englewood Cliffs, NJ.

Lacina, B. A. (1995) A Study of the Response of Geosynthetic Reinforced Flexible Pavement Test Sections to Dynamic Loading, MS Thesis, The Via Department of Civil Engineering, Virginia Tech, Blacksburg, VA.

Sehn, A. L. and Duncun, J. M. (1990) Experimental Study of Earth Pressure on Retaining Structures, The Via Department of Civil Engineering, Virginia Tech, Blacksburg, VA.

Smith, T. A., Brandon, T. L., Al-Qadi, I. L., Lacina, B. A., Bhutta, S. A. and Hoffman, S. (1995). Laboratory Behavior of Geogrid and Geotextile Stabilized Flexible Pavements, Final Report, Virginia Tech, Blacksburg, VA.

ACKNOWLEDGMENTS

TESTING AND ANALYSIS OF GEOTEXTILE-REINFORCED SOIL UNDER CYCLIC LOADING

ALAA K. ASHMAWY
GEORGIA INSTITUTE OF TECHNOLOGY, USA

PHILIPPE L. BOURDEAU
PURDUE UNIVERSITY, USA

ABSTRACT

Geosynthetic-reinforced soil masses are subjected to repeated loading in various applications such as embankments, unpaved road, and bridge abutments. Better understanding of the cyclic response of geosynthetic-reinforced soils is therefore needed. In this paper, triaxial test results of geotextile-reinforced silt subjected to cyclic loading are presented. The results show that significant improvement in terms of strength is introduced by the presence of the geotextile layers. Under cyclic loading, the cumulative plastic strains as a function of number of cycles are much lower for the reinforced specimens than for the unreinforced specimens. The amount of improvement seems to depend on the spacing between the geotextile layers, and to a lesser extent on the geotextile and interface properties. A simple analytical model is presented to interpret the test results. The model can be adapted in the future toward design of geosynthetic-reinforced embankments and abutments and similar reinforced earth structures subjected to cyclic loading.

INTRODUCTION

Cyclic loading conditions are frequently caused by traffic loading in transportation infrastructures. Examples include roadway and railway embankments, unpaved and paved roads, and bridge abutments. With the growing use of geosynthetics as a reinforcement material, attention must be given to the cyclic response of reinforced soil masses. Most reinforced-soil studies, to date, have focused on the monotonic behavior of such materials rather than their cyclic response. A comprehensive review on studies dealing with the cyclic response of geosynthetic-reinforced soils is given by Ashmawy and Bourdeau (1995).

Studies devoted to the cyclic response of reinforced soil can be divided into three main categories: (1) experimental, (2) theoretical, and (3) design-oriented. In the first category, an

experimental program is typically carried out on small- or large-scale reinforced soil specimens, and the response is examined as a function of reinforcement spacing or loading level. Examples of such approach include Leflaive (1985), Bathurst et al. (1986), and Raymond (1992). In the second category, analytical models are developed or numerical analyses are performed in an attempt to model the behavior of the reinforced soil mass. Only few studies belong to this second category, such as Madani et al. (1979) and Davies and Bridle (1990). In the third category, simple analytical models or empirical relationships are used to develop design methods. For instance, Giroud and Noiray (1981), Jaeklin (1986), and Houlsby and Jewell (1990) present different methods for geosynthetic-reinforced unpaved road design.

The objective of the present paper is two-fold: (1) to present experimental data showing the effect of geotextile reinforcement on the behavior of a compacted soil under triaxial loading, and (2) to introduce an analytical model to interpret the experimental data. The current study was performed in conjunction with a large-scale experimental program at the Swiss Federal Institute of Technology in Lausanne, Switzerland. Results obtained from the large-scale tests are presented elsewhere (Kharchafi and Dysli, 1994). The analytical model presented herein represents a first step toward the development of a design methodology for geosynthetic-reinforced earth structures subjected to cyclic loading.

EXPERIMENTAL PROGRAM

The experimental program consisted of cyclic triaxial tests on partially-saturated (as-compacted) unreinforced and reinforced silt. The soil was a natural glacial till, classified as CL, although a high percentage of particles fell within the silt and fine sand range. A large quantity of soil was first air-dried, clumps were crushed, and particles retained on No.4 sieve (larger than 4.75 mm) were discarded. Index and standard compaction properties of the soil are listed in Table 1. The reinforcement material was a non-woven thermally spunbonded polypropylene geotextile with a mass per unit area of 261 g/m^2. Stress-elongation curves for the geotextile are shown in Fig. 1.

The soil was mixed at two different water contents, 10% and 13.5%, and was then compacted in layers of equal height and density using a tamping rod, with geotextile discs placed in between, as shown in Fig. 2. Because a relative compaction of 90% was adopted throughout the testing

Table 1. Index and compaction properties of Crosby till.

LL	PL	PI	$w_{c\,optimum}$	$\gamma_{dry\,max}$ (kN/m^3)	G_s
19.5	15.5	4.0	10%	19.25	2.75
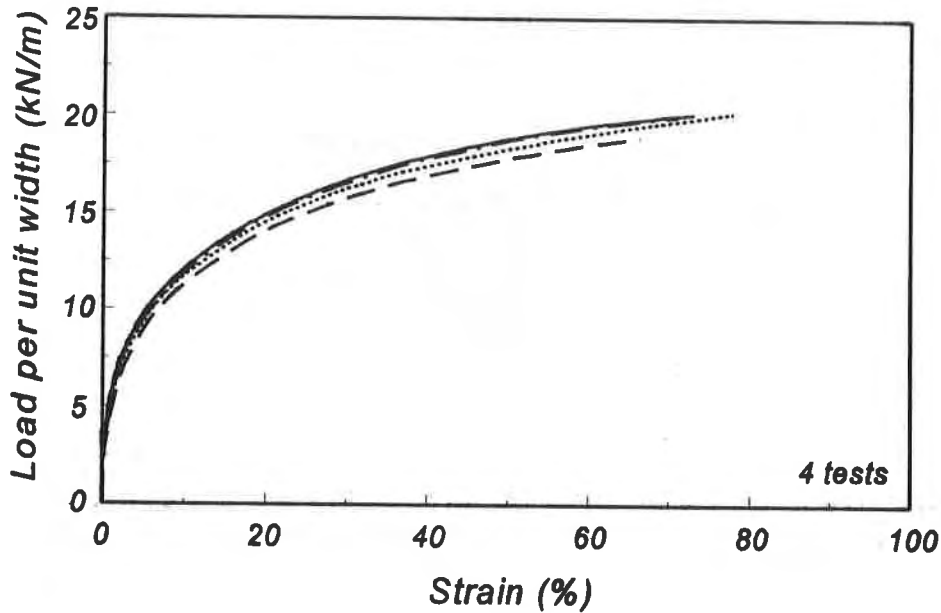
Figure 1. Stress Elongation curves for the non-woven geotextile.

program, the lower moisture content (10%) corresponds to a dry-of-optimum condition rather than optimum. The reason for this is that a lower compaction energy is required to achieve a 90% relative compaction. In turn, the higher moisture content (13.5%) represents a value that is slightly above optimum. The diameter of the triaxial specimen was 71 mm and the total length was 170 mm. Spacings (S) between the geotextile discs of 42.5 mm and 28.3 mm were selected, corresponding to 4 and 6 layers of soil along the specimen, respectively. Unreinforced specimens of the same soil were also prepared following the same procedure.

The prepared specimens were then placed in the triaxial chamber, and a 50 kPa confining pressure was applied. Based on previously performed monotonic test results on the unreinforced soil, unconsolidated undrained shear strength parameters for the partially saturated soil were determined. Based on these strength parameters, the shear strength values for the 10% (dry-of-optimum) and 13.5% (wet-of-optimum) soils at 50 kPa were 62 and 30 kPa, respectively. The unreinforced and reinforced specimens (Fig. 2) were loaded cyclically in a stress-controlled mode, each to a specific stress ratio, i.e., percentage of the monotonic strength of the unreinforced soil. A frequency of loading of 1 Hz was selected for all the tests, and the cumulative plastic strains were recorded as a function of number of cycles.

A servo hydraulic 810 MTS dynamic system was used for loading. The system consists of a loading frame, a hydraulic actuator, and a servo-control unit connected to both a data acquisition system and a hydraulic control valve. The apparatus is capable of generating triangular (ramp) and sinusoidal wave-forms at a maximum frequency of approximately 10 Hz, and of running in both
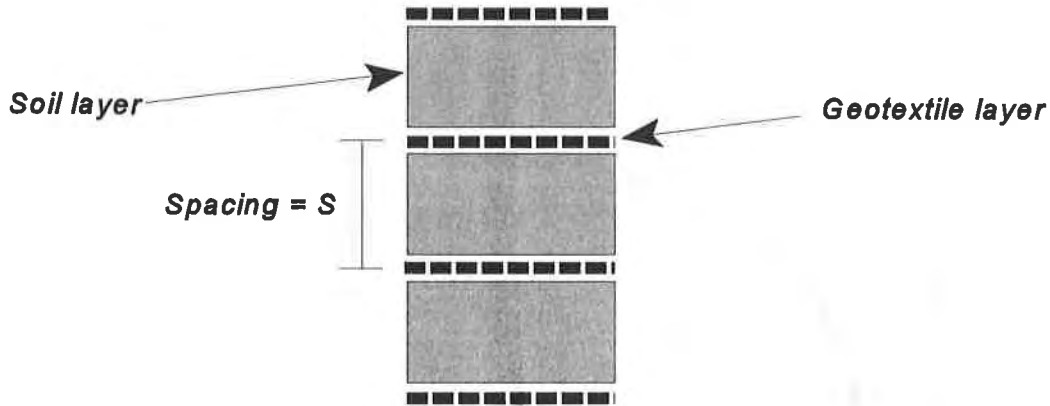
Figure 2. Placement of soil and geotextile layers within the triaxial specimen.

load (stress) or displacement (strain) controlled modes. An LVDT and a load cell were mounted on the frame and were connected to the controller unit. Pressure measurements were taken using Sensotec gage pressure transducers. A PC-based data acquisition and control system was connected to the instrumentation and to the hydraulic valve by means of an RS-232 communication cable.

Because the response of the geotextile-reinforced soil mass depends not only on the properties of the soil and the geotextile, but also on the interface conditions, direct shear tests were performed on the soil-geotextile interface. The soil was compacted in the bottom half of the shear box, and the geotextile was glued on the top half. Shearing along the interface was carried out following the procedure described in the ASTM standard method D 3080-72. Table 2 summarizes the interface Mohr-Coulomb parameters within the stress range of interest.

EXPERIMENTAL RESULTS

Unconsolidated undrained cyclic tests were performed on reinforced and unreinforced compacted Crosby till at both water contents (dry and wet of optimum). For the dry-of-optimum

Table 2. Mohr-Coulomb parameters for geotextile / soil interface, based on direct-shear tests.

	dry-of-optimum soil	wet-of-optimum
c_i (kPa)	0	0
ϕ_i (deg)	35	33
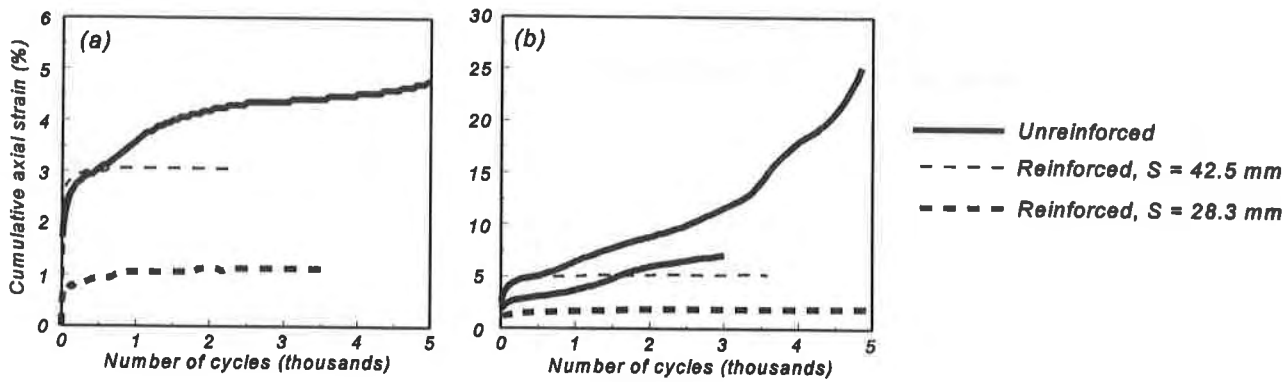
Figure 3. Strain vs. number of cycles (ε-N) curves for dry-of-optimum reinforced soil, cyclically loaded at (a) 60%, and (b) 80% axial stress ratio.

case (10% water content), the amplitudes of cyclic stress for the series of tests corresponded to approximately 60% and 80% of the monotonic strength of the unreinforced material (60% and 80% cyclic stress ratio). For the wet-of-optimum case, three series of tests were performed at cyclic stress ratios of approximately 70%, 100%, and 130%. The plastic axial strain vs. number of cycles were recorded, and the results (ε-N curves) are plotted for all tests in Figs. 3 and 4.

In Fig. 3, it can be seen that the behavior of the unreinforced material at 10% water content is brittle. The cumulative strain always increases with increasing number of cycles, but the rate of accumulation is highly irregular. For instance, in Fig. 3b, results from two tests on unreinforced specimens are significantly different. This suggests that localized failure planes develop within the specimen and cause the strain accumulate at faster rates in some cases. When geotextile reinforcement is used, the strains accumulate in a more predictable manner and reach a constant value after approximately a thousand cycles.

The behavior of the wet-of-optimum soil is much more plastic (less brittle). Cumulative plastic strain vs. number of cycles plots shown in Fig. 4 suggest that the plastic strains for the unreinforced material do reach an asymptotic value, even when the applied stress exceeds the unreinforced-soil monotonic strength. This can be explained by the fact that the monotonic strength is defined here as the strength corresponding to 20% strain. In addition, rate effects contribute to the response of the material. Since the monotonic tests were performed at a much slower rate of loading, a portion of the strain that develops may be attributed to creep. Unlike the dry-of-optimum case, where the unreinforced material behaved in a brittle manner, the role of the reinforcement in this case is only to reduce the magnitude and rate of plastic strain accumulation.

In Fig. 4a, test results on filter paper-reinforced soil are also displayed. Because the modulus of the filter paper and possibly the interface strength are much lower than those of the geotextile, the benefit obtained due to its use as reinforcement is much less. However, the effect of
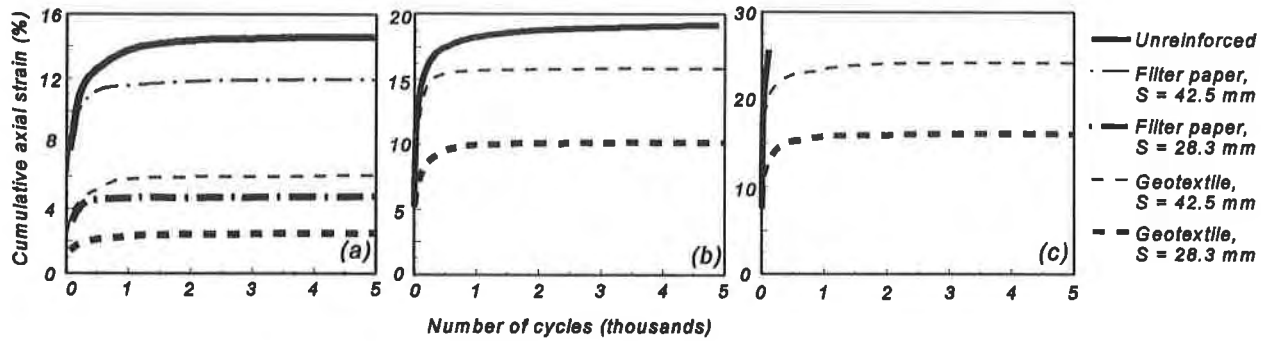
Figure 4. Strain vs. number of cycles (ε-N) curves for wet-of-optimum reinforced soil, cyclically loaded at (a) 67%, (b) 100%, and (b) 125% axial stress ratio.

reinforcement spacing seems to be more important than the properties of the reinforcement material. For instance, the use of filter paper at narrow spacing (28.3 mm) results in more improvement than when geotextile reinforcement is used at a wider spacing (42.5 mm). These results agree with the hypothesis proposed by Giroud and Noiray (1981) which states that the inclusion of reinforcement results in an immediate improvement in the bearing capacity of unpaved roads, regardless of the modulus or strength of this reinforcement.

ANALYTICAL PROCEDURE

In a triaxial test, the cylindrical soil specimen is presumably subjected to uniaxial compression loading after applying the cell pressure. Ideally, the strain field along the axis is homogeneous, and the specimen deforms uniformly in a pattern similar to that shown in Fig. 5a. In practice, however, such conditions are not likely to exist due to friction along the end platens. For plastic (non-brittle) soils, the deformed specimen assumes a barrel shape as shown in Fig. 5b. Higher friction along the loading plane results in the compression (Young's) modulus being overestimated. Most, if not all, standards (e.g., ASTM) require that the specimen height-to-diameter ratio be greater than 2 in order to minimize end friction effects. Since large height-to-diameter ratios result in buckling of the specimen, a ratio between 2 and 2.5 is required in ASTM standards.

When horizontal reinforcement layers are placed within the compacted specimen, the shape of the deformed specimen changes into a series of barrel-shaped elements as shown in Fig. 5c. This deformation mechanism has been verified during the experiment through visual observation. Because a homogeneous lateral strain field is assumed along the axis, the load-deformation characteristics of the specimen are not estimated appropriately. The larger the number of layers, and the higher the friction along the interface, the higher the apparent stiffness of the specimen.

An analytical solution for calculation of true shear modulus of an axisymmetric elastic specimen undergoing barrel-shaped deformation (Fig. 5b) was derived by Mohamed (1983). A
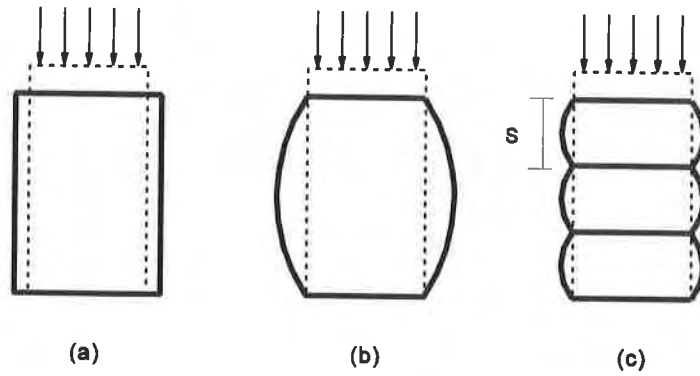
Figure 5. Deformed specimen shapes under axial loading: (a) ideal, (b) unreinforced, and (c) reinforced.

similar solution for the maximum axial stress, σ_a, for axisymmetric soil specimens reinforced with horizontal fabric layers was provided by Broms (1977):

$$\sigma_a = \frac{\sigma_{h0} \, K_{av}}{2 \, \tan^2\phi_m} \frac{h^2}{r^2} \left[\exp \frac{2 \, \tan\phi_m \, r}{h \, K_{av}} - 1 - \frac{2 \, \tan\phi_m \, r}{h \, K_{av}} \right] \tag{1}$$

where σ_{h0} is the confining stress, K_{av} is the lateral earth pressure coefficient, ϕ_m is the mobilized friction angle along the soil-geotextile interface, r is the specimen radius, and h is the initial specimen height.

As shown in Fig. 5c, the shape of the reinforced specimen is similar to a stacked series of barrel-shaped elements. Based on this deformed shape, and dividing both sides of Eq. 1 by the axial strain, ε_a, the apparent modulus, E_{app} , of the soil can be expressed for the reinforced triaxial specimens as:

$$E_{app} = 2 \, E \frac{S^2}{r^2} \left[\exp\frac{r}{S} - 1 - \frac{r}{S} \right] \tag{2}$$

where S is the spacing between the reinforcement layers, and E is equal to $(\sigma_{h0}/K_{av})/\varepsilon_a$ and is the "true" modulus of the soil. In Eq. 2, a value of K_{av} of 1 is used since the specimen initial loading is isotropic. The value of K_{av} will decrease during loading, but will remain relatively close to 1 due to the presence of the additional confinement provided by the reinforcement layers. It is also assumed that the mobilized coefficient of friction (tan ϕ_m) is equal to 0.5, i.e., $\phi_m = 26°$ in all the cases. The maximum values for ϕ_m are obtained from the direct shear tests and are listed in Table 2. Assuming that, on average, 3/4 of the maximum friction angle is mobilized, the corresponding value of tan ϕ_m is 0.49 and 0.46 for the dry- and wet-of optimum cases, respectively. For practical purposes, a value of 0.5 is adopted, resulting in Eq. 2. This Equation can always be expressed in

a more general form to account for the variation in the mobilized friction angle, ϕ_m, and the coefficient of lateral earth pressure, K_{av}. Although area corrections are not employed in the analysis, they can be introduced if the volume change of the specimen is recorded.

Equation 2 is applicable for linear elastic materials. Plastic strains, ε_p, can be expressed as a function of the cyclic stress, σ_{cyc}, and an equivalent modulus, E_p:

$$\varepsilon_p = \frac{\sigma_{cyc}}{E_p} \tag{3}$$

The equivalent modulus, E_p, is proportional to the elastic modulus, E, if the rate of plastic strain accumulation is a function of only the initial modulus. From Figs. 3 and 4, it can be seen that the "shape" of the ε-N curves are almost identical for the same water content, regardless of type of reinforcement and reinforcement spacing. Therefore, it can be concluded that this condition is satisfied.

Based on these assumptions, Eq. 2 and 3 can be combined to relate the plastic strain, ε_p, to a normalized strain, ε_n, as follows:

$$\varepsilon_p = \frac{r^2}{2 \, S^2 \left[\exp \dfrac{r}{S} - 1 - \dfrac{r}{S} \right]} \varepsilon_n \tag{4}$$

where ε_n is the equivalent strain for an ideally deformed specimen (Fig. 5a). In this case, the plastic strain, ε_p, is the strain measured not only for the reinforced, but also for the unreinforced specimens. In the unreinforced case, S is taken to be equal to the total specimen height, since the deformed specimen shape is similar to that shown in Fig. 5b.

The measured and normalized strains for the dry-of-optimum and wet-of-optimum cases are plotted as a function of the normalized stress in Fig. 6. Linear regression analyses were carried out on both data sets, and the regression parameters and correlation coefficients are given in Table 3. From the Figures and the regression data, it can be seen that the method was somewhat effective in normalizing the test results for the wet-of-optimum case. For the dry-of-optimum case, the data is highly scattered, possibly due to the inconsistent response caused by the brittle nature of the soil.

DISCUSSION

The methodology described above provides a useful tool for normalizing cyclic test data of reinforced soil specimens. The method, however, relies on the assumption that the cyclic
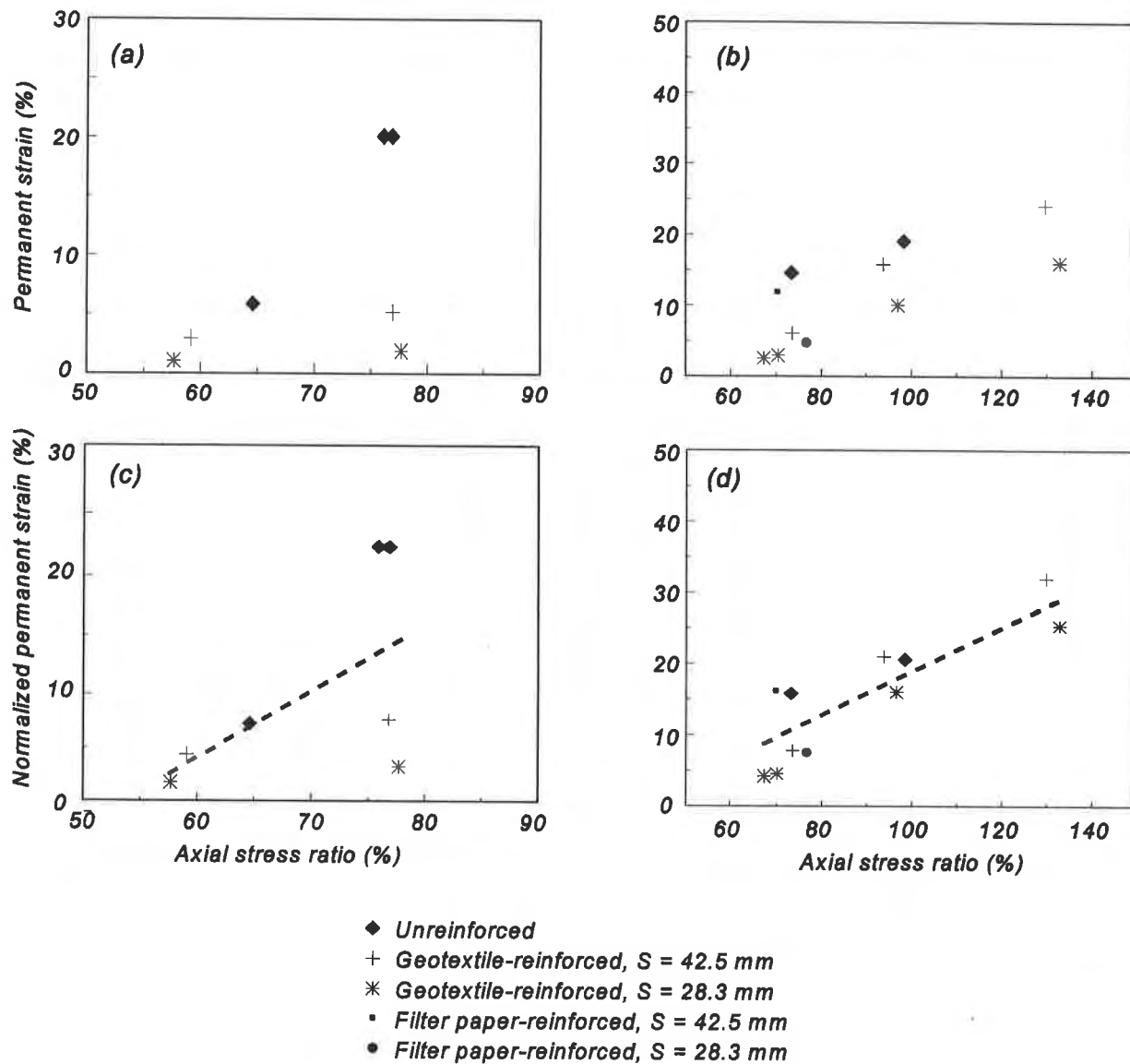
Figure 6. Permanent axial strain as a function of axial cyclic stress ratio: (a) measured, w_c=10% , (b) measured, w_c=13.5%, (c) normalized, w_c=10%, and (d) normalized, w_c=13.5%.

deformation of the soil is linked to the stress through an equivalent modulus. In other words, the material is modeled as an equivalent linear elastic material undergoing a strain ε_p when subjected to a stress σ_{cyc}. Because the wet-of-optimum soil was not as brittle as the dry-of-optimum soil, its behavior was more predictable. At high strain levels, for the unreinforced dry-of-optimum specimen, the specimen underwent excessively high deformation at high cyclic stress ratios, to the extent where it even becomes difficult to define a value for ε_p.

The analysis method can be applied toward the analysis of reinforced-soil structures provided that the assumptions made in the derivation are applicable. Although the solution may be modified

Table 3. Regression data for normalized cyclic test data.

Water content (%)	Constant	X-coefficient	Coefficient of correlation
10	-28	0.53	0.56
13.5	-14	0.33	0.87

for plane strain analysis if needed, it still provides an estimate of the relative improvement to be expected. However, for the large-scale structure under consideration, the mechanism of reinforcement has to be similar to that of the small-scale triaxial specimens presented in this study. Namely, the reinforcement has to extend across the loaded zone to provide an enhanced confinement condition once the shear stresses are mobilized along the interface. Such condition is present for instance in reinforced embankments where the reinforcement extends over the full width. For retaining walls and bridge abutments, an equivalent diameter or width of the structure has to be assessed based on either experience or numerical analyses. Once equivalent dimensions are established, the relative improvement can be estimated for different reinforcement materials and layer thicknesses.

For large-scale applications, it should be expected that the strength along the interface will be fully mobilized. The reason behind this is that at small overall strain levels for large-scale structures, the relative deformation at the interface between the soil and the reinforcement is likely to exceed the few millimeters needed to mobilize full interface strength. In the present solution, the reinforcement elements were assumed to be rigid. Although tensile elongation of the reinforcement should be expected for large-scale structures, it might not be necessary to account for this elongation since the response of the soil depends mainly on the strength mobilized at the interface, and not on the amount of elongation of the reinforcement. In cases where other reinforcement mechanisms such as membrane action or passive anchorage prevail the presented methodology should not be used.

It is also emphasized that predicting the response of reinforced soil masses under cyclic loading is not simple. Even when sophisticated models are implemented, high scatter in the prediction will always be present. Under cyclic loading conditions, the evolution of strains as a function of number of cycles is highly influenced by small initial variations in material properties and conditions. For instance, local initial defects are known to be the principal cause of faster degradation of materials, in general, under cyclic loading. The response of reinforced soil structures under cyclic loading in the field will be highly dependent on quality control during construction as well as long-term environmental conditions in the field. It should not, therefore, be expected that

accurate and reliable estimates of reinforced soil deformability or strength can be easily made without accounting for these sources of uncertainty.

SUMMARY AND CONCLUSIONS

Cyclic triaxial test results on geotextile-reinforced soil were performed to investigate the response of such materials under repeated loading conditions. The experimental study has shown that the inclusion of geotextile layers results in significant improvement in terms of the cyclic strength of the reinforced soil. A reduction in cumulative deformations as a function on number of cycles is observed when equally-spaced geotextile layers are placed within the soil specimen. This improvement in strength is mainly caused by the additional "enhanced" confinement as shear stresses are mobilized at the soil-geotextile interface. Experimental results also indicate that plastic strains cease to accumulate beyond roughly a thousand cycles, and that the shape of the strain vs. number-of-cylces curves is similar for the same soil. An equivalent normalized strain is formulated to predict the permanent deformation of the reinforced soil mass based on material and interface properties. The analytical procedure is yet to be extended for application in design and analysis of large-scale structures.

ACKNOWLEDGMENTS

REFERENCES

Ashmawy, A.K., and Bourdeau, P.L., 1995, "Geosynthetic-Reinforced Soils Under Repeated Loading: A Review and Comparative Design Study", *Geosynthetic International*, Vol. 2, No. 4, pp. 643-678.

Bathurst, R. J., Raymond, G. P., and Jarrett, P.M., 1986, "Performance of Geogrid-Reinforced Ballast Railroad Track Support", *Proceedings*, Third International Conference on Geotextiles, Vienna, Austria, Vol. 1, pp. 43-48.

Broms, B.B., 1977, "Triaxial Tests with fabric Reinforced Soil", *Proceedings*, International Conference on the Use of Fabrics in Geotechnics, Paris, France, pp. 129-134.

Davies, M.C.R., and Bridle, R.J., 1990, "Predicting the Permanent Deformation of Reinforced Flexible Pavements Subject to Repeated Loading", Performance of Reinforced Soil Structures, *Proceedings*, International Reinforced Soil Conference, Glasgow, pp. 421 425.

Giroud, J.P., and Noiray, L., 1981, "Geotextile-Reinforced Unpaved Road Design", *Journal of Geotechnical Engineering*, ASCE, Vol. 107, No. 9, pp. 1233-1254.

Houlsby, G.T., and Jewell, R.A., 1990, "Design of Reinforced Unpaved Roads for Small Rut Depths", *Proceedings*, Fourth International Conference on Geotextiles, Geomembranes and Related Products, The Hague, The Netherlands, Vol. 1, pp. 171-176.

Jaeklin, F.P., 1986, "Design of Road Base and Geotextile by Regression Analysis from Experience Data Sources", *Proceedings*, Third International Conference on Geotextiles, Vienna, Austria, Vol. 4, pp. 985-990.

Kharchafi, M., and Dysli, M., 1994, "The Mechanical Performances of Two Experimental Full-Scale Embankments Reinforced by Geotextiles", *Preprint*, Fifth International Conference on Geotextiles, Singapore.

Leflaive, E., 1985, "Sol Renforcé par des Fils Continus: le Texsol", *Proceedings*, Eleventh International Conference on Soil Mechanics and Foundation Engineering, San Francisco, Vol. 3, pp. 1787-1790.

Madani, C., Long, N.T., and Legeay, G., 1979, "Comportement Dynamique de la Terre Armée à l'Appareil Triaxial", *Proceedings*, International Conference on Soil Reinforcement, Paris, Vol. 1, pp. 83-88.

Mohamed, S.B., 1983, "An Absolute Calculation of the Rigidity Modulus of Protein Alginate Gels Using Forging Theory on Instron Data", *Journal of Texture Studies*, Vol. 14, pp. 353-376.

Raymond, G.P., 1992, "Reinforced Sand Behavior Overlying Compressible Subgrades", *Journal of Geotechnical Engineering*, ASCE, Vol. 118, No. 11, pp. 1663-1695.

USE OF GEOSYNTHETICS IN FAST-TRACK CONSTRUCTION OF RAILROAD SIDINGS OVER SOFT COMPRESSIVE ORGANIC SOILS

C.K. TAN
STS CONSULTANTS, LTD., USA

M.J. WHEELER
STS CONSULTANTS, LTD., USA

L.P. VANDER LEEST
WISCONSIN CENTRAL LTD., USA

ABSTRACT

Case histories are presented describing the use of geosynthetics for the design and construction of two railroad sidings in Wisconsin. The sidings measured 4,000 feet and 2,600 feet in length and required side slopes of 1.5H:1V and 2H:1V. Subsurface exploration indicated highly compressible organic soils of low shear strength beneath each of the sidings. A relatively rapid construction schedule was required at each site in addition to maintaining stability and operation of the adjacent mainline tracks. Instrumentation consisting of settlement plates and inclinometers was used along with vane shear testing to control the staged construction process and to evaluate performance. Geosynthetics contributed to the constructability of the projects as well as providing long term reinforcement of the siding embankments. Operation of the adjacent mainline tracks has not been adversely affected and instrumentation monitoring to date has shown successful performance of the siding embankments.

INTRODUCTION

During late 1994 Wisconsin Central Ltd. (WC) identified the need to construct extensions to two existing sidings at their Midway and Marsh sites. The Midway site is located in Walworth County, Wisconsin, in the Town of Midway. The Marsh site is located in the Town of Marsh in Washington County, Wisconsin. Figure 1 shows the general location of each of the siding sites. The sidings were required to increase efficiency of operation along heavily traveled corridor tracks. Construction of the siding extensions began in late 1995 and the sidings became operational during early 1996.

The siding extension constructed at the Marsh site measured approximately 2,600 feet in length with the Midway siding extension measuring approximately 4,000 feet. Centerline of the siding embankments was constructed 15 feet from the centerline of the corridor tracks. The height of the siding embankment at the Marsh site generally measured 8 to 10 feet with the Midway siding embankment height measuring 10 to 12 feet.

The siding sites at both Marsh and Midway are in low-lying areas identified as wetlands by the Wisconsin Department of Natural Resources (WDNR). Following lengthy discussions with the WDNR they became convinced that no practical alternate sites existed for construction of the sidings. Therefore, permission was granted to construct the sidings at the desired sites. As a condition for issuing permits for construction, the WDNR required that the exterior slopes of the siding embankments at Midway and Marsh be constructed at 1.5H:1V and 2H:1V, respectively, to minimize wetland impacts. Figure 2 shows a cross-section of the siding and corridor track embankments constructed at each of the sites.

SUBSURFACE CONDITIONS

Marsh Site. A total of 13 borings were drilled at this site. These borings were sunk along the eastern toe of the mainline track embankment. The borings were performed in two phases. The first-phase borings were drilled using a track-mounted drill rig in the winter when the ground was frozen. The second-phase borings were drilled in the early spring of 1995 using hand augers as the site was not accessible at this time to a drill rig that was bogged down on the very soft thawing surficial peat soils. In-situ vane shear tests were performed to determine pertinent soil strength parameters in several of the borings.

With the exception of the borings on the extreme north end of the siding site, significant thicknesses of organics were encountered during the subsurface exploration program. These organics typically extended to depths ranging between 3 meters and 5 meters or more below the ground surface. Figure 3 illustrates a typical soil profile of the subsurface conditions at the Marsh site. The surficial organics consisted of peat underlain by organic silt.

The peat layer generally had moisture contents ranging between 250% and 550%. In-situ vane shear tests indicated undrained shear strengths ranging between 2.5 kilopascal (kPa) and 15 kPa with remolded shear strengths ranging between 0 kPa and 5.0 kPa. Standard Penetration Test (SPT) values in the peat layer ranged between 1 and 5 blows per 30 cm penetration. A dry unit weight of approximately 2.0 kN/m^3 was determined with an estimated void ratio of 6.7. Results of a one-dimensional consolidation test on a representative sample of the peat layer indicated the material to be normally to slightly preconsolidated and highly compressible with a compression ratio of 0.45. The compression ratio is the slope of strain-versus-logarithm of pressure curve obtained from the consolidation test results.

The organic silt layer beneath the peat generally had moisture contents ranging between 200% and 300%. In-situ undrained shear strengths ranged between 12 kPa and 30 kPa with remolded shear strengths ranging between 2.5 kPa and 15 kPa. SPT values in the organic silt were generally 2 blows per 30 cm. The results of consolidated-undrained isotropically (CIU) triaxial test on a representative sample of the organic silt showed an undrained cohesion intercept of 7.5 kPa and a corresponding undrained friction angle of 20 degrees. In terms of effective stress, the organic silt had a drained cohesion value of 0 kPa and a corresponding drained friction angle of 28 degrees.

A high groundwater table generally existed along the siding site. Groundwater levels typically were found between depths of 0 meter and 1.8 meters.

Midway Site. Thirteen soil borings were advanced at the Midway site. Soil strength parameters in-situ were determined using vane shear testing in select borings. The borings were performed during the same period as for the Marsh site. They were also performed in two phases; Phase I was performed in the winter using a track-mounted drill rig, while Phase II was done in the early spring of 1995 using hand augers. A typical soil profile is shown in Figure 4.

The borings typically encountered organics, extending from the ground surface to depths as great as 9 meters. The organic soils consisted of peat, silts and clays. Moisture contents ranged up to 600% and organic contents up to 85% in the peat soils. The in-situ vane shear tests indicated shear strengths ranging between 7.5 kPa and 30 kPa with remolded shear strengths ranging between 0 kPa and 7.5 kPa. Dry unit weights ranging between 1.1 kN/m^3 and 2.5 kN/m^3 were determined on select peat samples. A compression ratio of 0.54 was determined on a representative sample of peat and the material was determined to be normally to slightly preconsolidated.

The results of a CIU triaxial test on a representative sample from the peat layer indicated an undrained cohesion intercept of 20 kPa and a corresponding undrained friction angle of 9 degrees. In terms of effective stress, the soil had a drained cohesion of 20 kPa and a corresponding drained friction angle of 18 degrees.

Groundwater levels at the site generally ranged from 0 meter to 1.5 meters below grade.

DESIGN ALTERNATIVES

Several different conventional design and construction options were considered during the preliminary stage of the projects. These included:

- completely removing and replacing of the highly compressible peat and organic soils with compacted fill;

- installing a wick drain or stone columns to accelerate consolidation of the organic deposits, and constructing the embankment section above using relatively low strength geotextile;
- constructing a conventional sheet pile or gravity retaining structure at the toe of the embankment.

These methods would require the use of relatively heavy construction equipment, some form of dewatering measures, and/or a temporary retaining system. These requirements would lead to prohibitive construction cost, longer construction time due to the very soft nature of the surficial peat, limited one-way access to the project sites and the need to maintain the stability and operation of the adjacent mainline tracks. For these reasons, the above conventional procedures were considered impractical.

It was decided that in order to meet the WDNR slope restriction condition and to meet the project time deadlines, a reinforced embankment that allowed the peat and organic soils to remain in place was the most practical alternative. Unlike some of the design and construction options described above, this option did not require the use of specialty contractors that would certainly increase the overall construction cost.

REINFORCED EMBANKMENT DESIGN

A properly designed reinforced embankment should have an adequate safety margin against global slope stability as well as internal stability of the reinforced mass. For both the Marsh and Midway sites, a typical slope section where the soft compressible organic deposits had the greatest thickness was selected for the evaluations. The global slope stability was analyzed using the computer program PCSTABL5 (1986) developed by Purdue University. The computer program uses limit equilibrium procedures to determine the minimum factor of safety. Both short- and long-term stabilities of the embankment slopes were analyzed using soil strength parameters obtained from the in-situ vane shear tests and the laboratory CIU tests. For the short-term analyses, the undrained field vane shear strength values were not corrected for strain rate and anisotropy effects, as suggested by Bjerrum (1972). This is because Bjerrum's correction factors were developed from data on soft clays, and are not necessarily applicable to highly plastic organic soils and peat. Instead of applying a strength correction factor to the measured undrained shear strength, the required minimum factor of safety for short-term loading and boundary conditions was increased from the customary value of 1.25 to a higher value of 1.5.

Due to bearing capacity concerns, it was decided that embankment construction at both siding sites should proceed in stages, consisting of placing the fill in a 2- to 3-foot height in any one stage to limit excess pore pressure development and to allow for excess pore pressure dissipation and consolidation of the foundation soils prior to placement of subsequent fill lifts. Based on results of the laboratory consolidation test, it was estimated that approximately 80% of

the excess pore pressure resulting from the 2- to 3-foot fill weight loading could be dissipated within a two-week period. Accordingly, the top few feet of the peat was assumed to have gained substantial strength from consolidation in the global slope stability analyses. The assumed strength gain was determined based on 90% consolidation. Results of the global slope stability analyses are summarized in Table 1. At both the Marsh and Midway siding sites, the computed minimum factor of safety of the reinforced embankment slope exceeded the established minimum acceptable value of 1.5.

Table 1. Results of Limit Equilibrium Slope Stability Analyses

Site	Side Slope Inclination	Drainage and Loading Condition	Failure Mode	Minimum Safety Factor	
				Unreinforced	Reinforced
Marsh	2.0H to 1.0V	Undrained	Block	1.1	1.5*
		Undrained	Circular	1.2	1.6*
		Drained	Block	1.5	1.8*
		Drained	Circular	1.8	2.0*
Midway	1.5H:1.0V	Undrained	Block	0.92	1.7
		Undrained	Circular	0.85	1.6
		Drained	Block	1.2	2.2
		Drained	Circular	1.2	2.0

* Notes: [1] A 90% strength increase in the top 2 feet of peat material was assumed due to consolidation effect.
[2] A minimum safety factor of 1.5 is required for undrained and drained conditions.
[3] Assumed three layers of geogrid, substituted with equivalent geotextile material during construction.

The length and vertical spacing of the geotextiles or geogrids required to provide internal stability of the embankment were determined using the procedure developed by Nelton Limited as given in the Geotextile Engineering Manual (1985). Granular fill was assumed in these calculations. Selection of the geotextile or geogrid was based on strength, permeability, survivability and ultraviolet degradation requirements. Typical reinforced embankment slope sections at the Marsh and Midway sites are shown in Figures 5 and 6, respectively. The required geotextile and geogrid material properties are given in Table 2.

Table 2. Geotextile and Geogrid Material Properties

Site	Material	Minimum Wide Width Tensile Strength (ASTM D 4595)	Minimum Puncture Strength (ASTM D 3787)	Minimum Permittivity (ASTM 4491)	Minimum Grab Strength (ASTM 4632)
Marsh	Geotextile	25 kN/m	0.53 kN	0.2 sec^{-1}	1.32 kN
	Geogrid*	12.5 kN/m (machine direction)	--	--	--
Midway	Geotextile	30 kN/m	0.53 kN	0.2 sec^{-1}	1.32 kN
	Geogrid*	12.5 kN/m (machine direction)	--	--	--

* Provided at base of embankment primarily for constructability purpose.

CONSTRUCTION

Construction Schedule. The construction schedule called for the trackage of Midway and Marsh to be placed in service as quickly as practicable. With winter approaching, it was decided to complete the grading, drainage, and placing of sub-ballast prior to freeze up. The Wisconsin Central Ltd. track forces could then work through the winter months placing the track materials on the furnished grade. Early in spring the ballast could be distributed, the track lined and surfaced, and raised to the required elevation, the new track could then be placed into service to benefit train movements on this busy transportation corridor.

Construction Sequence. Construction of the sidings at Marsh and Midway sites commenced on October 2, and October 26, 1995, respectively. The first phase of the construction involved removal of bushes and trees within the right-of-way of the new sidings, but leaving behind the root system and stump that would provide additional reinforcement to the embankment slope. This was then followed by placing a layer of geogrid at the base from the north to south end of the project site. The geogrid was provided primarily for constructability reasons, as it helped to provide access for construction equipment into the project sites.

A layer of select woven geotextile material was then laid over the geogrid. The first layer of fill was brought in by trucks and allowed to end dump and spread carefully over the geotextile using a light dozer. Due to the presence of groundwater, more than 2 feet (or 0.6 meters) of fill was allowed in the first lift operation. This first lift of fill was placed with only moderate compaction effort so as to prevent potentially damaging the underlying geotextile material.

Settlement plate and inclinometer readings along with in-situ vane shear testing were periodically performed during and within several days after placement of the fill to confirm that the foundation soils had gained sufficient strength to allow the placement of the subsequent fill.

The above process was then repeated until the full height of the embankment fill was attained. The subsequent fill was compacted using a vibratory roller. Field density tests were performed to confirm that a minimum compaction effort of 90% was attained based on the modified Proctor maximum dry density.

For proper anchorage, the geogrid and geotextile were extended at least 2 feet on to the existing mainline slope. A minimum of 3-foot overlap was allowed between two adjoining geotextile material.

FIELD MONITORING

Settlement Plates and Inclinometers. Two monitoring stations were selected at both Marsh and Midway siding sites to monitor the stability of the new fill embankment as it was being constructed. The monitoring results were also utilized to help determine when the staged construction process was ready for the next fill lift placement. Instrumentation installed at each of the monitoring stations included an inclinometer and several settlement plates and heave markers. The inclinometers were installed near the toe of the new siding embankment prior to fill placement. Since it was impossible to mobilize even a track-mounted drill rig to the site, these inclinometers were installed in holes made by hand augering. As a result, the bottom of these inclinometers was located within the soft organic clay layer due to practical limitation of hand augering equipment. However, the location at the top of the inclinometer casing was checked during each reading using a 'triangular' procedure with the other two survey points located far away from the construction.

At the Marsh siding site, maximum lateral deflections of 2.0 and 3.5 inches were observed at the two inclinometers locations when the siding embankment was completed to the proposed sub-ballast elevation with approximately 8 feet (or 2.4 meters) of fill in place. It appeared that most of the lateral movements occurred within a depth of 10 feet below the embankment toe grade. The maximum lateral movement, however, was measured at depths between 8 and 9 feet. At the Midway siding site, about 2 inches of maximum lateral deflection was observed at the inclinometer installed at Station 14+18. However, a relatively smaller maximum lateral deflection of 0.6 inch was recorded at the other inclinometer location. Again, the lateral movements occurred within the soft peat material.

The inclinometer readings along with field observation records clearly indicated that there was very little "mud wave" occurring during the fill placement. This could be due to the reinforcement effect on the soft peat and organic soils by leaving the rooting system and tree stump in place during the site preparation work and also with the use of geogrid and geotextile material. The greatest horizontal movements generally occurred near the top of the organic silt layer. Typical results of the inclinometer reading are shown in Figure 7.

At both the Marsh and Midway sites, approximately 3 to 4 feet of embankment fill was already in place when the settlement plates were installed. At Marsh site, the measured settlement ranged from 3.2 to 6.8 inches between October 9 and November 29, 1995, when the new siding embankment was raised to a height of 8 feet. The recorded settlement at the Midway site ranged from 3.2 to 16.8 inches (typically more than 8.5 inches) between the period of November 7 and December 1, 1995. During this period, the embankment fill was raised from about 3.5 feet to 8.0 feet. As expected, settlements at the Midway site were greater than those observed at the Marsh site as much thicker compressible soft foundation soils were found at the former site. Prediction of settlement due to fill placement at each site prior to construction proved difficult due to the complex drainage conditions within the organic soil layers and secondary consolidation characteristics of these materials. Settlement was also affected by the degree of lateral squeezing which occurred. However, recorded settlements were much less than what was expected.

Based on the above field settlement monitoring results, it was estimated that a maximum settlement of 14 and 32 inches would have occurred at the Marsh and Midway sites, respectively, from the placement of the 8-feet embankment fill. Additional settlements could be expected from immediate compression of the foundation soils and fill due to the soil weight of the ballast and sub-ballast material, and also from the subsequent consolidation and creep of the underlying peat and organic clay. Since the actual amount of lateral squeezing (or mud wave) during construction was much smaller than what was anticipated, the total maximum settlements of the sidings at the two sites are expected to be somewhat smaller than the predicted values of 3 to 5 feet estimated using laboratory testing results.

Field Vane Shear Test During Construction. The strength of the underlying peat material was tested using a Geonor Vane Borer during the filling process. This testing was used, in conjunction with the settlement and inclinometer readings, as a means to help determine when the next lift of fill could be placed. Results from the field vane testing indicated that approximately 50% to 80% of strength increase was obtained within a week after each lift of fill was placed. This consolidation rate was much faster than the predicted rate of two to three weeks based on results from one-dimensional laboratory consolidation test data and assuming two-dimensional drainage in the field. This may be due to the fact that a three-dimensional drainage condition was more likely prevailing in the field. The highly fibrous nature of the peat could also have contributed to the acceleration of the consolidation process.

CONSTRUCTION COSTS

Midway grading costs amounted to $435,000 that covered placement of 37,000 tons of granular material for track, geogrid and geotextile fabric along with the associated labor to complete the construction of the track embankment. The geosynthetics amounted to approximately $70,000 which was about 15% of the total cost of the grading and in turn resulted in only 5% of the entire track project.

Marsh grading costs were about $235,000 and like Midway's covered the required materials to completed placement of fill material as outlined in the bid specifications. The cost of the geosynthetics placed at this location amounted to $45,500 which was about 18% of the grading costs. The area adjacent to the siding site was a wildlife area which resulted in slightly higher costs to place the geosynthetics. The WDNR raised the water elevation in the area to attract the migrating water fowl, making placement of geosynthetics a little more difficult. However, the cost to place geosynthetics amounted to 6% of the total cost of track construction.

PERFORMANCE AND CONCLUSIONS

The use of geosynthetics allowed relatively rapid staged construction of the Marsh and Midway sidings over highly compressible soils of low shear strength. In addition, slope design requirements were met with use of geosynthetics as embankment reinforcement. Operation of the mainline corridor track embankments was not adversely affected both during the construction process and following completion of construction. The siding embankments are currently being effectively used and instrumentation monitoring has confirmed successful performance. WC operations were not affected by the construction with only minor track maintenance being required following construction.

Geosynthetic use at both the Marsh and Midway sites allowed significant cost savings when compared to other design and construction alternatives. Cost evaluation of other specific design types was not performed since the other design alternatives would have been substantially more expensive based upon information provided by various contractors. The cost to place geosynthetics at each of the project sites was only 5% to 6% of the total cost of the track construction.

ACKNOWLEDGMENTS

REFERENCES

Bjerrum, L., (1972) "Embankment on Soft Ground: State-of-the-Art Report," American Society of Civil Engineers Specialty Conference, Performance of Earth and Earth-Supported Structures, Purdue University, Vol. 2, pp. 1 - 54.

Carpenter, J.R., (1986) PCSTABL5 User Manual , Joint Highway Research Project, Purdue University and Indiana Department of Highways, 47 pp.

Christopher, B.R. and Holtz, R.D. (1985) Geotextile Engineering Manual, Federal Highway Administration, U.S. Department of Transportation, Vol. 2, Appendix D, pp. D-7 - D-26.

FIGURE 1: SIDING LOCATION SITES
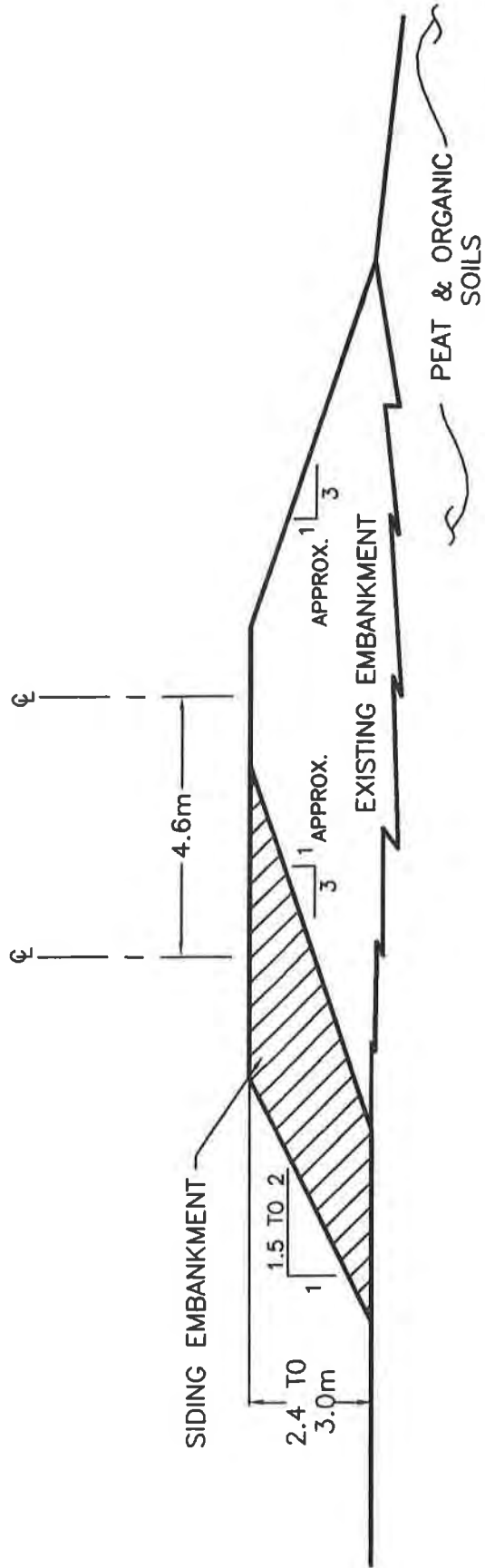
FIGURE 2: TYPICAL CROSS SECTION OF EXISTING TRACK
EMBANKMENT AND NEW SIDING
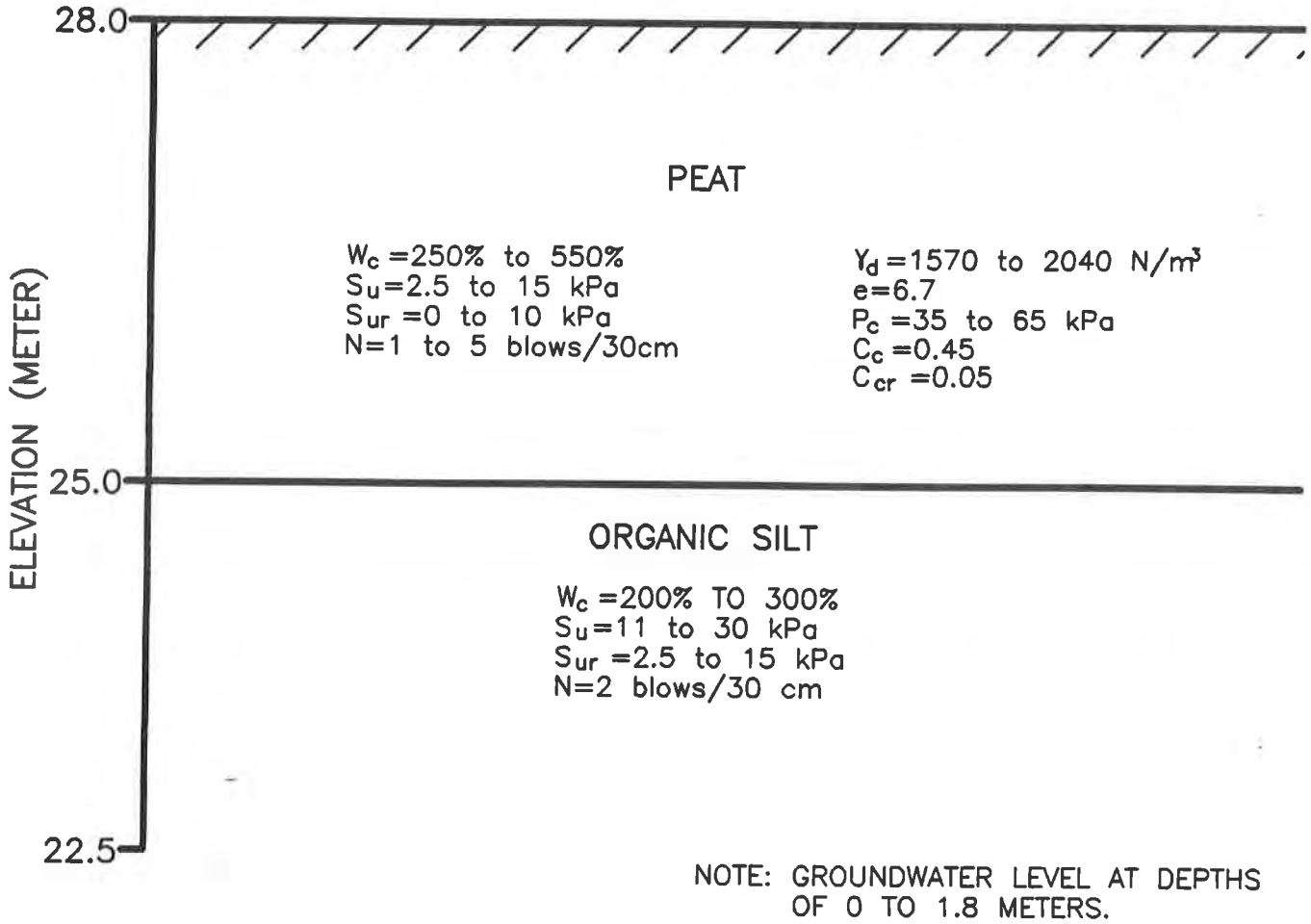
FIGURE 3: TYPICAL SOIL PROFILE — MARSH SITE

PEAT

W_c =350% TO 600%
S_u =7.5 to 30 kPa
S_{ur} =0 to 10 kPa
N=2 blows/30cm

γ_d =1570 to 3140 N/m³
e=7.6
P_c =30 to 55 kPa
C_c =0.54
C_{cr} =0.036

ORGANIC SILT

W_c =70% TO 600%
S_u =20 to 60 kPa
S_{ur} =1.5 to 7.5 kPa
N=4 to 6 blows/30cm

PEAT

W_c =200% to 600%
S_u =15 TO 20 kPa

SILTY CLAY/CLAYEY SILT
S_u =15 kPa W_c =50%

FINE TO MEDIUM SAND
N=13 blows/30cm
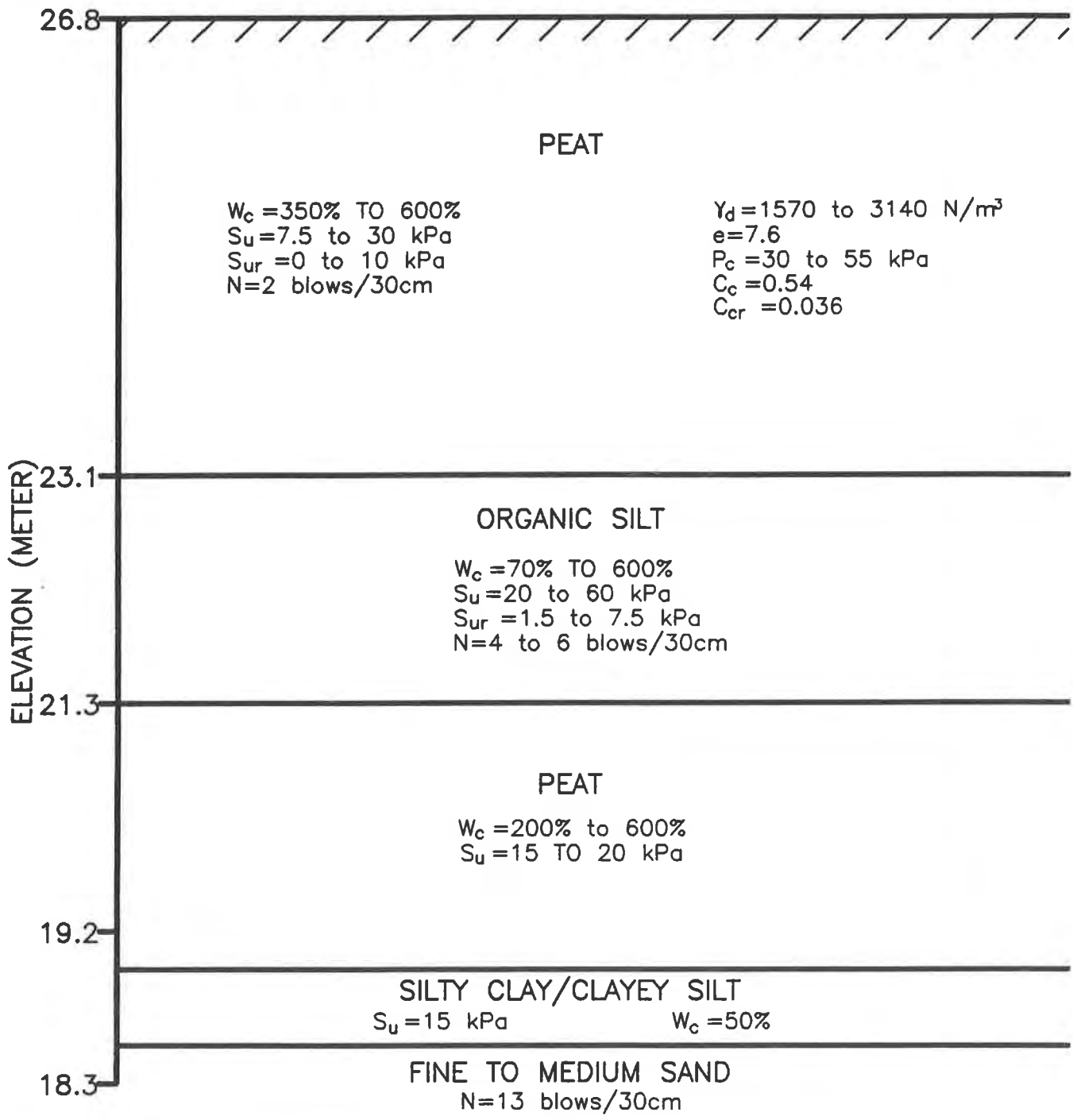
NOTE: GROUNDWATER LEVEL AT 0
TO 1.5m BELOW GRADE.

FIGURE 4: TYPICAL SOIL PROFILE — MIDWAY SITE

ELEVATION (METER)

26.8
23.1
21.3
19.2
18.3
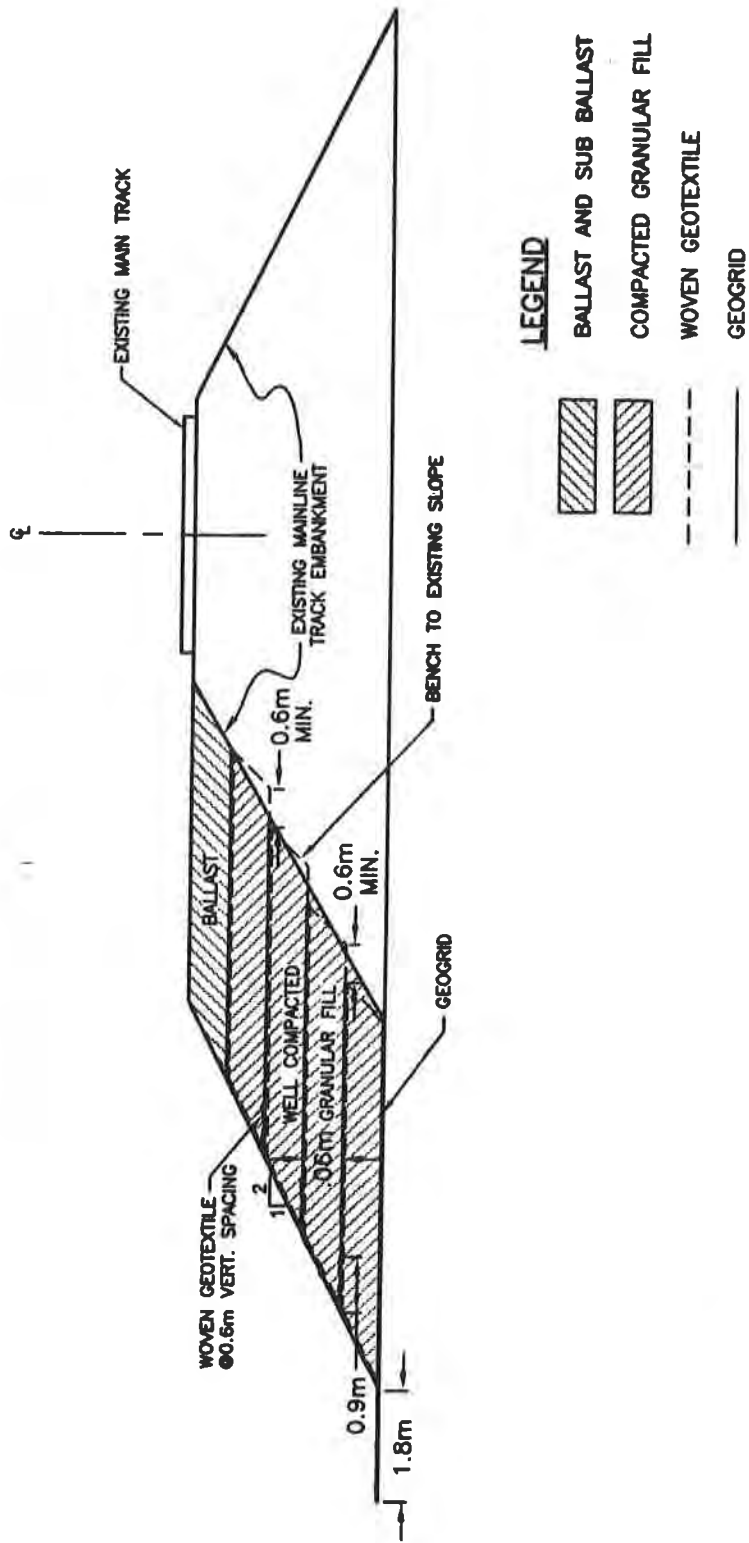
FIGURE 5: REINFORCED EMBANKMENT CROSS-SECTION DESIGN — MARSH SITE
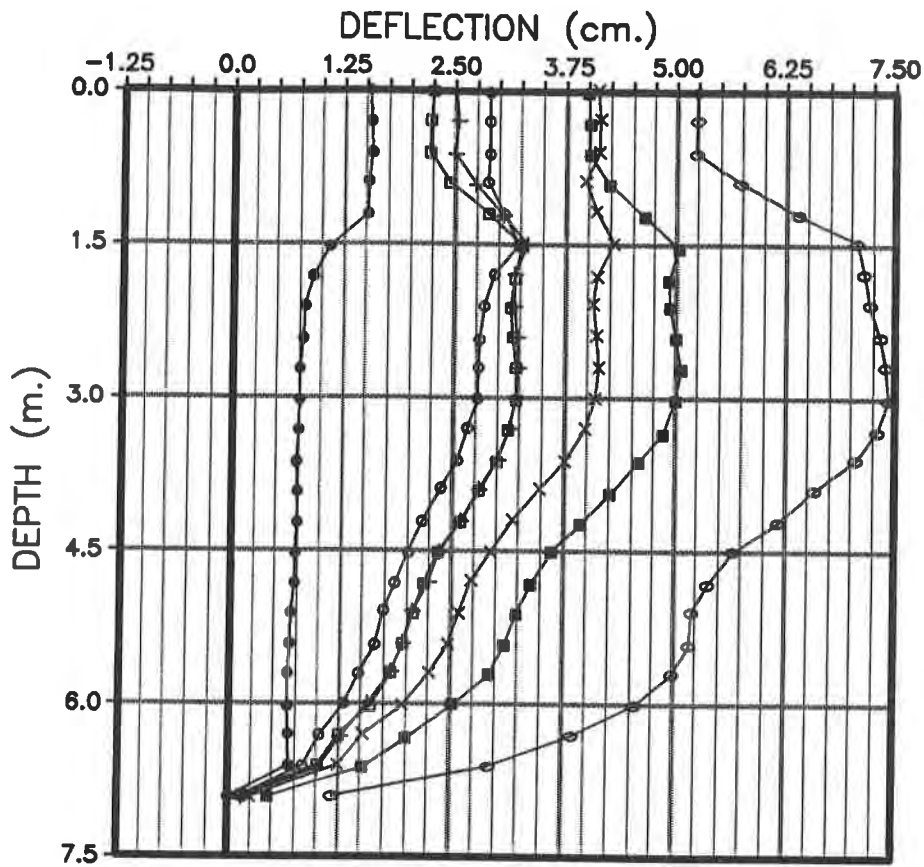
FIGURE 6: REINFORCED EMBANKMENT CROSS-SECTION DESIGN – MIDWAY SITE

FIGURE 7: TYPICAL INCLINOMETER MONITORING RESULTS

THE COST EFFECTIVENESS OF SEPARATION GEOTEXTILES: 9-YEAR UPDATE

C. J. SPRAGUE, P.E.
SPRAGUE & SPRAGUE CONSULTING ENGINEERS
GREENVILLE, SC, USA

ABSTRACT

In July 1987, Greenville County, South Carolina constructed a test road using low-cost pavements which included geotextile separators between the subgrade and the pavement structure. Three pavement cross-sections and three different types of geotextiles were evaluated in a 2500 m (8100+ ft) long trial section.

Visual pavement condition surveys have been made of the trial installation since its initial construction. In year 8, the entire road was resurfaced. Prior to resurfacing, localized areas of substantial distress were repaired or reconstructed, as required.

After 9 years, low-cost, light-weight geotextiles appear to be providing subgrade/base interface stability which has generally decreased the cost of pavement maintenance by 5 to 15% when compared to road sections without separation geotextiles.

INTRODUCTION

A trial installation was made on a 2500 m (8100+ ft) long low volume county road. The trial was undertaken to investigate low-cost pavement structures which incorporate separation geotextiles and has produced useful data related to survivability and short-term performance as reported by Sprague and Cicoff (1989, 1993) and Cicoff and Sprague (1991). An additional purpose of the trial was to assess the relative long-term performance of different pavement cross-sections with and without separation geotextiles.

The long-term performance of the installation has been determined through periodic inspections of the road surface. The road surface condition was characterized and ratings were entered into the County's Pavement Management System (PMS) for various segments of the road. The PMS then dictated the timing and type of maintenance of the various road segments. This allowed for the assessment of the ability to reduce maintenance costs when geotextiles are used with low cost pavement structures. The maintenance cost savings can then be compared to the nominal additional cost of including a geotextile.

INSTALLATION LAYOUT

Stockton Road, in southern Greenville County, South Carolina, was selected for this trial installation because it had been surfaced with aggregate twice in the preceding 18 months and was once again in need of additional surfacing. This indicated that the road subgrade was unstable when saturated and could benefit from the installation of a separation geotextile. The subgrade was a prodominantly silt and silty clay. Cone penetrometer measurements indicated typical strengths of 12 to 15 psi in the upper 1 to 2 inches of the subgrade .

The following cross-sections were used on approximately one-third of the road each:

-   65 mm (2-1/2 in) full depth asphaltic concrete binder course.

-   40 mm (1-1/2 in) asphaltic concrete surface course over 75 mm (3 in) compacted stone base.

-   25 mm (1 in) triple treatment surface course over 75 mm (3 in) compacted stone base.

Triple treatment is a surfacing technique used in South Caroline which involves three successive applications of asphalt emulsion and 10 mm (3/8 in) and smaller aggregate. After each application of aggregate, the surface is rolled with steel wheeled and pneumatic tired rollers.

After regrading the existing road surface, approximately 150 m (500 ft) of each type of geotextile was installed between the subgrade and each pavement section. The remaining areas of the road were used as a control for the long-term evaluation of each pavement section.

Typical properties of the separation geotextiles used are shown in Table 1.

Table 1. Typical properties of separation geotextiles

| | | Geotextile Designation | | |
| | | A | B | C |
Property	ASTM Method	Needle-punched Nonwoven	Slit-Film Woven	Needle-punched Nonwoven
Weight, g/m^2	D5261	140	140	200
Grab Strength, N	D4632	600/490	890/890	910/780
Grab Elongation, %	D4632	70/85	20/18	75/85
Puncture, N	D4833	270	360	400
Trap Tear, N	D4533	270/220	290/290	360/330
Mullen burst, kPa	D3786	1450	2650	2170
Water Flow, $l/min/m^2$	D4491	5700	200	5300
AOS, mm	D4751	.210	.425	.210

MONITORING PAVEMENT PERFORMANCE

In order to characterize the relative long-term performance of the various pavement sections and the appropriate level of maintenance to be employed at

the time of resurfacing, it was necessary to periodically inspect the road surface to track degradation. An objective visual inspection program was initiated. The program included quantitative assessments of the pavement surface by trained technicians performed on a periodic basis. The quantitative assessments were entered into a computerized pavement management system to facilitate tracking of the pavement performance relative to the other 2200+ km (1400+ miles) of roads in the county.

PAVEMENT CONDITION EVALUATION

Greenville County utilizes a computerized pavement management system as described by Sprague and Cicoff (1993). The basic data entered on the various pavement sections rely on surface distresses. Their quantity and severity establish the overall quality of a pavement. The pavement condition index, or PCI, is established on a ranking scale from 0 to 100. Pavement condition information is entered into and weighting and projecting calculations, and generation of priority listings are expeditiously handled by the computer program.

The PCI rankings of the pavement excluded distresses that are not related to the overall structural performance of the pavement. For purposes of this report, sample units without areas damaged by construction, utility work, and other localized distresses were intentionally selected. Sample units within each test section included the entire road width and contained approximately 240 m^2 (2600 ft^2). The sample units selected were typical of the pavement within each section. The results of PCI evaluations on various segments on Stockton Road are shown in Table 2. The data shows the gradual degradation of road surface to year 8 at which time the entire road was resurfaced, returning the PCIs of each test section to 100.

Table 2. Pavement condition survey results

Years of Service	65 mm Full Depth				40 mm over 75 mm Base				Triple Treatment			
	Cntrl	A	B	C	Cntrl	A	B	C	Cntrl	A	B	C
0	100	100	100	100	100	100	100	100	100	100	100	100
2	81	80	74	-	-	-	-	-	-	85	78	-
2.5	76	85	50	69	84	83	86	87	68	-	-	70
4.75	72	76	0	-	76	77	80	-	59	52	61	-
5.75	45	69	0	34	70	68	68	78	43	46	55	56
8	34	57	0	28	50	51	45	51	21	32	35	33
8	100	100	100	100	100	100	100	100	100	100	100	100
9	90+	90+	90+	90+	90+	90+	90+	90+	90+	90+	90+	90+

PROJECTING RATE OF DETERIORATION

A pavement performance curve characteristic of Greenville County roads was generated using PCI data on all 1400+ miles of roadway within the County's inventory. This deterioration rate curve is subsequently used to project the expected pavement performance for each pavement section using intermittent field evaluations. The general pavement performance curve is shown in Figure 1.
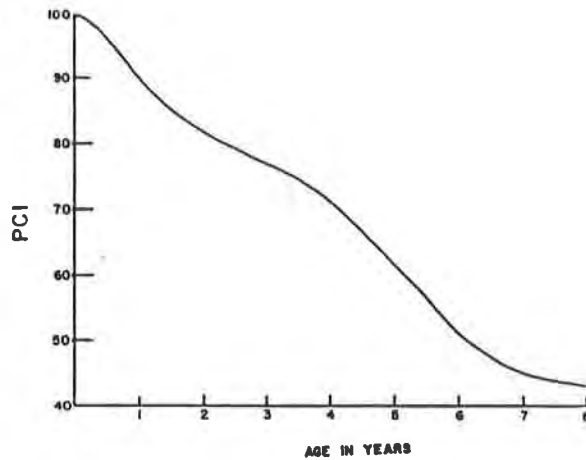
Figure 1. Pavement performance curve for Greenville County Roads

PAVEMENT PERFORMANCE

Full-depth Asphalt. The performance of the road section constructed of a 65 mm thick of asphaltic binder varied widely. The section underlain by the 140 g/m^2 nonwoven geotextile deteriorated at the slowest rate, followed by the control section, the section underlain by the 200 g/m^2 nonwoven geotextile and the section underlain by the slit film geotextile. The slit film material, because of its relatively slick surface which lead to slippage of the asphalt layer during placement, proved to be a detriment to a full depth asphalt pavement.

Asphalt over Stone Base. The performance of the road section constructed of a 40 mm asphaltic wearing course over the 75 mm stone base contained far less deviation than the other types of pavements. The sections incorporating woven and non-woven separation geotextiles performed similarly to the control section.

Triple Treatment over Stone Base. Where triple-treatment was constructed over a 75 mm stone base, pavement deterioration proceeded most rapidly. The sections incorporating separation geotextiles performed similarly. They all significantly outperformed the control sections. It should be noted that the triple treatment produces a relatively rough, coarse surface texture which is somewhat difficult to evaluate.

Comparing Pavement Types. The County had expected the pavements to achieve have life of 15 years (to PCI= 50). Yet, all sections performed below expectations by showing a rather rapid decrease in quality. Under the control conditions, the best overall performance was achieved by using a 75 mm stone base, with a 40 mm thick asphalt surfacing overlay. The full depth asphalt binder material, which was expected to have equal performance characteristics, experienced somewhat higher rates of deterioration overall, but actually provided the best performance of all test sections when constructed over geotextile A.

Although triple-treatment provides an all weather surface and protects the subgrade from moisture related failures, overall it performs very poorly as a structural material. Being the most flexible of the three designs, it was especially susceptible to rutting and associated distresses.

INITIAL CONSTRUCTION COSTS

Table 3 details the costs of constructing the pavements utilized in this test. Comparable direct and contracted prices for similar installations are currently being experienced. All hot-laid asphalt materials, as well as the geotextile and base under these materials, were placed in conjunction with the County's annual resurfacing program by a private contractor. The costs associated with construction of the triple treatment section reflect county labor, equipment and materials.

MAINTENANCE BASED ON PAVEMENT CONDITION

In Greenville County, as in many communities, the timing of pavement resurfacing, including associated repair and rehabilitative work is based on the availability of funding, the location of the road, and the road's pavement condition relative to other roads. Therefore, a road - or sections of a road - may deteriorate substantially prior to being included on the list of roads to be resurfaced in any particular year.

The extent and, therefore, cost of maintenance required to return a road to "as new" condition increases with decreasing pavement condition. The County must estimate the cost of this maintenance for all roads being considered for resurfacing in any given year so that a list of roads to be included in a given year's paving program can be developed for the available funding. Road locations and the amount of each type of maintenance activity are important details which must be included in the bid package for the annual paving program. A standard maintenance guide, such as shown in Table 4, relates the pavement condition to the type and cost of maintenance and facilitates the initial estimate of costs based on projected PCIs. Projected PCIs and the actual extent of proposed maintenance activities are verified by field observation.

Table 3. Stockton Road Initial Construction Cost Data ($/m^2)

Cost Basis	65 mm Full Depth				40 mm over 75 mm Base				Triple Treatment			
	Cntrl	A	B	C	Cntrl	A	B	C	Cntrl	A	B	C
Geotextile:												
Labor	–	.07	.07	.07	–	.07	.07	.07	–	.07	.07	.07
Material	–	.48	.48	.66	–	.48	.48	.66	–	.48	.48	.66
Base:												
Labor	–	–	–	–	–	–	–	–	.27	.27	.27	.27
Material	–	–	–	–	–	–	–	–	2.32	2.32	2.32	2.32
Equipment	–	–	–	–	–	–	–	–	.59	.59	.59	.59
Subcontract	–	–	–	–	2.74	2.74	2.74	2.74	–	–	–	–
Surface:												
Material	–	–	–	–	–	–	–	–	2.15	2.15	2.15	2.15
Equipment	–	–	–	–	–	–	–	–	1.02	1.02	1.02	1.02
Subcontract	4.19	4.19	4.19	4.19	2.13	2.13	2.13	2.13	–	–	–	–
Total	4.19	4.74	4.74	4.92	4.87	5.42	5.42	5.60	6.35	6.90	6.90	7.08

Table 4. Pavement maintenance cost schedule

PCI	Required Maintenance Activity	Cost ($/m²)
61 - 100	40 mm asphalt overlay	3.48
51 - 60	40 mm asphalt overlay w/ paving fabric	4.39
41 - 50	40 mm asphalt overlay w/ paving fabric & full depth patching (6.25%)	5.39
31 - 40	40 mm asphalt overlay w/ paving fabric & full depth patching (12.5%)	6.40
21 - 30	40 mm asphalt overlay w/ paving fabric & full depth patching (25.0%)	8.41
11 - 20	40 mm asphalt overlay w/ paving fabric & full depth patching (50.0%)	12.43
< 11	40 mm asphalt overlay w/ paving fabric & reconstruction	20.49

Unit Costs: 40 mm asphalt overlay @ $3.48/m²
paving fabric (installed) @ $0.91/m²
full depth patching / reconstruction @ $16.10/m²

EQUIVALENT UNIFORM ANNUAL COSTS

To account for different initial and maintenance costs when comparing pavement alternatives an annual cost comparison technique was chosen. The Equivalent Uniform Annual Costs (EUAC) were calculated for each pavement test section using both initial construction costs and maintenance costs incurred in year 8. The assumptions include an interest rate, i, of 7.5% and a resurfacing and/or restoration cost as shown in Table 4 depending on the given section's condition. The following equation by Newman (1977) was used to calculate EUAC:

$$EUAC = P(A/P,i,n) - F(A/F,i,n)$$

where: P = initial cost,
$A/P = i(1+i)^n / [(1+i)^n-1]$
$F = P - $ restoration cost
$A/F = i / [(1+i)^n-1]$

Table 5 summarizes the Equivalent Uniform Annual Costs for the various pavements installed for this project. The 60 mm full depth binder over the 140 g/m² nonwoven geotextile demonstrated significantly lower equivalent annual costs than the control pavement section. The conformability of the nonwoven may have assured continuity at the subgrade/pavement interface. The 200 g/m² nonwoven underperformed the control section, though poor road side drainage conditions were noted adjacent to the areas of maximum distress. The 140 g/m² woven slit film material was not suitable for use under full depth pavement.

For the pavement section constructed of a 40 mm asphaltic wearing surface over a 75 mm stone base, the equivalent annual costs were lowest for road sections utilizing a nonwoven separation geotextile. This indicates that the presence of a separation geotextile at the subgrade/stone base interface can enhance overall pavement performance. The slit film woven geotextile section slightly underperformed the other sections. Its performance may have been affected by its installation on a curve and slight grade.

The performance of triple-treatment over the 75 mm stone base has demonstrated a clear equivalent annual cost benefit when utilizing separation geotextiles when compared to no geotextile at all. The inherent flexibility of the triple-treatment section may benefit the most from the incorporation of a separation geotextile.

Table 5. Stockton Road, Cost Data and Pavement Lifecycle Costs ($/m^2)

	65 mm Full Depth				40 mm over 75 mm Base				Triple Treatment			
	Cntrl	A	B	C	Cntrl	A	B	C	Cntrl	A	B	C
Initial Cost	4.19	4.74	4.74	4.92	4.87	5.42	5.42	5.60	6.35	6.90	6.90	7.08
Maint. Cost (Yr. 8)	6.40	4.39	20.49	8.41	5.39	4.39	5.39	4.39	8.41	6.40	6.40	6.40
EUAC @ i=7.5%	0.93	0.78	2.31	1.17	0.88	0.83	0.92	0.84	1.28	1.13	1.13	1.14

CONCLUSION

Geotextiles provide subgrade/stone base interface stability which will generally increase the life and, therefore, reduce the maintenance costs of a pavement section. In most cases, life cycle costs for pavements incorporating separation geotextiles were lower than the costs associated with the control sections which did not utilize geotextiles. As expected, the greater the restoration cost, the greater the EUAC benefit of using separator geotextiles. Therefore, in general, it appears that the additional costs associated with including a separation geotextile are more than offset by the reduced life-cycle costs of the road. Annual cost savings ranging from 5 to 15 percent can be expected when using an appropriate separation geotextile with low volume paved roads.

ACKNOWLEDGMENT

REFERENCES

Cicoff, G. A. and Sprague, C.J. (1991), "Permanent Road Stabilization: Low-Cost Pavement Structures and Lightweight Geotextiles," Proceedings of the Fifth International Conference on Low-Volume Roads, TRR No. 291, Transportation Research Board, pp 294-310.

Newman, D.G. (1977), Engineering Economic Analysis, Engineering Press, p. 104.

Sprague, C.J. and Cicoff, G.A. (1989), "A Study of Permanent Road Stabilization: Low Cost Pavement Structures and Lightweight Geotextiles", Proceedings of Geosynthetics `89, San Diego, IFAI, pp. 316-323.

Sprague, C.J. and Cicoff, G.A. (1993), "A Study of the Cost- Effectiveness of Using Separation Geotextiles in Permanent Road Structures", Proc. of Geosynthetics `93, Vancouver, IFAI, pp. 49-63.

(Conversion: $/m^2 = 1.196 x $/yd^2)

Data Base Development for Determination of Long Term Benefit/Cost of Geotextile Separators

George R. Koerner
Geosynthetic Research institute, Drexel University, USA

KEY WORDS Geotextiles, separators, highway, long term, benefit/cost

ABSTRACT

The status of geotextiles used as separators in pavement cross sections has been described as being significantly underutilized. While geotextiles have been used as separators between soil subgrade and stone aggregate for over 25 years, their long term effectiveness have rarely been quantified. Thus a nationwide study is underway to assess geotextile performance in this application.

The intention of this paper is to describe how the background information is tabulated, how the performance of the pavements are being assessed and how the data is being analyzed for long term benefit/cost. A secondary goal of this paper is to serve as a solicitation for additional sites since a 20-year project is envisioned and this is the first exposure of the plan and its objectives.

INTRODUCTION

Proponents of geotextiles located between the soil subgrade and stone aggregate base course of highway pavements have suggested increased pavement life over the comparable situation in the absence of a geotextile. Indeed, some data is available in this regard, however, most is antidotal and qualitative. It is felt that a large data base is needed to assess the performance with and without geotextile separators at the same location and then a quantitative assessment of the performance of the respective sections over the lifetimes of the roadway is necessary. Even further, this assessment should be national in its scope. Thus all types of traffic, subgrade, climatic and environmental conditions can be included in the assessment. The situation is greatly heightened with the recent advent of design- build -maintain contracts for new and remedial construction of primary highways. In this regard, the successful contractor has the choice of the nominally higher initial cost with a geotextile, or the possibility of an ongoing and expensive maintenance program. In the author's opinion, the use of a geotextile should always be considered when using open graded stone base courses placed directly on soil subgrade.

The concept of geotextile separation can be illustrated by two simultaneous mechanisms that tend to occur over time. The first is that the subgrade soil tends to intrude into the voids of the stone base thereby compromising its drainage capacity. The second is that the stone base attempts to penetrate into the subgrade soil thereby compromising its strength. In both cases, the stone base is no longer effective when it is contaminated with fine grained particles from the subgrade soil from both drainage and strength perspectives. Therefore, the concept of including a geotextile to separate dissimilar materials so that the integrity and functionality of the stone base can remain as intended and designed seems to be intuitive but unfortunately is not quantified at this time.

While isolated case histories investigating the above geotextile application have been reported in the open literature, it is felt that a study to identify, characterize, and quantify the actual field performance of geotextiles installed as pavement separators is warranted.

It is envisioned that this study will be ongoing for up to 20 years. It should be recognized that the sites will take 5 to 10-years to show signs of pavement distress and/or deterioration. While project size is not particularly important, it is necessary to have sites which have an associated control section where no geotextile is placed for comparison purposes and to have a sufficient number of sites to develop a meaningful statistical data base.

BACKGROUND

In any engineering textbook on highway pavement design one will always note the use of stone base beneath the concrete or asphalt pavement surface. For concrete pavements, the purposes of the stone base are lateral drainage and a transition between the brittle behavior of the concrete and the plastic behavior of the subsoil. For asphalt pavements, the purposes are lateral drainage and bearing strength, Cedergren (1989).

It is assumed that the drainage function of the stone base must be preserved for the lifetime of the pavement system. If subgrade fines invade the stone base, it loses its drainage capability, moisture is retained and pavement life is decreased. A reason for the existence of potholes in pavements is due in part to poor drainage in the stone base material beneath the pavement.

The nature of the soil subgrade is an important consideration in any roadway design. Geotextiles are generally used when dealing with extremely weak saturated fine grained silt and clay soils. In cases where the CBR < 3, the deformation of the subgrade soil will be large, hence the geotextile will deform similarly and large scale tension is mobilized, sometimes called membrane tension. As described by Giroud and Noiray (1981), the potential mode of failure of the pavement system is drastically changed with the inclusion of the geotextile. This change results in an improvement in bearing capacity which results in a thinner base course being necessary than without the geotextile. The initial cost savings of stone versus the geotextile will generally justify the use of a geotextile. In this case reinforcement is the primary function of the geotextile. Separation for such a scenario is often considered a secondary function. Furthermore, filtration will also be a secondary function since saturated soils are usually involved.

When the soil subgrade has a CBR in the range of 3 to 7, the soil involved is considered marginal for a permanent paving surface (asphalt or concrete). However, many unpaved secondary roads are of this type. Various surface treatments of the stone base course are customary. Membrane reinforcement of the type just described is diminished. Separation and filtration become of greater importance. Justification for use of the geotextile is difficult because any possible decrease in stone base thickness is small. Thus the initial cost saving and justification for the cost of the geotextile is minimal.

Regarding the above situation of the soil CBR between 3 and 7, the concept of "stabilization" when using a geotextile is often referenced. The problem here is that stabilization is not as easily definable with respect to available design models as is reinforcement and separation.

Soil subgrades of CBR values of 7, and above, are the focus of this study. State DOT(s) often require a soil subgrade to have a CBR value of 7, or higher (some require 10 to 13) before a permanent paving surface (asphalt or concrete) is placed on the stone base. This is to avoid soil subgrade deformation which would prematurely crack the asphalt or concrete pavement. This being the case, membrane reinforcement generated by large scale deformation does not occur, leaving separation as the primary and essentially only function.

The above discussion frames the paradox of using geotextile separators for sites where the soil subgrade is firm and unyielding. Since the cost of the geotextile cannot be compared to the cost of reduced stone base, or pavement thickness, the only justification is for longer life. Yet one must wait for the pavement to show signs of distress or deterioration in order to make such an assessment. Additionally, one must have comparable sites with and without geotextiles separators to make a proper assessment. These two issues; (a) to determine the service life of pavements with geotextile separators, and (b) to compare the performance with comparable sections without geotextiles are the focus of the study. A 20-year time frame is envisioned.

ORGANIZATION OF THE DATA BASE

Example data base entry forms can be seen in the Appendix of this paper. The initial information on the form are dates and contact information. The form then details the pavement. The pavement is first characterized by a description of the roadway. Possible entries could vary from interstates (limited access freeways providing travel from state to state) to parking lots (areas in which vehicles temporarily occupy space). In addition to the description, the number of lanes in each direction and the width of each lane should be indicated.

The primary distinction between pavement types is concrete and bituminous. However, the specific type of pavement is important, e.g.,

- AC-asphaltic concrete pavement
- CC- continuously reinforced concrete pavement
- JPC- jointed plain concrete pavement
- JRC- jointed reinforced concrete pavement
- LMEPC- latex-modified emulsion paving course
- PCC- portland cement concrete pavement

In addition to identifying the pavement type, the average thickness of the layer should be indicated.

The base course and subbase course (if applicable) should be identified. Following are the usual categorizations;

- ABC -aggregate base course

- ATPBC -asphalt treated permeable base course
- BCBC- bituminous concrete base course
- CABC- cement aggregate base course
- CTPBC- cement treated permeable base course

The subgrade soils should be classified and characterized. In order to do so a number of soil characteristics need to be derived or obtained. At a minimum the subgrade soil's strength, moisture content, grain size and plasticity should be reported in the data base.

The geotextile should be described by manufacturer, style and polymer type. Several physical, mechanical and hydraulic properties are relevant. If the measured values of the site specific geotextile are not known, it is suggested that the manufacturers data be used or estimated.

The actual traffic conditions should be classified in terms of total traffic, traffic type, percent of total traffic and truck factor. From these values an equivalent single axle loads (ESAL) can be calculated. This value is a summation of the equivalent 80 kN single axle loads used to combine mixed traffic to design traffic for the design period. Different numerical values of ESAL will have a major effect on the performance of a pavement section. Knowing the ESAL for a particular site shall provide a datum upon which different sites can be compared.

The climatic conditions at the site are potentially important from a macroscopic point of view. Conditions such as FHWA region (which provides socio-political information), climatic zone, expansive soil regions, average solar radiation, average annual precipitation and average annual frost depth are all significant input parameters. Figures 1 (a) through (f) show the diversity of such conditions across the continental United States.

An identification of the type of under drain and/or edge drain at the site is important if applicable and should be noted on the form. Additionally, outlet spacing grade and profile of the test section should be identified.

The final section of the data base is an assessment of the existing condition of the pavement. The majority of the sites will utilize a visual assessment critique to judge the performance of the test sections. The information can be collected manually by teams of inspectors with written logs or video equipment and stored on tape. Some sites may utilize quantitative pavement assessment techniques such as deflectometers or road profilers. A deflectometer measures relative pavement deflection via impacting the road surface with a weight. The road profiler measures and records longitudinal profile, rut depth, and cross-slope data via a truck mounted accelerometer.

THE DATA BASE TO DATE

Table 1 presents the existing, but admittedly sparse, database. It is a compilation of work conducted on various projects over the past five years. The reason for relatively few sites is because a non-geotextile control section is needed for a life cycle cost comparison.
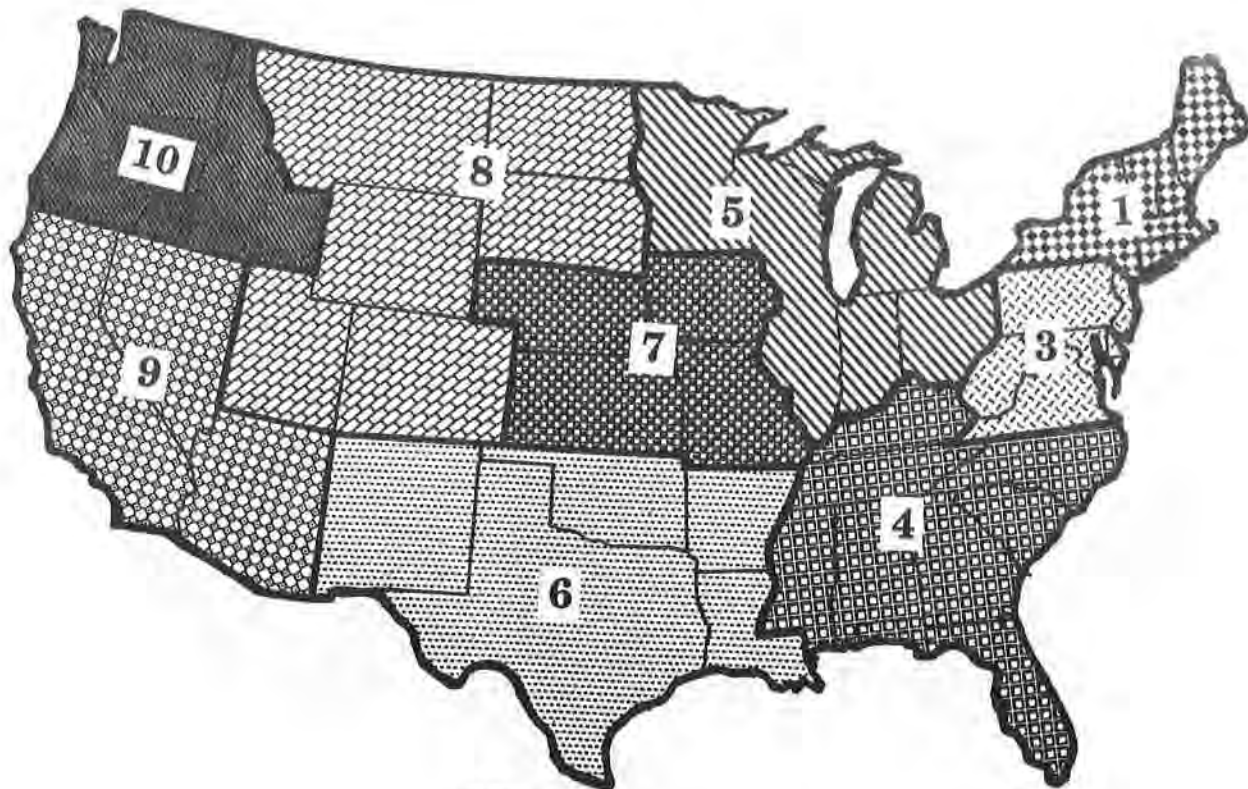
Figure 1 (a) FHWA regions of the USA

Region I -   High potential for moisture in pavement year round

Region II -   Seasonal variability of moisture in pavement

Region III -   Very little moisture in pavement during the year

Region A -   Severe winters with a high potential for frost penetration to appreciable depths into the subgrade

Region B -   Freeze thaw cycles in the surface and base. Severe winters may produce frozen subgrades, but long-term freezing problems are minor

Region C -   Low temperatures are not a problem. Stability at high temperature show be considered
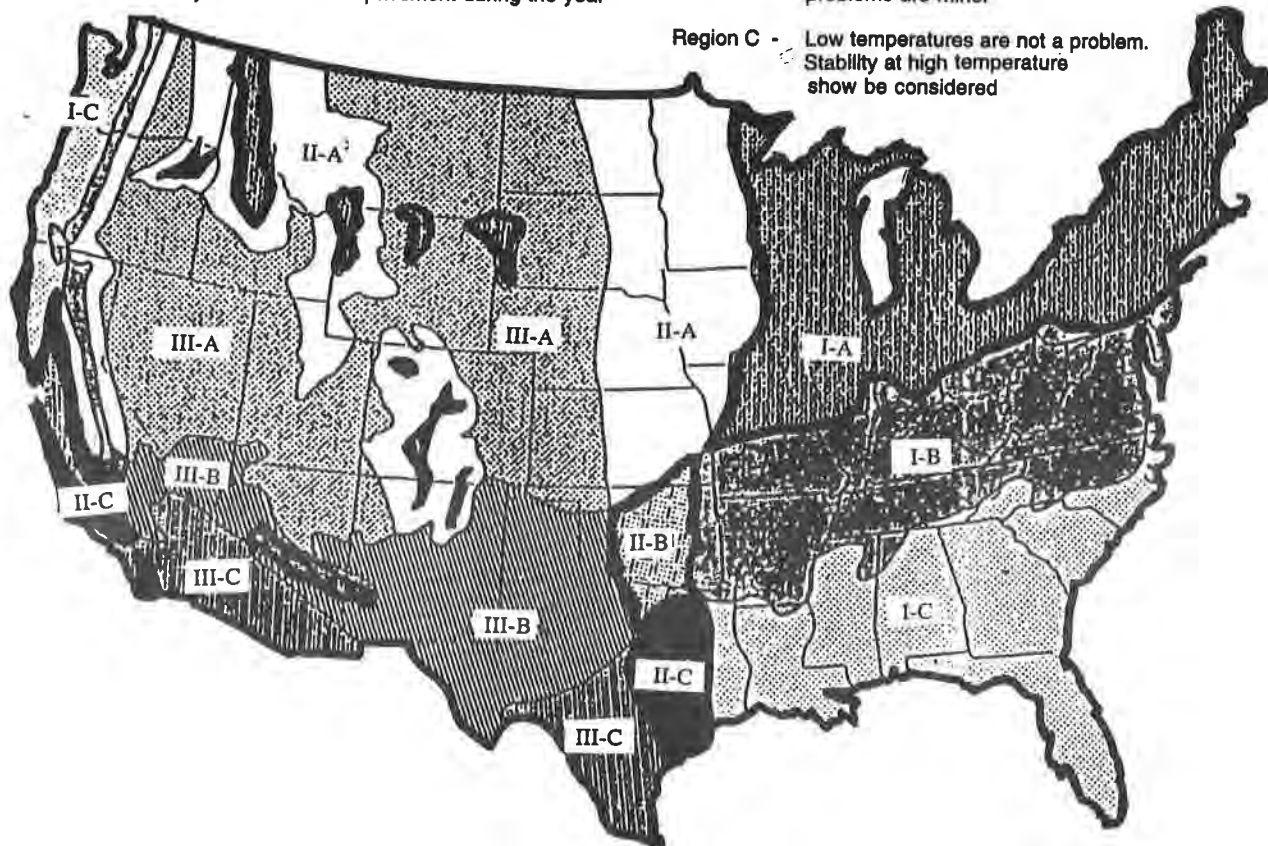
Figure 1 (b) Climatic regions of the USA

LEGEND

■ (black)	HIGH
▨ (hatched)	MODERATE
□ (white)	LOW
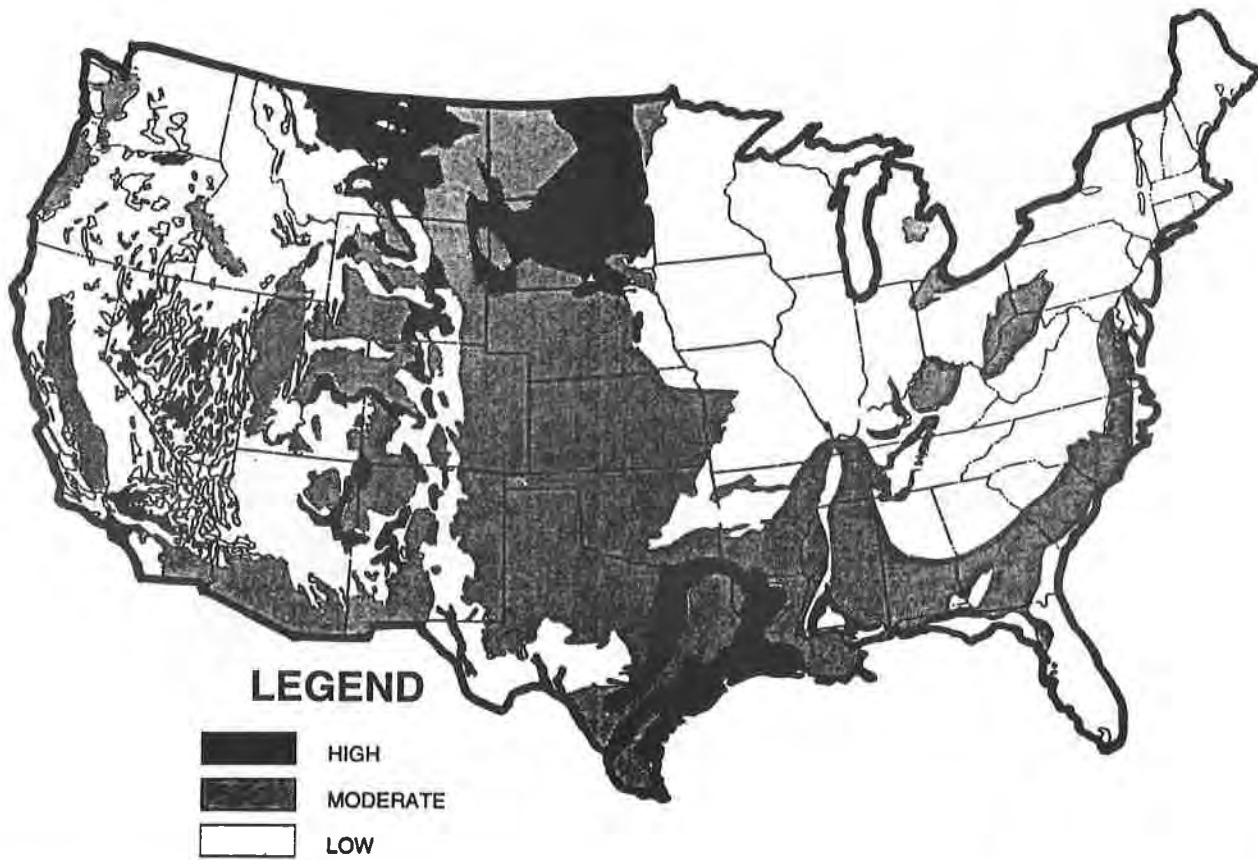
Figure 1 (c) Expansive soil regions of the USA

Note : Annual Solar Radiation
in Lanleys
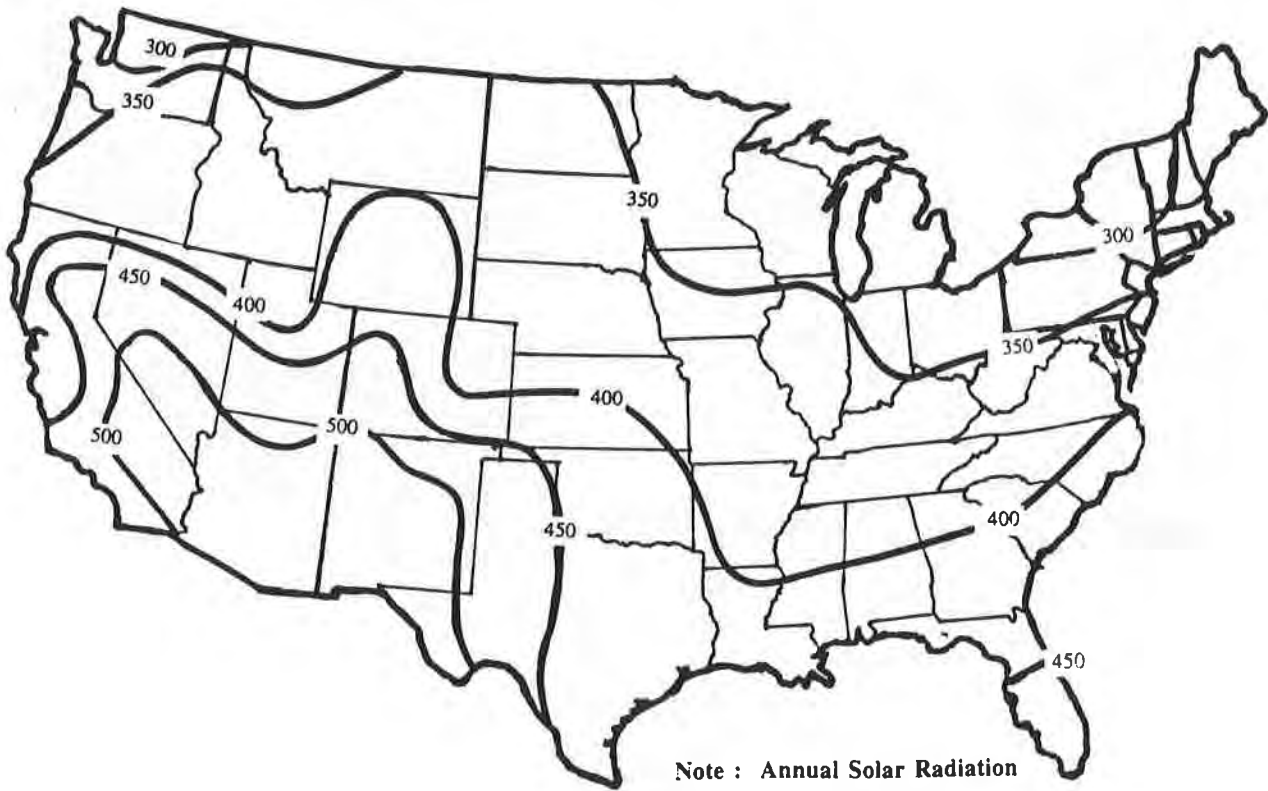
Figure 1 (d) Annual solar radiation of the USA

Figure 1 (e) Annual precipitation in the USA

AVERAGE ANNUAL
PRECIPITATION

☐	0 - 250 mm
▨	250- 510 mm
▨	510 - 760 mm
▨	760 - 1020 mm
■	above 1020 mm

Note : Depth in mm
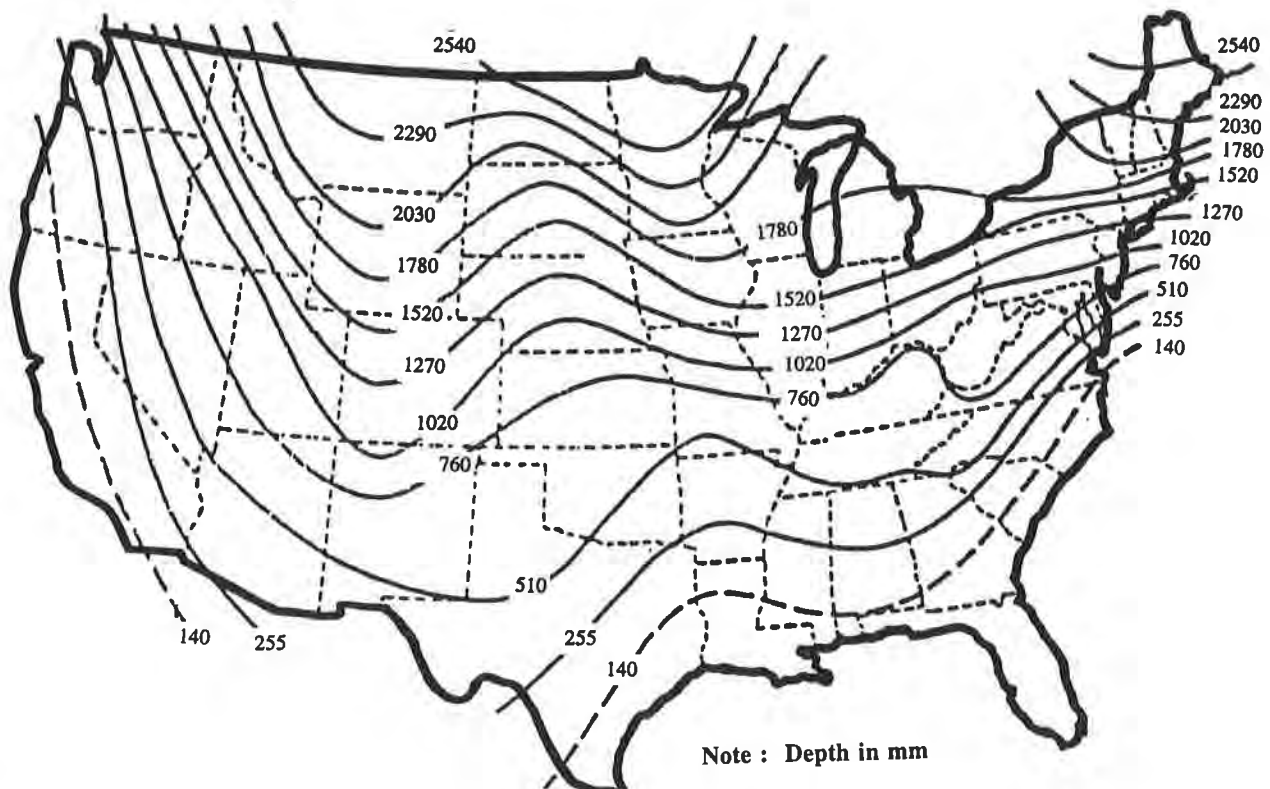
Figure 1 (f) Frost Depth in the USA

Most case histories in the literature do not have a non-geotextile control section. The perceived reason for not having control sections at sites where geotextile separators have been used in the past is that it changes the complexion of the project from conventional construction to a research and development effort.

Table 1 Geotextile separation data base

No.	Description & Reference	Geotextile	Pavement Section
1a	MN DOT, Winona County, CSAH 35	Propex 2090	50 mm asph. over 450 mm base
1b		Supac 4.5 NP	50 mm asph. over 450 mm base
1c	(personal communication with	Typar 3401	50 mm asph. over 450 mm base
1d	Randy Tilseth)	Mirafi 500X	50 mm asph. over 450 mm base
1e		Trevira 1127	50 mm asph. over 450 mm base
1f		Soil Control	50 mm asph. over 450 mm base
2a	WA DOT, SR 507, Bucoda Road	Typar 3401	50 mm asph. over 600 mm base
2b		Polyfelt TS500	50 mm asph. over 600 mm base
2c	Tsai, et. al. (1993)	Exxon GTF 150	50 mm asph. over 600 mm base
2d		Soil Control	50 mm asph. over 600 mm base
2e		Polyfelt TS700	50 mm asph. over 600 mm base
2f		Polyfelt TS 600	50 mm asph. over 600 mm base
3a	SC DOT, Greenville County	Hoechst 1112	40 mm asph. over 75 mm base
3b		Amoco 2002	40 mm asph. over 75 mm base
3c	Sprague and Cicoff (1993)	Hoechst 1125	40 mm asph. over 75 mm base
3d		Soil Control	40 mm asph. over 75 mm base
4a	Driveway, Springfield PA	Hoechst 1125	40 mm asph. over 150 mm base
4b		Typar 3401	40 mm asph. over 150 mm base
4c	Koerner & Koerner (1994)	Soil Control	40 mm asph. over 150 mm base
5a	LCS Bedford, VA	Amoco 2002	75 mm asph. over 100 mm base
5b		Tensar SS2	75 mm asph. over 100 mm base
5d		Soil Control	75 mm asph. over 100 mm base
5e		Amoco 2002	75 mm asph. over 150 mm base
5f		Tensar SS2	75 mm asph. over 150 mm base
5g	Smith, et. al. (1995)	Soil Control	75 mm asph. over 150 mm base
5h		Amoco 2002	75 mm asph. over 200 mm base
5i		Tensar SS2	75 mm asph. over 200 mm base
5j		Soil Control	75 mm asph. over 200 mm base

SOLICITATION FOR ADDITIONAL SITES

An assessment of the sites of Table 1 reveals that all five of the above projects had different agenda and goals. Some sites were intended to investigate different cross sections, while others were intended to compare different geosynthetic types. Still others were aimed at assessing different instrumentation techniques. The objective of the proposed effort is to illustrate the effectiveness of geotextile separators versus having no geotextile at all.

With this single objective in mind, it is proposed that an ideal geotextile separation field site should consist of a near straight section of well traveled roadway at least 200 m long without interruption of traffic signals within a 250 m in either direction. Four geotextiles extending the lane width, by 30 m in length each, are sewn together into a panel. This panel is placed on the soil subgrade and held tightly in place by stakes prior to placing stone base material. The base material is subsequently compacted with a vibratory steel wheel roller and then the pavement is placed. Two-30 m control sections without geotextile should be constructed at both ends of the geotextile panel patchwork. Geotextiles commonly used for this application are:

- woven slit film polypropylene geotextiles,
- continuous filament nonwoven needled polyester geotextiles,
- staple fiber nonwoven needled polypropylene geotextiles, and
- continuous filament nonwoven heat bonded polypropylene geotextiles.

The geotextile panel should be placed in the lane with the highest ESAL load. Prior to deployment of the geotextile, the subgrade soil of the site should be evaluated. Deployment of the geotextile should be supervised and documented. Subsequent lifts of subbase, base and pavement should be monitored and classified. Post construction monitoring of the test section should be conducted on a semiannual basis for approximately five years and on an annual basis thereafter.

The basis for installing such simple uninstrumented field sites is to spend resources installing many sites rather than few highly sophisicated ones. Such sections could be installed with little or no modification to the plans and specifications. Both the owner and the contractor can make minor adjustments needed to accommodate a rapid installation process. Long term monitoring of the project could be conducted by standard visual techniques or perhaps by several types of nondestructive testing methods. Such effort would entail no initial cost to the owner or the contractor . The only long term cost for the owner would be to monitor the site over time.

PAVEMENT EVALUATION

In order to characterize the relative long-term performance of different pavement sections, it is necessary to periodically inspect the road surface for distress and deterioration. A visual inspection program is to be initiated at all of the sites based on the AASHTO criteria, AASHTO (1993).

Each roadway segment is to be periodically surveyed by evaluators who note the type, severity and extent of the conditions exhibited by the pavement. At the end of each segment, the evaluator shall complete a survey form and send it to a central office for analysis.

ASSESSMENT CRITERIA

Information gathered from field surveys are entered into a pavement management program which calculates the performance with respect to time for each pavement segment. There are several software programs available which use different algorithms to predict pavement longevity. Two of the most popular programs are described below.

Micro Paver software for pavement management is available through the American Public Works Association. The program was developed by the US. Army Corps of Engineers in the mid 1980's. The quantity and severity of the observed distress establishes the overall quality of the pavement. Based on input from visual observations, a pavement condition index (PCI) is established on a scale of 1 to 100. Each of the distresses associated with a pavement section reduces the PCI from a top rank of 100. The algorithm of the Micro Paver software results in a PCI versus time curve. This decay curve is represented by a decreasing exponential function. The shape of the curve and hence the severity of the predicted highway decay is based on the nature of the visual observation in regards to when distress was observed after construction. It is generally believed that a pavement with PCI less than 50 is in need of resurfacing or other rehabilitative work, Sprague and Cicoff (1993).

The second method used to predict roadway service life is via AASHTO empirical equations used to calculate ESAL as developed by the Asphalt Institute. An annual average daily traffic (AADT) is used in the analysis along with a typical roadway annual growth rate. AADT is dependent on the type and proximity of the roadway to urban areas. Growth rates are dependent on economic conditions and demographics. Knowing the AADT and the growth rate, the variety of traffic that travels on the roadway needs to be characterized and subdivided into traffic classes. Each class is defined by traffic type, percentage range of total traffic and truck factor estimates. Finally the ADDT, multiplied by the percentage of each traffic type and truck factor, results in the number of ESAL applications per day. ESAL values can further be modified based on environmental distress factors such as swelling and frost heave. By accounting for swelling and frost heave the number of predicted ESAL applications is reduced. Knowing the ESAL value per year and an estimate of the roadways design speed, a service life can be calculated. This resultant service life carries the units of years. Like PCI, ESAL can be graphically presented as ESAL value versus performance time curves, AASHTO (1993).

LONG TERM BENEFIT/COST DETERMINATION

Regardless of the method used to assess the performance of the highway, a criteria will have to be established to determine the roadway performance with respect to cost. In so doing, different roadway sections can be compared based on a common present worth basis.

Like the pavement assessment criteria, the long term benefit/cost calculation can be performed in several ways. Carroll et. al. (1987) and Barksdale et al. (1989) suggest possible techniques. All of the techniques counterpoint that the added cost of the geotextile separator against the life-cycle cost of the pavement.

All of these techniques calculate how much longer a geotextile section of road will last compared to non-geotextile section of road. The assumption being that the service life of a road is defined when an overlay or "major" repair is required. Hence the non-geotextile pavement section may need an overlay constructed in x-years after the original construction of the pavement. As an example, if a pavement with a geotextile separator will last 40-years, versus a pavement without a geotextile lasting 20-years and then a 90 mm overlay for an additional 20-years, the costs can readily be calculated. In this case, the cost of the installed geotextile is directly comparable to the present worth of the cost of 90 mm of asphalt overlay.

SUMMARY

This paper has listed five field sites used as examples in order to evaluate the possible merits of geotextile separators between soil subgrades and base course materials in a roadway sections. In addition to compiling existing information, an ideal geotextile separator test site was proposed. Furthermore, pavement evaluation, roadway assessment criteria and methods for long term benefit/cost were discussed.

Hopefully this paper will stimulate interest in geotextile separators use in roadway applications. There are a estimated 10,000 km of new road constructed in the United States every year , DiMaggio and Cribbs (1996). It is felt that a project such as described herein is long overdue to provide economic justification for the use of geotextile separators in all of these new roadways.

It is hoped that this paper acts as a starting point for a data base of field sites to assess the long term benefit/cost of geotextiles used in the roadway separation applications. The paper should be considered as a solicitation for additional sites rather that a final record. The effort should be of value to the entire transportation community.

ACKNOWLEDGMENTS

REFERENCES

(AASHTO), (1993), American Association of State Highway and Transportation Officials AASHTO Guide to the Design of Pavement Structures, Washington, D C.

Carroll, R. G., Jr. and J. C. Walls, (1987), Granular Base Reinforcement of Flexible Pavements Using Geogrids" Proceedings of Geosynthetics '87 Conference, New Orleans, LA, pp. 46-57.

Cedergren, H. R., (1989), *Seepage, Drainage and Flow Nets*, J. Wiley and Sons, New York, pp. 367.

Barksdale, R.D., S.F. Brown, and C. Francis, (1989), "Potential Benefits of Geosynthetics in Flexible Pavement Systems," Notional Cooperative Highway Research Program, Report No. 315, Transportation Research Board, Washington, D C.

DiMaggio, J.D. and M.M. Cribbs, (1996), "The Role of Geosynthetics on Our Nations Highways," Proceedings of GRI-9 Conference on Geosynthetics in Infrastructure Enhancement and Remediation, GII Publications, Phila., PA, pp. 74-82.

Giroud, J.P., and Noiray, L., (1981), "Design of Geotextile Reinforced Unpaved Roads, "Journal. Geotechnical Engineering Division, ASCE, Vol. 107, No. GT9, September, pp. 1233-1254.

Koerner, R. M. and G. R. Koerner, (1995) "Separation: Perhaps the Most Underestimated Geotextile Function," Geotechnical Fabrics Report, Vol. 12, No 1, IFAI, St Paul, MN, pp. 4-10.

Smith, T. E., T. L. Brandon, I. L. Al-Quadi, B. A. Lacina, S. A. Bhutta and S. E. Hoffman, (1995), "Laboratory Behavior of Geogrid and Geotextile Reinforced Flexible Pavements." Final Report to ACF Inc., Blacksburg, VA, 94 pages.

Sprague. C. J. and G.A. Cicoff, (1993) "A study of the Cost-Effectiveness of Using Separation Geotextiles in Permanent Road Structures," Proceedings of Geosynthetics '93 Conference, Vancouver, BC, Canada, pp. 49-63.

Tsai, W. S., B. M. Savage, R. D. Holtz, B. R. Christopher and T. M. Allen, (1993) "Evaluation of Geotextiles as Separators in a Full-Scale Road Test," Proceedings of Geosynthetics '93 Conference, Vancouver, BC, Canada, pp. 35-48.

RESEARCH · EDUCATION · GEOSYNTHETIC INSTITUTE (GSI) · INFORMATION · ACCREDITATION · CERTIFICATION

ENTER DATE:	3-18-95
CONTACT CODE: 1B	INSTALLED: 1-6-85

SITE NAME	Winona CSAH 35
LOCATION:	Between CSAH 6 and CSAH 7
CITY, STATE, ZIP:	Winona County, MN

OWNER-PROJECT CONTACTS

FIRST NAME	LAST NAME	TITLE	PHONE
Randy	Tilseth	Materials Engineer	(612) 779-5604

NOTES:

GEOTEXTILE CONTACTS

FIRST NAME	LAST NAME	TITLE	PHONE
David	Guram	Geotextile Engineer	(770) 941-1711

PAVEMENT

ROADWAY DESCRIPTION	TYPE	THICKNESS
Collector Roadway	AC	50 mm

BASE MATERIAL

DESCRIPTION	TYPE	THICKNESS
Aggregate Base Course	AASHTO 57	450 mm

SUBBASE MATERIAL

DESCRIPTION	TYPE	THICKNESS
Not applicable	NA	NA

SUBGRADE SOIL

USCS CLASS	AASHTO CLASS	CBR	PLATE BEAR	Wc OPT.	Max Dry Density
ML	A-5	7	250 psi	18%	122 pcf

TYPE	CU	d10 (mm)	PI	% PASS 200	Insitu DENSITY
Inorganic Silt	11	0.01	10	36%	115 pcf

GEOTEXTILE

DESCRIPTION	STYLE
Needle Punched Nonwoven PP	SUPAC 4.5 NP Phillips

WEIGHT (oz/yd2)	GRAB (lbs)	PUNCTURE (lbs)	TEAR (lbs)	BURST (psi)	AOS (mm)	PERMITIVITTY (1/sec)
4.6	95/50	60	40	210	0.212	1.6

TRAFFIC

HIGHWAY CLASS.	TRAFFIC LIGHT	ADDT	TRAFFIC TYPE	% of TOTAL	TRUCK FACTOR		ESAL
Collector	NA	200	2A 4T	90	0.003	54	694
			2A 6T	7	0.28	392	
			4 A	2	0.62	248	
			5 A	0	1.05	0	

ENVIONMENT

FHWA REGION	Climatic Zone	Exp. Soil Potential	AVE. SOL. RAD.(lang.)	AVE. AN. PREC. (in.)	FROST DEPTH (in.)
5	1 A	Low	325	25	90

DRAINAGE

EDGE DRAIN TYPE	OUTLET SPACING (ft.)	GRADE (%)	PROFILE (cut-fill-ongrade)
NA	NA	2	Fill

PAVEMENT ASSESSMENT CRITERIA

VISUAL ID TECHNIQUE	DEFLECTOMETER	INT. ROUGHNESS INDEX	SUBGRADE FAILURE
Yearly inspection	NA	NA	NA

ATTACHMENT: Cross-section, plan view & photographs of the site

REVIEW OF THE UPDATED AMERICAN ASSOCIATION OF STATE HIGHWAY AND TRANSPORTATION OFFICIALS GEOTEXTILE SPECIFICATION

L. DAVID SUITS
SOILS ENGINEERING LABORATORY SUPERVISOR
NEW YORK STATE DEPARTMENT OF TRANSPORTATION
GEOTECHNICAL ENGINEERING BUREAU
ALBANY, NY USA

INTRODUCTION

Early in the history of the use of geotextiles in the United States, the American Association of State Highway and Transportation Officials (AASHTO), the American Road and Transportation Builders Association (ARTBA), and the Association of General Contractors (AGC) formed Joint Task Force 25 (TF 25) to develop guide specifications for the use of geotextiles on transportation agency projects. The Task Force was made up of representatives of the geotextile industry, private contractors, and state and federal transportation agencies. The resulting work was published in the AASHTO Specification Book as Specification M-288 on Geotextiles.

The material properties included in the original work of TF 25 were based on the experience in the use of these materials at the time. As, relatively speaking, the use of geotextiles in the United States was new, and there were very few, if any, accepted design methodologies for geotextiles, the task force took a conservative approach to its work. As experience was gained and design methodologies developed, the need to revisit Specification M-288 was realized. A joint AASHTO and Industrial Fabrics Association International (IFAI) Task Force was formed in 1994 to review and revise the specification. The resulting work was adopted by AASHTO in 1996. It is based on accepted design procedures, but also provides default material property values should the design procedures not be used.

TASK FORCE 25

Task Force 25 was formed early in 1982 with the charge to review tables of suggested geotextile property values for the FHwA Geotextile Manual that was being prepared at the time.

Following this review the Task Force continued to work with the goal of developing guide specifications for geotextiles used in paving, subsurface drainage, erosion control, sediment control(silt fences) and separation applications.

In 1986 the Task Force approved the five proposed specifications which included material property values and notes on construction and installation procedures. Between 1986 and 1990 the five individual specifications were merged into a single material specification, not including the construction and installation notes that appeared in the individual documents. In 1989 this single document was submitted to an AASHTO Subcommittee on Materials ballot as a revision to the existing AASHTO M-288 Specification for Geotextiles Used for Subsurface Drainage Purposes. As seen by the title the then existing specification was for drainage fabrics only. This revision represented an enlargement of the applications covered in the specification. The revisions were approved and the revised specification first appeared in the AASHTO 1990 " Standard Specifications for Transportation Materials and Methods of Sampling and Testing 15th edition," book as AASHTO Specification M-288-90 on Geotextiles. A final report of the Task Force's work was also issued in 1990 separate from the 15th edition of the AASHTO specification book. There were some minor clarification modifications done to the specification in 1992, and appeared as M-288-92 following those modifications. There were no changes made to the material properties however.

The material properties shown in M-288-92 represented the state of knowledge of the use of geotextiles in the listed applications at the time. As formal design procedures for the use of geotextiles were either nonexistent or in the development stages, the specification did not cover or encourage designing for the use of these materials, and did not promote the performance and economic benefits to following detailed design procedures.

JOINT AASHTO-IFAI TASK FORCE

In 1992, with the realization that knowledge on the use of geotextiles had grown at a rapid rate, and the fact that in reality the work of Task Force 25 was between five and ten years old, a proposal was presented to the AASHTO Subcommittee on Materials, Technical Section 4e, that it would be appropriate to start a formal review process of M-288 as it appeared then. The Technical Section agreed.

A preliminary review was done with a small task force in early 1993, with the formal Joint AASHTO-IFAI Task Force established late in 1993. The Task Force had Federal and State Transportation, academia, and industry(IFAI) representation.

M-288-90 as it appeared in the AASHTO Specification Book did not include the construction and installation guidelines that TF 25 had developed, as it was unclear at the time how to include them. One of the first tasks of the new task force was to approach AASHTO and work out the

logistics of including some form of the construction and installation notes in the eventual revised M-288. Once this was accomplished, the task force divided into two sub-groups; one to work on material properties; and one to work on the construction and installation notes.

REVISIONS TO SPECIFICATION M-288-92

<u>Material Requirements</u>

It is emphasized in the Scope of the revised document that the specification is not a design or construction specification, but is based on geotextile survivability from installation stresses. As such, selection of the geotextile is based on a knowledge of the anticipated installation stresses to which the geotextile will be exposed. The specification covers six applications in which geotextiles are used. They include: subsurface drainage, separation, stabilization, permanent erosion control, temporary silt fences, and paving fabrics.

The general strength requirements for the first four listed applications are broken into three classes of geotextiles, with Class 1 being the most robust, and Class 3 the least. Within each class the strength requirements are established based on elongation at break in the grab strength test. In each class the highest strength requirement being for materials that break at less than fifty percent elongation, and the least for those that break at greater than fifty percent elongation.. The requirements for the silt fence application are based on supported or unsupported fences. The paving fabrics being limited to fabrics with elongation at break greater than fifty percent.

Classes A & B in M-288-92 are defined as Class A being used where installation stresses are more severe than Class B applications, and by aggregate shape, trench depth, and the size and height of drop of armor stone. There were no definitive limits set to the installation stresses as far as differentiating between severe and less severe. Table 1 shows a basic comparison of M-288-92 applications and classes to those listed in M-288-96.

Table 2 shows comparisons of the general strength properties for each edition of the specification for the subsurface drainage, separation, stabilization, and permanent erosion control applications. The permittivity, apparent opening size, and ultraviolet stability requirements for each application are shown in subsequent tables.

Table 3 lists the class of default geotextile, and the designed for class for the subsurface drainage, permanent erosion control, separation, stabilization applications in M-288-96. By "designed for class" is meant; that with knowledge of field experience, laboratory tests, and/or certain site configurations, a lesser class may be used.

Tables 4 through 6 compare the apparent opening size, permittivity, and ultraviolet degradation requirements for the subsurface drainage, permanent erosion control, separation, and

stabilization applications.

Tables 7 and 8 show the comparisons for the two specifications for temporary silt fence and paving fabric applications respectively.

Table 9 list the designations for the test methods listed in the specifications.

Table 1- AASHTO Specification M-288 Applications/Classes

APPLICATION	YEAR	CLASS	
Subsurface Drainage	1992	A	B
Subsurface Drainage	1996	2	3
Sediment Control	1992	Self Supported	Wire Fence Supported
Temporary Silt Fences	1996	Unsupported	Supported
Erosion Control	1992	A	B
Permanent Erosion Control	1996	1	2
Paving	1992	-	-
Paving Fabric	1996	-	-
Separation	1992	High Survivability	Medium Survivability
Separation(CBR>3)	1996	2	3
Stabilization (1<CBR<3)	1996	1 (default)	2 3

Table 2 - Strength Requirements

PROPERTY	1992		1996					
	Class A*	Class B*	Class 1		Class 2		Class 3	
Elongation (%)	-	-	<50	>50	<50	>50	<50	>50
Grab Strength (N)	800 - 1200	356-800	1400	900	1100	700	800	500
Sewn Seam Strength (N)	710 - 1070	310 - 710	1260	810	990	630	720	450
Tear Strength (N)	220 - 445	110 - 310	500	350	400	250	300	180
Puncture Strength (N)	350 - 445	110 - 310	500	350	400	250	300	180
Burst Strength (kPa)	2000 - 2200	895 - 965	3500	1700	2700	1300	2100	950

* Ranges shown in Class A & B are based on application.

Table 3 - Default Geotextile Classes for M-288-96

APPLICATION	DEFAULT CLASS	DESIGN CLASS
Subsurface Drainage	Class 2	Class 3
Permanent Erosion Control	Class 2 for woven monfilaments Class 1 for all others	Class 2
Separation	Class 2	Class 3
Stabilization	Class 1	Class 2 or 3

Table 4 - Permittivity Requirements

APPLICATION	1992		1996 - Percent In-Situ Soil Passing 0.075mm		
	Class A	Class B	<15	15 to 50	>50
Subsurface Drainage	$K_{fabric} > K_{soil}$	$K_{fabric} > K_{soil}$	0.5 sec^{-1}	0.2 sec^{-1}	0.1 sec^{-1}
Temporary Erosion Control	$K_{fabric} > K_{soil}$	$K_{fabric} > K_{soil}$	0.7 sec^{-1}	0.2 sec^{-1}	0.1 sec^{-1}
Separation	$K_{fabric} > K_{soil}$	$K_{fabric} > K_{soil}$	Class 2 geotextile with 0.02 sec^{-1}		
Stabilization	-	-	Class 1 geotextile with 0.05 sec^{-1}		

Table 5 - Maximum Apparent Opening Size Requirements

APPLICATION	1992		1996 - Percent In-Situ Soil Passing 0.075mm		
	Class A	Class B	<15	15 to 50	>50
Subsurface Drainage	< 50% No. 200 - 0.6mm >50% No. 200 - 0.297mm	< 50% No. 200 - 0.6mm >50% No. 200 - 0.297mm	0.43 mm	0.25mm	0.22
Temporary Erosion Control	< 50% No. 200 - 0.6mm >50% No. 200 - 0.297mm	< 50% No. 200 - 0.6mm >50% No. 200 - 0.297mm	0.43mm	0.25mm	0.22mm
Separation	< 50% No. 200 - 0.6mm >50% No. 200 - 0.297mm	< 50% No. 200 - 0.6mm >50% No. 200 - 0.297mm	Class 2 geotextile with 0.60mm		
Stabilization	-	-	Class 1 geotextile with 0.43mm		

Table 6 - Maximum Strength Degradation Due To Ultraviolet Exposure

APPLICATION	1992	1996
Subsurface Drainage	70 % retained after 150 hrs	50 % retained after 500 hrs
Permanent Erosion Control	70 % retained after 150 hrs	50 % retained after 500 hrs
Separation	70 % retained after 150 hrs	50 % retained after 500 hrs
Stabilization	-	50 % retained after 500 hrs

Table 7 - Temporary Silt Fence Requirements

PROPERTY	1992 REQUIREMENTS		1996 REQUIREMENTS		
	Wire Fence Supported	Self-Supported	Supported	Unsupported	
				$\geq 50\%$ Elongation	$< 50\%$ Elongation
Grab Strength*	400 N	400 N - 50% max. elong. @ 200 N			
Grab Strength - MD	-	-	400 N	550 N	550 N
Grab Strength - XD	-	-	400 N	450 N	450 N
Permittivity	0.01 sec^{-1}	0.01 sec^{-1}	0.05 sec^{-1}	0.05 sec^{-1}	0.05 sec^{-1}
Ultraviolet Stability	70% retained after 500 hours	70% retained after 500 hours	70% retained after 500 hours	70% retained after 500 hours	70% retained after 500 hours
Apparent Opening Size	0. 84 mm max.	0.84 mm max.	0.60 mm max. avg. roll value	0.60 mm max. avg. roll value	0.60 mm max. avg. roll value

* Minimum in the weakest principle direction

Table 8 - Paving Fabric Requirements *?from :Daren*

PROPERTY	1992	1996
Grab Strength	356 N	500 N
Ultimate Elongation	50% @ break	$\geq$ 50%
Asphalt Retention	0.90 liters/sq m	manufacturer certification
Melting Point	135 deg C	150 deg C

Table 9 - M-288 Specification Test Methods

TEST METHOD	DESIGNATION
Grab Strength - Elongation	ASTM D4632
Sewn Seam Strength	ASTM D4632
Puncture Strength	ASTM D4833
Trapezoid Tear Strength	ASTM D4533
Burst Strength	ASTM D3786
Permittivity	ASTM D4491
Apparent Opening Size	ASTM D4751
Ultraviolet Degradation	ASTM D4355
Asphalt Retention	Texas DOT Item 3099
Melting Point	ASTM D276

Construction Installation Guides

As stated previously, the original TF 25 work included several notes on construction and installation of the geotextiles in an effort to ensure proper performance of them following installation. Unfortunately, these notes did not get published in M-288-90 or 92. At the start of the process of revising the specification the logistics were worked out for including construction and installation guides as appendices to the specification. These are to appear with the specification in the AASHTO specification book. The notes include directions on site preparation, material overlap, armor stone placement, post spacing for silt fences, embedment, damage repair, overlapping, direction of placement in water and on slopes, and installation suggestions for paving fabrics.

Proper installation is mandatory and critical for the long term proper performance of any

geosynthetic, and thus the importance of these notes being included with the material specification.

SUMMARY

The development of construction material specifications should be an ever evolving process, not ending with the initial document. Knowledge of performance, and types of materials are always changing. As a result, the manner in which such materials are specified needs to evolve with time.

The development and revisions to the AASHTO Specification M-288 are a prime example of the need for this process. The process which was followed in developing a cooperative effort between manufacturers and end users should serve as an example that can be followed in many other areas of the geotechnical engineering community.

A CASE STUDY INTO THE USE OF PAVEMENT REINFORCING GRID, MASTIC, AND MEMBRANE INTERLAYERS ON ASPHALT CONCRETE OVERLAYS

By : Theron J. Roschen, P.E.
Senior Civil Engineer
Sacramento County Public Works Agency, Transportation Division
California, U.S.A.

ABSTRACT

Traditional pre-overlay preparation of damaged pavement involved the removal of the distressed pavement to the depth of the failure plane and replacing the area with sound road building material. In those areas where it has been determined that the damaged pavement is on a stable base and that the distress is related to age hardening of the asphalt concrete coupled with weatherization, the use of: pavement reinforcing grids, reinforcing grids with water retarding fabric, asphaltic mastics and membranes, as an interlayer to an overlay may be shown to provide an alternative that is equivalent in performance to the removal and replacement of the damaged pavement. Furthermore, these products may prove to be economically advantageous when construction staging and traffic control are considered.

In August of 1995, the Sacramento County Transportation Division conducted two test sections that employed the use of nine (9) different pavement reinforcing grids, mastics, and membranes to bridge damaged but stable pavement. These were compared with sections where the distressed pavement was removed and replaced. Control sections without any pre-overlay preparation were also included. The installation and construction coordination issues were also observed.

This paper will examine the history that led up to the development of the various test products that were used, identify the source of pavement distress, and present the procedure used by Sacramento County for overlay design. The theoretical benefits of each product will be discussed and a fifteen (15) month post construction observation will be made. The costs of each product will be presented and compared with various reconstructive techniques that are used by Sacramento County in advance of an overlay.

PREFACE

Many existing roads are literally falling apart. The reasons behind their failure are ultimately derived from economics. Whether it be from an improvement standard for

development that opts for the less costly structural section, or be it untimely, inadequate, or unfunded maintenance treatments, roadways continue to deteriorate to a point where many municipalities are forced into a perpetual reactionary maintenance philosophy. More and more of the maintenance budget is siphoned off to perform "Band-Aid" type repairs rather than doing the correct, long lasting treatment the first time. To turn the battleship, designers must address the fundamental roadbase inadequacies or failures, and not just place a minimal overlay, and call it good. This involves the use of a pavement management system that focuses the overlay dollars onto the roads in poorest condition that carry the greatest amount of traffic, and have the courage (if you will), to commit the monetary effort to do what is necessary on those roads once you are there. Base repairs in advance of overlays are a necessary evil, and if interlayer treatments prove to be a viable alternative, then so much the better.

HISTORY

The idea of placing an interlayer in construction is not new. Ancient Egyptian builders used straw mats in the foundations of the pyramids and the romans used other woven fabrics in the construction of their roadways. Over sixty years ago in South Carolina coarsely woven cotton sheets were spread between coats of liquid asphalt as a road building technique to hold the asphalt in place and resist water seeping into the roadbed. For a while, at least, this idea seemed to work. Unfortunately the cotton fibers eventually lost strength from tire abrasion and rot. But, the idea of fabric holding the asphalt in place as a system to prevent water intrusion into the base was a sound one.

Since that time, numerous man-made fabrics have been tried with mixed results. The first known evaluations using man-made fabrics for paving, date back to 1966, and was started as part of the U.S. Army Corps of Engineer's research into emergency construction of pavements. The army Corps of Engineers was looking to replace the heavier and bulkier metal mesh planks that had been used for emergency military roads. A light weight non-woven polypropylene fabric was found to be the most successful. It produced a tough cloth that had good abrasion resistance and did not deteriorate from chemicals or rot. The inertness, light weight and construction toughness of the needle-punched fabric made for an ideal emergency road building material.

The fiber is produced from melting pellets of polypropylene resin which is then extruded through a spinneret (like a shower head). After being cut into short lengths about 100mm to 150mm (4" to 6")called staples, multiple fibers are then formed into a web and placed through a needle punch board. The needle punch process re-orients the fibers so that mechanical bonding is achieved. Another method called spunbound fabric randomly extrudes a continuous strand that produces a layer of given thickness, with little or no needle-punching. The fabric is then heat bonded on one side to prevent bleed-through of the tack

coat and minimize the sticking of construction tires to the fabric.

Many ASTM tests were developed to measure the material properties and performance of this new product. These tests include: Tensile properties, Temperature effects, Puncture resistance, Stiffness of the fabric, Burst strength, Ultraviolet effects, Water permeability, and Tearing strength. In May of 1970, The Federal Highway Administration initiated the National Experimental Evaluation Program or (NEEP). This program's goal was to reduce reflective cracking in bituminous overlays. Approximately 14 states participated in this program and it included pavement interlayer test sections containing: non woven Polypropylene, spunbound nylon, open weave polyester, fiberglass matting, woven glass, and a mixture of Polypropylene and nylon in a spunbound fabric. The non-woven polypropylene produced, by far, the best results.

In 1977 the Federal Highway Administration officially adopted it's use by issuing a report entitled "The use of fabrics in the construction and maintenance of low volume roads". In 1972 Caltrans placed their first extensive field test. These roads exhibited extensive map and block cracking, and had evidence of pumping subgrade. On one test section, a 25mm (1")overlay was placed over the asphalt-fabric interlayer and compared to a control section consisting of a conventional 62mm 2.5") overlay. The results showed that the fabric section had only 6% of the surface exhibiting cracking after 4 years. The much thicker and more costly control section exhibited 1%. On the other test section a 25mm (1") overlay was compared to the same thickness with the asphalt-fabric interlayer. The fabric section exhibited 33% less cracking than the control.

Concurrent with the development of paving fabric, was the introduction of geogrids in the early 1970s. These are polyethylene and polypropylene fibers that are manufactured into an open mesh with a rib spacing that varies from 12.5mm to 112.5mm (0.5" to 4.5"). Geogrids are stiffer than geotextiles and rely on their tensile resistance for strength. Early applications were primarily for drainage, erosion control, and haul road or railroad construction. Now these products are readily accepted by the civil engineering community for subgrade enhancement and are used in the reinforcement of earthen structures such as, slopes, embankments, and retaining walls. The effect of placing a stiff geogrid as an interlayer of an asphalt concrete overlay to extend the fatigue life or diminish rutting is relatively new and does not have enough comprehensive, time proven data, to reach any conclusions as yet.

Also in the early 1970's engineers were searching for a way to retard reflective cracks propagating up through asphalt overlays. These included the use of metal strips and plates, boards, and roofing materials all with varied success. It also became evident that geofabrics were not going to be the "cure all" as engineers tried to place them over ever-increasingly worse pavement surfaces. The development of Geomembranes, which are thin "impervious" sheets of rubberized or plasticized asphalt

combined with various geotextile fabrics, were primarily born out of the landfill industry when government regulations were enacted in 1982. Their uses were to provide lining and covering for liquid and vapor containment. Whether these products evolved on their own accord to address reflective cracking, or if the marketing of these products found the need, is really unimportant. These interlayer products have been shown to disperse the load over a distressed area and by reducing the stress at the crack. There is the added benefit of waterproofing the road were these products are placed that prevent moisture from penetrating to the base material and cause further structural degradation. Today there are many geosynthetic composites on the market. The placement of these membranes over entire bridge surfaces or in strips over cracks on roadways has increased over the years to the point were millions of square feet have been applied.

SACRAMENTO COUNTY OVERLAY DESIGN PROCEDURE

Before any overlay is contemplated, the existing pavement distress must be analyzed. Pavement failures are classified into three general categories, surface, bond, and structural. (See figure 1) Common failures in the Sacramento region are defined below:

SURFACE
Flushing - Smooth or shiny surface in the wheel paths caused by an over asphalted mix or rounded aggregates that compact under vehicle loading, reducing the free voids and forcing asphalt to the surface.
Raveling - A progressive loss of aggregate from the asphalt concrete from oxidation, weathering and/or traffic abrasion caused by poor compaction, materials, and/or mix design.
Rutting and Corrugations - Depression of the pavement in the wheel path or in stop/start zones caused by heavy traffic loading that overstresses the pavement and reconsolidates the asphalt and possibly the base sections. Rutting problems can incorrectly be interpreted as the pavement support section being under designed, however, another explanation is that the mix may contain rounded aggregates, excessive fines and/or inadequate compaction was achieved that caused a reconsolidation of the mat.
Alligator Cracking - A series of interconnected cracks caused by fatigue failure. Cracks begin at the bottom of the asphalt surface where the stress and strain forces are the highest and propagate upward as a series of parallel longitudinal cracks. Over time and repeated loads the cracks become connected and eventually spall out and form "potholes".
Block Cracking - Interconnected cracks that form rectangular blocks that range from 0.3m to 3m (1' to 10') squares and is caused by age hardening of the asphalt and a diminished ability to expand and contract with temperature fluctuations.
Longitudinal and Transverse Cracking - These cracks can be caused from poor compaction on construction joints, reflective cracks propagating through the asphalt concrete mat from underlying surface failures or slab joints, or shrinkage of asphalt concrete from age hardening.

CLASSIFICATIONS OF FAILURES

PAVEMENT FAILURES

- **Surface Failures**
  - Raveling
    - Lack of Asphalt
    - Age Hardening
    - Water and Wheel Action
  - Block, Transverse, Longitudinal Cracking
    - Age Hardening
    - Low Temperatures
    - Shrinkage
  - Shoving, Corrugations Flushing
    - Excess Asphalt
    - Excess Water
    - Smooth AC Aggregates
- **Bond Failures**
  - Slippage Cracks
    - Lack of Bond
    - Pavement Surfacing too Thin
    - Traffic Horizontal Loading
- **Structural Failures**
  - Fatigue Cracks
    - Excessive Pavement Deflections
    - Inadequate Design
  - Rutting
    - Inadequate Design
    - Excessive Moisture
  - Severe Distortion
    - Poor Foundation

FIG. 1

BOND
Slippage Failure - Slippage between layers of surfacing causing a break in the bond and movement in the upper layer due to insufficient tack coat, inadequate saturation of pavement fabric, or too thin an overlay.

STRUCTURAL
Longitudinal Shoulder Failures - A longitudinal crack that forms near the shoulder of an unimproved roadside ditch caused by a lack of shoulder support to the pavement structural section. Shrinkage of basement material from soil type and cyclical saturation conditions may also be factors.
Subgrade Rutting - Depression of the pavement in the wheel path caused by traffic loading that reconsolidates the base sections because of inadequately designed road section or excessive moisture in the base.
Fatigue Cracks - Transverse cracks formed by repetitive deflection of pavement due to an inadequately designed road section.

PROJECT PRELIMINARY SURVEYS

A preliminary survey of the street to evaluate the existing roadway for inadequacies in; grade, cross slope, skid resistance, accident history relating to pavement condition, conflicting stripe removal, and most importantly, pavement distress was conducted by the project engineer. Any of the aforementioned factors can be corrected by an overlay. The project engineer also "walked" the job with the maintenance supervisor and prepared a photolog of the road at about 30m (100') intervals. On this project a crack map was also prepared so that the baseline pavement condition was documented. During these visual inspections there was some intuitive appraisal of the pavement condition. However, a more objective evaluation was needed.

Sacramento County utilizes a computerized Pavement Management System that was developed by the Metropolitan Transportation Commission of the San Francisco bay area. Inspections are made once every year on non-residential streets and once every two years on residential streets. The severity and type of pavement distress are measured and a pavement condition index (PCI) is assigned (See figure 2). A deterioration curve of the PCI is generated by the computer. The deterioration rate is based upon extensive empirical data collected from bay area streets. The pavement management system also has the ability to give a recommendation for the timing of the appropriate surface treatment. The recommendations from the pavement management system are based upon field inspections of sample sections of a given roadway.

OVERLAY DESIGN

Sacramento County uses a design method that is a combination of the Caltrans structural design procedure and the pavement management system (PMS) developed by the Bay Area Metropolitan Transportation Commission. The information needed for this method

* <u>Step 1</u> Inspect sample units to determine type, quantity and severity level of pavement distresses.

Low Severity Longitudinal Cracks

Medium Severity Alligator Cracks
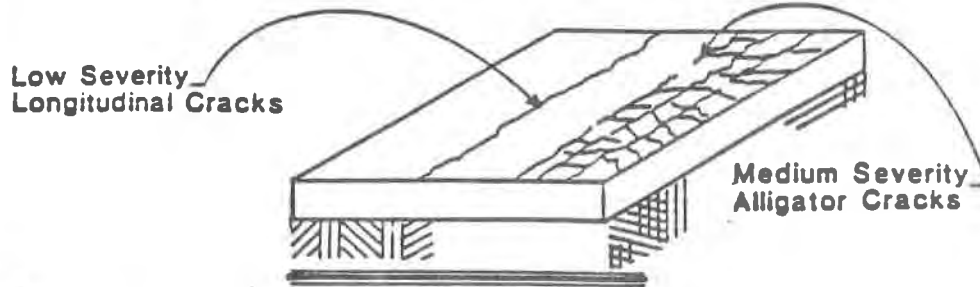
* <u>Step 2</u> Determine deduct values.

L,D&T Cracking

ALLIGATOR Cracking
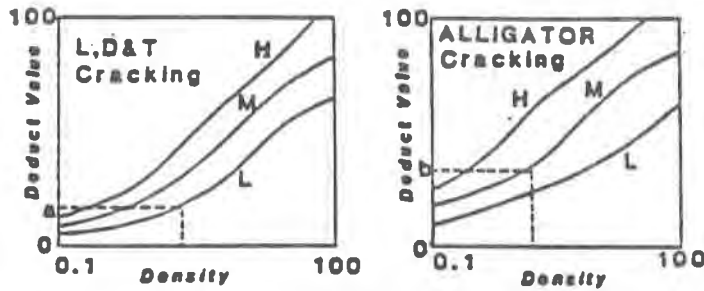
* <u>Step 3</u> Compute Total Deduct Value, TDV = a + b

* <u>Step 4</u> Adjust Total Deduct Value.

q = Number of entries with deduct value over 5 points
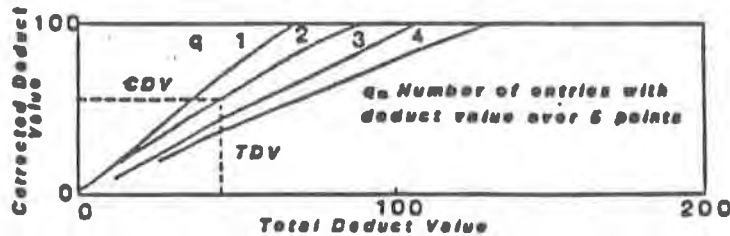
* <u>Step 5</u> Compute Pavement Condition Index, PCI = 100 - CDV, for each sample unit inspected.

* <u>Step 6</u> Determine Pavement Condition Rating

PCI

| 0 | 10 | 25 | 40 | 55 | 70 | 85 | 100 |

FAILED   VERY POOR   POOR   FAIR   GOOD   VERY GOOD   EXCELLENT

<u>RATING</u>
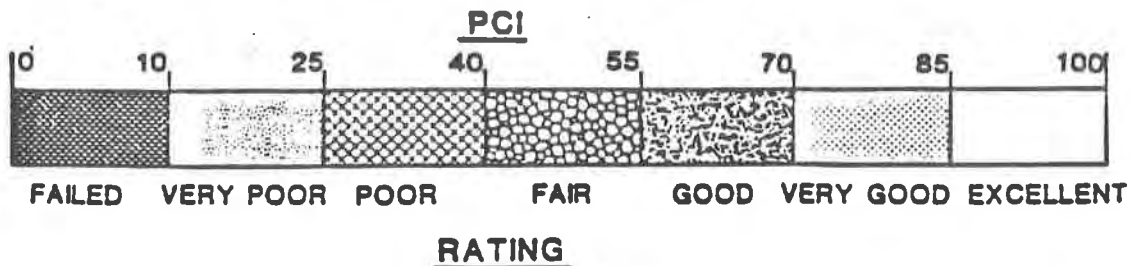
FIG.2   PCI Scale and Calculation Steps

include; existing road thicknesses and materials, PMS evaluation, R-Value testing of basement soil, and Traffic Index (TI) value.

The depth of each course of the pavement structural section is noted from the core samples or "As-Built" information. Each constituent is then converted to an equivalent thickness of asphalt concrete. Deductions are made from this equivalent thickness based on the pavement distress determined by the PMS and the effective full-depth asphalt concrete section (T_e) is determined. The actual required full-depth asphalt concrete section (T_r) is then calculated from the TI and R-values and compared with the effective existing structural section. The difference between the effective full-depth asphalt concrete section (T_e) and the required structural section (T_r) equals the required overlay thickness. Reductions in the (T_e) thickness are by the following factors:

PCI	Factor
100 - 71	0%
70 - 56	5%
55 - 41	10%
40 - 26	20%
< 25	Consider reconstruction

PROJECT DESCRIPTION (See figure 3)

In August of 1995, the Sacramento County Transportation Division executed a contract with Granite Construction Company for the placement of variable depth overlays of asphalt concrete on six roads in the County. The project contained over 22,000 tons of asphalt concrete and 6,800 tons of asphalt rubber concrete. Funding was provided by the Federal Surface Transportation Program administered by Caltrans with matching funds provided from the County Sales Tax revenues.

Sacramento County routinely removes and replaces damaged pavement with County Forces in advance of the contract overlay and places pavement reinforcing fabric on the road overlays to provide a water barrier and to inhibit reflective cracks. On this project however, two roadways contained test sections that employed the use of nine (9) different pavement reinforcing grids, mastics,and membranes. These interlayers were placed longitudinally in an asphalt concrete overlay to "bridge" damaged but stable, pavement and transversely over single cracks. These were compared with sections where the distressed pavement was removed and replaced with a new structural section, and other control sections without any pre-overlay preparation. The installation and construction coordination issues were also observed.

EXISTING PAVEMENT ASSESSMENT

The two roads selected for these tests were Elk Grove Boulevard and Elverta Road. Both roads are two lane rural roads that connect urban areas to regional collector roads. The average daily traffic for Elk Grove Boulevard is approximately 4,300 vehicles a day (5% trucks) and for Elverta Road is 7,600
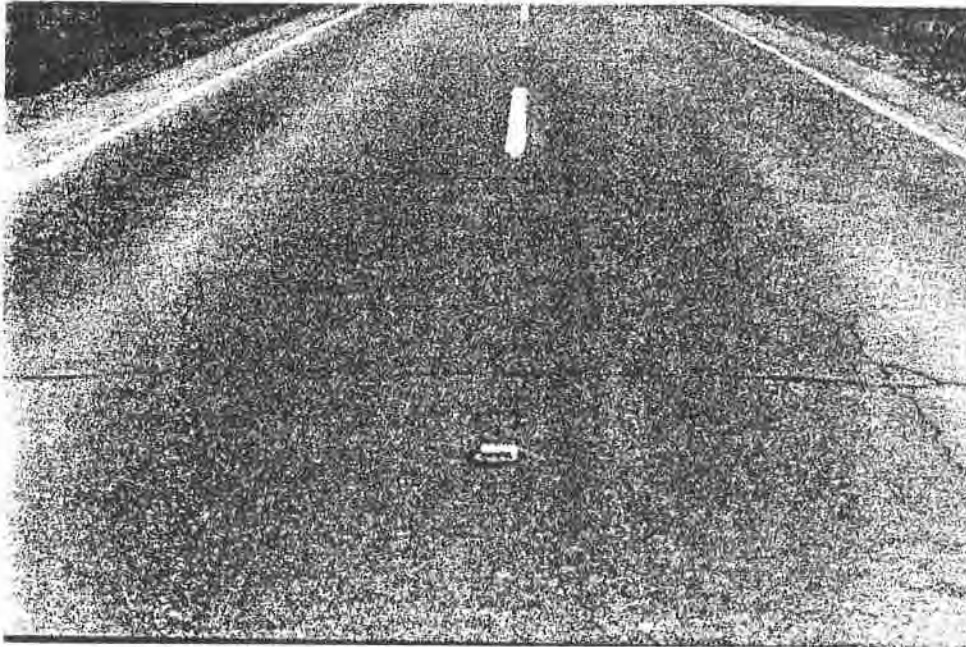
ELK GROVE BLVD.
Typical: Existing Condition - Transverse Block Cracking,
High Severity: Alligator Cracking in Outer Wheel Paths

ELVERTA ROAD
Typical Existing Condition
Moderate: Alligator Cracking, Raveling,
Minor: Pumping Through Skin Patches

FIG.3

vehicles a day (7% trucks). The available "As-built" information and maintenance history was gathered and it was discovered that Elk Grove Boulevard was constructed in 1917 with a 4.5m (15') wide 100m (4") thick Portland cement concrete (P.C.C.) road on compacted native material. A 60mm (0.2') AC overlay was place over the P.C.C. sometime in the 1950's when the road was widened to 7.9m (26'). The new road sections were constructed of 60mm (0.2') of asphalt concrete over 150mm (0.5') of aggregate base upon 150mm (0.5') of aggregate sub-base. In 1975 a 54mm (0.18') thick overlay was placed over the entire road surface. Current maintenance consisted of placing 9mm (3/8") asphalt concrete mix into the areas where alligator blocks had spalled out.

Elverta Road was constructed in 1967 with a 8.23m (27') wide traveled way with 2.4m (8') shoulders. The structural section is 75mm (0.25') of asphalt concrete over 225mm (0.75') of aggregate base upon 150mm (0.5') of lime treated base @ 4%. The shoulders were comprised of a double layer of chip seal over 225mm (0.75')of compacted aggregate base. Other maintenance activities consisted of the placement of a chip seal over the entire road in 1989. Between 1992 and 1994, several sections had "skin patches" of 9mm (3/8") asphalt concrete mix placed over the areas where alligator cracking had become prevalent, and crack sealant was placed sporadically.

R-Value testing on Elk Grove Boulevard yielded a value of 21. The PCI was 48 and the traffic index of 8 was used. This roadway had a longitudinal and transverse pattern that was characteristic to reflective cracks coming through from the joints in the underlying PCC roadway. In the widened sections a consistent depression of as much as 18.57mm (3/4") was observed in the outer wheel path in each direction. These depressions caused stormwater to pond in the rut and undoubtedly accelerated the deterioration of the pavement. This wheel path had medium severity alligator cracking with the pattern typically shaped in 150mm (6") diameter blocks. The blocks were stable and there was a slight discoloration of the pavement from the pumping of fines from the base. The asphalt aggregate mix showed evidence of severe age hardening.

R-Value testing on Elverta Road yielded a value of 35, a PCI of 42 and a traffic index of 8 was used. This roadway had longitudinal and transverse block crack patterns that gave way to random sections of alligator cracks. The blocks were stable with no evidence of pumping of fines from the base. The skin patches were now disbonding from the underlying layer and the asphalt aggregate mix showed evidence of severe age hardening.

As an example, following the overlay design procedure for Elk Grove Boulevard, the difference between the effective full-depth asphalt concrete section (T_e) (less the reductions for the PCI factor) and the required structural section (T_r), yielded a required overlay of 36mm (0.12'). The minimum overlay thickness based on the aggregate size in the mix is controlling the thickness. Therefor, the selected thickness was 39mm (0.13'). This assumes that the appropriate pre-overlay perpetration measure has been selected.

PRE-OVERLAY PREPARATION TECHNIQUES

Once the pavement failures had been identified a strategy for the pre-overlay preparation was formulated. There are several techniques that are summarized below. Each may be appropriate in the correct situation, but in any case, a clear understanding of the failure mode is essential for a dependable maintenance overlay.

Minimal Preparation - Broom cleaning or power wash of the road surface only.

Crack Sealing - After a broom cleaning of the road surface, debris in cracks less than 6mm (1/4") are blown out with a high pressure hose. Hot or cold modified asphalts are poured into the crack and stuck off flush with the surrounding pavement. The asphalts are typically modified with various fillers such as; finely ground mineral aggregate, rubber, or polyester fibers. The oil may be further modified with chemical polymers or latex products. Cracks can be routed out before sealing however, this can be a rather expensive process.

Seal Coats- Applied to areas were the cracks are greater than 3.1mm (1/8") and are connected in a large area. After a broom cleaning of the road surface, debris in cracks are blown out with a high pressure hose. A thin coat of asphalt emulsion is applied at a rate that fills the cracks and provides enough material to accept and retain an aggregate wearing surface. The area is then rolled with a rubber tire roller and allowed to cure. Excess chip may then be swept up.

Skin Patches and Leveling Courses - Hot or cold asphalt plant mix is spread over a clean roadway surface to eliminate differences in the transverse and longitudinal road profile.

Remove and Replace - Damaged pavement is removed with a saw cut, jack hammer, or grinder unit to a depth that reaches stable subgrade. The damaged section should be removed with a squared edge and about 0.3m (1') into sound pavement. Suitable aggregate base is compacted in place and remaining vertical faces are given a tack coat. The hole is then backfilled with plant mixed asphalt concrete, raked, compacted, and checked with a straight edge for uniformity. Full depth asphalt concrete may be used in lieu of the aggregate base. A rule of thumb is that 25mm (1") of asphalt concrete is equivalent to 50mm (2") of aggregate base.

On Elk Grove Boulevard, County Forces utilized a pavement grinder with a 0.9m (36") wide head that rotated at high speed to remove several of the most severe sections of damaged pavement from the wheel path and replaced it with 0.17m(7") of aggregate base and 50mm (2") of asphalt concrete. Several control sections were left un-repaired and the remainder of the damaged pavement was marked for the respective test interlayers. On Elverta Road, the preparation work consisted of a broom cleaning of the road. It should be noted that the pavement condition was fairly consistent through out the test section and therefor, not advantageous to any one product.

TEST PRODUCT DESCRIPTIONS, THEORY AND APPLICATION

The products used on this project do not represent the only products available nor does the use of the product represent an equal comparison to others.

All test products were laid on the day of the paving and no traffic was allowed upon them. Products 5 - 9 could have been placed in advance of the overlay. On Elk Grove Boulevard the entire road was allowed to be closed because there was a convenient parallel detour route. On Elverta Road, one half the road was closed and the traffic was moved onto the adjacent lane under a flagging operation. The manufacturer's representative were present during the installation. See figures 4 through 9.

GRIDS:

<u>**Test Product 1 Bayex GlasGrid**</u>® <u>**(8501)**</u>
Fiberglas open mesh grid 12.5mm square(0.5" X 0.5") coated with a high modulus elastomeric polymer and a pressure sensitive adhesive backing. Designed to take up thermal stress and resist the propagation of cracks through a new overlay mat with a tensile resistance of 560 lbs./in. and a typical elongation of less than 2%. The product is manufactured onto rolls of 1.5m (5') width, and come in 91.4m (300') lengths. Application is made by using a mechanical placement tractor followed by a rubber tire roller to establish the bond of adhesive backing. Remedial pavement preparation efforts must be made to clean, seal, and level the roadway. The recommended minimum overlay thickness is 37.5mm (1 1/2").
Installation: This product went down very efficiently and would not delay a normal paving operation. The adhesive backing worked properly provided the surface was level. Tack coat from adjacent test sections cause a release of the self adhesive backing. Some minor pick-up observed from asphalt deliver trucks.

Test Product 2 TENSAR AR
Rigid Polypropylene open mesh grid 45mm X 62.5mm (1.8" X 2.5"). Designed to control rutting and resist the propagation of cracks through a new overlay mat with a tensile resistance of 1,500 lb/ft. The grid mechanically combines with the asphalt pavement to reinforce and confine the overlay. The product is manufactured onto rolls of 1.9m (6.3') and 3.8m (12.6') widths, and come in 164' lengths. Application is made by using a mechanical placement tractor and attached to the existing pavement with a nailing pattern. Remedial pavement preparation efforts must be made to clean, seal, and level the roadway. The recommended minimum overlay thickness is 62.5mm (2 1/2").
Installation: This product was quite rigid and sections humped up even after nailing. This caused the grid to float up into the mat when the rollers passed over. This would not allow proper compaction as successive passes caused the mat to segregate. The overlay thickness was 25mm (1") thinner than recommended. This was an oversight on the behalf of the project engineer and the problems associated with this section should not necessarily be reflective of the products installation or performance. Nailing operation was time consuming and may be a delay to a paving work.

Elverta Road Pavement Reinforcing Mastic, Membrane, and Grid Test Sections
Measured From Centerline of Sorento Road West to El Rio Avenue

Bid Item	From (ft)	To (ft)	Eastbound Lane	Westbound Lane	Transverse Cracks > 1/2" 12" wide	Test Products (linear feet)								
						1 10' wide	2 12.6' wide	3 10' wide	4 12.6' wide	5	6	7 (36" wide)	8	9
16	2050	2260		X								210		
18	1840	2050		X							210			
20	1630	1840		X						210				
22	1890	2290	X						400					
24	1500	1890	X					390						
26	495	990		X			495							
28	0	495		X		495								
TOTAL (SQ. FT)						4950	6237	3900	5040	630	630	630		
(Linear Feet)						495	495	390	400	210	210	210		

Note: All measurements are approximate. The Engineer shall determine the exact limits of material placement based on their judgment of the pavement condition.

TJR:pmb [c:\data\ovrlay95.fed\ssect2.xls]

FIG.4

Elk Grove Boulevard Pavement Reinforcing Mastic, Membrane, and Grid Test Sections

Measured From Centerline of Grantline Road West to Bradshaw Road

Bid Item	From (ft)	To (ft)	Eastbound Lane	Westbound Lane	Transverse Cracks > 1/2" (12" wide)	1 (5' wide)	2 (6.3' wide)	3 (5' wide)	4 (6.3' wide)	5	6	7 (36" wide)	8	9
11	0	230*		X	200									X
11	0	500	X	X	360									X
12	0	400	X											400
13	500	750	X	X	180								X	
14	400	1000	X										600	
15	750	1000	X	X	180							X		
16	250	950		X								700		
17	1000	1500	X	X	360						X			
18	950	1055		X							105			
18	1350	1387		X							37			
18	1425	1773		X							148			
18	1000	1500	X	X	720						500			
19	1500	2500	X	X						X				
20	1500	2000	X							500				
21	2000	2500	X						500					
23	1597	1875		X				278						
23	1875	2000		X				250						
25	2000	2250		X			250							
27	2250	2597		X		250								
Linear Feet						250	250	528	500	500	790	700	600	400
(SQ. FT.)					2300 LF	1250	1575	2640	3150	1500	2370	2100	1800	1200
Transverse										720 LF	360 LF	180 LF	180 LF	560 LF
(SQ. FT.)					2300	0	0	0	0	720	360	180	180	560
Total Sq Ft						1250	1575	2640	3150	2220	2730	2280	1980	1760

Columns 1–9 = Test Products (linear feet)

Note: All measurements are approximate. The Engineer shall determine the exact limits of material placement based on their judgment of the pavement condition.

*Southbound Grantline Road to Westbound Elk Grove Boulevard ramp.

FIG.5

PRODUCT 8

GEOTAC PLACED OVER TRANSVERSE CRACKS
Elk Grove Blvd. October 10, 1995

PRODUCT 9

PETROTAC PLACEMENT
Elk Grove Blvd. October 10, 1995

FIG.6

PRODUCT 6

PAVEPREP PLACEMENT

Elk Grove Blvd. October 10, 1995

PRODUCT 9

PETROTAC WITH PAVEPREP IN FOREGROUND

Elk Grove Blvd. October 10, 1995

FIG.7

PRODUCT 1

GLASS GRID PLACEMENT
Elk Grove Blvd. October 10, 1995

PRODUCT 3

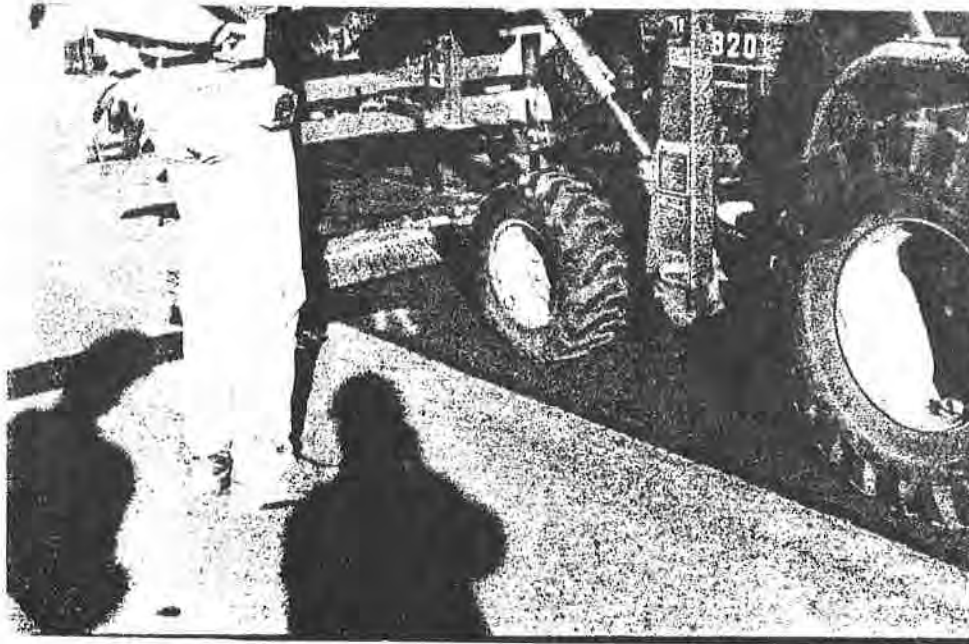**BITUTEX PLACEMENT**
Elk Grove Blvd. October 10, 1995

FIG.8

PRODUCT 2

TENSAR AR INSTALLED
Elk Grove Blvd. October 10, 1995

PROJECT ENGINEER AND PAVING OPERATION
Elk Grove Blvd. October 10, 1995

FIG.9

GRIDS WITH FABRIC:

Test Product 3 BITUTEX®-Composite

A combination of woven polyester grid 29.5mm square(1.18" X 1.18") coated with Styrol Butanien Rubber attached to a non woven polyester fabric. Designed to resist fatigue cracks through a new overlay mat with a tensile resistance of 841 lbs./ft. and a typical elongation of less than 20% and to prevent moisture from penetrating to the base material and cause further structural degradation. The product is manufactured onto 1.5m (5') wide rolls and come in 91.4m (300') lengths. Application is made by using a mechanical placement tractor onto a tack of asphalt emulsion, followed by a rubber tire roller to establish the bond. Remedial pavement preparation efforts must be made to clean, seal, and level the roadway. The recommended minimum overlay thickness is 37.5mm (1 1/2").

Installation: This product went down very efficiently and would not delay a normal paving operation. Some minor pick-up observed from asphalt deliver trucks.

Test Product 4 TENSAR ARC

Rigid Polypropylene open mesh grid 45mm X 62.5mm (1.8" X 2.5") laminated to a non woven polyester fabric. Designed to control rutting and resist the propagation of cracks through a new overlay mat with a tensile resistance of 1,500 lb/ft. and to prevent moisture from penetrating to the base material and cause further structural degradation. The grid mechanically combines with the asphalt pavement to reinforce and confine the overlay. The product is manufactured into rolls of 3.9m (13') width, and come in 50m (164') lengths. Application is made by using a mechanical placement tractor over an asphalt tack coat to saturate the fabric. Remedial pavement preparation efforts must be made to clean, seal, and level the roadway. The recommended minimum overlay thickness is 62.5mm (2 1/2").

Installation: This product was somewhat rigid but, went down efficiently and would not delay a normal paving operation.

REINFORCED FABRIC MASTICS:

Installation: These product all behaved essentially the same. They are temperature sensitive and could become more rigid in cold weather applications. On this project all products were supple and were readily placed. Rolls were heavy and somewhat difficult to handle. Roller operator stated that he could feel a bump as the equipment passed over the product in the transverse direction. A slight shadow was observed through the mat. However, after several days of traffic loading this was no longer observed.

Test Product 5 AMOCO Proquard

High density (80 lbs/cu. ft.) asphaltic mastic sandwiched between layers of high modulus woven polyester fabric and a non woven fabric 0.33mm (0.135")thick. Designed to be a stress relieving interlayer to dissipate the forces through the width of the product and reduce the tendency for the propagation of cracks through the overlay. The product is also designed to prevent moisture from penetrating to the base material and cause further

structural degradation. The product is manufactured into rolls of 0.3m(12"),0.5m (20"), 0.9m (36"), or 1.2m (48") width, and come in lengths that vary from 14.6m (48') to 31m (102') lengths. Application is made by hand onto a tack of asphalt, followed by a light hand roller to establish the bond of adhesive backing. There is minimal pavement preparation other than cleaning and sealing the roadway. This product can be placed days in advance of the overlay and be exposed to traffic. The recommended minimum overlay thickness is 37.5mm (1 1/2").

Test Product 6 PavePrep®SA

High density (80 lbs/cu. ft.) asphaltic mastic sandwiched between layers of polyester fabric 0.33mm (0.135") with an adhesive side packaged with a removable release liner. Designed to be a stress relieving interlayer to dissipate the forces through the width of the product and reduce the tendency for the propagating of cracks through the overlay. The product is also designed to prevent moisture from penetrating to the base material and cause further structural degradation. The product is manufactured into rolls of 0.3m(12"),0.5m (20"), 0.9m (36"), or 1.2m (48") width, and come in lengths that vary from 14.6m (48') to 31m (102') lengths. Application is made by hand followed by a light hand roller to establish the bond of adhesive backing. There is minimal pavement preparation other than cleaning and sealing the roadway. This product can be placed days in advance of the overlay and be exposed to traffic. The recommended minimum overlay thickness is 37.5mm (1 1/2").

Test Product 7 Perma GlasPave™

High density (77 lbs/cu. ft.) asphaltic mastic with a fine sand coating on one side with a high tensile, low elongation fiberglass reinforcing grid sandwiched between 3mm(0.12" thick) with a removable release liner on the other. Designed to be a stress relieving interlayer to dissipate the forces through the width of the product and reduce the tendency for the propagating of cracks through the overlay. The product is also designed to prevent moisture from penetrating to the base material and cause further structural degradation. The product is manufactured into rolls of 0.3m (12"), 0.6m (24"), or 0.9m (36") width, and come in lengths that vary up to 19.8m (65') lengths. Application is made by hand followed by a light hand roller to establish the bond of adhesive backing. There is minimal pavement preparation other than cleaning and leveling the roadway. This product can be placed days in advance of the overlay and be exposed to traffic. The recommended minimum overlay thickness is 37.5mm (1 1/2").

REINFORCED FABRIC MEMBRANES:

Installation: These product all behaved essentially the same. They are temperature sensitive and could become more rigid in cold weather applications. On this project the products were supple and were readily placed. Rolls were moderately heavy and somewhat difficult to handle. Roller operator stated that he could feel a bump as the equipment passed over the product in the transverse direction. A slight shadow was observed throughout the mat. However, after several days of traffic loading this was no longer observed.

Test Product 8 GEOTAC®

Rubberized asphaltic membrane with a top layer of polyester geotextile with an adhesive side packaged with a removable release liner. Designed to be a waterproofing interlayer in an overlay to prevent moisture from penetrating to the base material and cause further structural degradation. The product is manufactured into rolls of 0.3m (12"), 0.5m (20"), or 0.9m (36") width, and come in lengths that vary form 14.6m (48') to 31m (102') lengths. Application is made by hand followed by a light hand roller to establish the bond of adhesive backing. There is minimal pavement preparation other than cleaning and sealing the roadway. This product can be placed days in advance of the overlay and be exposed to traffic. The recommended minimum overlay thickness is 37.5mm (1 1/2").

Test Product 9 PETROTAC®

Rubberized asphaltic membrane with a top layer of polypropylene non woven fabric with an adhesive side packaged with a removable release liner. Designed to be a waterproofing interlayer in an overlay to prevent moisture from penetrating to the base material and cause further structural degradation. The product is manufactured into rolls of 0.3m (12"), 0.5m (20"), or 0.9m (36") width, and come in lengths that vary form 13.7m (45') to 31m (102') lengths. Application is made by hand followed by a light hand roller to establish the bond of adhesive backing. There is minimal pavement preparation other than cleaning and sealing the roadway. This product can be placed days in advance of the overlay and be exposed to traffic. The recommended minimum overlay thickness is 37.5mm (1 1/2").

COST COMPARISONS

Figure 10 illustrates the maintenance and rehabilitation treatments used by Sacramento County. The associated costs for these treatments were derived from typical publicly contracted projects and work performed by County Forces. The bid prices for the test products are also shown. On this project, County Forces removed and replaced damaged pavement with a pavement grinder to a depth of 225mm (9"), compacted the underlying subgrade, and replaced the area with 175mm (7") of compacted aggregate base and 50mm (2") of asphalt concrete(See figure 15). The costs for normal pre-overlay preparation methods vary from surface sealing to complete reconstruction. The costs for base repair techniques that would be typical and appropriate for these test roads ranged from jackhammer removal with County forces at $21.89 per square yard, to private contractor work at $17.50 per square yard, to grinder removal with County Forces at $10.28 per square yard. Test product costs ranged from $3.60 to $18.00 per square yard, and falls within the range of conventional repair costs. Each product has its' own properties for stabilizing and/or acting as a water barrier on the existing pavement. Their long term performance will determine if their use is economically justified.

SACRAMENTO COUNTY

Maintenance and Rehabilitation Treatments with
Associated Unit Costs in $ / SY in 1996

	MAINTENANCE TREATMENT	$/SY
1	RECONSTRUCT SURFACE & BASE (4" - 6")	17.50
2	RECONSTRUCT SURFACE (2.5")	9.81
3	THICK AC OVERLAY (2.5")	4.23
4	THIN AC OVERLAY (1.5")	2.53
5	THIN AC OVERLAY (1.5") RUBBER	4.81
6	AC OVERLAY (1.5") W/FABRIC	3.57
7	SLURRY SEAL	0.90
8	SINGLE CHIP SEAL	0.54
9	DOUBLE CHIP SEAL	1.02
10	RUBBERIZED CHIP SEAL (2% LATEX)	2.15
11	CHIP SEAL & SLURRY SEAL	1.47
12	MICRO SURFACING	1.45
13	SEAL CRACKS	0.05
14	SKIN PATCH (1") WITH COUNTY FORCES	3.36
15	REMOVE AND REPLACE SHALLOW PATCH (2" - 4") WITH COUNTY FORCES (CONVENTIONAL METHODS)	12.76
16	REMOVE AND REPLACE DEEP PATCH (4" - 6") WITH COUNTY FORCES (CONVENTIONAL METHODS)	21.89
17	REMOVE AND REPLACE DEEP PATCH (7" AB, 2" AC) WITH COUNTY FORCES (GRINDER UNIT METHOD)	10.28

GRIDS

Product 1	Bayex Glassgrid	6.75
Product 2	Tensar AR	3.60

GRIDS WITH FABRIC

Product 3	Bitutex	13.50
Product 4	Tensar ARC	9.00

REINFORCED FABRIC MASTICS

Product 5	Progaurd	13.50
Product 6	Paveprep SA	18.00
Product 7	PermaGlassPave	18.00

REINFORCED FABRIC MEMBRANES

Product 8	Geotac	9.00
Product 9	Petrotac	9.00

K:\SB\TJRREHAB.MNT

FIG.10

16 MONTH INSPECTION

At the writing of this paper, 16 months have passed since the original test installation. An inspection of the test sections did not show any evidence of pavement distress, other than the section with product 2 on Elk Grove Boulevard for the reasons described previously. This section has minor tearing in the surface in spots. These occurred very shortly after the original construction and it is interesting to note that in this section the mat has stabilized and only the surface tears are evident. No maintenance has been performed to date.

It is planned to conduct periodic follow-up inspections of these test sections and prepare supplemental reports. These reports will utilize the crack map that was prepared to pinpoint the condition of the pavement under the various test products and control sections.

CONCLUSION

The identification of the cause of pavement distress is essential to properly decide when to specify a geosynthetic interlayer in-lieu of the complete removal and replacement of damaged pavement. Hand in hand with this identification is the need to "design" the thickness of a maintenance overlay to satisfy structural needs and minimize reflective cracks. While long term evaluation of the test sections presented in this paper must be completed, it has been shown that most of these products can be installed without significantly impacting a paving operation. This is particularly true with those products that can be placed a day in advance of the overlay. The theoretical reinforcement and/or water barrier benefits of these products are based upon sound principles and the sections are performing well to date. Geosynthetic interlayers fall within the bracket of costs associated with more conventional base repair techniques performed by Sacramento County, and may prove to be an efficient, cost effective means of pre-overlay preparation that is equivalent in performance.

REFERENCES

Bushey, R.W., Sept. 1976 "Experimental Overlays to Minimize Reflective Cracking" <u>Caltrans, FHWA-CA-TL-3167</u>.

Donaldson, Ralph, Industrial Asphalt Incorporated & Rademacher, Paul, Executive Director of the Asphalt Paving Association. Personal interviews 1996.

Institute of Transportation Studies, 1984 University of California, "Pavement Maintenance and Rehabilitation Using Asphalt" <u>Course Notes, UCB-ITS-CN-84-1</u>.

Mahmoudi, K. G., Fall 1991 "Application of Geosynthetics in Improvement of Flexible Pavement Systems" <u>Masters Thesis, Cal. State Sacramento</u>.

Smith, R. E., August 1987 "Pavement Managers User's Guide for the Bay Area Pavement Management System (PMS)" <u>Metropolitan Transportation Commission</u>.

Acknowledgments

FULL SCALE DYNAMICAL TESTING ON REINFORCED BITUMINOUS PAVEMENTS

G. DONDI
D.I.S.T.A.R.T. DEPARTMENT
UNIVERSITY OF BOLOGNA, ITALY

ABSTRACT

Polymeric interlayers, such as geosynthetics, appear to be able to delay the surface cracking due to reflection of fissures from the underlying layers of damaged bituminous pavements. They are usually laid over a bituminous tack coat prior to the construction of an overlay. In our experimentation we examine the effectiveness of the insertion of geosynthetics in the top asphalt layers. In order to simulate the road pavement, we employed a steel box filled in the lower half with rubber. Above, two bituminous concrete layers with different interlayers were placed. In some specimens, deep artificial grooves were made in order to examine a damaged existing pavement. Then a laboratory research was undertaken to achieve a simulation of fatigue behaviour: a maximum of 500,000 cycles of loading at a frequency of 5 Hz were applied. The results of the reinforced specimens showed, although there was no improvement of the overall stiffness before the occurrence of a certain degree of cracking, the advantages of interlayers insertion in terms of reduction of displacements and rut depths. By virtue of the results it's possible to consider insertion of geosynthetics in bituminous pavement an effective rehabilitation works tecnique.

INTRODUCTION

Surface cracking, which is not always induced by traffic loads, is one of the main problems related to the durability of asphalt pavements. In fact, the rehabilitation of fissured road surfaces is often unsuccessful due to reflective cracking phenomena. The interposition of so-called "Stress Adsorbing Membrane Interlayers" (S.A.M.I.) is quite widespread and, in many cases, seems to be successful. Nevertheless, this geosynthetics application is not always rationally designed since a generally accepted design procedure still does not exist. We report the main questions, still pending, to which we are trying to give a reply, on the completion of our research, in the next months:

1. Which is the best type of geosynthetic (nonwoven geotextiles, geogrids, etc.) for asphalt reinforcement ?
2. Which is the best location for the synthetic interlayer ?
3. What is the minimum thickness for the asphalt overlay ?
4. Is the insertion of a geosynthetic in new roads construction to prevent the described phenomena opportune ?

The experimentation described in this paper deals with the behaviour of bituminous pavements containing synthetic interlayers. This subject has already been studied in the past by our University (Dondi and Righi, 1990), (Dondi, 1994), utilizing numerical methods. Recently a large number of experiments has been carried out. In an initial stage, for a preliminary static evaluation, we did some "three point bending" tests on bituminous mixes beams: without interlayers (UR), with nonwoven geotextiles (GX) and with polyester (PET) geogrids (GG).
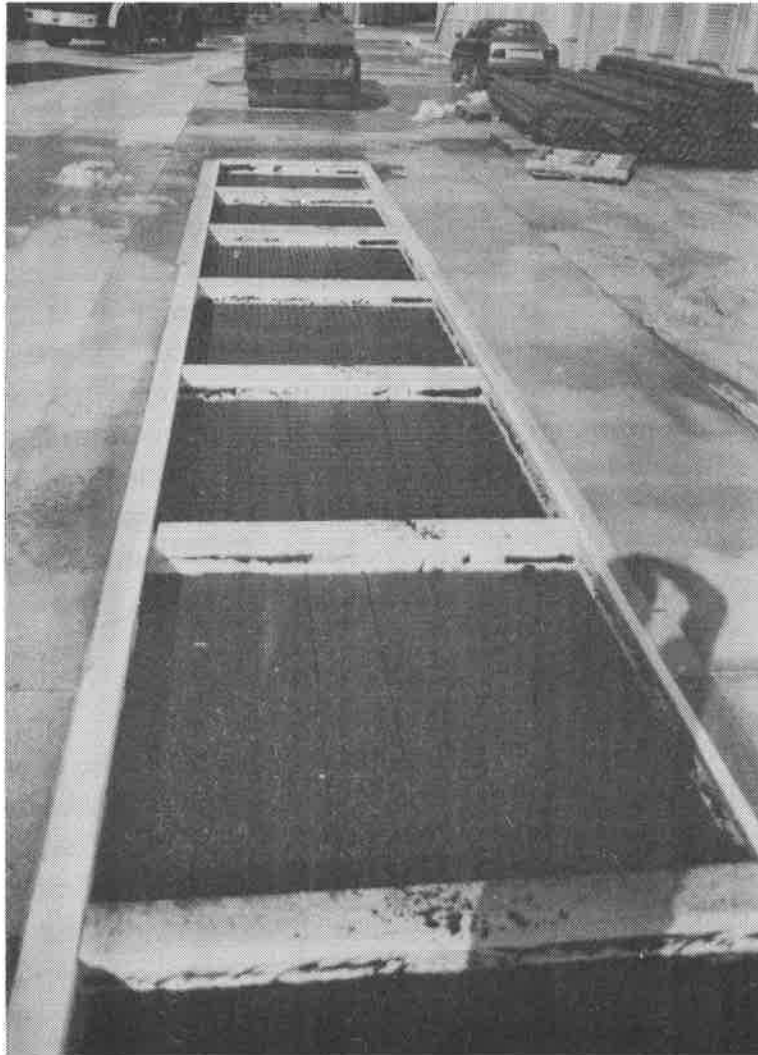

Figure 1. Samples preparation: longitudinal cuttings can be seen.

Then we created 24 specimens (1.4x1.4m) with many types of interlayers and degrees of disturbance (Fig. 1).It may also be interesting to describe the early stage of the experimentation, taking into account that, due to testing characteristics, it was impossible to consider a wider selection of interlayers. In this article we will consider only macro-reinforcement (Fig. 2); i.e. the interlayers that are well defined in the bituminous mix. The reinforcement of asphalt, as well known, requires high temperature resistant polymers: indeed with modified binders, during compaction, the mix reaches high temperatures (130-150 °C). For this reason it was necessary to use at least polypropylene (PP) or PET geotextiles.
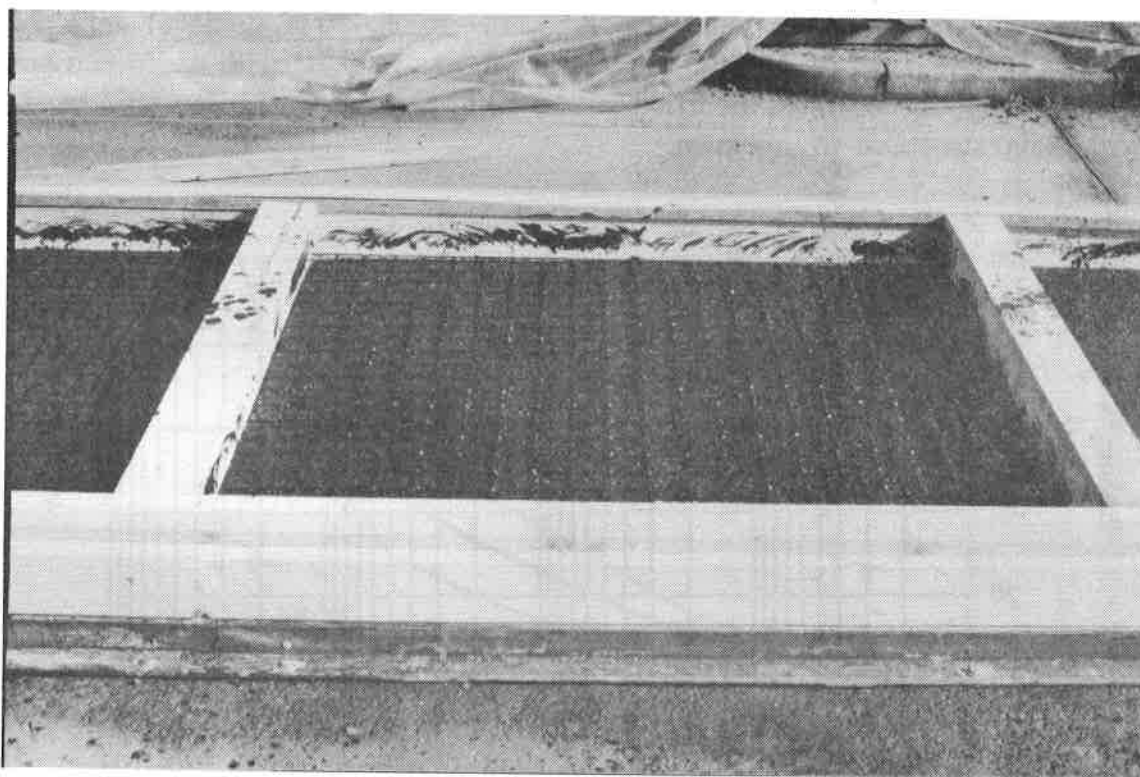
Figure 2. Detail of a polypropylene geogrid insertion in a specimen.

The insertion of nonwoven geotextiles in a flexible pavement generally causes a strength decrease despite a better overall behaviour. For this reason, some prefer stiffer geogrids or composites; furthermore, the latter theoretically seems to provide a better solution because improves the linking with the upper bituminous layer also without any tack coat upon the interlayer surface.

PRELIMINARY TESTS

In the first preliminary stage of the research we have verified, according to Judycki (1990), that the best loading methodology was, for many reasons, the three point bending: stresses and strains are more realistic. The samples were 100 mm wide, 85 or 100 mm high, and 600 mm long. The interlayer, when present, was placed 35 mm over the bottom of the sample. The rate of

loading was approximately 50 mm/min', as suggested also by Kunst e Kirschner (1993) and all the tests were carried out using a bituminous mix, with a 5% of 80/100 penetration grade bituminous binder.

The grain size distribution curve of the aggregate is represented in Fig. 3, with the binder fuse of the Italian National Roads Administration.

As an interlayer, we employed two geosynthetics currently used for road pavements: a nonwoven polypropylene geotextile (Grab Test, ASTM D-4632: 450 N, ε_f=55%) and a polyester woven geogrid (Tensile Test: 60 kN/m). The tack coat was realised with a cationic emulsion containing 70% of 80/100 bitumen, modified with 5 % of Styrene-Butadyene-Styrene (SBS-R) modifier with radial structural arrangement.
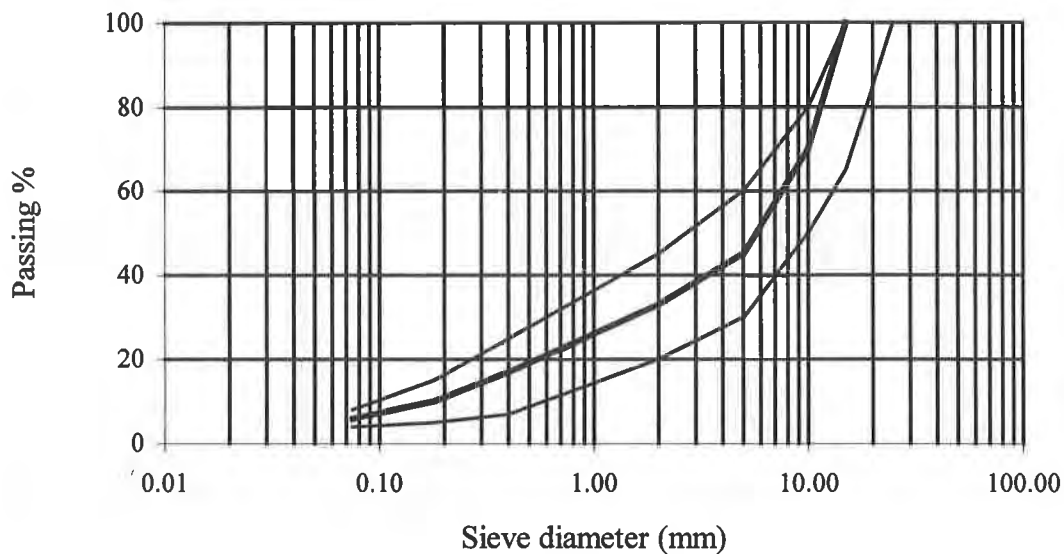
Figure 3. Grain size curve of the bituminous mix.

Typical results obtained in a three point loading tests on various samples show (Fig. 4) that when employing geogrids, there is a small increase of resistance, while with nonwoven geotextiles, the strength slightly decreases. But in both cases, even for large settlements, cracking never reaches the upper surface of the sample. The failure of specimens with geosynthetics, at displacements 2-3 times greater than the value recorded without interlayers, is due to sliding of the geosynthetic along the interface with bituminous concrete.

Furthermore, the most important aspect of synthetic interlayers is the increased capability of bearing high loads even after failure, i.e. a higher ductility (see Fig. 4). By employing criteria based on total deformation work balance, for interpreting the static tests (Dondi, 1995), we

obtained an increase ($\Delta\sigma_y$) of the equivalent ultimate strength, for the materials reinforced by geogrids, of more than 60%.

This last value of $\Delta\sigma_y$ appears to be more representative than the simple peak stress ratio of the improved mechanical properties.
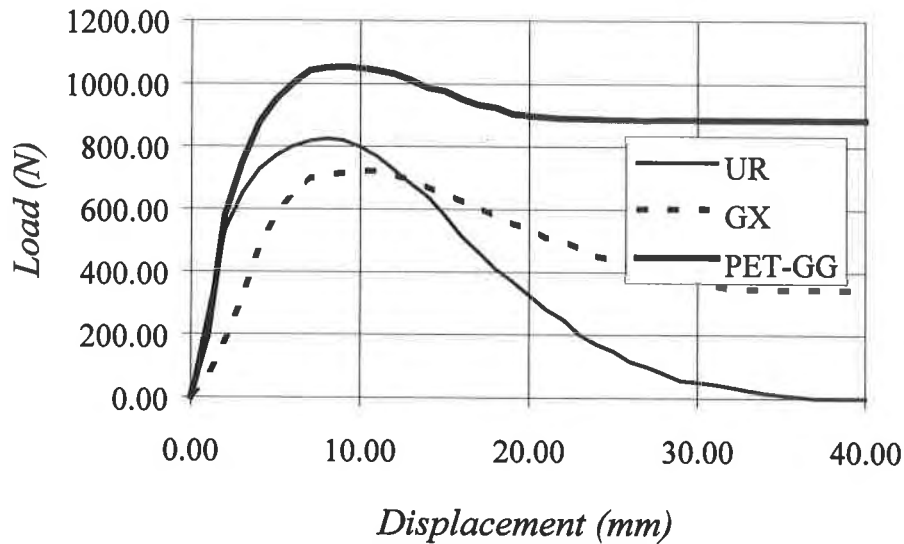
Figure 4. Comparison between "three point loading" tests on various samples.

The equivalent ultimate strength can be conventionally defined (Dondi, 1995) by the expression:

$$\sigma_y = L_y \cdot \frac{1.5 \cdot l}{b \cdot h^2} \tag{1}$$

where b, l, h represent respectively the cross section dimensions and length of the specimen and L_y is for hte equivalent yelding load, which is conventionally obtained by the results of the three point loading test.

The specimen behaviour, defined by the experimental load-displacement log, can be schematized by a two-straight line, as showed in Fig. 5. The sloping straight line has the maximum gradient (k) of the experimental curve and the total deformation work is represented by area (A) subtended by the two-straight line. The area is upper confined by a conventional deformation δ_u defined as:

$$\delta_u = \mu \cdot \delta_0 \tag{2}$$

where μ is the ductility, assumed equal 3, and δ_0 is the displacement corresponding to the maximum strength L_f. According to the previous considerations, the critical load L_y can be expressed by:

$$L_y = k \cdot \delta_u - \sqrt{(k \cdot \delta_u)^2 - 2 \cdot A \cdot k} \tag{3}$$
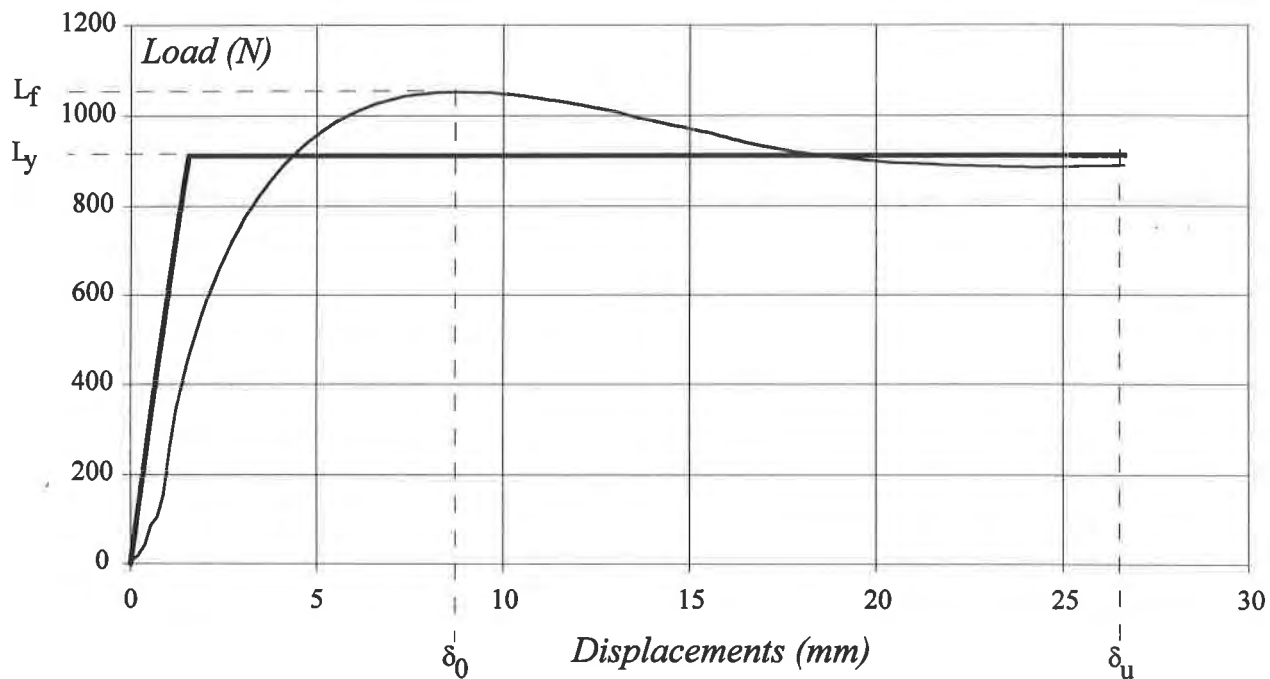
Fig. 5. Determination of the critical load L_y

DYNAMIC FULL SCALE LOAD TESTS

Encouraged by these results, we planned, in a second stage, to carry out more specific dynamic tests in order to better simulate traffic load conditions. The first step of this research project consisted in a comparison of the results obtained with numerical models such as BISAR (De Jong 1973) and F.E.M. non linear models (Fig. 6) such as FENLAP (De Almeida 1993). In particular, we tried to establish the different behaviour of semi infinite and confined multilayered system. It was discovered that, in order to avoid significative boundary effects, the minimum dimensions of squares specimen was approximately 1.5x1.5 m.

Therefore, we created a bituminous concrete strip, approximately 36 m long, in two stages (two layers): after completion of the first one, in some areas an artificial cutting was also realised to represent the rehabilitation of a fissured pavement; then various kinds of interlayers were inserted. The various samples have the characteristics shown in Table 1.

A steel box was then built to contain the asphalt samples and the underlying layers (Fig. 7). The load was applied by means of a circular steel plate, with a diameter of 0.3 m standing on a rubber layer with the function of minimizing stress concentration related to plate stiffness.
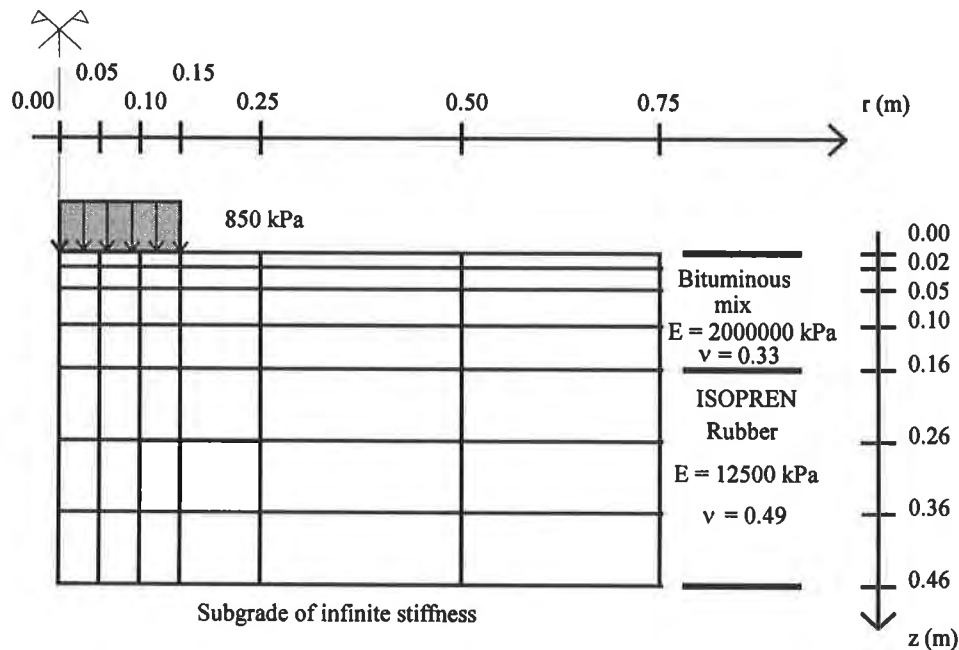
Figure 6 . Numerical mesh of the samples for numerical analysis.

To enhance only the behaviour of asphalt, and with the aim of reducing the uncertainties as much as possible, we decided to build the foundation bed with a rubber characterised by a simpler constitutive law than that of a granular material (Fig. 7). Therefore the asphalt samples, made outside in a single strip 36 meters long as described previously (see also Fig.1), were then cut away, brought in the laboratory, and disposed directly on the rubber settled down in the steel box. Hence the rubber represents, as far as stiffness is concerned, both the foundation and the subgrade layers. The asphalt specimens have a total thickness of 160 mm arranged as follows (Fig. 7):

1. a bottom 60 mm-thick asphalt layer, in some cases fissured (indicated in the text as "LE", whereas the other non-fissured samples are referred to as "NL") by cutting it with a steel tool for a depth of 50 mm;
2. the interlayer, when present, fixed with a cationic bituminous emulsion (1000gr/m^2 approximately) tack coat;
3. a top 100 mm thick asphalt layer.

Table 1. Characteristics of specimens tested

a) Non Lesioned bituminous concrete (NL)
a.1) Unreinforced Specimen (UR)
a.2) Specimen with nonwoven geotextile interlayer (GX)
a.3) Specimen with bi-directional woven polyester (PET) geogrid (GG) interlayer
a.4) Specimen with bi-directional polypropylene (PP) geogrid (GG) interlayer
a.5) Specimen with polypropylene (PP) geocomposite (GX+GG) interlayer
b) Lesioned bituminous concrete(LE)
b.1) Unreinforced Specimen (UR)
b.2) Specimen with nonwoven geotextile interlayer (GX)
b.3) Specimen with bi-directional woven polyester (PET) geogrid (GG) interlayer
b.4) Specimen with bi-directional polypropylene (PP) geogrid (GG) interlayer
b.5) Specimen with polypropylene (PP) geocomposite (GX+GG) interlayer
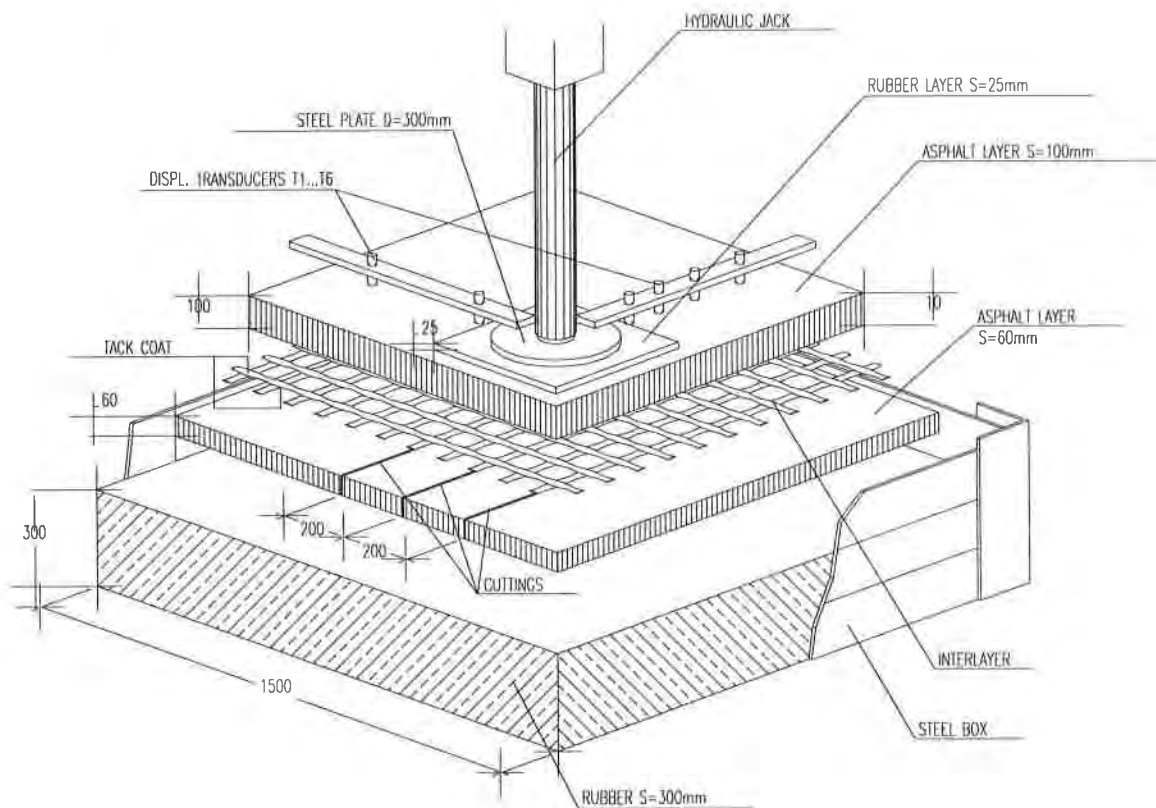
Figure 7. Sample composition.

The load was applied by a hydraulic jack, controlled by the data acquisition system, with a frequency of 5 Hz. The shape of the loading wave is approximately sinusoidal and has an initial amplitude (ΔV_o) of 60 kN, in the range 5-65 kN. During the tests and in some cases with very high displacements, it was necessary to reduce this amplitude in order to maintain the original frequency.

Two reference grids, 100x100 mm, and 50x50 mm in the central portion, were sketched on the surface of the samples previously covered with white paint, to allow reporting the failure pattern vs. number of cycles.

Surface displacements, at different distances from the loading plate, were monitored with inductive transducers connected to an Instron data acquisition system (Figg. 7 and 8).
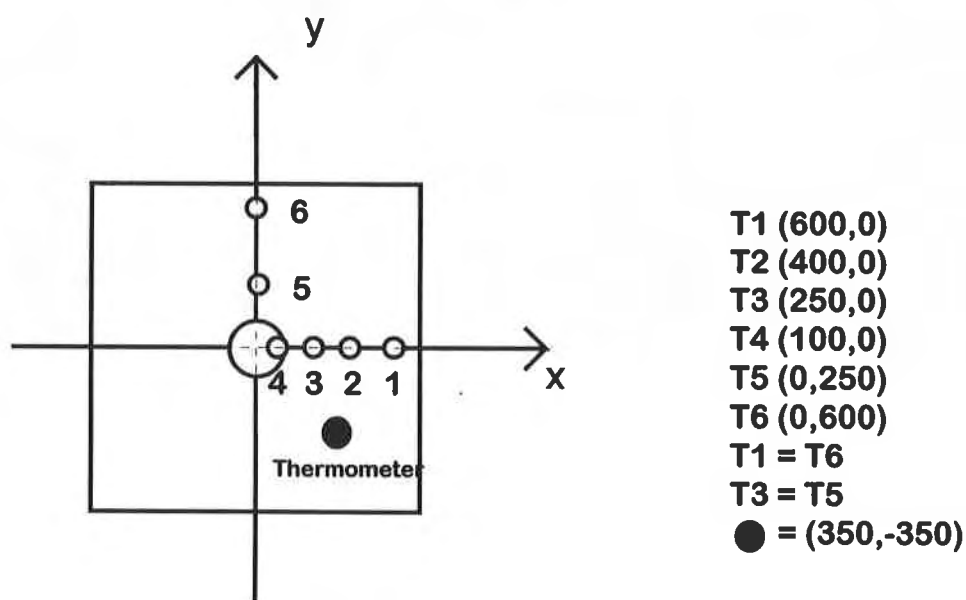
Figure 8. Location of transducers

RESULTS INTERPRETATION

Due to the fact that postprocessing requires a lot of time, we are presently only in a position to report partial data. All the samples, at the end of the tests (approximately three days long) showed very significant permanent displacements (Fig. 9), although the degree of damage was very different. It seems interesting, in particular, to compare the details of the results obtained on four samples.

These samples are:
1) Non-lesioned, with a nonwoven geotextile as interlayer (NL-GX);

2) Non-lesioned, without interlayers (NL-UR);
3) Lesioned, with a nonwoven geotextile as interlayer (LE-GX), (Fig. 10(A));
4) Lesioned, without interlayers (LE-UR), (Fig. 10(B)).
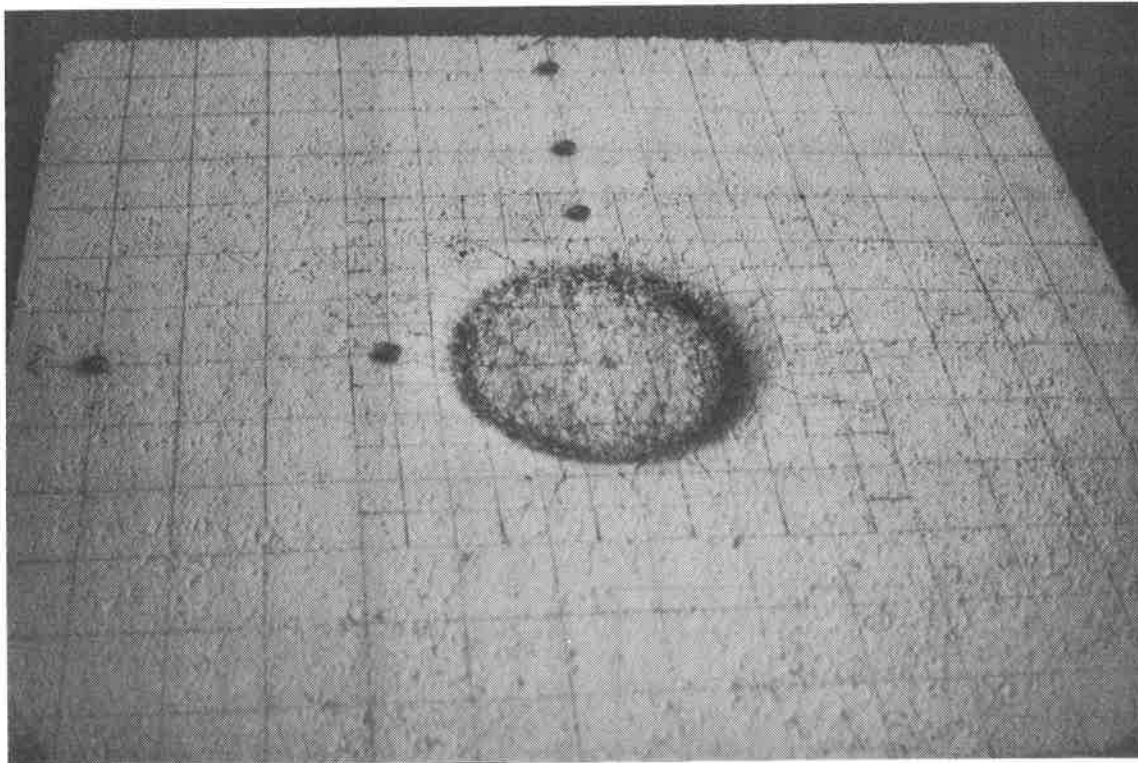
Figure 9. A specimen after 5×10^5 loading cycles

As described previously, it is to be pointed out that the failure behaviour of the various types of samples is quite different.

In non-lesioned samples (NL), cracking starts in radial directions on the free surface: this behaviour was previously observed by other authors (Kief et al., 1994) so we could assume that this is normal for pavements whose unique factor of degradation is repetitive loading. In lesioned samples (LE), the cracking pattern, as shown in Fig. 10 for 5×10^5 cycles, follows the alignment of artificial cuttings.

Permanent deformations are surprisingly similar for samples with (GX) and without interlayers (UR), while dynamic pseudo-elastic deformations follow a different behaviour: after 4×10^5 cycles, instantaneous settlements significantly increase in LE-UR sample while tend to be constant in the LE-GX specimen (see Fig. 11). Furthermore, cracks appear later in specimens and their extension is much smaller than in samples without geosynthetics.

When analysing the total viscoplastic settlement of fissured samples (see Fig. 11), the two curves for UR and GX samples are so close that no differences can be pointed out.

This is consistent because we didn't expect any stiffness increase consequent to the introduction of a nonwoven geotextile.
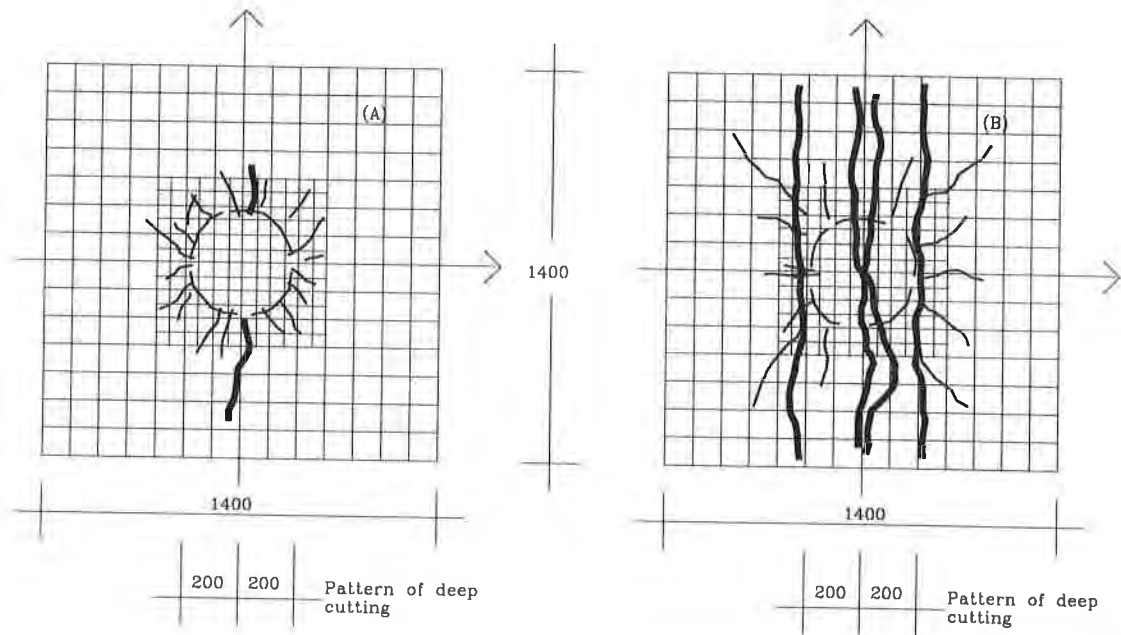
Figure 10. Cracking after 5 x 10^5 cycles in two similar samples: one, on the left, has an interlayer (LE -GX) and the other does not (LE -UR).

Taking into consideration the instantaneous fraction of the total displacement, we can see that, prior to a certain number of cycles (i.e. approximately 4x10^5, Fig. 11) the curves are quite similar. After this limit, there is a rapid increase of settlements in UR samples. However, the behaviour of GX samples is better even near failure because, due to the lower degree of surface breaking, downward water seepage is prevented. This certainly plays an important role in delaying the pavement degradation.

CONCLUSIONS

Macroreinforcement of bituminous mixes with geosynthetics, in particular with woven polyester geogrids (see Fig. 12) and composites, appears to be a powerful tool primarily in critical conditions such as heavy loads and for overlays of intensely fractured pavements. It has the advantage of allowing the recycling and, as pointed out in the first part of the article, there is a significant improvement of the ductility of bituminous layers. Actually, with polyester geogrids, there is also a slight increase in ultimate strengths, without interlayer failure.
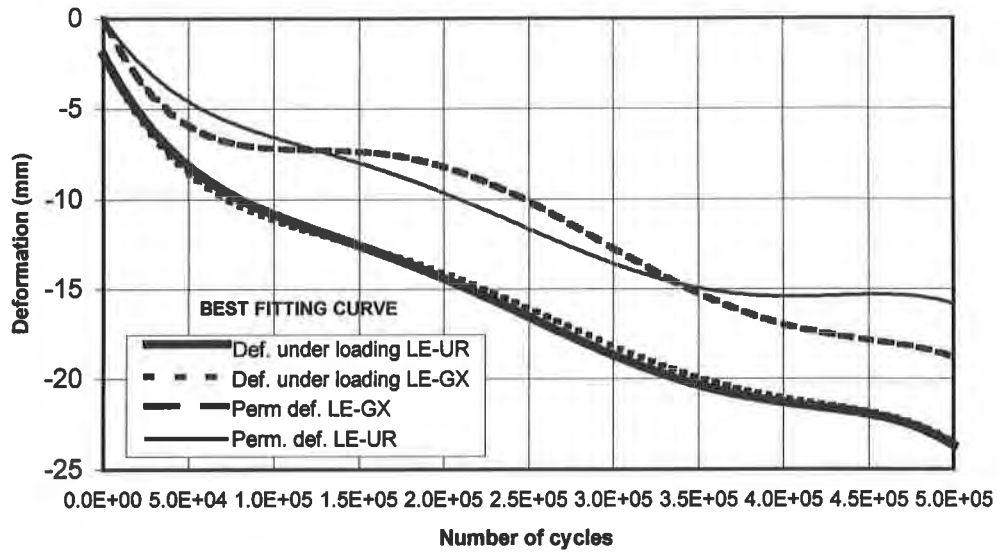
Figure 11. Settlement under loading surface vs. N° of cycles.

Failure mechanism is also different and, in any case, the presence of an interlayer delays the cracking reflection: this was also demonstrated by the experimentation carried out on full scale samples subjected to dynamic loading in order to better represent in situ conditions.
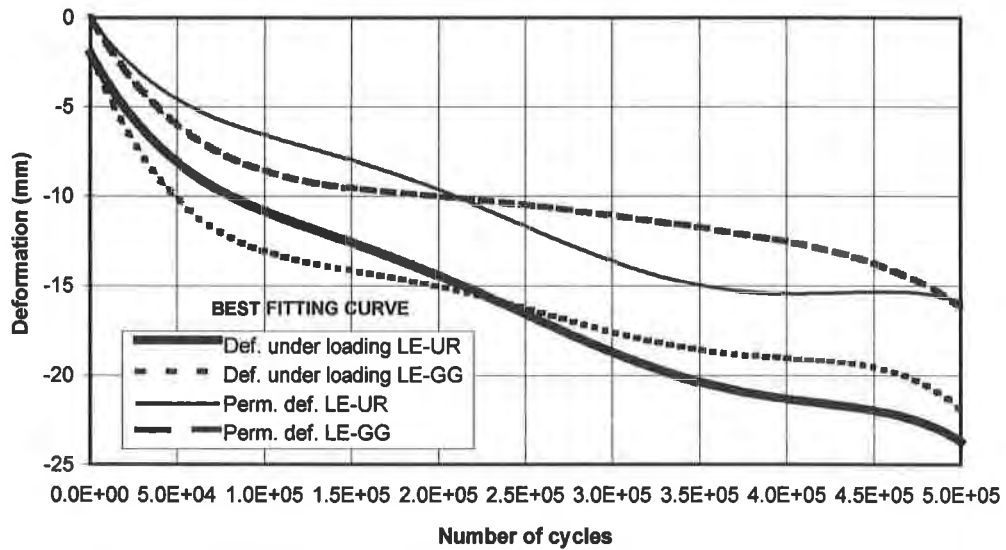
Figure 12. Settlement under loading surface vs. N° of cycles.

These tests, initially carried out with samples containing nonwovens, have substantially confirmed the results of static tests: the overall stiffness of the pavement doesn't increase, but

the degree of cracking is much lower. This confirms once more that nonwovens insertion in bituminous pavement rehabilitation works and with a good tack coat, is a guarantee of durability for the overlays.

The next step of this research project, while results interpretation is again in progress, consists of an in situ validation of laboratory tests. We have realised an experimental field by reproducing, in a lane of the Piacenza-Cremona-Brescia Motorway (A21) in Northern Italy (see Fig.13), some samples very similar to those tested in the laboratory. In order to take into account the real traffic volume and composition, we will also arrange for an instrumental section with an axles counter and an inductive load-measurement device.
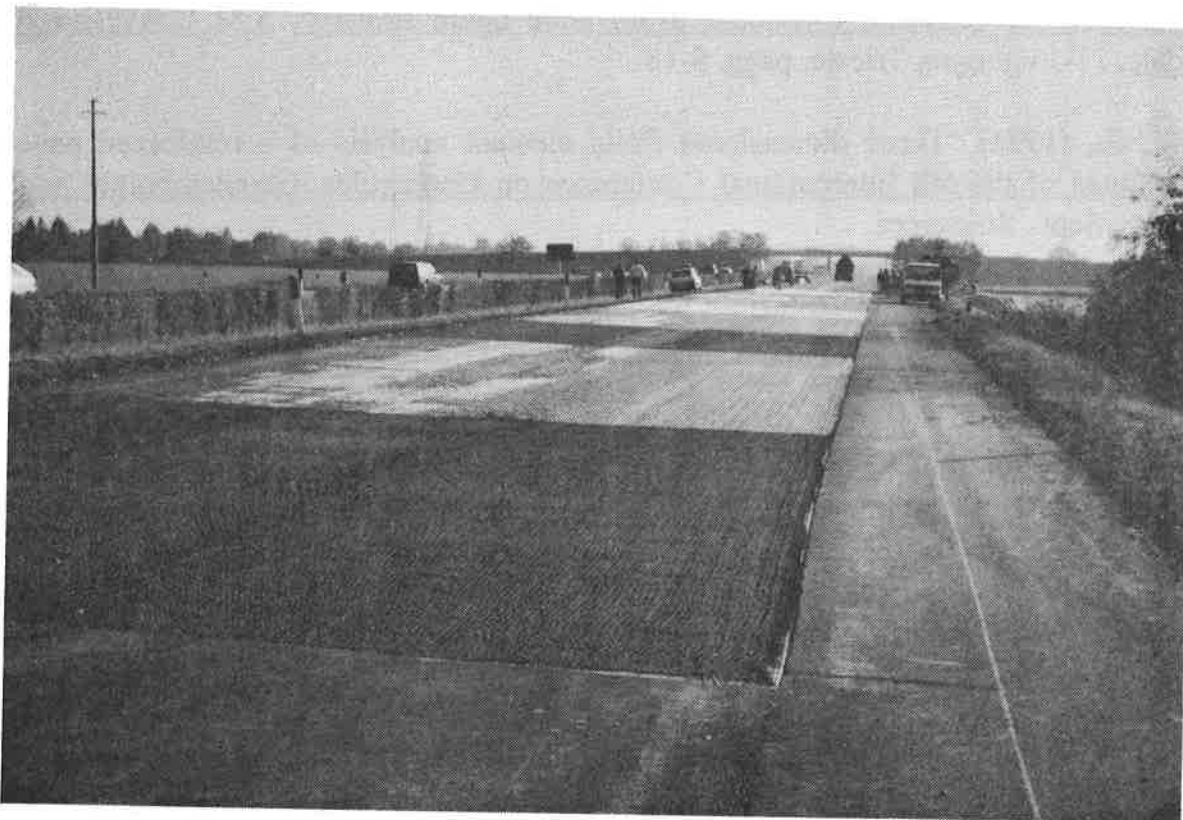
Figure 13. Experimental field in a motorway lane

ACKNOWLEDGEMENTS

REFERENCES

De Almeida Rocha, J. C. G., (1993) "Analytical Techniques for the Structural Evaluation of Pavements", Thesis submitted to the University of Nottingham, Department of Civil Engineering, for the degree of Doctor of Philosophy.

De Jong, D.L., Peutz, M.G.F., and Korswagen, A.R. (1973) "Computer Program Bisar, Layered systems under normal and tangential surface loads".

Dondi, G., and Righi, P.V. (1990) "Rinforzo delle sovrastrutture stradali", Quaderno AIPCR: "L' Impiego dei geotessili e prodotti affini nelle opere stradali", XXI Convegno Nazionale Stradale, 11-15 giugno, Trieste, pagg, 9-18.

Dondi, G., (1994) "Three dimensional finite element analysis of a reinforced paved road", Proceedings of the 5th International Conference on Geotextiles, Geomembranes and Related Products, Sept., Singapore.

Dondi, G., (1995) "Le pavimentazioni flessibili rinforzate mediante geosintetici", Estratto dagli Atti del Convegno Naz.:"La ricerca nel settore delle infrastrutture interportuali e aeroportuali", 28-29 giugno, Trieste.

Judycki, J., (1990) "Bending test of asphaltic mixture under statical loading", Proceedings of the fourth Intern. RILEM Symposium, October, Budapest.

Kunst, P.A.J.C., and Kirschner, R. (1993) "Comparative laboratory investigations on polymer asphalt inlays", Geosynthetics '93 Conference Proceedings, March, Vancouver, British Columbia.

Kief, O., Livneh, M., Ishai, I. and Altus, E. (1994) "Experimental and analytical approaches for studying reflective crack retardation", Proceedings of the 5th International Conference on Geotextiles, Geomembranes and Related Products, Sept., Singapore.

Economics

GEOSYNTHETICS 97
CONFERENCE
Long Beach, California USA

VALUE ENGINEERING: AN ALTERNATIVE LINER SYSTEM AT THE LA PAZ COUNTY REGIONAL LANDFILL

A. L. SHAFER, P.E.
Browning-Ferris Services, Inc., USA

S. PURDY, CEG
Vector Engineering, Inc., USA

D. TEMPELIS, P.E.
Browning-Ferris Industries, Inc., USA

ABSTRACT

The La Paz County Regional Landfill is a 65 hectare (160 acre) municipal waste site located near the western border of Arizona between the cities of Parker and Quartzsite. The site is operated under a public/private partnership between the County of La Paz and Browning-Ferris Industries, Inc. (BFI). The County owns the landfill and infrastructure and BFI is responsible for facility improvements, environmental compliance, and daily operations.

Following the initial permitting and construction of the first landfill cell, a value engineering review was conducted on the site design and permit requirements. Based on this review, substantial cost saving opportunities were identified. In order to implement the value engineering ideas, the site permit was modified and a new Solid Waste Facilities Plan was submitted to the Arizona Department of Environmental Quality.

This paper discusses the value engineering modifications that were conducted, the revisions to the permits, and the relative cost savings that were realized. The areas addressed include the liner system design, closure design, disposal capacity, and operations plan. Through the use of alternative liners a cost savings of well over 50 percent (as compared to the original permit) will be realized over the life of the landfill.

INTRODUCTION

The La Paz County Regional Landfill became operational under a public/private partnership on November 7, 1994, with the initial disposal of municipal waste into a newly constructed composite lined cell (Phase 1). The landfill is owned by the County of La Paz and operated by Browning-Ferris Industries of Arizona, Inc. (BFI), under an approved Solid Waste Facilities Plan.

The average depth to water at the site is approximately 152 meters (500 feet) with a groundwater gradient of about 0.009 meter/meter in a north-northwesterly direction toward the Colorado River, approximately 24 kilometers (15 miles) to the northwest. The subsurface lithology at the La Paz site consists of well-graded silty sands with some coarser gravels present at depth. In general, similar materials to those found at the surface extend more than 213 meters (700 feet) directly below the site (Bedinger, Sargent and Langer 1990). The average yearly precipitation at the landfill site has been

estimated to be about 13 centimeters (5.1 inches) per year based on data from the U.S. Department of Commerce, National Oceanic and Atmospheric Administration.

The liner system of the initial waste cell was constructed using a 1.5 millimeter (60-mil) high-density polyethylene (HDPE) geomembrane with an underlying 0.6-meter (2-foot) bentonite amended compacted soil liner (hydraulic conductivity less than 1 x 10^{-7} cm/sec) in accordance with the standards of 40 CFR 258 (Subtitle D) and the State of Arizona. Bentonite was trucked to the site from a borrow source in Utah and mixed with the on-site soils in a pug mill to attain the required hydraulic conductivity.
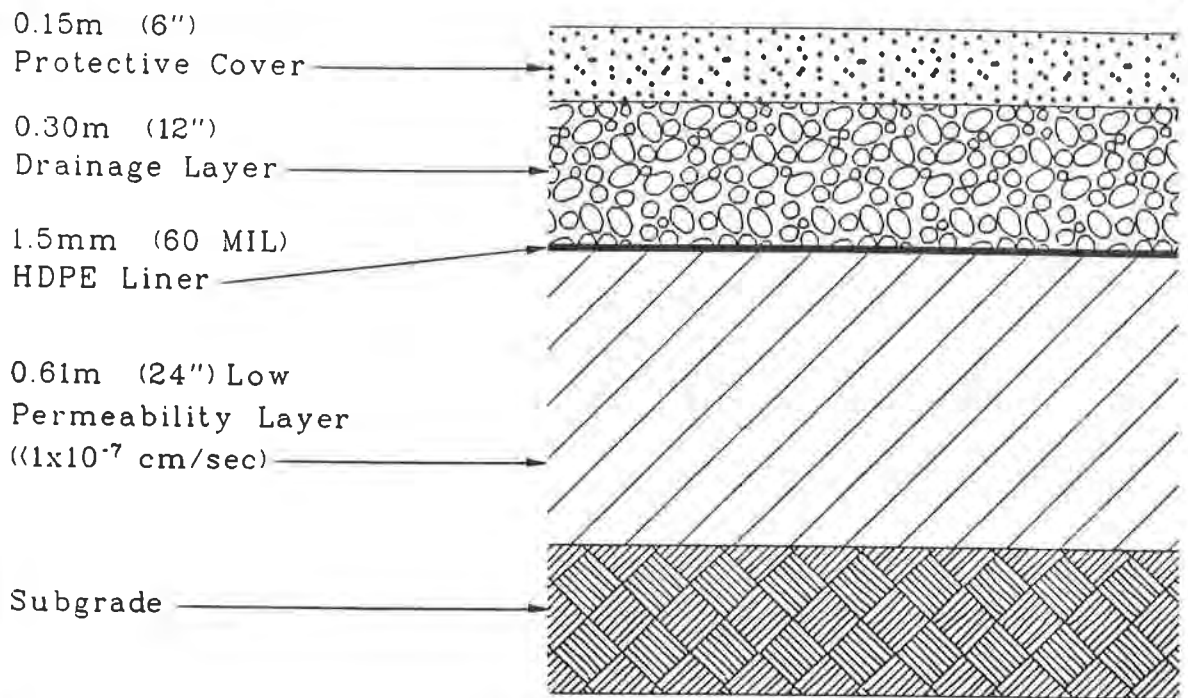
Due to the timing involved with the construction of the first landfill phase, a originally permitted liner system was installed. Since no on-site or nearby clays were available which could attain the requirement of less than 1 x 10^{-7} cm/sec, bentonite was mixed with the soils to achieve the desired hydraulic conductivity. This resulted in relatively high material, construction, and quality assurance costs on the project. After the Phase 1 Cell was operational, a value engineering analysis was performed to evaluate the potential for implementing cost saving design alternatives on subsequent phases of landfill construction.

Based on the value engineering analysis, it was determined that utilizing a geosynthetic clay liner (GCL) could result in lower material costs, increase the airspace available for refuse, and decrease the construction period and quality assurance costs. As required by Subtitle D, Section 258.40 (c), an engineered alternative must consider the hydrogeologic characteristics of the site and surrounding land; the climatic factors of the area; the volume of leachate; and physical and chemical characteristics of the leachate. These factors, as well as the viability of groundwater impacts and a comparison of the leakage rates for GCL and compacted soil liners were evaluated to demonstrate that a GCL liner alternative will ensure that the concentration values listed in Table 1, Section 258.40 of Subtitle D would not be exceeded in the uppermost aquifer at the relevant point of compliance.

The engineered alternative evaluation described above was submitted to the Arizona Department of Environmental Quality (ADEQ), and approval was granted to substitute a GCL for the 0.6-meter (2-foot)-thick originally permitted soil liner. The Phase 2 Cell at the La Paz County Regional Landfill was then designed and constructed utilizing a GCL in place of the 0.6-meter (2-foot) compacted bentonite amended soil liner. The following paper discusses the components of the engineered alternative evaluation dealing with the use of geosynthetics. The evaluation includes a comparison of leakage rates, constructability, and cost savings.

LINER SYSTEM COMPARISON

Originally Permitted Liner System. The liner system originally permitted for use at the La Paz County Regional Landfill consisted of a Subtitle D composite liner composed of HDPE geomembrane and an underlying 0.6-meter (2-foot) thick, bentonite amended compacted soil liner with a hydraulic conductivity of less than 1 x 10^{-7} cm/sec. In order to compare this liner system with the proposed alternative GCL system, the leakage through each of the liners was determined. Cross-sections of the originally permitted and proposed alternative liners are shown on Figure 1.

0.15m (6")
Protective Cover

0.30m (12")
Drainage Layer

1.5mm (60 MIL)
HDPE Liner

0.61m (24") Low
Permeability Layer
((1x10^{-7} cm/sec)

Subgrade

Originally Permitted Liner Detail

0.15m (6")
Protective Cover

0.30m (12")
Drainage Layer

1.5mm (60 MIL)
HDPE Liner

Geosynthetic Clay
Liner

0.30m (12") Prepared
Subgrade
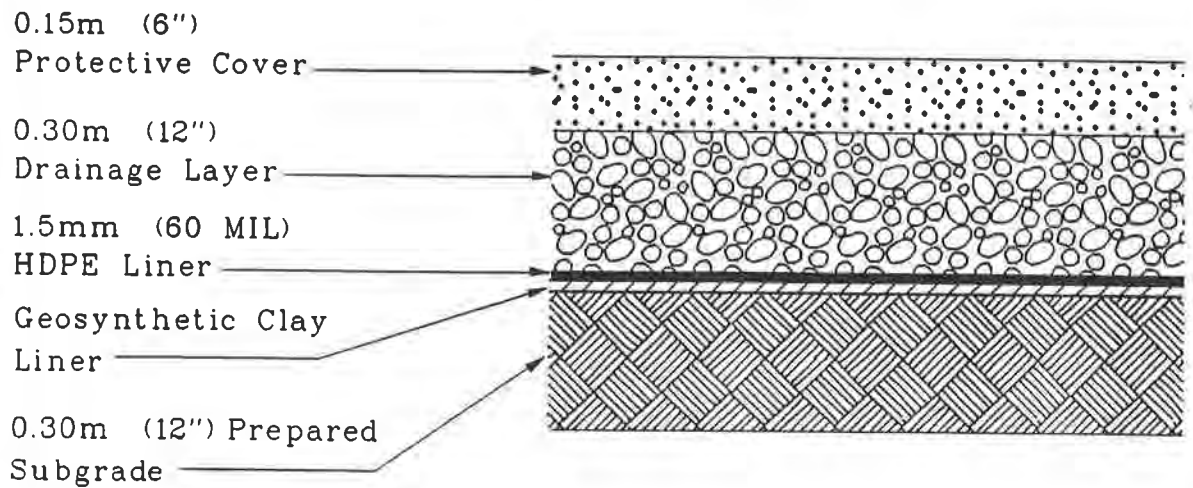
Alternative Liner Detail

Figure 1. Schematic of Liner Systems

Two documents that discuss leakage rates through liners have been published by the U.S. Environmental Protection Agency, Office of Solid Waste (EPA 1987, 1992). The purpose of these reports was to provide other governing agencies background information to assist in the development of performance standards and allowable leakage rates for operating facilities. The "background" document (EPA 1987) describes the development of leakage rate formulae and presents corresponding calculated results for many liner system configurations.

In order to compare the difference in flow rate from a standard one-square centimeter hole in a composite liner with good contact, a given clay hydraulic conductivity, and a head of 18.5 centimeters (7.3 inches) (maximum head on liner from HELP modeling conducted as part of the engineered alternative evaluation), the following equation by Giroud (1989) was used:

$$Q = 0.21h^{0.9}a^{0.1}k_s^{0.74}$$

Where: Q = flow rate (m^3/s)
           h = head over liner (m)
           a = area of hole (m^2)
           k_s = hydraulic conductivity of the subsoil (m/s)

For this formula, the flow rate from a composite liner with the prescriptive soil liner hydraulic conductivity of 1 x 10^{-7} cm/sec was determined to be 0.14 liters per hectare (0.09 gallons per acre) per day. This leakage rate assumes that good contact was achieved between the soil liner and HDPE geomembrane and that good construction quality assurance was performed.

Proposed Alternative Liner. The proposed alternative liner system for the La Paz County Regional Landfill consisted of replacing the 0.6-meter (2-foot) compacted soil liner with a GCL. There are currently two major types of commercially available GCLs. One type consists of bentonite encased between two geotextile fabrics and the second type consists of bentonite glued to a HDPE geomembrane.

The type of clay typically used in GCLs is sodium bentonite. Sodium bentonite is the name given to the highly plastic clay mineral montmorillonite, with sodium as the primary exchangeable cation. Bentonites used to fabricate GCLs are processed in an unhydrated state such that they appear to have a granular consistency. Upon hydration with water, the bentonite swells to form a continuous clay layer.

GCLs are shipped in rolls typically 3.7- to 5.3 meter (12- to 17.5-feet) wide and 25- to 61-meter (82- to 200-feet) long. They are installed by unrolling to form panels. Adjacent panels are overlapped, and for some products powdered bentonite is placed between the panels at overlaps. Large-scale laboratory testing (Daniel 1991) has shown that, when installed in accordance with the manufacturer's specifications, GCL overlaps are self-sealing and do not create a preferential pathway for liquid flow.

GCLs have been used in liner systems and cover systems for landfills, surface impoundments, and tank farms, as well as in other structures. When used in landfills, GCLs are often substituted for the compacted low-permeability soil component of a composite liner. The function of the GCL in the

composite liner is identical to that of a compacted soil liner which is to provide a low-permeability barrier to liquid flow through any defect in the overlying geomembrane.

The GCL material is manufactured under strict quality control (QC) guidelines. The QC requirements include conducting index and performance testing on both the supplied materials and finished product at specified frequencies. After the material is approved at the manufacturing plant, care is taken to keep the rolls dry, not stack them too high, and keep them from damage during handling. Prior to acceptance in the field, information concerning the manufacturer's name, product name, lot and roll number, and length, width, and weight must be submitted to the on-site CQA firm.

To analyze the leakage through a composite liner utilizing a GCL instead of a compacted soil liner, the hydraulic head over the liner determined from the HELP modeling discussed previously was again used. Good contact with the overlying geomembrane (a GCL with bentonite glued to the geomembrane would have excellent contact) was also assumed.

To determine the leakage from a composite liner with a GCL, the same equation as that utilized for the prescriptive liner was used:

$$Q = 0.21 h^{0.9} a^{0.1} k_s^{0.74}$$

Where: Q = flow rate (m^3/s)
          h = head over liner (m)
          a = area of hole (m^2)
          k_s = hydraulic conductivity of the subsoil (m/s)

While the same equation is used to determine leakage through the HDPE/GCL composite system, the head over the liner is much greater than the thickness of the GCL. In order to determine the average hydraulic gradient (i_{ave}) in a system with the head of leachate much greater than the thickness of the barrier layer, a curve developed by Giroud (1990) was used. From this curve, an i_{ave} of approximately 5 was determined.

Assuming the same defect size per hectare (0.4 cm^2 per hectare (1 cm^2 per acre)) and the same head on the liner (18.5 centimeters (7.3 inches)), the difference between the GCLs and the compacted soil liner is the hydraulic conductivity of the material and i_{ave}. GCLs with bentonite sandwiched between two geotextiles have hydraulic conductivities on the order of 1 x 10^{-11} to 5 x 10^{-11} m/sec (Cetco 1996 and Naue-Fasertechnik 1996). The hydraulic conductivity of the GCL with bentonite glued directly to geomembrane is a function of both the bentonite and the membrane. From the manufacturers literature, this the composite hydraulic conductivity is on the order of less than 1 x 10^{-11} m/sec (Gundle/SLT Environmental 1995). Manufacturers reported laboratory hydraulic conductivities vary vary with gradient and overburden pressure.

The leakage rates through the proposed alternative liner system were then calculated for the GCL. Since either type of GCL material would be acceptable for use as an alternative to the bentonite amended soil liner, the bentonite sandwiched between two layers of geotextile was used for the leakage calculation because it has a higher hydraulic conductivity. The leakage rate for the alternative liner system was then calculated to be 0.023 liters per hectare (0.015 gallons per acre) per day.

The leakage rate from the originally permitted liner system was determined to be 0.14 liters per hectare (0.09 gallons per acre) per day. Comparing this leakage rate to that of the alternative liner system shows that the alternative system leaks at a rate 6 times less than the originally permitted system. Wilson-Fahmy and Koerner (1995) have also concluded that the leakage rates through GCLs appear to be smaller than leakage rates through compacted soil liners.

COMPARISON OF CONSTRUCTABILITY

The above sections compared the leakage rates between the originally permitted Subtitle D composite liner and the proposed alternative composite liner utilizing a GCL. While the above discussions demonstrate that the leakage performance of the alternative liner is superior to that of the prescriptive liner, another factor to consider is the constructability in the field. In order to evaluate this performance in the field, the uniformity of the physical properties, durability, resistance to mechanical damage, and chemical compatibility must be considered.

Since GCLs are manufactured in a plant under strict quality control guidelines, consistency and uniformity of the product is quite high. For a bentonite amended soil liner (such as that installed in Phase 1); however, quality control is much more difficult. The contractor and CQA firm must rely on index property tests in the field in addition to laboratory hydraulic conductivity tests. The diversity of on-site materials used to mix with the bentonite could create variations in the final hydraulic conductivity of the soil liner.

Desiccation. A potential problem involving soil liners placed in a desert environment like Arizona is desiccation cracking. Since clay liners must be installed at moisture conditions above optimum, the potential for the material to dry and crack is very high. This potential for drying is not only extremely high when the clay liner is exposed, but is also high after the clay is covered by geomembrane due to the dry subgrade pulling moisture out of the clay.

Since GCLs are installed in a dry condition, they are not subject to desiccation cracking unless they become saturated and then dry out. Shan and Daniel (1991) found that if a GCL is hydrated and then dried, desiccation cracks form. However, they also found that when a GCL is rehydrated, it swells, and the hydraulic conductivity returns to approximately the original value.

Mechanical Damage. The potential for mechanical damage to a liner system due to construction operations was considered as part of the liner alternative demonstration. With respect to the alternative composite liner, aspects of construction are generally addressed in the project specifications and construction quality assurance (CQA) plan. Both the specifications and the CQA plan are developed to avoid construction-related damage to the liner system. For instance, the specifications typically require that all geomembrane seaming operations be performed under strictly controlled conditions, and that all seams be nondestructively tested in the field.

Mechanized construction equipment was not allowed to operate within about 0.5 meters (18 inches) of the alternative composite liner and the movement of the equipment was observed by CQA personnel to ensure that the geosynthetics were not inadvertently damaged. If damage did occur, it was identified through CQA monitoring activities, and repaired in accordance with the specifications and CQA plan.

It has been documented in the literature and manufacturer's data that GCLs have substantial self-healing properties. This is an advantageous characteristic should there be an inadvertent and undetected puncture of the alternative composite liner. Shan and Daniel (1991) reported the results of tests in which a GCL was punctured in a dry state and then permeated with water. The authors found that the GCL self-healed (i.e., little adverse effect on hydraulic conductivity) for puncture diameters up to about 2.5 centimeters (1 inch).

The potential for sharp objects in the subgrade (such as protrusions from thin lenses of hard material) to damage the geosynthetic components of a liner system were also considered as part of the landfill design. A compacted soil liner typically provides an excellent bedding layer for an overlying geomembrane. A GCL does not provide the same degree of bedding as a thick soil liner. However, at the La Paz County Regional Landfill, a 0.3 meter (1-foot) compacted subgrade layer composed of fine-grained materials was placed under the GCL. This layer provided protection for the alternative liner system.

The potential for mechanical damage to a liner system due to puncture by sharp objects in the waste was also considered as part of the design and operation of the landfill. The potential for puncturing the geomembrane by waste is the same whether the GCL or compacted soil liner is used. This potential is typically mitigated by the presence of drainage and operations layers.

Leachate Compatibility. Numerous reports have been published regarding the favorable compatibility of compacted soil liners with MSW leachates. These documents include a paper by Daniel and Liljestrand (1984). Similarly, no adverse impact of MSW leachate permeation on GCL permeability has been observed. Eith, Boschuk and Koerner (1990) found no difference between the permeability of samples permeated with water and those permeated with leachate.

Third Party Construction Quality Assurance (CQA). The final consideration involving the installation of a GCL versus a soil liner involves third party CQA. Since the GCL is a manufactured product, the inspection is very straight forward. The monitor must review the manufacturer's and conformance data, observe the subgrade preparation, ensure proper overlap, and inspect the sheet for defects. For the amended compacted clay liner, however, inspection can be difficult and requires very experienced monitors. This is because the monitors must observe the quantities and quality of bentonite added, the variation in the native materials, the final and individual lift placement thickness, the moisture content, the degree of compaction, the potential for interlift bonding, the presence of pumping soils, the protection from desiccation cracking, the surface grading, and the hydraulic conductivity.

Although the inspection of GCLs is more straight forward than that of compacted clay liners, careful observation of drainage/cover material placement is especially critical for GCLs. Since the GCLs are only about 0.6 centimeters (0.25 inches) thick, they are less forgiving to rips or tears. Close observation by CQA monitors (as described in the CQA plan for cell construction) will mitigate this potential problem. For smaller holes in the liner system, GCLs actually perform better than soil liners because of their swell capability and lower hydraulic conductivity.

As demonstrated by the above paragraphs, GCLs are much easier to install and perform third party quality assurance on than soil liners. The ease in constructability and the reduction in leakage rate, made GCLs an improvement to the amended clay liner currently permitted at the site.

COST COMPARISON

Substantial cost savings were realized on the Phase 2 expansion at the site by utilizing the GCL alternative liner system. Construction material and equipment costs were significantly decreased. Construction quality assurance and laboratory testing costs were also reduced using the liner alternative. Also, by removing the 0.6-meter (2-foot) compacted bentonite soil liner, additional airspace was gained.

Total tangible cost savings at this site when comparing Phase 1 construction (originally permitted liner system) with Phase 2 construction (alternative liner system) were on the order of 62 percent. Figure 2, presents a percentage breakdown of the components which comprised this tangible cost savings. Seventy-eight percent of the total tangible savings was contributed by lower construction costs. Five and 17 percent of the savings was contributed by gained airspace and lower CQA and laboratory costs, respectively. Phase 2 construction costs per hectare (acre) were 53 percent lower than Phase 1 construction costs. CQA and laboratory testing costs per hectare (acre) were 27 percent lower during Phase 2 construction than in Phase 1 construction. Figures 3 and 4 graphically present relative costs for construction, CQA, and laboratory testing activities for Phase 1 and Phase 2 construction. The relative construction costs shown on Figure 3 include material, labor and equipment costs. The gained airspace comprised the remainder of the total tangible cost savings.

Several intangible cost savings were not included in the values presented above. Several days were eliminated from the overall construction schedule by substituting the GCL for the 0.6-meter (2-foot) compacted bentonite amended soil liner. Therefore, inefficiencies in operations of the landfill due to on-site construction were eliminated on a more timely basis during the alternative liner phase of construction. Also, expensive natural resources such as water and bentonite were conserved.

CONCLUSION

Based on the calculations described in this paper, it has been shown that the proposed alternative liner system composed of a composite HDPE geomembrane with an underlying GCL leaks at a rate 6 times less than the original permitted liner system utilizing a compacted bentonite amended soil liner (Alternative Liner Report 1995). As discussed earlier in this paper other studies have also concluded that the leakage rates through GCLs appear to be smaller than leakage rates through compacted soil liners. This conclusion held true for both major types of GCLs and agrees with the site specific data presented in this paper.

In addition to demonstrating a lower leakage rate, GCLs were also shown to be superior to compacted soil liners from a constructability standpoint. Although compacted soil liners may be less expensive than GCLs if on-site materials are available, significant cost savings can be realized using GCLs if bentonite amendment or hauling from off-site borrow areas are necessary. Since no on-site clays were available at the La Paz County Regional Landfill, the engineered alternative evaluation utilizing GCLs resulted in a cost savings of over 62 percent.
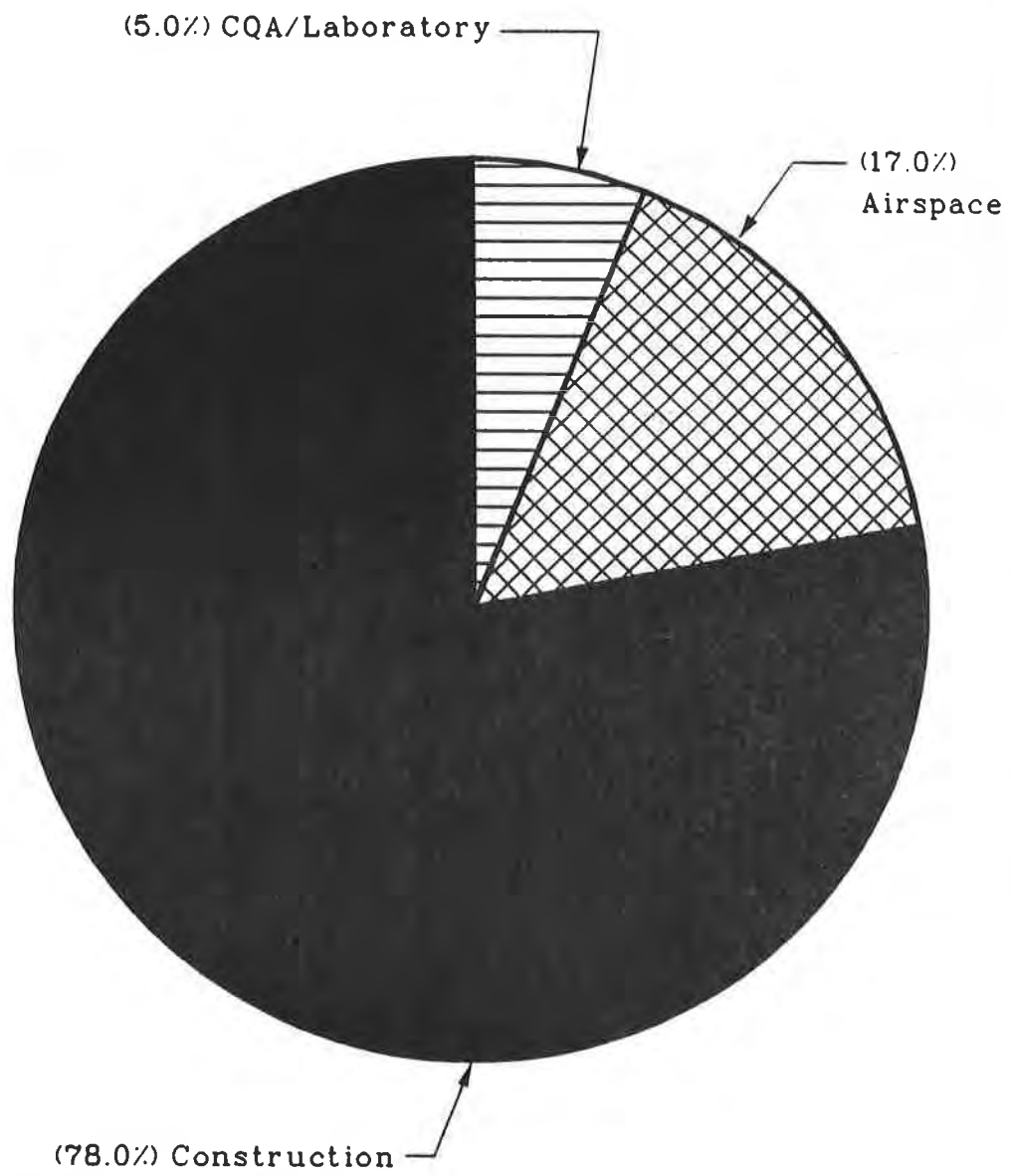
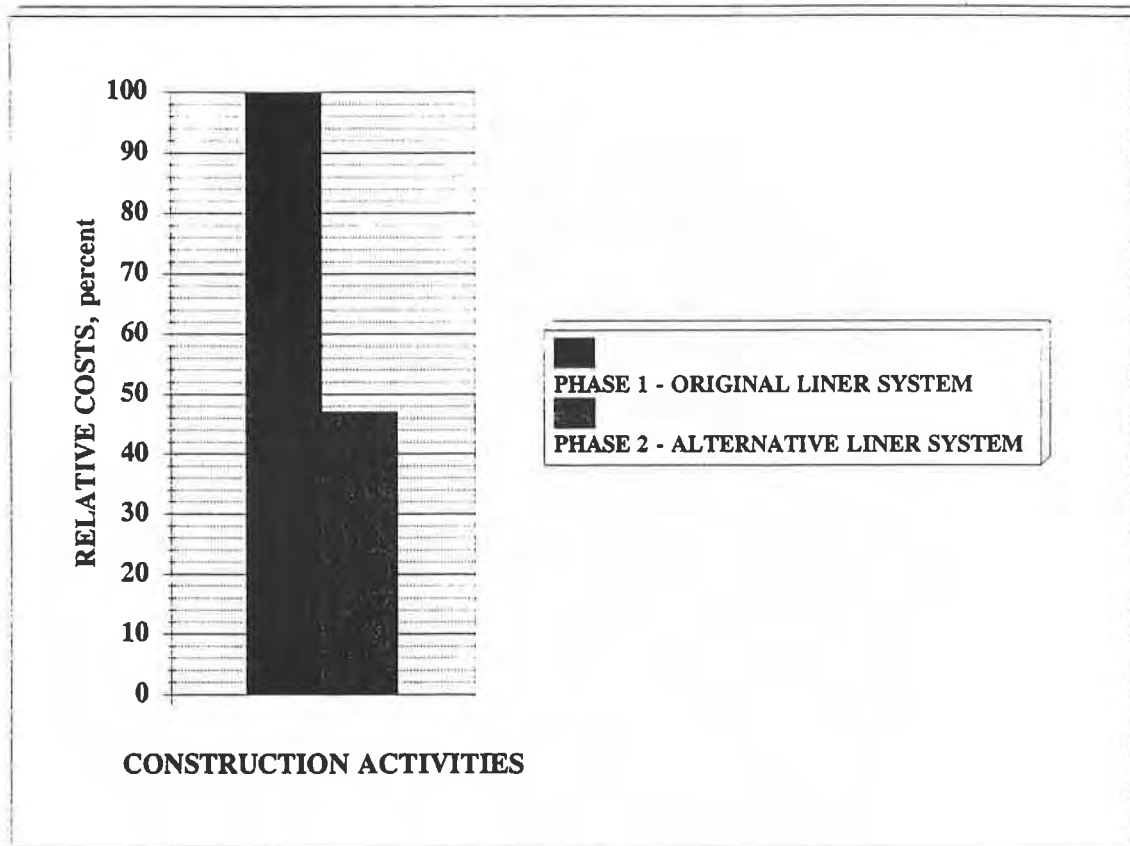Figure 2. Componets and Their Contribution to Tangible Cost Savings

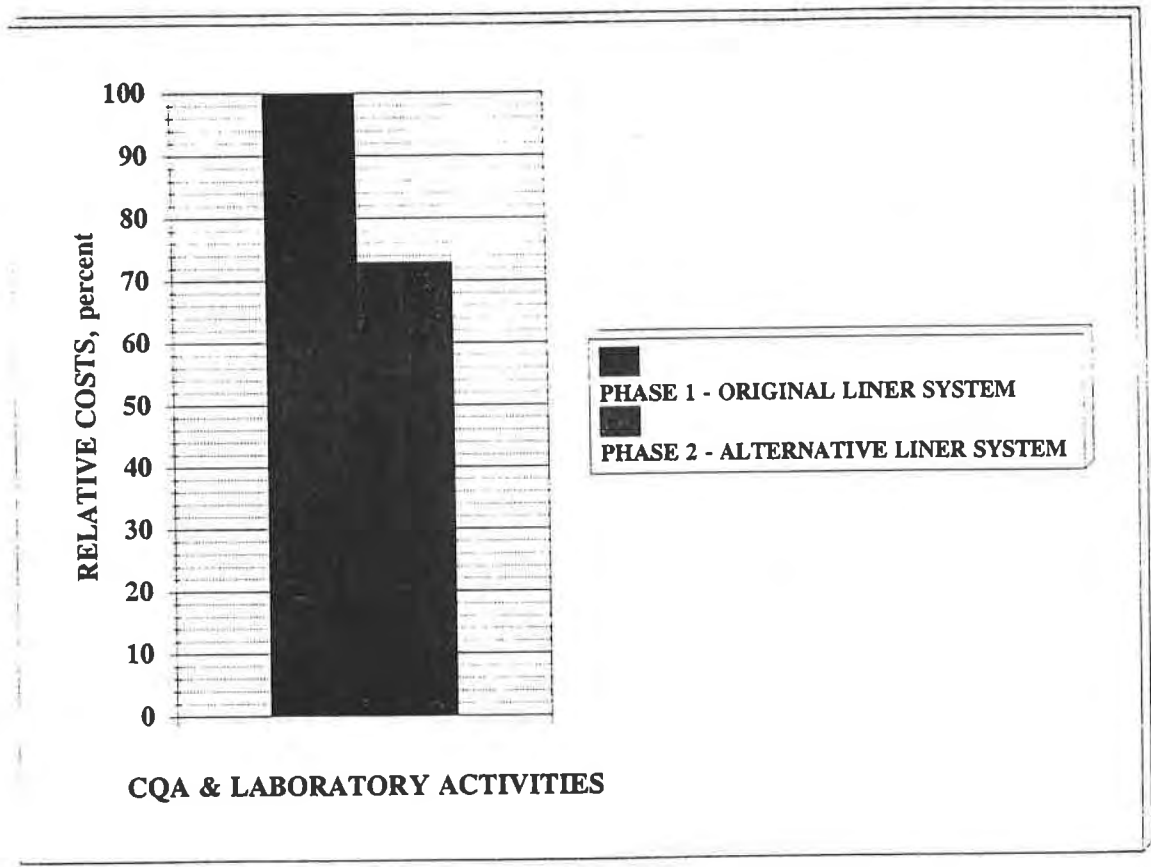Figure 3. Comparison of Phase 1 and Phase 2 Construction Costs

Figure 4. Comparison of Phase 1 and Phase 2 CQA and Laboratory Costs

REFERENCES

Bedinger, M.S., Sargent, K.A., and Langer, W.H., (1990), "Studies of Geology and Hydrology in the Basin and Range Province, Southwestern United States for Isolation of High-Level Radioactive Waste - Characterization of the Sonoran Region, Arizona", U.S. Geological Survey Professional Paper 1370 - D, U.S. Government Printing Office, Washington, D.C., 40 pp.

Boardman, T.B. and Daniel, D.E. (1995) "Hydraulic Conductivity of Desiccated Geosynthetic Clay Liners", ASCE Journal of Geotechnical Engineering, Vol. 122, No. 3, March 1996

Cetco (1996), Technical Specifications for Bentomat" and Claymax".

Daniel, D.E. and Liljestrand, H.M. (1984) "Effects of Landfill Leachates on Natural Liner Systems", Report to Chemical Manufacturers Association, University of Texas, Geotechnical Engineering Center, Austin, Texas, 86 p.

Daniel, D.E. (1991) "Geosynthetic Clay Liners", Geotechnical News, Vol. 9, No. 4, p. 28-33.

Eith, A.W., Boschuk, J. and Koerner, R.M. (1990) "Prefabricated Bentonite Clay Liners", Proceedings of the 4th GRI Conference on the Topic of Landfill Closures, Geosynthetic Research Institute, Drexel University, Philadelphia, pp. 204-226.

Giroud, J.P. and Bonaparte, R. (1989) "Leakage Through Liners Constructed with Geomembranes - Part I. Geomembrane Liners," Geotextiles and Geomembranes, Vol. 8, No. 1, pp. 27-67.

Giroud, J.P., Badu-Tweneboah, K., and Bonaparte, R. (1990) "Rate of Leakage Through A Composite Liner Due To Geomembrane Defects", Geotextiles and Geomembranes, Elsvier Science Publishers, Ltd., England, 1990.

Gundle/SLT Environmental (1995), Technical Specifications for Gundseal".

La Paz County (1994), La Paz County Main Landfill Aquifer Protection Permit No. P 101856 Petition for Permit Modification.

Naue-Fasertechnik (1996), Technical Specifications for Bentofix".

Shan, H.Y. and Daniel, D.E. (1991) "Results of Laboratory Tests on a Geotextile/Bentonite Liner Material", Geosynthetics '91 , Industrial Fabrics Assoc. Int., St. Paul, Minnesota, Vol. 2, pp. 517-35.

U.S. EPA (1987) Background Document on Proposed Leak Detection Rule, EPA/530-SW-87-015, Washington, DC.

U.S. EPA (1992) Action Leakage Rates for Leak Detection Systems. Supplemental Background Document for the Final Double Liners and Leak Detection Systems Rule for Hazardous Waste Landfills, Waste Piles, and Surface Impoundments." EPA/530-R-92-004, Washington, DC.

Vector Engineering, Inc. (1995) Alternative Liner Report for the La Paz County Regional Landfill, Parker, Arizona. Prepared for Browning-Ferris Industries of Arizona, Inc.

Wilson-Fahmy, R.F. and Koerner, R.M. (1995) "Leakage Rates through Holes in Geomembranes Overlying Geosynthetic Clay Liners", Geosynthetics '95, Nashville, Tennessee.

THE SIMS BAYOU FLOOD CONTROL PROJECT

Michael Diaz, P.E.
US Army Corps of Engineers (USA)

Deron N. Austin, E.I.T.
Synthetic Industries, Inc. (USA)

ABSTRACT

The US Army Corps of Engineers has been using a combination of cellular concrete mattresses and woven monofilament geotextile underlayments as flexible linings in high flow channels for nearly twenty (20) years. This successful system was employed on a 31 km flood control project in Houston, Texas (USA). In a joint venture with the Harris County Flood Control District, the Corps of Engineers contracted 5,550 linear meters of channel work to increase the width and depth of Sims Bayou to accommodate a 25 year storm event. The design and construction of this channel was challenged by the presence of predominately medium to stiff clays and silty clays from the bank line to several feet below the bottom of both the existing and proposed channel. To complicate matters, a 4.5 to 12.2 meter sand layer existed at depths of 1.5 to 6 meters below the proposed channel bottom. The combination of a cellular concrete mattress and a woven monofilament geotextile was selected to protect the critical channel slopes from erosion. The design required the selection of a geotextile that would prevent loss of foundation soil beneath the hard armor system, allow seepage relief and resist future heaving of channel slopes over the project life.

This paper details the feasibility study, design, installation, performance and cost-benefit of using 75,000 square meters of a woven monofilament geotextile beneath a cellular concrete mattress system on the first of many contracts on the Sims Bayou Flood Control Project. The paper includes installation photographs, a cost analysis, a basis for lining system selection and observations made during the first year of construction.

BACKGROUND

Located in the rapidly growing southern part of Houston, the 244-square km Sims Bayou watershed has represented flooding threats since the Committee on Public Works authorized a comprehensive flood damage prevention survey in 1948. Although funds were not made available until 1986, the Harris County Flood Control District began flood control rectification measures in the late 1970's in the lower reaches of Sims Bayou. The U.S. Army Corps of Engineers got involved after the project was authorized by Section 401(a) of the Water Resources Development Act of 1986 (PL-99-662). The authorized improvements included enlargement and rectification of 31 km of channel to provide a 25-year level of flood protection, installation of environmental quality improvement measures, construction of riparian habitat improvements and the establishment of 43.4 km of hiking and biking trails to be connected to

existing parks along Sims Bayou (Corps of Engineers 1989).

Due to its length, this flood damage prevention project was divided by the Corps of Engineers into nine (9) separate contracts. At the time of authorship, three (3) of the nine (9) contracts have been awarded and two (2) have been constructed. Although construction began on the first contract in 1994, completion is not expected until 2002. This paper details the design and construction experience for one of the first contracts as well as an overview of the entire project.

GEOTECHNICAL INVESTIGATION

Sims Bayou flows over the Beaumont clay formation, a well-known highly plastic soil exhibiting excessive shrink-swell characteristics. Although prior geotechnical investigations were conducted between 1957 and 1982, twenty six (26) Shelby tube borings were completed along the banks of Sims Bayou in the Fall of 1986. All samples were classified in accordance with the Unified Soil Classification System (USCS) and tested for grain size distribution, Atterberg limits, unconfined compression strength, unconsolidated undrained triaxial compression strength and direct shear (see Table 1). This investigation determined that predominately medium to stiff clays and silty clays existed from the bank line to several feet below the bottom of both the existing and proposed channel (Corps of Engineers 1989).

Table 1. Range of Soil Properties from Geotechnical Investigation
(Corps of Engineers 1989; Lindeburg 1992)

PROPERTY	Slickenslided Clay	Calcareous Clay
Soil Classifications (USCS)	CH	CL, CH
Plasticity Index (PI)	35 to 64	8 to 74
Dry Unit Weight (kg/m^3)	1,380 to 1,650	1,410 to 1,795
Moisture Content (%)	22 to 35	16 to 33
Unconfined Compressive Strength (kg/m^2)	9,000 to 31,690	6,850 to 58,690
Estimated Permeability (cm/sec)	> 5.0 x 10^{-8}	> 5.0 x 10^{-8}
Percent Sand (%)	1 to 20	1 to 30
Percent Fines (%)	80 to 100	70 to 100

During normal channel flow, a "perched" water table was encountered in the banks a few feet above the water surface in silty sand and sandy silt strata. This water table fluctuated with flow variations in the bayou. To complicate matters, a 4.5 to 12.2 meter thick sand layer was located at depths of 1.5 to 6 meters below the proposed channel bottom. This created an artesian condition that had apparently caused heaving in the existing channel bottom and was a major consideration in the rectification design.

CHANNEL LINING DESIGN & SELECTION

The design and selection of the lining system for channel rectification was challenging for the U.S. Army Corps of Engineers. The presence of highly plastic slickensided clays, artesian conditions, high channel flows, steep side slopes and local environmental concerns all presented difficult parameters. Although reinforced concrete paving and rock rip rap was proposed in the initial design, the advantages to these channel lining techniques conflicted with the goals of the Sims Bayou Flood Control Project. Due to its urban setting, the channel lining system needed to: (1) prevent disturbance of highly erodible silts and silty sands during the maximum design storm events; (2) enhance the aesthetic appearance by allowing the growth of vegetation; and (3) provide for groundwater recharge and infiltration of the aquifer. Although the U.S. Army Corps of Engineers realized the aesthetic and environmental benefits of turf reinforcement mats (TRMs), challenging soil conditions, uncertainty over vegetative establishment, concerns with proper anchoring of the mats and the need of overburden for uplift prevention forced the engineers to limit their solutions to porous hard armor systems. Based upon the project goals, the initial preferred system was a vegetated concrete cellular mat underlain by a woven monofilament geotextile. However, hydraulic stability, slope stability, channel bottom stability and filtration design analyses were all conducted by the Corps of Engineers before final selection.

Channel Bottom Stability   The channel bottom stability was determined by comparing the excess pore water pressure above normal water to the effective overburden pressure of the clay layer below the channel. Since factors of safety against hydrostatic uplift fell well below 1.0 in some channel sections, a satisfactory means of reducing pressure in the artesian sand layer and increasing overburden was needed to be developed. Although three (3) methods were considered for pressure control, a series of relief wells and piezometers was eventually selected and incorporated into the design (Corps of Engineers 1989).

Slope Stability   By modeling the mass of the concrete cellular mat as slope dead load, a commercially-available computer program was utilized to evaluate slope stability at various locations along Sims Bayou. Using peak shear strength and steady seepage conditions, a minimum factor of safety of 1.25 was determined for the various channel slopes. According to the Corps of Engineers design criteria, these values were just barely acceptable for the project (Corps of Engineers 1989). Lighter channel lining systems did not yield acceptable factors of safety.

Hydraulic Stability   Open channel flow analyses were performed using a commercially available computer program. The 25 year design storm event was modeled using the Hydraulic Engineering Circular No. 2 (HEC-2) approach. This created a maximum flood discharge of up to 1,335 cubic meters per second, maximum velocities of 2.1 m/sec and shear stresses of up to 30 N/m^2 (Corps of Engineers 1989). These values were well within the reported performance limits of concrete cellular mats.

Filter Selection.   Although the presence of clayey soils often results in the selection of a nonwoven geotextile, the engineers focused on eliminating the possibility of long-term clogging. Since previous research has shown a direct relationship between the percent open area (POA) of a geotextile and its clogging potential, the US Army Corps of Engineers determined that a woven monofilament geotextile would be the best filter underneath the cellular concrete mat

(Haliburton and Wood 1982). Since clayey soils on this project consisted of 5 to 85 percent of the particles passing the 0.075 mm mesh, a woven monofilament geotextile displaying a POA of equal to or greater than 4 percent was required in order to meet current US Army Corps of Engineers geotextile filter selection criteria (Al-Hussaini and Perry 1996).

Cost Analyses. Final selection of the concrete cellular mat could not be made without a detailed cost analysis of the various alternatives. Since the estimated total cost for all planned channel improvements along Sims Bayou was $243,235,000 (US) in 1989 (sixty-seven percent federal and thirty-three percent non-federal), the channel lining system was just one of many costs studied during the initial design phases (see Table 2).

Table 2. Cost Estimate for Channel Lining Alternatives
(Corps of Engineers 1989 with a 1.17 Inflation Factor)

Channel Lining System Alternatives	Estimated Unit Price	Depth of Treatment
Concrete Channel Lining	$39.94/ m^2	150 mm
Sand Filter Blanket	$5.11/ m^2	150 mm
	$45.05/ m^2	
Rock Riprap	$29.13/ m^2	550 mm
Blanket Stone	$41.38/ m^2	225 mm
	$41.38/ m^2	
Cellular Concrete Mat	$34.56/ m^2	120 mm
Woven Geotextile	$1.80/ m^2	n/a
Turfing	$1.38/ m^2	n/a
	$37.70/ m^2	

Based upon the result of the cost, slope stability, channel bottom stability, hydraulic and filtration analyses, the preferred system consisting of a vegetated cellular concrete mat underlain with a woven monofilament geotextile was selected for use in lining the Sims Bayou channel rectification project (Figure 1).
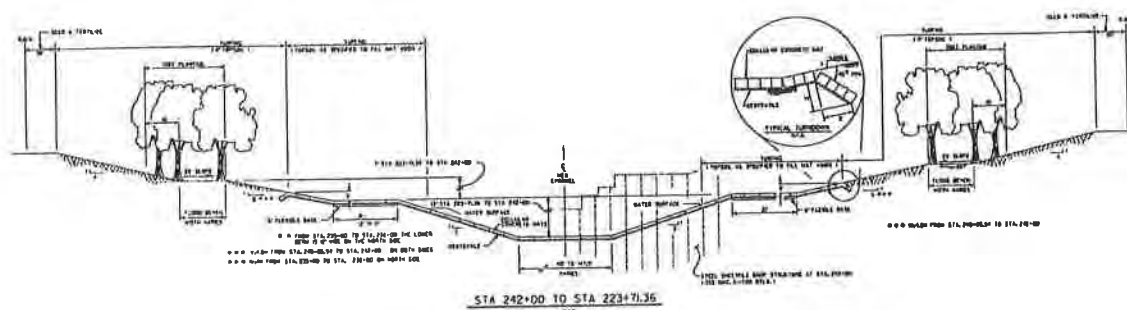

STA 242+00 TO STA 223+71.36

Figure 1. Typical Cross-Section for Channel Rectification
(Corps of Engineers 1993; Corps of Engineers 1994a)

SPECIFICATIONS

The US Army Corps of Engineers incorporated their standard specifications for the cellular concrete mat (Section 02279) and the woven monofilament geotextile (Section 02243). The cellular concrete mat was described as a pre-manufactured assembly of 27.56 MPa concrete blocks connected into a mattress using polyester revetment cables (see Figure 2). Once assembled, the specified mattress must display an open area of 18 to 23 percent to allow for vegetative establishment. The design required a 150 mm thick mattress under bridge overpasses and near large storm drains and 120 mm thick mattresses along all the remaining portions of the 31-km channel. The specified filter beneath the cellular concrete mat was a woven monofilament geotextile with a POA of 4 percent (see Table 3).
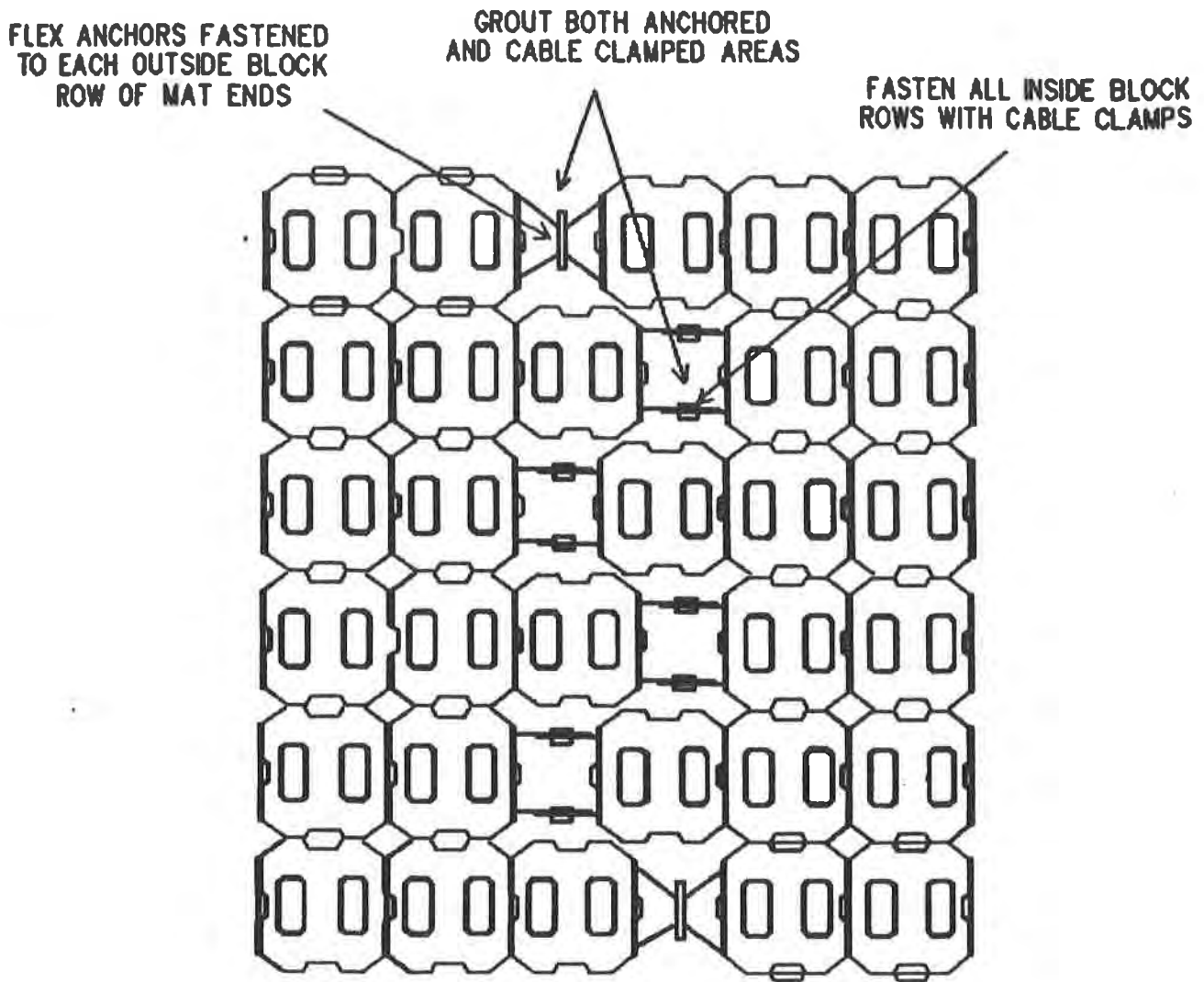
FLEX ANCHORS FASTENED
TO EACH OUTSIDE BLOCK
ROW OF MAT ENDS

GROUT BOTH ANCHORED
AND CABLE CLAMPED AREAS

FASTEN ALL INSIDE BLOCK
ROWS WITH CABLE CLAMPS

Figure 2. Cellular Concrete Mat

Table 3. Woven Monofilament Geotextile Filter Specifications
(Corps of Engineers 1994b)

Physical Properties	Specified Test Procedure	Current ASTM Test Procedure	Acceptable Values
Tensile Strength	ASTM D-1682	ASTM D-4632	1,110 N
Breaking Elongation	ASTM D-1682	ASTM D-4632	15 %
Seam Strength	ASTM D-1683	ASTM D-4884	90 % Retained
Puncture Strength	ASTM D-3787	ASTM D-4833	575 N
Abrasion Resistance	ASTM D-3884	ASTM D-4886	240 N
Bursting Strength	ASTM D-3786	ASTM D-3786	3,300 kPa
Permeability	ASTM D-4491	ASTM D-4491	0.010 cm/sec
Tear Strength	ASTM D-4533	ASTM D-4533	240 N
EOS	COE Method	ASTM D-4751	0.150 to 0.212 mm
Percent Open Area	COE Method	Under Development	4 %

CONSTRUCTION

The specifications required phased excavation of the new channel to minimize possible slope failures due to heaving from overburden or artesian pressures. Excavation of the portion of the channel above the lower berm, located 4 meters above the channel bottom, was completed 60 meters in advance of excavation below the lower berm. Artesian pressure was relieved prior to excavation of the channel below the lower berm (Corps of Engineers 1989).

The surface was initially prepared by compacting the subgrade. All depressions, obstructions, debris and rills were removed to provide a smooth bank for geotextile deployment. Synthetic Industries EROSION I woven monofilament geotextile was supplied to the contractor, Lecon Construction, Inc. in specially fabricated 5.5 meter wide rolls for easy installation. The geotextile was carefully installed to prevent damage to the product while not leaving it exposed for more than seven (7) days prior to placement of the cellular concrete mattress (Figure 3).

The cellular concrete mattress was installed using a crane equipped with a spreader bar. Adjacent mattresses were butted against each other and no more than a 75 mm gap was allowed. The protruding lateral cables were connected with approved sleeves. Duckbill anchors were then installed at predetermined intervals by carefully incising the geotextile and driving the anchors through the geotextile into the subgrade. For every twenty (20) anchors installed, the contractor was required to perform a duckbill pull-out capacity test. This test required that a load of 8.9 kN be maintained for 10 minutes without deforming more than 12 mm. The voids in the cellular concrete mats were filled with flexible base under the bridge overpasses. Select topsoil, seed and fertilizer were used as infill material along the rest of the project.
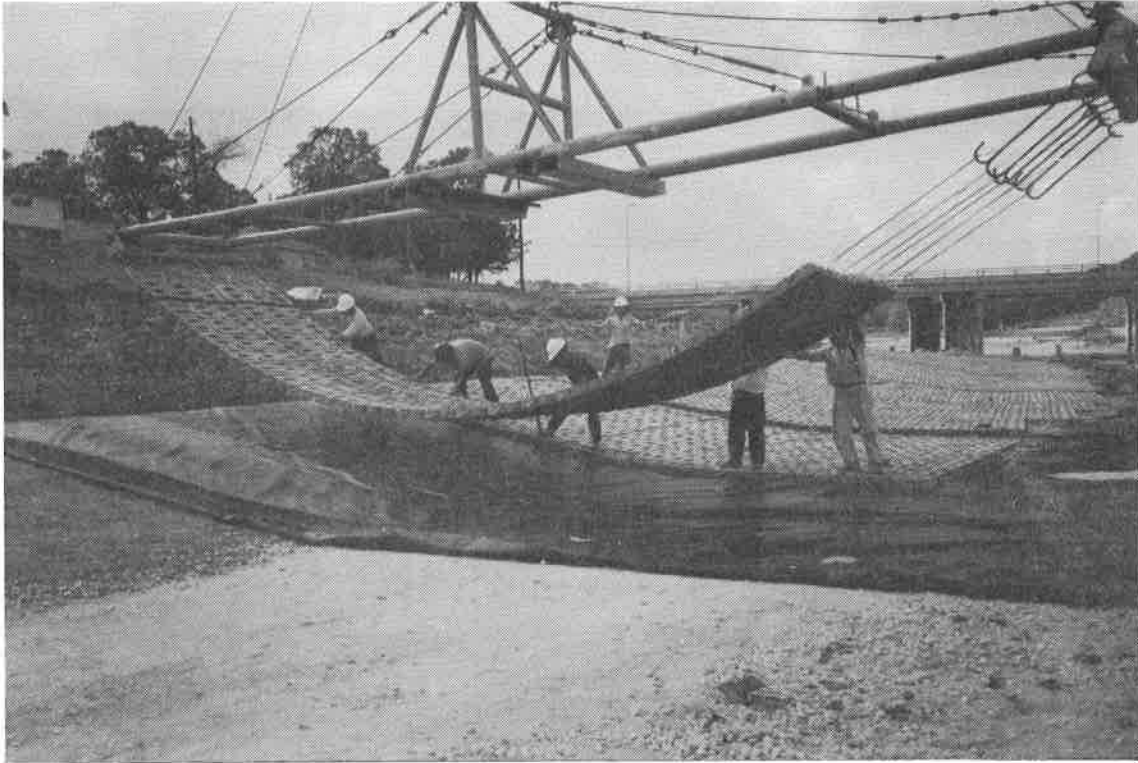
Figure 3. Photograph of Geotextile and Cellular Concrete Mat Installation

OBSERVATIONS & CONCLUSIONS

With two (2) contracts of the Sims Bayou Flood Control Project nearly complete, the woven monofilament geotextile and the cellular concrete block system is living up to its expectations. Although a 25 year design storm has not yet hit Houston, the channel lining system is stable and a healthy stand of vegetation has established (Figure 4). Although it is too early to draw conclusions regarding the long-term performance of the woven monofilament geotextile filter, the sedimentation levels in Sims Bayou are satisfactory and there appear to be no signs of channel uplift or slope instability. Some other general observations and conclusions are as follows:

- The US Army Corps of Engineers have been using the economical combination of cellular concrete mattresses and woven monofilament geotextiles as flexible linings in high flow channels for nearly twenty (20) years. The successful performance of this project will probably reinforce that trend.

- A woven monofilament geotextile was successfully installed beneath hard armor revetment systems in the presence of predominately medium to stiff clays and silty clays.

- Although the trend for moderate velocity open channels is toward "softer" lining solutions such as turf reinforcement mats (TRMs); highly erodible or infertile soil conditions, uncertainty over vegetative establishment, concerns with sufficient anchoring and the need of overburden for uplift prevention will sometimes force the engineers to utilize more expensive hard armor systems.

Figure 4. Photograph of Sims Bayou Channel Three (3) Months After Installation

ACKNOWLEDGEMENTS

REFERENCES

Anonymous, "Channel Improvements - Mile 0.0 to 19.3: Sims Bayou, Houston, Texas, Flood Damage Protection", General Design Memorandum, U.S. Army Corps of Engineers, Galveston District, Galveston, Texas, January 1989.

Anonymous, "Construction Plans for Channel Rectification - Hemingway to Reveille Park: Sims Bayou, Houston, Texas", Invitation Number DACW64-94-B-0054, Department of the Army, Galveston District, Corps of Engineers, Galveston, Texas, September 1994a.

Anonymous, "Construction Plans for Channel Rectification - Reveille Park to I-45: Sims Bayou, Houston, Texas", Invitation Number DACW64-94-B-0003, Department of the Army, Galveston District, Corps of Engineers, Galveston, Texas, November 1993.

Anonymous, "Specifications for Channel Rectification - Hemingway to Reveille Park: Sims Bayou, Houston, Texas", Invitation Number DACW64-94-B-0054, Department of the Army, Galveston District, Corps of Engineers, Galveston, Texas, September 1994b.

Al-Hussaini, M.M. and Perry, E.B., "Corps of Engineers Guide Specification for Use of Geotextiles as Filters", GeoFilters '96 Conference Proceedings, BiTech Publishers Ltd.,

Richmond, British Columbia, Canada, May 1996, pp. 11-19.

Calhoun, C.C. Jr., "Development of Design Criteria and Acceptance Specifications for Plastic Filter Cloths", Technical Report 5-72-7, U.S. Army Engineer Waterways Experiment Station, Vicksburg, MS, 1972.

Haliburton, T.A. and Wood, P.D., "Evaluation of the U.S. Army Corps of Engineer Gradient Ratio Test for Geotextile Performance", Second International Conference on Geotextiles Proceedings, Las Vegas, Nevada, USA, 1982, pp. 97-101.

Lindeburg, M.R., "Civil Engineering Reference Manual", 6th Edition, Professional Publications, Inc., Belmont, CA, 1992, p. 9-13.

SPECIFYING AND BIDDING SEGMENTAL CONCRETE FACED MSE WALLS ON U.S. ARMY CORPS OF ENGINEERS, ST. PAUL DISTRICT PROJECTS

Mark S. Meyers, PhD, PE
Neil T. Schwanz, PE
Geotechnical Engineers, U.S. Army Corps of Engineers,
St. Paul District, St. Paul, MN, USA

Ryan R. Berg, PE
Geotechnical and Geosynthetics Consultant, St. Paul, MN, USA

ABSTRACT

The U.S. Army Corps of Engineers St. Paul District has designed and constructed several geosynthetic reinforced mechanically stabilized earth segmental retaining wall (MSE SRW) systems in recent years. Most Corps of Engineers projects are constructed in challenging riverine environments. Specifying and bidding geosynthetic reinforced MSE SRW systems can be difficult, due to the limitations of federal procurement regulations, which do not allow for preapproved geosynthetic reinforced MSE SRW systems. Several unique approaches are now used to specify and bid geosynthetic reinforced MSE SRW systems based upon experiences and lessons learned from previous projects. A variety of approaches are used to address issues such as: foreseeable construction difficulties; design presentation; material specifications; bid items; allowable modifications to the presented design; design and shop drawing submittal requirements; and quantity determinations.

Specification and bidding of geosynthetic reinforced MSE SRW systems are discussed through the presentation of several case histories; each of which used a somewhat different specification and bidding approach. The discussions include key features of each project, the key design issues which led to the specification and bidding approach used, and lessons learned from each project. Data is presented which summarizes unit prices for various bid items, based on the specification and bidding approach utilized on each project. Key items to address in the design, specification, and bidding of geosynthetic reinforced MSE SRW systems are summarized. This paper is directed towards both government and private designers of geosynthetic reinforced MSE SRW systems.

INTRODUCTION

The St. Paul District of the U.S. Army Corps of Engineers (COE) has incorporated the use of geosynthetic reinforced mechanically stabilized earth segmental retaining wall (MSE SRW) systems

into civil works flood control and operation and maintenance projects. Since federal procurement regulations do not allow for preapproval of MSE SRW systems, several methods of specifying and bidding MSE SRW systems have been developed by the St. Paul District. These methods use specifications and bid items which provide fair and open competition among potential bidders. Other information provided in the contract documents varies from project to project, depending on the geotechnical nature of the site.

This paper presents a historical perspective on the use of traditional wall systems and factors leading to acceptance of MSE SRW systems for COE projects. The methods used to specify and bid MSE SRW systems are discussed. The use of these methods is illustrated in four case histories. Lessons learned from the specification and bidding of MSE SRW systems and the use and construction of MSE SRW systems are discussed. Comparative cost information for the case histories is documented and a comparative summary of the methods is presented.

HISTORICAL PERSPECTIVES

Use of Traditional Wall Systems. For nearly 100 years, the St. Paul District of the U.S. Army Corps of Engineers has designed and constructed various types of wall systems as major components of civil works flood control projects. The traditional wall systems include: concrete cantilever walls; I-walls; cantilevered sheetpile walls; and anchored sheetpile walls. These systems have been successfully constructed and perform well. However, they can be costly and may not provide an aesthetically pleasing project feature. A comparative summary of estimated costs of various traditional wall systems vs. MSE SRW systems is presented in the literature.

The majority of COE projects are designed for a 100- to 200-year project life. The project features are typically constructed in a riverine or reservoir environment. As such, additional design criteria and concerns need to be satisfied and addressed. Recently revised COE design criteria (USACE, 1989 and 1990) for retaining walls requires the application of strength mobilization factors (SMFs) to soil parameters. The use of SMFs typically results in longer footing width requirements for a given height of traditional concrete cantilever wall than in the past. Frost considerations and bearing capacity requirements also typically require more stringent embedment depths for wall system foundations.

Federal cost sharing agreements for most projects now require local sponsors to share 25 percent of the design and construction costs associated with standard flood control features and 50 percent of the design and construction costs associated with recreation features. As a result, the local sponsors have a vested interest in both the aesthetic appearance and the final costs of project features. Sustainability has become a major factor in the design and construction of COE projects.

Use of MSE Wall Systems. In the mid to late 1980s, MSE wall vendors began presenting the benefits of MSE wall systems to the St. Paul District. However, the design standards used by the COE did not allow for immediate acceptance of these wall systems. Technical concerns included

product performance and longevity. Non-technical concerns included sole source specifying and bidding of the MSE wall systems.

The late 1980s and early 1990s saw the introduction of MSE wall systems with geosynthetic reinforced backfill and concrete segmental retaining wall (SRW) units in private works. Since detailed information was not available regarding the performance of geosynthetic reinforcement and segmental block materials over time, especially in a riverine or reservoir environment, the MSE SRW systems were not considered for use by the COE. Technical factors considered to be potential problems included connection strength and performance, creep of the geogrid materials, freeze-thaw characteristics of the segmental block materials (especially when the toe is permanently submerged), damage to the block units from debris in the river during high flows, and movement of fines from behind a wall during rising and falling river stages (Meyers and Schwanz, 1993).

The use of MSE SRW systems in private work by others accelerated rapidly. Many vendors can supply a variety of types of geosynthetic reinforcement and SRW products. This allowed for the development of a generic material specification for the geosynthetic reinforcement and SRW products, thus removing the sole source specifying and bidding concerns for these products. The increased use of MSE SRW systems resulted in a greater amount of design and construction experience with these systems. Performance history was being generated and documented in research and case history publications. The St. Paul District was encouraged to use the MSE SRW systems and received advice regarding design methodologies and requirements and specification of the MSE SRW systems from outside, experienced consultants. These factors led to the use of MSE SRW systems in non-critical locations on flood control and reservoir projects in the St. Paul District starting in 1991.

ALTERNATIVE METHODS FOR SPECIFYING AND BIDDING MSE SRW SYSTEMS

General. Federal procurement regulations do not allow for pre-approval of the MSE SRW systems which have been developed by various vendors. Alternative methods for specifying and bidding the MSE SRW systems needed to be developed to allow for open and fair competition among suppliers. This required developing a wide open generic specification for geogrids and other geosynthetic reinforcement, SRW units, and geotextile filters, which spanned the range of product properties found in the literature. Sources of this information included the IFAI Specifiers Guide and manufacturer and vendor literature.

The St. Paul District has developed three alternative methods for specifying and bidding MSE SRW systems. These methods, summarized in Table 1, are discussed below. Use of the various alternative methods for specifying and bidding MSE SRW systems are illustrated in the case histories. Selection of the method to use is typically based on the geotechnical complexity of the site and problems anticipated to occur during the submittal review process. All methods require review and approval of shop drawings by a registered professional engineer experienced in the design of MSE SRW systems prior to submittal to the COE.

Table 1. Summary of Methods Used To Specify and Bid MSE SRW Systems

Method No.	1	2	3
Information Presented in Contract Documents	Complete Design	Alignment, Grades, and Generic Wall Section	Alignment, Grades, and External and Compound Stability Requirements
Summary of Method	External, compound, and internal stability completed by St. Paul District Shop drawings prepared by PE	Requires design of wall to be completed by a PE Shop drawings prepared by PE	External and compound stability completed by St. Paul District Internal stability completed by PE Shop drawings prepared by PE
Advantages of Method	Consistent bid information provided Cost of design by PE not required if presented design is used	Quickest way to meet internal design schedules and minimize design budgets	Consistent bid information provided COE assured that design criteria are satisfied Consultants very good at optimizing internal stability
Disadvantages of Method	Additional design time required to prepare contract documents COE internal stability analysis not likely to be optimized - Contractor will revise design to optimize product use	Complete wall design must be provided by a PE Difficult submittal review and approval process likely for non-generalized site conditions	Additional design time required by St. Paul District to determine external and compound stability requirements

Method 1: Present Complete Design. The basis behind this method is that the external, compound, and internal stability analyses are completed by the St. Paul District. The design and all information needed to construct the wall are presented in the contract documents. The major advantages of this method are: (i) the information presented in the contract documents gives all contractors something consistent to bid on; and (ii) the costs involved with having a professional engineer complete a preliminary design during the bidding process are eliminated. The disadvantages associated with this method include: (i) additional design time and detailing; and (ii) often, the internal stability analysis will likely be redesigned and optimized based on the specific SRW block and geosynthetic reinforcement selected by the contractor.

Method 2: Present Only Required Alignment and Grades. For this method, the required alignment and top and bottom of wall grades, and a generic cross section, are provided in the contract documents. This is the quickest way to meet internal design schedules and minimize design budgets. This method requires the construction contractor to have the MSE SRW system completely designed by a professional engineer.

Consulting engineers who generally design these wall systems are typically not familiar with COE design standards and the factors of safety required to complete the external and compound stability analyses (slope stability and bearing capacity). External and compound stability generally governs the required length of reinforcement on COE projects. Some designers still model the reinforced zone with an artificially high shear strength to prevent compound failure planes from passing through the reinforced soil mass, which can lead to unconservative external and compound stability factors of safety (Berg and Meyers, 1997). Most of the MSE SRW system design software used by consulting engineers, which is typically developed by vendors, do not compute an allowable bearing capacity. An allowable bearing capacity is supplied by the user as required input to the software. The designer must be particularly aware of sloping fills in front of the wall system and water elevations in computing an allowable bearing capacity. These factors can contribute to a difficult submittal review and approval process.

Method 3: Present Required Alignment and Grades and External and Compound Stability Requirements. The use of this method requires the St. Paul District to complete the external and compound stability analysis. The alignment, grades, and minimum reinforcement lengths and strengths required to satisfy external and compound stability design criteria are presented in the contract documents. The construction contractor is left to complete the internal stability analysis for review and approval by the COE. The advantage of this method is that the internal stability is the easier of the required analyses and consulting engineers are very good at doing this, especially with respect to optimizing the spacing of the reinforcement for the MSE SRW system selected for use by the construction contractor. Also, by providing the external and compound stability designs, the contract documents set guidelines which are consistent for all bidders and the COE is assured that all COE design standards are satisfied.

CASE HISTORIES

General. This section presents four case histories from various projects constructed or being constructed in the St. Paul District. A comparative summary of the case histories with respect to the specifying and bidding method, bid results, estimated alternate wall type costs, and an estimated savings of using the MSE SRW system over the alternate wall system(s) considered is presented in Table 2.

Case History No. 1: Rochester, Minnesota Flood Control Project, Stage 2B. Stage 2B of the Rochester, Minnesota Flood Control Project consisted of channel improvements through Soldier's Field Golf Course to optimize the hydraulic efficiency and capacity of the channel. The improvements required extensive widening and deepening of the existing channel and provided erosion protection for the channel side slopes.

The proposed channel improvements, utilizing 1V on 3H side slopes, would have required construction or repair of three greens and one tee box immediately adjacent to the channel, requiring closure of the golf course for a minimum of two seasons to establish a new green. The City of Rochester, who owns the golf course, was willing to permit golf course closure for one construction season, but closure for two seasons was unacceptable, as it would impact the course rating and result in loss of revenue and clientele. To alleviate this concern, the 1V on 3H channel side slopes were replaced with a wall system, which could be constructed without impacting the greens and tee boxes.

A traditional cantilever wall would require a footing dimension which would impact the greens during construction. An anchored sheetpile wall system with a concrete cap was selected as the wall system to be used in the areas of the greens. Although functional, this wall system lacked the aesthetic quality requested by the City.

The COE typically completes an internal Value Engineering (VE) study of completed design projects with construction costs in excess of $2 million. The VE study for Stage 2B completed in 1990 indicated a potential savings of $650,000 if a MSE SRW system were to be used in lieu of the anchored sheetpile wall system. An improved aesthetics benefit, although unquantifiable, would also be realized, which pleased the City of Rochester.

This was the first MSE SRW system bid by the St. Paul District. A precursor to Methods 1 and 3 was used to specify and bid the project. The contract documents for Stage 2B presented the government-designed MSE SRW system, including alignment, maximum top-of-footing elevations, SRW requirements, minimum reinforcement lengths, reinforcement properties, connection strength requirements, and backfill and compaction requirements. However, the construction contractor could choose to use the government design in its entirety, or redesign the reinforcement locations, spacing, and properties following AASHTO-AGC-ARTBA Task Force 27 recommendations. Such changes required submittal of computations or computer printouts identifying input parameters and

Table 2. Comparative Summary of Case Histories - Specification, Bidding, and Cost Data

Case History No.	Method Used	Bid Quantity m² (SF)	Bid Quantity Basis	Unit Price $/m² ($/SF)	Total Cost $1000s	Alternate Wall System	Alternate Wall Cost $1000s	Estimated Savings $1000s
1	3	1,560 (16,800)	Vertical Projection Above Ground	161.50 (15.00)	250	Anchored Sheet Pile With Concrete Cap	900	650
2	1	15 (160)	Vertical Projection Above Ground	161.50 (15.00)	2	Concrete Cantilever (See Note 1)	9	7
3	2	74 (800)	Vertical Projection Above Base	215.28 (20.00)	16	Concrete Cantilever (See Note 1)	44	28
4 RS 1A-1E	2	862 (9,280)	Vertical Projection Above Base	191.06 (17.75)	164	MSE Wall With Concrete Panel Facing	306	142
4 RS 1	3	706 (7,600)	Vertical Projection Above Base	204.51 (19.00)	144	MSE Wall With Concrete Panel Facing	251	107
4 RS 3	3	1,663 (17,900)	Vertical Projection Above Base	199.13 (18.50)	331	MSE Wall With Concrete Panel Facing	591	260

Note 1: MSE SRW system selected based on constructibility and aesthetic concerns only. A cost was not estimated for the alternative wall system. Cost indicated is approximate based on bids received for other concrete wall work on the project.

verifying the proposed design changes. A VE proposal would have been required to make changes to alignment, maximum top-of-footing elevations, minimum reinforcement lengths, or backfill and compaction requirements.

The construction contractor procured the services of a professional engineer to prepare shop drawings for submittal, review, and approval by the COE. The submittal proposed changes in reinforcement spacing and location and was accompanied by the appropriate computations and computer design results. The wall was completed in the summer of 1992. Although the MSE SRW system was not constructed in a consecutive manner or timeframe, it is the opinion of the authors that the wall was constructed much more rapidly than either a conventional retaining wall system or an anchored sheetpile wall system could have been constructed.

The as-constructed MSE SRW system required 1,560 square meters (m^2) of exposed wall surface (16,800 square feet (SF)) and 8,305 m^2 (89,400 SF) of reinforcement in three wall reaches. The wall system has performed as designed, as evidenced by high river stages followed by rapidly falling river stages in early April 1993.

Case History No. 2: Rochester, Minnesota Flood Control Project, Stage 2A. Stage 2A of the Rochester, MN Flood Control Project runs through downtown Rochester. The majority of the wall systems utilized for this reach of the project were determined to be critical features of the project due to high velocities under flood conditions, horizontal curves and S-curves along the alignment, a multiple level path system geometry, and lack of right-of-way between the channel and adjacent transportation corridors. As such, traditional wall systems were used on most of Stage 2A.

A single MSE SRW system was used as a grade control wall adjacent to a commercial building along the recreation trail in one small area of the Stage 2A project. This wall was approximately 9.1 m (30 feet) long and varied in exposed height from 0.6 m (2 feet) to 2.1 m (7 feet) for a total exposed wall surface area of 15 m^2 (160 SF). The foundation materials generally consisted of relatively clean granular materials and the groundwater level was below the level of influence of the wall. The wall was not subject to flooding. The backfill for the wall was nearly horizontal and the ground slope in front of the wall was horizontal. The design conditions were simple with no complicating factors requiring significant detailed analyses.

The MSE SRW system was selected for use because it was able to provide a low cost, easily constructed, aesthetically pleasing structure in this highly visible area. Two other areas of the project used low height SRWs similar in appearance to that proposed for this wall. Economics was not formally considered in the selection of this wall. However, a traditional concrete cantilever retaining wall would have required a much deeper and wider footing. This would increase excavation, backfill, wall height, and reinforcement requirements, resulting in a more costly wall system than the MSE SRW system selected for use.

The contract documents were developed utilizing Method 1, with the required alignment, grade, reinforcement lengths, and reinforcement spacing for the wall presented in the drawings. No modifications to the design were allowed, but the construction contractor was required to submit traditional shop drawings for review and approval by the COE. Minimum product requirements were specified. The construction contractor procured the services of a local professional engineer experienced in the design of MSE SRW systems to prepare the shop drawings and the wall was quickly and easily designed and constructed. Minimal analyses were completed for the design due to the uncomplicated conditions and low risk of damage or loss of life associated with wall failure.

Case History No. 3: Upper St. Anthony Falls Visitors Center. Upper St. Anthony Falls Lock and Dam, located in Minneapolis, Minnesota, is the most upstream lock and dam on the Mississippi River operated and maintained by the COE. Work to improve the accessibility for visitors to the site required the construction of a small retaining wall. The average height of wall was approximately 1.8 m (6 feet), with a maximum height of 2.4 m (8 feet), resulting in a total wall area of approximately 74 m^2 (800 SF). The foundation materials generally consisted of relatively clean granular materials and the groundwater level was below the level of influence of the wall. The backfill for the wall was nearly horizontal and the ground slope in front of the wall sloped gradually away from the wall to a roadway so that its influence on the bearing capacity was negligible. The design conditions were simple with no complicating factors requiring significant detailed analyses.

An MSE SRW system was selected for use on this project to provide a low cost, aesthetically pleasing structure in this highly visible area. The contract documents were developed utilizing Method 2, with the required alignment and grade for the wall presented in the drawings. The contractor was required to submit the complete wall system design and shop drawings for approval by the COE. Minimum product requirements were specified and a typical wall section was included to identify the basic wall requirements. The contractor procured the services of a local professional engineer experienced in the design of MSE SRW systems and the wall was quickly and easily designed and constructed. Minimal analyses were completed for the design due to the uncomplicated conditions and low risk of damage or loss of life associated with wall failure.

Case History No. 4: Lake Red Rock Multi-Purpose Trail Segment 4A. The Lake Red Rock Multi-Purpose Trail project is located along the northern shore of Lake Red Rock near Pella, Iowa. Lake Red Rock is the pool created by the COE Rock Island District Red Rock Dam. The Rock Island District is currently constructing a bituminous recreation trail along a portion of the perimeter of the pool. Retaining structures are needed in areas where right of way limits restrict the placement of sloping fill or cuts or in areas where the trail is adjacent to a high roadway embankment and the placement of fill needed for trail construction would be significant. The Rock Island District decided to use MSE SRW systems for the retaining structures and contracted with the St. Paul District to prepare the required design documents. Two approaches, Methods 2 and 3, were used in specifying and bidding the retaining structures as discussed in the following paragraphs.

A total of eight separate MSE retaining systems were used on this project, seven MSE SRW systems and one MSE reinforced slope. Five of the MSE SRW systems were relatively low height structures. Standard design conditions for these walls allowed the use of Method 2, specifying lines and grades in the contract documents and requiring the contractor to use a professional engineer to complete the design. The total design package for the five smaller walls was also required to be submitted for review and approval by the COE.

The remaining two MSE SRW systems, with total wall heights up to 16 feet (4.9 m), represented 2,369 m^2 (25,500 SF) of the total 3,321 m^2 (34,780 SF) of wall. They were constructed on the sideslope of an adjacent highway embankment. Significant portions of these walls would be inundated by the design pool of Red Rock Dam. Since the external and compound stability conditions were required to satisfy COE design criteria and procedures, and in order to insure equitable bids, it was decided to utilize Method 3 to specify and bid these wall systems. Therefore, the COE completed the external and compound stability (slope stability; bearing capacity; sliding analyses; overturning) and drain and filtration design in-house. These requirements were provided in the bid documents, along with required alignments and grades. The remaining design items, as well as a check of the slope stability, were required to be designed by a professional engineer and submitted for review and approval by the COE.

. The bid documents for the two larger walls included all external and compound stability criteria for the MSE SRW system. This criteria included: elevation of the top of the wall; wall embedment and bottom geogrid reinforcement elevation requirements; minimum geogrid reinforcement lengths; drain and backfill material gradations; geotextile materials; and required compaction and quality control testing; and minimum SRW concrete unit requirements. The contract documents included soil parameters and design criteria for the contractor to complete the internal and compound analyses, as well as a design check of the external stability. The construction contractor used a professional engineer to complete sufficient slope stability analyses and a bearing capacity check to verify the government design, as well as the internal stability analyses. Internal stability was analyzed in accordance with the NCMA design manual (Simac, et al, 1992).

This bidding approach worked very well and eased the submittal review process. The COE rigorous analyses of the external and compound stability for the larger, non-standard design walls required geogrid reinforcement lengths longer than some of the wall and slope heights. The presentation of these geogrid reinforcement requirements in the bidding documents eliminated the potential problems associated with shorter geogrid lengths generally assumed to secure a competitive bid versus the required geogrid reinforcement length based on detailed design performed after the contract is awarded.

LESSONS LEARNED

Specifying MSE SRW Systems. The St. Paul District's preferred use of the various alternative methods for specifying and bidding MSE SRW systems has been based upon experiences with various projects and site conditions. The St. Paul District typically uses Method 1 for very short, simple wall systems which require reinforcement, but where minimal time is projected to be spent reviewing the shop drawing submittals. Method 2 is utilized for wall systems of moderate height, such a wall which is less than 2.4 to 3 m (8 to 10 feet) in exposed height, and where difficult foundation conditions or other uncertainties do not exist at the site. In such cases, the contractor can usually provide an adequate design. Method 3 is used for almost all other cases.

Bid Items and Measurement and Payment. The selection of appropriate bid items and descriptions used in the measurement and payment discussions regarding the bid items in the contract documents evolved based on experience. Typically, the MSE SRW systems have one bid item, MSE Wall, which is bid either per exposed vertically projected wall surface area or per total vertically projected wall surface area (top of leveling pad to top of wall). This bid item includes all labor, SRW units, geogrid reinforcement, geotextile filter, leveling pad, drainage material, drain pipe and stubouts, excavation, backfill, and heavy equipment required to construct the wall as per the specifications. Note that the bid item is the vertical projection of the exposed or total wall area. For exposed projection, the bid item unit cost determined by the contractor must include the cost of all block and reinforcement below finished grade and must account for the batter required by the SRW system selected by the construction contractor.

Construction of MSE SRW Systems. Several advantages of constructing MSE SRW systems have been noted based on observations made during visits to COE construction projects where MSE SRW systems have been constructed. All of these advantages contribute to the lower cost of MSE SRW systems. These advantages are discussed in the following paragraphs.

The sequencing of construction appears to be much more flexible than construction of conventional wall systems. The Rochester 2B construction contractor moved his crews from wall to wall, regardless of whether the wall was completed or not, depending on adjacent construction activities, availability of equipment and materials, and whether the crew was needed elsewhere for a short period of time.

Dewatering costs can be minimized with MSE wall systems. The wall can be constructed to an elevation above which the dewatering system can be removed and/or above which flooding will not impact construction of the wall and adjacent areas. The Rochester construction contractor utilized this scheme and left the walls in a partially completed state for several weeks without impacting the project.

A line and grade construction crew with unskilled laborers can be utilized instead of a typical wall forming crew. A line and grade foreman is typically used to insure line and grade requirements

are met, especially for the first several courses of SRW units. The unskilled laborers then place the SRW units and the reinforcement as specified in the approved shop drawings.

Heavy construction equipment such as cranes are not needed to construct the wall. The SRW units weigh on the order of 38 to 45 kg (85 to 100 pounds) each and can be carried by one person. Some segmental block unit manufacturers supply a hand held device for carrying and placing the SRW units. The reinforcement, and geotextile, if required, is unrolled and placed by hand. A small loader is used to place backfill lifts, which are then compacted using hand-operated compaction equipment.

The St. Paul District geotechnical engineers have noted one disadvantage of MSE SRW system construction. This is the often unfamiliarity of construction details by COE inspectors and large construction contractors who generally are awarded COE construction contracts. MSE SRW system suppliers are required by the specification to provide experienced installers to assist the construction contractor during the early stages of the MSE SRW system. However, the installation learning curve for both the construction contractor and the inspectors can be substantial. Care for detail must be continual to insure bulges or misalignments are minimized.

CONCLUSIONS

The St. Paul District of the U.S. Army Corps of Engineers has successfully designed and constructed several MSE SRW systems in riverine and reservoir environments. Alternative methods for specifying and bidding MSE SRW systems have evolved over the last several years based on experiences with various methods. Today, three methods are utilized to specify and bid MSE SRW systems, depending on the geotechnical complexity of the site and problems anticipated to occur during the bidding and submittal review process. The three methods are presented, discussed, and supported by case histories in this paper.

The MSE SRW systems provide a cost-effective and highly aesthetic alternative to conventional wall systems for minimizing the affect of civil works flood control projects. In addition to cost savings and aesthetic value, other advantages of the MSE SRW systems include reduced construction time, flexibility of construction sequencing, minimization of dewatering costs, use of lower cost construction crews, and the absence of heavy construction equipment.

The St. Paul District's experience with MSE SRW systems has resulted in a great interest by other COE Districts to use these wall systems. Typically, these Districts and their local sponsors have selected MSE SRW systems after discussions with the St. Paul District geotechnical engineers and local sponsors and site visits to the projects where MSE SRW systems are used.

RECOMMENDATIONS

The methods used by the St. Paul District to specify and bid MSE SRW systems are presented in this paper. Based on a progressive use of MSE SRW systems, the methods have been refined. Use of the methods as discussed herein should minimize concerns during the bidding and shop drawing submittal and review processes. This recommendation is the opinion of the authors and does not necessarily represent the opinion of the U.S. Army Corps of Engineers or the St. Paul District.

REFERENCES

Berg, R.R., and Meyers, M.S., (1997), "Analysis of the Collapse of a 6.7 m High Geosynthetic-Reinforced Wall Structure", Geosynthetics '97 Conference Proceedings.

Meyers, M.S., and Schwanz, N.T., (1993) "MSE Segmental Block Wall System in a Riverine Environment", Geotechnical Fabrics Report, Volume 11, Number 4, pp. 22-27.

Simac, M.R., Bathurst, R.J., Berg, R.R., and Lothspeich, S.E., (1993) "Design Manual For Segmental Retaining Walls (Modular Block Retaining Wall Systems), First Edition", National Concrete Masonry Association, Herndon, Virginia.

U.S. Army Corps of Engineers, (1989) "EM 1110-2-2502, Retaining and Flood Walls", U.S. Army Corps of Engineers, Washington, D.C.

U.S. Army Corps of Engineers, (1990) "ETL 1110-2-322, Retaining and Flood Walls", U.S. Army Corps of Engineers, Washington, D.C.

PRICING STRATEGIES IN ENVIRONMENTAL CONSTRUCTION

CHARLES W. LOCKHART
SAMUEL W. TAYLOR
GOLDER CONSTRUCTION SERVICES
3730 CHAMBLEE TUCKER ROAD
ATLANTA, GEORGIA 30341

ABSTRACT

As with all types of construction, the economics of environmental construction projects are critical to project outcome. This is particularly relevant for environmental remediation projects, due to the negative cost impacts of the work. As opposed to a value-added construction project with revenue generating capabilities after completion, remedial projects represent sunk costs, often with little ability for recovery. However, the utilization of lump-sum contracting methods, in an attempt to control and minimize costs, often do not work on remedial construction projects due to the uncertainties inherent in the conditions to be encountered in the field. Alternative pricing strategies can be the key to a successful project outcome. Our experience has clearly demonstrated that there are cases where unit-price or cost-plus pricing, combined with proactive on-site third party construction management is the most advantageous way to execute many of these types of projects.

Introduction

Pricing strategies, in conjunction with contract scope of work and contract form, are the three essential ingredients of a construction project. There are years of experience in the building of capital projects which have defined this industry and avenues for success of the participants. However, the remedial construction market has introduced a new set of groundrules. This is basically due to the fact that the work is essentially on the cost, instead of the value side of the economic equation. Owners view these efforts as costs they do not want to incur, and may not even be totally responsible for. As a result, the overall climate of the project is changed from one of excitement at the creation of an asset, to one of "how do we get out of this." Contractors and owners have to recognize this change in climate and adapt to it so that each party properly shares the risks and rewards of the situation fairly. The pricing strategy and methods of payment are one of the keys to this.

The concepts of fast-tracking projects, and carrying them out in a design-build manner is also gaining favor in the landfill construction market, where multi-cell facilities can either be

accelerated or decelerated based on market demand. As a result, the scope of work and schedule for a project must be entirely flexible, and the resulting pricing strategy for the contract for design and construction must reflect this flexibility and provide a suitable sharing of risk and reward as well.

This paper is primarily focused on remedial construction. However, alternative pricing strategies can also be of benefit for the construction of conventional capital projects, such as landfills, where fast-tracking of design and construction, as well as the staging of construction to be responsive to the vagaries of the waste demand, is becoming more prevalent. In addition, the paper will provide a simple checklist that can be used as a guideline for evaluating when pricing other than lump sum may prove to be more suitable for the project. This topic has particular relevance given the dramatic increase in containment remedies for environmental remediation projects, and the increasing use of geosynthetic products in their construction.

METHODS OF PAYMENT

While there are numerous methods of payment used to reimburse construction contractors for the services which they provide, they usually fall into one of three general categories, namely Lump Sum, Unit Price, or Cost-plus. The appropriate method of payment is dependent upon the specifics of the project, and the inherent uncertainties associated with the contemplated work. The methods of payment must recognize the unique incentives and risks associated with each one (Figure 1).

Figure 1

Lump sum

The lump sum or firm-fixed price form of contract is utilized for projects where the design is complete, the scope of work, quantities and owner expectations are well defined, and there are few uncertainties. This method allows pure competitive bidding, with the contractor assuming almost all of the risks. Unfortunately, lump sum contracting is also utilized by owners when they have a limited budget, and use it as a method to attempt to put a cap on total project costs.

Unit-price

Unit price contracts are typically employed where the type and quality of the work are well defined, but the actual quantities may not be known with certainty at the time of bidding. The contractor develops his bid based on a price for each unit, utilizing a base estimate of quantities which is provided to each bidder. The actual reimbursement is determined by a measurement of the quantities. In this case, the risk of execution, quality and performance of the work is borne by the contractor, but the risks associated with the quantities is borne by the owner. Unit price bidding is appropriate where the project has quantity uncertainties, but competitive bidding is warranted. Examples are earthworks, highways, pipelines or other linear systems.

Cost plus

The third broad category of payment method is cost-plus. In this method, the contractor is reimbursed his "costs" for executing the work, plus additional amounts to cover his overhead and profit. The additional amount may be a fixed fee, a percentage, or a sliding scale tied to the total cost or schedule of the project. Since the cost for the work is open-ended with the cost-plus pricing method, the risks for total cost lie with the owner. This method is often utilized for fast-track construction, or other circumstances where the work commences prior to the design work being completed. The incentive for the owner to take on this additional risk is in the ability to complete the project sooner than the traditional design-bid-construct method may allow. This method under certain circumstances is also applicable to remedial construction, where the scope of work may change substantially from project onset to completion due to changing technology, regulatory environment or other outside factors.

Cost plus pricing has numerous variations. By reducing risk to the contractor, it can encourage innovation and use of new technologies. One example is a cost plus a fixed fee to cover overheads and profit. This creates an incentive for the contractor to complete the work as rapidly as possible with a minimum of reimbursable costs in order to maximize his profits during that period of time. Another example is cost plus a percentage. The percentage amount is applied to the reimbursable costs to cover the overhead and profit. However, this may reduce

incentive for the contractor to accelerate the work and complete it in a timely manner. One method to maintain this incentive is to incorporate a sliding scale percentage, so that if the job is drawn out, the coverage of the contractor's overhead and profit decline.

There are numerous incentives (or also penalties) which can be applied to all three types of contracts, including time or cost-dependent bonuses which give the contractor something to shoot for.

One example of an innovative pricing strategy regarding the installation cost of geosynthetic components has been utilized with great success. Simplistically, the strategy incorporates four pricing levels based on the time of year, related to climate, work levels and estimated field production efficiency. A base price (typically $ per square foot installed) is negotiated. Then an add/deduct percentage is utilized based on when the work is carried out. For example, if the work is carried out in the "high season" (i.e., summer/dry season, when typical contractor workload is high, the base prices are escalated by a percentage. If the work is carried out in the "low" season (i.e., spring/wet season when contractor workload is low), the prices are discounted. These add/deduct percentages are in the range of 5% to 15% above or below the base price. This strategy is obviously applicable to multi-phase, multi-year installation projects, such as landfills, but is an illustration of how flexibility and recognition of market forces can affect overall project schedule and cost.

Risks

From an owner/contractor perspective, the primary difference between the above methods is the allocation of total cost risk (Figure 1). Potential reward should be commensurate with risk; if contractors are asked to assume greater risk, they are entitled to greater potential profits. The spectrum is defined by lump sum pricing versus cost-plus pricing. Highly defined, conventional means/method projects usually attract a high number of qualified bidders, willing to develop a lump sum pricing for the work. In this scenario, the primary risk of total project cost is born by the contractor. In most cases, this is fair in that the owner has invested money and effort to carry out this level of definition and quantification, and therefore is entitled to shift the risk. Lump sum contracts can also provide a substantial incentive to contractors to develop cost saving means and methods, since they realize all of the cost savings.

Conversely, if the project is not quantifiable or conventional, then valid pricing will trend to unit-price or cost-plus, shifting the risk for total project cost to the owner, where it logically should reside. However, contractors should be willing to accept a lower profit as a trade-off for assuming lower risks. The relative concept of relationship of pricing and risk is depicted on Figure 2.
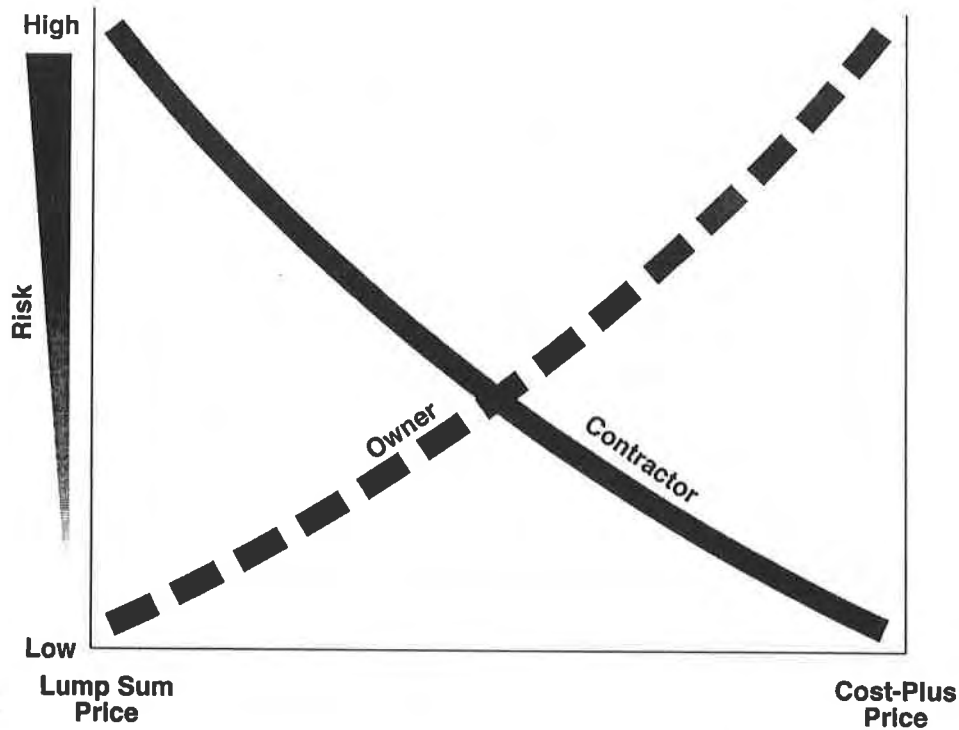
Figure 2

USE OF CONSTRUCTION MANAGEMENT TECHNIQUES

Professional Construction Management is a project delivery method that applies modern management techniques to project planning, design and construction in order to control time and cost and assure quality for the project owner.

Construction Management comprises a comprehensive array of services spanning all phases of the design and construction process. The program of services applied to a particular project should be one which is appropriate to the size, type, and complexity of the project and the needs of the owner. Construction management techniques are uniquely suited to projects where the risk of total cost resides with the owner. Usually, the Construction Manager (CM) is a member of the owner's project team and is responsible for developing and implementing a management plan that will achieve the goals of the owner and the project within the budgetary and schedule parameters established by the plan. The professional CM does not design or construct the project; the CM's task is to implement a management framework within which those processes may be carried out efficiently and effectively by the designers and the contractors. Compensation for professional CM services is usually based on a time and materials or fee basis and therefore is not dependent on the ultimate cost of the project, thus eliminating any conflict of interest in managing the costs of design and construction.

The Construction Management process is most effective when employed from the beginning of the project, allowing the CM, the owner, the design professional(s) and potential contractors to identify and resolve issues of value and constructability prior to completion. Scheduling and coordination are the keys to controlling time in the design and construction processes. The Construction Manager uses scheduling techniques to monitor progress and to anticipate critical events and concerns before they become problems. Project scope determines project cost, and opportunities for cost savings are greatest during design. The Construction Manager prepares independent cost estimates and reviews the on-going design for potential cost savings. During construction, the Construction Manager monitors progress, quantities, changes in scope or conditions, and other factors affecting cost to provide for a fair application of the contract terms.

UNIQUE ASPECTS OF REMEDIAL CONSTRUCTION

Environmental remediation projects introduce a unique framework to the question of optimizing construction pricing methodologies. This is primarily due to the negative cost impacts of the work; as opposed to "asset creation" construction projects which are usually linked with revenue generating capabilities after completion, remedial projects represent sunk costs, often with little ability for recovery. The situation is further compounded by a constantly changing regulatory environment and often by a requirement to utilize best available technology. This can result in prescriptive, proven remediation schemes being abandoned in favor of newer, but unproved technology at the whim of a regulator or advisory group with little regard to schedule and cost impacts.

Also, many of the "owners" are unfamiliar as well as uncomfortable with the uncertainties inherent with remedial construction. Typically, they are more familiar with the construction of capital facilities, often which are repetitive and with fewer uncertainties. Many of these projects, if not the majority, are executed through highly competitive lump sum bidding. Thus, owners may have a strong predisposition towards highly quantifiable design/specification packages, and hard-dollar lump sum bidding. Our experience is that often, when these conventional lump sum methods are applied to remediation construction, the owner and contractor expectations are not met, and often there are resultant schedule inefficiencies and rising costs associated with changes either to the scope or quantities, which are arguably compensatable to the contractor, but unpalatable to the owner. The net result can be unhappy participants and escalating claims or ultimately, litigation. We are suggesting that innovative pricing methods are more appropriate to these types of projects. The following examples, based on real project experience, illustrate these techniques. Given the sensitive nature of these projects, and the fact that one is ongoing, we must keep project names, locations and participants confidential.

CASE HISTORIES

Case History No. 1

Case No. 1 is illustrative of the positive impact of utilizing a cost-reimburseable contract with a resident construction manager. This environmental remediation project was initially set up as Lump Sum contract with some Unit Price elements. The scope of work included demolition of buildings, removal of contaminated soils, the placement of geosynthetic barrier layers and drainage layers, and rehabilitation of wetlands. In particular, the application of continuously sewn 16-ounce geotextile synthetic blankets over existing wetlands in an area in excess of 3 acres posed unique problems for the contractor to both price and subsequently install in the field. As the project was entering the third year of a two year construction schedule, the owner was facing a claim presented by the contractor which was greater than the proposed initial value of the contract. In addition, the project had a negative earned value for the moneys spent to date. At that time, the owner elected to resolve the outstanding claims, convert the contract to a cost-plus-fixed-fee contract, and engage a professional construction manager to provide construction management (CM) for the third (and final) year construction effort. Members of the CM team participated in negotiation and subsequent settlement of the outstanding claims and in establishing a cost-plus fixed fee contract (with incentives) for continuance of the project.

One of the keys to the project strategy was the addition of the Construction Manager. During construction the CM team was to provide contract administration and act as the owners agent in matters pertaining to the construction effort. One of the first steps was participation of the project team (owner, CM and contractor) in a "Teaming Session". This concept, initiated by the owner, defined the roles and expectations of the various parties and re-established a rapport among the Project Team so as to result in a spirit of cooperation in achieving the common goal. Broadly speaking the CM team's function was identified as:

- Participate as a member of the Project Team to complete the construction effort in an efficient manner such that the project was completed within the time allotted and the moneys budgeted

- Ensure that the contractor is fairly compensated for his efforts

- Satisfy the owner that value was received for money spent

In order to provide effective project administration and to make a meaningful contribution to the success of the construction effort, the CM Team's first priority was to review existing protocols of contract administration and either adopt them or establish new means of:

- Identifying and processing change orders

- Processing payment applications and submittals

- Communications between elements of the Project Team

Using management systems developed for use on landfill construction projects and adapted to remediation projects, the CM Team, in cooperation with the Contractor and the construction quality assurance (CQA) consultant, established the protocols and procedures appropriate to the cost-plus-fixed-fee nature of the new contract.

In addition to establishing contract administration systems, a construction schedule for the work to be performed was developed. A resource loaded network analysis construction schedule was submitted by the Contractor and reviewed by the CM Team. This review resulted in a Baseline Construction Schedule which was adopted by the Project Team. The Contractor's cost control accounting procedures were likewise reviewed and complimentary monitoring systems were implemented by the CM Cost/Schedule Engineer. With these systems in place the Contractor could commence construction activities.

Construction proceeded with the Project Team working collectively to achieve the goals established in the Teaming Session. Operations meetings were conducted daily with the Contractor's Project Manager, Superintendent and Foremen and weekly construction progress meetings were conducted to update the construction schedule and make plans for the forthcoming weeks efforts. Issues requiring resolution were discussed in the concept of achieving the common goal and, as a result of the cost-plus nature of the contract, decisions were reached without concerns regarding the Contractor's level of risk. Change orders effecting the cost of the project were reviewed with the knowledge that the cost of the change would be borne by the owner alone and that the Contractor would be rewarded at a pre-established percentage of the cost of the change.

At the start of construction the negotiated budget was established at just over $8.5 million. At the conclusion of the construction effort 10 months later, the total value of the contract, including changes, totaled $9.8 million. A major remediation project, which just 12 months earlier was mired in a major claim and fraught with animosity between the contracting parties, was completed at a cost of 15 percent over budget with no claims outstanding. The strategy of a cost-plus contract was declared a success by the owner.

Case History No. 2

The second case is the construction of a large, multi-cell municipal waste landfill. The liner system is a double composite liner, with textured liner on the slopes. The project was fast-tracked so that the design and construction could be carried out in close sequence. In order to

expedite the construction and alleviate concerns of both the owner and contractor over the degree of definition of the scope, the construction contract was structured to include unit prices for items of work for which the quantities are reasonably definable and cost-plus-fixed-fee for items which are not easily defined or quantified.

A Resident Construction Manager (RCM) has been actively involved in the project since its inception. The RCM acts as the owner's agent in all matters pertaining to the contract and as the primary interface between the owner and the contractor. In addition to being present on a full time basis during construction, the RCM participated in design coordination, preparation of bid documents, selection of the contractor, and in negotiations of certain items of the work deemed inappropriate to conventional methods of pricing construction activities such as lump sum or unit price. The cost-plus portion of the work is handled much as Force Account work is typically handled in that the Contractor and RCM each maintain an account of the labor and equipment hours associated with the effort and reconcile their respective accounts after an item of work is completed. Material incorporated into the cost-plus items of the project is measured and paid for by either pre-established unit rates or by Contractor paid invoices with an allowed mark-up of 5% for handling and a sliding scale of from 5% to 10% for profit. Pre-approved unit rates are applied to the labor and equipment hours agreed to and a fixed percentage rate, negotiated during selection of the Contractor, is allowed for overhead and profit. (While certified payrolls were not required, the owner is privy to the wage scale paid by the contractor and is able to accurately establish payroll costs for equipment operators and technicians.)

Innovative geosynthetic installation pricing has been developed at the site, based on time of year, production volume, and other factors which can increase the efficiency of the contractor's operation.

This contract is currently in its second year of construction and is progressing on schedule and within budget allowing for some major additional items of scope added by change orders. There are no known issues which are likely to result in a claim and again the owner is satisfied that he is receiving value earned for his construction expenditure.

PRICING STRATEGY

The concept of setting a well defined pricing strategy is the basis for bidding and should be undertaken for all projects, regardless of size or scope. In order to determine how a specific project matches up to the alternative pricing strategies, we recommend a simple checklist to guide owners. An example of such a list is indicated below.

Pricing Strategy Checklist

Level of Uncertainty	Low	High
1. Fast track/Design Build? (high if yes)		
2. Completeness of design		
3. Means and methods of construction		
4. Determination of quantities		
5. Determination of schedule		
6. Availability of experienced contractors		
7. Value of project		
8. Regulatory environment		
9. Owner experience/capabilities		

For each of the listed elements, if the level of relative uncertainty is "low", place a checkmark in the "low" column. If the relative uncertainty is "high", then place a checkmark in the "high" column. At the end of the evaluation, if a project has 2 or more checkmarks in the "high" column, then we recommend that alternative pricing strategies should be thoroughly considered, and depending on the size of the project, the use of a professional construction manager could assist and enhance the project outcome.

Obviously, the above list is overly simplistic, and is recommended as a guideline only. Owners /designers should develop their own criteria, and should consider including a relative weighting scale dependent on the importance of each factor. The key point is the need for a systematic analysis of pricing strategy relative to the project requirements.

SUMMARY AND CONCLUSIONS

Our experience has clearly demonstrated that there are cases where unit-price or cost-plus pricing, combined with proactive on-site third party construction management is the most advantageous way to execute remedial construction projects. As with all types of construction, the economics of remedial construction projects are critical to project outcome. This is particularly relevant due to the negative impacts of the work; as opposed to a value-added construction project with revenue generating capabilities after completion, remedial projects are represent sunk costs, often with little ability for recovery. However, our experience is that the utilization of lump-sum contracting methods, in an attempt to control and minimize these costs, can be problematic on remedial construction projects due to the uncertainties inherent in the quantities to be encountered in the field. In addition, the wrong methodology can set the stage for an antagonistic and unmotivated project team.

Pricing strategies , in conjunction with contract scope of work and contract form, are the three essential ingredients of a construction project. Due to the fact that the remedial construction market has introduced a new set of groundrules in that the work is essentially on the cost side of the economic equation, owners and contractors have to recognize this change in climate and adapt to it so that each party properly shares the risks and rewards of the situation fairly. The pricing strategy and methods of payment are one of the keys to this.

REFERENCES

Chen, W.F., (1995) The Civil Engineering Handbook. CRC Press, Inc., Boca Raton, FL.

Construction Management Association of America,(1988) Standards of Practice. CMAA, Reston, VA.

0113cwll.doc

PROTECTION OF PVC GEOMEMBRANES IN BAUXITE RESIDUE DEPOSIT

LEANDRO M. COSTA-FILHO
LPS CONSULTORIA E ENGENHARIA LTD, BRAZIL
EDWARD B. PACHECO
LPS CONSULTORIA E ENGENHARIA LTD, BRAZIL

ABSTRACT

For a bauxite residue deposit the impermeabilization of the slopes consists of a 0.8mm thick PVC geomembrane over a compacted clay layer. A protection for the PVC membrane against UV degradation and mechanical damage during the 5 year operation is required and consisted of a compacted soil layer. During construction, due to some difficulties associated with weather conditions, very wet soils in the borrow areas, and a very tight construction schedule, an alternative was sought, consisting of the use of shotcrete. In order to adjust construction procedures and evaluate alternatives of geomembrane protection during shotcreting, an experimental slope was prepared. The final solution consisted of a low mass per unit area non-woven geotextile on the geomembrane, a light wire netting and shotcrete prepared at a mix of 1:4:2 (cement, sand, crushed rock) with a water-cement factor of 0.5. Cost estimates for the original (compacted soil) and the alternative (shotcrete) solutions were of the same order and the shotcrete was then chosen due to the guarantee of finishing the work on schedule.

This solution was successfully applied on about 20,000m^2 of slope in the first stage of construction and another 15,000m^2 when the embankment was heightened. The use of a shotcrete protection layer for the geomembrane resulted in increase in storage capacity, reduction in borrow areas, reduction in execution time, a construction almost independent of weather conditions, greater erosion resistance and greater construction flexibility.

INTRODUCTION

The Bauxite Residue Deposit No. 5 at ALCOA aluminium plant in Poços de Caldas, MG, Brazil, has a storage capacity of the order of 1×10^6 m^3. The deposit, with a depth of 8 to 15m and crest length 1250m, is formed by embankment fills with internal slopes 2.5H:1V. At the bottom, a drainage layer consisting of sand with buried pipes covers the double impermeabilization system formed by a 0.8mm thick PVC geomembrane over a 60cm compacted clay layer. In the slopes the same impermeabilization system exists (3m wide clay layer under PVC geomembrane) but without drainage layer.

The construction had to be done under a very tight schedule, using only the available six months of relatively dry weather, since excess process water had to be stored in the deposit during the next wet season.

The common PVC geomembranes employed in this case require a protection cover, basically against mechanical damage and long-term ultraviolet radiation exposure . While at the bottom the drainage layer provides adequate protection, in the slopes the geomembrane would be exposed before and during filling of the deposit.

GEOMEMBRANE PROTECTION

Apart from UV degradation, PVC geomembranes require protection against different types of mechanical damage, such as:

- accidental tearing;

- wind effects;

- fall of debris (gravel, tools, etc.);

- vandalism

In industrial fills for solid waste storage a protection layer is nearly always required. In the present case the residue is disposed of as a pulp at low solids content and does not damage the geomembrane during placement and storage. Nevertheless, for the time span of 5 years before and during filling, predicted for Deposit No. 5, a protective layer is necessary on the side slopes.

During design, several alternatives for the protective cover were considered, which included:

- geotextile;

- geotextile impregnated with asphaltic emulsion;

- asphalt;

- soil cement;

- compacted soil.

A woven or non-woven geotextile was discarded mainly due to UV degradation and possible wind damage. Asphalt impregnated geotextile or an asphalt layer were discarded not only by their high cost but also by difficulties envisioned during placement and lack of technical experience on friction of asphalt with geomembrane at the slope angles used.

The soil-cement solution was not technically and economically attractive because:

- the locally existing soils consist of silty clays and clayey silts not easily mixed with cement, with the aggravating factor that they were found at elevated water contents.

- it is extremely difficult to execute an economical layer of soil cement on the 2.5H:1V slopes, over a geomembrane.

Therefore, a compacted soil cover was proposed, as shown in the cross-section in figure 1. For constructive reasons, the soil cover had a minimum width of 3m, compatible with conventional earth-moving equipment.

A series of stability analyses for the compacted soil cover was carried out. Interface shear strength parameters were determined by direct shear tests using compacted clay and drainage sand in contact with the PVC geomembrane. From the results, in order to obtain a minimum factor of safety of 1.25 at the end of construction of the soil cover, a soil berm was required for dike heights greater than 8m. A sand-layer was also required in contact with the geomembrane, as shown in figure 1.
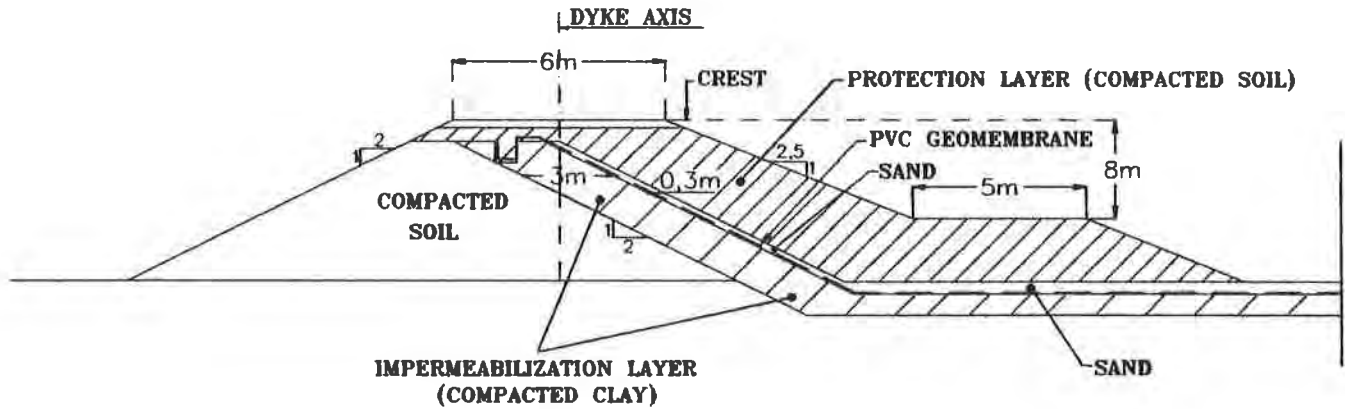
FIGURE 1 — DYKE CROSS SECTION — ORIGINAL SOLUTION

SOLUTION REEVALUATION

During construction some difficulties were found, such as above average rainfall and soils in the borrow areas wetter than expected. These factors, associated with the very tight construction schedule, forced a series of design adjustments. The placement of compacted clay for the protection layer in a restricted (3m wide, on average, along the whole perimeter) area, and with great care to avoid damage to the geomembrane, particularly created a serious constraint to the required overall schedule. Only light construction equipment could be used, with very low production. The sand layer at the interface posed additional difficulty for the construction.

An alternative solution for geomembrane protection was then sought in order to reduce the risk of construction delay. This alternative should effectively protect the geomembrane and be stable against sliding. Besides, its implementation should be independent of weather conditions. A layer of shotcrete was then selected as an alternative protection, but its use required the definition of shotcrete mix and thickness, need of reinforcing mesh and evaluation of possible damage to the geomembrane during shotcreting.

To clarify these questions and to adjust construction procedures, an experimental slope was prepared at the site.

EXPERIMENTAL SLOPE

An experimental slope was prepared at the site using the external soil slope of the Residue Deposit No. 4 with inclination 2H:1V. The use of a steeper slope than in the actual deposit was considered appropriate since the application of shotcrete would be tested under more severe conditions, the same occurring with the placement of the geomembrane. An area of about $500m^2$ of slope, with elevation difference between crest and base of 9m, was prepared. The 0.8mm PVC geomembrane was placed directly on the slope surface, previously cleared of any debris or loose material.

The following conditions were tested:

- shotcreting directly on the PVC membrane or on a non-woven low mass per unit area geotextile placed over the membrane;

- use of reinforcement made of a conventional steel mesh, a plastic geonet or a simple wire netting;

- thicknesses of 3.0 to 5.0cm for the final layer;

- mortar mixes 1:3, 1:4 and 1:5 (cement:sand), 1:4:2 and 1:6:2 (cement:sand:crushed rock), with the water cement ratio varying between 0.35 and 0.50.

Several combinations of the above conditions were tested. In all tests hand-operated conventional shotcreting equipment was used. The tests lasted for 5 days and a series of panels were open afterwards to observe the results.

The main conclusions of the tests were:

- placement of geomembrane, geotextile and reinforcing mesh and application of shotcrete on a 2H:1V slope did not present any difficulty;

- application of shotcrete directly on the geomembrane was not satisfactory due to the low adhesion between the two materials, with parts of the protection layer being easily detached. It should be noted however that, at least visually, there were no signs of damage to the geomembrane;

- the use of the geotextile, even of low mass per unit area ($200gr/m^2$), was successful in protecting the geomembrane and it could be observed that the geotextile was completely impregnated by the mortar;

- no distinctive difference could be noted between any of the reinforcing meshes tested and therefore it is concluded that even the simple wire mesh (of the type used in sports courts) was acceptable. In all cases this reinforcement was completely involved by the mortar, even when 3.0cm thick layers were formed. For the geonet reinforcement a thickness of 5.0cm was required

- small retraction cracks occurred in all tests, irrespective of layer thickness and type of reinforcement but without detachment of protection. An improvement was obtained when crushed rock (grain size 4.8 to 9.5mm) was used in the mix;

- overall stability of the protection layer was satisfactory during construction, despite the observed cracking. After the test program was completed, a trench was excavated at the base of the slope and a slip occurred parts of the protection layer. This would be expected due to the low frictional resistance between the geotextile and the geomembrane and indicates the need of an adequate support for the protection layer at its base.

A cost estimate was made for several alternatives among those tested. The results are shown in table 1.

NR	ALTERNATIVE				COST US$/m²
	MIX	GEOTEXTILE	REINFORCEMENT	THICKNESS (cm)	
1	Cement:sand 1:4	none	none	3.0 4.0 5.0	6.48 8.64 10.80
2	Cement:sand 1:4	yes	geonet	4.7	12.85
3	Cement:sand 1:4	yes	geonet	4.7	14.50
4	Cement:sand 1:4	yes	none	3.0	8.13
5	Cement:sand:gravel 1:4:2	yes	net wiring	3.0	8.83
6	Cement:sand 1:4	none	net wiring	3.0	8.34

TABLE 1 - COST ESTIMATES FOR SHOTCRETE ALTERNATIVES

Due to the small cost difference, alternative 5 was chosen, considering the technical advantages of using the geotextile and the reinforcement, as discussed above.

COMPARISON WITH THE ORIGINAL SOLUTION

The alternative chosen consists of a low mass per unit area geotextile on the geomembrane, a simple net wiring and shotcrete prepared at a mix 1:4:2 (cement:sand:crushed rock) with a water cement factor of 0.5. A minimum thickness of 3.0cm was adopted.

The cost of this alternative was compared with that from the original compacted clay protection.

For the compacted clay the following cost was computed:

- escavation and transport of clayey soil: 63250m^3 x US$ 1.10/m^3 = ... US$ 69,575.00

- soil spreading and compaction: 55000m^3 x US$ 0.75/m^3 = ... US$ 41,250.00

- sand layer at interface: 12000m^3 x US$ 11.00/m^3 = ... US$ 132,000.00

TOTAL: .... US$ 242,825.00

The cost of the shotcrete solution, after negotiations with the contractor, was US$ 239,224.00. This total cost corresponds to about US$ 12.00/m^2, higher than the estimates during alternative comparisons (table 1) due to uncertainties in production, equipment acquisition, etc.

However, other residue deposits, built afterwards, in which the same shotcrete protection solution was adapted, have unit prices of the order of US$ 9.00/m^2.

In any case it should be noted that these costs are much higher than for the 0.8mm PVC geomembrane itself, which is of the order of US$ 4.00/m^2 (inclusive installation).

The final choice of the shotcrete as protection was based on:

- technical feasibility of execution;

- guarantee of finishing construction on schedule;

- total cost comparable to the original solution.

CONSTRUCTION

Figure 2 presents the solution adopted for the internal slopes of Deposit No. 5.

Based on the observed behaviour in the initial stages of application of shotcrete protection, it was decided to introduce transverse and longitudinal joints made of flexible PVC tubes in order to reduce surface cracking.

It should be stressed however that cracking of the protection layer does not cause any problem to its functionality provided it is not so intense that cracks might cause detachment of chunks of mortar. On the contrary, cracks can be beneficial to the release of fluid pressures under the shotcrete due to infiltration from the crest or to water level drawdown in the deposit.

For the same purpose, 5cm diameter drainage tubes were installed at 3 elevations in the slope.

No difficulties were encountered during protection construction using conventional shotcrete projection equipment. Only under severe rainfall the work had to interrupted and could be resumed immediately after the rain stopped. The work finished well within schedule.
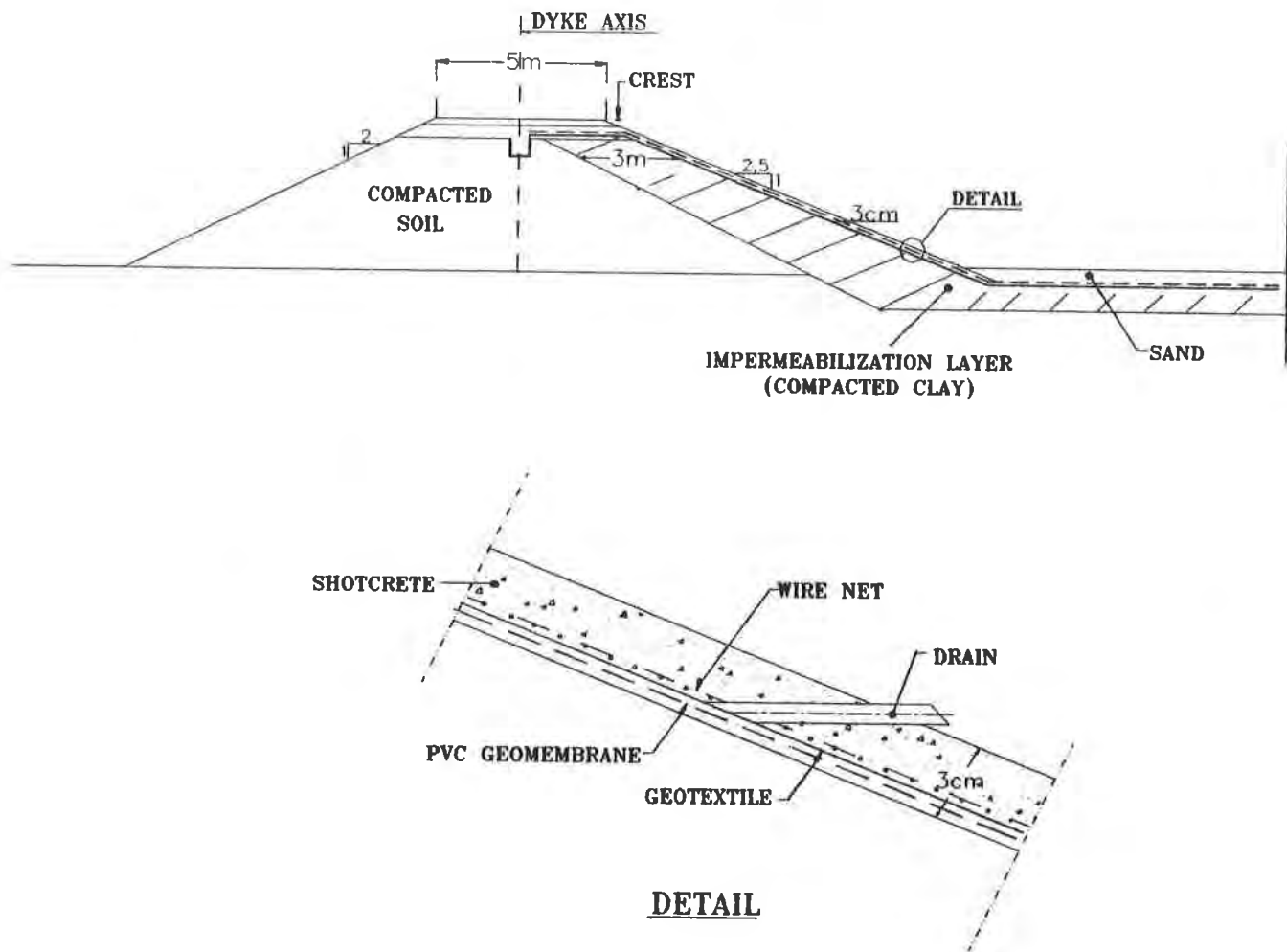
FIGURE 2 – DYKE CROSS–SECTION – PROTECTION WITH SHOTCRETE

Average production was 19m³/day (aprox. 630m² of slope surface), with peak productions of 30m³/day (aprox. 1000m²).

This solution was successfully applied in about 20,000m² of slope in the first stage of construction and another 15,000m² when the dikes were raised.

CONCLUSIONS

The use of shotcrete as protection for the PVC geomembranes on the slopes of Bauxite Residue Deposit No. 5 proved to be a technically satisfactory solution. No problems have been observed in the two years of exposure before and during operation.

The solution enabled the construction of the deposit to be finished in time, without undue difficulty, despite the severe weather conditions.

The following additional advantages were obtained with this type of protection:

- increase in storage capacity of the deposit by substitution of a 3m wide soil cover for a 3cm thick shotcrete layer;

- reduction in borrow areas, with associated rehabilitation;

- reduction in execution time for protection implementation;

- construction almost independent of weather conditions;

- less maintenance during operation, being resistant to superficial erosion;

- provides greater construction flexibility, considering the different activities involved in this type of work.

The main drawback in the shotcrete protection is its relatively high unit cost, despite the fact that for Deposit No. 5 this was not the case and the shotcrete solution was even cheaper than the original solution.

The same solution has already been applied in other bauxite residue deposits and could also be used in industrial waste fills. For solid waste industrial fills the shotcrete would also provide adequate protection during placement and spreading of waste.

ACKNOWLEDGEMENTS

GEOMEMBRANE LINERS: RELATIVE SIGNIFICANCE OF MATERIAL AND FINAL COSTS

By

Ian D. Peggs, I-CORP INTERNATIONAL, Inc.
Robert Denis, SOLMAX (Canada)
Dominic Berube, SOLMAX (Canada)

TOPIC: ECONOMICS

ABSTRACT

There are many factors that control the finished cost of an installed geomembrane lining system. In many instances, pennies are shaved off the costs of the geomembrane material itself, as if this is the most important cost factor. In many instances a geomembrane is perceived simply to be a thin plastic sheet that can conform to the subgrade, and which just needs melting and pressing together to make a joint; a pure commodity item. This view is acceptable only when the impact of leakage is insignificant. However, when the geomembrane is the critical barrier component of a lining system, it should not be treated in isolation as a commodity item. It should, rather, be considered as the key component that initiates a sequence of synergistic activities that, together, define the real cost and effectiveness of the lining system.

The selection of a geomembrane influences many subsequent installation related activities to the extent that what might be a good selection under given circumstances may be far more costly under other circumstances. Factors that can influence the final installed cost are examined and practical examples are given of where savings or additional costs have been incurred during liner installation projects.

It is clearly shown that low geomembrane and related service costs often lead to higher installed costs.

INTRODUCTION

The installation of a geomembrane liner in a facility where the provision of a hydraulic barrier is critical consists of several stages:

- design and specification
- material purchase
- subgrade preparation
- installation
- construction quality assurance
- testing

- covering

More often than not, the decision on which material to use is based on cost, with every effort being made to minimize costs by cents per square meter. It is known for proposals to be requested, a short list accepted, and these "successful" bidders requested to make their final best offer. The winner is then asked to sharpen their pencil and to give the best possible price. This is not the way to obtain an economical effective lining system, particularly when viewed in the long term. To this materials performance consultant, this international installer, and this project estimator, this philosophy is ill-advised. The real cost of a geomembrane is the final installed cost that will provide the required design lifetime without significant repair and maintenance costs.

As Well (1995) pointed out at the short course on "Geosynthetics: Lessons Learned from Failures":

" It is unwise to pay too much, but it is worse to pay too little. When you pay too much, you loose a little money - that is all. When you pay too little you sometimes loose everything because the thing you bought as incapable of doing the thing it was bought to do. The common law of business balance prohibits paying a little and getting a lot - it cannot be done. If you deal with the lowest bidder it is well to add something for the risk you run, and if you do that you will have enough to pay for something better."

John Ruskin (1819 - 1900)

The factors, over and above the cost of the material, that influence the ultimate cost of the geomembrane lining system are as follows:

- Quality of earthwork - subgrade and anchor trench
- Installation cost
- Competency of design
- Weather
- Quality of installation
- Installer's quality control costs
- Installer's administrative costs
- Independent CQA personnel costs
- Independent CQA testing
- Regulatory approval
- Maintenance

If delays to the project are caused by inferior performance at any of these stages, or if the installed lining system should fail due to inadequate input during any of these stages, the benefits gained by seeking the lowest material cost, or the lowest cost for any of the individual project components, will immediately be reduced or completely lost. Unfortunately the number of liner problems is presently increasing, not because of fundamental material failures, but because of a lack of knowledge of many of those associated with the design, installation, and CQA of the lining system.

DISCUSSION

A brief evaluation of the influences of the various components of the installation program on the cost of the lining system follows. All examples of field occurrences and events are real.

Material

There are two predominant factors that influence subsequent installation costs - the thickness of the geomembrane and whether it can be factory fabricated into larger panels (up to 5,000 m^2) or must be delivered to the site in rolls. Typically, HDPE geomembranes are always delivered to the site in rolls, thus all seams are field seams. While there are more seams in prefabricated panels manufactured from narrower rolls, most of them are factory seams that are made under a carefully controlled environment. However, there are fewer field seams in large panels of flexible geomembranes than there are in HDPE rolls. The basic choice between HDPE and other usually more flexible geomembranes is the increased strain tolerance of the more flexible geomembranes. The more flexible geomembranes are acceptable to USEPA in thinner gauges than HDPE (1.0 mm vs. 1.5 mm for basal liners, and 0.75 mm vs. 1.0 mm for caps). The more flexible geomembranes, in thinner gauges, can often be factory fabricated into larger panels for shipment to the field.

Geomembrane resin prices have been very volatile over the past few years as dictated by a broad market over which the geosynthetics industry has little control. The material cost for 1.5 mm HDPE is approximately $2.80/$m^2$, while that for 1.0 mm PVC is $2.50/$m^2$. At the same 1.0 mm thickness the PVC is considerably more expensive than HDPE at $1.90/$m^2$. A similar situation exists for PP geomembranes as for PVC geomembranes, but we will continue to use the HDPE/PVC comparison.

In most cases, and certainly in all waste containment applications, the geomembrane material should be selected based on its technical service requirements. It is too dangerous to assume that all geomembrane materials provide the same barrier function and to select a material based on cost alone. We will show that there are many more costs that can far exceed the cost ranges of the different materials and that it is economical to ensure that a good material and good installer are used on the project. The cost of material, as will be shown later, is approximately 4% of the costs of the complete landfill, and this barrier is the critical component of the waste containment.

Earthwork

The geomembrane installer and the CQA firm are usually required to approve the quality of the subgrade and the anchor trenches for accepting geomembrane. The assumption is generally made that the subgrade will be acceptable when the installer arrives on site. But it is not abnormal to see glass bottles, ends of metal pipe, stones, and tree roots sticking out of a supposedly "geomembrane-ready" subgrade. This is most likely to happen with low-cost general contractors. Several days can be wasted while remedial work is performed. Revenue-generating capabilities are delayed by several days, and standby costs for CQA and installer personnel are incurred. CQA expenses can amount to $600 per day for one person. Installer standby time can be $1,500 per day for a crew of 5. The same

can occur if the anchor trench corners are not rounded, if they are not straight, if there is loose soil in the trench, if stones are poking through the side wall, and if there is water in the trench.

Installation Cost

The installation time/cost is a function of the size of the site, the site contours, and the size of the rolls or panels of material. The latter determines the type of equipment and the number of people required to deploy, seam, and test the geomembrane. On smaller more complicated sites it may be possible to install about 3500 m^2 of 7 m wide HDPE rolls in a day, while it would not be difficult to install about 5000 m^2 of large PVC/PP panels. However, the PVC/PP panels would require more manual labor than the HDPE, while the HDPE would require more expert welders. On large level rectangular sites (where the detail work is a smaller proportion of the total work), with 10 m wide rolls of HDPE, it should be possible to install about 10,000 m^2 of both HDPE and PVC in one day. Thus on smaller sites the larger factory panels have the installation cost advantage, by about 12%. This is shown in Table 1.

TABLE 1

Approximate Installed Geomembrane Costs ($/$m^2$)

Area (m^2)	PVC (1 mm)	HDPE (1.5 mm)
< 10,000	10.30	11.40
10,000 - 50,000	8.40	7.90
>50,000	8.10	7.60

For an 80,000 m^2 landfill cap project, Keister (1994) reported being quoted deductions of between $3,000 and $20,000 if PVC rather than HDPE was used (of equal 1 mm thickness). Thus the installed cost for PVC was projected to be less costly even though the basic material cost was much higher.

Installation Quality

Here is where a major effect on total costs can occur, as clearly identified by Shepherd et al (1992). Two landfill cells of the same size were lined by different installers with the same CQA firm. Seams were repaired in one cell at 9 times the rate they were in the other cell. This cost extra time, the cost of CQA was doubled, and costs of testing were significantly increased.

In a similar vein, Calabria and Peggs (1996) reported an HDPE capping project in which several hectares of liner had been covered with cover soil before it was realized that the seam test results being generated by the installer's independent QC laboratory, and being reviewed by the owner's independent CQA firm, did not include the specified peel separation values. On retesting it was found that 50% of the previously passing samples now failed. Much liner had to be uncovered and hundreds

of meters of seams repaired. The installer claimed that BTEX (benzene, toluene, ethylbenzene, xylene) in the landfill gas was preventing the seams from being properly made despite the fact that there had been no problems on another section of the same cell the year before and despite the fact that repair seams could be properly made. On seam specimens that could be separated by hand it could be seen that soil and dirt were preventing good seams from being made. Thus, any saving in the cost of materials was obliterated by apparently poor seaming and apparently inattentive CQA and laboratory testing.

On another project the installer provided a panel layout drawing for the CQA firm to review. Normally such a drawing would generate a few comments that could easily be dealt with. In this case four drawings were reviewed before the layout was considered acceptable. Thus, the cost of CQA work for this simple task was four times larger than it should have been, not because of inefficient CQA but because of lack of forethought (or technical knowledge) by the installer. Use of an inexperienced CQA firm for this same task might have involved lower costs by accepting the first or second drawings, but any failure initiated at seams running across slopes would have again obliterated any savings.

In one project, the CQA firm identified a forthcoming shortage of material to both the general contractor and the installer, both of whom were relatively unfamiliar with the specific geomembrane material. No action was taken. Five days later work ceased for lack of material. It was a fine day during which the deployment could have been completed. The next few days it snowed. The related additional costs to the general contractor and owner were significant and required much negotiation. An experienced installer would have cost more but the project would have been completed weeks earlier.

Thus, it is more important to use a competent installer than to be concerned about material costs.

Design

In addition to the design being durable, the lining system must be constructible. For instance, if curved rather than straight walls and round pillars are designed, to which geomembranes must be attached by mechanical batten fasteners or by welding to cast-in extruded HDPE sections, installation (and CQA) times will be increased. If the cast in lock-strips are placed too low on the wall, failures can be expected since it is very difficult to ensure that the geomembrane is supported in the corner and that the edge of the geomembrane is flush with the wall and lock-strip. The geomembrane bridges the corner, the seam has residual stress, and the seam is highly stressed when the facility is filled. If joints between lock-strip sections or at corners are not properly welded together when the weld on the strip is to act as a waterstop, then leakage problems can be expected. This sounds like common sense, but it is surprising how many times, between designer and installer, such things occur.

The proper materials must be selected based on chemical resistance, substratum and superstratum soils, installation and covering temperatures, whether the liner will be left uncovered for some time, the potential for long term stresses, and maximum and minimum service temperatures. The materials

must be properly specified to be assured that these performance criteria will be met. All geomembrane materials do not behave the same. Even HDPE geomembranes from different manufacturers do not behave the same.

If the designer does not show what happens to the edge of a geomembrane between the end of a concrete wall to which the liner is fastened and an anchor trench 1 m away in which liner is buried, should the installer do nothing or apply their own solution? Regardless of whose problem it was, this situation caused the owner a great deal of money when erosion under the liner at the transition caused the liner to fail.

Thus design expertise can influence final costs of the lining system and whether the material or lining system will perform as intended under the expected environmental conditions. Clearly a liner failure due to improper selection of material, an omission in design, inability to install a liner effectively, or use of inappropriate superstratum, may far exceed any cost savings in material purchase.

Thus, it is more important to be concerned about designer expertise than it is to be concerned about material costs.

Weather

Geomembranes are installed in the Arctic and in the tropics. In some locations they experience constant low or high temperatures. They are installed at low temperatures and are covered with soil at high temperatures and vice versa. Ponds with uncovered liners are operated full at one temperature and empty at another, or are cycled at all temperatures. Service conditions influence the selection of geomembrane material. But so do the temperatures at which installation and first covering occur. While much attention may be paid to service temperatures, temperature fluctuations before the facility is put into service are mostly ignored. A 1 mm HDPE geomembrane may provide excellent service in a tropical environment but it requires considerable experience to successfully install such a geomembrane at high temperatures.

If installation and covering are to be done at the same steady temperature it only matters what that temperature is, since intermediate expansion and contraction of the geomembrane becomes insignificant. It is then only important as to whether the selected geomembrane can be installed at the installation temperature in a way that it will provide the required service conditions. For instance, if it is very important to have intimate contact between a 2.5 mm thick HDPE geomembrane and a subgrade clay in a lining system that must be installed at freezing temperatures, then that will be very difficult to do using typical North American procedures. It may be possible using more time consuming (and costly) German procedures in which small areas of the complete lining system are progressively built adjacent to each other. Alternatively a more flexible geomembrane material might be used that could be installed using the typical North American procedures in which the lining system is basically built complete layer by complete layer. The balance is between cost and performance under the project specific conditions. The cost of the geomembrane is not the only parameter of

concern. One can pay the low cost and the liner might or might not perform. One can pay a little more and be more assured that it will perform.

If installation is required at low winter temperatures and covering of the geomembrane will be done at high summer temperatures then the expansion coefficient (CTE) of the geomembrane material and its susceptibility to crease-induced stresses become of major significance in addition to service conditions. If the low expansion coefficient material has a higher cost than the high expansion coefficient material consideration should be given to the added cost of low CTE material compared to the possible costs of the several days taken to identify the unacceptable wrinkles, to cut them out, and to repair them.

If a PVC landfill cover is to be installed at low winter temperatures it is important that only installers with significant hot wedge fusion welding experience be considered for the project, together with a CQA firm that is fully conversant with all welding techniques for PVC, i.e. one that has experience in welding PVC with hot wedge fusion equipment. The CQA firm should not prevent a knowledgeable installer from fusion welding PVC at temperatures lower than 10°C simply because the specifications are only written for chemical seaming procedures. On one project, three weeks were wasted and independent consulting fees were incurred to convince the CQA firm that fusion welding would be acceptable. In this case a lack of knowledge (a consequence perhaps of selecting a lower cost installer) resulted in a far higher installed cost for the lining system.

But here is a major dilemma - how does one recognize a lack of expertise if one does not have that expertise oneself? There is no easy solution.

QC and CQA costs

The installer's QC costs are not a part of the material cost but are included in the installed costs. The QC costs for an HDPE geomembrane are approximately 3% of installed cost - for PVC they are approximately 2%. A similar relationship will extend to CQA costs depending on the size of the project and the thickness of the geomembrane. On average, the CQA costs for a large panel flexible geomembrane will be less than for a rolled geomembrane. Fewer field seams will require less welding and nondestructive testing equipment, thus fewer CQA monitors. Installation may be done more quickly given equivalent experience of installers and CQA firms.

The presently submitted rates for CQA "Site Superintendents" vary between $30/hr and $60/hr. Clearly this depends on whether the CQA firm is using a well-experienced installer being paid $20/hr or a summer student at $8/hr. This in turn determines whether the project will receive proactive CQA that will work with the installer to get the project finished, with maximum quality, ahead of schedule, or whether the project simply gets a data collector that contributes nothing to the quality of the installation. The latter may get completely "rolled" by an unscrupulous installer and have the project finished a week early but with poor quality. Or, to hide his lack of knowledge, the CQA superintendent may throw his weight around to show who is the "boss", and procrastinate, thus causing the project to last much longer than necessary.

The BTEX/dirt situation referenced earlier could be used as an example of how the CQA function can be overwhelmed by the installation function. It is easy for the latter to occur when the CQA function is performed from a car at the edge of a landfill cell when conditions are inclement - exactly the conditions when CQA should be at its most effective.

Shepherd et al. (1992) have stated, from extensive experience, that the additional cost of effective CQA is more than offset by the resulting earlier availability of the site for generating revenues.

CQA Testing

Conformance testing of geosynthetic materials should not be viewed as an opportunity for a second set of QC tests. This is not necessary. It is a waste of money. It is a waste of time. If the proper QC documentation has been obtained, conformance testing should just be a spot check of the material so should be done, in general, with fewer but strategic tests and at a lesser frequency than for QC testing. Thus, there will be an insignificant difference in the required conformance testing costs of the different geomembrane materials.

As with all the other components of the installation program, the quality and experience of the testing laboratory may be reflected in the rates charged by the laboratories. Seam tests can be obtained at base costs (for a single sample - no quantity discounts) varying between $18 and $60 for a set of 5 peel and 5 shear tests. The $18 tests will likely be offered by a laboratory that has not been accredited within the Geosynthetic Accreditation Institute-Laboratory Accreditation Program. Use such a lab and it may be found that samples do not meet specifications. After a second round of failing samples, a round of passing samples at another laboratory, and much consulting/CQA time, it might be found, for example, that specimens are being cut with scissors rather than by using a die stamp, or that sharp dies are not maintained. Suddenly the final cost of testing is far higher than $18 per sample.

Consider the costs of testing one seam sample. The following procedures are involved:

- recording the incoming sample
- cutting 10 specimens, but assuring seam is perpendicular to specimen axis
- marking 10 specimens
- testing 10 specimens, 1 minute each minimum
- visual examination of each specimen for location of break and amount of peal separation
- entering/printing data
- QC review of data
- faxing/mailing results
- filing and archiving all specimens

This takes at least 15 minutes time per sample plus the costs of tensile machines, dies, stamping machine, computers, software. Now you want an experienced tester who can tall you when there is an

anomalous result, and an experienced reviewer, plus you want immediate turnaround. As usual, one gets what one pays for.

The lab that failed to record the seam peel separations until 50% of the cap had been covered with soil would likely not have had the QC/tracking systems in place required for GAI-LAP accreditation. Undoubtedly its costs were probably lower than others. On the other hand, it is not necessary to pay $60 for a seam test when others can provide the right expertise and turn around time for $30 or $35. As always, it is a balance between cost and confidence in the service provided that must be struck.

If seam test results are proving acceptable at a frequency of every 150 m of seam length, the CQA firm may reasonably decrease the frequency of testing (increase distance between samples). On the other hand, if the temperature drops significantly the frequency of trial seaming or removal of seam samples/specimens may be increased. The testing costs are balanced against the quality of the completed seams.

Clearly, the costs of seam testing for large panel flexible geomembranes will be less than for 7 m and 10 m wide rolled geomembranes, but this will not likely be as significant a difference as that introduced by an inferior quality installer.

Regulators

Plans must be approved by regulators and construction reports must be approved by regulators before a facility can be placed into operation. This is a time consuming procedure. Regulators, like designers, installers, and CQA firms are comfortable with the known and with cases for which precedents have been set. Thus HDPE geomembrane lining systems, for example, can pass quickly through such regulatory channels, except in such regions where geomembranes are just starting to replace mineral lining systems. Thus, facilities can start generating revenues faster when the known materials or procedures are used. However, if there are unique difficulties (such as loss of plasticizer, oxidation, stress-cracking) with the known geomembrane (whether that is HDPE, PVC, EPDM, or CSPE) all the savings will be lost if the unique feature is responsible for a failure that a little extra cost up front might have prevented.

Overall costs

The cost of a landfill is very approximately $80,000/ha ($200,000/acre). The cost of a geomembrane lining system is very approximately 12% of that cost. The costs of design may be 15% and the cost of CQA about 10%

If the cost of the geomembrane is 30% of the cost of the lining system (4% of the landfill cost), concern over a 10% variation in the cost of the geomembrane material/installer amounts to 0.4% of the total landfill cost. This amount can be obliterated by a 3% increase in design costs and a 4% increase in CQA costs. On a typical 4 week installation project for small landfill cell an extra 1.5 days

in CQA time will overcome a 10% saving in geomembrane cost. As shown by Shepherd et al. (1992), a difference in quality between installers can vary the costs of CQA by 100%.

CLOSURE

Clearly there is no magic formula to identify the optimum cost of a lining system since each site has its own individual hydrogeological, subgrade, operating, environmental, and regulatory conditions. It is, however, clear that the only significant cost of the geosynthetic lining system is the cost of the installed geomembrane that will just provide the required service life with minimum maintenance costs.

The factors that influence the cost of an installed liner that will provide adequate service, in addition to the cost of the material are, most significantly:

- quality of design
- quality of installation
- weather during installation
- quality of CQA
- extent and quality of conformance/seam testing program
- technical knowledge of regulators.

It is not an easy matter to efficiently integrate all these components, but it is the authors considered opinions, from more than 40 man years of geomembrane and liner research, CQA, installation, testing, failure analysis, and leak survey experience that material cost is one of the least significant cost components of a lining system and that proper selection of material and experienced installer is the major step to assure a properly performing lining system. And for the optimum (most economical, assured performance) lining system, the complementary components of the program must be given the same attention.

As stated by Shepherd et al. (1992), the additional costs to assure that effective materials are installed in an effective way to provide the minimum required service will be more than offset by the earlier availability of a facility that will not fail and that will require the minimum maintenance.

So, note once again:

" It is unwise to pay too much, but it is worse to pay too little. When you pay too much, you loose a little money - that is all. When you pay too little you sometimes loose everything because the thing you bought as incapable of doing the thing it was bought to do. The common law of business balance prohibits paying a little and getting a lot - it cannot be done. If you deal with the lowest bidder it is well to add something for the risk you run, and if you do that you will have enough to pay for something better. "

John Ruskin (1819 - 1900)

The truth of this statement is demonstrated daily.

REFERENCES

Calabria, C. and Peggs, I.D., (1996) "Investigation of Geomembrane Seam Failures: Landfill Cover" Proceedings of the 10th GRI Seminar "Field Performance of Geosynthetics and Geosynthetic Related Systems", Philadelphia, PA, pp. 234-257.

Keister, B.A., (1994) "Capping: Geomembranes Control Groundwater Contamination from a Solid-waste Landfill", *Geotechnical Fabrics Report,* June/July 1994, IFAI, St. Paul, MN, pp. 18-23.

Shepherd J.A., Rivette, C.A. and Nava, R.C., (1992) "Landfill Liner CQA: A Summary of Real Costs and a Question of True Value", Proceedings of the 6th GRI Seminar, Philadelphia, PA, pp. 29-35.

Well, L.W., (1995) "Lessons Learned from Canal Reconstruction Using Composite Geomembrane", Proceedings of Short Course Geosynthetics: Lessons Learned From Failures, Nashville, TN, IFAI, pp. 237-249.

* * * * *

f:\papers\costsg97

Economics

GEOSYNTHETICS 97

CONFERENCE
Long Beach, California USA

FACTORS INFLUENCING DYNAMIC FRICTIONAL BEHAVIOR OF GEOSYNTHETIC INTERFACES

Anirban De
GeoSyntec Consultants, Walnut Creek, California, 94596, U.S.A.
(formerly, Department of Civil Engineering, Rensselaer Polytechnic Institute)

Thomas F. Zimmie
Department of Civil Engineering
Rensselaer Polytechnic Institute, Troy, New York 12180, U.S.A.

ABSTRACT

The interfacial friction behavior of various geosynthetic interfaces has been studied using different approaches. Results from both static and cyclic shear tests are presented. Comparisons have been made of the results obtained from both direct shear and shaking table tests. The use of a geotechnical centrifuge to simulate high normal stress conditions has been demonstrated. The results presented are expected to be useful in the design of landfill liners composed of multiple layered geosynthetics under both static and seismic conditions.

INTRODUCTION

The increased use of multi-layered liner systems for landfills with moderate to steep side slopes has raised concerns about stability against sliding. Due to their low friction values, the interfacial shear strength properties of different landfill liner interfaces are important parameters for design. In addition to this, many regulatory authorities have required landfills to be designed against seismic excitation, in view of concern about earthquake damage. Currently there is a need for additional technical guidance for engineers performing seismic design of landfill liner systems. Thus it is important to understand both static and dynamic frictional behavior of the geosynthetic materials that are commonly used in multi-layered landfill liner systems.

In this study, experiments to determine the interfacial shear strength of four common geosynthetic interfaces are discussed. Tests have been performed under both static and cyclic conditions using different equipment. The possible effect of sample size on the interfacial shear properties has been studied using different sized specimens in the tests. The challenge of simulating realistic normal stresses on the interface specimens during shear tests has been met by employing a high gravity environment induced by a geotechnical centrifuge.

EXPERIMENTAL PROGRAM

The interfacial friction behavior of different landfill liner interfaces was studied in this research. In this paper results are presented from tests on four interfaces, formed through different combinations of three types of geosynthetics. The interfaces that were tested are listed in Table 1. Further details about the interfaces and the geosynthetics involved are provided in De (1996).

Table 1. Description of geosynthetic interfaces

Interface	Upper Geosynthetic	Lower Geosynthetic
A	Geotextile: Polyfelt TS 700	Smooth Geomembrane: Gundline HD 60 mils
B	Smooth Geomembrane: Gundline HD 60 mils	Smooth Geomembrane: Gundline HD 60 mils
C	Smooth Geomembrane: Gundline HD 60 mils	Geonet (longitudinal)[1]: Tensar NS 1405
D	Smooth Geomembrane: Gundline HD 60 mils	Geonet (transverse)[2]: Tensar NS 1405

1 -Longitudinal   60° 60°   Direction of Shaking   2 - Transverse   30° 30°
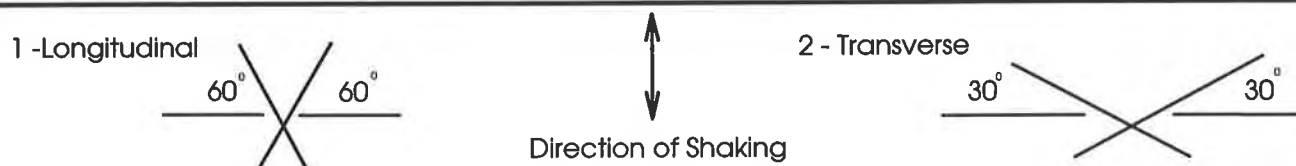
Interface A consists of a non-woven geotextile over a layer of smooth geomembrane. Interface B is composed of two layers of smooth HDPE geomembrane. While this interface is not usually found in landfill liners, it is a common component in seismic base isolator systems, and hence was included in this study. Interfaces C and D are both composed of a smooth geomembrane over a layer of geonet. The geonet contains strands that run at approximately 60° with each other. It was found through preliminary testing that the orientation of the geonet strands influenced the friction angle for the interface. Therefore two cases were considered for testing and the cases are illustrated in Table 1. Interface C contained the geonet in longitudinal orientation where the geonet strands were oriented at about 30° with the direction of sliding. Interface D contained the geonet in transverse orientation, where the angle between the strands and the direction of sliding was about 60°.

Direct shear tests were performed on specimens of two sizes. Large scale specimens with 300 mm (12 in) square dimension and smaller, circular specimens of 80 mm (3 in) diameter were tested. Both monotonic and cyclic tests were performed under stroke controlled conditions.

Tests were also conducted using an earthquake shaking table device to estimate the interfacial friction angle under dynamic conditions. Some of the shaking table tests were performed on board an 100 g-ton geotechnical centrifuge to simulate realistic prototype normal stresses experienced by landfill liner systems. The results from this approach are compared with those from the direct shear tests at the end of this paper.

DIRECT SHEAR TESTS

Direct shear tests were performed on specimens of two sizes, using two different devices. The large size specimens were tested in a direct shear device for geosynthetics. The smaller specimens were tested on a Norwegian Geotechnical Institute (NGI) direct simple shear device. The sample holding mechanism for the NGI device was simplified so that geosynthetic samples of circular cross section could be tested. No soil was used in either testing device, and the geosynthetics were laid in contact with solid metal plates. In each test, either a whole new specimen, or a new surface of a previously used specimen was tested. When a new surface of a previously used specimen was used, the latter test was performed at a normal stress higher than the former. Also, touching the surfaces before they were tested was avoided. Previous researchers (e.g. Lahlaf and Yegian (1991)) have noted that some geosynthetic interfaces are extremely sensitive to surface conditions and tend to get lubricated by human perspiration, when touched.

During the tests the normal force, the shear force and the displacement in the normal and the shear direction were measured. The cyclic tests were performed using a sinusoidally varying controlled stroke input under different values of normal stress. The frequency of excitation was 0.25 Hz for all the tests presented here. This frequency is lower than the range commonly encountered under seismic conditions. However limitations in the data acquisition system precluded the use of a higher excitation frequency. Results presented by De (1996) have shown that the values of dynamic interface friction angle do not appear to depend on the frequency of excitation within the range of seismic disturbances (0.5 to 5 Hz). The same amplitude of displacement was attained at the end of each cycle of excitation. This amplitude was fixed beforehand at a magnitude greater than the displacement required to mobilize the maximum shear strength in the sample.

The ratios of the maximum shear force and the normal force at any cycle during the cyclic testing provides an instantaneous value for the coefficient of dynamic friction. Thus, values of dynamic friction angle at different cycles during the testing can be calculated.

Tests on Large Sized Specimens Tests on the direct shear device for geosynthetics were performed on square specimens 300 mm (12 in) in dimension. This device was loaded by an MTS controlled servo-hydraulic actuator under both monotonic and cyclic conditions.

Monotonic tests were performed on the four interfaces at different normal stresses. Figures 1 and 2 show the plots of shear stress versus displacement for interfaces A and B. The curves tend to reach a maximum (peak shear stress value) relatively rapidly. After this the curve drops off; however some of the interfaces appear to exhibit a residual strength that is higher than the peak. For purposes of calculations of the coefficient of friction, the maximum (peak) shear stress value has been used. The values of friction angle measured under monotonic conditions for the different interfaces are presented in Table 2. It is worth noting that the two different orientations of the geonet (in interfaces C and D) do not reflect any difference in the value of static friction angle.
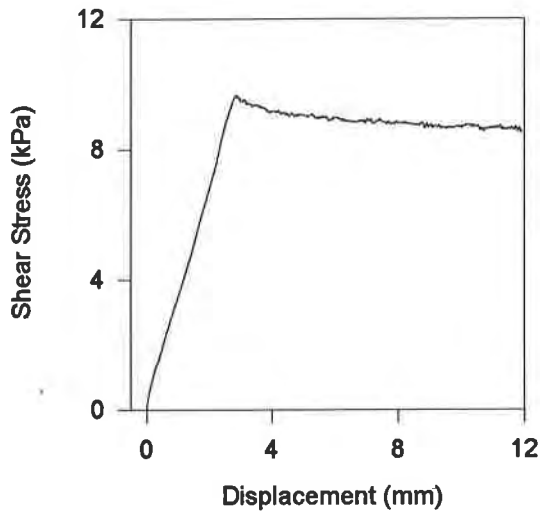
Figure 1. Monotonic direct shear test on Interface A
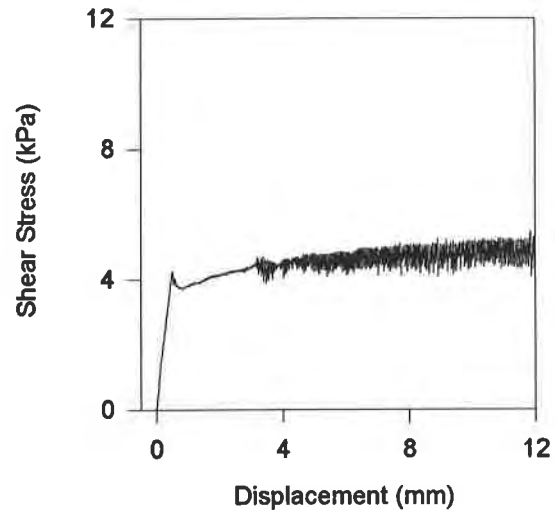
Figure 2. Monotonic direct shear test on Interface B

Table 2. Friction angles obtained from monotonic direct shear tests on large and small samples

Interface	Large sample (300 mm square)[1]	Smaller sample (80mm diameter)[2]
A	12°	11.7°
B	9.2°	13.6°
C	10.7°	11.3°
D	10.7°	11.3°

[1] Tested on direct simple shear device for geosynthetics
[2] Tested on modified NGI direct simple shear device

Figure 3 shows the plot of shear stress versus time from a cyclic test for Interface A. As mentioned previously, in the cyclic tests the same amplitude of displacement was attained after each stroke controlled cycle. It can be seen from this graph that the magnitude of shear stress reached at the end of each cycle tends to decrease with time. In other words, the shear strength of the interface appears to reduce with the number of cycles.
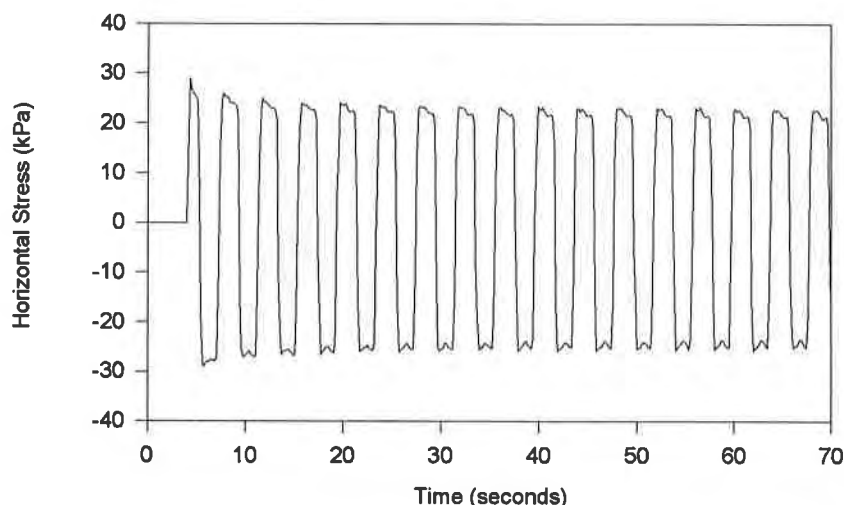
Figure 3. Cyclic direct shear test on Interface A

The ratio of the magnitude of the maximum shear stress attained at the end of each cycle and the normal stress provides the coefficient of dynamic friction angle for that cycle. This can be utilized to calculate the values of dynamic friction angle at different cycles of excitation. The results from such a calculation for interface A is shown in Figure 4 for four different normal stresses. It can be seen that for the first few cycles of loading, the friction angle has a value of about 12.5°. This value is comparable to the friction angle observed under monotonic conditions (Table 2). However, as the number of cycles of loading continues, the value of dynamic friction angle decreases continuously. This indicates that the geosynthetic interface offers reduced resistance to sliding. In the case of Interface A a significant drop is observed in about the first 25 cycles, after which the rate of drop diminishes. This same trend is observed in all four tests performed at different normal stresses.

The drop in shear resistance is most likely caused by polishing of the smooth geomembrane surface by the geotextile. This has also been observed by other researchers such as Mitchell et al (1990) and Yegian and Lahlaf (1992). Further evidence of this polishing is presented in De (1996) in the form of photographs of geomembrane sections taken under an optical microscope. These decreases in friction angles should be considered by designers when performing slope stability analyses.
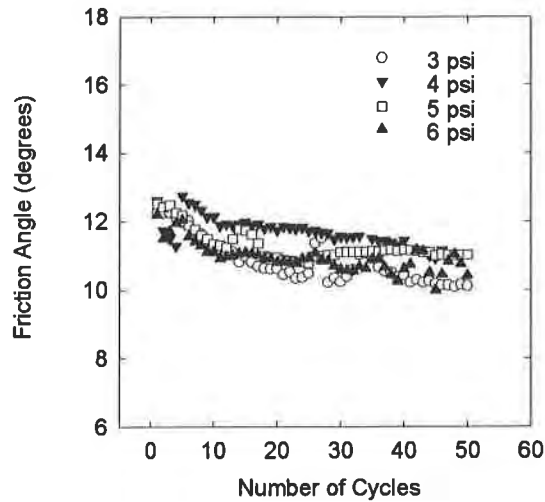
Figure 4. Variation in friction angle with number of cycles for Interface A

Figure 5 shows a plot of shear stress with time for a cyclic test performed on Interface B (smooth geomembrane over same material). In this case the magnitude of shear stress appears to increase with time (or number of cycles). Consequently, the dynamic friction angle increases with the number of cycles. This trend is shown in Figure 6 for tests performed under different normal stresses. The dynamic friction angle appears to change from 10.5° to about 19.5°. This is comparable to the value of static friction angle of 9.2° for the same interface. The results from the cyclic tests show minimal dependence on normal stress.
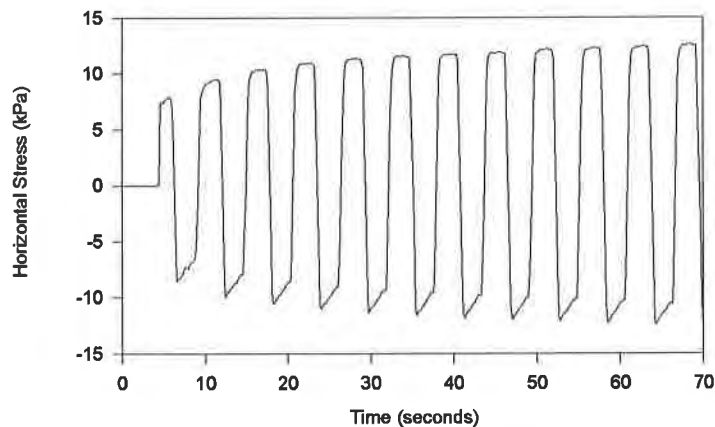
Figure 5. Cyclic direct shear test on Interface B
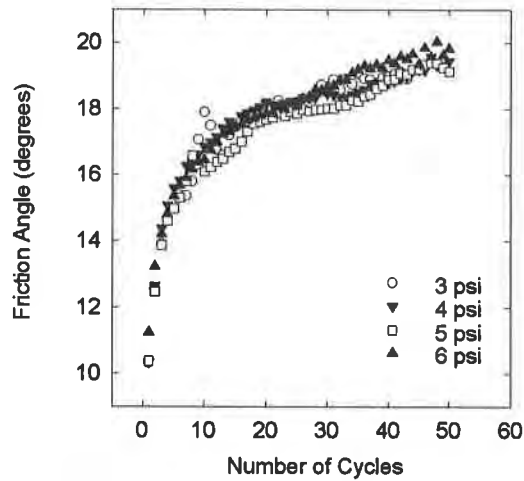
Figure 6 .Variation of friction angle with number of cycles for Interface B

Figures 7 and 8 show the variation in dynamic friction angle with the number of cycles for geonet in two different orientations over smooth geomembrane (interfaces C and D, respectively). For both orientations it can be seen that the friction angle is dependent on the normal stress, and the lowest normal stress shows the largest increase in friction angle with numbers of cycles. The dynamic friction angle for either orientation was about 10° for the first cycle of loading. This is very similar to the static friction angle of 10.7° for either orientation. After 50 cycles, the value was between 18° and 16° for the longitudinal orientation and between 18° and 14° for the transverse orientation.
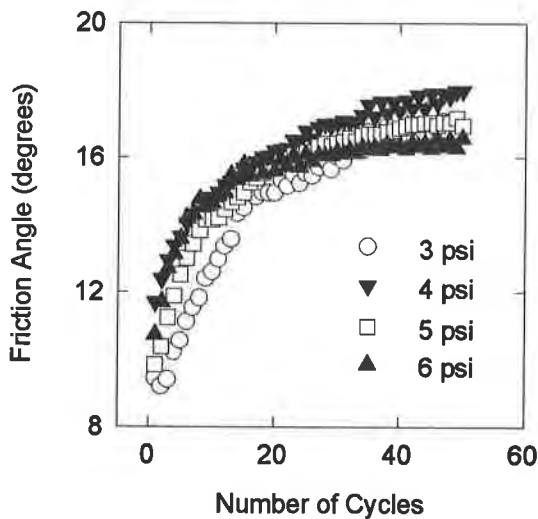
Figure 7. Variation of friction angle with angle with
number of cycles for Interface C
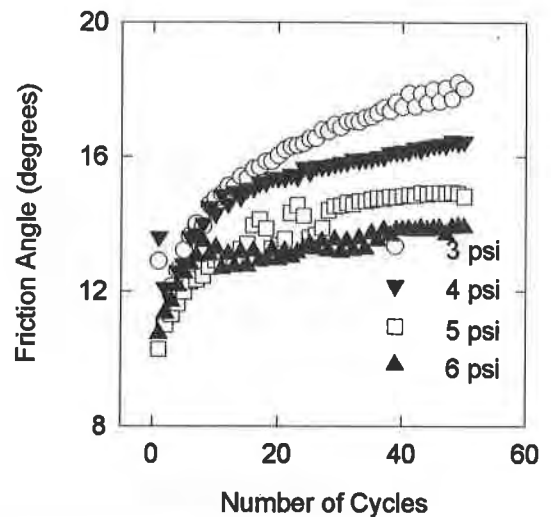
Figure 8. Variation of friction
number of cycles for Interface D

<u>Tests on Smaller Sized Specimens</u> Tests were performed using the Norwegian Geotechnical Institute (NGI) direct simple shear device on circular samples 80 mm (3 in) in diameter. The loading for monotonic tests was provided by an electric motor and for cyclic tests by a MTS controlled hydraulic actuator.

The experiments were performed in a manner very similar to those for the large scale samples. The friction angles measured in this device are shown in Table 2. For interfaces C and D the friction angles measured in the small samples were slightly higher than those measured in the large sized samples, and for interface A the friction angle was measured slightly higher in the large sample compared with the small sample. Practically speaking, the results for interfaces A, C and D are about equal for both sample sizes. The exception is Interface B, where there is a considerable difference between the measured friction angle values. One possible reason for this discrepancy may be due to the fact that for this interface (B) the peak shear stress is reached at a low value of displacement (Figure 2 versus Figure 1) and a much larger residual shear stress is obtained later. It is likely that the peak stress value was missed in the small scale samples and the residual strength provided the larger friction angle.

SHAKING TABLE TESTS

Shaking table tests were performed on pairs of geosynthetics with one geosynthetic mounted on the shaking table surface and the other laid over it with an overlying solid block providing the normal stress. The experimental setup used in the tests is shown in Figure 9. The table provides a sinusoidal base excitation which is transferred from the bottom geosynthetic to the top due to the shear strength of the interface. The contact area of interface tested in this apparatus was 445 mm x 292 mm (17.5 in x 11.5 in). A detailed description of the test procedure and theory is provided in Zimmie et al (1994 a & b).

Plan

Elevation

1 - Shaking Table
2 - Geosynthetic 1
3 - Geosynthetic 2
4 - Aluminum Frame
5 - Concrete Block
6 - LVDT
7 - Clamp for LVDT
8 - LVDT extension rod
9 - Metal bar
10 - Accelerometer
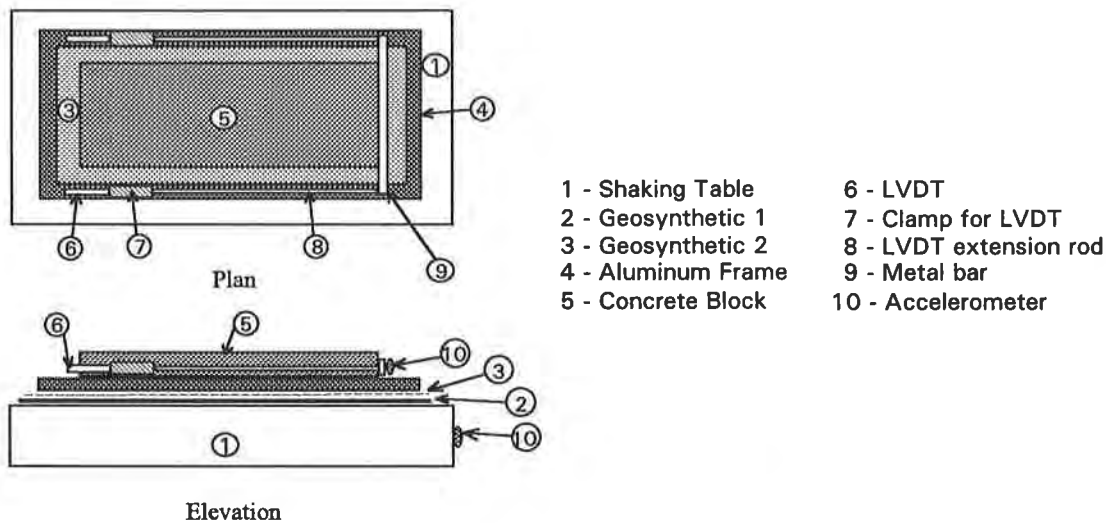
Figure 9. Experimental setup for shaking table tests

Figure 10 shows the freebody diagram of the block under shaking table excitation. The horizontal acceleration of the table a_t provides the frictional force, F, to the block which weighs W. As the amplitude of table acceleration is increased gradually, there will exist a limiting value of acceleration, a_b up to which the block will move with the table. At higher values of acceleration, slippage occurs between the block and the table.

The limiting value of frictional force will be a function of the dynamic friction angle, ϕ_d and can be obtained by equating the forces in the free body diagram. Thus the dynamic friction angle at the interface can be expressed as, $\phi_d = \tan^{-1}(a_b/g)$.
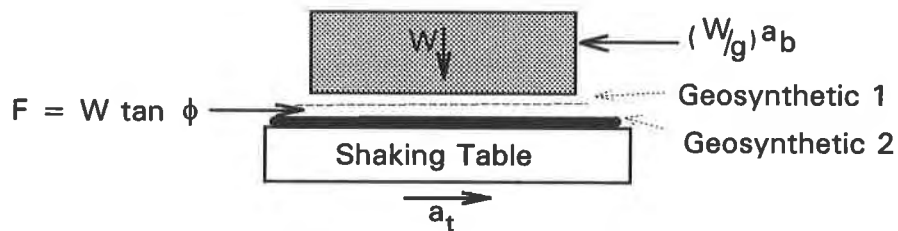
Figure 10. Freebody diagram for shaking table tests

During a test the values of acceleration at the block and the table are measured and their relative displacement. Sinusoidal excitation of gradually increasing amplitude is provided to the table. A resultant curve of the acceleration of the table (and the geosynthetic attached to it) versus the acceleration of the block (and the geosynthetic attached to it) may be plotted.

Figure 11 shows such a plot for interface A from tests performed at different frequencies of table acceleration. The figure shows an initial phase when both the table and the block accelerations are equal and are both increasing gradually. Later a point is reached when the block acceleration ceases to increase even as the table acceleration continues to increase (about 0.22 g in Figure 11). The amplitude of acceleration at which the block acceleration stops increasing indicates the point at which slip (relative displacement) between the geosynthetics is initiated. From this acceleration the dynamic friction angle can be calculated, by using the formula given above. Dynamic friction angles were calculated in this manner for the four interfaces studied in this paper. The values are presented in Table 3. The dynamic behavior of this particular interface (A) was found to be independent of the frequency of vibration (as shown in Figure 11). These observations and results are very similar to those obtained by other researchers (e.g. Yegian and Lahlaf (1992)).
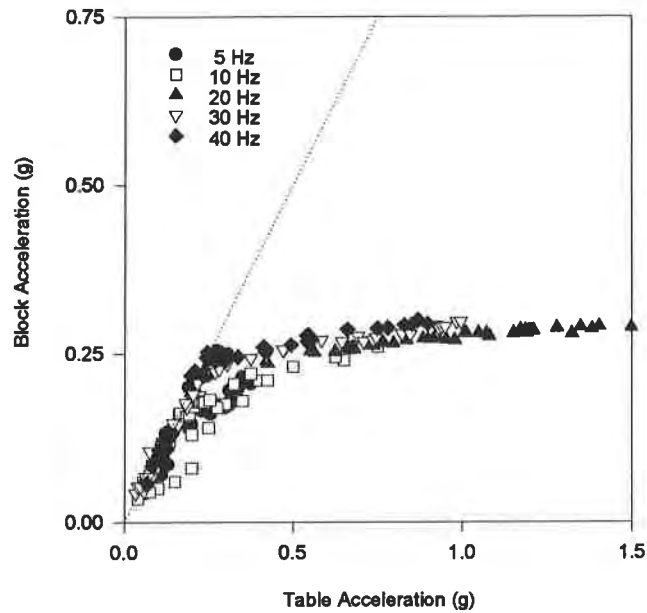
Figure 11. Shaking table tests on Interface A at different frequencies

Table 3. Dynamic friction angles obtained from shaking table tests

Interface	Dynamic friction angle
A	12°
B	14°
C	12°
D	12°

SHAKING TABLE TESTS UNDER HIGH g

Tests were performed utilizing high centrifugal acceleration fields to simulate normal stresses comparable to those experienced by landfill liner systems. For this purpose a 100 g-ton geotechnical centrifuge at Rensselaer Polytechnic Institute was utilized. The same model setup as described in the previous section was used. Centrifugal accelerations of 5, 10, 20 and 40 g were used to simulate normal stresses that were multiples of the normal stresses existing on the model at 1g. The same set of instrumentation used in the shaking table tests at 1g were used in the centrifuge tests. The frequency of excitation was scaled up proportionate to the g-level, following conventional centrifuge scaling laws.

Figure 12 shows the plots of table versus block accelerations recorded at different g-levels. From the plot the amplitude of acceleration at which slip (relative displacement) first occurs, can be determined. The results from high g tests on Interface A are shown in Table 4. In each case the slip at the interface is found to occur at approximately the same prototype acceleration, i.e. about 0.22 g (Table 4). The dynamic friction angle values for this interface, using different normal stresses, are found to be very similar.
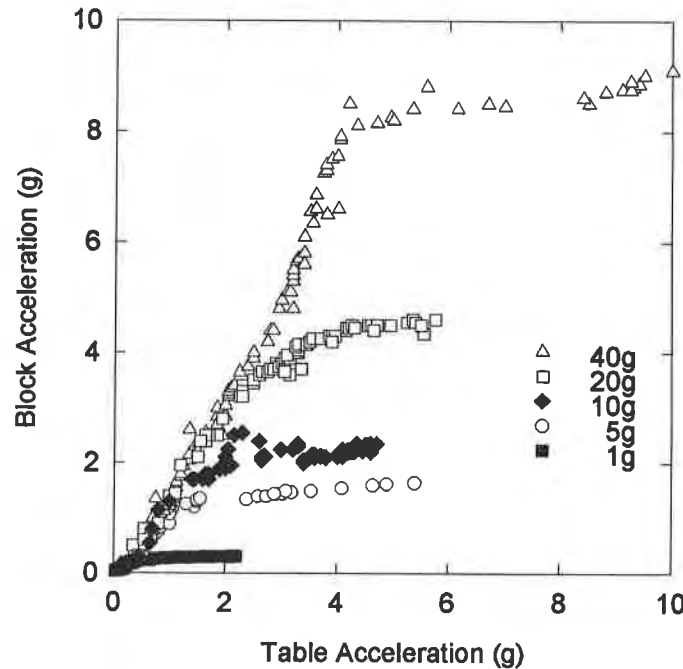
Figure 12. Table versus block accelerations from centrifuge experiments on Interface A.

Table 4. Dynamic friction angles at different g-levels and under different normal stresses for Interface A

g level	Normal Stress (KPa)	Model frequency (Hz)	Model acceleration at slippage (g)	Prototype acceleration (g)	Dynamic Friction Angle
1	2.1	5	0.215	0.215	12.1°
5	10.5	25	1.10	0.22	12.4°
10	21	50	2.1875	0.21875	12.3°
20	42	100	4.50	0.225	12.7°
40	84	200	8.75	0.21875	12.3°

SUMMARY AND CONCLUSIONS

Results from various kinds of friction tests on four different geosynthetic interfaces have been presented. Both monotonic and cyclic direct shear tests were performed on two different sized geosynthetic specimens. The results from these tests indicated little effect of specimen size in three out of the four interfaces.

The cyclic direct shear tests on the interfaces indicated that the dynamic friction angle of the interfaces tend to change with the numbers of cycles of loading. The nature of the change (whether increase or decrease) depends on the composition of the interface. The amount of change sometimes depends on the normal stress acting on the interface.

The results obtained from shaking table tests compare well with those from cyclic direct shear tests. The use of a geotechnical centrifuge to simulate higher normal stress conditions, similar to prototype landfill liners appears to be a viable method. However, careful attention must be paid to proper simulation of all conditions and scaling of all parameters involved.

It is important for designers to be aware of the changes in dynamic friction angles during cyclic loading. In the case of interface A designers may consider the drop in the value of friction angle while performing stability analyses. The dynamic friction angle of Interfaces B, C and D appeared to increase with the numbers of cycles of loading. Designers utilizing these interfaces for landfill cover and liner applications may consider ignoring the increases in order to achieve conservative design. However it may be important for designers of geosynthetic base isolation systems to take the increased friction angles into account.

REFERENCES

De, A. (1996) "Study of interfacial friction of landfill geosynthetics: static and dynamic", Ph.D. Thesis, Department of Civil Engineering, Rensselaer Polytechnic Institute, Troy, New York.

Lahlaf, A. M. and Yegian, M. K. (1991) "Dynamic Interface Shear Strength Properties Between Geomembranes and Geotextiles", Report No. CE-91/08, Northeastern University, Boston.

Mitchell, J. K., Seed, R. B., and Seed. H. B. (1990) "Kettleman Hills waste landfill slope failure. I: Liner-system properties", Journal of Geotechnical Engineering, ASCE, 116, 4, 647-668.

Yegian, M. K. and Lahlaf, A. M., (1992) "Dynamic interface shear strength properties of geomembranes and geotextiles" Journal of Geotechnical Engineering, ASCE, 118, 5,. 760 - 778.

Zimmie , T. F., De, A. and Mahmud, M. B. (1994a) "Study of geosynthetic interface friction" Centrifuge 94, 301-306. Balkema, Rotterdam.

Zimmie, T. F., De, A. and Mahmud, M. B. (1994b). Centrifuge modelling to study dynamic friction at geosynthetic interfaces", Proceedings of the Fifth International Conference on Geotextiles, Geomembranes and Related Products, Singapore, September 1994, pp. 415-418.

DEPTH AND WIDTH EFFECT ON PULL-OUT RESISTANCE OF WOVEN GEOTEXTILES IN SAND

RAJ P. KHERA
PROFESSOR, DEPARTMENT OF CIVIL & ENVIRONMENTAL ENGINEERING, NEW JERSEY INSTITUTE OF TECHNOLOGY, NEWARK, NJ, USA.
RAM M. R. KASTURI, SENIOR ENGINEER, LOUIS BERGER & ASSOCIATES, EAST ORANGE, NJ, USA
ISSA S. OWEIS, PRESIDENT, CONVERSE CONSULTANTS EAST, PARSIPPANY, NJ, USA
M. KHAIRUL ALAM, STRUCTURAL ENGINEER, BAKER ENGINEERING, ELMFORD, NY, USA.

ABSTRACT

Pull-out tests were conducted on geotextiles with widths 76 mm, 151 mm, and 305 mm, and embedded in a uniformly graded flint sand. For depth < 914 mm (3 ft) failure occurred in the sand mass and at greater depths failure occurred at the sand-geotextile interface. Within the sand the failure mass could be approximated by two half inverted elliptic cones at the strip ends and a prism in the middle. When the contribution of end half cones was discounted the unit stress on the geotextile was found to be independent of the strip width. Coefficient of lateral earth pressure varied between 0.4 and 0.52. Where failure occurred at sand-geotextile interface the angle of interface friction decreased with increasing depth and became essentially constant at 1.22 m depth.

INTRODUCTION

Geosynthetics are anchored by embedment in trenches located along the top of slopes to ensure slope stability as shown in Figure 1.

The depth of vertical trench for anchorage is usually 300 mm to 600 mm(1 ft to 2 ft). The anchor strength is frequently modeled in the laboratory by measuring the pull-out resistance of the fabric embedded in the given soil in a pull-out box as shown in Figure 2. Alternately, a direct shear test is used (ASTM D5321). In this test the geosynthetic is stretched over a block and placed in the upper half of the shear box and the soil is placed in the lower half of the shear box. The tests then yield the geotextile-soil interface frictional resistance. However, none of these methods truly represent the field conditions. Direct shear tests, though much more common in use, do not yield results similar to a true pull-out test where the geosynthetic is embedded in the soil either vertically or horizontally and then subjected to a force which causes it to be pulled out of the soil. Koerner (1994) states that stresses mobilized in a pull-out test are complex and need additional research.
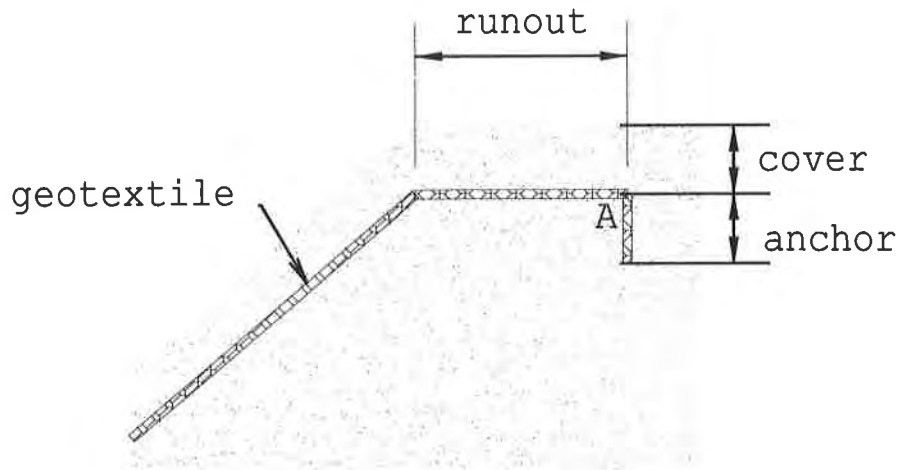
Figure 1 Runout distance and anchorage of geosynthetics
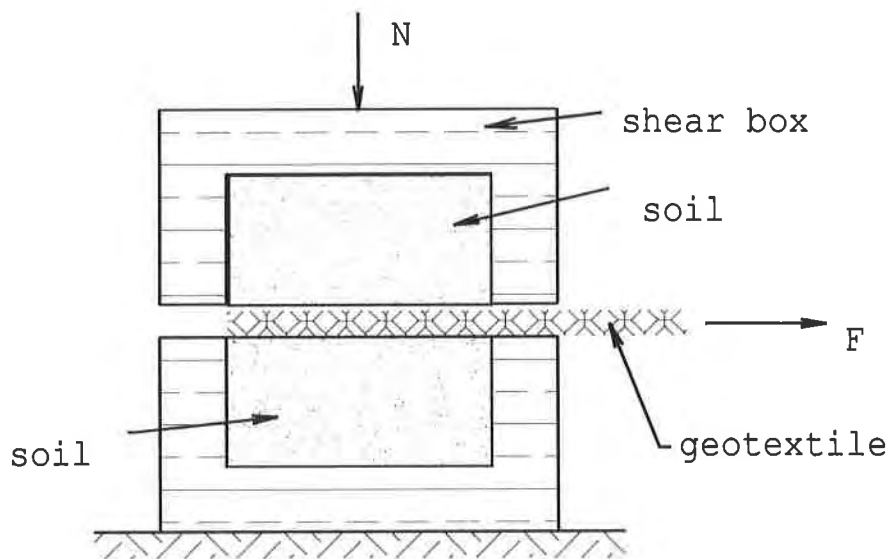
Figure 2 Conventional setup for pull-out resistance

Bacot et al. (1978) prepared a fill in the field where reinforcing strips were placed at different depths and pull-out tests were conducted in-situ. The friction angle for the fill material, which consisted of coarse grained soil, was about 24°. For a 50 mm (2 in.) wide strip, the interface friction angle between the strips and the fill was as high as 63°. The authors suggest that "a part of the reinforcements act as anchor and that the soil around the reinforcing strip is not at rest." The interface friction angle δ, dropped as the width of the strip was increased. Its value for 12 cm wide strip was 59°. Collios et al. (1980) reported similar values

for friction angles both from pull-out tests and direct shear tests. In pull-out tests they used equipment similar to that shown in Fig. 2, and the width of the geotextiles was the same as the shear box. Unlike Bacot et al. (1978) there was no soil past the edges of the geotextiles. Schlosser and Elias (1978) also reported from field test data a decrease in coefficient of friction as the width of strip increased from 15 mm to 50 mm (0.6 in. to 1.97 in.).

Rao and Pandey (1988) used three types of geotextile and Yamuna sand for pull-out tests using a scheme similar to that shown in Figure 2, as well as direct shear tests. Friction angle for Yamuna sand itself was 37°. From the pull-out tests the interface friction angle for one of the fabrics was computed to be 58° at a normal stress of 49 kPa (0.51 ton/ft²) and it dropped to 46° when the normal stress was 196 kPa (2.05 tons/ft²). The width of the geotextile was smaller than that of the box thus leaving the possibility that these too acted as anchors as postulated by Bacot, et al. (1978). In direct shear test, however, the interface friction angle for this sand and geotextile was 34° and it was independent of the normal stress. Similar trends were reported for other geotextiles and different sand.

There is no reasonable explanation for the very high values of interface friction reported from pull-out tests or the decreases in its value when the width of a strip is increased. The purpose of this paper is to show as to why the high interface friction angle reported for sand-geotextile is in fact not an interface resistance. Answer is also provided to the decrease in pullout resistance with increase in geotextile width and depth of embedment. Total resistance from the runout length and vertical anchorage where a according Koerner (1994) a frictionless pulley is assumed at 'A', as shown in Figure 1, is also investigated.

TESTING PROGAM

Geotextile. Two types of geotextiles with widths ranging from 76 mm to 305 mm (3 in. to 12 in.) were used. Both the fabrics were woven. One of the geotextile had a rough surface, a thickness given as 3.2 mm(1/8 in.), and a tensile strength of 275 N/mm (1550 lb./in.) width at 5 % strain. The other had a smoother surface, its thickness was given as 0.5 mm (1/50 in.) and tensile strength as 61N/mm (350 lb./in.) width at 15 % strain.

Aluminum Strip. The aluminum strip was 305 mm (1 ft) long, 75 mm (3 in.) wide, had a thickness of 4.8 mm (3/16 in.) and weighed 4.2 N (0.94 lb.).

Sand. The sand used was a poorly graded pure silica flint shot blasting sand with 80 % of the particle size between 0.84 mm and 0.425 mm. From direct shear tests its angle of friction 'ϕ' was determined to be 40° at a unit weight of 17.5 kN/m³ (111 lb./ft³) and for a normal stress range of 10 to 25 kPa.

<u>Testing Containers.</u> Initial tests were conducted in acrylic plastic containers 127 mm × 108 mm × 813 mm (5in. × 4.25 in. × 32 in.). As will be seen later this box was used only in the initial phase of testing. The data presented in this paper were obtained from either a plastic drum 559 mm (22 in.) in diameter or a wooden box 610 mm × 610 mm × 1220 mm (2 ft × 2 ft × 4 ft).

<u>Test Setup.</u> The geotextile was cut to the required width and its loose edges were heat welded. The depths of vertical anchorage ranged from 305 mm to 1.22 m (1 ft to 4 ft.) The horizontal embedment length ranged from 305 mm to 610 mm (1 ft to 2 ft). Where combined vertical anchorage and horizontal embedment (runout) were used, the cover on the runout length was 305 mm (1 ft). In order to assess the combined effect of runout and anchor, the laboratory test was set up as shown in Figure 3. For anchor with 305 mm (1 ft) cover a wooden enclosure as shown in Figure 4 was used to surround the geotextile before the cover sand was placed.
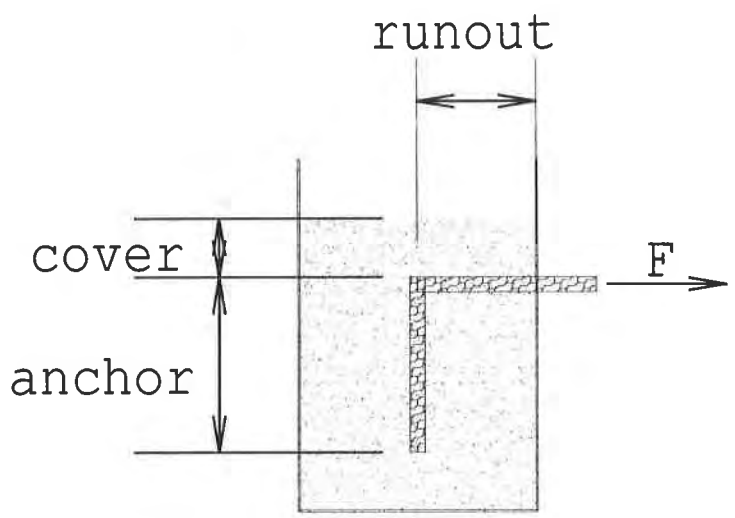
Figure 3 Test setup for combined anchorage and runout
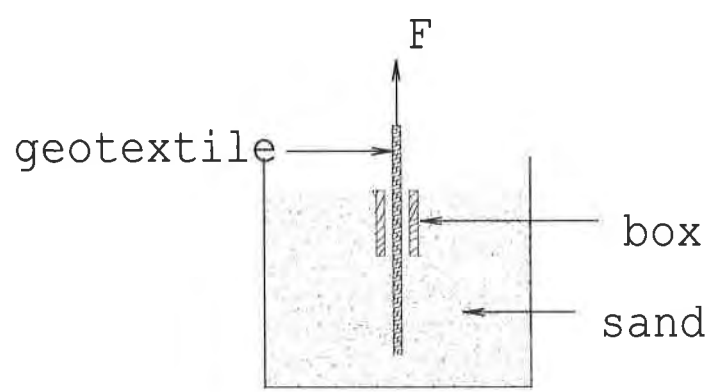
Figure 4 Wooden enclosure box to provide cover for anchorage

The sand was placed as described by Baker and Kondner (1966), by 'raining' it from 305 mm (1 ft) height from a suspended bucket. The final density of the sand was computed from the weight of the sand that was placed in the test container. The applied rate of deformation was about 15 mm/minute, deformation was measured by two dial gages, and the force was determined via a proving ring (Kasturi, 1990; Alam, 1991).

TEST RESULTS

Failure in Sand. Figure 5 shows the setup for vertical pull-out test in the acrylic box. Note the geotextile is placed with its width parallel to the face of the box and its face is located at a distance of 57 mm from the inside face of the box.
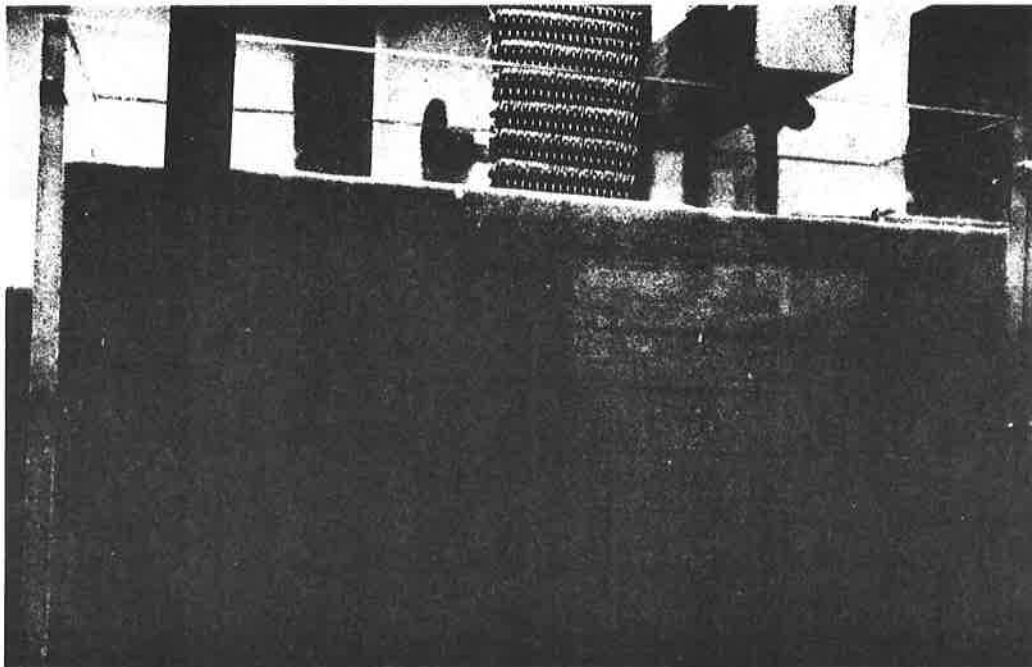
Figure 5 Setup for vertical pull-out test in acrylic box

After the pull-out test the results are shown in Figure 6. Even though the geotextile is at a considerable distance from the face of the box the upward movement of the sand is clearly observable to some depth.

The edge of the geotextile is set close to the end of the box in Figure 7. After the test the appearance of the soil movement is clearly observable. Note that to a considerable distance beyond the faces of the geotextile the sand has heaved from its original position. The heave also extends to a considerable depth.
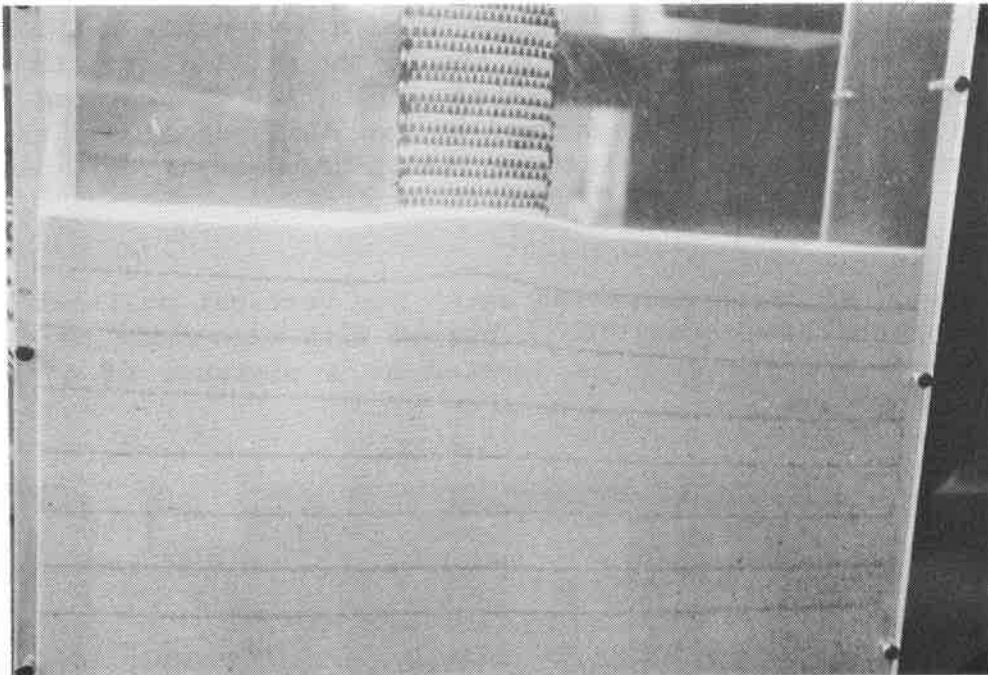
Figure 6 Sand movement after pull-out test
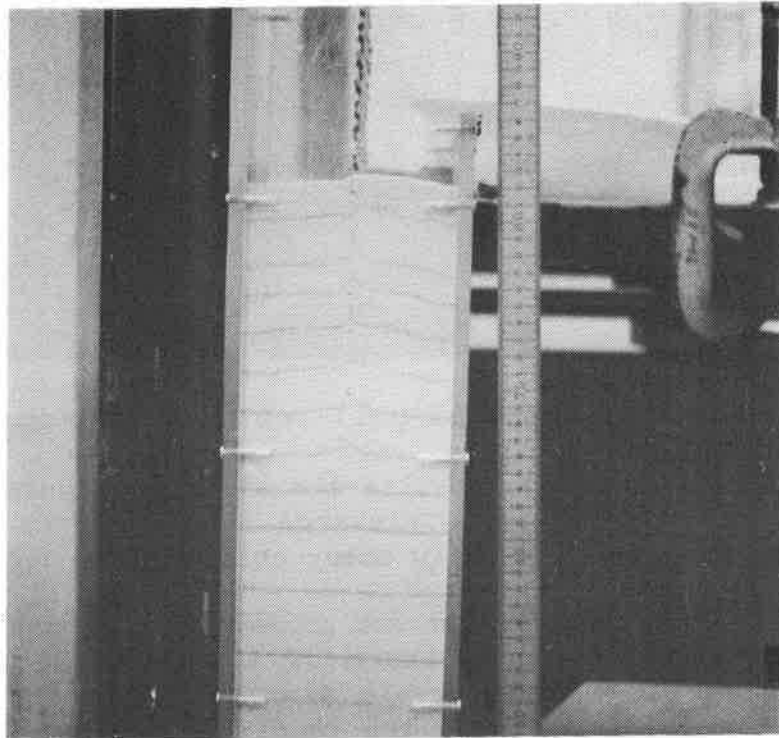
Figure 7 Heaving of sand along the edge

It is also to be noticed that the smaller dimensions of the acrylic container are interfering with the complete formation of the failure zone. Consequently, the acrylic box was replaced with larger containers. In the

larger containers the observation confirming this type of failure was the visible heaving of the sand at the surface after a pull-out test. The test data presented here were obtained from larger containers with minimum dimension of 559 mm which allowed free formation of the failure zones which had a maximum extent of 457 mm.

Based on the tests in the acrylic container and the apparent failure surfaces as observable in Fig. 6 and Fig. 7, the failure mode is depicted in Figure 8. The heaved sand mass is approximated as inverted half elliptic cones at the geotextile edges and an inverted prism having base sides parallel to the face of the geotextile and anchor depth as the height. The resistance to pull-out is provided by the weight of sand heaved and the frictional resistance between the heaving sand mass and the surrounding stationary soil. These forces are portrayed on the end cone in Figure 8.

The test results which are reported here were conducted in larger containers where it was not possible to see the movement of the sloil along the depth of embedment. For the tests where the soil surface surrounding the geotextile heaved consequent to the pullout test, its measurements were made as shown in the 'Top view' in Figure 8. The remaining dimensions were determined from the embedded length and width of the geotextile.

The results of the pull-out tests, in which failure occurred due to heaving of sand are shown in Table 1. For anchorage depths of 305 mm (1 ft) and 610 mm (2 ft) the heave extended considerably beyond the face of the geotextile as seen by the distances r_c and r_p in Table 1. The volume of the soil heaved for geotextile 'A' was somewhat smaller than for 'N'. For a given geosynthetic and depth of anchorage the contribution to pull-out resistance from the end cones is essentially the same regardless of the strip width.

Table 1.Test data where failure occurred due to heaving of sand

test no.	width mm	anchor depth mm	r_c mm	r_p mm	force F N	avg stress kPa	force in end cones N	stress less end cones kPa	K
'N'1V(3)	76	305	49	64	169	3.64	85	0.91	0.45
'N'1V(6)	152	305	49	64	231	2.48	75	0.95	0.40
'N'V1	305	305	49	64	414	2.23	81	1.14	0.43
'N'2V(3)	76	610	76	76	707	7.61	402	2.09	0.52
'N'2V(6)	152	610	76	76	903	4.86	356	2.01	0.45
'A'1V(3)	76	305	46	49	148	3.19	70	0.92	0.44

Typical force displacement for failure in soil (embedment 0.305 m) and failure at interface (embedment 1.219 m) are shown in Figure 9. Note that peak force is followed by a rapid drop in the force reaching almost an ultimate value. The drop in force was 48 % to 63 % where failure occurred in the soil as depicted in Figure 8 and for tests where failure occurred at

soil-geotextile interface the percent drop in the force ranged between 17 % and 36 %. The displacement at the peak force exhibited an increase from about 15 mm for embedment depth of 0.305 m to about 35 mm for the embedment depth of 1.219 m.
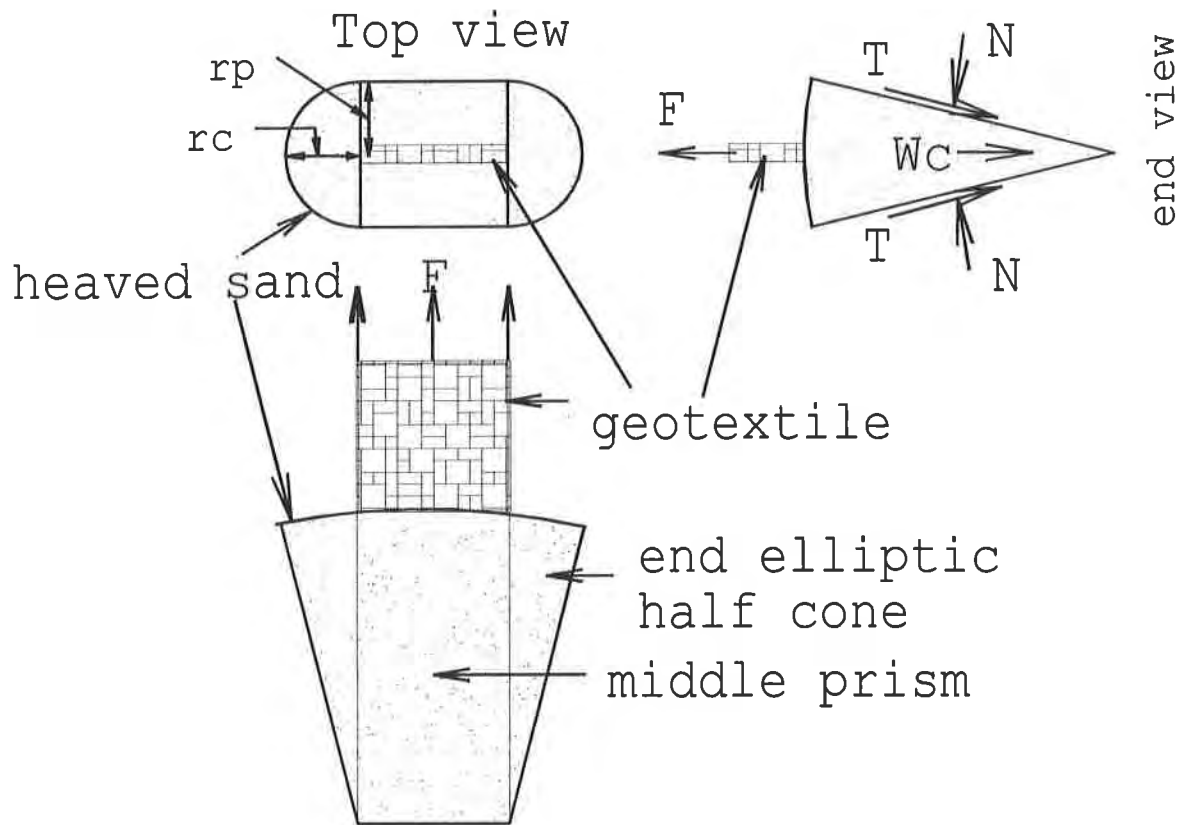
Figure 8 Failure mode for pull-out in vertical direction.

Effect of Width. As seen from Table 1 the average stress for 305 mm (1 ft) anchorage decreases from 3.64 kPa (76 lb./ft^2) to 2.23 kPa (46.5 lb./ft^2) as the width of the geosynthetic is increased from 76 mm (3 in.) to 305 mm (12 in.) Similarly for 610 mm (2 foot) anchorage the average stress decreases from 7.61 kPa (159 lb./ft^2) to 4.46 kPa (101.5 lb./ft^2) as the width of the geosynthetic is increased from 76 mm (3 in.) to 152 mm (6 in.). This trend agrees with the reported decreasing unit resistance with increasing geotextile width. However, if we discount the contribution of the end cones the unit resisting stresses for 305 mm (one foot) anchorage for the three widths range from 0.91 kPa (19 lb./ft^2) to 1.14 kPa (23.8 lb./ft^2). Similarly for 610 mm (2 feet) anchorage, if the contribution of the end cones is discounted, the unit resisting stresses for the two widths range from 2.09 kPa (43.7 lb./ft^2) to 2.01 kPa (41.9 lb./ft^2). The difference in these stresses is small and it can be stated that the pullout resistance is not affected by the geotextile width, if the effect of edges is accounted for.

The observed failure mode provides a clear explanation for the reported decrease in unit stress with increase in fabric width. Since in the field the geotextile width is very large, the contribution from the ends is bound to be negligible.
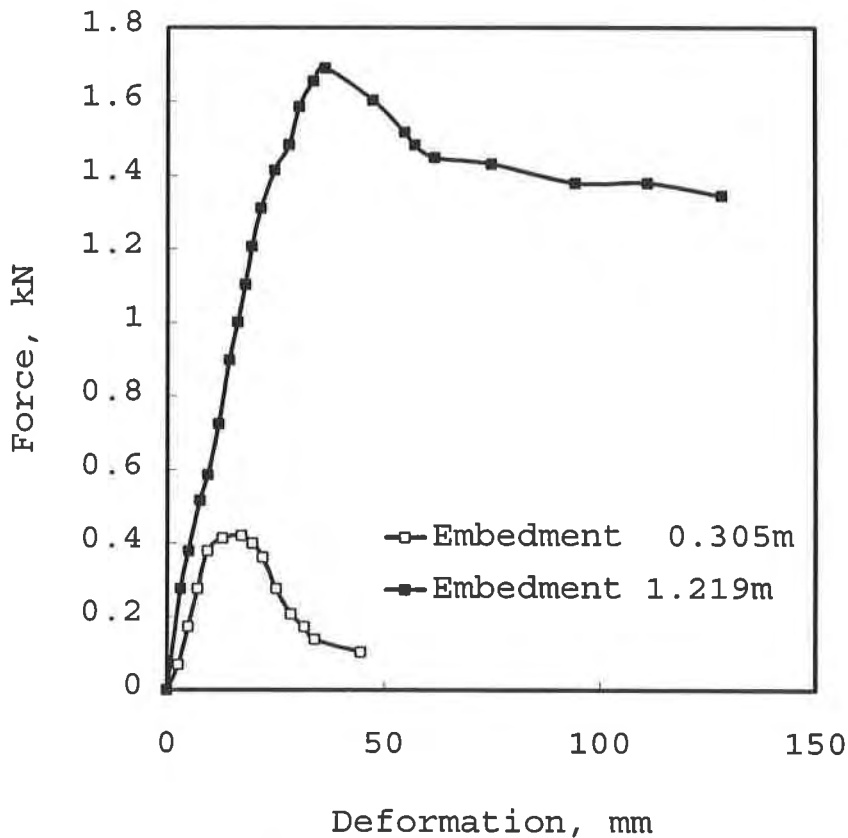
Figure 9 Typical force versus displacement curves in pullout tests.

The coefficient of lateral pressure varies between 0.40 and 0.45 for 305 mm (one foot) anchorage and for 610 mm (2 ft) anchorage its values are from 0.45 to 0.52. Though the variation for 610 mm (2 feet) anchorage is somewhat greater than for 305 mm (1 foot) anchorage, these values compare favorably with K_o of 0.36 as determined from the formula $K_o = 1 - \sin\phi$.

Effect of Geotextile Type. As seen from Table 1 the total resistance for geotextile 'A' in test 'A'1V(3) is 148 N (33.3 lb.) when compared with 169 N (38 lb.) for test 'N'1V(3) for geotextile 'N'. However, when comparing its K value (0.44 v/s 0.45) and unit stress without the contribution from the end cones (0.92 kPa v/s 0.91 kPa) the two fabrics seem to exhibit similar response. Because of the limited number of tests it is not possible to make any definitive conclusions.

Soil-Geotextile Interface Failure. For embedment depths ≥ 914 mm (3 ft) the failure occurred at the soil-geotextile interface as there was no observable heaving of the soil beyond the geotextile boundaries. At 914 mm (3 ft) depth the interface friction angle δ was computed to be 21.3°. The angle δ decreased to 17° at 1.067 m (3.5 ft) depth, and then to 15° for 1.22 m (4 ft) depth. Thus δ showed a decrease as the depth of embedment increased. In all these cases δ was determined based on lateral earth pressure coefficient K_o of 0.36. Thus the maximum normal stress on the embedded strip was 25 kPa. It may be postulated that a critical depth will be reached below which there will be no further increase in unit resistance. Looking at these results it appears that 1.219 m depth is close to the critical depth. Since 1.219 m (4 ft) anchorage depth is much greater than normally used in the field no further investigations were made.

The test results on an aluminum strip 1V-al, anchored 305 mm (1 ft) into the same sand, are given in Table 2. The interface friction angle δ was determined to be 15°. At this shallow depth the failure occurred unlike geotextile at the interface and not in the soil mass.

Table 2 Cases where failure occurred at sand-geosynthetic interface

test no.	width, mm	anchor depth, mm	force F, N	total average stress, kPa	$\delta°$
'N'V3	305	914	1379	2.47	21.3
'N'V3.5	305	1067	1526	2.35	17
'N'V4	305	1219	1690	2.27	15
1V-al	76	305	31	0.67	15

Combined Runout and Anchor Efficiency. When computing the capacity of the runout length Koerner(1994) neglects the contribution of the cover on the upper face of the geosynthetic. In the test setup as shown in Figure 3, because of the constraining effect of the container, the upper face of the geotextile does contribute to the total resistance of the geosynthetic. In order not to include this effect, test V1H14 was conducted without any cover, i.e., after 305 mm (1 ft) of anchorage the geotextile was laid flat on the surface of the sand and the pull-out test was conducted by applying force F in the horizontal direction. The efficiency was determined by dividing force F for this test by the force determined for test 'N'1V(3), where the pull-out force was applied in the vertical direction. The efficiency of test V1H14S1 with 305 mm (1 ft) anchorage, 418 mm (1.37 ft) runout length, and 305 mm (1 ft) cover was 1.23. For test V17H14S1, where the anchorage was 509 mm (1.67 ft) with other condition being the same as for V1H14S1, the efficiency was 1.28 . Thus in all instances for combined runout and anchorage the efficiency of the system was at least 120 %.

Table 3 Combined anchor and runout tests on 3 in. wide geotextile

Test	Anchor depth, mm	Runout , mm	Cover, mm	Pull, F N	Efficiency
V1S1	305	0	305	489	
V17S1	509	0	305	930	
H14S1	0	418	305	689	
V1H14	305	418	0	222	222/169=1.32
V1H14S1	305	418	305	1446	1446/(489+689)=1.23
V17H14S1	509	418	305	2068	2068/(930+689)=1.28

CONCLUSIONS

Based on the pullout tests on geotextile with widths 76 mm, 151 mm, and 305 mm, and embedded in a uniformly graded flint sand the following conclusions can be made.

For depth < 305 mm (3 ft) failure occurred in the sand mass and not at the geotextile-sand interface.

Failure mass could be approximated by two half inverted elliptic cones at the strip ends and a prism in the middle.

When the contribution from the end cones was excluded, the unit stress on the geotextile was found to be independent of the strip width.

For depths 914 mm (3 ft) or greater the failure occurred at sand-geotextile interface. Angle of interface friction decreased with depth and it became essentially constant at 1.22 m depth.

Geotextiles with vertical anchorage and runout offered 23% to 31 % greater pullout resistance when compared with the corresponding sum of independent vertical anchorage and runout resistances.

considering the last two paragraphs it can be stated that the actual resistance of the geotextile with anchorage less than 914 mm (3 ft) and a runout length will be greater than that computed based on the assumption of frictionless pulley as suggested by Koerner (1994).

REFERENCES

Alam, M. K. (1991) "Frictional resistance of Geotextiles", MS Thesis, Department of Civil and Environmental Engineering, NJIT, Newark, NJ.

Bacot, J., Iltis, N, Lareal, P., Paumier, T., and Sanglerat, G. (1978) "Study of the Soil Reinforcement Friction Coefficient", Proceedings ASCE Symposium, Earth Reinforcement, Pittsburgh, PA, pp. 157-185.

Baker, W. H., and Kondner, R. L. (1966) "Pull-out Load Capacity of Circular Earth Anchor Buried in Sand", HRR NO. 108, pp. 1-10.

Collios, A., Delmas, P., Gourc, J. P., and Giroud, J. P. (1980) "Experiment on Soil Reinforcement with Geotextiles", Proceedings Symposium. Use of Geotextiles for Soil Improvement, ASCE, Portland, OR, pp. 53-73.

Kasturi, R. M. R. (1990) "Anchor Trench Design For Geotextiles", MS Thesis, Department of Civil and Environmental Engineering, NJIT, Newark, NJ.

Koerner R. M. (1994) "Designing With Geosynthetics", Third Edition, Prentice Hall, Englewood Cliff, NJ, USA.

Rao, G. V., and Pandey, S. K. (1988) "Evaluation of Geotextile-Soil Friction", Indian Geotechnical Journal, V. 18 No. 1, pp. 77-105.

Schlosser, F., and Elias, V. (1978) "Friction in Reinforced Earth", Proceedings ASCE Symposium, Earth Reinforcement, Pittsburgh, PA, pp.735-763.

THE INFLUENCE OF GEOMEMBRANE SURFACE ROUGHNESS ON INTERFACE STRENGTH

J.E. Dove
The Georgia Institute of Technology, USA
J.D. Frost
The Georgia Institute of Technology, USA
J. Han
The Georgia Institute of Technology, USA
R.C. Bachus
GeoSyntec Consultants, Inc., USA

ABSTRACT

This paper summarizes the results of a study using the recently developed optical profile microscopy (OPM) technique as the basis for examining relationships between a quantitative surface roughness parameter and shear strengths of granular soil/geomembrane interfaces. The results show that interface friction is highly dependent on small increases in roughness for relatively smooth surfaces and that the beneficial effect of surface roughness becomes incrementally smaller as roughness increases. Practical applications of this work include: (1) development of correlations between surface roughness and interface shear strength using the surface roughness parameter, and (2) implementation of guidelines for optimal degree of geomembrane texturing and manufacturing quality control.

INTRODUCTION

Geomembranes are commonly designed to be in contact with soils or other geosynthetics. Textured geomembranes are used in applications where a higher level of interface shear resistance is required over what can be obtained using smooth geomembranes. Selection of a particular type of geomembrane is presently made on the basis of experience and/or through a design stage testing program of candidate materials. A new procedure called optical profile microscopy (OPM) was recently developed (Dove and Frost, 1996) and provides a quantitative measure of surface roughness for geomembranes. The OPM method can be used to provide new insight into the relationship between interface strength and texture, the development of optimum interface textures for specific applications, and manufacturing and construction quality control procedures for textured geomembranes.

It has been observed that the interface strength between granular soil and counterfaces of steel and polymer increases as the roughness of the counterface increases (Yoshimi and Kishida, 1982; Williams and Houlihan, 1987; Kishida and Uesugi, 1987; Bemben and Schulze, 1995; and Paikowsky et al., 1995). The upper bound of interface friction has been observed to be approximately equal to the effective stress friction angle of the soil. Stark et al. (1996) examined the interface strength between textured geomembranes and geotextiles and found that interface strength increased with an increasing degree of texturing. Several of the above studies quantified the surface topography using a stylus profilometer on specially prepared

steel surfaces which were relatively smooth compared with geotechnical surfaces. For geomembranes, there is at least three orders of magnitude difference in topographic relief between "smooth" and "rough" textures. It was found by Dove, et al. (1996) that it is difficult to obtain profiles of surfaces with this large difference in relief using conventional profiling equipment. Therefore, development of a quantitative roughness measurement method and hence obtaining a clear understanding of geomembrane interface behavior has been hindered by the difficulties associated with using traditional stylus devices in profiling the full range of geomembrane texture (Dove, 1996).

It has been observed that geomembrane surface topography affects the shearing mechanisms operating at the interface. Since surface roughness varies greatly between manufacturers and can vary to some extent between production lots and within a roll, an assessment of surface roughness is critical to proper understanding of the relationships between geotechnical materials for design practice. In this paper, the relationship between a static surface roughness parameter obtained using a stereology-based approach and sand/geomembrane interface strength is evaluated. Given that interface strength is a function of relative movement between surfaces and thus is a kinematic measure, it is likely that other surface roughness parameters which are determined with consideration of the direction of motion may yield alternative correlations between surface roughness and interface strength. On the other hand, a static measure such as used in this paper provides a robust roughness index for manufacturing and field quality control, and for examining interface strength behavior.

EXPERIMENTAL STUDY

Surface Roughness Parameter. Figure 1a shows a three-dimensional surface of an geomembrane sample. The roughness of the surface can be quantified by the surface roughness parameter, R_S, defined as:

$$R_S = \frac{A_s}{A_0} \tag{1}$$

where:
A_S = actual surface area;
A_0 = projected surface area.

Theoretically, values of R_S can range from 1.00 for a perfectly flat surface to infinity for highly textured surfaces. Most practical engineering surfaces have R_S values less than 5 and the geomembranes examined in this study have values less than 2.0. Use of R_S provides a value of roughness that is based on the three-dimensional characteristics of a surface instead of a two-dimensional profile trace given by conventional profilometers. This area-based measurement implicitly accounts for surface asymmetry and eliminates the effect of profiling direction on the value of roughness.

In practice, the surface roughness parameter is determined from the stereology relationship:

$$R_S = \overline{R_L \psi} \tag{2}$$

where:
R_L = the profile roughness parameter;
ψ = the profile structure factor.

The bar indicates that R_S is an average value of the product of R_L and ψ over several cross sections as described by Gokhale and Underwood (1990). R_L is defined as the actual length of a profile normalized by the projected length, (Figure 1b). The profile structure factor is determined from the distribution of line segment orientations, α, obtained from joining digitized points on a profile by straight lines, as shown in the insert of Figure 1b. The fraction of the length of profile in each of K orientation class intervals (0-180 degrees), $h_i\Delta$, are summed as indicated in Figure 1b. Details of this procedure are given by Dove and Frost (1996) and Gokhale and Drury (1990).
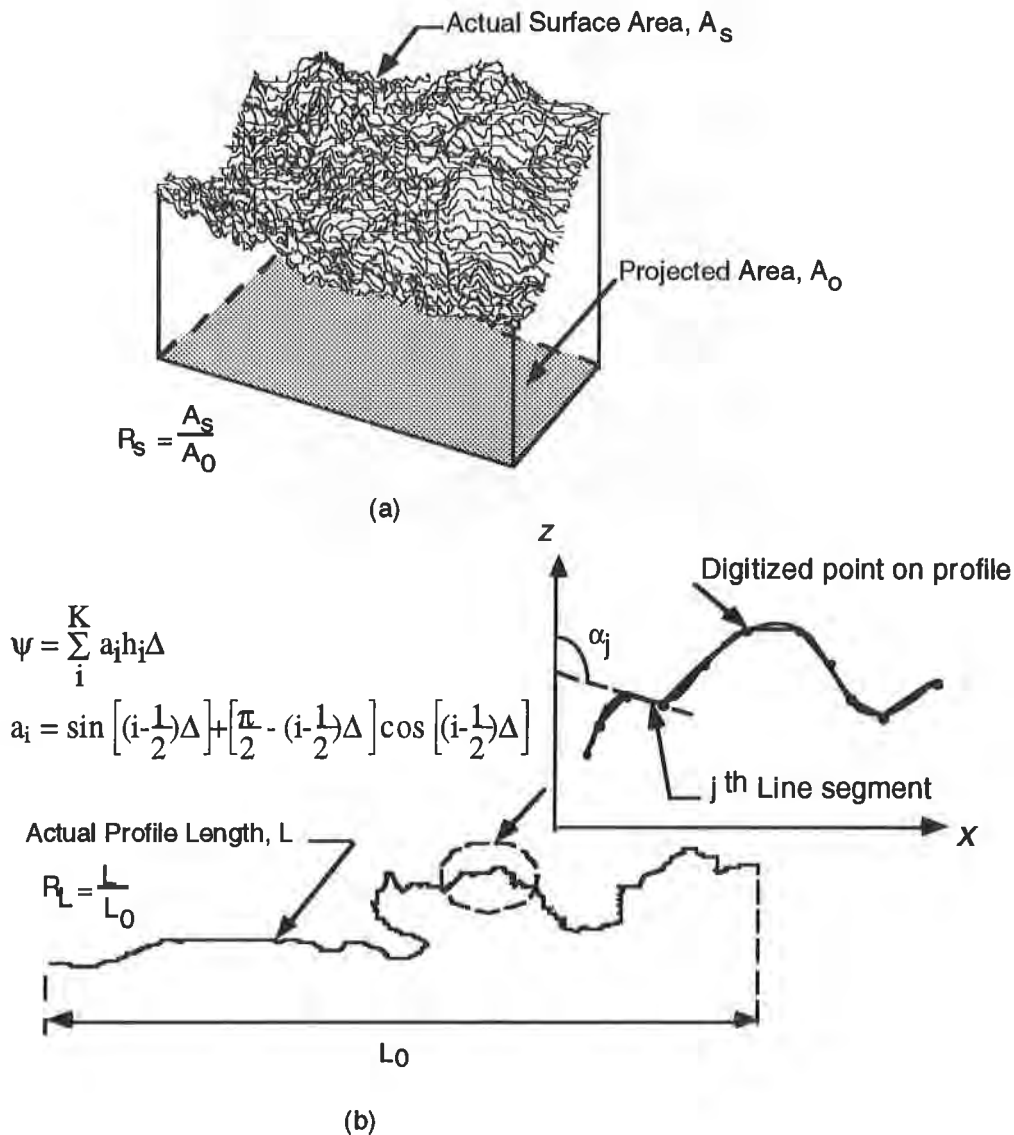
Figure 1. Definition of roughness parameters
(After Dove and Frost, 1996)

<u>Surface Roughness Characterization.</u>   One smooth and three textured HDPE geomembranes which are considered to be representative of the range of textures and texture patterns presently available to designers were utilized in this study. The samples included GSE Friction Flex supplied by GSE Lining Technology, Inc.; Dura Seal HD and Friction Seal HD supplied by National Seal Co. (NSC); and Poly-Flex Textured HDPE supplied by Poly-flex, Inc. The geomembranes were 1 mm or 1.5 mm in thickness.

Samples of geomembrane approximately 100 mm square are taken from selected locations on a roll. Gokhale and Drury (1990) determined that only three sections oriented at 120 degrees to each other are required to obtain an accurate measure of R_S (trisector approach). Accordingly, three specimen coupons approximately 50 mm in length are cut from the sample as shown on Figure 2.
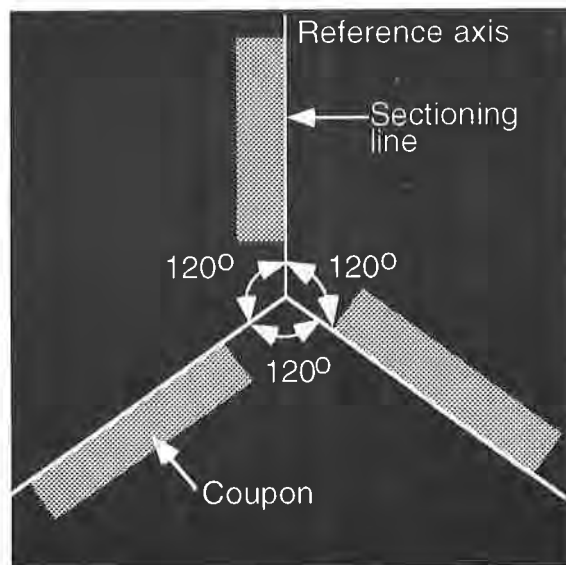
Figure 2. Geomembrane roughness specimen and coupons (plan view)
(Dove and Frost, 1996)

The three coupons are placed with the edges containing the sections positioned vertically into a mold filled with a plaster of Paris mixture. Once the mixture hardens, the surface of the plaster is then ground and polished to expose the three sections. The polished surface is then placed under an optical microscope and images are captured with a CCD camera and evaluated using an image analysis system. R_L, as defined in Figure 1b, is obtained directly from the image analysis system and ψ is computed from the orientation distribution of the line segments joining digitized points on the profile. The values of R_L and ψ are then averaged for the three profiles.

<u>Soil Properties.</u> Two standard Ottawa sands and a Upper Drain material from a landfill project in Illinois, USA were selected. Ottawa sands are typically used in research tests and their properties and behavior are well documented. The Upper Drain material was selected to corroborate the results obtained with the Ottawa sands.

Table 1 presents the index and strength properties of each soil. All soils are uniformly graded. The Ottawa sand grains are rounded to subrounded whereas the upper drain material

is primarily subangular with some subrounded particles. Ottawa 20/30 sand has 95 percent passing the No. 20 sieve and less than 5 percent passing the No. 30 sieve. Ottawa F-70 has 60 percent passing the No. 70 sieve and less than 5 percent passing the No. 140 sieve. The upper drain material has a maximum particle size of 2 mm and less than 2 percent passing the No. 200 sieve.

Table 1. Soil Index Properties

Soil	D_{50}, (mm)	$\gamma_{d, max}$ (kN/m^3)	$\gamma_{d, min}$ (kN/m^3)
Ottawa 20/30	0.6	17.4	14.9
Ottawa F-70	0.2	17.4	14.9
Upper Drain	0.7	17.5	14.6

Interface Strength Tests. Both 63.5 mm circular and 300 mm square direct shear boxes were used to perform interface shear strength tests. The tests were conducted at normal stresses ranging from 50 kPa to 300 kPa and a target relative density of 80 percent. Displacement rates of 0.01 and 0.04 inches per minute were used for the 63.5 mm and 300 mm shear boxes, respectively. Williams and Houihan (1987) found that the strengths of sand-geomembrane interfaces are insensitive to displacement rate.

Geomembrane samples were glued onto a plywood substrate and cured under a surcharge for 24 hours prior to shearing. The 300 mm shear box samples were clamped at one end and glued to a plywood substrate. Soil was placed dry and tamped to actual in-place relative densities ranging from 76 to 88 percent. All tests were conducted in the geomembrane machine direction. Specimens for roughness determination were collected directly adjacent to each shear test sample (in the machine direction). Roughness specimens were labeled according to the side being tested in shear and the direction of shear. The reference axis was in the machine direction.

RESULTS

Geomembrane Roughness. The range of R_S values determined for each geomembrane sample along with the average values and number of samples are summarized in Table 2. The last column of Table 2 gives the corresponding texture descriptor proposed by Dove and Frost (1996) and is based on the average value of R_S.

Table 2. Results of Surface Roughness Determinations

Geomembrane	Range of R_S Values	No. of Samples	Average R_S Value	Texture Descriptor (Dove and Frost, 1996)
NSC Dura Seal HD	1.05-1.13	18	1.07	Smooth
GSE Friction Flex	1.23-1.32	16	1.25	Slightly textured
NSC Friction Seal HD	1.35-1.78	17	1.50	Moderately textured
Poly-flex Textured HDPE	1.48-1.79	16	1.59	Moderately/heavily textured

The smooth geomembrane has R_S values ranging from 1.05 to 1.13; the latter value is for a specimen which was scarred from handling of the roll. Typically, R_S for smooth geomembranes ranges from 1.05 to 1.08. R_S values for the textured geomembranes used in this study are within the ranges found for the same geomembrane rolls in the previous study reported by Dove and Frost (1996). The National Seal Friction Seal HD has rows of texture elements oriented in the cross machine direction with a relatively smooth zone in between. It is seen that the R_S values have a range of 0.43 which the authors believe reflects the variability in the manufacturing process. It is the most highly asymmetric of the geomembrane samples used in the study.

<u>Effect of Surface Roughness.</u> All soil and interface friction angles presented herein are secant values computed for a cohesion intercept of zero. Figures 3 and 4 show the relationship between surface roughness and the peak and residual interface friction angles, respectively, for tests performed in the 63.5 mm diameter shear box. The individual plots correspond to different normal stress levels and contain the results of tests on several different sands. A distinct relationship is evident between the measured interface friction values and the surface roughness measurements and is discussed in more detail later. Similar plots (not shown) were generated for tests performed with the 300 mm square shear box. The larger shear box consistently gave lower peak soil and interface strength values than the 63.5 mm shear box for the same soil and geomembranes of similar roughness. Figure 5 is a comparison of results for geomembranes of varying roughness obtained with both shear boxes for the Upper Drain material at a normal stress of 100 kPa. From this figure it may be seen that the differences in peak strength increases from 2 degrees for smooth geomembranes to 6 degrees for moderately textured geomembranes. However, the trends in the data from each shear box are consistent. Peak strength differences between large and small shear boxes are normally attributed to relatively larger boundary (edge) effects, and stress and strain nonuniformities in the smaller box. It may be seen that these effects become more pronounced with increasing roughness.

Residual strength values were typically within 4 degrees as shown in Figure 5. It may also be seen that the difference is relatively constant with increasing roughness and the data trends are the same. The observed differences are likely due to boundary (edge) effects in the smaller box.

As observed from Figure 5, the results from each shear box are internally consistent and direct comparison of interface strengths can be made by using the normalized efficiency parameter as defined by Koerner (1990). Takasumi et al. (1991) examined data available in the literature and concluded that interface efficiency is not affected by shear box size. The peak efficiency is given by:

$$\text{Peak efficiency} = \frac{\tan\delta_{peak}}{\tan\phi_{peak}} \tag{4}$$

and the residual efficiency is defined as:

$$\text{Residual efficiency} = \frac{\tan\delta_{residual}}{\tan\phi_{residual}} \tag{5}$$
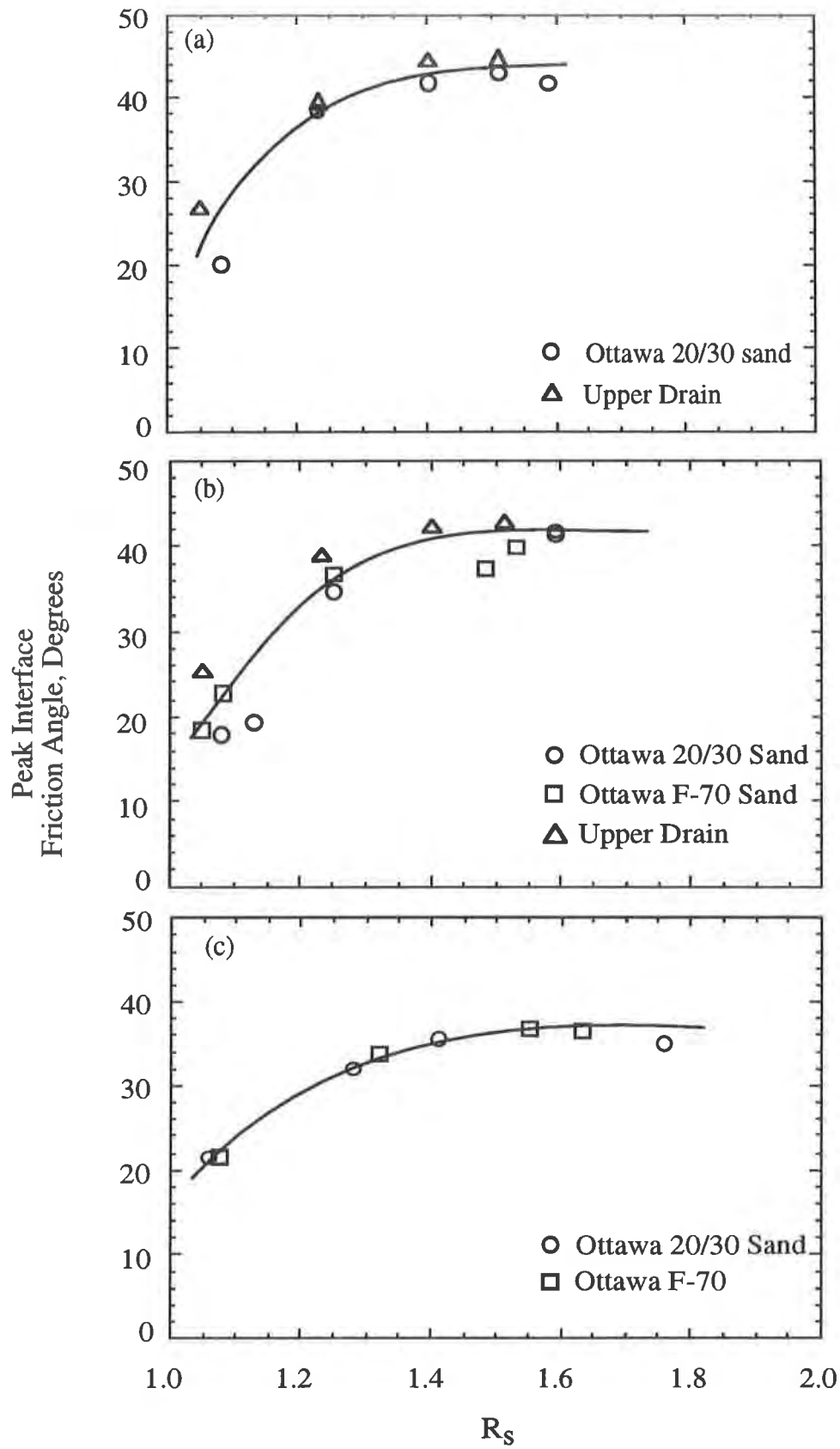
Figure 3. Peak interface friction, 63.5 mm shear
box: (a) 50 kPa, (b) 100 kPa, (c) 300 kPa
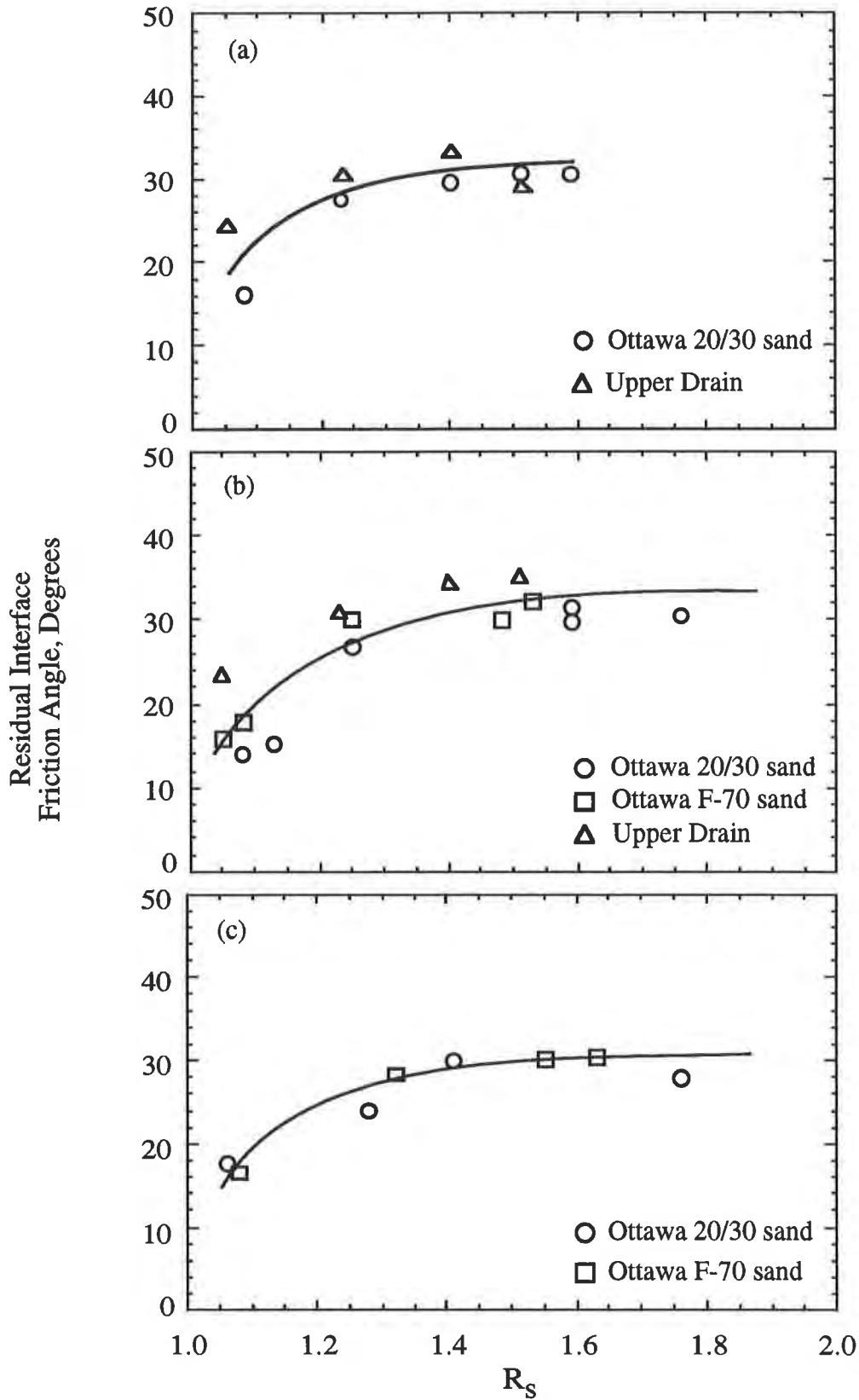
Figure 4. Residual interface friction, 63.5 mm shear box: (a) 50 kPa, (b) 100 kPa, (c) 300 kPa
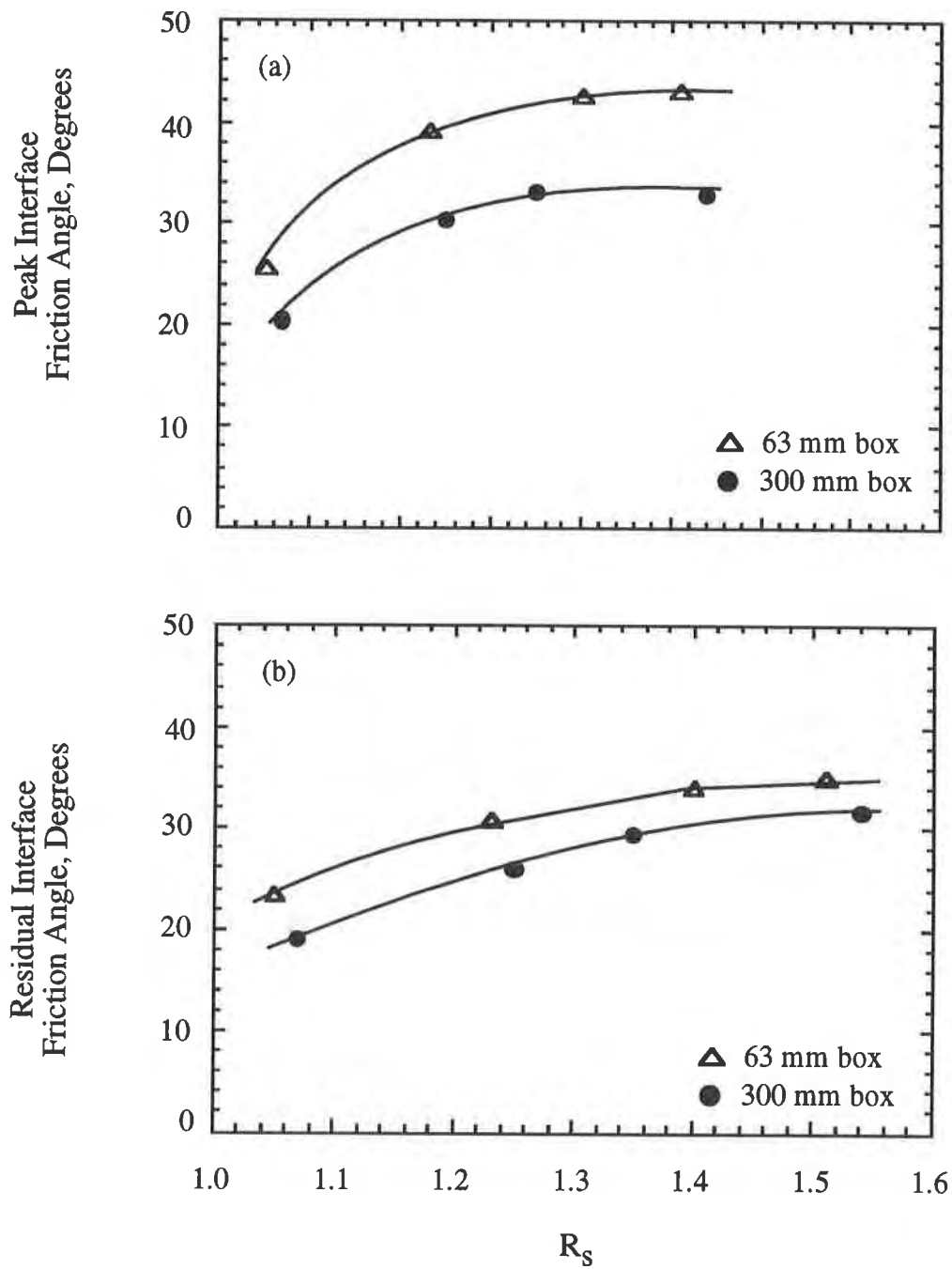
Figure 5. Shear Box Effects on Interface Friction: (a) Peak, (b) Residual. Upper Drain material, 100 kPa normal stress.

where:

δ_{peak} = peak interface friction angle;

$\delta_{residual}$ = residual interface friction angle;

ϕ_{peak} = peak soil friction angle;

$\phi_{residual}$ = residual soil friction angle.

The values of ϕ_{peak} and $\phi_{residual}$ used in Equations 4 and 5 are for tests on the same soil performed in the same shear box and at the same normal load as the corresponding interface tests. The effect of normalizing in this manner is to also normalize some of the boundary effects from each box. Figure 6 shows peak interface efficiency as a function of R_S for normal stresses of 50 kPa, 100 kPa and 300 kPa for both the 63.5 mm and 300 mm shear boxes. As can be seen, peak interface efficiency increases dramatically with small changes in roughness up to a critical R_S value. At R_S values greater than the critical value, little or no additional benefit is gained from increasing geomembrane roughness since the full soil internal friction is mobilized. This critical value of R_S ranges from 1.30 to 1.40 for the range of normal stresses and soils used in this study. In some cases, efficiencies marginally greater than 1.0 are realized. It is expected that these results will be similar for other soils with mean grain sizes greater than those tested in this study where the critical value would be expected to occur at larger R_S values. The relationships shown in Figure 6 are similar to those observed by Kishida and Uesugi (1987) and Paikowsky et al. (1995) for sands against steel surfaces.

Figure 7 shows the variation of residual efficiency with R_S. As seen in the figure, residual interface strength increases with increasing roughness until a limiting residual efficiency is asymptotically reached. At 50 kPa, a residual efficiency of about 0.85 to 0.95 appears to be the limit for the Upper Drain material. Efficiencies of about 1.0 are observed for Ottawa 20/30 sand. It is observed that for R_S values less than 1.1 (smooth surfaces), the data for Ottawa 20/30 sand are in close agreement with Ottawa F-70 sand and the Upper Drain material. In general, it was found that as roughness increases, the post-peak deformation required to achieve residual conditions decreases, and as normal stress increases at a constant roughness, the post-peak displacement required to reach residual conditions increases.

At a residual efficiency of about 1.0, the residual strength of the soil is assumed to be completely mobilized with shear occurring completely within the soil. However, below a residual efficiency of 1.0, slippage of soil grains or other more complex soil/interface interactions are probably occurring and full residual efficiency can not develop. For example, it is known that shear on a smooth geomembrane largely occurs at the interface and not in the soil, therefore the residual efficiency should be much less than 1.0. This agrees with the residual efficiency of 0.5 to 0.6 at R_S values of 1.05 to 1.11 shown in Figure 7. By increasing R_S to about 1.25 to 1.45, the soil reaches full residual strength mobilization as it becomes more involved in the shearing process through particle interactions with the counterface and through the associated steady state shear resistance. Current research is examining these mechanisms in greater detail.

It should be noted that roughness is only one characteristic of a surface and any value, no matter how determined, is not unique since surfaces with different texture patterns can have the same roughness value. A study of the interface behavior of such surfaces is currently underway. However it may be seen that beyond an R_S value of approximately 1.40, texture pattern makes little difference in efficiency or friction angle for sands with mean grain diameter
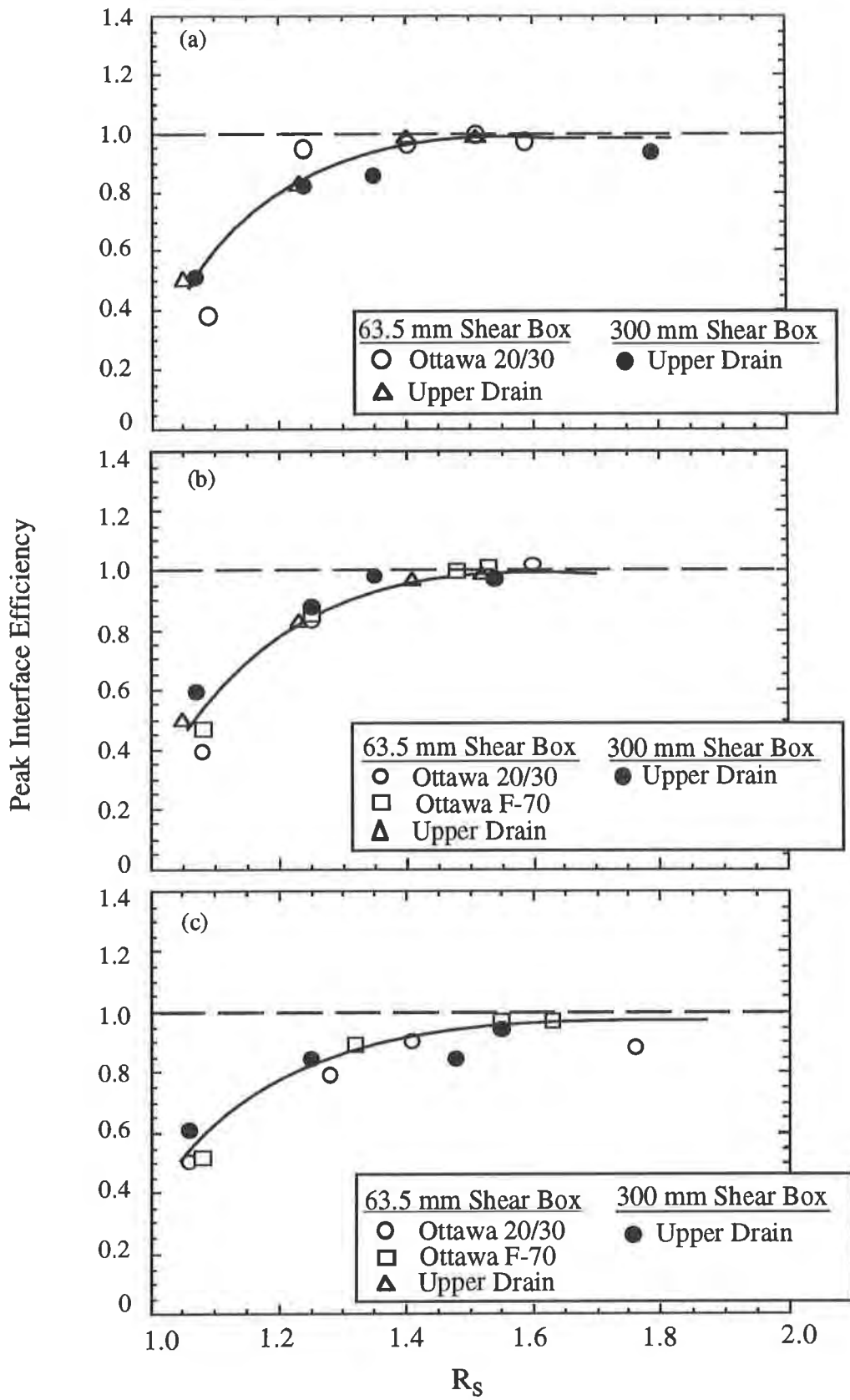
Figure 6. Peak interface efficiency: (a) 50 kPa, (b) 100 kPa, (c) 300 kPa
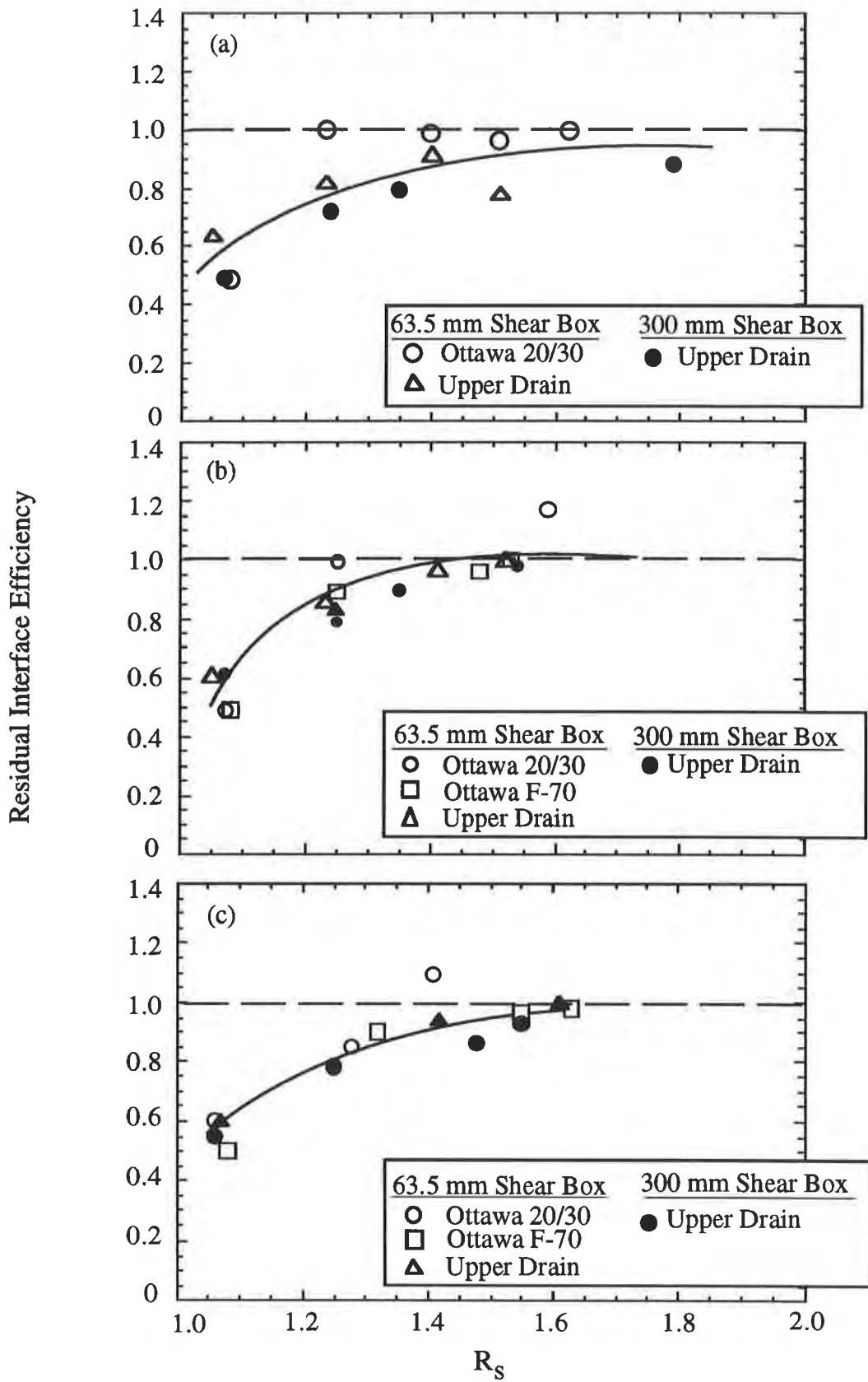
Figure 7. Residual Interface Efficiency: (a) 50 kPa, (b) 100 kPa, (c) 300 kPa

ranging from 0.2 to 0.7 mm as tested in this study. Since R_S is an aerial parameter, it is independent of profiling direction and surface asymmetry. If it is desired to obtain a roughness measure in a particular direction, the parameter R_L may be used. Correlations (not shown) similar to those of Figures 6 and 7 were obtained using R_L determined in the direction of shear.

Effect of Normal Stress. It is also observed that, for textured surfaces, interface friction angles generally decrease with increasing normal stress. However, for the smooth HDPE geomembranes used, the peak friction angle was observed to decrease with increasing normal stresses only up to about 50 kPa. Above 50 kPa, the peak friction angle increases due to indentation and shearing of the geomembrane polymer by the sand grains at the interface. This effect was more pronounced with the Upper Drain material which has a mixture of subrounded and subangular particles.

The effect of normal stress may also be observed in Figure 6. It is seen that the initial rapid increase in efficiency decreases with increasing normal stress. For example, by comparing the 50 kPa and 300 kPa plots, it may be seen that the rate of increase in peak efficiency with surface roughness decreases with increasing normal stress. The same effect is observed for the residual efficiencies of Figure 7. This is believed to result from the simultaneous increase in smooth surface interface strength behavior and a decrease in textured surface strength behavior. Another consequence of this normal stress dependency is that the strength envelope is curved instead of the typically assumed straight line. Fitting a straight line to this data produces erroneous "cohesion" intercepts for cohesionless materials.

CONCLUSIONS

The results show that surface roughness has a first-order effect on the strength of granular soil/geomembrane interfaces. Quantification of geomembrane surface roughness with the surface roughness parameter, R_S, obtained using the recently developed OPM method provides a means to establish the magnitude of the roughness effect and for examining interface response. Most importantly, it is observed that there is a limit to the beneficial effect of increasing roughness beyond an R_S value of about 1.4 for the granular soils tested. It has also been shown that interface strength is stress-level dependent for all textures. It is expected that R_S will be equally applicable to fine-grained soil/geomembrane interfaces.

For design applications using geomembranes in contact with granular soils, the critical value beyond which no benefit is obtained from increased roughness can be established for commonly specified materials. The relation between R_S and interface strength can provide a basis for improved quality assurance procedures since the design value or range of geomembrane roughness can be specified and maintained during construction. The behavior of the composite soil/geomembrane system can then be modeled for construction and service conditions.

ACKNOWLEDGMENTS

REFERENCES

Bemben, S. M. and Schulze, D. A., (1993) "The influence of selected testing procedures on soil/geomembrane shear strength measurements", Proceedings of Geosynthetics '93, Vancouver, BC, Canada, International Fabrics Association International, Vol. 2, pp. 619-631.

Dove, J.E. (1996) "Particle-geomembrane interface strength behavior as influenced by surface topography", Ph.D. Thesis, School of Civil and Environmental Engineering, Georgia Institute of Technology, 323 p.

Dove, J.E., Frost, J.D. and Dove, P.M., (1996) "Geomembrane microtopography by atomic force microscopy", Geosynthetics International, Vol. 3, No. 2, pp. 227-245.

Dove, J.E. and Frost, J.D., (1996) "A method for estimating geomembrane surface roughness", Geosynthetics International, Vol 3, No. 3, pp. 369-392.

Gokhale, A. M. and Underwood, E. E., (1990) "A general method for estimation of fracture surface roughness: Part 1. Theoretical aspects", Metallurgical Transactions A, Vol. 21A, pp. 1193-1199.

Gokhale, A. M. and Drury, W. J., (1990) "A general method for estimation of fracture surface roughness: Part II. Practical considerations." Metallurgical Transactions A, Vol. 21A, pp. 1201-1207.

Kishida, H. and Uesugi, M., (1987) "Tests of the interface between sand and steel in the simple shear apparatus", Geotechnique, Vol. 37, No. 1, pp. 45-52.

Koerner, R.M., (1990) "Designing with geosynthetics". Prentice Hall, Inc., Engelwood Cliffs, NJ, 652 p.

Paikowsky, S. G., Player, C.P., Connors, P.J., (1995) "A dual interface apparatus for testing unrestricted friction of soil along solid surfaces", Geotechnical Testing Journal, Vol. 18, No. 2, pp. 168-193.

Stark, T.D., Williamson, T.A. and Eid, H.T., (1996) "HDPE geomembrane/geotextile interface shear strength", Journal of Geotechnical Engineering, ASCE, Vol. 122, No. 3, pp. 197-203.

Takasumi, D.L., Green, K.R. and Holtz, R.D., (1991) "Soil-geosynthetics interface strength characteristics: A review of state-of-the-art testing procedures", Proceedings of Geosynthetics '91, Atlanta, Georgia, Vol. 1, pp. 87-100.

Underwood, E. E. and Banerji, K., (1987) "Quantitative fractography." Metals Handbook, ASM, Metals Park, OH, pp. 193-210.

Williams, N. D. and Houlihan, M. F., (1987) "Evaluation of interface friction properties between geosynthetics and soils", Proceedings of Geosynthetics '87, Vol. 2, New Orleans, LA, pp. 616-627.

Yoshimi, Y. and Kishida, T., (1982) "A ring torsion apparatus for evaluating friction between soil and metal surfaces", Geotechnical Testing Journal, Vol. 4, No. 4, pp. 145-152.

CORPS OF ENGINEERS GEOSYNTHETIC CLAY LINER INTERFACE TEST PROGRAM

K.L. PAVLIK
U.S. ARMY CORPS OF ENGINEERS, OMAHA DISTRICT
ATTN.: CEMRO-ED-GA (PAVLIK)
215 NORTH 17TH STREET
OMAHA, NE 68102-4978

ABSTRACT

The U.S. Army Corps of Engineers, Omaha District, has developed laboratory procedures for large specimen direct shear testing of geosynthetics to support its environmental mission. General procedures follow ASTM D 5321, "Determining the Coefficient of Soil and Geosynthetic or Geosynthetic and Geosynthetic Friction by the Direct Shear Method." This ASTM provides sufficient guidance for determining the frictional resistance for most geosynthetics, but lacks specific guidance for testing geosynthetic clay liners (GCLs). To better define GCL procedures, a test program was initiated specifically for geotextile based GCLs and their interfaces. The interface tested consisted of a Claymax 500SP against a Gundle 1.5 mm (60 mil) textured HDPE geomembrane.

INTRODUCTION

The U.S. Army Corps of Engineers, Omaha District (COE), purchased a Brainard-Kilman 113 direct shear machine and initiated a large specimen interface friction testing program to support its Hazardous, Toxic, and Radioactive Waste (HTRW) design and construction projects. The equipment has the capability of applying normal stresses of up to 69 kPa (10 psi) with a rigid load platen and up to 690 kPa (100 psi) with the bladder membrane apparatus. Procedures were developed for interface friction testing between geosynthetics, first without, and then with a GCL. General procedures followed the American Society for Testing and Materials (ASTM) D 5321, "Determining the Coefficient of Soil and Geosynthetic or Geosynthetic and Geosynthetic Friction by the Direct Shear Method." Various normal stress ranges were used in an effort to model previously reported testing. The internal shear resistance of the direct shear machine was determined by calibration procedures outlined in ASTM D 5321. The internal shear resistance was subtracted from the recorded shear force prior to plotting and

determining adhesion and friction angles. No large variations in the applied shear force were identified after movement of the traveling shear box had been initiated. However, no correlation's were developed to determine the effects of normal stress on machine resistance. Specimens were sheared in their machine direction with a constant effective specimen area until a post peak shear strength was determined. Specimens were inspected and observations noted at the end of each test.

Initially a geomembrane/geonet interface was tested in accordance with ASTM D 5321. These testing procedures are relatively straight forward and aided in familiarizing laboratory personnel with the equipment and its operation. A 300 by 300 mm (12 by 12 inch) geomembrane was placed in the upper box and sheared against a 360 by 410 mm (14 by 16 inch) geonet in the lower box. The tests were performed dry at a horizontal displacement rate of 2.5 mm (0.1 inch) per minute for up to 80 mm (three inches). Normal stresses of 210, 280, and 380 kPa (30, 40, and 55 psi) were applied by a bladder membrane. The manufacturer's load cell calibration results were used to determine the bladder membrane loading required for each of the applied normal stresses.

Once satisfied with the geomembrane/geonet test procedure and results, the COE performed interface friction testing on GCLs. ASTM D 5321 does not provide guidance for testing GCLs. However, ASTM guidance is currently under development titled "Determining the Internal and Interface Shear Resistance of GCL by the Direct Shear Method." Since no ASTM is currently available, the COE developed procedures for interface friction testing including specimen preparation, equipment modifications, and establishing a uniform gap between the upper and lower boxes. The interface used to develop the test procedures consisted of a geotextile based GCL and a 1.5 mm (60 mil) textured high density polyethylene (HDPE) geomembrane. The GCL was placed over a smooth, rigid substrate in the lower shear box. The geomembrane was placed in the upper shear box with an overlying smooth, rigid superstrate.

Normal stresses of 7, 14, and 28 kPa (1.0, 2.0, and 4.0 psi) were applied via the rigid load platen prior to adding distilled water. The manufacturer's rigid load platen rate equation and calibration data were used to determine the air pressure to apply for each of the normal stresses. The GCL specimens were then allowed to hydrate for 48 hours prior to shearing. Forty eight hours was chosen as the maximum length of time that could be allowed for hydration to keep testing costs within reason. In addition, this hydration time allowed uniform hydration of the GCL based on post test moisture content testing. A constant rate of displacement equal to 1.0 mm (0.04 inch) per minute was used to shear the interface.

SPECIMEN PREPARATION

Initially, GCL specimens were cut to fit in the 300 by 300 mm (12 by 12 inch) upper shear box. A template and permanent marker were used to mark the cut lines for the GCL specimens. The specimens were cut out using either a sharp utility knife or scissors. To minimize the loss of bentonite, two methods were employed to hydrate the bentonite along the cut lines. The first method used a sprayed mist to hydrate the edge of the GCL specimens immediately after cutting. Cutting the GCL on an incline, with the edge being cut facing upward, also aided in minimizing bentonite loss. The second method involved placing water along the cut line, allowing the bentonite to hydrate, and then cutting the specimens along the cut lines. Neither method proved superior to the other and both were slow and tedious processes. Two different types of GCLs were used to practice specimen preparation. One GCL contained powdered bentonite and the other contained granular bentonite. Minimization of bentonite loss on GCL specimens which contained powdered bentonite was more difficult than specimens which contained granular bentonite.

Due to difficulties in minimizing bentonite loss, the specimen preparation procedure was modified so that the GCL specimens were placed in the lower shear box. Specimens cut for the lower shear box were 360 mm (14 inches) wide and approximately 410 mm (16 inches) long. Although bentonite was still lost at the edges of the specimens, the as manufactured bentonite density was maintained within the area to be sheared. However, this method results in unconstrained swelling of bentonite outside the area where normal stresses are applied. During shearing, this could potentially result in a wave of bentonite forming at the leading edge of the upper shear box, resulting in erroneous high shear strengths. Based on limited test results, the COE did not consider this to be a significant problem. Therefore, unless requested otherwise, the decision was made to perform direct shear tests on GCLs by placing the GCL in the lower shear box due to the ease of specimen preparation and setup.

Although not used, another method for preventing bentonite loss involves sealing the edges of specimens after cutting and prior to setup. This can be done by removing a small amount of bentonite from the edges of the specimens, folding the geotextiles back onto the GCL and then stapling through the GCL and the edges of the specimens. The edges of the specimen could also be glued together to prevent bentonite loss. Either method would be acceptable provided the selected method minimized any effects to the test results. This could be accomplished by situating the sealed edges outside the shearing area (i.e. GCL in the lower shear box) with no increase in the overall thickness of the GCL between the upper and lower shear boxes.

EQUIPMENT MODIFICATIONS

<u>Textured Substrate.</u>   In discussions with other testing laboratories, it was discovered that slippage between the GCL and smooth substrate could be a problem.   To minimize this slippage and provide more uniform transfer of shear load onto the interface, a textured substrate was constructed.   Queried laboratories provided numerous different methods for creating a textured substrate.   The COE used a method developed by GeoSyntec Consultants, Inc. of Atlanta, Georgia. This method consisted of attaching wood files (Stanley Surform flat replaceable blades) to a rigid platen to form a textured surface.   Six wood files were glued to the bottom platen spaced approximately 8 mm (0.3 inch) apart as shown in Figure 1.   The files are 40 mm (1.6 inches) wide with chisel-like teeth and brackets that allow the files to be attached to a handle.   The brackets were ground off prior to attaching the files to the rigid platen with the teeth orientated in the same direction.
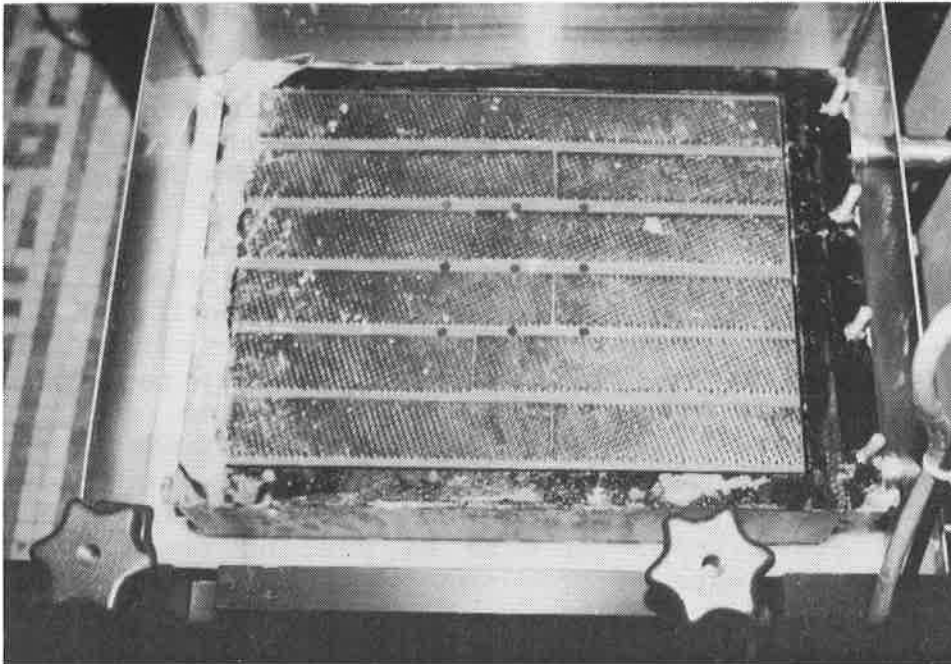
Figure 1.   Textured Substrate with Holes

<u>Hydration.</u>   Complete hydration of the GCL was a problem within the desired hydration time of 48 hours.   Initial test results indicated the GCL specimens were not fully hydrated in the center area because the GCLs only access to water was from the edges.   Tests with the textured substrate were more completely hydrated than with the smooth substrate, however, no series of test were completely hydrated.   The unhydrated area was approximately 60 to 80 cm^2 (9 to 12 in.^{2}) in size. To allow greater access of water to the center portion of the GCL, nine-8 mm (5/16 inch) diameter holes were drilled through the platen between the wood files as shown in Figure 1.   The underside of the

platen was then grooved, as shown in Figure 2, to connect each row of holes to the edges of the platen. This provided uniform hydration throughout the GCL that was confirmed by post test moisture content testing. Moisture contents, taken across the GCL, were typically in the 200 percent range.
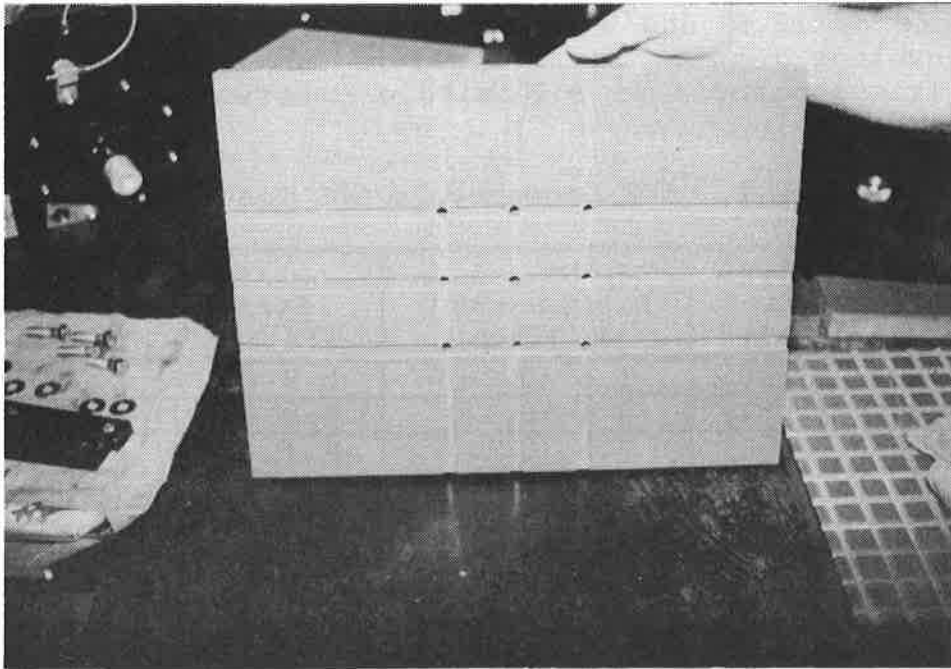
Figure 2. Grooves on Bottom of Textured Substrate

GAP BETWEEN BOXES

No guidance exists on determining the correct gap between the shear boxes. The gap between the shear boxes should be a function of the materials to be tested. The COE used a 6.1 mm (240 mils) gap for the geomembrane/GCL tests. This gap was used to ensure the geomembrane/GCL shearing surface was located between the shear boxes and to prevent the shear boxes from interfering with the shearing surface.

GCL TESTING RESULTS

A Claymax 500SP GCL and a Gundle Lining Systems, Inc. (Gundle) 1.5 mm (60 mil) textured HDPE geomembrane were selected for the test program. Specimens were sheared in the machine direction with the Claymax 500SP GCL positioned so that the Synthetic Industries 865 woven geotextile was in contact with the Gundle geomembrane. Reinforcement of the Claymax 500SP consists of stitching spaced at 100 mm (four inches) centers. The stitching was centered along the width of the specimen so that three of the stitch lines were within the shearing area.

A typical set of COE geomembrane/GCL test results are shown in Table 1 and Figures 3 and 4. Figure 3 is a plot of the horizontal displacement versus shearing force. Figure 4 shows the peak and post peak shear strength envelopes via a best fit line through their respective test sets and their projection to the intercept. The peak envelope results in an apparent adhesion of 5.8 kPa (0.85 psi) with a friction angle of 18.5° and a coefficient of variance of 0.999. The post peak envelope results in an apparent adhesion of 4.4 kPa (0.64 psi) and a friction angle of 9.9° with a coefficient of variation of 0.941.

Table 1. COE Geomembrane/GCL Test Data

Normal Stress kPa (psi)	Peak Shearing		Post Peak Shearing	
	Stress kPa (psi)	Displacement mm (inch)	Stress kPa (psi)	Displacement mm (inch)
7 (1.0)	8.3 (1.20)	1.5 (0.06)	5.9 (0.86)	66 (2.60)
14 (2.0)	10.4 (1.51)	3.6 (0.14)	6.3 (0.91)	79 (3.10)
28 (4.0)	15.2 (2.20)	3.0 (0.12)	9.4 (1.36)	79 (3.10)

No damage was observed in the GCLs which were inspected at the conclusion of each test. Bentonite was found on the geomembrane surfaces after every test.
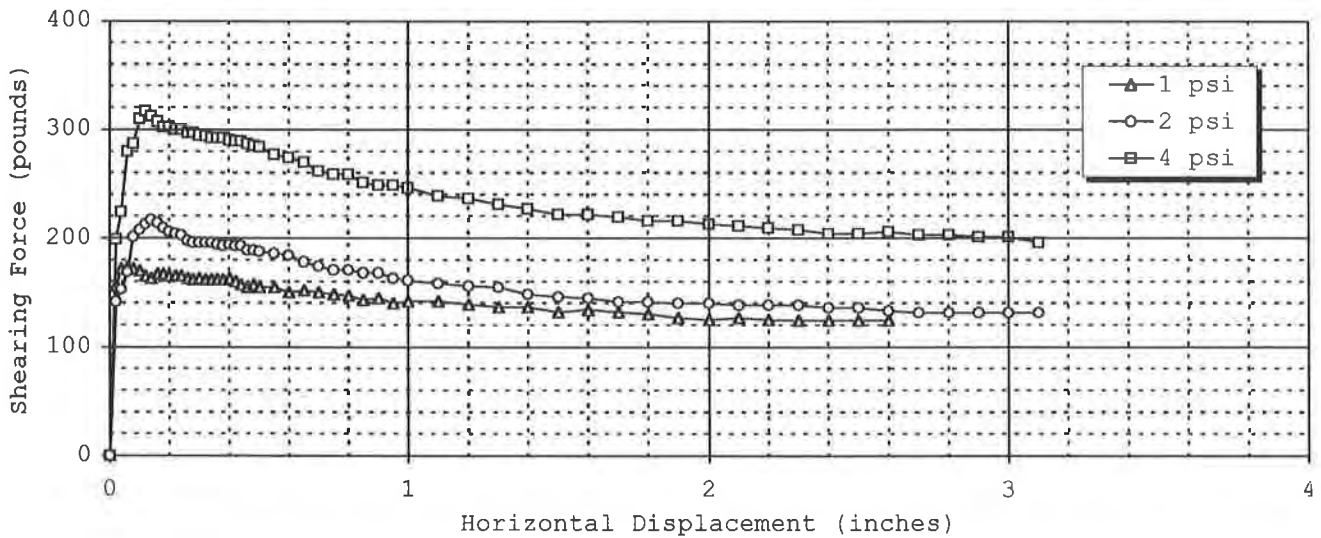
Figure 3. Displacement versus Shearing Force
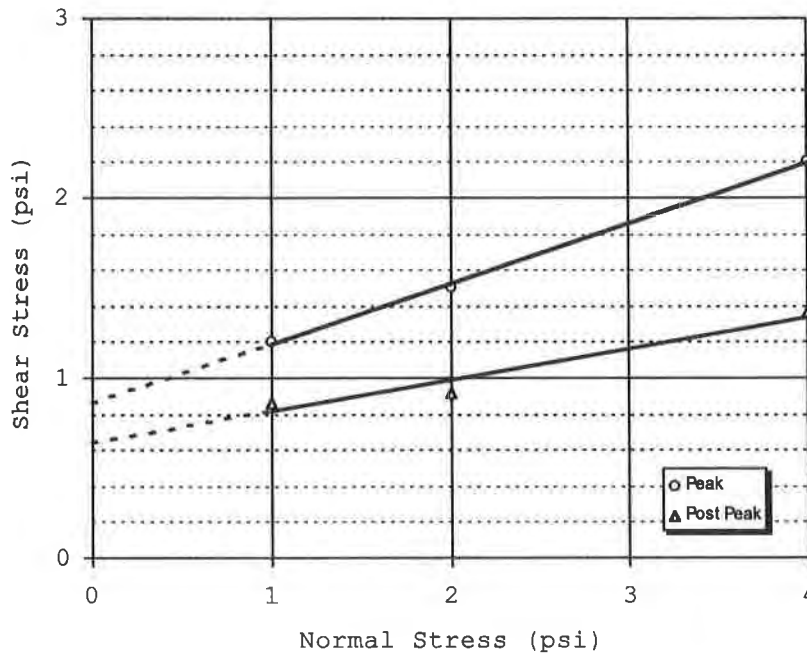
Figure 4. Shear Strength Envelopes

Similar testing results were supplied by CETCO and are summarized in Table 2. These tests were performed with a Claymax 500SP woven geotextile against a textured HDPE geomembrane, were hydrated, and sheared at a rate of 1.0 mm (0.04 inches) per minute. Residual friction angles were determined at a minimum of 80 mm (three inches) of displacement.

Table 2. Summary of Commercial Laboratory Test Data

Textured HDPE thickness mm (mil)	Normal Stresses kPa (psi)	Peak Friction Angle (degrees)	Peak Apparent Adhesion kPa (psf)	Residual Friction Angle (degrees)	Residual Apparent Adhesion kPa (psf)
1.5 (60)	2, 10, 14 (0.35, 1.4, 2.8)	35	0.5 (10)	26	1.0 (20)
1.5 (60)	19, 34, 48 (2.8, 4.9, 6.9	24	5.0 (100)	11	1.0 (20)
1.0 (40)	7, 14, 28 (1.0, 2.0, 4.0)	19	1.5 (32)	19	1.0 (20)
1.0 (40)	7, 14, 28 (1.0, 2.0, 4.0)	20	2.5 (53)	17	2.5 (53)
1.0 (40)	7, 14, 28 (1.0, 2.0, 4.0)	21	1.8 (37)	17	0.6 (13)
1.0 (40)	7, 14, 28 (1.0, 2.0, 4.0)	18	0.2 (5)	17	0.2 (5)

CONCLUSIONS

The COE has developed practical procedures for testing the interface friction between GCLs and other geosynthetics. These procedures are based on modifications to ASTM D 5321 to include specimen preparation and equipment modifications. Specimen preparation included a method for cutting out the GCL specimens so as to minimize bentonite loss. Equipment modifications consisted of construction of a nonslip substrate and providing water access to the center portion of the GCL. Limited COE testing to date has provided results similar to those from other commercial laboratories. Further work is required in development of test procedures for determining the effect of the wave created by placing the GCL in the lower box, the minimum time required to achieve uniform hydration of the GCL, and an appropriate gap spacing. Additional testing will be performed to develop procedures for determining the internal shear strength of GCLs and for testing soil/geosynthetic interfaces.

ACKNOWLEDGMENTS

The author wishes to express his appreciation to Dave Jaros and Steve Butler of the Omaha District HTRW Center of Expertise Geoenvironmental Branch for their assistance. Thanks also go to the support of the Omaha District Laboratory, namely Dick Schlenker, Elia Bahwawsi, and last but not least, Jeff Stanek.

REFERENCES

American Society for Testing and Materials (ASTM), (1992) "Determining the Coefficient of Soil and Geosynthetic or Geosynthetic and Geosynthetic Friction by the Direct Shear Method", D 5321, 5 p.

American Society for Testing and Materials (ASTM), (Draft) "Determining the Internal and Interface Shear Resistance of GCL by the Direct Shear Method", Draft 4, 7 p.

VARIABILITY ANALYSIS OF SOIL VS. GEOSYNTHETIC INTERFACE FRICTION CHARACTERISTICS BY MULTIPLE DIRECT SHEAR TESTING

K. R. CRILEY
VECTOR ENGINEERING INC., USA
D. SAINT JOHN
VECTOR ENGINEERING INC., USA

ABSTRACT

The performance of a single 3-point large scale direct shear interface test may be insufficient to accurately define the friction characteristics of a particular soil vs. geosynthetic or geosynthetic vs. geosynthetic relationship. In an effort to define the variable nature of these relationships the authors statistically analyzed the friction angles, adhesion, shear strength and final moisture contents of several multiple testing programs with up to 16 tests (48 points) each, for soil vs. a textured high-density polyethylene (HDPE) membrane.

The statistical data accumulated were utilized to create a range of expected friction angles and adhesions for any one soil type vs. a specific geosynthetic. The repeatability of the test is shown using the standard deviation of each set of data as a tool. There is an inherent risk, involved in using the data from any single test as a basis for construction design or performance evaluation. Multiple testing programs greatly reduce this risk.

INTRODUCTION

The interface friction angle and adhesion coefficient between a geosynthetic and soil are the primary and contentious variables used in the stability analysis and design of waste containment facilities. Geosynthetics are used to improve the protection of existing foundation soils and groundwater supplies from leakage of hazardous solutions. In new construction and in the expansion of existing facilities, the designer must have reliable and reproducible data in order to reduce his liability and risk, and ensure the owner/client has an economic and properly designed product.

The frictional characteristics of a specific soil vs. a geosynthetic is not a unique value that is easily reproduced or repeated. An understanding of the variability of the materials and the testing procedures must be understood in order to better understand and utilize the tests results. In reviewing and using test data from a group of tests, an acceptable design window or degree of accuracy (precision) should first be developed. With a better understanding of the data variability, the engineer can then utilize an acceptable range or tolerance of friction and adhesion values in his design and specifications.

Interface direct shear tests are performed to assist an engineer in evaluating the friction angle and adhesion coefficient for the various interfaces within the design. Design is primarily dependent on the interface with the lowest friction characteristics. The direct shear test, as a form of quality control, is also used to ensure product compliance to the values used in design.

The data presented here represents results from several different projects with specifications that required the contractor to provide interface direct shear tests on a frequency based on the square footage of

product (geosynthetics) placed on site. The lab's responsibility in performing these tests was to provide tests in accordance with the project specifications. Testing took place over several weeks, during different times over a two-year period. The results were not intended solely for use as research for this paper, thus are not weighted by any bias to create ideal results. Instead the data presents a good example of standard operation procedures following published test standards that could be expected in any testing program.

TEST STANDARD

Until the early 1990's, there was not a generally accepted test standard for measuring interface shear strength characteristics between two geosynthetics or a soil vs. geosynthetic interface. Common test methods included modified soil direct shear machines, which used a variety of box sizes, loading systems, displacement rates and other independently engineered systems. Pull-Out Boxes and Tilt Tables of differing design and procedures have also been utilized. All of these variables have an effect on the reproducibility of test data.

The Geosynthetic Research Institute in early 1986 developed and promoted a standard method, GS6 for conducting geosynthetic interface direct shear tests, and in 1991 the American Society of Testing Methods (ASTM) adopted the currently used D-5321 standard test method for "Determining the Coefficient of Soil and Geosynthetic or Geosynthetic and Geosynthetic Friction by the Direct Shear Method". The ASTM method was used for this testing program.

EQUIPMENT

Three similar direct shear machines were used for this project. The machines were purchased from a recognized dealer for soil and geosynthetic equipment. The drive system is electrically/mechanically driven, and capable of moving the shear box at selected displacement rates from 6.4 to 0.025 mm/min. (0.25 to 0.001 in./min.) under a maximum shear force of 44.4 kN (10,000 lb.). The units have 300mm (12 in.) square boxes. The lower box is the moving box with the top box fixed. The lower box is 100 mm longer in the direction of shear and contained a solid substrate for the tests. The lower box incorporated a bar clamp for attaching and holding the geosynthetic sample. The upper box contained the remolded soil sample, with a semi-ridged superstrate. Normal stresses greater than 41.4 kPa (6 psi) were applied using a pneumatic bladder and normal stresses less than or equal to 41.4 kPa (6 psi) were applied using dead weights. Air pressure to the bladder was controlled via a pneumatic regulator and measured with a digital pressure gauge. Shear force was measured using a 44.4 kN (10,000 lb) electrical load cell and horizontal displacement was measured with a 100 mm (4 in.) linear displacement transducer, with a readability of 0.025 mm (0.001 in.).

Test data was collected using a computer with a data logging program. The data recorded included time, shear force and normal displacement. At the end of each test the data was imported to a spread sheet file, where it was evaluated, and the final report was prepared.

Equipment calibration includes load cells, linear displacement transducers, horizontal displacement rate, the drive system friction and the normal load measurement. The normal stresses used were obtained from air pressure verses load calibrations, and not assumed as direct gage values. These measurement systems are calibrated on an annual basis and were current and operating within acceptable limits during the testing programs presented here.

TEST PROGRAM

The data for this study is from past projects that required multiple tests be conducted to help monitor conformance to project specifications. The projects, brand names and clients are confidential and will not be named in this paper. The scope of each testing program was to provide the client with interface friction angles and adhesion values for comparison to project specifications. Tests were performed on client supplied samples from on-site borrow soils and textured HDPE samples delivered to the site. In some instances, the HDPE samples were obtained from installed liner panels. Each test consisted of three separate normal stresses.

Five groups of data are presented. Each group represents separate testing programs conducted at different periods. There are two ranges of normal stresses presented: Groups I, II and III present data from low normal stresses of 7, 21 and 35 kPa (144, 432 and 720 psf); Group IV and V are for high normal stresses of 172, 414, and 689 kPa (3600, 8640, and 14400 psf). The data presentation summarizes final water contents, peak and post-peak shear stresses, friction angles and adhesions for each test in the group. Following are listed the groups and quantities of tests evaluated.

Group I	15 tests, Sandy Clay vs. 40 mil HDPE textured	Table 1
Group II	14 tests, Silty Sand vs. 40 mil HDPE textured	Table 2
Group III	15 tests, Sandy Clay vs. 40 mil HDPE textured	Table 3
Group IV	16 tests, Clayey Sand vs. 60 mil HDPE textured	Table 4
Group V	11 tests, Silty Sand w/Gravel vs. 80 mil HDPE textured	Table 5

SOIL SAMPLE PREPARATION

Bulk samples were delivered to the lab by the client. All of the soils in these projects consisted of fine grained soil with variable amounts of sand, silt and clay. Bulk samples for tests were first air-dried to a point where the soil was friable and easily reduced in size. The samples were next processed through a 4.75 mm (No. 4) sieve, then recombined and mixed to produce a homogenous sample.

Next individual test specimens were prepared. A standard mass of 5 kg was measured and sealed into a water tight container. Initial water contents were first determined. Then a calculated amount of water was added and thoroughly mixed with the soil to obtain the project specified water content. Large aggregates of soil were broken into smaller pieces to keep the individual aggregate sizes less than 10 mm (0.375 in.). Individual specimens were allowed to stand 20 ± 4 hours before compaction. Generally 3 to 6 test specimens were prepared at a time, then tested before preparing additional specimens. After moisture conditioning, the mass of each specimen was adjusted to a required amount, calculated to produce a known density when compacted to a predetermined volume.

For compacting the soil, the upper shear box was placed on a sheet of smooth HDPE on a firm concrete floor. The moisture conditioned soil specimens were loosely placed into the upper shear box, and spread uniformly across the shear box area then compacted to a predetermined height which provided the required density. All of the compacted specimens were dense and offered sufficient cohesion to the box sides, to

allow them to be transferred and mounted into the shear apparatus after compacting, without effecting the required density. The quantities of the sample were generally large enough to prevent any re-use of previously compacted specimens, however a minor amount of re-use did occur.

GEOSYNTHETIC PREPARATION

Samples were supplied from rolls cut in the field by the client, typically 1 meter long by the roll width. Upon receipt of each sample, the machine direction was noted and shear direction determined and marked on the sample. Three individual HDPE test specimens were cut from the field supplied sample for each tests. These specimens were identified with sample identification, test direction and the surface that was to be tested. HDPE specimens were cut to approximately 360 mm wide by 510 mm long (14 x 20 inches). For testing, each specimen was bolted to the lower shear box frame using a full width clamp. Under the HDPE, the lower substrate was made up of several layers of a special concrete fiber board, which provided a flat and firm base with a rough surface. New samples were used for each test point, re-use of previously tested specimens was not permitted.

TESTING PROCEDURES

The upper box with the compacted soil specimen was placed into the shear apparatus on top of the previously placed HDPE. The gap between the upper and lower metal frames was checked to assure that it would not contact the surface of the textured HDPE during shear, and the remaining clamps for the upper box were secured and tightened. A layer of geotextile was placed on top of the compacted soil followed by a layer of uniform fine gravel, a square load plate and then the upper pneumatic loading system or dead weights.

First the required normal load was applied, then tap water was added to inundate the soil sample. Normal stress and saturation were maintained for 20 ± 4 hours prior to shearing, and throughout the shearing stage of testing. After the saturation stage the sample was sheared. The displacement rate used for all tests was 1.0 mm / min.(0.04 in./min.). Tests were continued for a total horizontal displacement of 76 mm (3.0 in.). All test data, horizontal displacement, shear force and time were collected using a data acquisition system. Visual readings were obtained, recorded and compared to the computers test file for data verifications at the start and end of each test.

After shearing, the water surrounding the sample was drained before removing the normal load. This allowed for a more accurate measurement of the water content of the soil under load, presented as the final water content in the report. The normal load, plate, gravel and textile were removed, and a 200-300 g sample of soil was obtained from the center of the specimen for water content determination.

DATA INTERPRETATION & PRESENTATION

Data from each test point was imported from a data acquisition file to a spreadsheet file. This file was developed to perform all calculations and graphing needed to provide the final report. The determination of the individual peak (maximum) shear values from each test point was determined from shear stresses corresponding to a horizontal displacements less than 65 mm (2.5 inches). The term "post-peak" was used to define residual values that corresponded to the shear stress at or near 65 mm (2.5 inches) of horizontal displacement. In both cases, a visual check of the data was used to correct any unusual values; any suspect or questionable tests were re-run.

Table 1. Group I results, Sandy Clay vs. 40 mil HDPE textured

Test No.	Final Water Content, %			Peak Shear Strength, psf[1]						Post-Peak Shear Strength, psf[1]					
	Pt. 1	Pt. 2	Pt. 3	Pt. 1	Pt. 2	Pt. 3	φ	Tan φ	Adhesion	Pt. 1	Pt. 2	Pt. 3	φ	Tan φ	Adhesion
1	33.6	29.9	28.8	120	300	430	29	.55	50	110	280	390	26	.49	50
2	32.5	29.8	28.2	120	310	480	32	.62	30	100	280	460	32	.62	10
3	31.6	29.1	27.8	110	330	430	29	.55	50	90	300	410	29	.55	30
4	32.8	28.0	27.1	120	350	490	33	.65	40	100	340	470	33	.65	30
5*	32.0	30.5	26.0	130	320	690	42	.90	0	100	300	670	41	.87	0
6	28.7	35.6	28.9	170	350	520	31	.60	80	160	340	520	32	.62	70
7	30.9	29.3	27.1	210	310	480	25	.47	130	200	270	370	16	.29	150
8	31.4	30.2	28.0	130	290	450	29	.55	50	120	270	380	24	.45	60
9	30.3	29.0	27.8	150	310	500	31	.60	60	110	210	380	25	.47	30
10	30.1	29.9	28.8	140	290	440	28	.53	60	100	210	360	24	.45	30
11	31.6	31.0	28.6	140	290	450	29	.55	60	80	210	370	26	.49	0
12	32.8	31.3	29.8	130	380	400	25	.47	100	80	260	350	25	.47	30
13	33.1	31.3	28.2	140	290	470	30	.58	50	90	240	420	30	.58	10
14	32.4	29.1	28.7	110	280	460	31	.60	30	90	220	380	26	.49	20
15	34.4	28.4	28.0	130	280	470	31	.60	40	120	240	430	28	.53	30
Average Values:	31.9	30.2	28.1	137	312	477	30	.59	55	110	265	424	28	.53	37
Standard Deviation:	1.5	1.8	0.9	25.5	29.3	66.3	3.9	.10	30.7	31.8	43.6	82.7	5.6	.13	37.2
Maximum Values:	34.4	35.6	29.8	210	380	690	42	.90	130	200	340	670	41	.87	150
Minimum Values:	28.7	28.0	26.0	110	280	400	25	.47	0	80	210	350	16	.29	0

Normal Stress applied: Point 1 - 144 psf; Point 2 - 432 psf; Point 3 - 720 psf[1]

(1) 1 psf = 47.8 Pa   * Data suspect for point 3

Table 2. Group II results, Silty Sand vs. 40 mil HDPE textured

Test No.	Final Water Content, %			Peak Shear Strength, psf[1]						Post-Peak Shear Strength, psf[1]					
	Pt. 1	Pt. 2	Pt. 3	Pt. 1	Pt. 2	Pt. 3	φ	Tan φ	Adhesion	Pt. 1	Pt. 2	Pt. 3	φ	Tan φ	Adhesion
1	15.4	14.4	14.5	180	390	660	40	.84	50	180	380	660	40	.84	40
2	14.4	15.2	14.4	160	330	660	41	.87	10	150	330	640	40	.84	10
3	15.6	14.4	15.0	130	400	550	36	.73	50	130	400	540	35	.70	50
4	14.5	13.5	14.0	100	350	690	42	.90	0	80	340	650	41	.87	0
5	17.2	13.5	13.2	130	320	570	37	.75	10	120	310	540	36	.73	20
6	15.1	13.9	13.3	130	380	540	35	.70	40	120	350	530	35	.70	30
7	14.7	13.8	16.1	180	380	600	36	.73	70	170	370	590	36	.73	70
8	14.8	16.7	16.1	110	340	490	34	.67	30	110	330	470	32	.62	30
9	17.2	15.9	16.3	230	360	630	35	.70	110	230	350	620	34	.67	100
10	14.2	15.0	14.2	120	330	590	39	.81	0	120	320	580	38	.78	0
11	17.4	16.2	16.1	160	300	570	35	.70	40	150	290	560	35	.70	30
12	16.4	12.1	12.7	110	270	490	33	.65	0	100	250	450	31	.60	0
13	13.4	12.8	13.7	120	320	560	37	.75	0	100	300	550	37	.75	0
14	15.2	14.8	14.0	150	340	570	36	.73	40	140	330	560	36	.73	30
Average Values:	15.4	14.4	14.5	144	344	584	37	.75	32	136	332	567	36	.73	29
Standard Deviation:	1.2	1.3	1.2	35.6	36.3	60.2	2.7	.08	32.1	38.8	38.5	62.4	2.9	.08	29.2
Maximum Values:	17.4	16.7	16.3	230	400	690	42	.90	110	230	400	660	41	.87	100
Minimum Values:	13.4	12.1	12.7	100	270	490	33	.65	0	80	250	450	31	.60	0

Normal Stress applied: Point 1 - 144 psf; Point 2 - 432 psf; Point 3 - 720 psf[1]

(1) 1 psf = 47.8 Pa

Table 3. Group III results, Sandy Clay vs. 40 mil HDPE textured

Test No.	Final Water Content, %			Peak Shear Strength, psf[1]						Post-Peak Shear Strength, psf[1]					
	Pt. 1	Pt. 2	Pt. 3	Pt. 1	Pt. 2	Pt. 3	φ	Tan φ	Adhesion	Pt. 1	Pt. 2	Pt. 3	φ	Tan φ	Adhesion
1	33.4	29.7	25.6	140	350	580	37	.75	30	120	320	540	36	.73	10
2	33.3	32.5	31.5	120	290	440	30	.58	40	90	270	410	29	.55	20
3	29.4	29.6	28.2	140	280	380	23	.42	90	90	240	310	21	.38	50
4	34.8	31.0	24.3	110	290	500	34	.67	0	90	240	420	30	.58	0
5	33.4	29.2	28.0	120	330	410	27	.51	70	90	240	360	25	.47	30
6	32.5	27.8	28.4	120	310	460	30	.58	50	100	220	400	27	.51	20
7	34.1	28.1	27.8	100	300	450	31	.60	20	80	210	410	29	.55	0
8	32.7	27.6	26.7	100	300	450	31	.60	20	60	230	340	26	.49	0
9	31.5	29.9	28.8	130	280	400	25	.47	70	80	220	350	25	.47	10
10	31.3	30.1	29.4	130	270	460	30	.58	40	100	220	410	28	.53	10
11	31.9	29.5	28.5	120	290	460	30	.58	40	90	250	370	26	.49	30
12	31.0	29.5	28.3	120	260	450	30	.58	30	90	220	410	29	.55	0
13	33.7	29.0	27.5	90	300	410	29	.55	30	90	250	360	26	.49	30
14	34.9	29.7	27.9	130	280	450	29	.55	40	90	240	400	28	.53	10
15	33.3	29.1	28.0	110	350	480	33	.65	40	90	260	470	33	.65	0
Average Values:	32.7	29.5	27.9	119	299	452	30	.58	41	90	242	397	28	.53	15
Standard Deviation:	1.5	1.2	1.6	14.6	26.7	47.2	3.4	.08	22.5	12.5	27.3	55.7	3.5	.08	15.1
Maximum Values:	34.9	32.5	31.5	140	350	580	37	.75	90	120	320	540	36	.73	50
Minimum Values:	29.4	27.6	24.3	90	260	380	23	.42	0	60	210	310	21	.38	0

Normal Stress applied: Point 1 - 144 psf; Point 2 - 432 psf; Point 3 - 720 psf[1]

(1) 1 psf = 47.8 Pa

Table 4. Group IV results, Clayey Sand vs. 60 mil HDPE textured

Test No.	Final Water Content, %			Peak Shear Strength, psf[1]						Post-Peak Shear Strength, psf[1]					
	Pt. 1	Pt. 2	Pt. 3	Pt. 1	Pt. 2	Pt. 3	φ	Tan φ	Adhesion	Pt. 1	Pt. 2	Pt. 3	φ	Tan φ	Adhesion
1	16.0	14.6	12.5	2390	5400	8880	31	.60	210	2240	4270	6230	20	.36	970
2	14.8	13.9	13.1	2820	5580	9800	27	.51	1150	2560	5150	8330	23	.42	1350
3	15.4	14.0	13.8	2700	5730	9030	25	.47	1440	2310	5010	7990	23	.42	1170
4	14.6	14.3	14.2	2510	5800	8430	29	.55	730	2270	5430	7500	26	.49	790
5	15.5	14.2	13.4	2690	6250	9070	30	.58	770	2290	5660	7970	28	.53	660
6	15.6	14.7	13.5	2780	5410	9480	32	.62	360	2220	3470	5400	19	.34	570
7	15.4	14.6	13.6	2550	5930	9740	34	.67	160	2440	5210	7440	25	.47	930
8	15.6	14.0	13.3	2170	6090	9940	35	.70	0	2110	5460	7140	25	.47	800
9	15.7	13.9	13.1	2530	6310	9060	31	.60	620	2490	5580	8590	29	.55	550
10	15.9	13.8	13.1	2930	6380	10000	33	.65	630	2860	6180	9220	30	.58	870
11	14.7	14.2	13.5	3070	6710	10060	33	.65	880	2970	6070	9690	32	.62	720
12	14.8	13.7	12.6	3030	6090	10610	35	.70	330	2950	5790	9430	31	.60	720
13	16.1	13.4	12.5	2750	5850	10260	35	.70	100	2480	5640	8720	30	.58	490
14	14.9	14.1	12.7	3190	6480	10140	33	.65	890	3020	6310	9780	32	.62	820
15	15.4	13.4	13.0	2810	6380	9460	32	.62	770	2670	5810	8440	28	.53	910
16	14.7	13.7	13.2	2560	5820	9720	34	.67	140	2460	5280	8170	28	.53	610
Average Values:	15.3	14.0	13.2	2718	6013	9605	32	.62	574	2521	5395	8128	27	.51	808
Standard Deviation:	0.5	0.4	0.5	265.0	387.5	584.6	2.9	.07	411.0	292.8	713.4	1202.6	4.0	.09	228.3
Maximum Values:	16.1	14.7	14.2	3190	6710	10610	35	.70	1440	3020	6310	9780	32	.62	1350
Minimum Values:	14.6	13.4	12.5	2170	5400	8430	25	.47	0	2110	3470	5400	19	.34	490

Normal Stress applied: Point 1 - 3600 psf; Point 2 - 8640 psf; Point 3 - 14,400 psf[1]

(1) 1 psf = 47.8 Pa

Table 5. Group V results, Silty Sand with Gravel vs. 80 mil HDPE textured

Test No.	Final Water Content, %			Peak Shear Strength, psf[1]						Post-Peak Shear Strength, psf[1]					
	Pt. 1	Pt. 2	Pt. 3	Pt. 1	Pt. 2	Pt. 3	φ	Tan φ	Adhesion	Pt. 1	Pt. 2	Pt. 3	φ	Tan φ	Adhesion
1	15.6	12.7	13.2	2850	6010	10320	35	.70	240	2770	5710	9490	32	.62	460
2	15.2	15.0	14.8	2970	6300	9630	32	.62	830	2960	6230	9210	30	.58	1000
3	17.2	14.2	13.7	2840	6510	9920	33	.65	620	2660	6210	9250	31	.60	640
4	14.2	14.1	14.4	2690	5910	9720	33	.65	320	2640	5700	8770	30	.58	670
5	14.7	14.8	13.3	2930	6210	9610	32	.62	770	2860	5860	8540	28	.53	1100
6	16.5	14.9	12.3	2880	6690	10860	36	.73	250	2840	6470	10020	34	.67	550
7	15.2	14.3	14.1	3070	6840	10370	34	.67	770	3000	6760	10020	33	.65	840
8	16.3	14.5	14.1	2930	6800	11050	37	.75	260	2650	6470	10250	35	.70	220
9	15.1	14.2	13.5	2770	6990	9850	33	.65	750	2720	6880	8910	30	.58	1120
10	16.2	14.6	13.7	3150	6140	9610	31	.60	990	3000	5580	8540	27	.51	1150
11	15.9	13.6	13.8	3000	6010	10610	35	.70	260	2990	6000	10050	33	.65	530
Average Values:	15.6	14.3	13.7	2916	6401	10141	34	.67	551	2826	6170	9368	31	.61	753
Standard Deviation:	0.9	0.7	0.7	131.4	381.6	527.6	1.8	.05	286.5	146.4	440.8	639.2	2.5	.06	310.1
Maximum Values:	17.2	15.0	14.8	3150	6990	11050	37	.75	990	3000	6880	10250	35	.70	1150
Minimum Values:	14.2	12.7	12.3	2690	5910	9610	31	.60	240	2640	5580	8540	27	.51	220

Normal Stress applied: Point 1 - 3600 psf; Point 2 - 8640 psf; Point 3 - 14,400 psf[1]

(1) 1 psf = 47.8 Pa

The strength envelopes for both peak and post-peak stresses were calculated using a best-fit linear regression through the peak or post-peak shear stresses selected. The intercept with the shear stress axis was reported as the adhesion and the angle of the slope was reported as the friction angle.

Summaries of the test data are presented in Tables 1-5. Tests are numbered in the order they were performed.

FINDINGS

As discussed previously, the test groups were divided into two areas: Groups I, II & III were performed at the low normal stresses of 7, 21 and 35 kPa (144, 432 and 720 psf); Groups IV and V represent higher normal stresses of 172, 414 and 690 kPa (3600, 8640, and 14,400 psf.). Tables 6 and 7 summarize the average friction angles, adhesions, standard deviations and the coefficient of variation for these groups.

Table 6.

Summary of Peak Friction Angles, Adhesions, Standard Deviation & Coefficient of Variance						
Group No.	Average Friction Angle, ϕ	Standard Deviation	Coef. Varience	Average Adhesion, c	Standard Deviation	Coef. Varience
I	30	3.9	12.9	55	31	56.4
II	37	2.7	7.3	32	32	100.0
III	30	3.4	11.4	41	23	56.1
IV	32	2.9	9.1	574	411	71.6
V	34	1.8	5.3	551	287	52.1

Table 7.

Summary of Post-Peak Friction Angles, Adhesions, Standard Deviation & Coefficient of Variance						
Group No.	Average Friction Angle, ϕ	Standard Deviation	Coef. Varience	Average Adhesion, c	Standard Deviation	Coef. Varience
I	28	5.6	20.0	37	37	100.0
II	36	2.9	8.1	29	29	100.0
III	28	3.5	12.5	15	15	100.0
IV	27	4.0	14.8	808	228	28.2
V	31	2.5	8.1	753	310	41.2

The average peak friction angles for the low normal stresses, Groups I, II & III, ranged from 30° to 37°, and the standard deviations ranged from 2.7 to 3.9. The lower angles with greater variance were for sandy clays, while the silty sands show higher friction angles with less variance. The peak angles and standard deviations for the high normal stresses, Groups IV and V, varied less than the low normal stresses, and ranged from 32° to 34° with standard deviations of 2.9 and 1.8, respectively. The average post-peak friction angles for the low normal stress group ranged from 28° to 36°, and the standard deviations ranged from 2.9 to 5.6. The post-peak angles and standard deviations for the high normal stress group again varied less than the low normal stress group as did the peak values. The average post-peak angles for the high stress group were 27° and 31°, the standard deviations were 2.5 and 4.0. This data shows that there is less variation in test results at higher normal stresses than at lower stresses.

The adhesions from all the tests results gave the greatest amount of variability. In most cases, the standard deviation was greater than 50% of the average value of adhesion. Again the variance decreased with the higher normal stresses.

The standard deviations for the friction angles in group I, both peak and post-peak, are greater than the other groups. This was due to the fifth test's third point, which had shear stresses over 200 psf greater than the average. If this point is omitted the standard deviations for peak and post-peak friction angles reduce to 2.4 and 4.5, respectively. This indicates how a seemingly small change in water content for an individual test point will lead to misleading results.

The Mohr-Coulomb shear strength parameters, namely adhesion, c, and internal friction angle, ϕ, model the shear strength of the soil / geosynthetic interface over a wide range of confining pressure. The group I, III, IV, and V test results show a general trend of decreasing friction angle with increasing adhesion. This inverse relationship means that at a given confining pressure, the total shear strength, τ, where $\tau = c + \sigma \tan \phi$, may not vary as much as the variability of the Mohr-Coulomb parameters shown in tables 6 and 7. For an engineering analysis, the actual variation in the interface shear strength will depend on the confining stress at the interface.

The final water contents were all greater than the placement water content. This shows some increase in saturation occurred. The final water contents decreased with increasing normal stress, which follows standard consolidation theory, where increases in load force excess water to drain from the pore water system resulting in a denser soil mass and a lower water content. The standard deviations for these indicates that there was a very close control of specimen water contents. Measured shear stresses also reduced for a given test when the water content increased.

Other studies have noted similar results. Rivette, Spikula and Nava (1993) noted peak and post peak friction values based on six replicate tests, ranging from 32° to 38° for peak angles and 33° to 52° for post peak values. Again the range of adhesions were also greater for post- peak than peak friction angles. The authors also discuss the difficulty in repeatability with the test.

The author notes that in a sample reference program conducted by the American Association of State Highway Transportation Officials (AASHTO), similar standard deviations occurs for simple soils tests. These deviations range between 1.2 and 5.8 for the common tests, Atterbergs and gradation analysis, and

increase to 9.5 for a less common test, the R-Value. It is concluded that the standard deviations obtained from these data are very reasonable.

DISCUSSION

These tests are limited to a select group of soils and may not apply to other soil types. Soils such as fat clays with low permeability may have larger standard deviations due to the effects of pore pressure, poor drainage conditions and tests run too rapidly to allow for pore pressure dissipation. Project specifications set the required shear rate for these tests, and pore pressure during shear may have effected the results. Multiple tests on geotextile vs. a smooth geomembrane have not been successfully completed to show the variability of their relationships. An ASTM sub-committee conducted a round robin test using several labs, to evaluate the reproducibility of the current ASTM test standard. A geomembrane vs. geotextile were used in this study. The results were not acceptable due to a large variation in the data. Studies are currently underway to improve calibration methods and other variables before attempting another round robin.

Tests performed on presumably identical materials using presumably identical test methods do not, in general yield identical test results. Random errors inherent in every test procedure attribute to this. Test procedures may have unclear guidelines which lead to a difference of interpretation. Seemingly insignificant equipment variations have their influence. The factors that may influence the outcome of a test cannot be completely controlled. Similarly, the difference between test results from two or more groups of material will not indicate a quality difference if that difference is understood to be attributed to the test or material variability. A standardized test method, the personal, equipment, equipment calibration and the testing environment are key elements that must be controlled to properly evaluate a test and the test results accuracy.

Based on the authors experience and the experience of others, soil vs. geosynthetics interface frictional characteristics are not unique and are dependent on several user controlled test conditions. Substrates and superstrate types and usage may vary between labs. The type and usage of these can attribute to differences in tests results. Drainage conditions, shear rates, sample preparation and remolding/compaction methods can vary and also effect the results. This author strongly encourages the use of experienced labs and trained technicians. The participation in society organizations, accreditation and continual education is strongly recommended.

The intent of this paper is to present a large data base of similar tests, conducted on similar products, and demonstrate that the frictional characteristics of a particular soil vs. geosynthetic interface are not unique, and vary over a range of values. It is hoped that the data presented here will aid design engineers and increase their understanding of the possible ranges in frictional properties of soils and geosynthetics. This author encourages the use of multiple shear tests to minimize both the design engineer's and owner's risk.

It should be noted that the results presented here do not represent the request of a designer to assist in his/her design, but an after design requirement to assure compliance to the design!

The variability of the interface shear strength noted herein leads to several implications to designers. During the design phase the design engineer must specify enough tests to develop a statistically meaningful population. There is no firm rule as to the size of this population; the variations will depend upon the unique properties of the soils and the types of geosynthetic materials to

be used. For example, textured liner may result in higher variability than smooth material. The design engineer must consider the testing to be complete only when the population of data allows for reasonable statistical analysis.

During the design the engineer should also consider that the interface shear strength is not a singularity. There will be spatial variations and the design should include provisions for this. One approach is to use a probability of failure analysis in place of or to augment the conventional factor of safety approach. Another is to consider the consequences of local failures, then design a containment system that can tolerate such occurrences without breach. Simply using the minimum value is probably too conservative for most applications.

During construction these variations can be accommodated by allowing for both an average and a minimum test value in the specifications, and by specifying an adequate number of tests. The variation found in the design testing will be a good indicator of the variation to be expected during construction. Acceptance/rejection criteria based on a single test should be avoided.

REFERENCES:

GRI Test Method, Standard Test Method for "Interface Friction Determination By Direct Shear Testing", Geosynthetic Research Institute, Drexel University, 1991, pp. 1-10.

ASTM D 5321 (1992) "Standard Test Method for Determining the Coefficient of Friction of Soil and Geosynthetic or Geosynthetic and Geosynthetic Friction by the Direct Shear Method", American Society for Testing and Materials, Philadelphia, Pennsylvania.

Rivette, Chuck A, Spikula, Dan R., and Nava, Robin C. (1993) "Concerns and Experiences with Textured Geomembranes," Proceedings 7th GRI Conference on Liner Systems: Innovations, Concerns and Design, Industrial Fabrics Association International, St. Paul, MN. pp. 131-142.

ARML, Soil Proficiency Program, Report for samples 119 & 120, October 1995, AASHTO Materials Reference Laboratory, Gaithersburg, MD.

SHEAR STRENGTH OF GEOSYNTHETIC CLAY LINER SYSTEMS

FEKI N.*, GARCIN P.*, FAURE Y.H.*, GOURC J.P.*, BERROIR G.[+]

* IRIGM, University of GRENOBLE, France
[+] CEMAGREF, Anthony, France.

ABSTRACT

In order to follow the behavior of a liner system on the slope, it was decided to carry out a real scale experimentation at Montreuil/Barse (France). Two different systems are tested on slopes 1/1 and 1/2 of a landfill cell. The different components of the liner system are equipped for displacement measuring. At the same time a laboratory program is carried out to evaluate the shear strength of the materials and of their interfaces. The obtained characteristics are used to determine the theoretical stability of the different systems by limit equilibrium methods. The collected data, compared to the predicted stability, constitute an efficient way to validate these design methods.

INTRODUCTION

Four experimental cells were realized in an existent municipal waste landfill at Montreuil/Barse (France) with the support of the French Agency for the Environment (ADEME). The research was piloted by the French Research Institute of Agriculture and Environmental Engineering (CEMAGREF of Antony). The in situ experimental program was performed by a French waste management company CGEA-ONYX. Publics laboratories, CEMAGREF, LRPC of Nancy and I.R.I.G.M (University of Grenoble) were associated (Tanays et al, 1994).

One of these cells (square area of 50 x 50 m²) was constructed in order to study the behavior of a Geosynthetic Clay Liner (GCL) on the slopes 1/1 and 1/2. The GCL is covered by a granular soil to confine the bentonite in-between the GCL's geotextiles and to protect it against the mechanical and biochemical damaging.

Two kinds of cover soil were tested (Figure 1). On the slope 1/2, the GCL is covered by a gravel or by a silty sand layer. On the slope 1/1 the GCL is covered by silty sand layer. A geosynthetic cellular structure was used to confine it on the slope 1/1 and a geotextile was also

placed between the silty sand and the GCL as a mean of reinforcement. On the slope 1/2, the silty sand was unstable and was progressively eroded after big rainfalls.

The bentonite of the GCL is confined between two geotextiles stitched longitudinally. It was laid on the subgrade soil (clay), anchored on the top of the slope and covered with :
- 0.17 m of silty sand confined in geosynthetic cellular structure on the slope 1/1 (Figure 1a).
- 0.3 m of gravel or silty sand on the slope 1/2 (Figure 1b)

The stability of the liner system (granular soil, geotextile, GCL, etc.) is depending on the lowest shear strength part. This part could be either the interface between two successive layers or inside a layer itself, for example, in this case, the silty sand or the GCL. Then it is necessary to determine not only the mechanical properties of the different interfaces (friction between granular material and GCL or geotextile, or between geotextile and GCL, etc.) but also the internal shear strength of the GCL and of each layer.

To conduct the stability analysis of the liner system, an experimental program was carried out to evaluate the shear strength at critical interfaces using a large box. We detail the operative method which concern the fixation of geosynthetics, physical conditions of soils and application of vertical load.
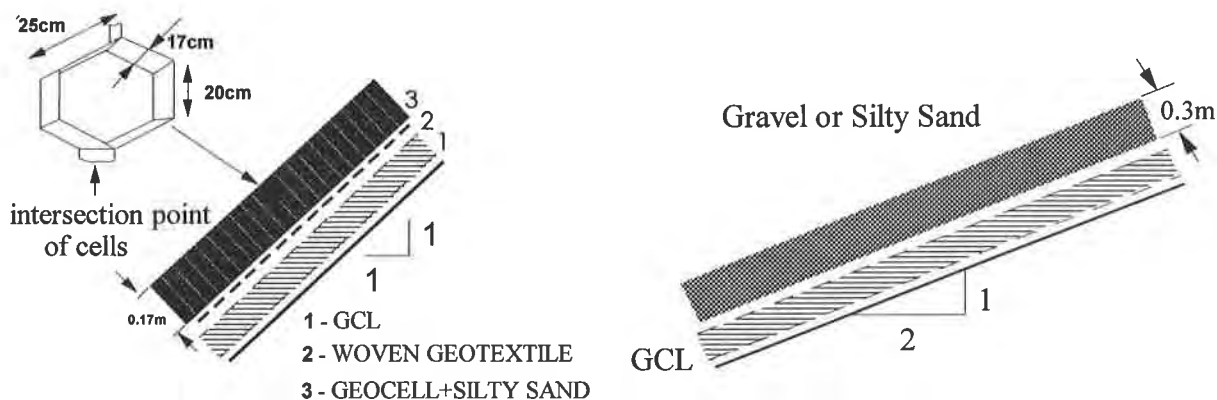
(a)- Cross section of the GCLiner system on the slope 1/1.

(b)-Cross section of GCLiner system on the slope 1/2.

Figure 1 : Cross section of the liner systems on 1/1 and 1/2 slopes for the experimental GCL landfill cell.

DIRECT SHEAR TESTS

In order to characterize the different materials used in the field and their interfaces, direct shear tests are realized in the I.R.I.G.M laboratory using a 300 mm x 300 mm direct shear testing apparatus. It is fitted with electronic gauges for monitoring the shear forces applied to test specimens and its horizontal displacement. The normal stress is applied by an hydraulic jack controlled by a steam gauge.

In this section we present the different experimental conditions used to determine the shear strength of the different interfaces and of the internal shear resistance of GCL. In all tests, the lower box moves at a constant rate of 1 mm/mn. The normal stress is distributed by a membrane and controlled with a steam gauge. Normal stresses applied on the sample interfaces during testing are 25, 50, 75 and 100 kPa.

Soil / GCL interface (Fig. 2) :

The lower GCL's geotextile (300 x 300 mm) is fixed on a rigid support (to assure the flatness of contact area). One extremity of the upper GCL's geotextile (500 mm length) is turn down around and glued to the PVC plate, the other is horizontally laid so that the contact area remains constant during the test. The PVC plate is setting on a rigid support.

The cover soil (gravel or silty sand) is compacted in the upper box with 50 mm thickness, with a dry density and a water content representative of field conditions. These combinations include :
- Silty sand/GCL
- Gravel/GCL.

Geotextile / GCL interface (Fig. 3) :

The GCL specimen is installed with the same procedure as described above but both sides of the upper GCL's geotextile are turn down around the PVC plate. The contact area initially 300 mm x 300 mm decreases during the test, then it must be taken into account to compute the shear stress.

In the upper box, the cover soil (silty sand) is surrounded by the woven geotextile to be tested. It is laid on the GCL. The silty sand is compacted to initial dry density of 16 kN/m^3 and at initial water content of 14%.

Internal GCL shear strength (Fig. 4) :

The lower GCL's geotextile is glued on a PVC plate fixed in the lower shear box. On one side it is anchored to the lower box and free on the other side. The upper GCL's geotextile is also glued on a PVC plate blocked inside the upper shear box.
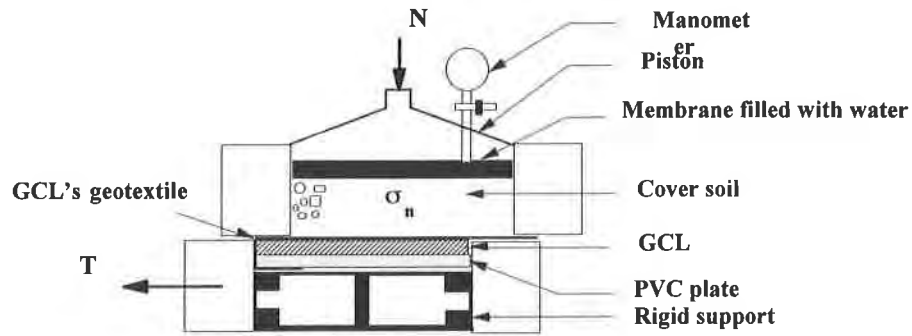
Figure 2 : tests condition for measuring shear strength of Soil / GCL interface
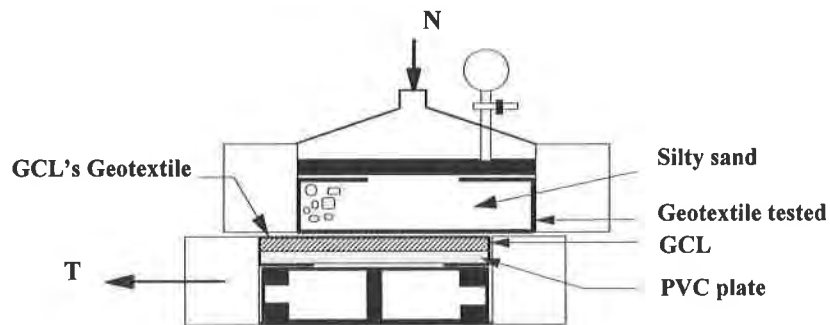
Figure 3: Test conditions for measuring shear strength of Geotextile / GCL interface
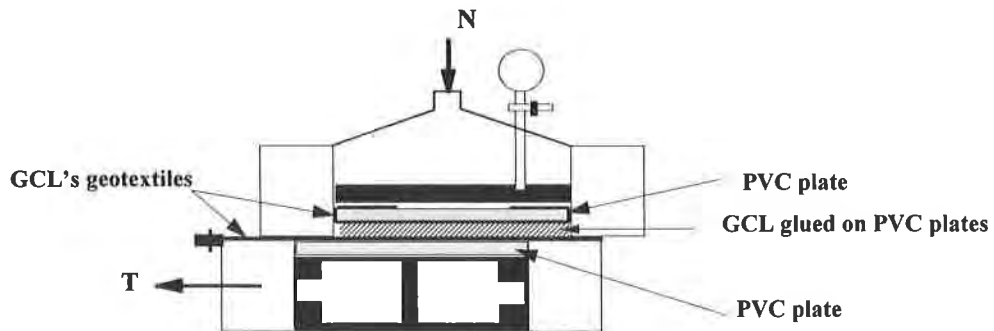
Figure 4: Tests conditions for measuring internal shear strength of GCLs.

TEST RESULTS

Soils internal shear strength :

First tests were realized to characterize the internal shear resistance of the soils (Gravel and silty sand and clay subgrade). The friction characteristics are given in Table 1.

Table 1 : Soil friction characteristics. $v = 1$ mm/mn; $25 < \sigma_n < 150$ kPa.

soil	unit weight (kN/m^3)	water content	ϕ (°)	c (kPa)
Clay	20	20%	0 °	60
Gravel	18	6%	41 °	0
Silty sand	19	13-14%	37 °	8

The mechanical properties of the different interfaces are called :

- ϕ_{g1}, C_{g1} : friction angle and cohesion of the Geotextile / GCL interface,
- ϕ_{g2}, C_{g2} : friction angle and cohesion of the silty sand /GCL interface
- ϕ_{g3}, C_{g3} : friction angle and cohesion of the gravel / GCL interface.

Geotextile / GCL Interface

GCL/GT interface samples are tested under 25, 50, 75 and 100 kPa. The relationship shear stress-shear displacement (Fig. 5) doesn't show any particular behavior. The slight peak obtained under 100 kPa, is due to the presence of the silty sand above the geotextile. It is important to note that the maximum shear stress is mobilized after a displacement of 10 mm under a normal stress of 25 kPa which is relatively important. The friction angle is 15° (Fig. 6).

Silty sand / GCL Interface

GCL/silty sand samples are tested under 50, 75 and 100 kPa. The shear stress continuously increases during the period of test (1 hour) (Fig. 7). This behavior seems to be related to the kind of soil. In fact the same observations are available for the sand/sand shear tests. The increase level of the shear stress is very low and require an important displacement. The maximum values of the shear stress obtained at the end of tests are considered to determine the interface shear strength. The found friction angle is 26° and the cohesion is 2 kPa (Fig. 8).

GCL/Gravel interface

The GCL/Gravel samples are tested under 25, 50 and 75 kPa (Fig. 9). The shear stresses increase with the normal stress and reach a constant stress level. The friction angle corresponding is 40° (Fig. 10). The interface properties values obtained are given in table 2.

Table 2 : Mechanical characteristics of the tested interfaces.

interface	normal stress (kPa)	interface characteristics
GCL/GT	25,50,75,100	ϕ_{g1}=15°, C_{g1}=0 kPa
GCL/Silty sand	25,50,75,100	ϕ_{g2}=26°, C_{g2}=2 kPa
GCL/Gravel	25,50,75	ϕ_{g3}=41°, C_{g3}=0 kPa

GCL internal shear strength :

In this section we present the principle of the test to check the GCL internal shear strength. Unfortunately it was not possible to test a stitched GCL. Tests were carried out only on GCLs linked by needlepunching.

This approach was only to show the feasibility of this kind of test. Of course, the results obtained on needlepunched GCLs are not completely comparable with stitched one.

The results concern dry specimens only. There is no problem to test wetted specimens : further researches are going on to look at the influence of wetting time, swelling, shearing speed, etc. Results are presented in Garcin (1997). The stress / displacement relationship shows a maximum shear stress very high and constant whatever the normal stress is, Figure 11. It corresponds to the fibers failure. The GCL behavior is analog to a quiet purely cohesive material. In fact the Mohr diagram, Figure 12 gives a small friction angle (8°) and a cohesion of 175 kPa.

After the peak the residual shear stresses are depending on the normal stress : it is a cohesionless behavior with a friction angle of 29°, Figure 12.

If GCLs are saturated, the peak behavior is the same, because it corresponds to the fibers failure. On a other hand, the shear residual stresses are very low : pure cohesive behavior is obtained with an undrained cohesion of 17 kPa (Garcin, 1997).

With that mechanical characteristics, the resistance of the dry GCL is good enough compared to the shear strength of geotextile / GCL interface or to the Silty sand / GCL interface.
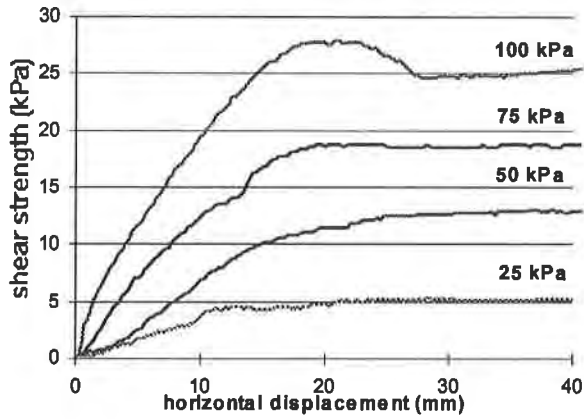
Fig. 5 : Shear stress for Geotextile/GCL interface.
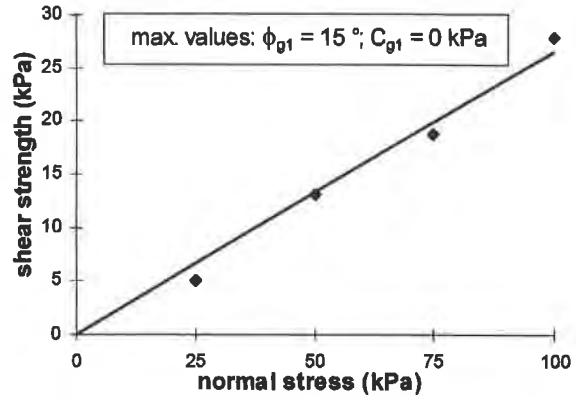
Fig. 6 : Mohr diagram for Geotextile/GCL interface.
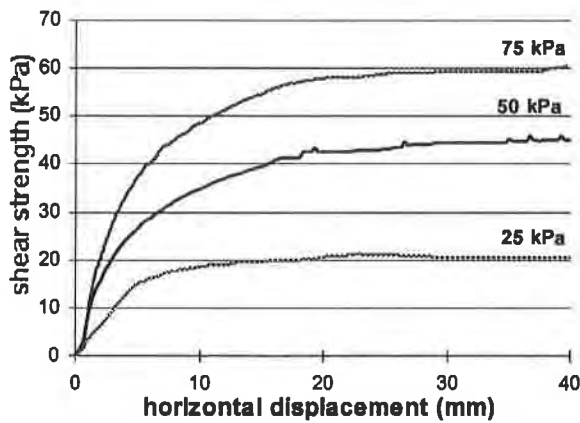
Fig. 7 : Shear stress for Silty sand/GCL interface
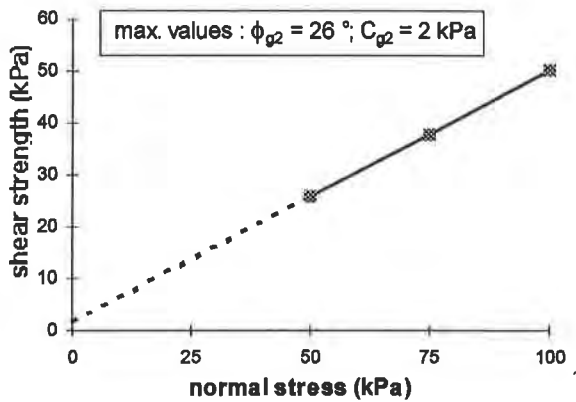
Fig. 8 : Mohr diagram for Silty sand/GCL interface.
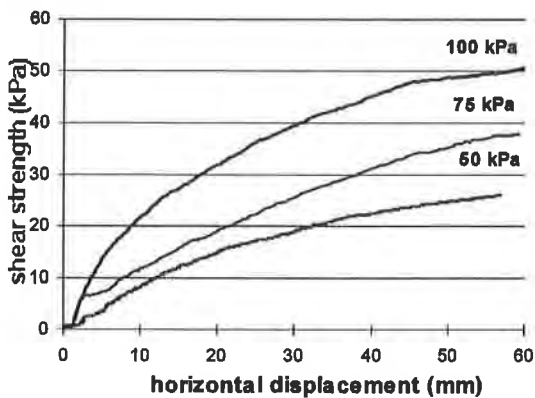
Fig. 9 : Shear stress for Gravel/GCL interface.
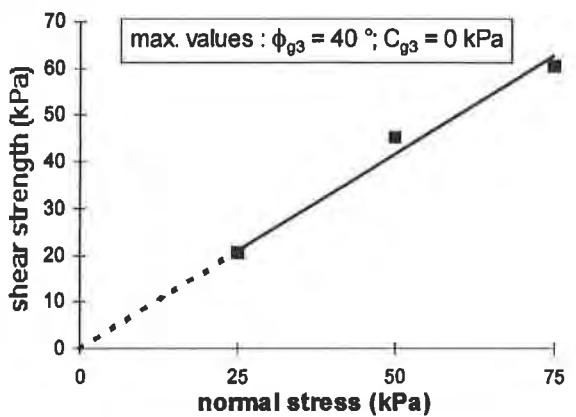
Fig. 10 : Mohr diagram for Gravel/GCL interface.
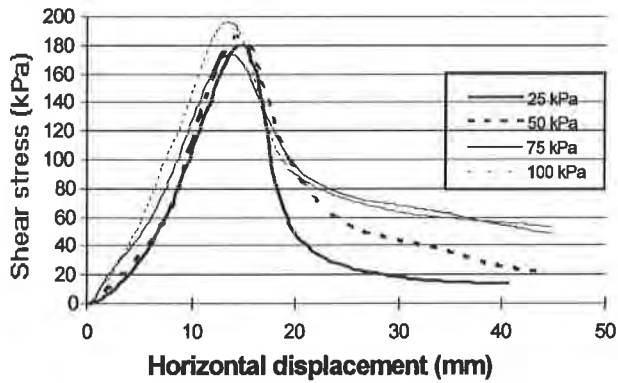
Fig. 11 : Shear stress / displacement relationship for GCL internal shear test.
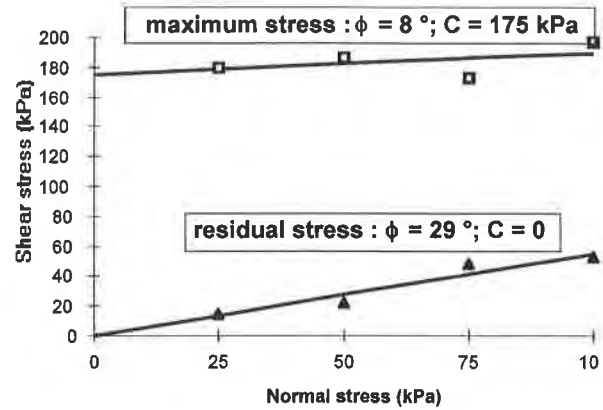
Fig. 12 : Mohr diagram for GCL internal shear test.

FULL SCALE EXPERIMENTATION DATA

The stability of the GCL after laying the cover soil on the slope, and after filling the cell with waste, is checked by measuring the displacements in each element of the lining system. The data presented in this paper are also available in Tanays et al (1994).

Lining systems are equipped for measuring the displacements in the GCL and in the cover soil. A example of the positions of the measuring points (landmarks) is given in Figure 13.
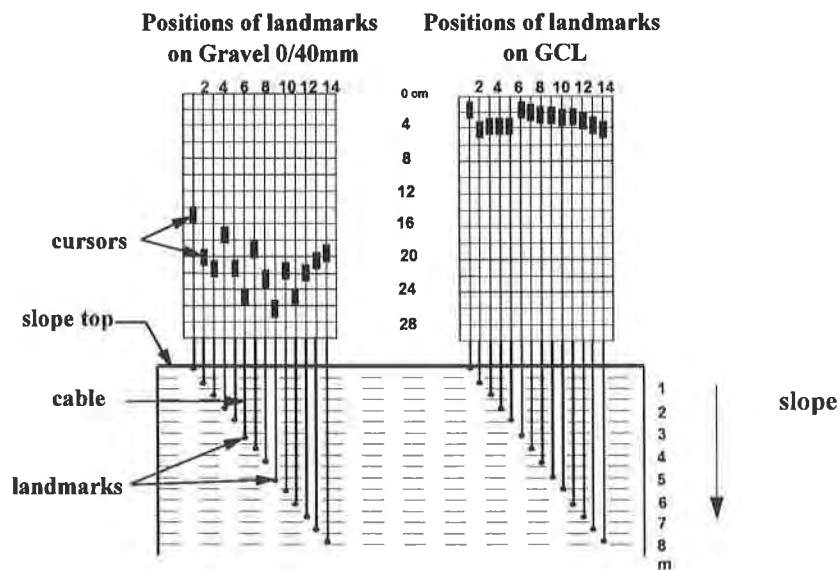
Figure 13 Example of instrumentation on the slope 1/2.

The displacements in the liner system are measured :
- For the slope 1/1 : 13 points in the GCL and 9 are fixed at the intersection of the alveolar structure filled with silty sand;
- For the slope 1/2 : 14 points in the GCL and 14 the gravel.

The landmarks are linked by thin metallic cables to a monitoring box. Displacements are measured by a cursor attached at each cable braced by counterweights. A 5 mm measuring error is estimated.

DISPLACEMENTS MEASURED

The displacements were measured before filling waste in the landfill cell. They are done for silty sand on 1/1 slope and for gravel for 1/2 slope.

Behavior of the lining system on the slope 1/2

The distribution of displacements along the slope is given for the GCL and the gravel, 43 days after placing the cover soil on the slope (Figure 14). The displacements in the GCL are very low with regard to the displacements in the gravel layer. They are more important on the slope toe. Note that the specific construction does not allow soil buttress at the toe. These measures remained unchanged for 500 days of observations.

Average strains calculated from the displacements of two consecutive points, show that the GCL is extended on the lower half of the slope. The maximum strain is about 1.5%.
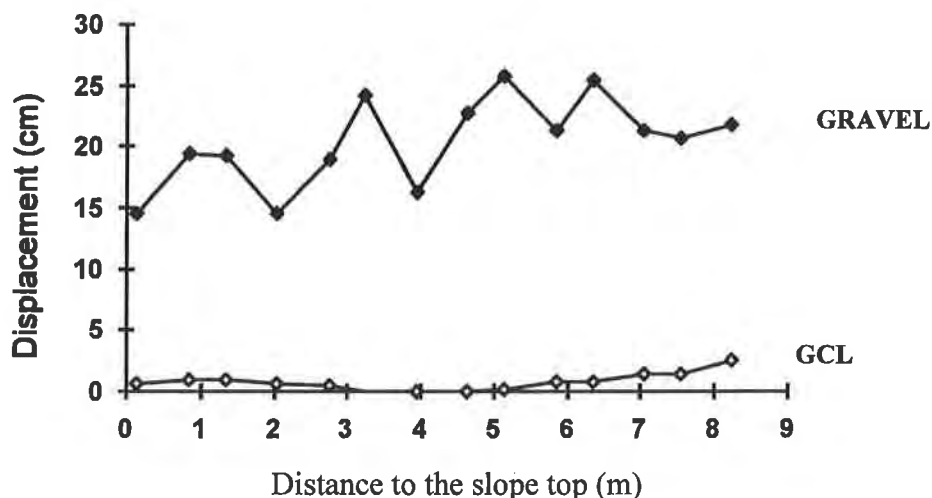
Figure 14: Displacements in the GCL and in the gravel along the slope 1/2, 43 days after installation.

Behavior of the lining system on the slope 1/1

The displacements in the GCL and the confined silty sand show a more important difference compared to the previous case (Figure 15).

The Silty sand displacements show a movement of about 30 mm, one day after its installation (14 Oct.94). These movements are significantly higher after 44 days and reach a displacement of 450 mm at mid-slope. Measurements done 3 months after the installation have shown a stabilization.

One day after its installation, the GCL is extended at the top of the slope and the average strain reached 5.5%. After this date, the displacement decreased significantly till 3 months of observations (Fig. 16). Due to the excessive strains (>2%), the important displacements are assumed to have caused partial failure of the GCL at different landmarks.
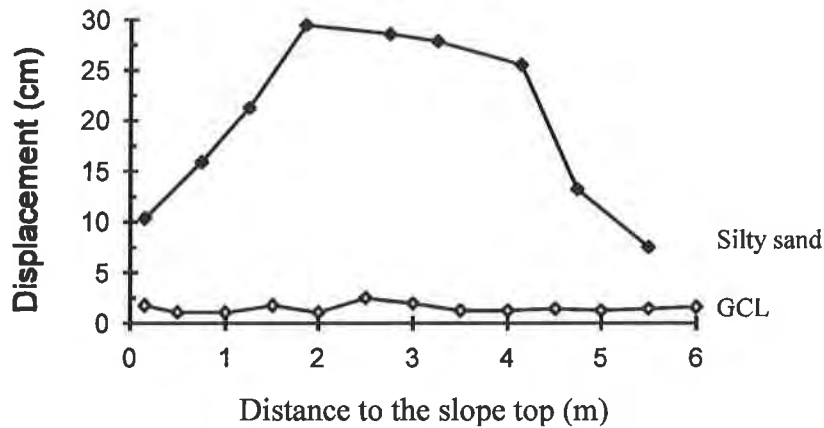
Figure 15 : Displacements in the GCL and in the confined silty sand just after installation 1/1 slope (13 Oct.94).
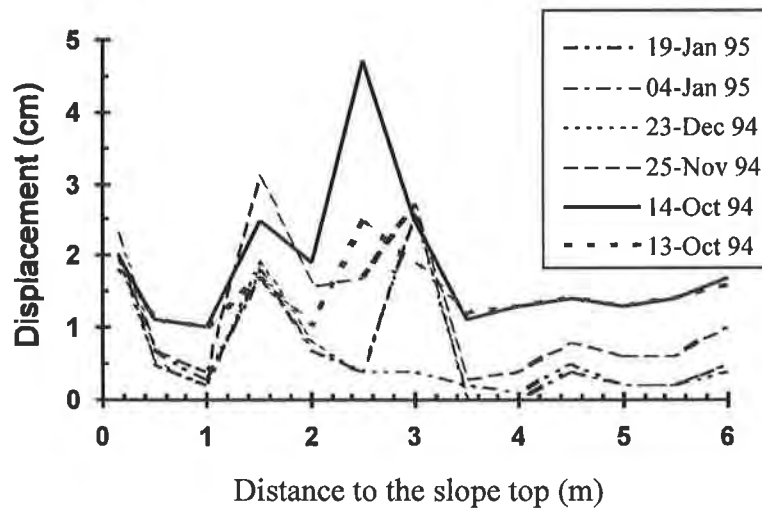
Figure 16 : Evolution of displacements on the GCL 1/1 slope (until 3 months after installation).

STABILITY ANALYSIS

In this paper the stability of the lining systems is only analyzed by limit equilibrium methods :
- Giroud (1989) and Koerner (1991) method based on limit equilibrium of two wedges ;
- The software ETAGE developed by the LCPC (Soyez et al, 1990) and based on the perturbation method.

The two methods give the safety factor and evaluate the necessary tension to ensure the stability of the lining system corresponding the desired safety factor.

The software ETAGE was developed for the stability study of lining systems where the length on the slope is very large with regard to the thickness of the cover soil. The failure surface is determined by a linear segment bounded at the top and at the toe of the slope by two circular arcs and supposed to pass above the segment CD as considered by Giroud-Koerner (figure 17).
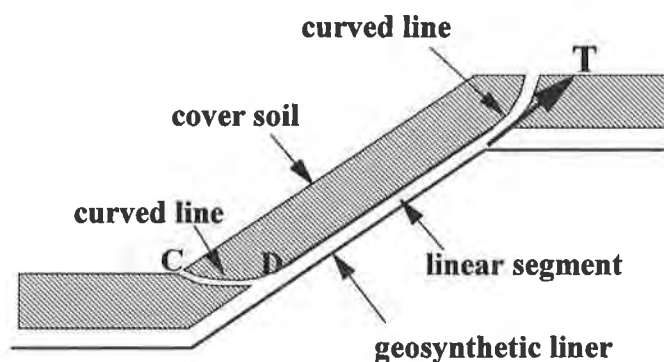
Figure 17 : Geometry of the failure surface used in ETAGE software.

If the security factor Fs, estimated by ETAGE computations, is found less than the desired safety factor Fr (given by the author), the resolution of the system is undertaken after adding a tensile force T supported by mean of the reinforcement (geotextile or geogrid). This force is calculated by $T = F_m(1 - F_s / F_r)$, where Fm is the average driving force calculated at the intersection points between the circular arcs and the linear segment (Figure 17).

The friction characteristics of the different materials and their interfaces determined by the shear tests (table 1 and 2) have allowed this stability analysis.

Stability analysis of the liner system on the slope 1/1

Two simulations are realized without and with the geotextile added between the confined silty sand and the GCL, to illustrate the beneficial effect of the woven geotextile used as a reinforcement. The computation have been done with :
- a unit weight of silty sand $\gamma = 19$ kN/m^3 and a soil thickness h = 0.17 m.
- a slope angle β =45° and a slope length L = 6.5 m.

Without geotextile, the tension T_{GC} is supported by the geocell only (Table 3).

With the geotextile, the failure surface is obtained at the interface GCL/GT, Table 4, and the total tension T_T calculated when Fs<1, is provided by both the geocell and the woven geotextile.

Table 3 : Slope 1/1 : Stability analysis without geotextile

silty sand		GCL/soil		method I		ETAGE	
$\phi(°)$	C(kPa)	$\phi(°)$	C(kPa)	Fs	T_{GC}(kN/m)	Fs	T_{GC}(kN/m)
37	8	26	2	1.80	0	1.86	0
37	0	26	0	0.84	5	0.77	5

Table 4 : Slope 1/1 : Stability analysis with geotextile.

silty sand		GCL/GT		method I		ETAGE	
$\phi(°)$	C(kPa)	$\phi(°)$	C(kPa)	Fs	T_T(kN/m)	Fs	T_T(kN/m)
37	8	15	0	1.05	0	1.05	0
37	0	15	0	0.81	8.1	0.63	9

The safety factors without reinforcement, calculated with the experimental shear characteristics, are greater than one. These results do not reflect the real behavior because the measured displacements of the confined silty sand were very large.

Tables 3 and 4 show also results assuming that the soil and the interface GCL/silty sand are cohesionless : due to the field conditions, high compaction of the soil is not allowed.

Then, without geotextile, the tension supported by the geocell is estimated to 5 kN/m. With the geotextile, the total tension is 9 kN/m. A greatest part of this tension should be effectively supported by the geotextile as it is more stiff (J=2500 kN/m). The real tension in the geocell would be determined if the tension in the geotextile could be measured.

Without buttress, the required total tension $T = [\gamma h L \sin \beta - \gamma h L \cos \beta tg\phi_{g1}]$, to obtain an equilibrium state (Fs=1), is 10.8 kN/m. The buttress force is estimated to 2 kN/m by the difference between tensions with and without buttress effect.

Stability analysis of the liner system on the slope 1/2

As the specific construction doesn't allow any soil buttress at the toe, the safety factors are calculated with this hypothesis. In ETAGE computations, the soil characteristics are decreased until zero at the buttress level.

.GCL-silty sand system :

The friction angle at the interface GCL/silty sand is slightly lower than the slope angle, which explain the failure occurred after laying the silty sand on the slope. The safety factor calculated by $F_s = tg\varphi / tg\beta$ (infinite slope hypothesis) is about 0.98.

The minimum safety factor, using ETAGE software, is roughly equal to the former F_s=1.01 (with γ=19 kN/m3, cover soil thickness h=0.30 m, length slope L=8.3 m, slope angle β=26.5°, soil friction angle ϕ=37°, and GCL/ silty sand interface friction angle ϕ_{g1}=26°). The critical state (slope β=26.56° and ϕ_{g1}=26°) and the low capacity drainage of the silty sand explain the failure of the slope 1/2.

.GCL-Gravel system :

The shear strength of the GCL/Gravel interface is high enough to ensure the stability of the liner system even without any buttress effect.

CONCLUSION

The difficulties to conduct shear tests with this type of geosynthetics, consists to find how to fix the GCL sample. Different types of anchorage are tested to achieve the one used for these tests.

To well approximate the shear characteristics, it is needful to conduct these tests with the same field conditions (normal stress, unit weight and water content of the cover soil). Also it would be necessary to complete these shear box tests by inclined plane tests because the normal stresses are generally low in the field.

These methods based on limit equilibrium methods under estimate the effect of soil strength. They have the advantage to be easy and rapid to use. They give a first approach on the liner system stability and the tension developed in the geosynthetic components and are enable to predict the important displacements measured. To have more realistic results, it is relevant to use numerical methods that take into account the strain compatibility and which give the displacements on the different components of the system (Villard et al, 1997).

ACKNOWLEDGMENTS

REFERENCES

Bressi G., Zinezi M., Montanelli F., Rimoldi P.(1995) « The slope stability of GCL layers in geosynthetic lining system ». Proceedings Sardinia 95, Fifth International Landfill Symposium, Italy; 2-6 Oct..

Garcin (1997) « Etude expérimentale du comportement hydraulique et mécanique des géosynthétiques bentonitiques ». Thèse de Doctorat de l'Université Joseph Fourier, Grenoble.

Giroud J.P. Beech J.F. (1989) « Stability of soil layers on geosynthetic lining system ». Geosynthetics'89 Conference, San Diego, USA.

Koerner R., Wu H. (1991) « Stability and tension considerations regarding cover soils on geomembrane lined sloped ». Geotextiles and Geomembranes 10, pp 335-355.

Long J.H., Gilbert R.B., Daly J.J. (1994) « Geosynthetic Loads Landfill Slopes : Displacement Compatibility ». Journal of Geotechnical Engineering, vol. 120, n°11, nov. 1994.

Tanays E., Letellier I., Berhnard C., Gourc J.P. (1994) « Behaviour of Lining Systems on Waste Landfills Slopes : An experimental Approach ». Fifth International Conference on Geotextiles, Geomembranes and Related Products. Singapore, 5-9 Sep.1994, pp 977-980.

Soyez B., Delmas P.H., Herr CH., Berche J.C.(1990) « Computer evaluation of the stability of composite liner ». Geotextiles and Geomembranes and Related Products, Balkema Rotterdam. pp 517-522.

Villard P., Gourc J.P., N. (1997), « Anchorage strength and slope stability of a landfill liner », Geosynthetic'97 (to be published)

INTERFACE STRENGTH TESTS AND APPLICATION TO LANDFILL DESIGN

HARI D. SHARMA, DONALD E. HULLINGS AND FRANCIS R. GREGURAS
EMCON, SAN JOSE, CALIFORNIA, U.S.A.

ABSTRACT

The purpose of this paper is to extend the database for interface friction values between geomembranes (specifically textured HDPE), geosynthetic clay liners (GCLs), soils, and admixed soils with emphasis on the stress/displacement behavior of soil/HDPE and various GCL interfaces. Interface strength data from 15 project sites, and 18 sets of tests between GCL/soil, GCL/geomembrane or internal GCL are presented. Two case studies for alternate base and sideslope liners, and a case study for an alternate cover liner are presented to illustrate how the data is used in actual design applications.

INTRODUCTION

With the development of higher landfills and more complicated multi-layer lining systems, the interface shear strengths in landfill design have become important. Interface strengths are critical for slope stability analyses and play a significant role in the ultimate capacity of landfills.

While the authors stress that there is no substitute for project-specific testing, a discussion of testing for various interfaces is relevant to design. This paper will discuss interface shear strengths between textured high density polyethylene (HDPE) geomembrane and either low permeability soil or geosynthetic clay liner (GCL). Current test methods and test variables will be discussed. Test results from various projects will be examined to develop relationships between soil properties and interface strengths and to evaluate the effect of certain test conditions. Most importantly, the application of interface shear strength testing to actual projects will be evaluated in three case studies.

DIRECT SHEAR TESTING AND INTERFACE STRENGTHS

It is generally agreed that direct shear testing is the proper method for developing interface shear strengths for landfill application. The American Society for Testing and Materials (ASTM) developed D5321 a decade ago specifically for this purpose. This is certainly not the only interface strength test procedures as other methods have been developed such as torsional ring, tilt table, and Texas double-ring (Gilbert, 1995). Testing discussed in the paper, however, was conducted in general accordance with ASTM D 5321 (ASTM 1995).

Many parameters are not well-defined by the ASTM D5321 method and are left to be determined by the engineer. The choice of parameters is important as it directly effects the results of testing. These parameters can be described as soil-related and geosynthetic-related parameters as summarized in Table 1.

Table 1
Possible Test Variables

Soil-Related	Geosynthetic-Related
Soil type	Geosynthetic type
Compaction	Sample preparation
Consolidation/Normal Load	Fixation
Strain rate	Strain rate
Saturation	Saturation

Parameters were determined to simulate field conditions with consideration for practical limitations on testing devices, time, and cost. An evaluation of all possible variations is beyond the scope of this paper, but the following factors were considered in our test program.

Box Size. 305-mm by 305-mm (12-inch by 12-inch) box was used in all the testing.

Fixation. In most cases, testing was performed to measure one interface with the geosynthetics firmly fixed by nailing, gluing or using a high friction striated plate.

Soil Type. Soils were generally low permeability soils, mainly silty clays (CL); silts (ML and MH) and clayey sands (SC) were also included. Soils are identified by type (according to the Unified Soil Classification System), plasticity index (PI), maximum dry density and optimum moisture content.

Geosynthetic Type. Geomembranes are textured HDPE from various manufacturers. The only other geosynthetic is GCL, again from a variety of manufacturers. The geosynthetic type is identified in either the text, tables, or figures.

Strain Rate. The rate used was about 1 mm (0.04 inches) per minute which is likely to result in partially drained conditions. Any exceptions are noted in the text.

Saturation. Except where noted, the interface was tested under submerged conditions and was allowed to saturated for a minimum of 16 hours before shearing. Geomembrane/soil interfaces are likely to be saturated under these conditions. GCLs were usually hydrated longer as they require at least 48 hours to hydrate.

Compaction. Compaction varied depending on the project requirements, but soil samples were generally compacted from 90 to 95 percent relative compaction at 2 to 6 percent above optimum moisture content (ASTM 1557). The effect of compaction was not evaluated in this study.

<u>Normal Stress</u>. Normal stress range from as low as 6.0 kPa to 24.0 kPa (125 to 500 psf) representing typical landfill covers and as high as 480 kPa (10,000 psf) to represent refuse loads on base and side slope liners.

STRESS/DISPLACEMENT BEHAVIOR OF SOIL/HDPE INTERFACES

Shear stresses are mobilized as displacements occur along geosynthetic/soil interfaces (actual strains generally are not used in direct shear test results). The peak strength, highest recorded stress throughout the whole range of displacements, is usually reached at small displacements (6-13 mm for 305 mm by 305 mm box). Behavior beyond displacement at peak can vary. Generally, two types of stress-displacement behaviors observed in direct shear tests are: (1) stress at large displacements is approximately equal to the peak strength as conceptually shown by curve A on Figure 1, and (2) for some interfaces stresses at large displacements are less than peak strength as shown on curve B. These behaviors are also discussed by Sharma and Hullings (1993). The minimum stress recorded for displacements beyond peak has been referred to as residual strength. As this term is somewhat misleading, the term post-peak strength will be used in this paper.

Evaluating post-peak behavior is important in determining shear strength parameters. Post-peak strengths (S_{pp}) may be as low a half the peak strength(S_p). This makes a significance difference in stability analyses with direct impacts on construction costs and landfill capacity. Reasons for drops in post-peak strengths may be related to soil behavior (soil properties, drainage, consolidation, etc.) or strictly the result of geosynthetic properties (e.g., breaks in stitching or needle punching of GCLs). The choice of which strength to use is a critical design decision that must take into account the stress-strain compatibility of the entire landfill system.

<u>Strain-Softening</u>. Post-peak interface strengths have been discussed in the literature with differences noted in behavior. Byrne (1994) noted drops in post-peak strengths in smooth geomembrane/highly plastic clay (PI=40 to 50) interfaces and referred to the drop in strength beyond peak as strain-softening. Tests were conducted at high strain rates (1 mm/min) to simulate field conditions at Kettleman Hills. Stark (1994) noted the same behavior for smooth geomembrane and the same type of clay using a torsional ring device. Post-peak strengths were 50 to 70 percent of peak strengths. Bemben and Schulze's (1995) tests on Connecticut River Valley glacial lake clay resulted in a 50 percent drop from peak strengths for plastic clay (PI=29) at the strain rate of 1 mm/min. Drops in post-peak strengths were less severe at lower strain rates (0.01 mm/min) approaching drained conditions. Fishman and Pal (1994) conducted drained shear tests with test data indicating some strain softening.

Cases are also cited, however, where no strain softening is noted for HDPE geomembrane and cohesive soil interfaces. In some of the first tests, Koerner and others (1986) noted that stress versus strain response curve for a range of clays and geomembranes were rarely strain softening. It should be noted that these tests were not conducted under submerged conditions. Ormans' (1994) tests on high plasticity silt indicated that peak and "residual" strengths were equal. The same was noted for Bee Canyon Landfill clay liner (Somasundarum and Khilmani 1991). While testing the effects of leachate on interface strength, Masada and others (1994) recorded no strain softening for a clay (PI=24) run under what was considered consolidated drained (CD) conditions.

Effect Of Plasticity On Strain Softening. A review of the literature indicates that strain softening may be related to soil plasticity. The effect of soil type on stress-displacement behavior was evaluated by comparing plasticity index (PI) to the ratio between post-peak and peak strengths (S_{pp}/S_p). Based on tests performed on 15 different low-permeability soils/textured HDPE geomembrane interfaces, the average S_{pp}/S_p ratio from tests under several overburdens is plotted against PI in Figure 2.

Although no direct relationship can be established, the general trend is decreasing s_{pp}/s_p ratio with increasing plasticity. The S_{pp}/S_p ratio is about 0.9 for PI values less than about 25 which indicates little strain softening for low plasticity compacted clays. Clays with higher plasticities (PI values over 30) have ratios as low as 0.4. Soils with high PI values but less fines (clayey sand) or elastic silt may have higher ratios than highly plastic clays. Further test data are required for such soils. Since the rate of pore pressure dissipation also decreases with increasing PI, Figure 2 could also reflect differences caused by negative pore pressures at lower displacements causing increased peak strength but not post-peak strength. This needs further evaluation.

Pore Pressures. Drainage conditions may play a role in strain-softening behavior. Dilative volume changes during shearing may induce negative pore pressures at the interface (Fishman and Pal, 1994; Bemben and Schulze, 1995). This suction pressure increases the effective confining pressure and hence the shear strength. It may be possible that strain softening in high plasticity clay is the result of undrained behavior at the interface. As the author's test program did not vary strain rate, this issue needs further evaluation.

STRESS/DISPLACEMENT BEHAVIOR OF GCL AND INTERFACES

The stress displacement behavior is even more complicated for interfaces involving GCL. The behavior may represent the interface between GCL/soil, GCL/geomembrane or internal GCL. While textured geomembrane may have some differences between products, GCL products vary more widely. GCLs can be adhesively bonded to a geomembrane or supported/attached to geotextiles. The geotextile supports may be woven or nonwoven and reinforced with stitching or needle punching. With so many variables, behavior is difficult to predict.

Behavior differs depending on the failure plane. Under low normal loads failure generally occurs along an interface with the GCL while at higher loads failure is through the GCL (internal). The normal load at which the failure plane changes depends on the material. Practical implications of such behavior are that under cover loads (i.e., normal stresses less than about 24 kPa) failures are along the interface while under large refuse loads failures may be through the bentonite.

The behavior between a GCL and soil may be similar to the behavior of the bentonite carrier and the soil. For GCL supported by geomembrane, the interface behavior between the geomembrane carrier and soil will be the same as geomembrane and soil. If the bentonite side is down against the soil, the strength would potentially be the strength of the bentonite. Unlike geomembrane-supported GCLs, geotextile-type GCLs may not behave like geotextile interfaces because of possible oozing and other effects of the bentonite. The GCL/soil interface typically has strengths slightly less than geotextile to soil depending on the degree of saturation of the bentonite.
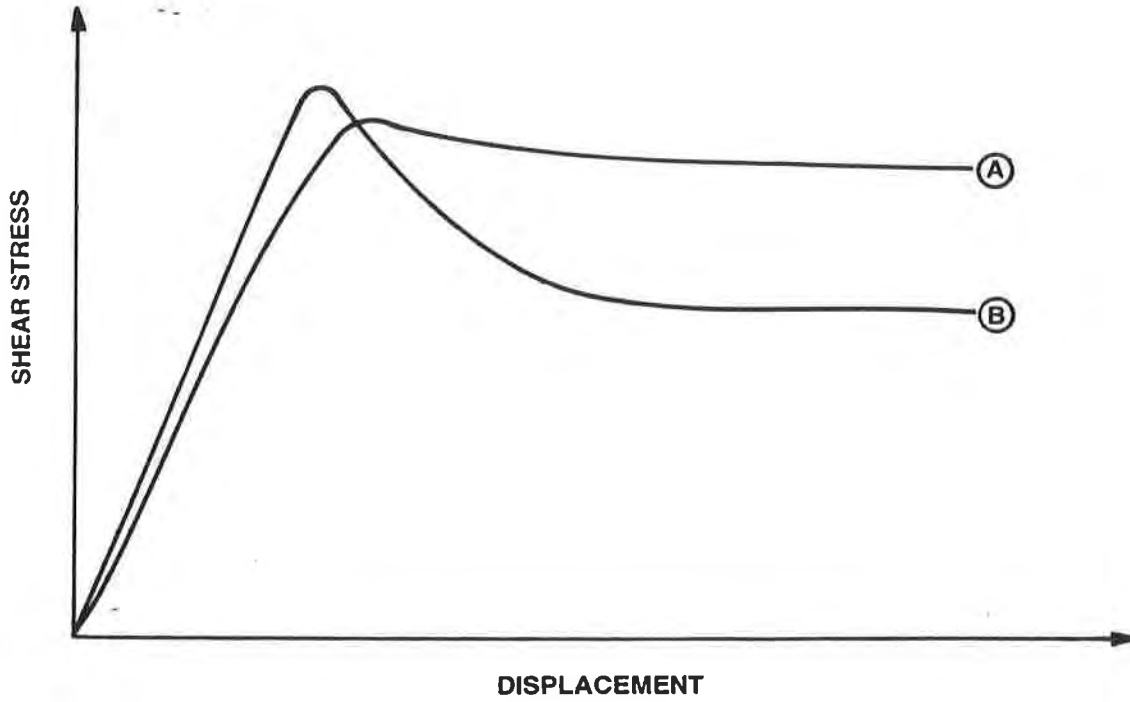
Figure 1. Idealized shear stress vs. displacement behavior
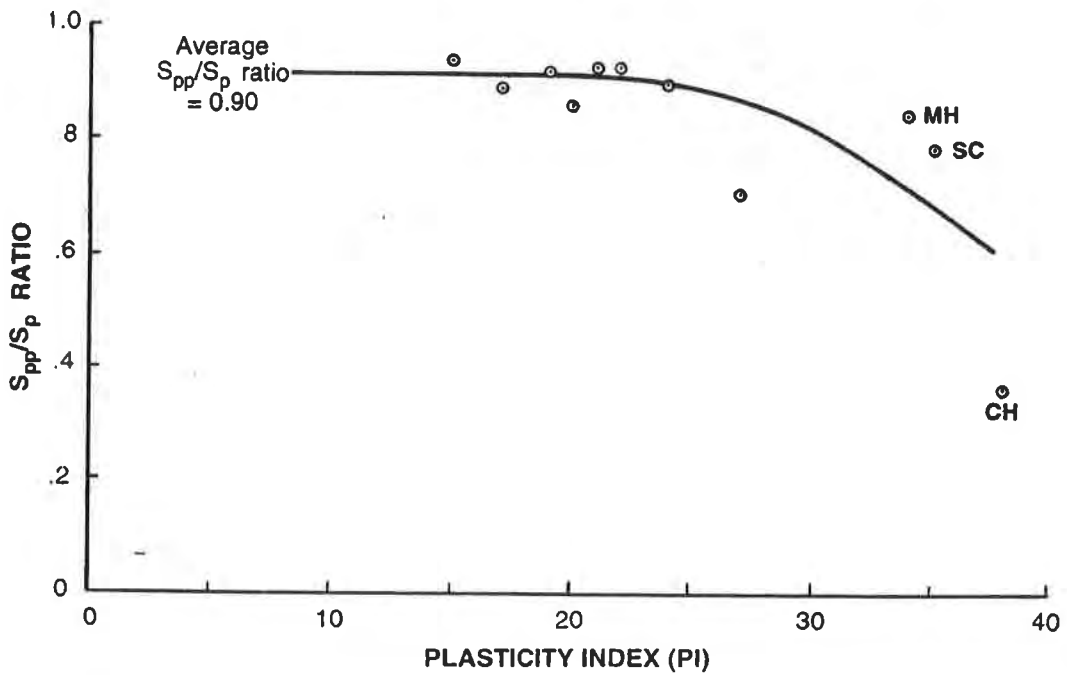
Figure 2. S_{pp}/S_p ratio vs. plasticity index

Similarly, the GCL/geomembrane behavior may be similar to geotextile/geomembrane behavior (for geotextile-type GCL). Geotextile/geomembranes have a pronounced peak as the geotextile fibers catch on the texturing. As fibers break or break loose from the texturing, the shear strength is reduced and may increase again as in GCL/geomembrane behavior. Byrne (1994) refers to this as slip-stick behavior. In his testing on three different GCLs the S_{pp}/S_p ratio ranged from 0.3 to 0.7.

SHEAR STRENGTH

The shear strength of a geosynthetic interface is generally not constant but increases with normal load. In this regard shear strength can be approximated similar to that of soils expressed in terms of friction angle and cohesion. Like soil strengths, geosynthetic interface strengths depend on soil type, normal load, and drainage conditions, among other parameters. The shear strength also depends on the stress/displacement behavior as discussed in the previous section.

<u>Strength Parameters For Soil/HDPE Interface</u>. Borrowing from traditional geotechnology, the interface strengths are often represented by cohesion and friction angle parameters. Often the cohesion term is referred to as adhesion (c_a) and the interface friction angle is represented by (δ).

A crucial mistake in interpreting test data is to assume linear behavior for conducting analyses. The shear strength versus normal load behavior is curvilinear but may be represented by multiple lines as suggested by the plot shown in Figure 3. Simple nonlinear equations, including that proposed by Giroud et al (1993) did not accurately fit the test data. The best-fit straight line for all normal loads can be misleading, especially at low loads where the parameters can dramatically overpredict shear strengths which would lead to obvious slope stability problems. Problems may also result in extrapolating data for higher normal loads. Data suggests that the curve may bend slightly downward at high loads and extrapolating data would again lead to overestimating the actual strengths.

When first interpreting interface shear strength data years ago, a single straight line was used to determine the friction angle and any c_a (or y-intercept) was ignored. It was felt that the c_a parameter may be test-related and could not be counted on in design. Ignoring the c_a also eliminated the possibility of overestimated strengths at low loads and was generally considered conservative. In addition to the best-fit straight lines, strengths were also represented by the friction angle corresponding to a representative straight line forced through the origin. While safe at low loads, such a line could overestimate strengths at higher loads.

For analysis, we have represented the strength behavior envelope as two or three line segments. The first segment generally goes through the origin and the last segment anticipates a small downward bend (i.e. lower slope). For each segment the slope and y-intercept is determined and used for finding the δ and c_a parameters over a given load range. No mathematical approach for segmenting the curves is proposed at this time. For specification purposes, various shear strengths at different normal loads are specified (e.g., 25 kPa shear strength at 100 kPa normal load and 90 kPa at 400 kPa normal load) and problems with interpreting data are avoided.

Strength Parameters For GCL And Interfaces. For GCLs a break in the curve for shear strength versus normal has a physical meaning and should be expected. At low normal loads the interface strength is largely frictional with the weakest plane being between the geomembrane and the GCL. At higher loads the internal shear strength of the GCL is lower than the interface strength. The interface strength is a measure of the combined strength of the bentonite (which have a small friction angle value under saturated conditions) and the strength of the reinforcement which is largely independent of normal load. The break in the curve is indicative of where the weakest plane shifts from the interface to inside the GCL, a typical relationship is shown in Figure 4. This behavior will be further discussed later in a case study.

CASE STUDIES FOR ALTERNATE BASE AND SIDESLOPE LINERS AND COVERS

Subtitle D (40 CFR 258) requires composite base and side slope liners below municipal solid waste landfills. The composite liner must consist of an upper flexible membrane liner (FML) underlain by a minimum 0.61m-thick low permeability (k $\leq$ 1 x 10^{-9} m/s) soil layer. If at a site this prescriptive liner standard is unreasonably and unnecessarily burdensome then an alternative liner system may be accepted provided it "is consistent with the performance goal" and "afford equivalent protection against water quality impairment". The following case histories demonstrate how interface strengths were interpreted and used in design applications for alternative liners and covers.

Case History 1. At a municipal solid waste landfill site in southern California obtaining low permeability soil was found to be very expensive. Therefore, a GCL was considered below the 60 mil HDPE geomembrane (FML) instead of a 0.61 m-thick (2-foot) compacted low-permeability soil layer. Extensive testing and evaluation have shown that various GCLs available in the market can provide equivalent protection with permeabilities two orders of magnitude lower than prescriptive clay. Strength criteria (both internal and interface) were evaluated for this project so that both the static and seismic stability criteria are met. This case history indicates how GCL and various interface strengths are considered in a design; and how one set of c_a and δ strength values are not representative of the strength parameters.

Figure 5 shows a typical cross-section of the landfill and the liner systems. The various interfaces, for the composite liner system that need to be considered in stability evaluation were: (1) subgrade-GCL, (2) GCL-internal, (3) GCL-textured side of geomembrane, (4) geomembrane-drainage layer, (5) geomembrane-operation layer. The subgrade at this site consists of sand, silty sands, and sandy silts. Operation layer consists of the material excavated from the site and is similar to subgrade materials. An evaluation of various material interfaces would indicate that the critical interfaces for this site would be: GGL-internal, and GCL-geomembrane.

In view of the above, direct shear tests in accordance with ASTM D 5321 were performed. The test procedure consisted of hydrating the GCL under 9.6 kPa (200 psf) normal load for 48 hours, because we considered that the GCL may become hydrated from moisture in the subgrade. Testing was done at a shear rate of 1 mm/min (0.04 inches per minute) for geosynthetic-to-soil interfaces. Different GCLs were considered and tested for this project and based on cost and technical feasibility a stitch-bonded geotextile-type GCL was selected. The shear strengths at 76.2 mm (3 inches) of displacement under various normal loads are presented in Figure 6.

TEST CONDITIONS

- Silty clay compacted to 93% at γ_{dmax} and OMC +3%
- Samples saturated in water for approx. 3 hrs. @ a normal pressure of 125 psf; full load applied overnight
- Shear @ 1.0 mm/min.

1kPa = 20.885 psf

$\tau_{peak} = 450 + 0.26\,(\sigma)\,psf$ $\tau_{peak} = 825 + 0.204\,(\sigma)\,psf$

$\tau_{post\text{-}peak} = 200 + 0.12\,(\sigma)\,psf$ $\tau_{post\text{-}peak} = 450 + 0.078\,(\sigma)\,psf$

$\tau_{peak} = \sigma$

$\tau_{post\text{-}peak} = 0.414\sigma$
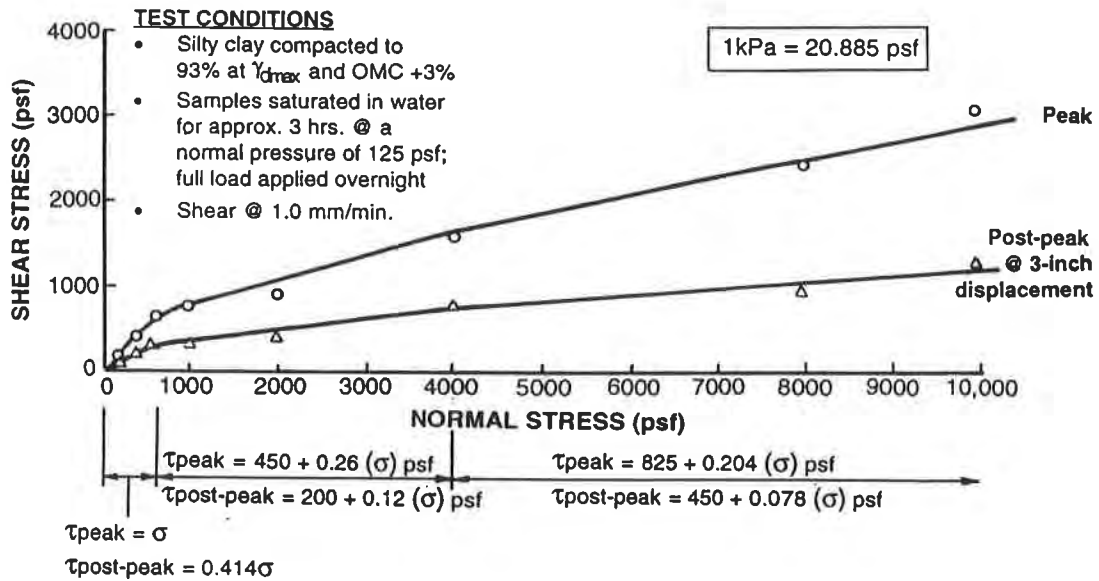
Figure 3. Typical shear stress vs. normal stress for low-permeability clay and textured HDPE

1kPa = 20.885 psf

LEGEND

⎯△⎯ GCL INTERNAL (from manufacturer)

··■··■··· GCL & CLAY INTERFACE

—·—○—·—· GCL & GEOMEMBRANE

⎯⎯ MINIMUM DESIGN STRENGTH ENVELOPE

GCL: Stitched geotextile type
GEOMEMBRANE: Textured HDPE
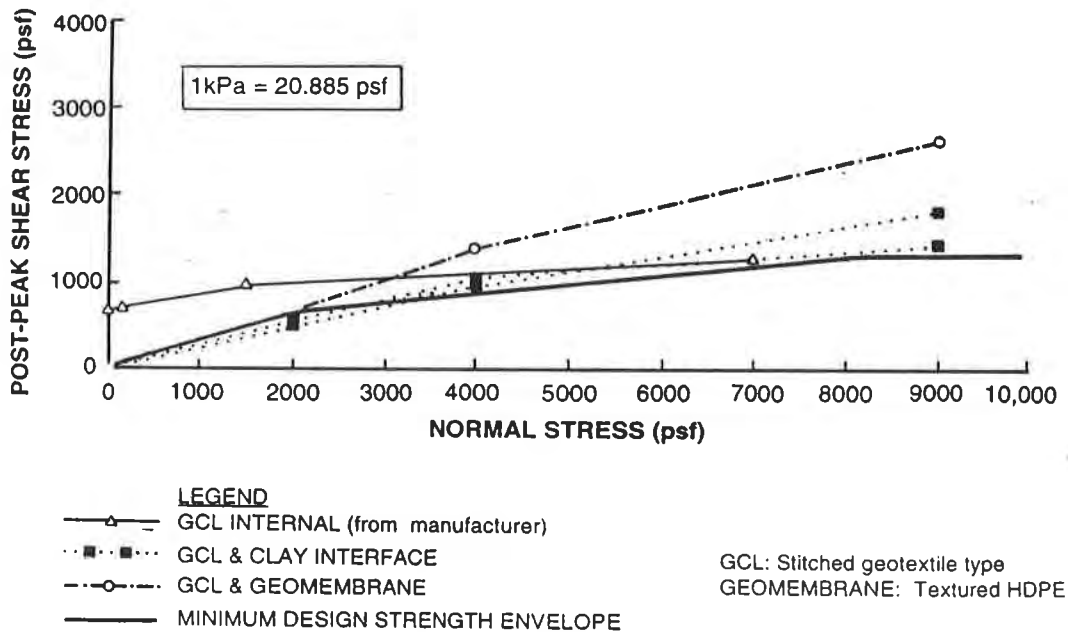
Figure 4. Typical shear stress vs. normal stress for GCL and textured HDPE
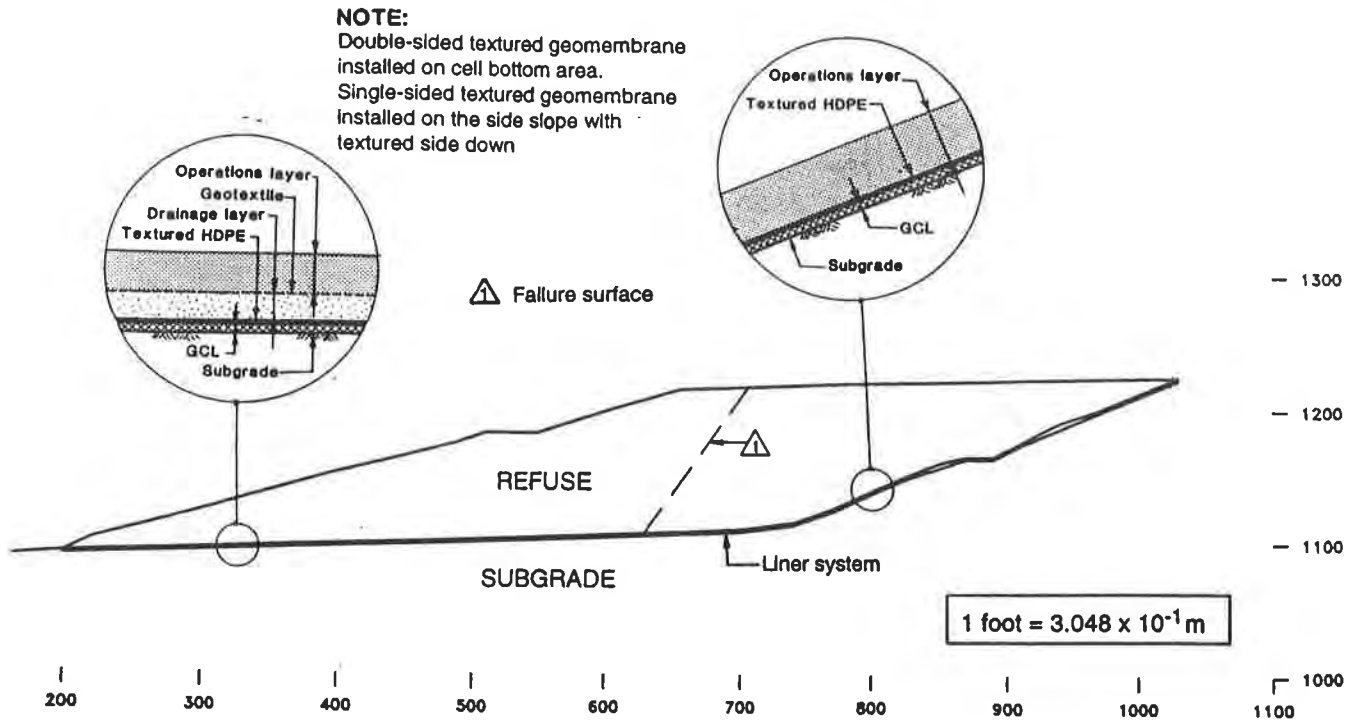
Figure 5. Liner system and static and seismic stability analyses typical section
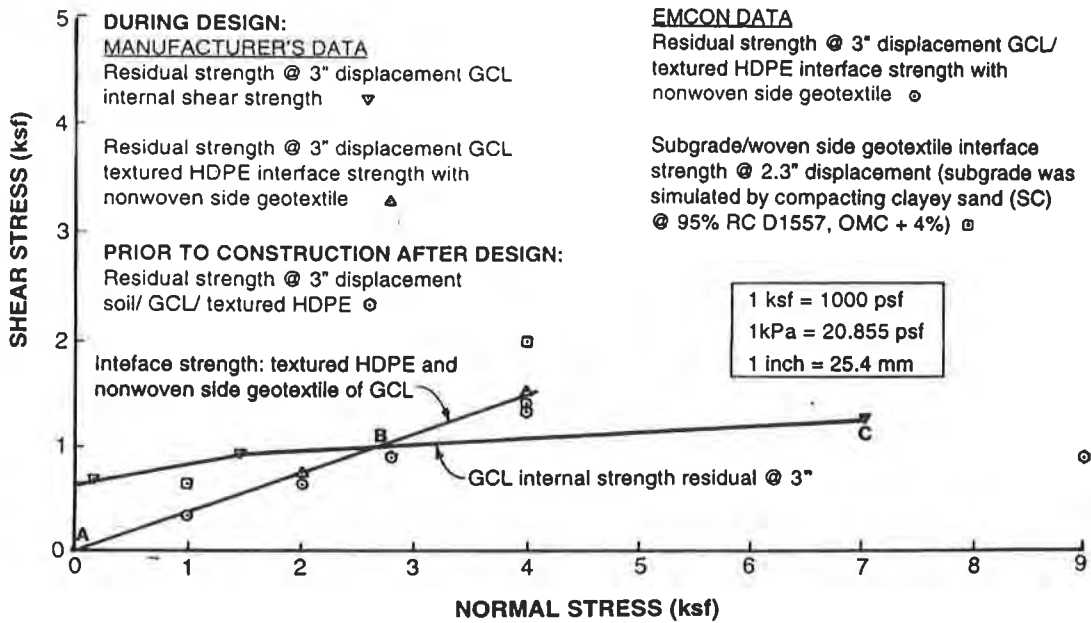
Figure 6. GCL internal and interface strength data

Static slope stability for the typical section (Figure 5) indicated a minimum static factor of safety of 1.53. Since the site is located in a seismic impact zone, the site seismicity was evaluated. The maximum probable earthquake (MPE) for the site used in the analysis consisted of a near earthquake with a magnitude of 6.7 with 0.42g rock acceleration and a distant earthquake with a magnitude of 8.0 with 0.22g rock acceleration. Analysis indicated that the seismic deformations resulting from MPE events were less than 305 mm (12 inches).

The construction of landfill cell was completed in 1995 and refuse has now been placed to its design height and has been performing satisfactorily.

Case History 2. At a municipal solid waste landfill in northern California obtaining clay for a 0.61 m-thick low permeability soil layer was found to be expensive since the clay was not available on or near the site. The options considered for the site were using (1) GCL (2) on-site soil (silty sand) mixed with imported clay and (3) on-site soil mixed with commercially available bentonite. Based on extensive laboratory testing and evaluation, the selected base liner system consisted of using an admixture of the on-site silty sand with bentonite overlain by a geomembrane.

Grain size, Atterberg limits and compaction tests and laboratory hydraulic conductivity tests were performed in accordance with ASTM D 5084. Three field infiltration tests were performed: (1) Double Ring Infiltrometer (DRI), (2) Air Entry Permeameter (AEP) and (3) Sealed Double Ring Infiltrometer (SDRI). The selected admixed material that met permeability (k) requirement of less than or equal to of 1×10^{-9} m/s had 90 percent soil and 10 percent bentonite by dry weight.

Direct shear testing was performed on textured HDPE geomembrane and on site soil and textured HDPE geomembrane and on-site soil admixed with 10 percent bentonite. The post-peak interface strength friction angle between geomembrane and on-site soil (without mixing bentonite) was about 24 degrees and between geomembrane and admixed soil was about 20 degrees in the normal load range of 48 to 432 kPa (1,000 to 9,000 psf). These tests did not indicate a bend in the shear-normal load relationship at higher normal test loads (432 kPa); this may be due to the sandy nature of the admix soil (SC). The sandy nature may also be the reason the admixed soil interface strengths were so high and had a S_{pp}/S_p ratio of about 0.8 even though the PI was a relatively high 34. This behavior, however, needs further evaluation.

Further details on these laboratory and field tests are presented in EMCON (1996). The landfill is constructed and is in successful operation for the last four years.

Case History 3. The site is a Class III municipal solid waste (MSW) landfill located along the California central coast. The current landfill is unlined and requires a prescriptive Chapter 15 final cover according to the California Code of Regulations (CCR) which requires from the top down (1) minimum 305 mm (12-inch) thick vegetative layer, (2) minimum 305 mm (12-inch) thick, low-permeable, compacted soil layer with a permeability equal to or less than 1×10^{-8} m/sec, (3) minimum 610 mm (24-inch) thick foundation soil layer.

The existing landfill face slopes ranged from 1.9 horizontal to 1.0 vertical (1.9H:1V) to 3.5H:1V with benches every 9 to 12 m (30 to 40 feet) of vertical elevation. The site soils consist of silty sand (SM) and elastic silt (MH) with the percentage of fines (minus U.S. Sieve size #200) varying from 34 to

68 percent. Atterberg limit indices (ASTM D 4318) measurements varied from 54 to 79 for the liquid limit and from 10 to 32 for the plasticity index. Laboratory compaction tests (ASTM D 1557) measured the maximum dry density at 1,136 and 1,240 kg/m^3 (71.0 to 77.5 pcf) at an optimum moisture content of 40.5 and 33.0 percent, respectively. A laboratory permeability test (ASTM D 5084) performed on a sample remolded to 85 percent of the maximum dry density (1,240 kg/m^3) at a 3.45 kPa (5 psi) confining pressure measured the permeability at 7.4 x 10^{-8} m/s.

The mean annual precipitation for the site is 584 mm (23 inches) with mean annual evaporation of 353 mm (14 inches). The design earthquake for the site are the MPE of magnitudes 6.3, 7.7 and 8.3 with rock accelerations 0.65g, 0.46g and 0.2g, respectively.

Because a clay soil was not available on site and to maintain an overall 1.2 m (4 feet) final cover thickness, the following alternative cover from the top down was proposed: (1) a 610 mm thick vegetative layer, (2) a geosynethetic clay liner (GCL) with a permeability no greater than 1 x 10^{-11} m/s and (3) minimum 610 mm thick compacted foundation layer.

A three-point interface shear strength test (ASTM D 5321) was performed for GCL against the vegetative and foundation soils. The normal stress loads were 6, 12, and 19 kPa (125, 250 and 400 psf). In addition, an interface shear strength test at a normal stress of 125 psf (6 kPa) was performed for a geocomposite against the vegetative soil. For each test, the soil specimen was compacted to 85 percent relative compaction (ASTM D 1557) at optimum moisture content to approximate field conditions on steep slopes. The GCL product used for testing was a stitched geotextile-type GCL. The nonwoven side of the GCL was tested against the vegetative and foundation soils. The geocomposite product used for testing was a HDPE geonet with nonwoven geotextiles heat bonded to each side. The hydration period, load application, and displacement rate procedures were as previously described in this paper. The post-peak results are presented in Figure 7. The strengths of overall system under low normal loads reflect interface shear strength; the internal strength of the GCL is not a factor. As shown in Figure, at low normal stress the strength envelope is linear.

An infinite slope analysis was performed using the methodology described by Lambe and Whitman (1969), and Sharma and Lewis (1994). The results of our slope stability analyses are presented in Table 2.

Table 2
Results of Static Stability Analyses

Slope Configuration	Composite Geonet	Factor of Safety Under Normal Seepage Condition	Factor of Safety Under Peak Seepage Condition
2H:1V	without	1.5	1.1
2H:1V	with complete coverage	1.5	1.5
2H:1V	3-m (10-foot) spacing (edge to edge)	1.5	1.3
2.5H:1V	without	1.8	1.3
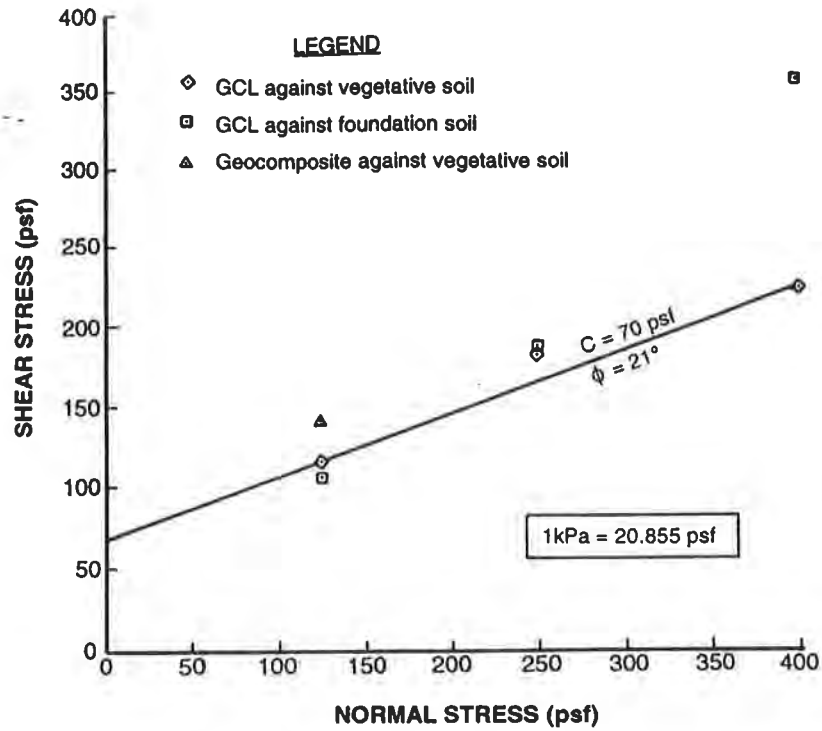
Figure 7. GCL/soil or geocomposite/soil interface shear strength
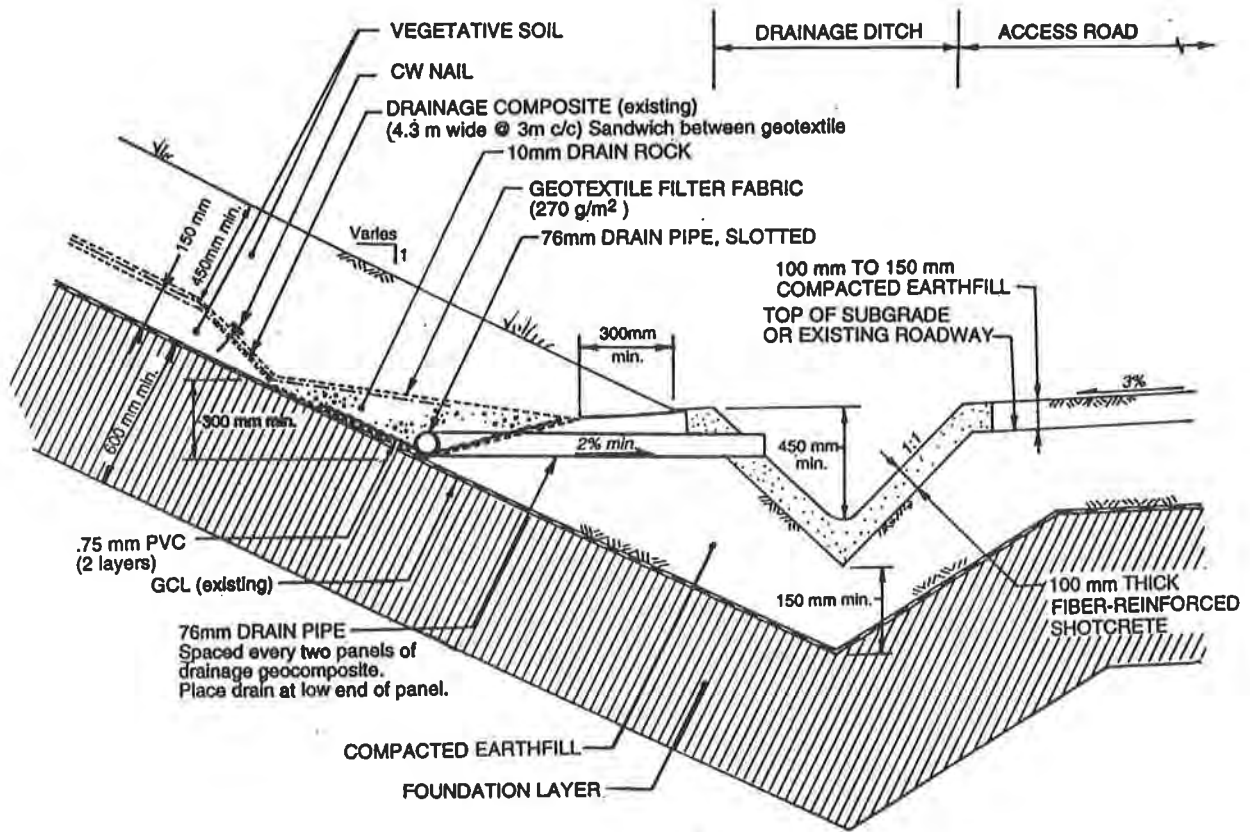
Figure 8. Cover system cross section

The selected cover system was to use GCL with geocomposite for slopes steeper than 2.5H:1V and GCL only for slopes flatter than 2.5H:1V. Seismic deformations were estimated using SHAKE, a yield acceleration computed using the methodology described by Matasoric (1993), and a procedure developed by Makdisi and Seed (1977) for calculating permanent deformations in dams and embarkments. Seismic deformations for these slopes were less than 306 MM (12 inches). Figure 8 shows a typical section of the constructed final cover system.

CONCLUSIONS AND RECOMMENDATION

Based on the test results, analyses, and discussions presented above, the following conclusions are drawn:

- Shear strength versus normal stress behavior, both for soil/HDPE geomembrane and GCL/HDPE geomembrane, is usually curvilinear and may be represented by up to three different c_a and δ values. The δ values may be significantly higher at low normal stresses (less than 24 kPa) than are at higher normal loads (greater than 380 kPa). While no physical meaning has been attributed to the bends in the curve for geomembrane/soil behavior, changes in the strength/normal stress behavior for GCLs may be attributed to a shift from interface strength to internal GCL strengths.

- Test results for soil/HDPE interface indicate that strain-softening (drops in post-peak strengths) occur and can be represented by a relation between post-peak to peak shear strength ratios (S_{pp}/S_p) and soil plasticity index . The ratio is about 0.9 for HDPE geomembrane/silty clays with a plasticity index (PI) less than 25. Ratios drop significantly (less than 0.5) for PI values above 30.

- At low normal stresses (less than 24 kPa), the shear strength envelope is linear and is applicable for final cover design. The curvilinear strength envelope is applicable to landfill base liner design.

- Alternative liners, as discussed in three case studies, can be evaluated, designed, and constructed to be "equivalent" to prescriptive standards. The proper evaluation of interface shear strengths for such applications is imperative.

This paper has further extended the existing database but presentation of more data and applications to actual projects, i.e., presentation of more case histories are recommended. Testing at various strain rates (with pore pressure measurements) and under high normal loads (above 500 kPa) are specifically suggested.

References

American Society for Testing and Materials (ASTM), Annual Book of ASTM Standards, Vol. 04.08 and 04.09, Philadelphia, 1995.

Bemben, S., and D. Schulze, "The Influence of Testing Procedures on Clay/Geomembrane Shear Strength Measurements," Proceedings of Geosynthetics '95, IFAI, Nashville, pp. 1043-1056.

Byrne, R., "Design Issues with Strain-Softening Interfaces in Landfill Liners," Waste Tech '94 Landfill Technology, Technical Proceedings, Charleston, South Carolina, 1994.

EMCON. "Interface Strengths and Alternative Liners for Landfills." EMCON internal report, 1996.

Fishman, K., and S. Pal, "Further Study of Geomembrane/Cohesive Soil Interface shear Behavior," Geotextiles and Geomembranes, 13(1994), pp. 571-589.

Gilbert, R., et al., "A Double Shear Test Method for Measuring Interface Strength," Proceedings of Geosynthetics '95, IFAI, Nashville, pp.

Giroud, J.P., Darrasse, J. and Bachos, R.C. "Hyperbolic Expression for Soil-Geosynthetic or Geosynthetic-Geosynthetic Interface Shear Strength", J. of Geotextiles and Geomembranes, Vol. 12, No. 3, Elsevier Publ. Co. (1993) pp. 275-286.

Koerner, R., J. Martin and G. Koerner, "Shear Strength Parameters Between Geomembranes and Cohesive Soils," Geotextiles and Geomembranes, 4(1986), pp. 21-30.

Lambe, T.W., and R.V. Whitman, Soil Mechanics, John Wiley & Sons, Inc., New York. 1969.

Masada, T., et al., "Modified Direct-Shear Study of Clay Liner-Geomembrane Interfaces Exposed to Landfill Leachate," Geotextiles and Geomembranes 13(1994), pp. 165-179.

Matasovic, H., "Seismic Response of Composite Horizontally-Layered Soil Deposits," Ph.D. Dissertation, Civil and Environmental Engineering Department, University of California, Los Angeles, p. 452, 1993.

Orman, M., "Interface Shear-Strength Properties of Roughened HDPE," Journal of Geotechnical Engineering, Vol. 120, No. 4, April 1979, pp. 758-761.

Somasundaram, S., and K. Khilnani, "Stability of High Refuse Slopes on Synthetic Lining Systems at the Bee Canyon Landfill," Proceedings of Geosynthetics '91, IFAI, Atlanta, pp. 145-158.

Sharma, H.D., and D. Hullings, "Direct Shear Testing for HDPE/Amended Soil Composites," Proceedings of geosynthetics '93, IFAI, Vancouver.

Sharma, H.D., and S.P. Lewis, Waste Containment Systems, Waste Stabilizations and Landfills: Design and Evaluation, John Wiley & Sons, Inc., New York, 1994.

Stark, T.D., and A.R. Poeppel, "Landfill Liner Interface Strengths From Tosional-Ring-Shear Tests," Journal of Geotechnical Engineering, Vol. 120, No. 3, March 1994, pp. 597-614.

AN EXPERIMENTAL CHARACTERIZATION OF SOIL-WOVEN GEOTEXTILE INTERFACE IN LARGE BOX PULLOUT TESTS

S. B. Mallick, D. J. Elton, S. Adanur

Auburn University, College of Engineering
115 Textile Building
Auburn, AL 36849

Phone : (334) 844-5497
Fax: (334) 844-4068

ABSTRACT

A laboratory research program was undertaken to determine the influence of fabric geometry and normal pressure on the stress-strain characteristics of soil-geotextile interface in pullout tests. Pullout tests were carried out in a large pullout box (91 cm × 61 cm × 46 cm). Three types of woven geotextiles were selected for the study. Three types of sand (coarse, medium and fine) were used as cover material for the pullout tests. Effects of fabric structure and normal pressure on the pullout test results were analyzed in terms of peak and ultimate pullout load, permanent strain along the length of the geotextile, total pullout displacement inside the box and interface friction angle. Pullout tests were conducted at 7, 21, 35 and 49 kPa normal pressures. The tests were performed at a constant displacement rate of 1 mm/min. Statistical Analysis System (SAS) software was used to perform Analysis of Variance (ANOVA) and Duncan's test of multiple comparison.

INTRODUCTION

Mechanical interaction between soil and a geotextile can be characterized by the shear strength developed between them. A high contact shear strength is desired when geotextile is used to reinforce soil and a low contact shear strength is desired when the soil and the geotextile are designed to move against each other. The shear strength is governed by the angle of internal friction developed between the soil and the geotextile. This shear strength, developed at the soil-geotextile interface, can be characterized by the stress-strain behavior of a geotextile, as it is subjected to pullout force.

Several researchers (1, 2, 3, 4) have demonstrated the effect of normal pressure and related soil dilatancy on the pullout performance of a soil-geotextile interface. For a soil-geotextile system, the coefficient of friction has been shown to decrease with an increase in normal pressure. Rao and Pandey (2) and Chang et al (3) demonstrated that the coefficient of friction of a soil-geotextile interface can exceed the coefficient of friction of soil itself. Ingold (5) reported that the interface friction angle of a soil-geotextile interface exceeded the coefficient of friction of the soil at low normal pressures. An opposite phenomenon was obtained by Murthy et al (4), who reported that the pullout coefficients of friction were less than those of sand (as obtained from direct shear test)

at three normal pressure levels.

Surface roughness has been found to have a significant effect on interface friction angle obtained in the pullout test (6). In these pullout tests, different sizes of glass beads were used to represent soils with different grain sizes. The coefficient of friction increased with an increase in surface roughness. The interlocking between the beads and the geotextile was observed to depend primarily on the ratio of the apparent opening size of the geosynthetic to the diameter of glass beads.

Collios et al (7) studied the effect of soil particle size and the deformability of geotextiles on direct shear and pullout test results. Test results show that the friction angle between the geosynthetic and cover materials increases with an increase in geotextile opening size.

There are two objectives in this study: (1) to evaluate the effect of fabric structure geometry on the pullout performance of woven geotextiles and (2) to evaluate the effect of normal pressure on the pullout properties of woven fabrics.

TEST PLAN

Materials. Three types of woven geotextiles and three types of sands were chosen for this study. The properties of these geotextiles are shown in Table 1. To observe the effect of fabric structure on pullout test results, three fabrics were chosen with similar polymer composition, comparable grab tensile strength and elongation, but with different structure and yarn construction. Three types of sands, coarse, medium and fine, were used for their different grain sizes. Sand properties are shown in Table 2.

Pullout Box. Figure 1 shows the schematic of the pullout box. The pullout box has an outside dimension of 91 cm (length) X 61 cm (width) X 46 cm (height). The box was made out of 2.5 cm thick plywood, with an aluminum cover.

Test Conditions. The pullout box was used in conjunction with the Instron Material Testing System for testing. Tests were conducted at a constant displacement rate of 1 mm/min. Four normal pressure levels, 7, 21, 35 and 49 kPa were used for pullout tests. Density of the compacted sand was measured with a balloon apparatus (ASTM D2167-66) before placing the geotextile. An average density of 1.46 to 1.63 gm /cc was reached for all three sands by manual compaction. A 5.1 cm long strip was marked on the geotextile sample as shown in Figure 2. After the test, the final length of the strip was measured. From the deformation of the strip, permanent strain at point A was calculated. One high precision dial gage was attached to the rear end of the geotextile sample to measure total pullout displacement inside the box. During the test, data on the pullout load, front end displacement, and the total pullout displacement of the rear end of the geotextile sample were measured. The calculated parameters included the strain at A, (Str_A) and the interface friction angle (I_ANG). Loading was stopped when the displacement exceeded 175 mm or if the geotextile failed in tension. The measured and calculated parameters were analyzed to determine the effect of normal pressure and structure of the geotextiles on pullout properties of geotextiles.

Table 1 Properties of Tested Geotextiles

| | WOVEN GEOTEXTILES | | |
	A	B	C
Structure	2 X 1 right Hand twill warp: slit film, weft: tape Yarn	Plain warp: tape yarn weft: slit film	Plain warp: monofilament yarn weft: tape yarn
Polymer	Polypropylene	Polypropylene	Polypropylene
AOS	40	70	40
Average Grab Tensile Strength (N) ASTM D4632	922.5	1003.2	841.5
Grab Elongation (%) ASTM D 4632	21.30	23.90	27.44
Wide width strip test (N) ASTM D4595	7540	9964	7532
Wide width elongation (%) ASTM D4595	25.54	34.82	33.67

Table 2 Sand Properties

| | SAND TYPE | | |
	Coarse	Medium	Fine
Average Diameter (mm)	1.03	0.8	0.3
Loose Density (kg/m^3)	1431.00	1431.00	1431.00
Compacted Density (kg/m^3)	1486.80	1577.12	1319.85
Shape (8)	Subangular	Subangular	Subangular

ANALYSIS OF RESULTS

The primary objective of the analysis was to evaluate the effect of normal pressure and geotextile types on the performance of woven geotextiles in pullout tests. The parameters analyzed included:

1. Peak or ultimate pullout load (L_PEAK)
2. Strain at A (Str_A)
3. Total pullout displacement, measured inside the box (T_PULL)
4. Interface friction angle (I_ANG)

Results obtained from pullout tests at the pressure levels of 7, 21, 35 and 49 kPa and with three types of sands, (coarse, medium and fine), were analyzed for each of the three geotextiles used.
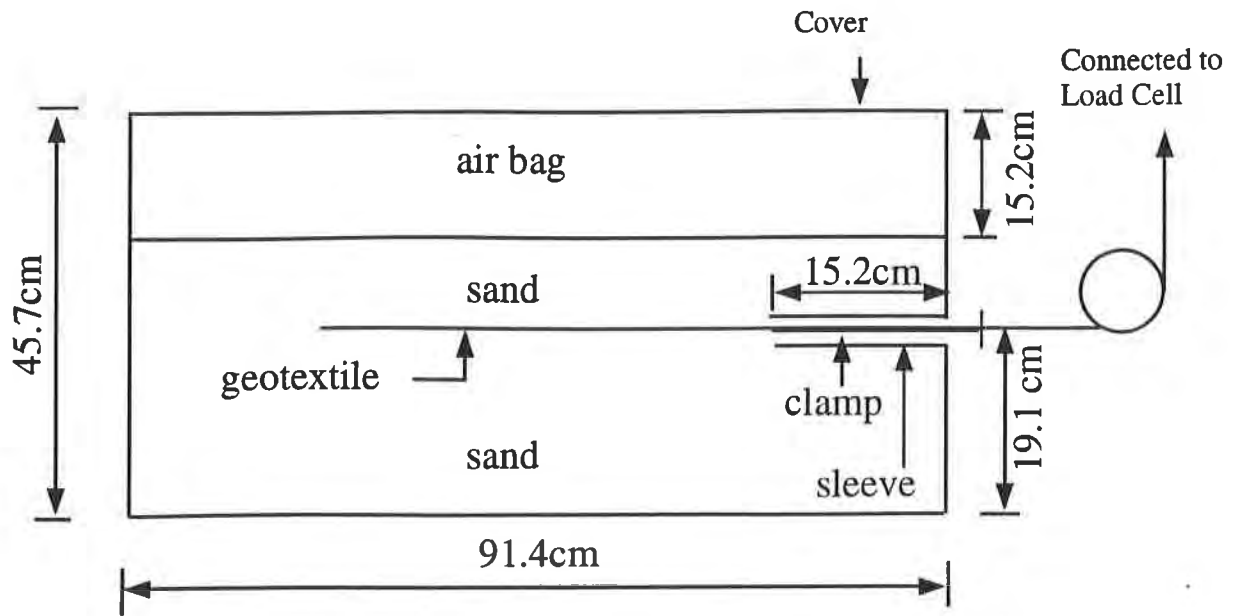
Figure 1 Profile of the Pullout Box
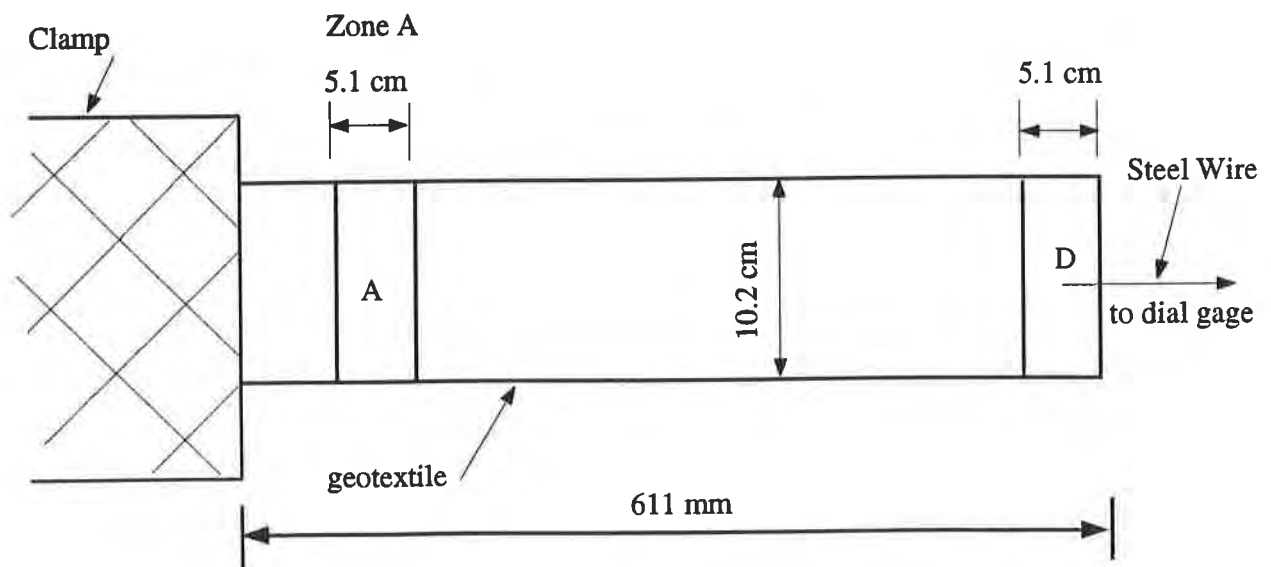
Figure 2 Area Marked for Strain Measurement

Statistical Analysis. The statistical analysis used in the study consisted of the analysis of variance (ANOVA), Duncan's Multiple Range Test, and regression. The Basic principle of Duncan's Multiple range test is briefly discussed below.

Duncan's Multiple Range Test. An Analysis of Variance reveals whether any difference exists between treatments. However, no inference can be made regarding the difference between any two particular treatments. A multiple range test allows the researchers to make pairwise comparison and check for any difference between two treatments. Basically the method uses the smallest difference, called LSD (Least Significant Difference), that would be declared significant, and compares the absolute value of each observed difference (for a pair of treatments). If the difference exceeds the LSD, the two treatments can be placed in two separate groups. This means that the average response for one treatment is significantly different from the average response of the other treatment. Duncan's Multiple Range test is a relatively new test (9). The test is less conservative than the other multiple comparison tests, but is widely used due to its simplicity. The basis for Duncan's multiple Range Test and LSD calculation procedure are as follows:

Test: $H_0 : \mu_1 = \mu_2, \mu_1 = \mu_3$, etc.   (Null hypothesis: all means are same)

   $H_A: \mu_1 \neq \mu_2, \mu_1 \neq \mu_3$, etc   (Alternative hypothesis: means are different)

Decision Rule: Reject $H_0 : |x_1 - x_2| \geq t^*D$; (for testing H_0)

where, t^* = t value for the degree of freedom = (n-k) and level of significance $\alpha = 0.05$

   D = Standard error

   t^*D = LSD, Least Significant Difference

Note: μ = population mean;   x = group mean

   n = total number of observation;   k = number of treatments

Effect of Geotextile Types on the Peak or Ultimate Pullout Load (L_PEAK). A typical plot of peak or ultimate pullout load (L_PEAK) against the normal pressures 7, 21, 35 and 49 kPa for geotextiles A, B and C and for the coarse sand is presented in Figure 3. The results show that geotextile B demonstrates the highest peak or ultimate pullout load of all the three geotextiles tested with all three types of sands. To determine any significant effect, analysis of variance (ANOVA) tests were conducted with a significance level (α) of 0.05. Results are shown in Table 3. The ANOVA test shows that the Probability > F is 0.07, which is slightly over the chosen significance level of 0.05. Duncan's multiple range tests were performed to group the geotextile types according to their effect on L_PEAK. The results are shown in Table 4. Geotextile B produced the highest average value of L_PEAK. Differences between the average value of L_PEAK for geotextiles A and B as well as for geotextiles A and C were not significant. Geotextile C produced the lowest average L_PEAK of all three geotextiles. The difference can be ascribed to the difference in the fabric geometry. Geotextile A is 2 × 1 right hand twill weave with slit film warp yarn and tape filling yarn. Geotextile B is a plain weave with a double tape warp and slit film filling yarn. Geotextile C has a plain weave structure with monofilament warp yarn and a tape filling yarn with a comparatively smooth fabric surface. Pullout resistance of geotextiles is primarily dependent upon three interaction mechanisms: skin friction, interlocking of sand particles and tensile strength of the fabric. Skin friction is affected by the fabric structure properties. Geotextile B had the roughest surface and the greatest surface area. The slit film filling yarn of geotextile B also may have locked

the sand particles inside the geotextiles during pullout, which in turn, resulted in a larger pullout resistance. Grab and wide width tensile strength tests on three geotextiles showed that geotextile B had the highest grab and wide width tensile strength of all three fabrics. Therefore, it can be concluded that the rough surface, greater surface area and the higher tensile strength of geotextile B resulted in the largest peak pullout resistance of all three fabrics. Examination of the geotextiles showed that the geotextile C had a relatively smooth fabric surface texture and lower surface area, and thus produced the lowest pullout resistance at peak.
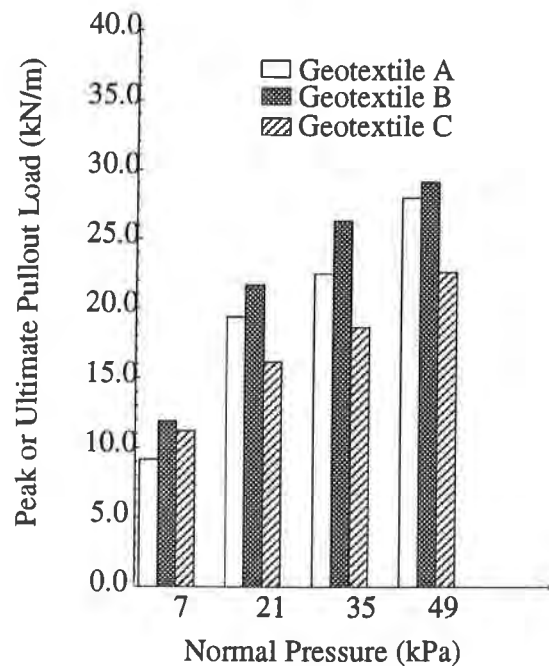
Figure 3 Effect of Geotextile Types on the Peak and Ultimate Pullout Load for Coarse sand

Table 3 Summary of Analysis of Variance on Pullout Test Results ($\alpha = 0.05$)

Independent Variables	Dependent Variables			
	L_PEAK	STR_A	T_PULL	I_ANG
Materials				
Sand	0.31	0.83	0.84	0.63
Fabric	0.07	0.04	0.46	0.42
Test Condition				
Normal Pressure	0.0001	0.0001	0.0001	0.0001

Number in the cell shows Probability >F (i.e., probability of making type I error. Type I error is the mistake of concluding there is an effect when in fact, there is none)

Table 4. Duncan's Multiple Range Test on Pullout Test Results (Gr. = Group)

Independent Variables		Dependent Variables							
Factor	Type /Value	L_PEAK (kN/m)		STR_A (%)		T_PULL (mm)		I_ANG (degree)	
		Mean	Gr.	Mean	Gr.	Mean	Gr.	Mean	Gr.
Fabric	A	21.1	AB	8.2	AB	50.0	A	53.8	A
	B	23.4	A	6.5	B	52,1	A	57.5	A
	C	19.2	B	8.9	A	30.5	A	53.7	A
Nor. Press (kPa)	7	11.9	D	2,0	C	118.4	A	69.9	A
	21	20.1	C	6.2	B	48.9	B	57.3	B
	35	24.3	B	7.3	AB	10.1	C	49.1	C
	49	27.9	A	8.5	A	54.6	C	44.0	D

Note: Means in the same group do not differ significantly

Effect of Geotextile Types on the Strain at A. Figure 4 shows a typical plot for the Str_A versus geotextile types for coarse sand. The trend of the data show that with the coarse sand, geotextile C produces greater strain at point A than the geotextile B. A significant effect of geotextile types was observed on Str_A (Table 3). Table 4 shows that geotextile C produced the highest average values for the strain at point A. Among the three, a significant difference was observed only between the average values of Str_A for the geotextiles B and C. Geotextile B has a plain weave structure with tape yarn in the warp and slit film in the filling direction. Geotextile C also has a plain weave structure with monofilament warp yarn and tape filling yarn. The difference between these two fabrics is the crimp in the warp yarn. The tape warp yarn of the geotextile B has practically zero crimp, whereas, geotextile C has crimp in high frequency and high amplitude in the monofilament warp yarn. When subjected to a pullout force in the warp direction, Geotextile C with higher crimp produces larger strain than geotextile B.

Best Fit Equation for Effect of Normal Pressure on Pullout Properties. One of the primary causes of geotextile failure in reinforced slopes is the slippage of geotextiles under pullout load. The normal pressure of soil above the geotextile plays a critical role in preventing the slippage. Results obtained from previous research and those obtained from this study show that normal pressure has a significant effect on laboratory pullout performance of geotextiles. Test results were analyzed to determine relationships between normal pressure and pullout properties. Regression analysis by a
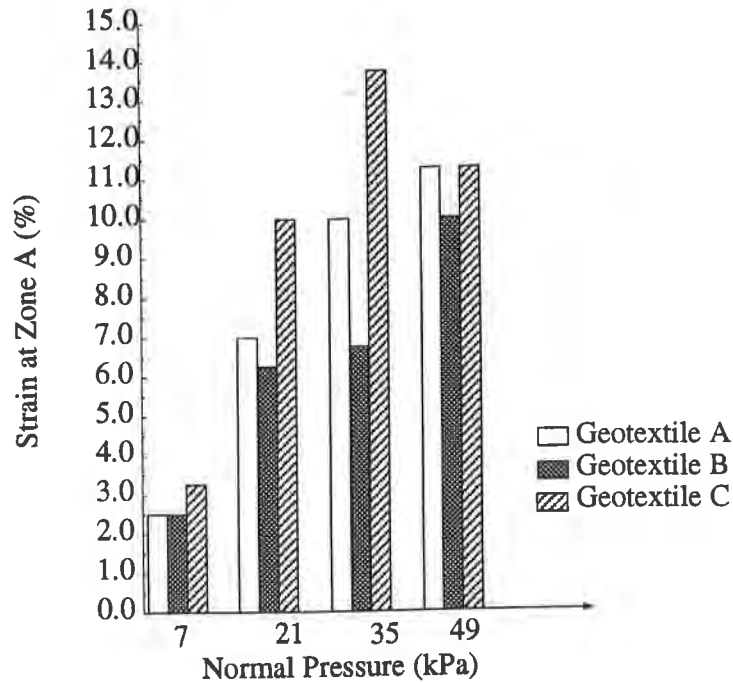
Figure 4 Effect of Geotextile Types on Strain at A for Coarse Sand

least square estimation procedure was performed on the data and the relationship corresponding to the highest coefficient of determination (R^2) is reported. In the analyses, the data from the tests on the different geotextiles with different sands were considered as a same set since the effect of sand and geotextile was found to be less significant compared to the effect of normal pressure (Table 3).

Effect of Normal Pressure on the Peak or Ultimate Pullout Load (L_PEAK). Figure 5 shows the plot of L_PEAK versus normal pressures for three types of geotextiles and three types of sands. The trend of the data shows that the pullout load increased continuously with the increase in normal pressures from 7 to 49 kPa for all three geotextiles. A significant effect of normal pressure was observed on L_PEAK (Table 3). Multiple Range Test showed that the average values of L_PEAK at all of the four normal pressure levels were significantly different (Table 4). The normal pressure level of 49 kPa produced the highest average value of L_PEAK, and the normal pressure level of 7 kPa produced the lowest average value of L_PEAK. As the normal pressure increased, indentation of sand particles also increased, which in turn resulted in a higher interlocking between the sand and geotextile. At higher normal pressure, sand density is also increased and the sand may dilate along the sand-geotextile interface during shear. Due to the restricted volume of the box, dilation of sand may have resulted in a higher surface area. This dilation, along with the interlocking effect, may have resulted in a higher L_PEAK at higher normal pressure. Figure 5 also shows the predicted relationship.
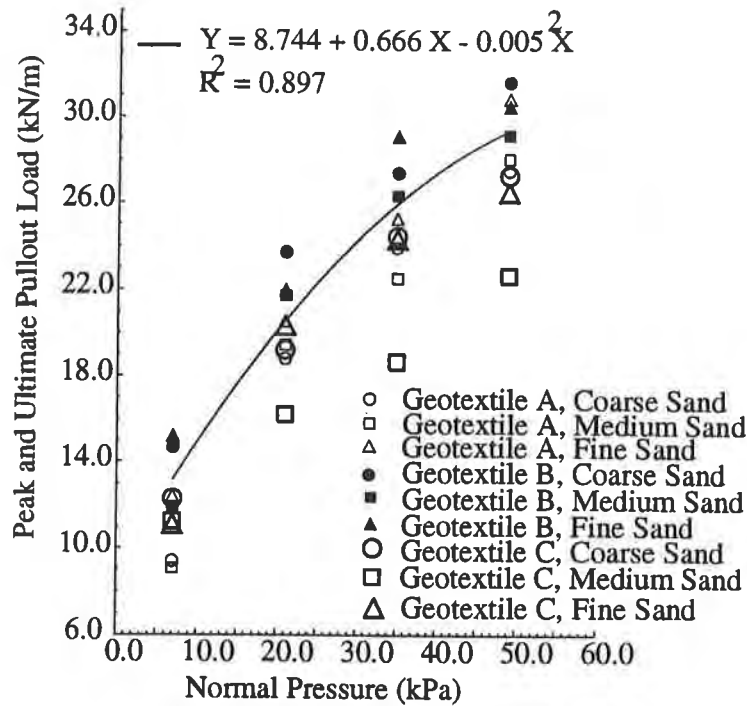
Figure 5 Effect of Normal Pressure on the Peak and Ultimate Pullout Load for Three Geotextiles and Three Sands

L_PEAK increases with the increase in normal pressure in the beginning. But its rate of increase gradually decreases with the further increase in the normal pressure and tends to reach an optimum L_PEAK . This relationship indicates that for the geotextile-sand combinations and the total pullout displacement of 175 mm selected for this study, L_PEAK cannot be improved significantly by only increasing the vertical load on top of the geotextile. As the normal pressure reaches 35 kPa, pullout or slippage of the geotextile inside the box is decreased to zero and the stretching of the geotextile provides the pullout resistance. Therefore, at higher normal pressures the pullout resistance is dominated by the tensile strength of the geotextile, not the frictional characteristics. After this certain level of normal pressure is reached, any further increase in normal pressure will only lead to stretching of the fabric which would finally result in the rupture of the sample during pullout. For a particular geotextile and soil combination, the relationship between L_PEAK and normal pressure can be determined for a given pullout displacement, by laboratory pullout testing and can be used to select the range of normal pressure for a desired L_PEAK value. A 0.897 coefficient of determination shows that the variable L_PEAK is sensitive to the change in normal pressure.

Effect of Normal Pressure on Strain at A (Str_A). Figure 6 shows the plot of Str_A versus normal pressure for the three geotextiles and three types of sands. The trend of the data shows that the strain at A increases, in general, with an increase in normal pressure. A significant effect of normal pressure was observed on the Str_A values (Table 3). Table 4 shows that the normal pressure level of 7 kPa produced the lowest average value of Str_A . The normal pressure levels of 35 and 49 produced similar average values of Str_A and were classified as group A which exhibits the highest

average value of Str_A. Average Str_A value for normal pressure level of 21 kPa was higher than that for 7 kPa but lower than that for 35 and 49 kPa. When a geotextile is subjected to a pullout force, under low normal pressure, the front part stretches under the pullout load and provides the pullout resistance. As the normal pressure increases, the stretching of the front part increases as was indicated by the continuous increased strain at A from 7 kPa to 21 kPa. At higher normal pressure (35 to 49 kPa), the strain at A reaches a maximum value and no significant difference was observed between the average values of Str_A at 35 and 49 kPa. Figure 6 also shows the relationship between strain at point A and normal pressure. It can be noted that at the low normal pressure levels, the strain at point A increases with an increase in normal pressure. The rate of increase of Str_A decreases at high normal pressure. At higher normal pressure, strains at point A tend to reach a peak for the selected geotextiles. A 0.657 coefficient of determination indicates a moderately good relationship between strain at point A and normal pressure.

Total Pullout of the Geotextile Sample (T_PULL). Total pullout of the geotextile sample was measured from the total displacement recorded by a dial gage attached to the free end of the geotextile as shown in Figure 2. The dial gage was placed outside the pullout box and a steel wire attached the dial gage to the free end of the geotextile sample. Inside the pullout box, a copper tube was used to protect the wire from the sand and reduce the friction. Figure 7 shows a continuous pullout load versus time plot with corresponding readings from dial gage. Dial gage records the movement of the end of the geotextile sample at point D, inside the box. Figure 7 shows that the sample reached the peak pullout load exactly at the moment when the dial gage number 3 recorded a movement at point D. Figure 7 indicates that pullout of a sample inside the box is also demonstrated by the nature of the pullout test plot . A peak pullout load indicates a slippage or pullout of the sample, whereas, continuously increasing nature of the pullout load versus displacement plot indicates zero pullout of the sample. Figure 8 shows the T_PULL versus normal pressure for the geotextiles A, B and C. The pullout displacement of the end of the sample decreased steadily with increase in normal pressure. For all three geotextiles, rate of decrease of the total pullout displacement with normal pressure was practically constant between 7 kPa to 35 kPa and then further reduced between 35 kPa to 49 kPa. For the geotextiles A and C, in the fine sand, the sample, did not move at all at 35 and 49 kPa. For the Geotextile B, total pullout displacement was measured as zero during the pullout test at 49 kPa. Therefore, it can be concluded that, in this case, the displacement measured at the front end of the geotextile was due to the stretching of the geotextile. A significant effect of normal pressure was observed from the analysis of variance tests (Table 3). Table 4 shows that T_PULL decreased with the increase in the normal pressure from 7 to 35 kPa. No significant change in the average values of the T_PULL was observed in between 35 to 49 kPa. At high normal pressure level, indentation of sand particles inside the geotextile results in an interlocking between sand and geotextile. This interlocking prevents the slippage (pullout) of the geotextile resulting in zero pullout displacement at point D at higher normal pressure levels. A decrease in T_PULL with an increase in normal pressure indicates that at higher normal pressure, a pullout test gradually becomes a tensile test, where the major part of the pullout resistance results from the tensile strength of the geotextile. Figure 8 shows the predicted relationship between total pullout and normal pressure. Total pullout decreases with increase in normal pressure. At 40 kPa

and above, pullout of the sample practically becomes zero, which indicates at high normal pressures, the pullout test simulates the insoil tensile test. A 0.782 coefficient of determination shows a good correlation between the variable T_PULL and normal pressure.

Effect of Normal Pressure on the Interface Friction Angle (I_ANG). Figure 9 shows the plot for the I_ANG versus normal pressures for the three geotextiles and three types of sands. In general the interface friction angle decreased continuously with the increase in normal pressures for all three geotextiles. To determine any significant effect, analysis of variance (ANOVA) tests were conducted with a significance (α) level of 0.05. Results are shown in Table 3. A significant effect of normal pressure was observed from the analysis of variance tests. Duncan's multiple range tests were performed to group the normal pressure levels according to their effect on I_ANG. The results are shown in Table 4. I_ANG decreased significantly with increase in normal pressure levels from 7 to 49 kPa. The decrease is significant at all four normal pressure levels. Figure 9 also shows the pressure levels, dilation of sand results in the interlocking between geotextile and sand, which in turn resists the sliding of the geotextile. This reduction in the pullout displacement, decreases the development of frictional force at the sand-geotextile interface which in turn results in a lower interface friction angle. A 0.931 coefficient of determination shows an excellent predicted relationship between the interface friction angle and normal pressure.

CONCLUSIONS

On the basis of this study the following conclusions can be made:

1.   Peak or ultimate pullout load increased significantly with an increase in normal pressure. The predicted relationship between peak load and normal pressure showed that the peak load tended to reach a constant value at higher normal pressures. Geotextile construction types had a significant effect on the peak pullout load. Due to the rough surface texture and greater surface area, geotextile B produced the highest peak and ultimate pullout load. Geotextile C produced a smaller peak pullout load than geotextile A.

2.   Normal pressure had a significant effect on the strain at point A. Strain at point A increased with an increase in normal pressures. The predicted relationship between strain at point A and normal pressure showed that at higher normal pressure, strain tends to reach a peak for the selected geotextiles. Geotextile types showed significant effect on the strain at point A. A high frequency and high amplitude crimp in the monofilament warp yarn of Geotextile C produced the highest average values for the strain at point A when subjected to a pullout load in the machine direction.

3.   Normal pressure had a significant effect on the total pullout displacement of the geotextile samples. As normal pressures increased, interlocking between the sand and the geotextiles decreased the displacement of the end of the geotextile inside the box. From the predicted relationship between normal pressures and total pullout displacement, it was observed that at the normal pressure level of 40 kPa and above, total average value of pullout displacement became practically zero.

$$Y = 12.44 + 0.345\,X - 0.003\,X^2$$
$$R^2 = 0.657$$

Strain at Zone A (%)

Normal Pressure (kPa)

○ Geotextile A, Coarse Sand
□ Geotextile A, Medium Sand
△ Geotextile A, Fine Sand
● Geotextile B, Coarse Sand
■ Geotextile B, Medium Sand
▲ Geotextile B, Fine Sand
○ Geotextile C, Coarse Sand
□ Geotextile C, Medium Sand
△ Geotextile C, Fine Sand
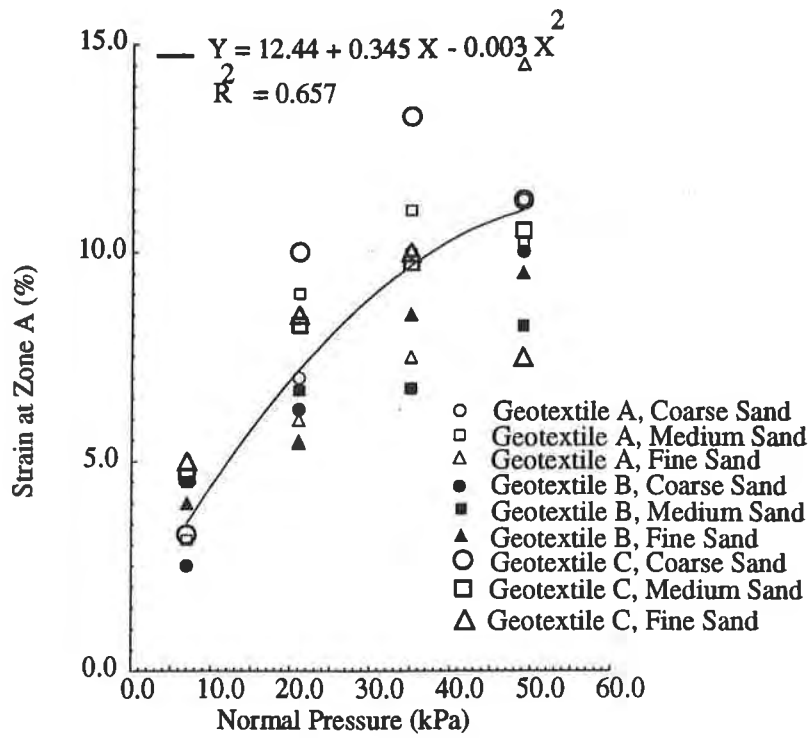
Figure 6 Effect of Normal Pressure on Strain at A for Three Geotextiles and Three Sands

Axis Y1

Axis Y2

2.0

Pullout Load (kN/m)

(X, Y1)

(X, Y2)

Total Pullout Displacement at the End of
the Geotextile (Point D) (mm)

Time (minutes)

—— Pullout Load versus Time
– – – Reading of Dial Gage No. 3 versus Time
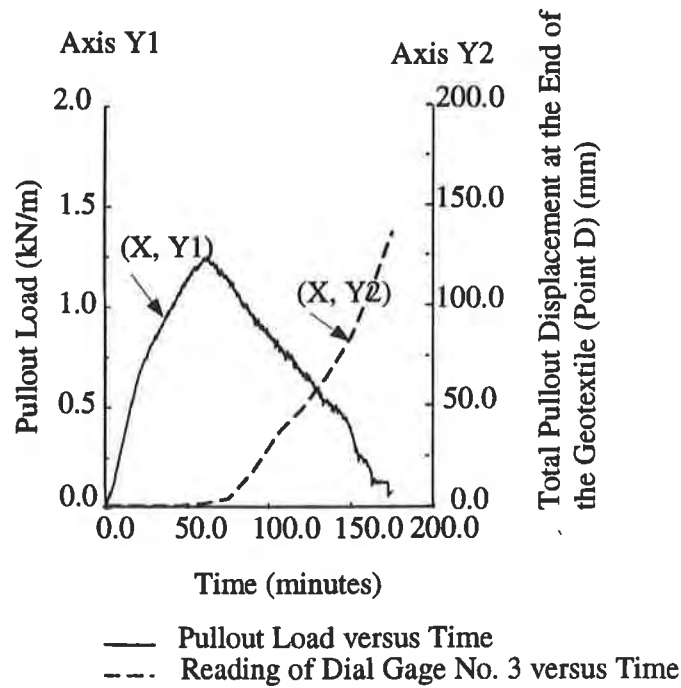
Figure 7 Pullout Load and Total Pullout Displacement with Time
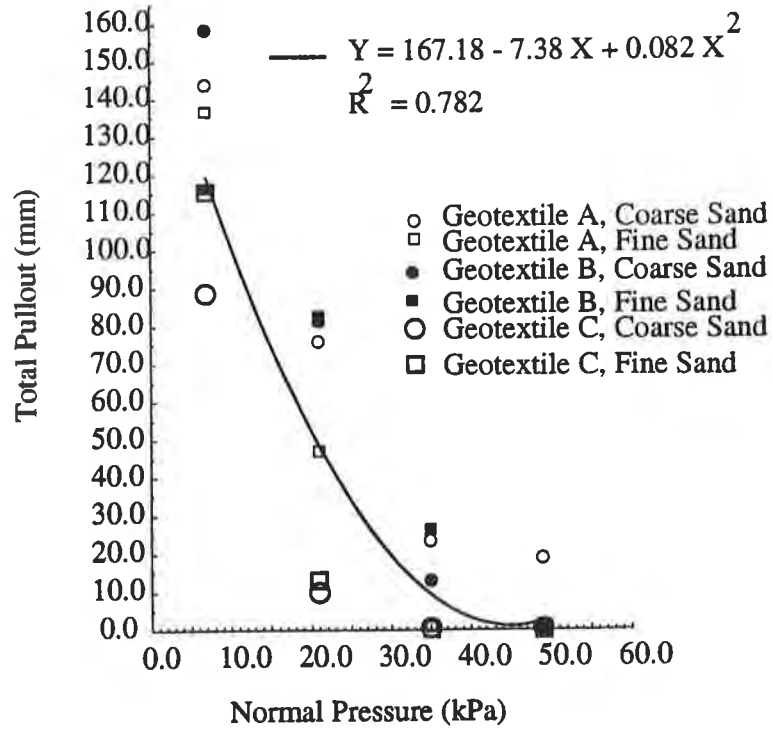
Figure 8 Effect of Normal Pressure on the Total Pullout Displacement for Three Geotextiles and Three Sands
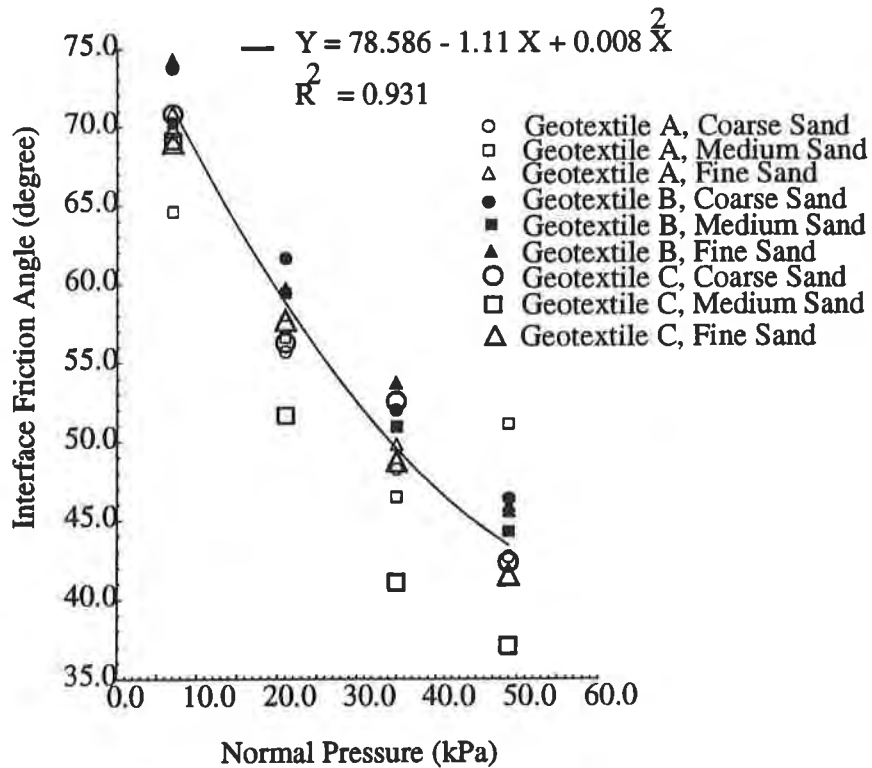
Figure 9 Effect of Normal Pressure on Interface Friction Angle for Three Geotextiles and Three Sands

4.   Interface friction angle decreased with an increase in normal pressure levels. A reduction in the pullout displacement, at high normal pressures, decreased the development of frictional force at the sand-geotextile interface which in turn resulted in a lower interface friction angle.

REFERENCES

1.   Brand, S. R., and Duffy, D. M.,"Strength and Pull out Testing of Geogrids", Geosynthetics' 87 Conference New Orleans, USA.

2.   Rao, G. V., and Pandey, S. K., "Evaluation of Geotextile-Soil Friction", Indian Geotechnical Journal, 18 (1), 1988.

3.   Chang, D. T. T, Wey, W. T, and Chen, T. C., "Study on Geotextile Behaviors of Tensile Strength and Pull Out Capacity", Geosynthetics'93 - Vancouver, Canada, p607.

4.   Murthy, B. R. S., Sridharan, A., and Bindumadhava, "Evaluation of Interfacial Frictional Resistance", Geotextiles and Geomembranes (12), 1993, p235-255.

5.   Ingold, T. S., "A Laboratory Investigation of Soil-Geotextile Function", Ground Engineering (1984), 17(8), p21-28.

6.   Kabeya, H., Karmokar, A. K., "Influence of Surface Roughness of Woven Geotextiles on Interfacial Frictional Behavior- Evaluation Through Model Experiments", Textile Research Journal, 63 (10), p604-610, (1993)

7.   Collios, A., Delmas, P., Gourc, J. P., and Giroud, J. P., (1980) "Experiments on Soil Reinforcement with Geotextiles", Preprint 80-177 The Use of geotextile for Soil Improvements. ASCE National Convention. Portland Oregon, p53-74

8. Holtz, R. D., Kovacs, W. D., "An Introduction to Geotechnical Engineering", Prentice Hall, Inc., Englewood Cliffs, New Jersey 07632, 1991

9. Steel, R. G. D., and Torrie, J. H., "Principles and Procedures of Statistics: A Biometrical Approach", Second Edition, McGraw-Hill Publishing Company, 1980

Seismic Design and Construction

TIME AND FREQUENCY DOMAIN MODELS FOR THE SEISMIC ANALYSIS OF GEOGRID REINFORCED SOIL WALLS

A. Carotti
Dept. of Structural Eng. - Politecnico di Milano University, Milan, Italy
P. Rimoldi
Tenax SpA - Geosynthetics Division, Viganò B. (Lecco), Italy.

ABSTRACT

This paper proposes a mathematical model for the dynamic behavior of geogrid reinforced soil retaining structures under bedrock horizontal excitation. A linear model of the soil without reinforcements (time and frequency domain) is firstly introduced, then a Newtonian non-linear model for the dynamics of soils with geosynthetic interlayer reinforcements is presented. The proposed theory has been checked with numerical simulation of case histories: a reduced scale model of a retaining wall and a full scale railway track retaining wall observed under a record of the Kobe earthquake.

INTRODUCTION

The present paper is aimed to the development of Newtonian multi-DOF (multi-Degrees-Of-Freedom) model for the seismic dynamics of a soil structure reinforced with geogrids or in general with geosynthetic layers.The model takes into account the few experimental observations available in the literature on the seismic behavior of reinforced soil structures, and it schematizes the effect of geogrids in terms of correction of the inherent stiffness and of the inherent damping of the embankment by adding the interlayer stiffness, the interlayer viscous damping and the interlayer Coulomb-type damping provided by the geogrids.The model is divided in two phases:

(i) linear Newtonian model for the dynamics of the soil structure without reinforcements;
(ii) non-linear Newtonian model of the soil dynamics with geogrids reinforcement.

The model has then been checked against the observation of two "geosystems" for which experimental results are available:

1) a reduced-scale sand embankment with geosynthetic reinforcements tested on a shaking table (Murata and Tateyama, 1994);
2) a retaining wall for railway embankment whose behavior, without reinforcement, is known under the 7.2 Richter scale Hanshin-Hawaji earthquake of January 17, 1995 in Japan (Tateyama at Al, 1995).

NEWTONIAN AND FREQUENCY DOMAIN MODELS FOR THE LINEAR DYNAMICS OF THE SOIL STRUCTURE WITHOUT REINFORCEMENTS

<u>Problem Statement. Modal Model.</u> From now on we will assume the following hypotheses, with axes and symbols as in Fig.1:

1. the free surface of the soil structure and the boundary with the bedrock, assumed to be perfectly stiff, are horizontal in the considered area;

2. the soil structure is far enough from any lateral boundary, so that the problem can be considered as indefinite horizontally;

3. the bedrock acceleration has the only horizontal component $\ddot{x}_{br}(t)$ which is assumed to be equal in every point of the bedrock itself;

4. the acceleration $\ddot{x}(z,t)$ of a point in the soil varies with the height on the bedrock, while it is constant in each horizontal plane;

5. the soil structure can be modeled as a stack of many layers, always in the assumption that the separating surfaces are horizontal (Fig.1).

Let's call H the total height, and H_i the thickness of the i-th soil layer. The indefinite equation of horizontal motion is:

$$\frac{\partial \tau_{zx}}{\partial z} - \rho \cdot \ddot{x}_s = 0 \tag{1}$$

where τ_{zx} is the shear stress, x_s is the absolute displacement of a generic point in the embankment, and ρ is the unit mass. If x(t) stands for the displacement of the generic point relative to the bedrock, we have:

$$x_s(z,t) = x(z,t) + x_{br}(z,t) \tag{2}$$

and Eq. (1) can be rewritten as:

$$\frac{\partial \tau_{zx}}{\partial z} - \rho \ddot{x} = \rho \ddot{x}_{br} \tag{3}$$

with the congruence condition on the shear strain γ_{zx}:

$$\gamma_{zx} = \frac{\partial x}{\partial z}$$

Let G be the elastic shear modulus of the soil and $\overline{G}$ its coefficient of viscous shear damping (proportional to the shear-strain velocity):

$$G \triangleq \frac{\tau}{\gamma}; \qquad \overline{G} \triangleq \frac{\tau}{\dot{\gamma}}; \qquad \dot{\gamma} = \frac{d\gamma}{dt} \tag{4}$$

Taking into account the Voigt-Kelvin constitutive law:

$$\tau_{zx} = G \cdot \gamma_{zx} + \overline{G} \cdot \dot{\gamma}_{zx} \tag{4'}$$

Eq.(3) can be rewritten as:

$$G \cdot \frac{\partial^2 x}{\partial z^2} + \overline{G} \frac{\partial^2 \dot{x}}{\partial z^2} - \rho \cdot \ddot{x} = \rho \ddot{x}_{br} \qquad (5)$$

The boundary conditions are:

$$\tau_{zx} = 0 \qquad \text{for } z = 0$$
$$x = 0 \qquad \text{at the bedrock}$$

In the case of a layered embankment, and in the hypothesis of a regular variation of the mechanical properties with the z axis, the system can be reduced to a monolayer system whose horizontal dynamics can be rewritten in the following way:

$$\frac{\partial}{\partial z} \left(G \cdot \frac{\partial x}{\partial z} \right) + \frac{\partial}{\partial z} \left(\overline{G} \cdot \frac{\partial \dot{x}}{\partial z} \right) - \rho \ddot{x} = \rho \ddot{x}_{br} \qquad (6)$$

Let's consider now the lumped mass model with parameters and symbols like in Fig.1 and 2: the multi-layer structure of the soil, with or without reinforcements, is discretized by concentrating, in correspondence of the i-th separation surface, the mass per unit area (that is for: L=D=1 in Fig. 1-3) given by:

$$m_i = \frac{1}{2} \left(\rho_{i+1} \cdot H_{i+1} + \rho_i \cdot H_i \right)$$

When we describe the interactions between two adjacent masses with two interlayers force fields according to Eq. (4), a conservative elastic field and a viscous-type dissipative field are obtained.

Let's introduce now the interlayers stiffness k_i, for the mass of thickness H_i and unit cross-section (that is for: L=D=1 in Fig.3):

$$k_i = \frac{\tau}{\gamma \cdot H_i} = \frac{G}{H_i} \qquad (7)$$

and the interlayer viscous damping c_i:

$$c_i = \frac{\tau}{\dot{\gamma} \cdot H_i} = \frac{\overline{G}}{H_i} \qquad (7)'$$

Let's consider now the 3 DOF system in Fig. 4 and let's indicate with M_i, K_i, C_i the same parameters as m_i, c_i, k_i, but related to a soil element of generic length L (that is, for D=1 in Fig. 3). When we introduce the elastic and viscous interlayer forces:

$$Fe_i = K_i \cdot x_i = k_i \cdot L_i \cdot x_i \qquad (7)''$$
$$Fv_i = C_i \cdot x_i = c_i \cdot L_i \cdot x_i \qquad (7)'''$$

then the interaction scheme of Fig.2 is obtained.

With reference again to Fig.4, and for a system with N layers, the Newtonian equation of motion for

the i-th layer (with i= 1..N) can be written as:

$$M_i \ddot{x}_{si} = K_i(x_i - x_{i-1}) + C_i(\dot{x}_i - \dot{x}_{i-1}) - K_{i+1}(x_{i+1} - x_i) - C_{i+1}(\dot{x}_{i+1} - \dot{x}_i) \tag{8}$$

$$M_i \ddot{x}_i - K_i x_{i-1} + (K_i + K_{i+1})x_i - K_{i+1}x_{i+1} - C_i \dot{x}_{i-1} + (C_i + C_{i+1})\dot{x}_i - C_{i+1}\dot{x}_{i+1} = -M_i \ddot{x}_{br}$$

As shown in Fig.2, Eq. (8) has the first and second items representing the elastic recall and the viscous friction incoming from the lower soil layer, while the third and fourth items represent the same forces from the upper layer: when, according to eq.(2), the absolute acceleration $\ddot{x}_{si}$ of i-th layer is disassembled into the acceleration relative to the bedrock $\ddot{x}_i$ plus the bedrock acceleration $\ddot{x}_{br}$, we obtain Eq. (8).

Let's introduce now the vector of the displacements relative to the bedrock:

$$x \overset{\Delta}{=} (x_1, x_2, ..., x_N)^T \quad , \quad x, \dot{x}, \ddot{x} \in R^{N\times1} \tag{9}$$

If a cyclic motion of the soil is postulated, with integral of motion x(t)= x × cos(wt+f), the matrix equation of the free motion is:

$$M \cdot \ddot{x}(t) + K \cdot x(t) = 0 \qquad
\begin{array}{l}
M \text{ diagonal mass matrix } (M \in R^{N\times N}) \\
K \text{ non - singular stiffness matrix}
\end{array} \tag{10}$$

The response in the physical space can be obtained as a superposition of the m modal contributions:

$$x(t) = \sum_1^m {}_jS_j \cdot p_j(t) \qquad S_j \in R^{N\times1} \tag{11}$$

in which $p_j(t)$ is the generalized motion of the j-th mode S_j. Introducing the vector p(t)=(p_1(t) p_2(t),... p_m(t))^T, Eq. (11) becomes:

$$x(t) = P \cdot p(t) \qquad P \in R^{N\times m} \tag{11'}$$

where

$$P = \begin{bmatrix} \cdot & \cdot & \cdot & \cdot & \cdot \\ \cdot & \cdot & \cdot & \cdot & \cdot \\ \cdot & \cdot & S_{ji} & \cdot & \cdot \\ \cdot & \cdot & \cdot & \cdot & \cdot \\ \cdot & \cdot & \cdot & \cdot & \cdot \end{bmatrix}$$

and S_{ji} is the i-th element of the j-th model shape (physically, the contribution of the j-th mode to the response of the i-th layer).

The modal analysis and the decoupling of the equations of motion can be extended to the system with viscous damping, by introducing a diagonal matrix $\bar{C}$ of the coefficients $\bar{c}_j$ with the form (Clough and Penzien, 1975):

$$\overline{C} = M \cdot \left[\sum_{1}^{N} {}_{j} \frac{\alpha \cdot \omega_j^2}{\overline{M}_j} S_j S_j^T \right] \cdot M \tag{12}$$

whose elements are:

$$\overline{c}_j = k \cdot \omega_j^2 \cdot \overline{M}_j \tag{12'}$$

and

$$\overline{M}_j = \sum_{1}^{n} {}_{i} S_{ji}^2 \cdot M_i \tag{12''}$$

is the j-th modal mass and M_i are the elements of the matrix M. The modal damping is defined as:

$$\overline{k}_j = \omega_j^2 \cdot \overline{M}_j \tag{12'''}$$

The uncoupled modal equations of motion of the soil structure under the bedrock acceleration $\ddot{x}_{br}(t)$ are:

$$\ddot{p}_j(t) + \alpha \omega_j^2 \dot{p}_j(t) + \omega_j^2 p_j(t) = -\Gamma_j \cdot \ddot{x}_{br}(t) = f_j(t) \qquad j = 1....m \tag{13}$$

where:

$$\alpha \triangleq \frac{\overline{G}}{G} \tag{13'}$$

and Γ_j is the modal participation factor:

$$\Gamma_j = (S_j^T \cdot M \cdot 1) / (S_j^T \cdot M \cdot S_j) \tag{13''}$$

The function:

$$f_j(t) = -\Gamma_j \cdot \ddot{x}_{br}(t)$$

is the modal forcing function at the bedrock.

It is possible to go back from the generalized model space, expressed in Eq. (13), to the physical space, through Eqs. (11).

Eq. (13) can be reformulated in the state space by introducing the following state vector r:

$$r \triangleq \left(r_1, r_2, ..., r_m, \dot{r}_1, \dot{r}_2, ..., \dot{r}_m \right)^T$$

Then Set (13) becomes:

$$\begin{cases} \dot{r} = A r + b \cdot \ddot{x}_{br} \\ x = E r \end{cases}$$

(14)

where:

$$A = \begin{bmatrix} 0_{m \times m} & & & I_{m \times m} \\ -\omega_1^2 & 0 & \cdots & 0 & -\alpha\omega_1^2 & 0 & \cdots & 0 \\ 0 & -\omega_2^2 & \cdots & 0 & 0 & -\alpha\omega_2^2 & \cdots & 0 \\ \vdots & \vdots & \ddots & \vdots & \vdots & \vdots & \ddots & \vdots \\ 0 & 0 & \cdots & -\omega_m^2 & 0 & 0 & \cdots & -\alpha\omega_m^2 \end{bmatrix}$$

$$b = \left(0_{1 \times m}, -\Gamma_1, -\Gamma_2, \ldots, -\Gamma_m\right)^T$$

$$E = \begin{bmatrix} S_1, & S_2, & \ldots, & S_m, & 0_{n \times m} \end{bmatrix}$$

Modelling the Soil Structure Response in the Frequency Domain. Bode Spectra and Power Density Spectra. The spectral analysis, which in the linear case is based on the Laplace transform technique, allows to obtain a compact representation of the response in the frequency band of practical interest (indicatively 0÷5 Hz) and the evaluation of the local amplification.

We will now assess the spectral response of the soil structure in the two following situations:
(i) the input at the bedrock is a sinusoidal accelerogram with slow varying frequency, the so called Sine-Sweeping excitation (Fig.5.a): the frequency response of the soil structure is obtained in terms of magnitude and phase plots (Bode plots);
(ii) the input at the bedrock is a multifrequency zero-mean non-stationary coloured noise accelerogram (Fig.5.b): the Power Spectral Density (PSD) of the soil response is obtained in this case.

(i) Frequency Response Transfer Functions. The spectrum of the response is obtained from a Sine-Sweeping accelerogram at the bedrock (Fig. 5.a), in such a way that the steady state is established for each frequency. The amplitude of the steady state response is plotted for each frequency. The transfer function Q_{ji} which ties the seismic acceleration $\ddot{x}_{br}$ to the response x_i of the i-th layer in j-th mode, is:

$$Q_{ji} = -\frac{\Gamma_j S_{ji}}{s^2 + \alpha\omega_j^2 s + \omega_j^2} \qquad \begin{array}{l} j = 1, \ \ldots, \ m \\ i = 1, \ \ldots, \ n \end{array}$$

(15)

where s is the Laplace complex variable.

(ii) Power Spectra of the wall Response. Let's consider the motion (13) of the generic j-th mode. The steady state response of the j-th mode under a stationary, ergodic, random forcing function, like in Fig. 5.b, is given by the PSD of the motion $p_j(t)$ of the j-th mode. Based on the Fourier transform of Eq. (13) (Clough and Penzien, 1975), the relationship between the PSD $\overline{S}_f$ of the forcing function and the PSD $\overline{S}_P$ of the soil modal response is:

$$\overline{S}_P(\omega) = \left|\overline{Q}(\omega)\right|^2 \cdot \overline{S}_f(\omega)$$

(16)

where $\overline{Q}(\omega)$ is the frequency response function of the system, obtained by the Fourier transform of Eq. (13) as:

$$\overline{Q}(\omega) = \frac{1}{\omega_j^2 \cdot \overline{M}_j \cdot \left[(1-\Omega^2) + i \cdot \left(\dfrac{\alpha \cdot \omega_j}{2} \cdot \Omega\right)\right]}$$

(17)

where:

$i = \sqrt{-1}$ = imaginary unit;

$\Omega = \dfrac{\omega}{\omega_j}$ = non-dimensional circular frequency;

ω = current circular frequency of the input.

NON-LINEAR DYNAMICS OF THE EMBANKMENT WITH GEOGRIDS REINFORCEMENTS.

Combined soil-and-geogrids stiffness and damping. Parameters estimation.
(i) Soil. For our problem with one only stress/strain component we will make initial reference to the non-linear Ramberg-Osgood law, which, with reference to Fig. 3 and for a pure shear deformation, can be written as:

$$\begin{cases} \hat{\alpha}\left(\dfrac{\tau-\tau_0}{B\cdot\tau_y}\right)^a + \dfrac{\tau-\tau_0}{B\cdot\tau_y} = \dfrac{\gamma-\gamma_0}{B\cdot\gamma_y} \\ \\ \tau_y = G_0 \cdot \gamma_y \end{cases}$$

(18)

When we apply shear load cycles to the soil (Prakash, 1981), as shown in Fig. 6.a, the parameters in Eq. (18) take the following values: for the first loading curves, B=1 and $\gamma_0=\tau_0=0$; for the successive ones, B=2, while γ_0 and τ_0 are the values at the moment of the last inversion of the loading-unloading cycle. The other parameters depend on the type of soil (Trifunac, 1980; Veletsas and Meek, 1974; Kansel et Al, 1976), with the following orders of magnitude:

$$a \sim 1 \div 3 \; ; \; \hat{\alpha} \sim 10^{-2} \div 10^{-3}; \; \gamma_y \sim 10^{-4} \div 10^{-6}$$

In Eq. (18), G_0 is the initial tangent modulus, that is the tangent at the origin to the first loading curve. Eq. (18) includes, as a particular case, the elastic case for $G_0=0$, and the elastic-perfectly-plastic case for $G_0=\infty$.

In a pure shear deformation regime, and seeking for a linearized equation of the Voigt-Kelvin type, the linearization is defined when the G e $\overline{G}$ parameters are identified. From the experimental knowledge of the (τ, γ) viscoelastic cycles under an armonic forcing function, it is possible to deduce the left or right extreme point P_0 (τ_0, γ_0) of the generic cycle in Fig.6a, and also the area L of the cycle. These two data allow to

identify the two force fields in the cycle:

- the conservative elastic force field whose characteristics constant is:

$$G = \frac{\tau_o}{\gamma_o}$$

(19)

The constant G represents the slope of the longitudinal axis of the generic elliptical cycle (see Fig.6.a);

- the dissipative force field of the viscous type: it is defined by the constant $\overline{G}$, which, based on the second Eq.(4), provides the pure shear stress when the soil element, in pure shear strain, passes at unit speed $\dot{\gamma} = 1$ (s⁻¹) through the undeformed shape (that is for $\gamma = 0$). From the experimental knowledge of the work L and remembering that the work L in an elliptical steady cycle coincides with the area of the ellipses itself, we have immediately:

$$\overline{G} = \frac{L}{\pi \ \omega \ \gamma_0^2}$$

(20)

where γ_0 and $\overline{G} \cdot \gamma_0$ are the two semi-axis of the elliptical cycle and ω is the circular frequency of the steady motion.

(ii) Geogrids. From laboratory tests (Montanelli and Moraci, 1997), we admit the following mechanical actions between the geogrids and the soil layers on top and bottom, as a consequence of the soil-geogrid interlocking:

1. an increase in the interlayer soil stiffness, proportional to the elastic stiffness of the geogrids. From monotonic tensile tests on geogrids (Fig.6b) the load strain curve has been reduced to a tri-linear curve and the stiffness value in each linear segment have been identified. We have focused the attention on the 1ˢᵗ stage, with strain threshold $\varepsilon_I = 0.03$. If L_g is the geogrid length in the direction of the seismic acceleration, F is the tensile force applied to the geogrid and Δl its elongation, we postulate that, in condition of interlocking between the geogrids and the soil layers, the contributed inter-layer stiffness is:

$$K_{g_i} = \frac{F}{\Delta l} = \frac{F}{\varepsilon_I \cdot L_g}$$

(21)

The length L_g can be sized in order to satisfy the condition of elastic response of the sheet within the 1ˢᵗ segment of the trilinear scheme of Fig. 6b. Adopting a safety factor FS=2.0, that is limiting to the response within the first half of the first segment, the condition of elastic stability for the geogrid between the i-th and the (i-1)-th soil layer is therefore:

$$\max(x_i - x_{i-1}) < (\varepsilon_I \cdot L_g) / FS$$

(22)

2. An increase of the interlayer viscous damping force, equal to the inherent viscous damping of the geogrid. From sinusoidal cyclic tests with frequency f = 1.0 Hz (see in Fig.6b one of the several tests performed at Tenax SpA Laboratory) and from the examination of an average elliptical cycle, the average viscous force

F_{visc} (force in counterphase to the velocity, when the displacement is nil) has been obtained, together with the value of the peak velocity (product of the peak displacement, obtained from the test plot, and of the circular frequency $\omega = 2\pi f$ of the test). From the ratio force/velocity the damping coefficient is immediately obtained. In details:

$$C_{gi} = \frac{F_{visc}}{\Delta l \cdot \omega} = \frac{F_{visc}}{\varepsilon \cdot L_g \cdot \omega} \tag{23}$$

where Δl coincides with the differential interlayer displacement $(x_i - x_{i-1})$, when perfect interlocking between soil and geogrids has been assumed.

3. An increase of the interlayer damping due to the Coulomb friction between the geogrid and the soil layers, under the weight of the soil above (already proposed in 1994 by Budhu and Halloum). The Coulomb friction due to the i-th geogrid (where N is the number of geogrid layers) is:

$$F_{Ci} = -tg\,\phi_{sg} \cdot g \cdot \sum_{k=i}^{n} M_k \cdot sign(\dot{x}_k) \ . \tag{24}$$

where the signum function $sign(\dot{x}_k)$ introduces the non linearity in the model. The direction of the opposing frictional force is determined by the sign of $\dot{x}_i$. In Eq. (24) ϕ_{sg} is the soil-geogrid interface friction angle; g is the gravity acceleration.

(iii) Non-linear Newtonian model with Geogrids. The Newtonian equations of motion for the N-DOF non-linear model with geogrids (N soil layers with N geogrid layers, see Fig.2 and 4, can be obtained from Eq.(8) of the model without geogrids, taking into account the elastic stiffness K_{gi}, the viscous damping C_{gi} and the Coulomb-type friction force F_{ci} induced by the geogrids, defined in Eq.s (21)÷(24).

Indicating with $\hat{M}$ the distributed load on top of the wall, the Newtonian equation of motion for the i-th layer is:

$$\begin{aligned}
M_i \cdot \ddot{x}_i = \ & -K_i(x_{i-1} - x_i) - C_i(\dot{x}_{i-1} - \dot{x}_i) + K_{i+1}(x_i - x_{i+1}) + C_{i+1}(\dot{x}_i - \dot{x}_{i+1}) - \\
& -K_{gi}(x_{i-1} - x_i) - C_{gi}(\dot{x}_{i-1} - \dot{x}_i) + K_{gi+1}(x_i - x_{i+1}) + C_{gi+1}(\dot{x}_i - \dot{x}_{i+1}) + \\
& +tg\phi_{sg} \cdot g \cdot \left(\sum_{k=i}^{n} M_k + \hat{M}\right) \cdot sign\,\dot{x}_i - tg\phi_{sg} \cdot g \cdot (\sum_{k=i+1}^{n} M_k + \hat{M}) \cdot sign\,\dot{x}_{i+1} = \\
& = -M_i \cdot \ddot{x}_{br}
\end{aligned} \tag{25}$$

where

$$g \cdot \left(\sum_{k=i}^{n} M_k + \hat{M}\right)$$

represents the total gravity load acting on the i-th geogrid layer.

NUMERICAL SIMULATIONS

We have checked the proposed mathematical model by applying it to the simulation of two different geodynamic systems, for which good descriptions are available in the literature:

1. a reduced-scale model of a sand wall with geogrid reinforcements, submitted to a non stationary sinusoidal excitation at the shaking table: the system is described in Fig.8 and in Murata and Tateyama (1994). Primitives and derived numerical data are provided in Tables 1 and 2. Modal frequency and damping parameters are summarized in Table 1. In our simulations only the 3 main geogrids of Fig. 8 has been taken into account.

2. a full-scale retaining wall for railway track embankment (Fig. 10) whose response under the Hanshin-Awaji Earthquake has been widely described in Tateyama et Al (1995). A summary of data is given in Tables A1 and A2. We have evaluated the effects of simulated geogrid reinforcements, under various seismic excitation conditions.

Reduced-scale reinforced wall. Let's refer to the reinforced structure in Fig.8. From Murata and Tateyama (1994), the amplification of the absolute acceleration at the top of the wall in respect to the seismic acceleration at the bedrock is evident. Let's define the "spectrum along the height" as a plot of the peak response displacement or acceleration of each soil layers (on the horizontal axis) versus the height h_i of the layers themselves (on the vertical axis). Such peak values are, in general, asynchronous. Results of this simulation are shown in Fig.9: Fig. 9.a gives the "amplification ratio" of the peak absolute acceleration of the soil layers versus the bedrock acceleration; Fig. 9.b gives the relative displacement of the layer ("displacement amplification"). Two spectra are provided, "without" and "with" geogrids, related to a monofrequency sinusoidal seism at the bedrock, with peak acceleration of $5 m/s^2$ at the frequency of 3.4 Hz (as considered in Murata and Tateyama, 1994).

In our numerical simulation, an $L_g = 3.5$ meters turns out in a $\Delta l_l / FS$ which is greater than the $\max(x_i - x_{i-1})$ of one order of magnitude. Assuming a mean differential displacement $< (x_i - x_{i-1}) >= 0.002$ m, we obtain a $C_{g_i} = 54.7 \, kN \cdot s / m$ damping coefficient. Other key numerical values for the same example are reported in Tables 1 and 2.

It is worth to note the reduction of the amplification ratio at the top of the wall obtained with geogrids: from an amplification ratio (AR) of 4.7 "without" geogrids, to an AR of 1.5 in the model "with" grids. Also the reduction of the displacement amplification from 42 mm to 7 mm is worth to be noted: it fit very well with the observed results.

Railway track embankment. Let us consider the soil structure in Fig. 10, reinforced with 15 geogrid sheets of 1.0 m length on each side of the wall (numerical data are given in Tables 1-2). It has been submitted to a simulated Kobe seism with peak acceleration of $8 \, m/s^2$. The accelerogram has been simulated with a non stationary zero mean gaussian noise filtered in the band (1.5, 2.5] Hz: an example is given in Fig.11. Fig.12 gives the response spectra along the height of the embankment; Fig.13 gives the corresponding Power Spectral Densities and Fig.14 the corresponding time histories.

CONCLUSIONS

From the indefinite equation of motion of a wall or embankment, in presence of a cinematic excitation at the bedrock, the Authors propose to model the wall as a multi-DOF lumped-masses system.

This technique afford advantages both in the description of the interlayer interactions, particularly when the wall is reinforced with geogrids; and in the interpretation of the phenomena through modal decoupling of the seismic dynamic response. Based on this scheme, the Authors propose to describe the soil-geogrid interaction as a local increase of both stiffness and damping. In this way the Authors have obtained a non-linear Newtonian model of the dynamics of reinforced walls.

The model has been validated on the base of the few available observations and then utilized to extrapolate the behavior of reinforced walls of different geometry under various excitations.

Results are encouraging and prelude to a systematic plan of numerical simulation. In the near future the Authors anticipate to develop a linear approximation of the non-linear model, which will furtherly facilitate the analysis and design of geogrid reinforced walls in seismic areas.

REFERENCES

Budhu M., Halloum H. (1994) "Seismic External Stability of Geotextile Reinforced Walls.", Fifth International Conference on Geotextiles, Geomembranes and Related Products, Singapore.

Clough, R.W., and Penzien, J. (1975), "Dynamics of structures", Mc Graw-Hill, New York.

Franklin A. G. (1982) "Seismic stability of embankment structures", Structural Safety, Vol. 1, p. 141.

Kausel E., Roesset J. M., Christian J. T. (1976) "Nonlinear behaviour in soil structure interaction", J. Geotechn. Engng. Division, ASCE, Vol. 102, N.GT11.

Montanelli F., Moraci N. (1997) "Behaviour of Geogrids under cyclic loads", Proc. Geosynthetics'97 Conf., Long Beach, California, USA.

Murata O., Tateyama M. (1994) "Shaking table tests on a large geosynthetic-reinforced soil retaining wall model. Recent Case Histories of Permanent Geosynthetic-Reinforced Soil Retaining Walls", Tatsuoka & Leshchinsky Editors.

Prakash S. (1981) "Soil Dynamics", New York.

Tateyama M., Tatsuoka F, Koseki J., Horti K. (1995) "Damage to Soil Retaining Walls for Railway Embankments During the Great Hanshin-Awaji Earthquake", First International Conference on Earthquake Engineering IS-Tokyo '95 Conf., Tokyo, Japan.

Tatsuoka F., Tateyama M., Koseki J. (1995) "Performance of Geogrid-Reinforced Soil Retaining Walls During teh Great Hanshin-Awaji Earthquake", First International Conference on Earthquake Engineering IS-Tokyo '95, tokyo, Japan.

Trifunac M. D. (1980) "Effects of site geology on amplitudes of strong motion", Proc. VII ECEE, Vol. 2, p. 145, Istanbul, Turkey.

Veletsos A. S., Meek J. W. (1974) "Dynamic behaviour of building - foundation systems", Earth.Engng.Struct.Dyn., Vol. 2, p. 121.

TABLE A1: NUMERICAL DATA FOR THE SOIL STRUCTURES IN FIG. 8 AND FIG. 10

	Structure in Fig.8	Structure in Fig. 10
dimensions HxLxD	H = 2.5 m L = 3.5 m D = 1 m	H = 8 m L = 13.8 m D = 1 m
soil density	ρ = 1400 kg/m^3	ρ = 18 (kN·s^2/m)/m^3
thickness of each soil layer (totally 3 layers)	H_i = H/3 = 0.83 m	H_i = H/3 = 2.7 m
mass of each layer	M_i = 4067 kg/m	M_i=6.62·10^3 Kgf·s^2/m
elastic shear modulus	G = 3000 kPa	G = 10000 kPa
viscous shear modulus	$\overline{G}$ = 0.0018·G = 20.4 kN·s/m^2	$\overline{G}$ = 0.0018·G = 18 kN·s/m^2
elastic stiffness coeff.	K_i = (G/H$_1$)·L·D = 1.20·10^6 Kgf/m	K_1 = K_2 =(G/H$_1$)·L·D = 5.17·10^4 kN/m K_3 = K_1/(L/2) = 7.5·10^3 kN/m
viscous damping coeff.	C_i = ($\overline{G}$/H$_i$)·L·D = 86.1 kN·s/m	C_i = ($\overline{G}$/H$_i$)·L·D = 93.7 kN·s/m
angle of internal friction	ϕ = 25° ; f_{ds} = 0.8	ϕ = 35°; f_{ds} = 0.8

TABLE A2: NUMERICAL DATA FOR THE SOIL STRUCTURES IN FIG. 8 AND FIG. 10

	Geogrids in Fig. 8	Geogrids in Fig. 10
number of layers	3	15
dimensions	L_g = 3.5 m	L_g = 2 m
dimensions of the mass between geogrids	H_g = 0.83m m_g = 4067 Kg	H_g = 8/15 m = 0.53 m m_g = 1920 Kg
elastic stiffness coefficient	K_{gi} = 74.3 kN/m	K_{gi} = 130 kN/m
viscous damping coefficient	C_{gi} = 54.7 kN·s/m	C_{gi} = 80 kN·s/m
Coulomb-type friction coefficient	F_{C1} = tg(ϕ_{sg})·g·m$_g$·3 = 43.5 kN F_{C2} = tg(ϕ_{sg})·g·m$_g$·2 = 29 kN F_{C3} = tg(ϕ_{sg})·g·m$_g$ = 14.5 kN	F_{C1} = tg(ϕ_{sg})·g·m$_g$·$\sum_{j=11}^{15} j$ = 650 kN F_{C2} = tg(ϕ_{sg})·g·m$_g$·$\sum_{j=6}^{10} j$ = 400 kN F_{C3} = tg(ϕ_{sg})·g·m$_g$·$\sum_{j=1}^{5} j$ = 150 kN
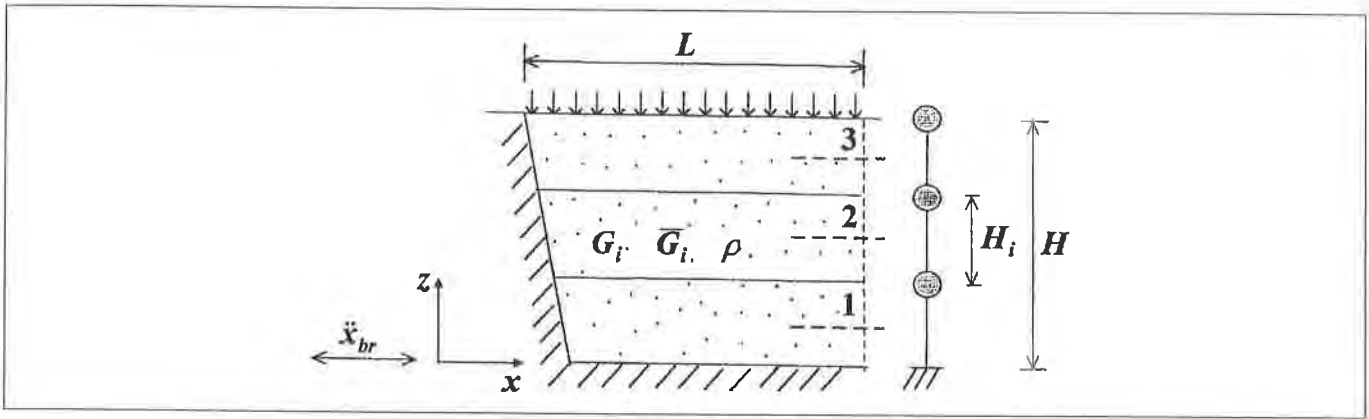
Figure 1 Scheme of the lumped-masses model

F_e : elastic force field
F_v : viscous force field
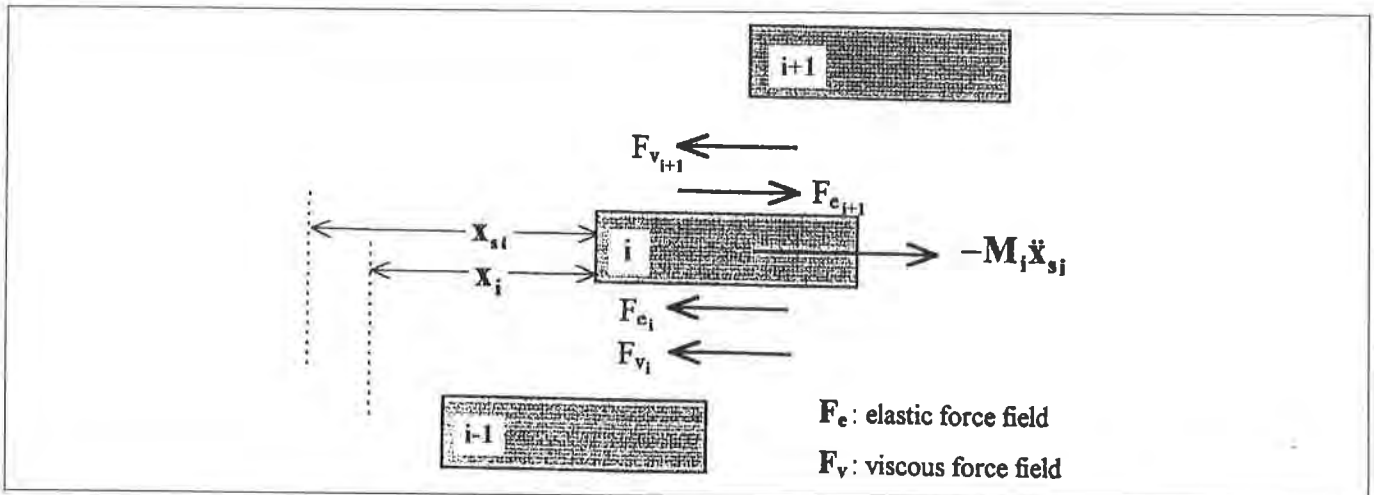
Figure 2 The interlayer interactions in seismic conditions

$$K \overset{\Delta}{=} \frac{F}{x}$$
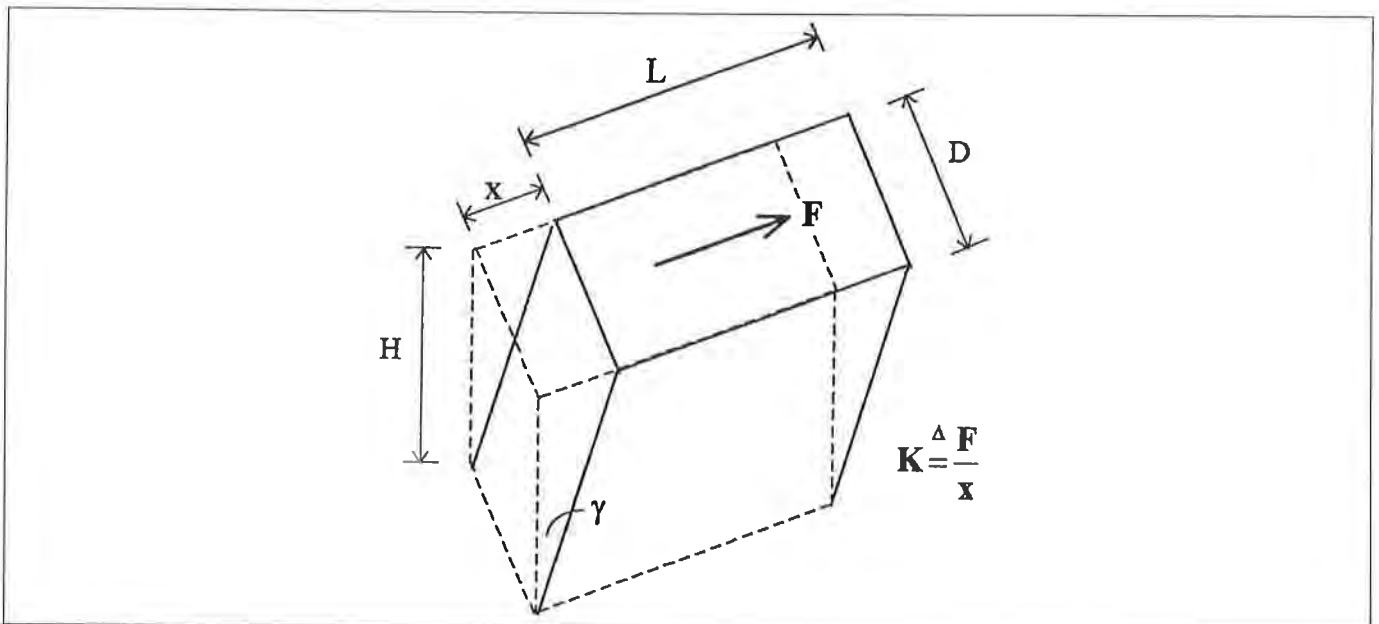
Figure 3 Scheme of the deformation of a soil layer
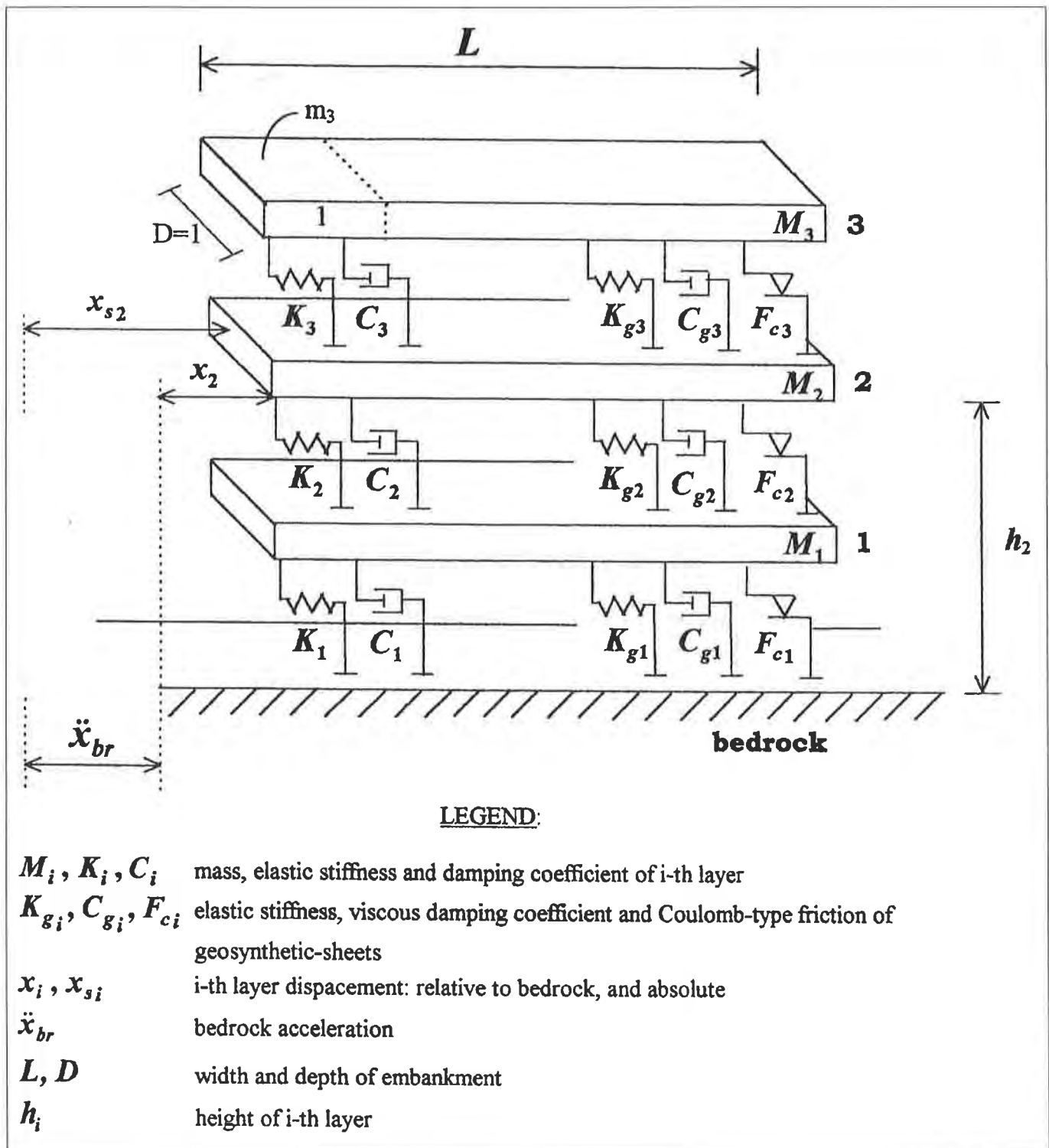
Figure 4 Example of a 3-DOF system with the stiffness and damping parameters

LEGEND:

M_i, K_i, C_i mass, elastic stiffness and damping coefficient of i-th layer

K_{g_i}, C_{g_i}, F_{c_i} elastic stiffness, viscous damping coefficient and Coulomb-type friction of geosynthetic-sheets

x_i, x_{s_i} i-th layer dispacement: relative to bedrock, and absolute

$\ddot{x}_{br}$ bedrock acceleration

L, D width and depth of embankment

h_i height of i-th layer
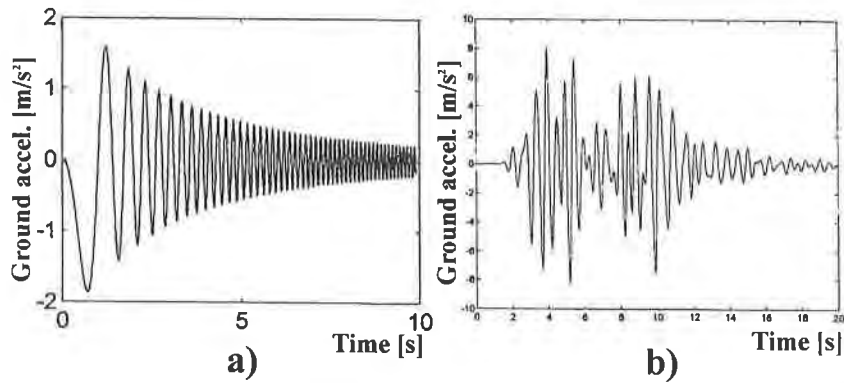
Figure 5 Two types of accelerogram at the bedrock: a) Sine-Sweep; b) coloured noise
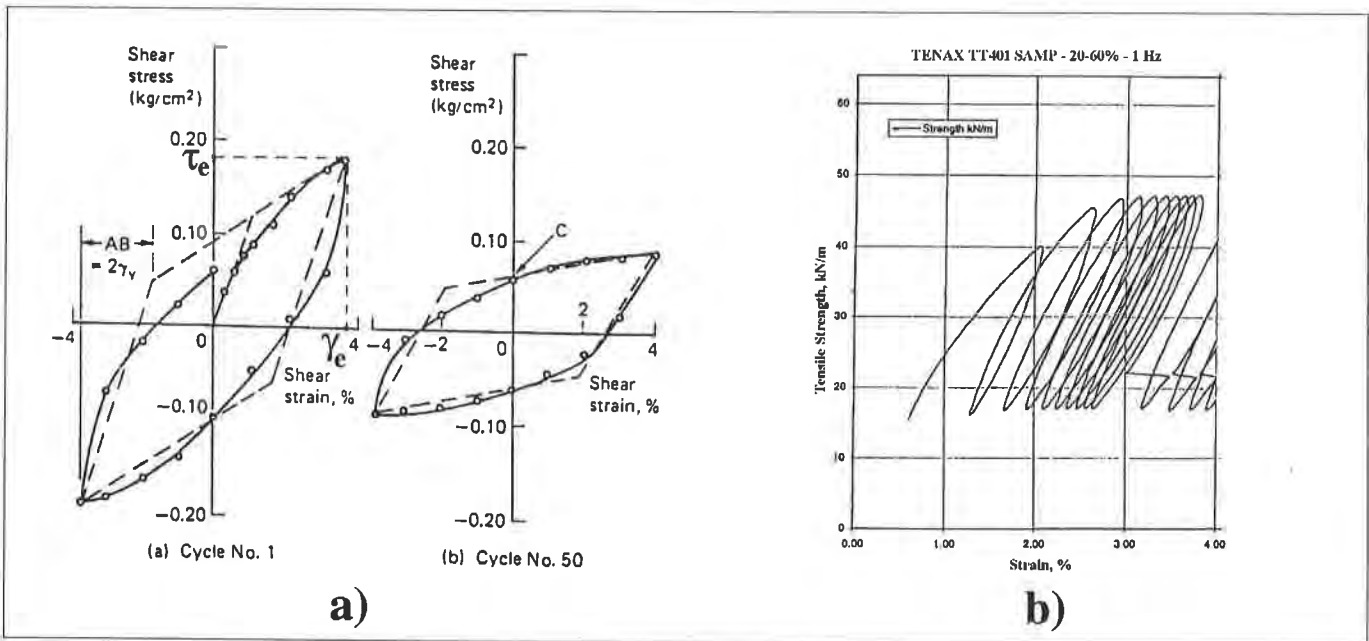
Figure 6 Typical stress-strain curves under cyclic loading: a) for a soil (from Prakash, 1981);
b) for a mono-oriented geogrid with 80 kN/m ultimate tensile strength
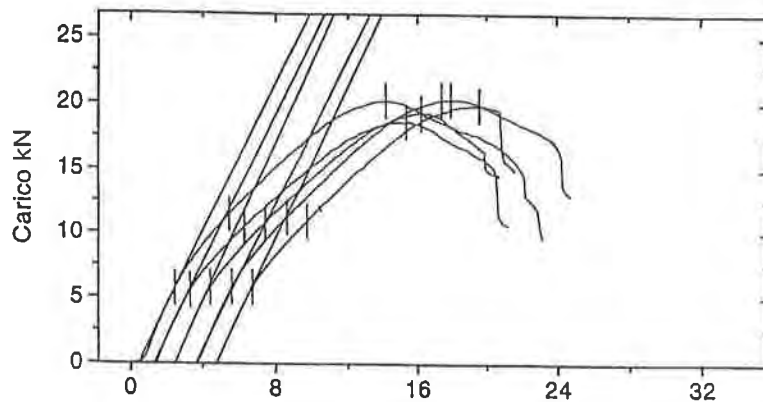
Figure 7 Typical stress-strain curves under monotonic loading
for a mono-oriented geogrid with 80 kN/m ultimate tensile strength
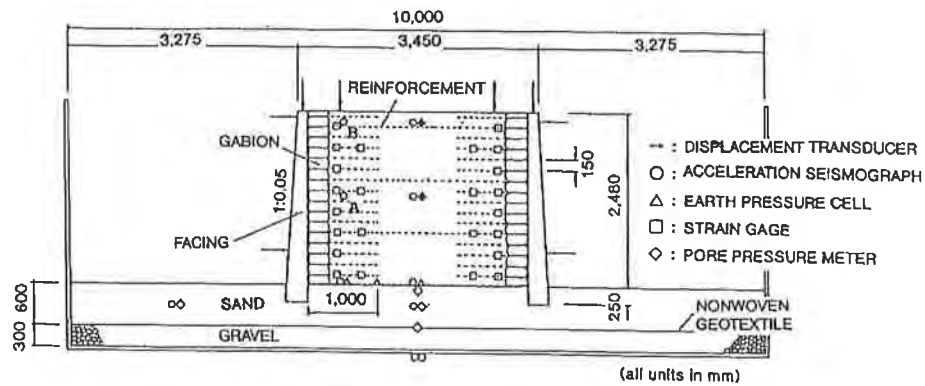
Figure 8 Reduced scale model of a reinforced wall,
tested on a shaking table (modified from Murata and Tateyama, 1994)
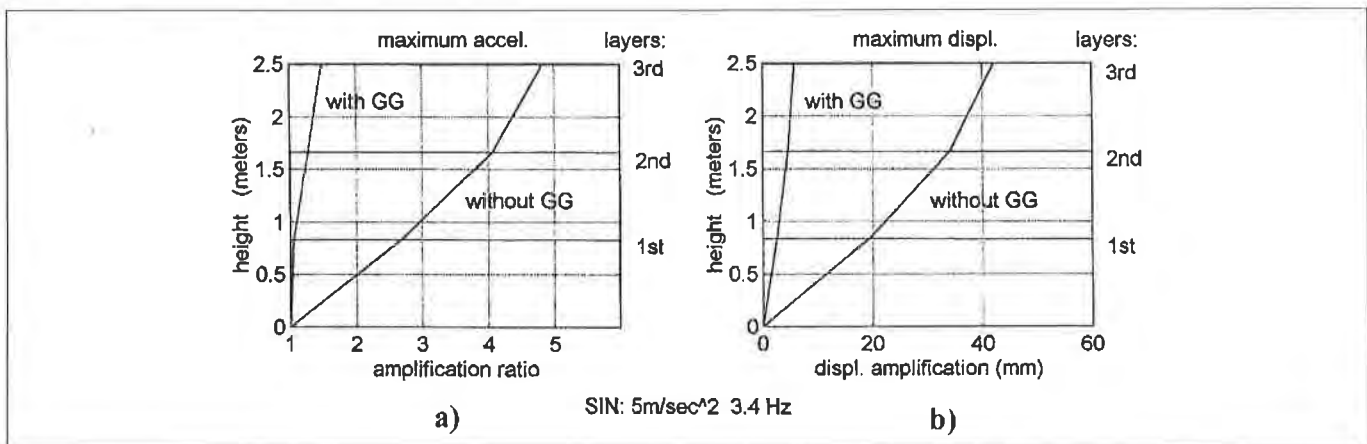
Figure 9 Plot along the height of acceleration and displacement for the structure in Figure 8
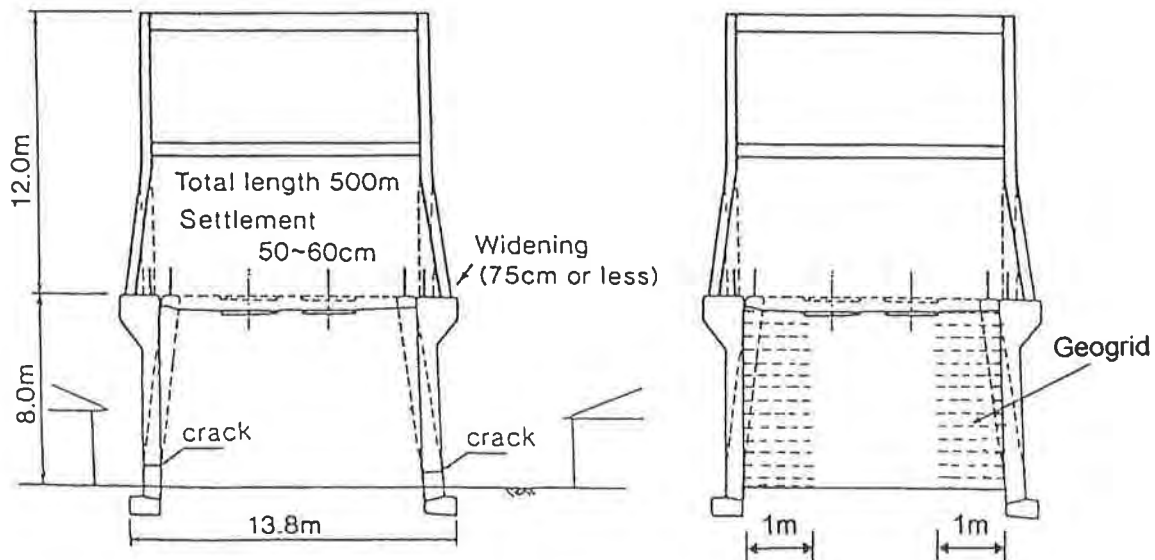
Figure 10 Retaining wall for track embankment (modified from Tateyama et Al., 1995)

simulation of KOBE seism   1995/01/17 05:46   N000E 8.206 m/s^2
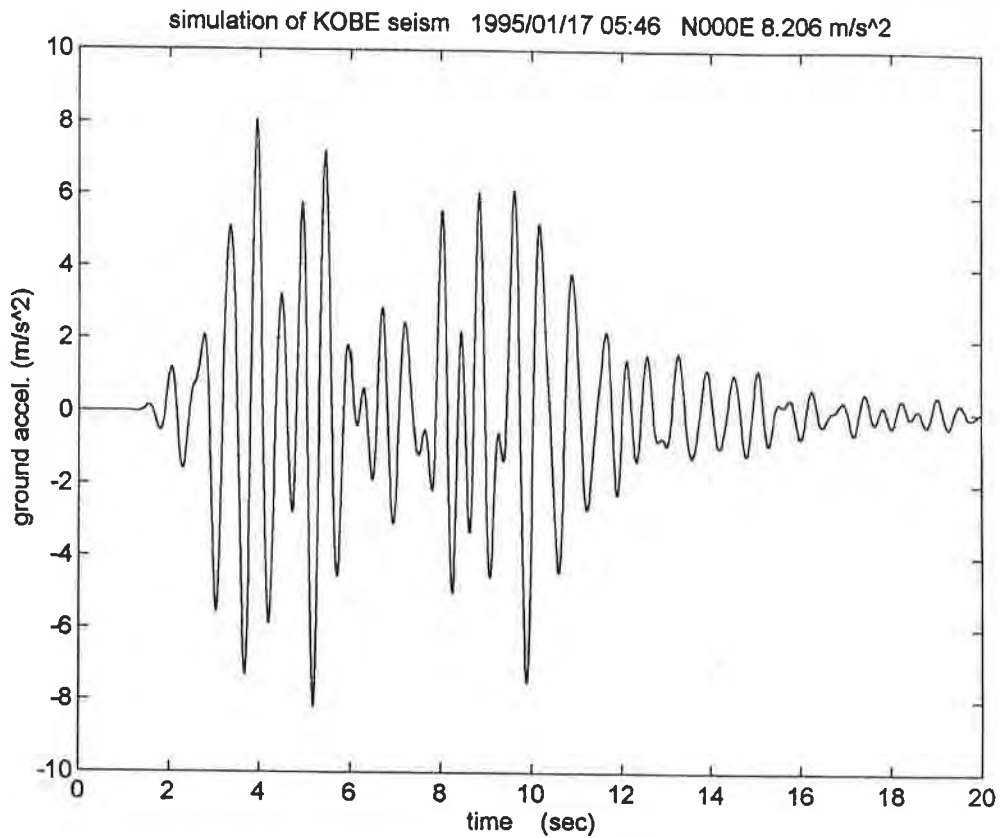
Figure 11 Simulation of the Kobe earthquake

a)

b)
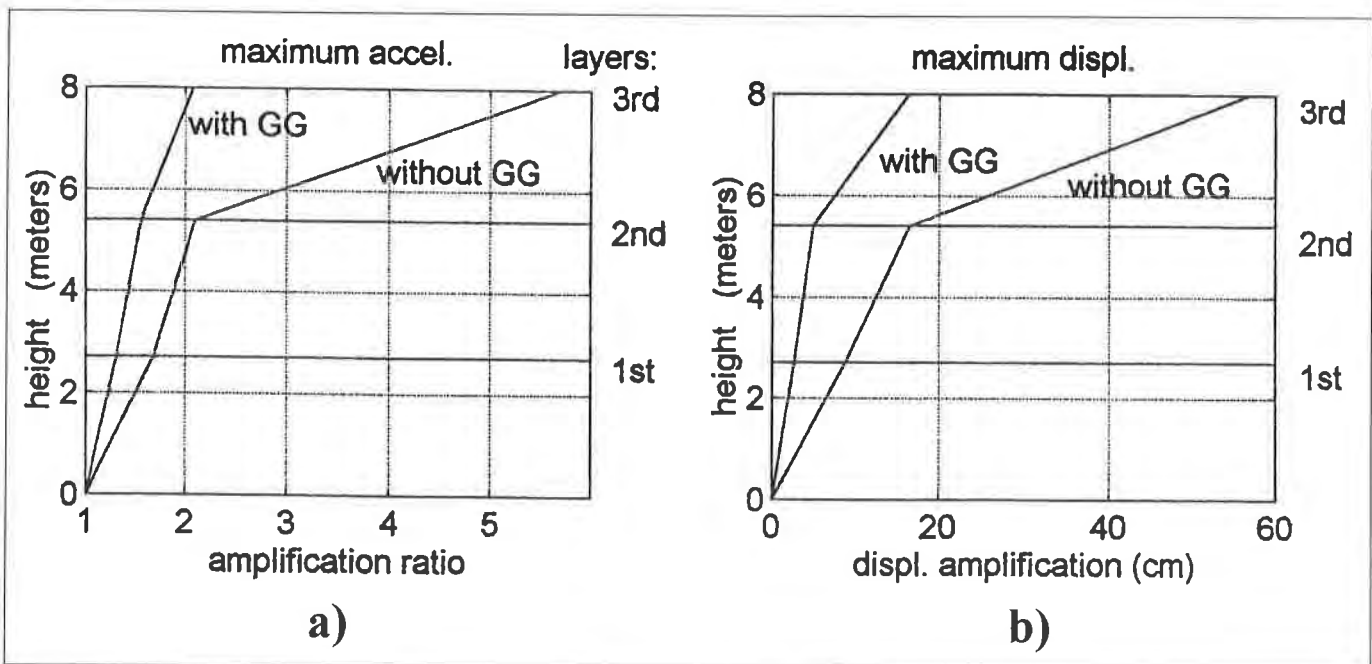
Figure 12 Plot along the height of acceleration and displacement
for the structure in Figure 10 under the seism in Figure 11
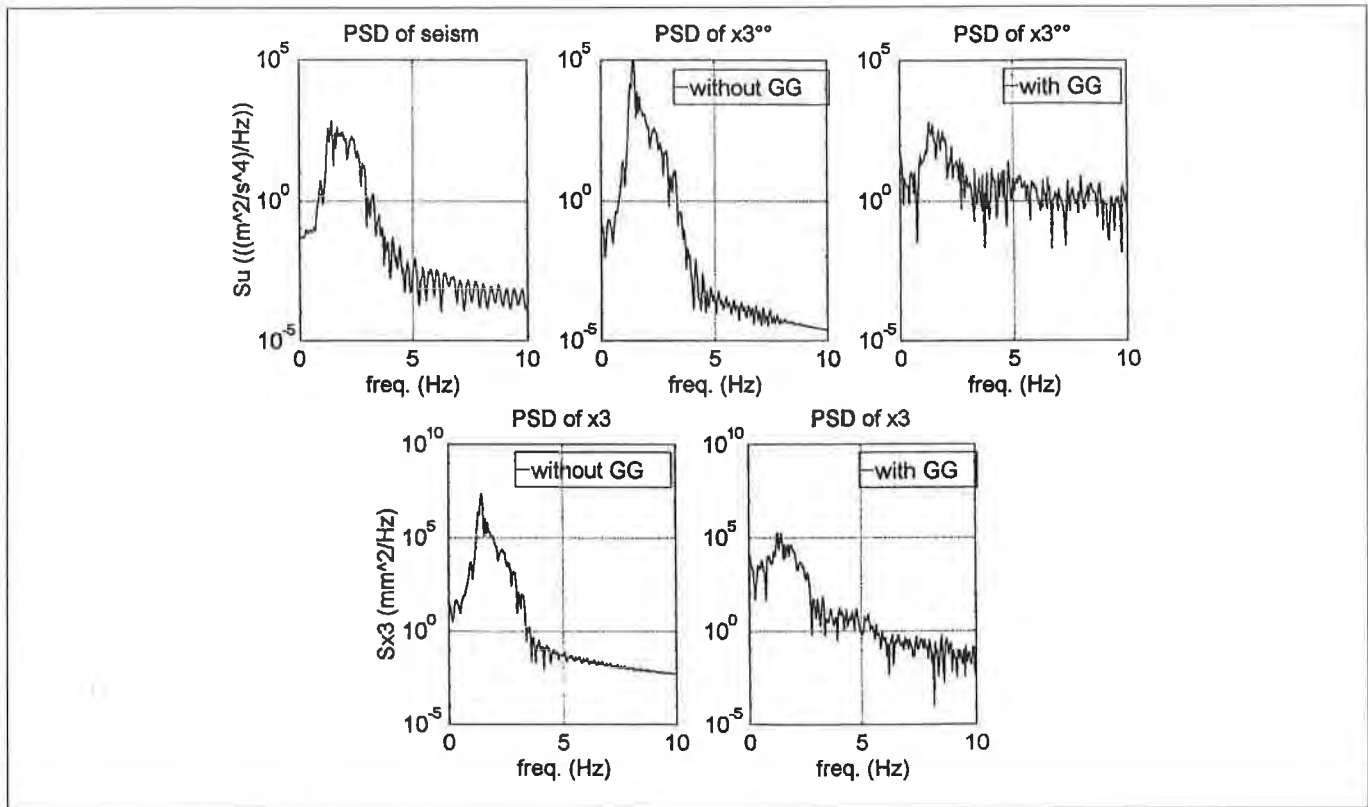
Figure 13 Power Spectral Densities for the structure in Figure 10 under the seism in Figure 11
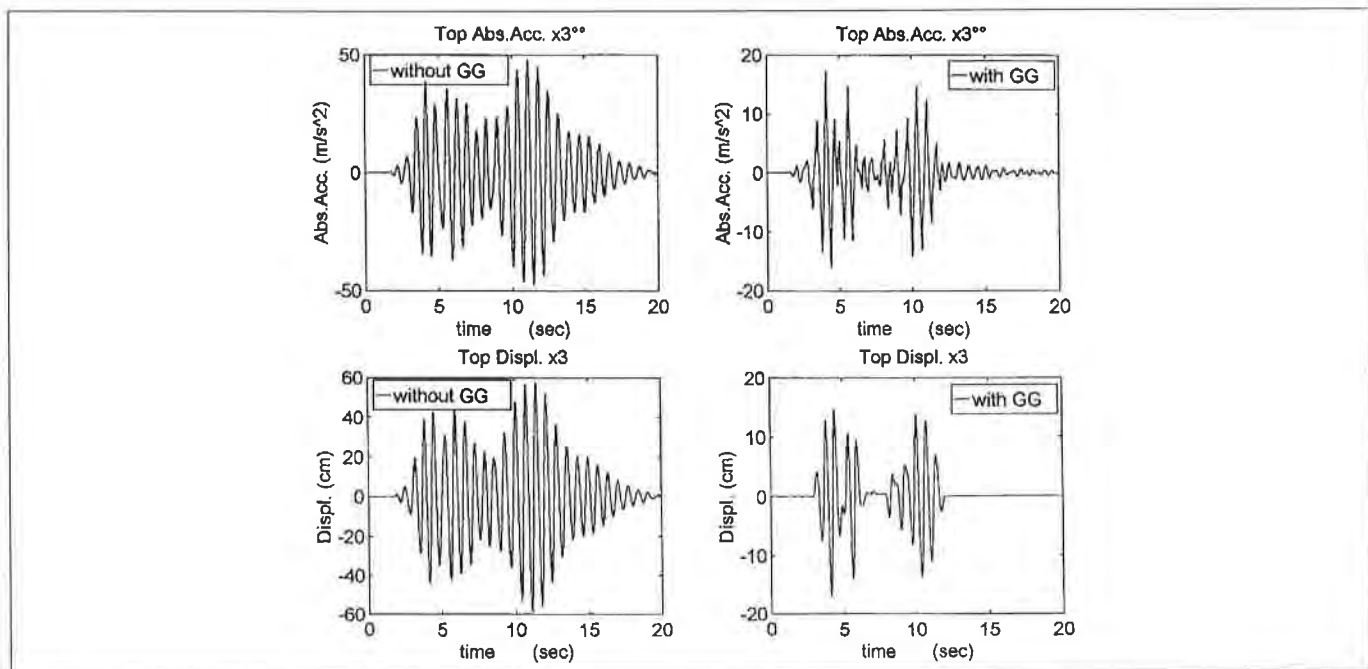
Figure 14 Time histories of acceleration and displacement at the top of the wall
in Figure 10, without and with geogrids

BEHAVIOR OF GEOGRIDS UNDER CYCLIC LOADS

MORACI NICOLA, UNIVERSITY OF REGGIO CALABRIA, ITALY
MONTANELLI FILIPPO, TENAX SPA, ITALY

ABSTRACT

This paper deals with the mechanical behavior of two geogrids in HDPE and PET for soil reinforcement applications. The behavior has been investigated by means of cyclic tensile tests conducted at different frequencies and load ratios for a duration up to 10,000 cycles. The above tests allowed the definition of the geogrid tensile properties under cyclic loads, such as the unload-reload tensile modulus and damping characteristics. The tests results allowed the definition of a method to predict the geogrid behavior that will be useful for future programmed test series in interaction with soil. Pre-stressed cyclic tests have been performed by means of tensile cyclic tests performed at relatively high frequencies with loads ranging around the long term design loads of the geogrids. The described testing methodologies and results are a valuable tool for qualitative prediction of the behavior of a geogrid when subject to repetitive loading such as traffic, train loading and earthquakes.

INTRODUCTION

In several applications, geogrids are subjected to cyclic or dynamic loads. These loads can be directly applied to the reinforcement by external conditions such as earthquakes, traffic and train loadings. The function of geogrid reinforcement can be such to be designed to withstand certain static loads, with additional cyclic loads, or to perform its reinforcement function only when subjected to cyclic loads. In the first instance a constant long term tensile load is present, and eventually additional loads are applied for a period of time, at either high or low frequencies. In the second instance, the long term applied load is quite low, but several and repetitive loads are applied up to values close to the maximum geogrid tensile strength.

Until now the geogrid tensile properties are usually determined by in-isolation monotonic tensile tests, and cyclic effects are taken into consideration by simply increasing the design safety factor. This approach cannot be considered satisfactory in order to analyze the mechanical

behavior of polymeric reinforcement under cyclic or dynamic loading. In fact, from the theoretical point of view, the design of the structures requires the knowledge of the constitutive laws of both interacting materials (soil and geogrid), and the definition of the interface laws between the two components (Bathurst and Cai, 1994).

This paper deals with the definition of the mechanical behavior of the geogrid material in isolation condition under cyclic loading. Isolation long term properties of the geogrids under static loads have been already studied by the authors (Moraci and Montanelli, 1996). The cyclic behavior of the geogrids has been investigated by means of sinusoidal tensile load cyclic tests carried out at different frequencies and load amplitude up to a duration of 10,000 cycles. Moreover, in order to simulate in sito conditions, tensile load cyclic tests have been performed with load levels ranging around the long term design load of the geogrid at different frequencies. A typical example is a geogrid loaded at 40% of its maximum tensile strength, and stressed with cycles ranging from 40 to 60% of its maximum tensile strength.

EXPERIMENTAL TESTING PROGRAM

The geogrids studied in the research have been an HDPE (High Density Polyethylene) extruded geogrid and a PET (Polyester) woven geogrid which nominal properties are reported in table 1.

Table 1. Nominal Geogrids Characteristics

Sample	Base Polymer	Mass per Unit Area μ g/m^2	Nominal Tensile Strength Tmax kN/m	Strain at Nominal Tensile Strength εmax %
GE-TEN	HDPE	750	80	13.0
GT-FOR	PET	500	80	12.5

To characterize the two types of geogrid, wide width tensile tests have been carried out. The tensile device has been equipped with hydraulic wide width clamps (Curtis type) for testing the extruded geogrid GE-TEN, while in-house roller type clamps have been designed and used for the woven type geogrid. The tensile strains have been recorded using a videoextensometer. The test results are reported in table 2.

Table 2. Monotonic Tensile Test Results in Accordance to ISO 10319:93

Geogrid	GE-TEN	GT-FOR
Tmax, kN/m	88.0	82.6
εmax, %	14.1	15.6
Jsec0,2, kN/m	1278	463
Jsec0,5, kN/m	980	449

where: Jsec 0.2 = Elastic secant tensile modulus between $\varepsilon = 0\%$ and 2% elongation
Jsec 0.5 = Elastic secant tensile modulus between $\varepsilon = 0\%$ and 5% elongation

The cyclic tests have been performed using a hydraulic press, controlled by an Instron 8580 digital multi-axis servohydraulic controller. The tensile cyclic loads have been applied using a haversine wave form oscillating from a load level equal to 1% of the nominal peak load (Tmax or nominal tensile strength) and different load ratios, such as 20%, 40%, 60% and 80%. Within the limit of the testing apparatus, the following frequencies have been investigated for all the levels of load ratios: 0.10 Hz, 0.25 Hz, 0.50 Hz and 1.00 Hz. All the tests have been carried out up to 10,000 cycles or geogrid fatigue failure. All tests have been performed at 20±2°C and at 65±10% relative humidity on a wide width type specimen.

In figure 1 are shown the details of the testing apparatus together with the clamping system for both geogrid types.
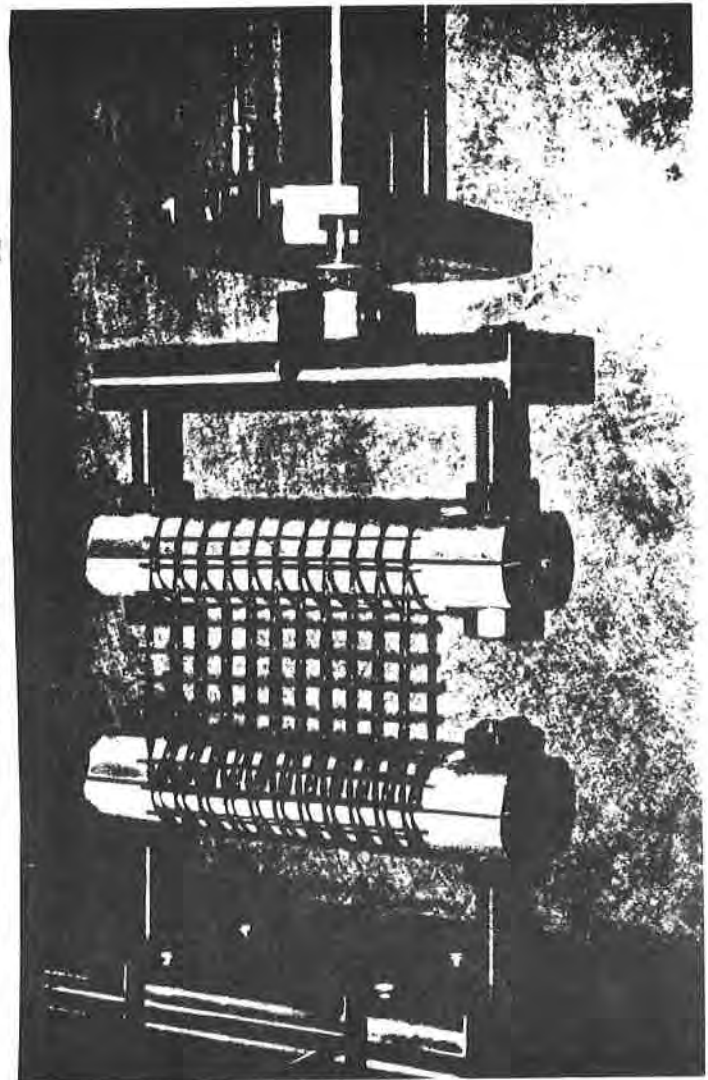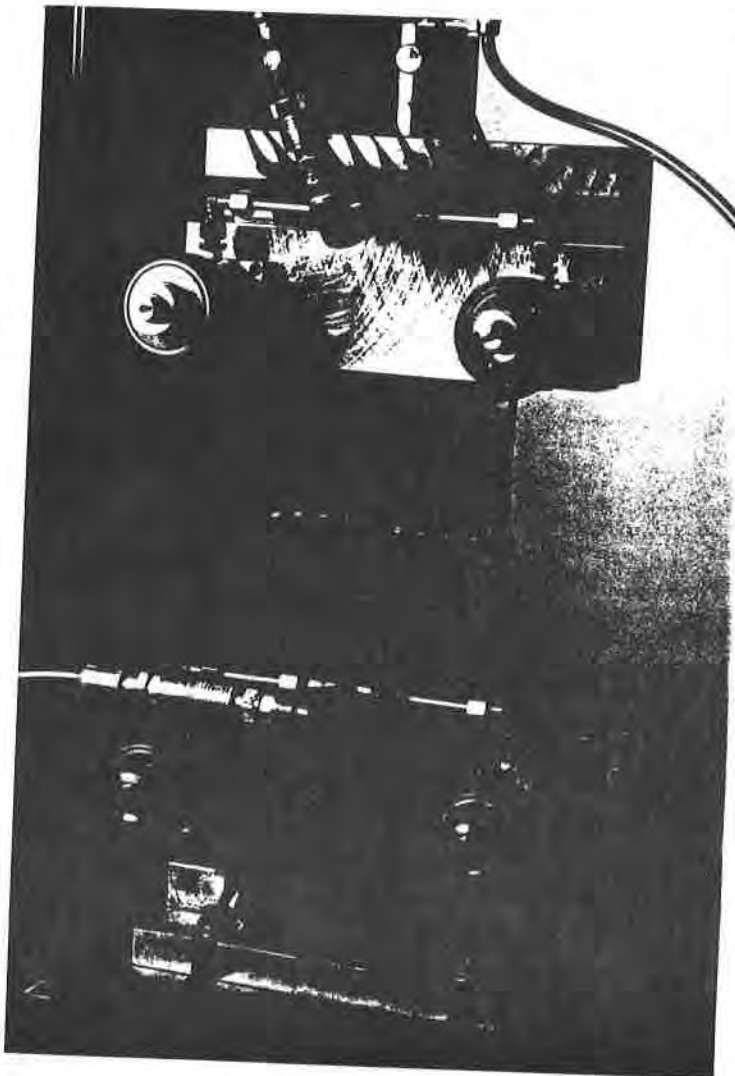
Figure 1. Geogrid Cyclic Test Apparatus showing:
a) GE-TEN Hydraulic Wide Width Clamps; b) GT-FOR Capstain Wide Width Clamps

The pre-stressed cyclic tensile load tests have been performed by means of cyclic tests, having a sinusoidal function conducted with load levels ranging around the long term design load of the geogrid at different frequencies, using the identical apparatus described above. The load amplitudes chosen for the experimental program have been mainly the following: from 20% to 40%, from 40% to 60% of the nominal peak load. These load levels have been selected to determine the geogrids behavior when subject to additional loading during its use; the geogrid is working at a stress level given by its long term design load and dynamic or cyclic loads are overimposed to the acting static loads. The following frequencies have been investigated: 0.1 Hz, 0.25 Hz, 0.5 Hz and 1.0 Hz. All the tests have been carried out up to 10,000 cycles or fatigue failure. All tests have been performed at 20±2°C and at 65±10% relative humidity.

The overall conducted testing program is briefly highlighted in table 3. In the following paragraphs only the behavior of extruded geogrid will be analyzed.

Table 3. Experimental Testing Program

Frequency	1.00 Hz	0.50 Hz	0.25 Hz	0.10 Hz
Geogrid	Load Ratio	Load Ratio	Load Ratio	Load Ratio
GE-TEN	0-20%Tmax	0-20%Tmax	0-20%Tmax	0-20%Tmax
GE-TEN	0-40%Tmax	0-40%Tmax	0-40%Tmax	0-40%Tmax
GE-TEN		0-60%Tmax	0-60%Tmax	0-60%Tmax
GE-TEN			0-80%Tmax	0-80%Tmax
GE-TEN	20-40%Tmax	20-40%Tmax	20-40%Tmax	20-40%Tmax
GE-TEN	40-60%Tmax	40-60%Tmax	40-60%Tmax	40-60%Tmax
GE-TEN	30-50%Tmax			
GE-TEN	60-80%Tmax			
GT-FOR	0-20%Tmax			0-20%Tmax
GT-FOR	0-40%Tmax			0-40%Tmax
GT-FOR				0-60%Tmax

Typical test results are shown in figure 2, 3 and 4 for either cyclic and pre-stressed cyclic tests carried out on GE-TEN and GT-FOR at 0.10 Hz. The load/strain cycles have been recorded and plotted following a log type acquisition program.

To analyze the cyclic behavior of the geogrid, the following parameters have been considered: the maximum cycle strain, ε_{tc}, in %; the unload and reload tensile modulus, Jur, in kN/m; the area of hysteresis loop, Aur, in kN/m*%; the applied tensile tension T in kN/m; the frequency in Hz and the cycle number (figure 5).
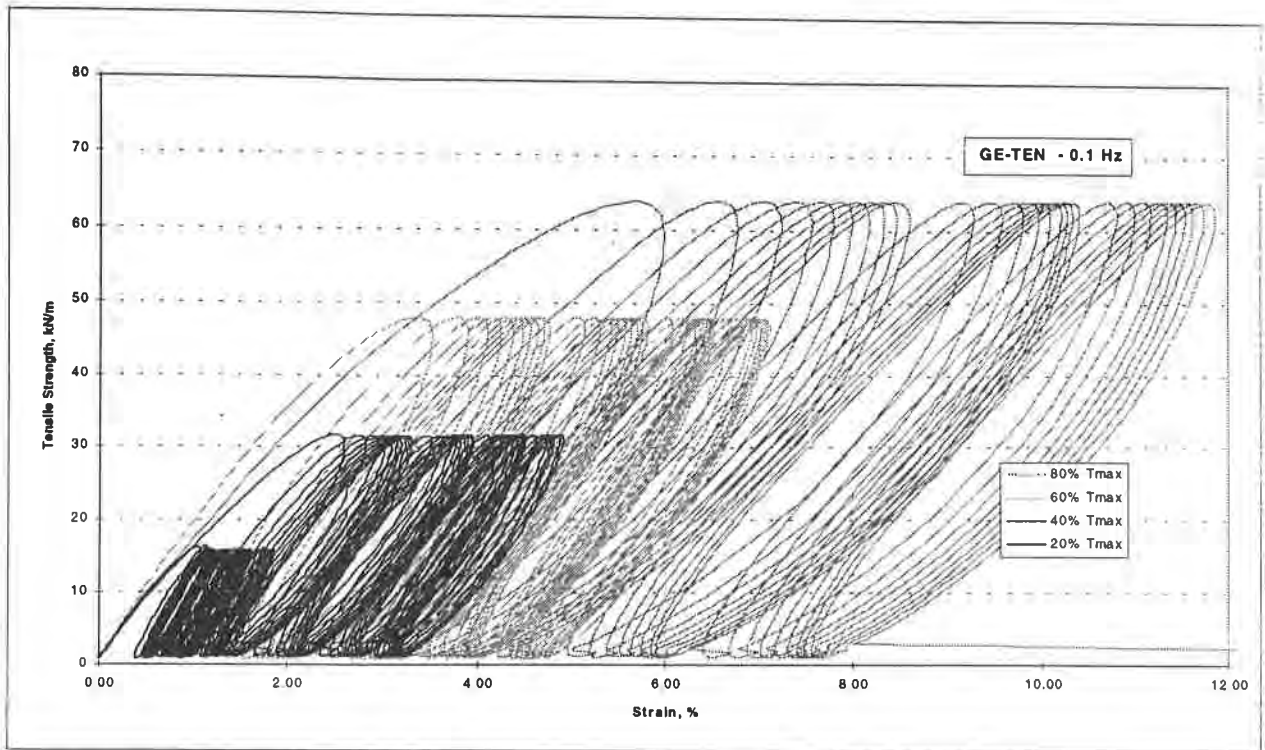
Figure 2. Cyclic Load Tests at 0.1 Hz on Geogrid GE-TEN at Different Load Ratios
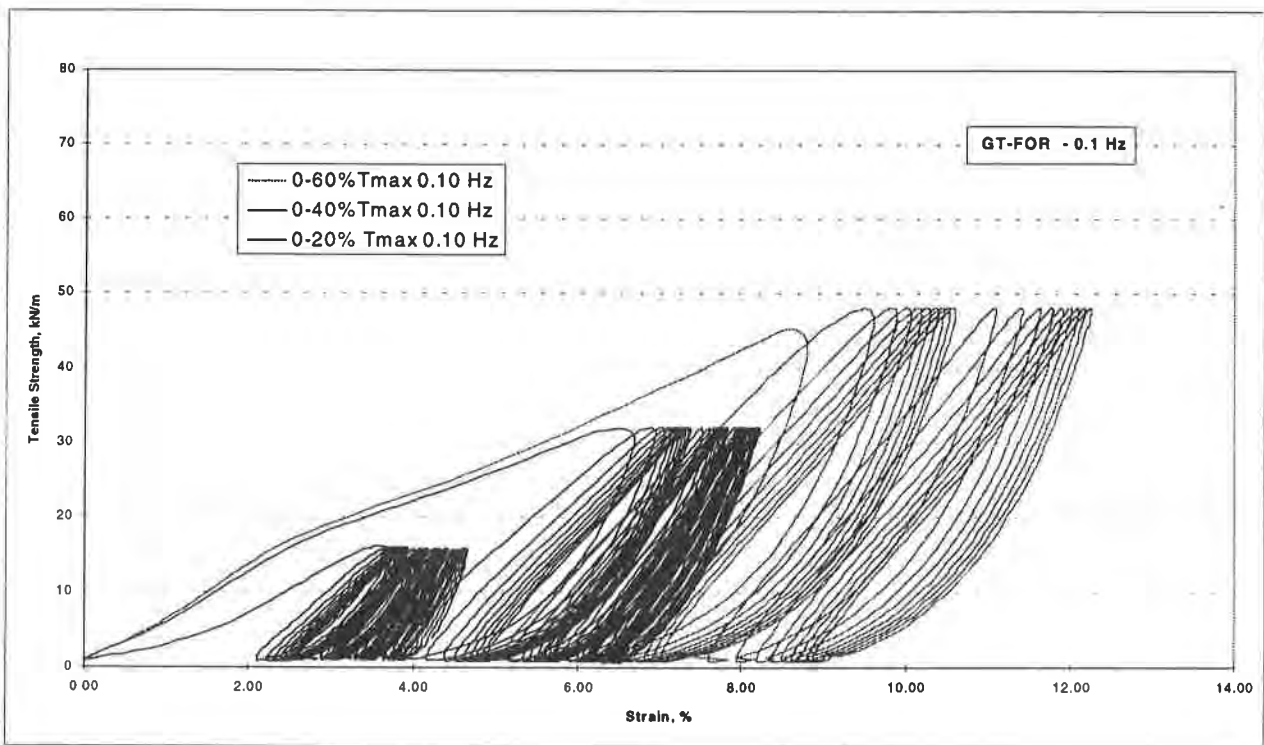
Figure 3. Cyclic Load Tests at 0.1 Hz on Geogrid GT-FOR at Different Load Ratios
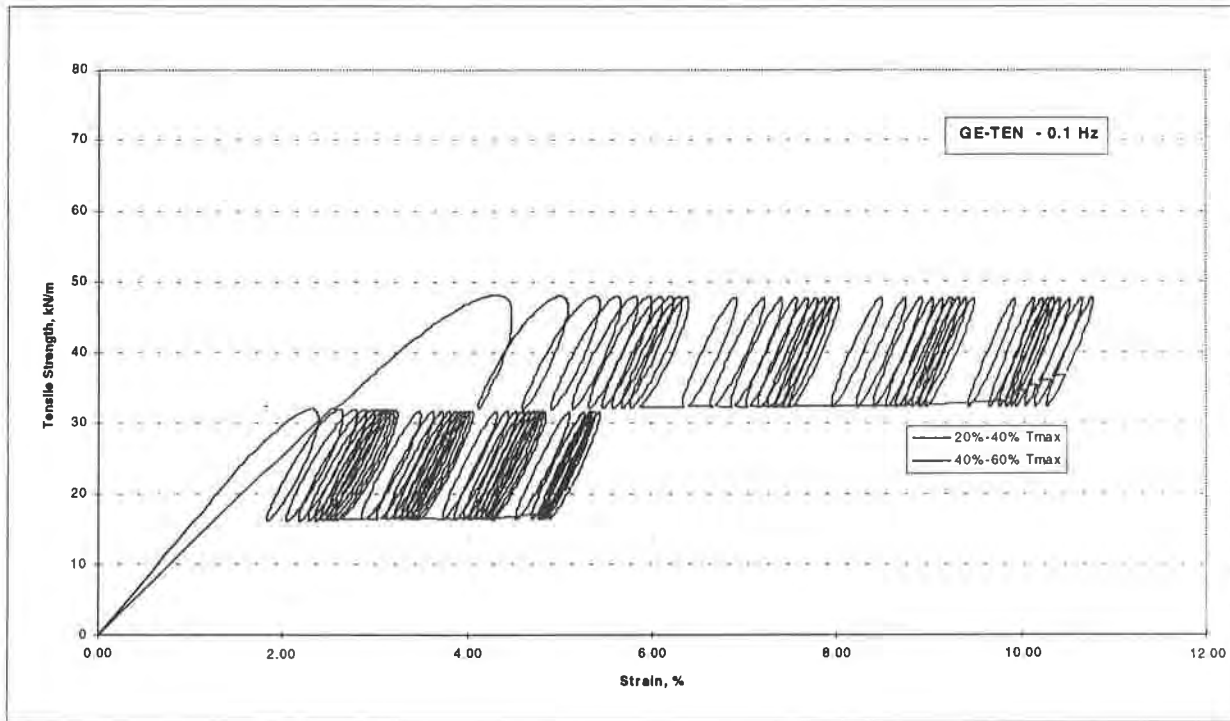
Figure 4. Pre-Stressed Cyclic Load Tests at 0.1 Hz on Geogrid GE-TEN at Different Load Ratios
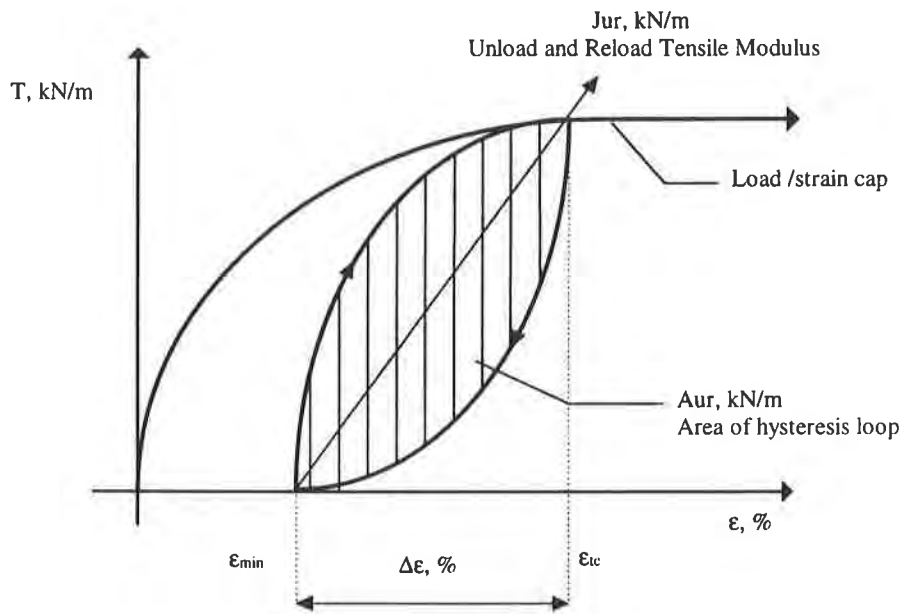
Figure 5. Characteristics of the Unload-Reload Cycle Loop

TESTS RESULTS AND ANALYSIS FOR GE-TEN GEOGRID

In figure 6 and 7 are plotted the maximum cycle strain versus cycle number for the geogrid GE-TEN. It is possible to notice how the results are gathered in groups having identical load level. Moreover, the lower is the frequency, the higher is the strain. Anyhow it is easy to see how predominant is the load level versus the cycle frequency in determining higher tensile strains. In figure 6 the geogrid GE-TEN fails after more than 1000 cycles ranging from 0-80% of Tmax. The strain curves up to 10,000 cycles and up to 60% load have a quasi-linear trend in the semi-logarithmic plane, in which the maximum cycle strains are almost proportional to the mean load and cycles. This behavior will be later analyzed. The above trend is confirmed by figure 8, in which are plotted the test results conducted at constant amplitude of 20% Tmax at a frequency of 1.00 Hz. The curves up to 60% Tmax or up to 1,000 cycles are quasi-linear with strains almost proportional to the applied mean load and cycles. The curves show a typical visco-elastic behavior. The analogy between this figure and constant load tensile creep curves is immediate. A second phase of this study will concentrate in analogies between creep and pre-stressed cyclic testing.

Now we will consider the effects of the applied cyclic load and frequency on the characteristic parameters of the material cyclic behavior: the unload-reload tensile modulus Jur (determined for a given tensional level) and the area of unload-reload hysteresis loop Aur, that is directly related to the damping potential of the material.
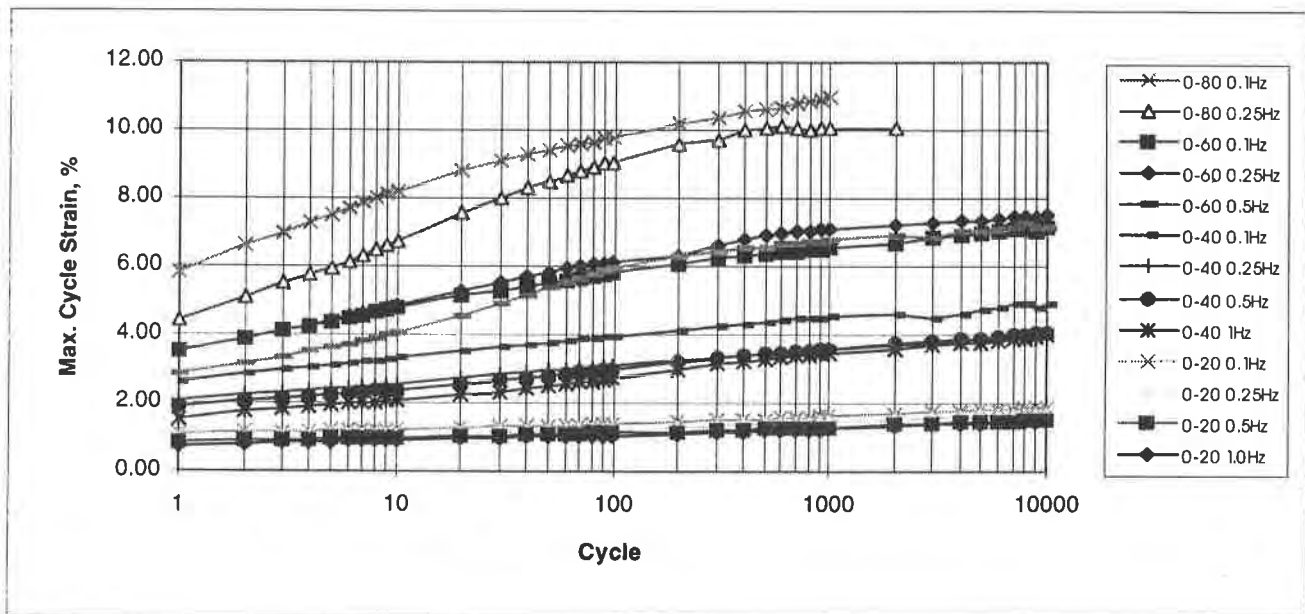
Figure 6. Cyclic Tests - Maximum Strain Cycle for Geogrid GE-TEN
for Different Load Ratios and Frequencies
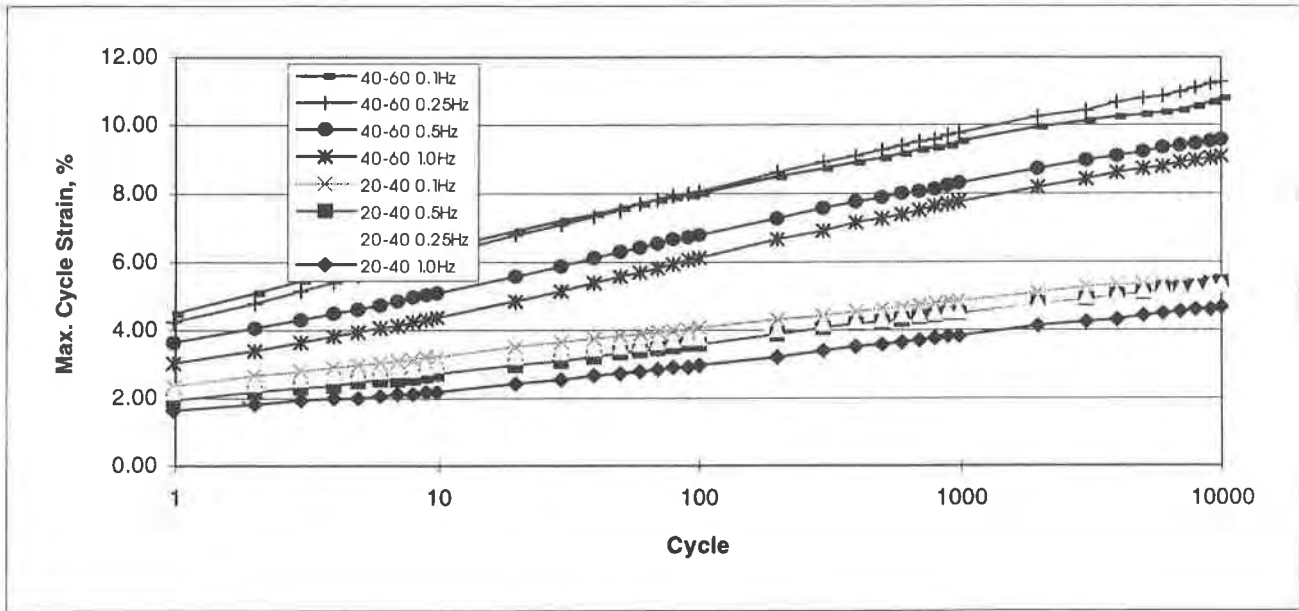
Figure 7. Pre-stressed Cyclic Tests - Maximum Strain Cycle for Geogrid GE-TEN
for Different Load Ratios and Frequencies

Figure 9 shows the unload-reload tensile modulus Jur versus cycle number for different loads and frequencies. The tensile unload-reload modulus increases during the first cycles (about 10 cycles) and consequently it remains mainly at a constant level with the increasing of the number of cycle, or even decreases for high level of loads. The tensile unload-reload modulus increases with the increasing of the frequency and with the decreasing of the applied load.
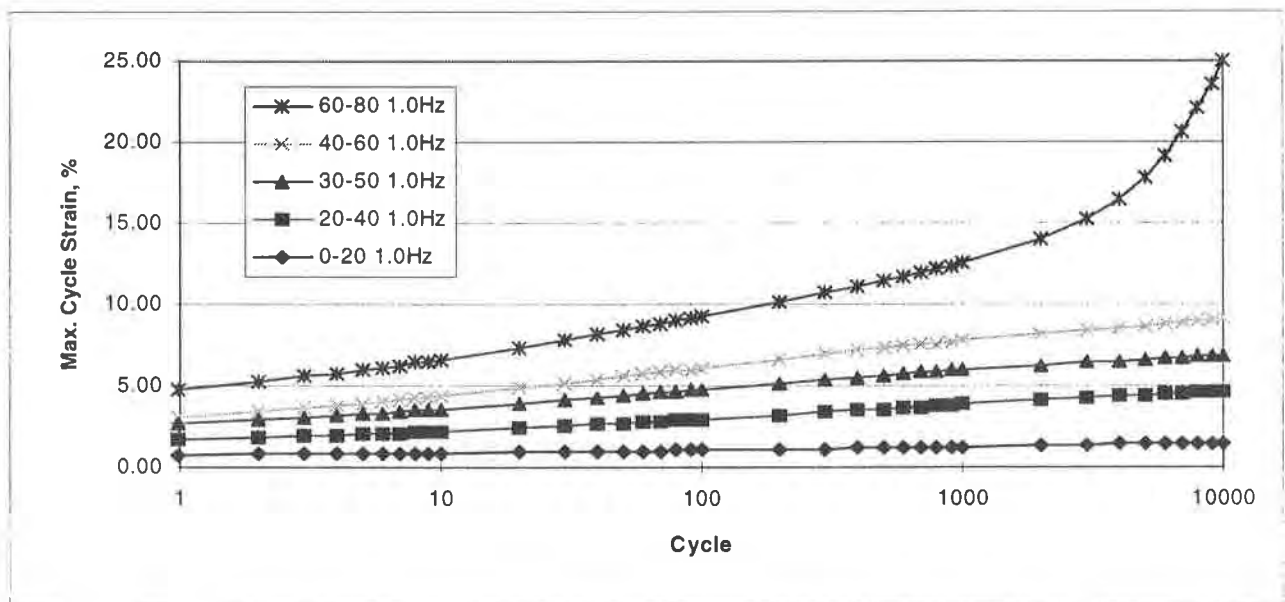
Figure 8: Constant Amplitude Tests - Maximum Strain Cycle for Geogrid GE-TEN
for Different Load Ratios and Frequency Equal to 1.00 Hz

When comparing the unload-reload tensile modulus with the monotonic tensile secant modulus (Jm) measured during a wide width monotonic tensile test at the same maximum load level, it is possible to obtain significant conclusions (figure 10). All the tests data yield a constant trend (up to cyclic load equal to 60% Tmax) ranging around a ratio between 1.5 to 2, whichever is the applied load or the testing frequency. For cyclic load equal to 80% Tmax, fatigue failure occurs and so the ratio Jur/Jm suddenly decreases. In particular, higher frequencies yield a higher ratio of Jur/Jm. Thus, it is possible to give a good estimate of the unload-reload tensile modulus up to 60% Tmax, from the results of a monotonic tensile test. Being the ranges of the ratio Jur/Jm so limited, the above prediction can be considered accurate for preliminary design at least within the test result conditions and parameters.

When plotting the unload-reload tensile modulus versus the strain (figure 11), the curves show a yield point after which the cyclic modulus decreases with increasing strain. This yielding behavior is more evident for high load levels and high frequencies.

It is interesting to compare the ratio of the maximum cycle strain (ϵ_{tc}) and the monotonic tensile strain (ϵ_{tm}) measured during a wide width monotonic tensile test at the correspondent maximum load level. This ratio is plotted versus the cycle number and for different frequencies in figure 12. For the typical range of long term design strength for the GE-TEN geogrid (T$\approx$ 20÷40%Tmax), the trend, in the semi-logarithmic plane, can be very accurately described by the following log regression: $\epsilon_{tc} = \epsilon_{tm} (a+b \log N)$ where the coefficients are given in table 4.

In figure 13 are presented the area of the hysteresis loop Aur in kN/m*% versus cycle number for different loads and frequencies. As in the case of the cycle modulus and strain, Aur is predominantly influenced by the load level and secondarily by the frequency. After few cycles (about 10), the value of Aur is mainly constant up to 10,000 cycles; thus it seems possible to consider the damping of the geogrid GE-TEN constant for long term cyclic applications under a given load level. Moreover, it is also possible to conclude that damping is directly proportional to strain level (depending on load level), figure 2, and inversely proportional to frequency and number of cycles (for N≤10 cycles), figure 13.

The pre-stressed cyclic testing results on the geogrid GE-TEN are presented in figure 14. Analogies with the above prescribed behavior are immediate, thus similar conclusions to the ones above presented may be drawn. In particular, it is possible to notice that for similar load amplitudes and cycle number, the pre-stressed conditions yield:

- a greater increase in the cyclic unload-reload tensile modulus, as it can be seen by comparing figures 9 and 14;
- a lower cycle deformation energy and a greater maximum cycle strain.
This behavior is due to the viscous effects related to the application of a static load during the time.
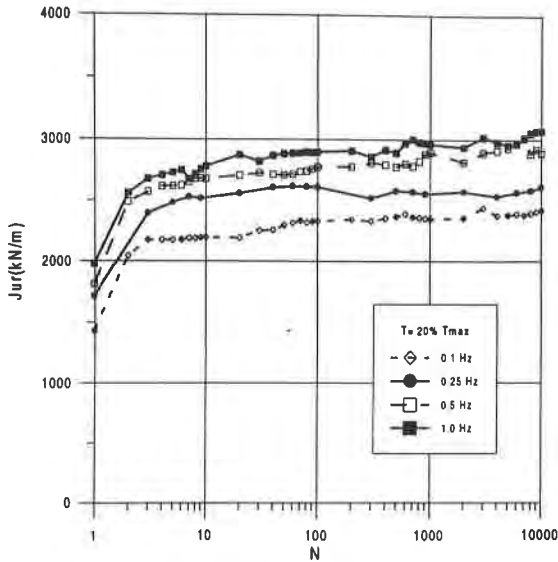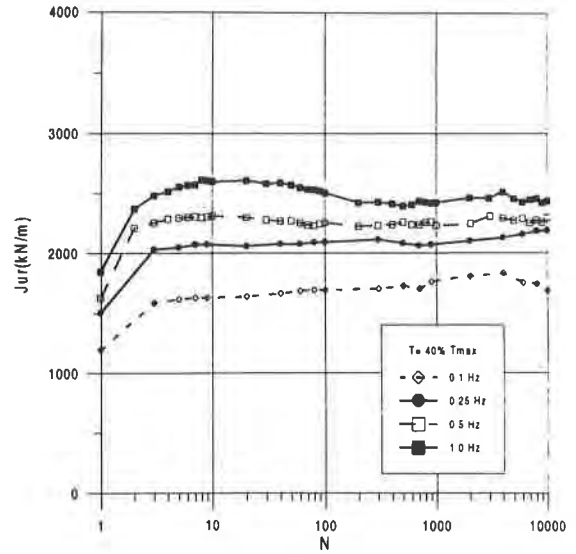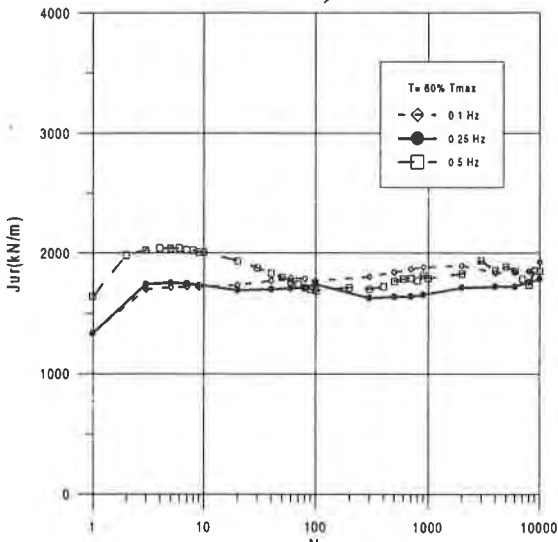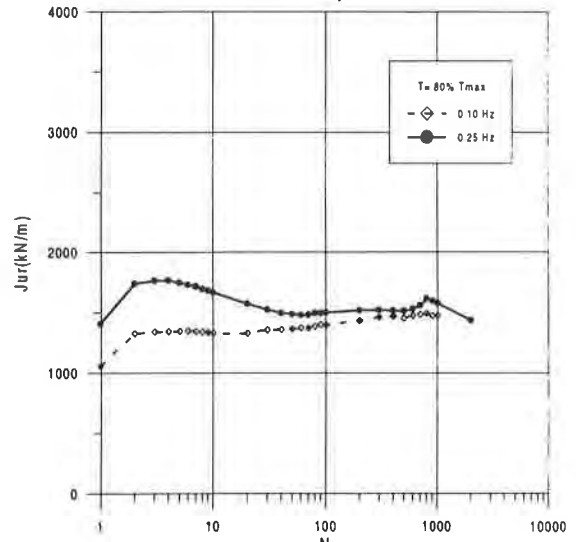
Figure 9. Unload-Reload Tensile Modulus Jur Versus Cycle Number for Different Loads for Geogrid GE-TEN: a) 0-20%Tmax, b) 0-40%Tmax, c) 0-60%Tmax, d) 0-80%Tmax.

The testing program has allowed the definition of design charts (figure 15), very useful when predicting the resulting deformation in a geogrid reinforcement under a given number of cyclic loading, when knowing the applied loads and frequencies.

These curves, defined as isocyclic curves, are valid for tensile sinusoidal loads ranging from 0 to the value of tensile strength reported on axis Y, for a temperature equal to 20°C, and for the specified frequencies (it is suggested to use these curves for tensile load up to 60%).
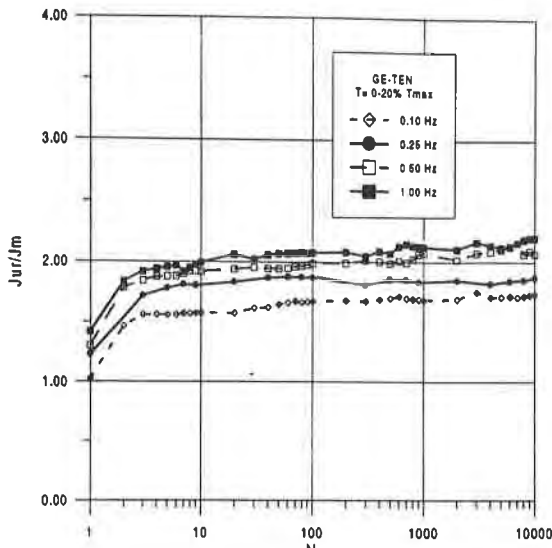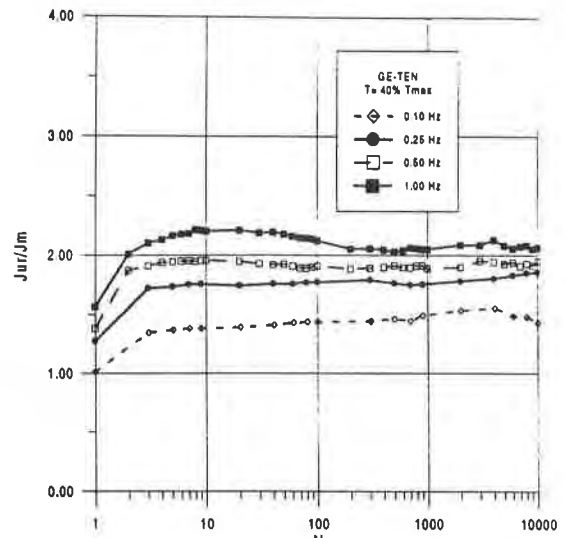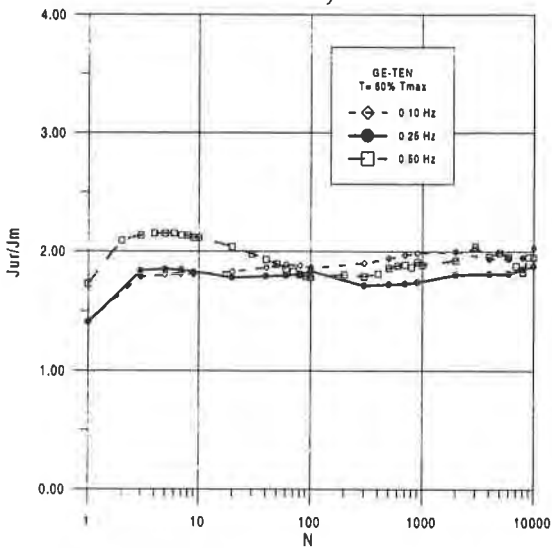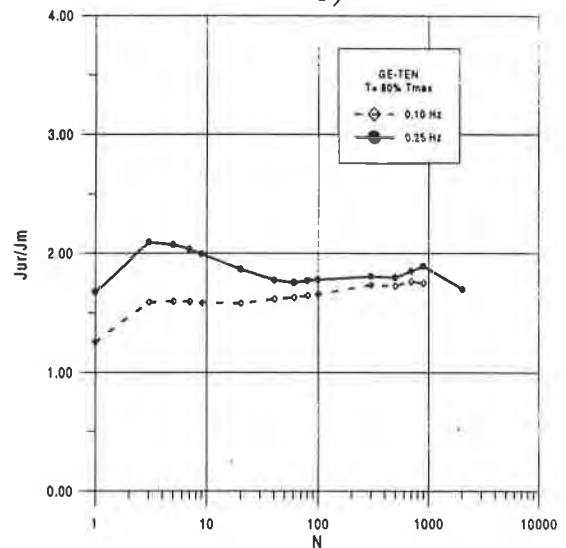
Figure 10. Ratio Jur/Jm Versus Cycle Number for Different Loads for Geogrid GE-TEN: a) 0-20%Tmax, b) 0-40%Tmax, c) 0-60%Tmax, d) 0-80%Tmax

CONCLUSIONS

The experimental analysis, related mainly to the definition of the behavior of the GE-TEN geogrid, has allowed the definition of the following considerations:

- the unload-reload tensile modulus is mainly function of the applied loads and secondarily of the cycle frequency. In particular, Jur increases with the increase of the testing frequency and with the decrease of the applied load level. The modulus increases during the first cycles (about

10) and afterward it remains mainly constant for T≤40%Tmax, while decreases for values of T>40% Tmax;
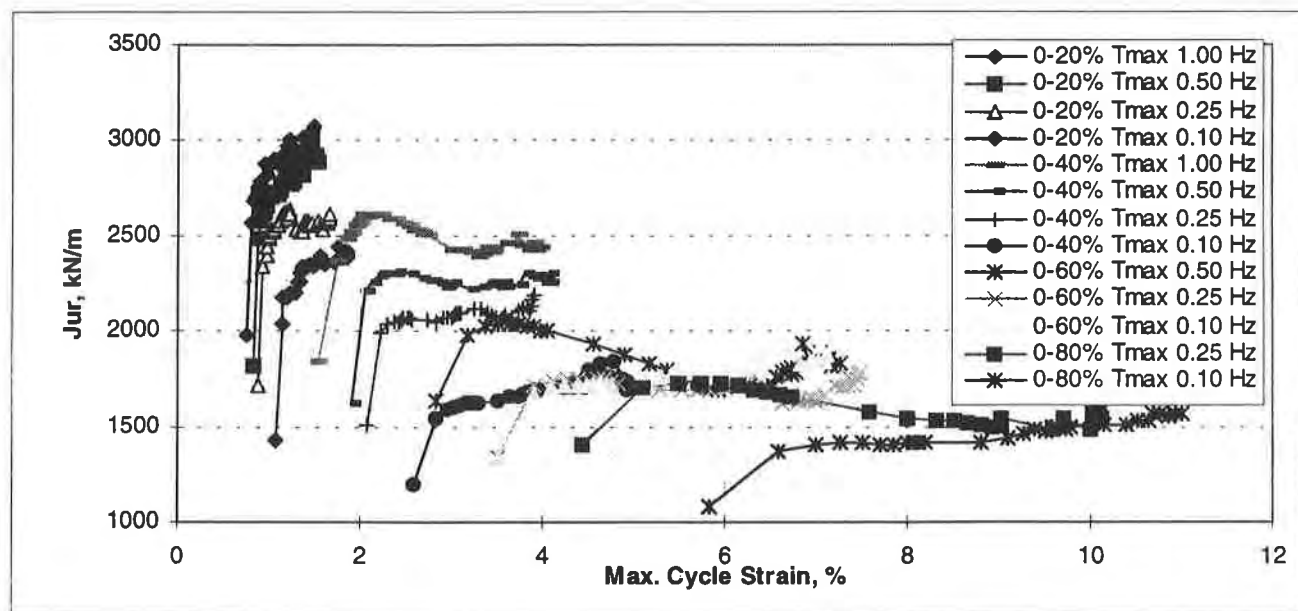
Figure 11. Unload-Reload Tensile Modulus Jur Versus Max. Cycle Strain for Different Loads and Frequencies for Geogrid GE-TEN

Table 4. Coefficients of the Strain Ratio Log Regression Lines Versus Cycle Number for Geogrid GE-TEN at 20°C.

Load Ratio	Frequency	a (-)	b (-)	R² (-)
0-20%Tmax	0.10 Hz	0.816	0.069232	0.98
0-20%Tmax	0.25 Hz	0.669	0.07001	0.99
0-20%Tmax	0.50 Hz	0.645	0.58100	0.93
0-20%Tmax	1.00 Hz	0.573	0.06295	0.99
0-40%Tmax	0.10 Hz	0.926	0.08177	0.98
0-40%Tmax	0.25 Hz	0.707	0.06978	0.99
0-40%Tmax	0.50 Hz	0.622	0.08230	0.99
0-40%Tmax	1.00 Hz	0.497	0.09233	0.99

- the ratio Jur/Jm up to a value of T≤60% Tmax is ranging within 1.5 and 2.0, where higher frequencies yield a higher ratio of Jur/Jm. Thus it is possible to provide a good estimate of Jur from the monotonic tensile strength tests.
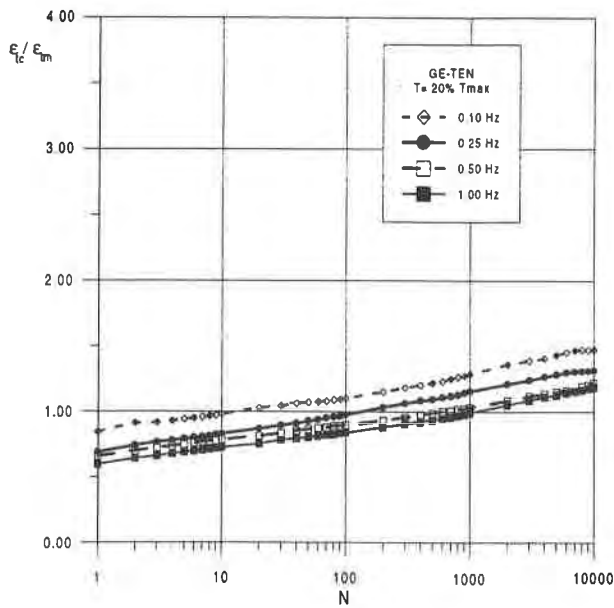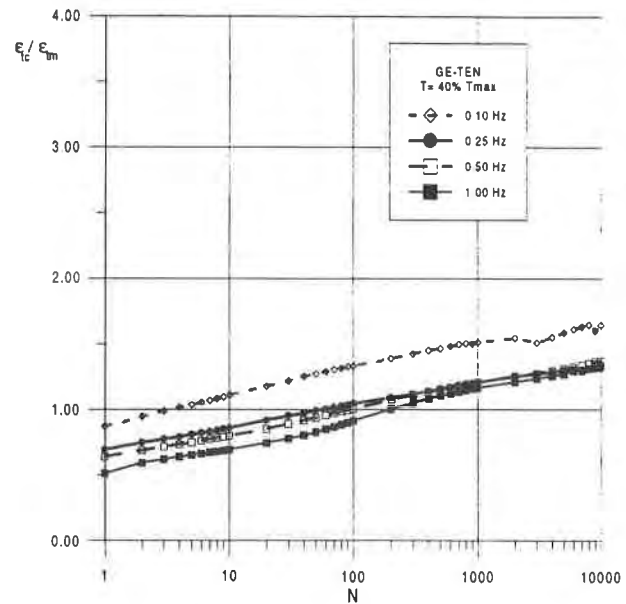
Figure 12. Normalized Maximum Cyclic Strain Versus Cycle Number for Different Loads for Geogrid GE-TEN: a) 0-20%Tmax, b) 0-40%Tmax

- when considering cyclic tests conducted at the same loading level and frequency for applied loads generally used in the design, the ratio $\varepsilon_{tc}/\varepsilon_m$, as a function of the cycles number, is linear on a semi-logarithmic plane. With this method it is possible to determine the total cyclic deformation after N load cycles, knowing the cyclic load applied and its frequency, using the relation:

$$\varepsilon_{tc} = \varepsilon_m \, (a+b \, logN);$$

where the values of the constant "a" and "b" are indicated in table 4.

- the deformation energy accumulated during the hysteresis loop Aur increases when the applied load increases and the frequency decreases. The hysteresis cyclic loop area decreases when the number of cycles increases and generally is mainly constant after a few loading cycles. So, damping of the geogrid GE-TEN can be considered constant for a determined load level and frequency. Moreover, damping is directly proportional to strain level (depending on load level), figure 2, and inversely proportional to frequency and number of cycles (for $N \leq 10$), figure 13. Of course, we can observe a rough increase of Aur only in correspondence of stressed ruptures of the material, in relation with the accumulation of deformations incompatible with the material resistance (the rupture deformations observed in cyclic conditions for T=80% Tmax are near to the one measured during the tensile standard tests).
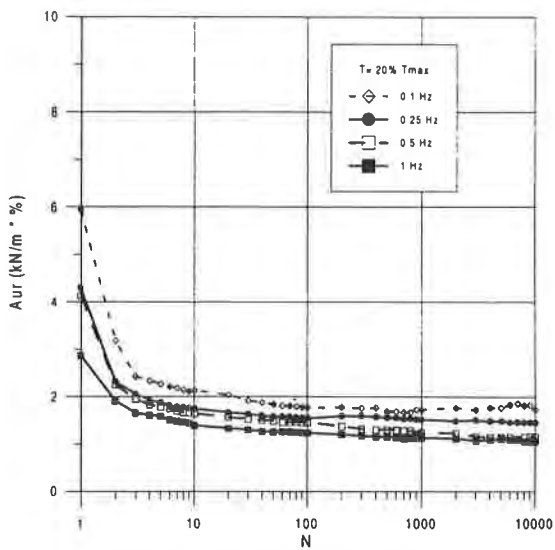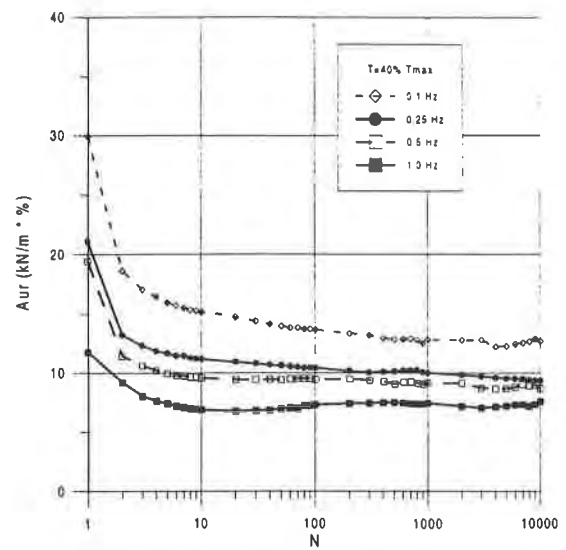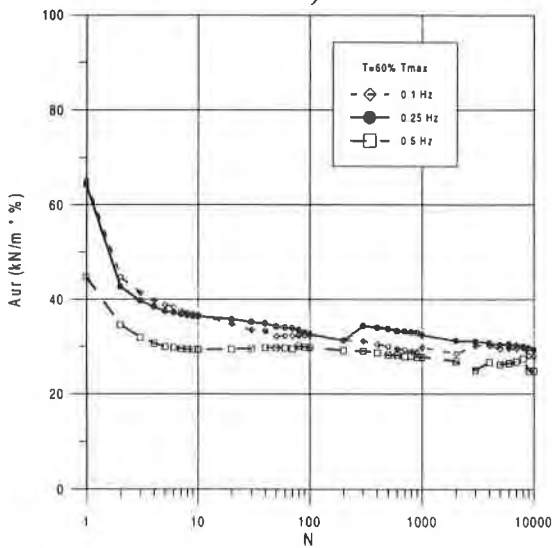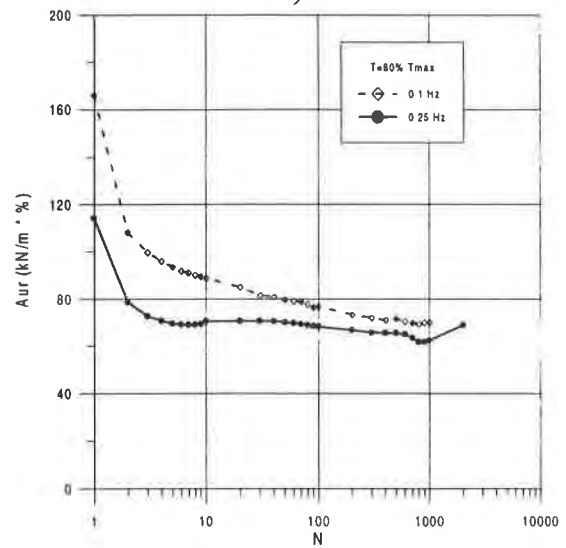
Figure 13. Area of the Hysteresis Loop, Aur Versus Cycle Number for Different Loads for Geogrid GE-TEN: a) 0-20%Tmax, b) 0-40%Tmax, c) 0-60%Tmax, d) 0-80%Tmax

- the pre-stressed cyclic tests produce on the material behavior an increase of Jur in relation to the one determined under cyclic tests performed with the same load amplitude. The improvement of the material behavior is highlighted by the low values of Aur measured during the tests. Finally, the total cyclic deformations after N cycles are bigger than the ones measured without pre-stress. This fact is connected to the permanent application with time of a static load (20% or 40% Tmax).
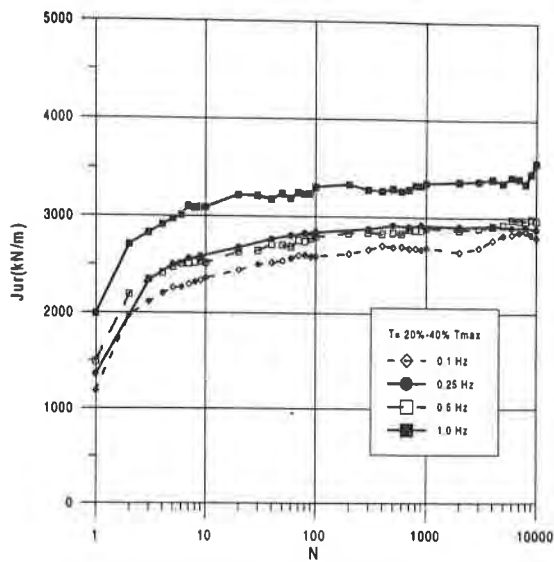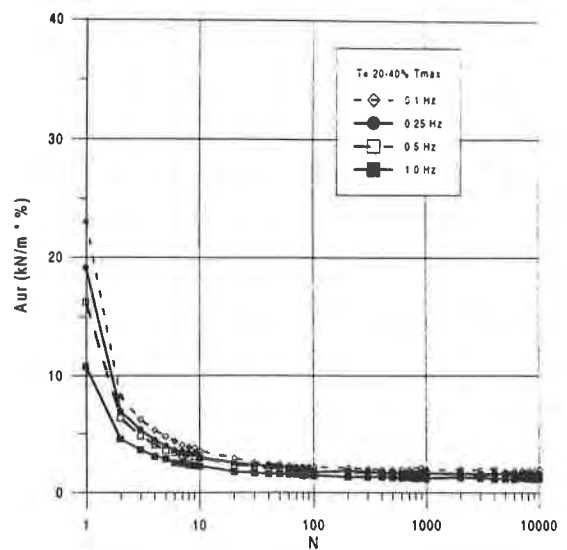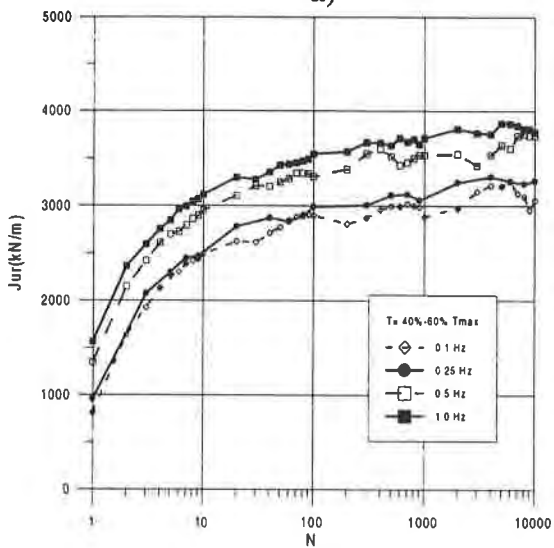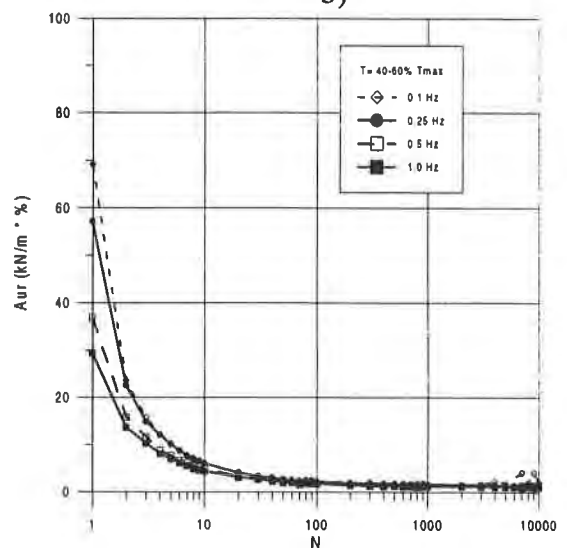
Figure 14. Jur and Aur Versus Cycle Number for Different Loads for Geogrid GE-TEN: a) and b) 20-40%Tmax, c) and d) 40-60%Tmax

ACKNOWLEDGMENT

We shall acknowledge the accuracy and experience during the extensive cyclic testing of Mr. Li Xiaojie.
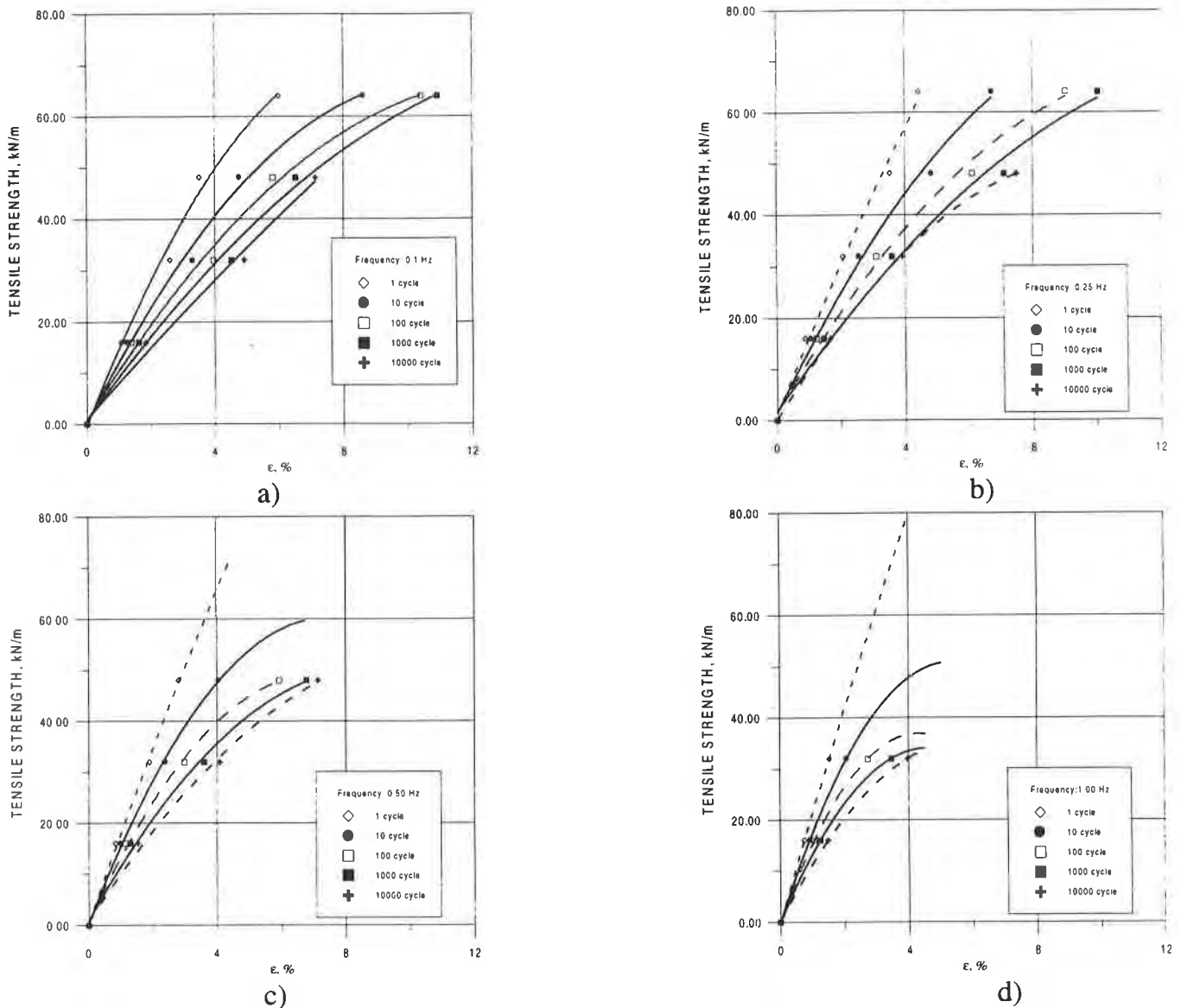
Figure 15. Isocyclic Curves of the Maximum Cyclic Load Versus Maximum Strain for Different Frequencies for Geogrid GE-TEN: a) 0.10 Hz, b) 0.25 Hz, c) 0.50 Hz, d) 1.00 Hz

BIBLIOGRAPHY

Bathurst, R.J. and Cai, Z., 1994, In-Isolation Cyclic Load-Extension Behavior of Two Geogrids, Geosynthetics International, Vol. 1, No.1, pp. 1-19.

International Organization for Standardization, 1993, Geotextiles - Wide Width Tensile Test, ISO 10319:93.

Moraci, N. and Montanelli, F., 1996, Short and Long Term Behavior of Geogrids under Static and Cyclic Load, IS Kyushu '96, Japan.

CYCLIC RESPONSE OF CLAY-GEOMEMBRANE INTERFACES AND THEIR IMPACT ON THE SEISMIC RESPONSE OF LINED LANDFILLS

Ronald C. Chaney
Humboldt State University
Arcata, California 95518

Richard Thiel
Thiel Engineering
Oregon House, CA 95962

Gregory N. Richardson
Richardson and Associates Engineering
Raleigh, NC 27603

Mark Cadwallader
Cadwallader Technical Services
Conroe, TX 77303

ABSTRACT

This study presents the results of cyclic shear tests on HDPE geomembrane/clay soil interfaces at strains < 1 % and investigates the effect of such interfaces on the seismic performance of landfills. Laboratory cyclic shear tests were performed on both textured and smooth HDPE geomembrane materials overlying a silty clay material.

INTRODUCTION

Recent RCRA Subtitle D regulations (40 CFR Part 258) established the requirements that MSW landfills must not be sited where they can be damaged by active ground faulting (258.13) and that they must be designed to resist the effect of regional earthquakes (258.14). Seismic design guidance developed by EPA (Richardson, et al., 1995) requires that, at a minimum, these facilities be designed to resist accelerations resulting from an event having a 90 percent probability of not being exceeded in 250 years.

The dynamic response of geomembrane/geotextile interfaces was previously investigated by Yegian et al. (1992) using a harmonic excitation shake table. They concluded that there is a limiting shear force, hence acceleration that can be transmitted from a geomembrane to a geotextile. Beyond this limit, relative displacements or slip will occur along the geosynthetic interface. In a proceedings of a workshop on research priorities for seismic design of a solid waste landfills (USC, 1994), it was noted that low shear strength interfaces may have a beneficial effect on the seismic response of a landfill in a manner similar to that of frictional base isolation systems for buildings. Yegian et al. (1995) more recently investigated the effect of irregular excitation on the response of geomembrane/geotextile interfaces. They showed the following: (1) that the magnitude of the reduction in the acceleration pulses varied with the peak acceleration of the ground motion (PGA) as well as with frequency content of the motion, (2)

spectral accelerations of the transmitted motion are reduced especially in the range of the predominant frequency of typical ground motions, (3) magnitude and pattern of the maximum and the permanent slips depend on the level of PGA and the frequency characteristics of the earthquake time history, and (4) the geosynthetic interface acts as a base isolator absorbing the wave energy through interface slip. Kavazanjian and Matasovic (1995) used non-linear dynamic response analysis that a potential benefit of low shear strength geosynthetic interfaces is a reduction of the peak acceleration response of the landfill.

CYCLIC LOADING ON A GEOMEMBRANE/CLAY INTERFACE

Shear tests were conducted to analyze the performance of the HDPE geomembrane/soil system interface under both static and cyclic loading. The laboratory program involved testing both textured and smooth HDPE geomembrane materials. The geosynthetic textured geomembrane materials tested were from three manufacturers (Gundle, STL and NSC). In addition Gundle's smooth HDPE geomembrane was also tested. Both static and cyclic shear tests were performed using a direct shear machine having a pneumatic loading system to apply the normal stress. The machine was fitted with a 102 mm (4 in.) diameter shear ring to perform the testing and shear loads were applied using a hydraulic actuator. Constant amplitude cyclic loads were applied at a frequency of 0.5 cycles per second. Cyclic load and displacement data were logged using a personal computer (PC) interface card which recorded 50 data points per second.

The clay liner material used was a white clayey sand whose properties are presented in Table 1.

Table 1 - Summary of Laboratory Test Material Properties

% Passing No. 200 Sieve	45.8%
Liquid Limit	24%
Plastic Limit	17%
Plasticity Index	7%
Maximum Dry Unit Weight (ASTM D698)	1.97 Mg/m^3 (123.4 pcf)
Optimum Water Content	11.5%

The clayey sand test specimens were compacted at approximately the soils optimum moisture content of 11.5 % to a relative compaction of 98 %. The compacted soil sample was placed in the top ring of the direct shear device. The lower ring was filled with rigid metal and porous discs. The liner coupon was attached with flat head screws to the top surface of the bottom ring. In this position, the geomembrane covered the rigid metal and porous discs. The upper and lower shear rings were placed together sandwiching the soil and liner and creating the interface to be tested. This "sandwich" with the soil over the liner coupon, was then consolidated. Consolidation was performed by applying a vertical consolidation load through a porous stone and loading cap on the soil sample. A loading hanger, pulled down by a pneumatic piston, applied the load to a top cap which transfers the force to the interface. The system was allowed to soak and compress over night under a consolidation

load of 193 kPa (28 psi), 359 kPa (52 psi), 414 kPa (60 psi), 828 kPa (120 psi). The change in specimen height was monitored and recorded.

After the consolidation was complete, a cyclic loading was applied. A hydraulic actuator applied the lateral shear loading to the liner/soil interface by acting on the top shear ring. The upper shear ring was moved a preset deformation. The single amplitude deformations used in this study were 0.18 mm (0.007 in.), 0.30 mm(0.012 in), 1.01 mm (0.04 in), and 2.03 mm (0.08 in). The specimen was cycled at 0.5 Hz for 10 cycles at each displacement level, starting with the smallest displacement and ending with the largest. The specimen was allowed to rest at its null location for 30 minutes between each of the four displacements. The load and displacement was monitored and recorded during the cyclic loading.

The static test sequence was performed using loading in only one direction. The loading rate for the static test was 0.01%/min. Results from the static tests (adhesion Ca, residual phi angle, and void ratio) are presented in Table 2.

Table 2 - Summary of Static Direct Shear Test Results

Interface	C_a kPa(ksf)	Phi(residual) (degrees)
Gundle HDPE(smooth)/Soil	5.8(0.12)	10.9
Gundle HDPE(textured)/Soil	25.4(0.53)	24.4

A summary of results from cyclic testing on both smooth and textured Gundle liner material are presented in Figure 1 . The results are plotted for a constant vertical stress as shear stress ratio/vertical stress (i.e. stress ratio) versus deformation. A review of the data by the authors shows that for a smooth liner material the effect of deformation level, vertical stress and the number of cycles on the stress ratio is minimal. In addition, stress ratio is effectively constant at 0.2 for the conditions investigated. This value of stress ratio corresponds to an angle of friction between the HDPE/clay interface of 11.3 degrees. This value is in agreement with results from static tests as presented in Table 2.

For the textured liner material the effect of the number of cycles of load application based on the authors observation of the data is minimal. The effect of increasing vertical stress is to move the curve from the top to the bottom of the range. The level of the stress ratio achieved increases with increasing deformation.

This data strongly suggests that the use of static interface shear strengths for smooth and textured geomembranes for dynamic analysis is conservative.

CYCLIC RESPONSE OF LANDFILLS

The response of landfills with geosynthetic interfaces under seismic loading can be investigated using either a limited number of computer models which incorporate slip elements or the SHAKE program. For programs which use slip elements information presented in Figure 1 can then be used directly. In contrast, a more common procedure is to use the SHAKE program to estimate the response of the landfill. This program requires information on the variation of shear modulus with shearing strain for the interface. To incorporate the interface data from Figure 1 equivalent "slip" elements must be developed or a true non-linear dynamic analysis must be used. To develop this information for SHAKE it was assumed that the deformation presented in Figure 1 occurred in a 1 ft (0.3 m) thick layer. The resulting shearing strain can then be calculated as the deformation divided by the layer thickness.

Plotting the secant shear modulus (G) from data presented in Figure 1 for both smooth and textured HDPE liner material versus the logarithm of the shear strain as a function of the vertical effective stress results in modulus degradation curves as presented in Figure 2. The G_{max} values at 0.001% shearing strain was estimated using an empirical equation by Hardin (1978). A review of Figure 2 shows that texture of the geomembrane does not appear to significally affect the shear modulus degradation curves. The effect of increasing vertical effective stress is also shown to increase the shear modulus for all shearing strain levels between approximately 0.001% thru 1.0%.

A normalized modulus degradation curve for both smooth and textured HDPE liner/clay interfaces is presented in Figure 3 as G/G_{max} versus the logarithim of the shearing strain. At strain levels below approximately .01 % curves are relatively flat indicating that the interface is undergoing basically elastic behavior. Above a strain level of approximately .01 % the G/G_{max} versus shearing strain curve undergoes degradation which indicates that the interface is undergoing plastic behavior.

RESPONSE OF LANDFILL UNDER SEISMIC LOADING

To evaluate the effect of an HDPE liner/clay interface on the seismic behavior of a landfill, a case study was investigated utilizing the idealized soil layers (Layer No. 1 and 2) as presented in Figure 7. Layer profile No. 1 consisted of a typical soil/waste column without a HDPE geomembrane/clay interface. In contrast, Layer profile No. 2 consisted of the same soil/waste column with a soft layer (HDPE geomembrane(smooth and textured)/clay interface) located at the bottom of the waste. The computer program SHAKE91 was used in this model study (Idriss and Sun, 1992). The approximate modulus degradation curve used for the soft layer was based on Figure 3 for smooth and textured geomembrane/clay interfaces. An earthquake time history (1987 Whittier Earthquake, Los Angeles-Obregon Park) with a peak horizontal acceleration of 0.43g was input at the top of the rock layer. The shear wave velocities of the MSW shown in Figure 4 were estimated from Idriss et al. (1995). The shear wave velocity is a function of the shear modulus (G) and the density (ρ) of the material as given by the below

equation. The density of the various layers was estimated from Idriss et al. (1995).

$$v_S = \sqrt{\frac{G}{\rho}}$$

(1)

The shear modulus of the HDPE geomembrane (smooth and textured)/clay interface was estimated knowing the vertical stress and results presented in Figure 2. Damping for the interface layer was assumed to be the same as clay.

Results of the analysis are presented as the Amplification Ratio versus the period (Amplification Spectrum) in Figure 5 for the cases of with and without a geomembrane (smooth and textured)/clay interface. The amplification spectrum is the ratio of the amplitude of motion at the top of the soil/waste column divided by that at the bottom of soil/waste column. A review of Figure 5 indicates that the fundamental period occurs between 2 to 2.5 seconds for the soil/waste columns studied. In addition, it is also seen that for the cases studied the soil/waste column amplifies the acceleration level by a factor of 3.8 from that imputed at the rock level. It is also shown that the HDPE geomembrane/clay layer (either smooth or textured) at the bottom of the waste column does not significantly affect the amplification ratio. These results are in basic agreement with those observed by Kavazanjian and Matasovic (1995). A review of shearing strains experienced during the seismic loading as calculated in the SHAKE program at the geomembrane (smooth and textured)/clay interface indicated that a strain level of only 0.15% was achieved. The small level of shearing strain level experienced therefore did not fully mobilize the available strength of the liner interface.

SUMMARY AND CONCLUSIONS

This study presented the results of cyclic shear tests on HDPE geomembrane/clay soil interfaces and investigated the effect of such interfaces on the seismic performance of landfills. Laboratory cyclic shear tests were performed on both textured and smooth HDPE liner materials overlying a silty clay material. Specific observations are as follows:

(1) Laboratory Test Program

a. For smooth geomembranes under either static or cyclic loading the stress ratio causing strain along the interface is constant. Use of the stress ratio from static tests is appropriate and relatively accurate for large cyclic displacements ($\leq$ 0.10in.).

b. For textured geomembranes the stress ratio causing strain along the interface increases with displacement. Use of stress ratio from static tests appear to be conservative for large cyclic displacements ($\leq$ 0.10in.).

(2) Case Study - Assuming cyclic deformations occurred over a 1 foot thick layer of material.

a. An approximate modulus degradation curve of G/G_{max} versus the logarithim of the shearing strain exists for both smooth and textured HDPE geomembrane/clay interfaces assuming a 1 ft. thick layer. The general shape of this relationship is approximately that previously identified for clayey soils.

b. For the idealized soil/waste columns studied under small strains, the fundamental period occurs between 2 to 2.5 seconds. This fundamental period is approximately the same for the conditions of either a geomembrane layer and without a geomembrane layer at the soil/waste interface.

c. For all the cases studied, the soil/waste column with and without a geomembrane/clay interface amplifies the acceleration level at the top of a 100 foot fill by a factor of 3.8 from that inputed at the basement rock level.

d. The small levels of shearing strain (0.15%) experienced at the bottom geomembrane/clay interface for the case studied did not fully mobilize the available strength of the contact. Therefore the bottom liner/clay interface studied does not appear to provide a slip surface and therefore does not modify earthquake response for the conditions modelled (Mag=6.1,a=0.43g). If the strain at the liner interface had been larger then the strength of the contact system would probably have governed the mechanical behavior.

ACKNOWLEDGEMENT

REFERENCES

Hardin, B.O. (1978). "The Nature of Stress-Strain Behavior of Soils", Proceedings Earthquake Engineering and Soil Dynamics, ASCE Pasadena, California, Vol. 1, pp. 3-89.

Idriss, I.M., Fiegel, G.L., Hudson, M.B., Mundy, P.K., and Herzig, R.(1995)"Seismic Response of the Operating Industries Landfill", Earthquake Design and Performance of Solid Waste Landfills, Geotechnical Special Publication No. 54, American Society of Civil Engineers, N.Y.,N.Y., pp.83-118.

Idriss, I.M. and Sun, J.I. (1992) "User's Manual for SHAKE91", Center for Geotechnical Modeling, Department of Civil and Environmental Engineering, University of California, Davis, California.

Kavazanjian, E. Jr., Matasovic, N., Bonaparte, R., and Schmertmann, G.R.

(1995) "Evaluation of MSW Properties for Seismic Analysis," Proceedings of the Geoenvironment 2000 Specialty Conference, ASCE, Vol. 2, pp. 1126-1141.

Kavazanjian, E. Jr., Matasovic, N. (1995). "Seismic Analysis of Solid Waste Landfills", Proceedings of the Geoenvironment 2000 Specialty Conference, ASCE, Vol. 2, pp.1066-1081.

Kavazanjian, E. Jr.,Hushmand, B., and Martin, G.R. (1991) "Frictional Base Isolation Using a Frictional Soil-Synthetic Liner System", Proceedings Third U.S. Conference on Lifeline Earthquake Engineering, Technical Council on Lifeline Earthquake Engineering Monography No. 4, ASCE.

Lahlaf, A.M., and Yegian, M.K. (1993). "Shaking Table Tests for Geosynthetic Interfaces", Geosynthetics '93, Vancourver, Canada, pp. 659-669.

Mitchel, J. K., Seed, R.B., and Seed, H.B.(1990) "Kettleman Hills Waste Landfill Slope Failure, I:Liner-system Properties," Journal of Geotechnical Engineering, ASCE, Vol 116, No. 4, pp. 647-668.

Richardson, G.N., Kavazanjian, E.,Jr., and Matasovic, N. (1996) "RCRA Subtitle D (258) Seismic Design Guidance for Municipal Solid Waste landfill Facilities", EPA/600/R-95/051Risk Reduction Engineering Laboratory, USEPA, Cincinnati, Ohio.

U.S. Environmental Protection Agency (1992). Title 40, Part 258, "Criteria for municipal solid waste landfills", Code of Federal Regulation, pp. 355©361.

USC (1994) "Proceedings of a Workshop on Research Priorities for Seismic Design of Solid Waste Landfills", G.R. Martin and E. Kavazanjian, Jr., editors, Department of Civil Engineering, University of Southern California, Los Angeles, March.

USGS (1991) "Probabilistic earthquake acceleration and velocity maps of the United States and Puerto Rico." Map MF 2120, United States Geological Survey.

Yegian, M.K., Yee, Z.Y., Harb, J.N.(1995) "Response of Geosynthetics Under Earthquake Excitations", Geosynthetics '95, pp.677-689.

Yegian, M.K., and Lahlaf, A.M.(1992) "Dynamic Interface Shear Strength Properties of Geomembranes and Geotextiles", Journal of Geotechnical Engineering, Vol. 118, No. 5, pp. 760-779.
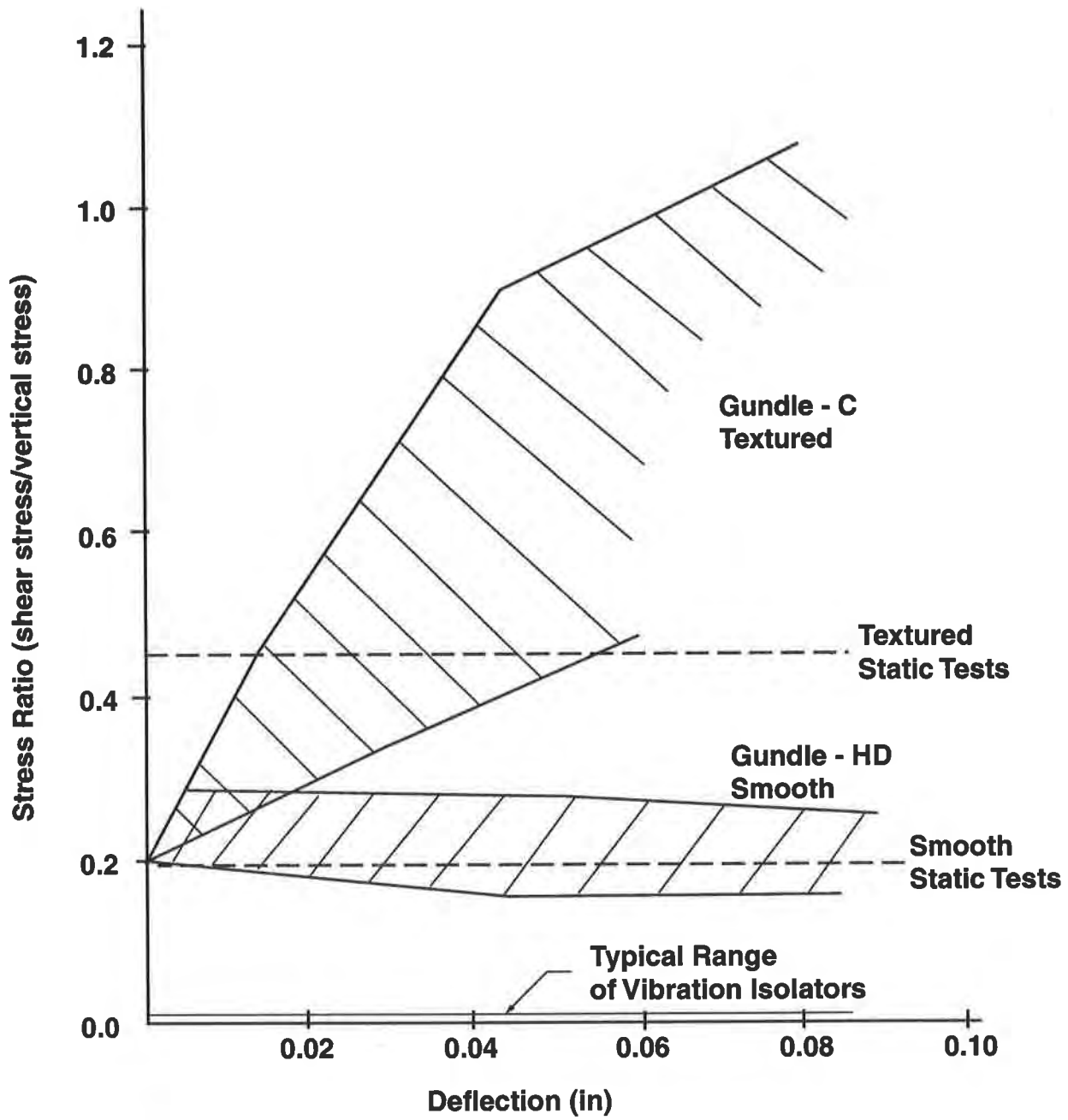
Figure 1 - Stress Ratio versus Deformation
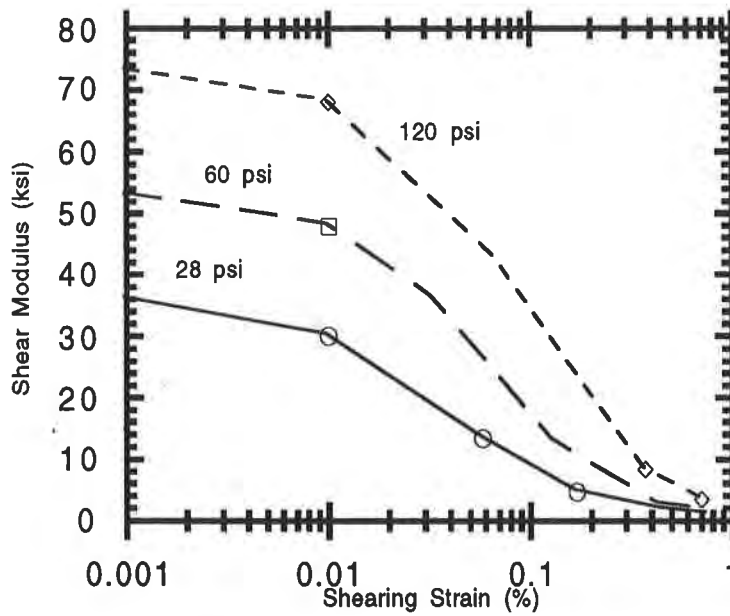
Figure 2 - Summary of Estimated Modulus Reduction
Curves, Geomembrane over 1 foot thick Clay Layer
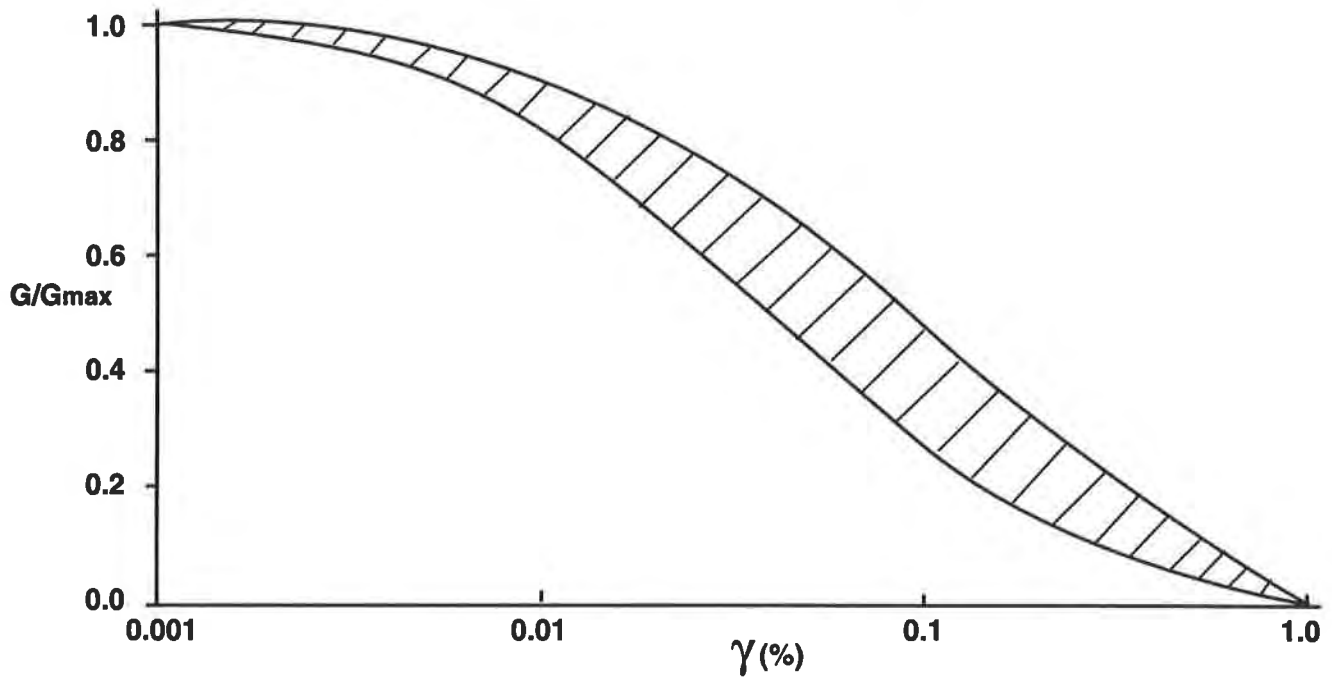
Figure 3 - Normalized Modulus Reduction Curve for HDPE
Liners/Clay Interfaces Assuming a 1 foot thick
layer.
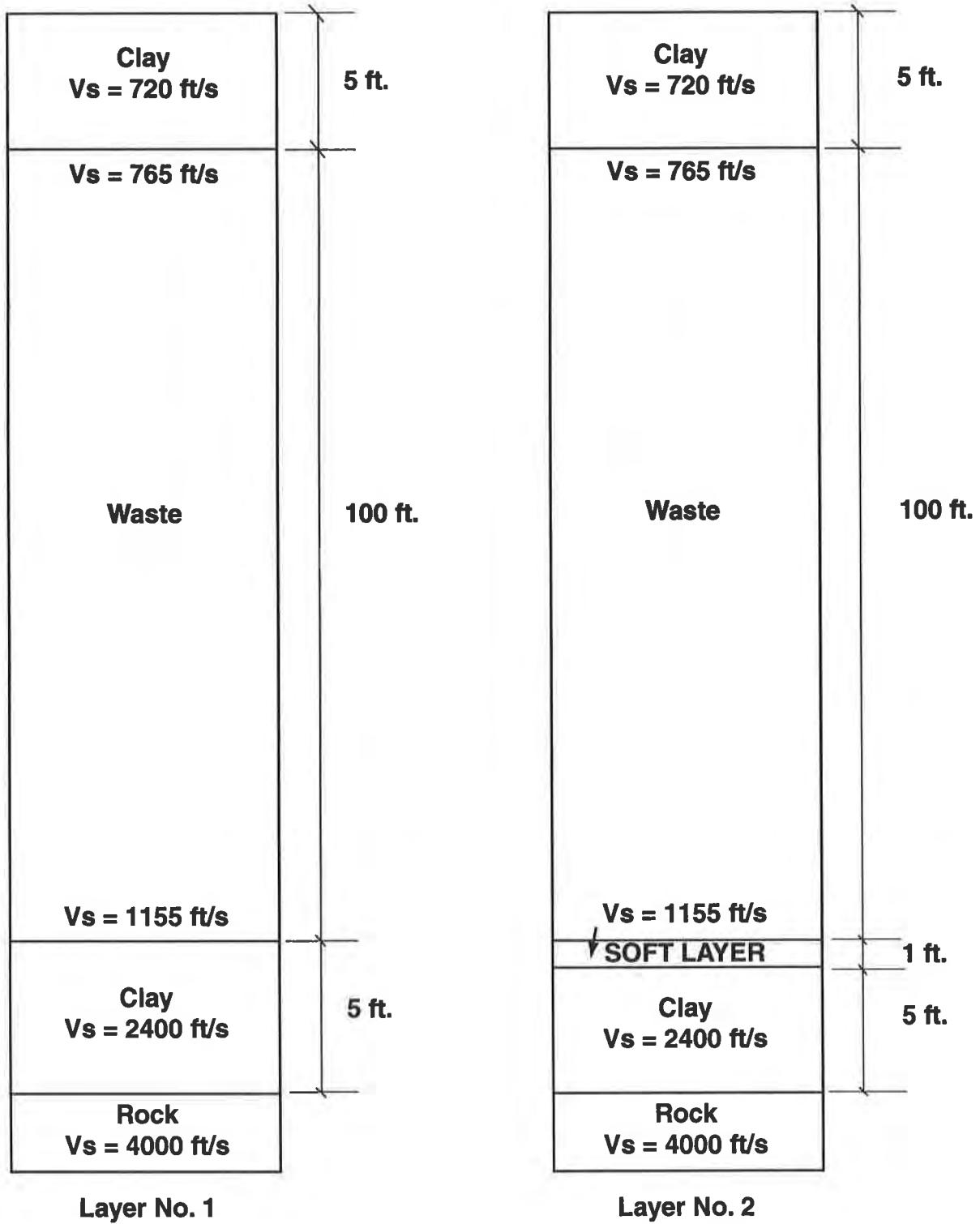
Figure 4 - Case Study Idealized Soil Layers

(1 ft. = 0.34048 m)
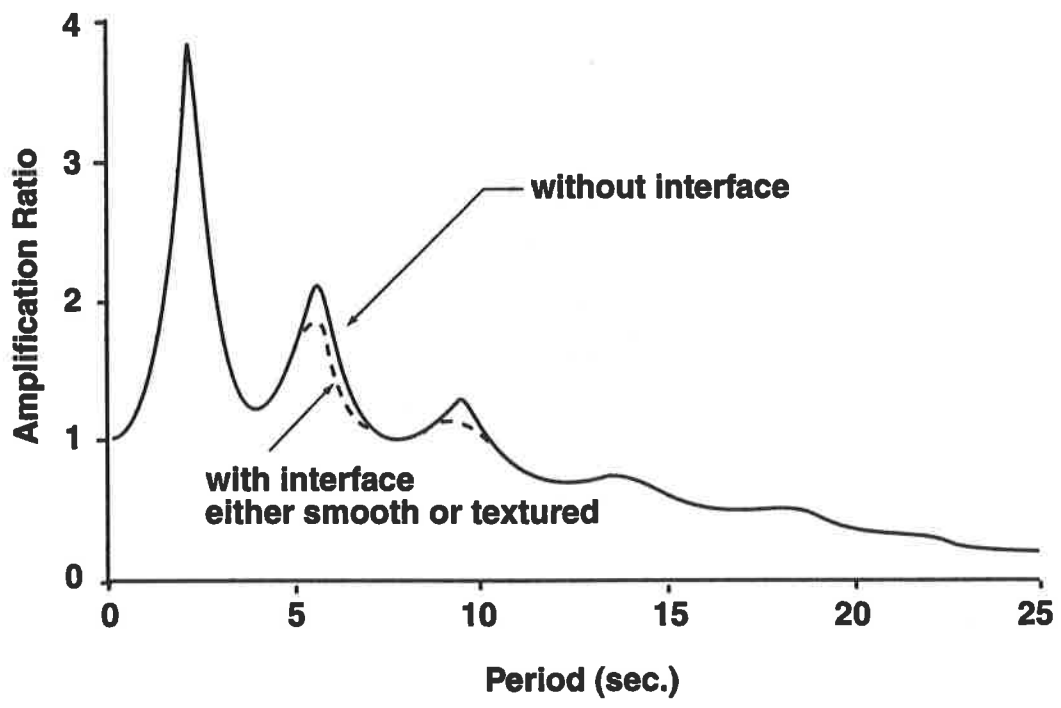
Figure 5 - Amplification Ratio versus Period for condition without and with (geomembrane / clay) Interface Conditions.

NEWMARK DEFORMATION ANALYSIS WITH DEGRADING YIELD ACCELERATION

Neven Matasovic
Edward Kavazanjian, Jr.
GeoSyntec Consultants, Huntington Beach, California, U.S.A.
Liping Yan
University of Southern California, Dept. of Civil Engrg., Los Angeles, California, U.S.A.

ABSTRACT

This paper presents a Newmark seismic deformation analysis in which a degrading yield acceleration has been implemented. The degradation of yield acceleration is modeled with a simple linear degradation model. Using a typical solid waste landfill composite cover configuration and actual interface shear strength testing results, the conservatism associated with seismic deformation analysis performed using the classical Newmark approach and a constant yield acceleration based upon residual and/or large deformation interface shear strength is investigated. The influence on permanent seismic deformation of the normal stress acting on the interface is also examined. Results indicate that Newmark seismic deformation analysis based solely on residual or large strain shear strength parameters is conservative.

INTRODUCTION

The most common approach to seismic deformation analysis used in geotechnical earthquake engineering practice is the "rigid block sliding on a plane" approach described by Newmark (1965). In that analysis, schematically depicted on Figure 1, seismically-induced permanent displacements of the block are calculated from the horizontal acceleration time history of the plane on which the block mass sits, $K_h(t) \cdot g$, and the yield acceleration, k_y. The yield acceleration is the horizontal acceleration that results in a factor of safety of 1.0 in a pseudo-static limit equilibrium analysis. As such, the yield acceleration is a function of material (or interface) shear strength and slope geometry.

The most common assumption regarding the yield acceleration used in Newmark analyses is that it remains unchanged during shaking. However, in his classical 1965 paper, Newmark recognized that the assumption of a constant shear strength, and therefore implicit assumption of a constant yield acceleration, might not always be appropriate. Newmark suggested that modifi-
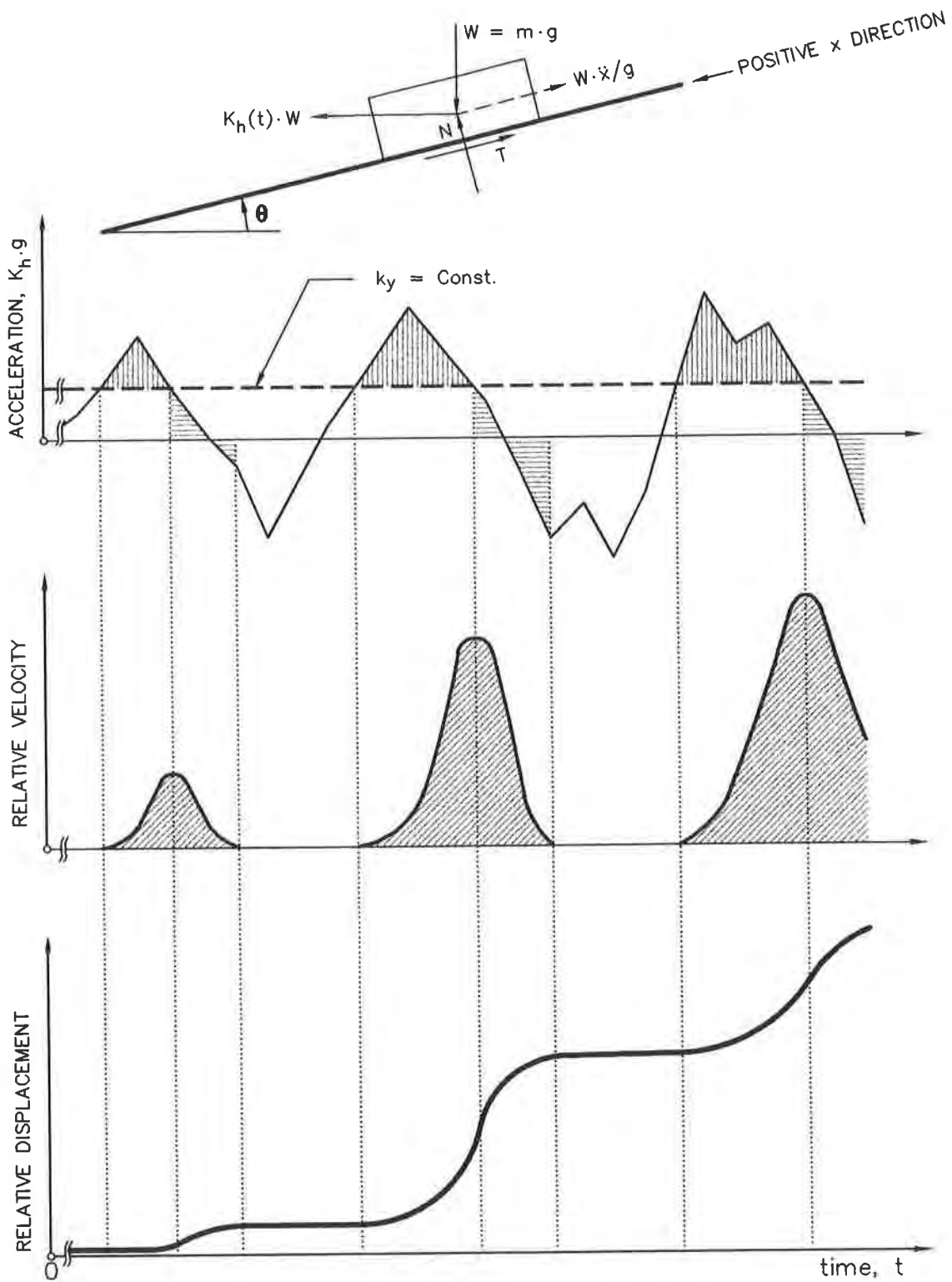
Figure 1. Basic elements of classical Newmark analysis

cation of the method to include cyclic degradation of the shear strength, i.e., degradation of yield acceleration, might be warranted. However, this suggestion has been largely ignored by the geotechnical community and, consequently, is not implemented in most commonly available computer programs for Newmark analysis. Faced with the necessity of choosing a constant value of yield acceleration for use in seismic deformation analysis of earthen structures, most engineers use a yield acceleration evaluated from residual or large deformation shear strength parameters to provide a conservative basis for design.

Calculation of seismically-induced permanent displacements is often an important consideration in the design of geosynthetic landfill cover systems. Typically, Newmark sugestion on degrading yield acceleration is ignored, i.e., classical Newmark seismic deformation analyses with a constant yield acceleration based upon residual interface shear strength parameters are employed in seismic design of composite landfill covers (Seed and Bonaparte, 1992). However, use of residual interface shear strength parameters to evaluate yield acceleration may result in an overly conservative assessment of seismic deformation potential.

In this paper we investigate the conservatism associated with seismic deformation analysis performed using the classical Newmark approach with a constant yield acceleration based upon large deformation or residual interface shear strength. In order to investigate that conservatism, we modified the classical Newmark analysis by introducing a degrading yield acceleration model and applied the modified analysis to a typical solid waste landfill composite cover system. Parameters for the degrading yield acceleration model were developed from the results of actual interface shear strength testing.

MODIFIED NEWMARK DEFORMATION ANALYSIS

The yield acceleration of a potential failure mass, k_y, is directly related to the shear strength on the failure surface. For a landfill cover system where geometry of the system is relatively simple and the failure surface follows a material interface, k_y will be directly related to the interface shear strength. Therefore, the yield acceleration will change whenever the interface shear strength changes.

The Newmark procedure is essentially a step-by-step numerical integration of time-dependent variables. In the numerical implementation of the Newmark analysis, k_y can easily be related to time or to the value of calculated permanent displacement. Consequently, a change (degradation) of yield acceleration with either time or displacement is relatively easy to implement into the computer programs for Newmark analysis (see e.g., Houston et al., 1987; Yan et al., 1996). However, analyses employing a degrading yield acceleration have not been widely used in practice. One challenge in employing such an analysis is to relate the change of k_y to engineering parameters that can be easily measured or quantified.

In our model, we assume that degradation of k_y starts when calculated permanent displacement reaches a certain threshold displacement value, δ_l. This threshold displacement

value is assumed to correspond to the peak of (an interface) shear force-displacement (or stress-strain) curve, as schematically indicated on Figure 2a. We further assume that degradation of k_y stops when a second threshold displacement value, δ_2, is reached. As indicated on Figure 2a, this second threshold displacement value is assumed to correspond to the large deformation or residual shear strength of the material (interface). Between these two threshold displacements, we assume the linear degradation of yield acceleration, as shown on Figure 2b.
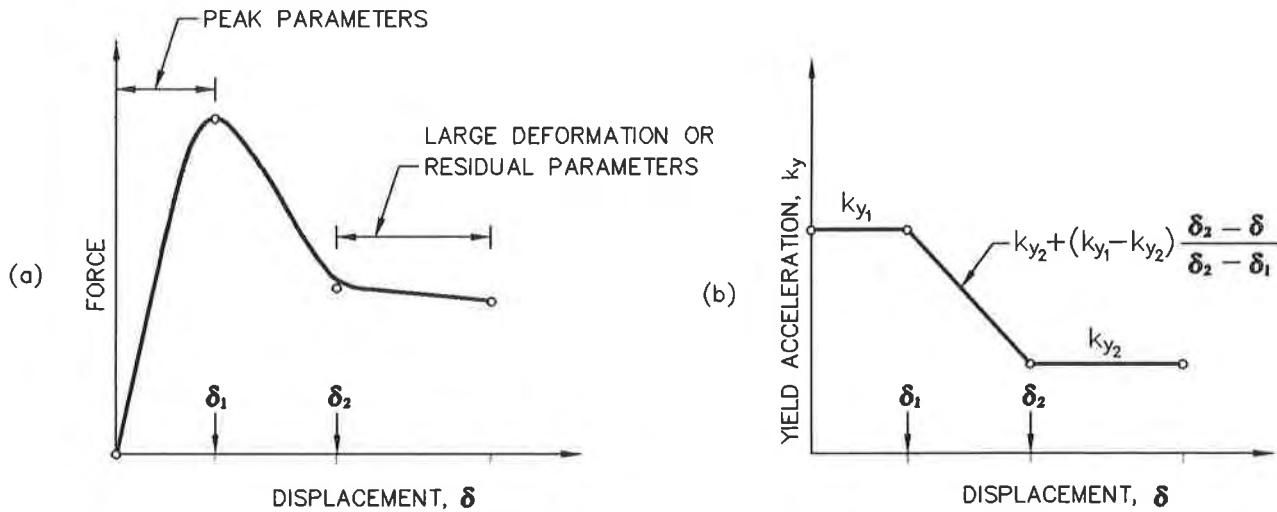
Figure 2. (a) Measured force-displacement curve; (b) Proposed yield acceleration degradation model for composite landfill cover interfaces

Figure 3 compares the integration scheme for a classical Newmark analysis, with k_y calculated from residual strength parameters, to that of the modified Newmark analysis with k_y following degradation law shown on Figure 2.

The accuracy of the modified Newmark analysis will depend on the accuracy with which the model parameters k_{y1}, δ_1, k_{y2} and δ_2 are determined. Factors influencing the evaluation of these parameters include the type of the test, specimen size, sample preparation procedure, testing rate, the deformation limit of the apparatus, and other details of the testing apparatus. It is beyond the scope of this paper to discuss these many factors involved in accurate determination of the model parameters. However, particular attention should be paid to the deformation limit of the testing apparatus as many testing devices do not induce sufficient displacement to induce true large or residual deformation conditions at the interface.
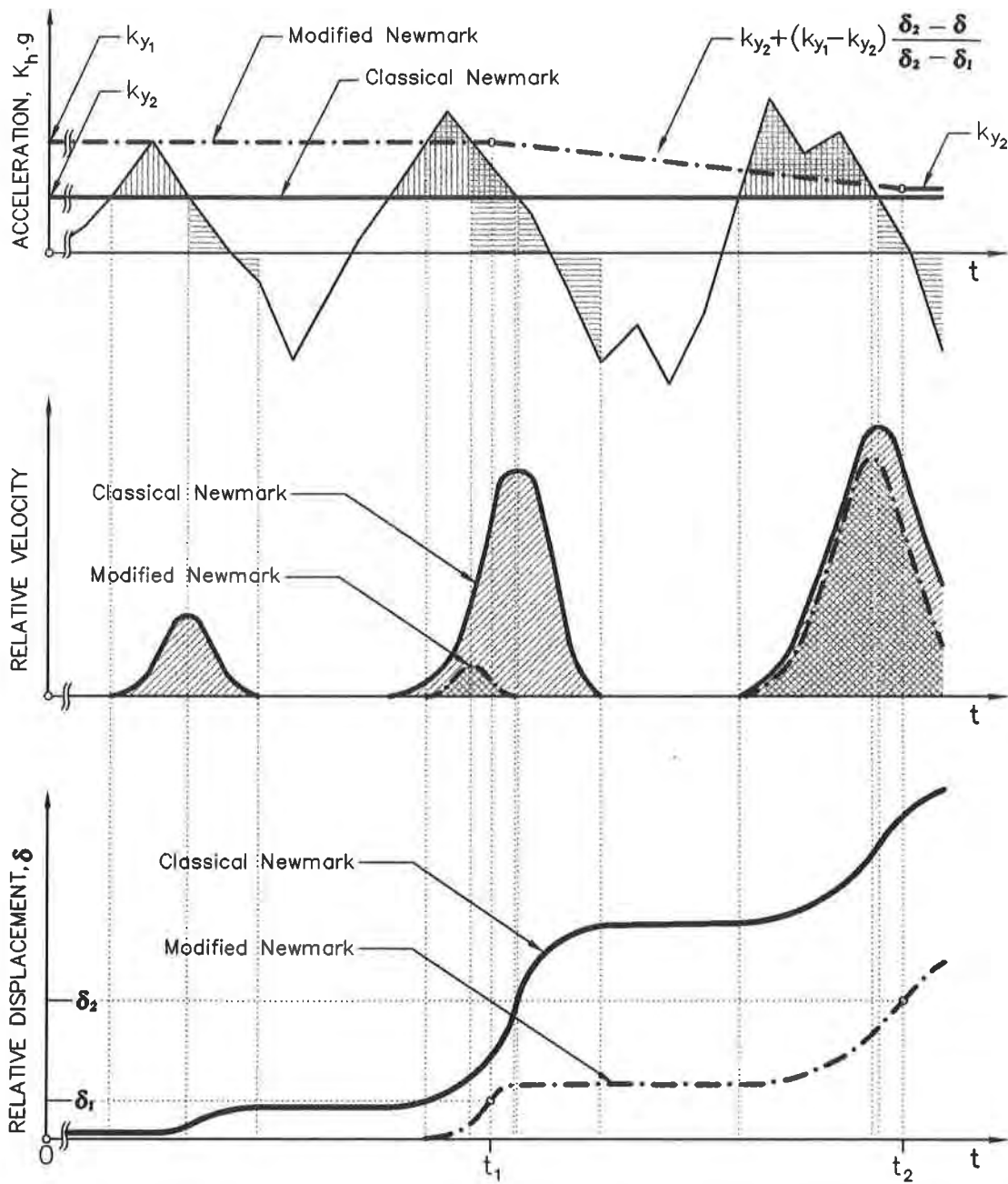
Figure 3. Comparison of classical and modified Newmark analysis
         integration schemes

EXAMPLE CALCULATIONS

A typical composite landfill cover system was selected to investigate the effect of a degrading yield acceleration in Newmark analysis. The cover system consisted of a vegetative cover soil over a double-sided geocomposite drainage layer, a textured geomembrane, and foundation soil. The cover slope inclination is 3.5H:1V (Horizontal : Vertical). Three different thickness of vegetative cover soil, 0.4 m, 1.2 m and 4.0 m were investigated. These thicknesses correspond to normal stresses, σ_n, of 6.9, 20.7 and 69.0 kPa at the bottom of the vegetative cover layer, respectively.

Direct shear testing results for a compacted soil-geotextile interface are shown on Figures 4 and 5. Figure 4 shows the load-deformation curves from the laboratory interface shear tests. The threshold displacements δ_1 and δ_2 indicated on Figure 4 were visually identified. Figure 5 presents an interpretation of the test results presented on Figure 4 in terms of interface shear strength parameters, a (adhesion) and ϕ (friction angle).
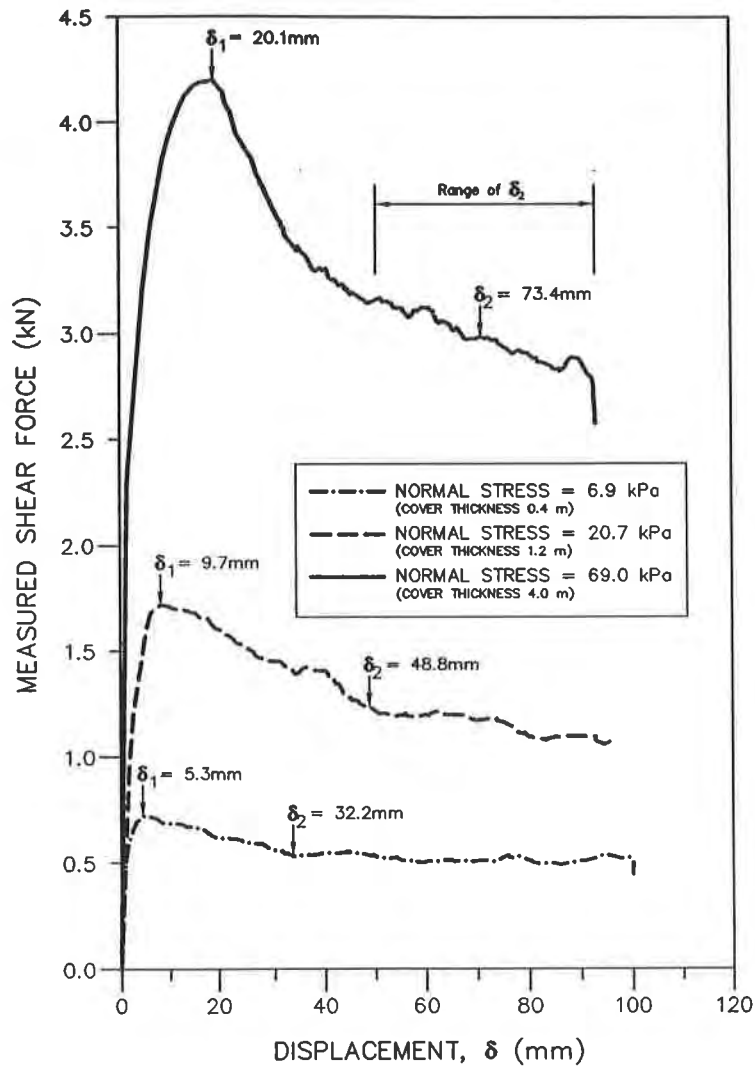
Figure 4. Compacted soil - geotextile interface direct shear testing results
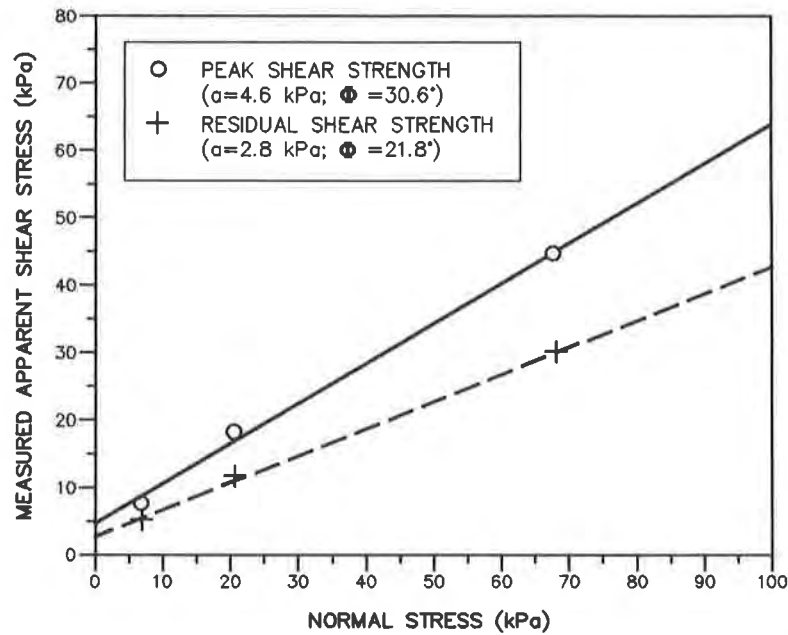
Figure 5. Interpretation of compacted soil - geotextile interface direct shear testing results

Table 1 lists the static factors of safety, FS_{STAT}, and corresponding yield accelerations, k_{y1} and k_{y2}, calculated along this interface for the three cover soil thicknesses using the infinite slope equations proposed by Matasovic (1991).

Table 1. Composite Landfill Cover Configurations Analyzed

Cover Thickness	Peak Parameters		Residual Parameters	
(Normal Stress)	FS_{STAT}	k_{y1}	FS_{STAT}	k_{y2}
0.4 m (σ_n = 6.9 kPa)	4.56	0.87 g	2.94	0.50 g
1.2 m (σ_n = 20.7 kPa)	2.90	0.46 g	1.91	0.23 g
4.0 m (σ_n = 69.0 kPa)	2.32	0.32 g	1.55	0.14 g

The Corralitos-Eureka Canyon Road accelerogram shown on Figure 6 was used as input into the seismic deformation analyses. This accelerogram was recorded during the 17 November 1989 Loma Prieta (Santa Cruz Mountains) earthquake of moment magnitude 6.9. The recording station was on bedrock, in the free-field, 14 km from the zone of energy release. The peak horizontal ground acceleration (PHGA) recorded at the recording station was 0.64 g. For the deformation analyses described below, this accelerogram was scaled to PHGA ranging from 0.1 to 1.1 g
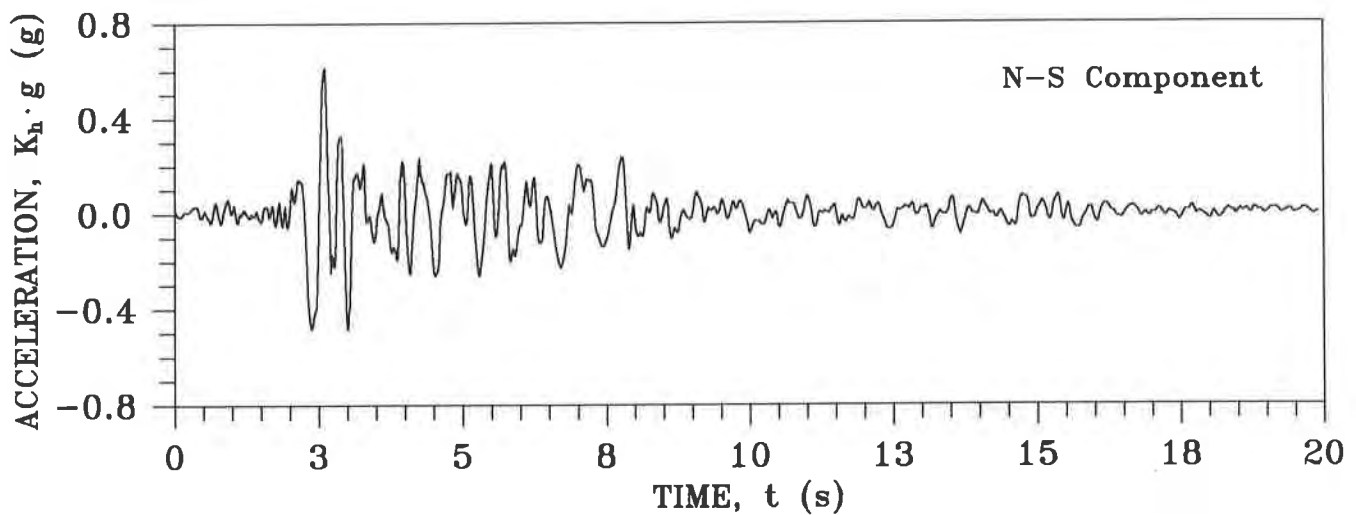
Figure 6. Corralitos - Eureka Canyon Road accelerogram

Classical Newmark deformation analyses using a constant yield acceleration were carried out for both peak and residual shear strength parameters. Modified Newmark analyses with a degrading yield acceleration were carried out using the degradation model shown on Figure 2b. Both analyses were carried out using computer program YSLIP_PM (Yan et al., 1996) for the three cover configurations listed in Table 1. The threshold displacement values indicated on Figure 3 were used in the modified analysis. Results are presented on Figure 6.

Figure 7 shows the results of the above described analyses for the three different normal stress levels (cover soil thicknesses). Calculated permanent displacements are presented as a function of the PHGA to which the accelerogram was scaled. Figure 7a indicates that at the lowest normal stress level (σ_n = 6.9 kPa), due to the relatively high value of k_{y1} (0.87 g), the seismic displacement response of the composite landfill cover calculated using the modified Newmark analysis is the same as that calculated using the peak shear strength parameters. At the intermediate normal stress level (σ_n = 20.7 kPa), the permanent displacement value calculated using the modified Newmark analysis reaches the first threshold displacement, δ_1, at approximately PHGA = 0.7 g. Beyond the first threshold displacement, the residual shear stress parameters rapidly start to influence the displacement response. The same trend can be seen on Figure 7c, which corresponds to the highest normal stress level (σ_n = 69 kPa) considered. All of the diagrams on Figure 7 indicate that Newmark analysis with residual shear strength parameters is conservative.
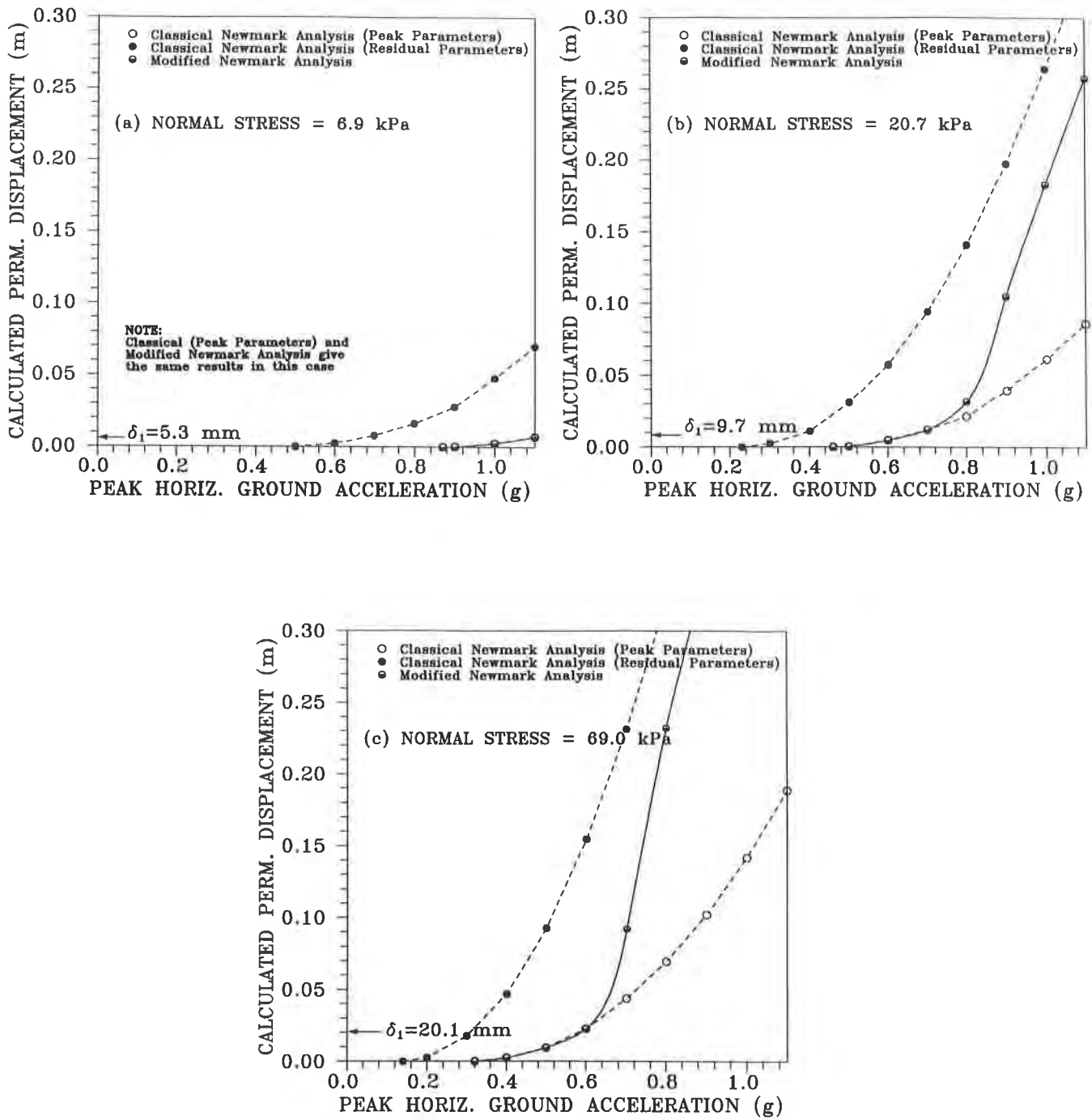
Figure 7. Comparison of classical and modified Newmark analysis at different normal
stress and peak horizontal ground acceleration levels

Threshold displacements δ_1 and δ_2 used in the above example calculations were selected by visual inspection of test results shown on Figure 4. However, the selection of δ_2 for the highest stress level on Figure 4 was subjective. In order to investigate the influence of δ_2 on the results of modified Newmark analysis, the analysis for the normal stress level of 69 kPa was repeated for a PHGA = 0.64 g with δ_2 varied from 20.1 mm (equal to δ, and corresponding to an instantaneous drop from the peak strength to the residual value) to 93 mm (the limit of the testing apparatus). Results of this parametric study are shown on Figure 8.
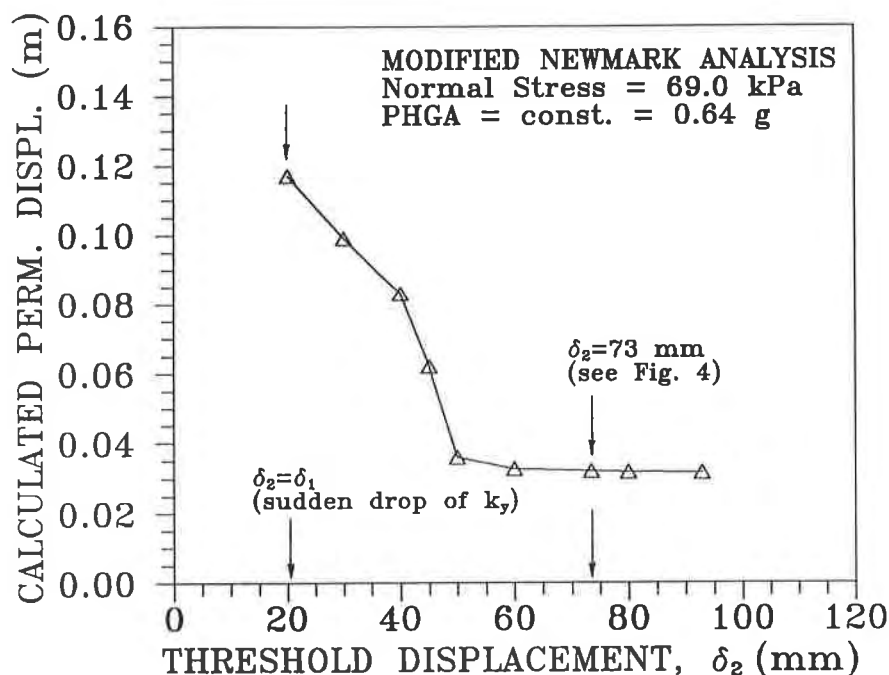
Figure 8. Influence of the second threshold displacement, δ_2, on the results of modified Newmark analysis

Figure 8 indicates that results parametric study were relatively insensitive to δ_2 values greater then 50 mm. The displacement value at which the results become insensitive to δ_2 value are likely to be problem specific and may depend upon peak acceleration, the frequency content of the accelerogram and a variety of other factors.

DISCUSSION AND CONCLUSIONS

The classical Newmark seismic deformation analysis can be modified by introducing a degrading yield acceleration into the analysis. For many strain softening materials (interfaces), such as those of geosynthetic landfill covers, this can be accomplished using a relatively simple linear degradation model. Analyses carried out using such a model clearly demonstrate that Newmark deformation analyses based solely on residual shear strength parameters are

conservative. Conversely, Newmark analyses based solely on peak shear strength parameters are unconservative. The degree of conservatism (or unconservatism) depends upon the value of the calculated seismic deformation compared to the threshold deformations at which the peak and residual strengths are mobilized.

The degree of conservatism can be qualitatively evaluated by comparing the calculated displacement based on the peak shear strength parameters with the threshold displacement δ_1. If the calculated permanent displacement based upon peak shear strength parameters is less than δ_1, the peak shear strength parameters govern the displacement response. If the calculated permanent displacement using peak shear strength parameters exceeds threshold displacement δ_2, then residual shear strength parameters govern the displacement response. However, our results indicate that even in this case, a deformation analysis based solely on residual parameters over-estimates the permanent displacements.

The decision on whether to base a geosynthetic landfill cover design on the residual or peak (interface) shear strength parameters, or on an analysis using a degrading yield acceleration, must consider a variety of other factors besides the value of maximum permanent displacement calculated on the basis of peak shear strength parameters. Factors such as creep and the cyclic nature of earthquake loading may accelerate the degradation of the interface shear strength to the value corresponding to the residual shear strength parameters. Therefore, evaluation of the appropriate interface shear strength values for use in permanent seismic deformation analysis still requires considerable engineering judgment.

ACKNOWLEDGMENTS

REFERENCES

Huston, S.L., Houston, W.N. and Padilla, J.M. (1987), "Microcomputer-Aided Evaluation of Earthquake-Induced Permanent Slope Displacements," Microcomputers in Civil Engineering, Vol. 2, pp. 202-222.

Matasovic, N. (1991), "Selection of Method for Seismic Slope Stability Analysis." Proc. 2nd International Conference on Recent Advances in Geotechnical Earthquake Engineering and Soil Dynamics, St. Louis, Missouri, Vol. 2, pp. 1057-1062.

Newmark, N.M. (1965). "Effects of Earthquakes on Dams and Embankments," Geotechnique, Vol. 15, No. 2, pp. 139-160.

Seed, R. B. and Bonaparte, R. (1992), "Seismic Analysis and Design of Lined Waste Fills: Current Practice," Proc. Stability and Performance of Slopes and Embankments - II, Vol. 2, ASCE Geotechnical Special Publication No. 31, Berkeley, California, pp. 1521-1545.

Yan, L., Matasovic, N. and Kavazanjian, E., Jr. (1996), "YSLIP_PM - A Computer Program for Simulation of Dynamic Behavior of a Rigid Block on an Inclined Plane and Calculation of Permanent Displacements of the Block," User's Manual, GeoSyntec Consultants, Huntington Beach, California, 21 p. (plus Appendix).

SEISMIC PERFORMANCE CHARTS FOR GEOSYNTHETIC REINFORCED SEGMENTAL RETAINING WALLS

R.J. BATHURST and Z. CAI
ROYAL MILITARY COLLEGE OF CANADA, CANADA
M.R. SIMAC
EARTH IMPROVEMENT TECHNOLOGIES, USA

ABSTRACT

A series of charts are presented that can be used to perform a preliminary evaluation of the seismic resistance of routine geosynthetic reinforced segmental retaining walls (RSRWs) designed for static load environments. The charts are based on a pseudo-static design method proposed by the first two writers and also serve to illustrate the effect of increasing horizontal ground acceleration on the destabilizing forces used in stability calculations for RSRW structures. An example problem is presented to demonstrate both the use of the charts and some important issues related to seismic performance of geosynthetic reinforced segmental retaining walls.

INTRODUCTION

The use of concrete block (segmental) retaining walls (SRWs) reinforced with geosynthetics has increased dramatically in recent years due to their ease of construction and low cost. A unique feature of SRWs is the use of mortarless dry-stacked modular concrete blocks to form the facia. The interlocking blocks provide transverse rigidity and shear capacity over the height of the wall. The stability of geosynthetic reinforced segmental retaining walls (RSRWs) under static loading has been adequately addressed by adopting conventional Coulomb wedge limit equilibrium methods as recommended by the National Concrete Masonry Association (NCMA) (Bathurst and Simac 1994; Simac et al. 1993; Bathurst et al. 1993). A design methodology has been proposed that extends the Coulomb approach to structures subjected to earthquake loadings (Bathurst and Cai 1995, Bathurst and Alfaro 1996). The method uses the classical Mononobe-Okabe (M-O) pseudo-static approach to estimate dynamic earth pressures. This paper is focussed on a set of charts that can be used to carry out a preliminary evaluation of the seismic resistance of routine RSRW structures and to provide insight into the quantitative effects of increasing horizontal ground acceleration up to 0.5g on the stability of static designed structures. An example problem is presented to demonstrate both the use of the charts and some important issues related to seismic performance of geosynthetic reinforced segmental retaining walls. In this paper, RSRW structures are assumed to be constructed with homogenous, compacted, cohesionless, unsaturated soils with peak friction angles ranging from 25 to 45 degrees and a horizontal backslope. The structures are restricted to firm foundations for which collapse of foundation soils or settlement is not a concern.
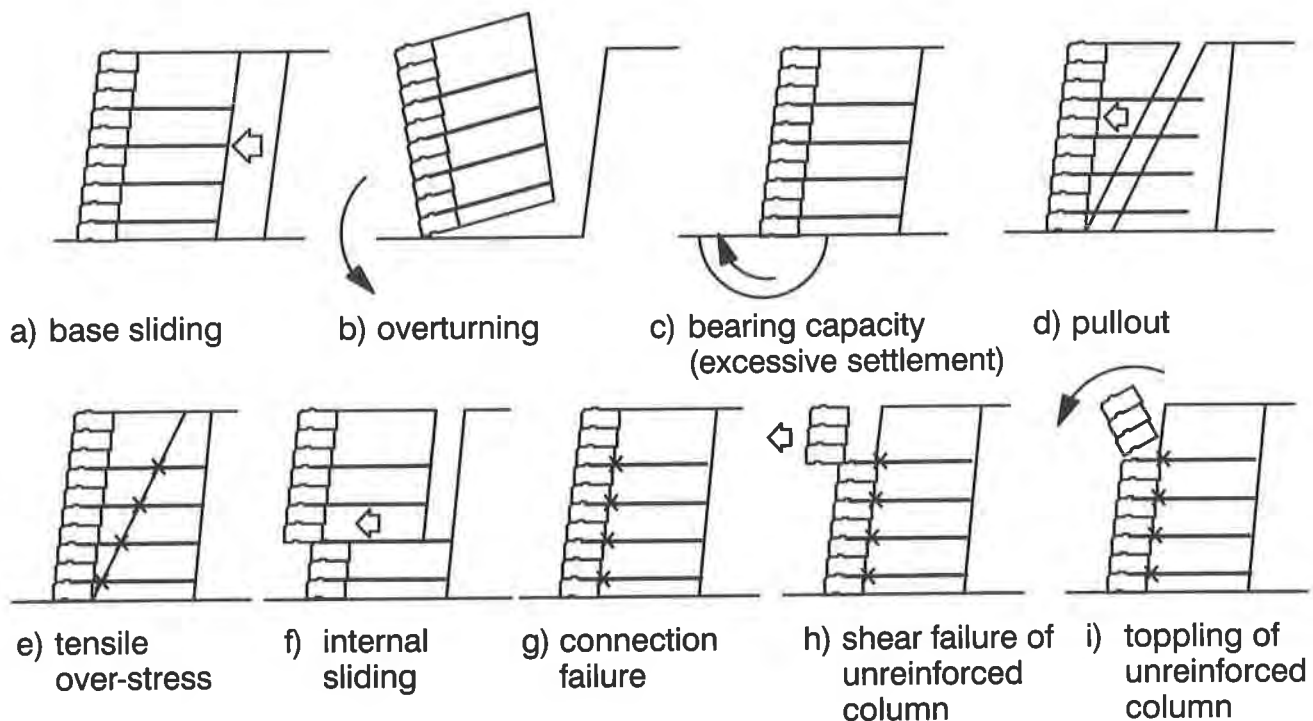
Figure 1. Modes of failure: External a), b), c); Internal d), e), f); Facing column; g), h), i) (adapted from Simac et al. 1993).

REVIEW OF PSEUDO-STATIC DESIGN METHODOLOGY

Potential Failure Modes. Potential failure modes for RSRW structures are illustrated in Figure 1. External failure mechanisms consider the stability of an equivalent gravity structure comprising the facing units, geosynthetic reinforcement and reinforced soil fill. Not included in Figure 1 is global instability which involves failure mechanisms passing through or beyond the reinforced soil mass. Modes of failure that require special attention in reinforced segmental retaining wall design and analysis are illustrated in the last four diagrams of Figure 1.

Dynamic Earth Pressure Theory. Pseudo-static rigid body approaches that use the Mononobe-Okabe (M-O) method to calculate dynamic earth forces acting on earth retaining structures are well established in geotechnical engineering practice (e.g. Seed and Whitman 1970). The M-O method can be recognized as an extension of the classical Coulomb wedge analysis and hence provides the designer with a consistent approach to that recommended by the NCMA for static loaded structures. The total dynamic active earth force, P_{AE}, imparted by a backfill soil (Figure 2a) is calculated as (Seed and Whitman 1970):

$$P_{AE} = \frac{1}{2}(1 \pm k_v)K_{AE}\gamma H^2 \tag{1}$$

where: γ = unit weight of the soil; and H = height of the wall. The dynamic earth pressure coefficient, K_{AE}, can be calculated as follows:

$$K_{AE} = \frac{\cos^2(\phi + \psi - \theta)}{\cos\theta \cos^2\psi \cos(\delta - \psi + \theta)\left[1 + \sqrt{\dfrac{\sin(\phi + \delta)\sin(\phi - \beta - \theta)}{\cos(\delta - \psi + \theta)\cos(\psi + \beta)}}\right]^2} \tag{2}$$

where: ϕ = peak soil friction angle; ψ = total wall inclination (positive in a clockwise direction from the vertical); δ = mobilized interface friction angle at the back of the wall (or back of the reinforced soil zone); β = backslope angle (from horizontal); and θ = seismic inertia angle given by:

$$\theta = \tan^{-1}\left(\frac{k_h}{1 \pm k_v}\right) \tag{3}$$

Quantities k_h and k_v are horizontal and vertical seismic coefficients, respectively, expressed as fractions of the gravitational constant, g. Following the approach used by Seed and Whitman (1970), it is convenient to decompose the total dynamic (active) earth force, P_{AE}, into two components representing the static earth force component, P_A, and the incremental dynamic earth force due to seismic effects, ΔP_{dyn}. Hence:

$$P_{AE} = P_A + \Delta P_{dyn} \tag{4}$$

or

$$(1 \pm k_v)K_{AE} = K_A + \Delta K_{dyn} \tag{5}$$

where: K_A = static active earth pressure coefficient; and ΔK_{dyn} = incremental dynamic active earth pressure coefficient. It should be noted that the partitioning of forces according to Equation 4 is not strictly correct since the failure wedge corresponding to P_A will become shallower with increasing magnitude of k_h and hence influence the magnitude of P_A. Bathurst and Cai (1995) have proposed the total active dynamic earth pressure distribution illustrated in Figure 2b for external, internal and facing stability analyses of RSRW structures. The normalized point of application of the resultant total earth force varies over the range $1/3 \le m \le 0.6$ depending on the magnitude of ΔK_{dyn} and the assumed point of application of the dynamic component of the total earth pressure distribution (the dynamic component is assumed to act at 0.6H above the base of the wall). The assumed pressure distribution is based on a review of the literature for conventional gravity retaining wall structures and is identical to that recommended for the design of flexible anchored sheet pile walls under seismic loads (Ebling and Morrison 1993). In the absence of ground acceleration, the lateral earth pressure distribution in Figure 2b reduces to the well-known triangular (static) active earth pressure distribution due to soil self-weight.

SEISMIC PERFORMANCE CHARTS

Assumptions. In order to simplify the charts in this paper a number of assumptions are made. The unit weight of the retained soil, reinforced soil and facing column are assumed constant. The horizontal backslope angle is taken as horizontal ($\beta = 0$); and the vertical seismic coefficient is taken as $k_v = 0$ which is a common assumption for pseudo-static design of conventional earth retaining structures. In addition, base ground accelerations are assumed to be transmitted uniformly through the entire structure. The reader is referred to the paper by Bathurst and Cai (1995) for a detailed dis-

a) forces and geometry   b) dynamic earth pressure distribution
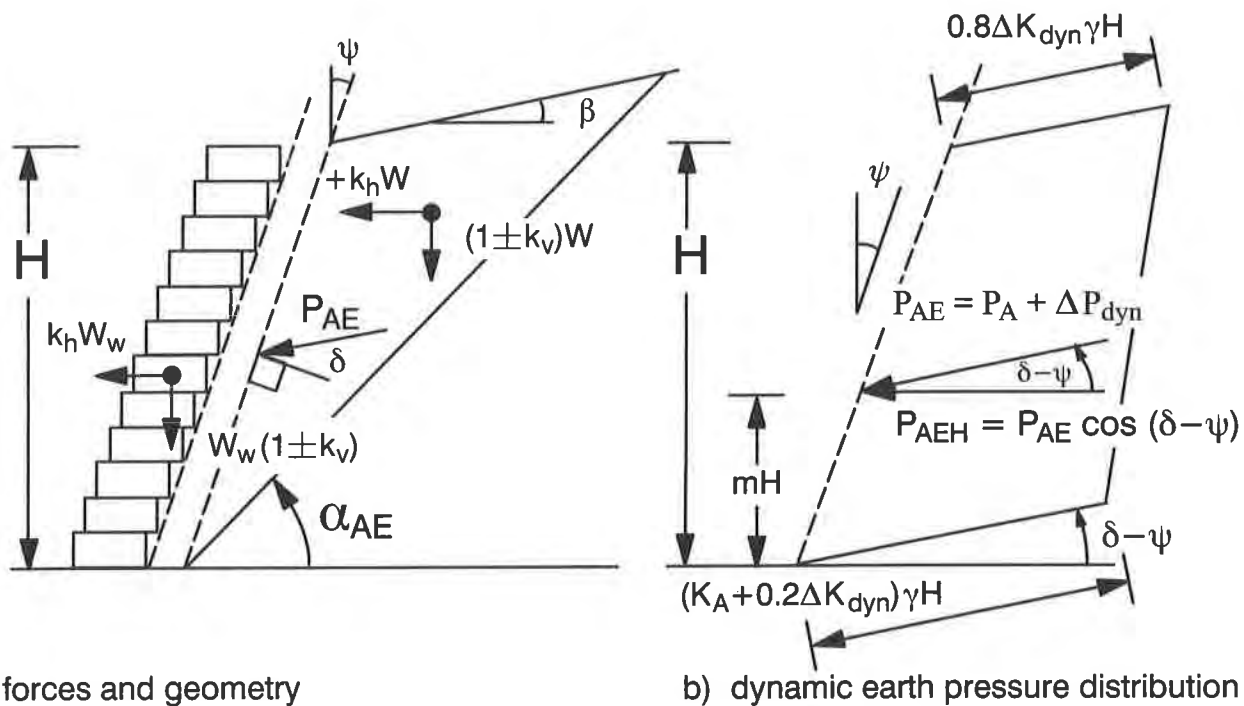
Figure 2. Dynamic forces and pressures used in pseudo-static seismic analysis of segmental retaining walls (after Bathurst and Cai 1995).

cussion of the principal assumptions in the pseudo-static seismic approach and issues related to the choice of appropriate k_h values for design.

Coefficient of Dynamic Active Earth Pressure. The horizontal component of dynamic active earth pressure, K_{AEH}, is introduced here since it is the horizontal component of dynamic active earth force, P_{AEH}, that is used in stability calculations (an approach that is consistent with the method adopted for static loaded structures by the NCMA). Hence:

$$K_{AEH} = K_{AE} \cos (\delta - \psi) = \frac{2 \, P_{AEH}}{\gamma H^2} \tag{6}$$

The results of calculations for the horizontal component of dynamic active earth pressure coefficient using Equations 1,2 and 6 are illustrated in Figures 3a and 3b. These figures illustrate that an increasing magnitude of horizontal ground acceleration results in increasing magnitude of destabilizing lateral earth pressures and forces used in stability calculations.

External Stability. Free-body diagrams for base sliding and overturning modes of failure are illustrated in Figures 4a and 4b, respectively. The term W_H in Figure 4 is the weight of the reinforced zone plus the weight of the facing column described by width L_W. The quantity $k_h \lambda W_H$ represents the horizontal inertial force of the composite mass. A value of $\lambda = 0.6$ has been used for this empirical constant in the analysis of both geosynthetic reinforced soil walls and walls that use steel reinforcement strips (Christopher et al. 1989). Parameter λ is assumed to be less than unity to account for the transient nature of the peak accelerations in the gravity mass and retained soils and the expectation that the inertial forces induced in the gravity mass and the retained soil zone will not reach peak values at the same time during a seismic event. The ratio of dynamic to static factors of safety for
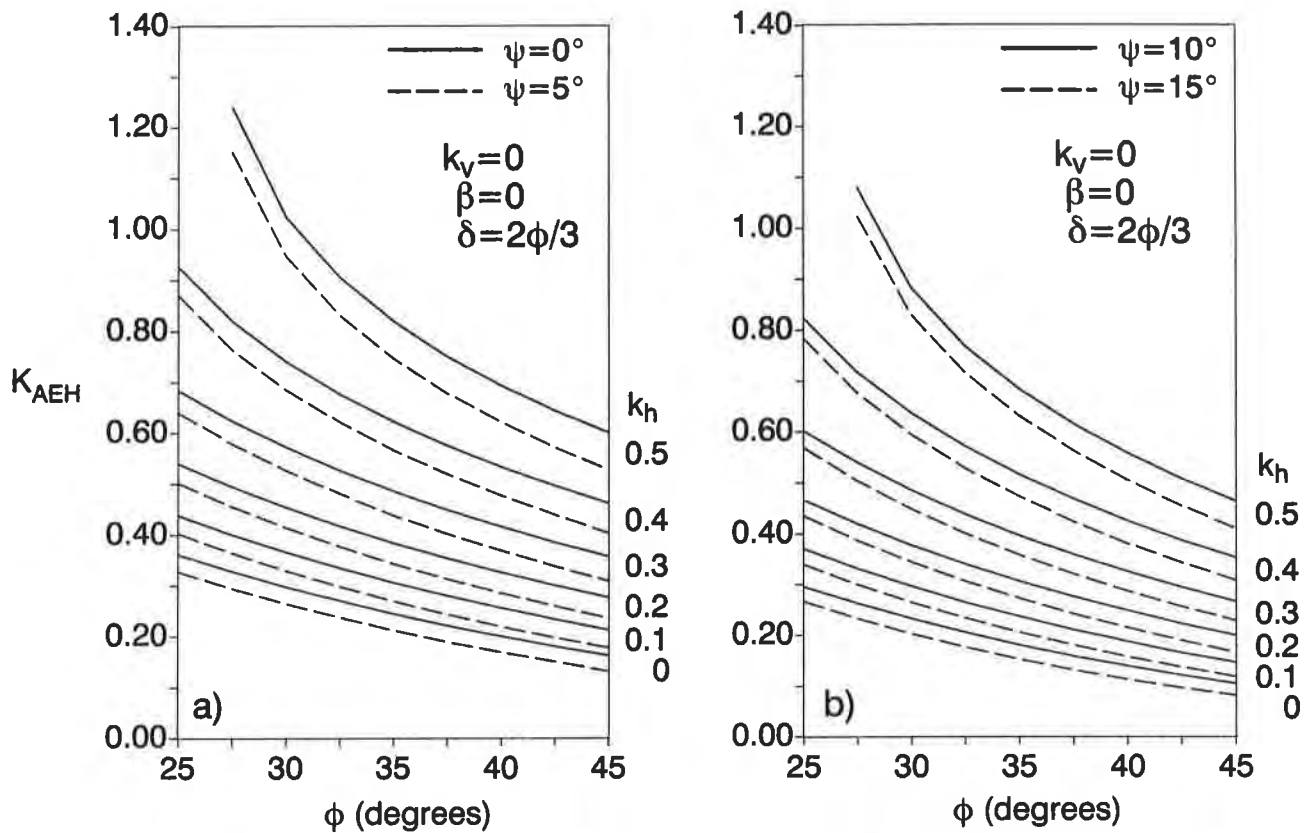
Figure 3. Horizontal component of dynamic active earth force coefficient, K_{AEH}.

a) base sliding

b) overturning
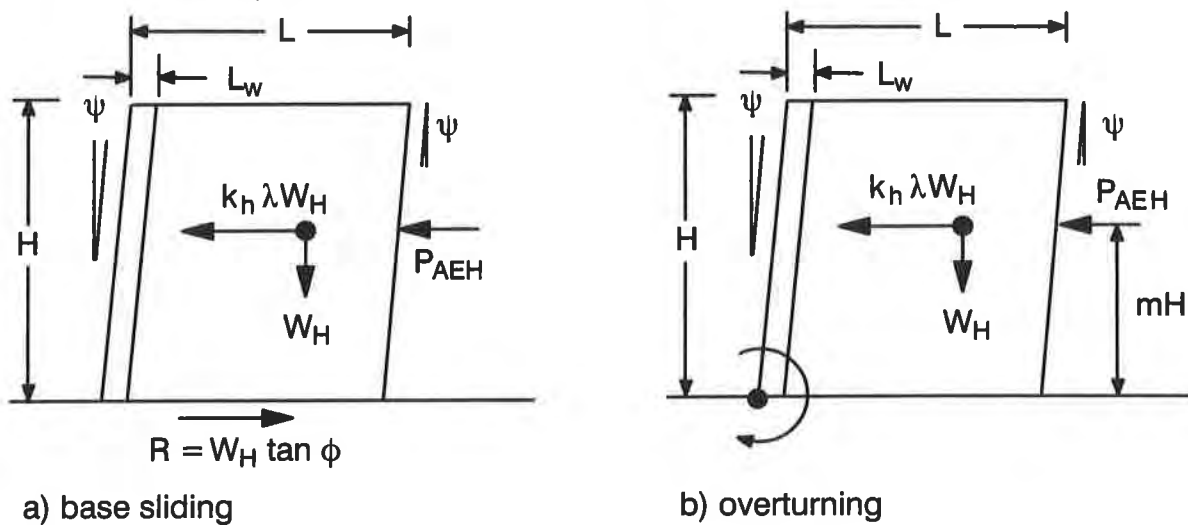
Figure 4. Forces and geometry for external stability calculations ($k_v=0$, $\beta=0$).

each of these two modes of failure is illustrated in Figure 5.

Internal Stability. The calculation of reinforcement forces is based on a contributory area approach in which each reinforcement layer resists the integrated lateral earth pressure partitioned between adjoining layers (area S_v in Figure 6). In the approach used here the incremental inertial force due to the facing column (quantity $k_h\Delta W_W$) also contributes to the reinforcement load, F_{dyn}. Force am-
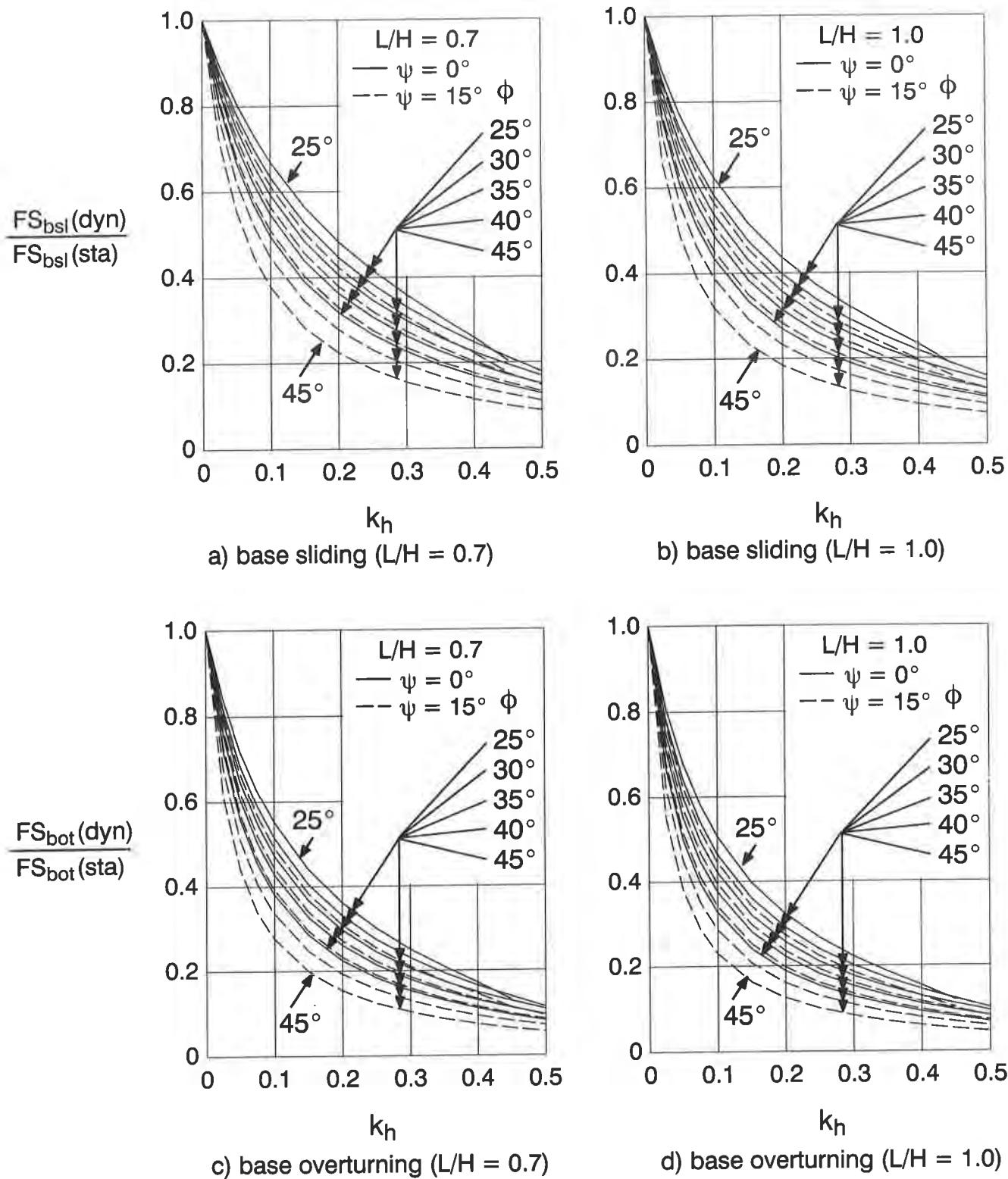
Figure 5. Ratio of dynamic to static factors of safety against external base sliding and overturning about the toe ($\beta=0$, $\delta=\phi$, $k_v=0$).

$0.8 \Delta K_{dyn} \gamma H \cos(\delta - \psi)$ — Dynamic earth pressure distribution

$k_h \Delta W_w$

$+ \quad S_v$

$=$

F_{dyn}

$L_w \quad (K_A + 0.2 \Delta K_{dyn}) \gamma H \cos(\delta - \psi)$ Reinforcement layer (typical)
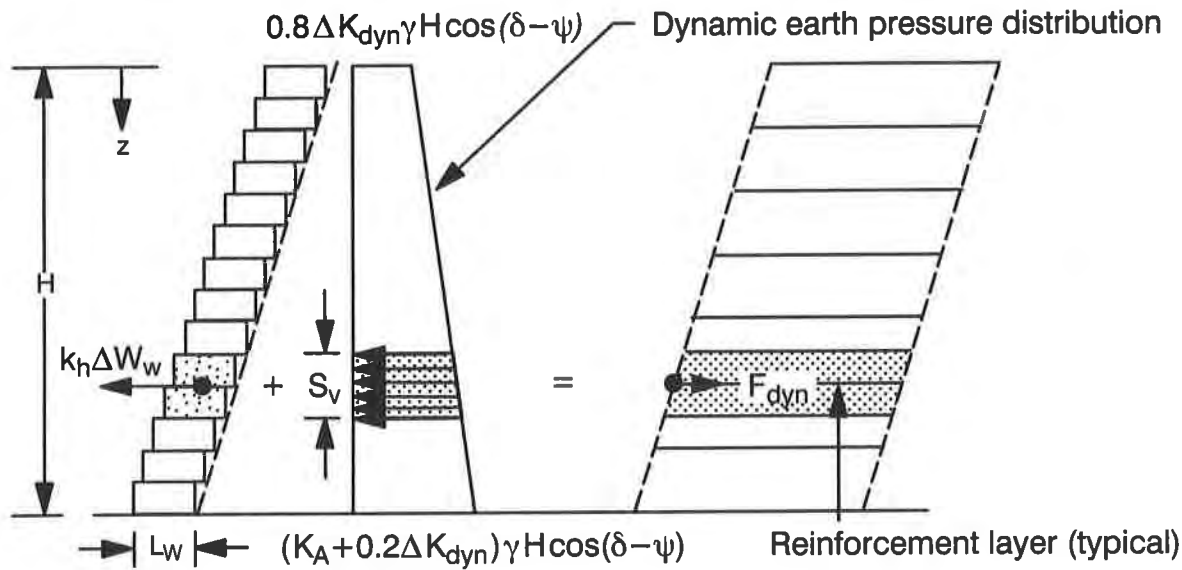
Figure 6. Calculation of reinforcement tensile load, F_{dyn}, due to dynamic earth pressure and wall inertia.

plification factors that can be used to estimate the total forces at the connections, in the geosynthetics layers and in the anchorage zones under seismic loading can be estimated using Figures 7a, 7b and 7c. A consequence of the M-O theory used in pseudo-static methods is that the internal failure surface becomes shallower as the magnitude of horizontal ground acceleration increases. An important implication of this effect is that reinforcement lengths calculated using the "tied-back wedge" approach will need to be lengthened in order that the internal wedge is contained by all reinforcement layers. The effect of increasing magnitude of k_h on the ratio of the minimum internal length of reinforcement layer required for static loading to that required under seismic loading conditions to just intersect the internal failure surface is illustrated in Figure 8.

Facing Column Stability. The results of pseudo-static analyses (Bathurst and Cai 1995) and shaking table tests (Bathurst et al. 1996) have illustrated that the most critical part of a reinforced segmental retaining wall during ground shaking is the unreinforced column directly above the topmost reinforcement layer. This portion of the wall can be analyzed as an isolated stubby gravity wall structure subject to the destabilizing earth forces and moments due to that portion of the lateral earth pressure distribution located above the elevation of the topmost layer of reinforcement. The ratios of dynamic to static factors of safety against interface sliding and overturning (toppling) for the top unreinforced column height are summarized in Figures 9 and 10. These charts differ from the external stability charts presented earlier (Figure 5) since the interface friction angle is taken as $\delta = 2\phi/3$ and the earth pressure distribution is truncated at depth z of the topmost reinforcement layer.

EXAMPLE PROBLEM

An example problem using the geosynthetic reinforced segmental wall shown in Figure 11 is introduced here to illustrate the use of the charts to perform a preliminary evaluation of the seismic stability of a static designed reinforced segmental wall. The wall dimensions have been taken from an actual structure reported by Bathurst and Cai (1995). The wall batter is less than 3 degrees and negligible error is introduced by assuming $\psi = 0$ in the charts. The soil parameter values assumed
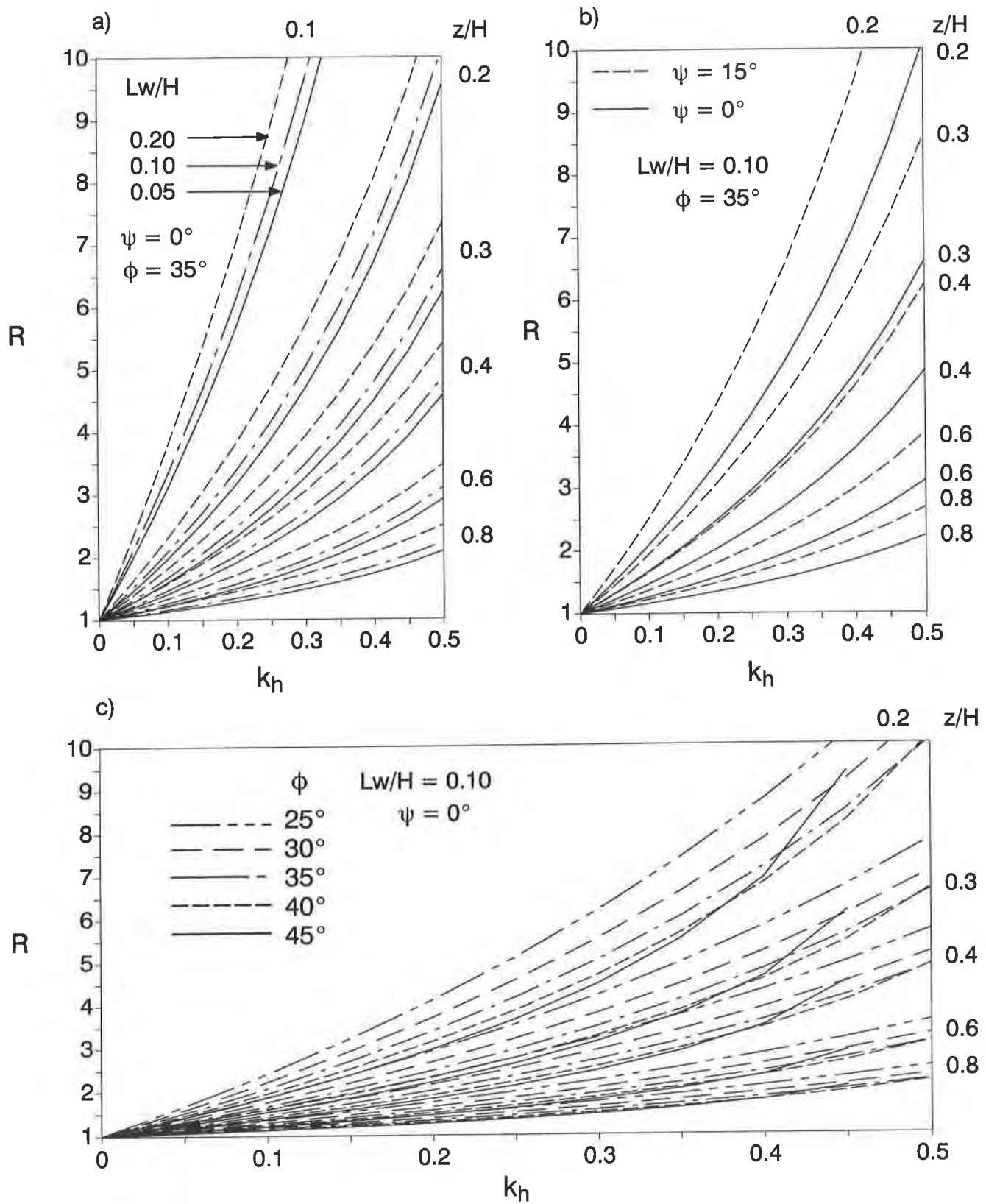
Figure 7. Reinforcement force amplification factor, R (β=0, δ=2ϕ/3, k_v=0).
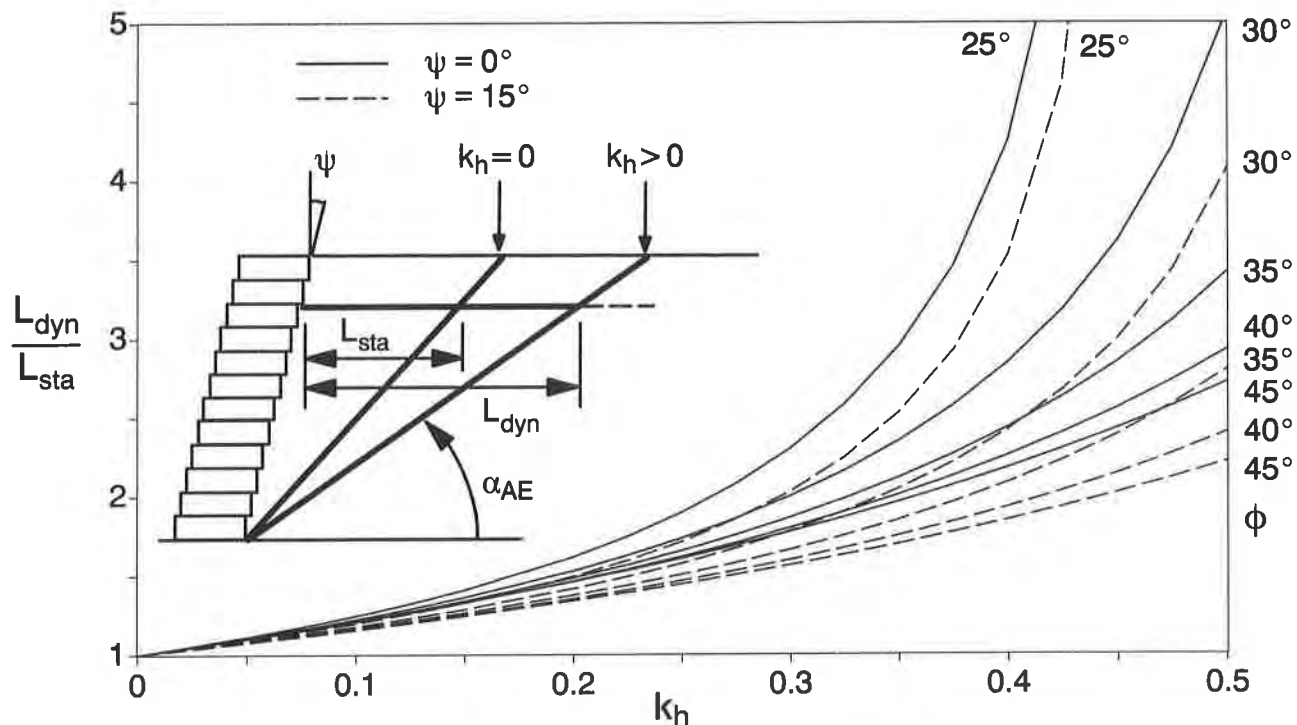
Figure 8. Ratio of dynamic minimum internal reinforcement length to static length required to just capture internal failure wedge ($\beta=0$, $\delta=2\phi/3$, $k_v=0$).

in the analyses are: $c=0$, $\phi=35°$, $\gamma=20$ kN/m^3. The available tensile reinforcement capacity is taken as the long-term allowable design strength of the geogrid reinforcement, $T_{allow}=27$ kN/m and for simplicity has not been adjusted upward to account for a larger design strength that may be reasonably assumed for the rapid loading condition (Bathurst and Alfaro 1996). Reinforcement anchorage capacities have been calculated assuming that the soil-geosynthetic interface friction angle is equal to the peak friction angle of the cohesionless soil. Block dimensions are 600 mm (toe to heel) by 200 mm high with a unit weight assumed to be equal to that of the soil. A range of parameters for interface shear between facing units and connection strengths have been considered to examine the influence of the magnitude of facing column strength parameter values on the stability of the facing column. A relatively poor block with Mohr-Coulomb parameters $a_u = 8$ kN/m (minimum shear strength term) and $\lambda_u = 24°$ (equivalent friction angle term) and a relatively better block with $a_u = 8$ kN/m and $\lambda_u = 50°$ are considered here. Corresponding connection strengths for the two blocks have been taken as $a_{cs} = 16$ kN/m (minimum connection strength term) and $\lambda_{cs} = 42°$ (equivalent friction angle term) and $a_{cs} = 16$ kN/m and $\lambda_{cs} = 67°$. These parameters values fall within ranges for typical segmental units on the market today (Bathurst and Simac 1994; Cai and Bathurst 1996). Two different reinforcement length to height ratios are also assumed: L/H = 0.7 and 1.0. The smaller value is a minimum aspect ratio value that is often prescribed in the literature for reinforced soil walls (e.g. AASHTO 1992). The results of static analyses are presented in Table 1. The calculated values were computed using program SRWALL (ver 1.1) written by the first writer which is a generic computer program for the stability analyses of routine (static) segmental retaining wall structures (Bathurst and Simac 1995). The high factors of safety for base sliding and overturning are a consequence of the relatively large L/H ratios assumed. Calculations show that the required aspect ratio to satisfy external stability factor of safety criteria for static loading is less than L/H=0.5. The static
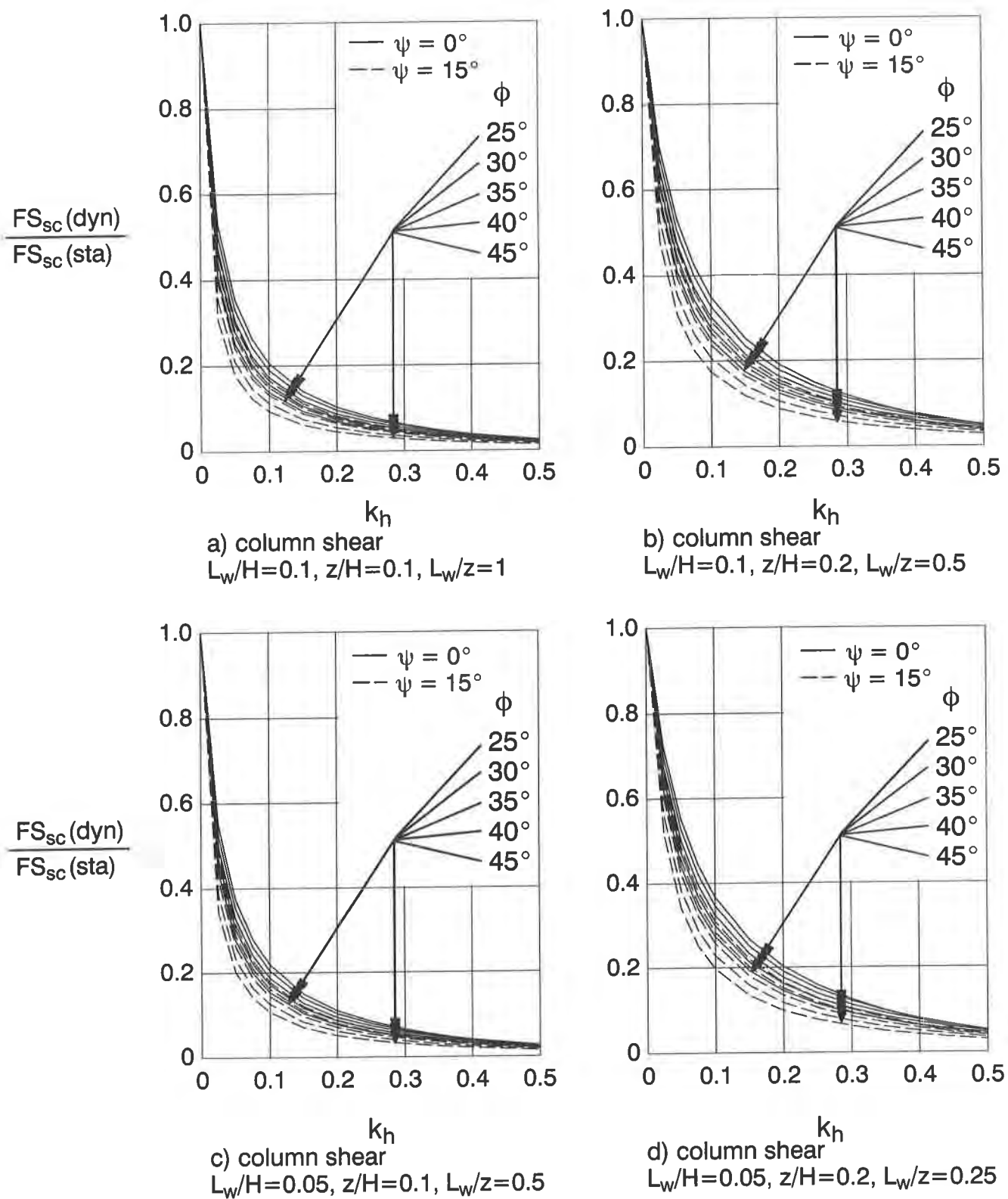
Figure 9. Ratio of dynamic to static factors of safety against sliding of the top unreinforced facing column ($\beta=0$, $\delta=2\phi/3$, $k_v=0$).
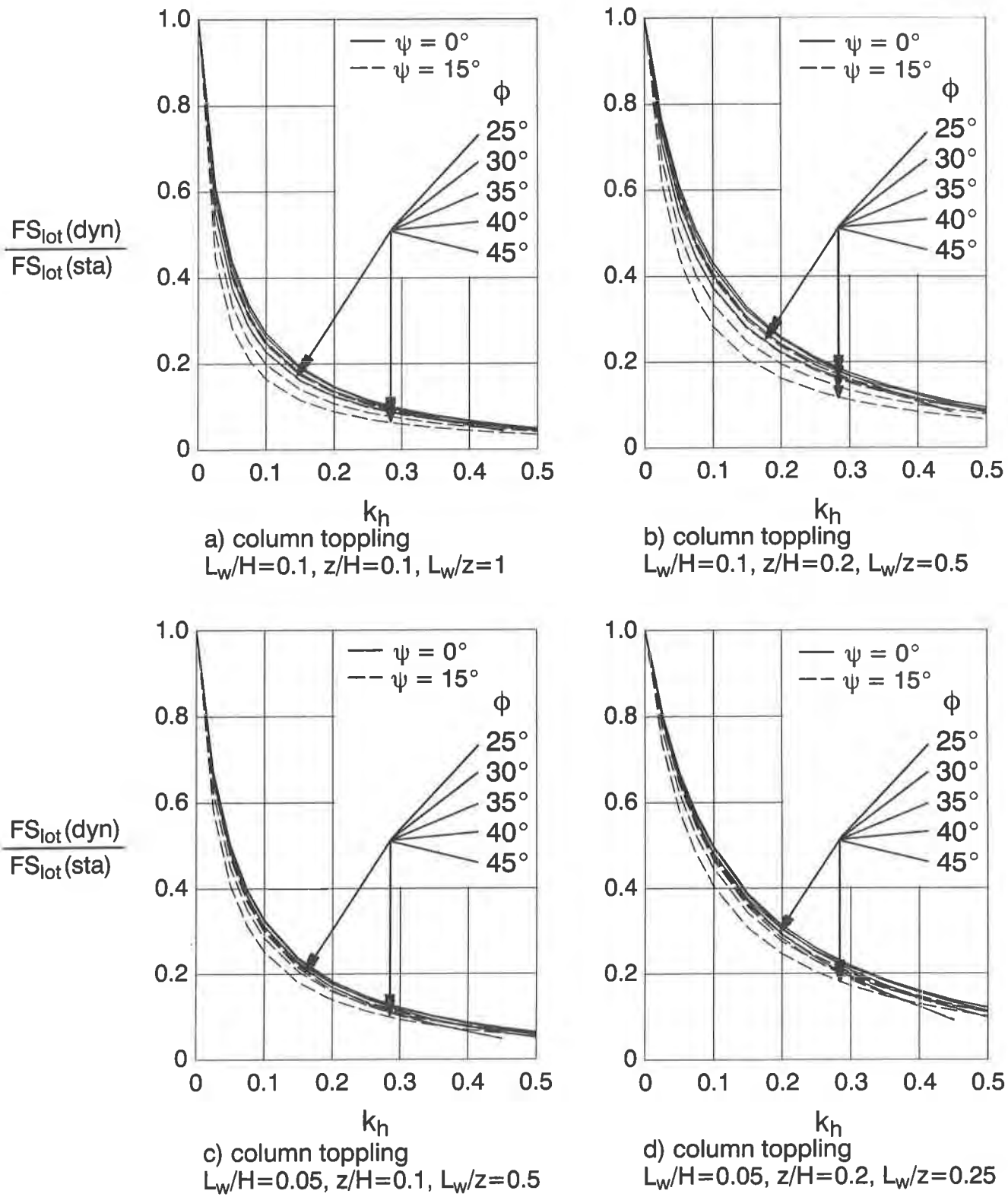
Figure 10. Ratio of dynamic to static factors of safety against toppling of the top unreinforced facing column ($\beta=0$, $\delta=2\phi/3$, $k_v=0$).
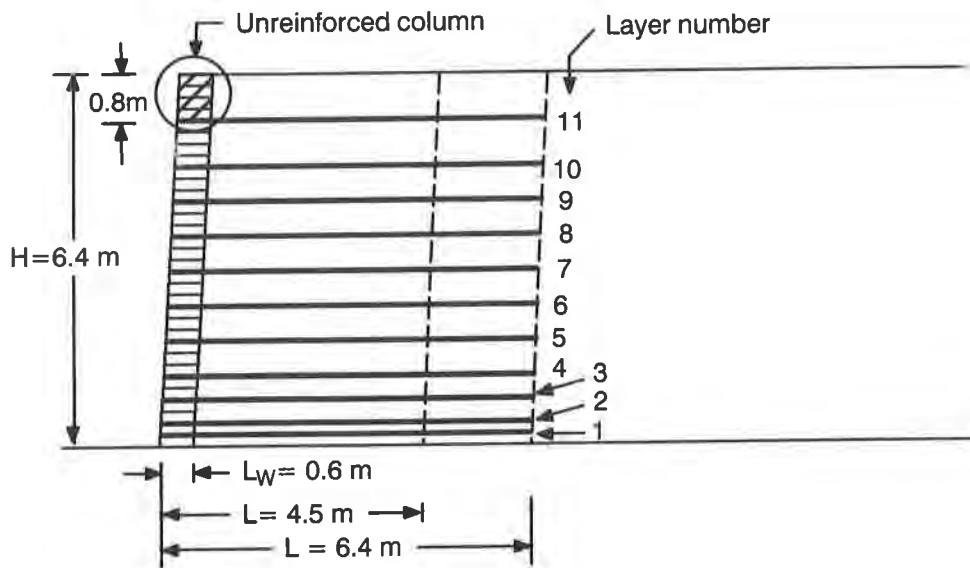
Figure 11.   Cross-section of example geosynthetic reinforced segmental wall.

factors of safety for the remaining failure mechanisms are also large due to the large width of the reinforced soil mass and the high density of reinforcement layers. The maximum permissible uniform horizontal ground acceleration coefficients to satisfy minimum prescribed factors of safety for each mode of failure under uniform horizontal seismic excitation are illustrated in the right hand columns of Table 1. The prescribed dynamic factors of safety have been recommended by Bathurst and Cai (1995) and are typically 75% of the static values following AASHTO (1992) recommendations for geosynthetic reinforced soil wall structures. The tabulated results show that seismic resistance is controlled by facing column stability (i.e. toppling and sliding of the unreinforced column at the top of the wall and connection strength). The maximum $k_h = 0.14$ value for the structure with L/H = 0.7 corresponds to a minimum reinforcement length in the top layer of 5.13 m (taken from the face of the wall) which is greater than the base width of 4.5 m. If a reinforcement length of 4.5m is used then the maximum permissible value of k_h for the example structure would be even lower. However, anchorage capacity using the pullout capacity model adopted by the NCMA will be proportional to anchorage length for $k_v=0$ and consequently the top layer needs only to be increased in length to achieve a satisfactory dynamic factor of safety against pullout of the top layer. Nevertheless, this exercise does demonstrate that a rigorous interpretation of the M-O model will typically require that the designer locally increase the reinforcement lengths at the top of the wall in order to provide sufficient anchorage length and to capture the internal failure surface that is a assumed in the "tied-back wedge" approach for internal design.

CONCLUDING REMARKS

The charts introduced here are restricted in scope but provide a guide for the designer when faced with the need to perform a preliminary evaluation of the seismic stability of a routine RSRW meeting typical minimum prescribed static factors of safety. However, the writers have noted that RSRW structures that just satisfy static factors of safety minimums will not satisfy the minimum default dynamic factors of safety recommended in Table 1 for even a modest seismic event. This conclusion is supported by the observation that the ratios of dynamic to static factors of safety (Figures 5, 9 and

10) and load amplification factor (Figure 7) vary steeply with increasing magnitude of horizontal seismic coefficient. Nevertheless, as illustrated in the example problem, inherent over-design of routine RSRW structures for static load environments may introduce acceptable margins of safety against most failure mechanisms during a modest seismic event. For example, the results of the dynamic analyses presented here suggest that a static designed wall is capable of resisting a seismic event corresponding to a peak horizontal acceleration of about 0.2g with only minor increases to the length of the top layer of reinforcement. In order to resist greater accelerations (and assuming use of the better of the two block systems), more reinforcement layers at the top of the wall, a shorter unreinforced column height and possibly even longer reinforcement lengths in the vicinity of the crest of the wall would be required. The designer should always carryout a complete dynamic stability analyses of any RSRW structure for which potential seismic loading is anticipated or prescribed. The reader is referred to the detailed description of the pseudo-static methodology proposed by the Bathurst and Cai (1995) in order to meet this requirement. Finally, it should be noted that a sliding block displacement method of design has been proposed by Cai and Bathurst (1996) that can be used to estimate seismic performance of reinforced segmental retaining walls based on displacement criteria. The results of displacement-based design methods may indicate for a given wall structure that acceptable levels of lateral movement of the structure are possible even though pseudo-static limit equilibrium methods of the the type described here result in factors of safety against collapse that are less than unity.

ACKNOWLEDGEMENTS

REFERENCES

AASHTO, 1992. Standard Specifications for Highway Bridges, 15th Edition, *American Association of State Highway and Transportation Officials*, Washington, D.C., USA, 686 p.

Bathurst, R.J. and Alfaro, M.C. 1996. Review of seismic design, analysis and performance of geosynthetic reinforced walls, slopes and embankments, *IS-Kyushu '96, 3'rd International Symposium on Earth Reinforcement*, Fukuoka, Kyushu, Japan, 12–14 November 1996, 30 p.

Bathurst, R.J. and Cai, Z. 1995. Pseudo-static seismic analysis of geosynthetic reinforced segmental retaining walls, *Geosynthetics International,* Vol . 2, No. 5, pp. 789–832.

Bathurst, R.J., Cai, Z. and Pelletier, M. 1996. Seismic Design and Performance of Geosynthetic Reinforced Segmental Retaining Walls, *Vancouver Geotechnical Symposium*, Vancouver, 6–7 June 1996, 24p.

Bathurst, R.J. and Simac, M.R. 1995. Software for Segmental Retaining Walls, *Geotechnical Fabrics Report*, September 1995, pp. 20-21.

Bathurst, R.J. and Simac, M.R. 1994. Geosynthetic Reinforced Segmental Retaining Wall Structures in North America, *5th International Conference on Geotextiles, Geomembranes and Related Products*, 6–9 September 1994, Singapore 24 p.

Bathurst, R.J., Simac, M.R. and Berg, R.R. 1993. Review of the NCMA Segmental Retaining Wall

Design Manual for Geosynthetic-Reinforced Structures, *Transportation Research Record*, 1414, pp. 16–25.

Cai, Z. and Bathurst, R.J. 1996. Seismic-induced Permanent Displacement of Geosynthetic Reinforced Segmental Retaining Walls, *Canadian Geotechnical Journal*, Vol. 31, pp. 937–955.

Christopher, B.R., Gill, S.A., Giroud, J.P., Juran, I., Schlosser F., Mitchell, J.K. and Dunnicliff, J. 1989. *Reinforced Soil Structures: Volume I. Design and Construction Guidelines*, Report No. FHWA-RD-89-043, Washington, DC., USA, Nov. 1989, 287 p.

Ebling, R.M. and Morrison, E.E. 1993. The Seismic Design of Waterfront Retaining Structures, *Naval Civil Engineering Laboratory Technical Report ITL-92-11 NCEL TR-939*, Port Huenene, CA, USA, 329 p.

Seed, H.B. and Whitman, R.V. 1970. Design of Earth Retaining Structures for Dynamic Loads, *ASCE Specialty Conference: Lateral Stresses in the Ground and Design of Earth Retaining Structures*, pp. 103-147.

Simac, M.R., Bathurst, R.J., Berg, R.R. and Lothspeich, S.E. 1993. National Concrete Masonry Association Segmental Retaining Wall Design Manual, *National Concrete Masonry Association* (NCMA), 2302 Horse Pen Road, Herndon, Virginia, USA, pp. 250, March 1993.

Table 1.   Results of stability analysis for example wall under static loading and maximum horizontal seismic coefficient to satisfy minimum factors of safety under seismic loading.

Mechanism	Factor of safety	Static			Seismic		
		Default minimum (NCMA)	Calculated minimum FS		Default minimum	Maximum k_h	
			L/H=0.7	L/H=1.0		L/H=0.7	L/H=1.0
Base sliding	FS_{bsl}	1.5	5.11	7.27	1.125	0.41	0.48
Base overturning	FS_{bot}	2.0	8.37	16.47	1.5	0.35	0.50
Reinforcement over-stressing	FS_{os}	1.2	2.32 [5]	2.32 [5]	1.0	0.27 [11]	0.27 [11]
Pullout	FS_{po}	1.5	4.95 [11]	19.04 [11]	1.125	0.14 [11] (L_{min}=5.13 m)	0.45 [11] (L_{min}=10.1 m)
Internal sliding	FS_{isl}	1.5	5.13 [1]	7.35 [1]	1.125	0.41	0.48
Unreinforced column toppling	FS_{lot}	2.0	8.45	8.45	1.5	0.21	0.21
Unreinforced column sliding	FS_{sc}	1.5	9.14 [a] 14.46 [b]	9.14 [a] 14.46 [b]	1.125	0.18 [a] 0.26 [b]	0.18 [a] 0.26 [b]
Connection	FS_{cn}	1.5	8.15 [a] 12.77 [b]	8.15 [a] 12.77 [b]	1.125	0.23 [a] 0.34 [b]	0.23 [a] 0.34 [b]

Notes: [5] reinforcement layer 5; [a] relatively poor block; [b] relatively good block

Mining

APPLICATION OF THE CELLULAR CONFINEMENT SYSTEM ON HEAP LEACHING OPERATIONS

WILLIAM A. CINCILLA ~ Denver office.,
GOLDER ASSOCIATES INC. USA
DANIEL F. SENF   df Senf @ Senf. org.
PRESTO PRODUCTS COMPANY - GEOSYSTEMS USA

ABSTRACT

For well over a decade, the Cellular Confinement System (CCS) has facilitated innovative solutions for a range of geotechnical problems, most notably those dealing with soil reinforcement for erosion control, earth retention and load support. Recently, the use of the CCS has been evaluated on a number of mining-related applications, including heap leaching. Heap leaching involves application of chemical solutions to a prepared "heap" of crushed ore and the recovery of those solutions via a liner and collection system. Metals are then extracted from these "pregnant" solutions. The industry-wide expanded use of heap leaching technology has provided a particular stimulus for the exploitation of large-tonnage, low-grade ores, particularly those of precious metals and copper.

This paper summarizes the important theoretical and practical features of the CCS and describes an innovative application which incorporates the CCS as the major component of the foundation of an "on/off" or "reusable" leach pad. The use of the CCS as an alternative to natural earth materials for liner and foundation support components are now being seriously considered on a number of international heap leaching projects where the physical, environmental and process engineering constraints favor reusable pads, especially when total project economics are considered.

BACKGROUND

Over the past decade mineral development, particularly in precious metals, has been significantly influenced by the emergence of heap leaching as a dominant extractive technology. Due primarily to its relatively low capital and operating cost, heap leaching has evolved as the preferred alternative for extraction of metals from large-tonnage, highly disseminated orebodies. In combination with parallel advances in process metallurgy, heap leaching technology (which has been pioneered primarily in the United States) has provided the stimulus for the exploitation of low-grade deposits that only a decade earlier would have been considered unattractive from an investment perspective.

Heap leaching can be broadly defined as the extraction of metals through the application of chemical solutions to "heaps" of either raw or processed (i.e. crushed and screened) ore. Solutions are typically applied using commercial-grade irrigation equipment at rates which slightly exceed the permeability of the ore. This application method maximizes particle wetting while preventing solutions from running off of the surface. As the solutions percolate through the ore, metals are dissolved into solution. The collected "pregnant" solutions are then processed to remove the metals and the remaining "barren" solution is reapplied to the ore after required modification with various chemical additives. This process is repeated until the metal concentrations in the pregnant solution are reduced to lower-than-acceptable levels. The ore is then classified as "spent" and is removed from active leaching. Figure 1 illustrates the basic components of a heap leaching operation.
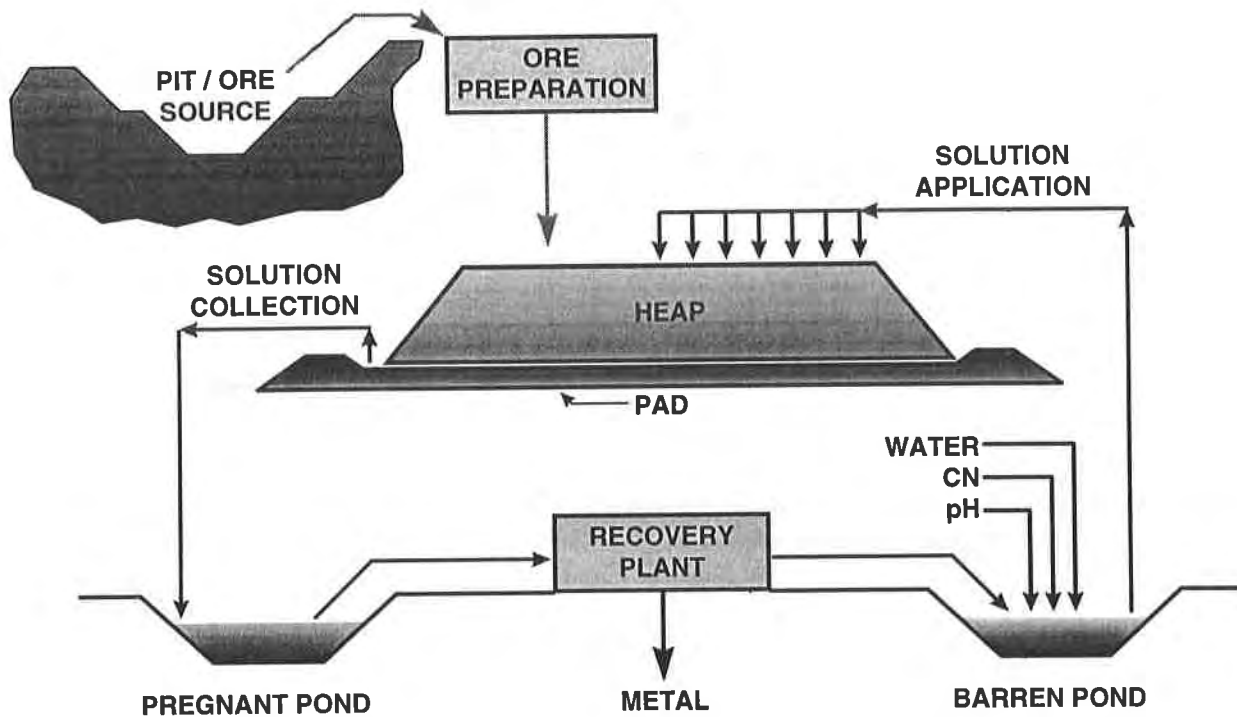
Figure 1 Schematic of the Heap Leaching Process

Liner systems, which are constructed beneath the heaps as "pads", control solution losses and allow the operation to comply with prevailing environmental protection standards. Since cyanide and strong acids are often used to affect the extraction of metals such as gold and copper, the "spent" ores must be rinsed once extraction has been completed to reduce residual concentrations of contaminants to acceptable levels. In a traditional heap leaching operation, rinsing takes place as a part of the closure and reclamation process and often involves significant investment in both time and capital (Van Zyl et al, 1988). The rapid expansion of heap leaching in the US gold industry parallels the widespread use of geomembranes, which have been the predominant choice for leach pad liner systems (Van Zyl, 1990).

Heap leaching of copper ores is carried out using an acid solution to dissolve the copper metal, which in turn is extracted using a number of processes including solvent extraction and electrowinning (SX-EW). Dump leaching, where unprocessed mine rock is leached, has been practiced in the copper industry for many years. More recently the trend has been toward "mine-for-leach" operations where more sophisticated crushing and classification techniques are used to increase metal recovery. Solution application rates and leaching cycle times are determined based on ore mineralogy and particle size distributions as well as other process-related variables.

Typically, heap leach pads are expanded both vertically (in lifts of designated height) and/or laterally to accommodate increased ore volumes. This means that the pad liner and solution delivery and recovery systems must also be expanded accordingly. The engineering implications of these expansions are sometimes complicated and expensive. As a result alternative leaching systems which make use of smaller "permanent" or "reusable" pads have been attempted but to date with only marginal records of success (Smith, 1993). Under these systems, ore is sequentially loaded, leached, rinsed and removed (reclaimed) from sections (panels) within the pad area in a nearly continuous fashion. Spent ore is then transported for disposal in separate dump areas. The failure of some of these reusable pads have largely been the result of issues related to materials handling (Dye, 1995). Limitations posed by the use of asphalt and concrete as the major options for permanent liner components also contributed to their problematic nature. The design of reusable pad systems include an "overliner" or drainage blanket above the primary liner to enhance solution recovery and to allow a working surface for equipment used for ore loading and removal. A number of systems have been implemented in an attempt to balance the design requirements for ore handling and solution recovery with mixed results.

In recent years environmental regulation and the continued requirement to increase operational efficiencies of the heap leaching process, via better solution management, have led to a re-evaluation of liner system design objectives. In particular to the potential for reusable pad alternatives. The result has lead to the predominant use of geosynthetic materials as the major components of heap leach pad liners and to the increasing evaluation of geosynthetic materials in mining applications in general (Van Zyl, 1990). These geosynthetic materials include geomembranes, geonets, geogrids, geotextiles and, most recently, geocells or what are often referred to as the cellular confinement system (CCS). The unique functional and behavioral properties of the CCS provides the basis for a new application as one of the primary components of the load support and solution recovery systems for reusable leach pads. This paper focuses on the use of the CCS as an alternative to materials such as asphalt and concrete for the construction of reusable heap leach pad liner systems. Use of the CCS has the potential to significantly contribute to the revival of reusable leach pad systems, which offer some distinct advantages over more traditional design approaches, especially when true costs of heap closure and reclamation are considered. In addition, cost and management of long-term environmental liabilities created by inactive heaps are becoming an important issue when evaluating the economics of a given mineral property. The CCS could provide the required level of operational performance and durability as well as the mechanism to reduce or eliminate some of the major environmental problems posed by heap leaching.

HISTORICAL OVERVIEW OF CCS DEVELOPMENT

The stimulus for the development of the CCS began in September 1975 when the US Army Corps of Engineers (Corps of Engineers) began researching the feasibility of constructing military bridge approach roads on soft soils such as beach heads (Webster and Watkins, 1977; Martin and Senf, 1995). The unique problems which the engineers faced in dealing with load support over soft soils resulted in the development of the first commercial lightweight CCS through a joint development effort between the Corps of Engineers and Presto Products Company of Appleton, Wisconsin. The first load-support application for the new product occurred in 1981, followed by applications related to erosion control and, most recently, earth retention, which was pioneered in Canada in 1986 (Bathurst, et al, 1993). These successes led to significant studies to further define the mechanics of cellular confinement and to establish practical guidelines for the technological application for a range of soil stabilization functions. (Martin and Senf, 1995)

The basic theory behind the function of the CCS is that cohesionless materials gain considerable shear strength and stiffness under sufficient confining stress conditions. These confining stresses are effectively produced in a CCS by means of the hoop strength developed by the high density polyethylene (HDPE) cell walls. The overall increase in the load carrying performance of the system is provided through a combination of the cell wall stresses, the passive resistance of the adjacent cells and through the frictional interaction between the infill soil and the cell walls (Martin and Senf, 1995). The lateral confinement provided by a network of cells produces a bridging action that improves the load/deformation characteristics of common granular fills and allows for significant reductions in the required thickness of structural support elements. In addition, the CCS prevents lateral spreading of the infill material under loading resulting in "no loss" of overall thickness of the load support system. Figure 2 illustrates the load support mechanisms developed by the CCS.
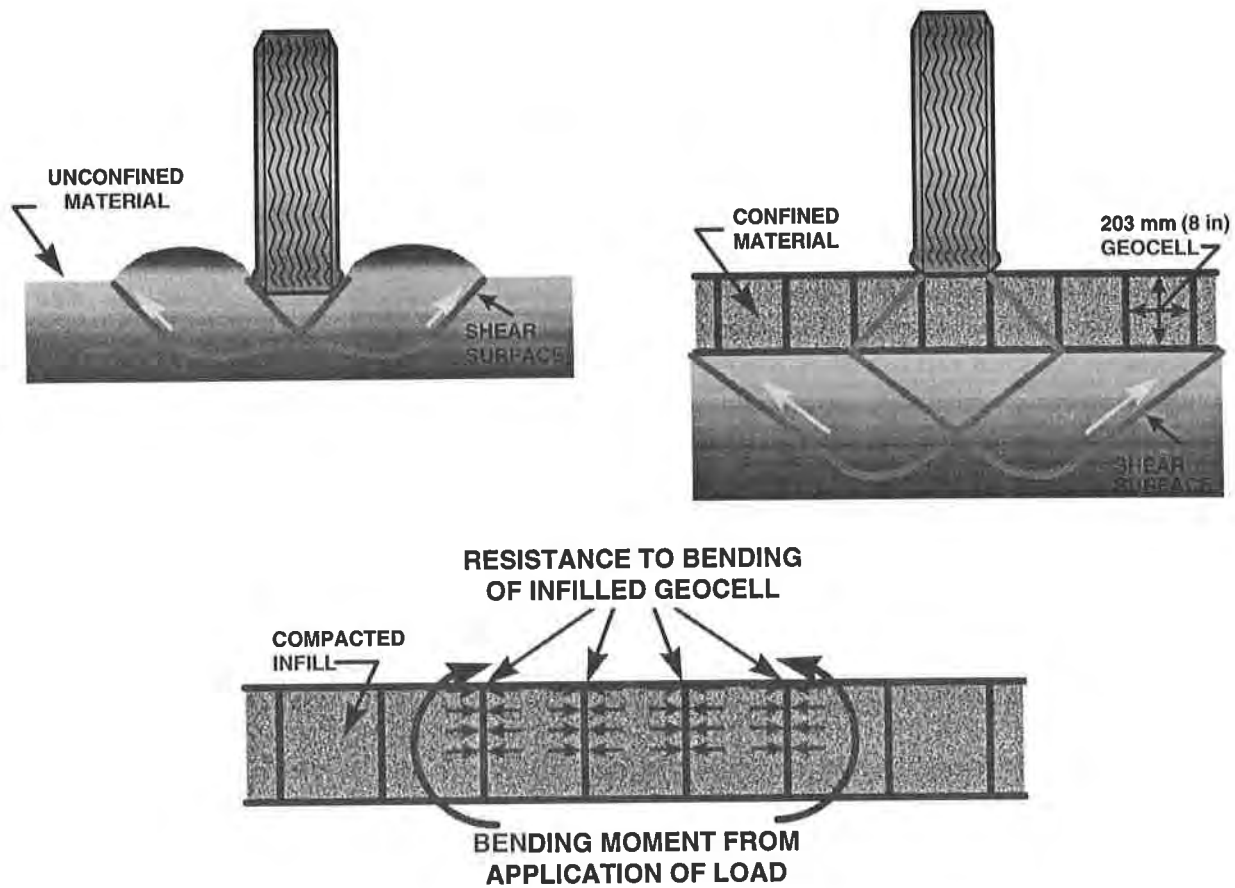
Figure 2 Load Support Mechanism as Developed by the CCS
(reprinted with permission of Presto Products Company)

Research has also shown that further improvements in performance of CCS systems can be achieved if the cell walls have a specific texture or perforations (Walls, 1992; Martin and Senf, 1995). CCS can be applied using less expensive locally-available granular fill materials and also provide the added benefit of drainage, thus allowing for the efficient control and removal of surface waters. These demonstrated functions of CCS were the most influential factors in evaluating their potential application in heap liner system design. Figure 3 illustrates the typical geometry of a CCS section.

The load bearing capacity of geocell-reinforced granular soils has been well documented (Bathurst and Jarrett, 1989; Bathurst and Karpurapu, 1993). These studies have led to the ability to predict the strength of the geocell/fill composite within a reasonable level of accuracy. In general, expected levels of performance of the CCS versus unconfined cohesionless fills are quite dramatic, with increases in performance on the order of 50% or more. In practical terms, cohesionless, granular fills reinforced with the CCS provide similar or superior levels of load distribution performance when compared with the performance provided by twice or more the thickness of the same unreinforced materials. Savings in granular fill costs, combined with chemical resistance and durability under rubber-tired vehicle traffic, make the CCS a viable component option for reusable heap leach pad foundation.
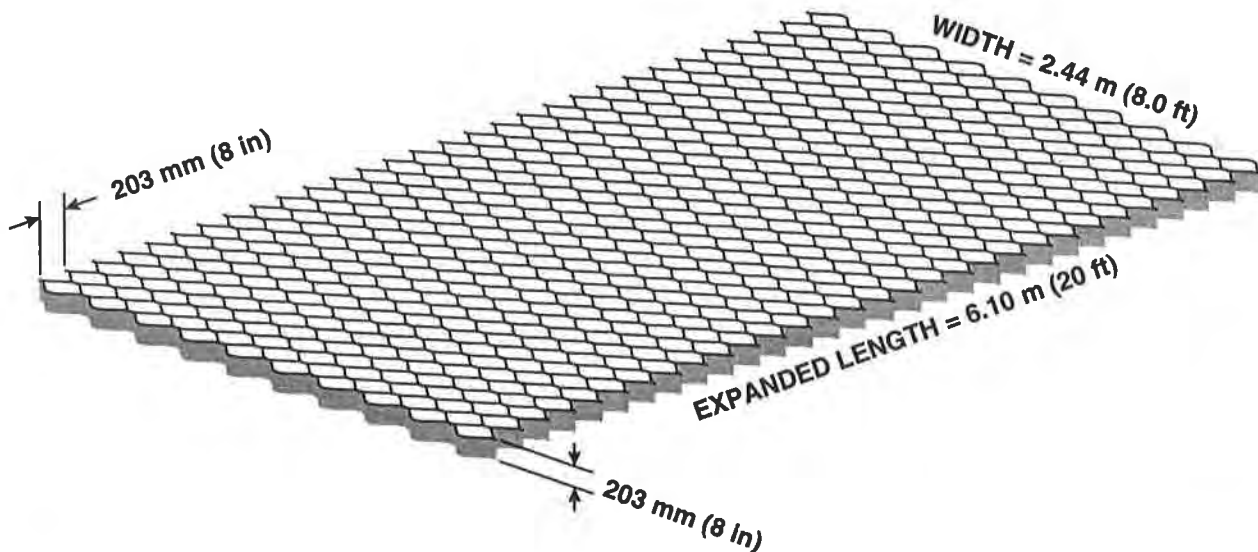
Figure 3 Typical CCS Section Geometry
(reprinted with permission of Presto Products Company)

HEAP LEACH PAD LINER SYSTEM DESIGN AND CONSTRUCTION

Heap leach pad liner designs have evolved significantly from the unlined "geological barrier" concepts which are still in limited use in some copper mines in the Southwestern United States and other areas of the world. Van Zyl (1990) provides an overview of current heap leach pad liner design philosophy in the US. For reusable leach pads, both asphalt and concrete have been used as the primary

liner system, since the principal selection criteria focus on the durability of the surface under heavy equipment traffic. For this reason, geomembranes have only recently been considered as a viable option, and only when applied in conjunction with relatively thick cushion or "overliner" layers of free-draining aggregate or select ore. However, the placement of these overliner materials presents a challenge in terms of maintaining the integrity of the geomembrane. In addition, operational controls necessary to insure that the (primary) geomembrane is not damaged during ore loading and unloading also present considerable challenges. The disadvantages of this type reusable system is soon apparent.

Operational problems have led to notable failures of reusable pads. For the most part these have been specifically related to handling problems during the unloading of highly-saturated spent ore. While some of these problems can be directly related to misapplication of the method based on unfavorable ore drainage properties, most of these reusable pads made use of the base layer of ore as the solution collection system resulting in less than optimum solution removal. The removal of partially drained ore also required that spent ore be placed in lined facilities, reducing some of the long-term environmental benefits of the concept. Since asphalt and concrete have well defined limitations in terms of chemical durability, the application of reusable pad concepts was impractical in copper leaching where strong acid (pH 0.8 to 2.0) leach solutions (raffinate) are commonplace.

The first documented use of geomembrane in a reusable heap leach pad was in Chile in 1993 at the Cerro Colorado Mine (Smith and Welkner, 1995). The design included a thick overliner layer (1.5 to 2.0 meters) which protected the geomembrane from inadvertent damage caused by ore loading and unloading. Based on the durability of the ore under acid attack, a limited amount of overliner replacement has been experienced thus far. However, with time, as fines are generated, the overliner will become more highly saturated gradually reducing trafficability and permeability. Reduction in overall effectiveness of the solution recovery system is the final outcome. The Cerro Colorado operation also includes special design components such as separate solution sedimentation ponds to handle fines generated during leaching and ore handling. The efficiency of copper extraction using SX-EW technology is relatively sensitive to pregnant solution quality; therefore, a great deal of attention has been paid to limiting the gross effect of fines.

When evaluating the potential for more universal application of reusable pad technology in copper leaching, the experience at Cerro, Colorado, as well as the collective experiences of gold heap leaching in North America were examined. The evaluation results indicated that several key criteria are critical to the selection process. These criteria included:

- General site constraints and topography;
- Ore volume and quality
- Availability, suitability and cost of on-site soils as liner/solution management system, components;
- Anticipated ore delivery rates;
- Mine life;
- Type of equipment to be used for ore transport, loading and unloading; and
- Constraints based on regulatory compliance, particularly for spent ore disposal.

The criteria given above sould be ranked based on site-specific conditions in order to qualitatively assess the viability of reusable and/or traditional expanding leach pad options. Figure 4 outlines some of the general options available for heap leaching, including a so-called "modified"

reusable pad where the footprint area is "reused" (thus optimizing the use of existing real estate) while the heap itself is expanded vertically in regular lifts. This modified reusable option has demonstrated advantages which are more significant relative to permanent reusable options if the spent ore below each active lift can function as a solution barrier when properly conditioned and compacted, or on those sites where limited space is available to dispose of spent ore. The geomembrane cost for expansion is nearly the same as expanding under a more traditional mode (i.e., vertical expansion with no interlift solution collection) and may incorporate an increased level of risk from a geotechnical perspective due to uncertainty in the prediction of differential settlement in the underlying parts of the spent ore heap beneath the active zone.
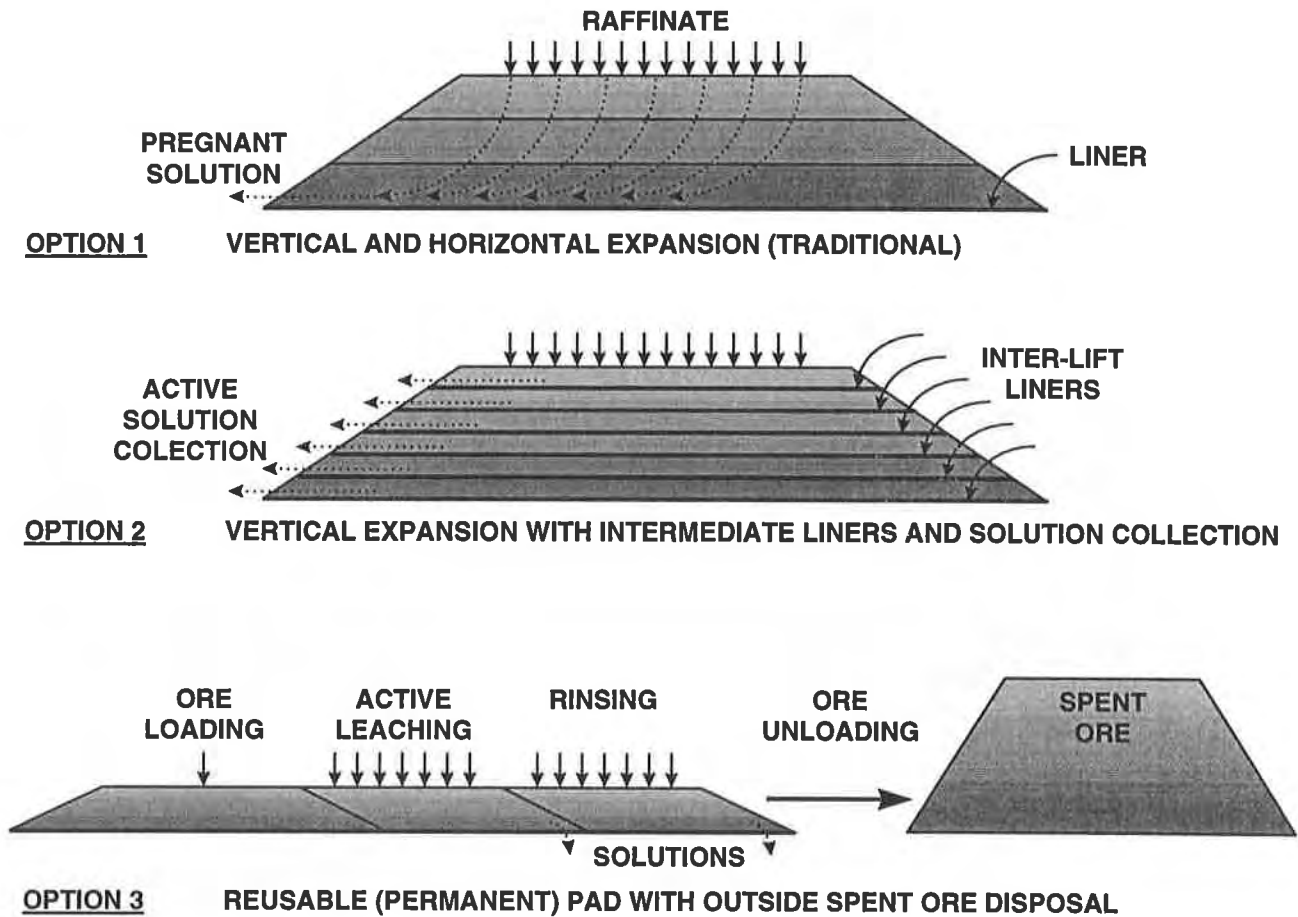
Figure 4 Overview of Leach Pad Options

The primary function provided by liner systems in traditional heap leach pads is to control solution, which is the lifeblood of the operation. The heap itself is, in a sense, a "plant" and any solution which is lost carries with it the extracted metals. In order to enhance solution recovery at the base of the heap and to prevent the excessive buildup of head on the liner, a system of perforated drainage pipes are usually included in the design above the primary liner system. By maintaining an efficient hydraulic break above the liner, the risk of developing instabilities related to the emergence of phreatic surfaces on

the exterior slopes of the heap are also minimized. The design of the solution recovery pipework systems is controlled by the hydraulic properties of the drainage media and the geometry of the pad base.

Solution application rates and leaching cycle times as well as the chemistry of the leaching solutions are determined based on metallurgical testing. Ore permeability plays an important role in this evaluation, as does the load permeability relationship since as the heap is loaded, permeability decreases. These variables can then be optimized to produce a theoretically balanced design which forms the basis for further evaluation of the leaching techniques to be used. In most cases, the testing which is carried out in support of heap leaching is done at a laboratory or on a bench scale. In some cases where the size and sensitivity of the operation demands additional work, near-production-scale field trials are often undertaken.

Figure 5 illustrates a typical design for a leach pad liner/solution recovery system. Numerous variations are possible. In the case of a reusable pad where the use of geomembranes is a potential option, the design process focuses on the durability and placement strategy for the drainage aggregate or select ore which will function as the overliner. Since this overliner must also provide the load support required for ore transport, loading and unloading equipment, the overliner selection process requires significant attention. It is during this selection process that the unique attributes and functional advantages of the CCS as a substitute for the traditional granular overliner becomes more apparent.
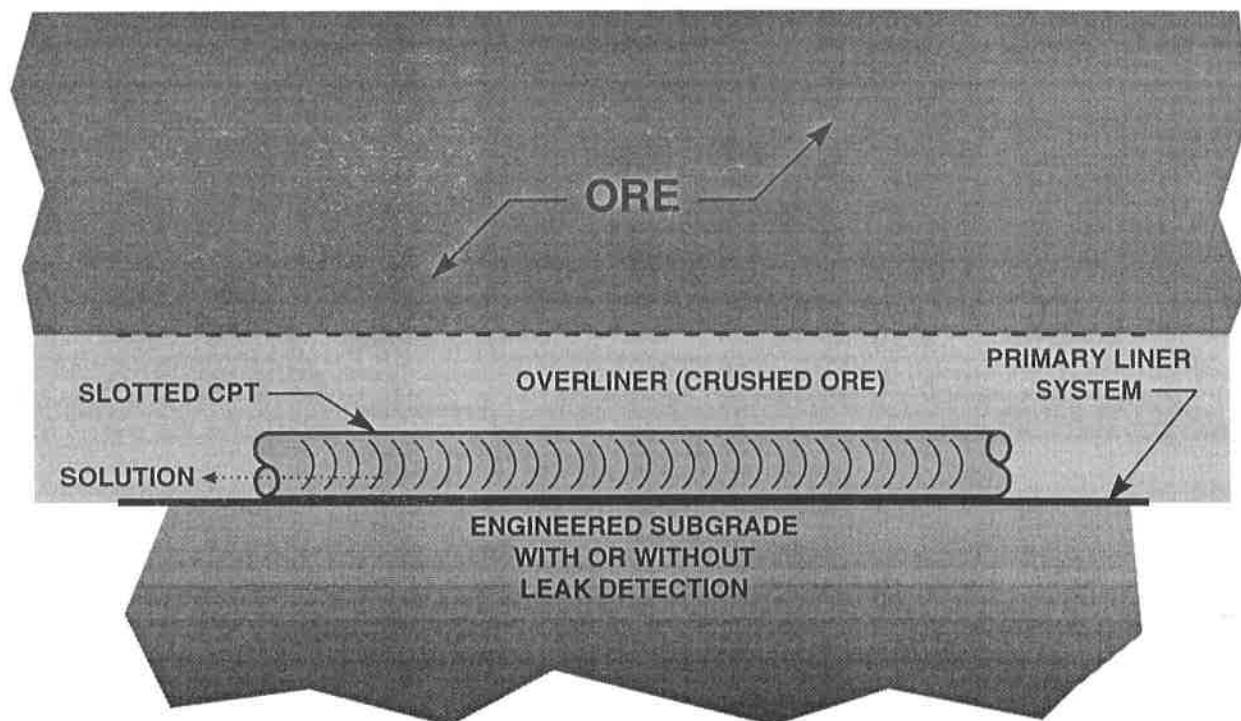
Figure 5 Typical Leach Pad Liner and Solution Recovery System Components

THE ROLE OF CCS IN ALTERNATIVE LINER SYSTEM DESIGN

The use of the CCS as a viable alternative for heap leach pad liner design was first investigated in 1995 during the conceptual design phase of a copper heap leaching operation in northern Chile. This section details the processes which led up to the recommendation of the CCS and the site-specific variables which influenced decision making. Although the example provided cannot be universally applied to other sites, it is recognized that the value gained through the evaluation of the CCS will lead to additional interest in reusable pad technology in general and to further the use of the CCS in providing alternative solutions for other mining-related problems.

The Case For The CCS. Site constraints dictated that the option of a reusable pad be assessed. Based on the production rate 10,000 metric tons per day (mtpd) of copper ore to be delivered to the pad, and the historical data from operations, a minimum cycle time and pad layout geometry for a reusable alternative were determined. Limitations on heap height to 4 meters, due mostly to loading equipment constraints and ore permeability and very limited access to other suitable sites, resulted in the development of a rectangular pad geometry with dimensions of 250 m by 400 m.

With these "hard" constraints established, a leaching system was developed which considered several alternatives for equipment for ore transport, loading and unloading. In addition, variables such as heap drain down time, the logistics of solution application system relocation and related operational issues were carefully weighed. This selection process resulted in the optimization of two major alternatives which included truck/stacker/front-end-loader and conveyor/stacker/front-end loader/truck equipment configurations. Since the liner system selection process was limited to geomembranes because of the extremely low pH of the raffinate solution (in the range of pH 0.9), the challenge was to develop an overliner concept that would be able to handle repeated traffic, yet allow for efficient removal of process solutions during active leaching. The CCS was chosen for further evaluation.

Liner Design Alternatives. Two primary alternatives were developed for the liner system. The first alternative consisted of a 1.5 mm-thick HDPE geomembrane constructed over a prepared engineered subgrade. Perforated corrugated polyethylene tubing (CPT) with a diameter of 203 mm were then installed above the primary liner and enclosed in a 1.0 m-thick overliner of selected, acid-resistant granular fill. This section would provide adequate protection for the geomembrane as well as efficient solution recovery. The potential cost and availability of the granular overliner stimulated the need to investigate alternatives which could reduce the volume of overliner. This need was evaluated while considering the need to protect the geomembrane.

Use of the CCS was then examined as a possible method for reducing the overliner thickness to an equivalent cost basis with that of the first alternative. The added benefit was that the working surface created by the CCS would provide a manageable boundary for removal of spent ore without the loss of expensive overliner material via over-excavation. Under the first alternative, as ore is removed, particular attention would need to be paid to the depth to which excavation was taking place, both from the perspective of liner damage and sacrificial loss of overliner beneath the spent ore. In this way the CCS was able to provide proven solutions to a number of problem areas at equivalent cost to the more traditional liner configuration.

The second (CCS) alternative consisted of the HDPE liner, above which was a 250 mm layer of the select granular fill with embedded CPT. A 203 mm cell depth CCS would then be installed above the base solution collection layer and would be filled with the identical select granular fill material. Ore would be loaded on this surface using radial stackers. Once the leaching cycle was completed, smooth-blade front-end loaders would be used to unload spent ore, which would be transported to outside dump areas for final disposal.

Even though there were no precedents set in the mining industry for such an application, there were similar industrial applications which were well documented and analogous to the heap leaching process, at least in concept. These examples were testaments to the functionality of the CCS in meeting the project demands. The most analogous related industrial applications included sanitary sewage sludge handling and dewatering. There, the CCS was use to contain and stabilize filtersand in a number of small-scale municipal waste water operations providing for efficient removal of dewatered sludge layers using front-end loaders without damage to the sand-filter layer. On reviewing these practical examples, the application to reusable heap leach pads was intuitive. Figure 6 illustrates the alternative reusable heap leach pad liner system which employs the CCS.
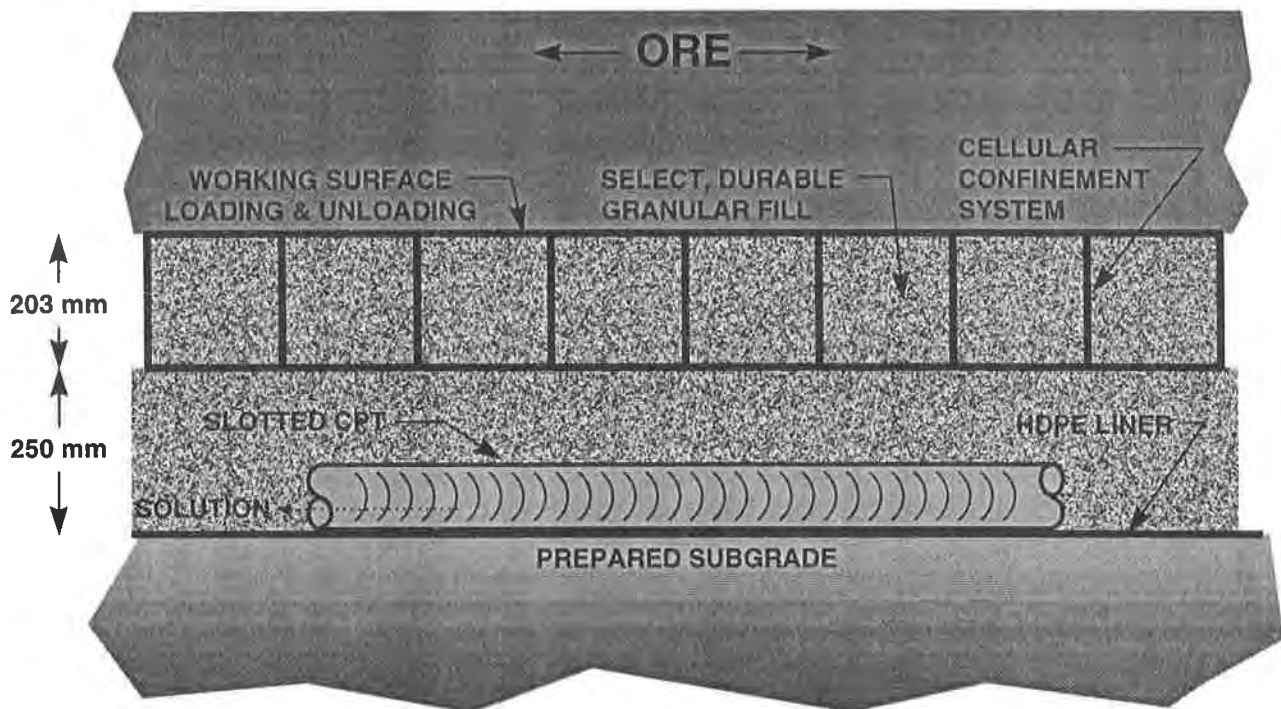
Figure 6 Typical Alternative Liner Section

Cost Analysis. The most significant factor in the selection of the CCS alternative as the preferred option for liner system design was that superior operational performance could be demonstrated at equivalent cost to the more traditional alternative. Table 1 illustrates the costs developed for the two liner system alternatives which take into account the longer term impact of replacement aggregate costs.

Using the CCS option, replacement was considered to be likely after a total of five years of continuous operation. A 10% aggregate loss factor was included in the monthly operating costs when the one-meter-thick overliner was used in lieu of the CCS. Using a net present value (NPV) approach, the option employing the CCS was shown to provide a marginal benefit. However, the operational advantages, combined with the reduced potential for generation of fines and associated degradation of process solutions weighed significantly in the tentative selection of the option employing the CCS.

Table 1 Concept-Level Cost Comparison - Reusable vs. Vertical Pad

	Item	Year One	Average Annual	7-Year Project	NPV @ 10%
Reusable Pad	Construction	$1,353,000		$1,353,000	
	Equipment	$1,290,000		$1,290,000	
	Operating	$2,445,500	$2,445,500	$17,118,500	
	Maint./Repl.	$264,300	$264,300	$1,850,100	
	Totals	$5,352,800	$2,709,800	$21,611,600	$15,595,142
Vertical Pad	Construction	$1,197,000	$1,197,000	$8,379,000	
	Equipment				
	Operating	$2,263,000	$2,263,000	$15,841,000	
	Maint./Repl.	$119,700	$119,700	$837,900	
	Totals	$3,579,700	$3,579,700	$25,057,900	$17,427,411

The costs which were developed for relative comparison of alternative concepts were conservative. Also, options other than reusable pads had been eliminated earlier during conceptual screening; therefore, application of the results on a more generic basis must be carefully considered. The application described in the previous discussions is still under final review at the time of preparation of this manuscript. A number of other potential projects have developed in the interim. One of the major objectives of this paper is to stimulate continued interest by the mining industry in reusable pad designs, particularly those for which the CCS application make sense.

DISCUSSION

The example of alternative design using the CCS was very site specific and issues related to the wider application of the technology in heap leaching in general did not greatly influence the decision-making process. Even though the CCS was shown to provide a viable, lower-cost alternative, the most significant technical, legal and cost advantages of using the CCS in this particular setting have yet to be evaluated. From a conceptual level, there are numerous reasons why reusable pads employing the CCS technology should be evaluated for all planned heap leach mineral processing operations. Significant reductions in environmental liabilities posed by groundwater pollution can be expected by concentrating the solution application in an engineered, dedicated processing area. In addition, the long-term economic and legal implications posed by closure and reclamation of large heap leaching operations have largely been ignored or greatly underestimated during the planning process. Since many of the deposits which first went into operation in the United States in the 1980s are nearing depletion, closure and reclamation issues are only very recently beginning to come to the forefront of discussion. With these pressures and the requirement to guarantee the long-term stability of inactive or closed heaps, there is great potential for the use of reusable pad methodology in future heap leaching development. The CCS can be shown to provide some technical and cost advantages that will enhance the design, construction and operation of these facilities.

ACKNOWLEDGMENTS

REFERENCES

Bathurst, R. J., and P. M. Jarrett, 1989 "Large-Scale Model Tests of Geocomposite Mattresses over Peat Subgrades," Transportation Research Record 1188, Transportation Research Board, Washington, D. C., pp. 28-36.

Bathurst, R. J., and R. Karpurapu, 1993, "Large-Scale Triaxial Compression Testing of Geocell-Reinforced Granular Soils," Geotechnical Testing Journal, GTLODJ, Vol. 16, No. 3, September, pp. 296-303.

Bathurst, R. J., R. E. Crowe, and A. C. Zehulak, 1993, "Geosynthetic Cellular Confinement Cells for Gravity Retaining Wall, Richmond Hill, Ontario, Geosynthetic Case Histories, International Society for Soil Mechanics and Foundation Engineering, March, pp. 266-267.

Dye, R. E., 1995, Personal Communication

Martin, S. and D. F. Senf, 1995, "Cellular Confinement: an important technology for soil stabilization applications," Geotechnical Fabrics Report, January/February.

Smith, M. E., and P. Welkner M., 1995 "Liner Systems in Chilean Copper and Gold Heap Leaching," Mining Engineering, January, pp. 53-57.

Smith, M. E., 1993, "The Gilt Edge Leach Pad: A Case History," in Proceedings, Geosynthetics '93, Vancouver, B. C., pp. 1203-1214.

Van Zyl, D. J. A., 1990, "Reliability-Based design of Heap Leach Pads and Ponds," in Proceedings, 4th Western Regional Conference on Precious Metals and the Environment, Lead SD, pp. 243-263.

Van Zyl, Hutchison and Kiel, Eds., Society of Mining Engineers, Inc., Littleton, CO. Introduction to Evaluation, Design and Operation of Precious Metal Heap Leaching Projects, 1988

Webster, S. L., 1979, "Investigation of Beach Sand Trafficability Enhancement Using Sand-Grid Confinement and Membrane Reinforcement Concepts," Report GL-79-20(1), Geotechnical Laboratory, U. S. Army Corps of Engineers Waterways Experiment Station, Vicksburg, MS, February

Webster, S. L., and J. E. Watkins, 1977, "Investigation of Construction Techniques for Tactical Bridge Approach Roads Across Soft Ground," Soils and Pavements Laboratory, U. S. Army Corps of Engineers Waterways Experiment Station, Vicksburg, MS, Technical Report S-77-1, September.

GEOTEXTILES IN WATER-BALANCE FINAL COVERS SYSTEMS
FOR ARID AND SEMI-ARID REGIONS

Gregory N. Richardson, Ph.D., P.E.
G.N. Richardson & Associates
Raleigh, North Carolina

Fess Foster, Ph.D.
Golden Sunlight Mine
Whitehall, Montana

ABSTRACT

During the past decade, considerable research has demonstrated the applicability of reclamation, i.e., final, covers that limit infiltration through manipulation of water storage capacities of the soil layers and natural evapotranspiration (ET) effects, i.e.,water-balance principles, as opposed to incorporating barriers such as compacted clay liners. Water balance covers rely on a two layered system to limit penetration of surface waters. The upper layer is a well graded loamy soil that will support vegetation and has sufficient water storage to typically hold a full season's precipitation. The premise is very simple: if we can hold all of the infiltration in the upper loam layer at times when the ET is minimal, the water will be removed by ET when the vegetative growth is maximum. Most arid and semi-arid vegetation are limited by the amount of stored water typically available in the ground; i.e., they run out of moisture in late summer or fall and become stressed. This paper presents background information and research being conducted to demonstrate the beneficial roles of geotextiles in such covers.

INTRODUCTION

During the past decade, considerable research has been performed to demonstrate the applicability of final covers that limit infiltration through manipulation of water-balance principles (Anderson et al., 1993; Melchior et al., 1994; Wing et al., 1993) as opposed to incorporating barriers such as compacted clay liners. The basic water balance equation is

$$\Delta S = P - Q - ET - L \tag{1}$$

where ΔS is the change in water storage in the upper soil layer, P is precipitation, Q is the runoff, ET is evapotranspiration, and L is seepage or percolation through the final cover. The design objective is to minimize L. As shown on Figure 1, water balance covers rely on a two layered system to limit penetration of surface waters. The upper layer is a well graded loamy soil that will support vegetation and has sufficient water storage to typically hold more than a full season's precipitation. The premise is very simple: if we can hold all of the infiltration in the upper loam layer at times when the ET is minimal, the water will be removed by ET when the vegetative growth is maximum. Most arid and semi-arid vegetation are limited by the amount of stored water typically available in the ground; i.e., they run out of moisture in late summer or fall and become stressed.

To keep the moisture in the loam layer in a water-balance cover, we use a simple phenomena first
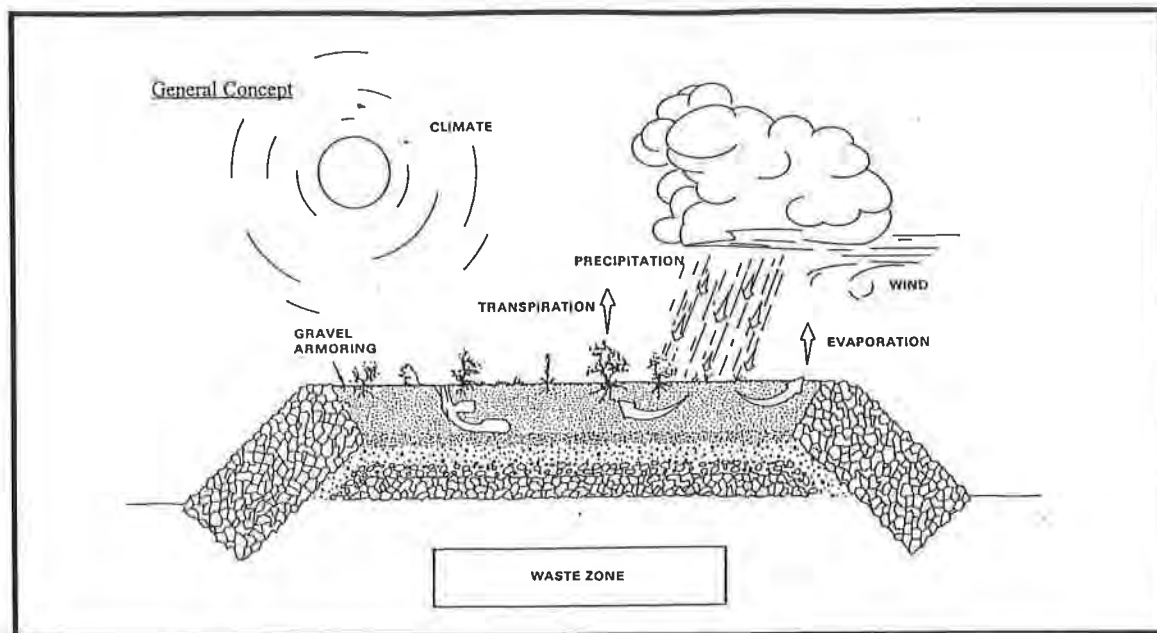
Figure 1. Two-Layer Water Balance Final Cover System

explored by L.A. Richards in the 30s. Richards observed that loamy soil layers in nature that were underlain by a coarse grained soil layer were always wetter that those that were underlain by a fine grained layer. His explanation, what is now referred to as Richard's Effect, essentially is that water is held in the loam by capillary tension. The coarse lower layer forms a capillary break that prevents moisture from being drawn downward by capillary forces and aids in retention of moisture in the upper loam. An excellent summary of such water-balance covers is presented by Benson et al. (1995).

The effectiveness of a capillary break depends essentially upon the difference in capillary suction between the loam and the granular layers at the capillary break. This effectiveness can be significantly diminished by the presence of fines in the coarse lower layer. It is particularly important that fines do not migrate vertically downward out of the loam. This will lead to a gradual blurring of the capillary break and reduced effectiveness of the capillary break. To prevent fines migration, a designer must incorporate either a graded natural filter zone or a geosynthetic alternative. Graded natural filter zones are constructed using relationships first established by Terzaghi (1922) as follows:

$$R_{15} = \frac{D_{15} \ of \ filter \ material}{D_{15} \ of \ material \ protected}$$

$$R_{50} = \frac{D_{50} \ of \ filter \ material}{D_{50} \ of \ material \ protected}$$

(2)

In general, current guidance for R_{15} and R_{50} (U.S.B.R., 1974) provide that R_{15} varies from 12 to 40 for subrounded particles and 6 to 18 for angular particles, and R_{50} varies from 12 to 58 for subrounded particles and 9 to 30 for angular particles. Separation of typical gravels and loams associated with a capillary break may require more than two layers of graded natural soil layers to satisfy the natural filter zone criteria, see Figure 2. Each filter layer must be a minimum of 15 cm (6-inch) thick for construction reasons. The development of a graded natural filter dulls the distinction between the two layers forming the water-balance final cover and adds to both the thickness and cost of the final cover.
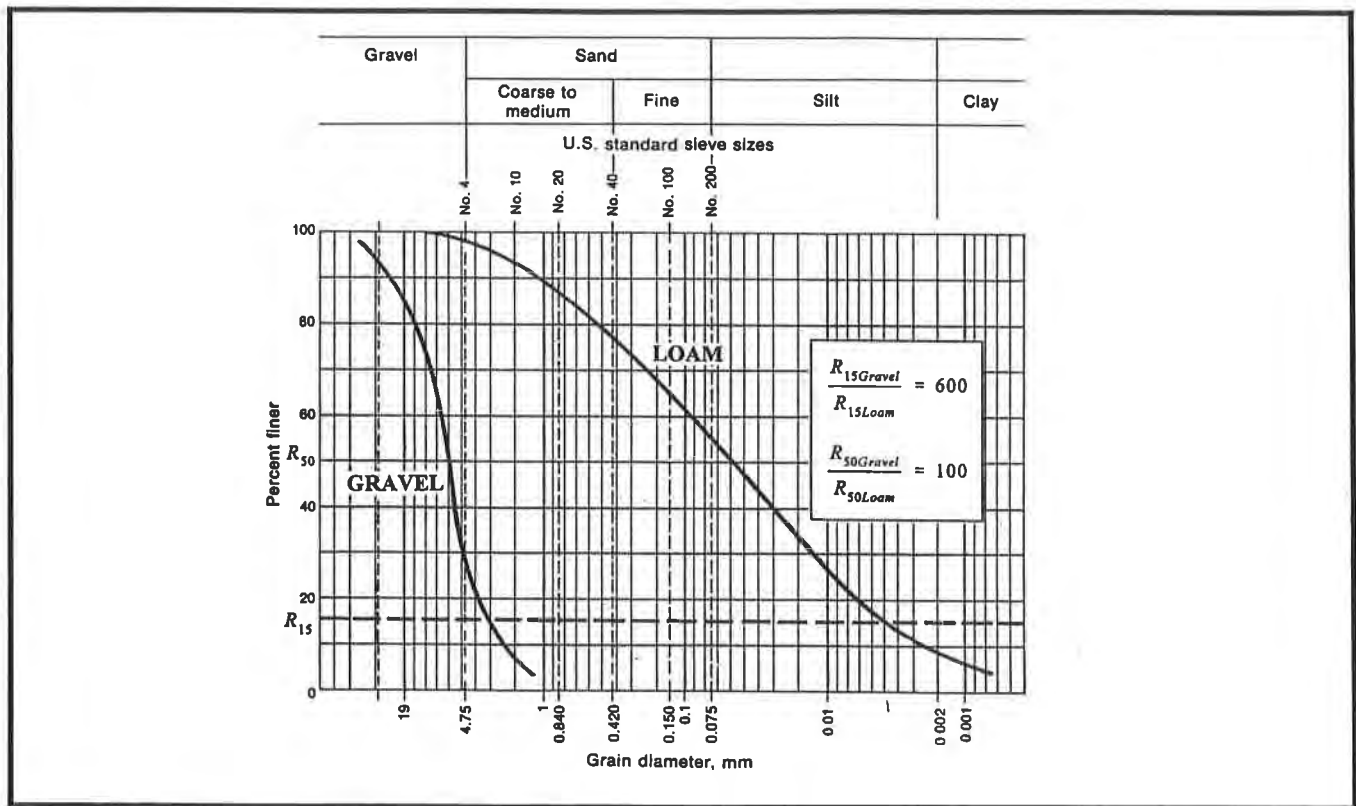
Figure 2. Grade Soil Filter Criteria

Geotextile filter criteria for soil retention is generally expressed as follows:

$$O_{95} < R_{95}\, d_{85} \tag{3}$$

where O_{95} is the maximum AOS of the geotextile, R_{95} ranges from 1 to 3, and d_{85} is the grainsize with 85% finer than for the loam. Interestingly, the geotextile does not have to be designed to resist clogging since the design goal is to prevent movement of water across the capillary break. Fines from the loam can migrate down to the geotextile and form a soil cake that has a permeability less than that of the loam (and therefore a greater soil suction) while water passing through the geotextile will wash the fines from the coarser stone beneath. Thus, the effectiveness of the capillary break using a geotextile may actually improve with time.

For the Loam soil shown on Figure 2, the maximum AOS of the geotextile is approximately 1.4 mm or a #14 sieve. Most woven or nonwoven geotextile satisfy this criteria.

Based on the above considerations, it is felt that a geotextile filter placed at the capillary break would reduce the cost and thickness of a water-balance final cover and provide a system that would actually improve in performance with time. This paper presents research being conducted to demonstrate the beneficial roles of geotextiles in such covers.

Water-Balance Evaluation of Final Cover Performance

The accepted approach for evaluating the performance of a water-balance final cover is the use of an analytical model and either actual or synthetic site weather data. This procedure is similar to that used in the EPA HELP (Schroeder et al., 1994) model commonly used to evaluate barrier style final covers. The HELP model cannot be used for evaluation of thick water-balance covers because it provides for capillarity related removal of soil water from only the upper evaporative zone (Fleenor, 1995). This causes HELP to over predict the amount of infiltration through thick final covers in arid and semi-arid regions. Alternative water balance models used in previous investigations by others include UNSAT-H (Fayer, 1990), TRACER3D (Morris et al., 1996), and RMA42 (Fleenor et al., 1995). These models attempted to provide improved algorithms for capillary forces within thick covers in arid regions. It is generally assumed that the HELP model will over predict infiltration through all final covers in arid and semi-arid regions.

Because of its conservative nature, the HELP model was used to estimate infiltration through potential mining reclamation final covers for waste rock. The cover profiles include 1) a vegetative layer directly over waste rock, 2) a capillary break cover constructed using a geotextile and a gravel layer, and 3) a capillary break cover constructed using a graded soil filter break as shown on Figure 3. The
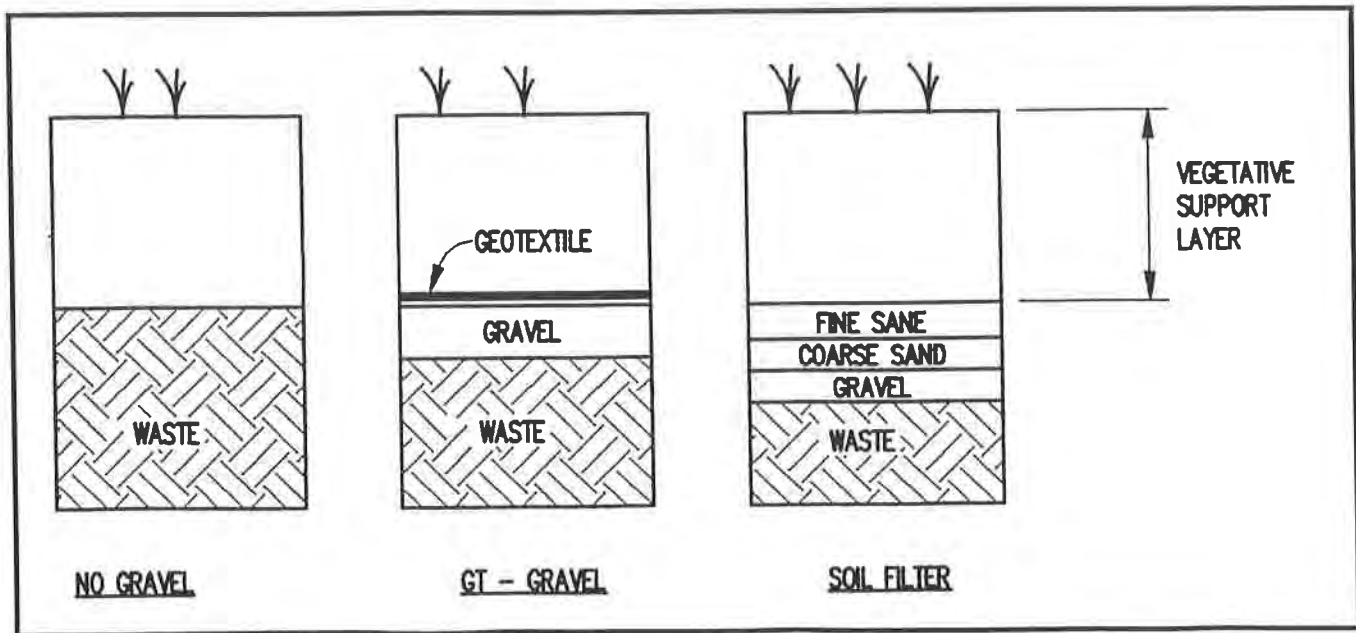
Figure 3. Cover Profiles Evaluated with HELP Model

thickness of the vegetative layer was varied from 24 to 48 inches. The average infiltration through the covers over a five year period is shown on Figure 4. The average annual precipitation during the five year period is 17.9 inches. The use of a 36 inch thick vegetative support layer and a geotextile/gravel capillary break system reduces the average annual infiltration to approximately 0.13 inch or 0.7% of the rainfall striking the cover. UNSAT-H analyses performed at this same site indicated an annual infiltration of only 2.49E-5 inches (Schafer & Associates, 1996) using a gravel capillary break layer that would also require a geotextile filter to construct and survive. This very small difference in predicted infiltrations between the HELP model and UNSAT-H must be examined with reference to the accuracy that important soil properties used in the evaluations can be defined.

The analysis of infiltration through a capillary break cover requires an accurate definition of the unsaturated hydraulic conductivity and volumetric moisture content for each soil as a function of the matrix suction, i.e., the capillary tension within the soil. A excellent summary of the difficulties of measuring these properties is presented by Meerdink et al. (1996). Typical examples of these relationships from applications at the Department of Energy Hanford facility are shown on Figure 5. The work of Meerdink et al., 1996 showed that significant difficulties exist in accurately defining the unsaturated hydraulic conductivity and volumetric moisture content relationships for an unsaturated soil even under research level field and laboratory efforts. This work did suggest the these relationships were reasonably well portrayed by empirical models developed by Brooks and Corey (1964, 1966) and Fredlund et al. (1994). The Brooks and Corey Model for volumetric moisture content verses soil suction, i.e., tension head, is incorporated in the HELP model commonly used for water-balance evaluations. All the models represent simple (complex?) Curve fitting algorithms used to best-fit available laboratory and field data. A discussion of testing methods to determine such data follows this section. These empirical models are expressed as follows:

Brooks-Corey Model

Volumetric Water Content vs. Matrix Suction

$$\frac{\Theta - \Theta_r}{\Theta_s - \Theta_r} = [\frac{\psi_b}{\psi}]^\lambda \quad when \;\; \psi > \psi_b$$

$$\Theta = \Theta_s \quad when \;\; \psi \leq \psi_b$$

(4)

where Θ is the volumetric water content (volume water divided by total volume), $_R$ is the residual water content, $_S$ is the saturated water content, ψ is the matrix soil suction, ψ_b is the air-entry suction pressure on the drying cycle (desorption) or the water-entry pressure on the wetting cycle (sorption), and λ is an empirical pore size distribution index.

Hydraulic Conductivity vs. Matrix Suction
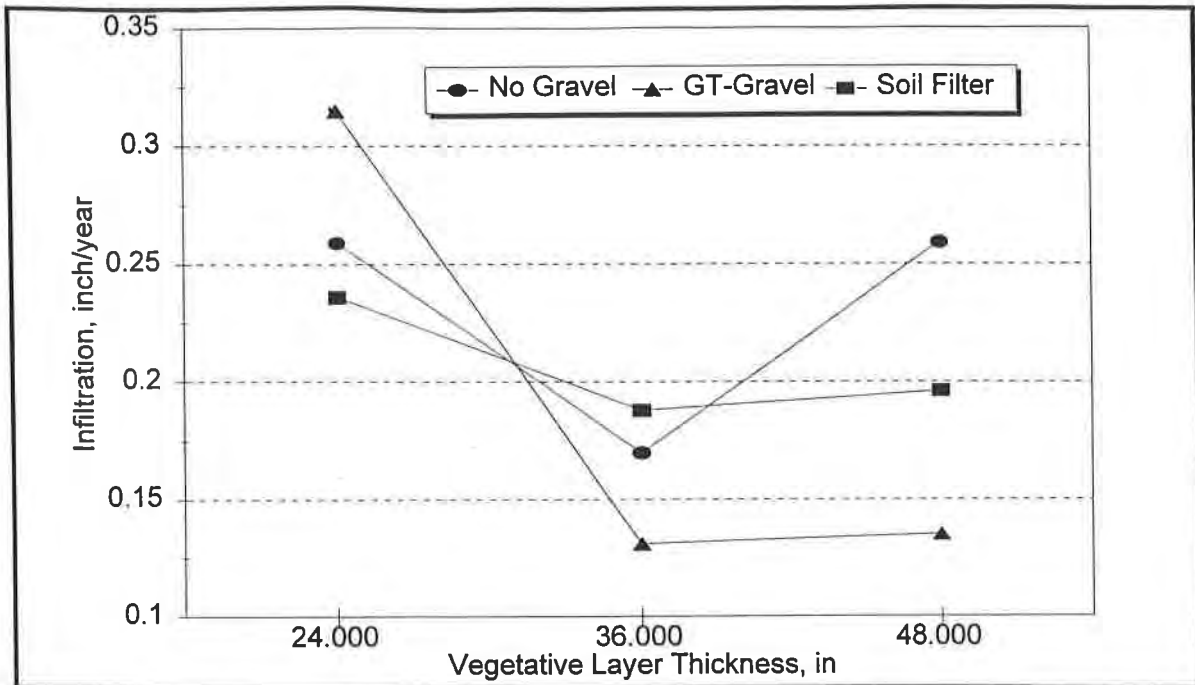
Figure 4. HELP Model Predicted Infiltration
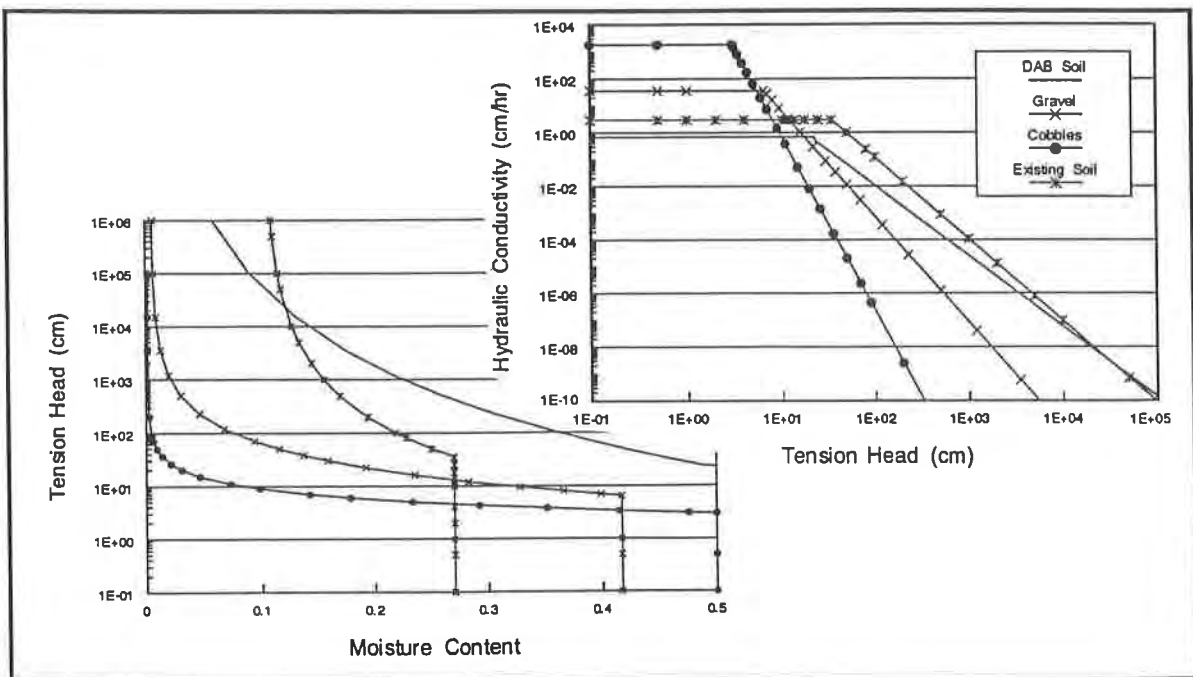
Figure 5. Unsaturated Soil Properties

$$K_r = K_s \left[\frac{\psi_b}{\psi}\right]^{2 + (5\lambda/2)} \quad \text{when } \psi > \psi_b$$

$$K_r = K_s \quad \text{when } \psi \leq \psi_b$$

(5)

where K_r is the permeability of the partially saturated soil and K_s is the permeability of the saturated soil.

Fredlund et al. Model

Volumetric Water Content vs. Matrix Suction

$$\Theta = C(\psi) \frac{\Theta_s}{[\ln(e + (\frac{\psi}{a})^p]^q}$$

(6)

where a, p, and q are empirical curve fitting parameters, and $C(\psi)$ is given as follows:

$$C(\psi) = 1 - \frac{\ln\left(1 + \frac{\psi}{C_r}\right)}{\ln\left(1 + \frac{1 \times 10^6}{C_r}\right)}$$

(7)

where C_r is related to the soil matrix suction at the residual water content.

Hydraulic Conductivity vs. Matrix Suction

$$K(\psi) = \frac{\int_{\ln\psi}^{b} \frac{\Theta(e^y) - \Theta(\psi)}{e^y} \Theta'(e^y) \, d\psi}{\int_{\ln\psi_a}^{b} \frac{\Theta(e^y) - \Theta_0}{e^y} \Theta'(e^y) \, d\psi}$$

(8)

where y = a dummy variable of integration representing $\ln \psi$, b = $\ln(106 \text{ kPa})$, ψ_a = air-entry pressure, and Θ' is the derivative of Equation 4 with respect to ψ.

Both the laboratory generation of empirical data and the empirical models for water content and permeability of partially saturated soils are complex and subject to considerable error. Given that the differences in water-balance models is commonly less than 1%, it is questionable whether the quality of soil data available for such analyses meets the mathematical accuracy of the models. It is also questionable that actual field construction will produce consistent properties within individual soil strata, i.e, the mathematics may be

more precise than life justifies.

Laboratory Evaluation of Partially Saturated Soil

A rigorous application of water-balance design requires knowledge of the relationships between matrix pressure within a partially saturated soil and (1) water content, and (2) permeability. The methods used to determine these relationships are discussed here to demonstrate their approximate and tedious nature.

<u>Matrix Suction vs. Water Content</u> ---- This relationship is commonly evaluated in the laboratory using the "filter paper" test, ASTM D-5298 Test Method for Measuring Soil Potential (Suction) Using Filter Paper. The test involves placing the partially saturated soil sample in contact with the filter paper for a sufficient time to establish equilibrium. Moisture from the soil will migrate to the filter paper until the suctions are balanced between the soil and filter paper. The water content of the filter paper is then evaluated and the soil suction is determined from known calibration curves for the filter paper. This procedure is applicable for fine grained soils only. For coarse grained soils and gravels the suction vs. Water content relationship can be measured using ASTM D-2325 Test Method for Capillary-Moisture Relationships for Coarse- and Medium- Textured Soils by Porous Plate Apparatus. Alternatively, the matrix suction can be determined in the laboratory or field using a soil tensiometer. Deaerated water is maintained under a low vacuum within the tensiometer and is in contact with pore water in the soil via the ceramic tip. A vacuum gauge on the tensiometer allows direct measurement of the soil or matrix suction. Considerable skill and effort is required to successfully utilize field tensiometer and their use is limited to relatively fine grained soils.

<u>Matrix Suction vs. Permeability</u> ---- A excellent summary of field measurement methods related to the measurement of permeability in partially saturated soils is given in ASTM D-5126 Standard Guide for Comparison of Field Methods for Determining Hydraulic Conductivity in the Vadose Zone. No standards exist, however, for measurement of hydraulic conductivity of partially saturated soils for either field or laboratory testing. Most field and laboratory methods rely on knowing the suction profile and flow rate within a given soil sample. This may be performed as a steady-state test by regulating the rate of water flow through the monitored sample or may be an 'instantaneous profile' measurement. Both methods rely on

defining the hydraulic head at a point within the sample as $i_w = \dfrac{dh_w}{dx}$. Knowing the flow rate and head,

the permeability of the partially saturated soil can be evaluated using Darcy's Law. This testing is very tedious and not generally available through commercial soils testing laboratories.

Alternative Laboratory Evaluation of Geotextile Enhanced Capillary Break

A simplified approach was taken to evaluate the benefits of a geotextile developed capillary break for mine reclamation covers. Simple flow lysimeters were constructed for the graded soil filter capillary break and geotextile filter alternatives as shown on Figure 6. The preferred capillary break alternative would simply be the capillary break that could retain the most water prior to allowing break through of the pore water. This was evaluated as follows:

1) The total dry unit weight of the soils placed within the lysimeters was obtained by knowing the water content and total weight of each soil placed.

2) The total weight of each lysimeter was monitored as water was gradually added to each lysimeter. Approximately .5 % water (by weight) was added to each lysimeter each increment of the wet up process. An approximately 48-hours increment between water additions was maintained. A tight fitting lid was placed over the samples to minimize evaporation during the tests.

3) The matrix suction near the geotextile enhanced capillary break was monitored for future field reference.

4) Water was added to each lysimeter until break through to the drainage layer occurred. The total water stored by each system prior to break through was obtained by subtracting the weight of the dry soil and lysimeter tank from the total final weight of the wetted lysimeter.
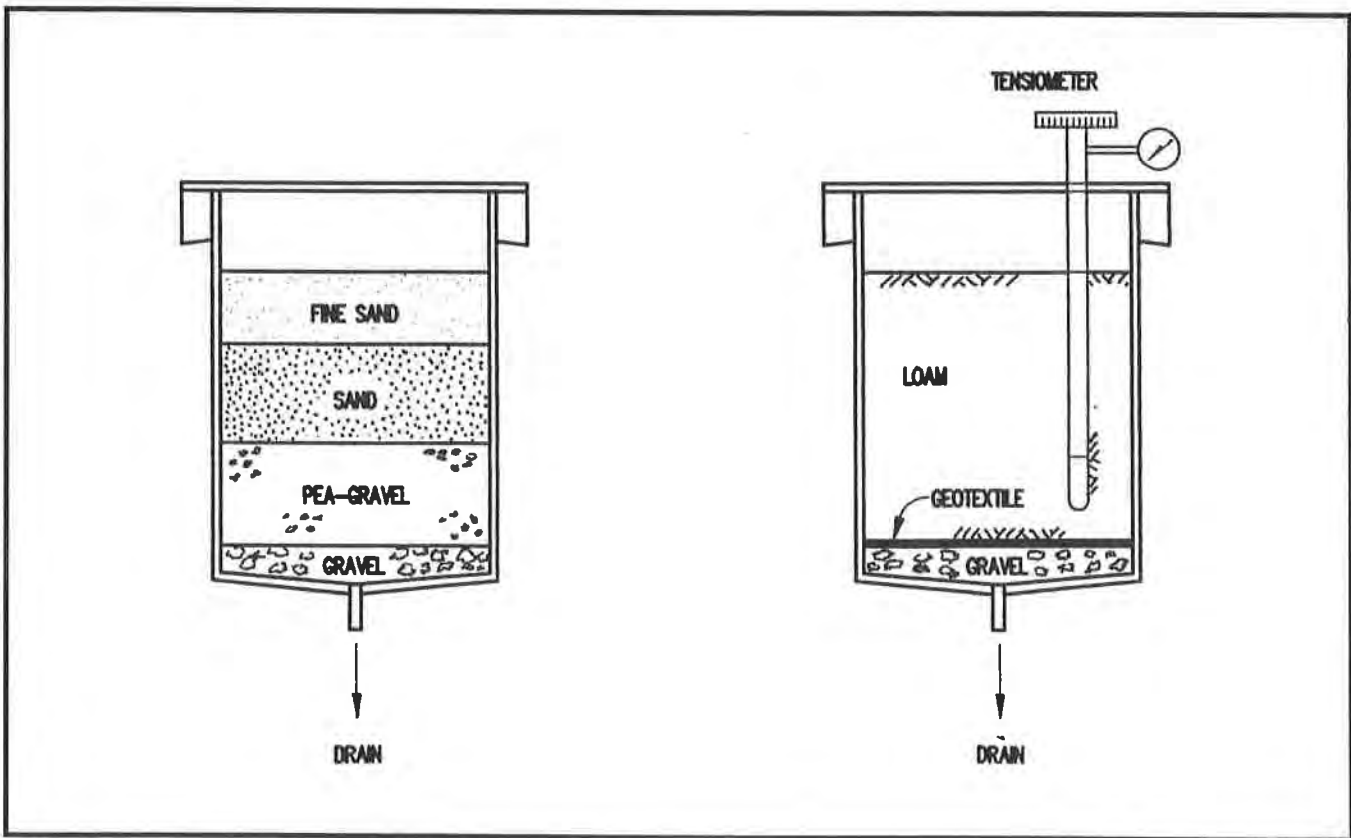
Figure 6. Lysimeters for Evaluating Capillary Break Performance

This test provides a quantitative estimate of the increased storage capacity provided by the use of a geotextile to form the capillary break. The results of the first series of tests are given in Table 2. All soils were placed in an air-dried state using minimal compactive energy. Future tests will evaluate the influence of wet-dry cycles on the break through water content.

Table 2 Laboratory Evaluation of Capillary Break Alternatives

Variable Measured	Graded Soil Filter	Geotextile Filter
Total Dry Soil Weight, lb.	135.5	117.8
Total Soil/Water Weight at Break Through, lb.	139.5	130.6
Water Stored at Break Through, inches of water	0.9	4.3

The ability to store more than three additional inches of water is very important in systems where the difference in predicted performance between the theoretical models is approximately 0.13 inches. This increase in the storage capacity of the water-balance cover without a corresponding increase in the depth to the capillary break is very important.

Long-Term Considerations For the Capillary Break Cover

The long-term performance of the geotextile supported capillary break must restrict the movement of vegetative roots through the capillary break and into the waste. By retaining soil water close to the surface, the combined topsoil and capillary barrier create a habitat for relatively shallow-rooted plant species and, thus, function as a de facto root-intrusion barrier (Cline et al. 1980; Hakonson 1986). Root growth is generally limited to regions within the soil where extractable water is available. Thus plant roots have no reason to penetrate through the geotextile to the dry gravel below. Lysimeter tests performed by the Department of Energy (Link,1994) showed that root mats tended to form at the capillary break interface. The root mat may provide a long-term alternative to the geotextile as the actual filter layer that maintains the capillary break.

Geotextile Selection Criteria

The geotextile used to created and maintain the capillary break must not be damaged during installation and must not allow the fines from the vegetative support layer to migrate to the coarse layer forming the capillary break. Thus clogging of the geotextile is not only acceptable, but actually preferred. Previously in this paper it was shown that almost all woven and nonwoven geotextiles satisfy the geotextile filter criteria for particle retention. To survive installation, the geotextile must have sufficient strength and ductility to resist the forces generated when the vegetative support layer is placed. Vegetative support layer soils may contain large stones since it is generally not economical to process these materials. Lacking field data on geotextile performance, it is recommended that the minimum strengths for separation as specified

by AASHTO M288-96 be used. These geotextile strength requirements are shown on Table 1. Note that no AOS requirement is required for this appilcation other than the AOS must be less than approximately 1.4 mm. These conditions allow the user to select the most economical of geotextiles available.

Table 1 AASHTO M288-96 Geotextile Specifications (1)

Application	Separation	
Class/ Property	Woven	Non Woven
1. grab strength, lb	250	160
2. elongation, %	<50%	≥50%
3. puncture, lb	90	60
4. burst, psi	390	190
5. trap tear, lb	90	60

(1) Minimum average roll values (MARV)

Summary

Both HELP and UNSAT-H analyses indicates that the use of a natural graded filter to form the capillary break actually increases the amount of infiltration in comparison to the use of a geotextile filter to form the capillary break. The exception being only when a very thin vegetative support layer is used. The substitution of a graded soil filter for vegetative support layers is, however, not a reasonable financial alternative. Irrespective of water-balance modeling concerns, the performance of the geotextile/capillary break cover produces a predicted infiltration rate of only approximately 1×10^{-8} cm/sec. The difference between zero infiltration and this very small level of infiltration is only approximately a tenth of and inch of annual infiltration. This infiltration rate would be difficult to measure in the field and can be improved on only by the introduction of problematic compacted clay barriers that have questionable long-term survivability due to freezing and dessication forces acting on clays in these regions.

The use of a geotextile to form the capillary break is recommended because of the following:

- The geotextile capillary break provides a significant increase in the water storage capacity above the capillary break without a corresponding increase in depth to the break,

- The geotextiles role is not diminished if it becomes clogged so the fabric can be selected based on known installation survivability criteria, and

- The long-term function of the capillary break does not depend upon the geotextile if the capillary break is placed within vegetation rooting depths.

The use of geotextile developed capillary breaks must of course be demonstrated through field trials and monitoring. It is reasonable, however, to begin such trials at this time.

References

Anderson, J.E., R.S. Nowak, T.D. Ratzlaff, and O.D. Markham, 1993. "Managing soil moisture on waste burial sites in arid regions," J. Environ. Qual., 22:62-69.

Benson, C.H. and M.V. Khire, 1995,"Earthen Covers for Semi-Arid and Arid Climates," Proceedings: Landfill Closures...Environmental Protection and Land Recovery, Geotechnical Special Publication No. 53, ASCE, NY,NY.

Brooks, R., and A. Corey, 1964. "Hydraulic Properties of Porous Media," Hydro. Paper No. 3, Civil Engineering Department, Colorado State University, Fort Collins, CO.

Brooks, R., and A. Corey, 1966. "Properties of Porous Media Affecting Fluid Flow," J. Irrigation and Drainage Div., ASCE, 92(2).

Cline, J.F., K.A. Gano, and L.E. Rogers, 1980. "Loose rock as biobarriers in shallow land burial," Health Physics, 39:497-504.

Fleenor, W.E. and I.P. King, 1995. "Identifying Limitations on Use of the HELP Model," Proceedings: Landfill Closures...Environmental Protection and Land Recovery, Geotechnical Special Publication No. 53, ASCE, NY,NY.

Foxx, T.S., G.D. Tierney, and J.M. Williams, 1984. Rooting Depths of Plants Relative to Biological and Environmental Factors, LA- I 0254-MS, Los Alamos National Laboratory, Los Alamos, NM.

Hakonson, T.E., 1986. Evaluation of Geologic Materials to Limit Biological Intrusion into Low-Level Radioactive Waste Disposal Sites, LA-10286-MS, Los Alamos National Laboratory, Los Alamos, NM.

Link, S.O., W.J. Waugh, and J.L. Downs, 1994. "The Role of Plants in Isolation Barrier Systems," In G.W. Gee and N.R. Wing (eds.), In-Situ Remediation: Scientific Basisfor Current and Future Technologies, pp. 561-592, Battelle Press, Richland, WA.

Melchior, K. Berger, B. Vielhaber, and G. Miehlich, 1994. "Multilayer Landfill Covers: Field Data on the Water Balance and Liner Performance," In G.W. Gee and N.R. Wing (eds.), In-Situ Remediation: Scientific Basis for Current and Future Technologies, pp. 411-425, Battelle Press, Richland, WA.

Meerdink, J.S., Benson, C.H., and M.V. Khire, 1996. "Unsaturated Hydraulic Conductivity of Two Compacted Barrier Soils," Journal of Geotechnical Engineering, American Society of Civil Engineers, Vol. 122, No. 7, July, pp. 565-576.

Morris, C.E. and J.C. Starmont, 1996. "Design of Capillary Barriers for Waste Site Containment," Proceedings 3rd International Symposium Environmental Geotechnology, San Diego, CA., pp. 513-522.

Reynolds, T.D., 1990. "Effectiveness of three natural biobarriers in reducing root intrusion by four semi-arid plant species," Health Physics, Vol. 59, pp.849-852.

Richards, L.A., 1931. "Capillary Conduction of Liquids in Porous Mediums," Physics Vol. 1, pp. 318-333.

Schafer & Associates, 1996. "Unsaturated Flow Modeling of Capillary Break Materials for Tailings Impoundment Reclamation," report to Golden Sunlight Mine, January 12.

Schroeder, P.R, et al, 1994. The Hydrologic Evaluation of Landfill Performance (HELP) Model: Engineering Documentation for Version 3, EPA/600/R-94/168b, Environmental Protection Agency, Cincinnati, OH.

Terzaghi, K., 1922. "Der Grundbruch an Stauwerken and seine Verhütung," Die Wasserkraft, Vol. 17, No. 24; Reprinted in From Theory to Practice in Soil Mechanics, John Wiley & Sons, New York, NY.

U.S.B.R., 1974. Earth Manual, 2 nd Edition, U.S. Bureau of Reclamation, Denver, CO.

Wing, N.R., and G.W. Gee, 1993. The Development of Permanent Isolation Surface Barriers: Hanford Site, Richland, Washington, U.S.A., WHC-SA-1799-FP, Westinghouse Hanford Company, Richland, WA.

OVERVIEW STUDY OF SEVERAL GEOMEMBRANE LINER FAILURES UNDER HIGH FILL LOAD CONDITIONS

A. J. BREITENBACH, P.E.
WESTEC, INC. - USA
5600 South Quebec Street, Suite 307-D
Englewood, Colorado 80111
Telephone: 1/303-290-9113
Telefax: 1/303-290-9904

ABSTRACT

This paper presents an overview study of the most probable causes for geomembrane liner failures under high fill load conditions, based on a post failure review of available literature, second-hand verbal information, and site or photo observations of 12 known heap leach pad slope failures that have occurred since 1985. Each slope failure may have unique site conditions, materials, or construction techniques, but a comparison of several case histories has shown a pattern of similarities with one or more likely causes for each failure.

Heap leach pad slope failures offer a wealth of information on the ultimate engineering performance and strength limits of geomembrane liner systems under high fill loads for the following reasons: 1) gold, silver and copper ore heap stacks are the highest existing fill structures in the world constructed on geomembrane liner systems; 2) heap fills generally consist of granular materials placed in controlled loose lifts, and are subsequently wetted and consolidated during leaching for developing moderately high in-place densities and driving force conditions on the liner surface; 3) pad grades typically are smoothed and graded to drain prior to geomembrane liner installation for potential planar or wedge-like slip planes along the most critical liner interface surfaces; and 4) downgradient pad toe areas are generally sloping downward for positive gravity flow into lined exterior ditches and ponds, and therefore, the heap fill must remain stable in stacked ore lifts on the planar liner surface generally without the support of large perimeter containment berms or excavated ground cells to buttress the toe area.

KEY WORDS: Geomembrane liners, Liner strengths, Liner failures, Heap leach pads.

INTRODUCTION

Currently, the highest geomembrane-lined fill structures in the world are low-grade gold and silver ore heap leach stacks in the western USA at 90 to 150 meters (300 to 500 feet) in vertical height. These records will soon fall by the wayside as unprecedented vertical design heap fill heights of 150 to 240 meters (500 to 800 feet) are being considered for geomembrane-lined gold and copper heap leach pad systems in the USA and internationally.

The most frequent number of geomembrane-lined slope failures occur on surficial lined fill cover slopes under low fill loads with an occasional rare occurrence beneath high fills on flatter grades. A slope failure indicates the overlying fill materials, liner system, and underlying foundation subgrade have reached the critical combined geometry, density, moisture and strength conditions for instability.

Lessons can be learned from each type of liner slope failure for application to all other lined facilities including hazardous and municipal solid waste landfills, tailings impoundments, heap leach pads, liner caps, and soil cover systems.

This paper will present an overview of the apparent causes of past heap leach pad slope failures on geomembrane liner systems. A schematic example of a geomembrane-lined heap leach operation is shown in Figure 1. A typical cross section of the most common geomembrane-lined composite leach pad liner systems is shown in Figure 2. Other less frequently constructed pad liner systems with direct geomembrane to geotextile interface contact are shown in Figure 3.

PAST LINER FAILURES

Geomembrane-Lined Slope Failures

The planar geomembrane liner surface generally has lower friction strength characteristics compared to the overlying cover fill and underlying bedding soil and foundation subgrade materials. Therefore the liner system requires special design, construction, and operational considerations to prevent instability along the most critical failure surface for solution containment (Breitenbach 1994).

In a review of published literature, second-hand information obtained from clients and colleagues, and site or photo observations, this author is aware of 12 known slope failures on geomembrane-lined heap leach pad facilities located predominantly in North America, with one failure occurring in South America and one in Australia.

The critical failure surface generally occurred by wedge failure along the liner surface. These geomembrane-lined slope failures were caused by several interrelated factors including the following most probable single or multiple causes listed below and summarized in Table 1 by frequency of occurrence for the 12 known sites:

- Placement of the first ore lift higher than 12 meters (40 feet) in vertical height with the exterior slopes stacked at the natural angle-of-repose;
- Placement of the first ore lift on downgradient pad toe grades steeper than 5 percent;
- Placement of the first ore lift in the downgradient pad liner direction;
- Placement of the ore heap fill on a weak foundation;
- Placement of underlying high plasticity clayey bedding materials at wet-of-optimum moisture content in direct contact with the geomembrane liner surface;
- Placement of geotextiles in direct contact with the geomembrane liner surface;
- Placement of ore lifts on snow or frozen ice sheets in direct contact with the geomembrane liner surface; and
- Placement of ore heap fill loads on poor to moderately compacted valley toe berm fills.

Each potential cause of failure should not be construed as a failure threshold limit for instability, but rather a cautionary indication of a potential problem to be considered in the design of the geomembrane liner system and subsequent ore heap fill construction. Adequately designed site grading fills by an experienced engineer in the critical downgradient toe areas of the heaps, in combination with geomembrane liner selection and experienced operator heap stacking operations, would have eliminated most of the 12 known slope failures.

The majority of the geomembrane-lined slope failures occurred on the more rigid (semi-crystalline) geomembrane liners during placement of the first ore lift. Textured geomembrane liner sheets and non-planar liner surfaces are frequently being designed and constructed at the downgradient toe of ore heaps in current practice to improve on the smooth surface friction strength of the less flexible geomembrane liners.

TABLE 1 - KNOWN GEOMEMBRANE-LINED SLOPE FAILURES AT 12 SITES

MOST PROBABLE CAUSE OF FAILURE	SITE 1	SITE 2	SITE 3	SITE 4	SITE 5	SITE 6	SITE 7	SITE 8	SITE 9	SITE 10	SITE 11	SITE 12
HIGH FIRST ORE LIFT		X				X	X			X	X	X
STEEP DOWNGRADIENT LINER TOE GRADE	X	X				X	X		X		X	
DOWNGRADIENT FILL PLACEMENT	X		X	X		X			X		X	
WEAK FOUNDATION					X			X		X		X
HIGH PLASTICITY WET-OF-OPTIMUM CLAY BEDDING FILL	X					X	X					
GEOTEXTILE TO GEOMEMBRANE DIRECT CONTACT			X	X						X		
SNOW OR ICE ON LINER SURFACE									X			
WEAK TOE BERM FILL						X						

GENERAL NOTES:

1. The leach pad sites with known slope failures are generally listed in chronological order (Site No. 1 in 1985 to Site No. 12 in 1993). Another 15 failures that have occurred as recent as 1996 are not listed due to insufficient information to confirm or determine the general cause of these failures.

2. The most probable causes of failure are generally listed from the most to least frequent occurrences, based on available post-failure information and verbal discussions.

3. The site locations and source of information are confidential until approved by the owners. Each site may not include all causes of failure, since follow up engineering studies at most of the sites are unknown or non-existent.

Other Types of Geomembrane Liner Failures

The list of probable causes for known geomembrane-lined slope failures does not include other types of geomembrane liner failures related to natural causes such a stress-cracking from climate exposure (Paradise Peak in Nevada), potential snow avalanche damage (Summitville in Colorado), or wind storm damage during liner installation (Ridgeway in South Carolina). It also does not include the more common man-made geomembrane leakage failures such as excessive foot traffic in exposed areas, poor quality liner materials and installation, or inadequate engineering inspection of the underlying bedding fill, geomembrane liner, and overlying cover fill operations.

These natural and man-made liner failures (deformations, punctures, pinholes, cracks, separations) can indirectly cause leakage and weakening of the geomembrane liner subgrade system beneath high fills. However this paper will focus on the more direct causes listed in this section with the most frequent causes illustrated for discussion purposes by an idealized ore heap wedge stability model.

CAUSE OF FAILURE

General

The greatest lessons learned in the advancement of engineered facilities are obtained by studying past failures. A slope failure on a geomembrane-lined fill structure provides clues to the material strengths and critical slope geometry limitations at which a failure will likely occur.

The engineering evaluation and analyses of a heap leach pad slope failure begins with a list of all pertinent known and unknown (assumed) factors. This list typically includes the density, moisture content, and strength parameters of the ore heap, liner system, and foundation subgrade (natural soil, bedrock or man-made fill) imposed on planned or as-constructed liner system surface grades, fill stack heights, exterior slopes, and loading conditions.

The known conditions for a post-failure stability model may include the following:

- The construction materials and geometry of the pad liner system;
- The granular ore heap and earth/rockfill containment dike construction techniques; and
- The actual failure plane reconstructed through the ore heap fill to the geomembrane liner surface or foundation subgrade based on observations.

The density, moisture content, and strength of the foundation, liner system, and heap ore fill can be determined from as-built records supplemented by the post-failure collection of representative material samples and appropriate laboratory testing, if the design and construction information is insufficient.

The unknown factors for a post-failure stability model may include the following:

- The actual solution level (phreatic surface) above the liner system at the time of failure;
- The potential leakage (if any) wetting the underlying bedding fill and subgrade prior to failure; and
- The amount of foundation settlement in the natural subgrade soils or site grading fill from the fill placement load conditions above the liner system.

Based on site specific planned, as-constructed, and post-failure information, supplemented by a review of past failures, the engineer can focus on modeling and evaluating the true cause of failure. The lessons learned from past geomembrane-lined slope failures indicate one or more causes can be considered for determining the sequence of failure, as discussed in the following sections.

<u>Cause No. 1 - Placement of the first ore lift higher than 12 meters (40 feet) in vertical height stacked at the natural angle-of-repose</u>. The majority of past geomembrane-lined fill slope failures have a tendency to occur during the first or second high ore lift placement and not at higher stack levels. The general exceptions are heaps stacked to higher levels with weak foundation conditions (see Cause No. 4).

There appear to be 3 basic interrelated reasons why "first lift" failure occurs on geomembrane liners including the following:

- The higher fill lifts allow some ore material segregation (weaker ore zones) to occur down a long angle-of-repose slope that is conducive to developing a wedge-like failure through the heap material to the geomembrane surface;
- Each individual ore lift is stacked at the natural angle-of-repose by radial stacker or truck end-dump and dozer operations for a surficial fill slope factor-of-safety at 1.0 for a fully drained infinite slope condition; and
- High lifts can create a relatively rapid first increment loading condition on low permeability bedding underliner soils placed above optimum moisture content for potential low-strength excess pore pressure conditions (see Cause No. 5).

After the first ore lift is placed at the natural angle-of-repose, subsequent lifts have a set back bench to develop an overall flatter slope for enhanced stability, as shown in Figure 4. Therefore each individual lift has a surficial slope factor-of-safety at 1.0 with higher factors-of-safety for the benched overall slopes in subsequent lifts.

A toe wedge failure along the liner interface surface is the most critical slip surface in the initial ore lifts. An idealized ore heap geometry with wedge failure planes analyzed at different heights is shown in Figure 5 at an overall exterior slope of 2H:1V and a 2 percent leach pad grade. Typical wetted strengths and densities are assumed for the ore and liner interface with the top of the Rankine wedge plane varied in 10 meter increments for illustration purposes. The computed static factors of safety versus heap fill heights for the idealized heap cross section are shown in Figure 6. Note that the two-dimensional model does not include the effects of increased density and strengths with depth for consolidation of a fully drained granular fill as the fill increases in incremental height. Simulated failure conditions may be more accurate in a three-dimensional model with strengths reflecting load consolidation (densification) in the ore heap.

The lowest factors of safety for the idealized study section occur in the first ore lift and increase with each 10 meter lift until the ore heap exceeds 30 meters in height. Subsequent lift heights above 30 meters for the idealized section show minimal changes in the factor of safety of a liner wedge failure, although the factors of safety for foundation failure (not shown in this example) will decrease with increased heap height. The results of these analyses show the importance of careful placement of the first 1 to 2 ore lifts to create and maintain a stable heap fill toe.

Cause No. 2 - Downgradient pad liner toe grades steeper than 5 percent. It is difficult to say when a pad site grade is too steep for fill placement on a geomembrane-lined surface due to the many site specific factors that affect the interface friction strength. As an example, a typical leach pad construction utilizes positive solution gravity flow on 1 to 3 percent typical downgradient pad toe grades with low hydraulic heads maintained above the pad liner system. Establishing a stable heap toe on flatter grades allows for buttressing and stabilizing the placement of subsequent horizontal fills against upgradient liner grades steeper than 30 percent.

Haul roads for initial ore truck traffic to the pad system present the most frequent localized slide problems from dynamic loads on steep liner grades under low confining cover fills. Some insight can be gained from these slides in understanding the affects of high fill loads placed directly on steep liner grades.

The placement of a liner cover fill or the first ore lift in a valley fill operation initially involves the construction of a haul road from the containment dike crest level down into the bottom valley bowl area for subsequent horizontal lift placement. The pad liner grades along the haul road are generally steeper than a 5 percent grade for most valley fills. Fill placement on steep

geomembrane-lined grades may cause some downgrade cover fill or geomembrane liner movement requiring repair. If some geomembrane slippage occurs on the hill slope during loading, then lower residual slide strengths may develop at the geomembrane/clayey bedding soil contact versus higher peak strengths before load-induced movement. The end result is a potential weakening of the geomembrane/bedding soil contact strength and increased tensile stress in the geomembrane liner material on the hill slope.

Cause No. 3 - Placement of the first ore lift in the downgradient pad liner direction.
There may be several interrelated reasons why downgradient ore fill placement on geomembrane liners causes a slope failure including the following:

- Segregation of ore materials in higher lifts stacked at the natural angle-of-repose for potential weaker ore lift zones in the critical downgradient direction (see Cause No. 1); and

- Potential residual versus peak strengths at the geomembrane/soil interface contact with the development of horizontal downgradient stresses in the geomembrane liner (see Cause No. 2).

Weaker ore zones dipping in the downgradient direction can create a classical Rankine wedge failure plane (Rankine 1857) through the ore fill to the lower strength planar geomembrane liner surface, although computer model wedge failure planes may vary for the lowest computed factor of safety.

This author believes there is some trade off in the potential residual strengths and natural segregation of placed fill material versus the rapid primary consolidation and increase in density and strength for a granular fill with controlled leaching (wetted and fully drained material). The ore strengths deep within the consolidated heap mass may be significantly higher than the less consolidated surficial loose lift materials on the heap slopes. The end result is that many heaps have remained stable at high stack lifts. However most of the known slope failures, excluding natural foundation failures, include downgradient stacking.

The combination of fill placement conditions for causing downgradient slope failures may also apply to upgradient fill placement. However, this author is not aware of any geomembrane-lined fill slope failures on fills placed in the upgradient pad liner direction.

Cause No. 4 - Placement of the ore heap fill on a weak foundation.
Ore heap pad liner systems are typically sited on competent natural or compacted soils and bedrock foundation subgrades. Where subgrade slide failures occurred beneath the stacked ore heap fills, these sites generally had pre-existing landslide features, adverse dipping weak bedrock formations, or low-permeability clayey soils with wet-of-optimum moisture content (see Cause No. 5). In some

instances, the clayey bedding fill was tested and found to be lower in strength than the flexible geomembrane liner/bedding soil interface contact due to the high plasticity or excess pore pressure characteristics of clays exhibiting less than 1×10^{-7} cm/sec hydraulic conductivity values.

Cause No. 5 - Placement of underlying high plasticity clayey bedding materials at wet-of-optimum moisture content. Past studies of liner leakage in landfill liners (Bonaparte et al. 1989) suggest that some wetting will occur in the bedding soil subgrade from geomembrane liner pinhole leakages and water vapor transport.

Laboratory tests indicate that placement of clayey soils at wet-of-optimum moisture content can reduce the hydraulic conductivity (permeability) in the bedding fill materials (Hermann and Elsbury 1987, Benson et al. 1994). This is a high-risk condition for high fill structures, since load-induced excess pore pressures may develop and cause undrained low strength conditions at the geomembrane/bedding soil interface contact, or initiate high plasticity soil creep movement.

Proper laboratory testing and engineering judgement are sometimes necessary for balancing the required soil strength versus low permeability characteristics of wetted clayey bedding soils, based on past studies (Daniel and Wu 1993) and observed geomembrane slide failures.

Cause No. 6 - Placement of geotextiles in direct contact with the geomembrane liner surface. The most successful leach pad liner system commonly used in North America and internationally is the composite geomembrane and clayey bedding liner system. There are a relatively small number of pad liner systems that incorporate a geotextile (geonet or geofabric) in direct contact with the geomembrane liner, which significantly reduces the interface liner strength compared to a direct underliner bedding soil and overliner cover fill interface contact with the geomembrane liner.

A leach pad liner failure (actually two failures about 2 weeks apart from each other on the same site under the same conditions) is known to have occurred on a 4 percent double geomembrane liner toe grade due to low interface friction strength characteristics at the geomembrane top liner to geofabric to geomembrane bottom liner surface contacts under a 5 to 6 meter (16 to 20 feet) thick first ore lift load placed in the downgradient direction. Another more extensive pad failure occurred on a 2 percent grade in Australia at the single lined geomembrane liner to geofabric contact on a granular subgrade under 5 to 7 meter (16 to 23 feet) thick first ore lift load placed in the downgradient direction. This low strength synthetic to synthetic interface condition has been well documented for the Kettleman Hills landfill failure that occurred in California (Mitchell et al. 1990).

Large-scale direct shear strength testing (ASTM D-5321 established in November 1992) and engineering judgement from past experiences are recommended for any geomembrane liner system that requires direct interface contact between geotextiles and geomembrane liners in the design of fill covers.

Cause No. 7 - Placement of ore lifts on snow or frozen ice sheets in direct contact with the geomembrane liner surface. Many cases have been observed where geomembrane pad liners were installed in the summer or fall seasons, but not covered with fill until the early winter season. Only one case of a slide failure due to snow burial is known to this author. Generally the black geomembrane liner surface prevents the build up of snow in solar heated areas exposed to sunlight.

This author has slipped and fallen on installed geomembrane liner surfaces enough times to know that a thin frost layer can significantly lower the liner surface friction strength to the point where walking up or down lined slopes is difficult to achieve without an anchored rope ladder. A snowpack cover buried and compressed beneath a fill has similar low strength effects on the geomembrane liner surface.

Cause No. 8 - Placement of ore heap fill loads on loose to poorly compacted valley toe berm fills. Most heap leach operations involve open pit mining techniques in which a large abundance of waste rock overburden material (non-ore rockfill) is available for pad construction at a low cost to haul and place by mine equipment as fill material. The amount of heap-induced load settlement on a loose to poorly compacted containment dike rockfill can vary depending on loose lift dump heights, haul equipment loads, rockfill gradations, rock particle strengths and other factors at each site, but likely can exceed 2 to 5 percent in vertical displacement (Breitenbach 1993). This amount of differential movement between the natural subgrade and the dike fill materials in a valley fill operation can develop lower residual strengths in the underlying clayey bedding soil liner and also in the overlying ore heap fill as lift heights increase.

It should be noted that the construction of high rockfills beneath heap leach pads with controlled lifts and compaction is common and generally has not been a stability problem. Adequately compacted berm and site grading fills add strength to the subgrade foundation as well as flatten the pad liner toe grades for solution control and heap stability.

CONCLUSION

This paper presented an overview study of several apparent causes of fill slope failures for geomembrane-lined systems beneath high fill structures such as gold, silver and copper heap leach pads. Lessons learned from geomembrane liner failures under high fill loads may also apply to other geomembrane-lined facilities such as solid waste landfills, tailing impoundments, liner caps, and soil covers.

In summarizing the overview of apparent causes for slope failures on geomembrane liner surfaces under high fill loads, and other experiences gained from conducting large-scale liner test fills and laboratory testing, this author has concluded the following:

- The known geomembrane-lined fill slope failures generally have several interrelated causes of failure rather than any single cause by itself;
- Slope failures generally occur along the geomembrane liner interface contact with underliner bedding fill or geotextile materials in most cases, except for a few cases where the subgrade foundation is weaker than the liner interface strength;
- The two-dimension cross sectional shape of the liner failure is typically a wedge from the crest of the fill down to the liner or a propagating wedge slip starting near the toe and extending to the crest of the fill with fill wedge planes at or steeper than the natural angle-of-repose;
- The failure contact in plan view on the liner surface, where the geomembrane liner is torn apart, approaches the shape of a circular arc such that a two-dimensional stability analyses should account for additional strengths gained in a three-dimensional failure wedge model to determine the true liner interface friction strengths at failure;
- Slope failures generally occur during the placement of the initial lifts of fill material on the liner surface with the exception of weak foundation failures that generally occur under subsequent higher fill loads above the 30 meter height;
- The more rigid medium to high density polyethylene (semi-crystalline) geomembrane liners generally have shown a significantly lower interface friction strength compared to the more flexible low density polyethylene and polyvinyl chloride liners, based on the known and probable leach pad slope failures as well as large-scale laboratory direct shear tests conducted for other projects; and
- The liner selection and design process for analyzing fill slope stability involves engineering experience and judgement of numerous parameter trade offs including some of the following options: smooth versus textured geomembrane sheets; planar versus non-planar liner surfaces; containment berm fills versus unsupported fill toe slopes; steep versus flat liner grades; high versus low initial fill placement lifts; and low permeability versus high strength conditions in critical underliner fills with high moisture content or high plasticity characteristics.

The geomembrane liner must function for the life of the facilities considering all pertinent site specific design conditions as well as planned construction and operation conditions. Some engineering judgment is required in the overall geomembrane liner selection and design to select the most practical liner system for construction. The success of liner projects can be directly attributed to an experienced team effort by the design engineer, followed by the liner fabricator/installer and construction testing personnel, and finishing with the earthwork contractor or operator of the facilities.

Most of the geomembrane-lined slope failures known to this author could have been avoided with proper leach pad liner design, construction, and stacking of the ore heap fills. The lessons learned from past geomembrane-lined slope failures can provide invaluable engineering judgement and contractor/operator guidance in minimizing inadequate design and construction practices.

REFERENCES

Benson, C.H., Zhai, H. and Wang, X, February, 1994, "Estimating Hydraulic Conductivity of Compacted Clay Liners", Journal of Geotechnical Engineering, ASCE, Vol. 120, No. 2, pp. 366-387.

Bonaparte, R., Giroud, J.P. and Gross, B.A., 1989, "Rates of Leakage Through Landfill Liners", Geosynthetics Conference Proceedings, San Diego, California, USA.

Breitenbach, A.J., March, 1993, "Rockfill Placement and Compaction Guidelines", Geotechnical Testing Journal, ASTM, Philadelphia, Pennsylvania, USA, Vol. 16, No. 1, pp. 76-84.

Breitenbach, A.J., August, 1994, "Design of Geomembrane Liners Beneath High Fill Structures", The Mining Record, Vol. 105, No. 33, pp. 8-10.

Daniel, D.E. and Wu, Y., February, 1993, "Compacted Clay Liners and Covers for Arid Sites", Journal of Geotechnical Engineering, ASCE, Vol. 119, No. 2, pp.223-237.

Hermann, J.G. and Elsbury, B.R., 1987, "Influential Factors in Soil Liner Construction for Waste Disposal Facilities", Geotechnical Practice for Waste Disposal '87, R. Woods, Ed.,ASCE, pp. 522-536.

Mitchell, J.K., Seed, R.B. and Seed, H.B., 1990, "Kettlemen Hills Waste Landfill Slope Failure", Journal of Geotechnical Engineering, Vol. 116, No. 4, pp. 647-660.

Rankine, W.J.H., 1857, "Theory on the Stability of Loose Earth Based on Ellipse of Stresses", Philosophical Transactions of the Royal Society, No. 147.
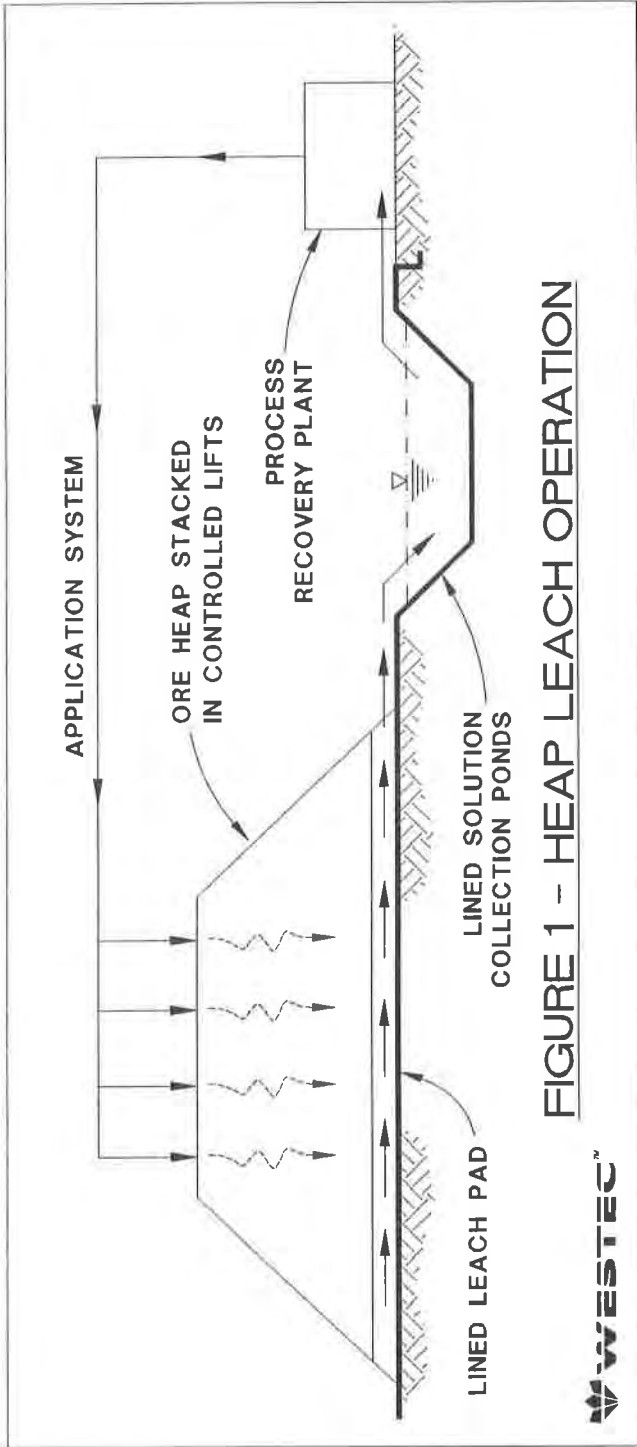
FIGURE 1 – HEAP LEACH OPERATION

APPLICATION SYSTEM

ORE HEAP STACKED
IN CONTROLLED LIFTS

PROCESS
RECOVERY PLANT

LINED SOLUTION
COLLECTION PONDS

LINED LEACH PAD

WESTEC™
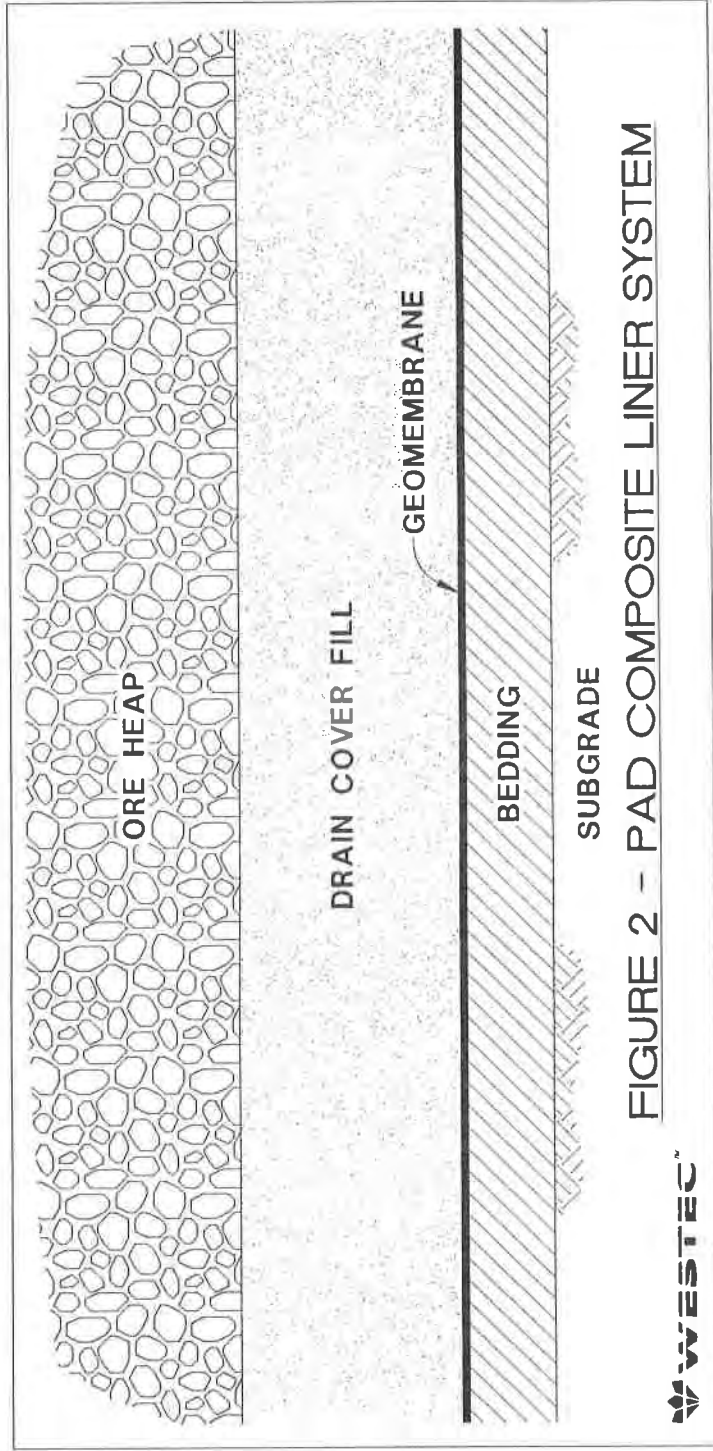
FIGURE 2 – PAD COMPOSITE LINER SYSTEM

ORE HEAP

DRAIN COVER FILL

GEOMEMBRANE

BEDDING

SUBGRADE

WESTEC™
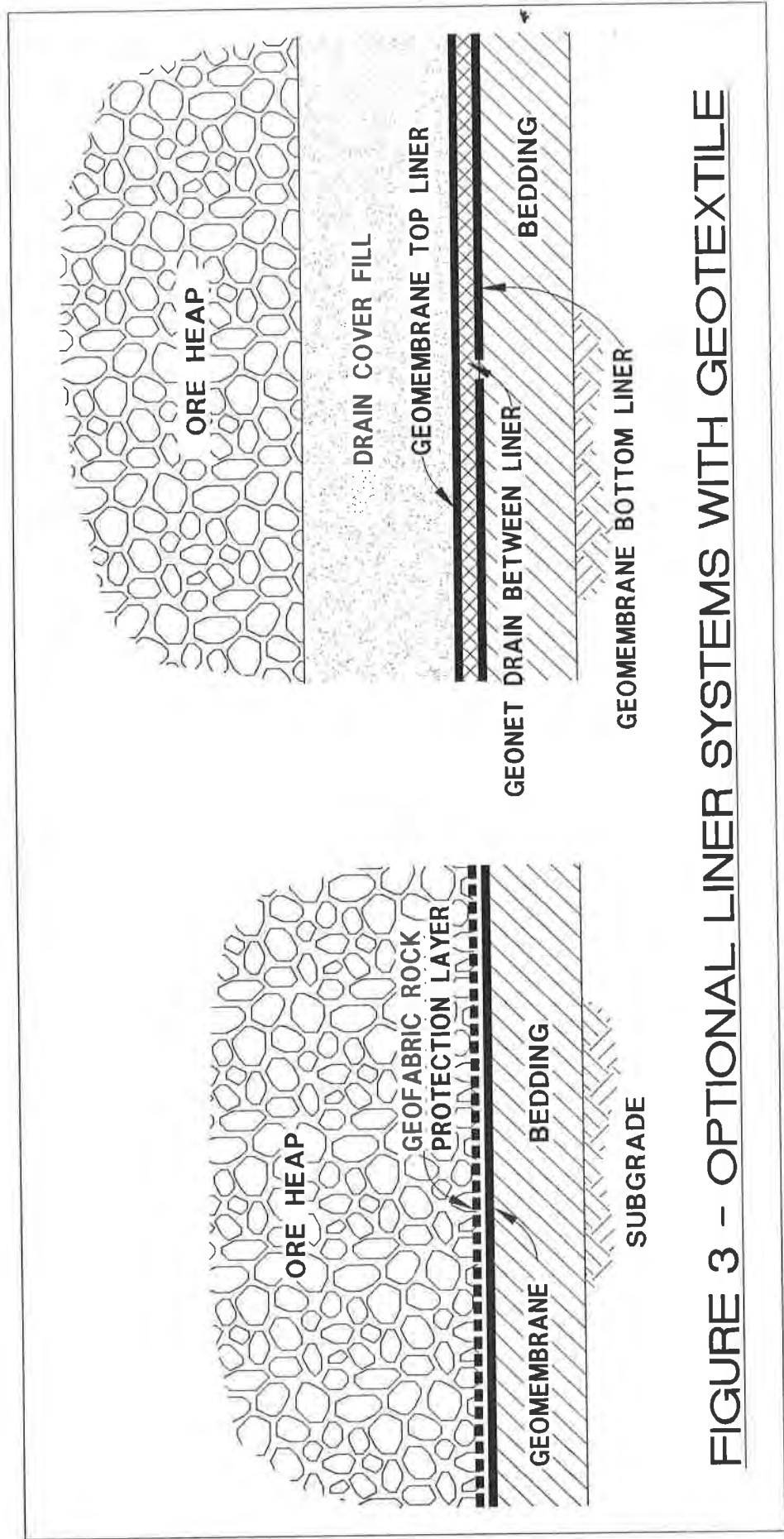
FIGURE 3 – OPTIONAL LINER SYSTEMS WITH GEOTEXTILE
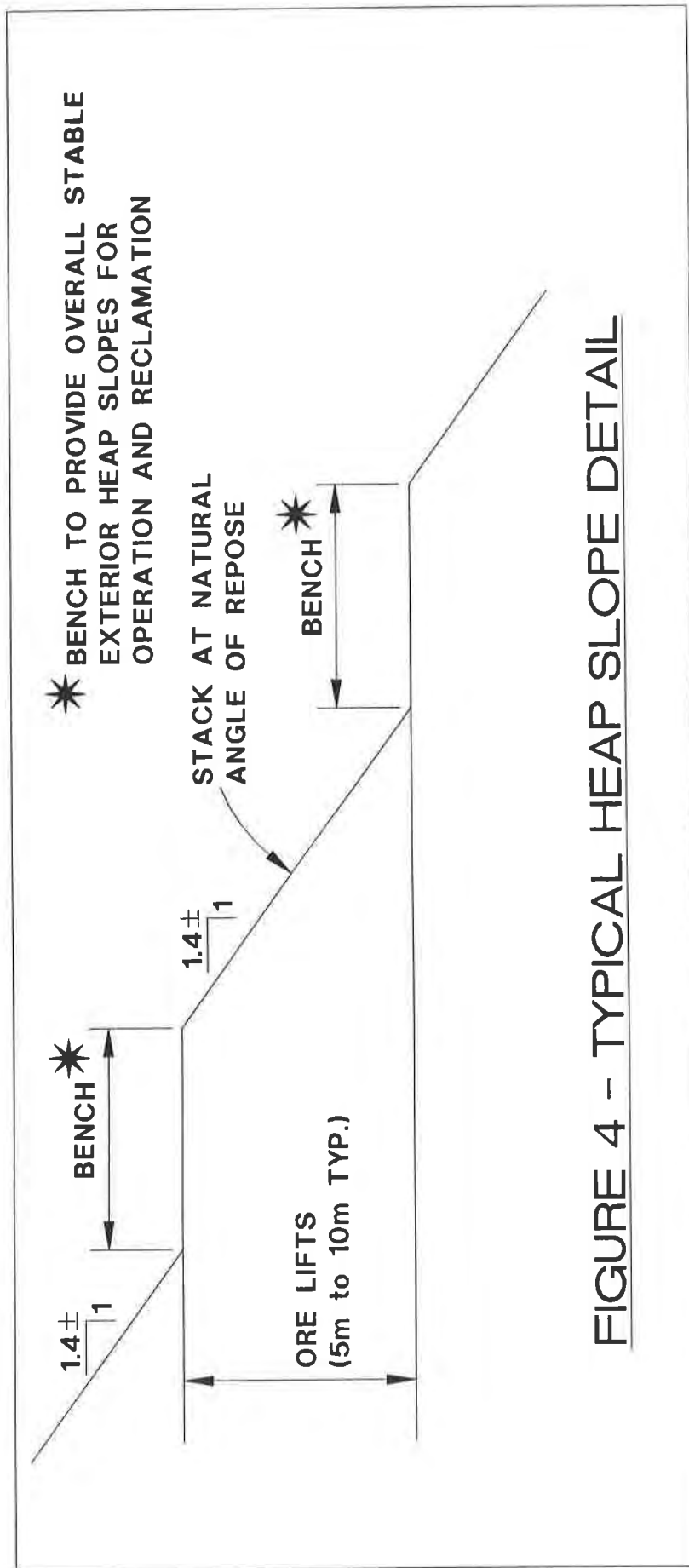
FIGURE 4 - TYPICAL HEAP SLOPE DETAIL

- BENCH TO PROVIDE OVERALL STABLE EXTERIOR HEAP SLOPES FOR OPERATION AND RECLAMATION

STACK AT NATURAL ANGLE OF REPOSE

BENCH

BENCH

1.4± 1

1.4± 1

ORE LIFTS (5m to 10m TYP.)
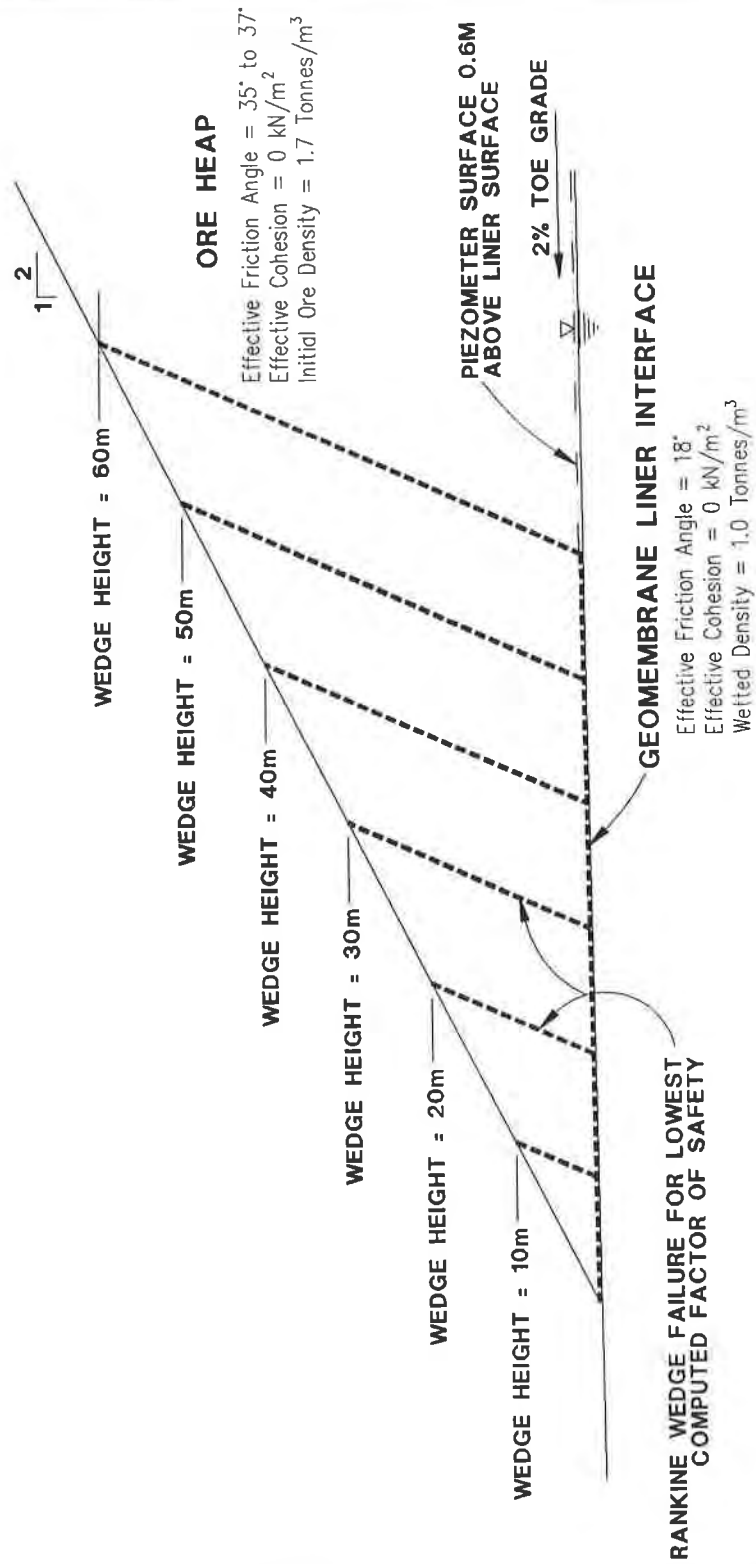
FIGURE 5 - IDEALIZED ORE HEAP SECTION

1
2

WEDGE HEIGHT = 60m

WEDGE HEIGHT = 50m

WEDGE HEIGHT = 40m

WEDGE HEIGHT = 30m

WEDGE HEIGHT = 20m

WEDGE HEIGHT = 10m

ORE HEAP

Effective Friction Angle = 35° to 37°
Effective Cohesion = 0 kN/m^2
Initial Ore Density = 1.7 Tonnes/m^3

PIEZOMETER SURFACE 0.6M
ABOVE LINER SURFACE

2% TOE GRADE

GEOMEMBRANE LINER INTERFACE

Effective Friction Angle = 18°
Effective Cohesion = 0 kN/m^2
Wetted Density = 1.0 Tonnes/m^3

RANKINE WEDGE FAILURE FOR LOWEST
COMPUTED FACTOR OF SAFETY

FIGURE 6 – FACTOR OF SAFETY vs ORE FILL HEIGHT FOR RANKINE WEDGE FAILURES

DESIGN, CONSTRUCTION, AND PERFORMANCE OF A SINGLE GEOMEMBRANE LINER SYSTEM AT A RESIDUAL WASTE DISPOSAL SITE IN WESTERN PENNSYLVANIA

K. H. KHILJI AND S. E. GOULD
GAI CONSULTANTS, INC., USA
T. W. HAMEL AND W. B. THOMAS
GPU GENERATION INCORPORATED, USA

ABSTRACT

This paper examines the effectiveness of a single geomembrane-lined deep valley coal ash/coal mine refuse disposal site to maintain ground-water quality after 10 years of operation. The site occupies over 81 hectares (ha) [200 acres (ac)] in western Pennsylvania. The effectiveness of the liner system was evaluated based on an assessment of the site's ground-water quality.

The liner system was designed in 1983. Selection of geosynthetics and drainage materials, interface shear values, and construction control methods were based on laboratory testing, field investigations, slope stability analyses, and construction load analyses. Diligent construction quality control was applied during all aspects of site development.

To examine the site's ground-water quality, the ground-water monitoring network was sampled approximately once every six weeks for one year (1994). Results of statistical analyses show that the liner system is effectively separating disposal site leachate from ground water and that the site is not degrading ground water.

INTRODUCTION

The Keystone Electric Generating Station and the East Valley Disposal Site are located approximately 56 kilometers (km) [35 miles (mi)] northeast of Pittsburgh in western Pennsylvania. In 1983, concerns for the environment prompted the Pennsylvania Department of Environmental Protection (PaDEP) to promulgate draft regulations governing the management of residual wastes, including coal ash generated by the electric power industry. These regulations addressed the use of liners at residual waste landfills to prevent or minimize the infiltration of leachate generated from deposited waste into the ground water.

In advance of the final regulatory requirements, the Keystone Station Owners Group committed to the design and construction of a lined residual waste disposal site. At the Keystone Station, approximately 51 ha (125 ac) have been lined with a single 1.3 millimeters (mm) (50 mil) thick polyvinyl chloride liner (Photograph 1). The site was initiated in 1984 and is the head of a valley fill designed for approximately 20 years accumulation of fly ash, bottom ash, coal refuse, and other plant wastes. The landfill embankment at completion will have depths exceeding 91 meters (300 feet). Development of the entire disposal site was divided into staged construction over a 12-year period. Construction was staged to limit the aerial extent of exposed waste and to defer the capital costs associated with liner installation. As areas were first constructed then soil covered in stages, prompt site stabilization was employed. This limited the volume of runoff, leachate, and erosion, and reduced the size and construction costs of the associated facilities.
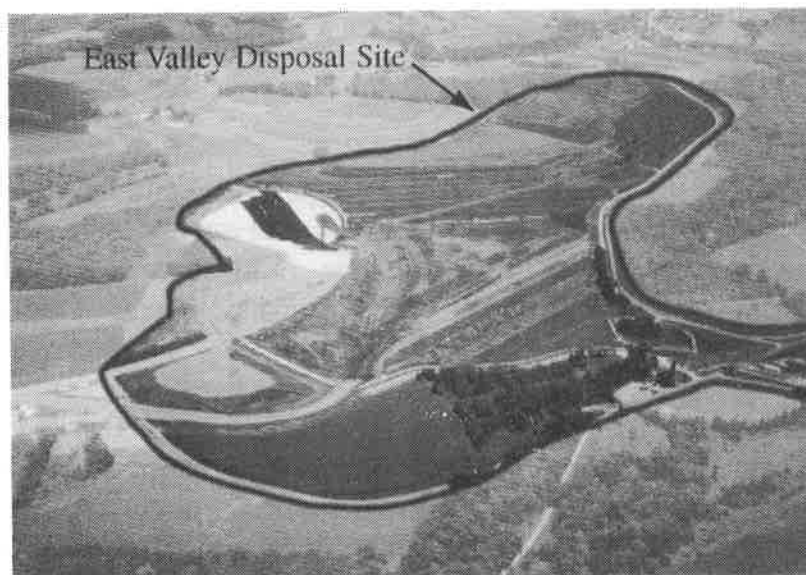
Photograph 1. East Valley Disposal Site.

The geomembrane liner system was installed across the valley bottom and up the valley side slopes which formed the base of the landfill. To maintain slope stability, the slopes were regraded to no steeper than 3H:1V (horizontal:vertical) and the geomembrane was installed between layers of permeable materials (Figure 1). At the base, a 30.5-centimeter (cm) [1-foot (ft)] thick sand layer (ground-water/leachate detection zone) collects and removes the ground water from beneath the liner. This layer discharges through perforated pipes which are trenched into the regraded ground surface. A woven separation geotextile layer was placed between the ground surface and the sand layer to limit fine particle migration. The geomembrane is protected by layers of nonwoven cushion geotextile on both sides. A 61-cm (2-ft) thick layer of screened bottom ash above the liner system directs leachate to a geotextile-wrapped rock drain, which flows to an equalization pond from which it is pumped to a treatment plant.

This paper describes the laboratory testing, stability analyses, construction methods, QA/QC, and performance evaluation based on ground-water monitoring.
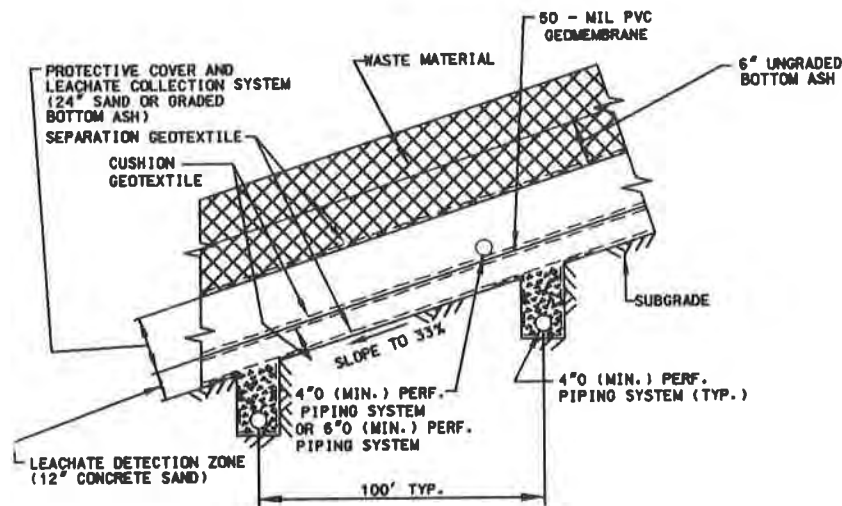
Figure 1. Single Geomembrane Liner System

LABORATORY TESTING

The engineering and mechanical characteristics at the interfaces of the various aggregates, geotextiles and the geomembrane were not known, but were considered critical due to the slopes and high embankment loads. Tests were performed to determine information regarding the following:

- Durability and abrasion of geotextiles and geomembranes placed on slopes when subjected to low and high vertical stresses, and

- Interface shear values for geotextiles, geomembranes and aggregates.

Materials evaluated by the testing program included various thicknesses of polyvinyl chloride (PVC), smooth high density polyethylene (HDPE), chlorinated polyethylene (CPE) and chlorosulfonated polyethylene geomembranes (CSPE); woven and non-woven geotextiles; fly ash, bottom ash, sand, site soil, and American Association of State Highway Transportation Officials (AASHTO) No. 8 aggregate.

Direct Shear Test. The shear characteristics of various geomembrane configurations were determined using modified American Society of Testing Material (ASTM) methods. Also, examination abrasion resistance characteristics of the synthetic materials were evaluated by visual examination. The material to be evaluated was placed in the shear plane and the device driven so that the shear resistance of the interfacing materials was determined. The geomembrane and geotextile materials were not anchored in the box but left to slide at the weakest interface. The soil or aggregates that would be above and below the synthetic materials were placed in the upper and lower shear box chambers to more closely model field conditions (Glogowski, 1992).

It was anticipated that the components of shear resistance for the interfacing materials would be somewhat variable depending on the normal stress conditions. Therefore, to model short and long term stability six different normal loads were used in the testing of each system model. Low normal stress conditions were used to determine stability during construction phases. Higher normal loads were used to assess long term slope stability, lateral deflection of materials on the geomembrane, and overall embankment stability.

The application of a geotextile on either side of the geomembrane provided suitable abrasion protection for the geomembrane. However, the introduction of the geotextile to a smooth HDPE geomembrane created low shear resistance values, which indicated that smooth HDPE systems would be limited in their application to sites with relatively flat slopes. Also, in the case of liner materials with "softer" surfaces (CPE and CSPE) some evidence of surface distress was created by lateral movement of the geotextile.

The lowest test-determined interface shear values (of the materials selected) were used to represent the liner system. Test results determined that the weakest interface was between the subgrade soil and woven geotextile. It is interesting to note that recent testing (1996) of a currently marketed nonwoven geotextile with the site soil, using a 30.5-cm [12-inch (in)] by 30.5-cm (12-in) direct shear test unit and following ASTM D5321-92, yielded nearly identical shear-normal values as the 1984 test results.

<u>Puncture Resistance Test</u>. The puncture resistance of the synthetic liner material was determined in a modified consolidation test apparatus. The lower chamber was filled with one of the candidate aggregate materials. The membrane material was fixed at the mid-level of the chamber so that a water-tight chamber was formed. The selected aggregate was then placed on top of the sample and load plate installed.

Normal loads approaching 1.5 times the anticipated embankment loadings were incrementally applied. After a normal load greater than 69 kPa (10 psi) was applied a 69 kPa (10 psi) water pressure was applied to the lower chamber. As the normal loads approached the anticipated embankment loads, the water pressure was cycled between 69 and 690 kPa (10 and 100 psi). The point of rupture of the membrane materials was noted. After maintaining 1.5 times the embankment loads for some time, the apparatus was dismantled, photographs of the membrane materials were obtained, and deformation and extent of failure was recorded.

Puncture resistance testing showed that although failure of the synthetic liner materials did not occur when bedded and covered with sand at loads approximately equivalent to 1.5 times the anticipated embankment loadings, significant distress of the geomembranes occurred. At particle contact points, geomembrane thickness was reduced to less than approximately 25% of the initial thickness.

For tests without geotextiles, when angular No. 8 gravel was used as bedding and cover material, 0.8 mm (30 mil) PVC failed at less than the anticipated embankment loadings and the

0.8 mm (30 mil) HDPE and 1.3 mm (50 mil) PVC failed at loads between the anticipated embankment loads and 1.5 times. With sand bedding and bottom ash cover, the 1.4 mm (55 mil) PVC resisted puncture at 1.5 times the anticipated embankment loads. CPE and CSPE materials showed excessive abrasion during direct shear and severe surface distress during puncture resistance testing, therefore, were not evaluated further.

In all tests with geotextile materials, significantly lower surface distress occurred. Also, it was possible for geomembranes that had previously failed under the anticipated embankment loadings to survive for the test period of two weeks when covered with geotextiles.

Geotextile Thickness Test. ASTM Standard D1777 was used to measure geotextile thickness under various loads. No relationship between thickness measurements under low loadings and higher loadings were observed. This gave rise to the thought that geotextile weight per unit area was a more appropriate factor in evaluating geotextiles used for geomembrane protection.

Testing Program Conclusions. Based on the testing program, it was concluded that:

1.   The application of geotextile material significantly reduced the effect of shear abrasion and point loads on the geomembranes,

2.   CSPE and CPE were susceptible to severe surface abrasion,

3.   Smooth HDPE had low shear resistance when protected with geotextile materials,

4.   A positive correlation does not exist between initial geotextile thickness and that measured under load, and

5.   The geotextile thickness did not reflect the protective qualities of the geotextiles monitored.

Therefore, protective geotextiles were initially selected based on the results of direct shear-abrasion testing and puncture resistance testing.

STABILITY EVALUATION OF THE GEOMEMBRANE LINER SYSTEM

The wedge method was used extensively in assessing the stability of extending the geomembrane system up the valley sides above the active waste surface, and in assessing the overall stability of the embankment, using the weakest interface in the liner system.

In some instances, the infinite slope analysis technique was also employed to evaluate the stability of the geomembrane system as it extended along the valley side slopes above the waste. Conventional circular arc stability analysis was conducted to evaluate local failures in the waste embankment.

A minimum static factor of safety of 1.2 was used for the liner extensions up the valley side slope since this was of a temporary nature. For this portion of the analysis, the underdrain leachate detection zone was assumed to control the build up of excess pore water. A minimum safety factor of 1.5 was used for the final site configuration (valley filled with waste).

EVALUATION OF WHEEL LOADS

Stresses beneath the wheels or tracks of construction equipment were calculated to develop curves of attenuation of vertical stresses with depth for track and rubber-tired vehicles. Boussinesq equations were applied to analyze shear stresses at the geomembrane for various equipment and slope conditions. Field tests were conducted on 0.8 mm (30 mil) PVC on flat and steep slopes, both with and without protective cushion geotextiles, to identify equipment restrictions and operating procedures to be employed in constructing the various layers of the system.

Small test pits were hand excavated in each of the above areas and geomembrane samples were obtained for visual inspection. Observations of reaction of the systems during placement and condition of the materials upon excavation formed the basis for the construction methods and QA/QC for the layers placed immediately over the liner.

THE SELECTED LINER SYSTEM

Based on the results of the laboratory and field testing and analyses, the following liner system was selected and installed:

- Subgrade:
  - Site soil compacted to 90% Modified Proctor Density (ASTM D1557).

- Underdrain/Leachate Detection Zone:
  - woven geotextile;
  - 30.5-cm (12-in) thick sand (PaDOT Type A) layer; and
  - 15.3-cm (6-in) diameter perforated SDR 23.5 acrylonitrile butadiene styrene (ABS) pipes at 30.5-m (100-ft) spacing.

- Primary Liner - a 1.3 mm (50 mil) PVC geomembrane sandwiched between two 339 g/m² (10 oz/sy) nonwoven cushion geotextiles.

- Leachate Collection Zone:
  - 61.0-cm (24-in) thick layer of bottom ash or sand screened to pass the 0.95-cm (3/8-in) sieve;
  - 15.3-cm (6-in) diameter perforated SDR 23.5 ABS pipes below central leachate drain; and
  - central leachate drain of geotextile-wrapped riprap-sized rock.

- Protective Cover Includes:
  - leachate collection zone;
  - woven geotextile; and
  - 15.3-cm (6-in) layer of unscreened bottom ash.

CONSTRUCTION METHODS AND QUALITY CONTROL

General Site Development. As stated previously, construction of the liner system began in 1984. The construction was started at the bottom of the upper valley and extended up the side slopes of the valley in subsequent years.

During each stage of the yearly liner construction, surface drainage from the surrounding runoff area was diverted to prevent excess water from entering the site during construction.

Clearing and grubbing of the site (staged construction) was completed as specified. Topsoil was stripped and stockpiled in predesignated areas out of the way of future development. Soil stockpile areas were assigned to meet the needs of cover soil for the waste disposal.

A network of diversion channels (see Photograph 2) were constructed to divert offsite runoff around the work areas. Areas were graded to eliminate slopes steeper than 3H:1V. Material excavated from these areas was either used as compacted fill or hauled to the soil stockpile areas for future use as soil cover on the disposal embankment. The subgrade consists of the top 15.3 cm (6 in) of the remaining in-place soil compacted to a minimum 90 percent Modified Proctor density. All surface stones larger than 15.3 cm (6 in) were removed. Any rock outcrop encountered during grading was overexcavated to a depth of 0.3 m (1 ft) and backfilled with compacted cohesive soil. After fine grading of the subgrade, the entire surface area was proofrolled with a 9,070-kg (10-ton) smooth-drum roller or a rubber-tired roller. Soft spots and seeps thus encountered were overexcavated and filled with appropriate fill (soil or drainage stone) and recompacted. The prepared subgrade was treated with an approved herbicide to prevent puncture of the liner by vegetative growth.

Photograph 2. Network of Collection and Diversion Channels.

<u>Ground-Water Underdrain/Leachate Detection Zone</u>. Ground-water underdrain/leachate detection pipes were installed on 30.5-m (100-ft) centers across the site. The 15.3-cm (6-in) diameter perforated ABS pipes were placed in AASHTO #57 stone envelopes encapsulated with nonwoven geotextile. Any springs encountered within the construction area were connected to the ground-water underdrain system. Woven geotextile was spread over the subgrade followed by the placement of an 0.3-m (1-ft) thick granular drain layer (PaDOT Type A concrete sand). Sand was placed in a single 30.5-cm (12-in) layer and compacted with a minimum of two passes of the bulldozer track area. The completed sand layer was fine graded to provide a uniform surface free of all windrows, bumps, and depressions. A layer of nonwoven geotextile was placed above the sand blanket to protect the PVC liner above the sand (see Photograph 3).

Photograph 3. Completed Sand Blanket Covered with Geotextile
Followed by PVC Liner Installation.

<u>Liner Installation</u>. A site-specific construction Quality Assurance/Quality Control (QA/QC) program was prepared prior to the start of liner construction. The program included procedures to be followed by both the installer and construction monitoring personnel so that the liner and associated geosynthetics, as well as their installation, would meet the specifications. The geosynthetic specifications were updated annually to keep pace with the rapidly advancing state of practice. The QA/QC program included the following items:

- Liner and associated geosynthetics testing results (conformance);
- Installation personnel experience requirements;
- QA/QC monitoring personnel experience requirements;
- Inspection of materials as delivered on site;
- Subgrade preparation approval;

- Installation procedures (laying, spreading, seaming, anchoring, weather conditions protection);
- Factory seaming tests (conformance)
- Field seaming tests and test frequencies (field and laboratory testing);
- Special details for liner connections to appurtenances;
- Daily field reports and documentation; and
- Patching and other repairs.

Prefabricated 1.33 mm (50 mil) PVC liner panels [not exceeding 30.5 m (100 feet) wide by 91.5 m (300 ft)], supplied by approved liner manufacturers were installed over the nonwoven geotextile (above the sand blanket) in the presence of the manufacturer's authorized personnel. The geomembrane was seamed using solvent bond lap joints. On slopes, the upslope panel was placed over the downslope panel. The contact area was wiped clean and bonding solvent was applied to both contact surfaces. All field seams were inspected visually and tested via air lance (ASTM D4437) over 100 percent of the seam. Samples removed from the field seams at specified intervals were tested in the laboratory for required peel and shear strengths. The approved liner was covered with another layer of nonwoven cushion geotextile (see Photograph 4).
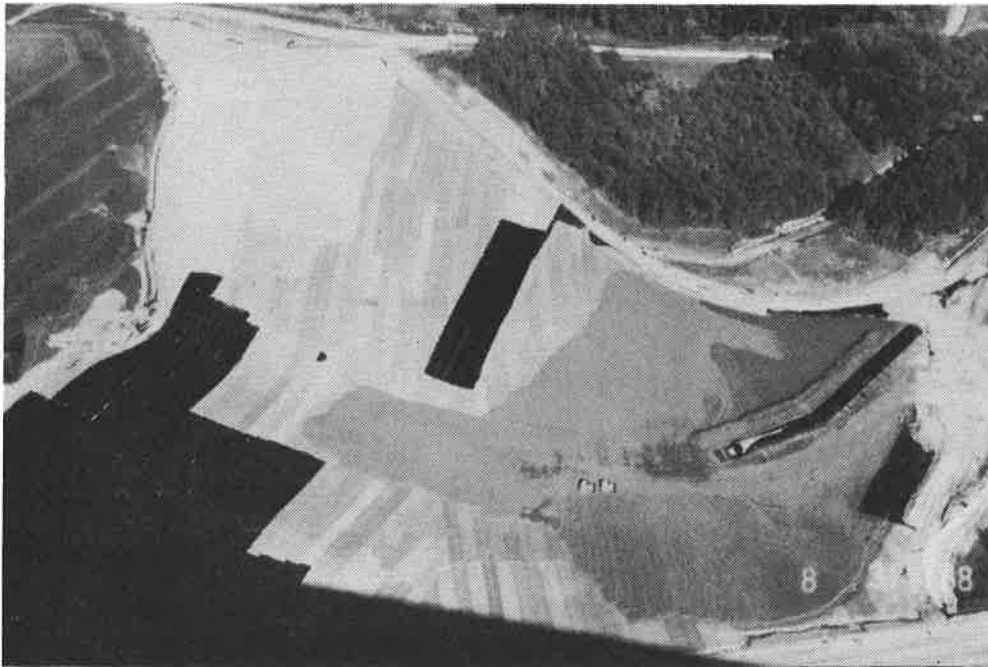
Photograph 4. Approved Liner Covered with Geotextile. Placement of 0.6-M (2-Ft) Layer of Graded Bottom Ash in Progress.

Leachate Collection Zone. Graded bottom ash [screened of particles larger than 0.95-cm (⅜-in)] was placed in one 0.6-m (2-ft) thick lift as soon as possible upon installation of the cushion geotextile over the liner. No vehicular traffic of any kind was allowed directly on the liner or

geotextile. Graded bottom ash was end dumped and pushed into place using a 140 hp dozer with a ground pressure not exceeding 48 kPa (7 psi). On slopes, the graded bottom ash was placed on the low side and pushed uphill. Vehicular traffic (other than one pass by the dozer track area) was kept to a minimum. The edge of the liner was placed in the anchor trench and covered with sand and soil cover as specified. Leachate collection drains were installed at required locations and connected to the previously installed central leachate drain or to the concrete pipe/weir box at the toe of the embankment.

Traffic/Waste Placement. No equipment was allowed to travel directly on any liner or geotextile material. Only a low-ground-pressure [48 kPa (7 psi)] dozer was allowed to travel above liner or geotextile areas, when there was the minimum of 0.6-m (2-ft) of cover (see Photograph 5). A minimum 1.8-m (6-ft) layer of cover material over the liner was required when operating vehicular traffic other than a low-ground-pressure dozer.
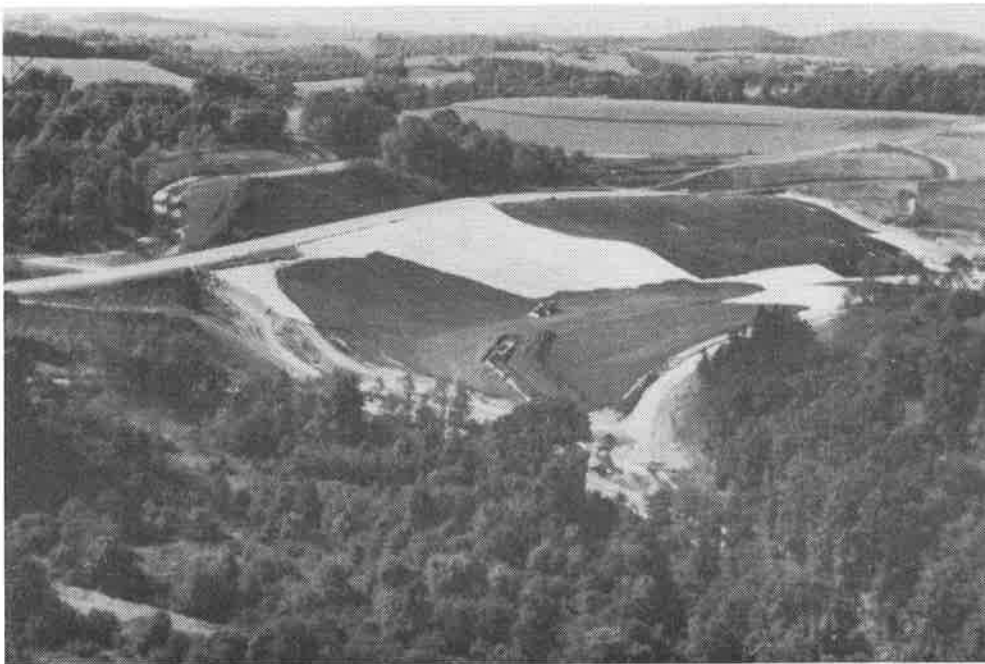
Photograph 5. Placement of 0.6-M (2-Ft) Layer of Graded Bottom
Ash. Leachate Collection Drain in the Foreground.

GROUND-WATER QUALITY ASSESSMENT

Introduction. A ground-water quality assessment was conducted to confirm observations from the disposal site's leachate collection and ground-water underdrain system. From visual observations (Photograph 6) and chemical analyses of the leachate and underdrain ground water (Table 1), it is apparent that the liner system is separating the leachate from the ground water.
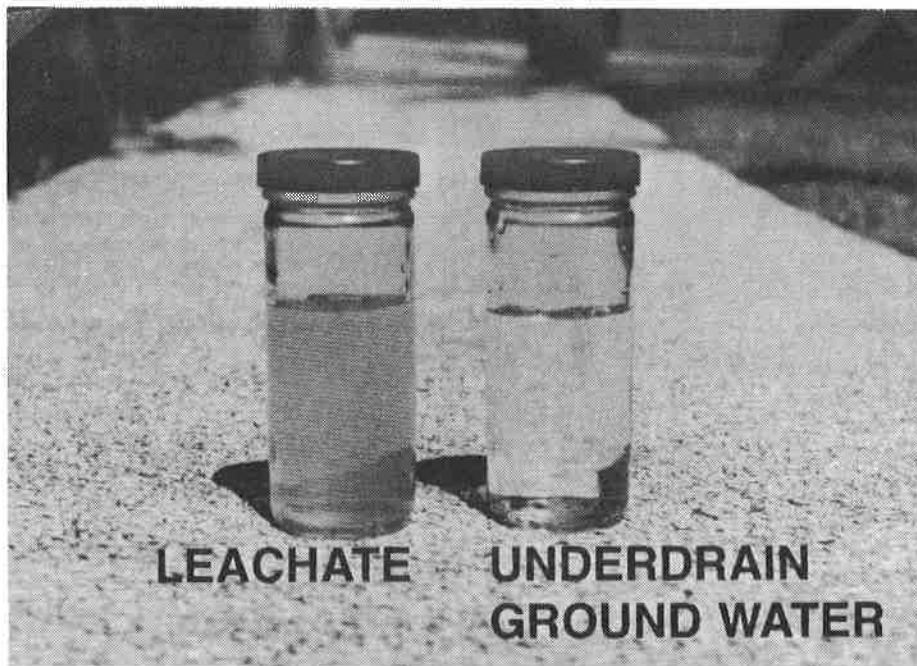
Photograph 6. Leachate and Underdrain Ground Water.

Table 1. Leachate and Underdrain Ground-Water Chemistry

Constituent/Parameter	Unit	Leachate	Ground-Water Underdrain
pH	S.U.	2.97	7.75
Specific Conductivity	μS/cm	7,330	434
Dissolved Iron	μg/L	803,400	40
Dissolved Manganese	μg/L	8,284	82

Note: Chemistry data collected during February 1996.

Aquifer Characteristics. The site's aquifer is characterized as a near-surface fractured bedrock, which varies in thickness from approximately 6 to 30 meters (20 to 100 feet). Ground-water flow through this fracture system follows the slope of the disposal site's valley topography. Therefore, ground-water flow is down the valley walls and out the mouth of the valley.

Ground-Water Monitoring Network. The monitoring network used to examine the site's ground-water quality consists of five monitoring wells: two background monitoring wells (MP-16 and MP-19), and three downgradient monitoring wells (MP-4, MP-17B, and MP-18) (Figure 2). These wells monitor the near-surface fractured bedrock aquifer. To detect the earliest occurrence of disposal site-related ground-water degradation, the downgradient monitoring wells were positioned across the mouth of the disposal site valley and close [i.e., within 61 m (200 ft)] to the toe of the disposal site. The downgradient monitoring wells

LEGEND

O	EXISTING MONITORING WELL
→	GROUND-WATER FLOW DIRECTION
1140 ——	GROUND-WATER CONTOUR AND ELEVATION (INFERRED WHERE DASHED)(MAY, 1994)
1000 ▬▬	STRUCTURE CONTOURS OF UPPER FREEPORT COAL HORIZON (CONTOUR INTERVAL 50 FEET)

REFERENCES:

1. BASE MAP TAKEN FROM: U.S.G.S. 7.5 MINUTE SERIES TOPOGRAPHIC QUADRANGLE ELDERTON, PA 1964, PHOTOREVISED 1973

2. STRUCTURE CONTOURS FROM GEOLOGIC ATLAS OF THE UNITED STATES, ELDERS RIDGE FOLIO, PA DATE OF MAPPING 1905

3. ALL WELL LOCATIONS ARE APPROXIMATE

SCALE: 1" = 2000'

Figure 2. Geology, Hydrogeology and Ground-Water Monitoring Network, East Valley Disposal Site

essentially monitor the entire fractured bedrock aquifer, and are designed to detect disposal site-related degradation migrating through the mouth of the disposal site valley.

To characterize background ground-water quality, a monitoring well was positioned at the head of the landfill valley and in the mouth of an adjacent valley. The monitoring well at the head of the landfill valley was intended to monitor ground-water migrating from the top of the valley. The well in the adjacent valley was positioned in a similar topographic setting as the downgradient wells, and was designed to monitor the same formations as the downgradient monitoring wells in the active valley.

Ground-Water Degradation Scenario. A theoretical ground-water degradation scenario was developed to determine if the established ground-water monitoring system is likely to detect degradation which originated since the existence of the disposal site (i.e., over the last 10 years). The one-dimensional Ogata-Banks equation (1967) (Domenico, 1990) was used to predict solute concentrations at the downgradient wells over time. The simulation assumed: the fractured bedrock aquifer as an equivalent porous media; a continuous source concentration equal to the leachate concentration at the disposal site valley head; and, an initial background ground-water solute concentration of zero. Only inorganic solutes which migrate at the same rate as the ground water were simulated.

Under these assumptions, solutes that originated from leachate at the disposal site valley head would be present in ground water at the downgradient wells in detectible concentrations in one to two years after the source was available. Furthermore, simulation results show that solute concentrations at the downgradient well locations would be near or equal the source concentration after the continuous source is available for a 10-year period. It is therefore concluded that the monitoring system described herein should have detected ground water degradation, if present at the site.

Ground-Water Quality Analysis. The five monitoring wells were sampled approximately once every six weeks from November 1993 to December 1994. Samples were analyzed for the constituents and parameters listed in Table 2.

Table 2. Parameters for Ground-Water Analysis

Dissolved Aluminum	Lead (Total and Dissolved)
Ammonia-Nitrogen	Magnesium (Total and Dissolved)
Bicarbonate	Mercury (Total and Dissolved)
Biological Oxygen Demand	Total Organic Halogens
Calcium (Total and Dissolved)	Orthophosphate
Chemical Oxygen Demand	Total Phenols
Chloride	Selenium (Total and Dissolved)
Fluoride	Silver (Total and Dissolved)
Iron (Total and Dissolved)	Zinc (Total and Dissolved)
Manganese (Total and Dissolved)	Benzene
Nitrate-Nitrogen	1,2-Dibromoethane
pH	1,1-Dichloroethane
Potassium (Total and Dissolved)	1,1-Dichloroethene
Sodium (Total and Dissolved)	1,2-Dichloroethane
Specific Conductance	Cis-1,2-Dichloroethene
Sulfate	Trans-1,2-Dichloroethene
Total Filterable Residue	Ethyl Benzene
Total Alkalinity	Methylene Chloride
Organic Carbon (Total and Dissolved)	Tetrachloroethene
Turbidity	Toluene
Arsenic (Total and Dissolved)	1,1,1-Trichloroethane
Barium (Total and Dissolved)	Trichloroethene
Cadmium (Total and Dissolved)	Vinyl Chloride
Chromium (Total and Dissolved)	Xylene
Copper (Total and Dissolved)	

The methodology developed to examine the ground-water quality data was designed in accordance with guidelines established by PaDEP. The methodology is based on a protocol

which utilizes statistically derived site-specific ground-water quality concentrations along with the United States Environmental Protection Agency (USEPA) Drinking Water Standards (USEPA, 1994a), to determine the presence or absence of ash/mine refuse related ground-water degradation at the site. This protocol uses statistical procedures and techniques described in USEPA documents (USEPA, 1989 and USEPA, 1994b) and recently published literature (Davis and McNichols, 1994).

For the purpose of this investigation, the statistically derived site-specific ground-water quality concentrations are referred to as potential degradation indicator levels (PDILs). The PDILs are compared to the data collected from the downgradient monitoring wells to assess the presence or absence of ground-water degradation. If a parameter's downgradient concentration exceeds its PDIL, it is concluded that the parameter's concentration in the ground water may be degraded as a result of the disposal site. If a parameter's downgradient concentration is less than the PDIL, it is concluded that the parameter's concentration in the ground water is not being degraded as a result of the disposal site.

The primary tool for constructing PDILs is MANAGES™ (Patel et al., 1993), an Electric Power Research Institute (EPRI) ground-water data management and statistical software package, and a commercial spreadsheet program. All the ground-water data collected during the assessment are stored in MANAGES™. Using the statistical and graphical tools provided in MANAGES™, the information required to develop PDILs can be obtained for each constituent and parameter. This information is manually transferred to a computer spreadsheet file where it is stored and further manipulated to develop the PDILs.

Results and Conclusions. None of the concentrations of parameters in the downgradient monitoring wells exceed their PDILs. Therefore, it is concluded the disposal site is not degrading ground water and the liner system is effectively separating leachate collected above the liner from ground water below the liner.

ACKNOWLEDGEMENTS

REFERENCES

Chester Environmental, (1994) Water and Air Management News. Volume 2, No. 1, Coraopolis, PA.

Construction Specifications, (1993) Stage 2B - 1994 Liner and Drainage Facilities Construction, Keystone, GAI Consultants, Inc., Monroeville, PA.

Davis, C. B. and McNichols, R. J., (1994) "Ground Water Monitoring Statistics Update: Part II Nonparametric Prediction Limits," Ground Water Monitoring & Remediation. Volume 14, pp. 159-175.

Domenico, P. A. and Schwartz, F. W., (1990) Physical and Chemical Hydrogeology. John Wiley and Sons, New York, pp. 636-639.

Gilbert, R. O., (1987) "Statistical Methods for Environmental Pollution Monitoring," New York: Van Nostrand Reinhold Company Inc.

Glogowski, Phillip E., (1992) Liner System Evaluation, Solid Waste Disposal Sites, Pennsylvania Electric Company, Project 89-342, GAI Consultants, Inc., Monroeville, PA.

Leggette, R. M., (1957) "Ground Water in Northwestern Pennsylvania," Bulletin W 3, Topographic and Geologic Survey, p. 215.

Mandel, J., (1964) The Statistical Analysis of Experimental Data. Dover Publications, Inc., New York, NY.

Patel, D. V., McCraw, D. A., Moser, D. B., Tye, T., Walther, D. E., Schurmann, M. W., Rusodimos, T., and McIntyre, D. L., (1993) "MANAGES™: Personal Computer Software for the Management and Evaluation of Ground Water Monitoring Data," V. 1.0. The Southern Company and Electric Power Research Institute.

Poth, C. W., (1973) "Summary Ground-Water Resources of Armstrong County, Pennsylvania," United States Geological Survey, Water Resources Division, Water Resource Report 34.

United States Environmental Protection Agency, (1989) Statistical Analysis of Ground-Water Monitoring Data at RCRA Facilities. Interim Final Guidance. Washington, D.C.

United States Environmental Protection Agency, (1994a) Drinking Water Regulations and Health Advisories. Office of Water. Washington, D.C.

United States Environmental Protection Agency, (1994b) EPA Regulations for Owners and Operators of Permitted Hazardous Waste Facilities. 40 CFR 264.97(i). Washington, D.C.

GEOSYNTHETIC USE IN MINING APPLICATIONS

Dirk Van Zyl, P.E., Ph.D.
Brian Simpson, P.E.
Golder Associates Inc.
Denver, Colorado, USA

ABSTRACT

Geosynthetics are widely used in mining applications. Such uses include geomembranes for containment and geotextiles for material segregation and drainage. This paper provides a broad overview of some of the uses of geosynthetics in mining. This overview is accomplished by considering uses in different mining applications. Heap leach facilities, tailings impoundments, waste rock dumps, and infrastructure are considered separately. It is clear that in general, geosynthetics are exposed to higher stresses in mining than in most general civil applications and that some issues are still not fully addressed when compared to other environmental applications. These issues are identified and discussed in further detail.

INTRODUCTION

Geosynthetics have been widely used in the mining industry over the last two decades. These uses include geotextiles for filter media, geomembranes for containment, and geogrids for reinforcing. In general, geosynthetics have performed satisfactorily and have improved the economics of mining projects. Some failures have occurred, mostly related to slope stability as a result of interface friction angles. Some of these failures have been reported in the literature (Poulter 1994) and (Breitenbach 1996) while in other cases, they were evaluated in various levels of details and kept confidential. This paper provides an overview of use of geosynthetics in mining applications. Various applications are considered as they relate to different mining facilities. Typical design approaches are discussed and outstanding issues where further research and evaluations are required, are identified.

REGULATORY AND ECONOMIC CONSIDERATIONS

The mining industry produces commodities which are sold on the free market based on commodity prices. During the development of a new mining project, economics are an important consideration. In the case of landfills and some other public projects, the cost of the project can be passed on to the consumer, however, this can not be done in the mining industry. The use of geosynthetics in the mining industry is therefore, a function of project economics and the economic use of natural materials.

In the US, the landfill and hazardous waste industries are regulated through federal statutes and regulations. Regulations promulgated under Subtitle C and D of the Resource Conservation and Remediation Act (RCRA) of 1976 and subsequent amendments control, to a large extent, the design details and usage of geosynthetics in the solid waste landfills and hazardous waste landfills. Much of this information has been used as background in the mining industry, however, such prescriptive federal regulations do not exist for the mining industry.

In the case of the mining industry, the various state regulations passed under the Clean Water Act (1977) and various state mine reclamation acts control the design considerations for geosynthetics. Most of these regulations are based on performance criteria instead of being prescriptive. This allows engineers who work in the mining industry flexibility to develop innovative designs and incorporate new materials as they become available. This aspect is important in maintaining the economic realities for the mining industry.

Environmental issues typically addressed in the mining industry deal with the protection of groundwater and surface water resources. Containment, therefore, is the most important consideration.

Various chemicals are used in the mining industry for the extraction of metals from minerals. Hydrometallurgical processes can be used for the extraction of gold, silver, and copper. In the case of gold and silver, cyanide solutions are used as a lixiviant. In the case of copper, sulfuric acid is used as a lixiviant. Flotation processes can also be used for mineral extraction. In this case, small amounts of organics and other chemicals are used. The resulting liquid usually contains low concentrations of chemicals. Mostly, all geosynthetics available on the market are compatible to the chemicals commonly used in the mining industry. Within the pH ranges (typically 2 to 10.5), geomembrane materials are resistant to corrosion and geotextiles can be safely used. Exposure to the elements is usually of more concern than exposure to the chemicals.

The following sections will discuss the use of geosynthetics in heap leach facilities, tailings impoundments, waste dumps, and mine infrastructure development.

HEAP LEACH FACILITIES

Heap leaching is widely used for the extraction of gold, silver, and copper. Low grade ores are stacked on the heap leach pad, lined with low permeability materials. The lixiviant is applied to the top of the heap and percolates through the heap under unsaturated conditions to the low permeability layer. The pregnant solution is then collected in lined ponds and the metal is removed through various processes (Van Zyl, Hutchison, and Kiel 1988). The two most important considerations, in terms of heap leach facilities where geosynthetics are used are containment and drainage.

Typical issues of concern in the design of heap leach facilities are:

- Coarse materials (sometimes up to a maximum particle size of 4 cm) are in direct contact with geomembrane materials.

- Static stresses imposed on the geomembranes are typically very high and, in some cases, heap heights can reach 125 m.

- The survivability of man-made drainage media that are used for leachate and leak collection under very high loads must be considered.

- Pond liners are exposed to mechanical and ice loading. Mechanical loading could be due to the dragging of pipes on the liner or the re-movements of pump barges within the ponds.

- Interface friction angles between the ore and the geomembrane and between the underlying low permeability soil liner and the geomembrane should be considered on a site specific basis.

An important design consideration is the overall behavior of geomembrane liner materials and the philosophy used in developing a liner system design. There are only two parameters which can be controlled during liner design, these are: the hydraulic head on the liner and the permeability of the liner. In the case of heap leach facilities, composite liners have been successfully used for containment. The hydraulic head on the composite liner is typically very low, that is, below one meter. In the case of valley leach facilities, higher heads can be present since the pregnant solution is contained in the pore space of the heap. A composite liner with a low hydraulic head is considered the optimum design for most heap leach facilities.

Surface solution ponds are often associated with heap leach pads. Barren and pregnant solutions are stored in lined impoundments or ponds. Pregnant solution ponds collect the solution which is percolated through the heap to extract the mineral resources. The solution is

then processed to remove the recoverable minerals and the resulting barren solution is sent to a lined pond for storage until new chemicals are mixed in to produce the desired lixiviant which is then re-applied to the heap. In the case of ponds where a high hydraulic head is present, a drainage layer with an extra geomembrane is placed on top of the composite liner. In this case, the purpose of the upper geomembrane is to reduce the head on the composite liner because any leakage through the upper liner will be removed via the drainage layer. The most important lining component is still the bottom composite liner in this case. Leakage through the upper liner is collected and removed from the leakage collection system. The upper geomembrane and drainage layer should not be referred to as the leak detection system since they are located above a composite liner which is the most important component of the overall system. Leak detection can only occur once leakage has entered the environment below the composite liner system.

Typical geomembrane types that have been used in heap leach operations include, polyvinyl chloride (PVC), high density polyethylene (HDPE), linear low density polyethylene (LLDPE), and, when available, very low density polyethylene (VLDPE). Other materials have been used for collection ditches and ponds in the past such as Hypalon and XR-5, but their use has decreased over the last decade. Polyethylene geonets have also been used as drainage media. Woven and non-woven geotextiles of various thicknesses and materials are also widely used.

The typical design approach for geomembranes include the following: 1) In order to evaluate the behavior of geomembranes under static loading from the heap, interface load testing is performed using the materials proposed in the design. This testing can be performed using large diameter load cells. The load cells have to be sufficiently large diameter to minimize scale effects. The typical size of granular material placed against geosynthetics may be on the order of 1.25 cm to 4 cm for mining applications. Typical ranges of required vertical load are 550 kPa to 2,000 kPa. The load is applied to the top of the load cell. The proposed liner, drainage and overliner materials are placed within the load cell in a manner similar to that proposed for the project. The vertical load is applied and maintained, typically 24 to 48 hours. Settlement of the samples can be monitored to verify the sample consolidation. At the completion of the loading cycle, the samples are removed from the load cell and visually inspected for damage. Damage is generally described subjectively based on:

- Number of abrasions;
- Indentations; and,
- Punctures.

A vacuum box test can also be performed to determine geomembrane integrity.

In addition to the above, the physical properties of the tested geomembrane can be obtained from standard geosynthetic tests and compared to results for virgin samples. Using this type of load test, results are obtained to make judgments about the compatibility of the materials and their behavior under static loading.

2) Another very important issue is the interface shear strength of geomembrane in contact with various materials. These tests are typically performed using large scale direct shear testing. Interface testing is typically performed using ASTM D5321 procedures. The interfaces are evaluated under a range of loading conditions including:

- Saturated conditions;

- Wetted interfaces (not saturated);

- Low to high normal loads (some flattening of shear strength envelope is common at high normal loads); and,

- Various shear rates.

The lining and drainage system may have numerous potential failure planes. Often, several different interfaces under the various loading conditions must be evaluated in order to determine the weakest (controlling) interface. Residual and peak envelopes should both be determined. Residual values are typically used for stability analyses.

For one particular heap leach project, Golder performed numerous interface shear strength tests using the large scale shearing device (30 cm by 30 cm) and several proposed geosynthetics and soil components. Both HDPE and LLDPE materials were tested and both peak and residual shear strength values were measured. The results of the testing indicated that the underliner (fine grained soil) component and the overliner (coarse grained drainage layer) did not significantly alter the interface strength over the load range considered. In addition, the measured peak and residual values were identical. The only significant variation encountered was a slight change in the friction angle with geomembrane type. Figure 1 shows the two trends for interface shear strength found for this particular project.

3) Leakage estimates are made using the expressions developed by Bonaparte, Giroud, and Gross (1989). It is typically assumed that one 10 mm^2 hole is present per 0.4 hectares of area.

Regarding the use of geosynthetics in heap leach facilities, a number of issues have not yet been addressed through research. These issues are, in many cases, more for curiosity than a specific technical design concern. One specific issue is the long-term behavior of various geomembranes under loading when in direct contact with granular materials. Load testing in the laboratory is typically done over a period of a few days at most, while loading in the field

will last during the length of operations (typically 2 to as much as 10 years). It is unknown whether creep deformation will occur or whether punctures could develop under the sustained static stresses. It is also unknown whether punctures developed under these loading conditions will be self-healing in nature (that is the particle may mostly fill the puncture and therefore not allowing significant leakage).

Very few heap leach facilities have been excavated to investigate the performance of geomembranes. A qualitative evaluation was made of a heap leach liner in Colorado during 1995. A heap leach facility was built on top of a tailings impoundment and was extended on a natural slope adjacent to the tailings impoundment. The natural slope was as steep as 2H:1V. Pad design consisted of a HDPE geomembrane on the natural ground with a layer of geonet and overlying HDPE. The heap was about 60 m, at its highest point. When the spent ore was excavated, samples of the geomembrane materials were examined. These investigations showed no specific distress of the geomembrane or the seams and no puncturing was observed in the few pieces that were evaluated.

Another issue of concern is the long-term behavior of geomembrane/geonet interface when subjected to high fluid pressures such as a very deep pond where a geonet is placed between two geomembranes. It is uncertain whether there will be penetration of the geonet into the geomembrane material under the imposed load and, thereby the potential for development of leaks in the geomembrane over the long-term. Some cases of partial penetration of the geonet into geomembranes have been observed. Typically, this occurs when the geomembrane is of lower density than the geonet resulting in the geonet being relatively stiff compared to the geomembrane.

The effect of consolidating materials on the interface forces along the sideslopes in valley fills is an issue which is typically not addressed. Varying settlement will occur throughout the heap due to the variations in thickness of the placed ore. This can result in displacements along the geomembrane on the sideslopes which can affect the stability of the heap. Residual shear strength values can be quickly approached with only minor movements along the geomembrane on the sideslopes. This issue can be evaluated using numerical methods (Byrne 1994) to determine the available shear strength based on the estimated displacements due to the consolidation settlements.

The use of geotextiles as a cover for drainpipes in heap leach facilities are not typically favored because some clogging has been observed. In the case of copper heap leaching, the presence of bacteria is part of the process. The potential remains of these bacteria have been blamed for clogging of geotextiles surrounding drain pipes. This issue has not been addressed in any detail to date relative to mining processes.

The potential for clogging of drainage systems in heap leach pads is important since the mineral values are recovered using the drainage system. In addition, if the geotextile clogs, high hydraulic heads may develop within the pad which could lead to stability problems. Also, for sulfide ores it is important to maintain an oxidizing environment for the leaching process to be successful. If a geotextile clogs and the ore begins to saturate, the recovery of the metal values declines.

TAILINGS IMPOUNDMENTS

Tailings are the fine materials which remain after extraction of metals from ore when extraction is done in a mill or concentrator. The grain-size distribution of tailings is typically that of very fine sand to silt. In many instances, tailings contain up to 60 percent minus 0.075 mm sieve size materials.

The containment of tailings liquid contaminants and drainage to reduce the head on the liner are major concerns in the use of geosynthetics for tailings impoundments. The control of the phreatic surface within the tailings impoundment is critical to the design of the containment system. Some impoundment designs use upstream construction techniques which rely on maintaining the phreatic surface away from the impoundment dam face in order to ensure stability. Geosynthetics are used as a permeability barrier during initial tailings placement in front of the dam since the tailings are placed as a slurry. In addition, geosynthetics are used to construct the bottom containment liner system and the underdrain system. Immediately following deposition of the tailings, dewatering is started utilizing an underdrain and surface pool (supernatant) management. The water management systems are used to lower the phreatic surface near the dam face to maintain drained soil behavior. Typical configurations of tailings impoundments are shown in Figure 2.

Issues that should be addressed during design are the liner and drainage system configurations and how they will behave under various heads. Tailings are deposited as a slurry, and the interaction of the slurry with the liner must be considered specifically under winter operations in cold climates. Beaches typically form and it is important to consider the effect of these beaches on the geomembrane behavior. After closure, it may be necessary to maintain the performance of the geomembrane for long-term containment. Long-term behavior of geomembrane and the overlying drainage layers is also an issue which must be addressed.

Typical geomembranes used for tailings impoundments include HDPE and LLDPE. VLDPE was also widely used when it was available, while PVC is not widely used because of its sensitivity to UV exposure. Woven and non-woven geotextiles are also used.

The typical design approaches include leakage estimates through liner systems based on one 10 mm^2 hole per 0.4 hectares. Operational plans are often compiled for tailings impoundments so that careful consideration can be given to potential interface forces which may develop on the liner as the tailings slurry consolidate. Variations of settlement throughout the impoundment result in widely variable stresses and strains within the geomembrane liner.

Some of the outstanding issues which should be addressed for tailings impoundments include the effect of settlement of tailings materials on the interface forces on slopes. Since tailings are deposited in slurry form with very high void ratios, significant consolidation occurs under self weight and under the weight of subsequent layers of tailings. The drag forces exerted by the consolidating tailings could lead to tearing or puncturing of the geomembrane. Experience shows that failures of this type have generally not occurred due to such interface forces, however, a better understanding of this should be developed.

Another issue is the clogging of geotextiles due to various chemical and bacteriological actions. Several researchers have studied the clogging of geotextiles under various situations but definitive design procedures for tailings impoundments are lacking. If geotextiles are used for drainage systems which contain sulfide tailings products, clogging of the geotextile may occur due to formation of precipitates at the interface of reducing and oxidizing environments. The tailings impoundment is often a reducing environment and the drainage system may be an oxidizing environment since it is usually open to the atmosphere.

The use of geotextiles within drainage systems for tailings impoundments can be a critical component for proper impoundment operation. As described previously, upstream tailings embankment construction requires careful management of the phreatic surface. Often, an underdrain system utilizing geotextile filters and separators is used to construct the underdrain system. If the geotextiles become excessively clogged during the impoundment operation, the phreatic surface may rise and jeopardize the impoundment embankment stability.

WASTE DUMPS

Waste dumps consisting of waste rock or mineralized rock contain too little ore to be economically processed. Waste rock dumps can be as high as 300 m or more and are typically formed through end dumping and dozing. Particle sizes range from silt size to very large rock, sometimes 2.5 m in diameter. The biggest issues associated with the use of geosynthetics in waste rock dumps is their use as drainage media. Woven and non-woven geotextiles are typically used in such drainage systems.

A typical design approach is to estimate the flow rates from site hydrological evaluations and spring and seep surveys. Geotextiles are used to separate the drainage material from the surrounding natural materials. The drainage materials can typically be 20-cm to 30-cm diameter rock. Geotextile layers under these conditions are subjected to very high loads.

An outstanding issue is the potential clogging of geotextiles due to various chemical and bacteriological influences. The significance of clogging of geotextiles in waste rock dumps is generally not as great as for heap leach pads and tailings impoundments. Most waste rock dumps are sufficiently coarse grained that excess pore pressures do not build up within the dump and jeopardize overall stability.

INFRASTRUCTURE

Mine infrastructure such as roads, airfields, etc. often include the use of geosynthetics. Materials segregation, reinforcement, and drainage are some of the biggest concerns in these conditions. Standard design procedures typical for development of highway projects and other public works are used and no specific outstanding issues specifically related to mining applications are known.

CONCLUSIONS

The mining industry presents many challenges for the design and use of geosynthetics for containment and drainage applications. Mining applications for geosynthetics are primarily the result of economic factors which push the design applications to less expensive, more effective components. Costs for mining projects are not directly passed on to the consumer since the mining industry produces commodities which are sold on the free market. The economic factors drive the designs of heap leach pads, tailings impoundments, and waste dumps to the engineering limits of the component materials resulting in minimum acceptable factors of safety, and "cutting edge" applications for materials.

REFERENCES

Bonaparte, R., Giroud, J.P., and Gross, B.A. (1989). "Rates of Leakage Through Landfill Liners", Proceedings, Geosynthetics 1989 Conference, San Diego, California, pp. 18-30.

Breitenbach, A.J. (1996). "Overview of Geomembrane Liner Failures," Proceedings, Tailings and Mine Waste '96, Colorado State University, Balkena Publishers.

Byrne (1994). "Design Issues with Strain-Softening Interfaces in Landfill Liners," Proceedings, New Directions in Geotechnical Engineering, Denver, Colorado.

Poulter, D.A. (1994). "Leach Pad Liner Stability on Slopes-Two Case Histories," Proceedings, Tailings and Mine Waste '94, Colorado State University, Balkena Publishers, pp. 205-214.

Van Zyl, D., Hutchison, I.P.G., and Kiel, J. (1988). "Introduction to Evaluation, Design, and Operation of Precious Metal Heap Leaching Projects", Society of Mining Engineers, Inc., Littleton, Colorado.
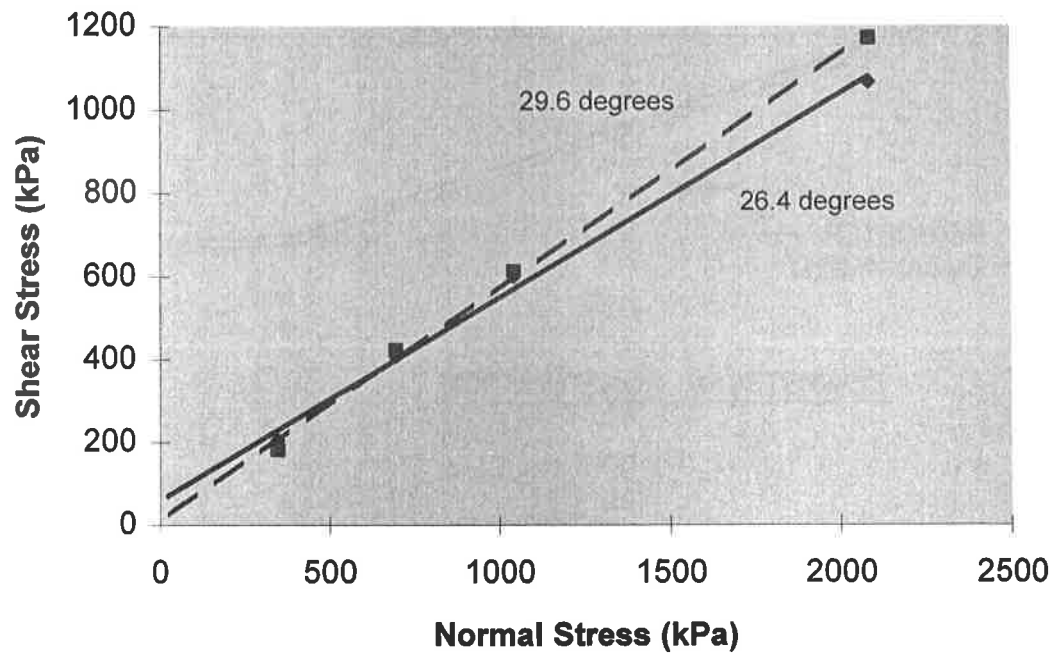
Dashed Line = Wetted interfaces, 100 mil smooth HDPE overlain by drain material (4 cm maximum), underlain by soil liner.
Solid Line = Wetted interfaces, 80 mil smooth LLDPE overlain by drain material (4 cm maximum), underlain by soil liner.

Figure 1 - Typical Shear Strength Test Results

TAILINGS SURFACE

FREEBOARD

PERIMETER
EMBANKMENT

DOWNSTREAM CONSTRUCTION

UPSTREAM RAISE

TAILINGS SURFACE

MAXIMUM TAILINGS ELEVATION
PRIOR TO RAISE

GEOMEMBRANE

PHREATIC
SURFACE

STARTER
EMBANKMENT

DRAINAGE SYSTEM

UPSTREAM CONSTRUCTION
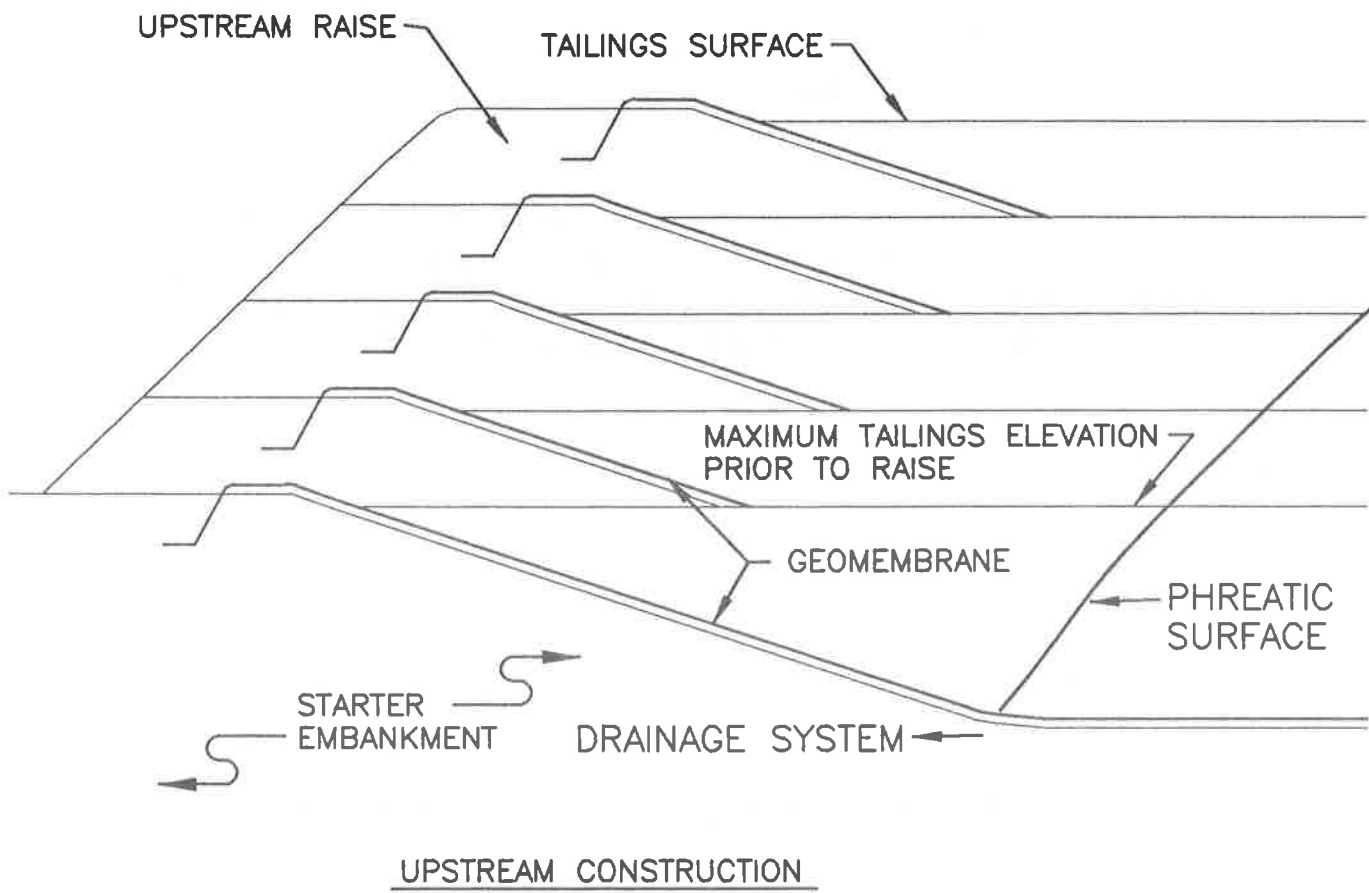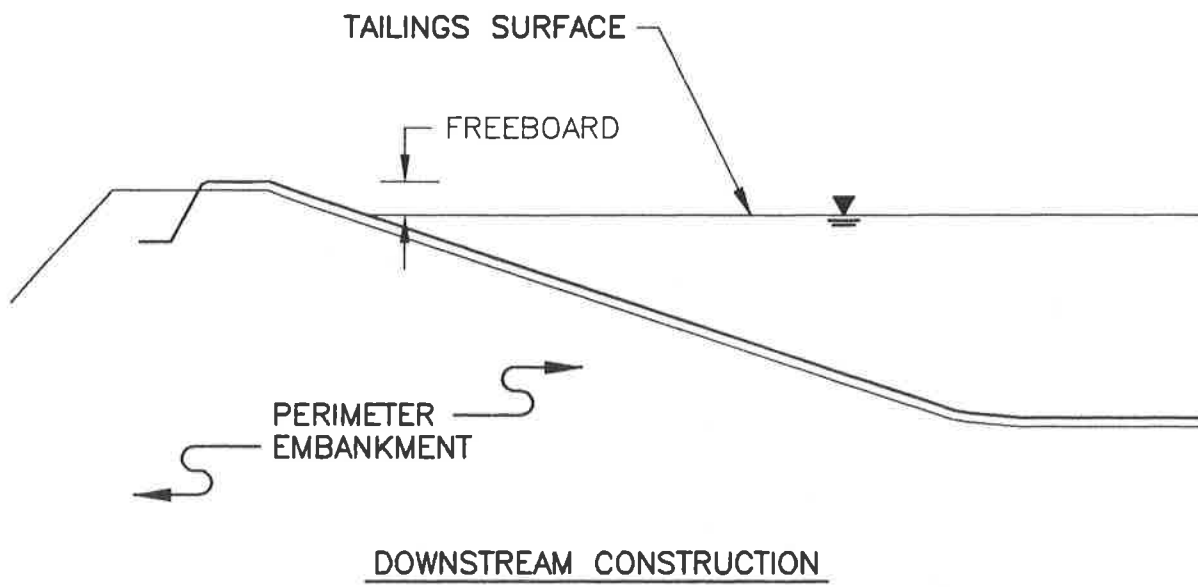
FIGURE 2 TYPICAL TAILINGS IMPOUNDMENT CONFIGURATIONS

Filtration

GEOSYNTHETICS 97
CONFERENCE
Long Beach, California USA

SIGNIFICANCE OF PERCENT OPEN AREA (POA) IN THE DESIGN OF WOVEN GEOTEXTILE FILTERS

JACEK MLYNAREK
SAGEOS, CANADA

GERARD LOMBARD
SAGEOS, CANADA

ABSTRACT

Design criteria for geotextile filters are discussed often among researchers and numerous design techniques based on empirical and theoretical considerations have been established. Most of the established techniques are for nonwoven geotextile filters. Few techniques have been proposed for woven geotextile filters.

The best known criteria for the selection of woven fabrics for use in filtration applications are those proposed by Calhoun (1972) whose work was incorporated by the U.S. Army Corps of Engineers into its construction guide for the specification and selection of geotextiles for filtration and erosion control applications (COE CW02215, 1977). Calhoun's criteria state that, wherever possible, one should use a fabric with the greatest Percent Open Area (POA) allowed by the criteria (specifically; a POA of up to 40% for soils containing 50% or less of particles passing the No. 200 sieve or a POA of up to 10% for soils having little or no cohesion and containing more than 50% silt by weight).

A recent trend in geotextile filter design has been to remove the POA parameter from filter design criteria altogether. Research data on the filtration behavior of geotextile filters have revealed, however, that the POA of a geotextile as well as its Maximum Percent Open Area (MPOA) are important parameters in the proper selection of a woven geotextile filter.

Research data on the filtration behavior of fifteen woven geotextiles and seven soils were gathered and the conclusions resulting from their analysis are presented in this paper. In this work, the incidence of observed piping phenomena is used to confirm the impact of three filtration properties, POA, MPOA, and characteristic opening size O_{95}, on woven filter performance.

It was found that filtration phenomena occurring at a soil/geotextile interface are extremely complex and require careful consideration. The gathered data support a general

conclusion that the POA is the main parameter which should be taken into consideration in any woven filter design process. It was also found that for some woven geotextile filters the POA varies when measured at different angles of light projection. It is therefore recommended that designers apply the greatest measured value of percent open area, the so-called Maximum Percent Open Area (MPOA), when designing woven filters.

KEY WORDS : Wovens, Filters, POA, Pore size, Design

INTRODUCTION

The first recorded use in the U.S. of a geotechnical fabric for erosion control occurred in 1958, when Carthage Mills developed a permeable synthetic woven fabric to replace a graded granular filter in a waterfront structure in Florida.

Before nonwoven geotextiles were introduced into the geotechnical products market, one of the most important criteria to consider when designing geotextile/soil filtration systems was Percent Open Area (Calhoun, 1972). According to the Corps, an appropriate POA promotes the initial passage of fines through the fabric thus developing an interim filter at the soil/geotextile interface. This contradicted later conventional design criteria for retention which ensured that soil particles do not pass through the geotextile. However, Giroud (1996) as well as other researchers such as Lafleur et al. (1993) and Austin et al. (1997) change the perception of geotextile filters behavior. Today, it is understood that geotextile filters and granular filters promote the formation of an interim filter in soil adjacent to the filter by promoting the initial passage of fines through the filter at the soil/filter interface.

In summary, the accepted qualitative hydraulic requirements for a geotechnical fabric in seepage/drainage applications are as follows :

1. The geotextile should not allow piping (e.g. retention and clogging) of the protected soil, except that some initial loss of fines may be acceptable to promote the formation of an interim filter in soil adjacent to the geotextile;

2. The fabric should not have a lower permeability than the soil and its presence should not cause an in-service reduction in permeability of the soil/geotextile system.

The question arises as to which property of a filter should be applied in the design process to ensure the promotion of an interim filter.

FILTRATION MECHANISMS

A geotextile installed in an earthen structure can be altered in time by many phenomena such as clogging, blocking, blinding, piping, and others. Clogging occurs when particles retain

within a geotextile structure. Particles and sediments can also be stopped upstream of a filter forming a layer which affect the filtration and drainage functions of the geotextile. The phenomena involved are defined as blocking and blinding mechanisms. The migration of fines in localized paths is referred to as piping.

Investigations into the mechanisms which affect the operation of geotextile filters show that following a filter's installation, fine particles within the zone closest to the filter migrate towards the filter. Fines with a smaller diameter than the geotextile openings and located adjacent to the fabric will be carried into the geotextile by flowing water. These fines will be evacuated into the drainage system or will be trapped permanently among the fibers. As fines are washed from the base soil, the coarser particles located at the interface will maintain their positions and a natural filtration zone will be formed immediately above the soil/geotextile interface. These larger particles will in turn stop smaller particles that will in turn stop even finer particles. As a consequence, coarse particles at the geotextile interface commence a filtration phenomenon within the soil itself and fines migration stops. It is clear that the geotextile filter acts essentially as the catalyst which induces the formation of the natural filter in the soil. For ideal performance of the geotextile filter, the hydraulic conductivity of the particles network at the soil/filter interface, as well as of the geotextile filter itself, should always be equal to or greater than the hydraulic conductivity of the parent soil (Giroud, 1996).

Thus, to achieve optimal results in filter performance, two phenomena must take place :

1. Following an initial period of instability which occurs during the formation of the soil filter, the hydraulic conductivity of the soil/geotextile system should remain relatively constant with time;

2. Following the initial period of soil piping (wash-out) which occurs during the formation of the soil filter, no further soil should be piped through the filter.

A simple solution to these critical phenomena is to select a geotextile filter with uniform openings small enough to retain the fines, yet large and frequent enough to allow any free fines within the adjacent soil to pass through the geotextile. This results in the formation of a bridge network or interim filter in the soil immediately adjacent to the fabric and provides the majority of future filtration and retention. Once this has been established, piping (loss of fines) ceases and the system is considered to be in equilibrium. At this point, the filter is actually contributing to the permeability of the geotextile/soil filtration system by retaining the interim filter in place and preventing it from collapsing into the drainage layer. If the initial release of fines through the fabric had not taken place, then clogging of the geotextile and/or blinding or blocking of the soil immediately adjacent to the geotextile could have occurred.

FILTRATION PROPERTIES OF GEOTEXTILES

To satisfy all of the filter criteria (by forming an ideal soil/geotextile filter system), the interaction between the base soil and filtration properties of the geotextile must be adequately

determined. The retention aspect of these criteria are related to pore size (distribution, maximum size, mean size), the frequency of the pores present, and their total area.

For woven fabrics, the weave or design is the manner in which the warp and weft are interlaced. This crossing of yarns during weaving produces various textures. The use of thread diagrams and cross-sections are ways of representing weaves. The basic structures of the most common weaves are presented in Figure 1, showing plain, twill, and satin weaves (Lu et al., 1996).

a) 1/1 Plein   b) 2/2 Twill   c) 4/1 Satin
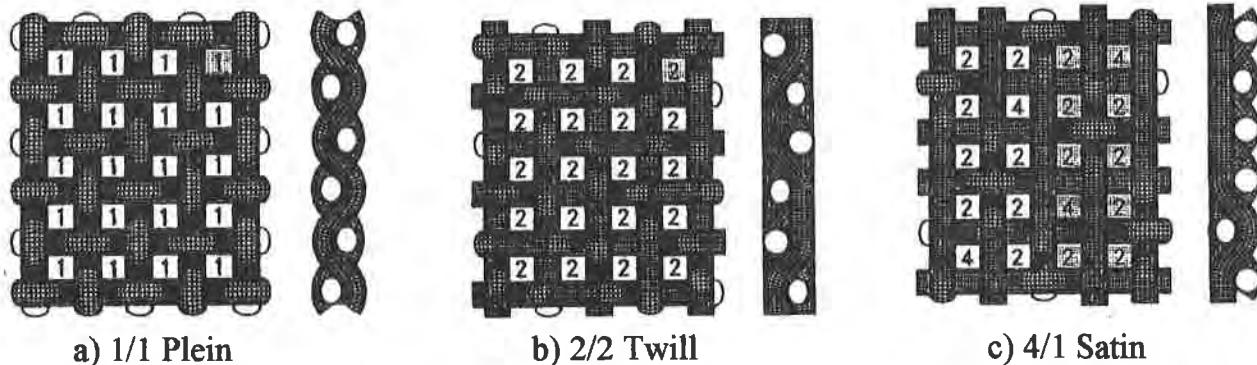
Figure 1 : Three basic weave models of woven filters (Lu et al., 1996)

In a plain weave, each weft yarn passes alternately over and under each warp yarn. It has the highest number of interlacing as compared with other weaves and therefore it produces the firmest fabrics, with square or rectangular openings.

Twill weave is similar to plain weave. The openings are straight through, but it differs in that each weft yarn alternately crosses over two and under two warp yarns, making a diagonal pattern.

In satin weave, the crossing points are less numerous than in plain weave. Each weft yarn crosses a specific number of warp yarns, for example four, so that one yarn floats above three other yarns in a perpendicular direction. This design is mainly used for esthetic purposes because of its lustrous effect.

The behavior of woven geotextiles is not only influenced by the type of weave but also by the structure of the elements used for the fabrication of the fabric, as shown in Figure 2. The yarns can be in the shape of monofilament round or oval, multifilament or tape flat (extruded or fibrillated). This parameter influences the rigidity, the thickness, and the opening size of the geotextile filter.

With simple basic woven structures as shown in Figure 3, the opening size and percent open area (POA) can be easily calculated (Kulichenko and Van Langenhove, 1992) :

Percent Open Area (POA) : $POA = S_V/S_T$

Open surface : $S_V = (a - d_1) \times (b - d_2)$

Total surface : $S_T = a \times b$

$a = 100/n_1$ $b = 100/n_2$

where :
n_1 - number of warp yarns per 100 mm
n_2 - number of weft yarns per 100 mm
d_1 - diameter of warp yarns (mm)
d_2 - diameter of weft yarns (mm)

$$POA = [(100/n_1 - d_1) \times (100/n_2 - d_2)]/[(100/n_1) \times (100/n_2)]$$

a)
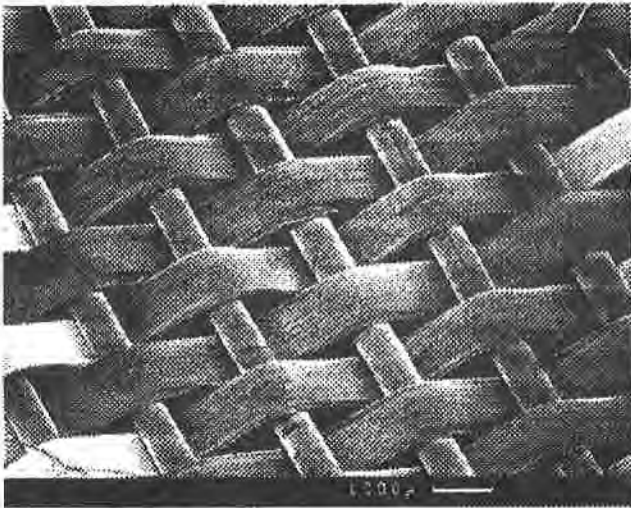
b)

c)
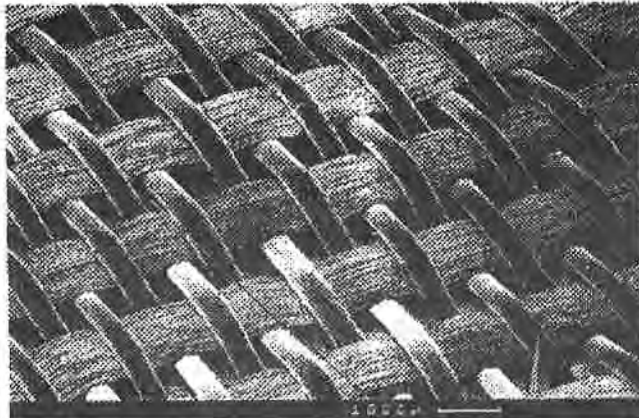
Figure 2 : Some types of woven fabrics
a) woven extruded monofilament;
b) woven fibrillated yarn
c) woven multifilament-on-monofilament
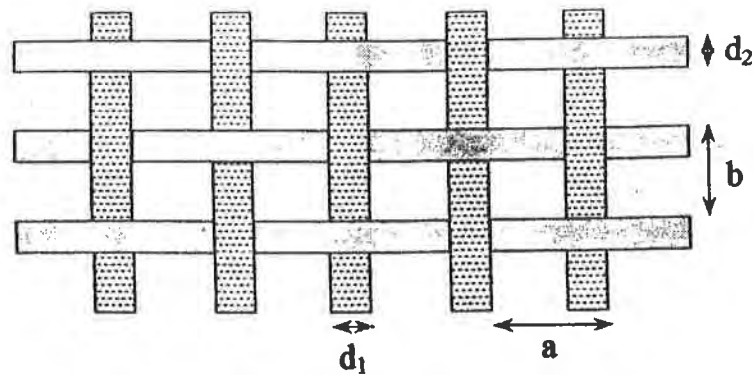
Figure 3 : Schematic presentation of simple woven structure

Optical methods constitute easy direct measurement techniques of the pore size of woven geotextiles (Islam and Bandra, 1996) by measurement of pick spacing or space between yarns. Optical methods can also be used to measure Percent Open Area (Calhoun, 1972).

In nonwoven fabrics, fibers or filaments are randomly distributed. The cohesion between fibers, e.g. strength of the fabric, is obtained at the final stage of the manufacturing process. This bonding action can be mechanical (needle-punching), thermal (heat-bonded), or sometimes chemical. Some non-woven structures are shown schematically in Figure 4. The type of bonding influences the rigidity, the thickness, the density, and the shape of pores of the geotextiles.

For nonwoven fabrics, simple calculation or direct measurement of pore size is impossible. Indirect measurement techniques have been developed : dry sieving - EOS (Calhoun, 1972; Garry and Raymond, 1983), dry sieving - AOS (CW-02215, 1977; ASTM D-4751, 1991), wet sieving - D_w (Saathoff & Kohlhase, 1986), hydrodynamic sieving - FOS (Fayoux, 1977; Rollin, 1985; Mlynarek et al.,1992), and pore size distribution - PSD (Rankilor, 1981; Mlynarek, 1985; Fischer, 1994; Bhatia and Smith, 1993, and Vermeersch and Mlynarek, 1996).

These techniques, initially developed for nonwoven products, were then used for all types of fabrics, whatever their basic structure. As a result of continuing efforts to establish uniform clogging criteria, the POA, along with its importance for filtration/drainage and erosion control applications, became only vaguely familiar, if at all, to many design engineers. Today, values for Percent Open Area are seldom seen in specifications. If they are mentioned, they are specified as values of secondary importance. The POA values are also rarely seen in guidelines which are published by various institutions and researchers. The POA property is not even mentioned in the ASTM STP 952 book on "Geotextile Testing and the Design Engineer" edited by Fluet (1987).

a)
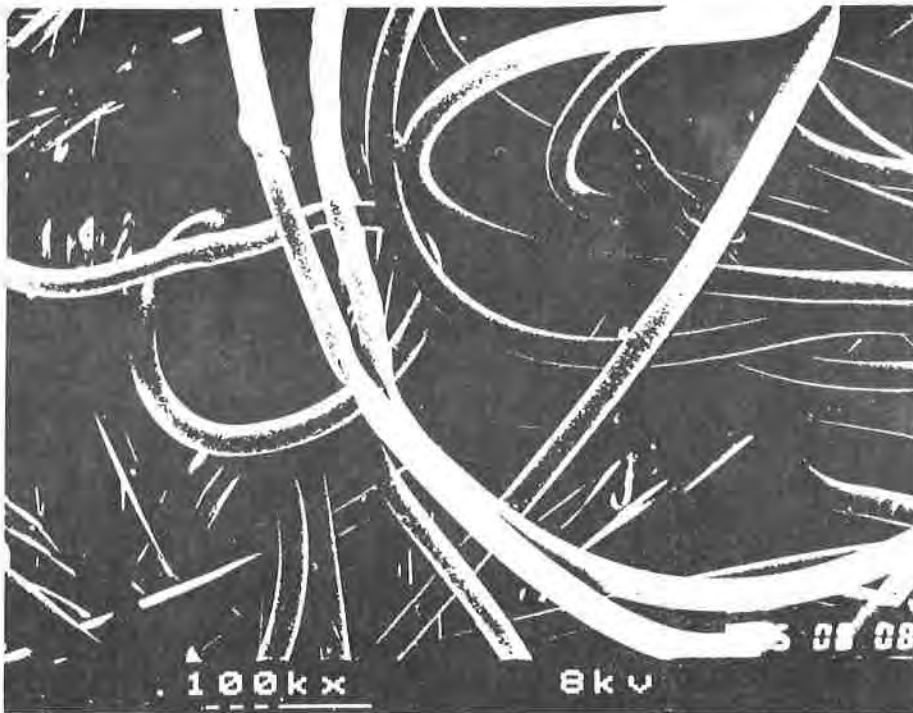
b)
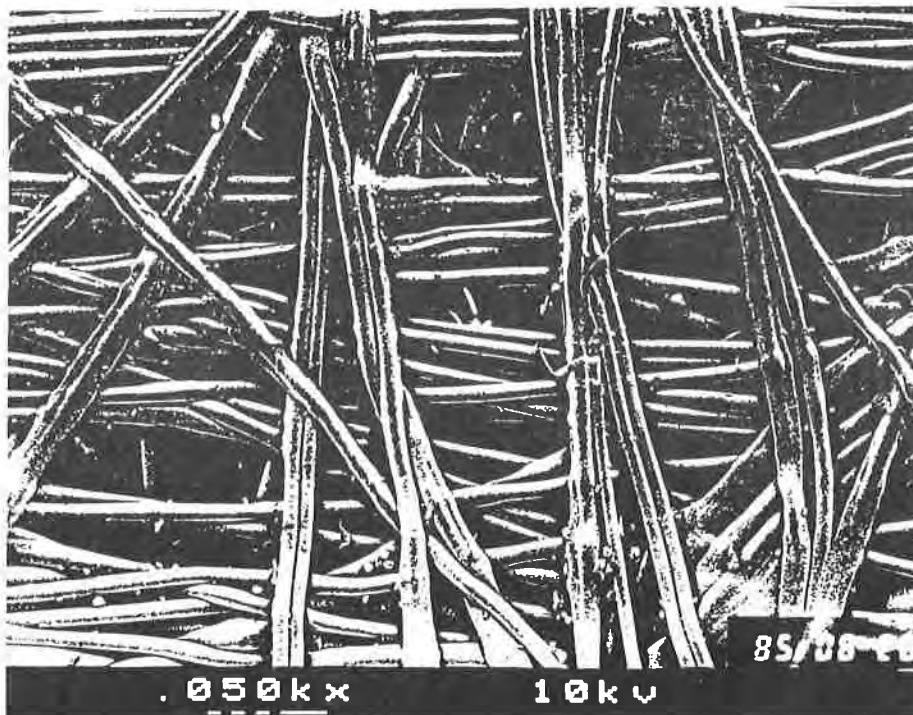
Figure 4 : Types of non-woven fabrics
a) needle-punched; b) heat-bonded

EVALUATION OF IMPORTANCE OF GEOTEXTILE FILTRATION PROPERTIES

Fluet (1987) concludes, after Calhoun (1972), Haliburton and Wood (1982), and Carroll (1981) that "fabric opening size and permeability coefficients do not indicate (geotextile) clogging potential". The question then arises as to which property of a geotextile does indicate this potential.

In an attempt to provide an answer to this question, several series of filtration compatibility tests (Mlynarek, 1993), and gradient ratio filtration tests (Austin et al., 1997) were carried out. Seven soils and fifteen woven geotextiles were tested to evaluate the importance of woven geotextiles' opening sizes and their Percent Open Area values on soil/geotextile system behavior. Gradient ratio values, overall hydraulic conductivities of soil/woven geotextile systems and the mass of fines passing through the geotextiles were used to estimate the overall behavior of soil/woven geotextile systems.

The results of these tests confirmed that filtration phenomena at the soil/filter interface are extremely complex. Soil internal stability, hydraulic conditions and geotextile's filtration properties are all related to each other and should always be considered as a single complex system. However, it can be concluded that piping and thus, clogging, phenomena are direct functions of the POA values of the geotextiles as shown in Figure 5.

Figures 6 and 7 show that there is little relationship between the mass of piped particles and the AOS and FOS values. The data points, however, are scattered and show some irregularity. A detailed analysis of the irregular points, shown in Figures 6 and 7, indicates some flaws in this relationship. It should be noted that for two woven products with almost identical opening sizes of 210 to 220 micrometers, the POA values vary between 0.5% to 19.2%. This is probably due to the difference in their structures as a result of manufacturing process differences. These results should warn engineers, first, that woven geotextiles can differ from each other, and second, against erroneous uses of opening size values in woven filter designs.

PERCENT OPEN AREA

The POA is a ratio of the total open area of geotextile (the void spaces between adjacent filaments and yarns) to the total specimen area. It is important to note that POA is a directly measurable value. Koerner (1994) mentions that a convenient way to measure the POA is to project a light through the geotextile onto a large, poster-sized piece of cardboard. The magnified open spaces can then be mapped by a planimeter.

The authors use a more sophisticated method of image analysis to measure the POA of geotextiles. In this method the geotextile is placed under an image analyzer microscope, and the openings are registered automatically and analyzed. The results of these analyses provide not only the POA value but also minimum, mean, and maximum opening size values as well as a histogram
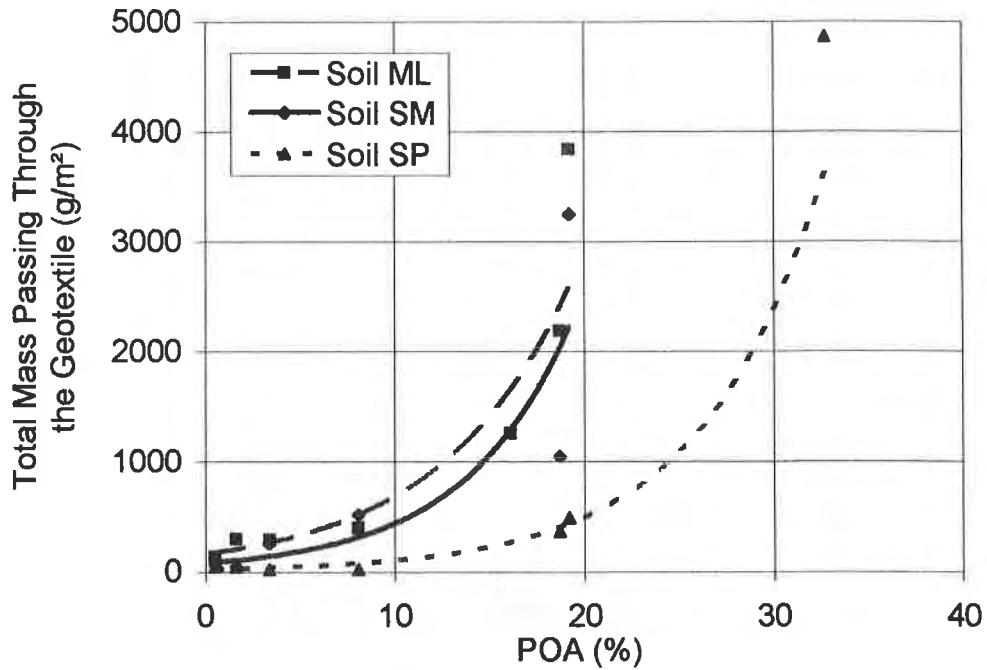
Figure 5 : Relationship between Percent Open Area of woven geotextiles and mass of fines which were piped out from soil/geotextile systems.
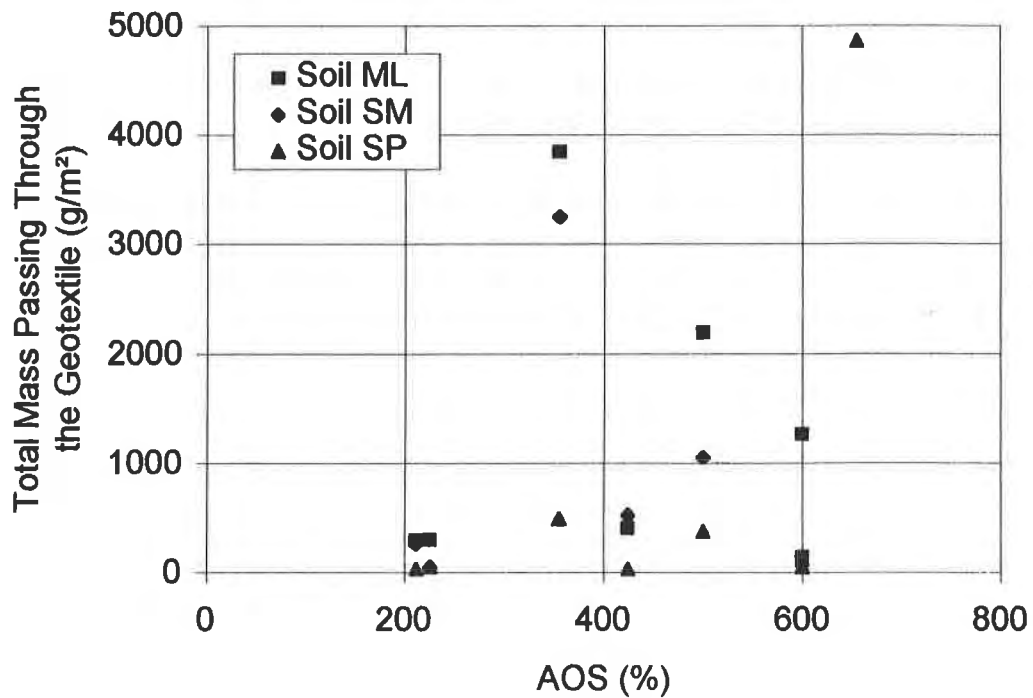
Figure 6 : Apparent opening size vs. total mass of fine piped out from a soil/geotextile system
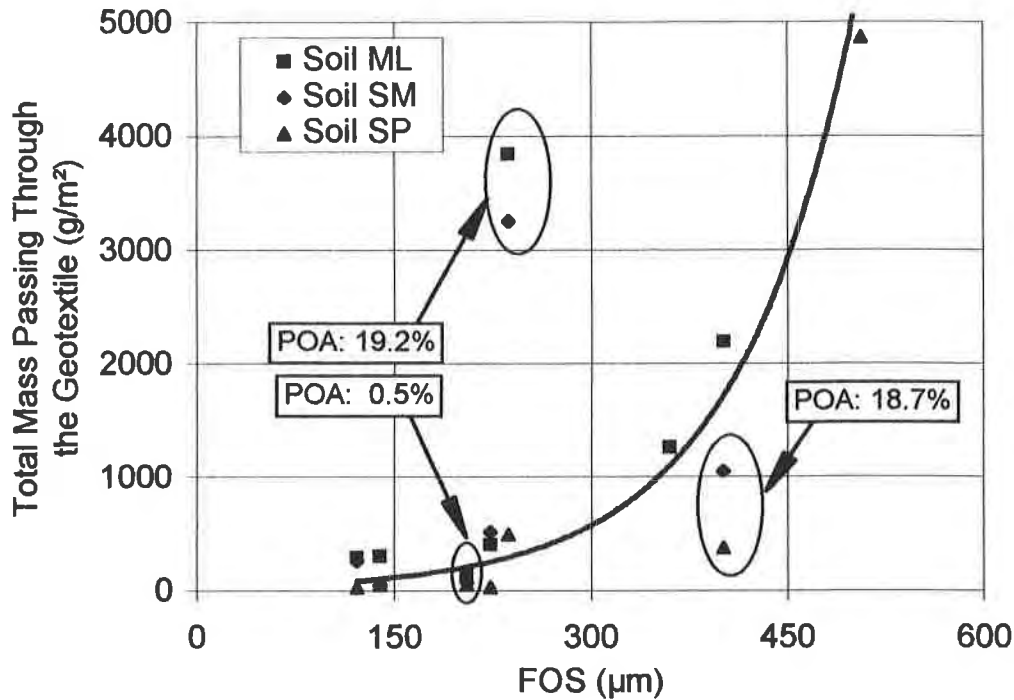
Figure 7 : Relationship between filtration opening size (FOS) and mass of fines
piped out from a soil/geotextile system

of the openings, as shown in Figure 8. With the histogram data we know not only the POA but also the frequency of pores of a specific dimension.

In addition, the image analyzer technique allows POA to be measured not only at a 90° angle of light projection but also under other angles and with rotation of the sample. The authors found that for some types of woven products, the POA can increase or decrease substantially when measured under light projected at different angles. This was particularly true for multifilament more complex woven geotextiles. Four types of basic pore models, which can influence the POA measurements, are shown in Figure 9.

Thus, it is suggested that for woven geotextiles the POA value should be reported by specifying two values, a percent open area (POA) value, measured under 90° angle light projection, and a maximum percent open area (MPOA) value, measured under different angles of light projection. It is suggested that the MPOA be measured under 30° and 45° angles of projected light and that the reported value of MPOA should indicate at which angle the maximum value was observed. An example of a simple method for specifying the filtration properties of a woven geotextile is shown in Table 1.

a)

b)
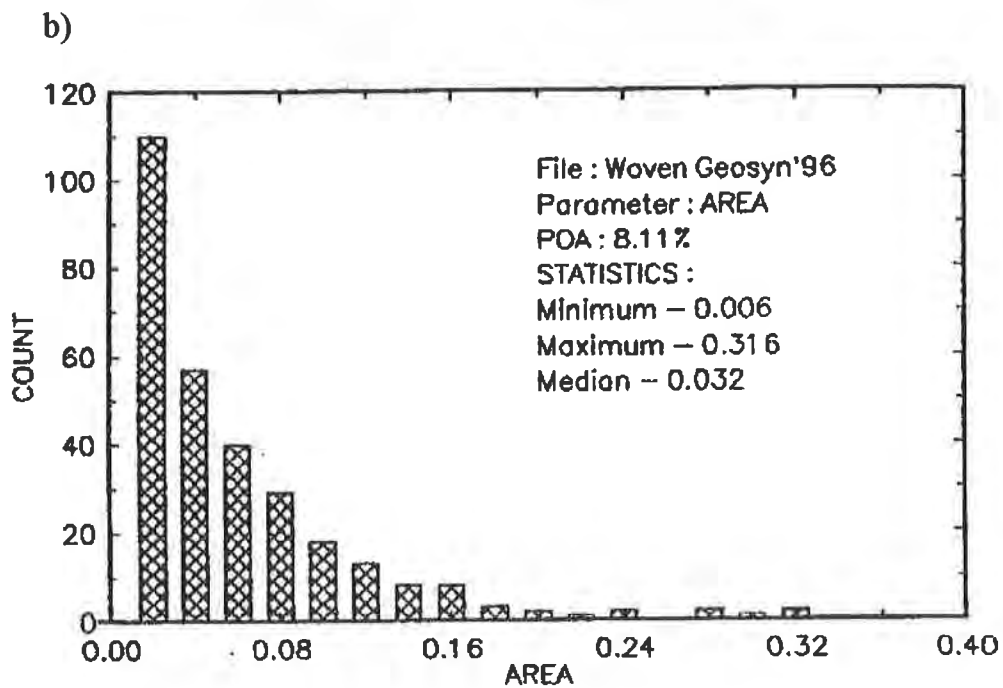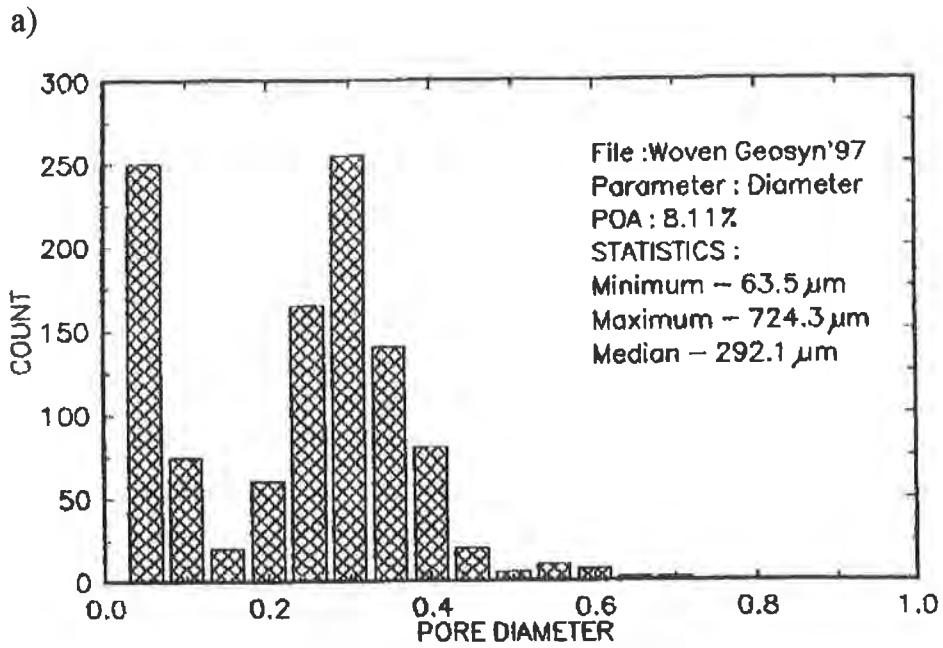
Figure 8 : Example of histograms obtained during POA measurement by image analyzer
a) by pore dimensions; b) by open surface

Adopting the recommendations outlined in this paper will have an influence on which fabrics are accepted for a particular filtration application and which are not. For instance, during this research, the authors examined a woven fabric which tests showed had a POA value of zero

(!) percent. Such a POA value would suggest that this woven product should not be considered for use in filter applications. This material's measured MPOA value, however, was 0.8% and the FOS was equal to 262 micrometers. Filtration compatibility test results revealed that this material exhibited excellent filtration behavior when used with silty soil. As a result, the product was recommended for filtration applications.

Pore type1   Pore type 2

Pore type 3   Pore type 4
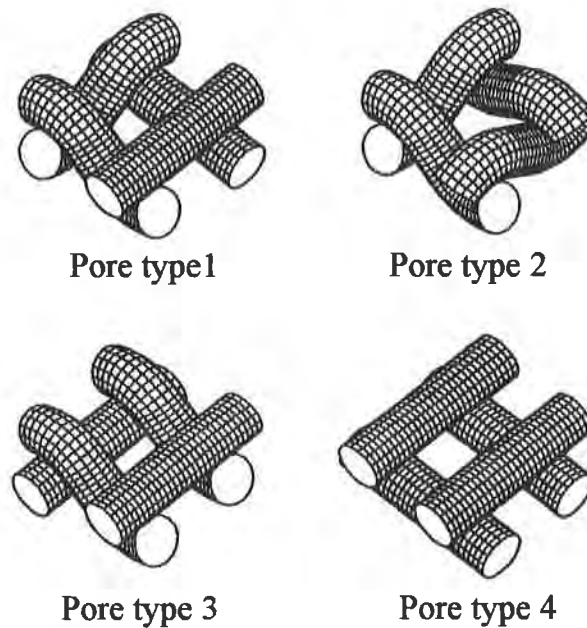
Figure 9 : Four types of basic pore models

Table 1 : Example of Specification of Filtration Properties of a Woven Geotextile

Parameter	Unit	Test Method	Value
Hydraulic Conductivity	m/s	ASTM D4491	1.20×10^{-3}
Permittivity	s^{-1}	ASTM D4491	2.03
Percent Open Area (POA)	%	SAGEOS GX 007-96	3.7
Maximum Percent Open Area (MPOA) under 45°	%	SAGEOS GX 007-96	8.1
Filtration Opening Size (FOS)	μm	CGSB-148.1-10	292

CONCLUSIONS

Based on an extensive evaluation of the available data on filtration behavior of woven geotextiles with different soils, as well as the authors' research results, it can be concluded that :

1. Woven fabrics present relatively simple structures in comparison to non-woven fabrics. Nevertheless, woven products, available on the market, show important differences between themselves.

2. For many woven products, it is possible to measure directly pore size characteristics such as opening sizes and percent open area.

3. The percent open area parameter governs a piping/clogging process during filtration through soil/woven geotextile systems. The direct relation between the mass of piped fines and the POA/MPOA values was found.

4. Knowledge of both the percent open area (POA) and the maximum percent open area (MPOA) of woven geotextiles is of great importance and it is recommended that both be used in design criteria.

5. POA values can differ substantially from MPOA values for the same woven product. It is recommended that the maximum value of open area should be used in design criteria.

6. Opening size has less importance during filtration through woven geotextiles and should not therefore be the primary filtration parameter to be considered in the design process.

ACKNOWLEDGMENTS

REFERENCES

ASTM D 4751 (1995). "Standard Test Method for Determining Apparent Opening Size of a Geotextile", 4th Edition of ASTM Standards on Geosynthetics, 1995

Austin, D.N., Mlynarek, J. and Blond, E. (1997). "Expanded Anti-Clogging Criteria for Woven Filtration Geotextiles", Proc. of Geosynthetics'97 Conference, Long Beach, 1997, in press.

Bhatia, S.K. and Smith, J.L. (1993). "Application of the Bubble Point Method in the Characterization of the Pore-Size Distribution of Geotextiles". J. of Geotechnical Eng.,ASCE., Vol.18, No.1, pp.94-105.

Calhoun, C.C. (1972). "Development of Design Criteria and Acceptance Specifications for Plastic Filter Cloth", <u>Technical Report S-72-7, US Army Corps of Engineers, Army Waterways Experiment Station</u>, Vicksburg, MI, June 1972, pp.55

Carroll, R.D. (1981). "Geotextile Filter Criteria", <u>Transportation Research Record 916</u>, Engineering Fabrics in Transportation Construction, Transportation Research Board, Washington, DC, 1983, pp. 46-53

Corps of Engineers, CW-02215 (1977). "Guide Specification for Plastic Filter Cloth", U.S. Army Corps of Engineers, Washington, USA, D.C.

Fayoux, D. (1977). "Filtration hydrodynamique des sols par les textiles", <u>Proc. Colloque int. sur l'Emploi des Textiles en Géotechnique</u>, Paris, France, Vol.2, pp.329-332.

Fisher, G.R. (1994). "The Influence of Fabric Pore Structure on the Behavior of Geotextile Filters", Ph.D. Thesis, University of Washington, Vol. 1 et Vol.2, p.502

Fluet J.E., (1987). <u>Geotextile Testing and the Design Engineer</u>, Ed. J.E. Fluet, ASTM STP,1987, pp.183

Garry, B.S. and Raymond, G.P. (1983). "Equivalent Opening Size of Geotextiles", <u>Geotechnical Testing Journal ASTM</u>, Vol.6, pp.65-77.

Giroud, J.P. (1996). "Granular Filters and Geotextile Filters", <u>Proc. of GeoFilters'96 Conf.</u>, Montreal, pp. 565 - 680.

Haliburton, T.A., and Wood, P.D. (1982). "Evaluation of the U.S.Army Corps of Engineers Gradient Ratio Test for Geotextile Performance", <u>2nd Int. Conference on Geotextiles</u>, Las Vegas, 1982, Vol.1, pp.97-101

Islam, A.T.M.S, and Bandara, P.P.U. (1996). "Yarn Spacing Measurement in Woven Fabrics with Specific Reference to Start-Up Marks", <u>J.Tex. Inst.</u>, 87, No.1, pp.107-119

Koerner, R., (1994). <u>Designing with Geosynthetics</u>, Prentice-Hall Inc., pp. 783.

Kulichenko, A.V., and Van Langenhove, L. (1992). "The Resistance to Flow Transmission of Porous Material", <u>J.Text. Inst</u>. Vol. 83, No.1, pp.127-132.

Lafleur, J., Mlynarek, J. and Rollin, A.L. (1993). "Filter Criteria for Well Graded Cohesionless Soils", <u>Proc. of the First Int. Conference on GeoFilters'92</u>, Karlsruhe 1992, Eds. J. Brauns, U. Schuler and M. Heibaum, pp. 97-106.

Lu, W.M., Tung, K.L. and Hwang, K.J. (1996). "Fluid Flow Through Basic Weaves of Monofilament Filter Cloth", Textile Research J., Vol. 66, No.5, pp.311-323

Mlynarek, J. (1985). "Hydraulic Conductivity and Pore Size of Non-Woven Filter Fabrics", Geotextiles and Geomembranes, Vol. 2, pp.65-77.

Mlynarek, J., Lafleur J., Rollin, A.L. and Lombard G. (1992). "Filtration Opening Size of Geotextiles by Hydrodynamic Sieving", Geotechnical Testing Journal, GTJODJ, Vol. 16, No.1, March 1993, pp. 61-69

Mlynarek, J. (1993). unpublished data on filtration compatibility tests (FCT) with woven geotextiles.

Rankilor, P.R. (1981). Membranes in Ground Engineering, Wiley & Sons Ltd., p. 377.

Rollin, A.L. (1985). "Filtration Opening Size of Geotextiles", ASTM Standardization News, May, pp. 50-52.

Saathoff, F. & Kohlhase, S. (1986) "Research of the Franzius Institute on Geotextiles Filters in Hydraulic Engineering", Proc. of the 5th Congress Asian and Pacific Regional Division, Seoul, 22p.

Vermeersch O.G. and Mlynarek, J. (1996). "Determination of the Pore Size Distribution of Nonwoven Geotextiles by a Modified Capillary Flow Porometry Technique", Recent Developments in Geotextile Filters and Prefabricated Drainage Geocomposites, ASTM STP 1281, S.K. Bhatia & L.D. Suits, Eds., ASTM, Philadelphia, pp. 19-34.

PORE SIZE DISTRIBUTION OF NON-WOVEN GEOTEXTILE FILTERS UNDER COMPRESSION STRESS.

O.G. VERMEERSCH
J. MLYNAREK
J.-F. DESROCHERS
SAGEOS, CANADA

ABSTRACT

In order to select geotextile filters for a particular application, hydraulic and mechanical properties should be known. The values of these properties are then applied in design. Three hydraulic properties of geotextiles are used in design for filtration and drainage: permittivity or permeability, characteristic opening size of pores, and transmissivity. Techniques have been developed to measure these properties and are now ASTM standard procedures.

The developed techniques used for permittivity and transmissivity address the measurement of these characteristics under compression. No one procedure has been developed to evaluate changes of the characteristic opening sizes of geotextile filters due to compression.

Based on the capillary flow technique, a procedure to measure the pore size distribution due to compression (PSDC) was developed. The capillary flow technique standard device has been modified in order to apply normal stresses. The details of the developed procedure are presented in the paper.

The results indicate that at low normal stress (50 kPa), a significant decrease of the maximum pore size (BBP) of nonwoven geotextiles occurs. It varies from 15% to 40% depending on the type of product. Moreover, it seems that nonwoven geotextiles, showing large maximum opening sizes (200 micrometers) under no normal stress, are more sensitive to the application of normal stresses than those with smaller opening sizes (100 to 130 micrometers).

More data are needed to confirm these results. A test program concerning this topic is in progress.

KEY WORDS

Geotextile, Pore Size, Pore Size Distribution, Compression, Nonwoven, Filtration, Separation

INTRODUCTION

Geotextiles are currently used as filters or separators in many different applications. They are used to wrap highway drains, to filter leachate in landfills, and to act as horizontal separators between subgrade soils and subbase aggregates. When designing as a filter or a separator, the current selection parameter of a geotextile consists of its opening size O_{95} measured without compression. However, in most of these applications, the geotextile is then submitted to static or dynamic normal stresses. Thus, it seems necessary to measure changes in the opening O_{95} as well as other openings, under compression. Only few previous papers deal with this subject [Rollin et al.(1981), Brochier (1984), Prapaharan & Holtz (1987), Elsharief (1992)].

It can be easily explained that the geotextile structure modification, due to a normal stress, affects the geotextile hydraulic properties. It is particularly noticed for nonwoven structures. Indeed, the thickness reduction induces a decrease in porosity which is, in turn, a parameter affecting the permeability, the transmissivity and the pore sizes.

This affirmation can be verified theoretically for both heat bonded and needle punched nonwoven geotextiles. Based on Lombard (1985) and Faure (1988) results, the following equations can be obtained.

$$PSDL(d) = 1 - \left(\frac{4\mu d}{\pi T_g D_F \rho_F} + 1 \right)^{\frac{T_g}{D_F}} \times \exp\left(-\frac{4\mu d}{\pi D_F^2 \rho_F} \right) \quad (1)$$

$$PSDF(d) = 1 - \left(\frac{4\mu d}{D_F(4\mu + 2\pi T_g \rho_F)} + 1 \right)^{\frac{2T_g}{D_F}} \times \exp\left(-\frac{4\mu d}{\pi D_F^2 \rho_F} \right) \quad (2)$$

where : PSDL(d): pore size distribution for heat-bonded geotextiles (according to Lombard)
PSDF(d) : pore size distribution for needle-punched geotextiles (according to Faure)
d: pore diameter (m)
D_F: fiber diameter (m)
T_g: thickness (m)
μ: mass per unit area of geotextile (kg/m²)
ρ_F: mass per unit volume of fibers (kg/m³)
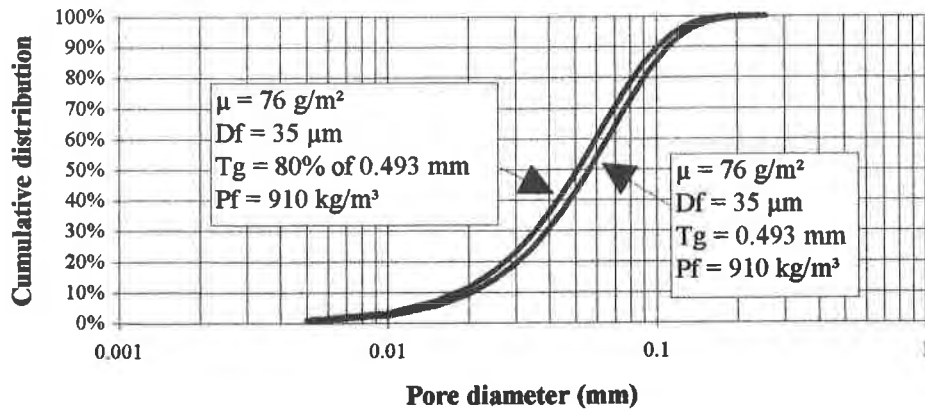
a)
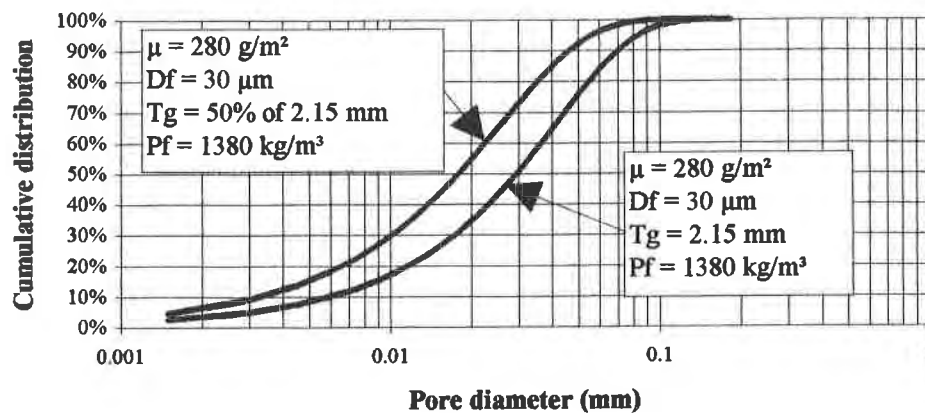
b)

Figure 1 : Theoretical pore size distributions
a) heat bonded nonwoven   b) needle punched nonwoven

The pore size distribution (PSD) of a given heat bonded geotextile can be easily computed using Eqn. 1, based on its standard properties: fiber diameter, thickness and porosity. This PSD is plotted in Figure 1a. Then, taking into consideration a reduction in thickness of 20 %, a second PSD is computed, and is also plotted in Figure 1a. A shift of the PSD to finer pores can be noticed.

Figure 1b shows the same experiment for a nonwoven needle punched product, and a shift of the PSD into finer pores is even more evident.

The encapsulation and image analysis technique was used by Brochier (1984), Rollin et al. (1981) and Elsharief (1992) to evaluate the geotextiles porometry under normal stresses. These researchers observed the influence of stress on the geotextile structure. Elsharief (1992) has observed that the 0_{50} pore size of some geotextiles could decreased about 20 % under as little as 15 % strain.

Prapaharan and Holtz (1987) used a mercury intrusion technique to measure the PSD of geotextiles and the changes in PSD under compression. They observed a 40 to 50 percent decrease in the O_{50} size of a needle punched geotextile under 54 % compressive strain.

Recently, the capillary flow porometry technique has been applied in geosynthetic engineering by Fisher (1994), Bhatia and Smith (1995), Vermeersch and Mlynarek (1996) and Vermeersch et al. (1996). Based on this technique, a research program has been conducted to adjust this procedure to determine the pore size distribution of nonwoven geotextile filters under compression (PSDC). The technique, including device modifications and preliminary results are presented and discussed in this paper.

TESTING DEVICE AND ITS MODIFICATIONS

The capillary flow technique is based upon the differential analysis of two test runs, a wet run carried out on a sample saturated with a wetting fluid and a dry run carried out on a dry sample. During each run, the measurements of the air flow rate and the applied pressure are registered. By comparing the differential flow between wet and dry runs, the PSD can be calculated.

The Coulter Porometer II, with a compressor as the pressure supply, was used in the program. The device is described in authors' previous paper, Vermeersch and Mlynarek (1996a). With this device, the wet run is carried out first, while the dry run is carried out automatically on the same sample used for the wet run, without any other manipulation.

Some modifications were made in the sample holder so that normal stresses could be applied for this project.

The regular sample holder device of the Coulter Porometer II (as shown in Figure 2) is composed of a sample body (1) and a sample cap (6) joined together to form a sealed chamber by means of a locking ring (7). A screen (2) as well as a filter screen (3) support the sample to be tested. The sealing against air leaks is given by an O-ring (5) held by the cap (6).

One of the most important issues to be solved concerning pore size distribution under compression was the application of uniform stress over the entire surface of the tested sample. A filter screen with circular openings 0.7 millimeter in diameter with 45% open area has then been chosen to apply a uniform stress on the surface of the sample. This filter screen was the same than the "standard" ones placed under the sample for measurement of PSD under no compression.

Thus, a set of two screens has been added: a stress screen (4) and this filter screen (3) (Figure 2). This set of screens was placed between the sample and the O-ring (5). With these modifications, it was possible to apply a uniform normal stress on the sample via the O-ring (5) and the sample cap (6), by means of the locking ring (7).
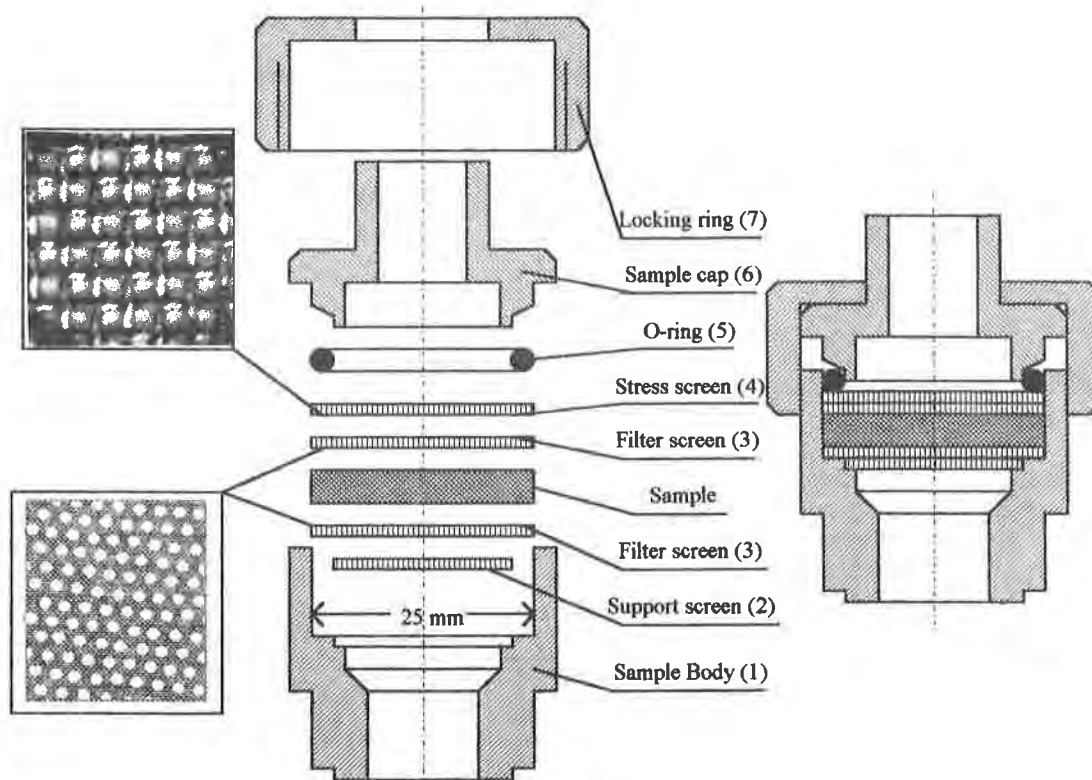
Figure 2 : Modified sample holder device (not in scale)

To eliminate possible leaks, a sealing tape (polytetrafluoroethylene thread seal tape) was applied around the screw of the sample body. In addition, to avoid leaks beside the sample, as shown in Figure 3, the periphery of the screen (4) was saturated in an epoxy resin. To achieve a sealed contact between the O-ring (5), sample cap (6) and support screen (4), the allowed minimum compression stress was fixed at 30kPa.
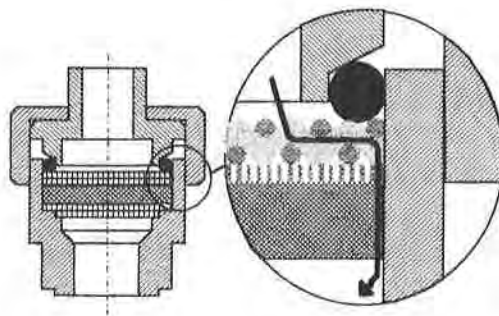
Figure 3 : Detail of possible leak beside the sample

Finally, to avoid stress absorption by a friction effect at the contact of the O-ring and the sample body, the O-ring was lubricated prior to the test with a silicone lubricant.

Device calibration procedure

In order to determine the stress applied on the sample during the porometry measurement, a device calibration procedure was performed. Its objective is to determine the relationship between the applied stress and the system (sample body, screens, sample, O-ring, sample cap) thickness. A dynamometer is used to calibrate the device. Typical results from the calibration procedure are shown in Figure 4.
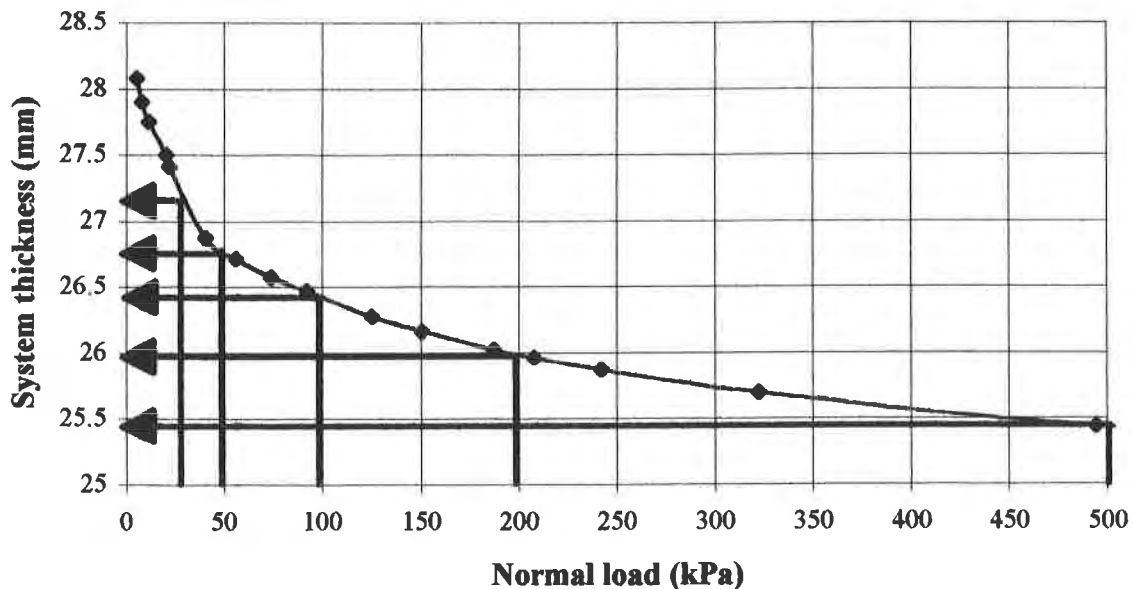
Figure 4 : Typical result from calibration procedure

It is noted that it is not possible to carry out calibration on the sample used for PSDC measurement due to sample irreversible deformation which can occur during stress application. Thus, different samples of the tested geotextile need to be selected for calibration and for final PSDC measurements. However, to limit effects of the non-uniformity of the products, the sample selected for calibration was similar in mass per unit area to the sample used for the PSDC measurement.

The calibration procedure includes the selection of samples of similar mass per unit area, the set-up of the device (placement of the elements), the testing (measurement of the systeme thickness under successive normal stesses - 30, 50, 100, 200, 500 kPa) and the data computation. Final configuration is shown in Figure 5.
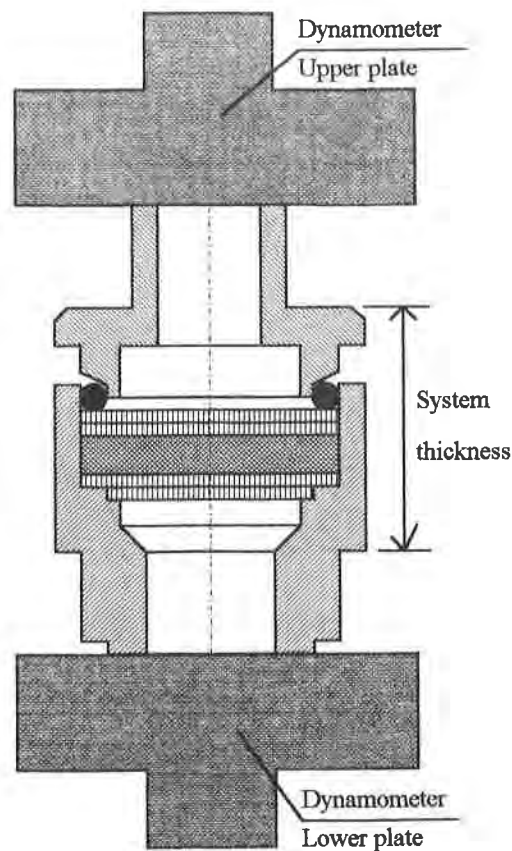
Figure 5 : Application of stress on the system

PSDC measurement procedure

The PSDC measurement procedure is based on the PSD ones presented by Vermeersch and Mlynarek (1996). It includes: the preparation of the device and its pressure control system, the sample preparation and its installation in the sample body, the testing and the data collection and PSDC computation.

PRELIMINARY RESULTS

Four (4) polypropylene (PP) nonwoven needlepunched geotextile products, from three (3) manufacturers, were selected to evaluate the applicability of the PSDC procedure for the determination of the pore size distribution under compression. The standard properties of the selected geotextiles are presented in Table 1.

Table 1 : Standard properties of selected nonwoven products.

Sample Id.	T_g - Thickness CGSB 148.1-3 (mm)	μ - Mass per unit area CGSB 148.1-2 (g/m²)	n - Porosity calculated (%)	FOS - Filtration opening size CGSB 148.1-10 (μm)
NP-A1	1.18	142	86.8	109
NP-B1	1.31	138	88.4	134
NP-B2	2.38	296	86.3	95
NP-C1	1.70	185	88.0	200

For each product, a series of samples (25 mm diameter) was selected and tested according to the calibration and PSDC procedures, described above. In addition, some PSD tests were conducted on samples with a low normal stress of 2 kPa.

The results, expressed in terms of bubble point (BBP) have first been plotted versus the applied normal stress and are shown in Figure 6. Two series of other plots are also presented. The first one, shown in Figure 7, consists of the cumulative pore size distribution of each product for four (4) selected pressures: 2kPa, 50kPa, 200kPa and 500kPa. The second one, presented in Figure 8, shows the differential pore size distributions for the same selected tests.
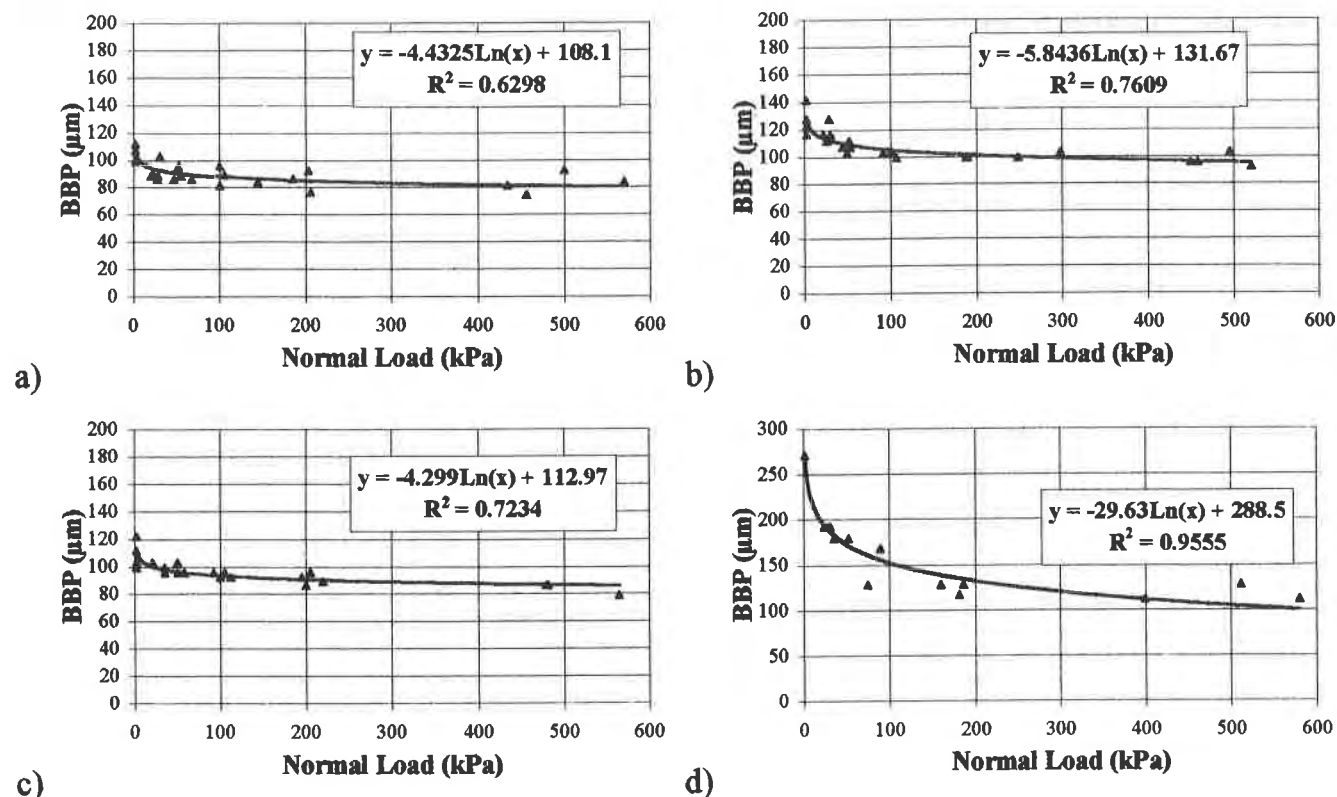
Figure 6 : BBP versus normal stress
a) NP-A1 b) NP-B1 c) NP-B2 d) NP-C1
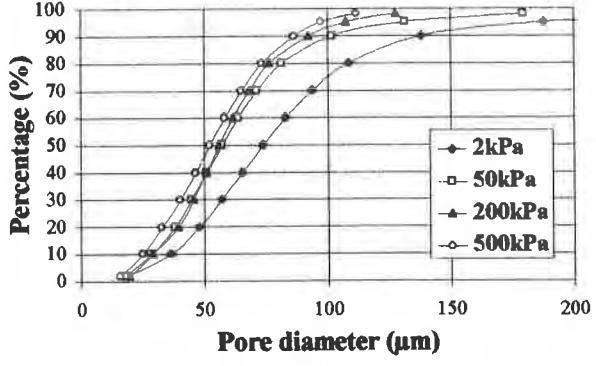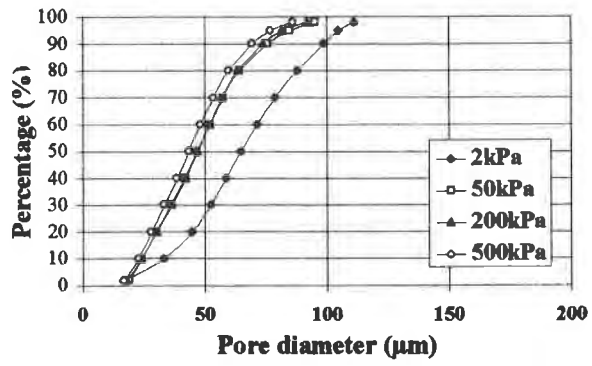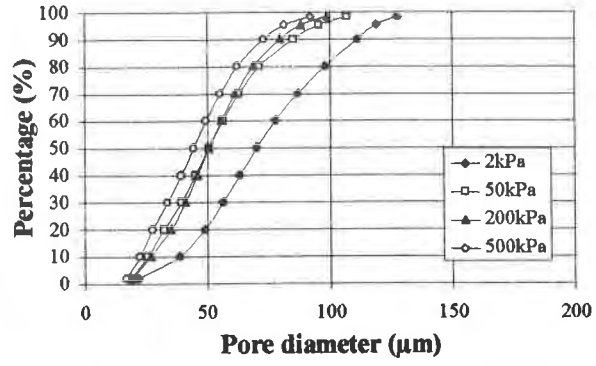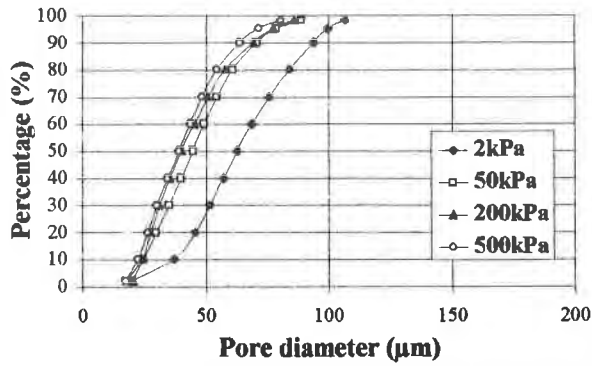
Figure 7: Cumulative PSD versus normal stress
a) NP-A1 b) NP-B1 c) NP-B2 d) NP-C1

a)
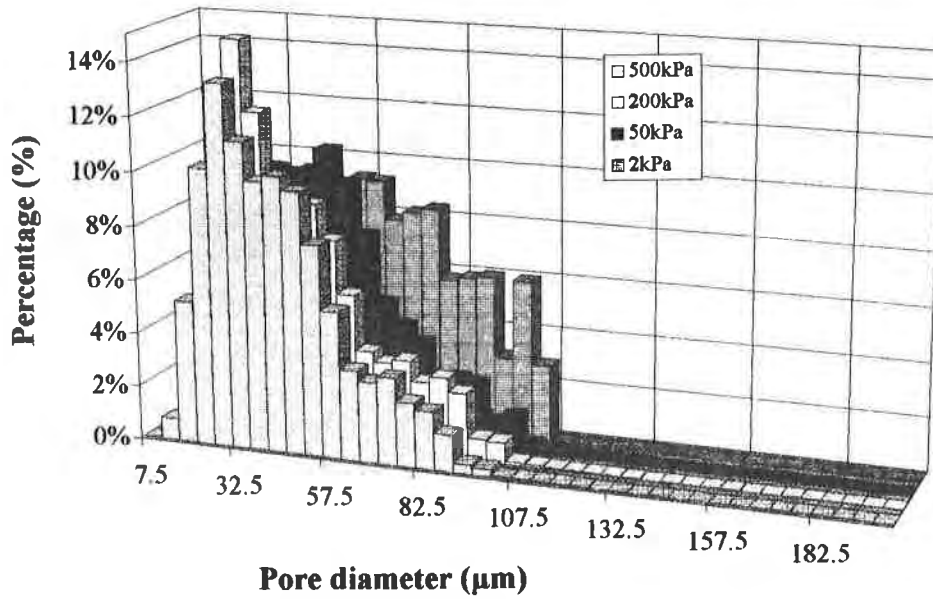
Figure 8 : Differential PSD versus normal stress   a) NP-A1

b)

c)
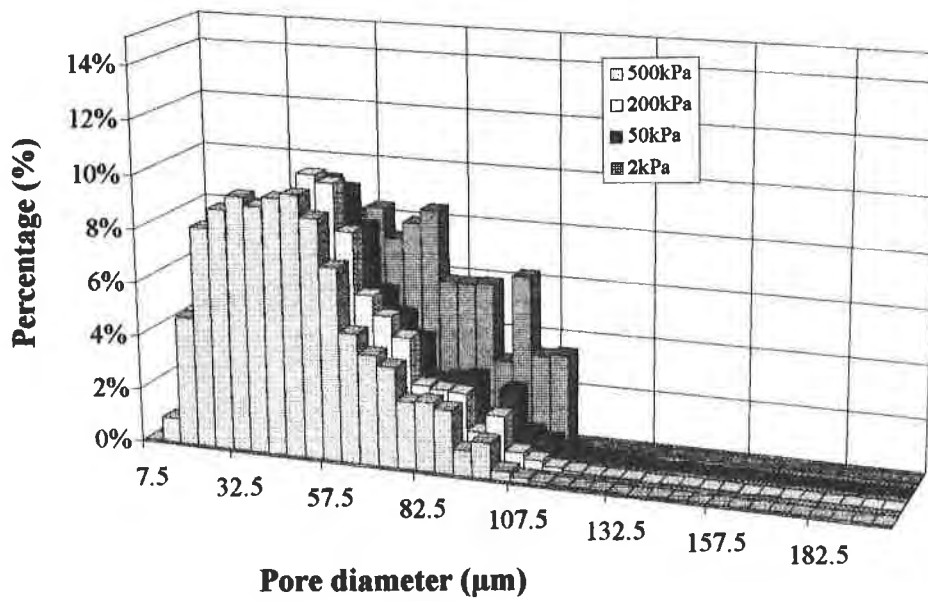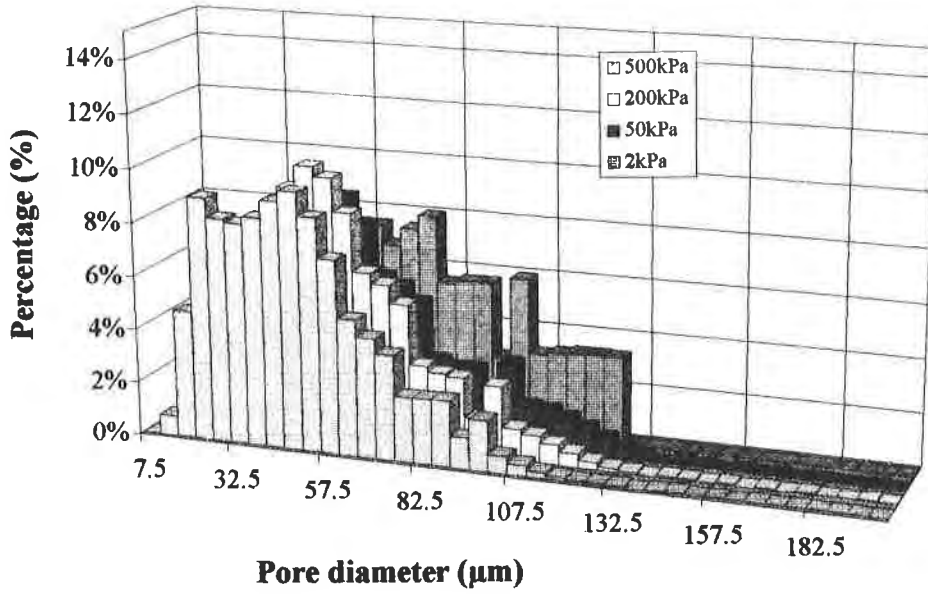
Figure 8 Con't: Differential PSD versus normal stress
b) NP-B1   c) NP-B2
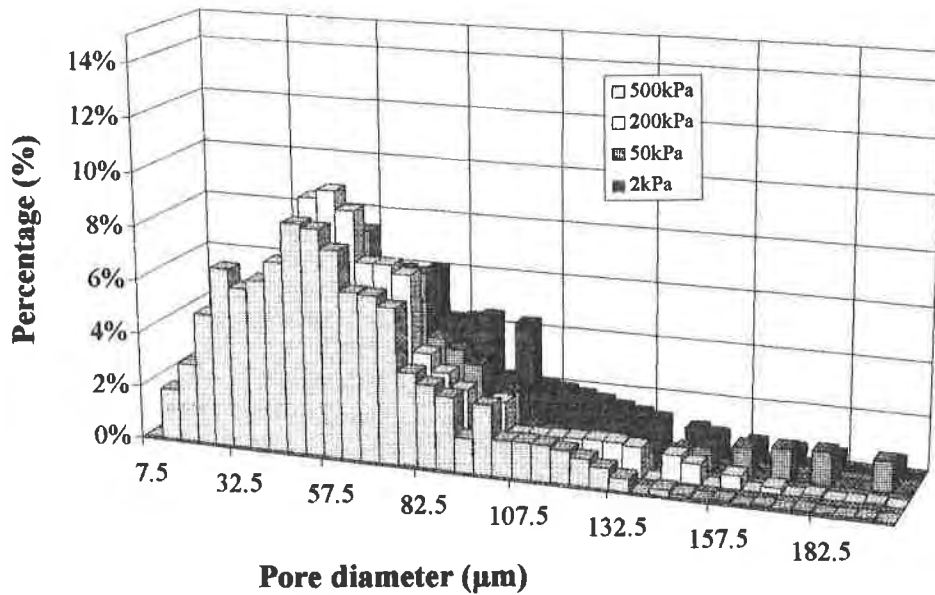
d)

Figure 8 Con't: Differential PSD versus normal stress   d) NP-C1

DISCUSSION

Figure 6 shows that the products are sensitive to the application of normal stress. It results in a shifting of their initial PSD (under 2 kPa) to finer pores, as shown in Figures 7 and 8.

The products NP-A1, NP-B1 and NP-B2, which present a filtration opening size (FOS) as measured by CGSB 148.1-10 in the range of 100-130μm behave in a similar way. A decrease in their BBP by 15% to 20% at 50 kPa and by 20% to 30% at 500 kPa is observed.

The NP-C1 product, with a FOS of 200μm, is more sensitive to normal stress than the other products. Its behavior is different and the BBP decreases by 40% at 50 kPa and by 60% at 500 kPa.

The PSDC of the products under 50 kPa and with 2 kPa normal stresses are shown in Figure 9 to illustrate differences in the PSD of different products.

It is noted that for the tested products, at a normal stress of 50 kPa, the O_{50} size decreases by about 25% in comparison to the O_{50} size measured under compression of 2kPa. This result is in agreement with Elsharief (1992) observations.

The nonwoven geotextiles with large maximum opening size (200 micrometers) under no normal stress, are more sensitive to normal stresses than the ones showing smaller opening size (100 to 130 micrometers).

More data are needed to confirm these results.

a)   b)
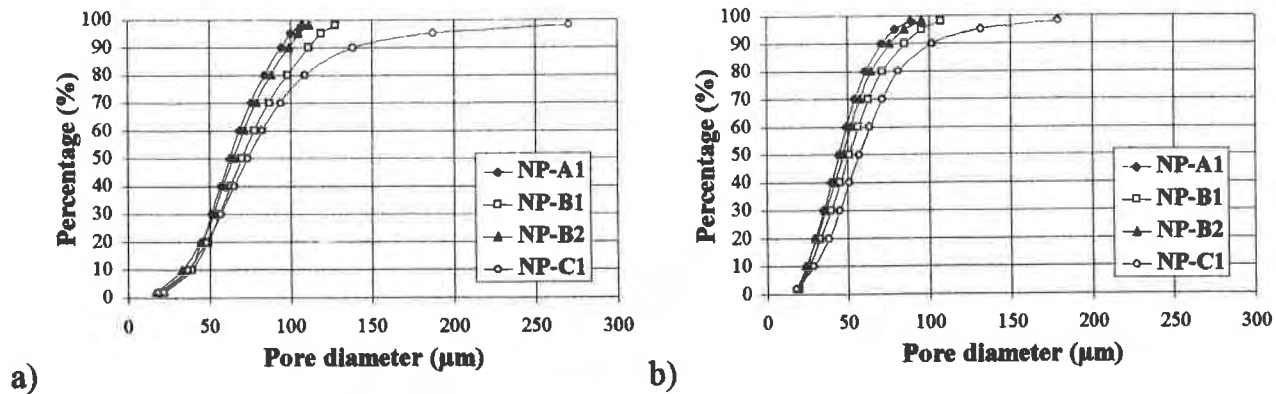
Figure 9 : Cumulative PSD for all tested products
a) 2kPa b) 50 kPa

CONCLUSION

A capillary flow technique procedure was applied to measure the pore size distribution under compression stresses (PSDC).

The results indicate that under a normal stress of 50 kPa, a significant alteration of the bubble point (BBP) of nonwoven geotextiles can occur. The maximum pore size of nonwoven geotextiles can decrease 15% to 40%. Moreover, at that stress, the O_{50} size is decreased by about 25% for the tested products. The alteration of the pore sizes is also observed for higher stresses, however with lesser magnitude.

It seems that nonwoven geotextiles showing large maximum opening size (200 micrometers) under no normal stress, are more sensitive to normal stresses than the ones showing smaller opening size (100 to 130 micrometers).

More data are needed to confirm these results. Additional tests are also recommended to determine the behavior of other types of geotextiles (heat bonded, woven) under normal stress. A test program concerning these topics is in progress.

Considering the applied procedure, it could be improved by attaching a pressure cell directly on the porometer to directly measure the normal stress during testing, thus, simplifying the PSDC procedure. No calibration procedure would be needed with such modification.

If a filter or a separator in service conditions is exposed to compression, the PSDC values should replace the pore size values presently used in filter design criteria.

REFERENCES

Bhatia, S.K. and Smith, J.L. (1995) "Application of the Bubble Point Method to the Characterization of the Pore-Size Distribution of Geotextiles", Geotechnical Testing Journal, GTJODJ, Vol. 18, N°1, March 1995, pp.94-105.

Brochier, P. (1984) Comportement des géotextiles en filtration et en séparation, M.Sc.A. Thesis, Chemical Engineering Dept., Ecole Polytechnique de Montréal, Canada, 217 p.

Elsharief, A.M. (1992) Laboratory Evaluation of Prefabricated Highway Edge Drains, Joint Highway Research Project, Purdue University, West Lafayette, Indiana, FHWA/IN/JHRP-92/20, 283 p.

Faure, Y.-H. (1988) Approche structurale du comportement filtrant des géotextiles, Ph.D. Thesis, Université Joseph Fourier - Grenoble 1, France, 344 p.

Fischer, G.R. (1994, The Influence of Fabric Pore Structure on the Behavior of Geotextile Filters, Ph.D. Thesis, University of Washington, D.C, 502 p.

Lombard, G. (1985) Analyse et comportement hydraulique des géotextiles thermoliés et thermosoudés, Ph.D. Thesis, Chemical Engineering Dept., Ecole Polytechnique Montreal, Canada, 271 p.

Prapaharan, S. and Holtz, R.D. (1987) "Pore Size Distribution of Nonwoven Geotextiles", Report to Hoechst-Celanese Corporation, Purdue University, West Lafayette, IN, 65 p.

Rollin, A., Masounave, J. and Denis R. (1981) "Prediction of Permeability on Nonwoven Geotextiles from Morphometry Analysis", Journal of Microscopy, 121 N° 1, pp.92-110.

Vermeersch, O.G. and Mlynarek, J. (1996) "Determination of the Pore Size Distribution of Nonwoven Geotextiles by a Modified Capillary Flow Porometry Technique", Recent Developments in Geotextile Filters and Prefabricated Drainage Geocomposites, ASTM STP 1281, Shobha K. Bhatia and L. David Suits, Eds., American Society for Testing and Materials, Philadelphia, PA, pp.19-34.

Vermeersch, O.G., Mlynarek, J and Lombard, G (1996) "Porometry Evaluation of Nonwoven Materials Based on the Bubble-Point Method", Proc. of 6th Annual TANDEC Conf., Knoxville, TN, Session 1, Paper 2, 14p.

EXPANDED ANTI-CLOGGING CRITERIA FOR WOVEN FILTRATION GEOTEXTILES

DERON N. AUSTIN, E.I.T.
SYNTHETIC INDUSTRIES, INC. (USA)

JACEK MLYNAREK, P.E., Ph.D.
SAGEOS GEOSYNTHETICS ANALYSIS SERVICE (CANADA)

ERIC BLOND, M.Sc.A.
SAGEOS GEOSYNTHETICS ANALYSIS SERVICE (CANADA)

ABSTRACT

Using a modified gradient ratio test procedure, an extensive filtration research program was conducted using three (3) fine-grained, cohesionless soils and ten (10) geotextiles. The purpose was to evaluate the filtration performance of each soil/geotextile combination and propose new anti-clogging criteria for woven monofilament geotextiles used as filters with fine-grained, cohesionless soils. Based upon the results, the authors suggest that: (1) current filtration design criteria include a new, expanded range of percent open area (POA) values for specific soil types; (2) the percent open area of a woven monofilament geotextile can be used to predict the gradient ratio for soils similar to those evaluated in this study; and (3) the mass of fine soils passing through the geotextile (i.e. piping) is not as critical as previously thought.

The research program includes: (1) an identification of the soils and geotextiles selected; (2) the predicted filtration behavior using recognized design procedures; and (3) the actual test procedures followed. The gradient ratio test results for all soil/geotextile systems are analyzed and observations are made concerning relationships between predicted and actual performance, index versus performance tests and the appropriateness of existing design and selection procedures for woven geotextiles used as filters in drainage. The conclusions of the paper are based upon the results from these gradient ratio tests and several other filtration studies on similar soils.

BACKGROUND

Unless the application is considered critical or severe, conventional geotextile filtration design procedures suggest that an appropriate nonwoven geotextile have a porosity greater than 50 percent and woven geotextiles have an open area greater than 4 percent. The exception to this rule of thumb is a gap-graded silty sand that contains less than 20 percent silt. These soils

are known to easily clog geotextiles beneath hard armor revetments in coastal zones. This has resulted in anti-clogging criteria for woven geotextiles of a percent open area (POA) greater than or equal to 15% (Fluet and Luettich, 1993). However, most current selection criteria used by the American Association of State Highway Transportation Officials (AASHTO), the Federal Highway Administration (FHWA) and the US Army Corps of Engineers (COE) do not take soil type into account when considering clogging behavior of geotextile filters.

Current Selection Criteria

AASHTO M288 is probably the most widely referenced geotextile specification in North America. It lists physical requirements for geotextiles used in subsurface drainage (Class A and B) and erosion control (Class A and B) applications (AASHTO, 1990). Although both applications allow for the use of woven geotextiles, there is no mention of POA in the specification. Therefore, no provisions to prevent clogging have been made by AASHTO either in design, selection or specification.

Published every four (4) years, geotextile requirements listed in Section 714 of the Standard Specifications for Construction of Roads and Bridges on Federal Highway Projects FP-92 and FP-96 are modeled after the AASHTO M288 specifications. As a result, there is no mention of POA in these specifications (FHWA, 1992; FHWA, 1996). Even though no provisions have been made to prevent clogging, the FHWA Geotextile Engineering Manual does give design guidance for anti-clogging criteria. In order to prevent clogging, FHWA recommends that a woven geotextile have a POA greater than or equal to 4 percent (Holtz et al, 1995).

The COE civil works construction guide contains probably the oldest nationally recognized geotextile specification in the world. Titled, "Geotextiles Used As Filters" and originally released in 1974, this guide includes provisions for filter design criteria for both woven and nonwoven geotextiles. In filtration applications where less than 5 percent passes the 0.075 mm sieve (U.S. Standard Sieve #200), an anti-clogging criteria for woven geotextiles of POA $\geq$ 10% is given. For all other soil types, the POA must be greater than or equal to 4 percent (Al-Hussaini and Perry, 1996). In addition to providing selection and specification guidance, the same requirements are listed in the design guide entitled "Engineering Use Of Geotextiles" (US Army/Air Force, 1994). As a result, all COE projects following the national specifications for woven geotextiles use a woven monofilament with a POA of at least 4 percent.

Examples of subsurface drainage and erosion control systems clogging due to the improper design and selection of the geotextile filter have been reported (Calhoun, 1972; Christopher and Holtz, 1985; Fluet and Luettich, 1993; Koerner et al, 1994).

GRADIENT RATIO TEST

The gradient ratio test is a well-accepted method to evaluate the filtration performance of geotextiles with cohesionless soils, such as sands and silts (Calhoun, 1972; US Army COE, 1977; Haliburton and Wood, 1982; ASTM, 1995). Using a rigid wall permeameter, a site-specific soil is placed above the geotextile and water is passed vertically through the system under a range of hydraulic heads. By comparing the hydraulic gradient of the soil system to that of the soil/geotextile interface, the clogging potential can be predicted.

ASTM Procedure

The original gradient ratio device and test procedure was developed in 1972 at the US Army Engineer Waterways Experiment Station (Calhoun, 1972). In 1990, the American Society of Testing and Materials adopted a version of this procedure as a test method for geotextiles entitled, "Standard Test Method for Measuring the Soil-Geotextile Clogging Potential by the Gradient Ratio". The method is recommended for evaluating the performance of soil/geotextile filtration systems under controlled test conditions and gradient ratio values obtained may be used as an indication of the soil/geotextile system clogging potential and permeability. Gradient ratio values are calculated with readings from one (1) manometer below and four (4) manometers above the geotextile. The manometers above the geotextile are located at levels of 25 mm (1 inch) and 75 mm (3 inch). The hydraulic gradient is set at one (1.0) and measurements are made at specified times. After 24 hours, the gradient is raised to 2.5, 5.0 and 7.5 and the readings are repeated (ASTM, 1995). It is assumed that any change at the soil/geotextile interface can be detected by the manometers during the pre-defined testing period.

A gradient ratio of approximately 1.0 indicates that the geotextile has no effect on the hydraulic conductivity and the soil is internally stable. A gradient ratio of less than 1.0 may indicate internal instability of the soil and the soil/geotextile system, with some fines possibly moving out of the system. A gradient ratio greater than 1.0 indicates that the filtration system is showing signs of blinding or clogging (ASTM, 1995).

SAGEOS Procedure

Two parameters of the ASTM D-5101 test procedure were recently criticized by many geotechnical and geosynthetic engineers. First and foremost, it is felt that the location of the manometer nearest to the geotextile so far from the geotextile surface that the test cannot accurately determine the behavior at the soil/geotextile interface. Secondly, ASTM D-5101 can only test soil/geotextile filtration behavior in unidirectional, downward flow conditions (ASTM D-35 Committee Meetings: Denver, CO, June 1995 and Atlanta, GA, January 1996). As a result, SAGEOS Geosynthetics Analysis Service of Canada modified the ASTM gradient ratio device and procedure by: (1) adding an additional manometer 6 mm (1/4 inch) above the geotextile surface in an effort to more accurately measure the filtration phenomena at the soil/geotextile

interface; and (2) testing the soil/geotextile system in the downward and upward flow directions. A cross-section of this modified device (SAGEOS) is shown in Figure 1.
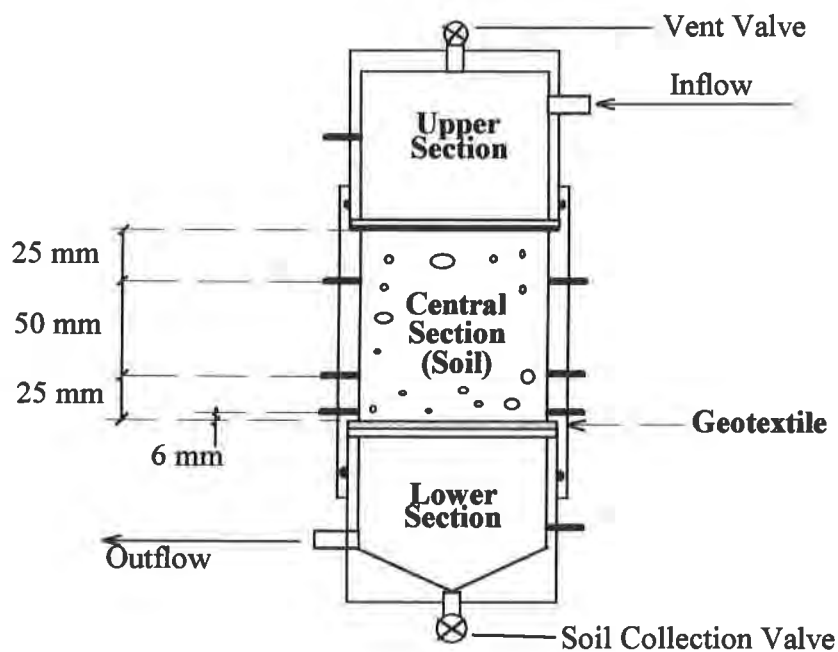
Figure 1. Schematic of SAGEOS Gradient Ratio Test Device

Significance of Results

Four (4) distinct filtration behaviors can be determined using the results from the gradient ratio test: (1) bridging of soil at the soil/geotextile interface; (2) blinding of the soil and/or the geotextile at the soil/geotextile interface; (3) clogging of the geotextile; and (4) passing of soil through the geotextile (i.e. piping). By analyzing gradient ratio values, system permeability, mass of soil trapped within and mass of soil passed through the geotextile, the filtration behavior can be predicted.

As previously stated, the nearest manometer to the soil/geotextile interface with the SAGEOS device is much closer than that in the ASTM device, showing the filtration phenomenon at the soil/geotextile interface with more accuracy. Because of this accuracy, previously accepted gradient ratio values of 1.0 to 3.0 seem inappropriate when evaluating hydraulic gradients only 6 mm (0.25 inch) from the interface. Ideally, soil particles having a smaller diameter than openings in the adjacent geotextile and will be carried through the interface. As fines wash out from the base soil, coarser particles at the soil/geotextile interface will not mobilize and a natural filtration zone will form. Therefore, the lower limit of acceptable values for such conditions have been reduced as follows:

$$0.5 < \mathrm{GR_{SAGEOS}} < 3.0 \ \text{ and } \ 0.75 < \mathrm{GR_{ASTM}} < 3.0$$

For these evaluations, the gradient ratio calculated using the manometer located 6 mm (0.25 inch) from the soil/geotextile interface is designated as $\mathrm{GR_{SAGEOS}}$ whereas the value obtained from the 25 mm (1 inch) manometer is referred to as $\mathrm{GR_{ASTM}}$.

Piping Phenomena

If a geotextile cannot retain the soil, the permeability at the soil/geotextile interface increases and soil particles pass through the geotextile. The distribution of water head during the gradient ratio test when piping is occurring typically has the shape shown in Figure 2. Gradient ratio values are typically less than 0.75 (ASTM) and 0.5 (SAGEOS).
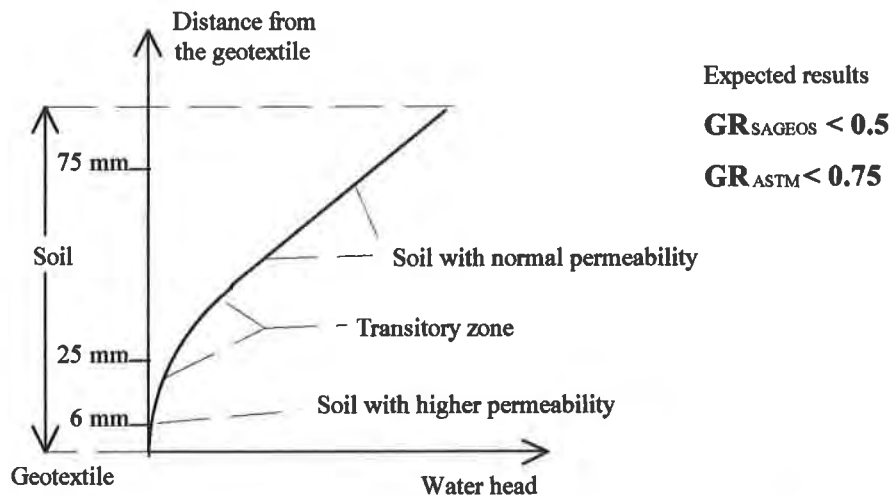
Figure 2. Typical Distribution of Water Head During Piping

Bridging Phenomena

When the construction of the geotextile is such that the soil actually spans the openings and rests on the yarn surface, the water head distribution is nearly linear. Although the permeability at the soil/geotextile interface will be slightly higher than that of the soil itself, very little fines will pass through the system. This type of behavior is the most desirable when conducting gradient ratio tests on cohesionless soils.

Blinding/Clogging Phenomena

Blinding is the filtration phenomena that results from surface blocking of geotextile openings. Systems displaying these characteristics typically have permeabilities very close to

the soil itself and exhibit very small amounts of fines passing through the geotextile. Clogging develops when soil is trapped within the geotextile structure. The distribution of water head in a gradient ratio test experiencing blinding or clogging is shown in Figure 3. Gradient ratio values of greater than 3.0 typically indicate that the filtration systems is experiencing the blinding or clogging phenomena.
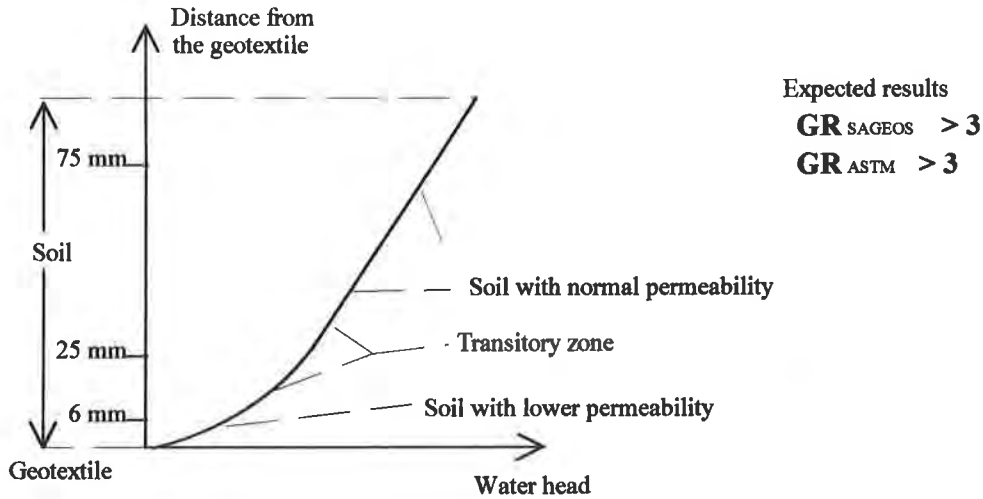
Figure 3. Typical Distribution of Water Head During Blinding/Clogging

In summary, the mass of soil passing through the geotextile is relatively high during piping and the mass of soil particles passing through the geotextile during blinding is low. If clogging occurs, the mass of soil trapped inside the geotextile will be high. Results from the gradient ratio test can be analyzed using the chart presented in Figure 4.
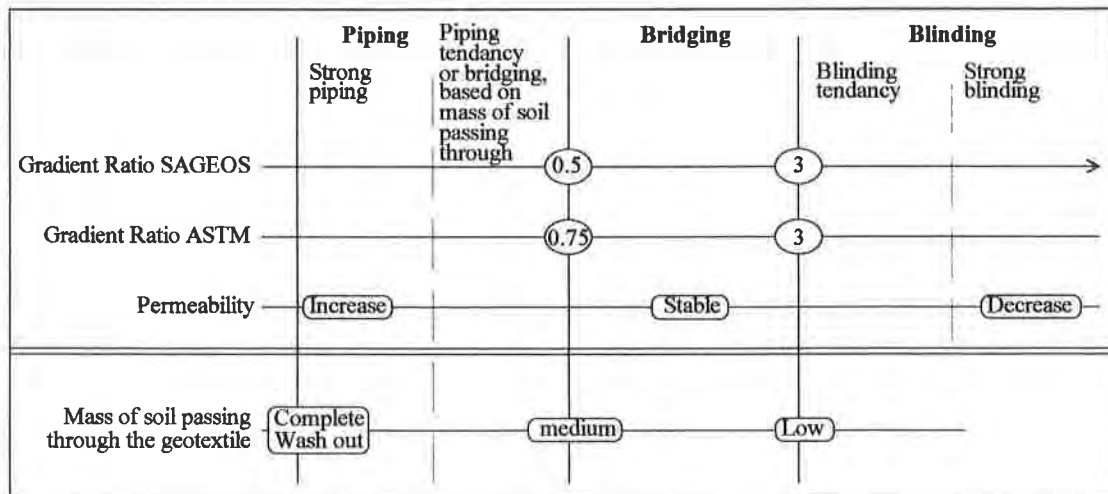
Figure 4. Analysis Chart for Gradient Ratio Test Results

RESEARCH PROGRAM

The research program was designed to evaluate the filtration behavior of several fine-grained soils with various geotextiles under high hydraulic gradients. The soils and geotextiles were selected from the types most commonly encountered in North America and used in filtration applications. Failure of some systems was expected in order to apply upper and lower limits to existing anti-clogging criteria.

Soils

Three (3) cohesionless soils were selected due to their troublesome nature and experience in previous filtration tests. A grain size analysis was conducted on each soil to determine the particle size distribution values required for typical filtration design and selection (d_{10}, d_{15}, d_{30}, d_{60}, d_{85}, and d_{90}), the coefficient of uniformity, C_u (d_{60}/d_{10}) and the coefficient of curvature, C_c ($d_{30}^2/d_{60} \times d_{10}$). The soils used in the study were classified as a silty sand (SM), a poorly-graded sand (SP) and a silt (ML) in accordance with the Unified Soil Classification System. These soils had the grain size distribution as shown in Figure 5.
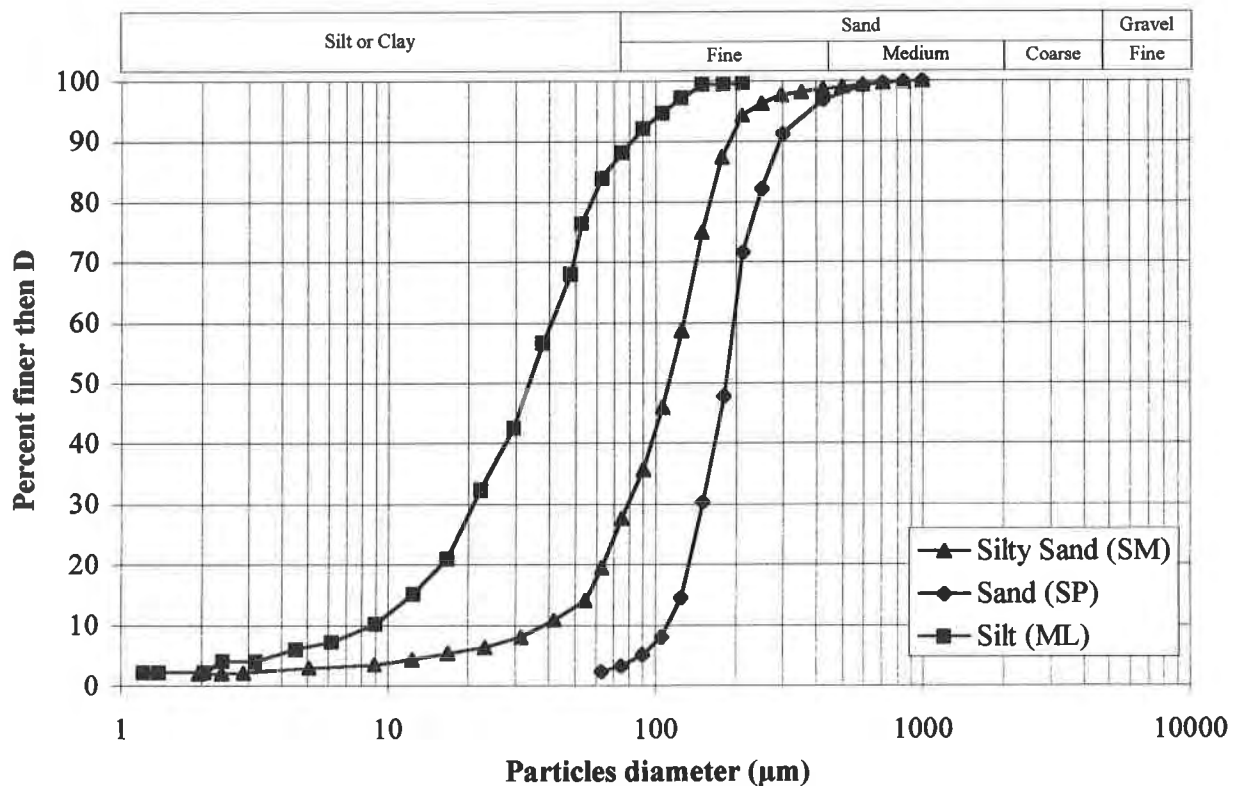
Figure 5. Grain Size Distribution of the Soils Used in Gradient Ratio Tests

Geotextiles

The physical and hydraulic properties for each geotextile were determined. Properties included mass per unit area, thickness, mass per unit volume, filament diameter, permeability, permittivity, filtration opening size (FOS), apparent opening size (AOS), porosity (nonwoven), percent open area (woven) and maximum percent open area (MPOA). Ten (10) different geotextile styles were supplied by Synthetic Industries, Inc. and Carthage Mills. These are generically identified as shown in Table 1.

The properties were measured in accordance with relevant ASTM and Canadian General Standards Board (CGSB) standard procedures. POA, maximum percent open area (MPOA) and filament diameter was measured according to SAGEOS internal laboratory testing procedures. Values for porosity were calculated. These properties are summarized in Table 1. The MPOA was measured under a microscope connected to an image analyzer. The specimen was slowly turned in order to continuously measure the areas of pores under different angles of observation. The maximum measured area of pores is the MPOA of the geotextile. Previous research has suggested this parameter be included into the design criteria for woven geotextile filters (Mlynarek, 1994; Mlynarek, 1997).

Table 1. Selected Properties of Geotextiles Tested

Geotextile Type	Geotextile Composition	Porosity (%) Calculated	AOS (µm) ASTM D4751	FOS (µm) CGSB 148.1-10	POA (%) SAGEOS	MPOA (%) SAGEOS	Permittivity (1/sec) ASTM D4491	Permeability (cm/sec) ASTM D4491
A	WPP - ST x MF	na	226	139	1.63	1.63	0.41	0.028
B	WPP - ST x ST	na	600	205	0.48	0.48	0.07	0.0032
C	NWPP - SF,NP	86.8	180	95	na	na	2.1	0.52
D	NWPP - SF,NP	86.4	150	73	na	na	1.0	0.48
E	WPP - MF x MF	na	212	122	3.4	3.4	0.72	0.023
F	WPP - MF x MF	na	425	224	5.7	5.7	1.6	0.064
G	WPP - MF x MF	na	500	401	12.1	13.1	6.5	0.43
H	WPP - MF x MF	na	355	238	19.2	19.2	15	0.93
J	WPP - MF x MF	na	600	361	16.1	19.5	7.5	0.51
K	WPP - MF x MF	na	655	506	32.7	34.6	25.4	1.7

Notes

"na" indicates that the property is not relevant to that type of geotextile
"WPP" indicates woven polypropylene geotextile
"NWPP" indicates nonwoven polypropylene geotextile
"ST" indicates geotextile contains a slit tape/film yarn in one direction
"MF" indicates geotextile contains a monofilament (i.e. round or oval) yarn in one direction
"SF" indicates geotextile contains staple fibers
"NP" indicates geotextile is produced by needlepunching fibers

Geotextile Qualification

Three geotextile filter design procedures were used to determine what properties are required for each soil/geotextile combination to yield acceptable gradient ratio values. Applying the criteria for retention and clogging to the three soils proposed for use resulted in the recommended geotextile opening sizes (O_{95}), percent open area and porosity values shown in Table 2. Comparing the values shown in Table 2 to the values to the O_{95}, POA and porosity of the ten (10) geotextiles described in Table 1, a prediction of filtration behavior was made (Table 3).

Table 2. Recommended Filtration Properties for the Various Geotextiles

Soil Type (USCS)	Holtz et al. (1995)	Luettich et al. (1992)	Mlynarek (1995)
Sand (SP)	$O_{95} < 265$	$O_{95} < 281$	$183 < O_{95} < 265$
	W: POA > 4% NW: n > 50%	W: POA > 4% NW: n > 30%	W: POA > 4% NW: n > 30%
Silty Sand (SM)	$168 < O_{95} < 280$	$O_{95} < 239$	$112 < O_{95} < 171$
	W: POA > 4% NW: n > 50%	W: POA > 4% NW: n > 30%	W: POA > 4% NW: n > 30%
Silt (ML)	W: $37 < O_{95} < 66$ NW: $37 < O_{95} < 119$	$O_{95} < 95$	$50 < O_{95} < 66$
	W: POA > 4% NW: n > 50%	W: POA > 4% NW: n > 30%	W: POA > 4% NW: n > 30%

Notes

"W" indicates woven geotextile criteria
"NW" indicates nonwoven geotextile criteria
O_{95} as determined by filtration opening size (FOS) tests. Values expressed in microns (μm)
"n" indicates porosity

Table 3. Predicted Filtration Behavior of the Various Soil/Geotextile Combinations

Geotextile Properties			Predicted behavior according to...		
Type	FOS (μm)	POA (%)	Holtz et al. (1995)	Luettich et al. (1992)	Mlynarek (1995)
A	226	1.63	SP: Blinding SM: Blinding ML: Piping	SP: Blinding SM: Blinding ML: Piping	SP: Blinding SM: Blinding ML: Piping
B	600	0.5	SP: Blinding SM: Blinding ML: Piping	SP: Blinding SM: Blinding ML: Piping	SP: Blinding SM: Piping ML: Piping
C	180	na	SP: Bridging SM: Blinding ML: Bridging	SP: Bridging SM: Bridging ML: Bridging	SP: Blinding SM: Blinding ML: Piping
D	150	na	SP: Bridging SM: Blinding ML: Bridging	SP: Bridging SM: Bridging ML: Bridging	SP: Blinding SM: Blinding ML: Piping
E	212	3.4	SP: Blinding SM: Blinding ML: Piping	SP: Blinding SM: Blinding ML: Piping	SP: Blinding SM: Blinding ML: Piping
F	425	8.1	SP: Bridging SM: Bridging ML: Piping	SP: Bridging SM: Bridging ML: Piping	SP: Bridging SM: Piping ML: Piping
G	500	18.7	SP: Piping SM: Piping ML: Piping	SP: Piping SM: Piping ML: Piping	SP: Piping SM: Piping ML: Piping
H	355	19.2	SP: Bridging SM: Bridging ML: Piping	SP: Bridging SM: Bridging ML: Piping	SP: Bridging SM: Piping ML: Piping
J	600	16.1	ML: Piping	ML: Piping	ML: Piping
K	655	32.7	SP: Piping	SP: Piping	SP: Piping

Notes

"SP" indicates a poorly-graded sand
"SM" indicates a silty sand
"ML" indicates a silt

Test Procedure

In addition to the adding the manometer 6 mm above the geotextile, the ASTM procedure was modified to simulate rapid changes of hydraulic gradients, which is consistent with the use of geotextiles as filters in erosion control and subsurface drainage applications. A hydraulic gradient of two (2) was used at the beginning of each test to evaluate the influence of non-critical (i.e. laminar) conditions on filtration behavior. After the filtration curve stabilized (or after three days of testing, whichever came first), the hydraulic gradient was increased rapidly to five (5). This gradient was maintained until the filtration curve was judged stable and then decreased rapidly to two (2); stabilized and then increased rapidly to a gradient of eight (8); stabilized and decreased rapidly to two (2); and finally stabilized and increased rapidly to five

(5). The direction of flow for the first and second cycle was done in the downward direction whereas flow was reversed in the upward direction for the third cycle. This three-step cycle allowed for dynamic flow conditions to be evaluated during the tests.

TEST RESULTS & ANALYSES

Results for each soil/geotextile combination were plotted and presented as shown in Figure 6. Although most observations were made using the gradient ratio values and mass of soil passing through the geotextile, the system permeability was also plotted for each test using the criteria previously described (Figure 4). An example of the visual assessment of the data is shown in Figure 7.
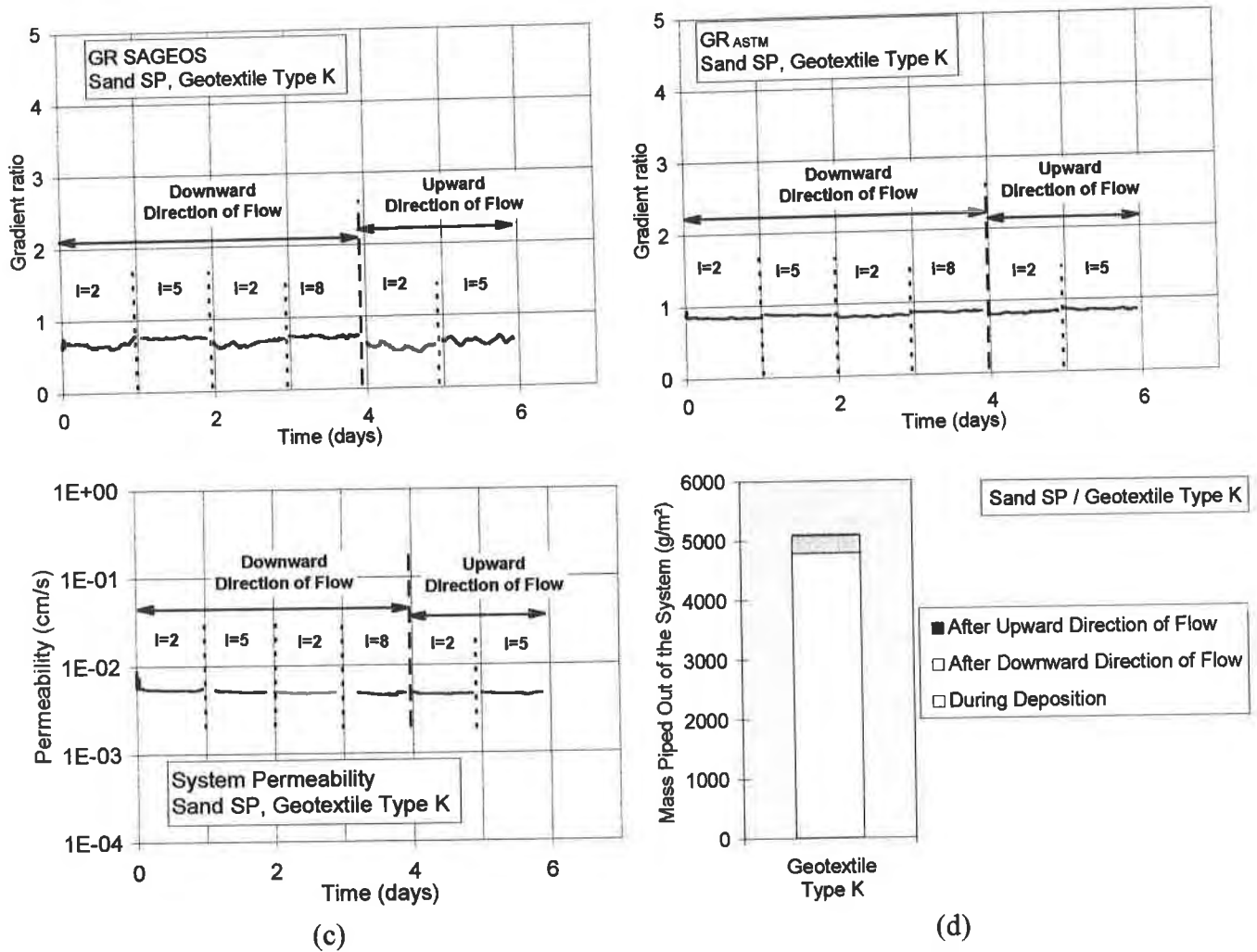
Figure 6. Typical Presentation of Gradient Ratio Test Results
[Sand (SP)/Geotextile Type K Results Used in Above Example]
(a) SAGEOS GR; (b) ASTM GR; (c) Permeability; (d) Mass of Fines Passed
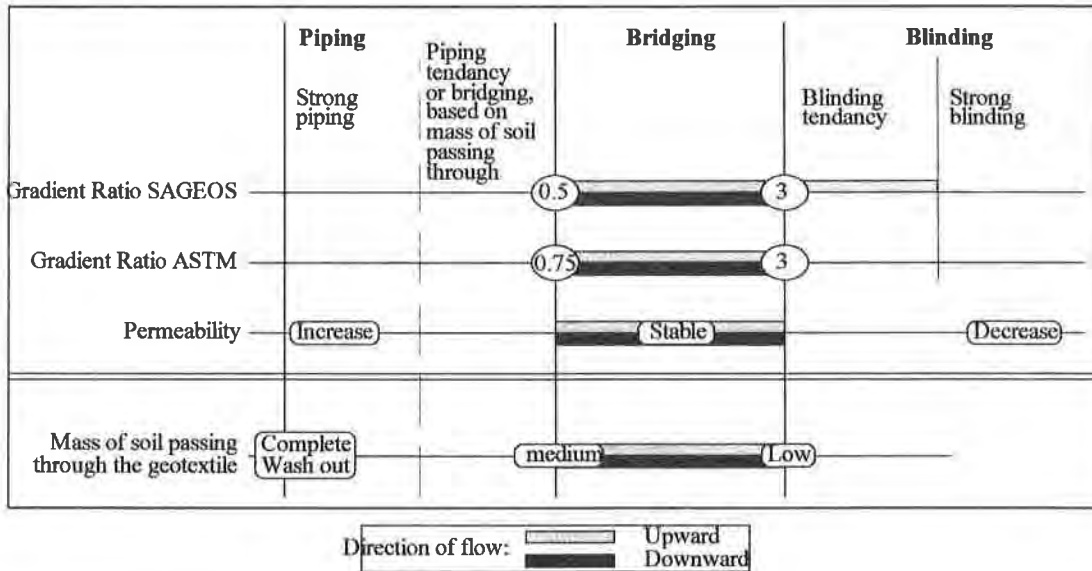
Figure 7. Typical Analysis Chart for Gradient Ratio Test Results
[Silty Sand (SM)/Geotextile Type B Results Used in Above Example]

Sand (SP)/Geotextile Systems

Most of the geotextiles tested demonstrated good filtration behavior (i.e. bridging) with the poorly-graded sand (SP). Based on the gradient ratios, Geotextile Type C, G and H indicated a tendency for piping. Geotextile Type B showed a tendency for blinding/clogging. Although the mass of fines passing from most of these systems was not significant (ranging from 0 to 390 g/m^2), Geotextile Type K system lost a significant amount of soil during the test (4860 g/m^2) even though it demonstrated excellent filtration behavior in terms of gradient ratio values.

Silt (ML)/Geotextile Systems

Based upon the gradient ratio values, Geotextile Types A, B, C, E and J exhibited good filtration behavior (i.e. bridging) while four (4) of the systems, Silt (ML)/Geotextile Types D, F, G and H, indicate a tendency for piping. A significant passing of fines during placement of the soil was noticed for systems containing Geotextile Types G, H and J (1930 g/m^2, 3800 g/m^2, and 1080 g/m^2, respectively). However, the loss of fines decreased significantly once the tests were

underway. It is also important to note none of these systems showed a tendency for blinding/clogging.

Silty Sand (SM)/Geotextile Systems

Based on the gradient ratio values, Geotextile Types A and B demonstrated good filtration behavior (i.e. bridging) while the systems containing Geotextile Type C, D, E, F, G and H indicate a tendency for piping. Of these systems, only Geotextile Types G and H indicated a significant passage of fines (1050 g/m^2 and 3250 g/m^2, respectively). None of the filtration systems showed a tendency for blinding/clogging. The behavior of all systems is summarized in Table 4.

Table 4. Observed Filtration Behavior from Gradient Ratio Tests

Geotextile Type	Observed behavior based on...	
	Gradient Ratio Value	Mass of Passing Fines
A	SP: Bridging SM: Bridging ML: Bridging	SP: Bridging SM: Bridging ML: Bridging
B	SP: Blinding SM: Bridging ML: Bridging	SP: Blinding SM: Bridging ML: Bridging
C	SP: Piping SM: Piping ML: Bridging	SP: Bridging SM: Bridging ML: Bridging
D	SP: Bridging SM: Piping ML: Piping	SP: Bridging SM: Bridging ML: Bridging
E	SP: Bridging SM: Piping ML: Bridging	SP: Bridging SM: Bridging ML: Bridging
F	SP: Bridging SM: Piping ML: Piping	SP: Bridging SM: Bridging ML: Bridging
G	SP: Piping SM: Piping ML: Piping	SP: Bridging SM: Piping ML: Piping
H	SP: Piping SM: Piping ML: Piping	SP: Bridging SM: Piping ML: Piping
J	ML: Bridging	ML: Piping
K	SP: Bridging	SP: Piping

Notes

"SP" indicates a poorly-graded sand
"SM" indicates a silty sand
"ML" indicates a silt

OBSERVATIONS

After the testing was complete, observations were made concerning modifications to the gradient ratio test procedure and device, correlation of results to the predicted behavior and relevancy of the passing of fines during the test to field drainage applications.

Modifications to Gradient Ratio Test

By adding a manometer in the vicinity of the soil/geotextile interface (approximately 6 mm from the geotextile), the gradient ratio test procedure seems to yield values that are more consistent with the observed behavior. Additionally, the mass of fines passing through the geotextile should be measured during test preparation, immediately after soil deposition and at the end of the test. The total amount of fines passing is clearly an indicator of piping.

Geotextile Filter Design Procedures

The accuracy of the three (3) selected filtration design procedures can be evaluated by comparing the predicted results from Table 3 to the actual results in Table 4. All three procedures successfully predicted the piping phenomenon observed with Geotextiles H, J and K. However, of the 26 gradient ratio tests conducted in this study, the retention and clogging criteria successfully predicted the filtration behavior in 42 percent (Holtz et al, 1995; Luettich et al, 1992) to 50 percent (Mlynarek, 1995) of the soil/geotextile systems. These results compare very favorably to comparisons previously made to observed behaviors of installed subsurface drainage systems (Koerner et al, 1994).

Index Properties Versus Filtration Behavior

A correlation between the observed behavior of each filtration system and the index properties of the relevant geotextile was attempted. A relationship between the gradient ratio and percent open area was discovered and is shown Figure 8. Although other research has shown the mass of fines piping through a filtration system has a direct relationship to the AOS and FOS of the geotextile, this was not observed during this research program (Mlynarek and Lombard, 1997). However, a possible relationship between the total mass of soil passing during a gradient ratio test and the POA of the geotextile was discovered as shown in Figure 9. Thickness of the nonwoven geotextiles tested in this program did not influence the filtration behavior of the systems. This observation is supported by previous research (Rollin et al, 1994).
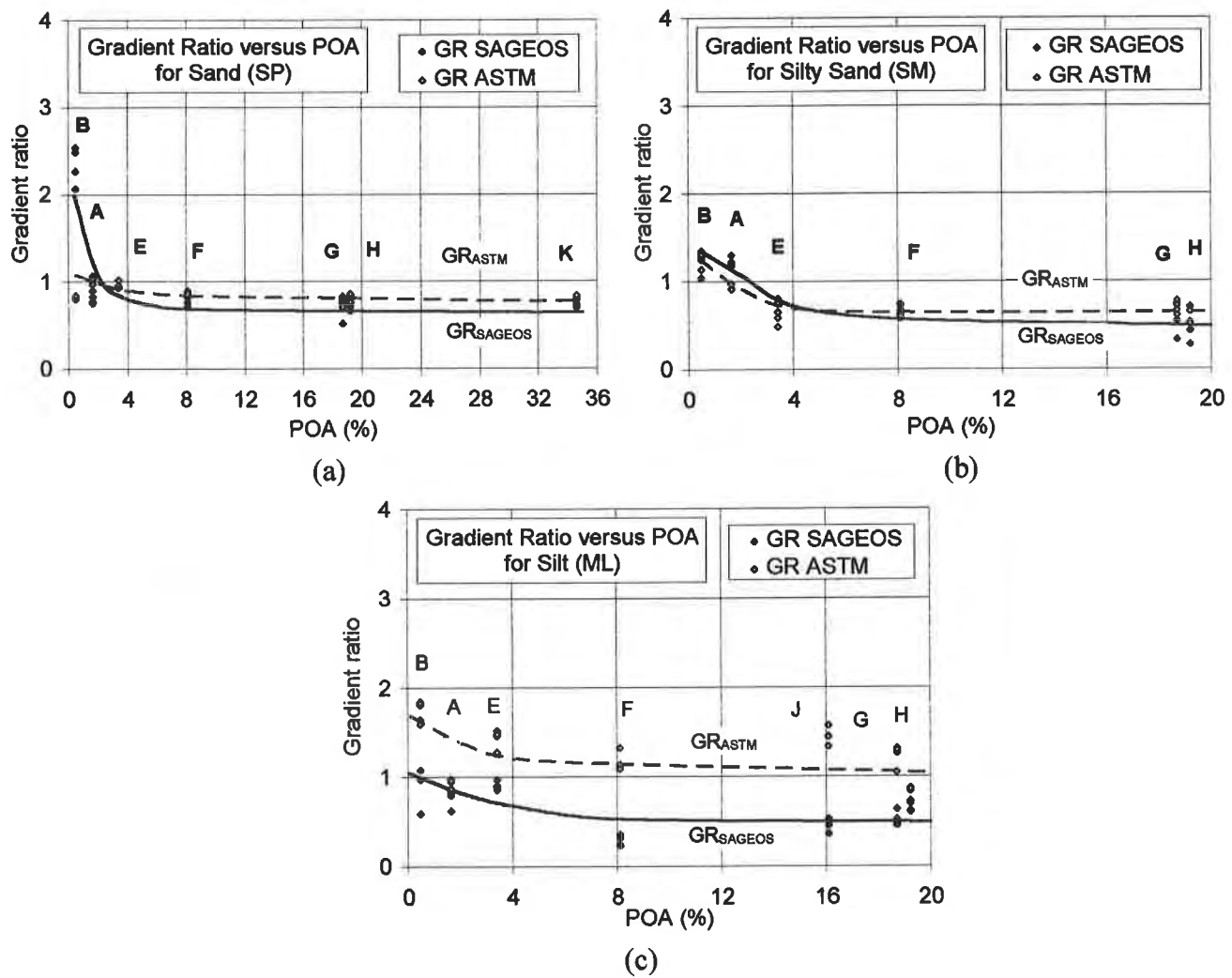
Figure 8. Relationships Between Gradient Ratio and Percent Open Area for Woven Geotextiles
(a) for Sand (SP); (b) for Silty Sand (SM); (c) for Silt (ML)
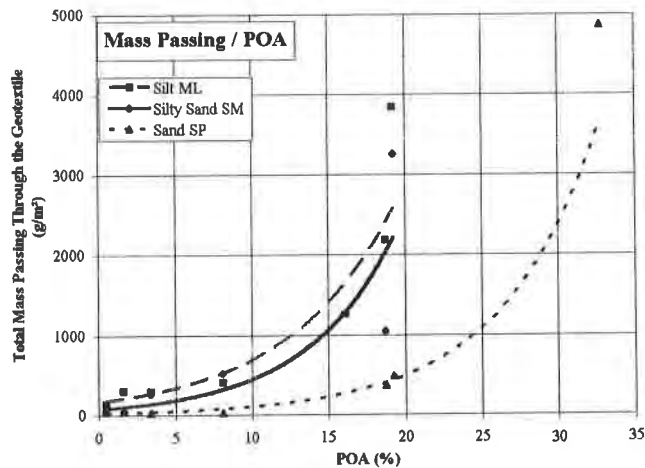
Figure 9. Mass of Soil Passing versus POA

Passing of Fines

Based upon these test results, the gradient ratio values and the mass of passing or piped particles should both be analyzed when evaluating the filtration behavior of geotextiles. Although it is commonly accepted that low gradient ratio values indicates soil piping, many of the systems evaluated had a gradient ratio well below 1.0 and no significant wash out of fines was observed. This means that these soil/geotextile systems developed excellent filtration behavior without building excess pore pressure. More than likely, the geotextile filter behaved as a catalyst to develop an excellent filtration system. Therefore, the mass of piped fines should be used to estimate the potential for piping.

The currently published acceptable limit of the mass of fines passing through the geotextile during a filtration test is 2500 g/m² (Lafleur et al, 1992). This value is defined as the acceptable quantity of particles that can be trapped in a drainage system without disturbing its overall performance. However, this value does not take into account the size of the drainage system. Although most of the geotextiles in this research program would also be used on banks and shorelines as filters beneath hard armor systems, a drainage pipe would represent the most critical situation where excessive loss of fines might cause it to clog.

Assuming the soil that enters a drainage pipe through the openings in the geotextile filter settles in a very loose state (e.g. dry unit weight, $\gamma_d = 10$ kN/m³) and is located 100 meters from the end of the pipe, calculations were made to determine the acceptable mass of fines trapped in a 100-meter long pipe of various diameters and slopes. The soil may accumulate at the lowest point in the pipe, possibly due to differential settlement. This is presented in Figures 10 and 11.
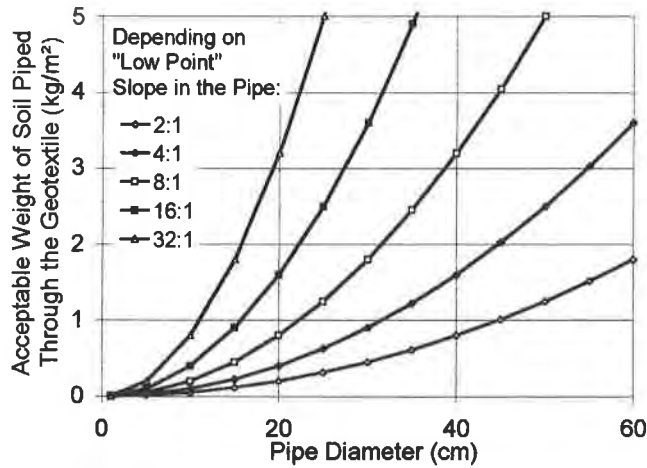
Figure 10. Acceptable Quantity of Soil in a Drainage Pipe.
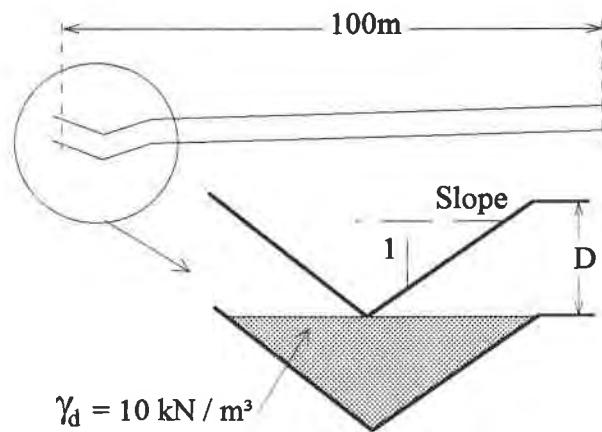
Figure 11. Configuration of the Lowest Point in a Drainage Pipe

For example, a 15-cm diameter drainage pipe with a low point slope of 16H:1V could accept up to 900 g/m^2 of fines from the geotextile filter over 100 meters length without impeding the flow. Therefore, the acceptable mass of particles passing through the geotextile filter becomes a design parameter that should be considered when choosing a drainage pipe diameter or a geotextile for hard armor underlayment.

Current Selection Criteria

The accuracy of selection criteria used by the American Association of State Highway Transportation Officials (AASHTO), the Federal Highway Administration (FHWA) and the US Army Corps of Engineers (COE) was also studied. Since these techniques do not take soil type into account when considering clogging behavior of geotextile filters, the results of these tests could be used to refine these nationally-recognized standards.

Since blinding was observed in the Sand (SP) system containing woven geotextile with a POA of less than 0.5% (Geotextile Type B) and piping was not noticed for woven geotextiles with POA values of up to 19.2% (Geotextile Type F), additional gradient ratio tests are recommended using woven geotextiles with a 19%<POA<32% to discover an upper limit for poorly-graded sands. Although none of the geotextiles tested indicated blinding potential in the Silty Sand (SM) and Silt (ML) systems and the woven geotextile with a POA of 16.1% (Geotextile Type J) indicated piping, it appears that the upper limit is 8%<POA<16%.

Based upon this research program, AASHTO should revise their geotextile selection criteria to included a minimum POA of 4%. Although the anti-clogging criteria established by FHWA and the COE seems to be sufficient for course sands, the POA for poorly-graded sands could be lowered to 1.6% without the risk of clogging. However, an upper limit of approximately 20%<POA<30% should be established in order to prevent the loss of excessive fines. Silt and silty sands may have a lower limit for POA of 0.5% and an upper limit of 8%.

CONCLUSIONS

An extensive gradient ratio research program was conducted using three (3) fine-grained, cohesionless soils and ten (10) geotextiles. All relevant properties of the selected soils and geotextiles were evaluated, their filtration behavior was predicted using three recognized design procedures and the results of the tests were analyzed and observations were made concerning relationships between predicted and actual performance, index versus performance tests and the appropriateness of existing design and selection procedures for woven geotextiles used as filters in drainage. Based upon the results from these gradient ratio tests and other referenced documents, the following conclusions can be made:

- The gradient ratio test is a very important tool used to predict the filtration behavior of geotextiles in cohesionless soils. By adding an additional manometer approximately 6 mm above the soil/geotextile interface, the accuracy of the test can be improved.

- Measuring the mass of fines passing during a gradient ratio test is also an excellent way to help assess the filtration behavior of the geotextile.

- Although piping was observed in many of the soil/geotextile combinations, the mass of fines passing is not as troublesome as it appears. The amount of fines passing through a woven geotextile with a POA of 32% is not enough to create stability problems. Furthermore, a drainage system can use a woven geotextile that passes some fines during a gradient ratio test as long as the flow capacity of the drainage pipe is considered during the design.

- Percent open area (POA) is the single most important property in the selection of a woven geotextile filter and has a direct correlation to gradient ratio with the soils tested in this study, namely poorly-graded sand (SP), silty sand (SM) and silt (ML).

- Although the limit of acceptable gradient ratio values assumed prior to testing was $0.5 < GR_{SAGEOS} < 3.0$ and $0.75 < GR_{ASTM} < 3.0$, the authors recommend that the range be modified to $0.8 < GR_{SAGEOS} < 1.0$ and $0.95 < GR_{ASTM} < 1.5$. When following either the ASTM or SAGEOS test procedures, gradient ratio values above 2.0 are considered risky.

- Considering all three (3) soils evaluated, Type E was the best performing geotextile filter.

- The minimum anti-clogging criteria recommended by the Federal Highway Administration (FHWA) and the US Army Corps of Engineers (COE) of POA > 4% is applicable for course sands. However, it is possible that this value could be lowered to 1.6% for fine, poorly-graded sands (SP) and may have an upper bound of 20 to 30%.

- The recommended anti-clogging criteria for silty sand (SM) and silt (ML) is $0.5\% < POA < 8.0\%$.

- The thickness of a nonwoven geotextile has no correlation to filtration performance.

ACKNOWLEDGEMENTS

REFERENCES

Anonymous, (1995), <u>ASTM Standards on Geosynthetics</u>, 4th Edition, American Society for Testing and Materials, Philadelphia, Pennsylvania, USA.

Anonymous, (1994), <u>Engineering Use of Geotextiles</u>, Joint Departments of the Army and Air Force, TM 5-818-8/AFJMAN 32-1030, Washington, D.C., USA.

Anonymous, (1977), <u>Guide Specification for Plastic Filter Cloth</u>, CW-02215, US Army Corps of Engineers, Washington, D.C., USA

Anonymous, (1990), "Standard Specifications for Geotextiles, Designation M288-90", <u>Standard Specifications for Transportation Materials and Methods of Sampling and Testing - Part I Specifications</u>, Fifteenth Edition, American Association of State Highway Transportation Officials (AASHTO), Washington, D.C., USA.

Anonymous, (1992), <u>Standard Specifications for Construction of Roads and Bridges on Federal Highway Projects FP-92</u>, U.S. Department of Transportation, Federal Highway Administration, Washington, D.C., USA, Section 714.

Anonymous, (1996), <u>Standard Specifications for Construction of Roads and Bridges on Federal Highway Projects FP-96</u>, U.S. Department of Transportation, Federal Highway Administration, Washington, D.C., USA, Section 714.

Bhatia, S.K., Huang, Q. and Hawkins, W.M., (1995), "The Soil-Geotextile Interface Stability Under Sudden Change in Hydraulic Conditions," <u>Geosynthetics '95 Conference Proceedings</u>, Nashville, Tennessee, Industrial Fabrics Association International, St. Paul, Minnesota, USA, p. 469-481.

Calhoun, C.C. (1972), <u>Development of Design Criteria and Acceptance Specifications for Plastic Filter Cloth</u>, Technical Report S-72-7, US Army Waterways Experiment Station, Vicksburg, Mississippi, USA, June 1972, p. 55

Christopher, B.R. and Holtz, R.D., (1985), <u>Geotextile Engineering Manual</u>, Report No. FHWA-TS-86/203, Federal Highway Administration, Washington, D.C., USA.

Fluet, J.E. and Luettich, S.M. (1993), "Geotextile Filter Criteria for Gap-Graded Silty Sands", <u>Geosynthetics '93 Conference Proceedings</u>, Industrial Fabrics Association International, St. Paul, Minnesota, USA, p. 469-481.

Haliburton, T.A., and Wood, P.D., (1982), "Evaluation of the US Army Corps of Engineers Gradient Ratio Test for Geotextile Performance", Proceedings from the 2nd International Conference on Geotextiles, Las Vegas, Nevada, USA, Vol.1, p. 97-101.

Holtz, R.D., Christopher, B.R. and Berg, R.R., (1995), Geosynthetic Design and Construction Guidelines, Publication No. FHWA HI-95-038, NHI Course No. 13213, Federal Highway Administration, Washington, D.C., p.31-47.

Koerner, R.M., Koerner, G.R, Fahim, A.K. and Wilson-Fahmy, R.M., (1994), Long-Term Performance of Geosynthetics in Drainage Applications, NCHRP Report 367, Transportation Research Board, Washington, D.C., USA.

Lafluer, J., Mlynarek, J. and Rollin, A.L., (1992), "Filtration of Broadly Graded Cohesionless Soils", Journal of Geotechnical Engineering, American Society of Civil Engineers, New York, New York, Vol. 115, No. 12, p. 1747-1768.

Luettich, S.M., Giroud, J.P. and Bachus, R.C., (1992), "Geotextile Filter Design Guide", Geotextiles and Geomembranes Journal, Special Issue on Geosynthetics in Filtration, Drainage and Erosion Control, Vol. 11, Nos. 4-6, p. 355-441.

Mlynarek, J., Lafleur J. and Rollin, A.L., (1992), "Filter Criteria for Well-Graded Cohesionless Soils", Proceedings of the First International Conference on Geofilters, Karlsruhe, Germany, p. 97-103.

Mlynarek, J., (1995), "Geotextile Design for Filtration", Notes from Short Course on Geosynthetics, Canadian Geotechnical Conference, Vancouver, British Columbia, Canada.

Mlynarek, J. and Lombard, G. (1997), "Significance of Percent Open Area (POA) in the Design of Woven Geotextile Filters", Geosynthetics'97 Conference Proceedings, Long Beach, California, Industrial Fabrics Association International, St. Paul, Minnesota, USA, p. 469-481 (in press).

Rollin, A.L., Mlynarek, J., Hoekstra S.E. & Berkhout, H.C. (1994), "Geotextile Thickness : A Relevant Filter Design Criterion", Proceedings of the 5th International Conference on Geotextiles, Geomembranes and Related Products, Singapore, Vol. 2, p. 695-698.

Author Index

Author Index

Subject Index

The pages listed indicate the first page of the paper in which the reference is found.

Subject Index

GFR

Geotechnical Fabrics Report

Fifteenth year and growing...

Published nine times a year, GFR is the geosynthetics industry's most respected and credible magazine. It provides 16,000 civil engineers, contractors and installers with the latest information on design techniques, product developments and cost-saving solutions.

For a limited time, you can receive one full-year subscription for only $28.* This subscription includes the Specifier's Guide—the ultimate reference for the geosynthetics industry.

To stay informed, just fill out the required information below and fax to 612/222-8215, or mail to

Geotechnical Fabrics Report
345 Cedar St., Suite 800
St. Paul, MN 55101-1088 USA
phone 612/222-2508, e-mail gfr@ifai.com.

> **Need extra copies of the 1997 GFR Specifier's Guide? Extra copies are available for only $20* each.**

☐ **Yes,** send me additional copies of the Specifier's Guide for only $20 each, plus postage and handling.

☐ **Or better yet,** start my subscription to Geotechnical Fabrics Report. I'll receive 8 issues plus the Specifier's Guide for only $28.*

We will bill you. *Introductory offer. Only valid for new subscriptions; Canada and Mexico $32; All other countries $39.

What is your title?
(Check ONE only.)

☐ Owner/Corporate Executive (G1)
☐ Chief/Staff Engineer (G2)
☐ Geotechnical Engineer (G3)
☐ Consulting Engineer (G4)
☐ Civil Engineer (G5)
☐ Research & Development (G6)
☐ Purchasing (G7)
☐ Sales/Marketing (G8)

☐ Professor (G9)
☐ Librarian (G10)
☐ Student (G11)
☐ Other. Please specify.(G99)
_____

What is your primary business?
(Check ONE only.)

☐ Engineering Firm/
   Engineer in Private Practice (GA)
☐ Government Agency (GB)
☐ Contractor (GC)
☐ Geosynthetic Installer (GD)
☐ Installation/Fabrication Equipment (GE)
☐ Installation/Fabrication Accessories (GF)
☐ Testing Service/Equipment (GG)

☐ Geosynthetic Producer/Distributor (GH)
☐ School/Association/Publication/Library (GI)
☐ Commercial/Industrial (GJ)
☐ Waste Management/Landfill (GK)
☐ Other. Please specify.(GW)
_____

Name: _____   Complete mailing address: _____

Phone: _____   Fax: _____   E-mail: _____

Signature: (required) _____   Date: _____

Geosynthetics '97 Conference Proceedings

Volume 1

High-Strength Reinforcement
Marine
Geosynthetics Durability
Student Session
Remediation and Containment
Erosion Control

Volume 2

Pavement Systems
Economics
Interface Friction Testing
Seismic Design and Construction
Mining
Filtration

GEOSYNTHETICS

97

CONFERENCE
Long Beach, California USA